

KAPPA

Dynamic Data Analysis

v5.30

The theory and practice of Pressure Transient Analysis, Rate Transient Analysis, Formation Testing, Production Logging and the use of Permanent Downhole Gauges

Olivier Houzé, Didier Viturat, Ole S. Fjaere et multi alii

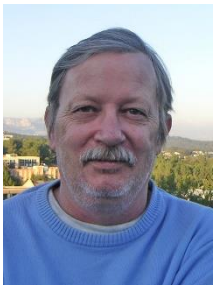
Main authors



Olivier Houzé (OH)
Engineer from Ecole Polytechnique (1982) and MSc in Petroleum Engineering from Stanford University (1983); four years with Flopetrol (Schlumberger) as a well test field engineer; co-founder of KAPPA in 1987; original author of Saphir; author of several SPE papers and co-author of the SPE Monograph on Pressure Transient Testing (2009); SPE Distinguished Lecturer (2013); SPE Board, Technical Director for Reservoir (2012-15); recipient of the SPE Lester C. Uren Award (2019)



Didier Viturat (DV)
Engineering Degree from Ecole Centrale de Lyon (France, 1975) and from the IFP school (France, 1976). Thirteen years as a Field Engineer, Reservoir engineer and Instructor with Flopetrol and Schlumberger Testing. Eight years as Reservoir Engineer with Geoservices and Geopetrol. Head of technical support, principal trainer and consultant in KAPPA Engineering since 1999. Author of several papers on Well Test Analysis methods



Ole S. Fjaere (OSF)
BSc in Petroleum Engineering from Rogaland Regional College (Norway, 1975). Ten years with Flopetrol (Schlumberger) as a well test and wireline operator, well test interpretation engineer and line management. Joined KAPPA in 1989 as an instructor and consultant in Pressure Transient Analysis. Experience in training and many field studies worldwide. Initiated the integration and the content of the QA/QC in Saphir based on a practical field experience with SHELL Gabon

Credits to

Past project contributors: **Tom Blasingame, Dilhan Ilk**, **Simon Trin**

Technical author: **Véronique Chassignol**

Artworks: **Claire Turner, Benoît Berthoud**

Reviewers: **Joop de Wit, Kevin Siggery**, **David Wynne**

Other contributing authors



Olivier Allain (OA)
Ecole Nationale des Ponts et Chaussées (1987); MSc and Engineer degrees in Petroleum Engineering from Stanford University (1987, 1988); Technical Director of KAPPA since 1991



Vincent Artus (VA)
PhD in Reservoir Engineering from IFP (2003); Post-doc at Stanford University (2004) and Research engineer at IFP; joined KAPPA in 2005; currently in charge of all numerical developments



Eric Tauzin (ET)
Engineer from ENSEEIHT (1992) and MSc in Petroleum Engineering from Stanford University (1995). Joined KAPPA in 1998. Head of software development, in charge of KAPPA-Workstation since 2013



Dasha Latysh (DL)
Degree in Applied Mathematics at Ufa SAT University (2007). MSc in Petroleum Engineering from Tomsk Heriot-Watt (2008). 2 years in Rosneft. Joined KAPPA in 2010. Development support in France



Irina Kostyleva (IK)
BSc Novosibirsk Univ., MSc in Pet. Eng. at Heriot-Watt Univ. (2008), PhD at Imperial College London (2015). Joined KAPPA in 2015, Technical Support lead on Citrine and Unconventional Resources



Juan Carlos Nunez (JCN)
Engineer degree UCV-Venezuela (2009); MSc Petroleum Economics & Management at IFP (2011). 3 years Reservoir Engineer with Repsol. Joined KAPPA in 2014, Technical Support lead on Azurite



Nicolas Kotlar (NK)
Engineer degree from UNMDP Argentina (2009), MSc in Reservoir Engineering from YPF (2011). Two years with YPF. Joined KAPPA in 2013 & 2018. Technical support lead on Emeraude



Daniel Nakaska (DN)
Degree in Electrical Engineering from Queens University (2006). Seven years with Fekete as Reservoir Engineer. Two years with Anderson Thompson. Joined KAPPA in 2017 as Citrine's Project Lead



Dave Belanger (DB)
BSc in Mechanical Eng. UC Berkeley (1981); 10 years with Schlumberger, 25 with Chevron as petrophysicist and Sr Research Engineer (USA, Kazakhstan and Angola). Joined KAPPA in 2016

1 – Introduction

OH

Based on the number of registered downloads, this book is quite popular in the E&P industry! This may be somewhat related to the fact that it is free…

However, we hope it is not only that, and that the evolving content of this PDF book justifies the substantial effort invested to write, print and read it.

1.A What is this book for?

Since its first version this book was written to be used as…

1. a stand-alone technical book regularly updated on the methodologies related to the analysis of dynamic data

2. a set of reference notes for KAPPA training courses on:
    a. Pressure Transient Analysis / Rate Transient Analysis
    b. Unconventional Resources (URAP)
    c. Production Logging
    d. Formation Tests
    e. Permanent Gauges and Intelligent Fields
    f. In-house courses of various, flexible content

3. a technical reference manual for KAPPA software products

This book is NOT about software functionalities. Tutorials, online videos and online Help exist for that purpose. We focus on the methodology related to the analysis of dynamic data.

However, we shamelessly take and produce screenshots from our software products. Though there are certainly other very good commercial software around we are not there to make advertising for our competition ☺.

Incidentally we do not promote such or such method because it is integrated in our software products. It is the other way around: by default, we implement in priority what we believe in, though we may add methods for which we are not enthusiastic, but which do not hurt. We refuse to implement what we think is wrong, whatever the commercial pressure. But, in these cases, we try to explain why…

1.B What is new in this version?

This new release (v5.30.01, January 2020) integrates a new chapter (18) in thermal analysis and simulation. As this was part of our numerical developments we have taken this opportunity to completely reorganize and substantially update our chapter on numerical models (14). We have also substantially updated our chapter on PL (17) in order to integrate our latest developments on Emeraude.

In the chapter of reservoir models (7) we have added the description of two fall-off models related to polymer injection and water injection in fractured formations. We have also kept on improving our chapter on unconventional resources (10) with the addition of analytical models, segmented DCA and anomalous diffusion.

The rest is basically update of screenshots and minor improvements.

We hope you will enjoy reading it as much as it was a painful process to put it together…

OH

…a boring note on Copyrights

Sorry to talk about this dull detail but this is a sign of the times. This book is the intellectual and commercial property of KAPPA. It is available on our WEB site at no cost to registrants. You are welcome to download it and print it for your own use. If you are in the academic world, or even if you are a professional instructor, you are welcome to have it printed for your students. You are also permitted to take any part of it and integrate it into other media on the condition that the copyright of KAPPA is added and visible. This applies to the copies of the copies, etc.

You are NOT allowed (and KAPPA reserves the right to take legal action and would):

- To commercialize this book in whole or in part;
- To use any part of this book in any media format without a clear reference and acknowledgement to KAPPA.

We have seen in the past that some of our diagrams and figures, available from our software, on-line help or the support material we deliver with our courses, have been used in other publications. KAPPA has no objection to this however we do ask, and expect, to be acknowledged. Since the foundation of the Company KAPPA has regularly and systematically officially registered its software and supporting diagrams and figures. In addition the figures we insert in our published documents are bitmap exports of vector (Illustrator™) original documents that we also keep and register. So we can prove both the chronological and technical history of our supporting material.

1.C What is Dynamic Data Analysis?

Dynamic Data are the result of transient measurements of fluxes (rates) and physical properties (pressures, temperatures, saturations, etc) when petroleum and other fluids are moved around the reservoirs, generally to and from some wells. This occurs at different scales in time and space, from the shortest formation tests to the full production life of the wells. **Dynamic Data Analysis** includes all methodologies and tools developed by our industry to analyze these dynamic data and forecast their behavior at these different time scales.

When KAPPA was created in 1987, the main and almost only source of dynamic data was the well test operations. Analyses of acquired data were called well test interpretation. Though producing periods could theoretically be used, the essence of well test interpretation was to analyze the relatively smoothed shut-in periods, whether build-ups or fall-offs. Things changed when the same methods were extended to other operations where shut-ins are recorded, such as formation tests and unplanned shut-ins recorded by permanent gauges. Well test interpretation was progressively rebranded **Pressure Transient Analysis**, or PTA (see chapter 3). For KAPPA this is the scope of **Saphir**, initially released in 1988.

In the late 1990's, engineers started looking at rates and pressures at the time scale of the well production life. They initially tried to use PTA software products, but this did not work, as models and hypotheses at this time scale had to be different. Decline Curve Analysis, or DCA, had be initiated in the 1920's based on empirical observation of rate decline. In the 1980's, methods were enhanced with superposition, loglog plots, Blasingame plots and all the models already developed for PTA. All these tools became **Rate Transient Analysis**, or RTA (see chapter 4). For KAPPA, this is the scope of **Topaze**, initially released in 2003.

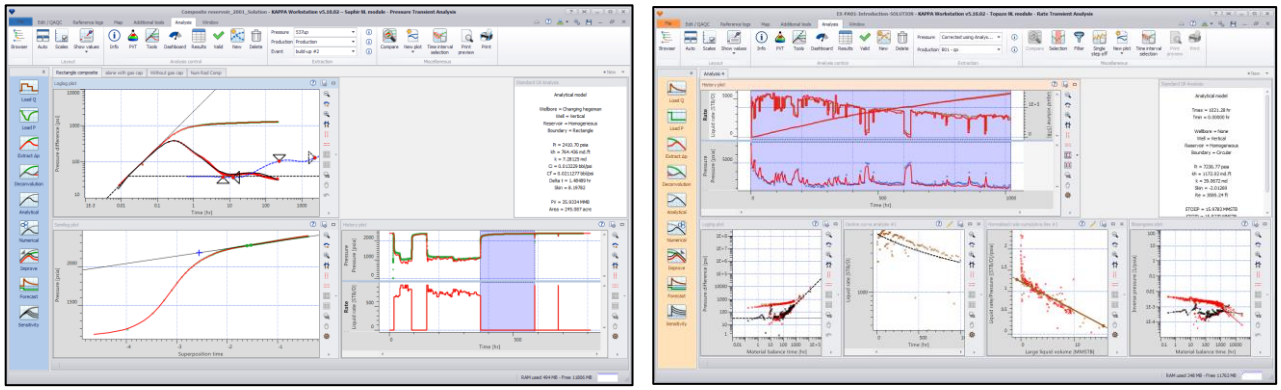


Fig. 1.C.1 – Pressure Transient Analysis (Saphir) and Rate Transient Analysis (Topaze)

The development of **Permanent Downhole Gauges**, or PDG, brought an unexpected source of PTA and RTA data. The number of recorded points was massive and reservoir engineers had their first experience of data overflow. This overflow was addressed with the development of smart filters and dedicated client-server applications (see chapter 16). Then came information overflow: It is not about the volume of the recorded data, but the large number of potential information which may be extracted from the analysis of these data. Engineers would never have the time to process everything and would proceed by exceptions. This was the origin of Intelligent Fields projects, which combine permanent acquisition and storage in historians, a federating data model and some specific workflows.

Automatic processes now do most of the ground work while engineers focus on exceptions that require remedial decisions. Initially released by KAPPA as the Diamant module in 2003, this workflow is now integrated in a client-server process named **KAPPA Server**.

To match the observed data, both PTA and RTA started using analytical models (see chapter 13). The development of the Bourdet derivative and high accuracy gauges produced an explosion of the publications of new analytical models, whether at the level of the wellbore (see chapter 5), the well geometries (see chapter 6), the reservoir diffusion (see chapter 7) and the reservoir extent (see chapter 8).

There has been a growing interest in using numerical models (see chapter 14) to address the limitations of analytical models in terms of geometries and diffusion equations. These models have been increasingly used in the past ten years, thanks to unstructured grids, enhancements in numerical inversion techniques and PC power, allowing the use of these models without significantly increasing the overall duration of an analysis.

In a more traditional way, numerical models are also used for forward reservoir simulation and history matching. An interesting application of unstructured grids is the ability to adapt the grid to the time scales and special details of the model. This allows using variations of the same model for PTA, RTA and history matching. In KAPPA this process achieved using a **multipurpose numerical model**, simultaneously available and adapted in Saphir, Topaze and our full-field reservoir model, **Rubis**, initially released in 2008.

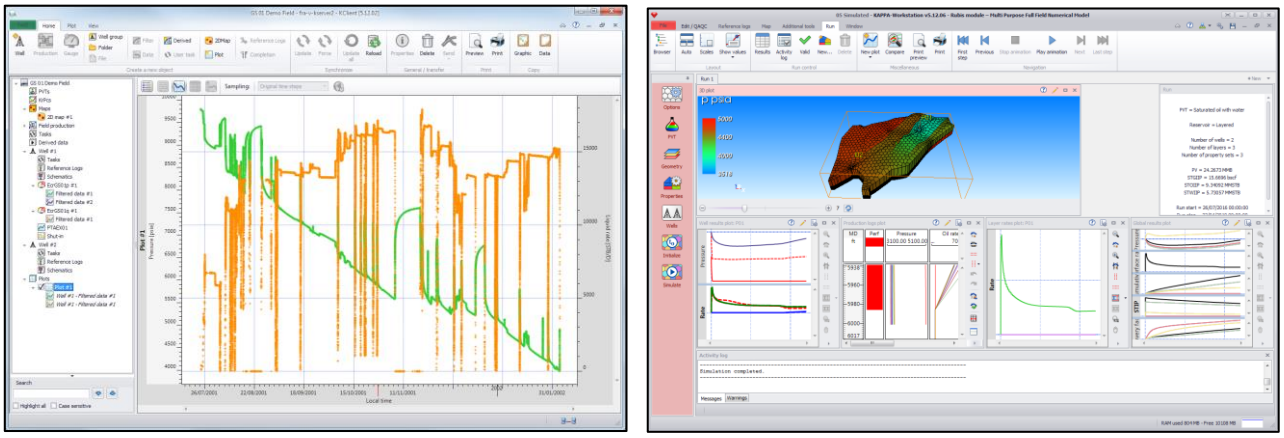


Fig. 1.C.2 – PDG processing (KAPPA Server) and Full-field numerical model (Rubis)

Previous generations of **Formation Testing** operations (see chapter 11) were designed to find static pressures. Multiple stations would provide an initial static pressure gradients and initial fluid contacts. The last generation of formation testers is much more sophisticated. It allows taking multiple PVT samples in a flow sequence that is a good candidate for Pressure Transient Analysis. Multiple observation probes allow a vertical understanding of the system but require specific processing and modeling. KAPPA has now integrated in the KW 5.20 package **Azurite** dedicated to the formation Testing analysis using the latest analysis methods.

Though one would wish to have a perfect understanding of the underlying physical behaviors and use the different methodologies and modeling capabilities available for the analysis of dynamic data, lack of time, and sometimes lack of data, make the process nearly impossible to apply when an engineer has to handle hundreds of wells on a daily basis.

This is particularly the case for unconventional resources (see chapter 10), where thousands of wells are drilled and fractured without virtually any metrology. In these cases pragmatism dictates the use of empirical decline curves, to which physical models may be substituted when a few wells have been properly monitored, interpreted and modeled. This area is called **Field Performance Analysis**. For KAPPA this is the scope of **Citrine**, developed in cooperation with DeGolyer and MacNaughton, and initially released in 2014.

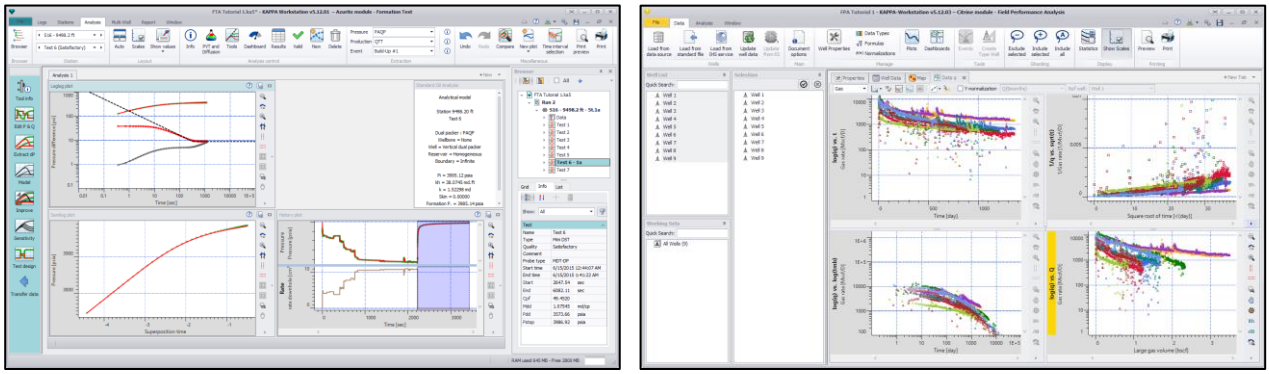


Fig. 1.C.3 – Formation Testing (Azurite) and Field Performance Analysis (Citrine)

Production Logging, or PL tools used to be run when something was wrong with the well production. In the past twenty years this perception has evolved. PL is now a full scale reservoir tool, especially in multilayered formations and for complex well geometries (see chapter 17). In KAPPA this is the scope of **Emeraude**, initially released in 1996.

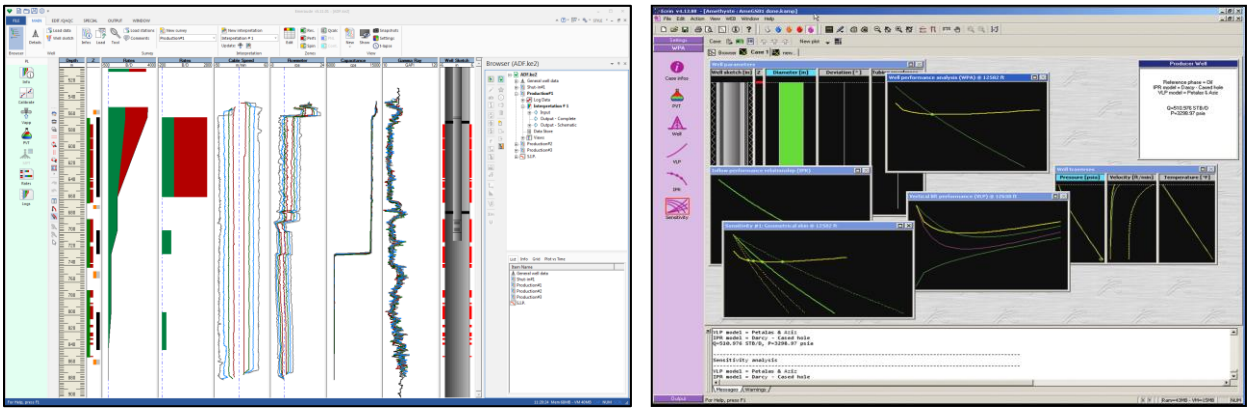


Fig. 1.C.4 – Production Logging (Emeraude) and Nodal Analysis (Amethyste)

If we consider that all the above deal with transient data (even very long transients) **Nodal Analysis** is somewhat at the junction between the transient and the steady state or pseudo-steady state worlds. Though it generally uses steady-state models it is applied in transient analysis to correct responses to datum. It shares the IPR's with the PTA, and used the same well models and flow correlations as the PL (see chapter 15). In KAPPA, this is the scope of **Amethyste**, initially released in 2009.

Traditionally analysis and forecast have been focusing on pressures and rates. **Temperature** was a secondary information. The temperature channel would traditionally be used as a correcting factor to calculate the pressure from the gauge sensor raw measurements. A constant reservoir temperature would be used to define the PVT properties in the reservoir. Temperature gradients would be used to calculate wellbore profiles in Nodal Analysis, and sometimes, in Production Logging, the temperature response could be used as a Plan B when the mechanical spinner has failed. Things are changing today with the spread of fiber-optics installation, and the development of temperature models for both wellbore and even the diffusion in the reservoir. The changes in temperature profile are also a smooth indicator of shut-ins when pressure is too noisy. Using temperature is a work in progress, and for KAPPA temperature processing is now present in Rubis, Emeraude, Amethyste and KAPPA Server.

In summary, the analysis of dynamic data has become a patchwork of techniques which cover various ranges of time and space. The diagrams below are a horizontal and vertical schematic sections of the areas covered by these different techniques. The reality is naturally more complex and the boundaries between these techniques are naturally fuzzy:

- Purple: Nodal Analysis allows, among other things, to model the pressure change between the sand face and any point in the wellbore, including the well head.
- Green: Production Logging addresses the flow in the wellbore at the sand face, with the ability of identifying phase contribution of the different producing zones.
- Yellow: Formation Testing covers a relatively small drainage area but with a resolution far better than classical well testing.
- Blue: PTA assesses the well and the reservoir within a zone called radius of investigation (blue disk), which can be increased with deconvolution (blue circle)
- Orange: RTA assesses and forecasts the productivity of the well in its drainage area.
- Red: Full-field Numerical Modelling and Field Performance Analysis consider the whole reservoir production for more or less sophisticated analysis and history matching.

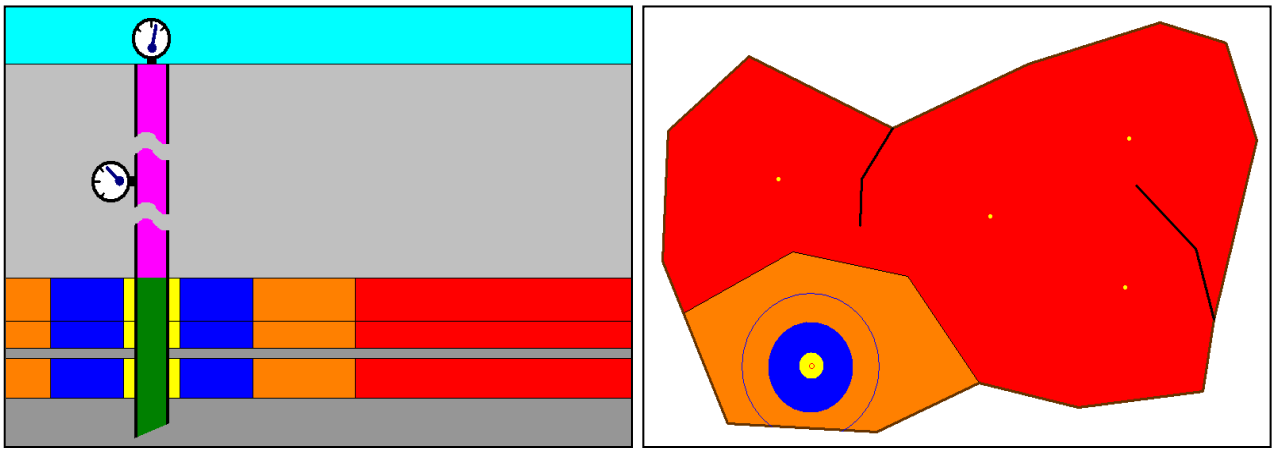


Fig. 1.C.5 – Schematics in the X-Y and X-Z planes of Dynamic Data Analysis

1.D Book content

1 – Introduction

2 – Theory: Includes the hypotheses, equations and solutions at the root of the models and methods implemented, especially in PTA and RTA.

3 – Pressure Transient Analysis (PTA): Short history, followed by a presentation of the classical and modern methods; operational issues, test design and quality control.

4 – Rate Transient Analysis (RTA): Short history, followed by a presentation of the classical and modern methods developed for the analysis and forecast of production data.

5 to 8 – wellbore (5), well (6), reservoir (7), boundary (8) models: itemized review of models used in both PTA and RTA. We split models by category, progressing away from the wellhead, moving from wellbore, to well, reservoir and finally boundaries.

9 – PVT: black oil models and EOS (pseudo-functions presented in chapter 13).

10 – Unconventional Resources: Definitions and issues; presentation of the analyses tools and models specific to the productions in shale / CSG plays.

11 – Formation tests: Processing and analysis of formation test data.

12 – Other test operations: slug tests, multilayer and interference tests; minifrac analysis.

13 – Analytical models: specific issues related to analytical models: derivation, use of image functions, superposition, use of pseudopressures and pseudo-times (first version).

14 – Numerical models: Additional capabilities and specific issues related to numerical models in order to handle complex geometries and nonlinear diffusion effects.

15 – Nodal Analysis: IPR, VLP, Flow Correlations, Nodal analysis and sensitivity (work in progress).

16 – Permanent Downhole Gauges and Reservoir Surveillance: Processing of PDG data, data overflow, information overflow; solutions and workflows developed by the industry.

17 – Production Logging

This introduction to production logging covers the governing principles, typical tools, operations and interpretation methods.

18 – Thermal analysis and simulation

This chapter explores the different applications of temperature data, followed by a summary of the key theoretical concepts on thermodynamics. The different thermal methods offered by KAPPA are described.

1.E Other books for reference

If you want to learn how to perform DDA the KAPPA book you have in your hands right now is certainly the most practical you will find ☺. If you do not believe it, or if you wish to expand your reading, we invite you to plough through some, or for the real masochist, all of the following learned tomes:

For normal people:

1. 'Advances in Well Test Analysis': SPE Monograph Vol. 5 by Robert C. Earlougher, Jr. in 1977: This is a monument. Get one even if the content is a bit outdated (no Bourdet Derivative). It will remain for a long time a mine of references.
2. 'Transient Well Testing': SPE Monograph Vol. 23, published in 2009 though it was supposed to get out in 1990. Ten different authors (including OH), 850 pages that are sometimes pretty heterogeneous, but still a must-have.
3. 'Modern Well Test Analysis, a computer-aided approach' by Roland Horne, Petroway Inc. 1995: The first book which really integrated the current methodology based on the Bourdet derivative. Still today a very good complement.
4. 'Well Test Analysis: The use of advanced interpretation models', by Dominique Bourdet, Elsevier 2002: Three good reasons to get it: (1) with the Bourdet derivative, Dominique certainly made the single most important contribution to modern Pressure Transient Analysis and, indeed, to Rate Transient Analysis; (2) Dominique started KAPPA with Olivier Houzé in 1987, and he left in 1991; (3) his book is very close to our philosophy. It now lacks Rate Transient Analysis, deconvolution and numerical models, but it is still a must-have.

For those from the dark side who love equations and wish to understand everything:

1. 'Conduction of Heat in Solids', Carslaw & Jaeger: A mother lode from where the petroleum industry has been mining many ideas. Equations need adaptation, but they are all there.
2. 'Handbook of Mathematical Functions', Abramowitz & Stegun: All you need to navigate your starship through Laplace Space and Bessel Functions. A must-have if you write code.
3. Raj Raghavan: 'Well Test Analysis', Prentice Hall 1993: Raj just loves equations. Do not try to count. He must have been paid by the Integral and this is, actually, the strength of this book. An excellent set of theoretical references.

There are other very good books, apology for not referencing them all…

1.F How many equations do you want?

As we know people love or hate equations. Of course people want to have 'practical' training; because the silly alternative is 'impractical' training. But it would be a mistake to completely turn our back on the equations, and 'dumb down' the learning.

Although we know that people with a solely academic background may miss the point if they do not understand the practical world, likewise it makes little sense for wholly practical people to have no understanding of the theoretical background.

Engineers with an excellent practical experience but no theory may be making mistakes of which they are blissfully and completely unaware.

So, as with anything else, this is just a matter of common sense.

Knowing the theory means knowing the assumptions, and knowing the assumptions means knowing the limitations of the theory.

There is one thing for sure: PTA and RTA are not just about knowing how to operate the software. That's the easy bit. The software is just a tool. It is the Engineer who makes the interpretation.

So we have decided to provide two levels of reading in this book, and we leave you to choose:

- The main, white sections will only show the practical side of things, the qualitative explanations, and the behavior equations, i.e. those you would have to apply for, say, a specialized analysis using your own spreadsheet. It will also show basic equations, but not the details of derivation of these equations. You will be spared disappearing into dimensionless and Laplace space (Captain).
- If you would like, at least once in your life, to follow the process of the derivation of the diffusion equation, line source solution, finite radius well, closed systems, gas pseudopressures, the yellow sections are just for you.

2 – Theory
OH – OSF – DV

2.A Diffusion equation

2.A.1 Darcy's law

Darcy's original experiment (Henry Darcy, France, 1856) is shown below. It was initially set to study the pressure loss due to the flow of water in sand filters.

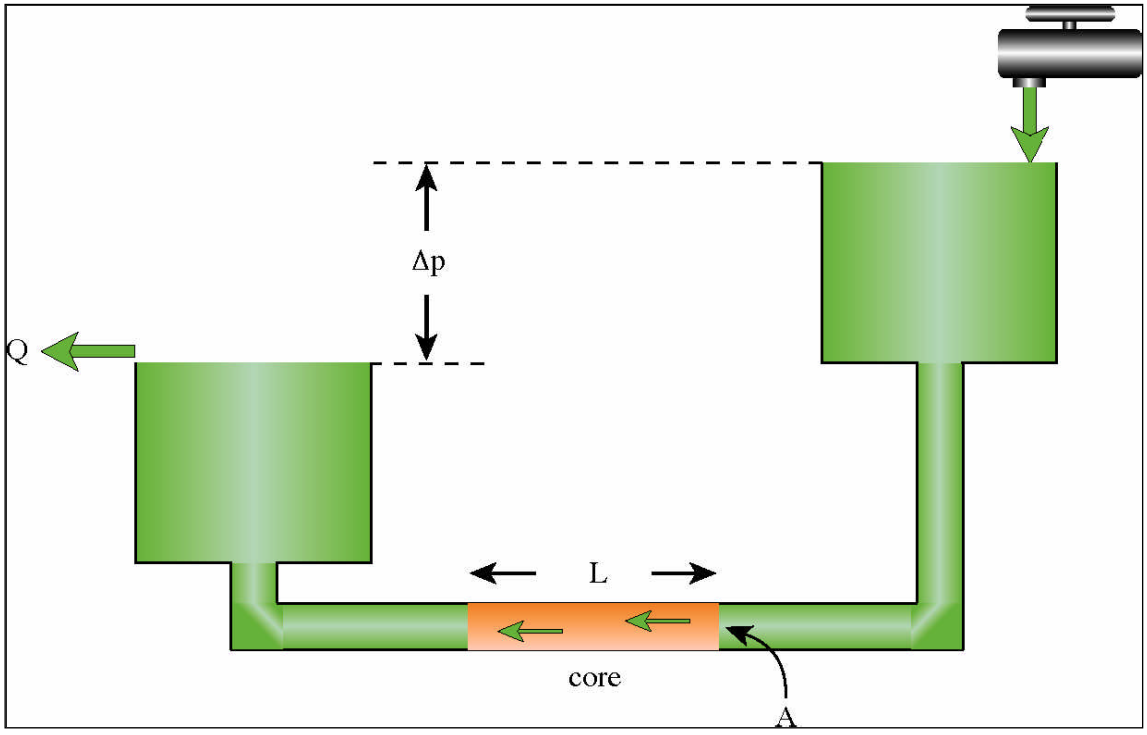


Fig. 2.A.1 – Darcy's experiment

In this experiment, Henry Darcy established a linear relation between the horizontal flow rate across a section of porous medium and the pressure gradient across the same section.

Using today's conventions, in Field Units, the relation discovered by the Darcy's experiment can be written:

$$\frac{\Delta p}{L} = -887.2\frac{Q\mu}{kA}$$

Its differential form can be given in linear coordinates for linear flow and in cylindrical coordinates for radial flow. For radial coordinates the flow rate is assumed to be positive for a producing well, i.e. flow towards the well:

Darcy's law in linear coordinates, in the x direction: $$\frac{\partial p}{\partial x} = -887.2\frac{q_x\mu}{k_x A}$$

Darcy's law in radial coordinates: $$r\frac{\partial p}{\partial r} = 141.2\frac{q\mu}{kh}$$

Darcy's Law states that the pressure drop between two points, close enough to consider all parameters to be constant, will be:

- proportional to the flowrate density (q/A)
- proportional to the fluid viscosity (μ)
- inversely proportional to the reservoir permeability (k)

Darcy's Law is a fundamental law in dynamic data analysis. It is used to model the flow in several compartments in the reservoir:

- At any point of the reservoir, it is one of the three equations that will be used to define the diffusion equation (see next section).
- When the well is flowing, it determines the pressure gradients at the sandface.
- Close to reservoir boundaries it determines that the pressure gradient towards a no-flow boundary is flat, or it allows the determination of the inflow from the pressure gradient.

Darcy's law assumes a linear relation between the flow of fluid in one direction and the pressure gradient, corrected for gravity, in the same direction. This assumes that the density of flow is small enough to avoid turbulent behaviour.

When there is turbulence, a quadratic term is added and Darcy's law is replaced by the Forchheimer's equation. We then speak about non-Darcy flow. In most cases, non-Darcy problems will be solved with a numerical model.

2.A.2 The diffusivity equation

The diffusivity equation describes how, in an elementary piece of rock, the pressure will react in time as a function of the local pressure gradient around this piece of rock.

There may be as many diffusivity equations as there are assumptions on what is happening downhole. The basic theory in Dynamic Data Analysis uses the simplest possible diffusivity equation, assuming the following:

- The reservoir is homogeneous and isotropic.
- The fluid is single-phase and only slightly compressible.
- Gravity effects are ignored. If they were not the diffusivity equation would be written in terms of potential and not pressure.
- Darcy's law applies.
- Reservoir and fluid properties are independent of the pressure.

Under these conditions, the diffusivity equation is derived from the combination of:

(1) The principle of conservation of mass
(2) Darcy's law
(3) Slightly compressible fluid equation

Some more complex versions of the diffusivity equation will have different components: Darcy's law may be replaced by the Forchheimer's equation, and more complex PVT models may be used: real gas diffusion, multiphase black oil correlations or an Equation of state.

Derivation of the diffusivity equation:

The diffusion equation is derived from the combination of three elementary equations:

The law of **conservation of mass**: this is a 'common sense' law that states that nothing is ever created or lost; things just move or transform themselves (Antoine Lavoisier, France, 1785). The formulation for an elementary piece of rock is that 'mass in' minus 'mass out' = 'accumulation'.

We consider the flow in the x direction of a fluid through a (small) area A, between x and x+δx and between time t and t+δt. Considering that 1 bbl/day = 0.23394 ft^3/hr, we get the following equation

Conservation of mass: $Mass_{in} - Mass_{out} = Accumulation = Mass_{after} - Mass_{before}$

Conservation of mass: $\left[0.23394\rho q_x \delta t\right]_x - \left[0.23394\rho q_x \delta t\right]_{x+\delta x} = \left[\rho\phi A\delta x\right]_{t+\delta t} - \left[\rho\phi A\delta x\right]_t$

Differential form: $-0.23394\ \frac{\partial \rho q_x}{\partial x} = A\frac{\partial(\rho\phi)}{\partial t}$

The second equation we will use relates the rate in a direction to the pressure gradient in this direction. The simplest among these equations is **Darcy's law** (Henry Darcy, France, 1856), which establishes a linear relation between the speed and the pressure gradient, the linear factor being a function of one reservoir property (the permeability) and one fluid property (the viscosity).

Darcy's law in the x direction: $q_x = -\frac{k_x A}{887.2\mu}\frac{\partial p}{\partial x}$

So we get: $-0.23394\frac{\partial}{\partial x}\left[-\frac{k_x A\rho}{887.2\mu}\frac{\partial p}{\partial x}\right] = A\frac{\partial(\rho\phi)}{\partial t}$

This simplifies to: $\frac{\partial(\rho\phi)}{\partial t} = 0.0002637 k_x \frac{\partial}{\partial x}\left[\frac{\rho}{\mu}\frac{\partial p}{\partial x}\right]$

It is from the equation above that we will start when dealing with real gas. Now we are going to focus on slightly compressible fluids. The first term can be developed as:

First term: $\frac{\partial(\rho\phi)}{\partial t} = \frac{\partial(\rho\phi)}{\partial p}\frac{\partial p}{\partial t} = \left[\rho\frac{\partial\phi}{\partial p} + \phi\frac{\partial\rho}{\partial p}\right]\frac{\partial p}{\partial t} = \rho\phi\left[\frac{1}{\phi}\frac{\partial\phi}{\partial p} + \frac{1}{\rho}\frac{\partial\rho}{\partial p}\right]\frac{\partial p}{\partial t}$

New differential form: $0.0002637\frac{k_x}{\rho\phi}\frac{\partial}{\partial x}\left[\frac{\rho}{\mu}\frac{\partial p}{\partial x}\right] = \left[\frac{1}{\phi}\frac{\partial\phi}{\partial p} + \frac{1}{\rho}\frac{\partial\rho}{\partial p}\right]\frac{\partial p}{\partial t}$

The two terms between brackets in the second member of the equation are the formation compressibility and the fluid compressibility:

Formation compressibility: $c_f = \frac{1}{\phi}\frac{\partial\phi}{\partial p}$

Fluid compressibility: $c_{fluid} = \frac{1}{\rho}\frac{\partial\rho}{\partial p}$

New differential form: $$\frac{\partial p}{\partial t} = 0.0002637 \frac{k_x}{\rho\phi\left[c_f + c_{fluid}\right]} \frac{\partial}{\partial x}\left[\frac{\rho}{\mu}\frac{\partial p}{\partial x}\right]$$

The last equation required is PVT related, in order to assess the relation between the fluid compressibility and the pressure. The simplest equation that can be used is the **slightly compressible fluid**, assuming that the fluid compressibility is constant, i.e. independent of the pressure. So we get a total constant compressibility:

Slightly compressible fluid: $$c_t = c_f + c_{fluid} = \text{Constant}$$

Also we can consider that: $$\frac{\partial}{\partial x}\left[\frac{\rho}{\mu}\frac{\partial p}{\partial x}\right] \approx \frac{\rho}{\mu}\frac{\partial^2 p}{\partial x^2}$$

We finally get the diffusion equation in the x direction:

Diffusion equation; direction x: $$\frac{\partial p}{\partial t} = 0.0002637 \frac{k_x}{\phi\mu c_t}\frac{\partial^2 p}{\partial x^2}$$

The process above was dealing with the flux in only one direction. If we consider now the flux through an arbitrarily small cube in all three directions, we get:

Generic diffusion equation: $$\frac{\partial p}{\partial t} = 0.0002637 \frac{\left[k_x \frac{\partial^2 p}{\partial x^2} + k_y \frac{\partial^2 p}{\partial y^2} + k_z \frac{\partial^2 p}{\partial z^2}\right]}{\phi\mu c_t}$$

If we consider an isotropic reservoir, all permeability components are equal to a unique permeability, k:

Isotropic diffusion equation:

$$\frac{\partial p}{\partial t} = 0.0002637 \frac{k}{\phi\mu c_t}\left[\frac{\partial^2 p}{\partial x^2} + \frac{\partial^2 p}{\partial y^2} + \frac{\partial^2 p}{\partial z^2}\right] = 0.0002637 \frac{k}{\phi\mu c_t}\nabla^2 p$$

The operator on the right end side is called the Laplace operator, or Laplacian. It is also written Δp, but we will avoid this form in order not to cause confusion with the pressure change in time, also noted Δp.

2.A.3 Diffusion in a homogeneous isotropic reservoir

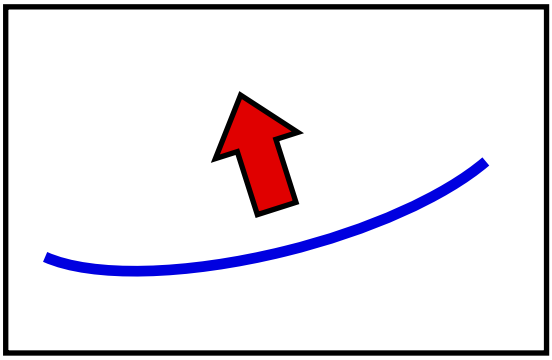
When combining the law of conservation of mass, the simplest pressure gradient equation (Darcy's law) and the simplest material balance relation (slightly compressible fluid assumption), we get the simplest version of the diffusion equation, given below in three different forms:

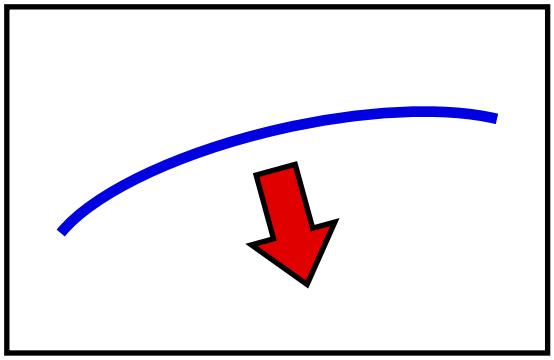
General form: $$\frac{\partial p}{\partial t} = 0.0002637 \frac{k}{\Phi\mu c_t}\nabla^2 p$$

Radial flow: $$\frac{\partial p}{\partial t} = 0.0002637 \frac{k}{\Phi\mu c_t}\frac{1}{r}\left[\frac{\partial}{\partial r}\left(r\frac{\partial p}{\partial r}\right)\right]$$

Linear flow: $$\frac{\partial p}{\partial t} = 0.0002637 \frac{k}{\Phi\mu c_t}\frac{\partial^2 p}{\partial x^2}$$

Physical meaning: If we look at the last relation and consider the flow in only one direction:





- If the curvature of the pressure profile is positive, the pressure will locally increase. If the curvature is negative the pressure will decrease. The speed of the pressure change, in whatever direction, will be proportional to this curvature.
- If the permeability is large, the pressure change will be fast. Basically, the more permeable the formation, the quicker the formation fluid will react to a local pressure disturbance.
- If the viscosity is large, the pressure change will be slow. Basically, the more viscous the fluid, the slower the formation fluid will react to a local pressure disturbance.
- The ratio k/μ, to which the speed of reaction is proportional, is also called the mobility.
- If the porosity is large, the pressure change will be small, and therefore, at a given time, relatively slow. Basically, the more porous the formation, the lower the pressure change that will be required to produce / receive the same mass of fluid.
- If the total compressibility is large, the pressure change will be small, and therefore, at a given time, slow. Basically, the more compressible the formation is, the lower the pressure change required to produce / receive the same mass of fluid.
- The term $1/\phi c_t$, to which the amplitude of the reaction is proportional, is also called the storativity.
- Mobility and Storativity seems to play the same role in the diffusion equation. However the mobility will also be found in the inner boundary conditions and this is where the role of the different parameters will diverge.

Generally, the diffusion equation used in most analytical models is the radial formulation. The reference point of such a radial solution is the producing or injecting well. This system of coordinates is well suited to model radial flow to and from the well. In the following we will stay in radial coordinates.

The diffusion equation shown above describes the flow of what we call a homogeneous reservoir where this same, unique equation will be applied everywhere in the reservoir. More complex reservoirs can be modelled, and this diffusion equation will be replaced by formulations involving different pressures at the same point (double-porosity, double-permeability reservoirs) or changing diffusivity and mobility in different locations (composite reservoirs). The different reservoir models are detailed in the chapter on the subject.

2.B Initial, well and outer boundary conditions

The diffusion equation describes how the fluid pressure in a local piece of rock will locally react to a pressure disturbance. This equation defines how the system will react far from the boundaries and the wells.

In order to define a problem completely we need to know a starting point, i.e. the initial state of the system, and how the fluid flow will be constrained at the well and at the natural limits of the reservoir.

2.B.1 Initial conditions

The most common condition, and the only easy state to model analytically, is to assume that at a reference time 0, corresponding to the time when the sequence of production starts, the reservoir was at initial uniform pressure p_i. This simple equation can be written:

In Cartesian coordinates: $\forall x, y, z \quad p(t=0, x, y, z) = p_i$

Assuming a radial symmetry: $\forall r \quad p(t=0, r) = p_i$

In the case of a multilayer analysis, if the reservoir layers are commingled there could be one such equation for each independent layer. If the pressure difference between the different layers is not the static gradient in the wellbore, it means that cross-flow will occur between the different layers as soon as the well is perforated, even if it is not flowing.

It is also possible to start a problem with a dynamic pressure situation. This will be, typically, the 'restart' of a simulator run from which one wants to run a test on a new, additional well. This kind of situation is however only possible when using a numerical model.

2.B.2 Well conditions

All equations above (diffusion, initial and outer boundary conditions) lead to a nicely uniform reservoir at initial pressure, forever. What changes this million-year-old equilibrium is the disturbance created by man-made producing or injecting wells. We generally take 0 as the time of the initial disturbance.

The simplest realistic model is a vertical well, of radius r_w, fully penetrating the formation. The inner condition is nothing more than Darcy's law calculated at the sandface. In the case of a homogeneous reservoir this will write: Finite radius well: $\left[r \frac{\partial p}{\partial r} \right]_{r_w, t} = 141.2 \frac{qB\mu}{kh}$

As the flow rate q is generally given at standard conditions, the volumetric downhole rate q_{sf} is calculated by multiplying the standard rate by the reservoir volume factor B. In the simplest cases this volume factor is considered constant. Otherwise a PVT equation must be used to dynamically calculate the volume factor.

An unrealistic but very convenient model of well condition is the line source, corresponding to the same Darcy's law but for the limit case of a well of radius zero.

Line source well: $$\lim\left[r\frac{\partial p}{\partial r}\right]_{r\to 0,t} = 141.2\frac{qB\mu}{kh}$$

The line source problem is interesting because it is easier to solve, faster to run and the calculation of this solution at $r=r_w$ is a good approximation of the finite radius solution and for any practical purpose it is exactly the same solution within the formation, when $r>r_w$. It is the solution of choice to simulate interference tests and image wells for boundary effects (see the chapter on boundary models).

Other inner boundary conditions correspond to Darcy's law applied to more complex well geometries (fractures, limited entry, horizontal, slanted, multilateral, etc), and are detailed in the chapter on well models.

In most cases, the production of the well will be affected by wellbore effects, generally modelled using what we call the wellbore storage. This notion is developed in the Wellbore chapter.

In these cases there is a time delay in the production / shut-in, and the well condition also includes a wellbore component. The simplest model is a constant wellbore storage applied to a well opened and shut in at surface. The modified equation, for a finite radius well, with wellbore storage:

$$\left[r\frac{\partial p}{\partial r}\right]_{r_w,t} = \frac{141.2\left[qB + 24C\frac{\partial p}{\partial t}\right]\mu}{kh}$$

2.B.3 Outer boundary conditions

Another set of equations is needed to define how the fluid reacts close to a natural boundary. This could be the outer boundary of the system, or even intermediate faults.

The simplest condition to model analytically is that there is no boundary at all, i.e. that the reservoir is of infinite extent in all directions. The equation for such system is:

Assuming radial symmetry: $$\lim\left[p(r,t)\right]_{r\to\infty} = p_i$$

Naturally and unfortunately, no reservoir is infinite. However, in pressure transient analysis this model is easier to generate and will match the data over the duration of the well test, as long as the test is short enough for no lateral boundary to be seen.

Infinite reservoir models are unlikely to be used in rate transient analysis, where such a hypothesis is unlikely to be met over the extended time range of such analysis.

2.C Line Source Solution in a homogeneous infinite reservoir

We now consider the simplest problem we can find: the diffusion in a homogeneous infinite reservoir, starting at initial uniform pressure p_i, produced by a vertical line source well. The introduction to dimensionless terms and the derivations for this model are shown in the Chapter 'Analytical models - 13.B - Dimensionless problems'.

2.C.1 The Line Source Solution

The solution in dimensionless terms is given in the paragraph '13.B - Dimensionless problems'.

To get the physical solution, the dimensionless parameters are replaced by their real values.

The solution at any point and time, for a Line Source well producing a homogeneous infinite reservoir, is then given by the following:

Line Source Solution:

$$p(r,t) = p_i - \frac{70.6qB\mu}{kh}\left[-E_i\left(-\frac{948.1\Phi\mu c_t r^2}{kt}\right)\right]$$

A typical line source response is displayed in the figures below, on a loglog scale (with the Bourdet derivative) and a semilog scale. For first readers, the notions of loglog and semilog plots are described in the PTA methodology chapter.

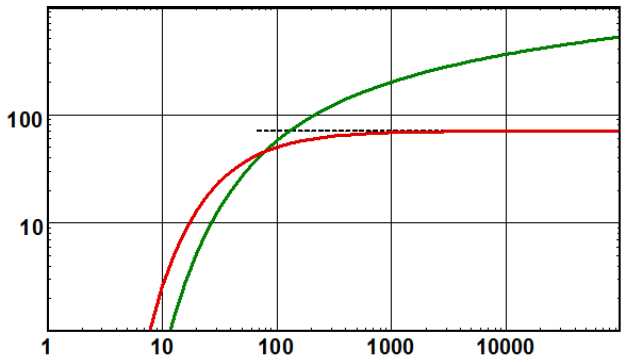


Fig. 2.C.1 – Line source loglog plot

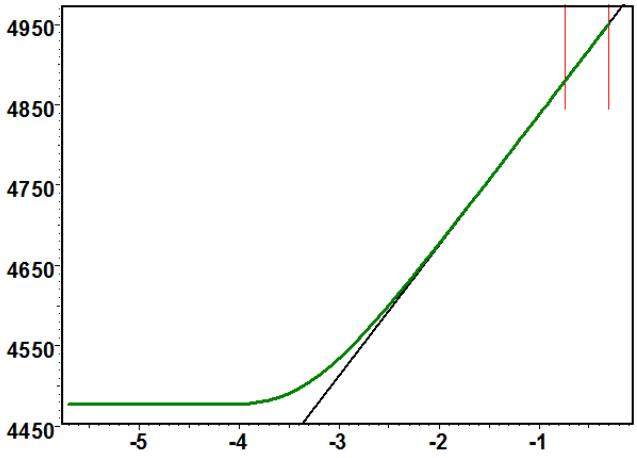


Fig. 2.C.2 – Line source semilog plot

The line source equation shows that the pressure change is a unique function of the parameter group r^2/t, or more conveniently $r/\sqrt{t}$. This has an important implication on the physical understanding of the diffusion process. If one considers, for example, the time it requires for the pressure change to reach a certain value (for example 1 psi), it will amount to a certain value of $r/\sqrt{t}$ that we will calculate from the Line Source Solution, and therefore the relation:

Radius of investigation:

$$r_{inv} = a\sqrt{t}$$

In the chapter on boundary models we recommend at one does not use the notion of radius of investigation, as it may be misleading when one considers how such result is used afterwards. However, it is an interesting means of understanding the diffusion process. To extend this notion to cases where the flow geometry may not be strictly radial, we may consider that the area of investigation is proportional to r^2, and we therefore have:

Area of investigation: $A_{inv} = bt$

If the flow is not strictly horizontal and/or the thickness h is not constant, we will use:

Volume of investigation: $V_{inv} = ct$

Although the following is valid at any point in the reservoir, we will now focus on the well response, that will be taken at r=r_w. As demonstrated in the previous section, there is a value of time above which the Line Source Solution reaches a 'regime' where one can use an approximation of the highest interest to the well test interpretation engineer. It is the semilog approximation and this regime is called **Infinite Acting Radial Flow**, or **IARF**.

IARF: For $t \geq \frac{379200\Phi\mu c_t r_w^2}{k}$ $\quad \left(p_i - p_{wf}\right) = \frac{162.6qB\mu}{kh}\left[\log\Delta t + \log\frac{k}{\Phi\mu c_t r_w^2} - 3.2275\right]$

Convention: ln(x) is the natural logarithm; log(x) is the decimal logarithm

IARF is characterized by linearity between the pressure change and the logarithm of time. This is why we also call this the semilog approximation. The slope of the response allows the calculation of the permeability-thickness, kh.

But before we develop further the IARF, we are going to introduce two other effects commonly accounted for in Pressure Transient Analysis: Wellbore storage and Skin effect.

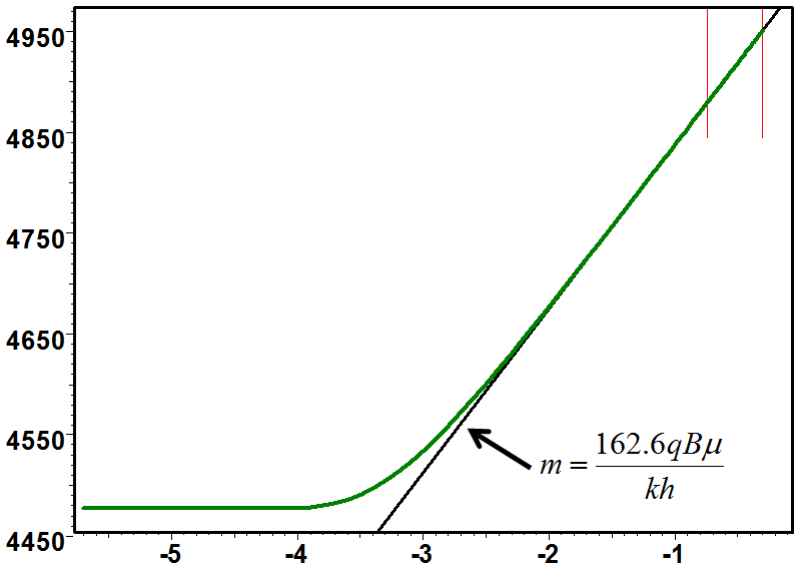


Fig. 2.C.3 – Semilog plot (note : the X-axis is a linear scale of log (Δt))

2.D Wellbore storage and skin

2.D.1 Wellbore storage

In most cases the valve used to open the well and shut it in is not exactly at sandface level. In most cases it will be at surface. Even in the case of downhole shut in there is always a volume that will act as a cushion between the sandface and the valve. As a result, wellbore dynamics create a time lag between the sandface and the surface, or the valve, or the choke. This is what we generally call wellbore storage.

Let us take the case of a well opened and shut in at surface. When you open the well the initial surface production will be coming from the decompression of the fluid trapped in the wellbore. In the initial seconds or minutes of the flow the sandface will not even 'know' that the well is opened and the sandface rate will remain virtually zero. Naturally, at some stage we get to a mass equilibrium, i.e. the sandface mass rate reaches the surface mass rate. This is the time of the end of the wellbore storage. Conversely, if the well is shut in at surface, the surface rate will go immediately to zero while the sandface does not know about it. The time of wellbore storage is this transition time between the effective shut-in time and the time at which the reservoir stops flowing into the well.

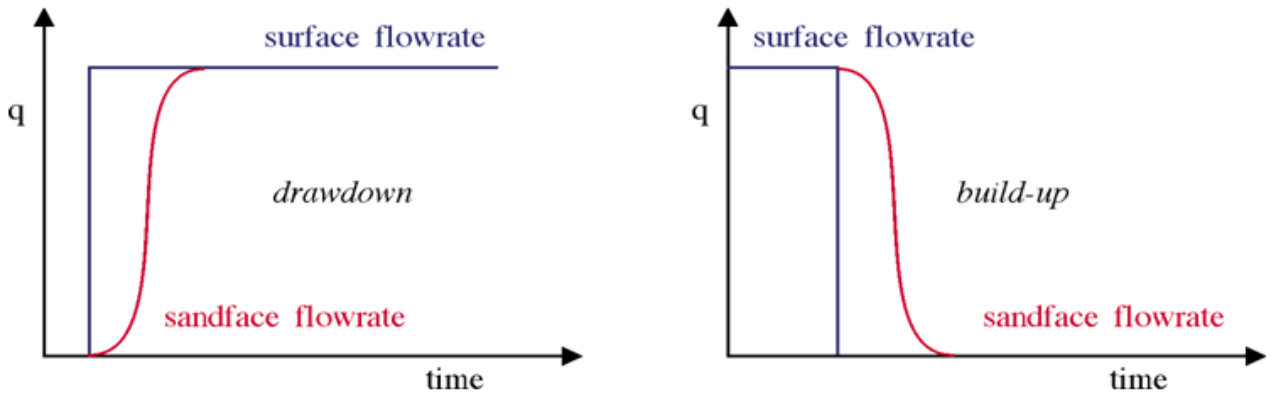


Fig. 2.D.1 – Wellbore storage

There are two main types of wellbore storage. The first one is modelled by the compression or decompression of the wellbore fluid in the wellbore volume. This is expressed as:

Wellbore storage by fluid compression: $C = V_w c_w$

Where V_w is the wellbore volume and c_w the fluid compressibility.

The second type of wellbore storage is linked to the rise of the liquid level present in the wellbore. A simplified version is expressed as:

Wellbore storage from liquid level: $C = 144\frac{A}{\rho}$

Where A is the flow area at the liquid interface, ρ is the fluid density.

The relation between the surface and the sandface rate is then given by:

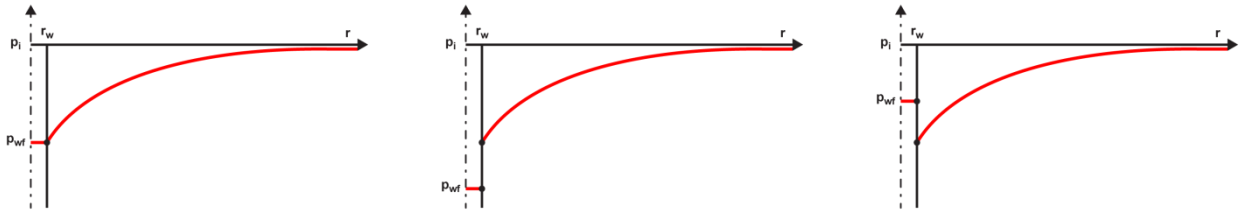
Wellbore storage equation: $$q_{sf} = qB + 24C\frac{\partial p}{\partial t}$$

The simplest wellbore storage model implies that C is constant. However this is not always the case, and the various models of storage are described in the Wellbore chapter.

2.D.2 Skin

The skin effect quantifies the difference between the productivity of a well in an ideal case and its effective productivity in reality:

- If, after drilling, completion, cementing and perforating, the pressure drop for a given production into the wellbore is identical to the one you would forecast in the ideal case for the same geometry, the skin is zero.
- Very often, the reservoir near the wellbore had been invaded and the effective permeability around the well is lowered, thus a higher pressure drop results for a given production. The skin is then positive.
- Conversely, a stimulated well will have better productivity, hence a lower pressure drop for a given production. The skin is then considered negative.
- Skin may not be constant in time. During the initial 'clean-up' period in a well test, skin has a tendency to reduce. Conversely, over long period of times, completed wells may get damaged reducing productivity, hence an increasing skin.



Non damaged skin = 0 Damaged Skin > 0 Stimulated Skin < 0

Fig. 2.D.2 – Skin sign convention

We will consider that a well has a constant skin when the additional pressure drop, or Δp_{skin}, is proportional to the sandface rate. The skin S is a dimensionless factor representative of a pressure change, and integrates the same coefficients as the one in Darcy's law:

Constant skin S: $$\Delta p_{Skin} = p(r_w, t) - p_{wf}(t) = 141.2\frac{q_{sf}\mu}{kh}S$$

Where p is the pressure in the formation, at a given time, at distance rw, i.e. just beyond the sandface, while p_{wf}, at a given time, is the well flowing pressure.

A way to model a positive skin effect is to consider an equivalent composite system, with an invaded zone, or skin damage zone of radius r_{ws} larger than r_w and permeability k_s lower than k.

Darcy's law gives the relation between the equivalent skin factor, r_s and k_s:

Skin from a radial composite equivalent: $$S = \left(\frac{k}{k_S} - 1\right)\ln\left(\frac{r_{ws}}{r_w}\right)$$

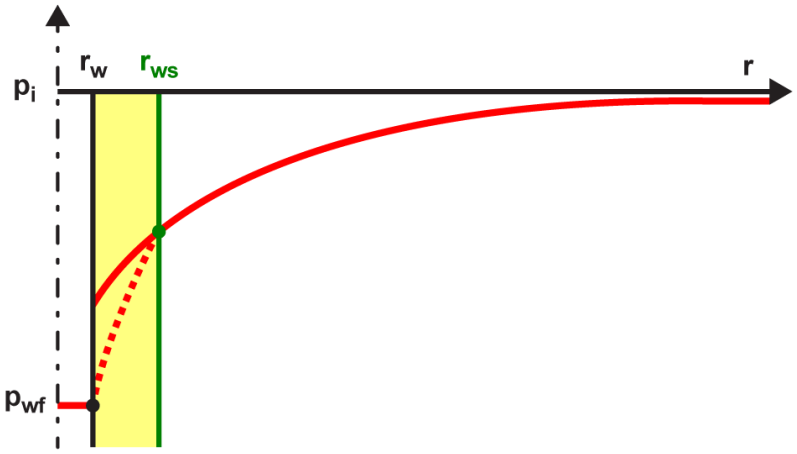


Fig. 2.D.3 – Equivalent composite system

Another way to model skin is the notion of equivalent radius, applicable to both positive and negative skins. The idea is to consider that the well with skin has the same productivity as a larger or smaller well with no skin. If the skin is positive, the equivalent wellbore radius will be smaller than r_w. If the skin is negative, the equivalent wellbore radius will be larger than r_w. The equation, again, straight from Darcy's law, can also be found at the limits when the permeability k_S above tends to infinity (open hole), and will be given by:

Equivalent wellbore radius: $$S = -\ln\left(\frac{r_{we}}{r_w}\right) \quad \text{or} \quad r_{we} = r_w e^{-S}$$

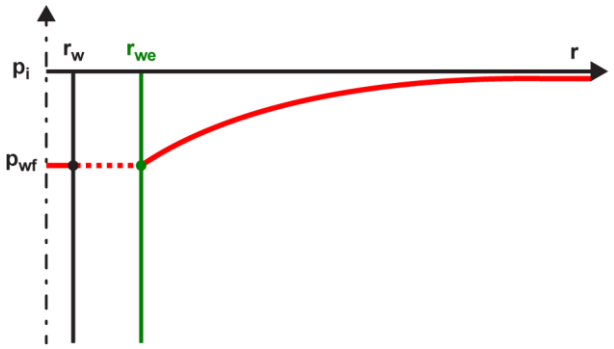


Fig. 2.D.4 – Skin: equivalent wellbore radius

We now consider the case of a homogeneous, infinite reservoir produced by a vertical well with constant wellbore storage and constant skin.

2.D.3 Derivation

We now have a slightly more complex problem to solve:

Homogeneous radial diffusion: $$\frac{\partial p}{\partial t} = 0.0002637 \frac{k}{\Phi \mu c_t} \frac{1}{r} \left[\frac{\partial}{\partial r} \left(r \frac{\partial p}{\partial r} \right) \right]$$

Finite radius well: $$\left[r \frac{\partial p}{\partial r} \right]_{r_w, t} = 141.2 \frac{q_{sf} \mu}{kh}$$

Initial pressure & infinite reservoir: $$p(t=0, r) = p_i \qquad \lim \left[p(r,t) \right]_{r \to \infty} = p_i$$

Wellbore storage & skin: $$q_{sf} = qB + 24C \frac{\partial p_{wf}}{\partial t} \qquad p - p_{wf} = 141.2 \frac{q_{sf} \mu}{kh} S$$

We will now repeat the definition of the dimensionless terms and add dimensionless sandface rate and dimensionless wellbore storage. The Skin, being dimensionless, does not need any conversion:

Dimensionless radius, time & pressure:

$$r_D = \frac{r}{r_w} \quad t_D = 0.0002637 \frac{kt}{\Phi \mu c_t r_w^2} \qquad p_D = \frac{kh}{141.2 qB\mu} (p_i - p)$$

Dimensionless sandface rate & storage: $$q_D = \frac{q_{sf}}{qB} \qquad C_D = \frac{0.8936C}{h \phi c_t r_w^2}$$

We now get the equivalent dimensionless problem:

Homogeneous radial diffusion: $$\frac{\partial p_D}{\partial t_D} = \frac{1}{r_D} \left[\frac{\partial}{\partial r_D} \left(r_D \frac{\partial p_D}{\partial r_D} \right) \right]$$

Initial pressure & infinite reservoir: $$p_D(t_D = 0, r_D) = 0 \qquad \lim \left[p_D(r_D, t_D) \right] = 0$$

Finite radius well: $$\left[r_D \frac{\partial p_D}{\partial r_D} \right]_{r_D = 1, t_D} = -1$$

Wellbore storage & skin: $$\left[r_D \frac{\partial p_D}{\partial r_D} \right]_{r_D = 1, t_D} = -q_D \qquad p_{wfD} = p_D + q_D S \quad q_D = 1 - C_D \frac{dp_{wfD}}{dt_D}$$

The solution process will be the same as the line source problem and will not be detailed here.

For the finite radius problem (without storage, without skin), the general form is like the line source:

Generic Modified Bessel solution: $$\overline{p}_D(u, r_D) = A(u) K_0(r_D \sqrt{u}) + B(u) I_0(r_D \sqrt{u})$$

As the line source, the infinite reservoir conditions arrives at B(u)=0. The only difference is that we now calculate the well equation at r_D=1 and not r_D=0. This gets us to a different value for A(u):

From the inner boundary condition: $$A(u) = \frac{1}{u\sqrt{u}K_1\left(\sqrt{u}\right)}$$

If we define the function: $$K_0^1(x) = \frac{K_0(x)}{xK_1(x)}$$

The finite radius solution at the well is $$\bar{p}_D(u) = \frac{1}{u}K_0^1\left(\sqrt{u}\right)$$

In the wellbore storage and skin solution we eliminate q_D and p_{wfD} in the top equations, we take the Laplace transform, etc, etc. In fact, we can make the generic demonstration that, if we know the Finite Radius solution of a given problem in Laplace space, wellbore storage and skin can be added by the following transform:

We obtain a modified Bessel equation and solve for inner and outer boundaries; a term K_1 appears corresponding to the finite radius well condition, and we finally get the following results:

Adding wellbore storage & skin: $$\bar{p}_{wfD}(u) = \frac{1}{u}\left[\frac{S + u\bar{p}_{FRD}(1,u)}{1 + uC_D\left[S + u\bar{p}_{FRD}(1,u)\right]}\right]$$

In the homogeneous infinite case: $$\bar{p}_{wfD}(u) = \frac{1}{u}\left[\frac{S + K_0^1\left(\sqrt{u}\right)}{1 + uC_D\left[S + K_0^1\left(\sqrt{u}\right)\right]}\right]$$

The problem is then solved in real space by taking the inverse Laplace transform using Stehfest numerical algorithm. Though the solution is more complex, the difference between this solution and the Exponential Integral solution will stabilize when wellbore storage effects vanish, the residual difference remaining is the skin factor. This links to the IARF by:

After wellbore storage: $$p_{wfD}(t_D) \approx -E_i\left(-\frac{1}{4t_D}\right) + S$$

Dimensionless IARF: for $t_D \geq 100$ $$p_{wfD}(t_D) = \frac{1}{2}\left[\ln t_D + 0.80907 + 2S\right]$$

2.D.4 Behavior

The two figures below show the drawdown response of a vertical well with wellbore storage and skin in a homogeneous infinite reservoir. The plot on the left shows the response on semilog scale, with the pressure as a function of log(t). The plot on the right shows the loglog plot of log(Δp) and derivative vs log(Δt).

The derivative is developed in the chapter on 'PTA – General methodology'. The derivative shown on the right is the absolute value of the slope of the semilog plot on the left. When the model on the left becomes a straight line, the derivative stabilizes horizontally. The level of this stabilization is the slope of the model on the left. As all responses end up parallel on the left plot, then all derivatives merge to the same level on the right plot.

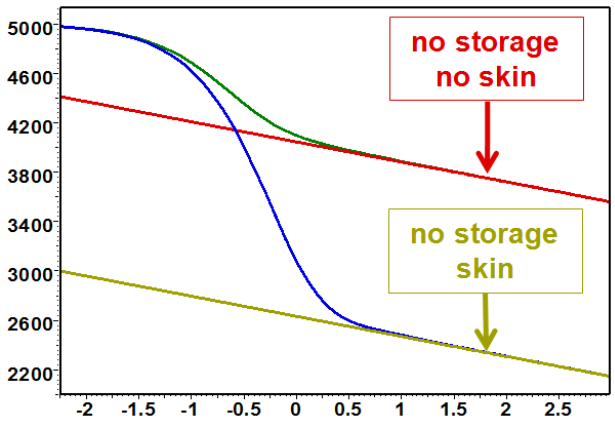


Fig. 2.D.5 – Finite radius solution, semilog plot

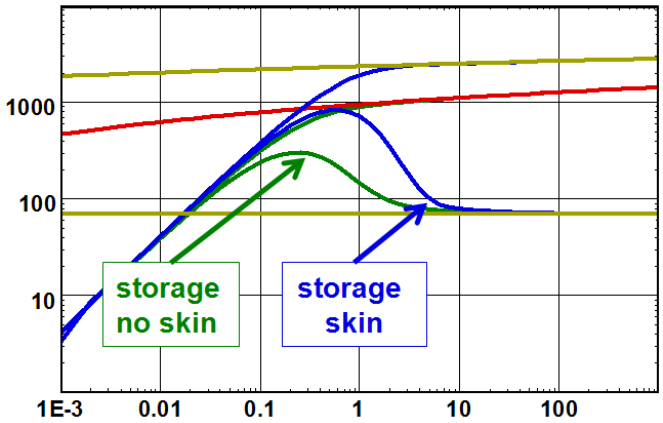


Fig. 2.D.6 – Finite radius solution, loglog scale

At early time, the flow is governed by wellbore storage and there is a linear relation between pressure change and elapsed time:

Early time pure wellbore storage: $$p(\Delta t) = p_i - \frac{qB}{24C}\Delta t$$

At late time, Infinite Acting Radial Flow (IARF) is reached, and there is a linear relation between the pressure change and the logarithm of the elapsed time:

IARF Equation: $$p(\Delta t) = p_i - \frac{162.6qB\mu}{kh}\left[\log(\Delta t) + \log\left(\frac{k}{\Phi\mu c_t r_w^2}\right) - 3.228 + 0.8686S\right]$$

2.E Outer boundary conditions

The previous sections only considered reservoir of infinite extent. An outer boundary will be made up of one or several sections of various type and shape combinations. In this section we will introduce the most usual types of boundaries, solve the case of a simple closed system and introduce the notion of pseudo-steady state (PSS).

2.E.1 Major types of boundaries

The most common type of boundary or boundary section is sealing, or no flow. It is given by applying Darcy's law orthogonally to the boundary surface, with a rate equal to zero:

No-flow boundary section: $$\left[\frac{\partial p}{\partial \vec{n}}\right]_{\Sigma} = 0$$

The second most common type of boundary or boundary section is an approximation of pressure support (gas drive or water drive) considering that the pressure remains constant:

Constant pressure boundary section: $$[p]_{\Sigma} = p_i$$

There are many other types of boundaries: leaky boundaries, conductive boundaries, water drives and gas caps. They will be described in detail in the chapter on boundary models.

In this section we focus on closed systems constituted by only no-flow sections, as we want to introduce the notion of pseudo-steady state (PSS), the main regime of interest in Rate Transient Analysis (RTA).

The simplest case of a closed system (because it is the simplest to model analytically) is a reservoir of circular shape centered at the well and of radius r_e. Such model may be used to simulate the behavior of a really closed system or the production of a well in its drainage area:

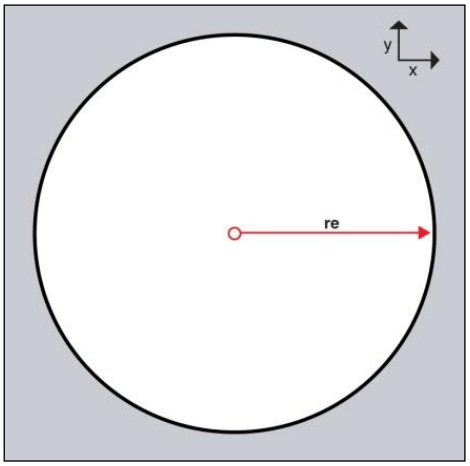


Fig. 2.E.1 – Closed circular boundary

2.E.2 Derivation for a circular reservoir

We consider a finite radius well to which we will add later wellbore storage and skin. Because it is an easy extension we are going to solve both cases of no-flow and constant pressure.

The problem is defined by the following set of equations:

Homogeneous radial diffusion: $$\frac{\partial p}{\partial t} = 0.0002637 \frac{k}{\Phi \mu c_t} \frac{1}{r} \left[\frac{\partial}{\partial r} \left(r \frac{\partial p}{\partial r} \right) \right]$$

Finite radius well: $$\left[r \frac{\partial p}{\partial r} \right]_{r_w, t} = 141.2 \frac{q_{sf} \mu}{kh}$$

Uniform initial pressure: $$p(t = 0, r) = p_i$$

Boundary equation, closed circle: $$\left[\frac{\partial p}{\partial r} \right]_{r_e, t} = 0$$

Boundary equation, ct pressure circle: $$p(t, r_e) = p_i$$

Dimensionless parameters are exactly the same as for the infinite finite radius solution and will not be repeated here. We end up with the following dimensionless problem:

Homogeneous radial diffusion: $$\frac{\partial p_D}{\partial t_D} = \frac{1}{r_D} \left[\frac{\partial}{\partial r_D} \left(r_D \frac{\partial p_D}{\partial r_D} \right) \right]$$

Initial pressure & finite radius well: $$p_D(t_D = 0, r_D) = 0 \qquad \left[r_D \frac{\partial p_D}{\partial r_D} \right]_{r_D = 1, t_D} = -1$$

Closed circle OR Ct pressure circle: $$\left[\frac{\partial p_D}{\partial r_D} \right]_{r_{eD}, t} = 0 \quad \text{OR} \quad p_D(t_D, r_{eD}) = 0$$

As for the line source problem we move the diffusion equation into Laplace space and get the following generic solution using modified Bessel functions:

Solution of the diffusion equation: $$\bar{p}_D(u, r_D) = A(u) K_0(r_D \sqrt{u}) + B(u) I_0(r_D \sqrt{u})$$

The terms A(u) and B(u) will be defined by the initial, inner boundary (well) and outer boundary equations. Long story short we end up with the following solutions:

For a closed circle: $$\bar{p}_{FRD}(u) = \frac{\frac{K_0(\sqrt{u})}{u\sqrt{u} K_1(\sqrt{u})}}{1 - \frac{K_1(r_{eD}\sqrt{u})}{I_1(r_{eD}\sqrt{u})} \frac{I_1(\sqrt{u})}{K_1(\sqrt{u})}} - \frac{\frac{I_0(\sqrt{u})}{u\sqrt{u} I_1(\sqrt{u})}}{1 - \frac{I_1(r_{eD}\sqrt{u})}{K_1(r_{eD}\sqrt{u})} \frac{K_1(\sqrt{u})}{I_1(\sqrt{u})}}$$

For a ct pressure circle: $$\bar{p}_{FRD}(u) = \frac{\frac{K_0(\sqrt{u})}{u\sqrt{u} K_1(\sqrt{u})}}{1 + \frac{K_1(r_{eD}\sqrt{u})}{I_1(r_{eD}\sqrt{u})} \frac{I_1(\sqrt{u})}{K_1(\sqrt{u})}} - \frac{\frac{I_0(\sqrt{u})}{u\sqrt{u} I_1(\sqrt{u})}}{1 + \frac{I_1(r_{eD}\sqrt{u})}{K_1(r_{eD}\sqrt{u})} \frac{K_1(\sqrt{u})}{I_1(\sqrt{u})}}$$

To the finite radius solution we can add wellbore storage and skin in Laplace space:

Adding wellbore storage & skin: $$\bar{p}_{wfD}(u)=\frac{1}{u}\left[\frac{S+u\bar{p}_{FRD}(u)}{1+uC_D\left[S+u\bar{p}_{FRD}(u)\right]}\right]$$

The problem is once again transferred to real space using the Stehfest algorithm. The behavior is studied in the next section. As for IARF we will use an interesting late time approximation:

Late time approximation: $$p_{wfD}(t_D)=\frac{2t_D}{r_{eD}^2}+\ln r_{eD}-\frac{3}{4}+S$$

This will be the origin of the pseudo-steady state behavior. Converting the dimensionless radius back dimensionless variables to physical variables we get the PSS equation:

PSS equation: $$p_{wfD}(t_D)=\frac{2\pi r_w^2}{A}t_D+\frac{1}{2}\ln\left(\frac{A}{C_A r_w^2}\right)+0.4045+S$$

C_A is the Dietz shape factor, characteristic of the shape of the reservoir and the position of the well in the reservoir. In the case of a well at the center of a closed circle we get C_A=31.62.

2.E.3 Pseudo-Steady State flow

At late time the pressure response of a well flowing at the center of a homogeneous reservoir of circular shape will be approximated by:

Circular PSS equation: $$p(t)=p_i-0.03723\frac{qB}{\phi c_t h r_e^2}t-141.2\frac{qB\mu}{kh}\left[S+\ln\frac{r_e}{r_w}-\frac{3}{4}\right]$$

We see that the slope of this linear approximation is inversely proportional to the square of the circle radius. More generally the slope will be inversely proportional to the reservoir area.

In the case where the reservoir thickness is not the constant h the slope will be inversely proportional to the volume of the reservoir (or the drainage area). In other words quantifying the PSS slope will provide an estimate of the reservoir volume and therefore the reserves.

The figures below show the drawdown response of a vertical well with wellbore storage and skin in a homogeneous reservoir and under three boundary configurations: an infinite reservoir (green), a circular reservoir of 6,000 ft of radius (blue) and an even smaller reservoir with a radius of 3,000 ft (red). Responses are shown on a linear scale (left) and a loglog scale (right) together with the Bourdet derivative defined in the PTA chapter.

During production, when the boundary is detected, the behavior deviates from Infinite Acting Radial Flow to reach Pseudo-Steady State according to the equation above. PSS is characterized by linearity between the pressure change and the elapsed time on the linear scale.

On the loglog plot PSS is characterized by a unit slope of the Bourdet derivative. Though it is slower, the pressure change also tends towards merging with the pressure derivative on the same unit slope.

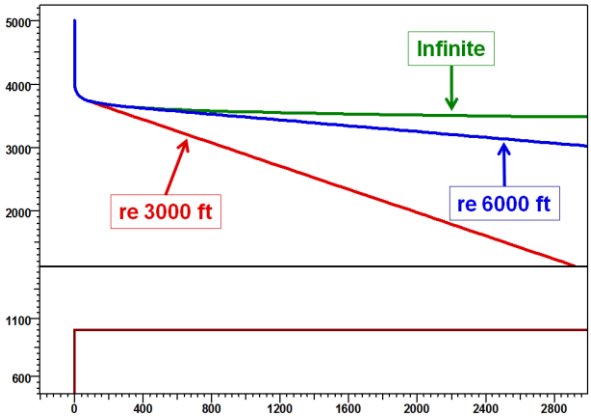


Fig. 2.E.2 – Finite radius PSS solution, linear scale

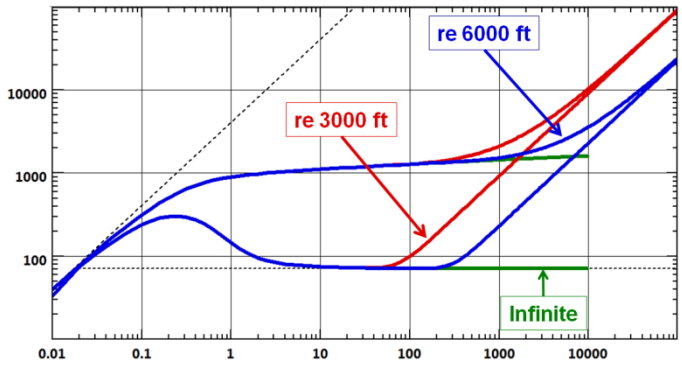


Fig. 2.E.3 – Finite radius PSS solution, loglog scale

Comparing the two circular responses:

- Drawing a straight line on the linear plot will show that the slope of the 're 3,000 ft' line is twice larger than the slope of the 're 6,000 ft' line.

- Looking at the time of deviation from IARF on the loglog plot, we see that this occurs 4 times earlier for the 3,000 ft case than for the 6,000 ft case.

In both cases we see the inverse proportionality of the slope and the time of divergence to the square of the reservoir radius or, more generally to the reservoir area.

The circular model is only one example of closed systems, and Pseudo-Steady State exists for all closed systems. It is a regime encountered after a certain time of constant rate production.

Although it is a flow regime of interest for Pressure Transient Analysis, it is THE flow regime of interest in Rate Transient Analysis. Pseudo-Steady State may sometimes not only be seen as a result of reaching the outer boundary of the reservoir; in a producing field, for example, there is a time when equilibrium between the production of all the wells may be reached, and, for each well, Pseudo-Steady State will occur within the well drainage area.

For a slightly compressible fluid, Pseudo-Steady State is characterized by a linear relation between the pressure change and the time. When PSS is reached, the pressure profile in the reservoir will 'freeze' and the pressure will deplete linearly and uniformly throughout the connected reservoir. Things are somewhat different when the PVT becomes complex.

2.F Complex production histories – Superposition in time

2.F.1 The principle of superposition

Derivations as shown before assumed a constant rate production. In practice we need to model more complex flow histories. This is done using the principle of superposition. We generate the solution of a complex problem as the linear combination and superposition, in time and/or space, of simpler components. The most popular superpositions are:

- Simulation of complex production histories by linear combinations of simple drawdown solutions with different weights and starting times. This is called superposition in time, the equations are developed in the chapter 'Analytical models - 13.C - Superposition in time'.
- Simulation of simple linear boundaries by linear combinations of infinite well and interference solutions coming from virtual wells (also called image wells).

For any problem involving a linear diffusion equation, the main superposition principles are:

- Linear combinations of solutions honoring the diffusion equation also honor this equation.
- At any flux point (well, boundary), the flux resulting from the linear combination of solutions will be the same linear combination of the corresponding fluxes.
- If a linear combination of solutions honors the diffusion equation and the different flux and boundary conditions at any time, then it is THE solution of the problem.

A series of rules for superposition in time are built from these principles, they are detailed in the chapter 'Analytical models - 13.C - Superposition in time'.

2.F.2 Build-up superposition

We consider a production at rate q of duration t_p, followed by a shut-in:

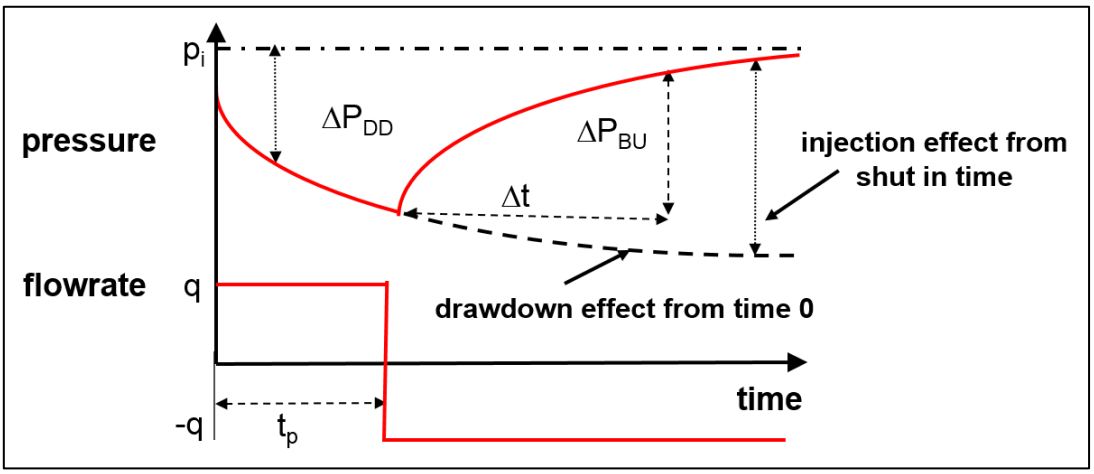


Fig. 2.F.1 – Buildup superposition

The build-up pressure (see details in the chapter 'Analytical models - 13.C - Superposition in time') is then:

$$p_{BU}(t_p + \Delta t) = p_i - \Delta p_{DD}(t_p + \Delta t) + \Delta p_{DD}(\Delta t)$$

In term of delta p, it is:

$$\Delta p_{BU}(\Delta t) = \Delta p_{DD}(t_p) + \Delta p_{DD}(\Delta t) - \Delta p_{DD}(t_p + \Delta t)$$

Therefore:

$$\Delta p_{BU}(\Delta t) < \Delta p_{DD}(t_p) \ \ and \ \ \Delta p_{BU}(\Delta t) < \Delta p_{DD}(\Delta t)$$

Note: the build-up response will be 'flatter' than the drawdown response, and the pressure will never get back above initial pressure…

2.F.3 Multirate superposition

Multi-rate superposition is the natural extension of the build-up superposition to any type of production history. A sequence of rates q_1, q_2, …, q_n, of respective durations T_1, T_2, ... T_n, with respective starting times $t_1=0$, t_2, ... t_n.

More derivation details are given in 'Analytical models - 13.C - Superposition in time'.

The multirate superposition general function is finally:

$$p(t) = p_i - \sum_{i=1}^{n} (q_i - q_{i-1}) \Delta p_{unit}(t - t_i)$$

We have shown how multirate solutions can be derived from elementary drawdown solutions. Horner time, superposition time, etc, will be introduced in the PTA methodology chapter.

2.G Other means to solve and model a diffusion problem

The three models presented so far were solved analytically. Analytical models are fast and accurate. Unfortunately a lot of problems are too complicated to be directly solved analytically. This section presents the main tools used in the industry to provide such solutions.

2.G.1 Superposition in space of analytical models (image wells)

It is possible but relatively complex and CPU intensive to model linear boundaries and radial diffusion at the same time. However, for some geometries, linear boundaries can be replaced by a superposition of interferences from virtual wells. This is called the method of image wells, which in turn requires the notion of superposition in space.

The principle application is detailed in the chapter 'Analytical models - 13.D - Superposition in space'.

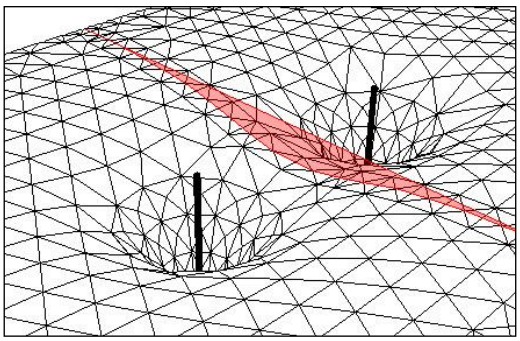


Fig. 2.G.1 – 3D representation of the pressure profile with an image well

Note: in case of multiple faults, if the number of image wells is limited the sum of the image solutions constitute the exact analytical model. Conversely, when the sum is infinite the resulting solution could be classified as a semi-analytical solution (developed in 'Analytical models - 13.D - Superposition in space').

This is correct, but still solutions using image wells are an important category of models that we wanted to single out.

2.G.2 Boundary elements

A particular case of approximate analytical solutions are boundary elements. The principle is to honor the boundary condition by adding to the infinite solution an integral function on the boundary that will 'compensate' for the infinite solution to honor this boundary condition.

This solution has the advantage of focusing on the boundary only, and solves a 3-D problem with a 2-D solution, or a 2-D problem with a 1-D solution.

However there are two major shortcomings: (1) each block delimited by a boundary must be homogeneous, and (2) it involves the inversion of a densely populated matrix, and this can be very computer intensive.

Because of these two shortcomings, numerical models are currently preferred and more developed in the industry.

2.G.3 Numerical models

The application to PTA and RTA of specifically designed numerical models is one of the major technical developments of recent years, especially for KAPPA.

Numerical models address the two major limitations of the modelling methods presented above: they can model complex geometries, and they can model nonlinear diffusion problems for which the superposition in time and space of analytical models will not work.

Numerical models are the subject of a dedicated chapter in this book.

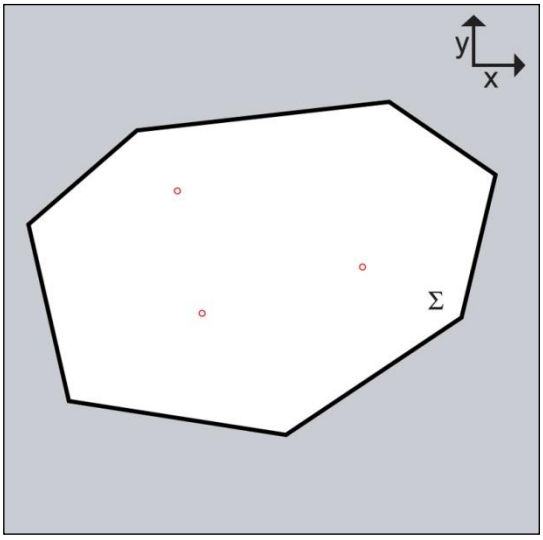


Fig. 2.G.2 – Boundary elements

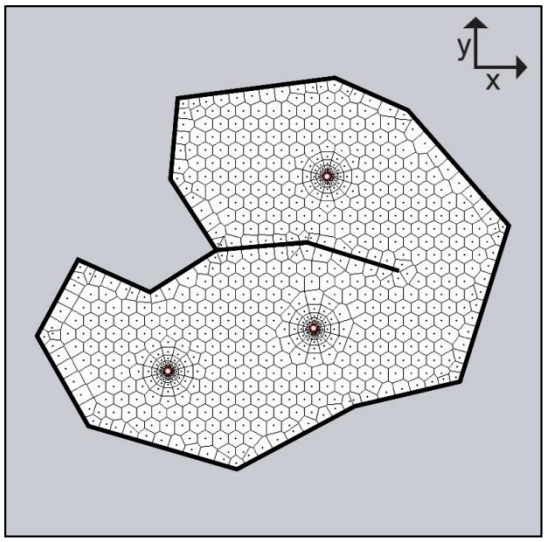


Fig. 2.G.3 – Numerical model

2.H Physical meaning of Diffusion

In Pressure Transient Analysis and Rate Transient Analysis, we use the diffusion assumptions described in the previous section to process measured data, analyze them using models and finally forecast the well and reservoir response. To do this we have two groups of parameters; the 'known' parameters that we will input and the 'unknown' parameters that we calculate.

In the process, we may be tempted to ignore the impact of the known parameters and focus on unknown parameters. Worse, engineers with improper training may use software defaults for 'known' parameters without considering the impact on the results.

This section is a summarized guide to the influence of all parameters involved in the diffusion process, whether we input or calculate them.

2.H.1 Reference case

To do this we select a reference case, with arbitrarily long production and shut-in periods.

You may wish to reproduce the whole process in the chapter below by running successive test designs in Saphir and compare the results using the multi-gauge or multi model option.

We simulate the simplest model that can reproduce the three following flow regimes: Wellbore Storage and Skin, Infinite Acting Radial Flow and Pseudo-Steady State. We model a vertical well in a circular homogeneous reservoir centered at the well:

Input parameters: r_w=0.3 ft; h=100 ft; ϕ=10%; c_t=1.e-5 psi-1; μ=1 cp

Flow rate history: q=1,000 stb/day with B=1; 1,000 hours of flow; 1,000 hours of shut-in

Interpretation 'results': p_i=5,000 psi; C=0.01 bbl/psi; Skin=0; k=10 mD; r_e=1,500 ft

The result of such design, on both production and buildup, is shown below. The loglog plot shows both drawdown and buildup periods.

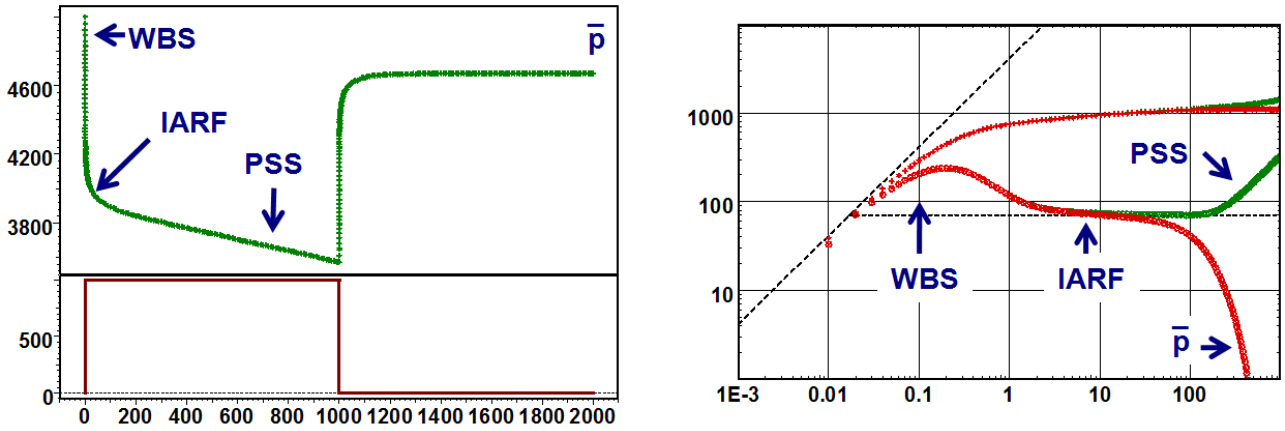


Fig. 2.H.1 – Test Design of the reference case: history and loglog plots

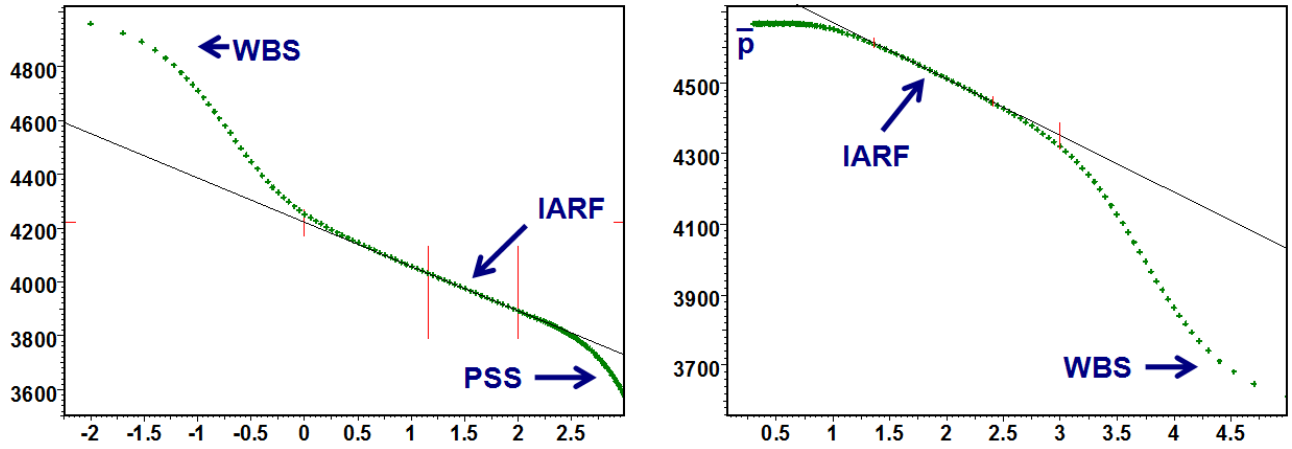


Fig. 2.H.2 – Semilog plot (drawdown) and Horner plot (buildup)

As developed in the PTA chapter we can observe the following:

- The early time hump of the derivative is the transition between pure wellbore storage (early time unit slope; the magnitude of the hump is the skin).
- Infinite Acting Radial Flow (IARF) corresponds to the stabilization of the Bourdet derivative.
- At late time, the production (drawdown) period shows a unit slope corresponding to Pseudo-Steady State, whilst during the shut-in the pressure stabilizes at the average pressure and the derivative takes a dive (also see the chapter on 'Boundary models').

In the following we are focusing on the production (drawdown) and study the effect caused by changes in both 'known' and 'unknown' parameters.

In this design we know ALL parameters. In the following, however, we will make a split between 'unknown' and 'known' parameters. 'Unknown' parameters are those for which we generally look for in a Pressure Transient or Rate Transient Analysis.

In the case of the simulated example, they are the wellbore storage coefficient, the skin factor, the reservoir permeability and the radius of the circular boundary.

'Known' parameters are those we generally assume to be given as an input in order to calculate the 'unknown' parameters from the analysis. Usually, they are r_w, h, ϕ, c_t and μ.We will show how sensitive the response is to the 'known' and 'unknown' parameters, and how an error in the estimation of such parameters will impact our analysis.

2.H.2 Effect of 'unknown' parameters

2.H.2.a Wellbore storage

The figure below presents the response with all default parameters except for the wellbore storage. Values for C are 0.001, 0.003, 0.01, 0.03 and 0.1 (stb/psi).

The value of C has a major effect, which is actually exaggerated by the logarithmic time scale. You can see on the linear history plot that all responses seem to be the same, however.

Infinite Acting Radial Flow: When the influence of wellbore storage is over all responses merge together, both in terms of pressure and derivative. Wellbore storage does not play any role except that it masks infinite acting radial flow on a time that is proportional to the value of C.

PSS: Wellbore storage does not affect the late time response.

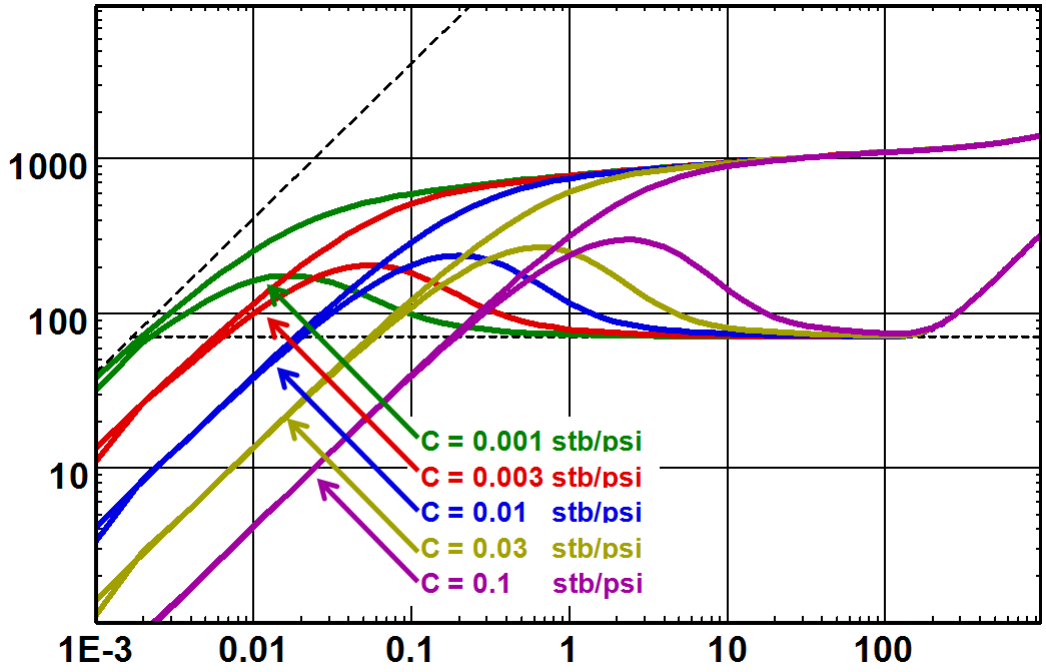


Fig. 2.H.3 – Effect of wellbore storage, loglog plot

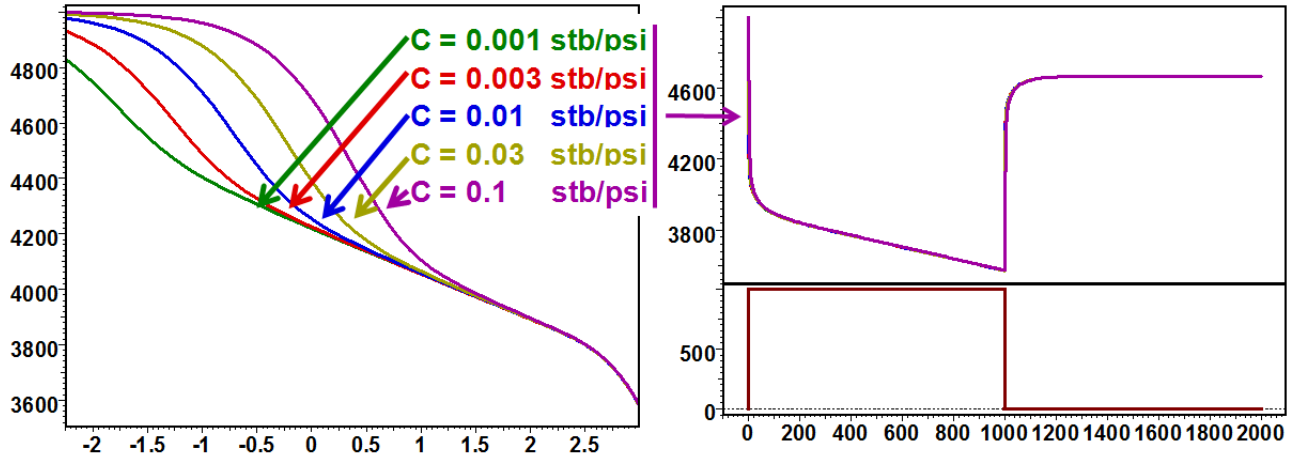


Fig. 2.H.4 – Effect of wellbore storage, semilog and history plot plot

2.H.2.b Skin

Below is shown the response with all default parameters and a variable skin. Values for skin are -3, 0, 2, 5 and 10.

Storage: Skin does not change the position of the early time unit slope (pure wellbore storage) but affects the amplitude of the hump. A larger skin will produce a larger hump, hence delaying the time at which Infinite Acting Radial Flow is reached.

IARF: Once IARF is reached, the skin has no effect on the vertical position of the derivative, but has a cumulative effect on the amplitude of the pressure.

PSS: Skin does not have an effect on the time at which PSS is reached or on the derivative response at the end. However the cumulative effect on the pressure remains and all responses 'bend' and remain parallel when PSS is reached (see history plot below).

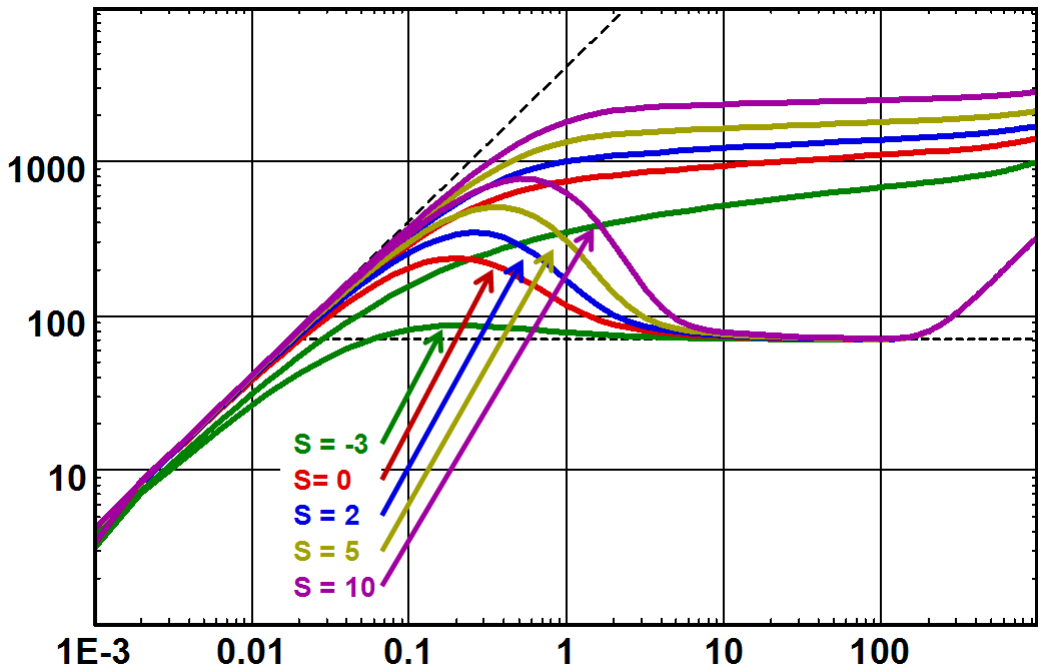


Fig. 2.H.5 – Effect of skin, loglog plot

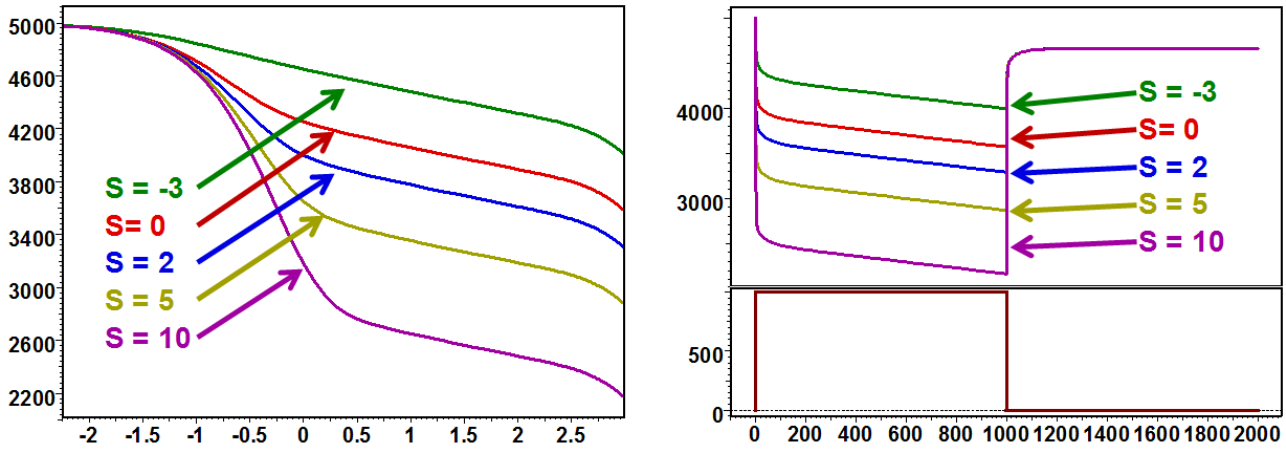


Fig. 2.H.6 – Effect of skin, semilog and history plot

2.H.2.c Permeability

The figure below presents the response with all default parameters except the permeability. Values for k are 2, 5, 10, 20 and 50 mD.

Storage and IARF: The derivative responses have the same shape but they are translated along the wellbore storage line of unit slope. When the permeability is higher, the reservoir reacts faster and deviates earlier from pure wellbore storage. The level of stabilization of the derivative, i.e. the slope of the semilog plot, is inversely proportional to k. For this reason the responses diverge on the semilog plot, the different slopes being inversely proportional to k.

PSS: At late time all derivative signals merge to a single unit slope. This is linked to the fact that permeability has no effect on the material balance equation.

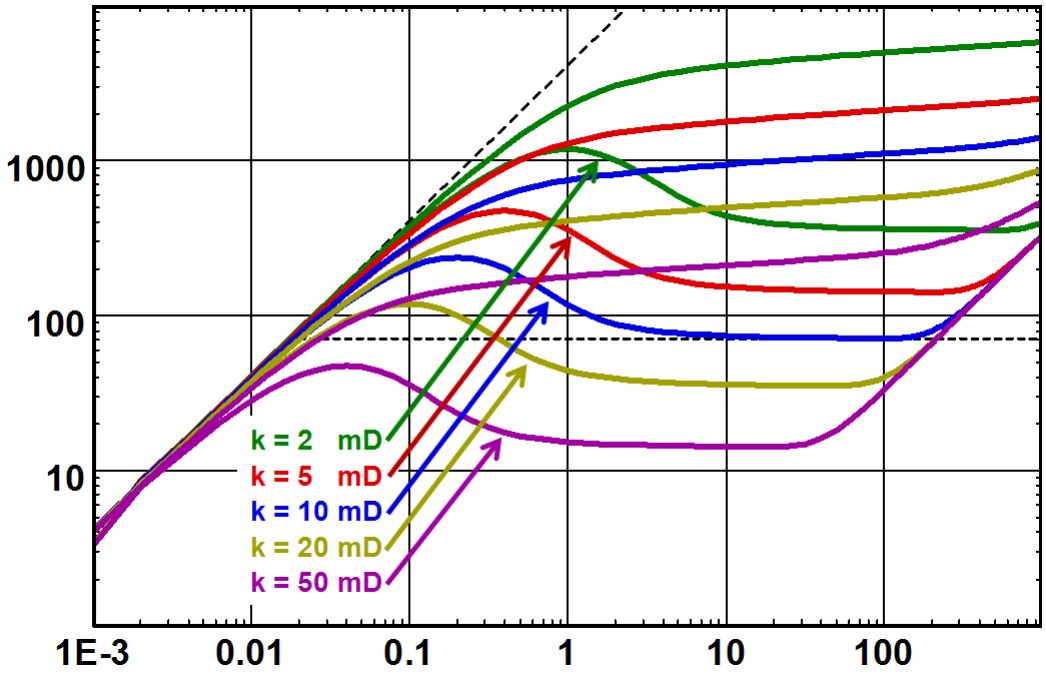


Fig. 2.H.7 – Influence of the reservoir permeability, loglog plot

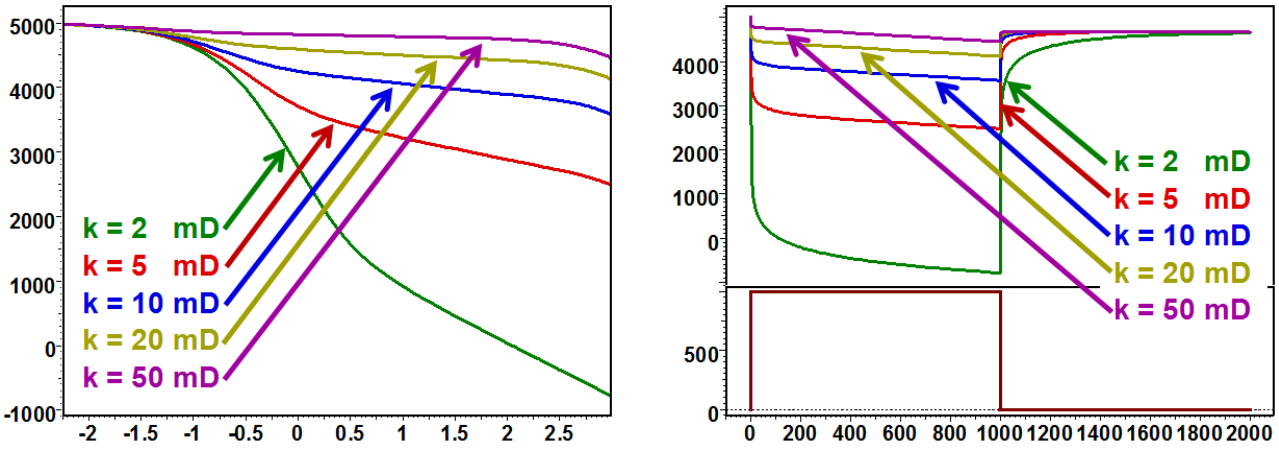


Fig. 2.H.8 – Influence of the reservoir permeability, semilog and history plot

2.H.2.d Reservoir size

Below is presented the response with all default parameters except the reservoir size, the radius r_e. From the reference case we have successively divided / multiplied by 1.5, and the values of r_e are 667, 1000, 1500, 2250 and 3375 ft.

The time at which PSS occurs depends on r_e. As the governing group in the diffusion equation is t/r^2, when r_e is multiplied by 2 the time at which PSS occurs is multiplied by 4. When PSS occurs the slope of the pressure response, on the history plot, is inversely proportional to the volume of the reservoir, and therefore inversely proportional to r_e^2.

In the shut-in the pressure stabilizes to the average pressure obtained by simple material balance. Unlike the cases above, the pressures, for a given production, do not stabilize at the same value. Again the depletion ($p_i - p_{av}$) is inversely proportional to the reservoir pore volume, i.e. inversely proportional to r_e^2.

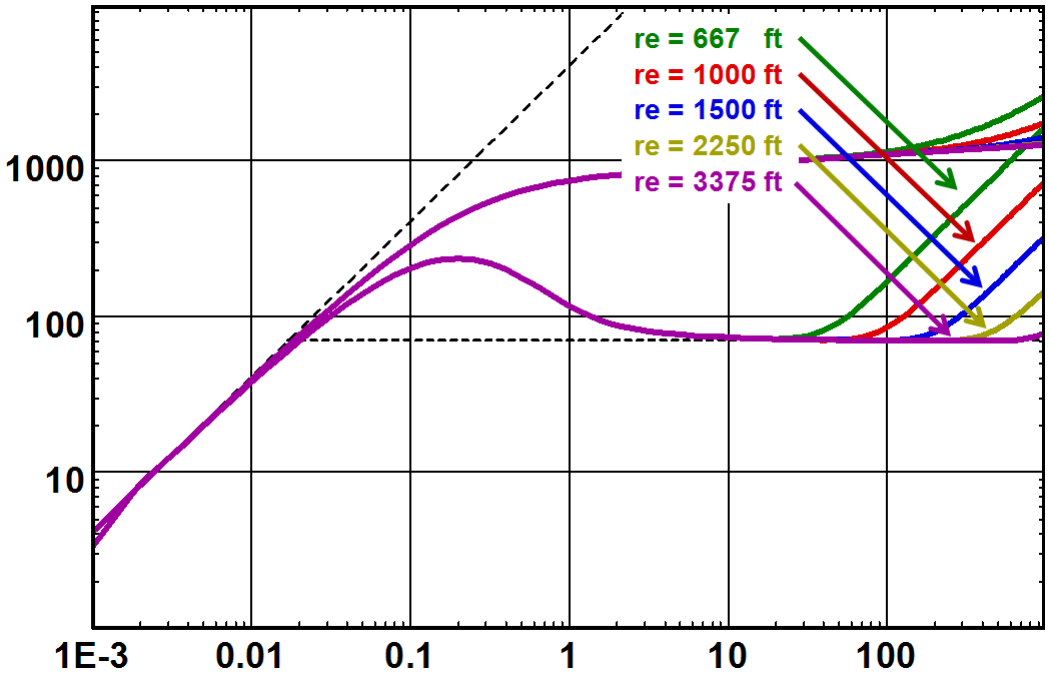


Fig. 2.H.9 – Effect of the reservoir size, loglog plot

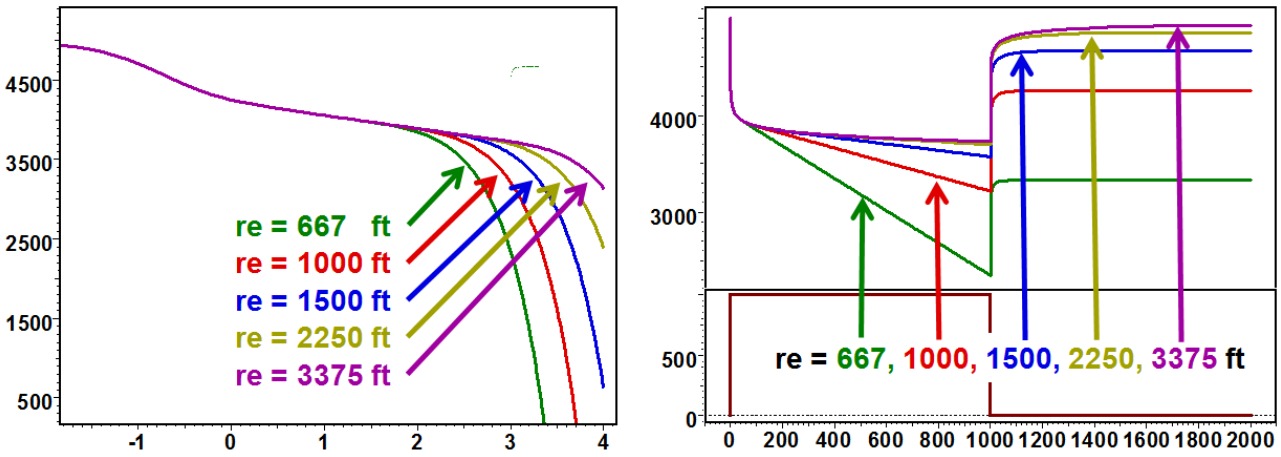


Fig. 2.H.10 – Effect of the reservoir size, semilog and history plot

2.H.3 Effect of 'known' parameters

2.H.3.a Wellbore radius

The response with all default parameters but varying the wellbore radius is illustrated below. Values of r_w are 0.1, 0.3, 1 and 3 ft.

The effect of a change in the wellbore radius is strictly the same as the consequence of a skin change: Early time amplitude of the derivative hump, no middle time and late time effect on the derivative, but a shift in the pressure that stays constant once wellbore storage effects are over. The equivalence between wellbore radius and skin is hardly a surprise, as skin can also be defined with respect to an equivalent wellbore radius. The well response is in fact a function of the equivalent wellbore radius $r_{we} = r_w.e^{-Skin}$.

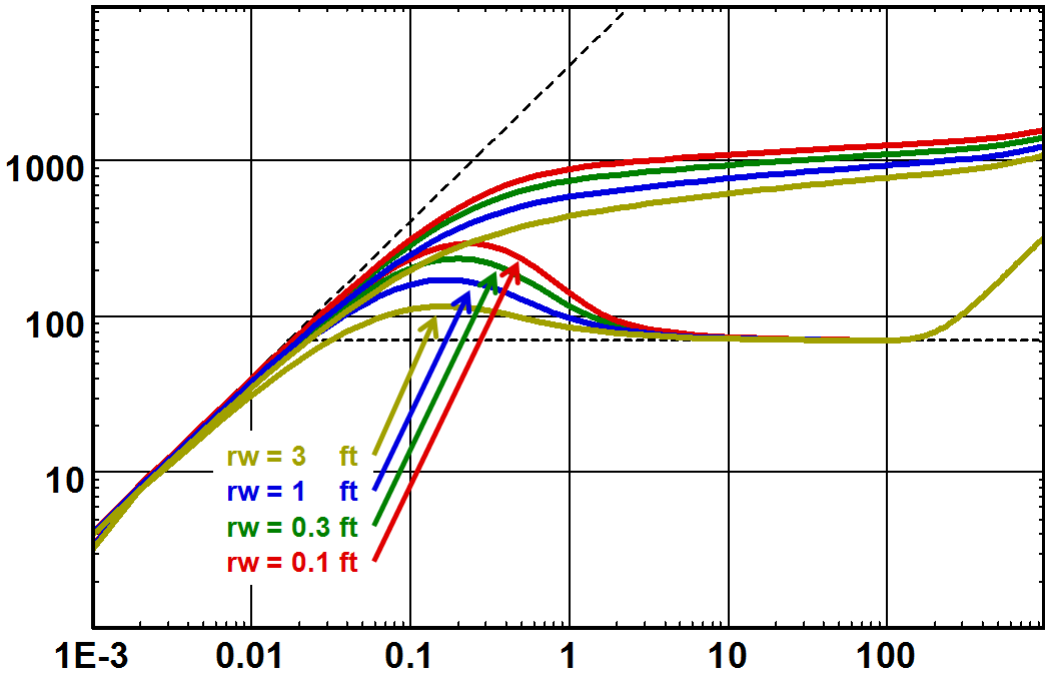


Fig. 2.H.11 – Effect of wellbore radius r_w, loglog plot

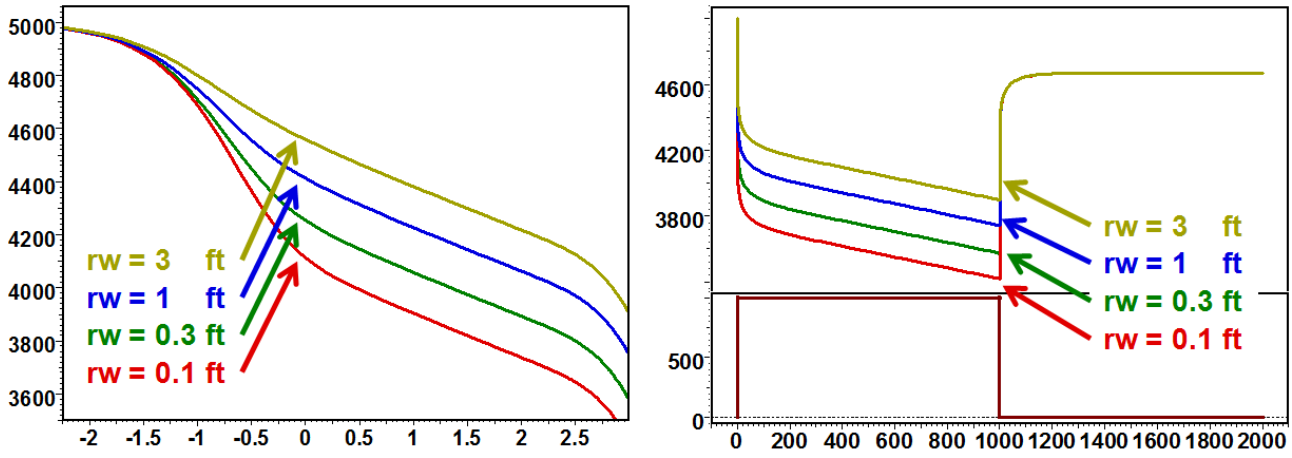


Fig. 2.H.12 – Effect of wellbore radius r_w, semilog and history plot

2.H.3.b Porosity

The figure below presents the response with all default parameters but varying the porosity. Values for ϕ are 3%, 10% and 30%.

Storage and IARF: Porosity behaves like the skin or the well radius. A smaller porosity produces a higher hump on the derivative but does not change the derivative IARF level. The equivalence between porosity and skin is used in two different areas. In interference tests the skin has a marginal influence, and the pressure amplitude is used to assess the porosity.

Hydrogeology: Hydrogeology will assess a value of skin (generally zero) and use the absolute value of the pressure change to assess the Storativity S, i.e. the porosity.

For a given reservoir size, the time for PSS is proportional to ϕ. Underestimating the porosity by 10% will provide an overestimation of the reservoir bulk volume of 10%, and therefore an overestimation of the boundary distance. The total pore volume will remain correct.

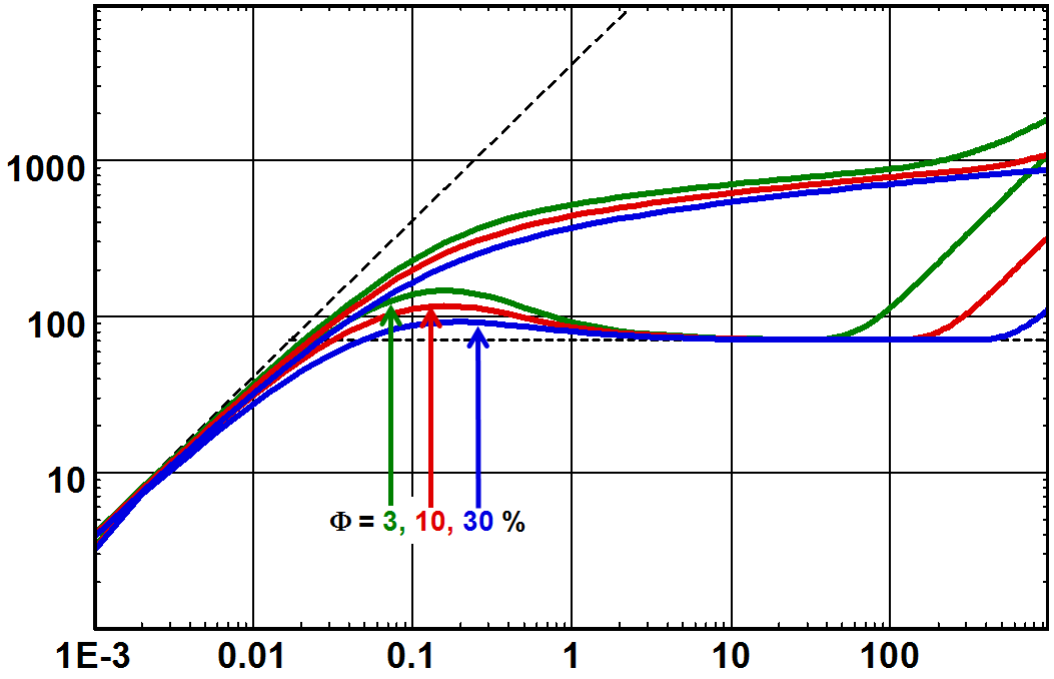


Fig. 2.H.13 – Effect of the reservoir porosity, loglog plot

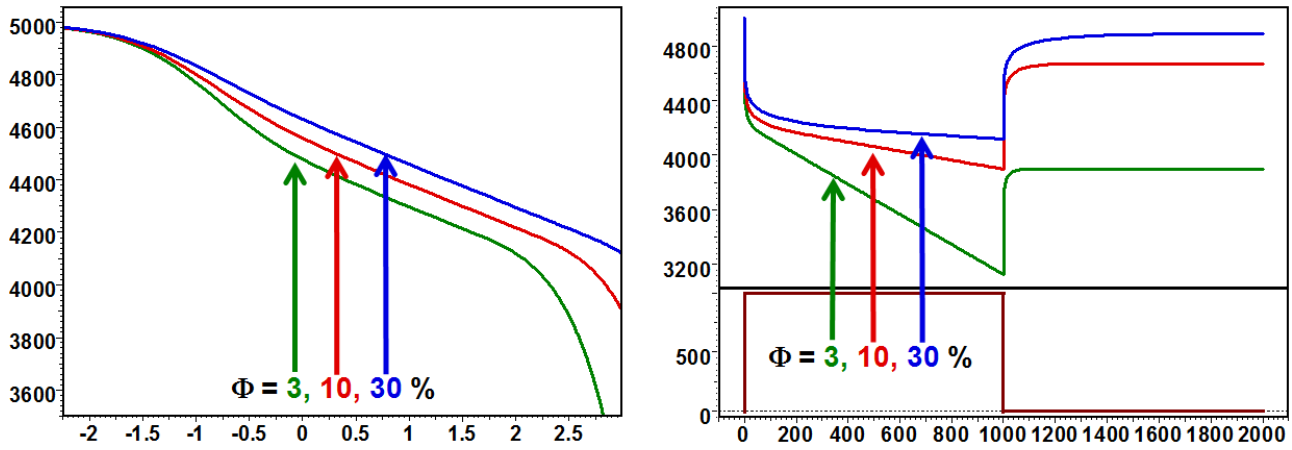


Fig. 2.H.14 – Effect of the reservoir porosity, semilog and history plot

2.H.3.c Total compressibility

Illustrated below is the response simulated with default parameters varying the total compressibility. Values for c_t are 3.e-6, 1.e-5 and 3.e-5 psi-1. The sensitivities at Early Time (Storage), Middle time (IARF) and late time (PSS) are strictly the same as for the porosity: A smaller compressibility produces a higher hump of the early time derivative. Compressibility does not affect the derivative level when IARF is reached but has a cumulative effect on the pressure. At late time, compressibility affects the time at which the boundary is detected and the material balance equation. As for porosity, under-estimating c_t by 10% will provide an over-estimation of the reservoir size by 10%, and therefore an over-estimation of the boundary distance. In fact, on all parts of the response, the influence of porosity and compressibility will be a function of their product $\phi.c_t$.

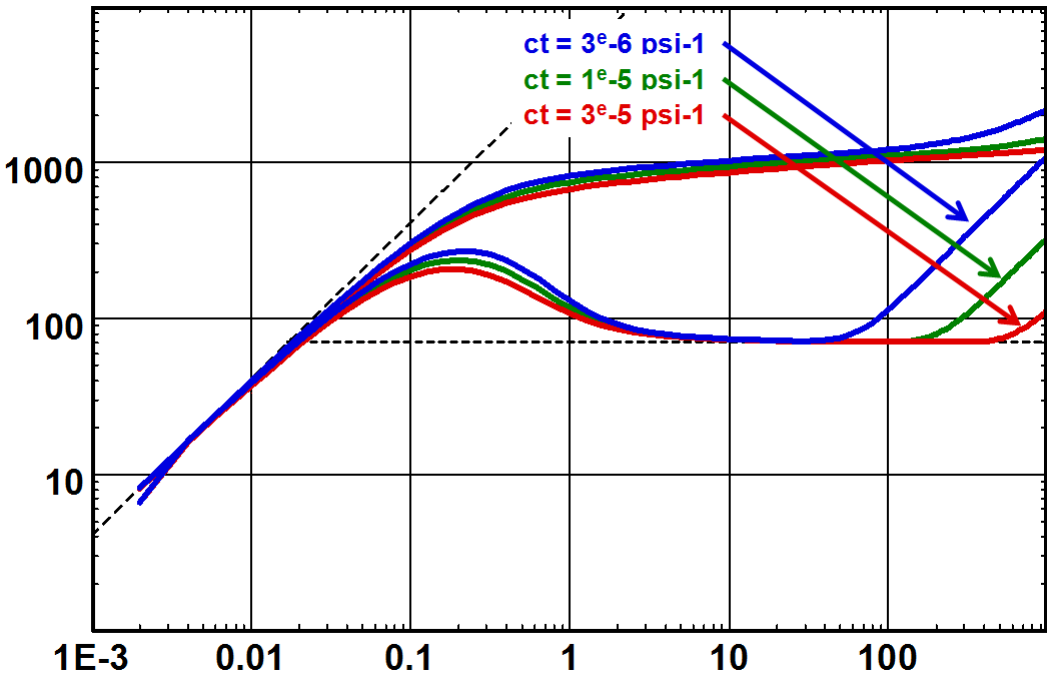


Fig. 2.H.15 – Effect of total compressibility, loglog plot

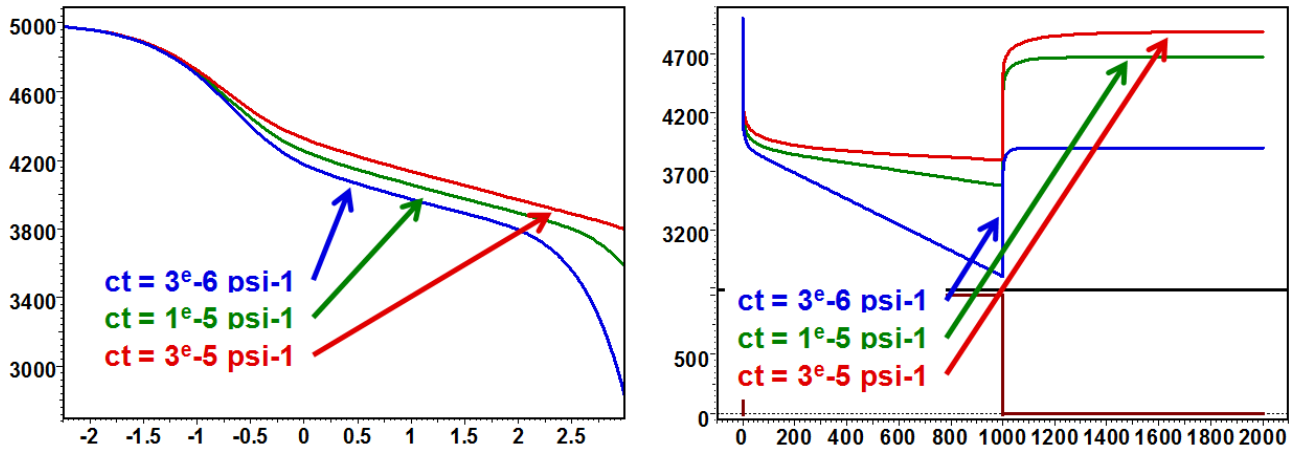


Fig. 2.H.16 – Effect of the total compressibility, semilog and history plot

2.H.3.d Viscosity

The next figure illustrates the response with default parameters but varying the fluid viscosity. Values for μ are 0.2, 0.5, 1, 2 and 5 cp. If we compare the response with the Fig. 2.H.8 illustrating the effect of a permeability change (above), we see that the sensitivity to viscosity is exactly opposite to the sensitivity to permeability. At early time (Storage) and middle time (IARF), the derivative responses have the same shape but translated along the wellbore storage line of unit slope. When the viscosity is lower, the reservoir reacts faster and deviates earlier from pure wellbore storage. The levels of stabilization of the derivative and the semilog slopes are proportional to μ. At late time all derivative signals merge to a single unit slope. In other words, the sensitivity on 1/μ is the same as the sensitivity to k on all parts of the response. This means that we have another governing group with k/μ, also called the mobility.

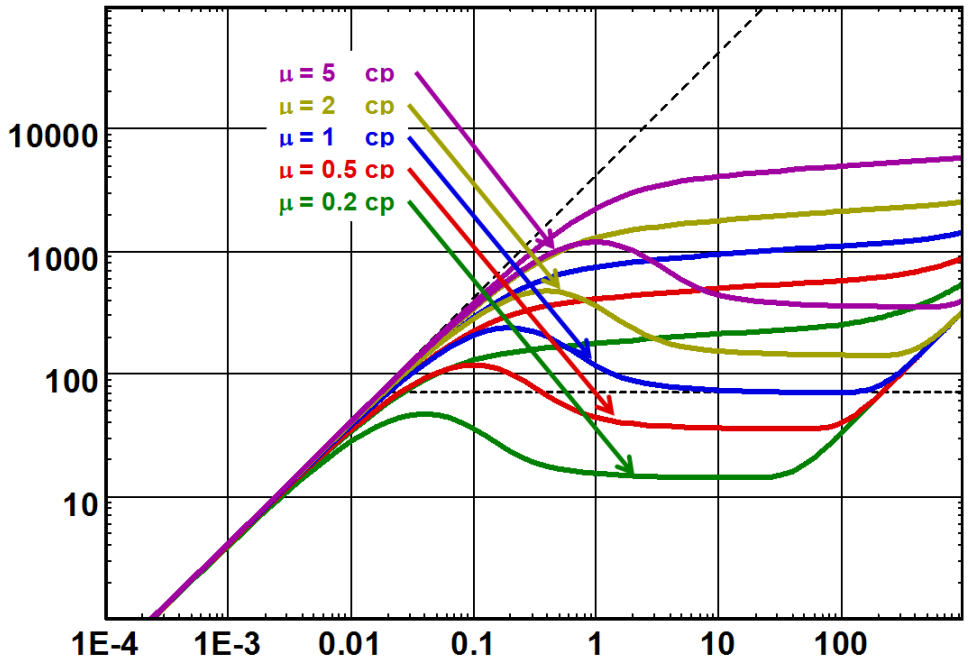


Fig. 2.H.17 – Effect of the fluid viscosity, loglog plot

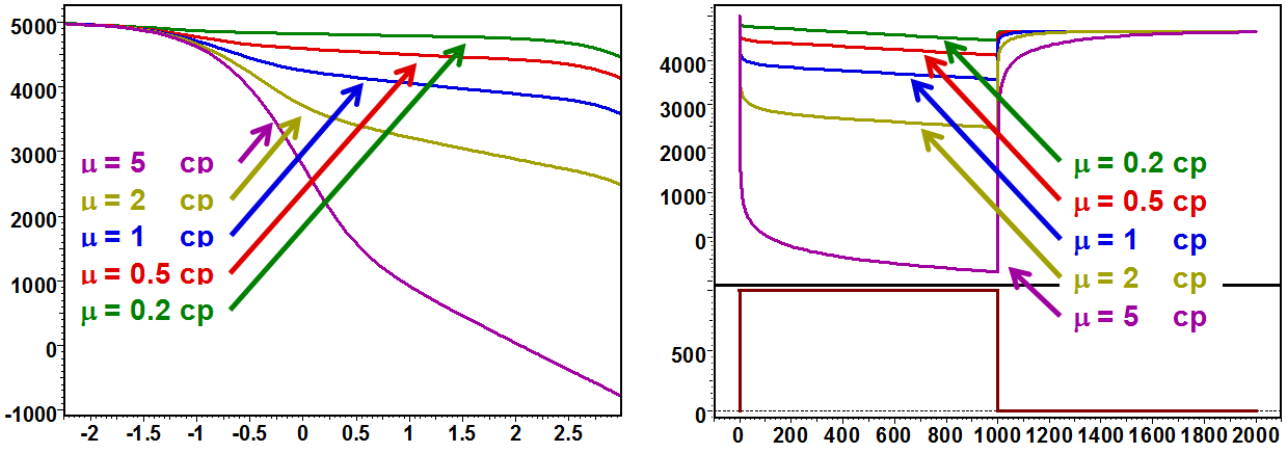


Fig. 2.H.18 – Effect of the fluid viscosity, semilog and history plot

2.H.3.e Thickness

Illustrated below is the response with all default parameters constant and a varying net drained thickness. Values for h are 20, 50, 100, 200 and 500 ft.

Storage and IARF: Changing the thickness has a similar effect to changing the permeability and an effect opposite to changing the viscosity. In other words, the governing group that defines the early time response, apart from wellbore storage and skin, is kh/μ.

PSS: Unlike permeability and viscosity, the reservoir thickness also has an effect on the late time material balance calculation. Also, the time at which the derivative deviates from IARF towards PSS does not change, and therefore the influence of the thickness on the position of the PSS straight line is similar to the sensitivity to the reservoir porosity or the compressibility.

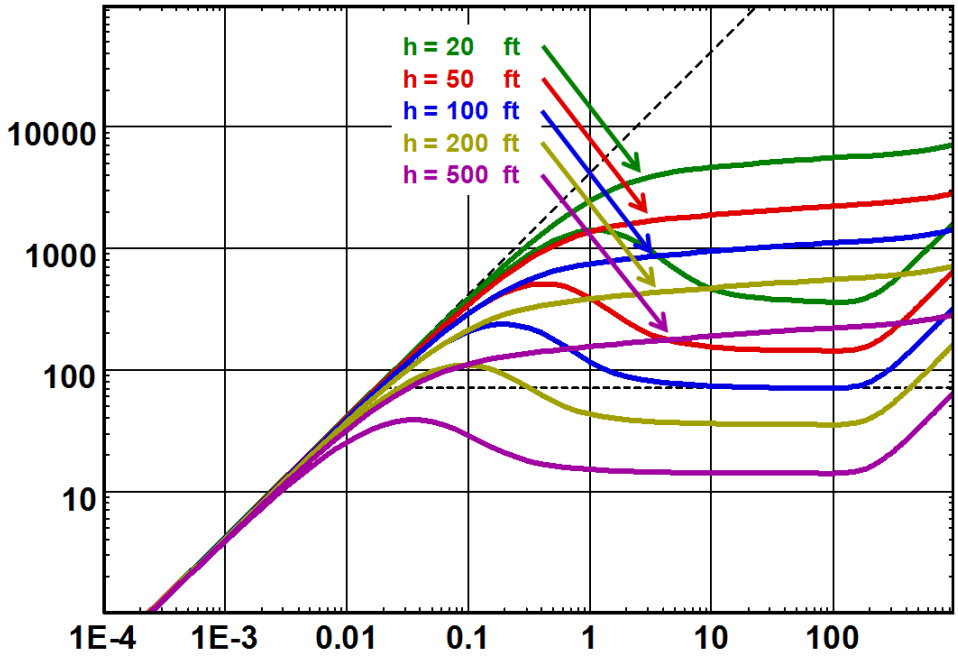


Fig. 2.H.19 – Effect of the reservoir thickness, loglog plot

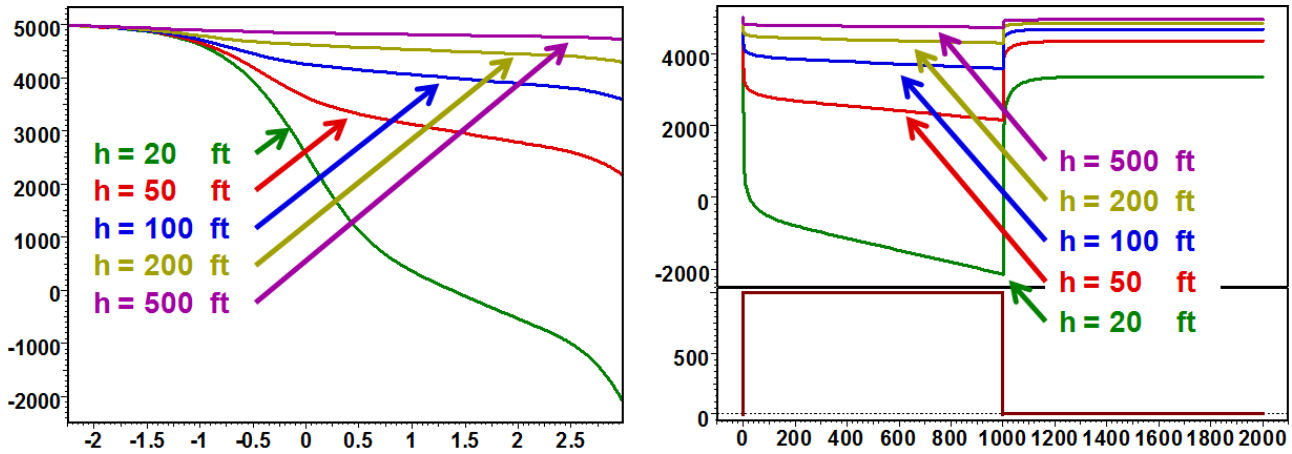


Fig. 2.H.20 – Effect of the reservoir thickness, semilog and history plot

2.H.3.f How about rates?

We are not referring to superposition effects, but to the plain value of the rate, i.e. the effect of a systematic error on the rate values and/or the formation volume factor B.

Fig. 2.H.22 below illustrates the response with all default parameters constant, but with a variable rate for each simulation. Values for qB are 600, 800, 1000, 1200 and 1400 rb/d.

The result of varying qB corresponds to a straight multiplication of the pressure change from pi. The loglog response is shifted vertically, and the semilog and history plots are vertically compressed or expanded, the fixed point being the initial pressure.

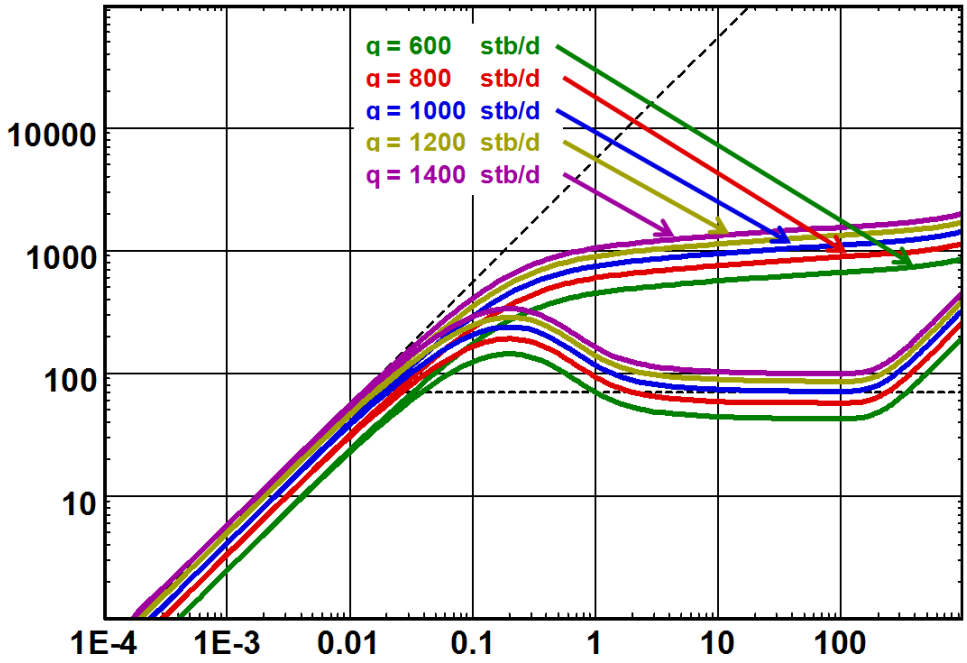


Fig. 2.H.21 – Effect of the rate– qB, loglog plot

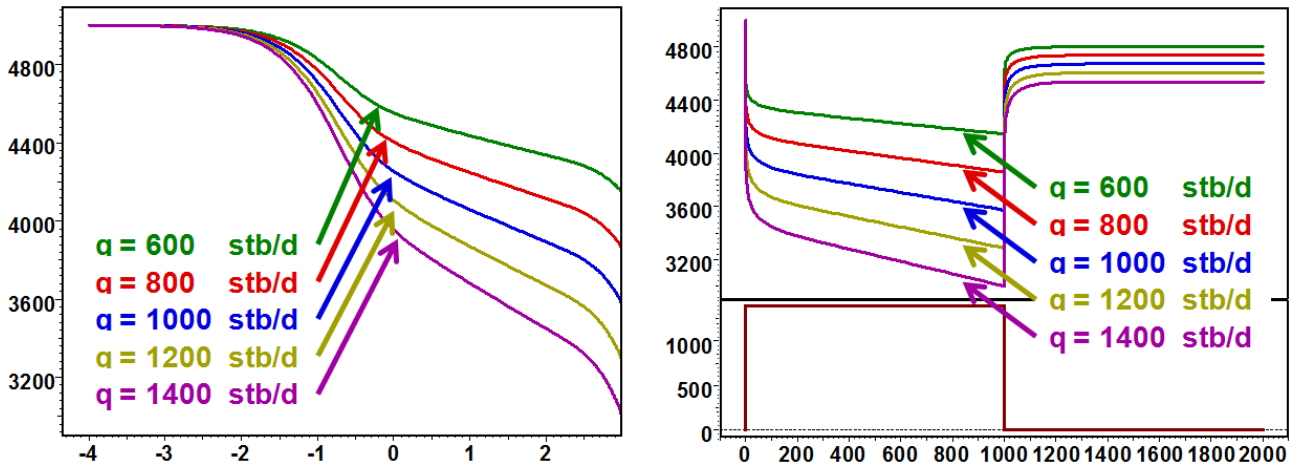


Fig. 2.H.22 – Effect of the rate– qB, semilog and history plot

2.H.4 Conclusions

2.H.4.a on this series of designs

Beyond the arbitrary split between input and output parameters set in the methodology of Pressure Transient Analysis, we see that several groups of parameters govern the response of the well / reservoir system.

- Pure wellbore storage: The absolute position of the early time unit slope is only a function of the wellbore storage C.
- Transition from pure wellbore storage to IARF: The shape of the hump, which originally was set to $C_D e^{2.Skin}$ when dealing with type curves, is actually a function of C and $r_w e^{-Skin}$, and is also slightly affected by ϕ and c_t. The whole curve is translated along the unit slope as a function of k, μ and h, the governing group being kh/μ.
- IARF: The governing group is kh/μ defining the semilog slope, hence the level of the derivative stabilization when IARF is reached.
- There is a residual effect of rw, skin, ϕ and c_t that defines the constant term of the IARF straight line. Generally the Skin factor is calculated from this constant term.
- At late time the parameters that govern the position of the PSS unit slope are r_e, ϕ, c_t and h. The governing group is $\phi.c_t.h.r_e^2$. You may actually prefer the group $2\pi.r_e^2.h.\phi.c_t$, and you get $V_{pore}.c_t$, where V_{pore} is the reservoir pore volume. What we arrived at here is nothing more than material balance.
- There is a residual effect of all factors that affected the transient diffusion before PSS was reached, and which constitute the constant term of the PSS straight line.

2.H.4.b on the equations

If we consider the IARF equation given in previous section:

$$p(t) = p_i - \frac{162.6qB\mu}{kh}\left[\log(t) + \log\left(\frac{k}{\Phi\mu c_t r_w^2}\right) - 3.228 + 0.8686.Skin\right]$$

…and if we re-shuffle it a bit, we get:

$$\Delta p(t) = \frac{162.6qB}{\frac{kh}{\mu}}\left[\log(t) + \log\left(\frac{kh}{\mu}\right) - \log(h\Phi c_t) - 3.228 - 2\log\left(r_w e^{-Skin}\right)\right]$$

One can see that the slope is a function of kh/μ, and that there is a constant term that shows, among other things, the residual effect of $r_w e^{-Skin}$, ϕ and c_t.

If we consider the PSS equation given previously:

$$p(t) = p_i - 0.234\frac{qB}{\phi c_t hA}t - 141.2\frac{qB\mu}{kh}\left[\frac{1}{2}\ln\left(\frac{A}{C_A r_w^2}\right) + 0.4045 + Skin\right]$$

…and if we re-shuffle it a bit again, without worrying about calculating a few constants, including the value of the shape factor for a circle, we get:

$$\Delta p(t) = a_1 qB \frac{t}{2\pi r_e^2 h \phi c_t} + a_2 qB \frac{a_3 + \ln\left(r_e^2\right) - \ln\left(r_w e^{-Skin}\right)}{\frac{kh}{\mu}}$$

Or…

$$\Delta p(t) = a_1 qB \left[\frac{1}{V_{pore} c_t} t + f\left(r_w e^{-Skin}, \frac{kh}{\mu}, r_e \right) \right]$$

One can see that the slope is a function of the porous volume times the compressibility, while the constant term is a function of all the transients that happened before PSS occurred.

2.H.5 Effect of errors on the different input parameters

What we have seen so far is the sensitivity of a test / production design on the different parameters. In the case of a real analysis we will input the 'known' parameters, calculate the model response and vary the 'unknown' parameters until the model matches the measured response. This will 'calculate' the 'unknown' parameters.

What we will do now is consider that the truth is our reference case. From this reference case we will change one of the 'known' parameters to a wrong value, off by, say, 10%. Then optimize the model by varying the 'unknown' parameters to match the reference case and see how this affects these parameters (the results from Pressure Transient or Production Analyses).

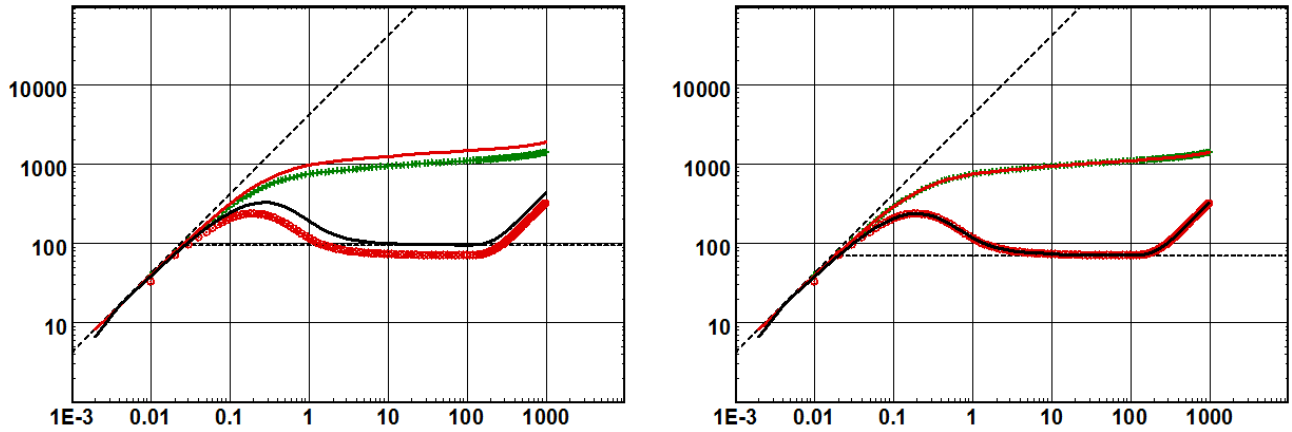


Fig. 2.H.23 – h at 25% below 'true' – Left plot is the model using all other 'exact' unknown Right plot is the match after optimization of the unknown parameters kh is OK – k is 33% above 'true' – re is 15% above 'true' – Skin at -0.14 instead of 0

The action here is fairly straightforward, so we will spare you the figures and only show you the results:

- Well radius: If we over-estimate r_w by 10%, the calculated skin will be over-estimated with a shift of 0.1. The general rule is that the false skin induced by this incorrect r_w will be in the ratio (rw_{wrong}/rw_{right}). All other parameters will be OK.
- Porosity: If we over-estimate ϕ by 10%, k and kh will be OK, there will be a marginal error on the skin, the reservoir size will be underestimated by 10%, and hence the boundary distances will be underestimated by 5%.
- Compressibility: Same as above. If we over-estimate c_t by 10%, k and kh will be correct, there will be a marginal error on the skin, however the reservoir size will be underestimated by 10%, hence the boundary distances will be underestimated by 5%.
- Viscosity: If we over-estimate μ by 10%, k and kh will be overestimated by 10%, there will be no error on skin and the reservoir size will be evaluated correctly.
- Thickness: If we over-estimate h by 10%, kh will be correct and k will be underestimated by 10%. There will be a marginal error in the skin, the reservoir size will be underestimated by 10%, and hence the boundary distances will be underestimated by 5%.
- Rate: If we over-estimate q.B by 10%, C, k.h and k will be overestimated by 10%. The reservoir size will also be overestimated by 10%, and hence the boundary distances will be overestimated by 5%. There will also be a minor skin difference.

This is summarized in the table below:

	Storage & Skin		Permeability		Boundary	
	C	**Skin**	**k.h**	**k**	**Area**	**Distance**
r_w ↑ 10%	-	↑ 0.1	-	-	-	-
ϕ ↑ 10%	-	ε	-	-	↓ 10%	↓ 5%
c_t ↑ 10%	-	ε	-	-	↓ 10%	↓ 5%
μ ↑ 10%	-	-	↑ 10%	↑ 10%	-	-
h ↑ 10%	-	ε	-	↓ 10%	↓ 10%	↓ 5%
q.B ↑ 10%	↑ 10%	ε	↑ 10%	↑ 10%	↑ 10%	↑ 5%

2.I The case of dry gas

2.I.1 The PVT of real dry gas

When the problem is no longer linear, the superposition of drawdown solutions is replaced by more complex semi-analytical models or numerical models. Superposition time functions may no longer be strictly valid, but they will be kept as diagnostic tools. Ultimately, only nonlinear numerical models will be strictly valid.

In some cases we can try to keep using the principle of superposition by substituting the pressure, and in some cases the time, with a function of the pressure that makes the equation a bit more linear. This is the case for the nonlinear diffusion of dry gas, where we will use what is called pseudopressure and pseudotime.

We have considered so far that the reservoir fluid was slightly compressible and that viscosity and compressibility were constant. This assumption is not valid for gases.

Regarding compressibility, the PVT relation is given by:

Ideal gas: $PV = nRT$

Real gas law: $PV = ZnRT$

The gas viscosity is also a function of pressure and temperature. The Z factor and viscosity may be input from tables at a given temperature or we may use correlations. The correlations for Z factor (Beggs & Brill, Dranchuk et al, Hall and Yarborough) and for viscosity (Lee et al, Carr et al) can also be matched using flash reference data. From the Z factor table / correlation, one can then calculate the volume factor and compressibility correlations.

The two figures below give a typical relation between Z and μ as a function of p at a given T:

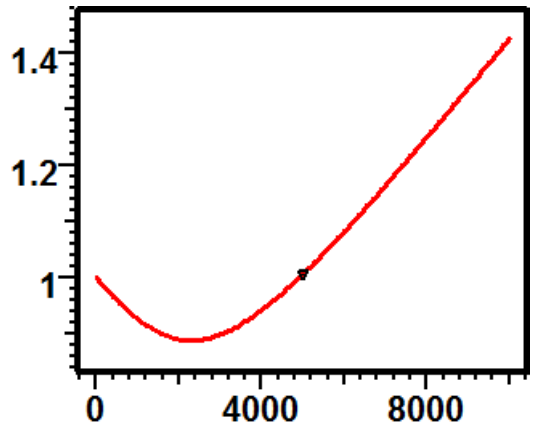


Fig. 2.I.1 – Z factor vs p [psia]

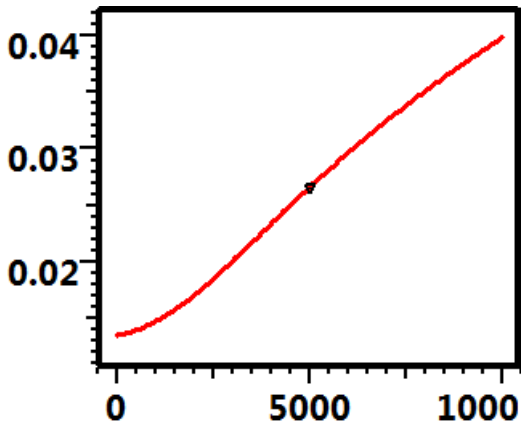


Fig. 2.I.2 – μ_g [cp] vs p [psia]

Volume factor and compressibility are then calculated from the Z factor:

Volume factor and compressibility: $B_g = \frac{Zp_{sc}T}{pT_{sc}}$ $c_g = -\frac{1}{B_g}\frac{dB_g}{dp} = \frac{1}{p} - \frac{1}{Z}\frac{dZ}{dp}$

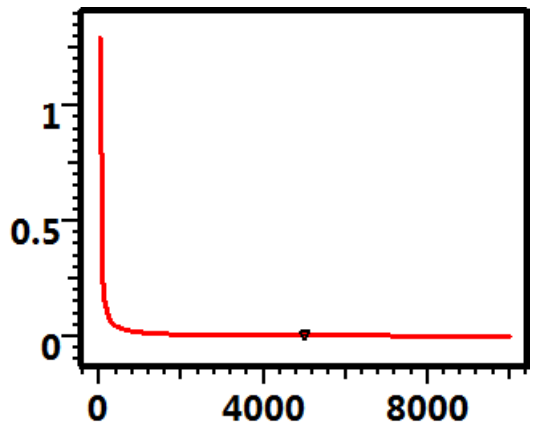


Fig. 2.I.3 – B_g [SCF/RCF] vs p [psia]

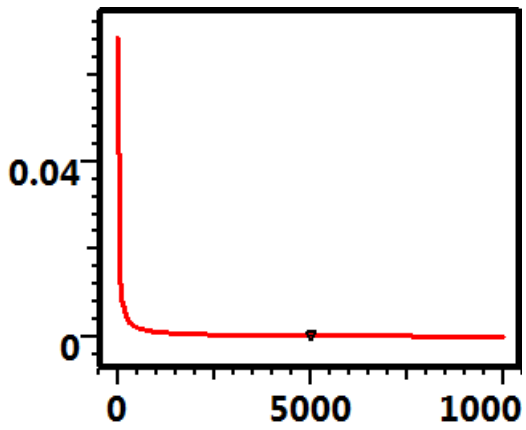


Fig. 2.I.4 – c_g [psi^{-1}] vs p [psia]

We could just use these PVT elements straight into a numerical simulator. However we would be short of diagnostic plots if we were just blindly simulating and matching.

The idea is to rearrange the equations by changing variables in a gas diffusion equation that looks like the slightly compressible fluid equation. If we do so we could extend the methodology and diagnostic plots developed for the linear process to the nonlinear process of gas diffusion. This is done by introducing pseudopressures.

2.I.2 Derivation of the real dry gas diffusion

We deviate from our initial derivation just before the slightly compressible fluid assumption:

Raw diffusion equation:
$$0.0002637k_x \frac{\partial}{\partial x}\left[\frac{\rho}{\mu}\frac{\partial p}{\partial x}\right] = \frac{\partial(\rho\phi)}{\partial t}$$

The real gas law gives:
$$PV = ZnRT \quad \text{where} \quad n = \frac{m}{M}$$

This gives the gas density:
$$\rho = \frac{m}{V} = \frac{M}{RT}\frac{p}{Z}$$

Diffusion equation becomes:
$$0.0002637k_x \frac{\partial}{\partial x}\left[\frac{M}{RT}\frac{p}{\mu Z}\frac{\partial p}{\partial x}\right] = \frac{\partial}{\partial t}\left[\frac{M}{RT}\frac{p}{Z}\phi\right]$$

Which simplifies to:
$$\frac{\partial}{\partial t}\left[\frac{p}{Z}\phi\right] = 0.0002637k_x \frac{\partial}{\partial x}\left[\frac{p}{\mu Z}\frac{\partial p}{\partial x}\right]$$

The first term develops as:
$$\frac{\partial}{\partial t}\left[\frac{p}{Z}\phi\right] = \phi\frac{p}{Z}\left[\frac{1}{\phi}\frac{\partial\phi}{\partial p} + \frac{Z}{p}\frac{\partial}{\partial p}\left(\frac{p}{Z}\right)_T\right]\frac{\partial p}{\partial t}$$

The gas compressibility is written:
$$c_g = \frac{1}{\rho}\left(\frac{\partial\rho}{\partial p}\right)_T = \frac{RTZ}{Mp}\frac{\partial}{\partial p}\left(\frac{Mp}{RTZ}\right)_T = \frac{Z}{p}\frac{\partial}{\partial p}\left(\frac{p}{Z}\right)_T$$

So:
$$\frac{\partial}{\partial t}\left[\frac{p}{Z}\phi\right] = \phi\frac{p}{Z}\left(c_f + c_g\right)\frac{\partial p}{\partial t} = \phi c_t \frac{p}{Z}\frac{\partial p}{\partial t}$$

And the diffusion equation becomes:

$$\phi c_t \frac{p}{Z}\frac{\partial p}{\partial t} = 0.0002637 k_x \frac{\partial}{\partial x}\left[\frac{p}{\mu Z}\frac{\partial p}{\partial x}\right]$$

Or:

$$\frac{p}{Z}\frac{\partial p}{\partial t} = 0.0002637 \frac{k_x}{\phi c_t}\frac{\partial}{\partial x}\left[\frac{p}{\mu Z}\frac{\partial p}{\partial x}\right]$$

We add the viscosity μ on both sides of the equation:

Gas diffusion equation:

$$\frac{p}{\mu Z}\frac{\partial p}{\partial t} = 0.0002637 \frac{k_x}{\phi \mu c_t}\frac{\partial}{\partial x}\left[\frac{p}{\mu Z}\frac{\partial p}{\partial x}\right]$$

2.I.3 Diffusion of real dry gas

2.I.3.a Standard pseudopressures

In order to extend the methodology of Dynamic Data Analysis to gas cases, one introduces a function of the pressure called the pseudopressure. It is given by:

Gas pseudopressure:

$$m(p) = 2\int_0^p \frac{p}{\mu Z} dp$$

The Derivation leading to this equation is detailed in the 'chapter 13 - Analytical models - 13.E - The use of pseudofunctions'.

The Field unit for pseudopressures is psi²/cp. A typical the product μz response as a function of pressure, and for a given temperature, is shown below. There is a rule of thumb regarding the behavior of this function:

- Below 2000 psia, μZ is fairly constant, and m(p) behaves like p^2
- Above 3000 psia, μZ is fairly linear, and m(p) behaves like p

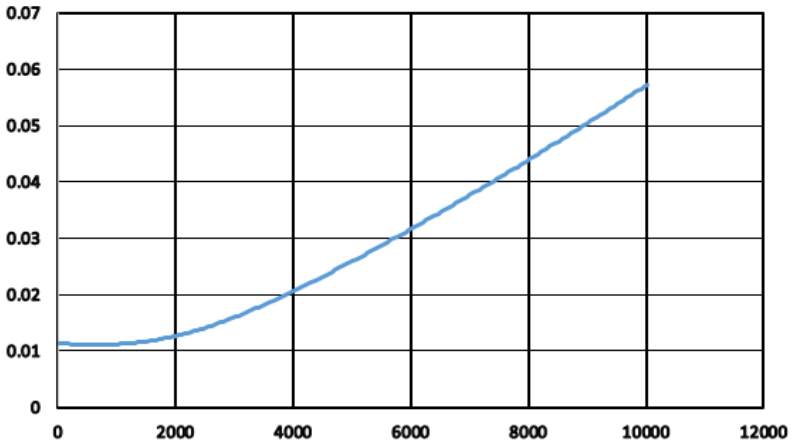


Fig. 2.I.5 – μz vs p [psia)

Gas diffusion equation:

$$\frac{\partial m(p)}{\partial t} = 0.0002637 \frac{k}{\Phi \mu c_t}\nabla^2 m(p)$$

The principle of traditional real gas analysis is to replace the pressure by the pseudopressure and interpret the data as if the fluid was slightly compressible.

However, there is an important shortcoming in this method. Although the equation looks the same, it will only be linear as long as we can consider the diffusion term $k/\phi\mu c_t$ constant. This is valid as long as the average reservoir pressure does not substantially decrease which is a reasonable assumption for a standard, relatively short, well test. In the case of extended tests such as limit tests and production well tests, this may not be the case.

2.I.3.b Normalized pseudopressures

The gas diffusion equation remains valid if we multiply the pseudopressures by a fixed number. Because the unit and orders of value of the standard pseudopressures are not intuitive, one possibility is to use normalized pseudopressures by selecting a reference pressure p_{ref}, with the condition:

Normalized pseudopressures: $$m_{Norm}(p) = p_{ref}\frac{m(p)}{m(p_{ref})}$$

Normalized pseudopressure at: p_{ref}: $$m_{Norm}(p_{ref}) = p_{ref}$$

The normalized pseudopressures have the dimension and unit of the pressure, it follows the same diffusion equation and it coincides with the pressure at p_{ref}:

Normalized pseudopressures: $$\frac{\partial m_{Norm}(p)}{\partial t} = 0.0002637\frac{k}{\Phi\mu c_t}\nabla^2 m_{Norm}(p)$$

2.I.4 Non-Darcy flow

The diffusion equation used as the basis of the methodology in Dynamic Data Analysis is based on three components: the conservation of mass, a PVT equation and Darcy's law. We have seen above that the gas PVT required some adjustments in the equations and the method: pseudopressures, changing storage, material balance. In complement there are some cases, and especially for gas, where the assumption of Darcy flow is invalid. Sections of the reservoir, generally close to the well, will flow at such speed that turbulence will occur and have a strong impact on the well response. We now need to add a turbulence component to the flow equation, replacing Darcy's law by a second degree equation, such as Forchheimer's.

Darcy's law expressed in terms of speed, in SI units: $$\frac{\partial P}{\partial x} = \frac{\mu}{k}\cdot u$$

Forchheimer's equation, same references and units: $$\frac{\partial P}{\partial x} = \frac{\mu}{k}\cdot u + \beta\cdot\rho\cdot u^2$$

β is called the turbulence factor. There are two main options to address non-Darcy flow:

- The first is to focus on the impact of non-Darcy flow on the well productivity. This is what was done historically using rate dependent skin. Normal diffusion is used, but an additional, rate related skin component is added.
- The other way is to model non-Darcy flow by numerically integrating the Forchheimer equation in the model.

A diagram of the two options is shown in the figure below:

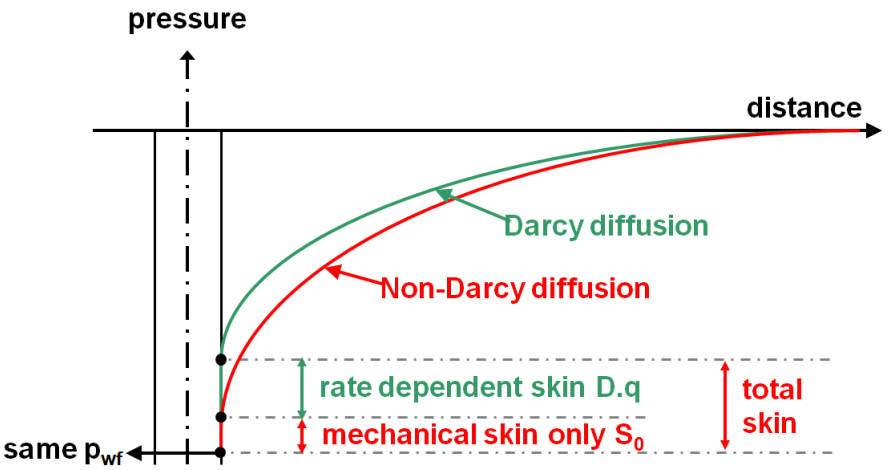


Fig. 2.I.6 – Two ways to model non-Darcy flow

The application of these two approaches is detailed in the chapter 'PTA General methodology' and in 'Rate Transient Analysis – The case of dry gas'.

3 – Pressure Transient Analysis (PTA)

OH – OSF – DV

3.A Introduction (with a short history)

The following sections present the classical and modern methodology and tools developed for Pressure Transient Analysis (PTA). We will present the typical path recommended to perform an analysis and to design a test. The final sections are dedicated to operational considerations on well testing i.e. what data to gather and its validation

When PTA was still called Well Test Interpretation, analyses were performed on data acquired during dedicated operations called well tests. Typical well test set-up is shown in the figure below. Temporary equipment is installed downhole and at surface, the well is put on production under a predefined program and the diagnostic is performed, generally on a shut-in period after a clean-up phase, an initial shut-in and a stable production phase during which producing rates are measured at the separator.

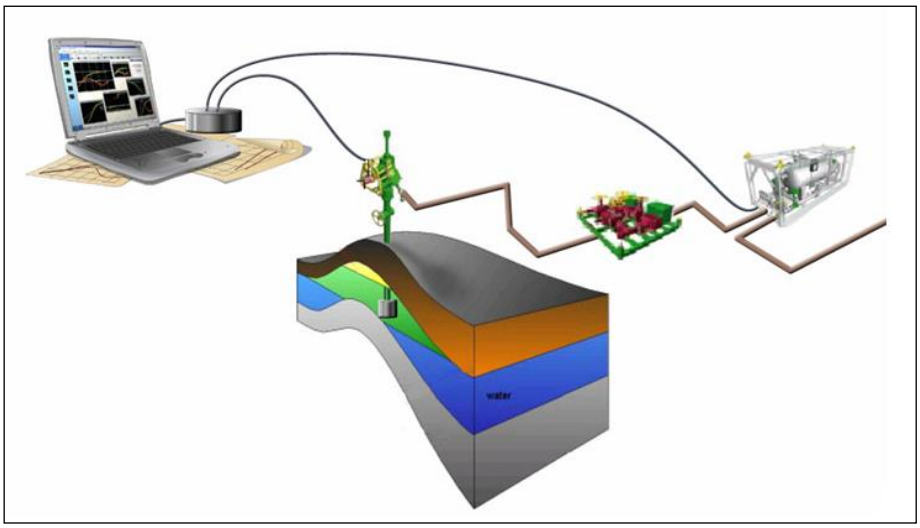


Fig. 3.A.1 – Typical well test setup

The data absolutely required to perform a PTA are the rates, the pressures (preferably downhole), the fluid PVT and a few additional parameters (well radius, pay zone, etc) required to switch from a qualitative to a quantitative analysis.

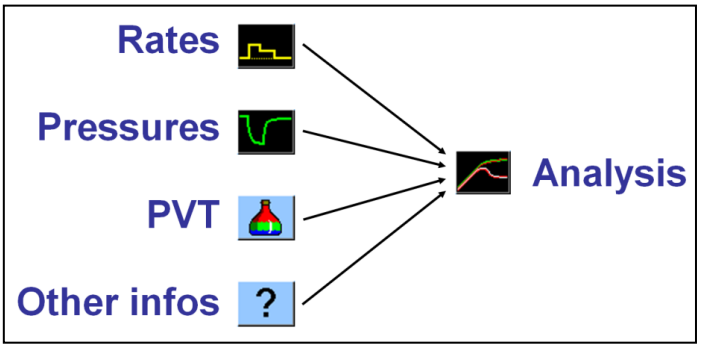


Fig. 3.A.2 – Required data for Analysis

The main flow regime of interest is the Infinite Acting Radial Flow, or IARF, which occurs after well effects have faded and before boundaries are detected. IARF may not always be seen. IARF provides an average reservoir permeability around the well, the well productivity (skin). When the well is shut in we also get an estimate of the reservoir static pressure (p* or pi). The first PTA methods were specialized plots (MDH, Horner) introduced in the 1950's to identify and quantify IARF. Other specialized plots dedicated to other flow regimes followed through.

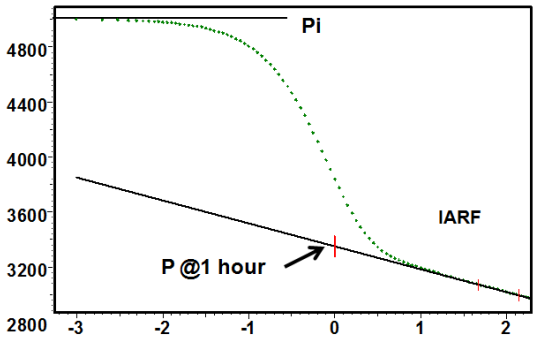


Fig. 3.A.3 – MDH plot

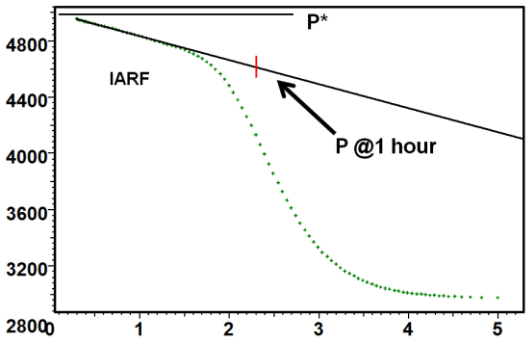


Fig. 3.A.4 – Horner plot

In the 1970's loglog type-curve matching techniques were developed to complement straight lines. One would plot the pressure response on a loglog scale on tracing paper and slide it over pre-printed type-curves until a match is obtained. The choice of the type-curve and the relative position of the data (the match point) provided physical results. These methods were of poor resolution until the Bourdet derivative was introduced.

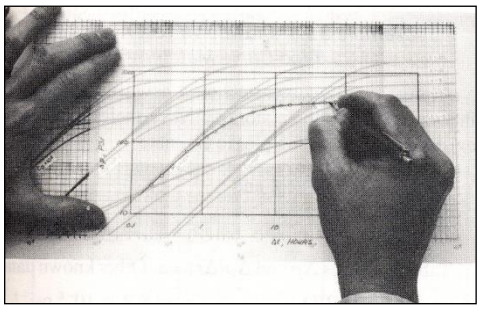


Fig. 3.A.5 – Manual Drawdown type curve matching

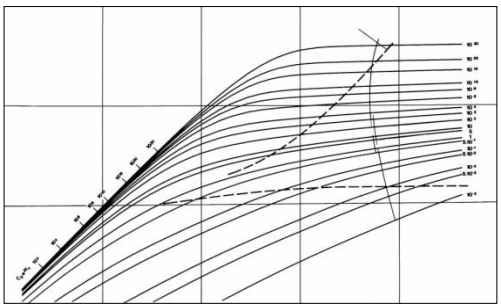


Fig. 3.A.6 – Drawdown Type Curve

In 1983, the Bourdet derivative, i.e. the slope of the semilog plot displayed on the loglog plot, increased the resolution and reliability of a new generation of type-curves.

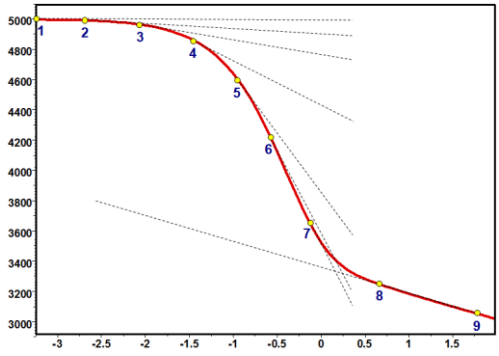


Fig. 3.A.7 – Superposition plot

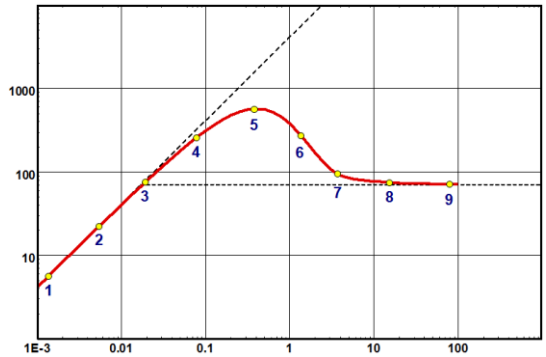


Fig. 3.A.8 – Derivative plot

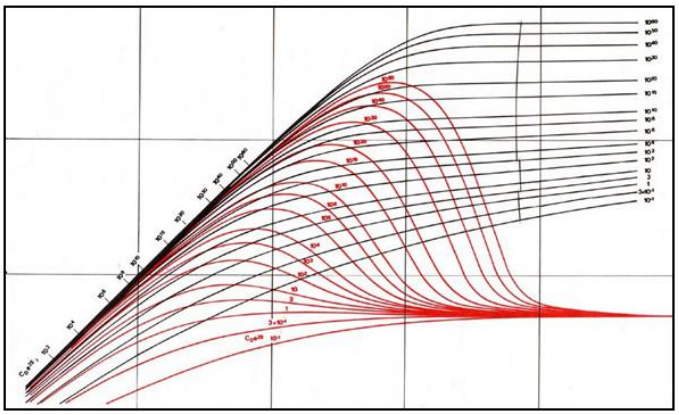


Fig. 3.A.9 – Bourdet derivative type curve

Type-curve techniques turned obsolete in the mid-1980s with the development of PC based software and the direct generation of more and more sophisticated analytical models, taking into account the complete pressure and flow rate history.

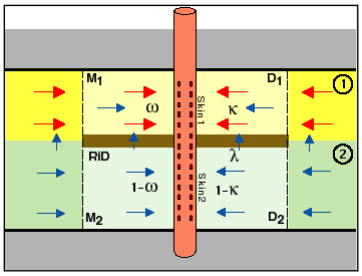


Fig. 3.A.10
2K Composite reservoir

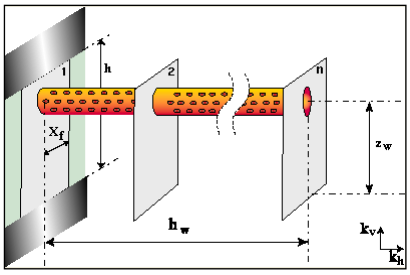


Fig. 3.A.11
Fractured horizontal well

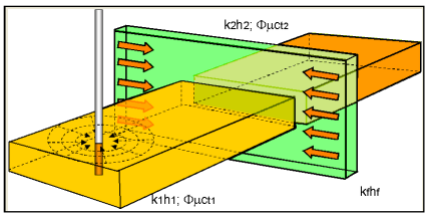


Fig. 3.A.12
Conductive fault

The core diagnostic tool remained the Bourdet derivative. Solutions were no longer unique, and the engineer was challenged to search for the most consistent answer by considering information available from all sources. The match of the model on the real data governed the validity of these analysis, while straight-line methods were made redundant. Beyond superposition and the use of more sophisticated models, PC based software allowed nonlinear regression to improve results by history matching the data with the models.

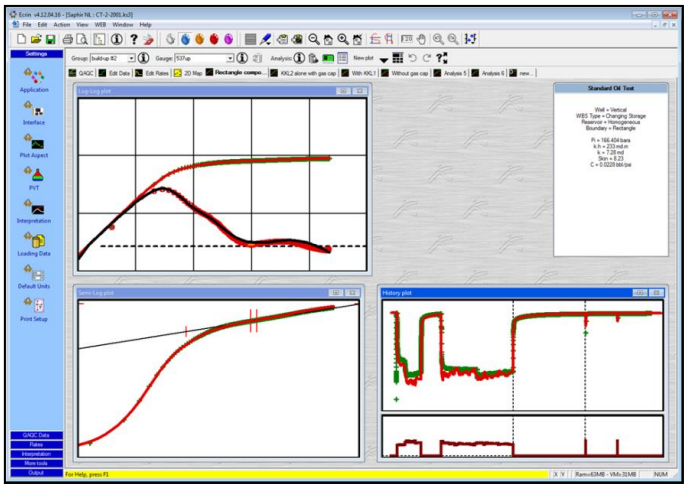


Fig. 3.A.13 – 1990-2000's – PC based PTA

Despite the spread of more and more complex analytical models and various pseudo-pressures developed to turn nonlinear problems into pseudo-linear problems accessible to these analytical models, there was a point where analytical models would not be able to handle the complexity of some geometries and the high nonlinearity of some diffusion processes. The 1990's saw the development of the first numerical models dedicated to well testing, though the spread of usage of such models only took place in the early 2000's.

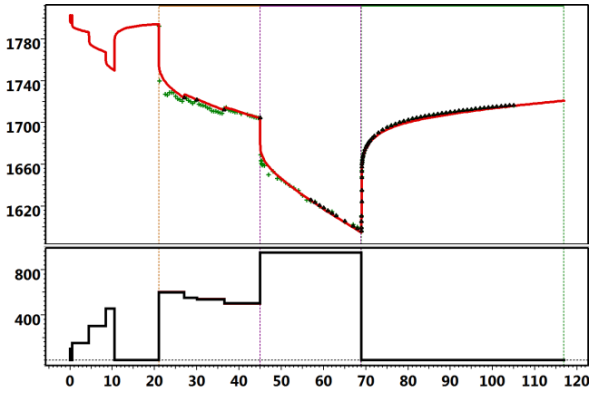


Fig. 3.A.14 – History match

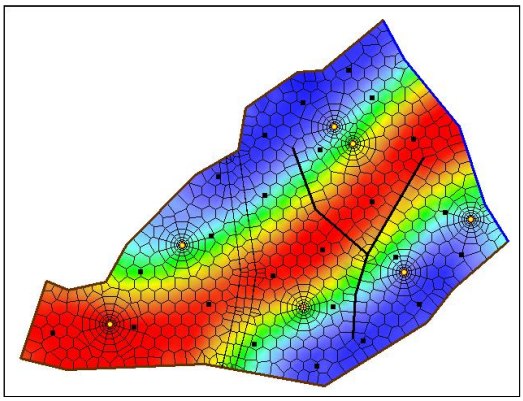


Fig. 3.A.15 – Numerical models

One would expect that most developments to come will be technology related, with more powerful processing, higher graphics and higher amount of data available. For sure we are also going to see in the years to come expert systems that will be able to approach the capacity of human engineers, in a more convincing way than the work done on the subject in the 1990's.

However the surprise is that we may also see fundamental methodology improvements. The 'surprise' of the past decade has been the successful publication of a deconvolution method which, at last (but we caveats) can be useful to combine several build-ups in a virtual, long and clean production response. Other surprises may be coming…

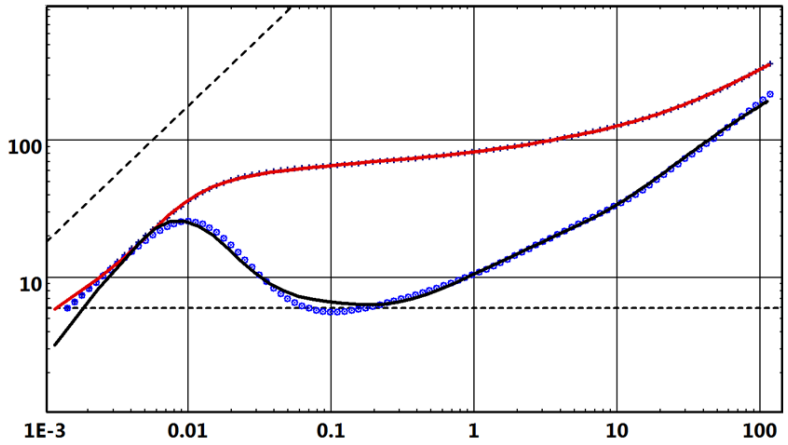


Fig. 3.A.16 – Deconvolution

In the next two sections we will make a clear distinction between the traditional tools (the 'old stuff') and modern tools (the 'right stuff'). Traditional tools had their use in the past, and they are still in use today, but have become largely redundant in performing analysis with today's software. Modern tools are at the core of today's (2016) modern methodology, and they are of course on the default path of the processing.

3.B The old stuff

Twenty years ago, the core of well test interpretation was the dual use of specialized plots and type-curve matching:

- Specialized plots correspond to a selected scale where some flow regime of interest such as infinite acting radial flow, linear flow, bilinear flow, spherical flow or pseudo-steady state are characterized by a straight line. The slope and the intercept of this straight line will generally give two parameters of the system.
- Type-curve matching consists in sliding a plot of the data, generally on a loglog scale, on pre-printed type-curves. The relative position between the data and the type-curve, also called the time match and pressure match, provides two quantitative parameters. The choice of type-curve will give additional information.

We will start with the semilog plots, the main specialized plots used to quantify the main flow regime in PTA: Infinite Acting Radial Flow, or IARF.

3.B.1 IARF and Semilog plots

We have seen in Chapter 'Theory' that IARF is the main regime of interest in Pressure Transient Analysis. In the case of a production at a constant rate, IARF is characterized by linearity between the pressure change and the logarithm of time. We will see that such linearity is also found for more complex production history, provided that the right time function is used.

3.B.2 Drawdown response and MDH plot

In the case of a constant production from time 0 to infinity, the IARF is characterized, for a finite radius well in a homogeneous reservoir, by the equation:

$$\left(p_i - p_{wf}\right) = \frac{162.6qB\mu}{kh}\left[\log\Delta t + \log\frac{k}{\Phi\mu c_t r_w^2} + 0.8686S - 3.2275\right]$$

In the case of more complex well geometries and reservoir heterogeneities, the constant term may be more complicated, as it will integrate the cumulative effect of these geometries and heterogeneities. Still the response will have the same shape. The value of skin S calculated from the equation above may not be the right value in terms of well damage according to Darcy's law, but it will have some meaning. It is called the 'equivalent skin'.

The Miller-Dyes-Hutchinson (MDH) plot is a graph of the pressure or the pressure change as a function of the logarithm of time. IARF is characterized by a linearity of the response.

Drawing a straight line through these points gives a slope and an intercept:

IARF straight line: $$Y = \frac{162.6qB\mu}{kh}\log\left(\Delta t\right) + b = m\log\left(\Delta t\right) + b$$

Where: $$b = \Delta p_{LINE}\left(\log(\Delta t) = 0\right) = \Delta p_{LINE}\left(\Delta t = 1hr\right)$$

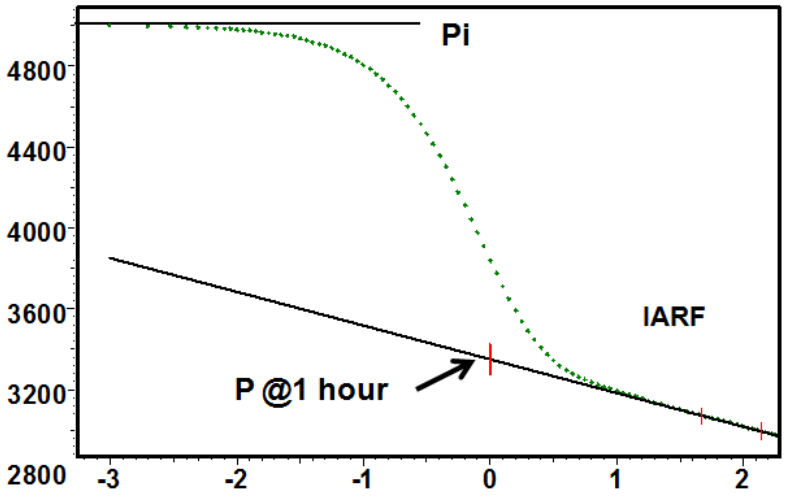


Fig. 3.B.1 – Drawdown MDH plot

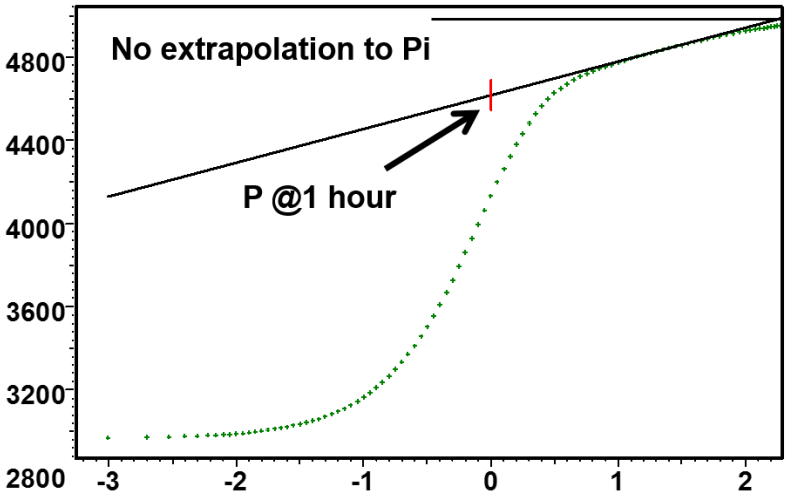


Fig. 3.B.2 – Buildup MDH plot

Important: The value of b corresponds to the value of Δp on the straight line, not on the data.

Permeability and the skin are then given by:

Permeability: $$k = \frac{162.6qB\mu}{mh}$$

Skin factor: $$S = 1.151\left[\frac{\Delta p_{LINE}(\Delta t = 1hr)}{m} - \log\left(\frac{k}{\Phi\mu c_t r_w^2}\right) + 3.228\right]$$

3.B.3 Build-up response and Horner plot

The MDH plot, with the simple log(Δt) time function, results directly from the log approximation to the drawdown solution for infinite-acting radial flow. In order to use semilog analysis for any flow period other than the first drawdown, it is necessary to take into account superposition effects.

How to get the Horner plot:

Build-up superposition: $\Delta p_{BU}(\Delta t) = \Delta p_{DD}(t_p) + \Delta p_{DD}(\Delta t) - \Delta p_{DD}(t_p + \Delta t)$

IARF approximation: $\Delta p_{DD}(X) = \frac{162.6qB\mu}{kh}\left[\log(X) + \log\left(\frac{k}{\Phi\mu c_t r_w^2}\right) - 3.228 + 0.8686S\right]$

If Δt is large enough to reach IARF, so will t_p+Δt. A lot of terms cancel out and we get:

Build-up superposition: $\Delta p_{BU}(\Delta t) = \frac{162.6qB\mu}{kh}\log\left(\frac{\Delta t}{t_p + \Delta t}\right) + \Delta p_{DD}(t_p)$

Rearranging: $\Delta p_{BU}(\Delta t) = \frac{162.6qB\mu}{kh}\log\left(\frac{t_p \Delta t}{t_p + \Delta t}\right) + \left[\Delta p_{DD}(t_p) - \frac{162.6q\mu}{kh}\log(t_p)\right]$

If the production time was too short, IARF was not reached during the flow period and $\Delta p_{DD}(t_p)$ cannot be turned into a log approximation. The constant term on the right of the equation becomes unknown. In this case, the analysis described below will give the permeability, but not the skin factor. If the production time was long enough, then the term t_p can also be turned into a logarithmic approximation and we get:

IARF at t_p: $\Delta p_{DD}(t_p) - \frac{162.6qB\mu}{kh}\log(t_p) = \frac{162.6qB\mu}{kh}\left[\log\left(\frac{k}{\Phi\mu c_t r_w^2}\right) - 3.228 + 0.8686S\right]$

So: $\Delta p_{BU}(\Delta t) = \frac{162.6qB\mu}{kh}\left[\log\left(\frac{t_p \Delta t}{t_p + \Delta t}\right) + \log\left(\frac{k}{\Phi\mu c_t r_w^2}\right) - 3.228 + 0.8686S\right]$

We introduce the Horner Time as: $\frac{t_p \Delta t}{t_p + \Delta t}$

Infinite-acting radial flow for a build-up is characterized by linearity between the pressure response and the logarithm of Horner time. Drawing a straight line through this point gives a slope and an intercept:

IARF straight line: $Y = \frac{162.6qB\mu}{kh}\log\left(\frac{t_p \Delta t}{t_p + \Delta t}\right) + b = m\log\left(\frac{t_p \Delta t}{t_p + \Delta t}\right) + b$

If the producing time t_p was long enough to reach IARF, the IARF approximation for a build-up will be similar to the drawdown relation, replacing time by Horner time, and will be given by:

IARF for a build-up: $\Delta p_{BU}(\Delta t) = \frac{162.6qB\mu}{kh}\left[\log\left(\frac{t_p \Delta t}{t_p + \Delta t}\right) + \log\left(\frac{k}{\Phi\mu c_t r_w^2}\right) - 3.228 + 0.8686S\right]$

After transformation, we get the equation of the Horner plot straight line in terms of pressure:

$$p_{BU} = p_i - \frac{162.6qB\mu}{kh}\log\left(\frac{t_p + \Delta t}{\Delta t}\right)$$

Permeability-thickness product and the skin are then calculated.

Permeability-thickness product: $k = \frac{162.6qB\mu}{mh}$

Skin factor if t_p is large enough: $S = 1.151\left[\frac{p_{1hr} - p_{wf}}{m} + \log\left(\frac{t_p + 1}{t_p}\right) - \log\left(\frac{k}{\Phi\mu c_t r_w^2}\right) + 3.23\right]$

Note that the time function is such that the data plots 'backwards', as when Δt is small, at the start of the build-up, the Horner function (log (tp+Δt)/Δt) will be large, and when Δt tends to infinite shut-in time the Horner time tends to 1, the log of which is 0.

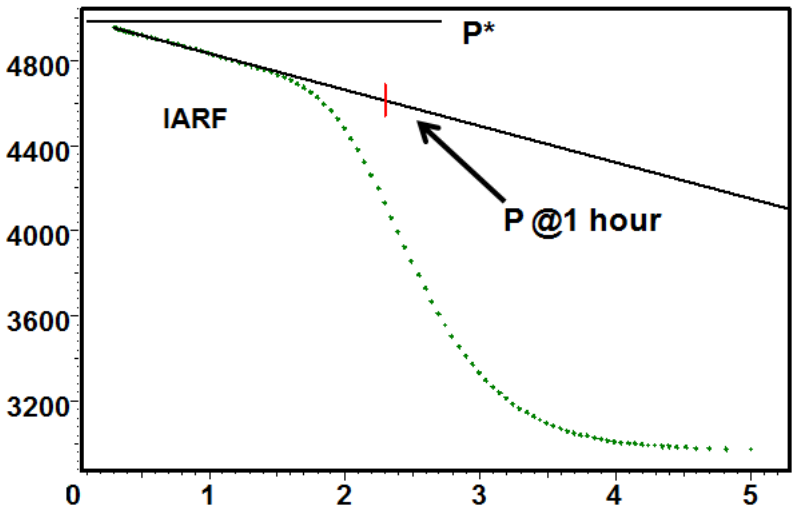


Fig. 3.B.3 – Horner plot

If the reservoir were truly infinite, the pressure would continue to build-up in infinite-acting radial flow and eventually intercept the y-axis at pi, the initial pressure. However, as no reservoir is infinite, the extrapolation of the radial flow line at infinite shut-in time is called p*, which is simply an extrapolated pressure.

If the reservoir is infinite: $p_i = p^*$

It is important to notice that the calculation of the permeability is valid even in the case of a short production before the shut-in, while the validity of the calculation of skin is conditioned to a producing time long enough, so IARF was reached before t_p.

3.B.4 Shut-in after a complex production and superposition plot

When a shut-in follows a complex production / injection history, the process is equivalent to that for a simple build-up, but the Horner time must be replaced by the superposition time function defined by:

$$Sn(\Delta t) = \sum_{i=1}^{n-1} \frac{q_i - q_{i-1}}{q_n - q_{n-1}} \log(t_n - t_i + \Delta t) + \log \Delta t$$

A plot of pressure versus superposition time is the 'general semi-log' plot:

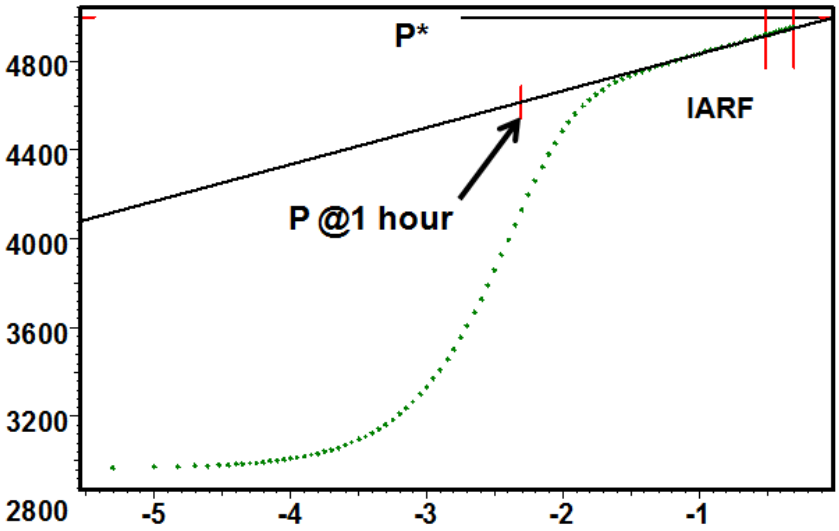


Fig. 3.B.4 – General semilog: superposition plot

Calculations of permeability is the same as for the Horner plot, and the skin factor is calculated by taking one point on the straight line, say (X,Y), and is given by:

$$S = 1.151\left\{\frac{Y - p_{wf}}{m} - X - \log\left(\frac{k}{\Phi \mu c_t r_w^2}\right) - \sum_{i=1}^{n}\left[\frac{q_i - q_{i-1}}{q_n - q_{n-i}} \log(t_{n+1} - t_i)\right] + 3.23\right\}$$

3.B.5 Complex productions and rate normalized superposition plot

In some cases the engineer will want to interpret producing periods when the rate is not stabilized, or the rates data will be sandface rate, and therefore the value of the rate will not instantaneously go down to zero during the shut-in period. These cases are a little more complex than the cases above. However the principle of the semi-log analyses will be kept with the following modifications:

For a multi-rate production or injection (whether rates are measured at surface or downhole), the adequate semi-log plot will still have the same superposition time as the X axis, but the pressure will be replaced by:

$$\frac{Q}{q(t)}[p_i - p(t)]$$

Where Q is a reference value for normalization, that will be generally chosen to be the last stabilized rate of the interpreted period so that the function tends to Δp at late time.

For a multi-rate build-up or fall-off using sandface rates, the Y axis will still be

$$p(t) - p_{wf}$$

but the calculation of the superposition time will allow rates to be changed during the period. Furthermore the reference rate will not be the difference of rates before N and N-1 (this has no meaning when dealing with continuous downhole rate measurements), but the last stabilized rate before shut-in.

3.B.6 Using type-curves

Loglog type-curvesType-curve matching originally consisted in plotting a loglog plot of the pressure response versus time on tracing paper that could then be slid over a set of pre-printed type-curves, the log cycles being square and of the same size in both plots. The selection of the type-curve matching the data can provide one or several parameters, and the relative positions of the two plots in the X and Y direction, also called the match point, will give two other interpretation results.

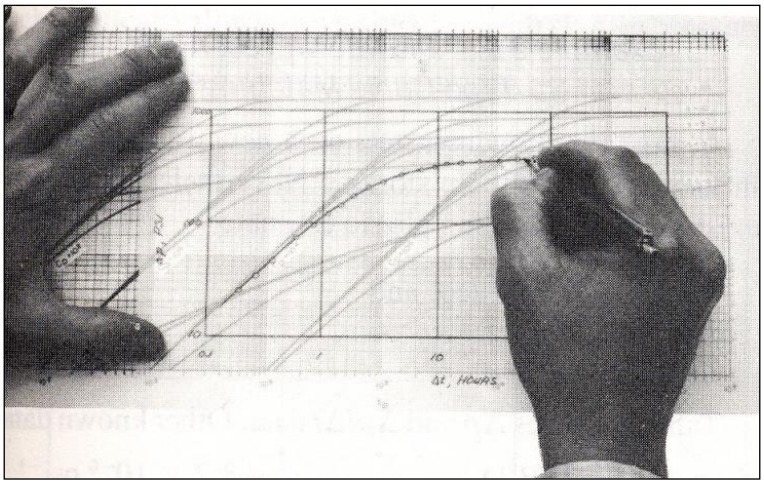


Fig. 3.B.5 – Type-curve matching

The type-curve used for wellbore storage and skin in an infinite homogeneous reservoir (in the following Figure), the pressure match (relative positions in the Y direction) will give the permeability. The time match (relative positions in the X direction) will give the wellbore storage, and the selection of the curve will give the skin factor.

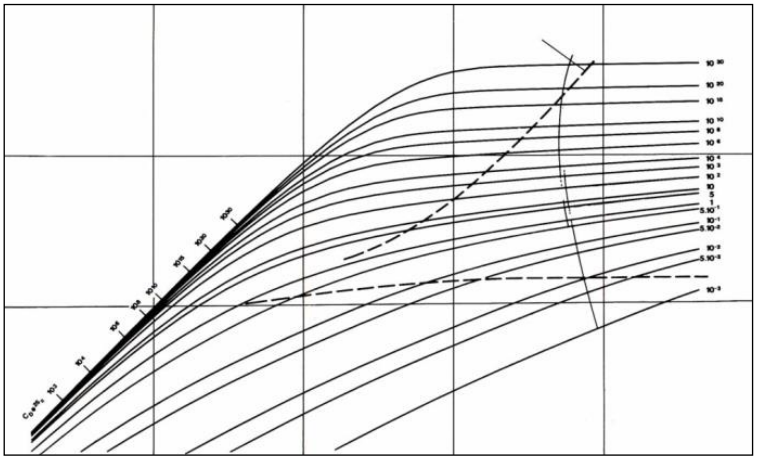


Fig. 3.B.6 – Wellbore storage and skin type-curve

The origin of type-curves

We have seen in Chapter 'Theory' that diffusion problems were solved by replacing the real variables by dimensionless variables that eliminate other parameters influence in order to arrive at a set of equations that are solved, hopefully quite simply and once and for all, in dimensionless space. Two critical variables are the dimensionless time and dimensionless pressure.

Dimensionless time: $$t_D = 0.0002637\frac{k}{\Phi\mu c_t r_w^2}\Delta t = A\Delta t \text{ where } A = f(k,\mu,r_w,...)$$

Dimensionless pressure: $$p_D = \frac{kh}{141.2qB\mu}\Delta p = B\Delta p \text{ where } B = g(k,h,\mu,...)$$

This is still used today in modern software to generate analytical models. The solution is solved in dimensionless space, then the variables are converted to real variables and superposition is applied to the solution, and then matched with the real data.

However, this was not possible, or at least not easy, before personal computers and related software were available. So the 'trick' was to use a simple and remarkable property of the logarithmic scales, historically used to create slide rules. Taking the logarithm of the equations above we would get:

Logarithmic relations: $$\log(t_D) = \log(\Delta t) + \log(A)$$

and $$\log(p_D) = \log(\Delta p) + \log(B)$$

In other words, the dimensionless response, also called a type-curve, and the real response, taken on a loglog scale, have the same shape. By translation, it is possible to match the data on the dimensionless response and this is called a type-curve match. The value of the translation, also called match point, in the X direction (the time match) and in the Y direction (the pressure match) will give A and B, which in turn provides two quantitative pieces of information. The time match will give different, model dependent, information. The pressure match will typically give the permeability-thickness product.

3.B.7 Other specialized plots

Infinite Acting Radial flow is the most important but not the only flow regime characterized by linearity of the pressure response when plotted versus the right time scale. Different flow regimes require a specific plot of pressure versus the appropriate time scale to quantify parameters specific to the flow regime.

The main flow regimes are:

Regime	Model	Linearity vs
Infinite Acting Radial Flow	Homogeneous Infinite	logarithm of time
Pseudo-Steady State	Closed systems	time
Pure wellbore storage	Wells with storage	time
Spherical flow	Limited Entry wells	inverse of square root of time
Bilinear flow	Fractures with Finite Conductivity	fourth root of time
Linear flow	Fractures	square root of time
Linear flow	Channel shaped reservoirs	square root of time
Semi-linear flow	U-shaped reservoirs	square root of time
Semi-radial flow	Sealing fault	logarithm of time
Partial radial flow	Intersecting fault	logarithm of time
Early time IARF	Horizontal well	logarithm of time
Linear flow	Horizontal well	square root of time

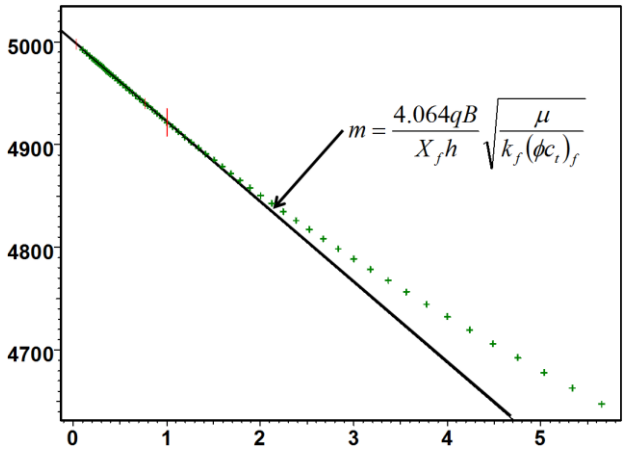


Fig. 3.B.7 – Square root plot

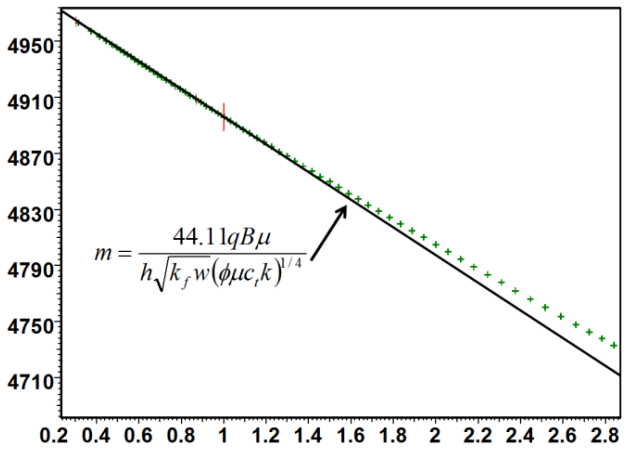


Fig. 3.B.8 – Fourth root plot

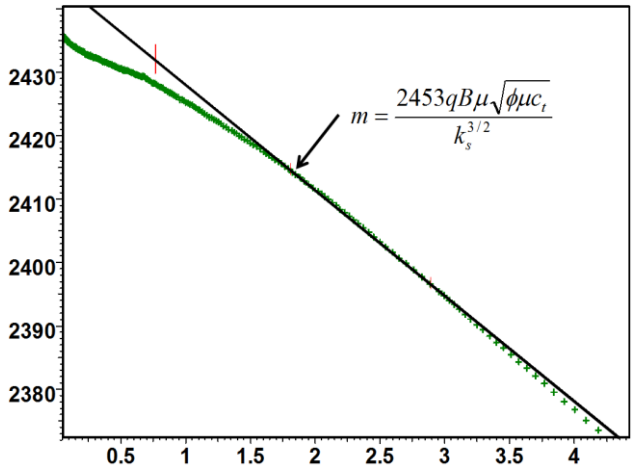


Fig. 3.B.9 – One over square root of time plot

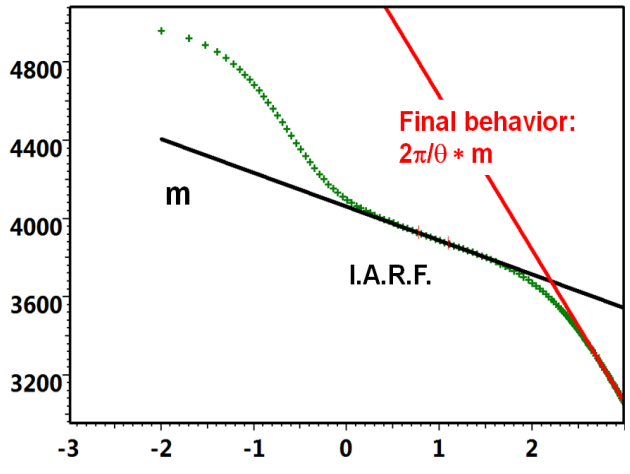


Fig. 3.B.10 – MDH plot for intersecting faults

3.B.8 IPR & AOF

A common measure of the performance of any gas, or oil, well is its ability to deliver against atmospheric pressure. It is certainly unrealistic if we consider the bottom hole pressure; however this measurement provides an input value for IPR calculations, and it is an accepted 'universal indicator' for gas wells. It is called the 'Absolute Open Flow' potential of the well. The concept of AOF is more useful if one uses wellhead instead of bottomhole pressures, as this indicates now the maximum achievable flowrate.

In order to evaluate the AOF, the well is tested at multiple rates. The bottom hole pressure is measured during each drawdown and buildup. These data are plotted on the adequate plot in order to deduce the leading parameters values for the equations governing the rate and the stabilized flowing pressure relationship. The most classical plot is Δm(p).vs q, on a log-log scale , leading to the C and n parameters values of the Rawlings and Schellhardt equation:

$$Q = C(m(\bar{p}) - m(p_{wf}))^n$$

The same equation is used to describe the Inflow Performance Relationship and to create the very useful IPR plot m(pwf) versus q.

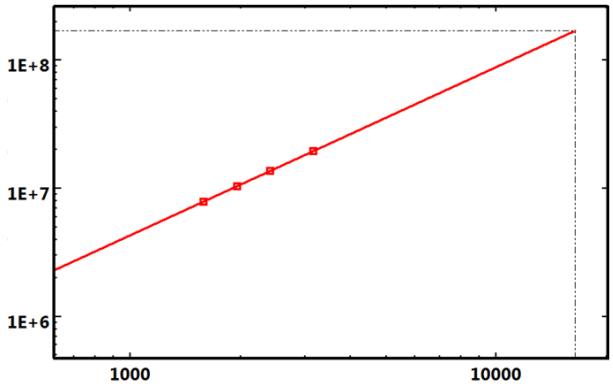


Fig. 3.B.11 – AOFP plot

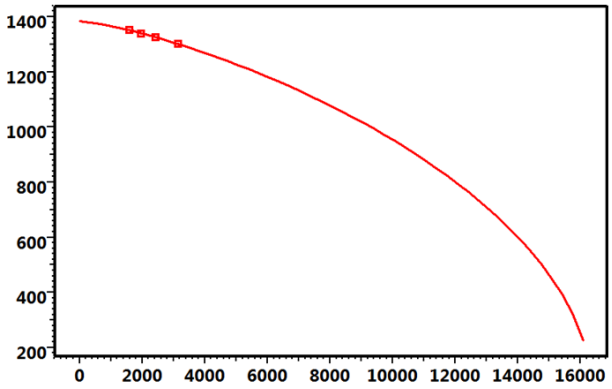


Fig. 3.B.12 – IPR plot

The AOF is obtained by extrapolating the deliverability curve to a Δm(p) value corresponding to a flowing bottom hole pressure of 14.7 psi.

Cullender and Katz improved later the method in order to reduce the well test duration by using short and non stabilized flow period data. The various well test types and IPR and AOF methods are detailed in the chapter on Well Performance Analysis.

3.C The 'right' stuff

To speak about 'right stuff' vs. 'old stuff' is deliberately provocative. Old stuff is not always wrong. Old stuff was smartly developed to adapt to what we had before modern PC's: slide rules, graph paper, basic calculators, programmable calculators, etc. Old stuff has been of great benefit to the industry and was on the critical path to get the modern tools we have today.

What is sometimes wrong is to continue using old techniques that are less accurate than more recent developments. What is definitely wrong is to continue using such tools today, simply out of inertia, while everybody knows that their limitations are successfully addressed by more modern techniques. What is near criminal is using the good old stuff to address completely new problems that were never encountered when this good old stuff was developed.

Simpler is better when simple is right.

3.C.1 Before the Bourdet Derivative

Until 1983, PTA methodology was a manual process alternating type-curve matching and specialized analyses. Type-curves without derivative had poor diagnostic capabilities. The results from specialized plots would help position the data on the type-curve.

For example, drawing the IARF straight line on the Horner plot would give a permeability that could be used to set the pressure match on the type-curve. Selecting a type-curve would give the approximate time of start of IARF, which in turn would help define the Horner plot line. For gas we would complement this with AOF / IPR analyses.

The shortcomings of this methodology were numerous:

- Type-curves with pressure only had very poor resolution on a loglog scale.
- Type-curves were generally printed for drawdown responses, and ruined by superposition.
- Type-curves were set for a discrete number of parameter values.
- Specialized plots required a pure flow regime that may never have been established.
- Skin calculation on the Horner plot required that IARF was reached during the drawdown.
- Drawing a straight line through the two last pressure points was a common practice.
- The process required moving back and forth between at least two or more different plots.

To most engineers the replacement of manual techniques by computer based analysis in their day-to-day work occurred in the 1980s, and came from three major breakthroughs:

- Electronic downhole pressure gauges, either run with memory or on electric line, became cheap and reliable, detecting repeatable behaviors far beyond what the previous generation of mechanical gauges could offer.
- The spread of Personal Computers allowed the development of PC-based pressure transient analysis software. The first PC based programs appeared in the 1980's, initially reproducing the manual methods on a computer. Since then, new generations of tools have been developed, with modern methodology at its core.
- The Bourdet derivative is certainly the single most important breakthrough in the history of Pressure Transient Analysis. It is still today (2016) the cornerstone of modern technology.

Let us start with the Bourdet derivative…

3.C.2 Definition of the Bourdet Derivative

As any breakthrough idea, the principle of the Bourdet derivative is very simple:

The Bourdet Derivative is the slope of the semilog plot displayed on the loglog plot…

… to be more accurate, it is the slope of this semilog plot when the time scale is the natural log. It has to be multiplied by ln(10)=2.31 when the decimal logarithm is used in the semilog plot. The semilog plot is not 'any' semilog plot (MDH, Horner, etc). To be correct the reference logarithmic time scale must be the superposition time.

For the first drawdown: $\Delta p' = \dfrac{d\Delta p}{d\ln(\Delta t)} = \Delta t \dfrac{d\Delta p}{d\Delta t}$

In the more general multirate case, and in particular for shut-ins: $\Delta p' = \dfrac{d\Delta p}{d\sup(\Delta t)}$

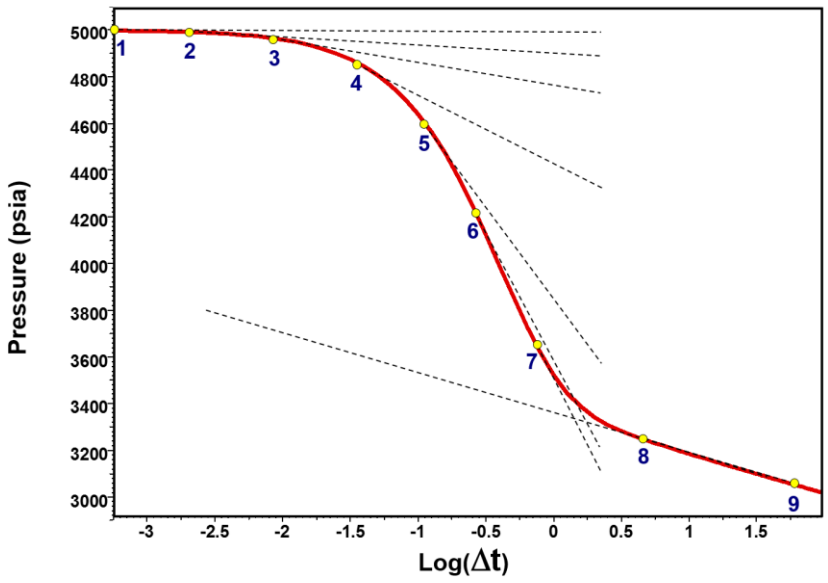


Fig. 3.C.1 – Bourdet derivative, semilog plot

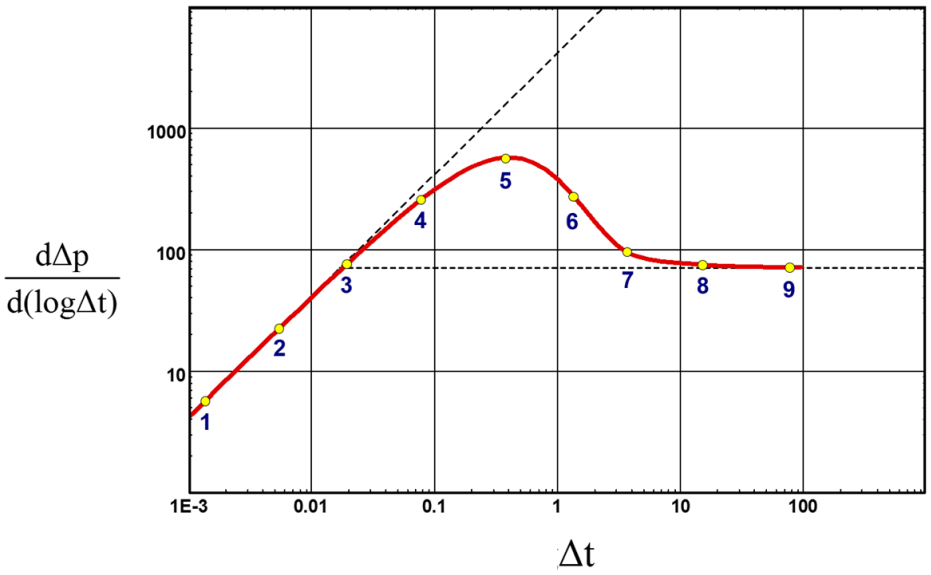


Fig. 3.C.2 – Bourdet derivative, loglog plot

3.C.3 Bourdet Derivative & Infinite Acting Radial Flow (IARF)

When IARF occurs we have the approximation: $\Delta p = m' \sup(\Delta t)$

Where m′ is the slope of the semilog straight line. In the following the drawdown response is a specific case of the multirate response, and the logarithm of time is the specific superposition time for a drawdown. The derivative is therefore:

Derivative when IARF has been reached: $$\Delta p' = \frac{d\Delta p}{d \sup(\Delta t)} = m'$$

When IARF is reached, the derivative stabilized to a level equal to the slope of the semilog straight line. This property was the main reason for the development of the derivative, as it is easy and straight forward to identify IARF on the loglog plot, something which is virtually impossible on the semilog plot. One can say that the derivative is a 'magnifying glass' of the semilog behavior, conveniently placed on the same plot, used historically for type-curve matching.

Combined with the early time unit slope during wellbore storage, the derivative provides an immediate way to define the pressure and the time match on the loglog plot, just by positioning a unit slope line on the wellbore storage regime and positioning the horizontal line on the IARF response.

This alone would have made the Bourdet derivative a key diagnostic tool. The delightful surprise was that the derivative could do much more, and that most well, reservoir and boundary models carry a specific signature on the derivative response. It is this remarkable combination that allowed the derivative to become **THE** diagnostic and matching tool in Pressure Transient Analysis.

3.C.4 Bourdet Derivative & Wellbore Storage

Pure wellbore storage effects are only observed at very early time when the well pressure behavior is dominated by the well fluid decompression or compression.

In case of pure wellbore storage: $\Delta p = C\Delta t$

Even for multirate solutions at early time: $\sup(\Delta t) \approx \ln(\Delta t)$

The derivative is therefore: $\Delta p' = \Delta t \frac{dC\Delta t}{d\Delta t} = C\Delta t = \Delta p$

At early time, when pure wellbore storage is present, pressure and the Bourdet derivative curves will merge on a unit slope straight line on the loglog plot.

Other early time flow regimes, such as linear and bilinear flow, covered in more detail later, will exhibit a different and specific behavior for both pressure and the Bourdet derivative.

3.C.5 The original idea behind the Bourdet Derivative

The simplest and most frequently used analytical model in Pressure Transient Analysis is the case of a vertical well, with wellbore storage and skin, producing a homogeneous reservoir of infinite extent. This 'new' formulation of the derivative by Bourdet et al. was solving at once this case, on a single loglog plot, and in a very accurate way:

When plotting the pressure and the Bourdet derivative on a loglog scale, at 'late time' the derivative would stabilize, and the stabilization level would define the type-curve pressure match (hence the permeability) in a unique way. The only possible movement then would be left and right to define the time match.

At early time the Pressure and the Bourdet derivative would merge on a single unit slope, that was also found on the type-curves, hence providing a unique value of this time match, and an instant calculation of the wellbore storage.

Luckily enough, the shape of the derivative (drawdown) type-curve and the Bourdet derivative of the data (multirate) was seldom affected by the superposition, unlike the pressure data, so it was reasonably valid to match the data derivative with the type-curve derivative, hence getting a unique identifier of the type-curve (generally C_De^{2S}), which in turn would give the value of Skin.

So, on a single action, a type-curve using the Bourdet derivative would provide the definitive answer on a single, accurate diagnostic plot.

This was already brilliant, but it turned out that the Bourdet derivative could bring much more for all type of models, whether by identification of other flow regimes or by the signature that the Bourdet derivative would carry for such or such model…

3.C.6 Bourdet Derivative & other flow regimes

We are not going to describe exhaustively the list of flow regimes that can be successfully identified using the Bourdet derivative. The short answer is: 'a lot'. The table below shows a list of the most frequently used flow regimes in PTA, together with the chapter of the DDA book where this will be covered in more details:

Model	Regime	Δp slope	Δp' slope	DDA chapter
Storage	Storage	1	1	Wellbore
Fracture	Linear	0.5	0.5	Well
Fracture	Bilinear	0.25	0.25	Well
Limited Entry	Spherical	-	-0.5	Well
Homogeneous	IARF	-	0	Reservoir
Channels	Linear	0.5 (late)	0.5	Boundary
Closed	PSS	1 (late)	1	Boundary

As an appetizer, below is a loglog plot of some of these flow regimes:

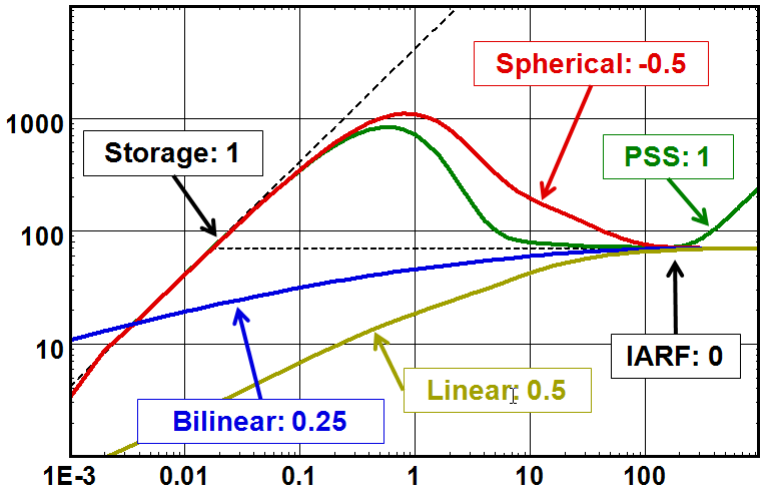


Fig. 3.C.3 – Bourdet Derivative and various flow regimes

3.C.7 Bourdet Derivative & Other models

The use of the Bourdet derivative does not stop with flow regimes. The Bourdet derivative can display the signature of numerous well, reservoir and boundary behaviors. Again the loglog plot below shows some typical behaviors detected from the observation of the Bourdet derivative.

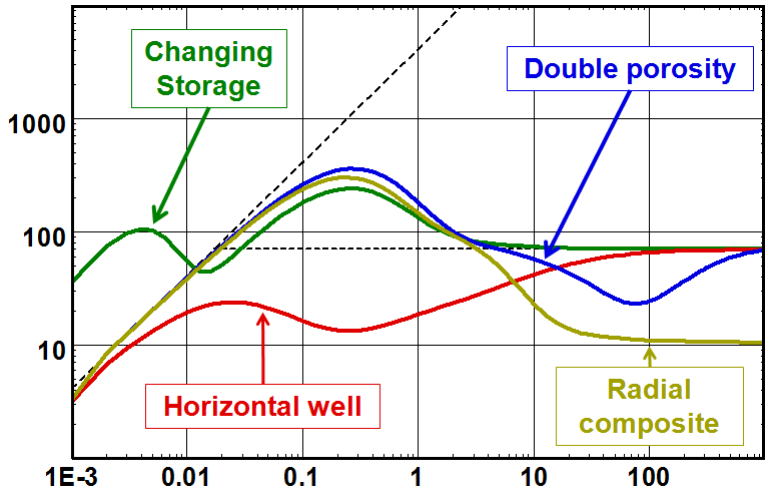


Fig. 3.C.4 – Bourdet derivate and other models

3.C.8 Modeling

The actual measured data is matched to a full model response selected by the interpreter from the identified flow regimes, including the appropriate well and boundary models and the actual production history.

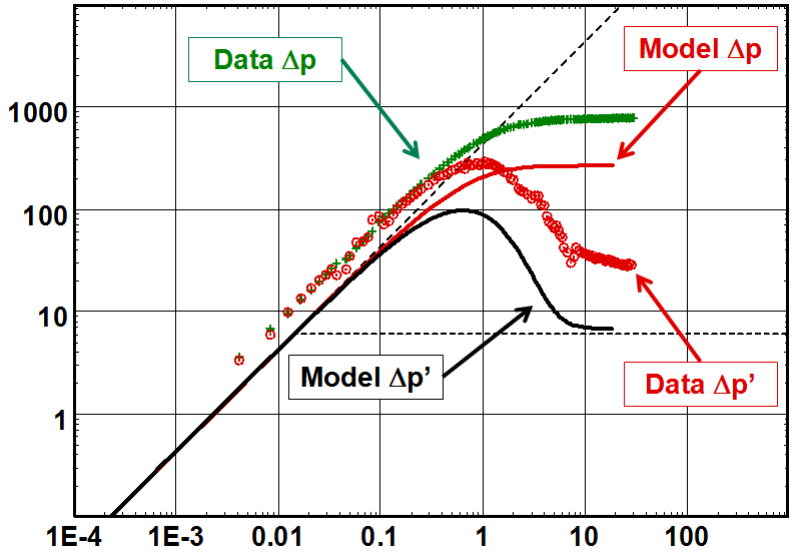


Fig. 3.C.5 – Modeling

3.C.9 Other types of derivative

It also exist other derivatives, adapted to other flow period or regimes than the infinite acting radial flow.

Their objective is to exhibit a constant value horizontal line when a specific flow regime is observed.

Drawdown

This is a derivative of the pressure/pressure difference with respect to the logarithm of elapsed time. Since no superposition is taken in to account, strictly speaking, it is valid for the very first drawdown only.

Buildup

This is a derivative of the pressure/pressure difference with respect to the logarithm of buildup time (see table below). Strictly speaking, it is valid for a build up following a single constant rate drawdown.

The time function is $\frac{(t_p + \Delta t)}{\Delta t}$

Agarwal

This is a derivative of the pressure/pressure difference with respect to the logarithm of Agarwal time: $\frac{t_p.\Delta t}{(t_p + \Delta t)}$

dp/dt

This is a derivative of the pressure/pressure difference with respect to the elapsed time. The derivative tends to be flat when the flow is dominated by depletion of a small and constant compressibility fluid. During reservoir dominated flow, the derivative exhibits a monotonically decreasing trend. Any fluctuations/humps etc. may be indicative of some wellbore disturbance.

Spherical

This is a derivative of the pressure/pressure difference with respect to the logarithm of spherical time function : $f_{sup}\left(\frac{1}{\sqrt{\Delta t}}\right)$

This derivative stabilizes at a constant value during spherical/hemispherical flow.

Linear

This is a derivative of the pressure/pressure difference with respect to the logarithm of linear time function : $f_{sup}\left(\sqrt{\Delta t}\right)$

This derivative stabilizes at a constant value during linear flow.

Chow Group

Chow group takes the form: $\frac{\Delta p}{2\left(\frac{d(\Delta p)}{d(\log \Delta t)}\right)}$

3.D The use of modern deconvolution

Deconvolution in Pressure Transient Analysis has been the subject of numerous publications. Deconvolution could tentatively be used (1) to remove wellbore storage effects in order to get to IARF earlier, (2) to turn a complex noisy production history into an ideal drawdown ready for interpretation, (3) to explore boundaries not detected by individual build-ups.

Despite the good hard work done on the subject, true deconvolution is fundamentally unstable. To add stability into the deconvolution process one has to make assumptions that bias the response. Until recently, when a new paper was published on the subject, the natural question would not be "does it work?" but rather "where's the trick?".

This is no longer the case. A set of publications, initiated by Imperial College and complemented by bp (e.g. SPE #77688 and SPE #84290), offer a method that actually works, especially, although not exclusively, to identify boundaries from a series of consecutive build-ups. There is a trick, and there are caveats, but the trick is acceptable and the method can be a useful complement to PTA methodology.

Saphir offered on October 2006 the first commercially available version of this method. It was since improved by adding additional methods and it is now a totally recognized and helpful method, able to provide additional information, unseen through other techniques.

3.D.1 What is deconvolution? Why do we need it?

3.D.1.a The need

Analytical models are developed assuming a perfectly constant production as drawdown type-curves. In reality a well test, or a well production, is anything but constant. Rates vary in time, and the producing responses are generally so noisy that we usually focus on shut-in periods only.

In the simulated example shown on the plot below, the total production history is 3,200 hours, and the build-up is only 100 hours long. What we see on the loglog plot corresponds to only 100 hours of diffusion. We use the superposition of the rate history in the derivative calculation, but this is only to correct superposition effects; we really only see 100 hours of diffusion.

But there is more than 100 hours of information in the total response. Pressure has been diffusing for 3,200 hours, some locations far beyond the radius of 100 hours of investigation have felt the effect of the production and this information has bounced back to the well. So there is more information somewhere in the data, but not in the build-up alone.

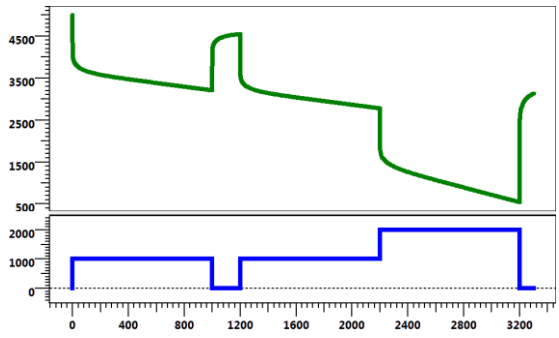


Fig. 3.D.1 – History: $p_w(t)$ & rates

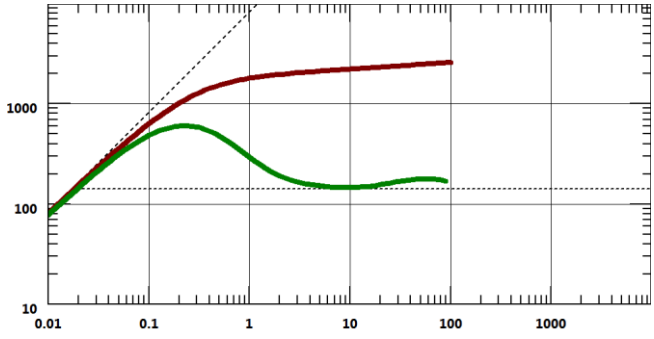


Fig. 3.D.2 – Build-up: $\Delta p_w(t)$ & $\Delta p'_w(t)$

The idea behind deconvolution is, in this example, to recreate from the real data, the ideal pressure response to a constant production over the same period (see below). If such a response was created, we could extract a loglog response of 3,200 hours duration, and the virtual data extracted this way would show much more of the reservoir than the 100 hour build-up could possibly reveal alone.

In other words, if we extract the deconvolved data from the real pressure response without assumptions, we will be able to get a much longer response, or the same response for a much shorter test.

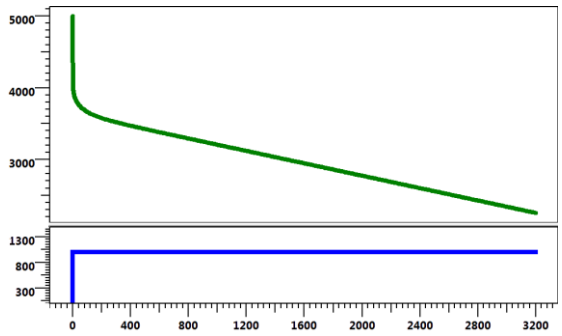


Fig. 3.D.3 – Deconvolution: $p_u(t)$

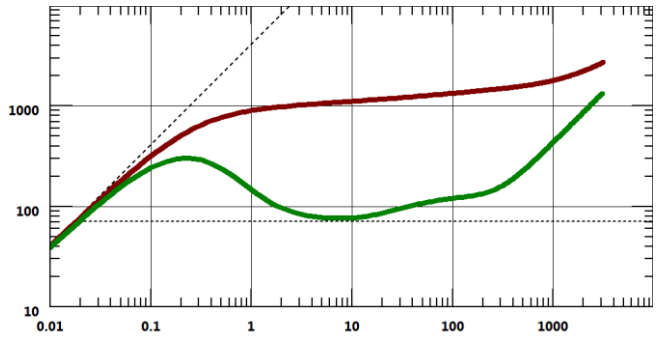


Fig. 3.D.4 – Deconvolution: $\Delta p_u(\Delta t)$ & $\Delta p'_u(\Delta t)$

In theory we may not even need to shut the well in. With deconvolution we would make a stepwise construction of an ideal constant pressure response and be able to perform a Pressure Transient Analysis whenever we have some rates and pressures recorded at the same time. One of the Holy Grails of transient analysis has been found?

3.D.1.b Mathematical formulation

Before looking at deconvolution, we need to know a little about what constitutes convolution. The mathematical definition of the convolution of two real functions is:

$$[f \otimes g](t) = \int_0^t f(\tau) g(t-\tau) d\tau$$

Convolution is what we do when we apply the principle of superposition (see Chapter 2) in order to get the pressure response $\Delta p(t)$ for a complex rate history q(t) knowing the ideal pressure drop $\Delta p_u(t)$ for a constant, unit production. We have:

$$\Delta p_w(t) = \int_0^t q(\tau) \frac{\partial \Delta p_u(t-\tau)}{\partial(t-\tau)} d\tau = \int_0^t q(\tau) \Delta p'_u(t-\tau) d\tau$$

Where $$\Delta p'_u(t) = \frac{\partial \Delta p_u}{\partial t}$$

In other words: $$\Delta p = q \otimes \Delta p'_u = q' \otimes \Delta p_u$$

Note that, when the rate history is a step function, the calculation of this integral will bring the 'usual' superposition equation, seen in Chapter 2:

$$p(t) = p_i - \sum_{i=1}^{n} (q_i - q_{i-1}) \Delta p_u(t - t_i)$$

What we know from the test data is the pressure response $\Delta p(t)$ and the rate history q(t). What we are interested in is $\Delta p_u(\Delta t)$, the ideal response for a constant production. The process of getting a convolution component (Δp_u) from one convolution component (q) and the convolution product (Δp) is called deconvolution.

We will not get into the details of the past work on deconvolution. There was what we call 'blind' deconvolution, i.e. a stepwise 'de-superposition' of the pressure data assuming nothing. This is an unstable and divergent process. There was also 'constrained deconvolution', such as moving to Laplace space and dividing the Laplace pressure response by the Laplace rate history. The weak point was generally in the assumptions made. Other deconvolution targets were more limited, such as getting an early IARF response by deconvolving the early time build-up with the 'assumed' downhole rates corrected by wellbore storage. However all these attempts had limited success. Deconvolution was considered a nice but unrealistic idea.

However, a new approach has recently been developed by Imperial College and bp. This approach has generated much enthusiasm, and although it is valid and useful, it is most important to bear in mind the assumptions and the limitations, as there are, indeed, some. It is based on a change of variable corresponding to what we really look for, ie the derivative on a loglog scale.

We define $\sigma = \ln(\Delta t)$ and $z(\sigma) = \ln\left[\frac{dp_u(\Delta t)}{d\ln(\Delta t)}\right] = \ln\left[\frac{dp_u(\sigma)}{d\sigma}\right]$

With this change of variable, the convolution equation becomes:

$$p(t) = p_i - \int_{-\infty}^{\ln t} q\left(t - e^{\sigma}\right) e^{z(\sigma)} d\sigma$$

3.D.2 Deconvolution Method 1 (von Schroeter et al., 2004)

This method was initially presented by von Schroeter et al. (Imperial College) in 2004. The suggested reference SPE Paper is #77688.

3.D.2.a Problem unknowns

Instead of looking numerically for the pressure response for a unit rate $\Delta pu(\Delta t)$, we change the unknown and consider the response upon which we will base our diagnostic. i.e. the logarithm of the pressure derivative response as a function of the logarithm of time:

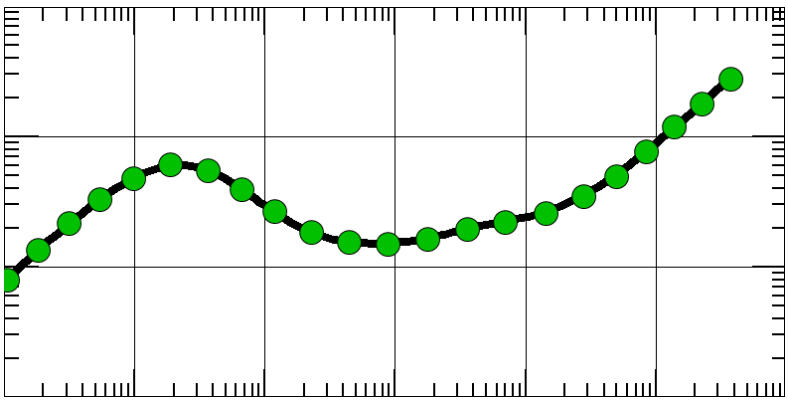


Fig. 3.D.5 – 1st (and main) unknown: z(σ)

$$\sigma = \ln(\Delta t) \quad \text{and} \quad z(\sigma) = \ln\left[\frac{dp_u(\Delta t)}{d\ln(\Delta t)}\right] = \ln\left[\frac{dp_u(\sigma)}{d\sigma}\right]$$

The principle of the new deconvolution method is to find the derivative curve z(σ) which, using a modified convolution expression, will match the data. The curve z(σ) is defined as a polyline or a spline. It has an initial point, as (0,0) makes no sense on a loglog scale. Its time range is the elapsed time between the beginning of the production history and the last data point we will try to match (3,200 hr in the previous example).

The curve z(σ) is the main unknown. There are two additional sets of optional unknowns: the first is the initial pressure p_i, which may or may not be known. The last unknown is a tolerance to errors in the rate history, which we need to introduce for the optimization process to converge.

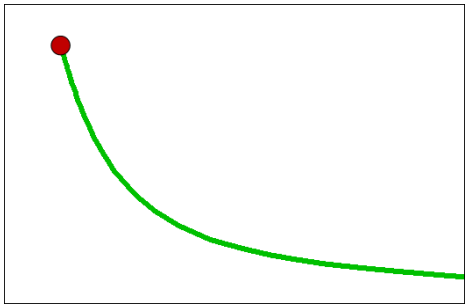


Fig. 3.D.6 – 2nd unknown: p_i

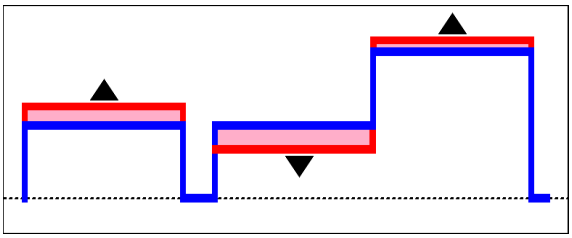


Fig. 3.D.7 – 3rd unknown: Δq's

3.D.2.b Problem objective function

The three unknowns above are adjusted, in a nonlinear regression process, to minimize an objective function. This objective function has three components.

Naturally, the first and main component of the objective function we want to minimize is the standard deviation between the convolved model and the pressure data (Fig. 3.D.8 below). This may be all pressure data or, more likely, a series of time intervals where the pressure data is considered reliable. Typically, successive build-ups are a good candidate, unless the producing pressures are exceptionally smooth as in the case of clean gas tests for example.

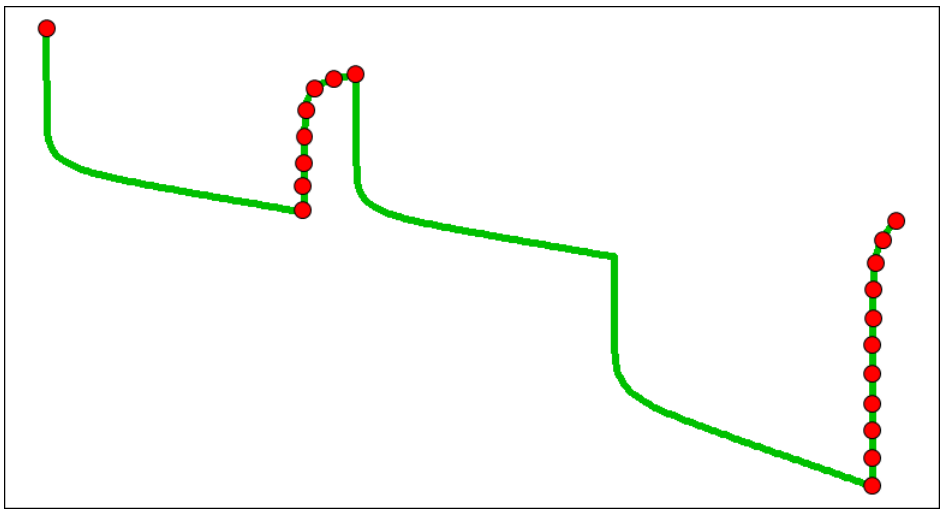


Fig. 3.D.8 – 1st objective function
minimize distance between simulated and real data

The second component of the objective function is the total curvature of the derivative response. When several derivative responses provide an equivalent match, the idea is 'the simpler the better'. Among the candidate responses, the one with the smallest total curvature is selected. In other words, if several variations give a good fit, the one that transits smoothly between the points is preferred to those that oscillate.

The third and last component of objective function is the modification in the rate values required to obtain a match. Again, for the same quality of match, the solution that requires the smallest changes in the rates is selected.

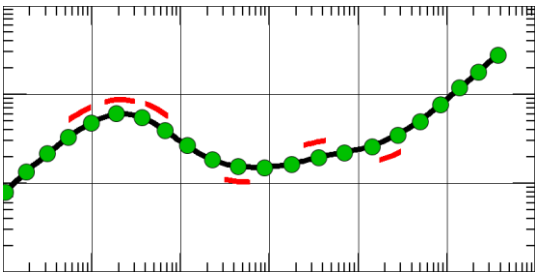


Fig. 3.D.9 – 2nd objective function minimize total curvature

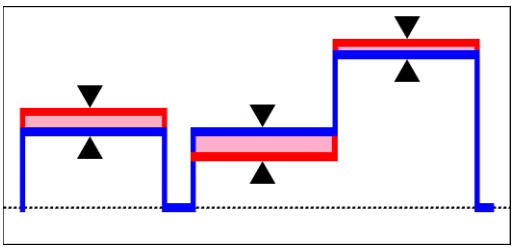


Fig. 3.D.10 – 3rd objective function minimize rate correction

3.D.2.c Deconvolution in plain English

This essence of this new deconvolution method is optimization. Instead of optimizing model parameters at the end of the interpretation, we take a discrete representation of the derivative we are looking for, and we shift it and bend it until it honors the selected data after integration, to give us a unit pressure change response from the derivative, and convolution, to take the rates into account.

Because we need to account for some uncertainties on the rates and for better behavior of the optimization algorithm, we allow the rates to change a bit, but we try to make this change as small as possible.

We want the resulting derivative curve to have the same kind of signature as the various analytical and numerical models we use. To achieve this we make sure that the total curvature of the response is reasonable, i.e. the resulting curve is not too twisted.

Once we get our deconvolved derivative, we integrate to get the pressure response and show both pressure and derivative on a loglog plot. As this is the theoretical response for a constant rate, we match the deconvolved data with drawdown models, not superposed models.

Because this deconvolved response is not data, but 'only' the result of an optimization that may be imperfect, we keep an eye on the real data by superposing the model and looking at the history match on the real, not the deconvolved signal.

3.D.2.d Field data application

The history plot below shows 3,000 hours of permanent pressure and rate recordings. The three longest build-ups are extracted and shown on a loglog scale below.

The green and red build-ups are strictly telling exactly 'the same story', while the blue build-up is consistent at late time but diverges at early time, with apparently a different wellbore storage and skin.

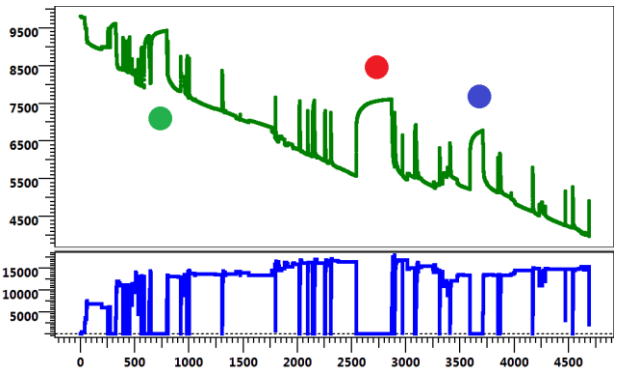


Fig. 3.D.11 – Production and pressure history

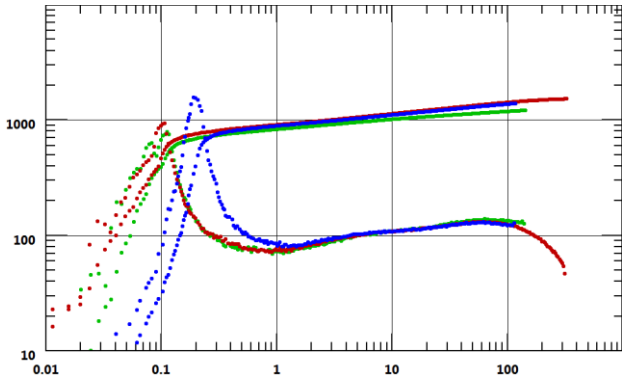


Fig. 3.D.12 – Normalized loglog plot

If we apply the von Schroeter et al. method on the two coherent build-ups (green and red) the process is successful and the resulting deconvolution is shown in the figure below. The late derivative dip in both build-ups does not correspond to a pressure support but the beginning of a closed system. The late time unit slope in the deconvolution derivative will provide a fair estimate of the well drainage area. Because we had two build-ups the deconvolution process could also back calculate a consistent value for the initial pressure.

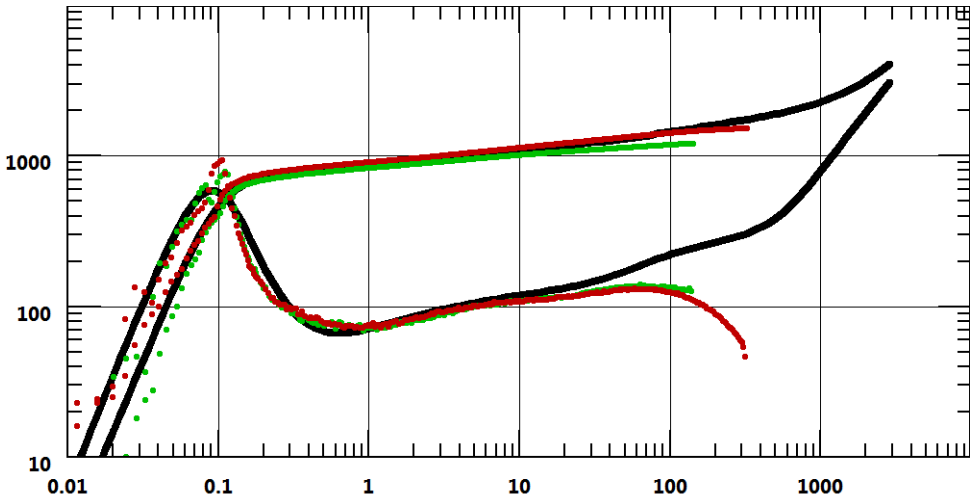


Fig. 3.D.13 – Deconvolution with the two consistent BU's

3.D.2.e Main limitation of von Schroeter et al. method

We take the same real example as in the previous section, but we consider the third build-up later in the same well production history. If we extract and compare the derivative response of the three build-ups, they tell more or less the same story at late time but the early time response is inconsistent with the two initial build-ups.

If we calculate the convolution with no constraint from the three build-ups, or even using any of the two first build-ups and the last, we get an erratic deconvolved signal (see figure below). Coming back to Earth, we should remember that deconvolution is, after all, only a nonlinear regression process.

Any engineer that has been using nonlinear regression on analytical models knows how this process is impressive when it succeeds and pathetic when it fails. It is the same here. The inconsistencies at early time have forced the spline to oscillate to the best, actually least bad, fit for the early time of the three build-ups. This had a residual effect at late time and the spline had to oscillate again to get back on track. It is frustrating, because we do not really care about the early time, and the late time of the three build-ups were telling more or less the same thing. But the process has failed, because it is just a brainless numerical process that is not able to incorporate this early / late time distinction. Hence, the process is doomed, looking for a global solution that does not exist.

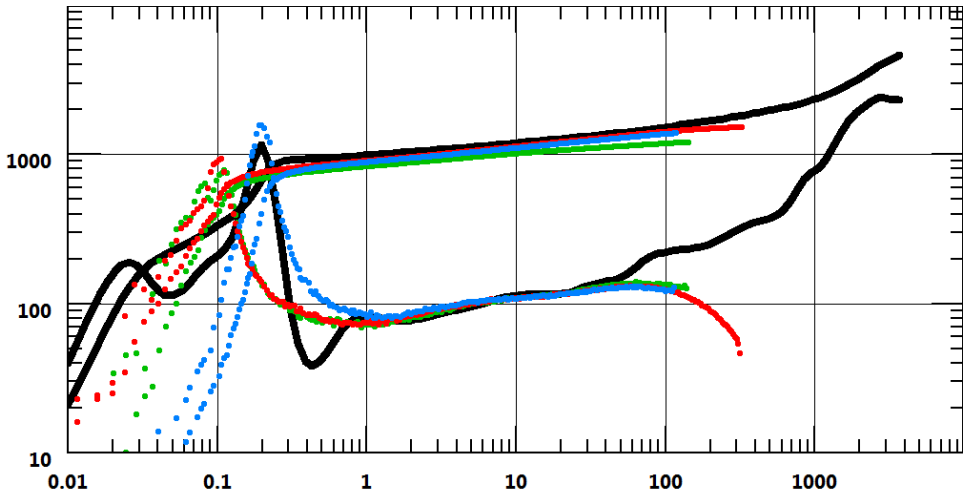


Fig. 3.D.14 – Deconvolution from the three BU's

If we want to use deconvolution for, say, volumetrics from PDG data, we are likely to see the wellbore storage and skin change over time. We face here a major potential limitation of the deconvolution. It also kills any hope to have the deconvolution become a single button option that would give the engineer a reliable late time response at no risk.

To be fair to the von Schroeter et al. method, it could give a more stable answer if we increased the smoothing of the algorithm. This amounts to give more weight to the 'minimum curvature' part of the error function at the expense of the 'match data' part. The algorithm then sacrifices the accuracy of the match in order to get a simpler, smoother derivative curve.

The danger of using smoothing is to hide a failure of the optimization and get a good looking but absolutely irrelevant deconvolution response. Such irrelevance could be detected when comparing the reconvolved pressure response to the recorded data on a history plot. However this problem is one of the main, frustrating shortcomings of the original von Schroeter et al. method.

3.D.3 Deconvolution Method 2 (Levitan, 2005)

It is possible to perform a deconvolution for a single build-up if we combine the shut-in data with a known value of initial pressure (see the consequences below in the paragraph 'Pi influence on the deconvolution').

The workaround suggested by Levitan is to replace a single deconvolution for all build-ups by one deconvolution for each build-ups.

As deconvolution can be done using pi and any build-up, the idea of the Levitan method is to perform one deconvolution for each build-up with a common value of initial pressure. The first guess of pi may produce divergent deconvolution responses. The value of pi is reiteratively changed until one gets a consistent late time response for all deconvolutions. Because each deconvolution only honors one build-up data at a time, there will not be any instability at early time.

This process is easily accessed in Saphir: this Levitan et al. deconvolution method is proposed when multiple periods are extracted: 'Separate deconvolutions with a common pi' (Levitan et al). The checkbox 'force Pi to:' is automatically tagged 'on' and pi must be entered manually. This option calculates automatically one deconvolution per extracted period. The results working on the 3 build ups is shown below:

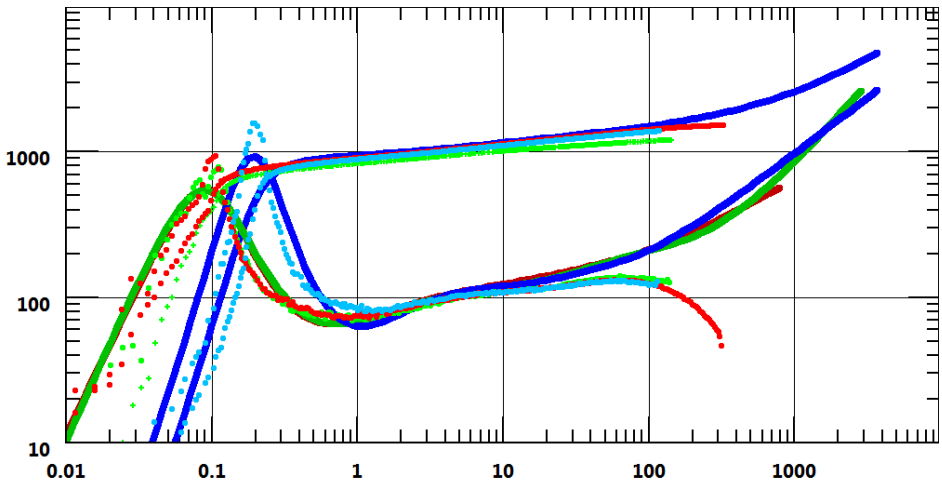


Fig. 3.D.15 – Automatic 'separate deconvolution with a common pi'

When ignoring the Pi:

The process would be a bit more complicated if we did not have a couple of coherent build-ups to start with. If we had, say, only Build-up #1 and Build-up #3, we would have to 'play' with the initial pressure until the late time behaviors are coherent and give the same reservoir size. Attempts at deconvolution with values that are both too low too high for pi are shown in the plots below.

This becomes a trial-and-error process, until the late time behavior is coherent for the two build-ups although this just may not be possible. We see on the plots below that the late time behavior are reasonably coherent but crossing each other.

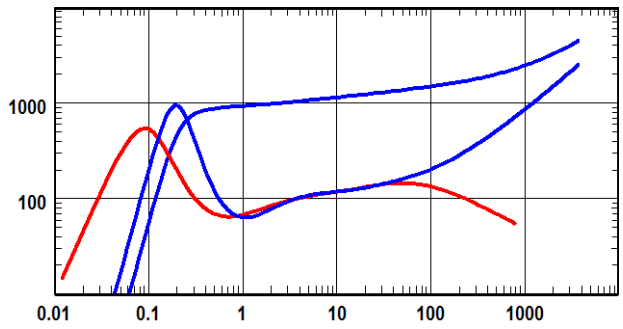


Fig. 3.D.16 – Separate deconvolutions initial pressure too low early build-up 'below' late build-up

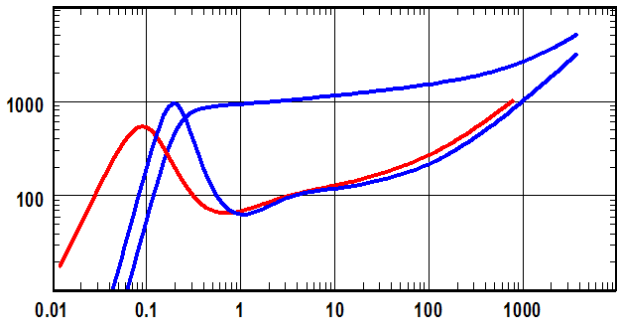


Fig. 3.D.17 – Separate deconvolutions initial pressure too high early build-up 'above' late build-up

The Levitan method addresses the main limitation of the von Schroeter et al. method. However two problems remain:

a) It requires a re-iterative process where the initial pressure is assessed and corrected until the coherence of all convolutions is reached. Attempts to add an optimization loop on pi have failed so far.
b) A deconvolution using a given build-up and a single additional point (the initial pressure) will not provide additional, intermediate behaviors that we may detect if we were running a single optimization on all build-ups. Some information is therefore potentially lost in the separation process.

3.D.4 Deconvolution Method 3 (Houzé et al., 2006-2010)

When we extract several shut-ins from PDG data and compare them together on a rate normalized loglog plot, they often, remarkably exhibit the same behavior at late time but vastly differ at early time, with different wellbore behaviors and apparent skin factors.

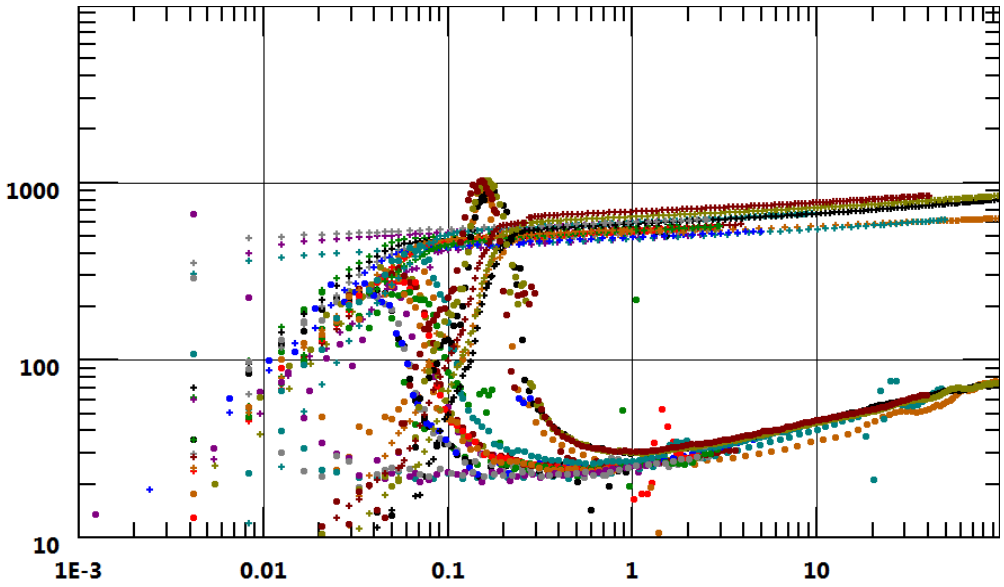


Fig. 3.D.18 – Multiple build-ups from PDG data

This inconsistency ruins the stability of the von Schroeter et al. method and forces the engineer to go into the tedious process of trial and error of the Levitan method.

When the inconsistency comes from different behavior at early time, a solution is proposed.

To illustrate this we can run a very simple simulation, or test design, of two systems with different wellbore storages and skins but the same reservoir / boundary model. In this example we use the simplest homogeneous infinite behavior but it applies to more complex systems. The loglog plot of both responses is shown below left. Simulation 1 has a constant wellbore storage. Simulation 2 has a larger, changing wellbore storage and a higher skin value.

The plot below right compares both simulations on a linear scale and displays the difference between them. During the production phase, the simulations differ with an early time transient corresponding to the different wellbore effects and the skin. When wellbore effects fade the difference stabilizes at a level corresponding to $\Delta P_{Skin}(\Delta Skin)$. When the well is shut-in there is again a transient behavior, but when the wellbore effect fades the difference stabilizes to zero. We will call this limit time the convergence time.

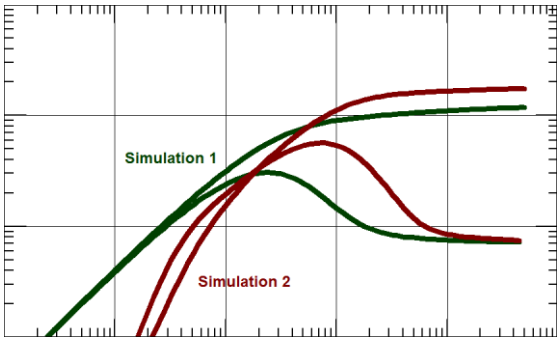


Fig. 3.D.19 – Two simulations: log log plot

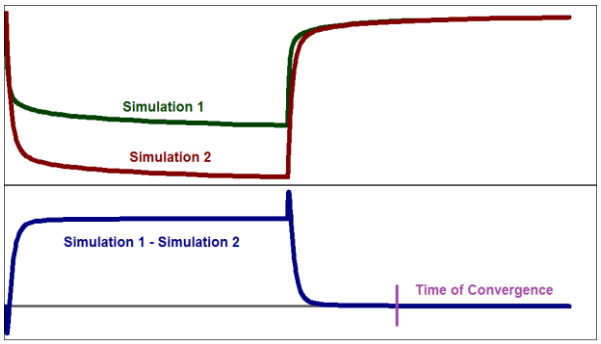


Fig. 3.D.20 – Two simulations: linear plot

On the loglog plot, pressures do not merge at late time because we are plotting $\Delta P(\Delta t) = P_{Shut\text{-}in}(\Delta t) - P_{wf}(\Delta t=0)$. The $P_{Shut\text{-}in}$ values converge, and ΔP stabilizes at $P_{wf1} - P_{wf2}$

The deconvolution is an optimization on P, not ΔP. We will get a stable process, not affected by early time discrepancies, if we run an optimization on one build-up and the last part of the other build-ups after convergence.

The Houze et al. method (called 'Deconvolution on one reference period and the end on the other periods' in Saphir), allows specifying which period (blue in our case) will be taken as a reference and all its data taken into account and the other periods (green and red) will be taken into account at late time after the convergence time specified by the user.

It gives a single deconvolution matching with the reference period early time and corresponding to all the periods at late time as shown below:

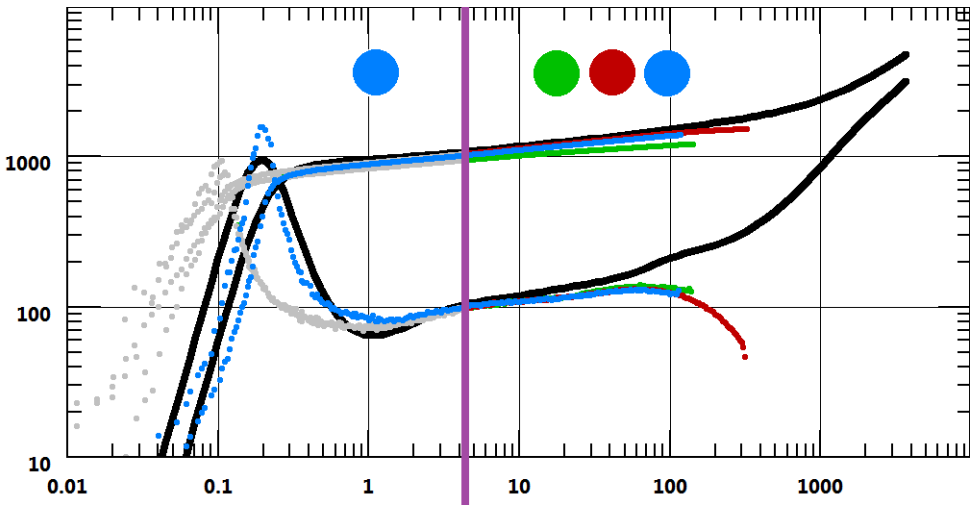


Fig. 3.D.21 – Deconvolution with a period reference early time and all periods late time

3.D.4.a Variant 1: Using Levitan method after Method 3

The main variable in the Levitan method is the initial pressure. Method 3 brings a value for pi which is meant to be compatible with all selected build-ups and is a good candidate for the Levitan method. Without any engineer interaction, the initial pressure resulting from Method 3 is used to execute the Levitan method immediately after Method 3, with no more trial-and-error.

From experience, this combination does not bring much. The problem with the Levitan method is that each deconvolution will be the simple combination of a given build-up and a single value of initial pressure. Even if we add one or two log-cycles between the build-up and the deconvolution, all this addition will be coming from a single pressure value, and therefore deconvolution will have no chance to pick-up intermediate behaviors.

3.D.4.b Variant 2: Using Method 3 on all build-ups

Method 3 consists in picking the convergence time, selecting a build-up and running the optimization. This can be successively applied to all build-ups.

Compared to the Levitan method, we get the same number of deconvolution responses and the post-processing is the same. However it has the advantage of using a 'proven' convergence time instead of a wildly guessed initial pressure, and there is no reiteration. In complement, each deconvolution uses positive information from all build-ups, and it is possible to pick intermediate behaviors that are beyond the reach of the Levitan method.

There is no guarantee that the late behavior of all deconvolution curves will be the same. This will be the case only if the material balance information is consistent. If not, it will point out that the deconvolution process may not be valid, either because of poor data or because the hypotheses behind this deconvolution are not valid

3.D.4.c Remaining limitations

The deconvolution method presented in this paper clears some of the limitations of the von Schroeter et al. method without some of the inconvenience of the Levitan method. However limitations remain and should not be overlooked:

- Deconvolution works if convolution, i.e. the principle of superposition is valid. This in turn implies that the equations governing our system are linear. This rules out any nonlinearity such as nonDarcy flow, multiphase flow, etc. In such case the optimization will give 'something' but this something may be plain wrong and misleading.
- For any practical purpose, the new deconvolution only works on shut-in periods. This observation is the basis of this Method 3, which otherwise would not be valid.
- Attempts to integrate interference wells in the deconvolution process have failed so far.
- Deconvolution apparently adds one or two log cycles but there is no magic. We had this information before. When interpreting a build-up, a properly trained engineer checks the coherence of the model on the pressure history plot. If the simulation was inconsistent it was the sign that 'something' had affected the long term response that was not detected during this build-up. Adding this 'something' would often amount to adding some late time boundary behaviors, in order for the model to follow the data throughout the well history. The new deconvolution just does that, but in a very elegant way.
- Deconvolution is not a video game that turns bad data into good ones… When successive build-ups are inconsistent, the deconvolution optimization will fail. At best it will be specularly, but in the worst case it will look OK and will be misguiding.
- With Method 3 different wellbore storage and skin factors may be handled. However the rest of the model must remain constant. The idea of getting all shut-ins from ten years of a permanent gauge, then run a deconvolution is perfectly ludicrous. In real life the system changes and the convolution of a single model over several years just does not make sense.

3.D.5 Pi influence on the deconvolution

In the case illustrated in the figures below, we have run a test design with a homogeneous infinite model. So we know that the right response is homogeneous infinite. It starts from an initial pressure of 5,000 psia. There was a 400 hours constant rate production period followed by a 100-hours shut-in.

When the deconvolution is run with too high a value of pi (red dot), there is an additional depletion compared to the infinite case. In order for the deconvolution to honor both the build-up and the initial pressure, it will have to exhibit at late time an increase of the derivative level, typical of a sealing boundary. Conversely, if we entered too low a value of pi (blue dot), there needs to be some kind of support to produce depletion smaller than the infinite case. The deconvolution will exhibit a dip in the late time derivative.

In other words, deconvolution honors the data of the first 100 hours of the build-up, and then uses the flexibility of the 400 last hours to 'bend' in order to be compatible with the entered value of pi. Why is the shape so smooth? Because, on top of this, the optimization process minimizes the total curvature of the derivative curve.

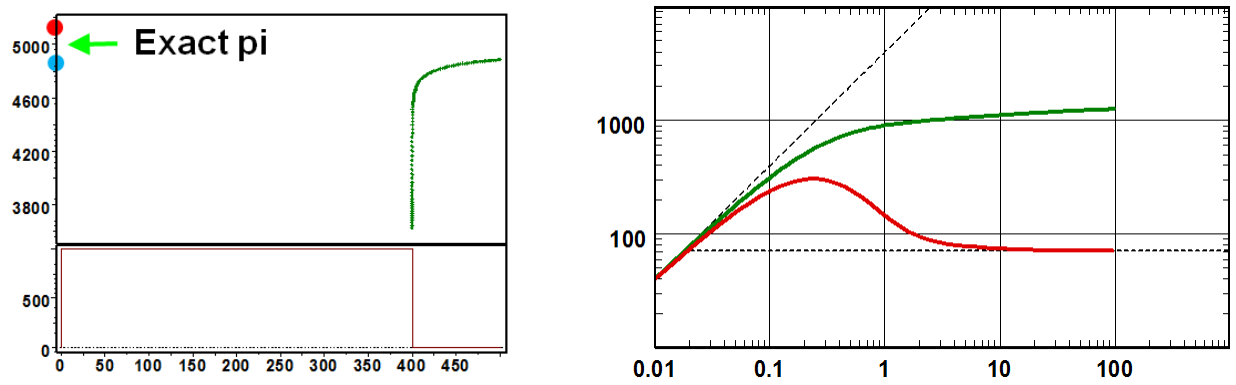


Fig. 3.D.22 – Deconvolution of a single build-up with different values of pi
For an infinite reservoir - Left: Simulation; Right: extracted build-up

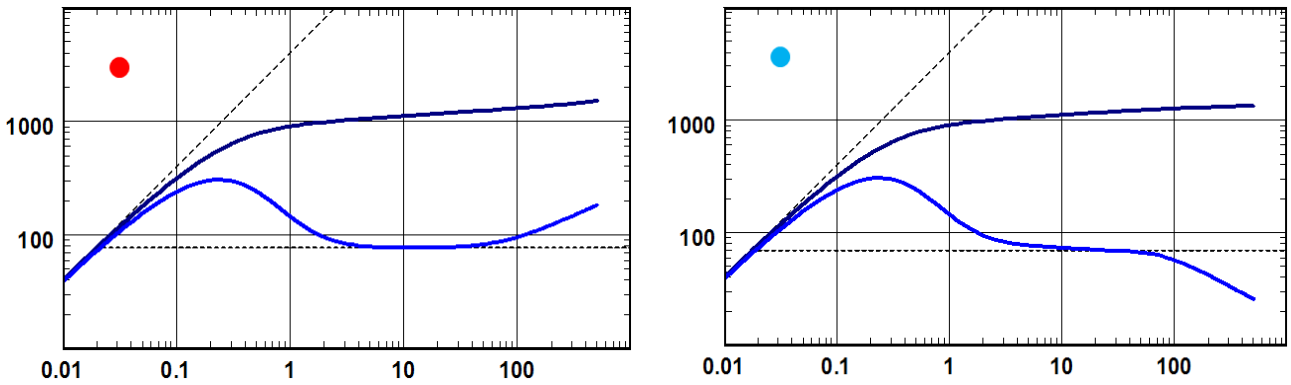


Fig. 3.D.23 – Deconvolution with pi too high (red) or too low (blue)

How does this work?

We had 400 hours of production and 100 hours of shut-in. Deconvolution is attempting to provide 500 (theoretical) hours of constant production. The first 100 hours of the spline representation are rigid, because they have to match the build-up. We have a loose tail between 100 and 500 hours. The regression moves the tail up or down in order to match the initial pressure pi after superposition, i.e. to match the depletion during the producing phase.

If the initial pressure is higher than the infinite case, the depletion is greater, and the reservoir has to be bounded. If the initial pressure is lower, the depletion is less and the derivative of the deconvolution will tail down and exhibit pressure support.

Now, there are hundreds of tail responses that could produce a specific depletion. Which one is picked? The simplest one, because the regression selects the solution with the lowest curvature, i.e. the one that will go smoothly from the part of the response that is fixed to whatever PSS level. The first part of the data is rigid, the last part is more or less set by the depletion and the transition is as smooth as possible.

Naturally, if we had more intermediate data, like some reliable flowing pressures, this would 'firm up' the deconvolution algorithm. The optimization first focuses on matching the data before trying to get a smooth response.

3.D.5.a Implementation in Saphir 5

The implementation in Saphir gives access to two of the above mentioned methods, through a very logical workflow.

The periods to analyze must be first selected for extraction, they may be picked interactively:

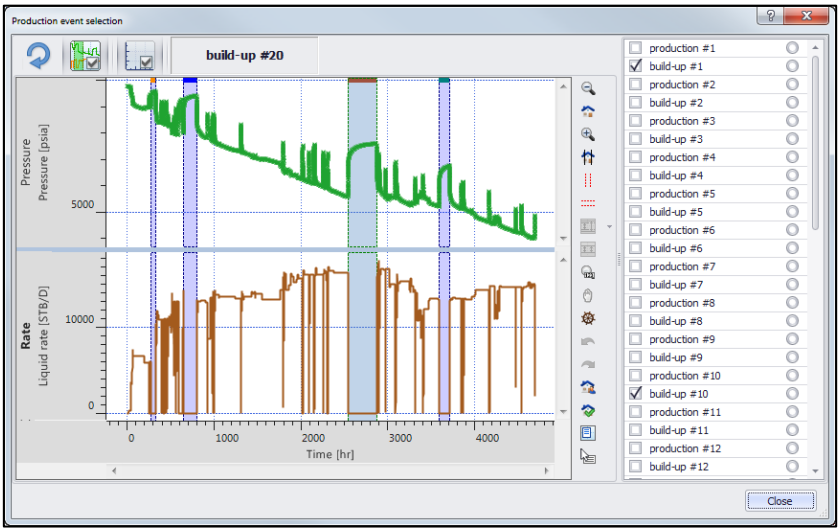


Fig. 3.D.24 – Selecting the periods

Having selected one or more build-up, when the deconvolution process is called its dialog offers possible methods:

- Deconvolution on one period as reference, and the end of the other periods (Houze et al.)
- Separate solutions with a common Pi (Levitan et al.)

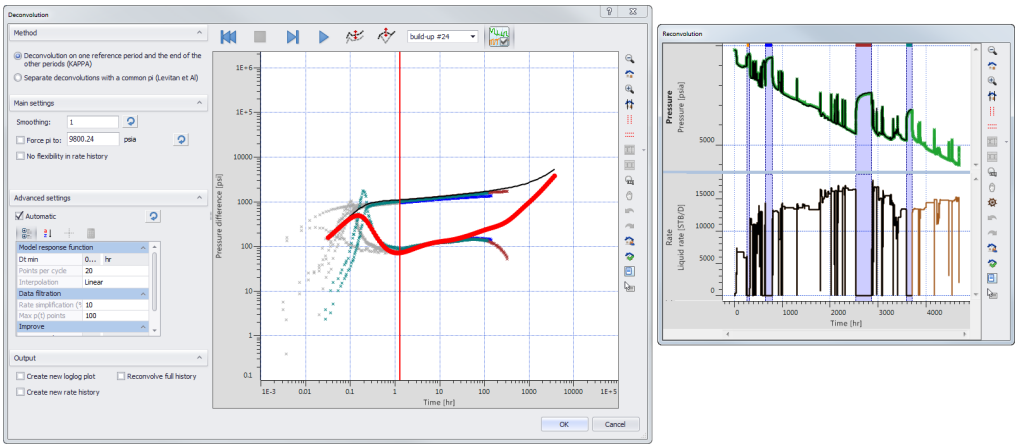


Fig. 3.D.25 – Deconvolution on one period as reference and reconvolved data

The Pi can be forced to a fixed value to improve the process efficiency.

The rate history correction can be desactivated.

It is possible to superimpose the deconvolved signal and the individual build-up data in a rate normalized way. The reconvolved responses corresponding to the build-ups can also be plotted.

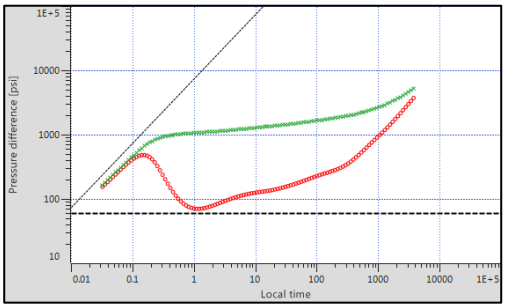


Fig. 3.D.26 – Deconvolved response

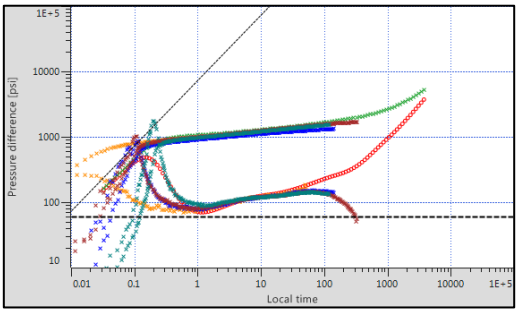


Fig. 3.D.27 – Compared to BU data and reconvolved response

3.D.6 Using sensitivity to assess the validity of a deconvolution

The early time part of the deconvolution response is constrained by the build-up data, and the tail end is adjusted to honour other constraints, such as the pressure drop between the successive build-ups. When no constraint is applicable to a part of the data, the deconvolution picks the smoothest possible path to minimize the curvature. There may be intermediate boundary effects in the 'real' reservoir, but we have no way to know. An issue is to assess which part of the deconvolved data is positive information, and which part is just a smooth transition between positive information.

This is a very serious issue, and may be one of the main dangers of the deconvolution process. When we interpret data and choose the simplest model that honors whatever we have, we know the assumptions we make. When we add a closed system to a model matching individual build-ups in order to reproduce the depletion, we know that we are taking the simplest model, but that there may be additional and intermediate boundaries that we may not see. In its apparent magic, deconvolution presents a long term response that is NOT positive information but just a best match. So how can we discriminate positive information and information by default?

One element of answer is to calculate a sensitivity. The deconvolution parameters include the points of the z(σ) response, the curvature of this response and the rate changes. Looking in the Jacobian of the deconvolution matrix we can see the sensitivity of the match to the individual points of the z(σ) response. In Saphir we normalize this and show it as a vertical sensitivity band for each point of z(σ).

This band does not quantify the real, physical, uncertainty. It only provides a blunt statistical description of the problem around the solution point and answers the question, "By how much can I move this node until the match is affected?" If the sensitivity is high, we are close to positive information and the uncertainty band is narrow. If, on the contrary, moving a point up and down has no or little effect on the global response, then we know that this section of the response may not be very relevant. In order to illustrate this we have taken two extreme examples.

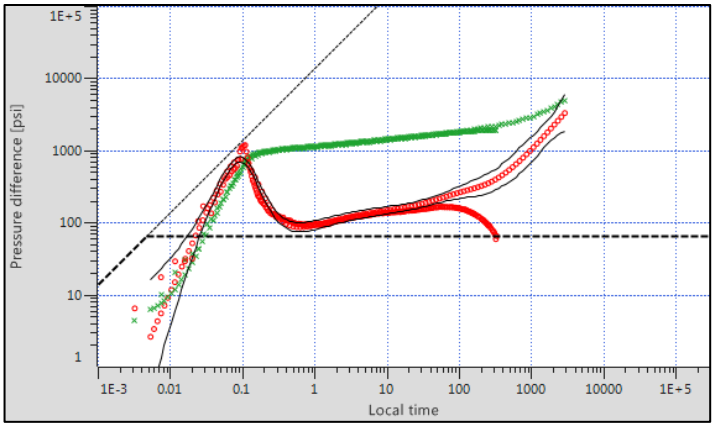


Fig. 3.D.28 – Sensitivity representation single build-up and no pi (1/2)

In the above figure we have done what we should never do: calculate a deconvolution with a single build-up WITHOUT imposing a value of pi. The problem is completely under-defined, because we can move the tail end of the deconvolution and get a perfect match of the data by compensating pi. So the tail end is completely irrelevant and it shows on the sensitivity plot.

In the below left figure, we have run the deconvolution with the two build-ups of the original example. We let pi be calculated by the deconvolution process. As one can see, the sensitivity is much better, but intermediate behavior could have been different. What made the deconvolution pick the selective curve was its smoothness. Now, in the right side figure the same deconvolution was run but the value of pi was fixed. This makes the sensitivity graph even better.

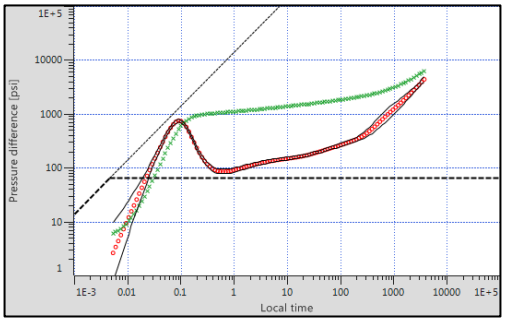


Fig. 3.D.29 – Sensitivity representation two build-ups and no pi

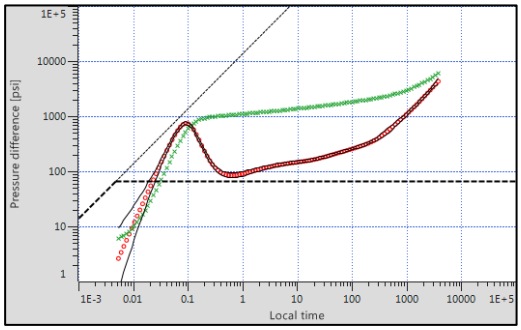


Fig. 3.D.30 – Sensitivity representation two build-ups and pi

3.D.7 Conclusion

The recent deconvolution is a nonlinear regression on a model derivative, without knowing the model. The main unknown are these derivative points on a loglog scale. We curve is bent, integrated and superposed in order to best fit the data of interest, generally consecutive and reasonably consistent build-ups. Additional unknown may be the initial pressure and some slack on the rate history. Additional constraints include a minimization of the curvature and of the amplitude of the rate changes.

This new deconvolution provides, in one run, a synthesis of information present in different parts of the pressure / rate history. When you combine two build-ups that are far apart in time, you do not only check their coherence but you integrate, in the deconvolved response, the information of depletion that took place between these two build-ups.

There is nothing really that a conscientious and trained engineer could not do before having this tool, but all this information is calculated in a single run, early in the interpretation process, instead of being a trial-and-error, last minute analysis following the interpretation of the individual build-ups.

So the tool is useful and interesting, but we must emphasize its uses and limitations:

- For any practical purpose, today it only works on shut-ins.
- It should not be used as a black box. It is only an optimization process, and optimization processes are typically impressive when they work and pathetic when they do not. Any error in the deconvolution process will be carried over during the rest of the interpretation.
- Deconvolution should be considered a complement to, not an alternative to, standard build-up analysis. It can be useful, early in the interpretation process, to run a deconvolution and see if it carries any information that could be integrated in the engineer thinking process, but the reference and ultimate decision should come from a match on the real data (typically the history match and the individual build-ups), not only the match on the product of an optimization process that carries some assumptions.
- To work at once it requires us to bundle together coherent, typically build-up, responses. When build-ups are incoherent, it is still possible to run individual deconvolutions based on the same value of pi, and modify pi until the different deconvolutions are coherent.
- Deconvolution only works if superposition works and if the system does not change in time. Superposition works if the running equations are linear. If the flow is nonlinear (e.g., material balance depletion, nonDarcy, multiphase, etc) deconvolution will fail and may be misguiding. Same will apply, even if the diffusion is perfectly linear, if other wells are interfering with the analyzed pressure response (multi-well case).

So, as with any new tool there is the ‘buzzword’ syndrome. It should not be oversold nor overbought. Deconvolution is NOT the silver bullet that will provide your reserves that we could not see before.

Still, it is great to have something new in an area where the last really innovative theoretical tool was the 1983 Bourdet derivative.

3.E Modern PTA methodology

Modern Pressure Transient Analysis is based on the use of PC based PTA software products. The key for any modern software is to combine user friendliness and a powerful technical kernel, with both analytical and numerical capabilities. In terms of methodology, the central diagnostic tool is the loglog plot, showing both pressure and the Bourdet derivative used for the diagnostics and the match with the selected model(s). The sections below describe the typical path of today's Pressure Transient Analysis. It was our understanding of what this typical path should be that led us to implement this in Saphir.

Once the interpretation is initialized the first task is to get a coherent and representative set of rate and pressure data. This includes loading the data, quality check and validation and editing to prepare for analysis. One or several periods of interests, typically buildups, will then be extracted and the diagnostic plot created and the data diagnosed. The interpretation engineer can select one or several candidate analytical and/or numerical models, set their parameters and generate these models. For candidate models that are retained, the engineer can refine the parameters, either manually or using nonlinear regression. Once the model parameters are finalized, the user may assess the sensitivity and/or cross-correlations of the parameters using confidence intervals from the nonlinear regression and run sensitivity analysis. Finally, a report is issued.

The path above is the default path when all goes well. In reality, for complex problems, it may be a trial-and-error process where the interpretation engineer may decide to go backwards before continuing forward again when a segment of the process is not satisfactory.

3.E.1 Initialization

The data and the operation need first to be reference in time and spavce. The interpretation engineer must then input information required to identify the test and select the main options that will set up the interpretation process: the type of test (standard, interference). The engineer may start with a standard analysis, nonlinear numerical, shale gas or coalbed methane (CBM), multilayer analytical or linear numerical, or a formation tester type of analysis. The final input will be the parameters that are assumed to be known which are required to calculate the interpretation results: porosity, net drained vertical thickness, well radius, etc.

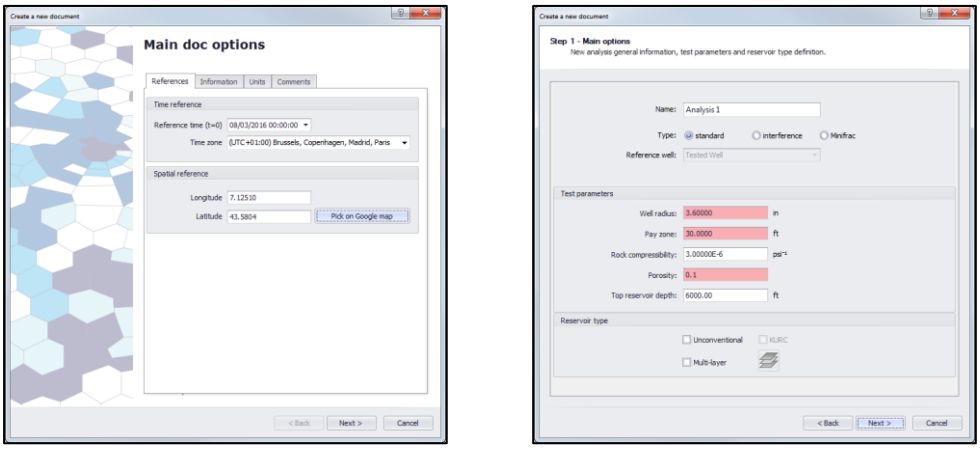


Fig. 3.E.1 – Time and Spatial references and General conditions

Then the type of fluid has to be determined, that will determine the function of the pressure to be used, for a slightly compressible fluid, only a few PVT properties, assumed to be constant, are needed: formation volume factor, viscosity, and total system compressibility.

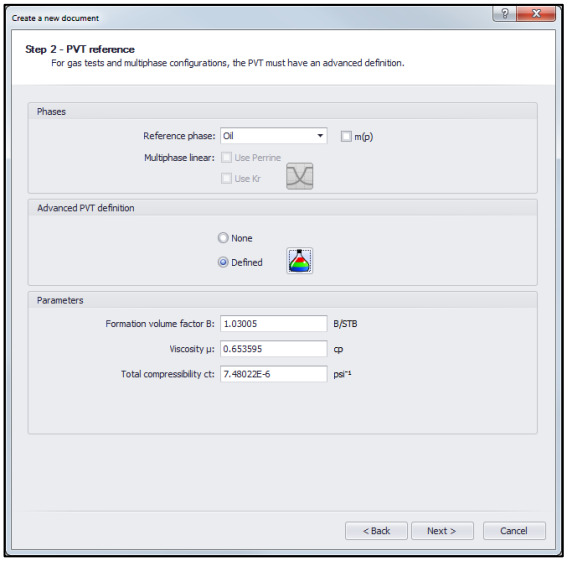


Fig. 3.E.2 – Slightly compressible fluid

For other phase combinations, a choice of correlations or input of PVT tables is required to calculate the pseudo pressure and pseudo time functions.

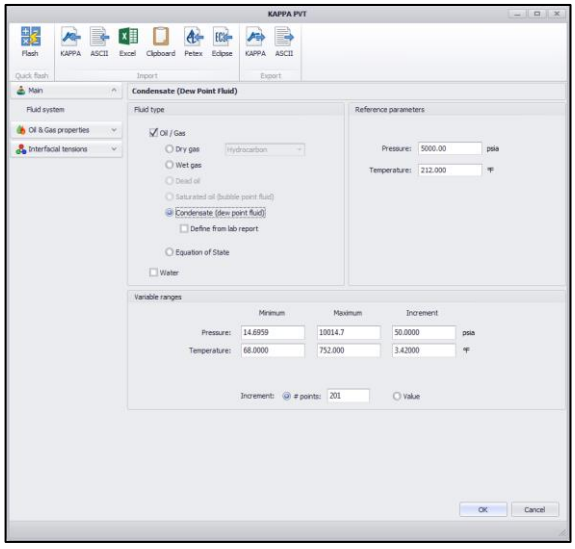


Fig. 3.E.3 – Defining the PVT

3.E.2 Loading Data

Import from flat ASCII files, manual input and copy-paste from a spreadsheet are the main methods used to load data. However, data is increasingly read from databases sometimes with a direct real time link to the running acquisition systems of service companies during the test.

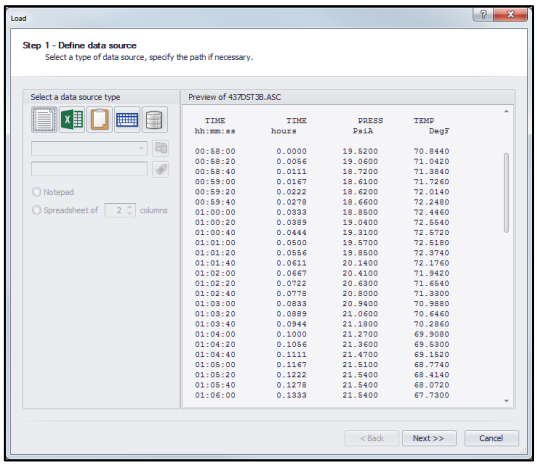


Fig. 3.E.4 – Loading Data: Define data source

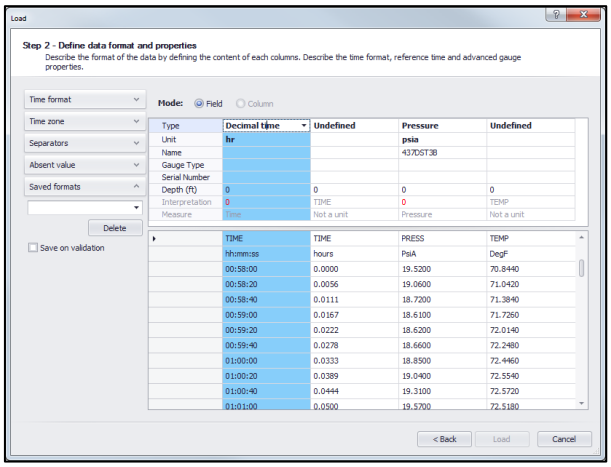


Fig. 3.E.5 – Loading Data: Define data format

Unlike for open-hole logs and despite several attempts in the past, as of today (2010) no industry-standard ASCII format has emerged to execute the load with a click. In Canada the EUB has published a format (PAS) for compulsory electronic submission of test data and results, but this remains very oriented towards local legal procedures. So software packages have to provide the engineer with the flexibility to interactively define the file format, in order to cover the wide variety of existing files.

Originally, the amount of data was a real issue because of limited available memory running under DOS, the cost of computer memory, and the fact that the size of the data arrays had to be declared and set by the software programmers at compilation time. All these limitations have gone. Today's software can easily handle multiple gauges and volume of gauge data acquired during a well test which is sometimes more than a million data points.

The recommended procedure is to load all data acquired from all gauges during the well test, and not just a filtered subset. Filtering can always been applied later, on duplicate data sets. However, things are changing with the spread of permanent downhole gauges and the increased usage of production data in Pressure Transient and Rate Transient Analysis. The amount of production data is one order of magnitude higher, and is much less smooth than a typical buildup. Smart filters, such as wavelets, are increasingly required to reduce the volume of the data, retaining any trends and significant changes and at the same time eliminate noise. The processing of Permanent Downhole Gauge (PDG) data is covered in another chapter.

3.E.3 Quality Control

Quality Control is an essential part of the interpretation, too often overlooked in the past, it includes:

- Validation of the gauges: identification of failures, drift, clock failure, resolution, etc.
- Identification of operational problems.
- When applicable, identification and correction of tidal effects.
- Discrimination of wellbore effects from reservoir effects.

Quality Control has fortunately become a growing concern. Previously, an interpretation engineer would often consider the buildup data only and match it with, for example, a radial composite model; whilst all too readily ignoring the possibility that the test behavior could indeed be related to wellbore phase redistribution. An efficient tool to diagnose wellbore effects is the dynamic calculation of the difference between the gauges measuring the same data. The value of the difference itself is of little interest as long as it stays within the gauges accuracy. However, variations of the difference may be a valuable source of information.

When two pressure sensors are set at the same depth, as with a dual gauge carrier, their difference can be used to check their synchronization (time shift) and their coherence. Gauge failure and gauge drift may be identified.

When the gauges are set at different levels, as in a tandem configuration, any change of the pressure gradient occurring between the gauges may be detected. In the presence of phase segregation problems, the proper placement of dual gauges may help qualifying and even quantifying these problems. The engineer will avoid pointlessly interpreting and using a complex reservoir model behavior that has absolutely nothing to do with the reservoir.

In the absence of dual gauges, one can calculate the derivative of the gauge versus time, and plot it on a linear or log-log scale. This will act as a 'magnifying glass' of the pressure behavior.

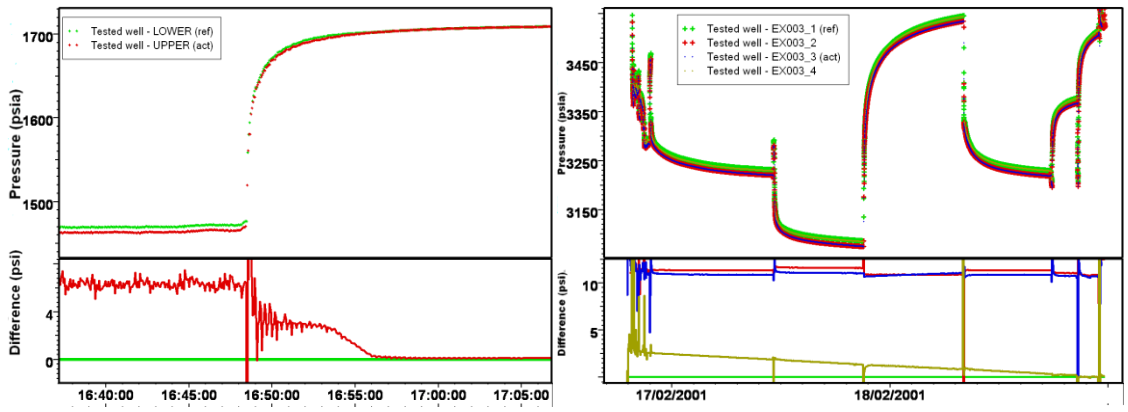


Fig. 3.E.6 – Data Quality control using dual gauges and Drifting gauge

Even though people associate the difficulty of well test interpretation to the modelling part, a lot of thinking takes place at this stage of the interpretation, as it defines the starting point from which the diagnostic will take place. Failing to identify any operational problems can potentially jeopardize the whole interpretation process.

There is a side advantage in performing a comprehensive Quality Control: after going back and forth between the data and the well test report, the interpretation engineer will know what happened during the test, even if he/she was not on-site.

3.E.4 Editing data

Loaded data may be the result of careful post-processing by the data acquisition company, in which case no or little editing may be needed. But very often the interpretation engineer will have to gather data of unequal quality and from different sources. Pressures will often be acquired downhole in real time or with a memory gauge, while rates will still be measured at surface and come from the well test report with a different time sampling.

Beyond the usual cleaning of irrelevant data and the correction of load errors, the main challenge will be to end up with at least one coherent, synchronized set of rate and pressure data. To get there the engineer may have to perform the following tasks:

- Get all data acquired electronically to the same reference time.
- If not already loaded, create the rate history graphically by identifying the pressure breaks and get the rate values from the well test report. Use a facility to automatically identify the shutin periods and automatically correct the production history from volumes to rates.
- Refine the production history, when the time sampling of rate measurements is too crude.
- Conversely, if the production history goes into useless details, simplify the rate history to reduce the CPU time required to run the models.

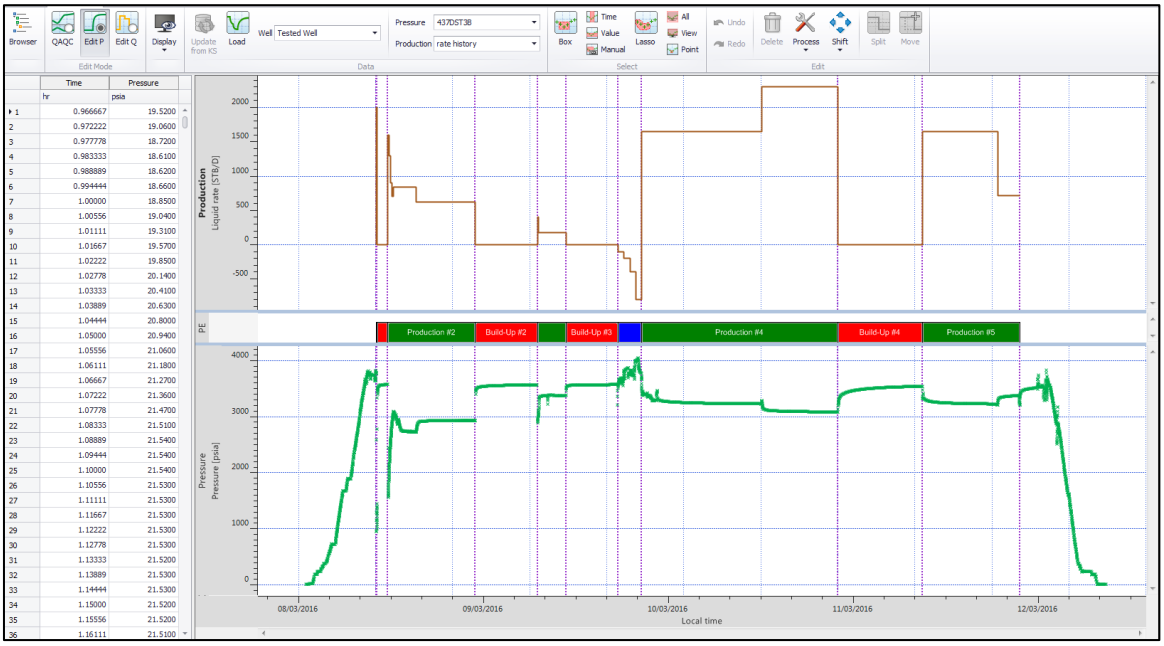


Fig. 3.E.7 – Editing data:
Pressure and production history adjustment

3.E.5 Extraction and diagnostic

Once the data have been synchronized and validated, the analysis itself will start. The engineer will focus on one or several gauges, one or several flow periods, and will create the appropriate diagnostic tools, starting with the loglog and the semilog plots. When several gauges are used, they will be overlaid. When several production and/or shutin periods are extracted, they will be rate-normalized, then overlaid. In the case of Saphir, this extraction is followed by an automatic positioning of a horizontal line for IARF on the Bourdet derivative and a unit slope line for pure wellbore storage on both pressure and the Bourdet derivative. This positioning is set by a relatively simple filtration, the main goal being to put these lines in the same 'range' as the data. Surprisingly, this sort of processing works quite well in the case of simple responses, giving an instantaneous estimate of the wellbore storage and permeability-thickness product. In case of complex behavior, the software may have selected the wrong level of the derivative for IARF and or the wrong unit slope for wellbore storage. The interpretation engineer will then interactively move the two straight lines in order to properly position these flow regimes.

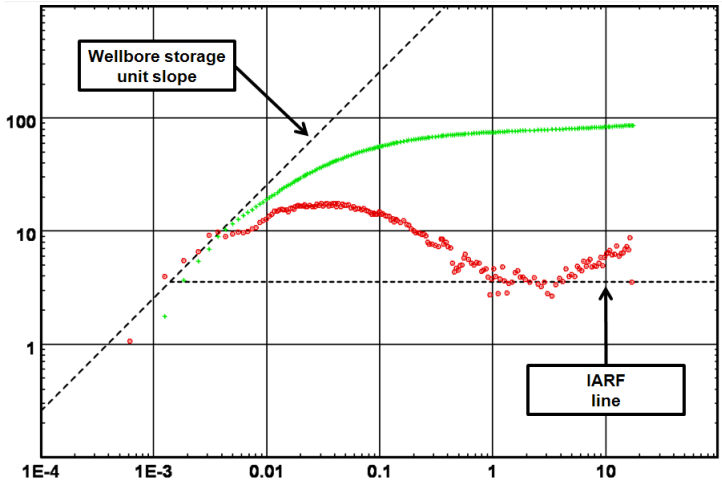


Fig. 3.E.8 – Match lines

During the extraction process, and possibly later, the engineer may decide to control the derivative smoothing, apply a logarithmic filter, and in the case of a shut-in, control the last flowing pressure.

3.E.6 Deconvolution

The new deconvolution method developed in the last few years was presented in a previous section. Extraction of the deconvolution may occur right after the extraction of the individual shut-ins, or much later after the interpretation of the individual shut-ins.

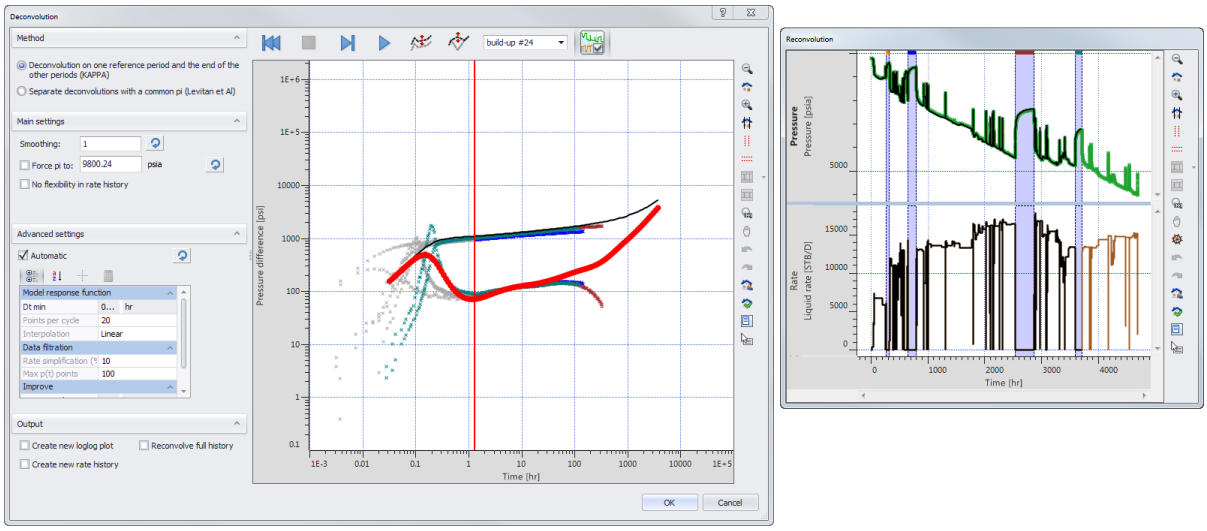


Fig. 3.E.9 – Deconvolution dialog

3.E.7 Diagnostic

After extraction, data problems overlooked in the initial quality control may become apparent, requiring further data editing, and a new extraction.

Looking at the derivative response will generally be the starting point of this process. Individual features in the derivative signature will be considered, validated or rejected, and potentially associated to a well, reservoir or boundary model. These possible assumptions must then be compared to what is already known from other sources.

Depending on the diagnostic, the loglog and semilog plots can be complemented by other specialized plots to identify specific flow regimes by straight line analysis. However this approach has been made largely redundant by the introduction of the modern approach. The engineer will have the choice of the pressure function, the time function and the type of superposition that will be applied to the time function; raw function, tandem superposition for simple buildups, or multirate superposition.

Depending on the prior knowledge and the complexity of the response, the problem may be very quickly restricted to one or two alternatives, or the range of possibilities may remain large. For exploration wells, the uncertainty in the explanation may stand, and alternative explanations may be presented in the 'final' report. Further tests and increased knowledge of the reservoir could allow, later, narrowing down the range of possibilities, months or years after the initial interpretation.

3.E.8 Model generation

The engineer, after diagnosing the behavior, will then select one or several candidate models. The process below will be duplicated for each considered model.

The objective is to use the modelling capability of the software to match in part or in totality the pressure response. This will consist of selecting one or several models, which may be analytical or numerical. Then, entering a first estimate of the model parameters, running the model and comparing the simulated results with the real data, on all relevant plots.

AI based Model advisers may be used to speed up the process by detecting if a derivative response can be explained by a certain combination of well, reservoir and boundary models, and produce a first estimate of the model parameters with no user interaction.

Today's software products offer a wide choice of analytical models. Typically the user will select a wellbore, a well, a reservoir and a boundary model. Unfortunately, our ability to solve problems mathematically is limited, and all combinations of well, reservoir and boundary models may not be available. This is sometimes frustrating to the engineer, as in this case only portions of the response can be matched at any one time.

There are many ways to estimate parameters: (1) from the results of specialized plots that may have been created in the analysis; (2) from straight lines drawn on the loglog plot (wellbore storage, IARF, fractures, closed systems, etc.); (3) from interactive features picking the corresponding part of the derivative signature; (4) by manual input.

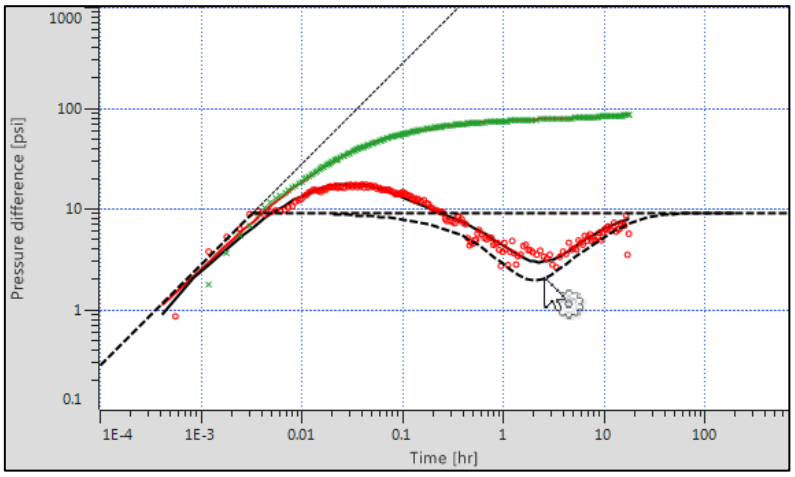


Fig. 3.E.10 – Interactive pick

For complex analytical models, only a few parameters, or relationships between parameters, will be determined in a unique way from the well test response. The other parameters or missing relations will be input from other sources of information. If this missing information is not available, the problem will remain under-specified.

The previous remark on parameter estimation is even more critical when using numerical models, where the geometry will essentially be built from prior knowledge of the reservoir, and only a few 'global' unknowns will be deduced from the test.

It is no longer a technical problem to transfer information and data directly and dynamically between applications, and there are dozens of public or proprietary protocols to do so (OLE, COM, DCOM, Corba, etc.). As a consequence models generated from third party applications may be transferred and run in pressure transient analysis software. The most common example is a 'standard' reservoir simulator run.

The model is generated and compared to the data, in terms of both pressure and Bourdet derivative on the history plot, the loglog and semilog plots. In case other specialized plots are used, the model will also be compared on these different scales. At this point, the engineer may decide to reject the candidate model, or keep it and refine the parameter calculations.

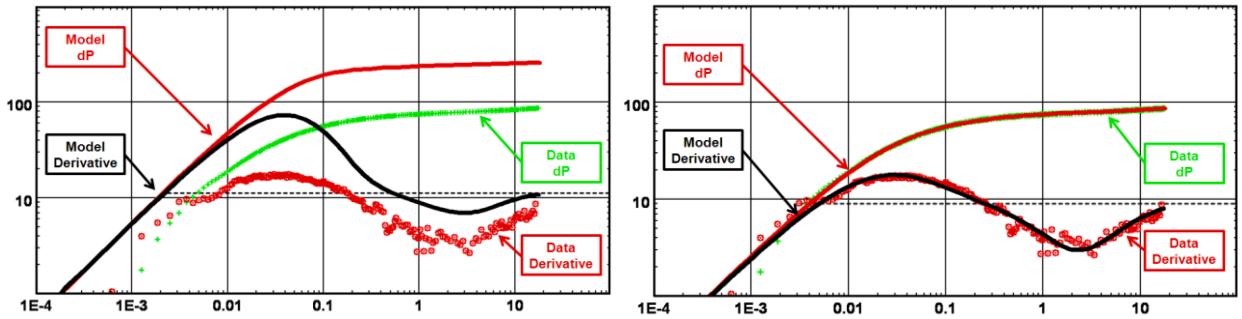


Fig. 3.E.11 – Initial and Final model match

3.E.9 Model refinement

Modification of the parameters: Before leaving the parameter refinement to an optimization routine, the engineer should deal with the gross parameter errors if there are any. This will increase the chance for the regression to succeed and converge faster, and it will secure the choice of the model. Software will generally provide facilities to ease this process. For example, parameters may be corrected if the engineer shifts the match on the loglog plot. However, an experienced interpretation engineer with a good understanding of the sensitivity to the model parameters will often do it faster by changing the values by hand.

Nonlinear regression: The principle is to use numerical optimization to refine the parameter estimates by minimizing an error function, generally the standard deviation between the simulated pressures and the real pressures at carefully selected times. The derivative may also be integrated in the error function. The most commonly used optimization algorithm is Levenberg-Marquardt, but there are many variants.

Among the model parameters, some may be fixed by the engineer. For the others, the engineer may control their upper and lower limits. The data points on which the error function will be calculated may also be user controlled. One major choice will be whether the optimization is restricted to the analyzed period, or if it is extended to data outside the analysis. In the first case, the match at the end of the optimization process will be as good as or better than the starting point. If the optimization is performed on points beyond the analyzed period, the overall history match will be improved, but potentially at the expense of the quality of the match on the period used for the diagnostic.

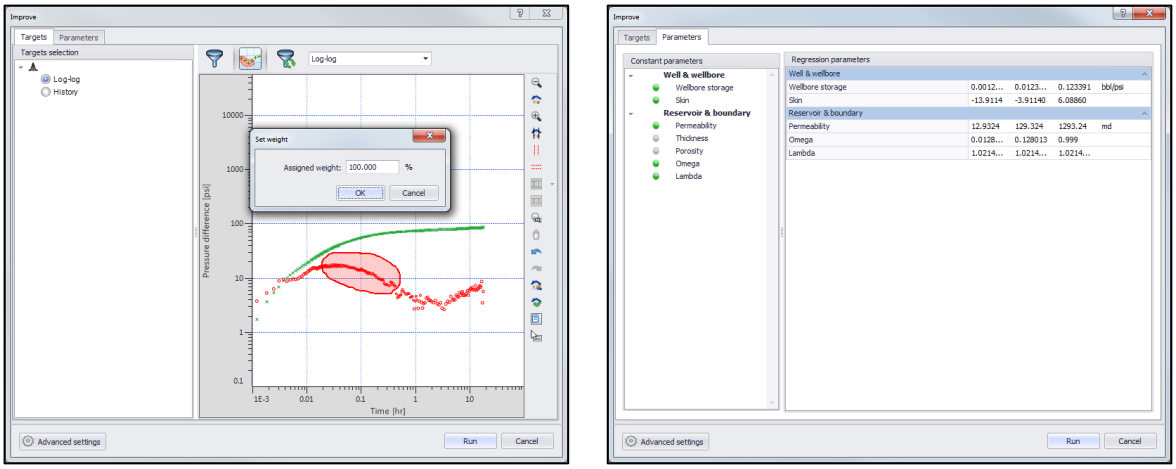


Fig. 3.E.12 – Setting weight to the regression points and controlling the optimization bounds

3.E.10 Sensitivity study

At the end of the nonlinear regression it is also possible to recover the confidence intervals. They can be used to assess the sensitivity to individual parameters and eventual parameters cross-correlations.

One can also run and display series of model generations corresponding to different values of a given parameter in order to compare them on a single loglog plot. This is, to a certain extent, the modern version of the type-curves, where dimensionless drawdown solutions are replaced by the generation and extraction of detailed models with user preset ranges of parameters. The figure below shows the sensitivity to the distance between a well and one single sealing fault.

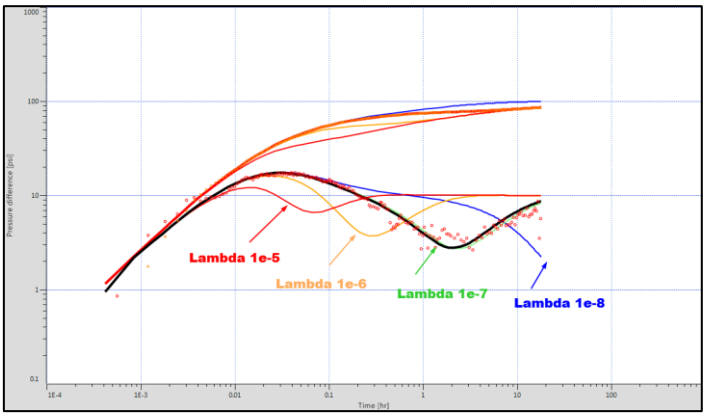


Fig. 3.E.13 – Sensitivity to the Lambda factor

3.E.11 Reporting Guidelines

A typical interpretation report will be split into two components: the 'mechanical' part, basically the result tables and plots generated, directly or indirectly, by the Pressure Transient Analysis package, and the 'verbose' part, where the engineer will report the objectives, the operations, the interpretation, the confidence one could have on his interpretation, and possible recommendations for well treatments and/or future tests.

There has never been an industry standard for reporting, except the Canadian EUB format that is restricted to very basic results. Typically, professional interpretation reports will be generated with two possible set-ups:

- A header document, from a word processor, with some 'copy-paste' of plots and results from the PTA software, but with most of the 'mechanical' report delivered as an annex.
- An integrated document, typically from a word processor, where some plots and tables are dynamically connected to the PTA software using some OLE or COM automations. The advantage of this solution is that it is much more flexible. Once a model template has been set up the reporting process will get shorter and shorter from one interpretation to the next.

In any case the engineer must keep in mind that an interpretation is, at best, a best guess at a given time, and 'truth' can evolve with time. The key word here is 'interpretation'.

'The reservoir is a circle of radius 4123.93 ft'.

This is probably the worst possible statement we can imagine in PTA. The reservoir is very unlikely to be an exact circle. What we have in PTA is a range of models that we KNOW to be over-simplified. We simplify to turn the qualitative into quantitative, and one must always be factual. Also, the number of significant figures of a result must be reasonable, or at least not ridiculous. It is not because the nonlinear regression finished at a given number that we must keep all the significant figures of this number. So a much more reasonable statement would be: 'If we consider that the late time behavior is linked to a close system, a reasonable match was obtained with a circular reservoir with a radius of 4,100 ft.'

'The more I know about well testing, the more I worry'. H.J. Ramey Jr, 1989

3.F Test design

Pressure Transient Analysis is performed on data that were acquired during dedicated operations (well tests) or from permanent gauges. In order to optimize a coming well test, one can use the modelling capabilities of the PTA software to run a test design, i.e. simulate the response of a well test from the parameters or range of parameters we expect. It is then possible to play with the different scenarios and adapt them to the various constraints and the test objectives.

In order to run the scenarios the engineer must rely on known information and data or make reasonable assumptions. To explore 'what-if' scenarios, sensitivity studies are carried out and based upon these the engineer can choose both downhole and surface equipment including, amongst others, pressure gauges with adequate accuracy and resolution. Surface equipment must be selected which includes facilities to measure the flowrate of gas, oil and water. This done, the engineer can make the safest and most economical plan to reach the test objectives.

3.F.1 Safety

Safety is the primary concern in all well testing operations and is the mandatory objective that must be met before any other. With the safety constraints applied the objectives of the test must be defined, operational limitations identified and scenarios considered that clearly show if the objectives will be met and if not, why not. The safety aspects of well testing are covered in a variety of documents and books available on the internet and elsewhere. All companies have their own procedures and standards and they should all be fairly common as they have to conform to rules and regulations set down by the various regulatory bodies overseeing different parts of the world. This section is just to remind the reader that Hazard and Operational studies (HAZOPS) for well test operations exist and they must always be applied to ensure safe practice and operation.

3.F.2 Objectives

It sounds obvious but you must know what you want to achieve. What are the ultimate results you would like to obtain from the considerable investment involved in running such a test, and what are the results going to be used for. An assessment of the value of the results is also necessary to avoid 'overkill' and unnecessary expenditures. Below is a non-exhaustive list of parameters one may want to determine in a well test:

- Well model (fractures, partial penetration, slanted and horizontal well parameters)
- Reservoir model (double porosity, layer and composite parameters)
- Boundary model (distance and type of boundaries)
- Permeability
- Skin
- Heterogeneities (double-porosity, layer and composite parameters)
- Static pressure
- Layer parameters (properties and pressure)
- Layer contributions

3.F.3 What data, what quality at what cost?

In order to gather the data necessary to meet the test objectives it is required to define the type of tools that will achieve this. How critical is the accuracy of the downhole measurements and what are the requirements with respect to surface flow rates? What is the requirement with respect to frequency of sampling?

As a general rule the higher the sampling rate of a tool, the better it is for pressure transient analysis. This is certainly the case with respect to downhole pressure and temperature measurements, but is less critical with the surface flow rate measurements.

The tools must be carefully selected. The downhole gauges must have accuracy adequate for the expected pressure response. If the differential pressure during a test is expected to be small (e. g. high permeability and low formation damage) then the accuracy and resolution becomes an important issue. It is also important to consider if high sampling rate of a tool will have an adverse effect on its accuracy. How to program a memory gauge or decide to use real time surface read-out gauge is an issue that needs to be resolved.

If multiphase production is expected in the wellbore or even in the formation then certain considerations must be addressed. To decrease the wellbore volume, downhole shutin may be considered to minimize the chances of phase segregation during a buildup and careful placement of the gauge in the test string is important.

The below figure illustrates the programmed change in pressure acquisition rate just prior to a buildup. The increase in sampling rate increases the noise.

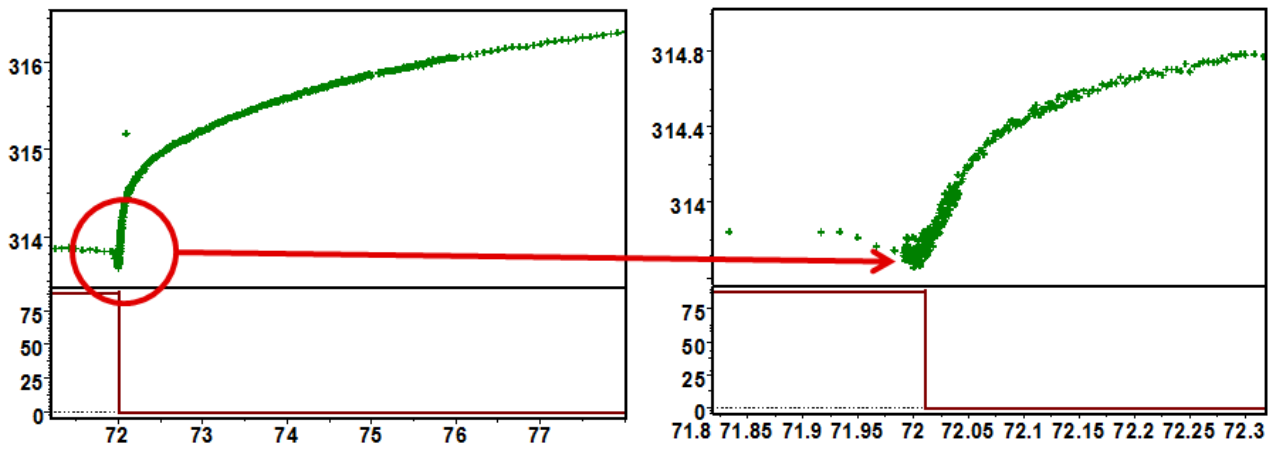


Fig. 3.F.1 – Increase in acquisition rate

When the diagnostic plot is affected by noise the recognition of the flow regimes becomes more difficult and the choice of the correct interpretation model becomes ambiguous. See following illustration.

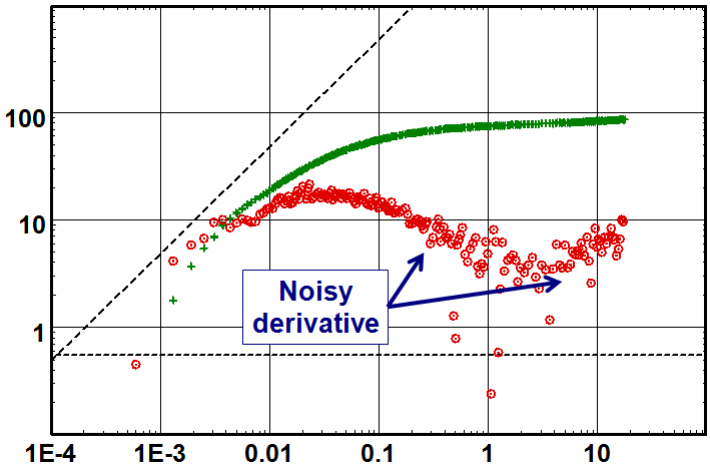


Fig. 3.F.2 – Ambiguous model identification

The behaviour of the period that will be analysed is very dependent upon the previous history and in particular any disturbances immediately before the period in question. If flow rate changes or small shutin periods immediately prior to the subject period cannot be avoided, at least the value of the flow rates should be captured. This is a detail that should be stressed in any test program.

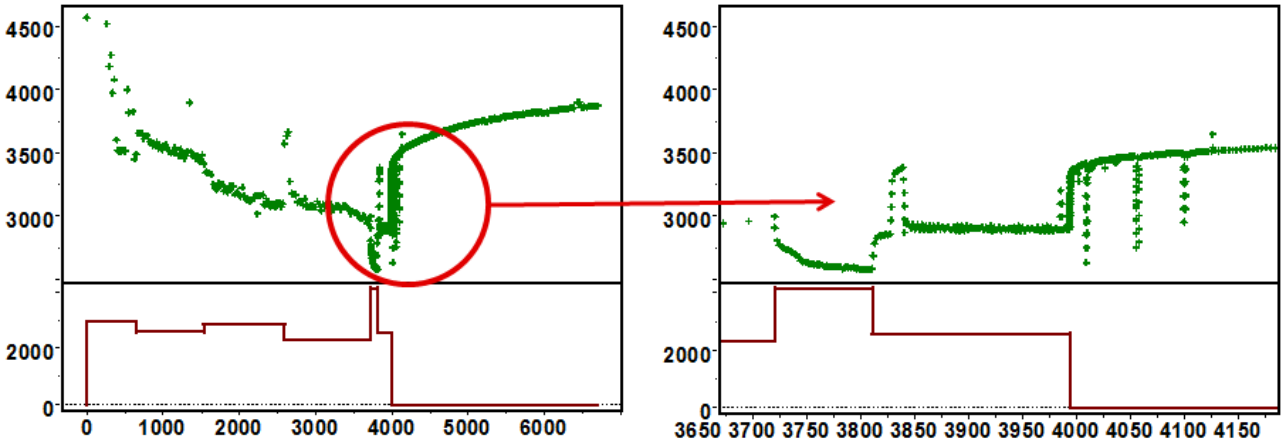


Fig. 3.F.3 – Disturbing the period for analysis

During a buildup that was designed for analysis purposes avoid as far a safety permits any surface operations that may jeopardize the usefulness of the period. The example below illustrates a real case where some surface operations affected the buildup period and rendered it for all practical purposes useless for any analysis with confidence.

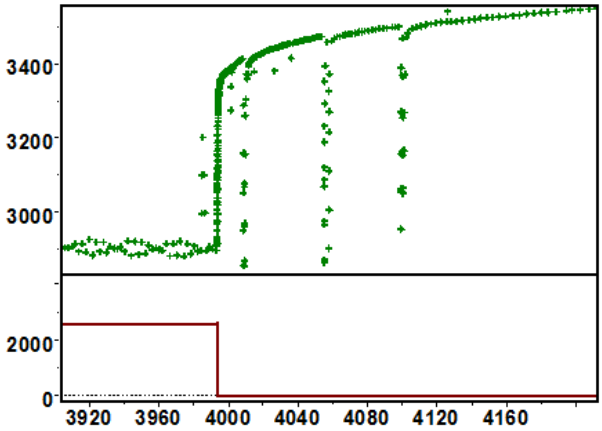


Fig. 3.F.4 – History plot

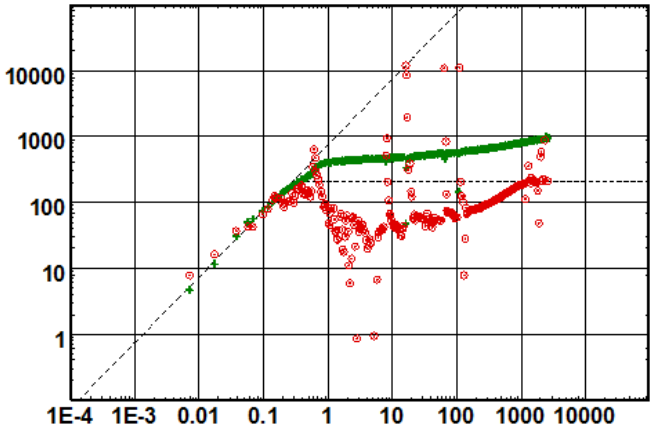


Fig. 3.F.5 – Loglog plot

3.F.4 Type of test

There are several different tests mainly depending upon the type of well.

- Exploration
- DST
- Formation testing
- Appraisal
- Production
- Dynamic gradient
- Static gradient

The planning of any of these types of tests involves setting a scenario to theoretically evaluate if the objectives of the tests will be met.

3.F.5 Scenario

In order to set a scenario some of the information is usually known and some are assumed. The quality and quantity of the known parameters are dependent upon the amount of work already carried out on a prospect, if the planned test is to be carried out in a known field, if the well has already been tested at some earlier stage, etc. The below table summarises some of the data necessary to set the scenario which will be used to theoretically simulate the test which will be used for the final program.

Well completion	PVT parameters	Rock properties	Reservoir description
rw Perforated interval hw Estimated damage Depth Deviation	Specific gravity Volume factor B Viscosity μ Compressibility co, cg, cw Estimated Pi (initial pressure)	Net pay h porosity ϕ formation compressibility cf or cr Estimated permeability k	Distance to limit Limit types Estimated Pi (initial pressure)

In order to illustrate the concept we will devise a scenario where the main objective of the test is to determine skin, permeability and the distance to a seismic defined fault at some distance away from the well (1500 ft).

The analysis of nearby wells has indicated the nature of the reservoir to be homogenous with a permeability-thickness of some 1000 mDft. The skin is of course unknown but believed to become positive after drilling in this relatively high permeability rock. PVT parameters are known in this saturated reservoir, and porosity and net drained thickness have easily been determined from open hole logs in advance of the planned test.

The well has been on production in excess of a year. The well will be shut in to run two memory gauges in tandem and set in a nipple 100 ft above top of perforations. The sampling rate of the gauges is set at a minimum sampling of one second. The below plot illustrates how a five second sampling rate with a quartz gauge of 0.01 psi resolution and 1 psi noise should look on a diagnostic loglog plot.

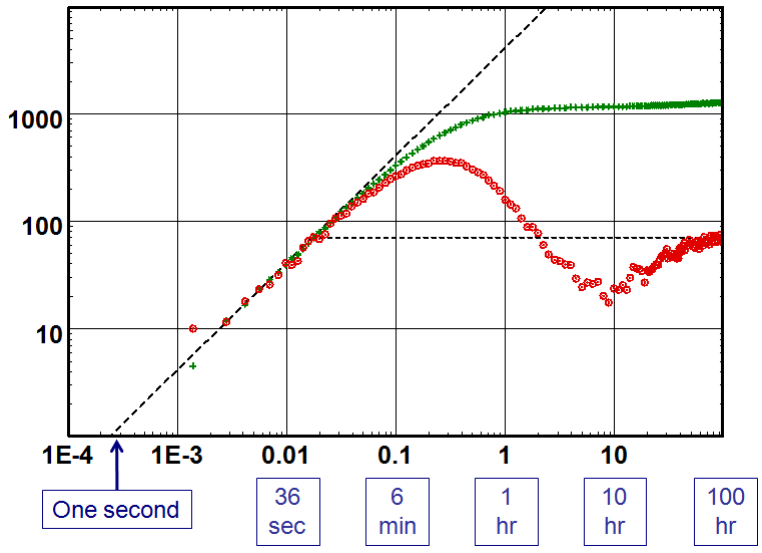


Fig. 3.F.6 – Logarithmic scale

The duration of the shutin that permits for the running and setting of the gauges is set to 24 hours to allow the pressure to stabilize. Then a one single constant production step of 1000 stb/d for 24 hours. This will be followed by a build up of 100 hours. The 100 hours was chosen as the limit of buildup time. The reason is not necessarily to build up for the actual 100 hours, but it is a duration that, from most practical viewpoints is the limit of most buildups in production wells due to the production loss. This allows determining the optimum buildup time in order to find the permeability, skin and distance to fault. The test design option of the software was then used to calculate different scenarios and 'what if' sensitivities. The simulated pressure history is shown in the figure below.

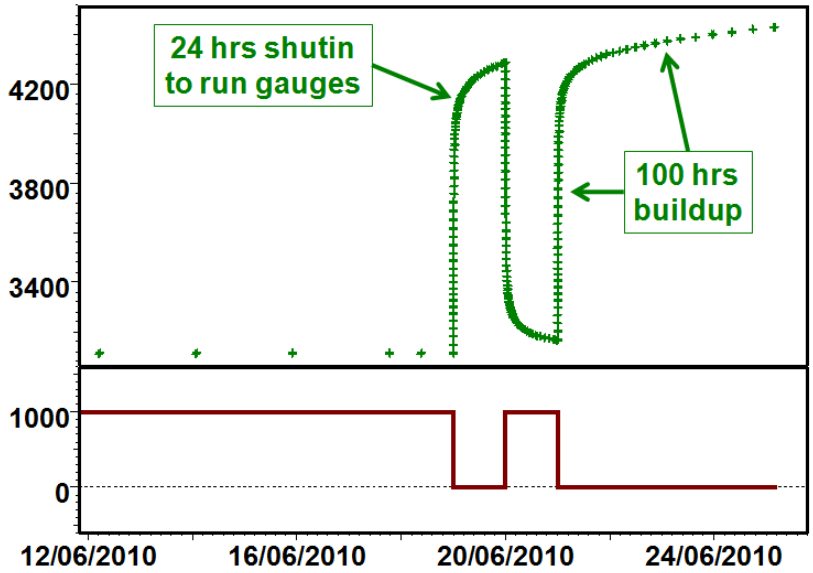


Fig. 3.F.7 – Simulated pressure history

The defined production history and the model were used to study the sensitivity to the skin by running various models and make a comparison. From the figure below it can be seen that infinite acting radial flow will be reached for skin equal -2 at 7 hours shutin time, and skin of 5 at 14 hours shutin time. The combination of skin above 5 and the fault will mask the radial flow thus permeability cannot be determined with any confidence. The sealing fault is detected after about 25 hours shutin time, however the doubling of the slope will only happen after the end of the 100 hours shutin.

The next figure illustrates that when the storage increases above 0.01 bbl/psi and the skin is maintained at +10, then radial flow will not be reached and the identification of the fault becomes ambiguous.

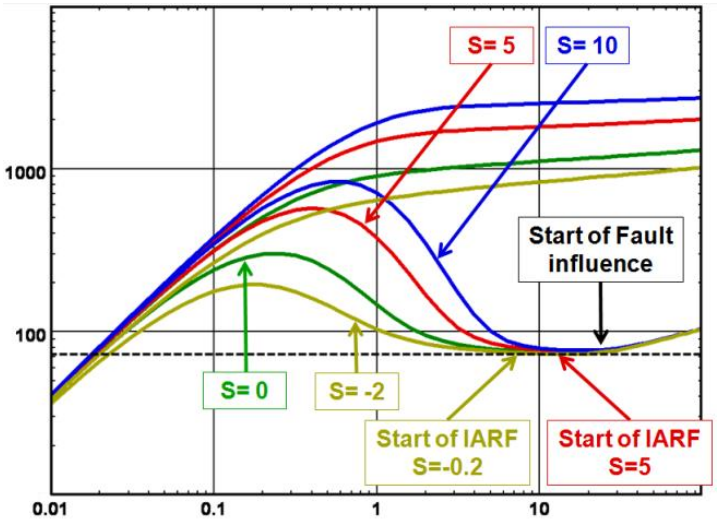


Fig. 3.F.8 – Skin sensitivity

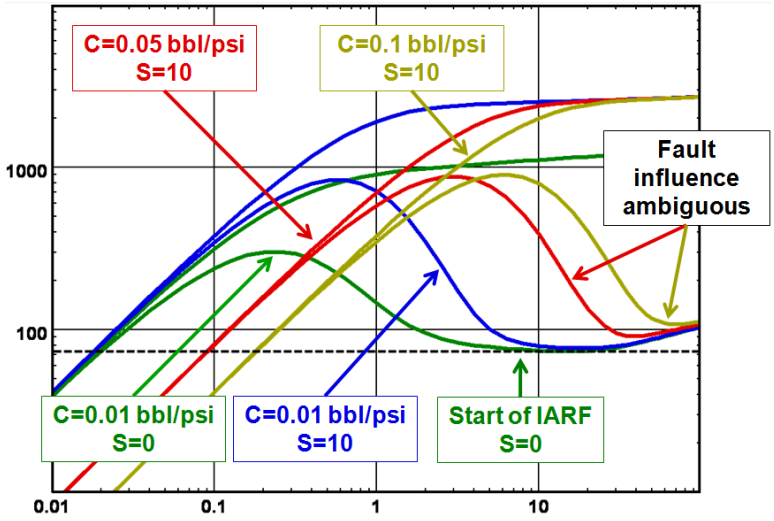


Fig. 3.F.9 – Wellbore storage sensitivity

3.F.6 The final program

A final program is issued and contains all the necessary information to allow the field personnel to safely carry out the well test and assure that all necessary equipment is available.

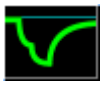
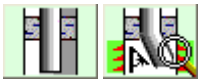
Specific responsibility levels and who is accountable for what part of the operation is defined in the document.

Each phase of the operation is identified and durations of flow and shutin periods are clearly defined. Usually a flow sequence is defined with one single and constant flowrate, this is sometime confusing and the field personnel may try to achieve such a constant flowrate by continuously adjusting the choke. To increase the chances of obtaining a solid analysis from the data it is however recommended to avoid any choke changes during a single defined flowing period as long as the flow rates are measured.

Finally the program is just that, a program; proper field supervision is of course indispensable and adjustments to the plan must be continuous as conditions change.

3.G Operational considerations: Gathering data

It is absolutely necessary, before running a test, to really identify what the test objectives are and which data should be acquired. Part of this work will be achieved with the test design. However, in complement the engineers and operators on site will need to clearly know what information is needed. The following table can be used as a guide, but the list is by no means exhaustive.

	Type of data	**PTA**
	Production history	Yes
	Pressure history	Yes
	PVT, correlations, tables or constraints	Yes
r_w	Wellbore radius	Yes
Φ	Porosity	Yes except interference
h	Net vertical drained thickness	Yes
	Field map with surrounding wells based on seismic interpretation	Preferably
	Production history of surrounding wells	Preferably
	Complete completion log preferably with a permeability log. Core and core analysis	Preferably
	Completion diagram and geometry, deviation, perfos, gauge depths.	Preferably
	All gauges, well test and operations reports	Yes
	Choice of flow correlations or availability of lift curves from third party software	If pressure far from sandface

3.H Quality Assurance and Quality Control

3.H.1 Introduction

During the early 1980's the oil industry, especially in Northern Europe, went through a totally justifiable drive to increase the quality and efficiency of work carried out in most of the commonly related services involved in the production of oil and gas.

Quality control manuals and procedures had to be presented to prove that every effort was fulfilled by the involved parties to assure that work, equipment and preparation procedures were documented and followed. These documents had to be approved by a 'controlling body' before the company was qualified as an approved contractor. The QA/QC manuals described and identified the procedures to follow, backed up by checklists, tests, inspections and certification by approved inspectorates.

This drive was mainly directed towards offshore construction and sub-sea technology to optimize equipment performance and the quality of engineering works, including the safety of oil and gas installations and oil field operations.

Service companies were no exception, but QA/QC was limited to planned and regular calibration of mechanical and electronic measuring devices. As service companies claim no responsibility for any loss or damage due to faulty measurements and interpretations, there was no procedure to validate measured data before analysis.

However methods were developed in the early 1990's. They allow quality control of downhole pressure and temperature measurements, and they ensure that the data is valid and usable by the engineer for further analysis. Such validation increases the confidence in the results of the analysis and eliminates, to a large degree, errors that could lead to major mistakes in the decision process of optimum development and production of petroleum reserves.

3.H.2 Background

The introduction of the Bourdet derivative revolutionized the approach to PTA. It gave us deeper sensitivity and multiplied our analysis ability. It also complicated the diagnostics by revealing phenomena unseen and not understood until this time.

This sensitivity had a price: as both reservoir response and operational problems affect the same pressure response, too often the Bourdet derivative response to fluid movements in the wellbore, phase segregation and temperature anomalies would wrongly be associated to a reservoir feature and interpreted as such.

It was necessary to enable the engineer to differentiate between the representative data of the reservoir response and the part caused as a result of a signal from other phenomena.

The techniques described in this chapter were developed as a result of severe interpretation problems encountered in many fields and led to the introduction of the concept of Differential Pressure Analysis.

It will be shown how the use of pressure differentials measured between pressure gauges placed at different levels in the test string can help the interpreter to identify the pressure data that is valid for interpretation, and enable him to save time by eliminating useless data caused by anomalies and wellbore phenomena. The method brings 'Quality Control' one step further, and should be an integral part in the overall QA/QC programs of any company dealing with downhole measurements of pressure and temperature.

3.H.3 The concept of Differential Pressure Analysis

The analysis is based upon the difference in pressure measured between tandem pressure gauges, the simplest case, or a combination of pressure differences if multiple gauges are used during a pressure survey.

The study of these differences can reveal the following problems and has a direct impact on the choice of the data measurements for a valid PTA:

- Detect phase segregation in the wellbore;
- Establish phases for pressure correction;
- Identify the movement of the fluid interface movements (water / oil / gas);
- Identify temperature anomalies or other gauge technical problems;
- Check the gauge accuracy and resolution;
- Identify gauge drift;
- Other technical or electronic malfunctions;
- Selection of the most representative data channel, if any.

By convention the pressure difference between gauges is calculated so that that an increase in the 'difference channel' represents an increase in the fluid density between the gauges sensing points, and a decrease a reduction of the fluid density, i.e.:

$$\Delta p = p_{lower} - p_{upper}$$

The 'difference channel' behaviour is the same whatever the gauge offset. The upper gauge may well read a higher pressure than the lower gauge, possibly due to a gauge problem or just because of accuracy, but the 'difference channel' would have the same identifiable shape.

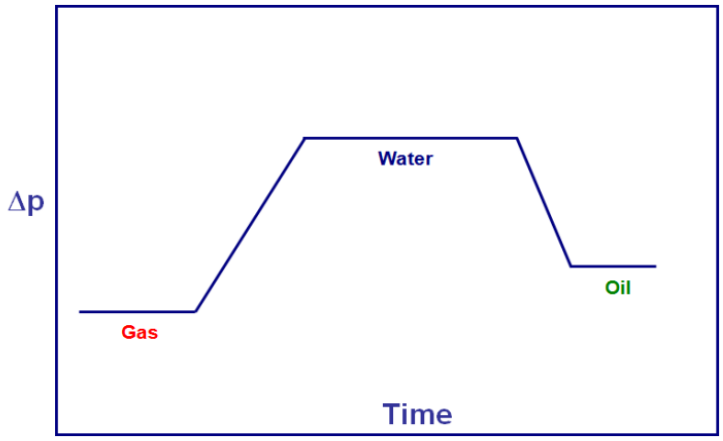


Fig. 3.H.1 – Difference channel

3.H.4 Basics

The simple analysis is based upon the study of the pressure and temperature differences between two or more gauges placed in the test string at different depths. The figure below shows schematically what happens to the pressure at the different sensors, if a 'gas-oil' interface is moving downwards and passes the sensors.

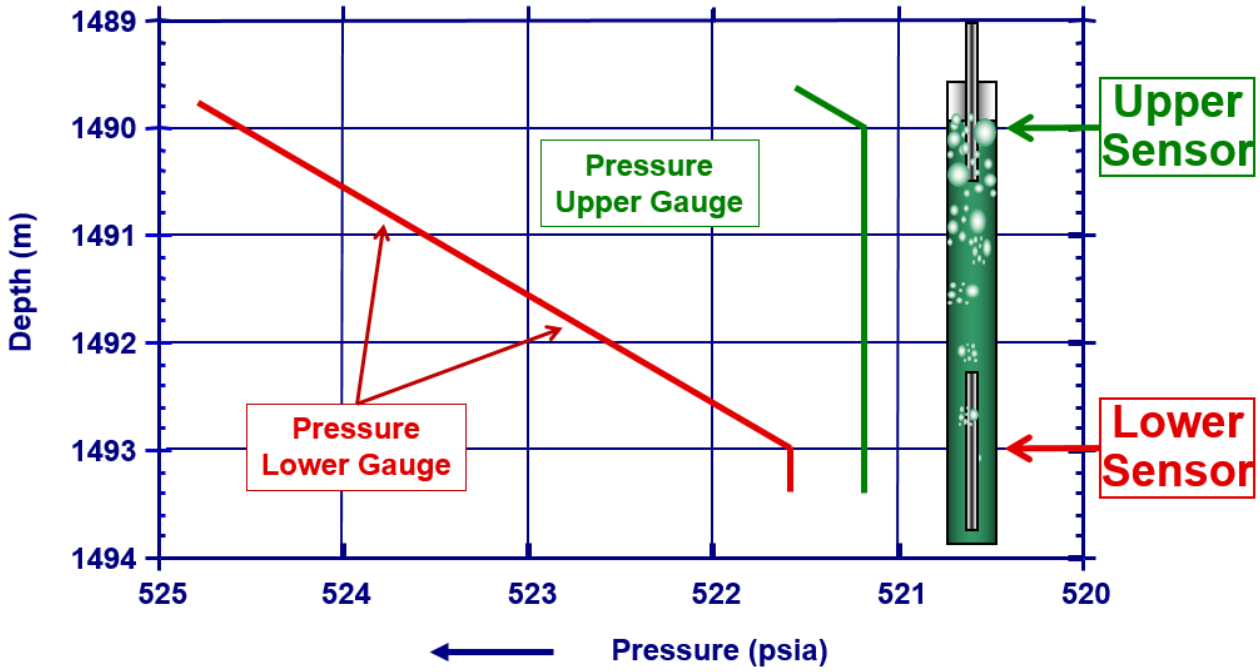


Fig. 3.H.2 – Fluid movement downwards

The example assumes that any background behavior is following a constant transient (trend) or is in Pseudo-Steady state (PSS).

Once the gas-oil interface hits the upper sensor, the pressure at this sensing point remains 'constant' while the interface moves towards the lower pressure point.

The pressure at the lower sensor declines linearly if the fluid interface movement is constant. It becomes constant again after the interface has moved below the lower pressure sensor. The difference in pressure between the two sensing points is represented by the difference in fluid gradient between oil and gas.

The following illustration represents the 'difference channel' between the two sensing points, and by simple analysis it can be determined what fluid phase changes have caused the observed phenomenon (see QA/QC).

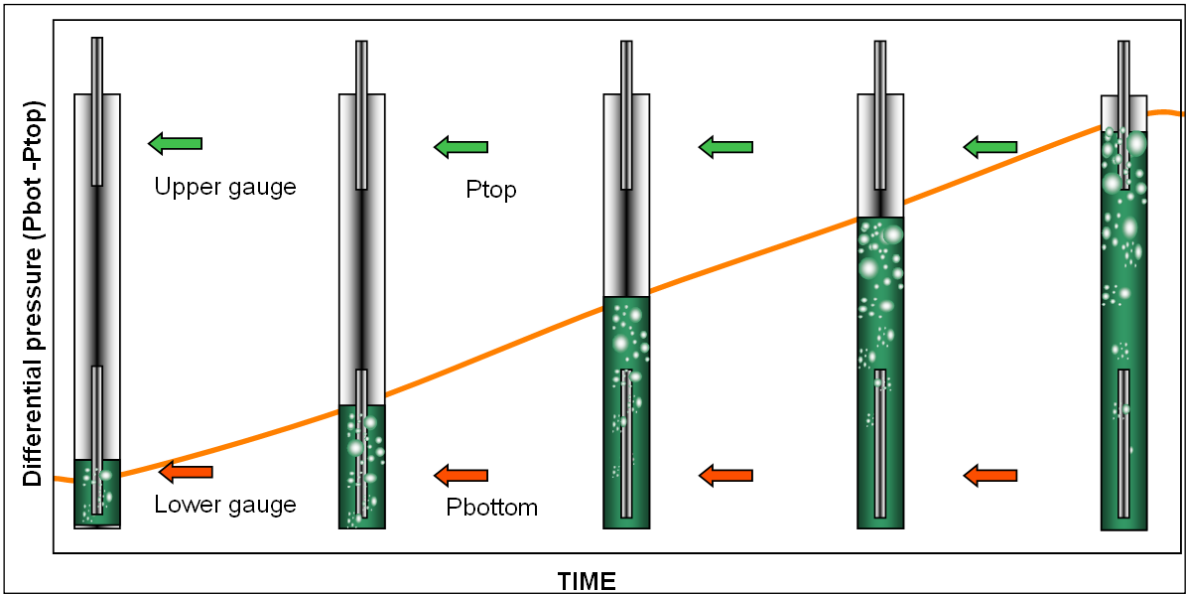


Fig. 3.H.3 – Pressure difference

3.H.5 Pressure correction

Clearly it would be desirable to be able to correct for any perturbation in the pressure caused by the 'phase segregation', which also in the majority of cases has an adverse effect on the Bourdet derivative used for the diagnostics in pressure transient analysis.

In practice this has proved to be near on impossible although using models that takes into account changing wellbore storage can sometimes reproduce the observed effects, but with little added quantitative value. The important task is to identify the problem and discount the period of perturbation when the data is being analysed by simply ignoring this part of the data and being able to explain why the data was ignored.

The simple identification that a problem exists will also help the engineer in making static pressure corrections. The fact that the pressure gauges sensing points are seldom at the level of the sandface is often overlooked by the interpretation engineer.

Classically, the static pressure (pi, p*, p bar, final build-up pressure) is corrected:

- From the gauge depth to the sandface using a static well static gradient.
- From the sandface to a common reservoir datum using the reservoir gradient taking into account any gradient changes.

This correction is usually done manually and is essential to establish reservoir pressure trends, declines and depletion rates.

In the past the dynamic pressure was not corrected as this involved advanced modeling with multiphase flow. Today many such flow models are available. The advanced correction of dynamic pressure data is covered in the chapter on wellbore models.

3.I More on QA/QC

3.I.1 Diagnosing phase segregation from differential pressure

Differential Pressure Analysis is an intelligent evaluation observed anomalies, and an attempt to identify the fluid phases in the wellbore near the gauge sensing points. It gives a reasonable idea of wellbore occurrences and the fluid distribution.

This only gives approximate results and it cannot be used for all types of wellbore phenomena. Nevertheless it enhances the operational understanding and allows for an intelligent correction to reservoir datum with more confidence. Such analysis will also enhance the confidence in the material balance calculation and the identification of drainage patterns.

Practically it involves a choice of several recognizable events on the difference channel (blue circles in the figure below) and transfers the different delta pressure values to a simple spreadsheet. Estimation of fluid gradients is based on the known fluid densities and resulting changes in the pressure gradient, that makes the total picture logical by applying a global gauge offset.

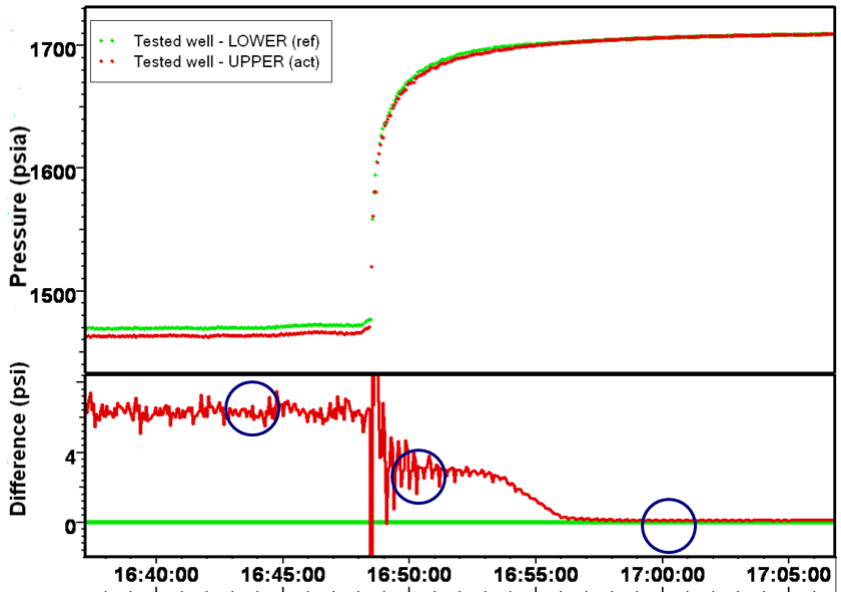


Fig. 3.I.1 – QAQC plot with events marked on difference channel

This method does not only reveal wellbore anomalies. It also determines the pressure gauge offset, which will have to be within the range of the gauge manufacturer's claimed accuracy and resolution.

DIFFERENTIAL PRESSURE ANALYSIS

Events	From Difference Channel		dp Gradient	Assumed Fluid	Assumed Gradient	Calculated dp	Implied Offset	Observed dp	Residual difference
	Time	dp							
	(hrs)	(psi)	(psi/ft)		(psi/ft)	(psi)	calculated	corrected	(psi)
[1]	[2]	[3]	[4]	[5]	[6]	[7]	[8]	[9]	[10]
Event 1	17.10	6.30	0.69	Friction	0.714	6.510	-0.210	6.510	0.000
Event 2	17.18	2.90	0.317	Oil	0.341	3.110	-0.210	3.110	0.000
Event 3	17.33	0.20	0.02	Gas	0.045	0.410	-0.210	0.410	0.000

Distance between sensors: 9.12 ft **Assumed Accuracy Offset:** -0.21 psi

Column (2) and (3) are read directly from the difference channel from the quality control plot. Column (4) is the differential gradient calculated from column (3). Column (5) and (6) are intelligent guesses or assumptions by the user that will normalize column (8), i.e. the same implied gauge offset applies whatever the assumed fluid phase is present.

The implied offset is then entered by the user in its appropriate box below the table, and the residual differences will become close to zero or zero, if the correct assumption as to the fluids present in the wellbore have been made.

The implied offset becomes the gauge offset which has to be within the gauge specifications to be acceptable to the operator.

This analysis gives a much better idea as to which of the fluid gradients to use to correct the gauge pressure to top of sandface.

Another product of this approach is being able to decide which part of the data is really valid for pressure transient analysis as all data affected by the segregation or fluid movements must be discounted in the interpretation process. The impact of not knowing and understanding the wellbore environment is now described.

3.I.2 Impact on the diagnostic

The impact on the Pressure Transient Analysis can be substantial, as illustrated below. The upper gauge is affected by phase segregation and the shape of the derivative is clearly distorted, resulting in the wrong choice of interpretation model.

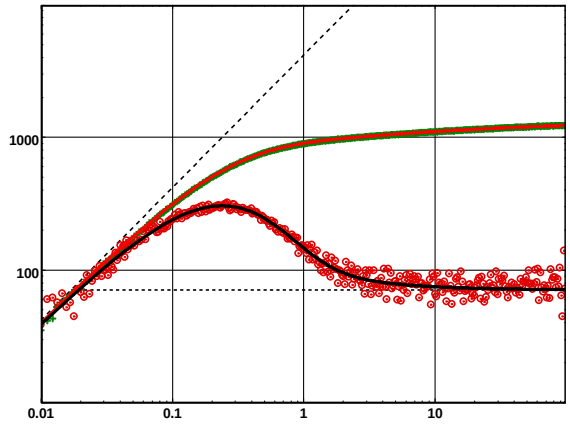


Fig. 3.I.2 – Lower gauge; homogeneous

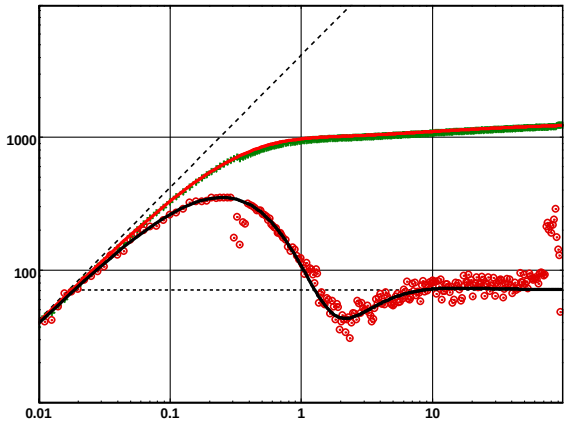


Fig. 3.I.3 – Upper gauge; double porosity

3.I.3 Gauge drift

Gauge drift is caused by unstable electronic components and fatigue of the sensing material used in the instruments. Strain gauges are particular susceptible to this problem.

Drift during a relatively short well test is uncommon, especially today as the quality of electronic gauges has increased immensely. However, it still does happen, and a severe drift will lead to a wrong PTA diagnostic.

The drift problem is more common during long term measurements and can therefore be a real problem in permanent downhole gauges (PDG).

In any case it is important to check the data for validity through the QA/QC procedures described in this document before attempting any serious analysis. To identify a drifting gauge it is necessary to have two or more measurements and study the difference channel constructed between a reference gauge and all the other gauges.

The following figures illustrate the difference channel and the impact on the analysis of the drifting gauge id we did not know that such drift exists.

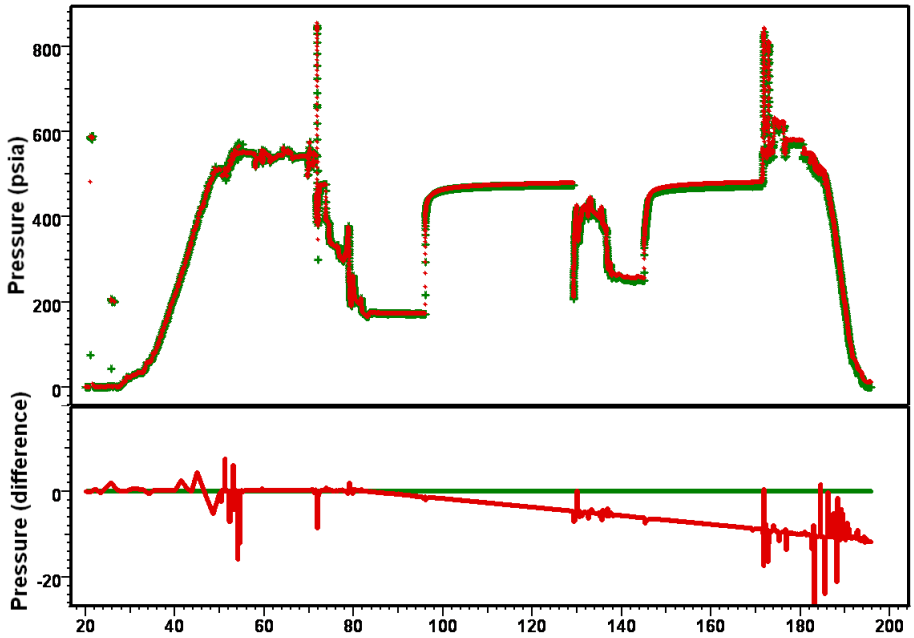


Fig. 3.I.4 – QA/QC plot with difference

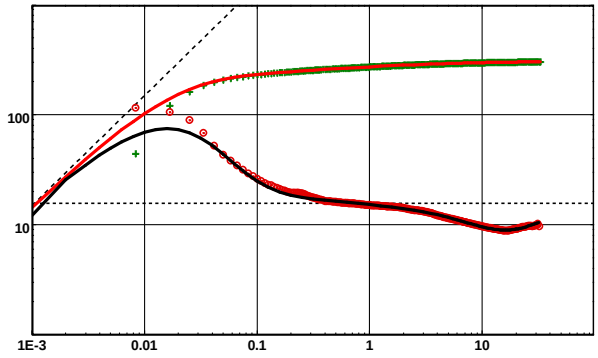


Fig. 3.I.5 – Match non drifting gauge, no fault

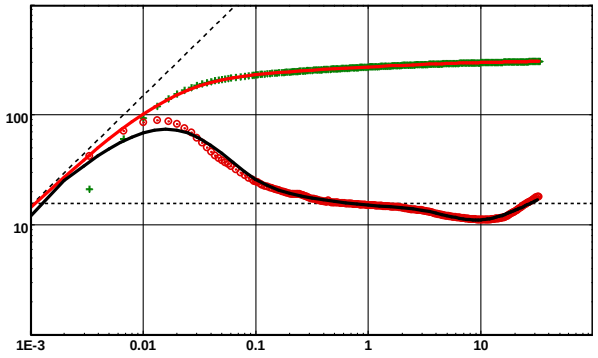


Fig. 3.I.6 – Match drifting gauge, with fault

3.I.4 Phase redistribution

When different phases are produced the redistribution of fluids in the wellbore at shut-in may be almost instantaneous and produce what is called 'gas humping'. This may (seldom) be seen in a water / oil case also. At shut-in the fluid mixture separates and a total reversal of fluids occurs in the wellbore. The heavier fluid moves to the bottom of the well and the lighter fluid, usually gas, accumulates at the top. This can produce a hump in the pressure at shut-in sometimes above the reservoir pressure.

Only when the two phases are stabilized will the buildup return to a normal pressure difference and the response may be analyzed.

The below figure illustrates how the pressure at the sandface at early time can actually rise above reservoir pressure. Imagine a well with a well head pressure A. The upper part of the well is filled with a liquid/gas mixture of a certain weight and in the lower part of the well gas is predominant (admittedly, a rather theoretical assumption). The gas phase at the bottom is considered weightless. In between the two phases is a frictionless piston. The gauge pressure at the bottom of the well is therefore the wellhead pressure plus the weight of the oil mixture, A+P. Lets now assume that we turn this cylinder upside down, the wellhead pressure stays at A+P and the bottom hole pressure increases to A+2P. This induces an abnormal rise in the bottom hole gauge pressure that can be above reservoir pressure.

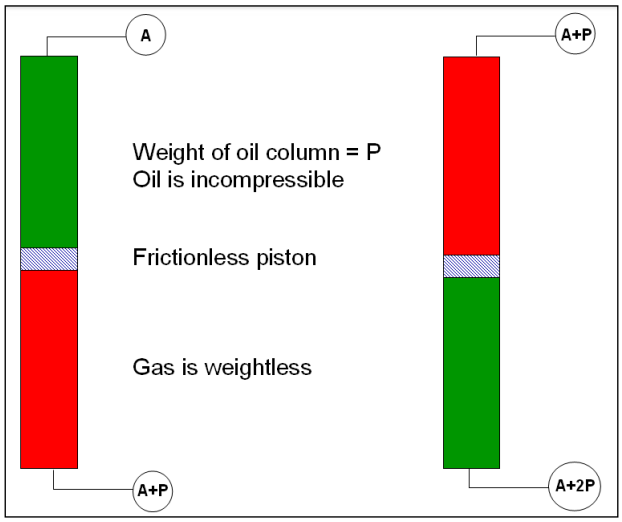


Fig. 3.I.7 – Gas humping

See the following figure that illustrates the hump caused by this phenomenon. This is a classical feature in Pressure Transient Analysis.

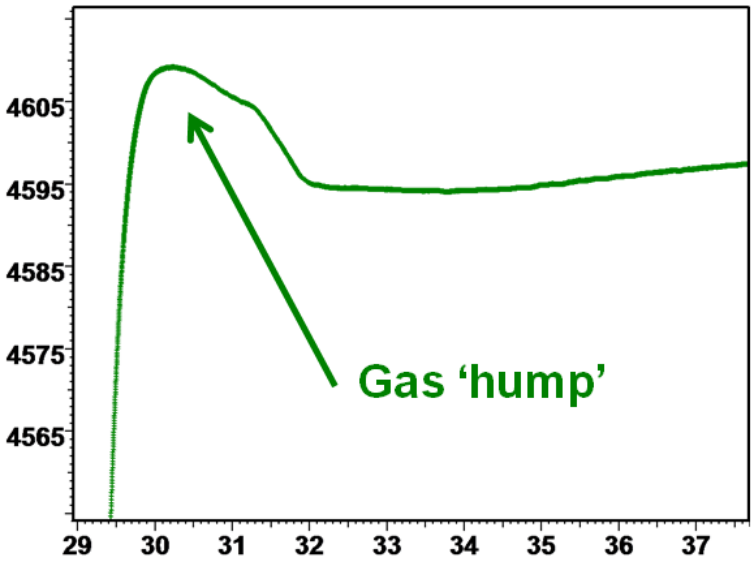


Fig. 3.I.8 – Gas humping

3.J The case of dry gas

3.J.1 Diffusion of real dry gas

As mentioned in the 'Theory' chapter, in order to extend the methodology of Dynamic Data Analysis to gas cases, we introduce a function of the pressure called the pseudopressure. It is given by:

Gas pseudopressure: $$m(p) = 2\int_0^p \frac{p}{\mu Z} dp$$

Using the gas pseudo pressure instead of the pressure, the diffusion equation remains valid *the same methodology presented above can apply.*

In addition to these methods, the gas case presents few particularities presented here.

3.J.2 Correcting the pressure to sandface

Usually the pressure gauge is not set at the sandface due to mechanical constraints in the completion. Because of this, the results obtained from the pressure transient analysis are at the level of the gauge and not the sandface which, in terms of pressure (Pi) and skin (S), will not reflect the true sandface conditions.

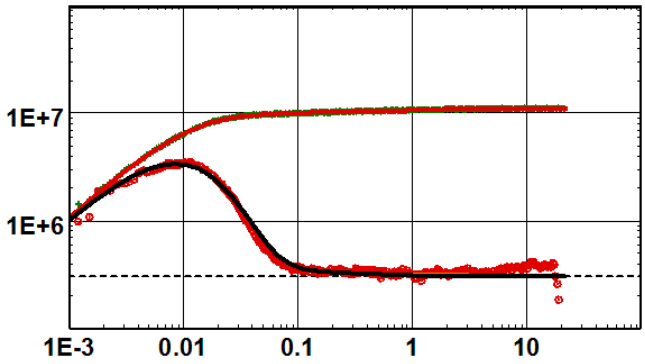
It is necessary first to define the vertical pressure profile in the well. The Saphir/Topaze internal flow correlations or an actual lift curve generated by some specialized program (i.e. Amethyste) can be used for this.

The available correlation for gas is an external lift curve or the internal Cullender & Smith method, but with two modifications for handling water and condensate.

The correlation is based on the gas properties as defined in the PVT setup, and a general friction factor is calculated using the Colebrook and White equation. Note that when you deal with a condensate case with equivalent gas gravity and total rates, the proper gradient and rates are used in the correlation to account for the condensate presence. The presence of water can be accounted for, based on a constant water to gas production ratio.

The solution selected in Saphir is to include both the hydrostatic and friction pressure loss in the model and correct the generated model response to the actual gauge depth, and then to return all the results at the sandface.

In fact, the gauge pressure is not transformed, nor corrected hence it is the model that is brought to the level of the gauge.



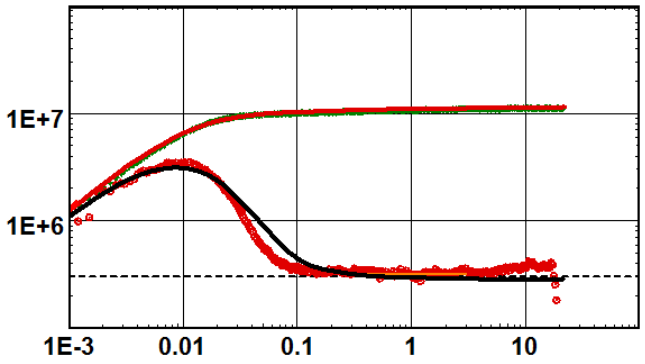
Well & Wellbore parameters

C	=	0.0287	bbl/psi
Skin0	=	4.41	
dS/dQ	=	0.0033	[Mscf/D]-1

Reservoir & Boundary parameters

Pi	=	1384.38	psia
k.h	=	2520	md.ft

Fig. 3.J.1 – Analysis at gauge level



Well & Wellbore parameters

C	=	0.0732	bbl/psi
Skin0	=	4.41	
dS/dQ	=	0	[Mscf/D]-1

Reservoir & Boundary parameters

Pi	=	1418	psia
k.h	=	2520	md.ft

Fig. 3.J.2 – Analysis after model correction to gauge level

You can observe that results (Pi and skin) are now returned at the sandface and that the rate dependent skin attributed to the formation is now a lot smaller and should be attributed to the pressure loss through, in this example, the 1000 ft of 1.5”ID tubing.

Once the sandface parameters have been returned by the model match, the sandface pressure can be properly corrected to a common reservoir datum though the, hopefully appropriate, knowledge of the fluid gradients in the reservoir.

3.J.3 Gas material balance

The issue of material balance in gas diffusion has become increasingly critical in recent years with the spread of permanent gauges. The origin is the same as for changing wellbore storage. Even with the use of pseudopressures, the diffusion equation can be considered linear for as long as the diffusion terms left outside the time and pressure variables remain constant. This time, we are not facing problems of changing wellbore storage, a process only linked to the pressure in the wellbore, but to the whole diffusion process throughout the reservoir.

Diffusion equation:

$$\frac{\partial m(p)}{\partial t} = 0.0002637 \frac{k}{\Phi \mu c_t} \nabla^2 m(p)$$

As soon as we have a pressure gradient in the reservoir, the diffusion term, and especially the product μc_t, will become different from one reservoir block to the next.

Although one could consider that it also happens during any well test, this becomes critical when the reservoir average pressure declines in the reservoir and/or in the well drainage area. It is therefore necessary to adjust the models or the data.

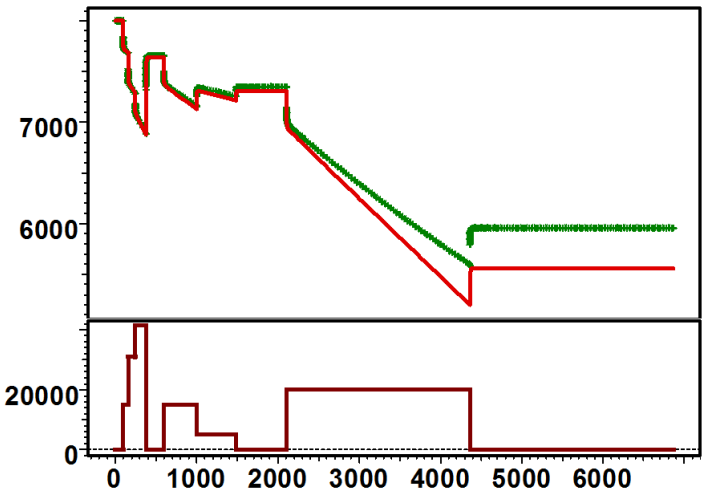


Fig. 3.J.3 – Match without a material balance correction

If we look at a real gas simulation for a long term limit test, or a production survey using permanent gauges, and use it to match with an analytical model where the diffusion was taken at initial pressure, we can see a divergence between the simulated pressure and the measured data, even though the reservoir geometries and the PVT used are strictly the same.

There are again three ways to handle this problem:

3.J.3.a Using pseudotime functions

The pseudotime function is calculated with the reservoir, or drainage area, average pressure:

See more details in the chapter '13.E - The use of pseudofunctions'.

This method was useful at the time when one only had type-curves as models. Today computers can do much better and faster. The main shortcoming was that the initial estimate of the volume and the initial pressure was made before the model was matched. The model would give a value of initial pressure and volume, which might not be the same as the initial guess, hence requiring another modification of the data, another match, and so on. The process would however, converge quickly.

3.J.3.b Integrating the material balance correction in the analytical model

The theory behind this solution is the same, but the use of a model makes the process simpler and more coherent. The model includes a reservoir size and an initial pressure. So the initial gas in place can be calculated as an integral part of the model. At any time step the algorithm calculates the average pressure from the cumulative production using p/Z, and replaces the viscosity and total compressibility in the superposition by the one coming from the average pressure. So at any time step the simulated pressure is coherent with the material balance of the model. The optional derivation is shown below:

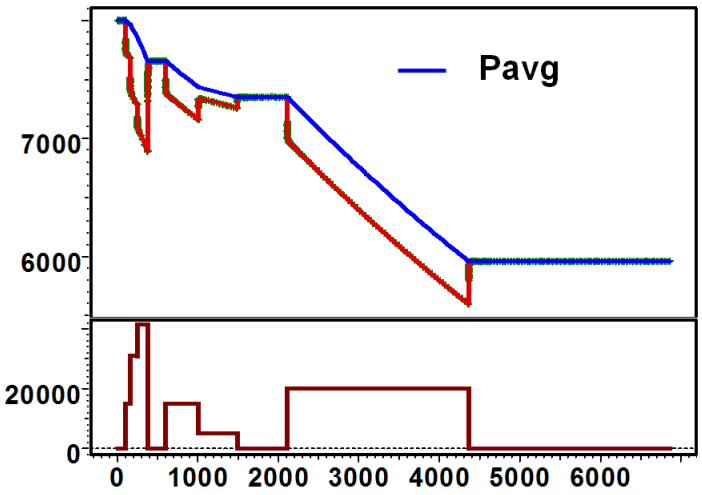


Fig. 3.J.4 – Match with a material balance correction

3.J.3.c Using a numerical model

The use of a numerical model is, conceptually, even simpler. As the gas equation is entered at the level of each cell, the material balance is automatically honoured, not only globally, as above, but at the level of each cell. Solving the problem numerically is by far the most rigorous approach.

As the problem is nonlinear, this requires Saphir NL and the use of a nonlinear solver, but in the case of single gas this will rarely require more than one iteration. So this sort of model, for reasonably simple geometries, will be both fast and accurate.

For information, the case presented above is an actual simulation using Saphir NL.

3.J.4 Non-Darcy flow

As mentioned previously, there are two main options to address non-Darcy flow: using a rate dependent skin model or integrating the Forchheimer equation in a numerical model.

3.J.4.a Simulating non-Darcy flow with a rate dependent skin model

There are two complimentary approaches to determine the rate dependency caused by high flow velocities and turbulence using the simplified assumption that the relationship is linear. In an analytical model the non-Darcy flow effect is simulated by an additional skin using the linear function of the rate.

$$S_{total} = S_0 + (ds/dq)q \qquad ds/dq = D$$

This is illustrated in the figure above. D is called the (linear) non-Darcy flow coefficient.

In order to access the rate dependency it is necessary to conduct a multi flowrate test, these tests are described in the chapter Well Performance Analysis.

The classical way of determining the skin versus rate relationship is to use semilog analysis of each flow period if this analysis is valid. Then plot the resulting skin versus the corresponding rate as illustrated in the figure below. This will return the skin without turbulence ie: the mechanical skin, the intercept of the assumed straight-line, S_0 and the rate dependency D derived from the slope. Here it is important to remember that a flow/after flow test with only one single shut-in may not produce the required results as a semilog analysis of a producing period may be impossible due to the inherent fluctuation of the rates masking the pressure response where semilog analysis is valid.

It is therefore recommended to use the type of tests that have intermediate shut-ins, isochronal or modified isochronal, where we stand a better chance of obtaining the skin from the analysis of these shut-ins. The plot of skin versus rate is done automatically in Saphir. The results can then automatically be transferred and the model generated with regression to improve the model match as necessary.

If the skin versus rate plot fails because semilog analysis is not valid, the rate dependency parameters cans still be set in the model dialog using an initial guess. Then the model match can be refined by regression.

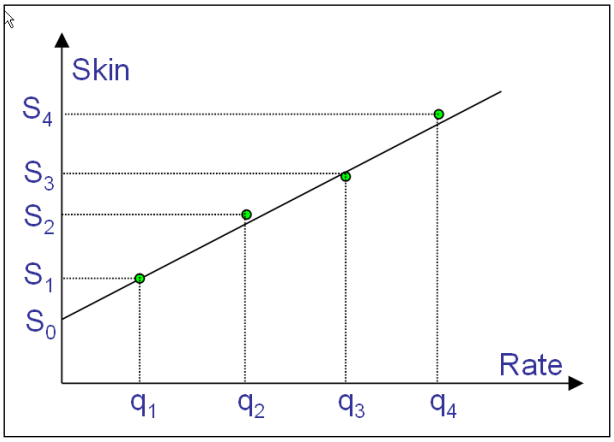


Fig. 3.J.5 – Skin versus rate plot

The figures below show the comparison between a simulation run with a constant skin and a rate dependant skin:

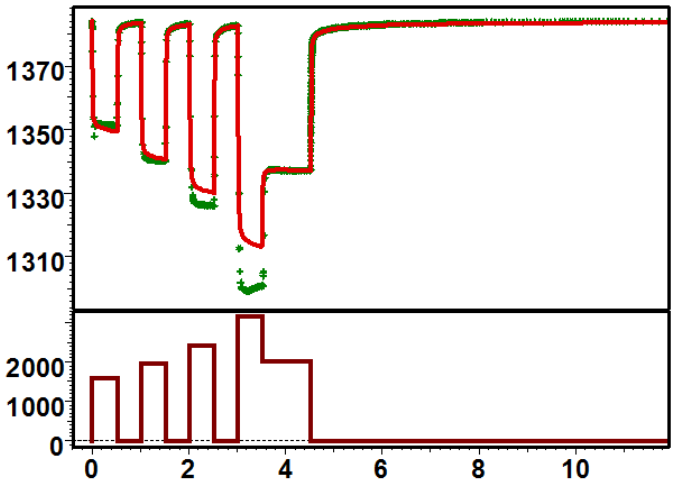


Fig. 3.J.6 – Isochronal test matched with a constant skin

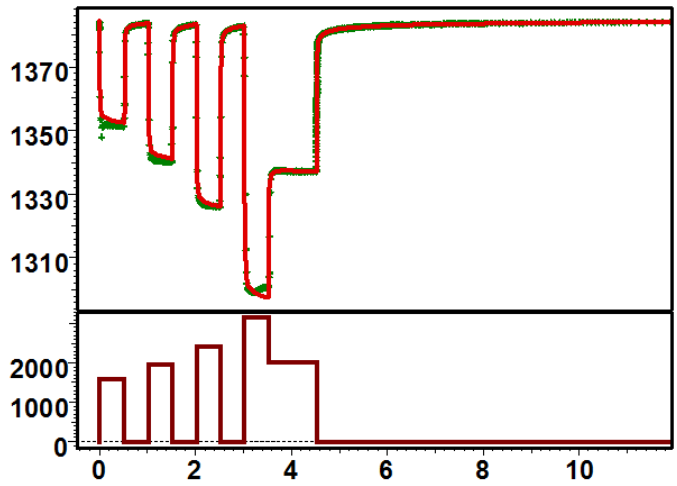


Fig. 3.J.7 – Test data matched with a rate dependant skin

3.J.4.b Simulating non-Darcy flow with a numerical model

In a numerical model the (non linear) non-Darcy flow effect is included in the flow equation through the value of the (non linear) non-Darcy flow coefficient, β which appears in the Forchheimer equation:

$$\frac{\partial P}{\partial x} = \frac{\mu}{k} \cdot u + \beta \cdot \rho \cdot u^2$$

It can be evaluated from the linear assumption described above using ds/dq with:

$$\beta \approx ds/dq \cdot \frac{2\pi r_w \cdot h \cdot \mu}{k}$$

or from an empirical equation:

$$\beta = \frac{0.005}{\left[\Phi \cdot (1 - Sw)\right]^{5.5} \cdot k^{0.5}}$$

4 – Rate Transient Analysis (RTA)

OH – DV – TB

4.A Introduction (with a short history)

Rate Transient Analysis (RTA) and PTA are both about getting pressure and rate data and do 'some kind' of analysis. They converged recently but they do not share the same history…

RTA started with the empirical observation of rate decline. In 1919 Arnold tried to establish a relation between the first year production and ultimate recovery. In 1924 Cutler published production decline responses on a linear plot.

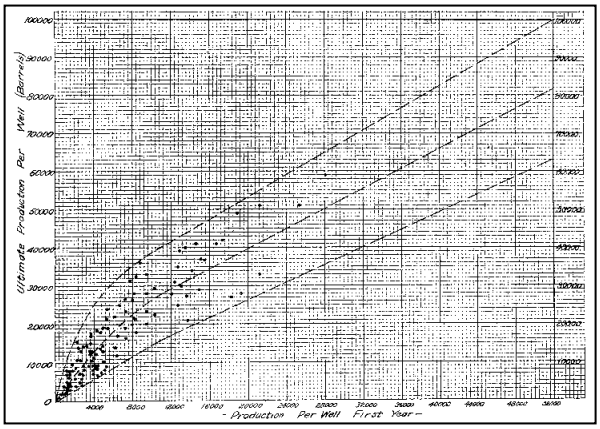


Fig. 4.A.1 – Arnold plot (1919)

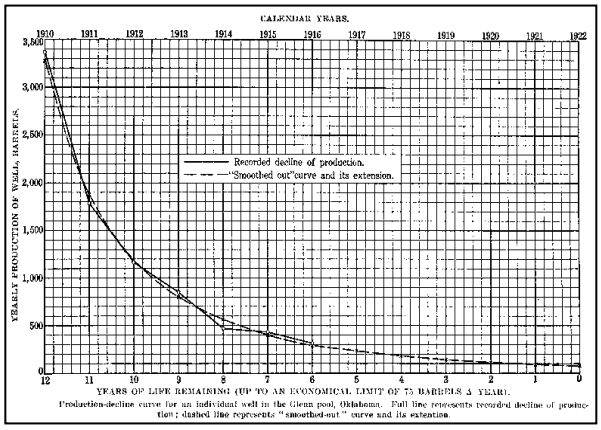


Fig. 4.A.2 – Cutler plot (1924)

In the 1940's Arps published a formulation of constant pressure production including exponential, hyperbolic and harmonic decline responses. The first loglog, well test style type-curves came with Fetkovich in the 1970's, still assuming constant flowing pressure at a time where PTA was already about superposition and convolution. Ten years later Carter extended it to the gas case.

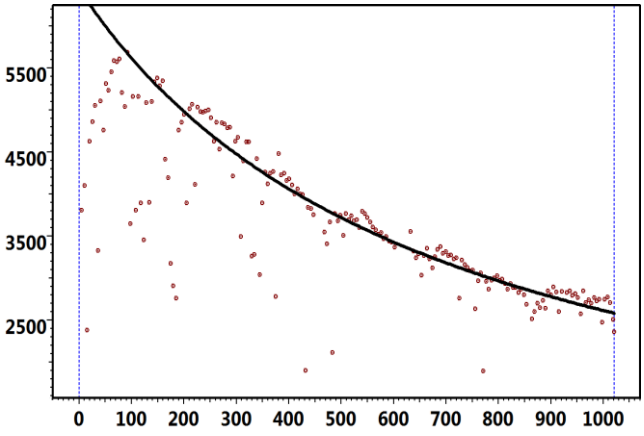


Fig. 4.A.3 – Arps plot

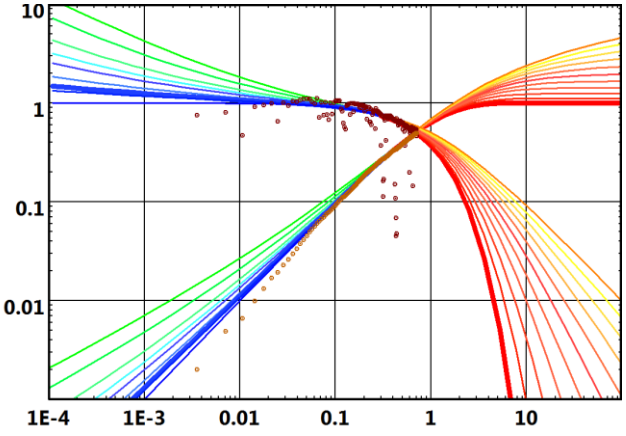


Fig. 4.A.4 – Fetkovich type curve

Other type-curves were later published to address further complex configurations including layered and fractured reservoirs. By the end of the 1970's at this stage the methodology was somewhat equivalent to the standard procedure in PTA in the late 1970s. The Arps plot was the counterpart of the Horner plot, and the constant pressure type-curves were the counterpart of the PTA constant rate type-curves.

Superposition and derivative came ten years later, shortly after the publication of the Bourdet PTA derivative. Two formulations of a loglog plot were made available. The Blasingame plot showed productivity index and derivative on the time scale, while the loglog plot showed rate normalized pressure, providing a response similar to its PTA counterpart. In both cases, on the time axis, the logarithm of elapsed shut-in time was replaced by the logarithm of the material balance time, in order to align long term Pseudo-Steady State (PSS) responses.

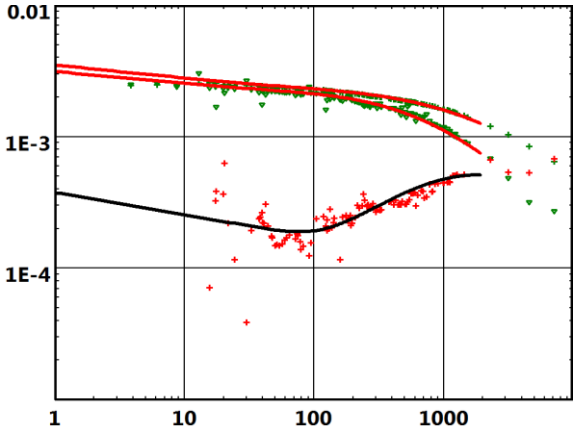


Fig. 4.A.5 – Blasingame plot: Normalized rate Pressure

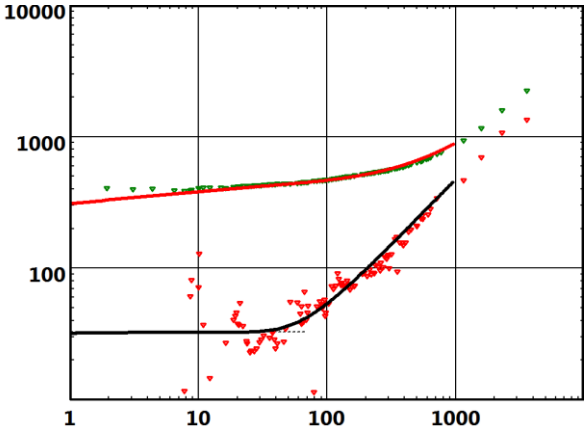


Fig. 4.A.6 – The loglog plot: Normalized pressure rate

At this stage, RTA's theory had caught up with PTA. However, while the Bourdet derivative and PC based software had an immediate and dramatic impact on day-to-day PTA, this did not happen as fast for RTA, where most work continued to be done using Arps and Fetkovich methods, generally as an annex to a production database.

The use of modern RTA methods and modern software only developed early 2000s, partly due to the development of permanent pressure gauges. When engineers started receiving long term continuous pressure data, the first reaction was to load this into a PTA program: "I have rates; I have pressures, so I treat this as a well test". However PTA methodology was not designed for this type of data. Material balance errors and over-simplifications using Perrine's approach for multiphase flow property evaluation were among the most frequently encountered errors.

Another recent factor for the development of modern RTA was the recent investments in unconventional plays, where RTA, because of the very slow and long transient responses, somehow replaced PTA as an analysis tool. In this opportunity, new Rate Decline Curves have been developed, they are presented more in detail in the Chapter 10-D.

4.B The old stuff

4.B.1 Arps

Decline Curve Analysis methods, as formalized by Arps in 1945, have been for many years the conventional technique for analysis and forecasting of well production data. Decline type-curves are based on an empirical rate-time and associated cumulative-time equation, which can be expressed in the general form:

$$q(t) = \frac{q_i}{\left[1 + bD_i t\right]^{\frac{1}{b}}} \qquad Q(t) = \frac{{q_i}^b}{D_i(1-b)}\left(q_i^{1-b} - q(t)^{1-b}\right)$$

where: q_i is the initial rate, D_i is the decline factor, and b a parameter varying between 0 and 1, defining the decline type. Three types are usually considered: hyperbolic, exponential and harmonic.

Exponential decline, $b = 0$

It can be shown that the general decline equation tends to an exponential decline when b tends to 0:

$$q(t) = q_i e^{-D_i t} \qquad Q(t) = \frac{q_i - q(t)}{D_i}$$

Harmonic decline, $b = 1$

$$q(t) = \frac{q_i}{\left[1 + D_i t\right]} \qquad Q(t) = \frac{q_i}{D_i}\ln\left(\frac{q_i}{q(t)}\right)$$

Hyperbolic decline, $b \in]0,1[$

The expressions are those above.

Decline curve equations are applicable only after the transient part of the response has ceased, i.e. during boundary dominated flow. A general approach consists in the determination of the three parameters directly, by non-linear regression. The traditional usage however, is centered on the use of some specific presentations where linearity is sought after the value of b has been fixed. Practically, the following scales / linearity can be used:

$\log(q)\ vs\ t:$ Linear plot if the decline is exponential, concave upward otherwise.

$q\ vs\ Q:$ Linear plot if the decline is exponential, concave upward otherwise.

$\log(q)\ vs\ Q:$ Linear plot if the decline is harmonic, concave downward otherwise.

Most RTA software allows the scale to be set to the above and more. The regression of the decline is non linear, i.e. it is possible to have the value of b determined from the regression rather than assuming a value of b linked to the particular scale.

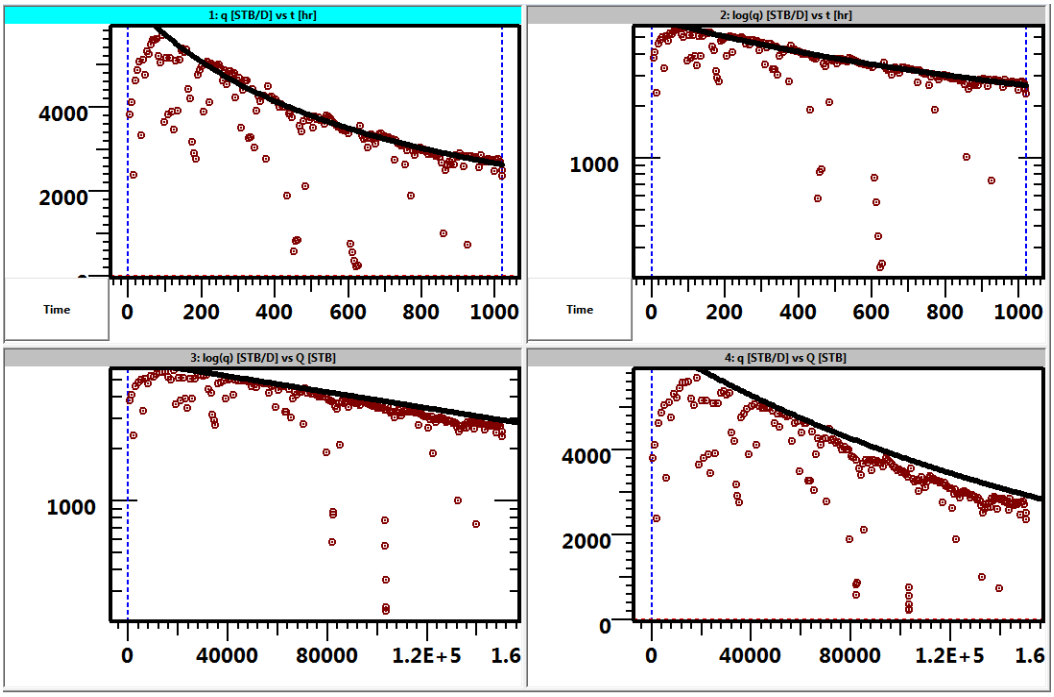


Fig. 4.B.1 – Arps

Once the decline parameters have been obtained, and since the analytical expression of the rate and cumulative are known, it is possible, from a given abandonment rate, to calculate the corresponding abandonment time, and hence the recovery at abandonment.

The abandonment rate is usually defined as either q_a or the ratio $\frac{q_a}{q_i}$.

The abandonment time is noted t_a and the recovery at abandonment $N_p(t_a)$. The figure below illustrates this extrapolation of the Arps plot.

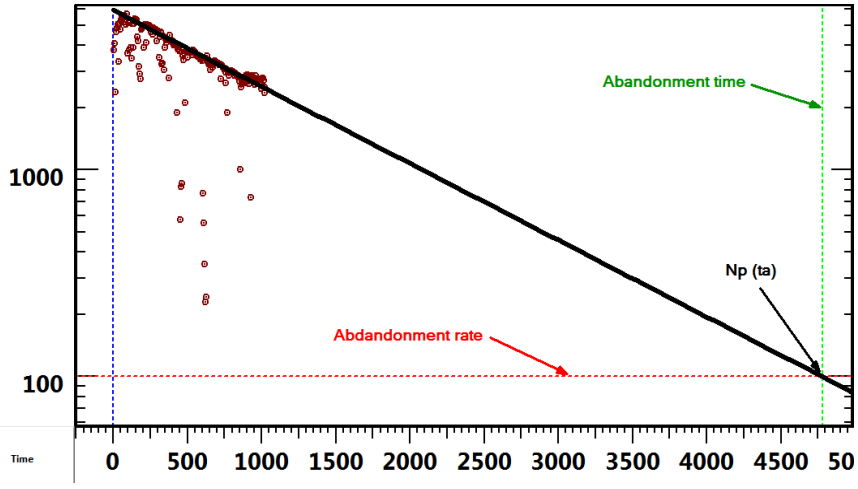


Fig. 4.B.2 – Abandonment

Exponential decline is widely used because of the simplicity of the associated graphical methods. It leads to conservative reserves estimates. Besides, it can be demonstrated that exponential decline is the late time behavior of a constant pressure production in a closed reservoir, with a slightly compressible fluid assumption.

The equation governing the PSS behaviour is:

$$\Delta p = mQ + bq$$

With $\Delta p = p_i - p_w$

Q = cumulative production

q : instantaneous production rate

and $m = \frac{1}{Nc_t}$

Differentiating the two terms of the equation with respect to the time:

$$\frac{d\Delta p}{dt} = m\frac{dQ}{dt} + b\frac{dq}{dt}$$

Under constant production well pressure conditions

$$\frac{d\Delta p}{dt} = 0 = m\frac{dQ}{dt} + b\frac{dq}{dt}$$

We have

$$\frac{dQ}{dt} = q$$

Therefore

$$\frac{dq}{dt} = -\frac{m}{b}q \text{ or } \frac{dq}{q} = -\frac{m}{b}dt$$

$$\int\frac{dq}{q} = -\frac{m}{b}\int dt \text{ or } \ln q = -\frac{m}{b}t + cst$$

$$q = \exp(-\frac{m}{b}t + cst)$$

that can be written $q = q_i \exp(-\frac{m}{b}t)$

There are many situations however, where the general hyperbolic decline is more adequate. This is the case in solution gas drive reservoirs.

In our opinion, and given the power of the non-linear regression, it is better to try and determine all three parameters, including b, systematically.

Above all, it is important to stress that decline curves have many limitations:

- The bottom-hole pressure must be fairly constant.
- The well behavior is assumed constant, e.g. no change in skin with time.
- The drainage area of the considered well is constant, i.e. the producing behavior of surrounding wells must also be stabilized.

A refinement can be made for the case where the decline in the oil rate is caused by an increase in the water cut, mostly in water drive reservoirs with unfavourable mobility ratio. If one replaces the oil rate by the oil cut, f_o the Arps equation can be used for wells with variable gross production. The same plots can be made and extrapolated: $\log(f_o)$ vs t, f_o vs Q and $\log(f_o)$ vs Q.

4.B.2 Fetkovich

In 1980, Fetkovich introduced a type-curve combining the theoretical response of a well in a closed reservoir, and the standard Arps decline curves. The motivation behind this work was to come up with a loglog matching technique applicable to both the transient part of the data and the boundary dominated flow period. By presenting both periods, the Type-Curve would avoid incorrectly matching transient data on decline curves.

A determining preliminary step was that the exponential decline can be shown to be the long-term solution of the constant pressure case. The Fetkovich type-curve is derived assuming a slightly compressible fluid and constant flowing pressure. Extension to gas can be made with the appropriate dimensionless rate expression, as described below. The original type-curve presented by Fetkovich displayed rate only. A composite presentation including the cumulative was later introduced to bring more confidence in the matching process and to reduce the effect of the noise.

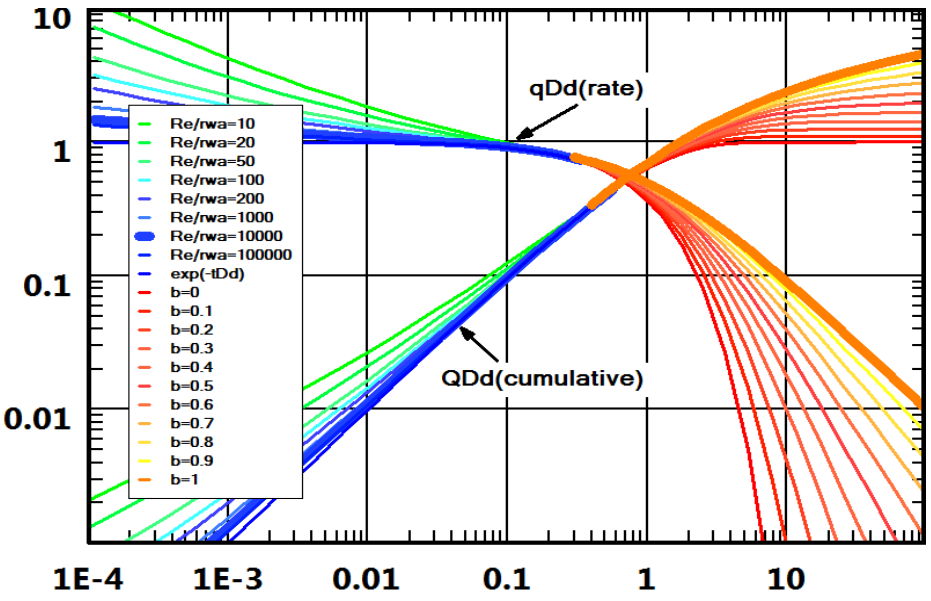


Fig. 4.B.3 – Fetkovich type curve

In the above figure the left region of the curves (green to blue) corresponds to the transient part of the response. On the right hand side, are the Arps decline curves (red to yellow). Note the legend on the left: the red Arps curve is for an exponential decline (b=0), the last yellow curve is for a harmonic decline (b=1).

The Fetkovich type-curve displays dimensionless values q_{Dd}, Q_{Dd} versus t_{Dd} as defined below. The dimensionless variables can be expressed in terms of the Arps decline curve parameters, or in terms of the transient response parameters. The duality is due to the composite nature of the type-curve showing once again a merge of a theoretical closed reservoir response, and the empirical Arps stems.

All the following equations are in Oil Field Units.

Time

Decline curve dimensionless time: $t_{Dd} = D_i t$

Dimensionless time: $t_D = 0.0002637 \frac{k}{\Phi \mu c_t r_w^2} \Delta t$

Related by: $t_{Dd} = \frac{t_D}{\frac{1}{2}\left[\left(\frac{r_e}{r_w}\right)^2 - 1\right]\left[\ln\left(\frac{r_e}{r_w}\right) - \frac{1}{2}\right]}$

Rate

Decline curve dimensionless rate: $q_{Dd} = \frac{q(t)}{q_i}$

Dimensionless flow rate, oil: $q_D \ \ oil = \frac{141.2 q(t) \mu B}{kh\left(p_i - p_w\right)}$

And the equivalent expression for gas is:

$$q_D \ \ gas = \frac{50300 T q(t) p_{sc}}{T_{sc} kh\left(m\left(p_i\right) - m\left(p_w\right)\right)} \text{ ; with } m(p) = \int_0^p \frac{2pdp}{\mu Z}$$

q_{Dd} and q_D are related by: $q_{Dd} = q_D\left[\ln\left(\frac{r_e}{rw}\right) - \frac{1}{2}\right]$

Cumulative production

Decline curve dimensionless cumulative: $Q_{Dd} = \frac{Q(t)}{Npi}$

Where N_{pi} defines the ultimate recovery.

A match will bring values of r_e and kh, D_i and q_i. The type of decline, b is not linked to any of the match ratios, obtained by selecting the correct type-curve. From the external boundary distance, the reservoir pore volume can be calculated. From the Arps parameters, the future performance can be forecast; N_{pi} can be calculated as well as N_p for any specified abandonment rate.

4.B.3 Gas material balance $\overline{P}/Z$ vs Q plot

In case of dry gas reservoir a classical method can also be applied, using the $\overline{P}/Z$ vs Q plot. The method assumes to get several reliable static average pressure values in the well history.

The method is based on the simple material balance equation:

$$Gi = \frac{QB_g}{B_g - B_{gi}}$$

Where Gi is the gas initially in place and Q the cumulative gas production.

Estimating the Bg by:

$$B_g = \frac{0.00504\,TZ}{\overline{P}}$$

The equation becomes:

$$\frac{\overline{P}}{Z} = \left(-\frac{P_i}{GZ_i}\right)Q + \frac{P_i}{Z_i}$$

This equation indicates that a plot of $\frac{\overline{P}}{Z}$ versus Q extrapolates to the gas initially in place Gi.

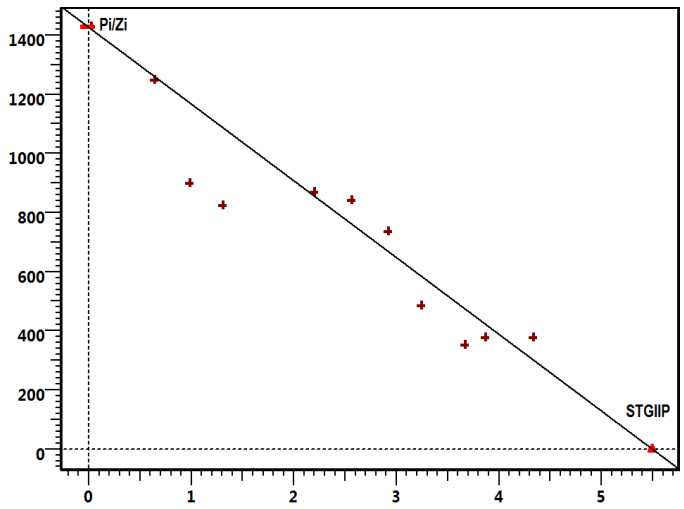


Fig. 4.B.4 – $\overline{P}/Z$ vs Q plot

The validity and the accuracy of this method depend directly on the validity of the static pressure and of the PVT parameters.

4.C The right stuff

4.C.1 Blasingame plot

Previous sections have described the conventional Decline Curve Analysis methods, and their extension using Fetkovich type-curves. We recall that the latter were obtained by combining a theoretical model response and the empirical decline stems of Arps.

Broadly speaking, one could say that the introduction of type-curve matching techniques in production analysis has opened the way to applying methods developed for well test interpretation to the analysis of production data. The main limitation in the Fetkovich type-curve is the assumption of constant flowing pressure. Blasingame and McCray noted that using a pressure normalized flow rate when the bottom-hole pressure varies significantly did not remedy the problem. They sought functions that would transform the variable pressures/variable rates solution into an equivalent constant pressure or constant rate solution. They introduced two specific time functions, t_{cr} the constant rate time analogy, and t_{cp} for constant pressure. For the liquid case, the constant rate analogy time function is defined as the ratio of the cumulative and the flow rate:

$$t_{cr} = \frac{Q(t)}{q(t)}$$

When the normalized rate $\frac{q(t)}{p_i - p_w(t)}$ is plotted versus this function on a loglog scale, the boundary dominated flow period follows a negative unit slope line:

The Black Oil Pseudo Steady State flow rate equation is:

$$\frac{q_o}{\Delta p} = \frac{1}{b_{o,pss} + m_{o,pss}\bar{t}}$$

With:

$$m_{o,pss} = \frac{1}{Nc_t}\frac{B_o}{B_{oi}} \quad ;$$

$$b_{o,pss} = 141.2\frac{\mu_o B_o}{kh}\left[\frac{1}{2}\ln\left[\frac{4}{e^{\gamma}}\frac{1}{C_A}\frac{A}{r_w^2}\right] + s\right];$$

and

$$\bar{t} = \frac{N_p}{q_o}$$

When the Pseudo Steady States dominates $\frac{q_o}{\Delta p}$ is function of $\bar{t}$ at exponent (-1).

Therefore a loglog plot of $\frac{q_o}{\Delta p}$ vs $\bar{t}$ will show a negative unit slope straight line.

Note: Periods of very low rates give artificially high values of $\bar{t} = \frac{N_p}{q_o}$ then the equation $\frac{q_o}{\Delta p} = \frac{1}{b_{o,pss} + m_{o,pss}\bar{t}}$ tends to $\frac{q_o}{\Delta p} = \frac{1}{m_{o,pss}\bar{t}}$ the points are found on the same -1 unit slope straight line.

Based on this result, Palacio and Blasingame introduced type-curves that could be used for variable flowing pressure conditions. In order to improve the type-curve analysis the Bourdet derivative was also considered. However, due to the noise inherent to the production data, the derivative was not applied to the normalized flow itself but to its integral. More precisely, the Palacio-Blasingame type-curve plot shows the following:

Normalized rate:

$$PI(t) = \frac{q(t)}{p_i - p_w(t)}$$

Normalized rate integral:

$$PI\ Int. = \frac{1}{t_e}\int_0^{t_e} PI(\tau)d\tau = \frac{1}{t_e}\int_0^{t_e} \frac{q(\tau)}{p_i - p_w(\tau)}d\tau$$

Normalized rate integral derivative:

$$PI\ Int.Derivative = \frac{\partial(PI_{Int})}{\partial \ln(t_e)}$$

All three curves are plotted against t_e on a loglog scale:

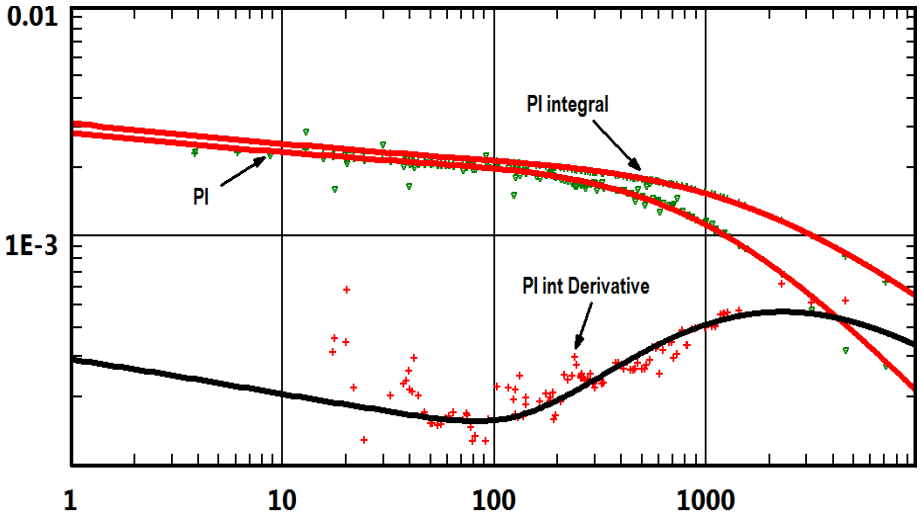


Fig. 4.C.1 – Blasingame plot

The traditional method of using this presentation is in conjunction with type-curves for a particular well model (see figure below).

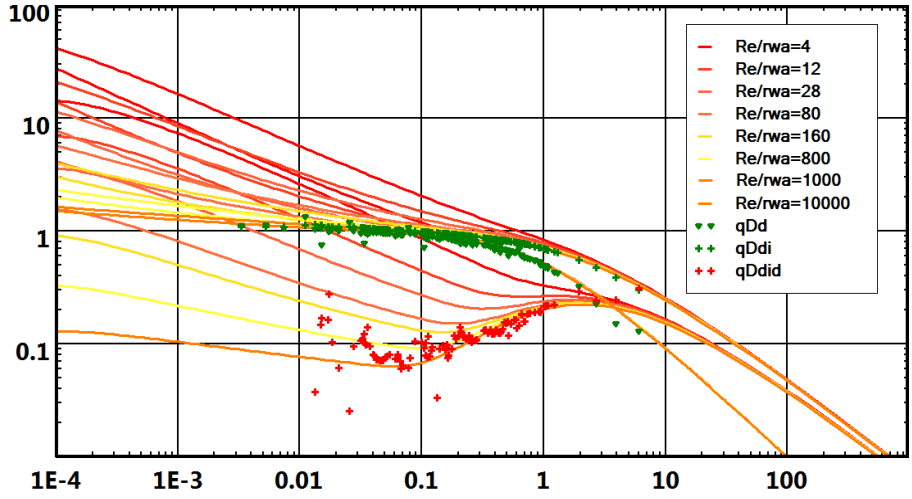


Fig. 4.C.2 – Blasingame type curve

This plot is used as a diagnostic tool, where the data and a model response are compared. The model can be any model, analytical or numerical, single or multi-well, etc. One can either display the 'true' model response, i.e. the response to the full pressure history, or the response to a single pressure step. The single step response shows the signature of the model in a clear, and usable form, whereas the response to the real history is usually very erratic, because the equivalent time is jumping back and forth in time.

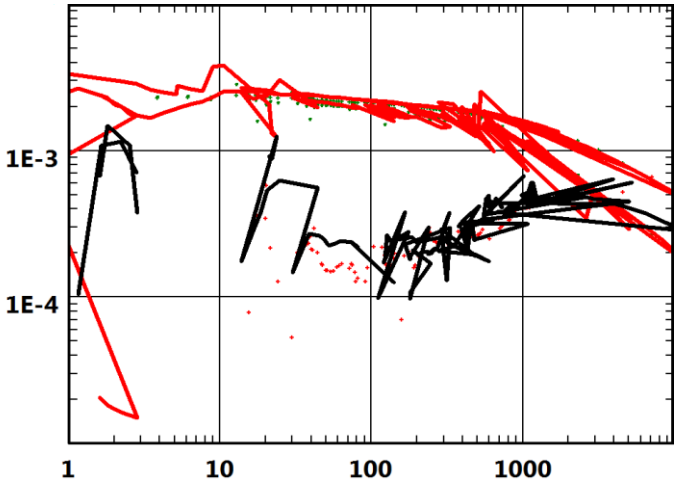


Fig. 4.C.3 – Blasingame plot with 'true' model response

4.C.2 Loglog plot

By replacing the time with an equivalent time, defined as the ratio of the cumulative to the flow rate, one can transform a variable flowing pressure test into a constant rate equivalent, at least for a liquid case. The parallel with constant rate solution can be taken one step further if, rather than working with a pressure-normalized rate, we work with rate-normalized pressure.

In other words for the liquid case, if we plot $\frac{p_i - p_w(t)}{q(t)}$ versus $t_e = \frac{Q(t)}{q(t)}$ on a loglog scale the boundary dominated flow will exhibit a unit slope line, similar to pseudo-steady state in Pressure Transient Analysis. Furthermore, if we take the derivative of the normalized pressure with respect to the logarithm of t_e, the transient part will exhibit a stabilization at a level linked to the mobility.

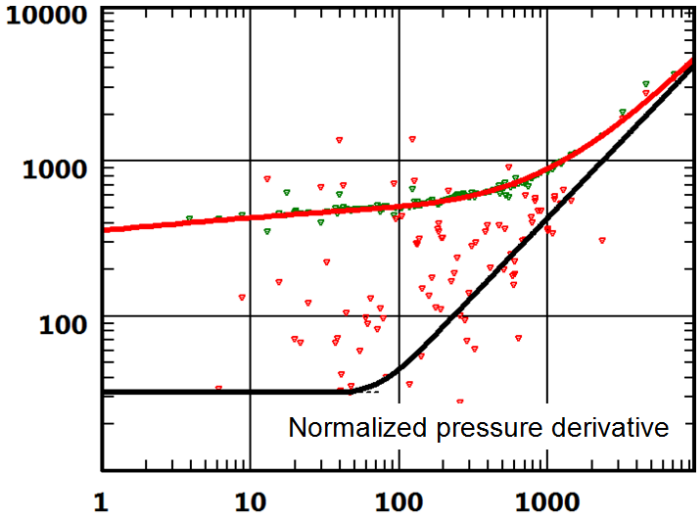


Fig. 4.C.4 – Loglog plot with normalized pressure derivative

The similarity with PTA is thus complete. Yet, the noise level on the derivative is usually too high, see the figure above. One workaround is to work with a normalized pressure integral, in a manner analogous to what was done on the Palacio-Blasingame type-curves.

Integral of normalized pressure: $$I(t_e) = \frac{1}{t_e}\int_o^{t_e} \frac{p_i - p_w(\tau)}{q(\tau)} d\tau$$

Bourdet derivative of the Integral of normalized pressure: $$I'(t_e) = \frac{\partial I(t_e)}{\partial \ln(t_e)}$$

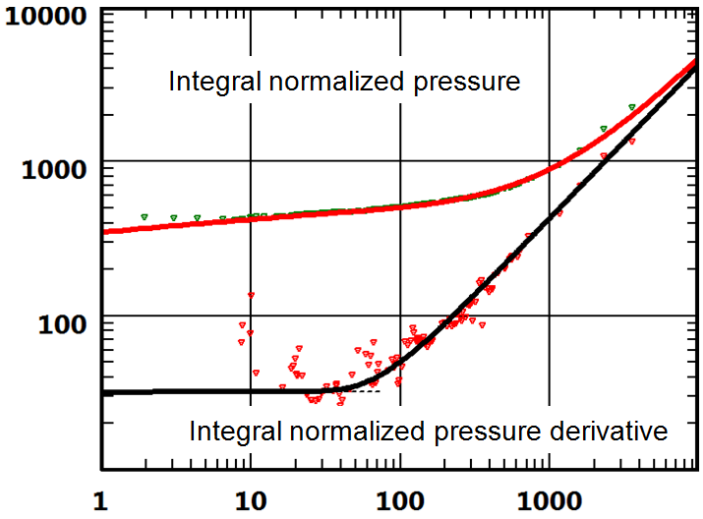


Fig. 4.C.5 – Loglog plot, integral of normalized pressure and derivative

Using the integral preserves the signature of the flow regimes while significantly reducing the noise. Hence such definitions provide a diagnostic tool where most of the usual well test methods can be used. In particular, it is clearly possible to get an estimate of the reservoir kh from the derivative stabilization level. The kh being known, one can then get a first estimate of the reservoir size from the unit slope late time trend. These calculations are an integral part of the loglog plot. It is possible to either display the 'true' model response, i.e. the response to the full pressure history, or the response to a single pressure step. The single step response, used in all the figures above, shows the signature of the model in a clear and usable whereas the response to the real history is usually very erratic, because the equivalent time is jumping back and forth in time as illustrated in the figure below.

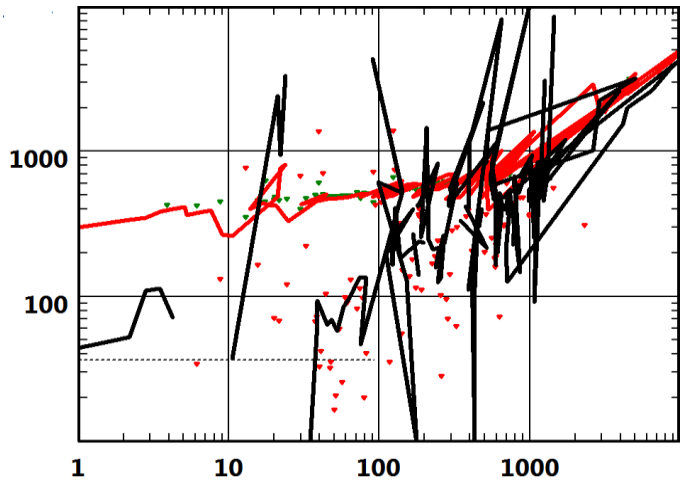


Fig. 4.C.6 – Loglog plot with 'true' model response

4.C.3 Material balance (Normalized rate-cumulative) plot

Agarwal et al. presented a Cartesian plot of dimensionless rate q_D versus dimensionless cumulative Q_{DA}.

They show that the responses corresponding to distinct reservoir sizes all exhibit a straight line with a negative slope during boundary dominated flow, and all curves converge to the same value on the X axis, equal to $1/2\pi$. In other words, the following relation is established in all cases during boundary dominated flow:

$$q_D = \frac{1}{2\pi} - Q_{DA}$$

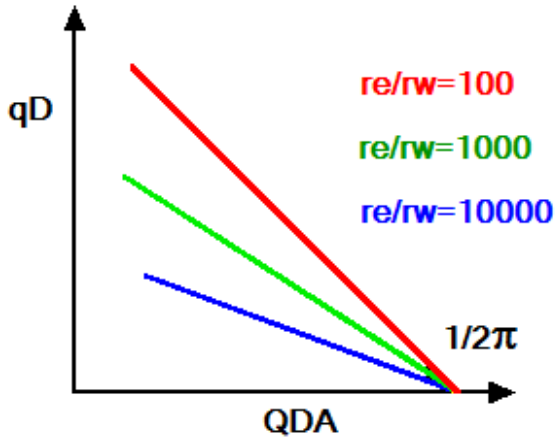


Fig. 4.C.7 – Agarwal et al plot

The expression of the dimensionless variables varies depending of the fluid type and a specific treatment must be applied in each case.

Oil

For an oil case, the expression of the dimensionless parameters is defined below:

$$q_D = \frac{141.2qB\mu}{kh(p_i - pw)} \quad \text{and} \quad Q_{DA} = \frac{0.8936QB}{\phi hAc_t(p_i - p_w)}$$

All equations are in Oil Field units.

The dimensionless cumulative production can be expressed in terms of the fluid in place, in STB/D:

$$N = \frac{\phi hA}{5.615B}$$

$$Q_{DA} = \frac{0.8936Q}{5.615Nc_t(p_i - p_w)} = \frac{Q}{2\pi Nc_t(p_i - p_w)}$$

So the linear relationship between dimensionless rate and cumulative becomes:

$$\frac{141.2qB\mu}{kh(p_i - pw)} = \frac{1}{2\pi} - \frac{0.8936QB}{5.615Nc_t(p_i - p_w)}$$

Using the full definition of the dimensionless variables requires an a priori estimate of PV, basically what we are after. Therefore the method presented by Agarwal-Gardner is iterative. However we see from the above equation that if we plot $\frac{q}{p_i - p_w}$ versus $\frac{Q}{c_t(p_i - p_w)}$ boundary dominated flow will exhibit a straight line which intercept with the X axis gives directly N.

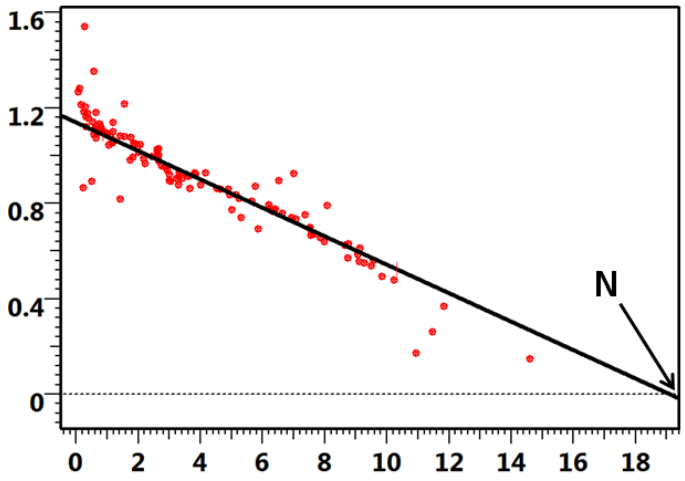


Fig. 4.C.8 – Material balance plot

Note: In the case of constant flowing pressure, it is interesting to draw a parallel between this rate cumulative plot and the rate cumulative plot used in traditional decline curve analysis. The traditional decline methods yield a maximum recovery rather than fluid in place. The relation between the two methods is established by considering a recovery factor of RF= $c_t(p_i - p_w)$.

4.C.4 Flowing gas material balance plot

The principle is to get from flowing data a plot that resembles a normal P/Z plot made in terms of reservoir average pressure. As always the problem with this kind of analysis is that one needs the results sought to build the plot, leading to an iterative procedure.

The Material Balance equation in gas in terms of pseudo pressure is written:

$$m(\bar{p})_n = m(p_i)_n - \frac{G_{pn}}{G_i c_{t1}}$$

Where the normalized pseudo pressure and equivalent time functions are defined as:

$$m_n(p_i) = \frac{\mu_i z_i}{2 p_i} \int_{p_{base}}^{p} \frac{2p}{\mu\, z}\, dp$$

and

$$G_{pn} = \left(\mu_g c_t\right)_i \int_0^{G_p} \frac{1}{\overline{\mu}_g \overline{c}_t} dG_p$$

The P.S.S equation is:

$$m(\overline{p})_n - m(p_{wf})_n = b_{a_pss} q_g \qquad \text{eq(1)}$$

Where:

$$b_{a_pss} = \frac{b_{pss}}{m\left(P_{ref}\right)}$$

Combining P.S.S. and Material Balance equations:

$$\frac{m(p_i)_n - m(p_{wf})_n}{q_g} = \frac{1}{c_{ti} G_i} \left[\frac{1}{q_g} \left(\mu_g c_t\right)_i \int_0^{G_p} \frac{1}{\overline{\mu}_g \overline{c}_t} dG_p \right] + b_{a_pss}$$

If we define the pseudo material balance time:

$$t_{ca} = \frac{1}{q_g} \left(\mu_g c_t\right)_i \int_0^{G_p} \frac{1}{\overline{\mu}_g \overline{c}_t} dG_p$$

Using the equality derived from the P.S.S. equation:

$$t_a = \frac{\mu_i c_t^i}{q(t)} \frac{Z_i G_i}{2 p_i} \left[m(p_i) - m(\overline{p}) \right]$$

equation (1) can be changed to give:

$$\frac{m(p_i)_n - m(p_{wf})_n}{q_g} = \frac{t_{ca}}{c_{ti} G_i} + b_{a_pss} \qquad \text{eq(2)}$$

The principle of the flowing material balance method is:

Create a plot of $\frac{m_n(p_i) - m_n(\overline{p})}{q_{(t)}}$ versus t_a

As the system goes into pseudo steady state flow, the points will converge towards a straight line: the intercept at ta = 0 hrs is b.

Having b:

1. The equation (1) is used to calculate $\overline{p}$ from pw, b, and q(t).
2. $\overline{p}/Z$ is plotted versus Q:

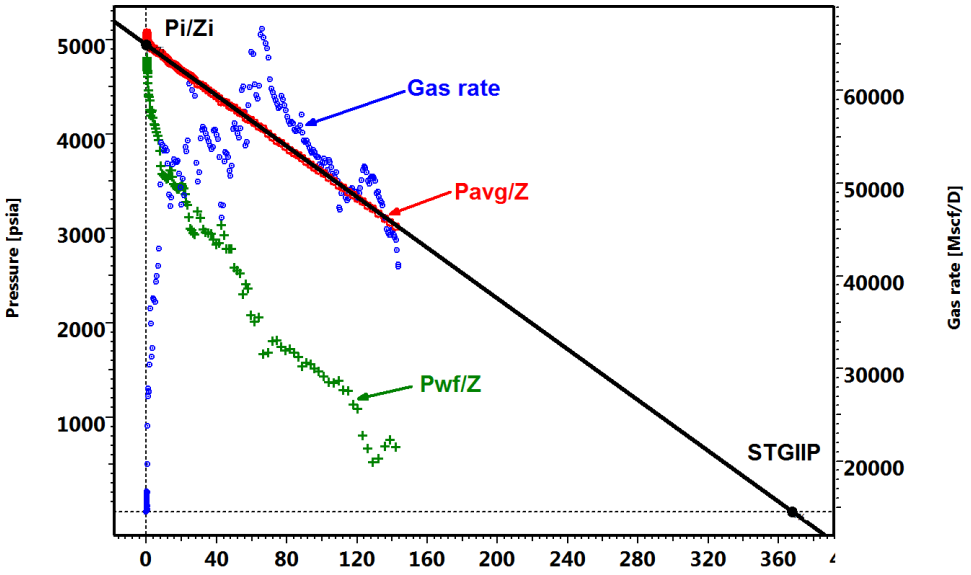


Fig. 4.C.9 – $\overline{p}/Z$ versus Q plot

3. A straight line is drawn through the Pavg/Z and extrapolated to get Gi.

Only problem is that the time function used by the first plot, *ta* involves the reservoir average pressure hence it requires an estimate of the reserves.

In this Topaze example, the complete procedure follows:

(1) Estimate Gi beforehand.

(2) By selecting a time range where the system is believed to be in pseudo steady state, the software performs an automatic regression to determine b using equation (1) and the method defined above.

(3) Then the straight line method will be applied in the plot $\overline{p}/Z$ versus Q, Pi/Zi can be input to find Gi (STGIIP).

Like most of the methods extrapolating a behavior the constraint is that the well status and production conditions must be constant in the interval used for the analysis.

4.C.5 P-Q diagnostic plot

The two methods presented above require selecting data set during the P.S.S. flow period.

Kabir et al. presented a cartesian plot of P vs q which provides a simple way to perform a diagnosis.

The life of a production well can be divided in three type of behavior:

1. The infinite acting radial flow
2. A period during which the production is maintained and imposed by the completion.
3. The Pseudo Steady State, when the well behavior is boundary dominated.

During the P.S.S. it is demonstrated that the slope dp/dq is governed by the equation:

$$\frac{dp_{wf}}{dq} = \frac{0.2339Bq}{\Phi h c_t A} \Big/ \frac{dq}{dt}$$

In a closed system, the rate has an exponential decline, therefore, the slope dp/dq will be constant and function of the drained volume.

A typical P vs Q plot behaviour would be:

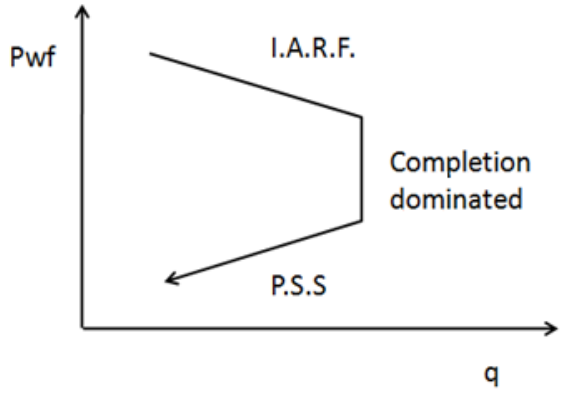


Fig. 4.C.10 – Typical P vs Q plot

That allows diagnosing the various behaviour types on a p vs q plot of any well field data:

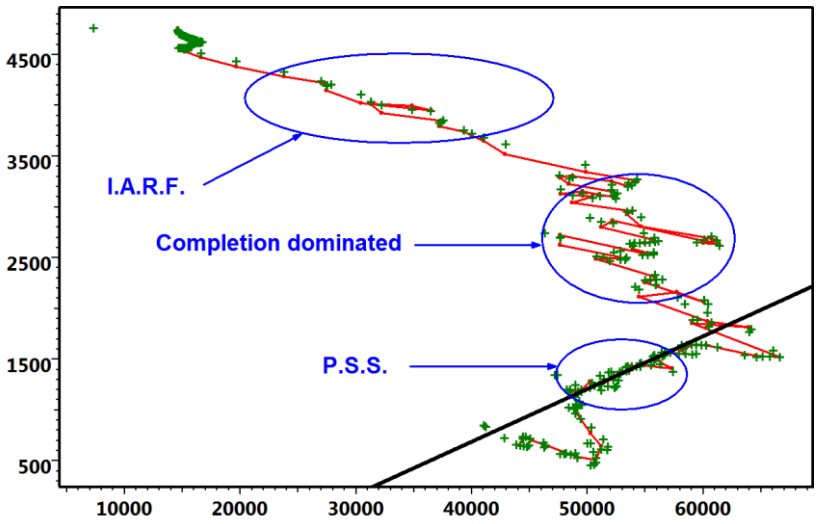


Fig. 4.C.11 – Field example P vs Q plot

Then, the adequate subset of points can be selected to be used in the corresponding methods. It also allows comparing the behaviours from wells to wells in order to detect a possible compartmentalization: if the plot exhibits two different slopes in the P.S.S., that tends to demonstrate that they are depleting two different compartments.

4.C.6 History plot

For complex cases and noisy data where no specific behavior is seen on these diagnostic plots, the linear plot of pressure and rates vs. time becomes the main tool. There is no real diagnostic, just an optimization process. Under these conditions, it is not realistic to expect to estimate more than a productivity index, mobility and a drainage area. In the absence of any other information, the simplest analytical solution, homogeneous circular reservoir, will usually be suitable to model the well drainage area. The use of more complex models can be acceptable if complementary information is available from other sources, and the number of parameters allowed to change in the optimization process is reduced to a minimum.

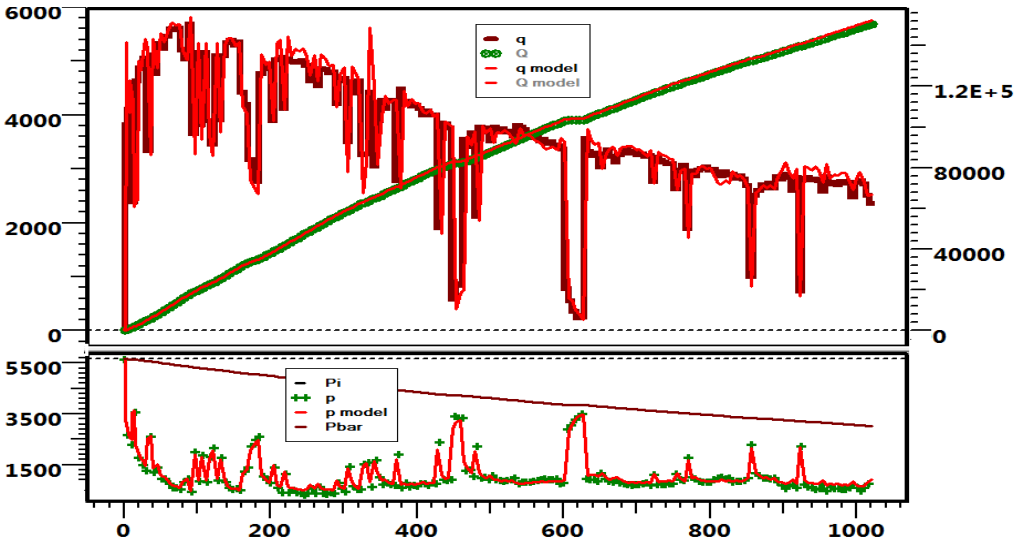


Fig. 4.C.12 – Production history match

4.D The case of dry gas

In this paragraph we present the way the methods created for oil production analysis are modified and adapted to take into account the gas properties specificity.

The original methods specific to gas (and only to gas) production analysis are directly presented in the chapters 'Old Stuff' and 'Right Stuff'.

4.D.1 Diffusion of real dry gas

As mentioned in the 'Theory' chapter, in order to extend the methodology of Dynamic Data Analysis to gas cases, we introduce a function of the pressure called the pseudopressure. It is given by:

Gas pseudopressure: $$m(p) = 2\int_0^p \frac{p}{\mu Z} dp$$

Using the gas pseudo pressure instead of the pressure, the diffusion equation remains valid the same methodology presented above can apply.

In addition to these methods, the gas case presents few particularities presented here.

4.D.2 The old Stuff

4.D.2.a Fetkovich

It is worth noting that specific methods or extensions have been studied for gas production, such as the Carter type-curve. When using the Fetkovich type curve with gas, the expression of the rate match is modified to use the pseudo pressure m(p), in a similar manner to what is done in Pressure Transient Analysis. In addition, Fraim and Wattenbarger suggested the use of a normalized time rather than time itself, with the following definition:

$$t_n = \int_0^t \frac{(\mu c_t)_i}{\mu(\bar{p}) c_t(\bar{p})} dt$$

The gas diffusion equation can then be re-written in terms of pseudo pressure m(p):

$$\frac{\partial m(p)}{\partial t} = 0.0002637 \frac{k}{\Phi \mu c_t} \nabla^2 m(p)$$

When the pressure varies significantly, the term μc_t and therefore the diffusion term varies. If we introduce the pseudotime:

$t_n(t) = \int_0^t I(p_{wf}(\tau)) d\tau$ where $I(p) = \frac{(\mu c_t)_i}{\mu(\bar{p}) c_t(\bar{p})}$

The diffusion equation becomes: $\frac{\partial m(p)}{\partial t_n} = 0.0002637 \frac{k}{\Phi(\mu c_t)i} \nabla^2 m(p)$

Note: the use of the normalised pseudo time requires the knowledge of the average pressure at each step, that makes its use difficult.

They demonstrated that the real gas constant pressure solution, when plotted using normalized time, exhibits a boundary-dominated period that matches the exponential decline. The major drawback however, is that the normalized time expression requires an a priori knowledge of the average pressure, hence of the reserves. The method is thus iterative in nature.

Note: if the normalized time is not used a gas response in depletion mode will not necessarily follow the exponential decline.

Using Fetkovich type-curves

It is important to remember that the Fetkovich type-curve is based, for the depletion part, on the Arps decline curves. Like the decline curves it suffers some limitations:

- It is assumed that the bottom-hole pressure is fairly constant. Fetkovich suggests that if the pressure is smooth, and uniformly decreasing, one could use a Δp normalized rate.
- The well behavior is assumed constant, e.g. no change in skin with time.

The drainage area of the considered well is constant, i.e. the producing behavior of surrounding wells must also be stabilized.

4.D.2.b Gas material balance $\overline{P}/Z$ vs Q plot

This method is specific to gas. It is not an 'adapted' oil method to gas, it is presented in the chapter 'The old stuff'.

4.D.3 The right stuff

4.D.3.a Blasingame plot

The cornerstone of the Blasingame plot is the linearity between the normalized rate $\frac{q(t)}{p_i - p_w(t)}$ and $\frac{1}{t_e}$ during boundary dominated flow. This relation, valid for a slightly compressible fluid, does not apply to gas unless the rate is normalized with respect to $\Delta m(p)$ and the time is modified as follows:

$$\bar{t}_{egas} = \frac{\mu_{gi} c_{ti}}{q_g(0)} \int_0^t \frac{q_g(t)}{\mu_g(\bar{p}) c_t(\bar{p})} dt$$

In the PSS oil flow rate equation $\frac{q_o}{\Delta p} = \frac{1}{b_{o,pss} + m_{o,pss}\bar{t}}$, the slope $m_{o,pss}$ is a function of the fluid compressibility, which is highly pressure dependent in gas cases.

The objective is to keep the linearity and the PSS flow rate equation for gas in the same shape as for oil:

$$\frac{q_g}{\Delta p_p} = \frac{1}{b_{g,pss} + m_{g,pss}\bar{t}_{egas}}$$ with a constant slope $m_{g,pss}$

We take the varying viscosity and compressibility into account by introducing the 'pseudo' pressure and 'pseudo' normalized time:

$$p_p = \frac{\mu_{gi} z_i}{p_i} \int_{p_{base}}^{p} \frac{p}{\mu_g z} dp$$

$$\bar{t}_{egas} = \frac{\mu_{gi} c_{ti}}{q_g(t)} \int_0^t \frac{q_g(t)}{\mu_g(\bar{p}) c_t(\bar{p})} dt$$

The slope is then: $$m_{g,pss} = \frac{1}{G c_t}$$

The intersect becomes:

$$b_{g,pss} = 141.2 \frac{\mu_{gi} B_{gi}}{kh} \left[\frac{1}{2} \ln \left[\frac{4}{e^{\gamma}} \frac{1}{C_A} \frac{A}{r_w^2} \right] + s \right]$$

The consequence of not using this time function is that the linearities expected during the various flow regimes may be distorted.

It is not necessary in the Blasingame plot since this plot only provides a basis for comparing the data and a model response calculated for the particular case. Handling the non linearities is the model responsibility, not that of the plot. If the model is representative, the model and the data will be consistent. So it does not matter whether such or such period exhibits a linearity or not.

This is different when using a type curve as the type curve embeds modelling assumptions. That is why this time function is used in Topaze in the match with the Blasingame type curve.

4.D.3.b Loglog plot

The linearities expected during the various flow regimes may be distorted when the diffusion does not follow a linear equation, with gas or in multiphase cases, it is important to realize that the loglog plot, like the Blasingame plot, only provides a basis for comparing the data and a model response. Handling the non-linearities is the model responsibility, not that of the plot. If the model is representative, the model and the data will be consistent. It does not really matter whether such or such period exhibits linearity or not. When using a type-curve this is different as the type-curve embeds modelling assumptions.

4.D.3.c Material balance (Normalized rate-cumulative) plot

The boundary dominated flow obeys the same equation:

$$q_D = \frac{1}{2\pi} - Q_{DA}$$

Provided that the dimensionless rate and cumulative production be defined as:

$$q_D = \frac{1422.T.q}{kh\left(m(p_i) - m(p_w)\right)} \quad \text{and} \qquad Q_{DA} = \frac{4.50.T.z_i.G_i.\left[m(p_i) - m(\bar{p})\right]}{\phi hA.p_i.\left[m(p_i) - m(p_w)\right]}$$

All equations are in Oil Field units.

Unlike the oil case, we cannot find a simple expression of a normalized cumulative that is independent of the fluid in place. This is because the gas in place is involved in a non-linear fashion in the expression of the dimensionless cumulative. However by extension with the previous method for oil we can choose to plot:

$$\frac{q}{m(p_i) - m(p_w)} \quad \text{versus} \quad Q_{DA} = \frac{G_i.\left[m(p_i) - m(\bar{p})\right]}{\left[m(p_i) - m(p_w)\right]}$$

The value of 'X' at the intercept is:

$$\frac{G_i.\left[m(p_i) - m(\bar{p})\right]}{\left[m(p_i) - m(p_w)\right]} @\ Intercept = \frac{\phi.h.A.p_i}{4.50.2.\pi.T.z_i} = \frac{PV.p_i}{4.50.2\pi.T.z_i} = \frac{PV.p_{i.}.p_{sc}.T}{4.50.2\pi.T.B_{gi}.Tsc.p_i} = \frac{PV}{B_{gi}} = Gi$$

Note: the X-axis value $Q_{DA} = \frac{G_i.\left[m(p_i) - m(\bar{p})\right]}{\left[m(p_i) - m(p_w)\right]}$ depends on the gas in place *Gi* value, therefore a change in the straight line coefficients changes the intersect therefore the abscissa of the data, in other word moving the straight line will move the data points through which we draw it, it becomes an iterative process that converges easily.

4.D.3.d Flowing gas material balance plot and P-Q diagnostic plot

Like the P/Z vs q plot, these methods, specific to gas, and not 'adapted' oil analyses methods, are presented in the chapter 'The right stuff'.

4.D.4 General major gas issues

4.D.4.a Correcting the pressure to sandface

Usually the pressure gauge is not set at the sandface due to mechanical constraints in the completion. Because of this, the results obtained from the pressure transient analysis are at the level of the gauge and not the sandface which, in terms of pressure (Pi) and skin (S), will not reflect the true sandface conditions.

It is necessary first to define the vertical pressure profile in the well. The Saphir/Topaze internal flow correlations or an actual lift curve generated by a specialized program (Amethyste) can be used for this.

The available correlation for gas, in Topaze, is an external lift curve or the internal Cullender & Smith method, but with two modifications for handling water and condensate.

The correlation is based on the gas properties as defined in the PVT setup, and a general friction factor is calculated using the Colebrook and White equation. Note that when you deal with a condensate case with equivalent gas gravity and total rates, the proper gradient and rates are used in the correlation to account for the condensate presence. The presence of water can be accounted for, based on a constant water to gas production ratio.

The solution selected in Topaze is to include both the hydrostatic and friction pressure loss in the model and correct the measured pressure to the sandface depth.

An important consequence is that the dependent skin attributed to the formation can be a lot smaller because a large part is now attributed to the pressure loss through.

4.D.4.b Gas material balance correction

The Rate Transient Analysis is performed on large duration data set and the material balance in gas diffusion is a critical issue.

The diffusion equation can be considered linear for as long as the diffusion terms left outside the time and pressure variables remain constant. Diffusion equation:

$$\frac{\partial m(p)}{\partial t} = 0.0002637 \frac{k}{\Phi \mu c_t} \nabla^2 m(p)$$

As soon as we have a pressure gradient in the reservoir, the diffusion term, and especially the product μc_t, will become different from one reservoir block to the next.

If we look at a real gas simulation for a long term production survey and use it to match with an analytical model where the diffusion was taken at initial pressure, we can see a divergence between the simulated pressure and the measured data, even though the reservoir geometries and the PVT used are strictly the same.

There are two ways to handle this problem in Rate Transient Analysis.

Integrating the material balance correction in an analytical model

The model includes a reservoir size and an initial pressure. So the initial gas in place can be calculated as an integral part of the model. At any time step the algorithm calculates the average pressure from the cumulative production using p/Z, and replaces the viscosity and total compressibility in the superposition by the one coming from the average pressure. So at any time step the simulated pressure is coherent with the material balance of the model. The optional derivation is shown as follows:

We consider the total gas in place at initial pressure. V_{res} is the pore volume occupied by the gas. T_{res} is the fluid temperature at reservoir conditions. G_i is the initial gas in place at standard conditions.

Real gas equation at initial pressure: $$p_i V_{res} = Z_i nRT_{res}$$

Same amount of fluid at standard conditions: $$p_{sc} G_i = nRT_{sc}$$

So we get immediately G_i: $$G_i = \frac{p_i}{Z_i} \cdot \frac{V_{res} T_{sc}}{p_{sc} T_{res}}$$

We now consider, at time t, the same situation after a total cumulative production of Q(t). We now want to calculate the average reservoir pressure:

Real gas equation at initial pressure: $$\bar{p} V_{res} = \bar{Z} n(t) RT_{res}$$

Same amount of fluid at standard conditions: $$p_{sc}\left(G_i - Q(t)\right) = n(t) RT_{sc}$$

So we get immediately G_i: $$G_i - Q(t) = \frac{\bar{p}}{\bar{Z}} \cdot \frac{V_{res} T_{sc}}{p_{sc} T_{res}}$$

We calculate the average pressure from: $$\frac{\bar{p}}{\bar{Z}} = \frac{p_{sc} T_{res}}{V_{res} T_{sc}} \left(G_i - Q(t)\right)$$

Using a numerical model

The use of a numerical model is, conceptually, even simpler. As the gas equation is entered at the level of each cell, the material balance is automatically honoured, not only globally, as above, but at the level of each cell. Solving the problem numerically is by far the most rigorous approach.

As the problem is nonlinear, this requires Topaze NL and the use of a nonlinear solver.

4.D.4.c Non-Darcy flow

As mentioned in the 'Theory' chapter, there are two main options to address non-Darcy flow: using a rate dependent skin model or integrating the Forchheimer equation in a numerical model.

Simulating non-Darcy flow with a rate dependent skin model

A rate dependant skin model may be used in the pressure and rate history simulation:

$$S_{total} = S_0 + (ds/dq)q$$

The required parameters values are:

$$S_0 \quad and \qquad ds/dq$$

These values result from a necessary well test data analysis. The methods are developed in the Chapter 'PTA - General Methodology'.

Simulating non-Darcy flow with a numerical model

In a numerical model the (non linear) non-Darcy flow effect is included in the flow equation through the value of the (non linear) non-Darcy flow coefficient, β which appears in the Forchheimer equation:

$$\frac{\partial P}{\partial x} = \frac{\mu}{k} \cdot u + \beta \cdot \rho \cdot u^2$$

It can be evaluated from the 'Rate dependant skin' linear assumption described above using ds/dq with:

$$\beta \approx ds/dq \cdot \frac{2\pi r_w \cdot h \cdot \mu}{k}$$

or from an empirical equation:

$$\beta = \frac{0.005}{\left[\Phi \cdot (1 - Sw)\right]^{5.5} \cdot k^{0.5}}$$

4.E Modern RTA methodology

Modern Rate Transient Analysis is based on the use of PC based RTA software products. The key for any modern software is to combine user friendliness to a powerful technical kernel, requiring both analytical and numerical capabilities. In terms of methodology, the central diagnostic tools are the Blasingame and loglog plots, which are used whenever such a diagnostic is possible. However, because of the very scattered nature of production data, the ultimate diagnostic tool will often be the history plot, where the coherence of the model and the data, in terms of simulated pressures, rates and cumulative productions, will be the final decision tool for the interpretation engineer.

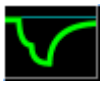
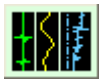
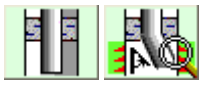
Once the interpretation is initialized and production data loaded, the first task will be to extract the interval of time on which the analysis will be performed. If the pressures are not available, only the 'old' tools can be used. If both rates and pressures are available, the interpretation will be performed with the four main diagnostic tools. The interpretation engineer can select one or several analytical and/or numerical models, set their parameters and generate these models for comparison with the actual data. For models that are believed applicable, the engineers can refine the model leading parameters, either manually or by using nonlinear regression.

Once this is finalized, the engineer may use the model(s) to forecast future production by defining a scenario of producing pressures. The user can then run a sensitivity analysis on a selection of the model parameters.

The path described is the default path when all is well. In reality, for complex problems, it becomes a trial-and-error process where the interpretation engineer may decide to go back and forth as needed when part of the process is unsatisfactory.

4.E.1 Preparing a project and loading data

The initialization procedure is largely the same as that used in PTA. The interpretation engineer inputs PVT data, geometric well and reservoir information, the following table can be used as a guide:

	Type of data	**Required for RTA**
	Production history	Yes
	Pressure history	Old stuff: No Right stuff: Yes
	PVT, correlations, tables or constraints	Yes
r_w	Wellbore radius	Yes
Φ	Porosity	Yes
h	Net vertical drained thickness	Yes
	Field map with surrounding wells based on seismic interpretation	Preferably
	Production history of surrounding wells	Preferably
	Complete completion log preferably with a permeability log. Core and core analysis	Preferably
	Completion diagram and geometry, deviation, perfos, gauge depths.	Preferably
	All gauges, well test and operations reports	Yes
	Choice of flow correlations or availability of lift curves from third party software	If pressure far from sandface

The load option imports flat ASCII files, allows manual input, copy-paste from spreadsheets, and increasingly input through links to databases or intermediate repositories using advanced filtering tools.

After the load, the cumulative production is automatically calculated by integration of the production history, and is displayed on the history plot together with the rate. Pressures is loaded and displayed in the history plot.

Quality control is not as critical as in PTA, because wellbore effects are normally not dominant, except when the pressure is recorded at surface. In this case, the validity of the well intake curves used to correct the pressure to sandface during extraction can become a potential weak point.

4.E.2 Editing data

Loaded data may be the result of careful post-processing after the data has been acquired, in which case no or little editing may be needed. However, often the interpreter will gather data of unequal quality from different sources. Pressures will often be acquired downhole in real time or with a memory gauge or come from permanent gauges (PDG), while rates are mostly measured at surface but in some cases, can also come from permanent measuring devices downhole.

Beyond the usual cleaning of irrelevant data and the correction of load errors, the main challenge is to end up with at least one coherent, synchronized set of rate and pressure data. To get there the engineer may have to perform the following tasks:

- Synchronise all data acquired electronically to the same reference time.
- If rates are not loaded from a file, create the rate history by identifying the pressure breaks and get the rate values from hard copy reports.
- Refine the production history, when the time sampling of rate measurements is too crude.
- Conversely, if the production history goes into useless detail, simplify the rate history to reduce the CPU time required to run the models.

4.E.3 Extraction and diagnostics

Once the data have been synchronized and validated, the analysis itself will start. The time range over which the extraction of the data will take place is defined and the following plots are built by the software in addition to the history plot:

- ARPS plot
- Fetkovich type-curve plot
- Fetkovich plot
- Blasingame plot
- Loglog plot
- Normalized rate-cumulative plot

At extraction time the option to invoke a defined lift curve or flow correlation to correct the pressure profile from the measurement depth to sandface can be chosen.

The loglog plot (see below) is used for diagnostic purposes to identify the two main flow regimes hopefully present in production data, infinite acting radial flow (IARF) and pseudo steady state (PSS). The pressure match is fixed to coincide with a stabilization of the derivative of the normalized pressure integral and the time match is fixed to the unit slope line of PSS at late time. The pressure match and the time match are adjusted by click and drag of the mouse. The loglog plot is linked to the Blasingame and the Fetkovich plot so any change in the loglog match is mirrored in the others. In case the data is of high quality and the sampling frequency is high enough it is sometimes possible that more than the IARF transient develop thus extending the diagnostic possibilities to approach those of PTA and both well and reservoir models can be recognized in the test data. This is however rare in low frequency data typically used in rate transient analysis.

If the loaded pressure history contains any decent build-ups with high frequency pressure data or a link to a database that allows the repopulation of this data without a filter then the interpreter is in luck. This data can be transferred to a PTA module to determine all of the classical parameters including the model and these can be transferred back to the RTA package and finally the modelling can begin; adjusting for parameters that can typically change over the longer time intervals involved in rate transient analysis (i.e. skin).

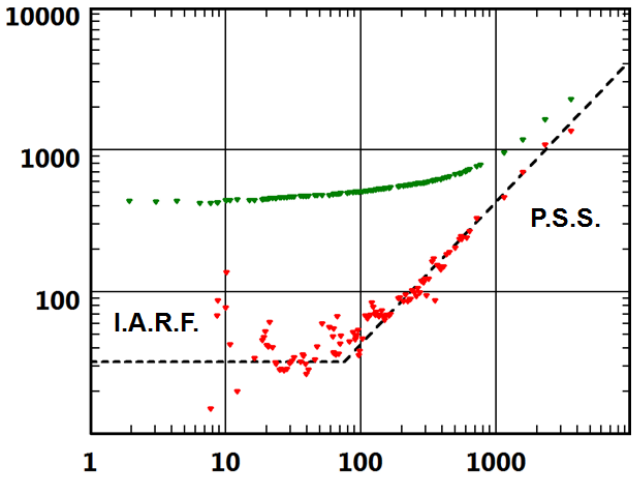


Fig. 4.E.1 – Match on the Loglog plot

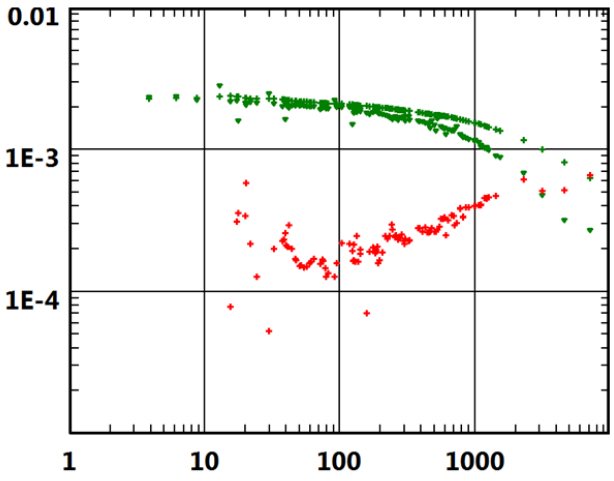


Fig. 4.E.2 – Blasingame plot

4.E.4 Model generation

After the diagnostics candidate models, analytical or numerical, are selected and an attempt is made to obtain a match between the models and the real data in all the relevant plots including the history plot. To obtain a match the interpreter will run with a first estimate of the model parameters generally obtained by generating the default, or automatic, model based on the initial match made in the loglog plot as described in the previous section. The default model is the homogenous model with constant skin in a closed circle. At generation time a first estimate of the constant skin is automatically made by the software.

After a comparison between the model and the data, changes can be made to the model parameters and any known well configuration can be imposed such as knowledge of the well being fractured, horizontal or partially penetrating. In the event that PTA was performed on part of the pressure data the model used can be transferred to the rate transient analysis.

Finally the objective is to vary the model parameters until there is a reasonable match between the model and the data in all relevant plots, including the history plot.

4.E.5 Model refinement

Before using the software non-linear regression routine to optimize the model parameters and the match, the engineer should manually deal with the gross parameter errors and change the values until the model and the data are closer. An experienced analyst with a good understanding of the sensitivity to the various model parameters should get a fit, by changing the parameters by hand, between the model and the data very quickly. This will increase the chance for the regression to succeed and converge faster.

The principle of non-linear regression is to use numerical optimization to refine the parameter estimates by minimizing an error function, generally the standard deviation between the simulated and real values at selected times. The most commonly used optimization algorithm is Levenberg-Marquardt, but there are many variants. The engineer has the possibility to run with some or all the leading parameters of the model and he can also fix the upper and lower limits of the allowed parameter variation. The data points on which the error function will be calculated may also be controlled. See figure below:

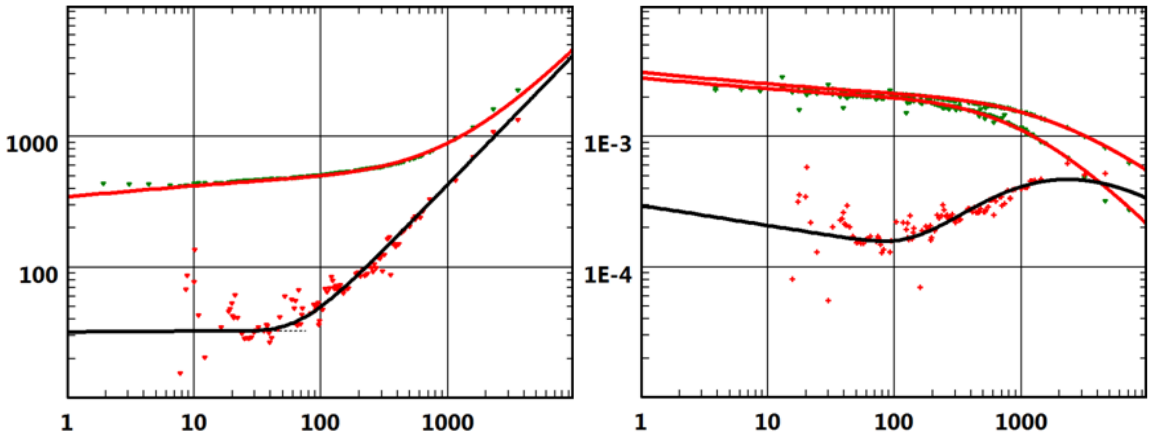


Fig. 4.E.3 – Final match after optimization

4.E.6 Deconvolution

4.E.6.a Principle

The deconvolution in RTA is primarily a denoising exercise.

While PTA deconvolution seeks a constant rate response to reconstruct a multiple rate pressure signal, RTA deconvolution looks for a constant pressure response to reconstruct a multiple pressure rate signal. Despite the parallel on the principle, an important difference lies in the fact that the original extraction interval and the one after deconvolution remain the same.

In other words, RTA deconvolution does not extend the diagnostic plot in duration, but is expected to provide a smoother and more easily interpretable loglog plot.

4.E.6.b Basic theory

In data mining, supervised learning is the case where both the target, y, and the input, x, are measured and the objective is to find the patterns which relate y and x. Once these patterns are identified, they can be used for further prediction.

In case of RTA deconvolution, the target is the measured production data while the input are features, which are functions of pressure and time. Mathematically, the features can be written as:

$$x^{(i)} = \begin{bmatrix} \sum_{j=1}^{i-1} \left(\Delta P^{(j)} - \Delta P^{(j-1)}\right) \\ \sum_{j=1}^{i-1} \left(\Delta P^{(j)} - \Delta P^{(j-1)}\right) \log\left(t^{(i)} - t^{(j)}\right) \\ \sum_{j=1}^{i-1} \left(\Delta P^{(j)} - \Delta P^{(j-1)}\right) \left(t^{(i)} - t^{(j)}\right) \\ \sum_{j=1}^{i-1} \left(\Delta P^{(j)} - \Delta P^{(j-1)}\right) \sqrt{\left(t^{(i)} - t^{(j)}\right)} \end{bmatrix}$$

where $x^{(i)}$ above contains four features, defined at time i. In the above example, the first feature represents rate as a superposition of pressure drop changes, the second feature represents infinite acting radial flow, and the third represents wellbore storage and pseudo-steady state flow while the fourth feature represents linear flow.

In this approach, the flow rate $q^{(i)}$ at time i is represented to be a linear combination of the features $x^{(i)}$:

$$q^{(i)} = \theta^T x^{(i)} + \varepsilon^{(i)}, i = 1,2,3, \dots, n$$

where θ is a N_f dimensional vector with unknown constants (N_f being the number of features employed), ε captures the measurement error and other discrepancies and n is the number of flow rate and pressure measurements.

In matrix form, this can be represented as:

$$\mathbf{q} = \theta^T \mathbf{X} + \varepsilon$$

where q is a n-dimensional vector and X is a n x N_f matrix.

Assuming that the mean of the error is zero, the exercise then becomes that of minimizing the mean-square error function:

$$J(\theta) = \frac{1}{2} \sum_{i=1}^{n} \left(\theta^T x^{(i)} - q^{(i)}\right)^2$$

Since this is a linear system of equations, the unknown θ can be solved directly by:

$$\theta = (X^T X)^{-1} X^T q$$

4.E.6.c Model Regularization

One danger in data mining methods is to over fit the data, which degraded the predictive capability of the model. Ridge regression (a type of model regularization technique) is widely used to address the overfitting issue by reducing the prediction variance. Instead of minimizing the function J(θ) above, ridge regression minimizes:

$$J(\theta) = \frac{1}{2}\sum_{i=1}^{n}\left(\theta^T x^{(i)} - q^{(i)}\right)^2 + \lambda\sum_{j=1}^{p}\theta_j^2$$

Where $\lambda \geq 0$ is called the tuning parameter and controls the relative weight on a better fit and smaller parameters. A ten-fold cross-validation is used to select an appropriate value of λ [2].

Once λ is determined, θ can be evaluated as:

$$\theta = (X^T X + \lambda I)^{-1} X^T q$$

where I is the identity matrix.

Once the relationship between the pressure drop and the rate has been learned, one can predict the rates given the selected features, proposed pressure drops and constants θ:

$$q_{pred} = X_{pred}\theta$$

References

[1] Tian, T. and Horne, R. N., 'Applying Machine Learning Techniques to Interpret Flow Rate, Pressure and Temperature Data from Permanent Downhole Gauges', SPE 174034.

[2] Hastie, T., Tibshirani, R. and Friedman, J., 'The Elements of Statistical Learning, 2nd Edition', 2009.

4.E.6.d Implementation in Topaze

The user can select whether the target data to be used should be rates or cumulative production.

A Features panel allows the user to select which features to include in the regression process:

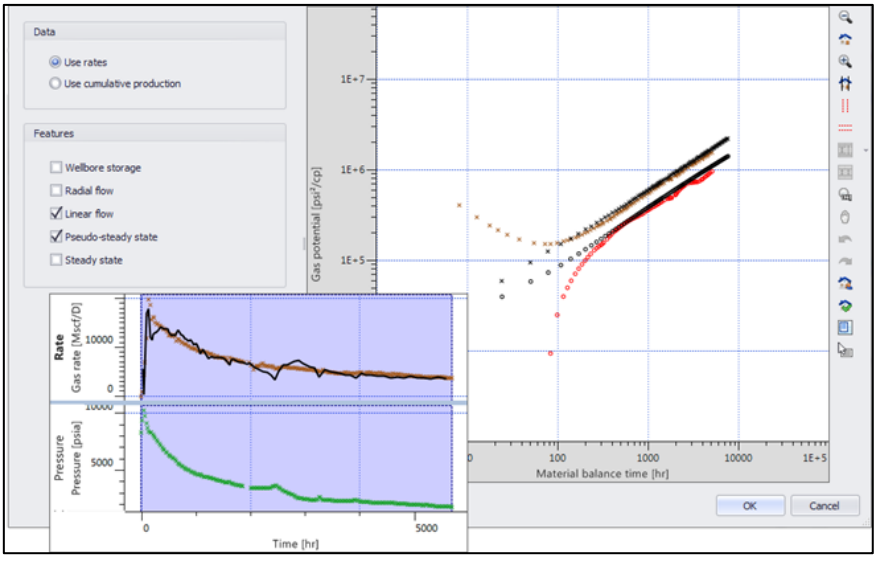


Fig. 4.E.4 – Topaze RTA deconvolution dialog

4.E.7 Forecast

Once the model has been selected a production forecast can be easily performed by defining a flowing (producing) pressure scenario. See the figure below illustrates this with a constant pressure production for 100 days.

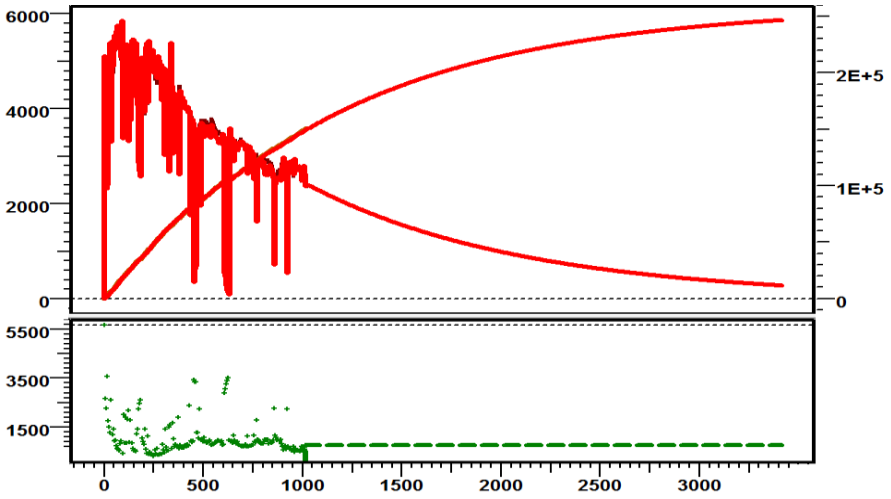


Fig. 4.E.5 – Forecast 100 days constant pressure production

4.E.8 Sensitivity study

At the end of the nonlinear regression it is also possible to recover some confidence intervals. They can be used to assess the sensitivity to individual parameters and any eventual parameters cross-correlations.

Another possibility is to run and display a series of model generations corresponding to different values of a given parameter, in order to compare theses on the history.

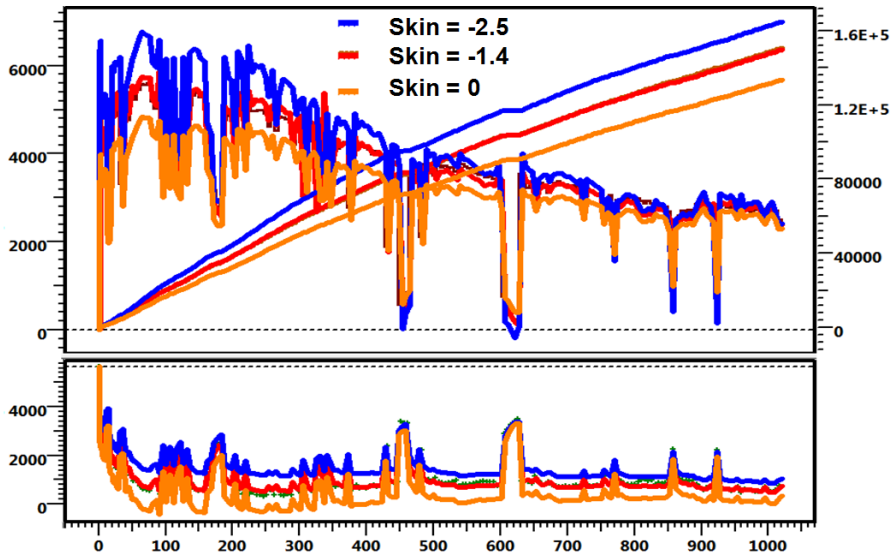


Fig. 4.E.6 – Sensitivity to skin

4.E.9 Reporting Guidelines

A typical analysis report will be split into two components: the 'mechanical' part, basically the result tables and plots generated, directly or indirectly, by the Rate Transient Analysis package, and the 'verbose' part, where the engineer will report the objectives, the operations, the analysis, his confidence in the results and forecast, and possible recommendations for stimulation, workover and continued or future measurements and equipment to use.

Typically, professional analysis reports are generated with two possible set-ups:

- A header document, from a word processor, with some 'copy-paste' of plots and results from the RTA software, but with most of the 'mechanical' report delivered as an annex,
- An integrated document, typically from a word processor, where some plots and tables are dynamically connected to the RTA software using some OLE or COM automations. The advantage of this solution is that it is much more flexible. Once a model template has been defined, the reporting process will get shorter and shorter from one analysis to the next.

4.F RTA versus PTA

4.F.1 Introduction

The comparative table below shows a summary of the common and different aspects of the PTA and RTA techniques.

The main aspects will be detailed later in this paragraph.

	Pressure Transient Analysis (PTA)	**Rate Transient Analysis (RTA)**
Theoretical bases	Same equations, superposition, analytical and numerical model. Some assumptions are, however, specific.	
Time range	Hours, Days, sometimes Weeks	Weeks, Months, Years
Periods of interest	Mostly shut-ins Clean productions possible	Producing phases But build-ups may be included
Data sources	Well test measurements Formation tests Permanent gauges (PDG)	Measured/allocated production surface pressure readings Permanent gauges (PDG)
Reservoir areas of interest	Whatever volume of investigation during the test and/or the shut-in	Well or group drainage area
The good old plot(s)	MDH, Horner	Arps
The good old type-curve(s)	McKinley, Gringarten	Fetkovich
Modern diagnostic plots	Loglog with Bourdet derivative	Loglog & Blasingame with Bourdet derivative
Main flow regime of interest Main corresponding results	Infinite Acting Radial Flow kh & skin	Pseudo-Steady State (PSS) drainage area & shape factor
Diagnostic capability	High to very high	Average to low
Long term validity	Average to low	High to very high

4.F.2 Common tools

RTA and PTA methods share the same assumptions in terms of the use of the diffusion equation and limiting conditions. Most of the analytical and numerical models developed in PTA may be used in RTA with minor adjustments, such as the ability to use the pressures as the input to simulate the rates with superposition.

Modern RTA and PTA share a similar path. After loading, synchronizing and extracting data, one first tries to run a diagnostic using specialized plots and straight lines. An analytical or numerical model is then run, and an optimization process adjusts the parameters to minimize the difference between the simulated model response and the observed data.

4.F.3 PSS vs. IARF

The main regime of interest in PTA is Infinite Acting Radial Flow (IARF). We look primarily for a stabilization of the Bourdet derivative. When IARF is detected, specialized analysis will give a value of mobility and a total equivalent skin factor. We can refine this and diagnose other well, reservoir and boundary behaviors from various parts of the response; however the starting point will always be IARF.

The main regime of interest in RTA is Pseudo Steady State (PSS). We look primarily for a unit slope on the Loglog or the Blasingame plot. Specialized analysis will determine the size of the well drainage area from the slope, and the intercept will be a function of three main factors: the well productivity index, the mobility and a shape factor. More complex models could be used, but there may not be enough information to determine the additional parameters. However the pressure transient results may be used to determine these.

4.F.4 Diagnostic capabilities

One of the key steps in PTA is the diagnostics, where, based on the derivative behavior the engineer decides which model could most appropriately be used to perform the analysis. This is made possible by very clean data and constant production i.e. zero, during the build-up.

Production history may be so scattered that the responses will be dominated by transients. In this case there is no way to identify pseudo steady state behavior. This may happen even though the well is still producing and the pressure is declining globally.

Despite the lack of pure PSS behavior it will be possible with a model to history match the data and obtain a reliable drainage area estimate and even sometimes discriminate mobility, skin and shape factor. No specialized plot will show such a behavior. So the use of models and optimization is likely to change the way RTA is performed completely, even more radically than happened with PTA.

4.F.5 Validity of the PTA hypothesis in Rate Transient Analysis

PTA can provide a clean snapshot of what the well and reservoir system is at a given time. RTA covers a much wider time range, and some of the assumptions valid during a single well test will not be true over the well producing history. The three main differences are related to the well productivity, the drainage area and multiphase production.

PTA models account for rate-dependent skin. It is also known that the well may be cleaning up during the initial production phase. So the well productivity may not be constant during a well test. However this is a reasonable assumption for a single build-up, and optimization will be possible with a single mechanical skin model. In RTA this is unlikely. Well productivity does change over time, and no optimization process is reasonably possible over a long period of time without considering a time-dependent skin.

In PTA, boundary effects are generally material boundaries, even though interfering wells can produce the same effects as boundaries. In RTA we consider the well drainage area. Except when there is only one producing well, part or all of the drainage area boundaries are immaterial, depending on the flow equilibrium between the neighboring wells. The drainage area will change in time when new wells are produced, or even when the flow rates change asymmetrically. To account for these changes, a multi well model, either analytical or numerical, may be required.

In PTA we approximately handle multiphase cases using pseudo-pressures or considering that saturations are constant and the flow can be modelled with an equivalent single-phase fluid as in Perrine's method. In RTA, solutions exist that consider that individual fluids develop PSS independently. However these solutions make a global correction for multiphase production but they are unable to forecast the breakthroughs. There is a point where only a history match with a numerical model can account for multiphase production.

5 – Wellbore models

OH – OSF – DV

5.A Introduction

Until we are able to beam the fluid directly from the pore space into the ship cargo bay we will need to use this route called the wellbore. Wellbore effects are seen very differently, depending where you stand:

- For the Pressure Transient Analysts anything related to the wellbore is a nuisance. Wellbore effects will spoil the early part of the pressure response, and may even persist throughout the whole test or shut-in survey.

  So to the PT-Analyst Wellbore Effects = BAD.

- Production Analysts are a little luckier, because they work on a time scale where transient effects are not that important, and addressing wellbore effects amounts to connecting a lift curve. In fact, playing with the lift curves and implementing 'what if' scenarios is part of their jobs.

  So to the Production Analyst Wellbore Effects = OK.

This Manichean split can be presented another way:

- The steady-state component of wellbore effects is a key element of the well productivity. It may be modeled using lift curves, or VLP curves, and this in turn requires flow correlations that are present in both Production Logging and Well Performance Analysis, a.k.a. Nodal Analysis™ (Trademark of Schlumberger).

  Correction to datum may be either applied to the data in order to correct the real pressure to sandface, or integrated in the model in order to simulate the pressure at gauge level. Correction to datum and integration of VLP curves are detailed in the PTA (QA/QC) and the Well Performance Analysis chapters of this book.

- The transient component of wellbore effects often ruins the life of the PT-Analyst. The action at the origin of a sequence of flow (opening and shut-in of a valve, change of a choke) is occurring at a certain distance from the sandface, and any wellbore volume between the operating point and the sandface acts as a cushion. This induces a delay between what we want to see and what effectively occurs at the sandface.

  In welltest operations, it is highly recommended to reduce this nuisance as much as possible by means of downhole shut-in tools.

  In Rate Transient Analysis it is not much of an issue, as transient wellbore effects occur at a time scale of little interest for rate decline.

This chapter deals with the modeling of some of the simplest transient wellbore models, and is mainly applicable to Pressure Transient Analysis only.

5.B Constant Wellbore storage

The simplest wellbore model is the constant wellbore storage

As introduced in the 'Theory' chapter, the wellbore storage introduces a time delay between the rate we impose at the operating point (typically the choke manifold at surface) and the sandface rate. The wellbore storage equation was introduced in the 'Theory' chapter:

Wellbore storage equation: $$q_{sf} = qB + 24C\frac{\partial p_{wf}}{\partial t}$$

Not surprisingly, the constant wellbore storage model assumes that the wellbore storage factor C is constant. The below figure illustrates the behavior of the sandface rate during the opening and shut-in of a well.

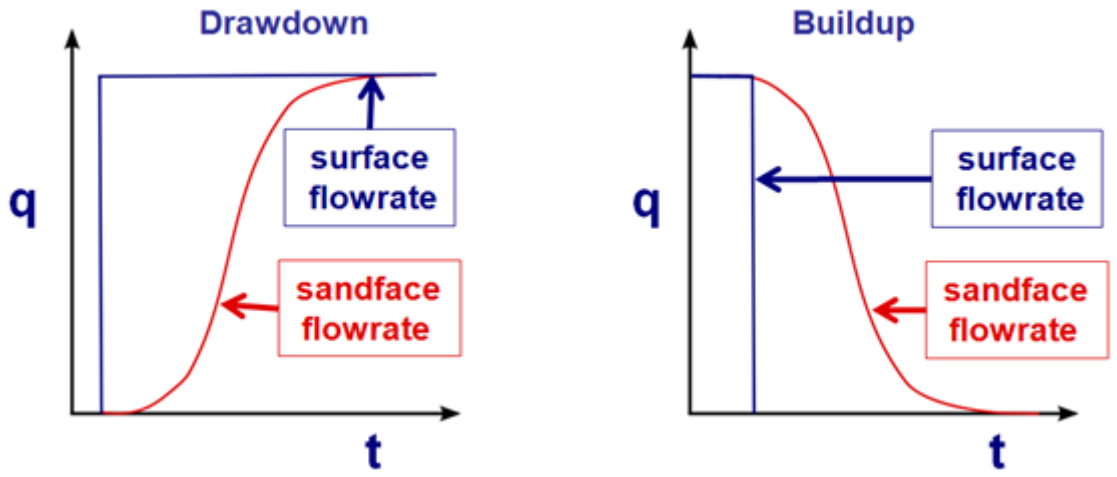


Fig. 5.B.1 – Wellbore storage

5.B.1 Loglog analysis

Fig. 5.B.2 with various constant wellbore storage constants is illustrated below. Pure wellbore storage is characterized by the merge of both Pressure and Bourdet Derivative curves on the same unit slope.

At a point in time, and in the absence of any other interfering behaviors, the Derivative will leave the unit slope and transit into a hump which will stabilize into the horizontal line corresponding to Infinite Acting Radial Flow. The form and the width of the hump is governed by the parameter group Ce^{2S}, where S is the Skin factor.

The horizontal position of the curve is only controlled by the wellbore storage coefficient C. Taking a larger C will move the unit slope to the right, hence increase the time at which wellbore storage will fade. More exactly, multiplying C by 10 will translate the curve to one log cycle to the right.

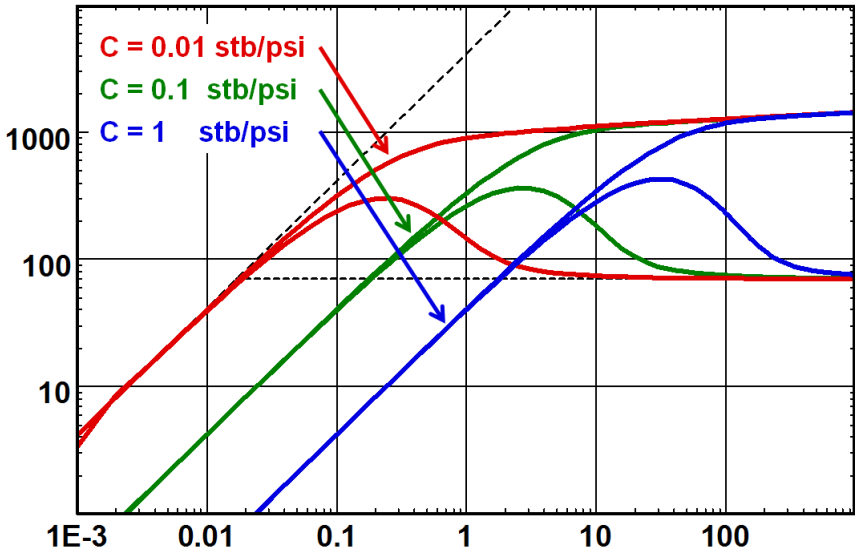


Fig. 5.B.2 – Wellbore storage loglog response

5.B.2 Specialized analysis (Cartesian plot)

A unique slope on the loglog plot corresponds to a linearity of the pressure response on a Cartesian plot. This Cartesian plot may show either P or ΔP vs. Δt.

Below is shown a Cartesian plot of pressure versus time.

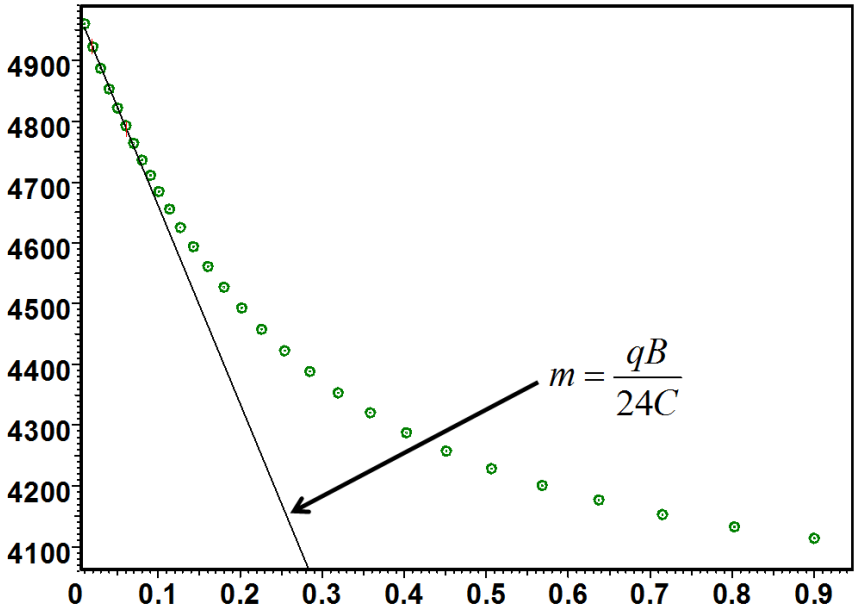


Fig. 5.B.3 – Cartesian plot of pressure vs. elapsed time

The early time straight line corresponding to the pure wellbore storage is given by:

Wellbore Storage Straight line: $\Delta p = \frac{qB}{24C}\Delta t = m\Delta t$

So one can get the wellbore storage constant with:

Specialized plot result: $C = \frac{qB}{24m}$

5.B.3 Sensitivity analysis on the wellbore storage coefficient

The figure below presents the response with wellbore storage values, C of 0.001, 0.003, 0.01, 0.03 and 0.1 (stb/psi).

The value of C has a major effect, which is actually exaggerated by the logarithmic time scale. You can see on the linear history plot that all responses seem to be the same, however.

When the influence of wellbore storage is over both the pressure change and the derivative merge together. Wellbore storage tends to masks infinite acting radial flow on a time that is proportional to the value of C. Wellbore storage will also tend to mask other flow regimes that can be present in a well test. Early time well responses such as linear, bi-linear, spherical and hemispherical flow will disappear if the storage effect is considerable. Effects of heterogeneous reservoirs can also be masked by wellbore storage. The wellbore storage effect on other well and reservoir models are covered in the individual chapters of these models.

Wellbore storage does not affect the late time pseudo steady state response.

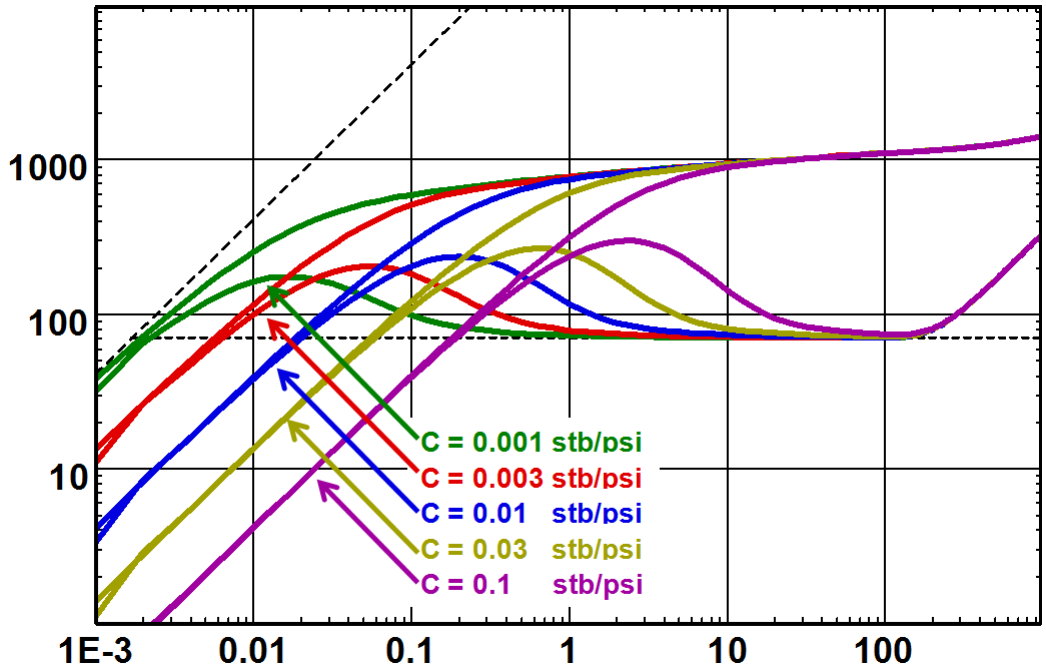


Fig. 5.B.4 – Effect of wellbore storage, loglog plot

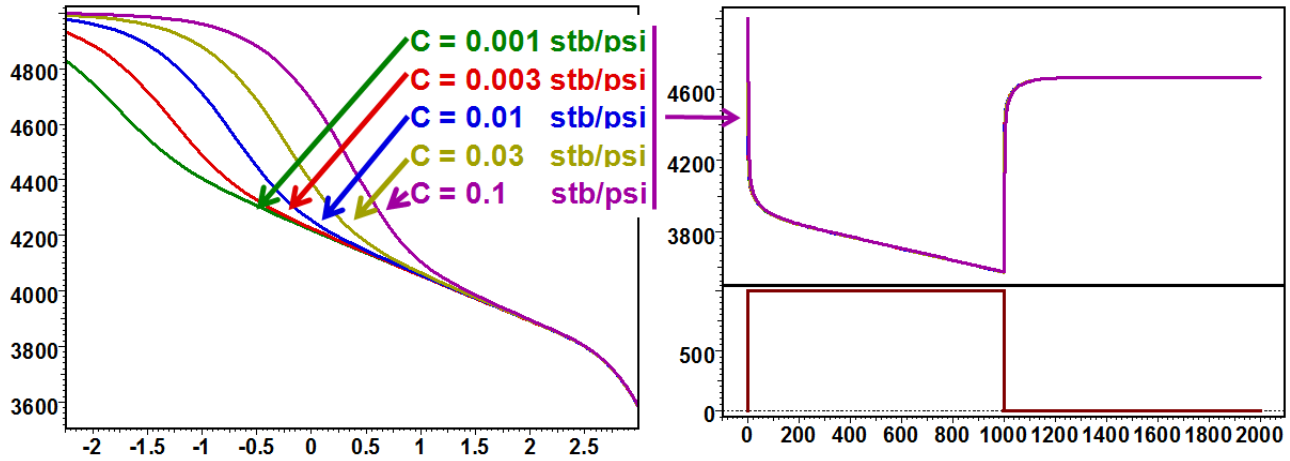


Fig. 5.B.5 – Effect of wellbore storage, semilog and history plot

5.C Changing wellbore storage

The most frequent case of changing wellbore storage is related to the compressibility change of the wellbore fluid.

A classic example is gas. When the well is flowing the pressure in the wellbore will decrease, and the gas compressibility will increase. In this fixed volume this will result in an increase of the wellbore storage parameter. The opposite will occur during the shut-in, where the increase of pressure will result in a decrease of the wellbore storage. Though it occurs in any gas test, this behavior will be visible, and become a nuisance, in the case of tight gas, where the high pressure gradient in the formation results in a high pressure drop in the wellbore.

Another typical example is an oil well flowing above bubble point pressure in the reservoir. At a stage (sometimes immediately) there will be a point in the wellbore above which the pressure gets below bubble point. In this place the oil compressibility will be progressively dominated by the compressibility of the produced gas, hence an increase of the wellbore storage which will evolve in time.

In both cases, the wellbore storage will be increasing during the production and decreasing during the shut-in.

Other sources of changing wellbore storage may be various PVT behaviors, change of completion diameter of a rising or falling liquid level, phase redistribution, falling liquid level during a fall-off, etc.

In some cases the wellbore effect will be so extreme that any modeling is hopeless. In this case the engineer will focus on matching the derivative response after the wellbore effect has faded, accepting that the early time response cannot be matched and may induce a (cumulative) incorrect value of the skin factor.

There are three main ways today to model changing wellbore storage:

- Analytical, time related wellbore storage
- PVT correction using the pseudotime function and a constant storage value
- Numerical, pressure dependent storage model

5.C.1 Analytical models

Most analytical formulations of changing wellbore storage involve an initial value of wellbore storage C_i, a final value C_f, some assumption for a transition function (Hegeman, Fair, etc) and a time at which this transition occurs. The main characteristic of these models is that the transition occurs at a given value of Δt, and is NOT related to the value of the pressure.

The figures below illustrate increasing and decreasing wellbore storage as modeled by the Hegeman model of changing wellbore storage.

The matching consists in setting the wellbore storage straight line on the FINAL value of wellbore storage, pick a second position corresponding to the INITIAL value of storage, and then pick the median time when the transition occurs. The initial model generation will seldom match the response perfectly, but this model, combined with a robust nonlinear regression, has the capacity to adjust to virtually any single trend early time response.

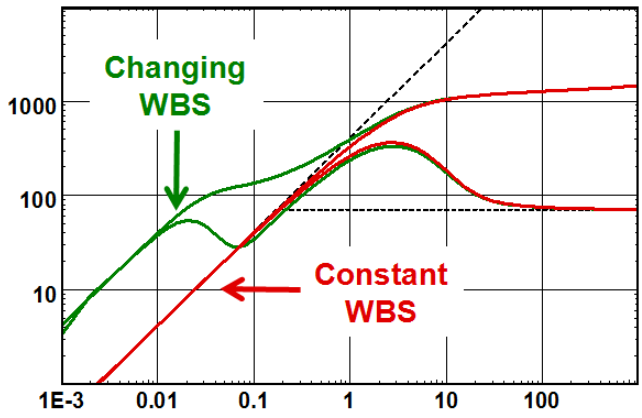


Fig. 5.C.1 – Increasing storage

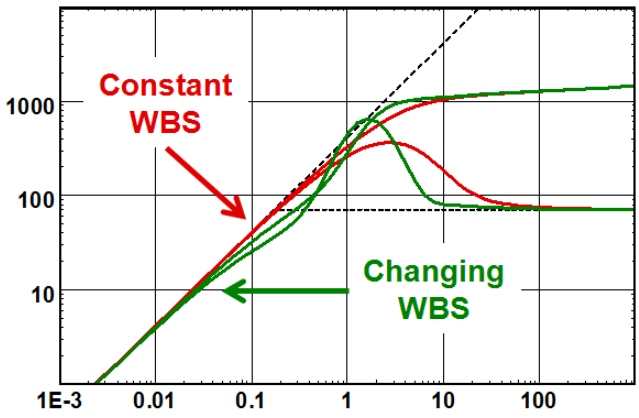


Fig. 5.C.2 – Decreasing storage

In practice, the Hegeman model is sharper and has more capabilities to match real data. This is related to the choice of transition function and does not mean that this model is physically better. Actually it does not mean that ANY of these models are correct, and they should be used with care for the following reasons:

- The models are just transfer functions that happen to be good at matching real data. There is no physics behind them. They may end up with an initial, final storage and transition time that makes no physical sense.
- These models are time related. There will be a wellbore storage at early time and a wellbore storage at late time. This is not correct when the model is pressure related. In the case of production, the real wellbore storage at early time will correspond to the storage at late time of the build-up, and the reverse. So, the superposition of a time related solution will be incorrect on all flow periods except the one on which the model was matched. This aspect is often ignored and/or overlooked.
- These models are 'dangerous' to the extent that they work beautifully to match 'anything that goes wrong' at early time, even when the use of such model is not justified. They are the early time version of the radial composite model at intermediate time. Actually, combining changing wellbore storage and radial composite will match any rubbish data.

5.C.2 Combining pseudo-time and a constant storage model

When the pressure drawdown is large the non-constant compressibility leads to a changing wellbore storage therefore a distortion in the early time of the loglog plot. The changes in μc_t can also be included in the diffusion equation and pseudo-time can be used during the extraction of the period to be analyzed.

Pseudo-time: $t_{ps}(t) = \int_0^t I\left(p_{wf}(\tau)\right) d\tau$ where $I(p) = \frac{1}{\mu(p) c_t(p)}$

The following figures show a loglog response before and after pseudo time correction. The use of pseudo time is detailed in the chapter on '*13.E - The use of pseudofunctions'*.

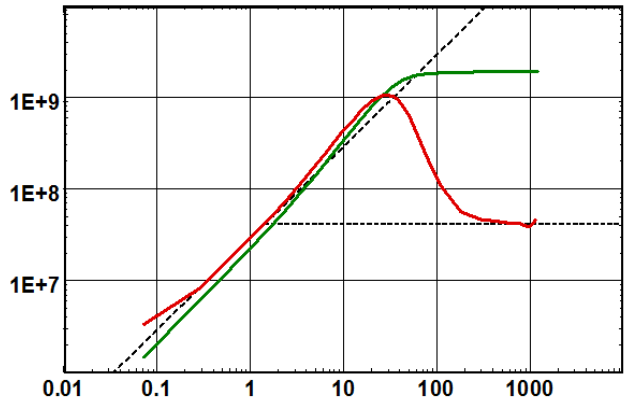


Fig. 5.C.3 – Without pseudo-time

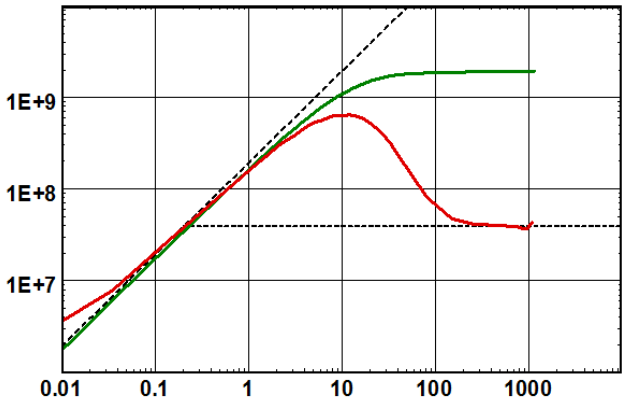


Fig. 5.C.4 – With pseudo-time

5.C.3 Numerical pressure dependent wellbore storage

The principle is to use a wellbore model which, at any time, uses the pressure to define the wellbore storage parameter. In order for the model to be stable, the wellbore storage has to be calculated implicitly at each time step. As the problem is not linear, this can only be done using a non linear model.

This is by far the most relevant way to simulate pressure related wellbore storage. The figure below illustrates a buildup matched with the changing wellbore storage model (Hegeman), the extracted buildup corrected for pseudo time and matched with this model, and the match with the non linear numerical model with pressure dependent wellbore storage.

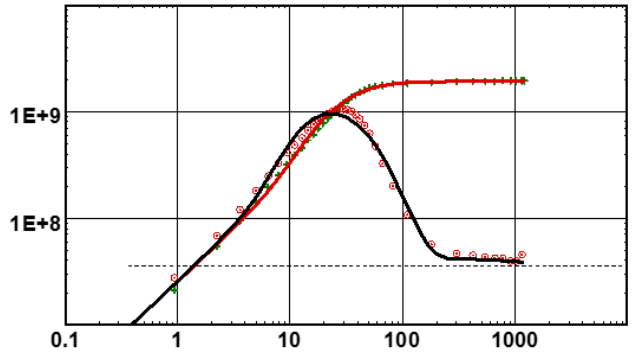


Fig. 5.C.5 – Changing wellbore storage match

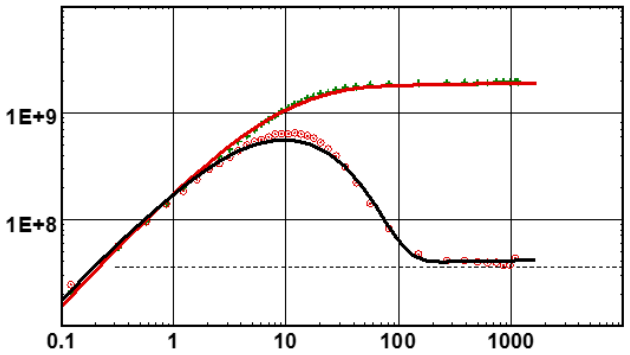


Fig. 5.C.6 – Pseudo time match

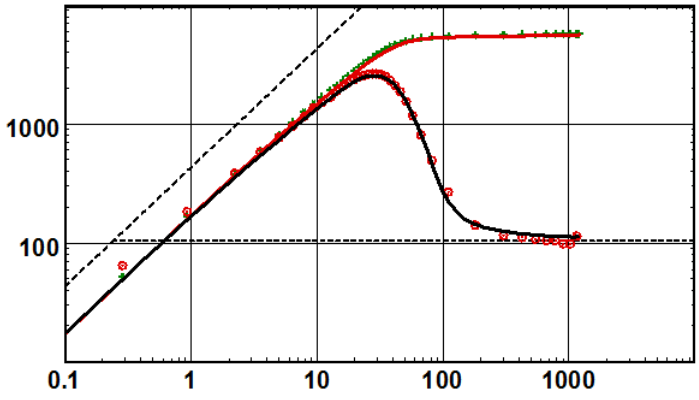


Fig. 5.C.7 – Match with non linear numerical model: Pressure dependent wellbore storage

6 – Well models

OH – OSF – DV

6.A Introduction

The geometry of the well, its trajectory in the formation, the way it is completed and/or stimulated, have a major impact on transient responses and the long term well productivity.

For the PT-Analyst, in most cases the well model will dominate the transient response after the wellbore storage has faded and before IARF is established.

The flow geometry around the well may create characteristic flow regimes, with a specific signature of the Bourdet derivative and linearity on a given specialized plot. Some long lasting flow geometries may also be identified by the Production Analyst.

After radial flow is reached the well model will produce a total equivalent skin, which can be calculated using the standard straight line method (MDH, Horner, Multirate semilog). This total skin is the sum of the 'real' skin, resulting from the well damage or stimulation, and a geometrical skin which will define the difference in productivity between the current well geometry and a fully penetrating vertical well.

However textbook responses are not that frequent. Wellbore effects may hide some specific well regime. Some well configurations, such as horizontal wells, will have a longer term impact, will be sensitive to heterogeneities and will seldom exhibit the expected behavior.

The problem of identifying and quantifying well behaviors is not trivial, and it is not expected to become any better in the years to come. Additional developments are very likely to blur the message even more:

- In extremely low permeability formations the geometry of the well may affect the pressure response for years, and IARF may never be reached for the practical duration of the well life. This is the case of fractured horizontal wells in shale gas formations, and it is developed in the unconventional gas chapter of this book.
- Increasingly complex and 'intelligent' completions, multi-drain wells, may be a dream for the production engineer but they are a nightmare for the analyst. The sensitivity of the solution to local heterogeneities, the lack of unique solutions, and the absence of any pure flow regime make the analysis almost impossible.

For these reasons, what is taught in this chapter may become less and less relevant when this sort of configuration becomes the norm. When no formal analysis technique is available we will end up using these complex models for test design and productivity design, and we will use history matching with a very limited number of diagnostic tools.

6.B Vertical well with Constant Skin

The simplest model is a vertical well fully penetrating the reservoir producing interval.

This is the model used to derive the basic equations in the chapter on 'Theory'. This model is sometimes called 'wellbore storage & skin', reference to the original type-curves of the 1970's. The reason is that the two only parameters affecting the loglog plot response will be the wellbore storage and the skin factor. However, wellbore storage is a wellbore effect and skin is used in complement of all other models.

So we will stick to the term 'vertical well', considering that 'fully penetrating' is the default status of a vertical well, otherwise the model will be called 'limited entry' or 'partial penetration' (see other sections in this chapter).

The behavior of a vertical well in a homogeneous infinite reservoir has already been presented in previous sections and is shown here as a reminder. The loglog and semilog plots below show the response for various values of the skin factor (S).

On the loglog plot, the shape of the derivative response, and with a much lower sensitivity the shape of the pressure response, will be a function of the group $C.e^{2S}$.

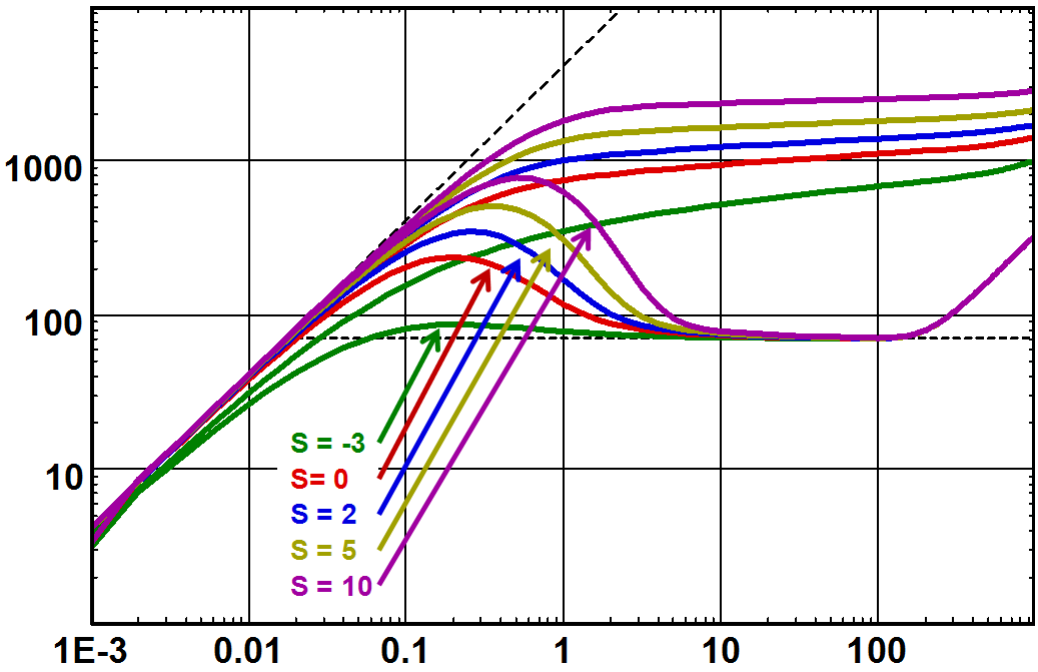


Fig. 6.B.1 – Effect of skin, loglog plot

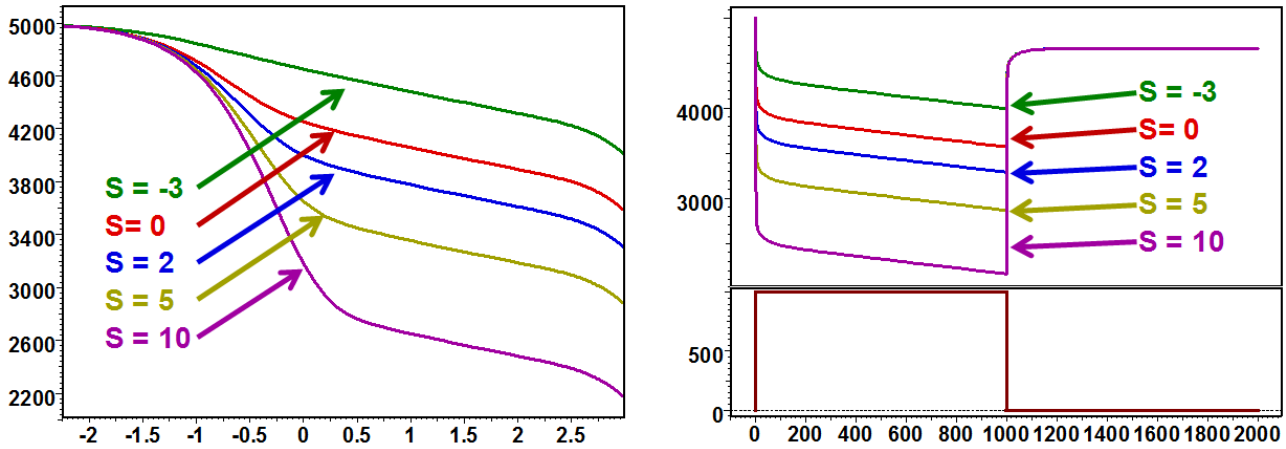


Fig. 6.B.2 – Effect of skin, semilog and history plot

The shape of the hump, which originally was set to $C_De^{2.Skin}$ when dealing with type curves, is actually a function of C and r_we^{-Skin}.

If we consider the IARF equation given in previous section:

$$p(t) = p_i - \frac{162.6qB\mu}{kh}\left[\log(t) + \log\left(\frac{k}{\Phi\mu c_t r_w^2}\right) - 3.228 + 0.8686.Skin\right]$$

…and if we re-shuffle it a bit, we get:

$$\Delta p(t) = \frac{162.6qB}{\frac{kh}{\mu}}\left[\log(t) + \log\left(\frac{kh}{\mu}\right) - \log(h\Phi c_t) - 3.228 - 2\log\left(r_w e^{-Skin}\right)\right]$$

One can see that the slope is a function of $k.h/\mu$, and that there is a constant term that shows, among other things, the residual effect of r_we^{-Skin}, ϕ and c_t.

6.C Vertical Well with Changing Skin

In this section, we keep the assumption of a vertical well fully penetrating the formation. However we now allow the skin factor to be changing over time and/or as a function of the producing rate.

6.C.1 Rate dependent skin

In high rate wells, especially but not only in gas wells, the flow velocity may become considerable and in some cases the flow becomes turbulent. When this happens, Darcy's law no longer applies and will be replaced by Forchheimer's equation:

$$\frac{dP}{dx} = \frac{\mu}{k} \cdot u + \beta \cdot \rho \cdot u^2 , \ \beta = \frac{0.005}{[\Phi \cdot (1 - Sw)]^{5.5} \cdot k^{0.5}}$$

The exact problem is nonlinear and can be solved numerically, as described in chapter on 'Numerical models'.

However, it can be simplified and analytical models can be used with a fair approximation by adding a rate dependent component to the skin factor. Under these conditions, the effective skin factor S' for a given rate q will be given by:

$$S' = S_0 + Dq \quad or \quad S' = S_0 + \frac{dS}{dq} q$$

D is called the non-Darcy flow coefficient. In order to assess the rate dependency the skin has to be solved for several rates.

In gas well testing the most common method is to plan for an isochronal or modified isochronal test, but this is done mainly to determine the deliverability of the well. Such a test procedure includes multiple buildups after different flowrates and the engineer can then profit for 'free' the fact that the buildups can be analyzed for skin and define the rate dependency. This can then be used in the model.

The following figures illustrate the loglog plot with four buildups with different skins and the corresponding history match using a constant skin in the model. It can be seen that the match is not consistent with the measured data.

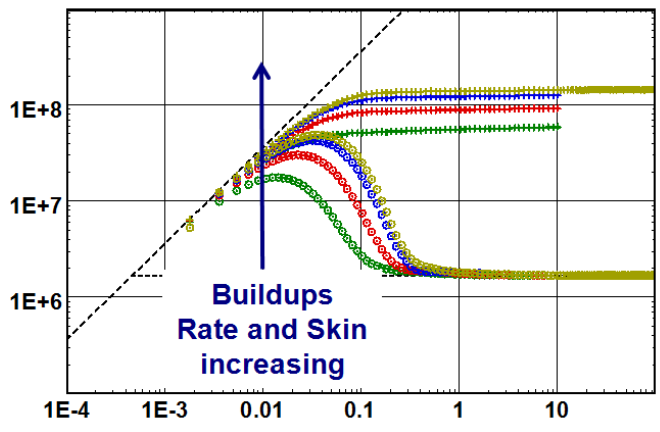


Fig. 6.C.1 – Loglog plot

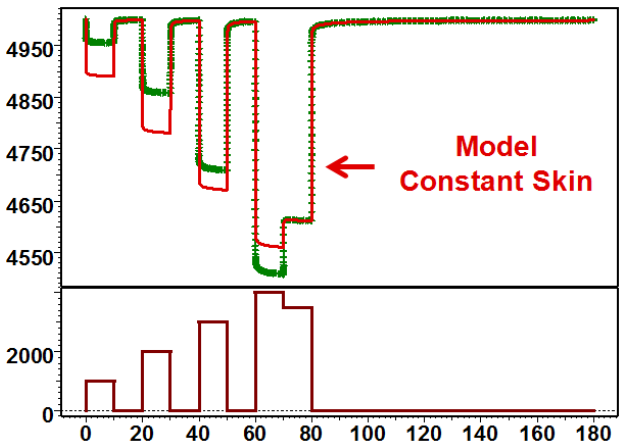


Fig. 6.C.2 – History match, constant skin

The next figures illustrate the 'skin versus rate' plot, which is used to evaluate the rate dependency and the skin if no turbulence was present. From this we can determine a rate dependent skin model. Finally we see n the history match plot that the model is consistent with the measured data.

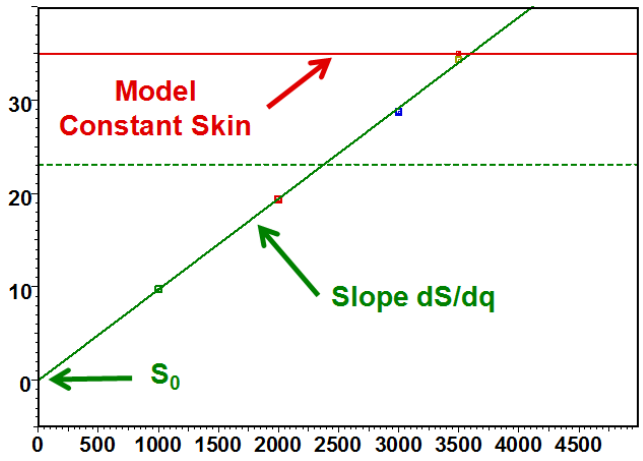


Fig. 6.C.3 – Skin vs. rate plot

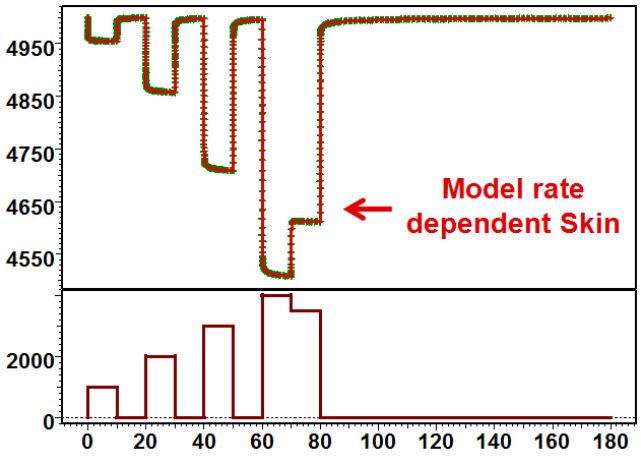


Fig. 6.C.4 – History match, rate dependant skin

6.C.2 Time dependent well model

After a stimulation job or a full workover, there is often a voluntary change from one well model to another. This can typically be the change of the well conditions from a wellbore storage and skin type to a fracture model after a 'frac' job. The skin can also change but the transformation of the model is more radical than just an improvement or deterioration of the skin. The other well models are discussed and developed later in this chapter but since the change of the full well model is similar to that of just a straight forward time dependent skin, we will briefly discuss it here.

The most common example of a well model transformation is when a well is subject to fracture stimulation. Typically the well is damaged and no fracture is intersecting the well during the first status or time period of a well test. Then the well is subject to the 'frac' job and the well model is changed to fracture model. It is possible to model this using a time dependent well model. The history is divided into time periods with a certain status, and each status can have the following definitions:

- Status with constant wellbore storage and skin
- Status with changing wellbore storage
- Rate dependent skin for each status
- Status with infinite, uniform flux or finite conductivity fractures
- Each status can have a different geometry limited entry
- Each status can have a different horizontal well geometry

The figure below illustrates the loglog match of the well behavior before and after a fracture stimulation job. The model matches the whole history of the test sequence including the fracture treatment.

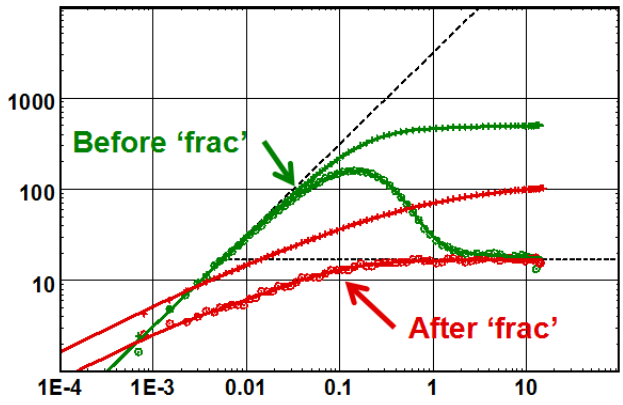


Fig. 6.C.5 – Changing well loglog match

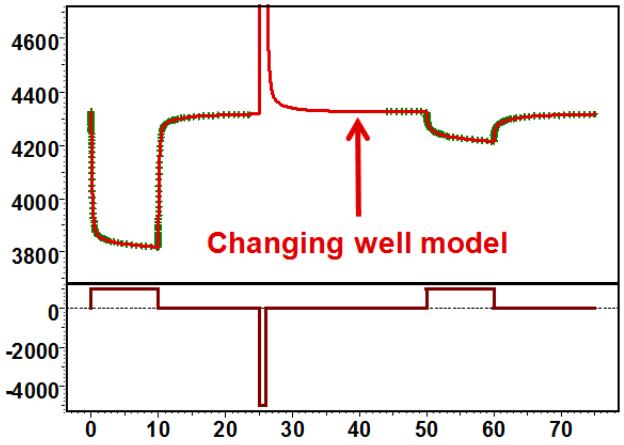


Fig. 6.C.6 – Changing well history match

6.C.3 Time dependent skin

When the well is cleaning up one will see a decrease of skin with time. Conversely a well may get progressively damaged during its producing life, hence an increase of the skin factor.

These effects may be modeled by allowing the mechanical skin to vary over the well life. This may actually be combined with a rate dependent component, though solving for both may often be an under-specified problem.

In Saphir, time dependent skin is just a subset of the changing well model where each status is assigned a skin. The figure below illustrates a well that is cleaning up matched with a constant and changing skin model.

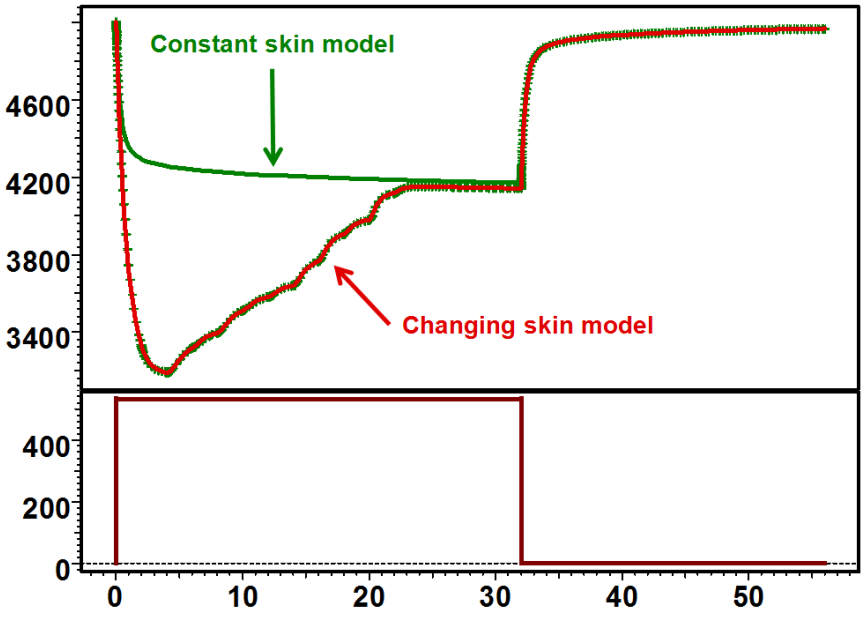


Fig. 6.C.7 – Well cleaning up

6.D High conductivity fracture

6.D.1 Hypotheses

Acidizing and fracturing are the basic choices when one wants to improve the productivity of a well. Acidizing requires an injectivity which will make it the typical treatment of choice for stimulating wells in high to medium permeability formations.

At the opposite, fracturing requires a mechanical stress induced by the resistance to the flow, and will be typically performed in low permeability formations. An extreme case today is the production of shale gas formations, which only occurs through series of fractures created along a horizontal drain. In a fracture job the bottom hole pressure rises above the fracture gradient of the formation, but within the pressure range allowed by the completion. Once the fracture is initiated, the bottom hole pressure is kept while a proppant such as sand or ceramic beads is included in the fracturing fluid. As the fracture 'screens out', the induced fracture faces remain open.

Rock mechanics suggests that in most cases the fracture has symmetrical 'bi-wing' geometry. The model we use in well testing assumes that the fracture wings are two perfect rectangles, each of length X_f, the half fracture length. For fully penetrating fractures the rectangles height is the formation thickness.

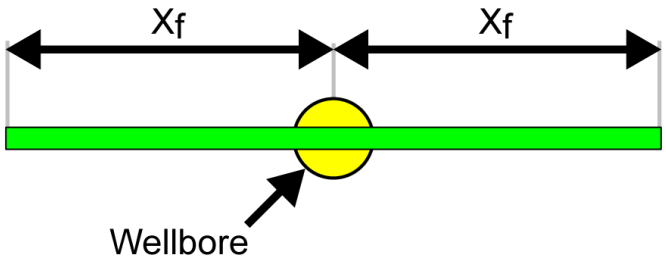


Fig. 6.D.1 – Schematic of a fracture model in the horizontal plane

There are two main types of fractured models: the high, or 'infinite conductivity' and the 'finite conductivity'. In the high conductivity we assume that the pressure drop along the inside of the fracture is negligible. In the low conductivity case we simulate diffusion within the fracture (see specific section).

There are two main high conductivity fracture models: the **Uniform Flux** model assumes a uniform production along the fracture. The **Infinite Conductivity** model assumes no pressure drop along the fracture. The latter is the one that makes sense physically. The former was initially developed because it is pretty straightforward to generate analytically. It is also used with a 'trick' (see below) to simulate the infinite conductivity response without the CPU cost of the true, semi-analytical solution.

6.D.2 Behavior

At early time only the part of the reservoir in front of the fracture will significantly contribute to the well production, orthogonal to the fracture plane. This is what we call the **linear flow**, and this is a characteristic feature (see figure below).

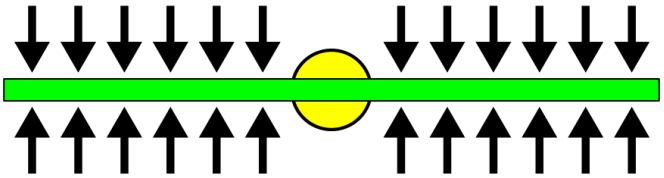


Fig. 6.D.2 – Early time linear flow

This linear flow is a particular case of a flow through a section of constant area A. Other examples of such flow are late time linear flow between two parallel faults. When such flow occurs there is a linear relation between the pressure change and the square root of the elapsed time, given by the following relation:

$$\Delta p = \frac{8.12\,qB}{Area}\sqrt{\frac{\mu\Delta t}{k\phi c_t}}$$

Where '*Area*' is the flowing section in ft². In the case of a fracture, the flowing section is the area of the fracture rectangle, so $Area = 2X_f h$. We then get:

$$\Delta p = \frac{4.06\,qB}{hX_f}\sqrt{\frac{\mu\Delta t}{k\phi c_t}} = \sqrt{\frac{16.52\,q^2B^2\mu}{h^2\phi c_t}}\frac{\sqrt{\Delta t}}{\sqrt{kX_f^2}}$$

The flow will then progressively deviate from the early linear flow while the rest of the formation starts impacting the well production, and the area of investigation becomes elliptical. When the production continues the ellipse grows into a large circle and we reach Infinite Acting Radial Flow. At this stage the fracture behaves like a standard well with a **negative skin**.

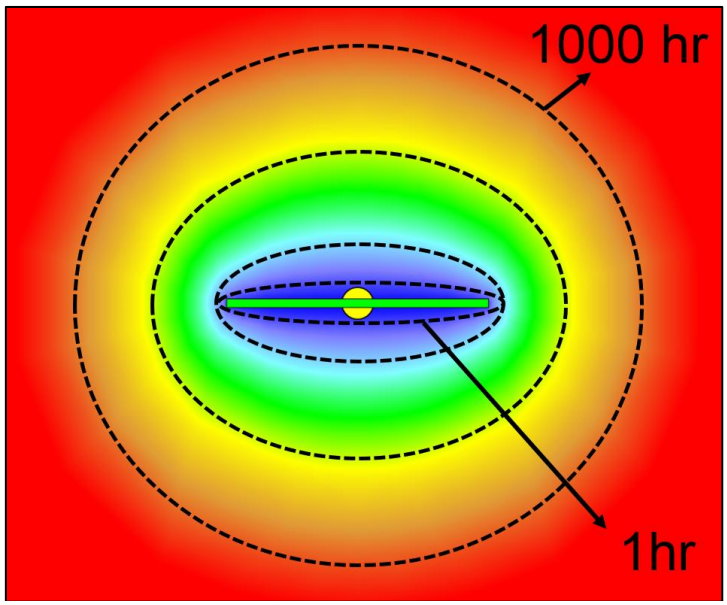


Fig. 6.D.3 – Evolution of the area of investigation

The figure below shows the normalized density of flow from the formation into the fracture. The red curve corresponds to the Uniform Flux fracture. At very early time the infinite conductivity solution will follow this profile. However this changes rapidly until it stabilizes at late time to the blue curve, showing that most of the flow at late time comes from the tips of the fracture, which are more exposed to the rest of the formation than the center part.

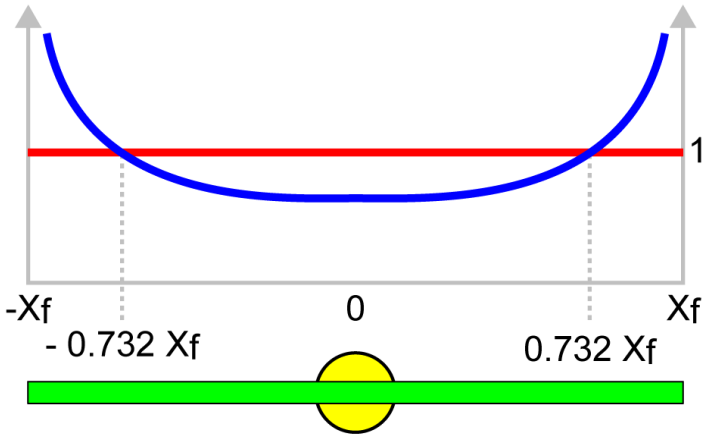


Fig. 6.D.4 – Flow profile along the fracture at early and late time

6.D.3 Loglog Analysis

From the previous section, the pressure change during the early time linear flow is:

$$\Delta p = m\sqrt{\Delta t} \quad where \quad m = \sqrt{\frac{16.52 q^2 B^2 \mu}{h^2 \phi c_t}} \frac{1}{\sqrt{k X_f^2}}$$

In the equations above, all parameters are inputs except the permeability and the fracture half length. During the linear flow, the result of any analysis will therefore provide a relation between permeability and fracture half length by determining the value of kX_f^2.

The Bourdet derivative at early time is given by:

$$\Delta p' \approx \frac{d\Delta p}{d\ln(\Delta t)} = \Delta t \frac{d\Delta p}{d\Delta t} = \Delta t \frac{m}{2\sqrt{\Delta t}} = \frac{1}{2} m\sqrt{\Delta t} = \frac{1}{2}\Delta p$$

On a decimal logarithmic scale this writes:

$$\log(\Delta p) = \log(m) + \frac{1}{2}\log(\Delta t) \quad and \quad \log(\Delta p') = \log(\Delta p) - \log(2)$$

The early time flow regime of a high conductivity fracture is characterized on a loglog plot by a half unit slope on both the pressure and derivative curves. The level of the derivative is half that of the pressure. At later time there is a transition away from this linear flow towards Infinite Acting Radial Flow, where derivative stabilizes (see figure below).

The position of these two half slope straight lines will establish a link between the time match and the pressure match, providing a unique result for kX_f^2. Fixing the stabilization level of the derivative will determine the value of k, and the half fracture length will be calculated from kX_f^2. If there is no clear stabilization level the problem will become underspecified.

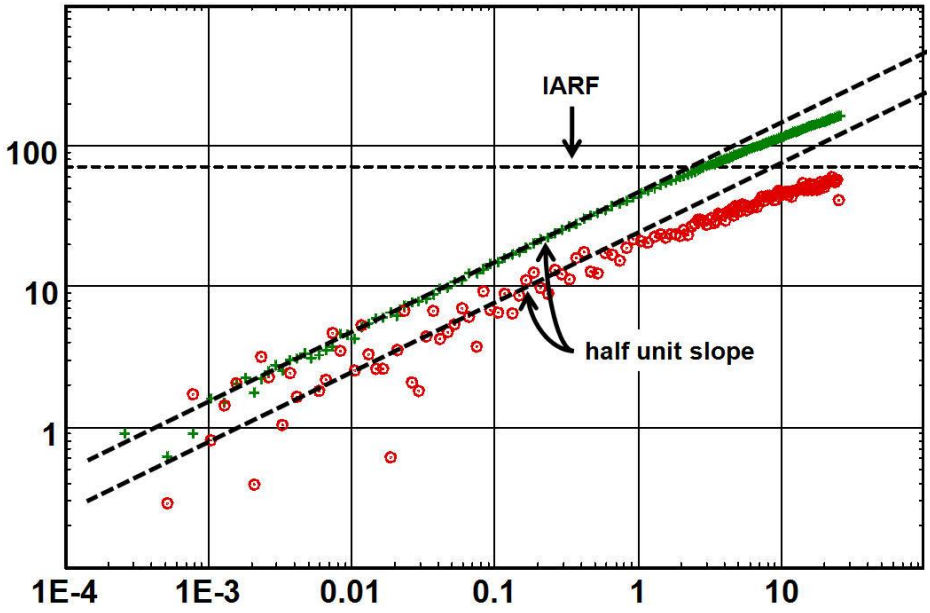


Fig. 6.D.5 – Infinite conductivity fracture behavior

6.D.4 Sensitivity to different parameters

6.D.4.a Choice of fracture model

The description above applies to both Infinite Conductivity and Uniform Flux models. It may be interesting at this stage to compare both solutions for the same parameters, see figure below.

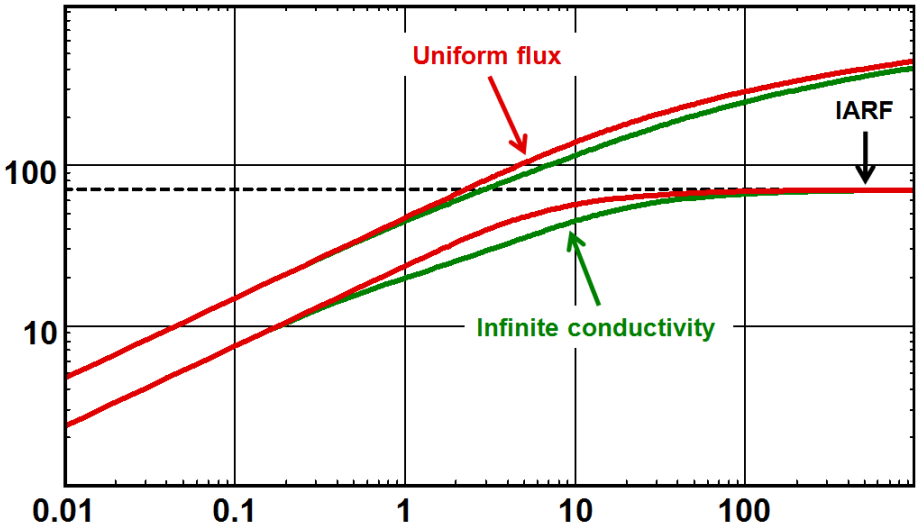


Fig. 6.D.6 – Uniform Flux vs. Infinite Conductivity

These solutions differ only slightly when plotted on a loglog scale. Purists consider that the uniform flux solution is physically incorrect and only the infinite conductivity solutions should be used. In real life the uniform flux transients generally offer a better match, and this can be explained by the fact that the productivity of the uniform flux fracture, for a given length, is slightly lower than the infinite conductivity, and that this, possibly, better simulates the slight pressure losses in the fracture.

The Uniform Flux model was published because it was fairly easy to calculate. The infinite conductivity fracture was solved semi-analytically (at high CPU cost) but it was shown that an equivalent response could be obtained by calculating the (fast) uniform flux solution at an off-centered point in the fracture ($x=0.732.X_f$). This position corresponds to the intercept of both flow profiles, as shown in the 'behavior' section.

6.D.4.b Sensitivity to the half fracture length

The loglog plot below is the comparison of several infinite conductivity responses for different values of X_f, all other parameters, including the formation permeability, staying the same. Because the permeability does not change, the pressure match remains constant, and the loglog response is shifted left and right. Multiplying the fracture length by 10 will shift the responses two log cycles to the right. This will shift the early time half slope down one cycle.

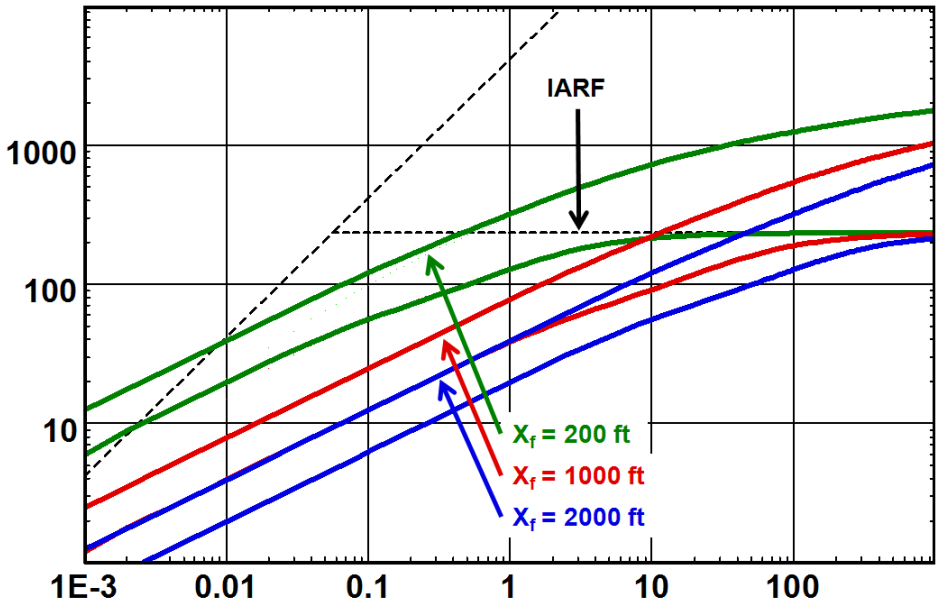


Fig. 6.D.7 – Sensitivity to X_f

6.D.4.c Sensitivity to the reservoir permeability

The loglog plot below is the comparison of several infinite conductivity responses for different values of permeability, all other parameters, including the fracture half length, staying the same. Multiplying the permeability by 100 will shift the stabilization of the derivative down two log cycles, but the half slope of the linear flow will only be shifted down one log cycle.

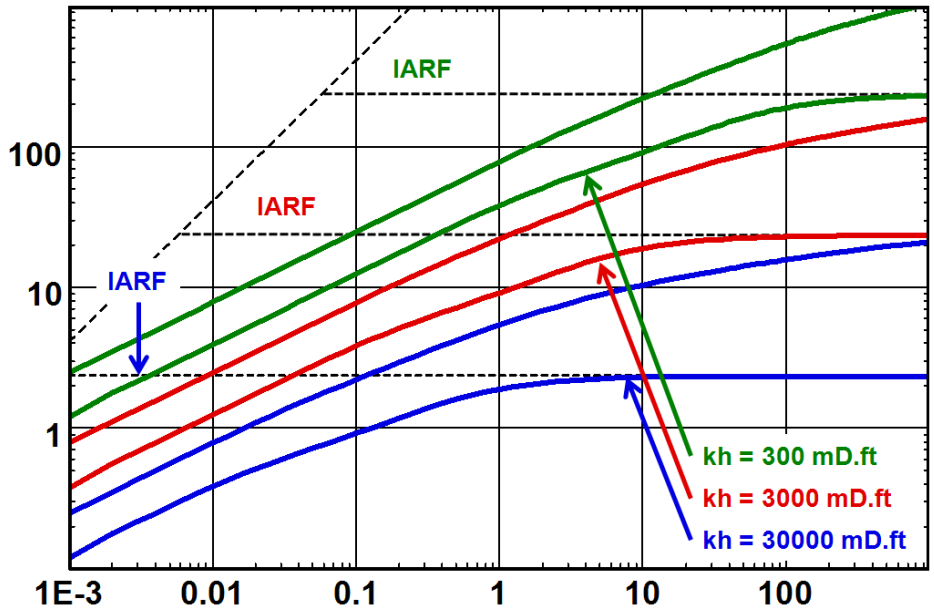


Fig. 6.D.8 – Sensitivity to kh

6.D.5 Specialized Analysis

Let us repeat it. The loglog analysis with the Bourdet derivative (a.k.a. the 'right stuff') has all what is needed to perform the complete analysis of a fractured well. Positioning the half slopes of both pressure and Bourdet derivative exactly does what we will be showing below. The advantage of the loglog approach is that it will be valid even if a pure linear flow is not detected, and a successful nonlinear regression will not require pure behaviors to occur. Anyway, the specialized analyses have a historical value and do not hurt, anyway.

From the previous section, the relation between pressure and time during the linear flow is:

$$\Delta p = m\sqrt{\Delta t} \quad where \quad m = \sqrt{\frac{16.52 q^2 B^2 \mu}{h^2 \phi c_t}} \frac{1}{\sqrt{k X_f^2}}$$

A straight line can be drawn on a cartesian graph of pressure change versus $\sqrt{\Delta t}$:

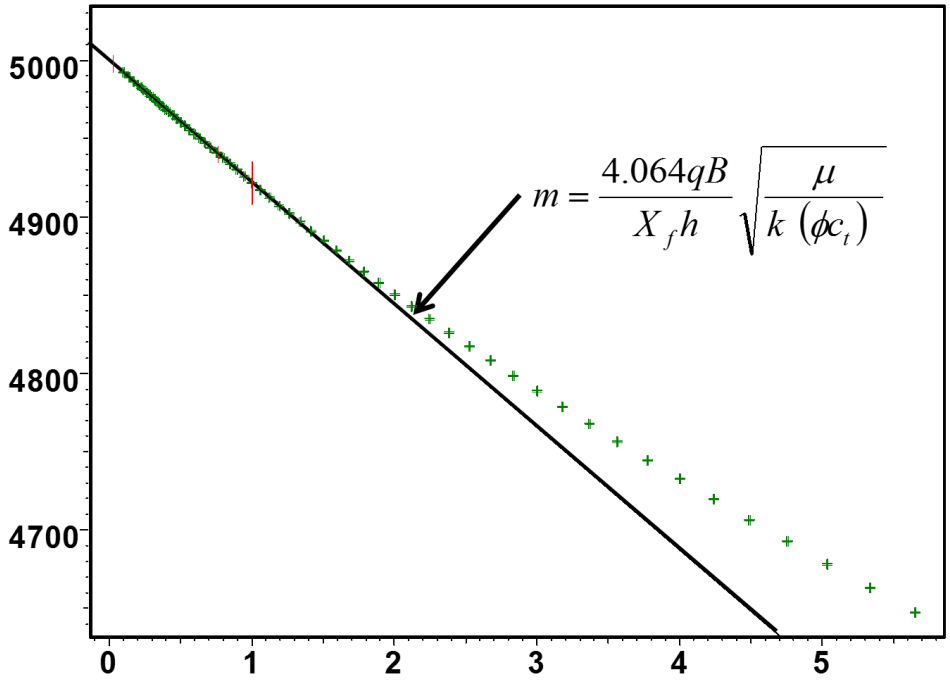


Fig. 6.D.9 – Square root plot

From this plot we get a value of kX_f^2, and therefore X_f if we do know k.

$$kX_f^2 = \frac{16.52 q^2 B^2 \mu}{m^2 h^2 \phi c_t} \quad and/or \quad X_f = \frac{4.06 qB}{mh}\sqrt{\frac{\mu}{k\phi c_t}}$$

Applying superposition? **NO!**

In a specialized plot (except the linear plot) it is possible to replace a time function by its rate superposition. For example we could use the tandem square root plot in the case of a build-up. This is the case when we assume that the flow regime we are studying is actually the superposition of these flow regimes. We do this for Infinite Acting Radial Flow or late time effects such as the linear flow between parallel faults. This does NOT apply here, or to any other early time behavior, and we should use the pure time function, not the superposed one. The only exception may be for shale gas, where the 'early time' behavior actually lasts years, and where superposition may be applicable.

6.D.6 Adding wellbore storage

The original publications on fracture solutions were without wellbore storage and skin. It is not that it was absent, but the solution with two additional parameters (C and S) was too complex to be turned into readable type-curves especially as the influence of skin is particularly messy.

Wellbore storage will affect the early time data by masking the linear flow. If the storage effect is high enough no fracture flow may be diagnosed from the loglog plot and the interpreter can no longer justify that a fracture may exist if the total skin is not highly negative. It will also become increasingly more difficult to make a choice between a low or high conductivity fracture, and the half fracture length X_f can no longer be determined from the square root plot.

If a fracture job had been done on the well this could be an indication that the job had not been very successful or that the fracture had propagated up or down rather than laterally.

The below figure illustrates the effect of wellbore storage on the linear flow in the loglog plot.

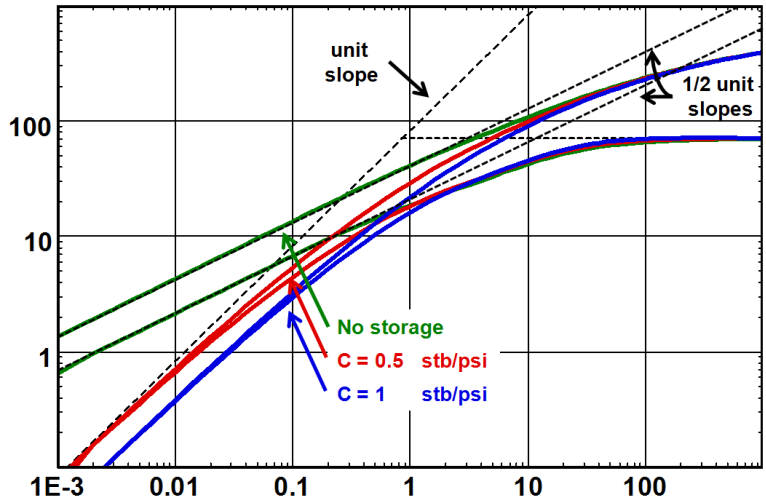


Fig. 6.D.10 – Loglog plot influence of wellbore storage

6.D.7 Skin effect

Total skin; geometrical skin; model skin: The concept of skin in configurations that are not based on a standard vertical well are sometimes confusing. This section describes the different skin components, and how they may be combined.

6.D.7.a Fracture Geometrical Skin

When we run a standard straight line analysis on a logarithmic scale (MDH, Horner, Superposition) we calculate a value of the skin factor. This is what we call the **Total Skin** S_T. This calculation may take place at any time after the extraction of the build-up, and is independent of the model chosen. The Total Skin is given by the equation:

$$\Delta p_{Skin} = 141.2 \frac{q_{sf} \mu}{kh} S_T$$

where Δp_{Skin} is the pressure difference between our data and the response of a standard, undamaged, fully penetrating vertical well.

When we generate a high conductivity fracture model with no specific damage or stimulation other than the fracture itself, and then perform a IARF straight line analysis, we will get a negative skin. This negative skin is not due to any pressure loss or gain at the sandface, it is just due to the geometry of the well. This is what we call the **Geometrical Skin** S_G. We can also link this geometrical skin to the equivalent wellbore radius. This is the radius of a theoretical vertical well that would have the same productivity as the fracture. The geometrical skin and equivalent radius depend on our choice of fracture model:

$$Uniform\ Flux: \qquad S_G = -\ln\left(\frac{X_f}{2.718 r_w}\right) \qquad r_{weq} = \frac{X_f}{e} \approx 37\% X_f$$

$$Infinite\ Conductivity: \qquad S_G = -\ln\left(\frac{X_f}{2.015 r_w}\right) \qquad r_{weq} = \frac{X_f}{2.015} \approx 50\% X_f$$

Another way to present this is that an infinite conductivity fracture with a half length of 200 ft will have the same productivity of a theoretical vertical well with a radius of 100 ft. If the well radius is 0.3 ft, the geometrical skin S_G will be -ln(333)= -5.8.

The figure below shows the equivalent wellbore radius for an Infinite Conductivity Fracture (blue) and a Uniform Flux Fracture (orange).

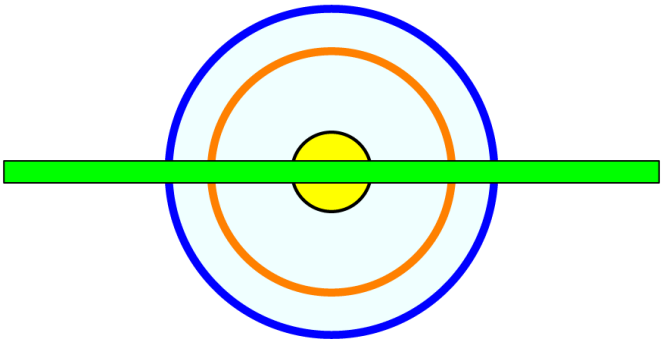


Fig. 6.D.11 – Equivalent wellbore radius

6.D.7.b Model Skin and Total Equivalent Skin

In complement there may be a pressure loss or gain at the sandface, which is quantified with the **Model Skin** S_M. At this stage one has to be careful about the convention of how the skin is defined. There are two ways to define the Skin factor in a fractured well model, and these are accessible in the Saphir settings page, Interpretation option, Skin tab:

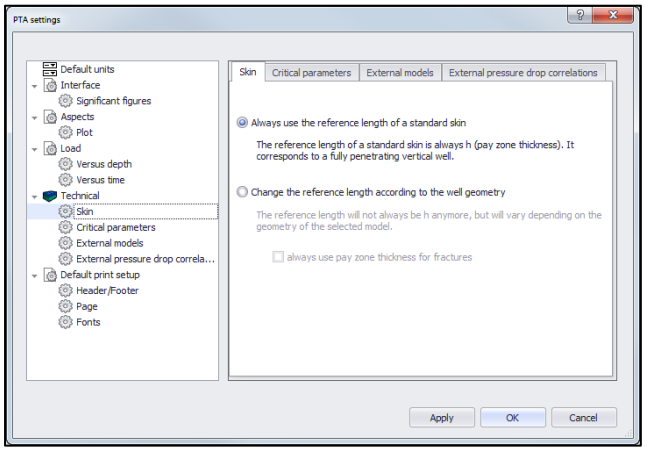


Fig. 6.D.12 – Skin convention dialog in Saphir

The **Standard Skin** considers that we keep the standard vertical well sandface as the flow area through which the skin factor is applied. This is as if the skin pressure drop was occurring at the well and not at the fracture sandface.

There are two ways to define the **Fracture Skin**:

$$A_{Flow} = 2\pi r_w h$$

Because the reference areas are the same, under this convention the component skins add up, and the total equivalent skin S_T will be:

$$S_T = S_G + S_M$$

and $A_{Flow} = 4X_f h$

Because the reference areas are different, under this convention the component skins will need a normalization to add up, and the total equivalent skin S_T will be:

$$S_T = S_G + \frac{\pi r_w}{2X_f} S_M$$

6.D.7.c Influence of skin

The figure below illustrates the influence of fracture skin on the behavior of the pressure change and the derivative. There is no effect on the derivative but the pressure change will no longer show the half slope behavior of linear flow as the pressure change become flatter as the fracture skin increases.

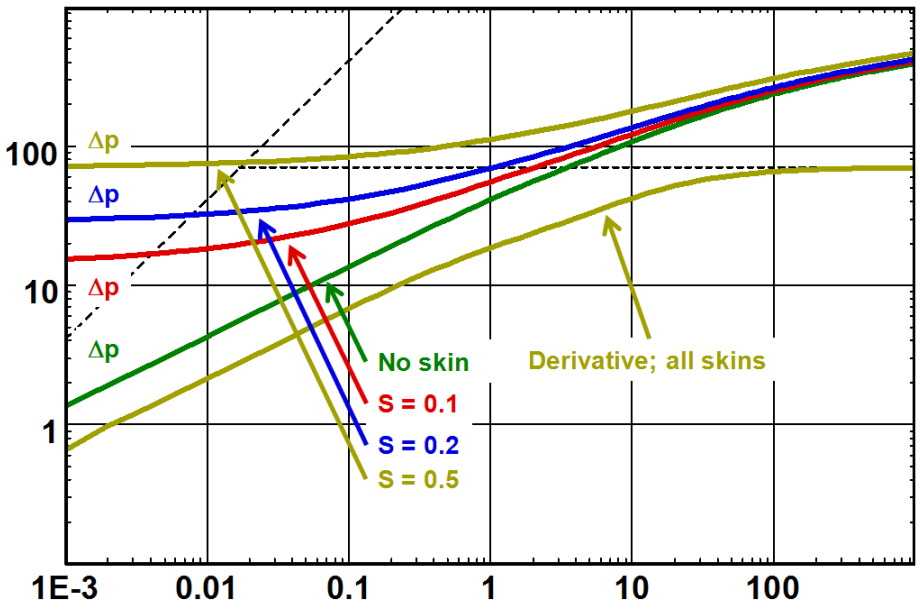


Fig. 6.D.13 – Fracture skin influence

6.E Low conductivity fracture

6.E.1 Hypothesis

The fracture geometry is the same as that of the high-conductivity models, but now it is assumed that there is a significant pressure gradient along the fracture.

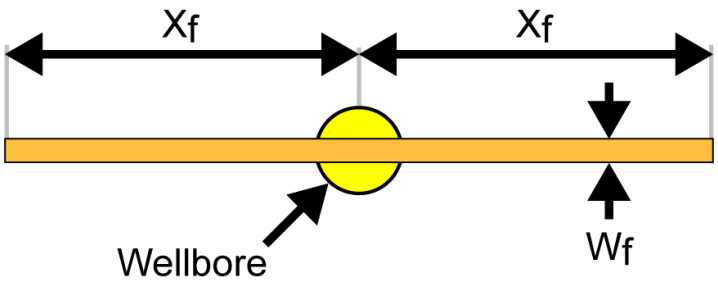


Fig. 6.E.1 – Schematic of a fracture model in the horizontal plane

6.E.2 Behavior

In the absence of storage, the first flow regime is linear flow along the fracture axis, this simultaneously induces a linear flow orthogonal to the fracture, the amplitude of which changes along the fracture length, i.e. there is a non-uniform flux into the fracture, in contrast to the high-conductivity models. This bi-linear flow regime, with linear flow along two axes, gives rise to a pressure response proportional to the fourth root of time. Both the loglog and the Bourdet derivative plots exhibit quarter slopes during bi-linear flow. Bi-linear flow is followed by the usual linear flow, characterized by a 1/2-unit slope on the loglog.

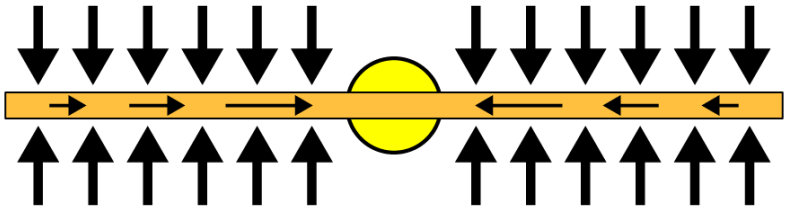


Fig. 6.E.2 – Early time bi-linear flow

The bi-linear flow regime is usually happening at very early time, and is not always seen. It represents the time at which the pressure drop along the fracture is significant, and in reality this time is very short. Even when there is no storage effect, the data sometimes does not exhibit a ¼-slope and can be matched directly with a high-conductivity fracture model. However, the general model for an 'induced fracture' fractured well must be the finite-conductivity fracture model, as there will always be a pressure drop along the fracture, however small. This is however, not significant compared to the linear pressure drop in the reservoir into the fracture.

There are two additional parameters that needs to be specified in this model; the fracture width (w) and the fracture permeability (k_f), in fact it is the permeability thickness of the fracture that is specified (k_fw).

When the fracture conductivity is very high, the model approaches the infinite-conductivity response, with a ½-slope developing immediately. Conversely, with low k_fw the pressure drop along the fracture is significant almost to the onset of radial flow (IARF). When such flow occurs the relationship between the pressure change and the fourth root of elapsed time is given be the flowing relationship:

$$\Delta p = \frac{44.11 q B \mu}{h\sqrt{k_f w}\left(\phi \mu c_t k\right)^{1/4}} \Delta t^{1/4}$$

6.E.3 Loglog Analysis

From the previous section, the pressure change during bi-linear flow is:

$$\Delta p = m\sqrt[4]{\Delta t} \quad where \quad m = \frac{44.11 q B \mu}{h\sqrt{k_f w}\left(\phi \mu c_t k\right)^{1/4}}$$

$$\Delta p' \approx \frac{d\Delta p}{d\ln(\Delta t)} = \Delta t \frac{d\Delta p}{d\Delta t} = \Delta t \frac{m}{4\sqrt[4]{\Delta t}} = \frac{1}{4} m\sqrt[4]{\Delta t} = \frac{1}{4}\Delta p$$

On a decimal logarithmic scale this writes:

$$\log(\Delta p) = \log(m) + \frac{1}{4}\log(\Delta t) \quad and \quad \log(\Delta p') = \log(\Delta p) - \log(4)$$

During bi-linear flow the pressure change and the Bourdet derivative follows two parallel straight lines with a slope of one quarter (1/4). The level of the derivative is a quarter of that of the pressure change.

This is followed by the onset of linear flow and the pressure change and the Bourdet derivative follow then two parallel straight lines of half slope (1/2) with the level of the derivative half that of the pressure change.

When radial flow is reached we have the usual stabilization of the derivative curve.

The following figure illustrates this behavior on the loglog plot.

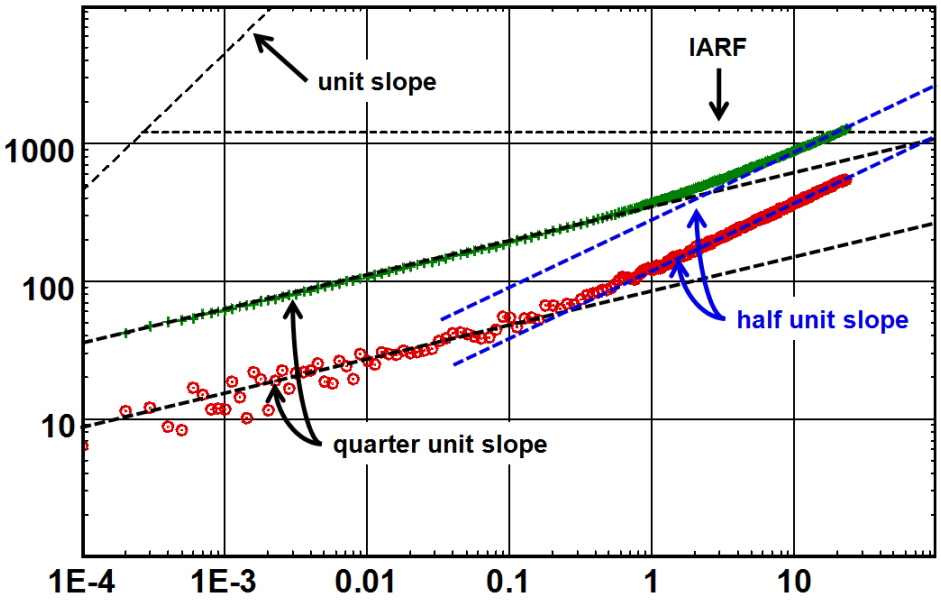


Fig. 6.E.3 – Finite conductivity fracture behavior

6.E.4 Sensitivity to different parameters

6.E.4.a Sensitivity to $k_f w_f$

For larger fracture conductivities the solution approaches that of an infinite conductivity fracture and the bi-linear flow will disappear completely as the derivative and the pressure change is shifted lower and lower, the ¼ slope will be completely replaced by the linear ½ slope. See the illustration in the figure below.

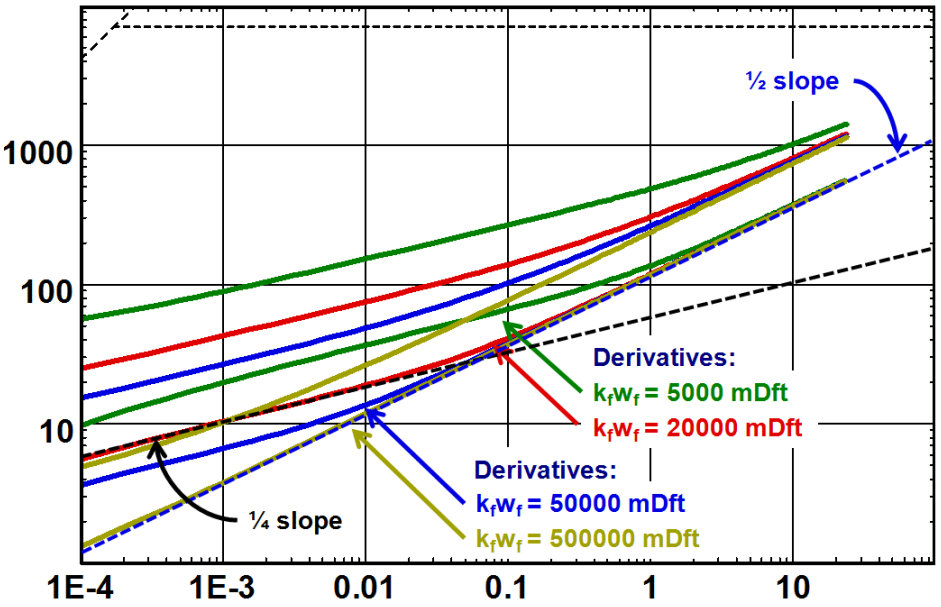


Fig. 6.E.4 – Finite conductivity fracture, sensitivity to $k_f w_f$

With very low fracture conductivity the linear flow will not develop and the bi-linear flow will be dominating until the unset of infinite acting radial flow.

6.E.4.b Sensitivity to the half fracture length

Keeping $Fc_D = \frac{k_f w_f}{kX_f}$ constant the pressure change and the Bourdet derivative curves shift to the right as the fracture length increases. The longer the fracture, the longer it takes to reach IARF. The following figure illustrates this.

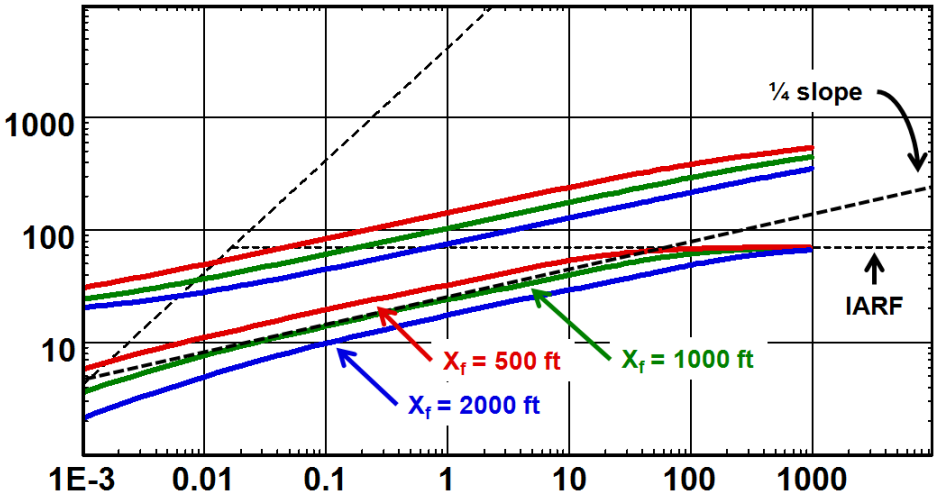


Fig. 6.E.5 – Constant Fc_D; sensitivity to half fracture length, X_f

In practice, massive hydraulic fracturing is only common in very low permeability formations. We typically encounter this sort of stimulation in Tight Gas, Shale Gas and Coal Bed Methane (CBM), type of reservoirs. This topic is covered in the chapter on 'Unconventional Reservoirs'. It suffices to say here that these types of wells would not be economically viable or would not produce at all without this sort of stimulation. It is now becoming popular not only to induce one single fracture in the well, but horizontal wells are selectively 'fracced', and multiple individual low conductivity fractures may exist. It goes without saying that the analyst's task can become more than just challenging.

It is easy to imagine that for a period subject to pressure transient analysis the time to reach infinite acting radial flow will be prohibitively long, and in some cases the transient will never reach this flow regime at all (well, maybe after thousands of years). Thus one can understand that lacking some of the flow regimes the interpretation of massive hydraulically fracced wells can be quite difficult.

It is therefore always recommended that a pre frac test be carried out to determine the permeability thickness product of the formation (kh).

6.E.5 Specialized analysis

The data that matches the quarter unit straight line in both the pressure change and the Bourdet derivative is in bi-linear flow. A plot of the pressure change versus the fourth root of elapsed time, $\sqrt[4]{\Delta t}$ will be on a straight line of slope:

$$m = \frac{44.11qB\mu}{h\sqrt{k_f w}(\phi\mu c_t k)^{1/4}} \text{ and } k_f w = 1945\sqrt{\frac{1}{\Phi\mu c_t k}}\left(\frac{aB\mu}{hm}\right)^2$$

The figure below illustrates the fourth root plot.

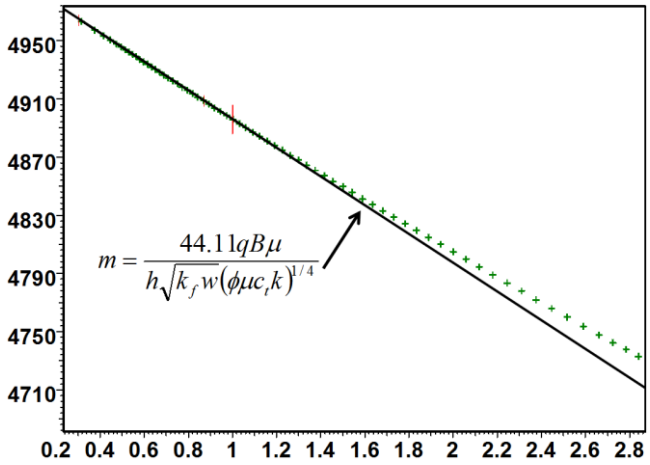


Fig. 6.E.6 – Fourth root plot

6.E.6 Adding wellbore storage

Wellbore storage will affect the early time data by masking both bi-linear and linear flow. The storage effect does not need to be very high in order to mask the fracture flow completely. The interpreter is faced with data that cannot prove that a fracture exists; only the very negative skin associated with the fracture and a marked increase in productivity will give him some arguments that the stimulation job was indeed successful or partly successful.

In fact, the analyst is often faced with this dilemma. From a design point of view the fracture job may be judged successful as we know what we pumped and the proppant disappeared, so the fracture must be in the ground. But often, the frac will propagate up or down, and parallel short fractures maybe induced thus masking the very long fracture that was designed for. It is just not manifesting itself in the bottom hole pressure data.

The figure below illustrates the effect of wellbore storage on the early time behavior.

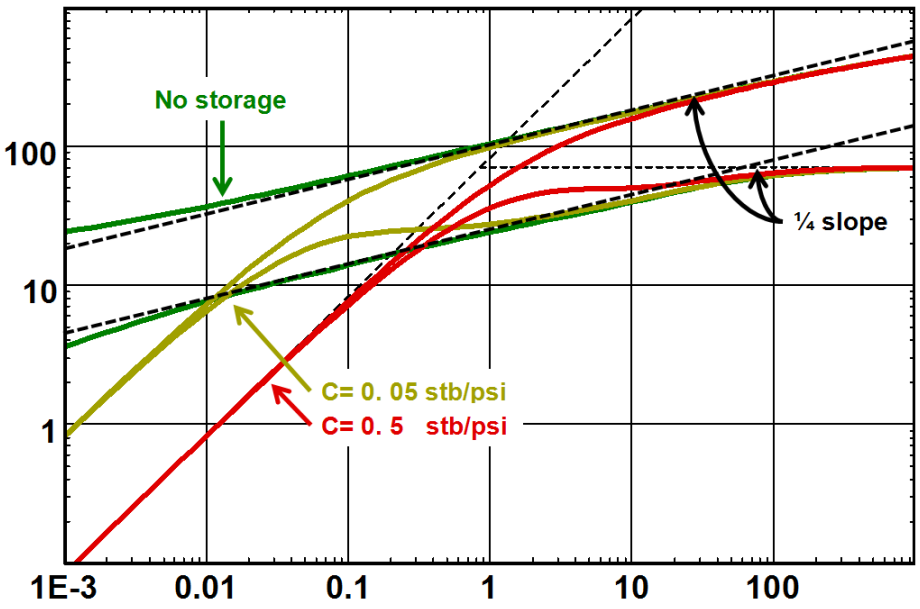


Fig. 6.E.7 – Wellbore storage influence

6.E.7 Skin effect

The total (semilog) skin of a fractured well is negative due to the fracture geometry. The mechanical skin of the fracture (damage) is the difference between the total skin and the geometrical skin. The total skin is given by the equation:

$$\Delta p_{Skin} = 141.2 \frac{q_{sf} \mu}{kh} S_T$$

where Δp_{Skin} is the pressure difference between our data and the response of a standard, undamaged, fully penetrating vertical well.

6.E.7.a Fracture Geometrical Skin

The skin of the finite conductivity fracture is defined by the geometrical skin defined for an infinite conductivity fracture and a correction factor to allow for the pressure drop caused by the low fracture conductivity.

The geometrical skin expresses the relation between the half fracture length and the skin for values of $\frac{k_f w}{k X_f} > 300$ and:

$$S_G = -\ln\left(\frac{X_f}{2.015 r_w}\right) \qquad r_{weq} = \frac{X_f}{2.015} \approx 50\% X_f$$

6.E.7.b Model Skin and Total Equivalent Skin

In complement there may be a pressure loss or gain at the sandface, which is quantified with the **Model Skin** S_M. At this stage one has to be careful about the convention of how the skin is defined. There are two ways to define the Skin factor in a fractured well model, and these are accessible in the Saphir settings page, Interpretation option, Skin tab:

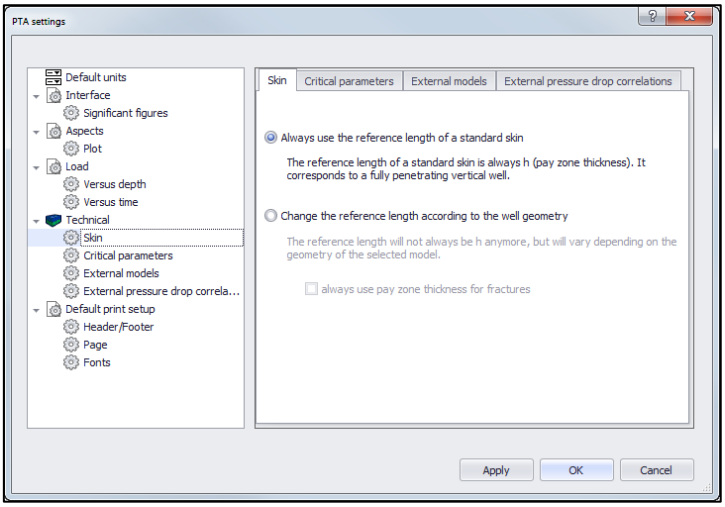


Fig. 6.E.8 – Skin convention dialog

The **Standard Skin** considers that we keep the standard vertical well sandface as the flow area through which the skin factor is applied. This is as if the skin pressure drop was occurring at the well and not at the fracture sandface.

There are two ways to define the **Fracture Skin**:

$$A_{Flow} = 2\pi r_w h$$

Because the reference areas are the same, under this convention the component skins add up, and the total equivalent skin S_T will be:

$$S_T = S_G + S_M$$

If one consider $A_{Flow} = 4X_f h$

The reference areas are different, under this convention the component skins will need a normalization to add up, and the total equivalent skin S_T will be:

$$S_T = S_G + \frac{\pi r_w}{2X_f} S_M \text{ Influence of skin}$$

The figure below illustrates the influence of fracture skin on the behavior of the pressure change and the Bourdet derivative. There is no effect on the derivative but the pressure change will no longer show the quarter slope behavior of bi-linear flow as the pressure change become flatter when the fracture skin increases.

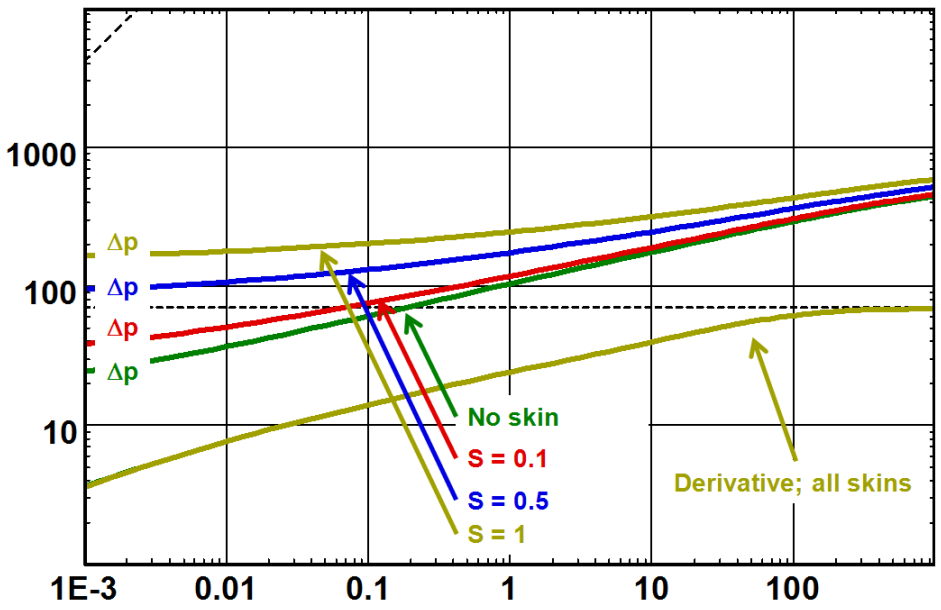


Fig. 6.E.9 – Fracture skin influence

6.F Limited entry well

6.F.1 Hypothesis

This model assumes that the well produces from an interval smaller than the net drained interval. The drained interval is not always fully perforated to avoid gas coning or cusping and/or water production from an underlying or lateral aquifer or bottom water. In this case the limited entry is voluntary. Partial penetration can also happen as a result of field operations gone awry; problems such as perforations off depth and plugging of perforations are amongst many reasons that a well has limited contribution to production.

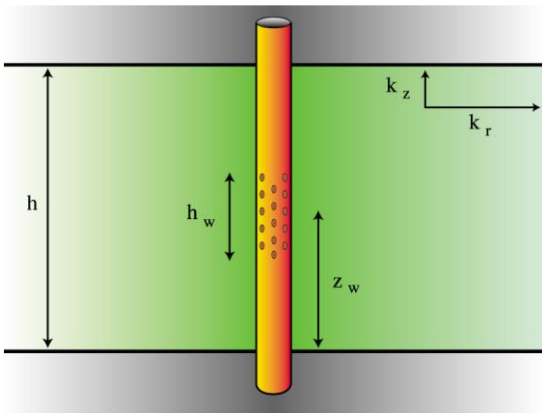


Fig. 6.F.1 – Limited entry schematic

The partial penetration effect also comes into play with all sorts of formation testing tools where the point of production can be just one single small ID probe, thus the pressure measurements maybe affected by the partial penetration spherical flow regime right through the measurement time. This particular test type is covered in the chapter on 'PTA - Special test operations'.

6.F.2 Behavior

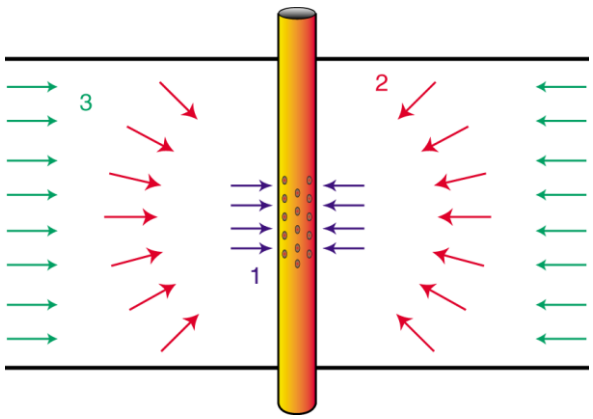


Fig. 6.F.2 – Limited entry flow regimes

In theory, after wellbore storage, the initial response is radial flow in the perforated interval h_w (see figure above), shown as '1'. This 'stabilization' gives the product $k_r h_w$ (the subscript $_r$ stands for radial) and it can be imagined that if there were no vertical permeability this would be the only flow regime present before the influence of any lateral boundaries. In practice this flow regime is more often than not masked by wellbore storage.

In flow regime '2' there is a vertical contribution to flow, and if the perforated interval is small enough a straight line of slope –½ (negative half slope) may develop in the Bourdet derivative, corresponding to spherical or hemi-spherical flow. The pressure is then proportional to $\frac{1}{\sqrt{\Delta t}}$.

The relation of the pressure change and the 'one over the square root' of the elapsed time is:

$$\Delta p = \frac{70.6qB\mu}{k_s r_s} - \frac{2453qB\mu\sqrt{\phi\mu c_t}}{k_s^{3/2}}\frac{1}{\sqrt{\Delta t}}$$

With: $$k_s = \left(k_r^{\,2} k_v\right)^{1/3}$$

Finally, when the diffusion has reached the upper and lower boundaries, the flow regime becomes radial again, and the stabilization now corresponds to the classical product, $k_r h$.

In any model where there is a vertical contribution to flow, there must also be a pressure drop in the vertical direction, and vertical permeability has to be considered along with the radial permeability. The pressure drop due to the flow convergence (flow regime 2, spherical flow) is a 'near-wellbore' reservoir effect caused by the anisotropy. If the spherical flow is seen in the data it may be possible to separate the 'damage' and 'geometric' components of the total skin determined from the second IARF period.

6.F.3 Loglog Analysis

From the previous section, the pressure change during spherical flow is:

$$\Delta p = a - m\frac{1}{\sqrt{\Delta t}} \quad where \quad m = \frac{2453qB\mu\sqrt{\phi\mu c_t}}{k_s^{3/2}} \quad and \quad a = \frac{70.6qB\mu}{k_s r_s}$$

$$\Delta p' \approx \frac{d\Delta p}{d\ln(\Delta t)} = \Delta t\frac{d\Delta p}{d\Delta t} = \Delta t\frac{m}{2\Delta t^{3/2}} = \frac{1}{2}m\frac{1}{\sqrt{\Delta t}} = \frac{1}{2}(a - \Delta p)$$

The characteristic flow regime is spherical flow until upper and lower boundaries have been reached and then followed by radial flow in the reservoir.

The interesting flow regime here is spherical flow during which time the pressure change is proportional to $\frac{1}{\sqrt{\Delta t}}$, the Bourdet derivative will follow a negative half unit slope straight line. From this flow regime it is possible to determine the spherical permeability ks, then, knowing kr, to deduce the anisotropy $\frac{k_v}{k_r}$. The below figure illustrates the behavior of a well with partial penetration.

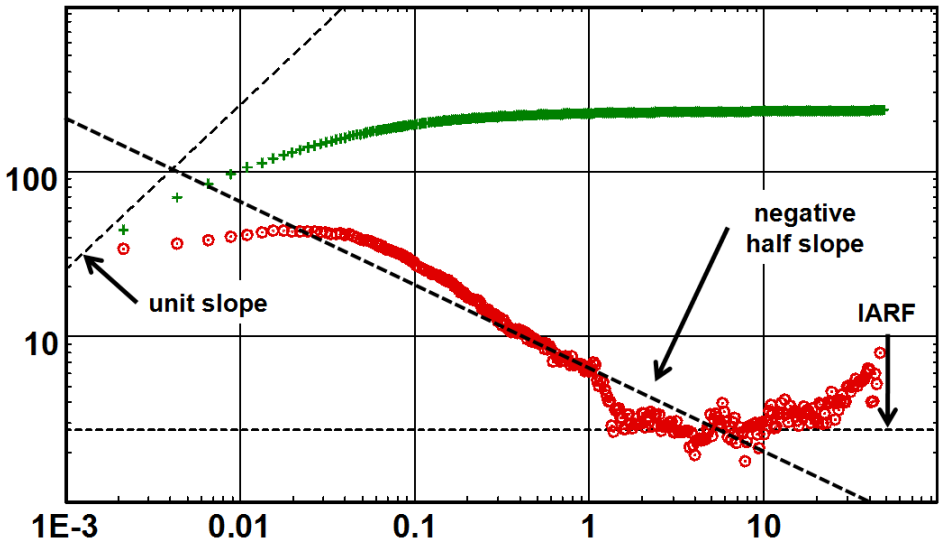


Fig. 6.F.3 – Limited entry well behavior

6.F.4 Sensitivity to different parameters

6.F.4.a Sensitivity to the anisotropy

As the anisotropy contrast becomes large the spherical flow regime becomes longer and the geometrical skin more severe. If the open interval is close to either the upper or lower boundary hemispherical flow will develop which is seen as a translation of the negative half slope in time, it develops later. If either of the boundaries is a constant pressure boundary (gas cap or active aquifer can act as a constant pressure boundary) then the Bourdet derivative will turn down. The below figures illustrates the sensitivity caused by the anisotropy on the Bourdet derivative in the loglog plot.

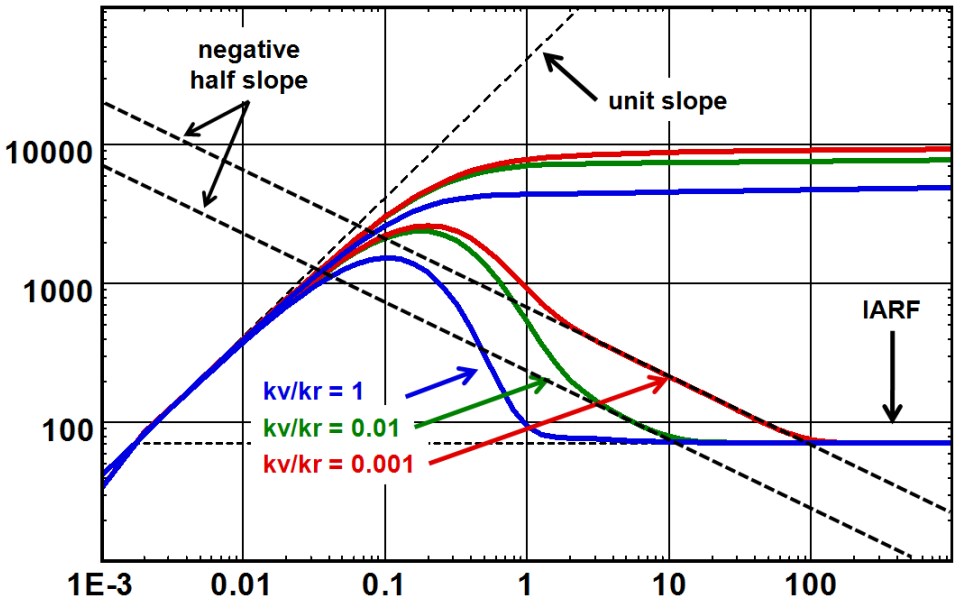


Fig. 6.F.4 – Sensitivity to anisotropy

The following figure shows the difference between spherical and hemi-spherical flow.

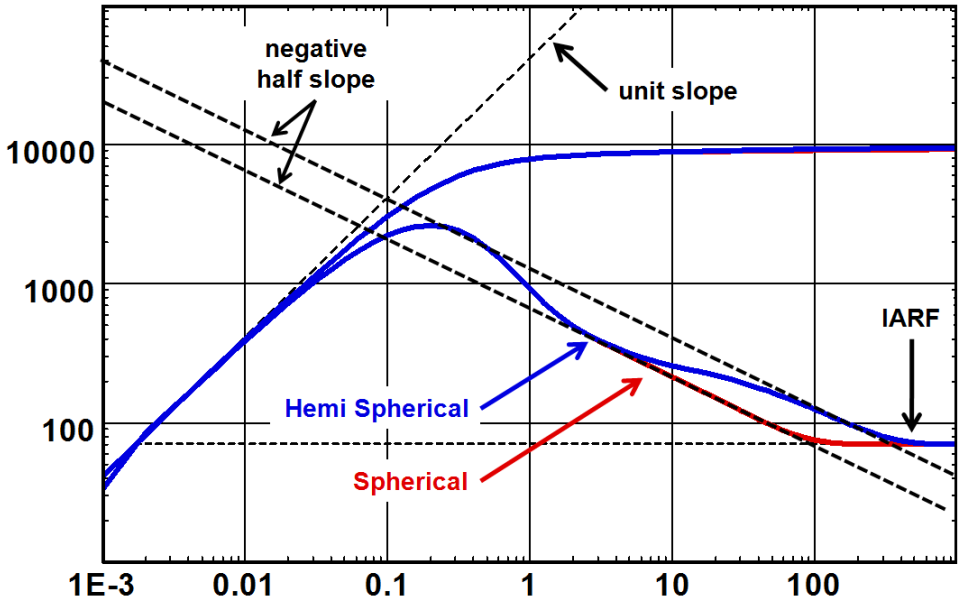


Fig. 6.F.5 – Spherical and hemi-spherical

6.F.4.b Sensitivity to the vertical distance to a constant pressure boundary

The next figure illustrates the influence of the proximity to a constant pressure boundary. The closer the perforated interval is to the boundary the stronger is the effect form it.

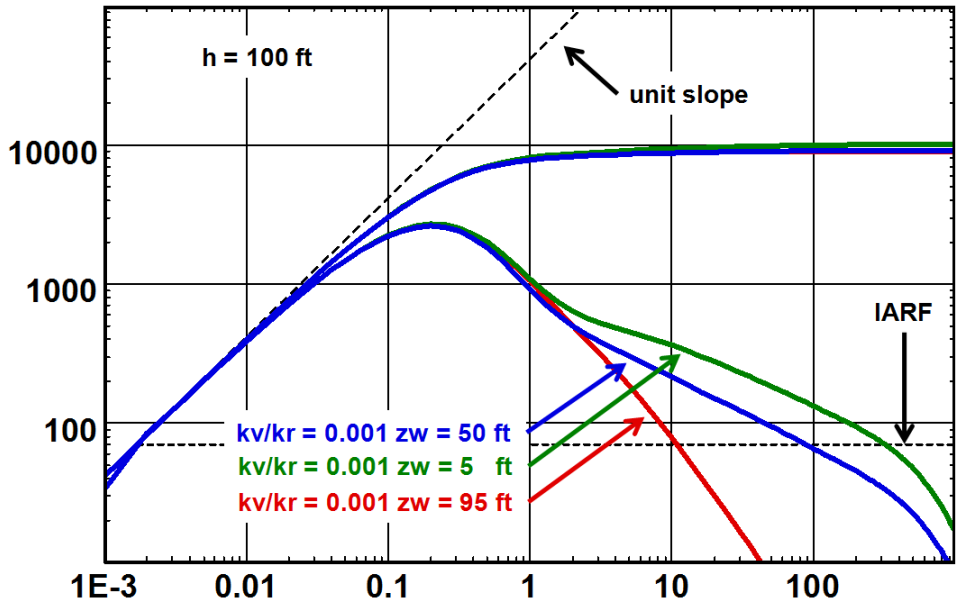


Fig. 6.F.6 – Limited entry with Gas Cap

With a high enough vertical permeability the spherical flow may not be seen at all; this is also dependent upon the ratio h_w/h, the fraction of the producing interval that is contributing and the level of wellbore storage. As k_v decreases the negative half slope spherical flow derivative becomes increasingly evident. The geometrical skin also increases.

6.F.5 Specialized analysis

The data that matches the negative half unit slope straight line on the Bourdet derivative in the loglog plot will also will also be on a straight line if the pressure change is plotted versus $\frac{1}{\sqrt{\Delta t}}$ in a cartesian plot. The straight line has a slope of:

$$m = \frac{2453 q B \mu \sqrt{\phi \mu c_t}}{k_s^{3/2}}$$

The anisotropy can then be determined $\frac{k_v}{k_r} = \left(\frac{k_s}{k_r}\right)^3$

This is valid when the contribution interval is such that spherical flow develops. If the open interval is close to the upper or lower boundaries then hemispherical flow will develop and the slope of the specialized plot has to be divided by two.

The below figure illustrates the specialized plot of pressure change versus $\frac{1}{\sqrt{\Delta t}}$.

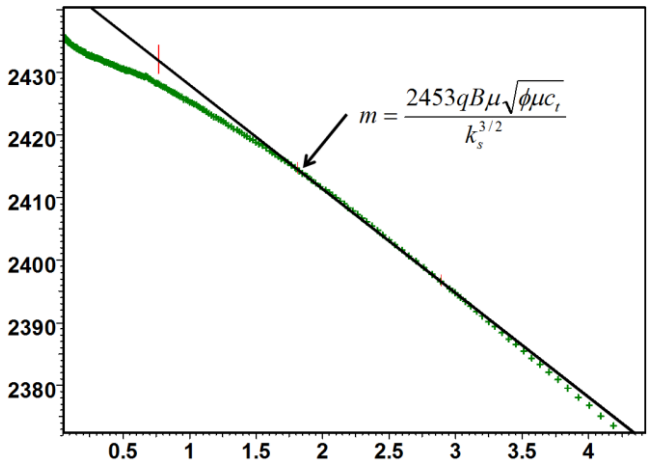


Fig. 6.F.7 – One over square root plot

6.F.6 Adding wellbore storage

Wellbore storage will quickly mask the spherical flow regime. In a well where there is no voluntary partial penetration the interpreter can easily miss the effect and as the limited entry can result in a high geometrical and thus a high total skin this can often be misdiagnosed as damage alone when coupled with the storage effect. Stimulation of a limited entry well will therefore often have no results.

The following figure illustrates the effect of increasing wellbore storage on a limited entry well.

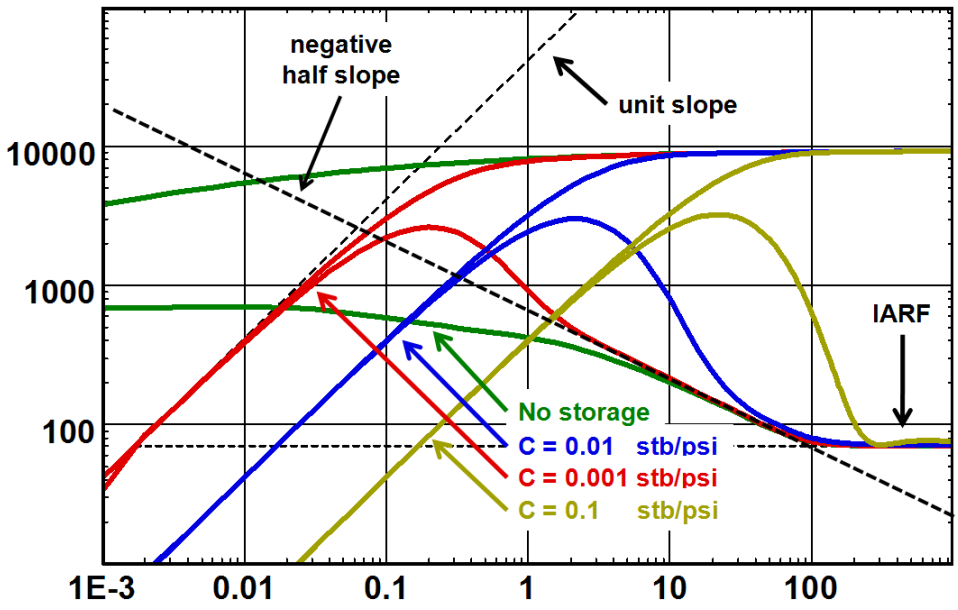


Fig. 6.F.8 – Sensitivity to wellbore storage

6.F.7 Skin effect

6.F.7.a Skin components

The total skin of a limited entry well is invariably positive due to the partial penetration. The mechanical skin of the open interval is the difference between the total skin and the geometrical skin.

A variety of correlations has been presented in the literature to estimate the geometrical skin. In Saphir the geometrical skin is determined by the difference between the model skin and the model skin for a fully penetrating vertical well with no skin damage, thus the various skin components adds up directly:

$$S_M = (S_T - S_G)$$

At this stage one has to be careful about the convention of how the skin is defined. The skin referring to the perforated interval hw is related to the skin related to h by:

$$S_M(h) = S_M(h_w)\frac{h}{h_w}$$

The skin can be referred to the perforated interval and the skin components needs to be normalized to add up, the total equivalent skin S_T will always be:

$$S_T = S_M(h) + S_G = S_M(h_w)\frac{h}{h_w} + S_G$$

6.F.7.b Influence of skin

The figure below illustrates the influence of the mechanical skin on the pressure change and the Bourdet derivative. There is no effect on the derivative so a change in skin will not mask the spherical flow regime.

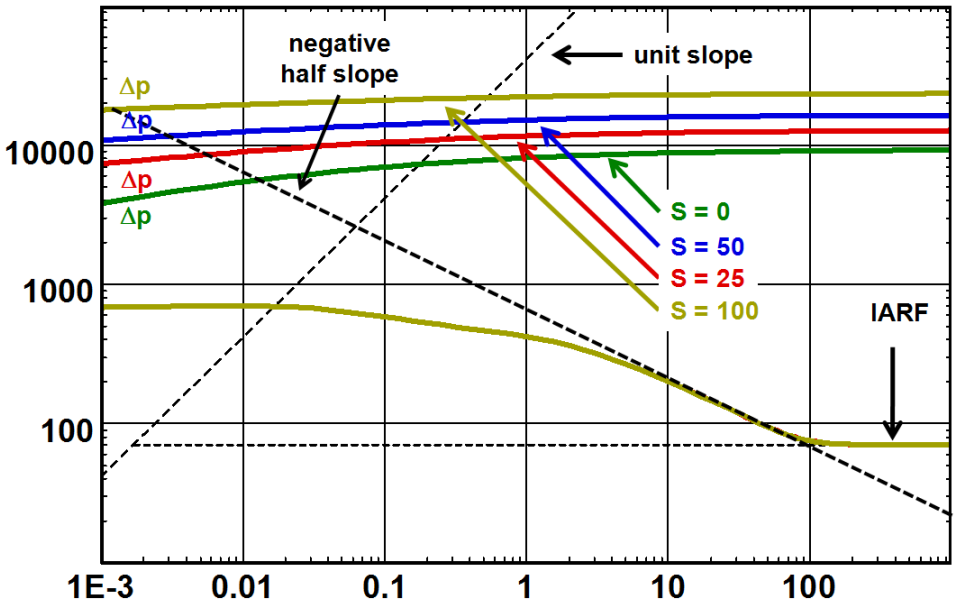


Fig. 6.F.9 – Limited entry skin sensitivity

There are often questions about how positive a skin can be in reality. The reality has to be seen in the proper light, that is with the appropriate reference. Imagine a test carried out with a 2 inch probe of a formation tester. The skin is determined to be 1 with reference to the probe dimension. If the test had reached radial flow a classical semilog analysis would reveal a skin (total skin) of 600 calculated with the appropriate net drained interval of 100 ft. So yes, very positive skin values may exist, the trick is to know what they mean.

6.G Horizontal wells

Horizontal wells are with no doubt a dream for the production engineer. However, they are a bit of a nightmare for the interpretation engineer trying to perform Pressure Transient Analysis. The nightmare started in the early 1990's, when the first horizontal well solutions were integrated into PTA software. It was quickly found out that the wells producing the textbook response given by the theory were in minority.

After the fact, the reason is pretty straightforward: the reality is far more complex than what we model. When dealing with vertical wells, we are making the same mistakes, but there is an enormous and fortuitous averaging effect taking place around the vertical well, and the response will be close to what theory predicts. In other words, we were lucky in the start when we used simplistic models for vertical wells and Infinite Acting Radial Flow and it worked (just). No such luck with horizontal wells, as the response is very sensitive to the assumptions that we make, whether it is the homogeneity of the formation, the part of the horizontal well that will produce effectively (the part of the horizontal section that is contributing to the production), the well geometry (the first rule of horizontal wells being that they are not horizontal) and multiphase flow behavior in the wellbore.

This warning is to say, yes fine, there are horizontal well models, and they give some theoretical behavior that will be described in this section. In the next section you will find 'textbook' data and some not so 'textbook' but overall you will realize that we can indeed make sense of the majority of data sets and achieve consistent analysis results. When we cannot, it is better to explain why and avoid at all costs inventing all sorts of schemes to try to explain the unexplainable.

6.G.1 Hypothesis

The well is assumed to be strictly horizontal, in a homogeneous formation which is also strictly horizontal and of uniform thickness h. As a start, we will consider that the reservoir is isotropic in the horizontal plane, but we will allow vertical anisotropy and other parameters to be defined as in the limited entry well.

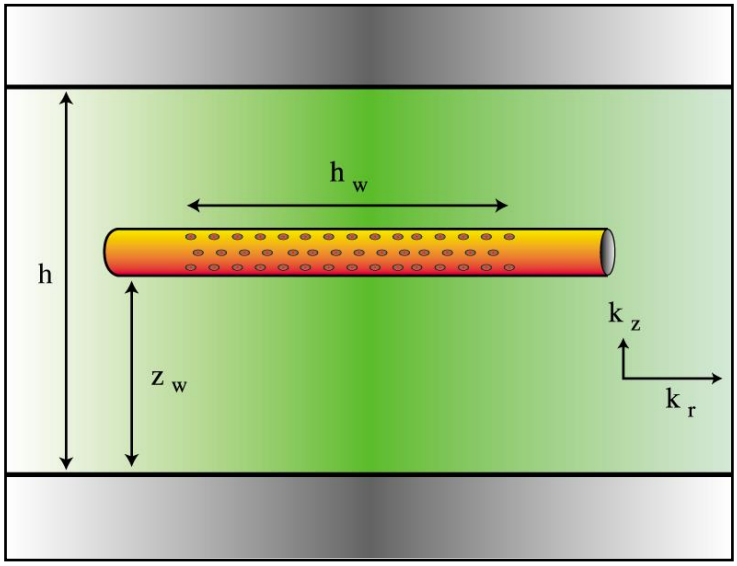


Fig. 6.G.1 – Horizontal well geometry

6.G.2 Behavior

The first flow regime, often obscured by wellbore storage, is pseudo-radial flow in the vertical plane, analogous to radial flow in a vertical well (see below figure). The average permeability combines the vertical and a radial (horizontal) component with horizontal anisotropy. In most cases the horizontal anisotropy is ignored and the permeability combination is just that of vertical and radial permeability. The thickness corresponds to the producing well contributing length. The level of the horizontal derivative, or the slope of the semilog straight-line, is therefore:

$$(kh)_{early} = h_w \sqrt{k_v k_r}$$

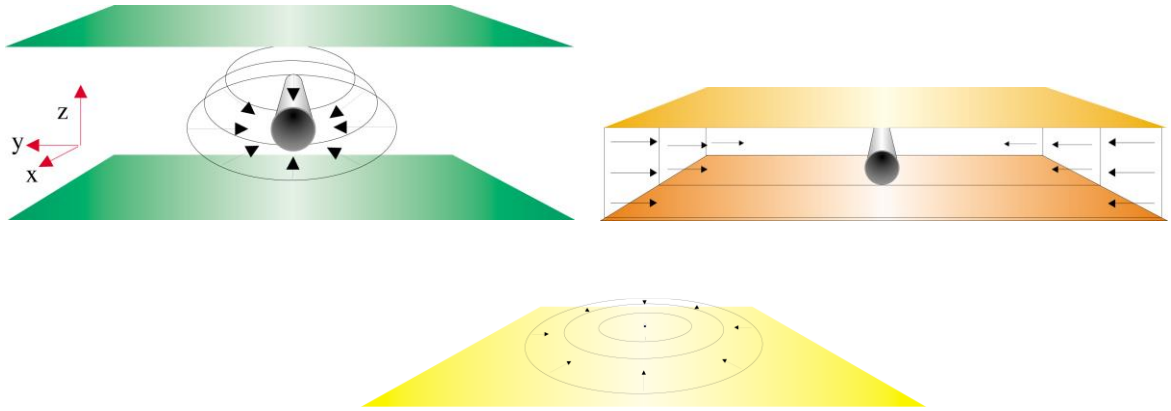


Fig. 6.G.2 – Main flow regimes: Pseudo-radial, linear flow and radial

If the vertical permeability is relatively large, the geometrical skin will be negative and the second flow regime is linear flow between the upper and lower boundaries. The Bourdet derivatives will follow a 1/2-unit slope.

$$(kh)_{linear} = k_r \left(\frac{h_w}{2} \right)^2$$

When the vertical permeability is small the geometrical skin becomes positive and the behavior of the second flow regime will be similar to that observed in limited entry wells.

The final flow regime is radial flow equivalent to that in a vertical well, with the second derivative stabilization representing the usual kh if the reservoir is considered isotropic.

$$(kh)_{late} = k_r h$$

6.G.3 Loglog analysis

The below figure illustrates a typical horizontal well behavior of a real horizontal well. Despite the changing wellbore storage at early time the 'early radial flow' is developed before linear flow sets in.

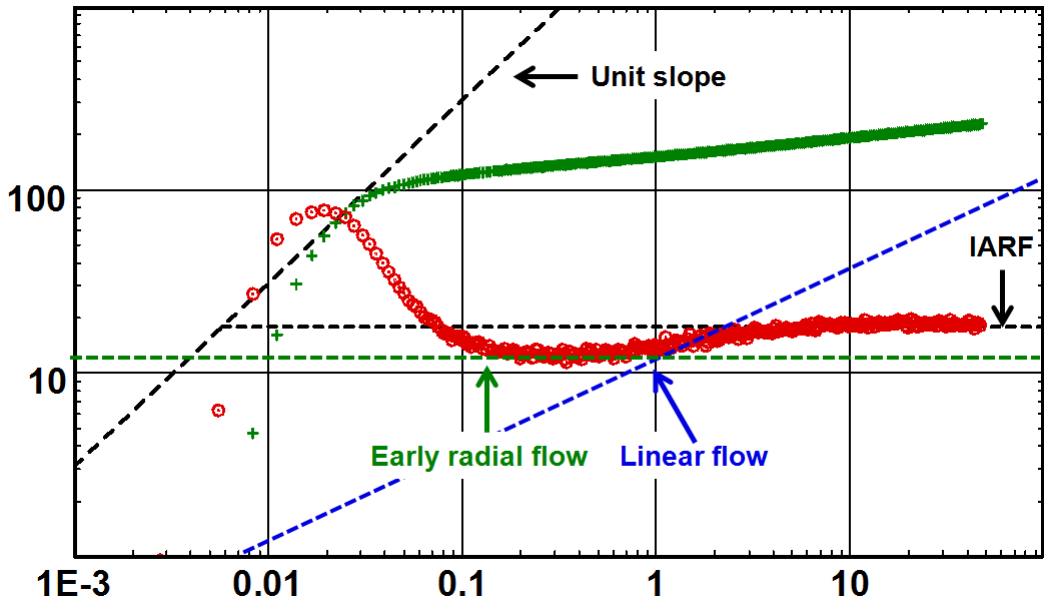


Fig. 6.G.3 – Horizontal well behavior

Looking end-on into a horizontal well is equivalent to looking down a vertical well. The first flow regime after storage in a vertical well is radial flow, and in a horizontal well the same applies. However due to the anisotropy the flow around the wellbore is not circular, but elliptical, as the diffusion will typically propagate more slowly in the vertical direction. Had the reservoir been totally isotropic in all directions then the diffusion around the horizontal well would be perfectly radial.

Once the diffusion has reached the upper and lower boundaries the flow becomes linear (if the geometrical skin is negative), equivalent to the parallel faults geometry in a vertical well but because of the finite length of the horizontal wellbore it cannot stay linear forever. Eventually the diffusion has reached sufficiently far from the wellbore that the dimensions of the horizontal section become irrelevant, and the flow again becomes radial, equivalent to radial flow in a vertical well.

6.G.4 Sensitivity to different parameters

6.G.4.a Contributing horizontal section, h_w and position

In a reservoir with no gas cap or aquifer, the well would typically be positioned as centrally as possible between the upper and lower boundaries, in which case the boundaries would be seen simultaneously and there would be a clean transition from radial to linear flow. The following figure illustrates the behavior with variable contributing horizontal sections (h_w),there is no wellbore storage.

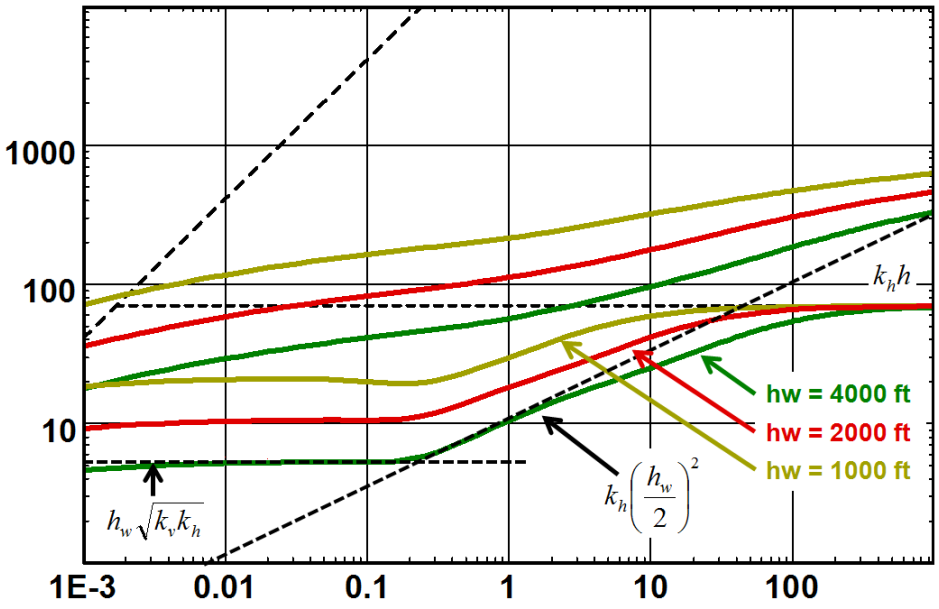


Fig. 6.G.4 – Horizontal well loglog response, variable horizontal drains

If the well is closer to one or the other boundary, there will first be a doubling of the derivative, as if seeing a fault in a vertical well, before the second boundary brings on the linear flow. The following figure illustrates this.

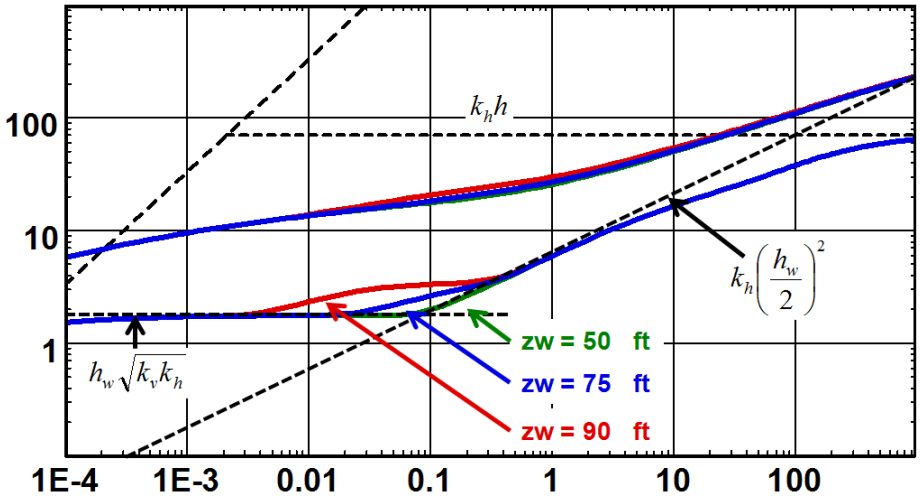


Fig. 6.G.5 – Horizontal well loglog response, variable well placements, zw

If the upper or lower boundary is a gas cap or an aquifer, the well will probably be positioned close to the other sealing boundary. In that case there will again be a doubling of the derivative, similar to the 'fault' response in a vertical well, followed by a constant pressure response. In each case the doubling of the derivative will not always be fully developed before the arrival of the next flow regime, be it linear flow or a constant pressure boundary.

6.G.4.b Sensitivity to the anisotropy

Further, below, we are illustrating the behavior for a horizontal well with a variable k_v/k_h. When the permeability contrast increase, the shape of the Bourdet derivative looses the classic 'finger print' of the horizontal well. The shape of the derivative approaches that of a partial penetrating well.

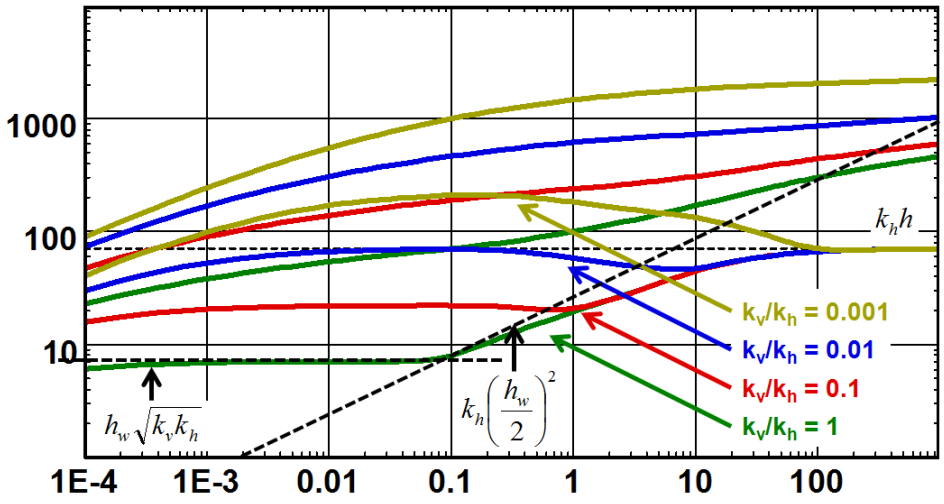


Fig. 6.G.6 – Horizontal well loglog response, variable vertical anisotropy

6.G.5 Adding wellbore storage

Wellbore storage will very quickly mask the 'early time radial flow'. Significant wellbore storage will also mask the half unit slope straight line of the linear flow. Both factors increase considerable the challenge facing the interpretation engineer since experience has shown that it is common not to develop infinite acting radial flow in the reservoir. Without any recognizable clear flow regimes to deal with, the task is certainly compounded and a consistent analysis can only be achieved if the reliability of the 'known' data is high. Refer to the following figure that shows the behavior with different wellbore storage constants.

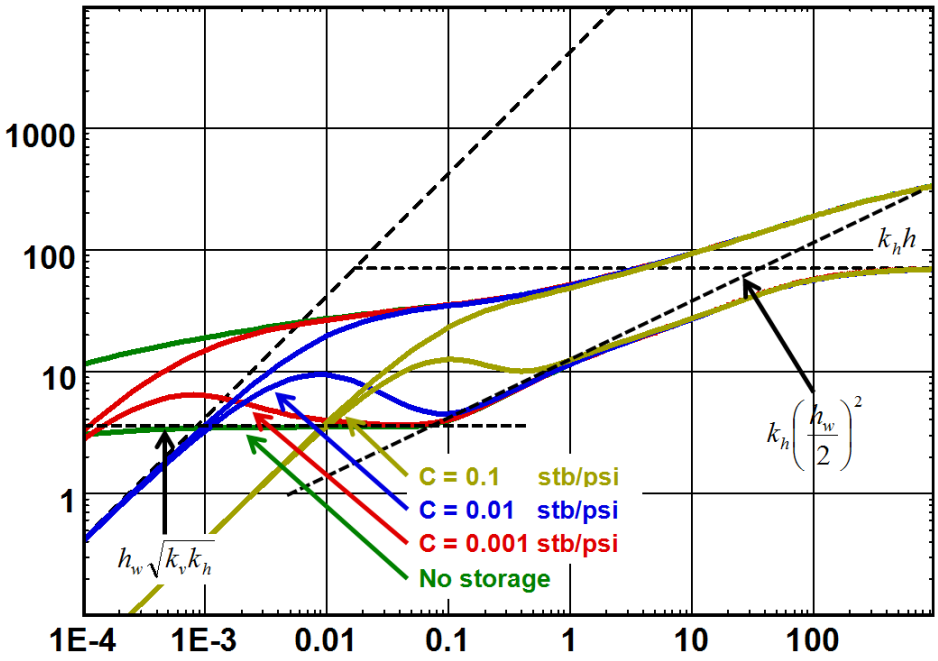


Fig. 6.G.7 – Sensitivity to wellbore storage

6.G.6 Skin effect

When the contrast between horizontal and vertical permeability (anisotropy) is small the geometry of a horizontal well will induce a negative skin components that reflects directly why we would want to drill horizontal wells in the first place. The mechanical skin S_M is the difference of the total skin S_T and the geometrical skin S_G.

A variety of correlations has been presented in the literature to estimate the geometrical skin. In Saphir the geometrical skin is determined by the difference between the model and the model for a fully penetrating vertical well with no skin damage.

$$S_T = \left(S_M + S_G\right)$$

The infinitesimal skin S_M is constant at the wellbore; however several references can be used to normalize the different skins.

If the skin is referred to the horizontal contributing length then:

$$S_T = \frac{h}{h_w} S_M + S_G$$

And including the anisotropy:

$$S_T = \frac{h}{h_w}\sqrt{\frac{k_r}{k_v}} S_M + S_G$$

The figure below illustrates the influence of the skin on the behavior of the pressure change and the Bourdet derivative. There is no effect on the derivative as long as the skin is 0 or positive. If the skin S_M becomes negative then both the pressure change and the derivative will mask the early time radial flow and the shape at will approach the behavior of the fractured well.

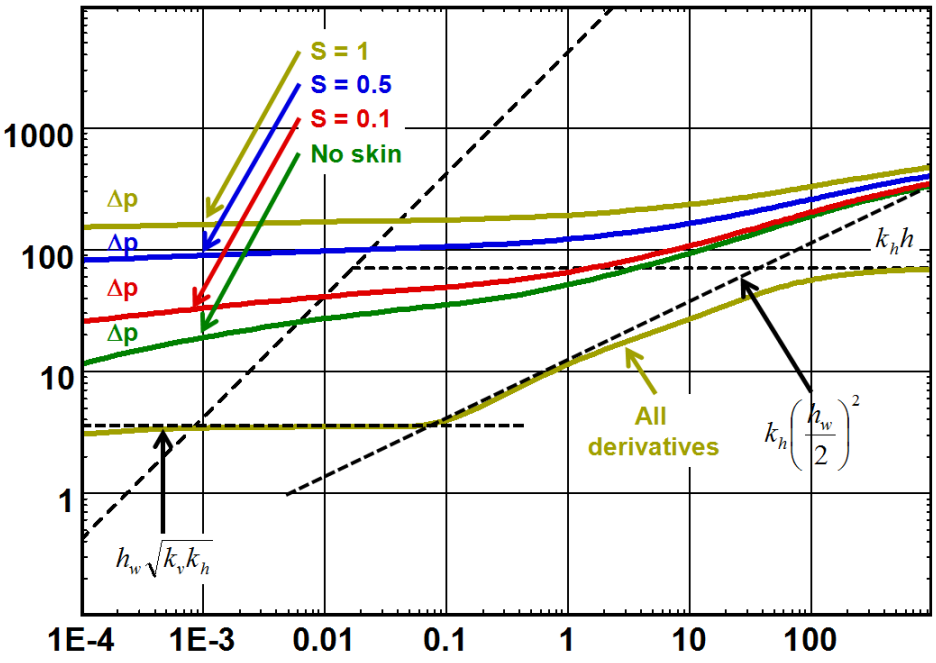


Fig. 6.G.8 – Horizontal well, sensitivity to skin

6.H More on horizontal wells

6.H.1 The flow regimes and incomplete data

During a test we should be able to easily identify the main flow regimes during the period that is being analyzed. Unfortunately this is the theory and 'real life' is not so accommodating. In fact it is rare to see a real test that exhibit the 'late time' or reservoir radial flow. The 'early' radial flow is often masked by wellbore storage and unfortunately too often by phase segregation in the wellbore. The well maybe close to an unidentified upper or lower boundary so what may look like 'early' radial flow is in fact just a boundary response. The reservoir is by most accounts not homogeneous so in addition, the analysis is complicated by having to use reservoir models with additional parameters to describe the heterogeneities.

In addition we know that most 'horizontal' wells are not horizontal at all and in almost all real cases they cut through various dipping layers.

The analysis of a horizontal well response is a challenge indeed.

Unfortunately there is not much we can do to produce miracles. The challenge is to recognize that a flow regime has been masked by another and if not, make the right diagnostics.

When a flow regime is missing in the response we have to rely on the 'known' parameters that were discussed in a previous chapter of this document. And, we are in luck, Saphir has some tools that are very useful and can help us produce a complete analysis with confidence even if the data recorded is incomplete.

6.H.1.a Early time radial flow

Let's say we have recorded a buildup in a horizontal well, but the test was stopped in the middle of the linear flow period, see the below figure.

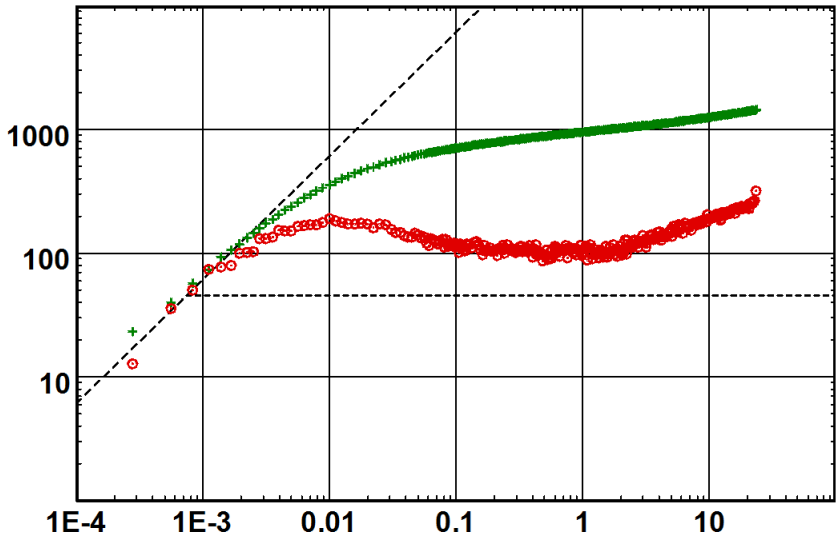


Fig. 6.H.1 – Loglog plot of incomplete data

Further, if we assume that seismic and log data is complete and that we have already good knowledge of expected horizontal contribution (h_w), vertical drainage (h) and the ratio of anisotropy, the below outlines a procedure that will help in the analysis of incomplete data.

The semilog plot will give:

$$(kh_w)_{early} = h_w\sqrt{k_v.k_r} = 162.6\frac{qB\mu}{m_{semilog}}$$

and the skin: $$S_{\left(k_v,k_r,h_w\right)} = S_M\frac{h}{h_w}\sqrt{\frac{k_r}{k_v}}$$

with: $h=h_w$

We can also trace the 'early time radial flow' line on the loglog plot to determine $(kh_w)_{early} = h_w\sqrt{k_v.k_h}$, and S_M directly.

'Knowing' h_w and k_v/k_r we estimate quickly what k_r should be if the 'known' parameters are right. We also 'know' the pressure match: $PM = 1.151k_rh/162.6qB\mu$ and can quickly place the infinite acting radial flow line on the right level on the loglog plot.

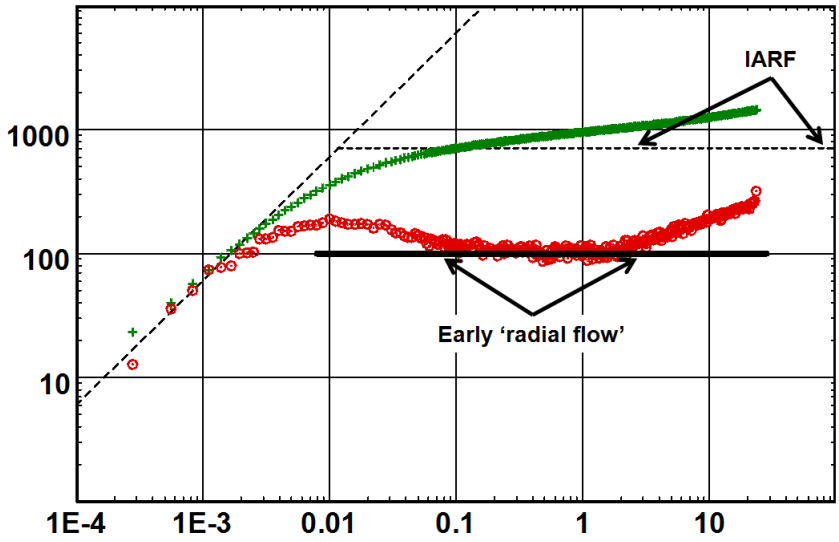


Fig. 6.H.2 – Loglog plot with 'early time' line and pressure match

6.H.1.b Linear flow

A plot of the pressure change versus $\sqrt{\Delta t}$ will return the length of the contributing drain (h_w) if k= k_r and h=h. The special 'Channel' line in the loglog plot will also return this parameter.

$k_h\left(\frac{h_w}{2}\right)^2 = 16.52\left(\frac{qB}{mh}\right)^2\frac{\mu}{\Phi c_t}$, m is the slope of the straight line in the pressure versus $\sqrt{\Delta t}$ plot.

If we match the IARF line with the 'early time' radial flow and we replace the value of h with h_w the line in the square root plot and the specialized line, 'Channel' in the loglog plot, will return the vertical net drained, h as follows: $h = (L_1 + L_2)_{Model}\sqrt{\sqrt{\frac{k_v}{k_r}}}$

This gives us a double check that our approach is consistent despite the missing data. The below plots illustrates the square root plot and the 'Channel' special line in the loglog plot.

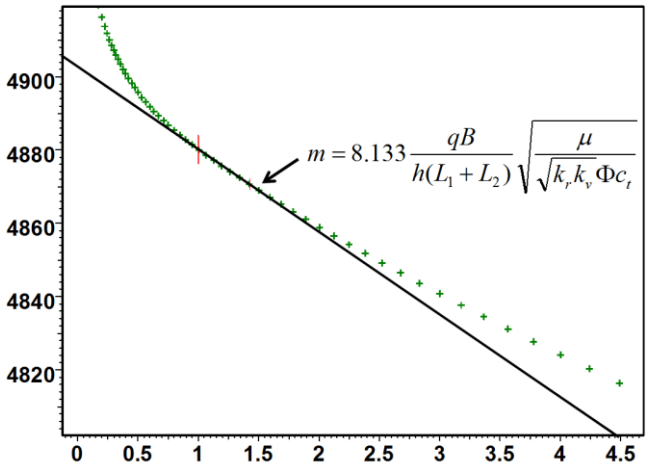


Fig. 6.H.3 – Square root plot

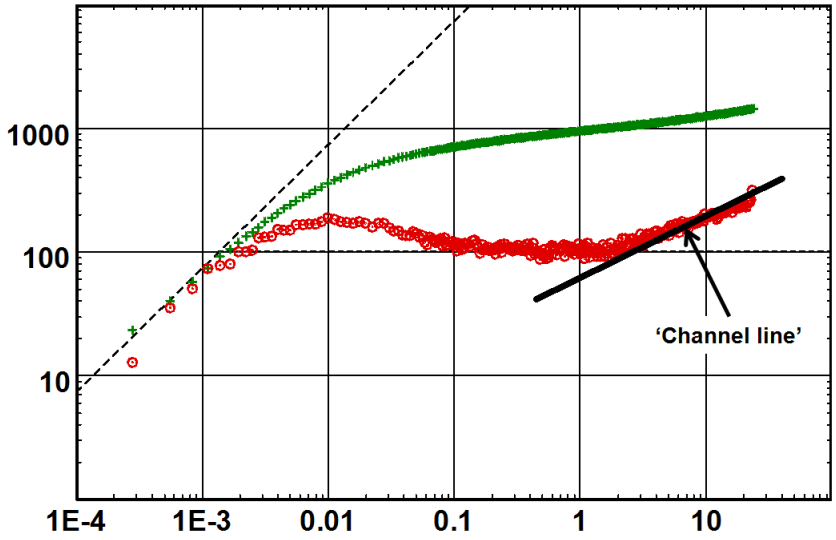


Fig. 6.H.4 – Loglog 'Channel' line

Finally we have enough information to be able to generate the model with the appropriate 'known' and 'unknow' parameters. The model match is illustrated below.

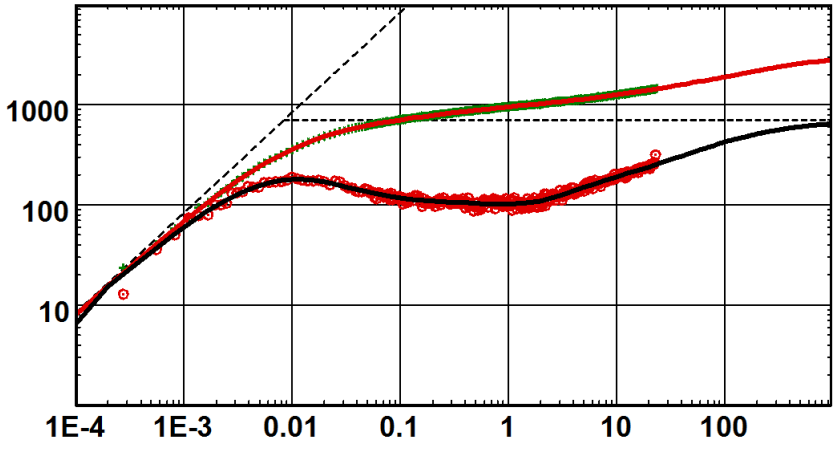


Fig. 6.H.5 – Final model match

In addition we can use a 'poly' line to set the level of 'early' radial flow, the linear and the 'late' radial flow. Just using the input of the 'known' parameter and transferring the 'poly' line results to the model we see that the results from the line gives a model very close to the data. A quick 'improve' of the leading parameters of the model will give us a perfect match with very reasonable results, see the figures below.

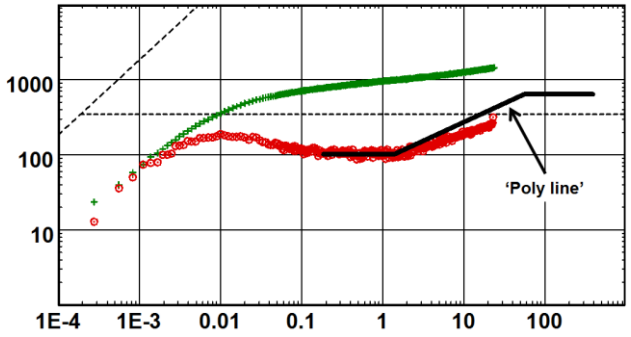


Fig. 6.H.6 – Loglog plot with 'poly' line

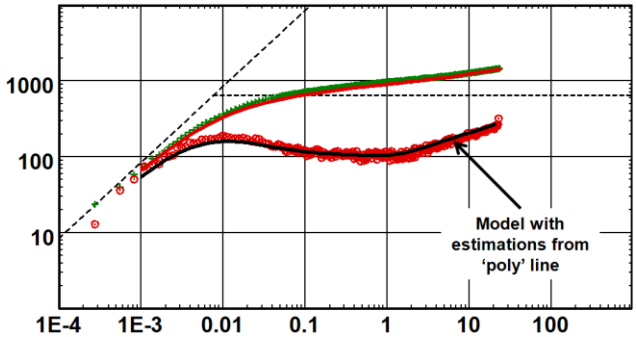


Fig. 6.H.7 – Loglog plot with model from 'poly' line

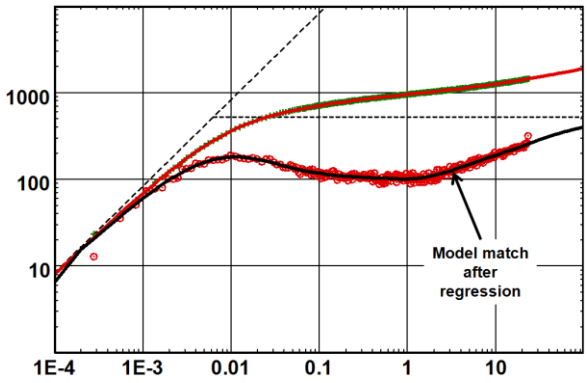


Fig. 6.H.8 – Loglog plot with model after regression

6.H.2 Horizontal anisotropy

The figure below illustrates the horizontal well behavior where the reservoir is anisotropic, vertically k_z/k_r = 0.01 (constant) and horizontally k_x/k_y, k_x is along the well and k_y is perpendicular to k_x. It shows clearly that the most efficient horizontal well crosses perpendicularly to the high permeability direction.

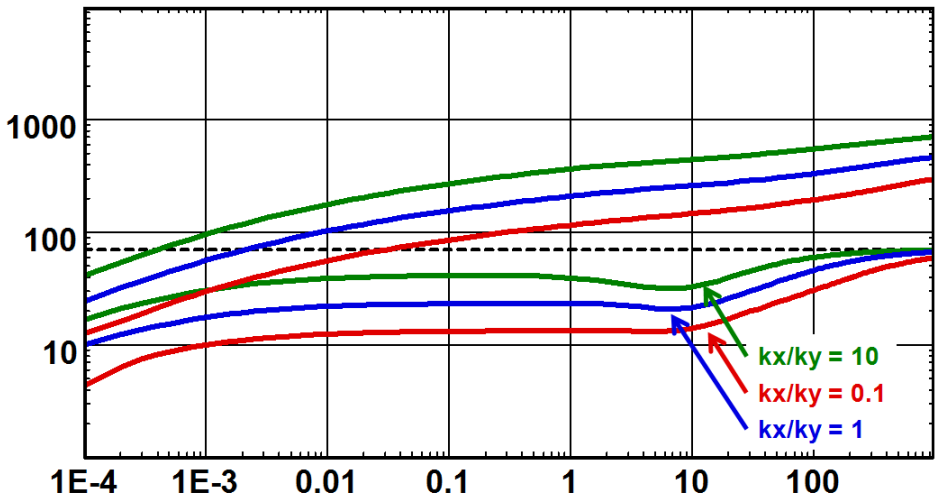


Fig. 6.H.9 – Horizontal well loglog response, variable horizontal anisotropy

6.H.3 Fractured horizontal well

When facing the challenge of producing very low permeability reservoirs (for example shale gas reservoirs), the completion type of choice is usually the fractured horizontal well in order to maximize productivity and increase the drainage area, as extremely low mobility is limiting significantly the extent of drainable volume further from the well. Consequently, this model is well adapted to unconventional gas analysis and production forecasting.

For those interested in the particular problem of production analysis in unconventional gas reservoir, it is further developed in the KAPPA shale gas papers: *The Analysis of Dynamic Data in Shale Gas Reservoirs – Part 1 and Part 2 (OH et al.).*

In a tight matrix environment, the production from the interface drain - reservoir is negligible compared to the multiple fractures contribution. Consequently, the productivity index will be less sensitive to the drain damage than to the fracture quality. This will be illustrated below.

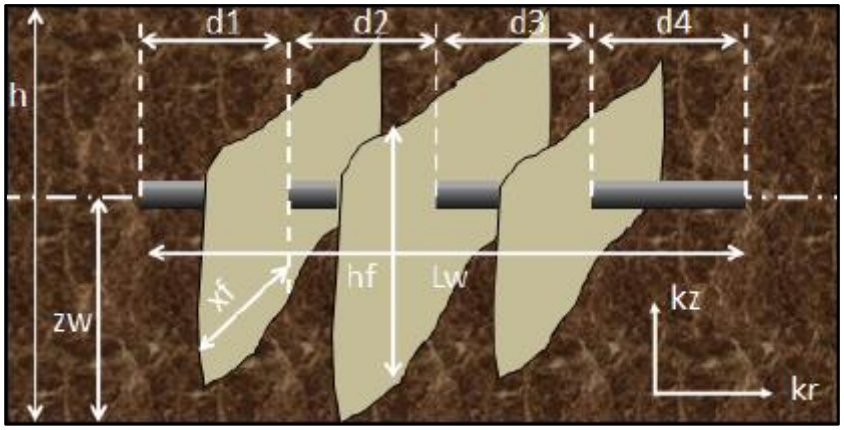


Fig. 6.H.10 – Fractured horizontal well

After the effects of wellbore storage, linear or bilinear flow behavior develops due to the fractures (1/2 or 1/4 unit slopes or both), then the response may correspond to radial flow in the vertical plane orthogonal to the horizontal borehole, with an anisotropic permeability $k = \sqrt{k_v k_r}$, this flow regime is usually always masked by the fracture influence.

As the top and bottom boundaries are sealing, the response shows the behavior of a vertical well between two parallel sealing faults and the derivative should follow a positive half unit slope during this linear flow, however there is no easy way to determine if the half slope is caused by the fractures or the horizontal wellbore between the upper and lower boundary.

At later time stabilization in the derivative is observed corresponding to infinite acting radial flow (IARF) in the horizontal plane relative to kh.

6.H.3.a Sensitivity

The below figure illustrates the behavior with various well configurations, flow through the fracture only, through the drain only and through both. It shows clearly that the contribution of the drain is negligible.

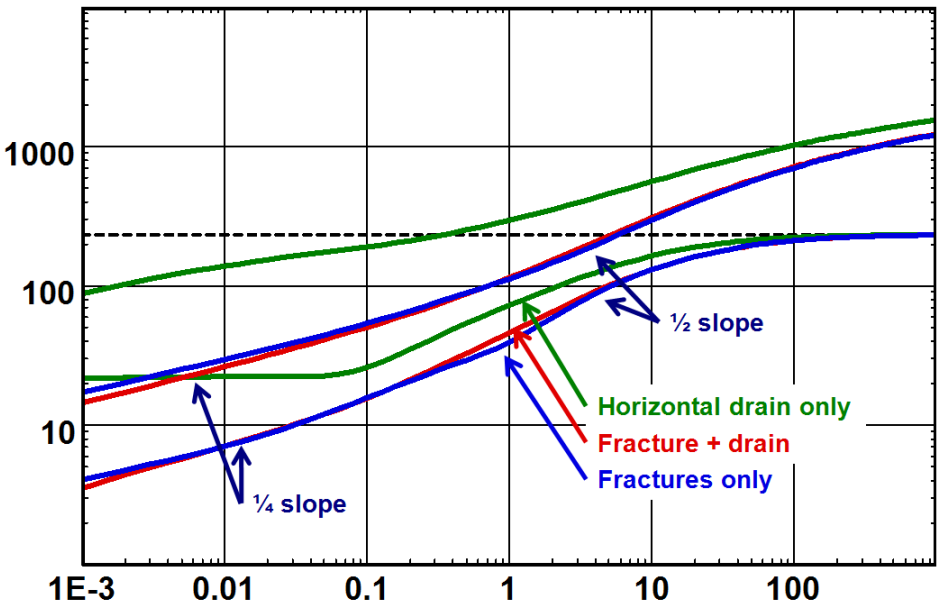


Fig. 6.H.11 – Flow through fractures, drain or both

The horizontal well behavior is totally dominated by the presence of the fractures, the typical shape of the horizontal well disappears and is replaced by the dominant behavior of the low conductivity fractures with the characteristic shape of bi-linear (¼ slope) and linear (½ slope) flow. The rules discussed in the previous section will no longer apply.

The Horizontal fractured wells behavior is therefore dominated by the fracture quality, fracture half length, conductivity and number. The spacing also plays an important role in the behavior as seen in the following figure that show the influence of the length of the horizontal drain with equal number of identical fractures. The shorter the drain, with the equal number of fractures, the steeper the transition from bi-linear to infinite acting radial flow becomes and the less the overall shape resembles that of a horizontal well.

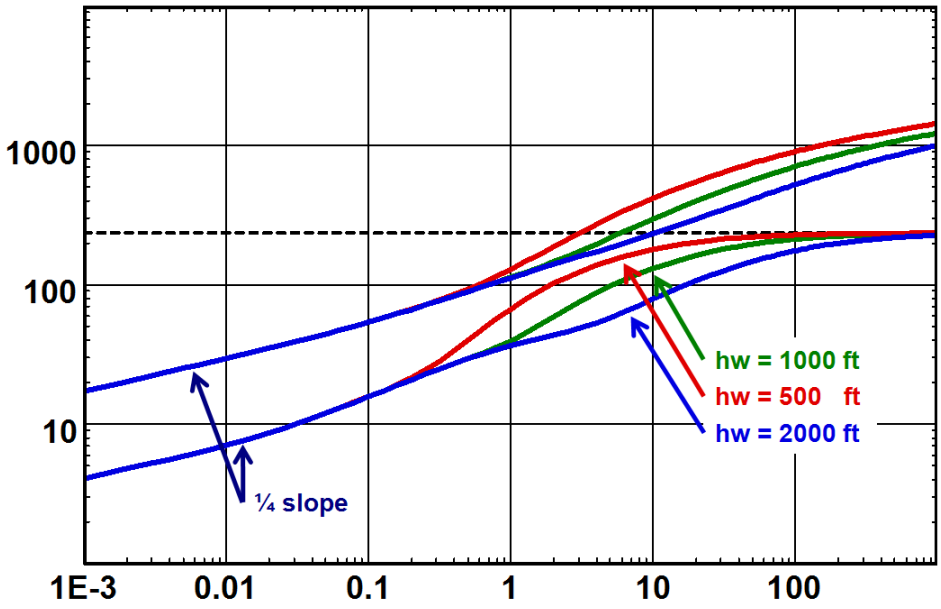


Fig. 6.H.12 – Equal number of identical fracture, sensitivity to horizontal drain length

The figure below illustrates the influence of the half length of the fractures. In this case there are four fractures at equal spacing. When the half fracture length is small it is possible to observe the classical 'early time' radial flow of the horizontal well behavior. This is however the rare occasion when we deal with multiple fractured horizontal wells.

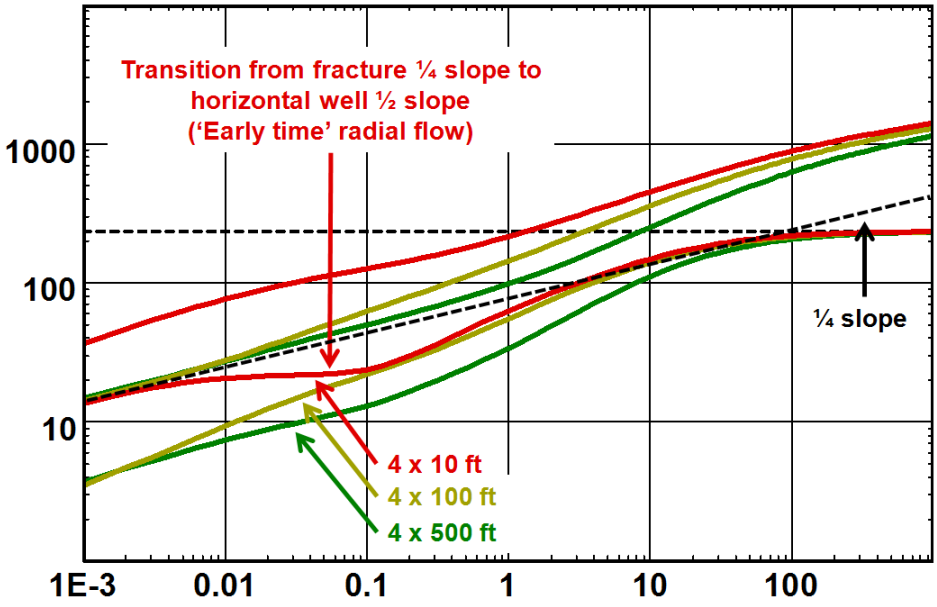


Fig. 6.H.13 – Influence of half fracture length

6.H.3.b Adding wellbore storage

The wellbore storage effect will mask the fracture flow regime, see the following figure.

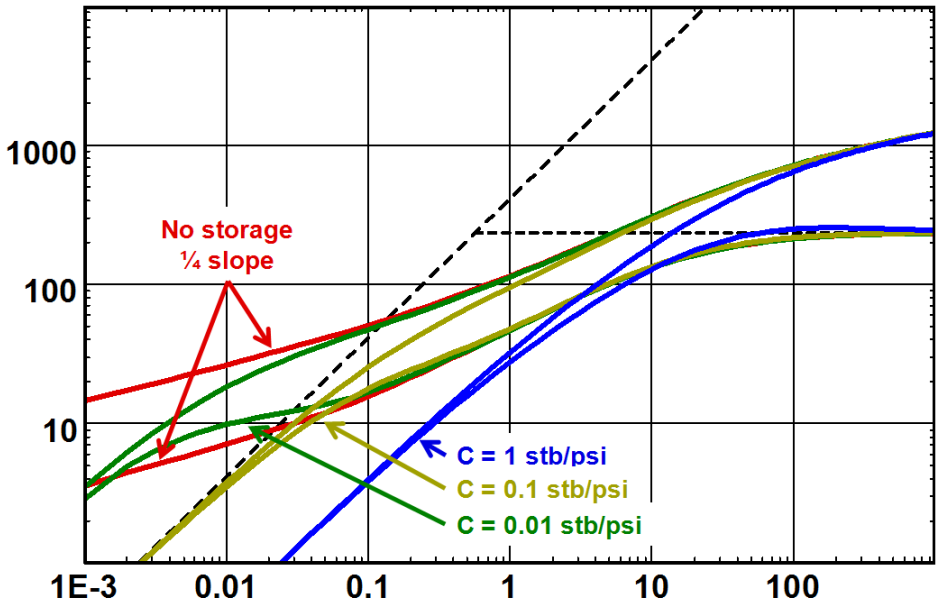


Fig. 6.H.14 – Influence of wellbore storage

6.H.3.c Skin

When a situation with multiple fractures in a horizontal well is facing us we are invariably up against low or 'no' permeable rock. In most cases we are dealing with 'unconventional gas'. Thus the damage of the actual well(bore) becomes a non issue.

The skin will not influence the derivative, thus we will retain the diagnostic tool, and be able to recognize the flow regimes present in the signal when no other influence is present, such as high or changing wellbore storage and phase segregation.

The figure below illustrates the multiple fracture model with the influence of skin.

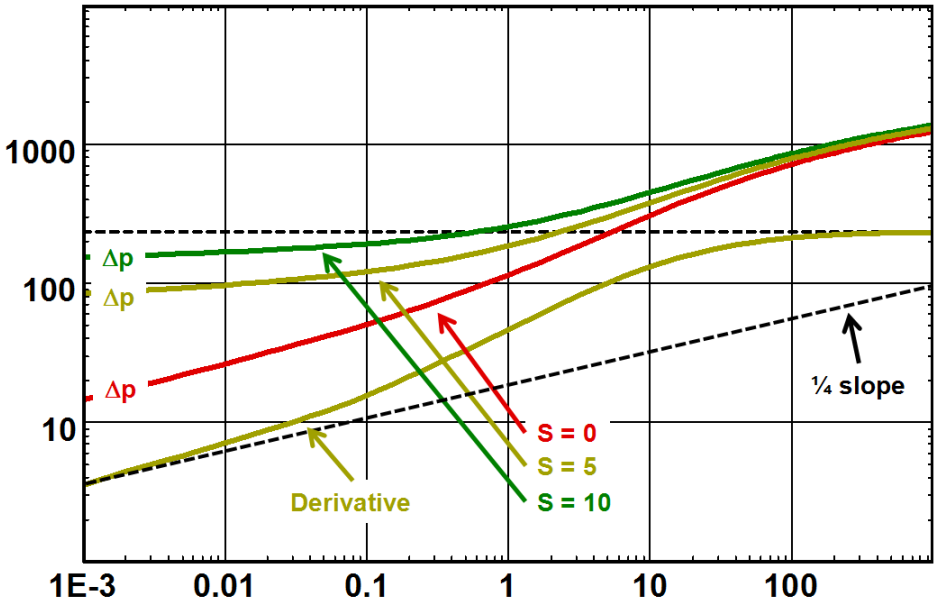


Fig. 6.H.15 – Skin influence

6.H.4 Field examples

Below we are illustrating two model matches with real data. The first well has a near textbook behavior of a horizontal well with changing wellbore storage at early time.

The second well is in an area where the vertical permeability is very low. This gives rise to the typical but unorthodox behavior of a horizontal well with positive geometrical skin.

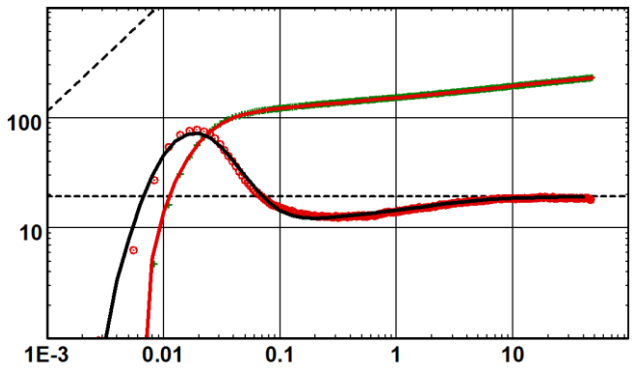


Fig. 6.H.16 – Horizontal well: Negative geometrical skin

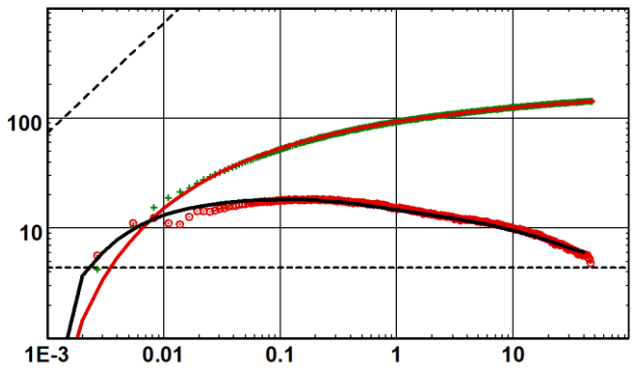


Fig. 6.H.17 – Horizontal well: Positive geometrical skin

6.I Slanted wells

As with horizontal wells, slanted wells are designed to increases productivity by maximizing reservoir contact. In fact the horizontal well is just a subset of the generalized slanted well solution.

We have seen in low vertical permeability formations that horizontal wells are not very efficient.

An answer to this problem is the slanted well which maximizes the communication length with the formation while crossing it totally. Even zero vertical permeability formations are connected to the well over the complete thickness.

Generating analytical solutions to simulate and study such wells is quite easy. The challenge is to select the adequate model and to define the various corresponding parameters.

Common questions are: "my well is deviated, do I have to consider it as a slanted well?" or "my well is sub-horizontal, do I analyze it as a horizontal or slanted well?", and then the series of questions: "Which thickness do I use if my formation is not horizontal, do I use the measured depth or the true vertical depth?" In addition the slanted well can either be fully penetrating or with a selected interval perforated or open to flow. The well will invariably cross different layers so this will also have to be considered in the solutions.

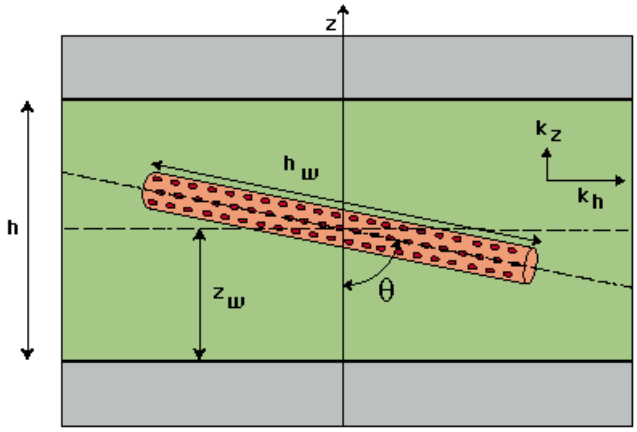


Fig. 6.I.1 – General slanted well

The answer to these questions is simple after understanding that we do not analyze the formation geometry but the pressure behavior, therefore the parameters or the criteria we use are the parameters influencing this behavior. The selection of the model is imposed by the shape of the pressure curve, not by the geometries.

Of course, the diagnostic will not tell you if the well is vertical, slanted or horizontal, you are already aware of that (hopefully). It will tell you how it behaves and how it has to be treated.

The following sections illustrates the typical sequences of flow regimes and pressure behaviors that characterize the different well types.

Analytical solutions respect certain assumptions such as the negligible effect of gravity on fluid flow. This means that the analytical slanted well model describes the cases of slanted wells in a horizontal formation, or if you want, a vertical, slanted or a horizontal well in a slanted multilayer formation. The parameter to consider is the angle between the well and the main flow direction.

Initially the impact of this geometry description is on h and h_w:

- h is the net drained thickness, perpendicular to the flow direction (not systematically TVD or MD).
- h_w is the contributing producing well length.

6.I.1 Behavior

There are, like in the horizontal well, some main flow regimes that can develop. If the angle with the vertical is large, the well is approaching a horizontal well. The dip of the layer is such that the well follows the formation stratigraphically, then the equivalent behavior will be that of a horizontal well and three distinct flow regimes may develop.

'Early time' radial flow in the plane normal to the well, this regime is usually masked when the slant is such that the well is close to a vertical well. Wellbore storage will also in most cases mask this behavior.

Linear flow between an upper and lower boundary if the well angle approaches the horizontal.

Reservoir radial flow if the test is long enough.

The below figure illustrates the loglog behavior of a real slanted well where all the main flow regimes have developed.

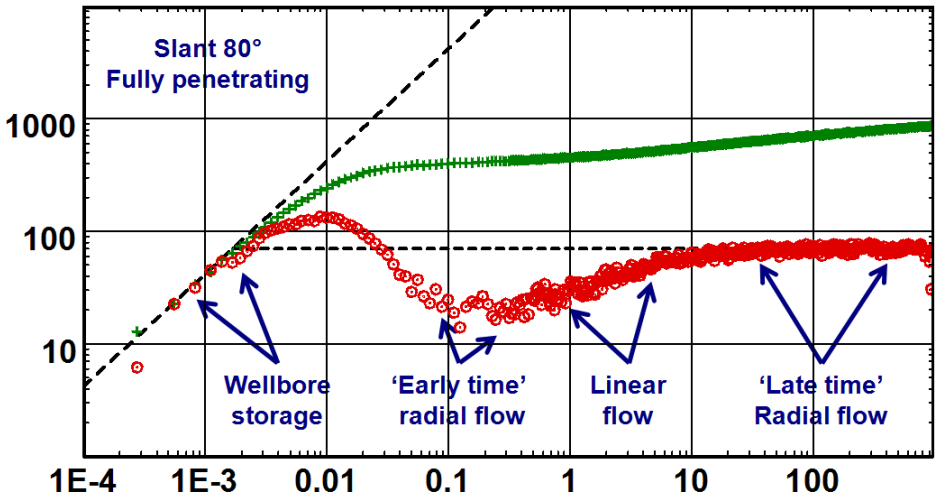


Fig. 6.I.2 – Slanted well response

6.I.2 Sensitivity to different parameters

To illustrate the response of the slanted well various models were generated with various scenarios. None of the scenarios are intended to reflect a real well but are run to see the response to various situations of some interest. The comparison to the horizontal well response is shown in various settings.

The below figure illustrates the response of a fixed contributing length of a fully penetrating vertical well, the same penetration at an angle of 45 degrees and the equivalent horizontal well response. One can easily see that the horizontal well with the same penetration length as the vertical well is a poorer well due to the anisotropy.

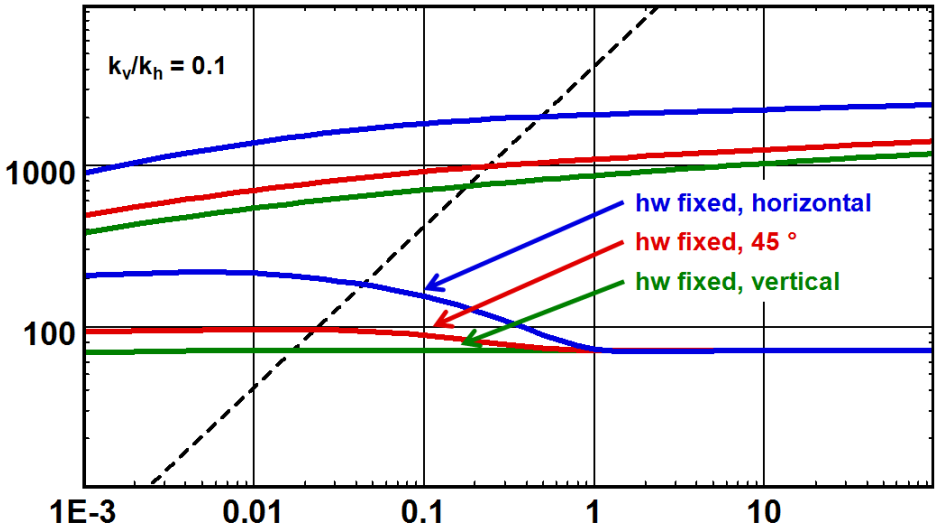


Fig. 6.I.3 – Slanted well fixed penetration

The next figure illustrates the behavior when the well is fully penetrating from top to bottom boundaries with various inclination angles. The reservoir in this case is isotropic. It is possible to observe the phenomenon caused by the end effects; flow at the extremities of each of the slanted wells, as well as the 'early time' radial flow $h_w\sqrt{k_r k_v}$ equivalent to the response in a pure horizontal well.

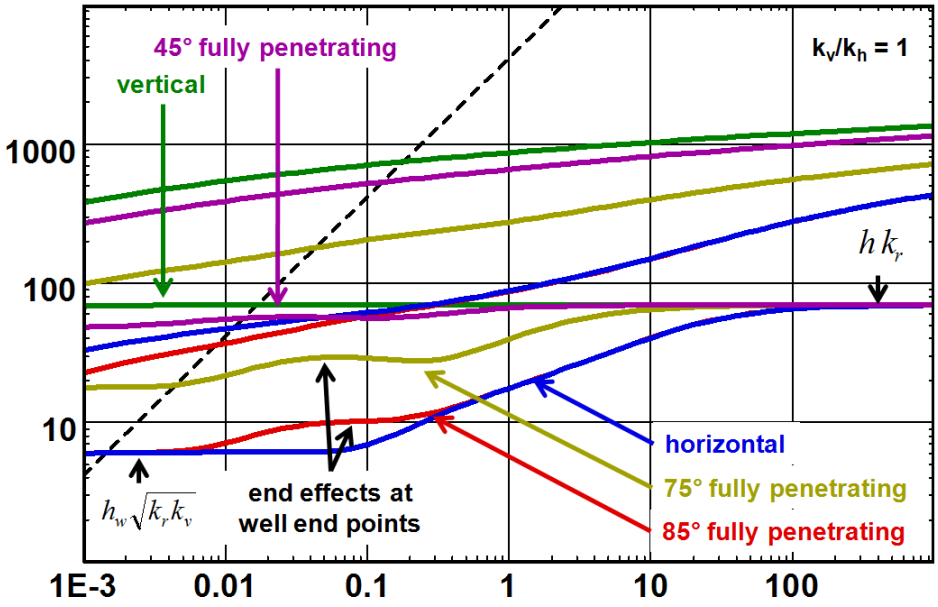


Fig. 6.I.4 – Slanted well variable penetration

The following is a comparison of a horizontal well in a highly anisotropic rock with various slanted wells, all with the same contributing length. It can be seen that crossing the reservoir with a well at an angle is advantageous because of the anisotropy.

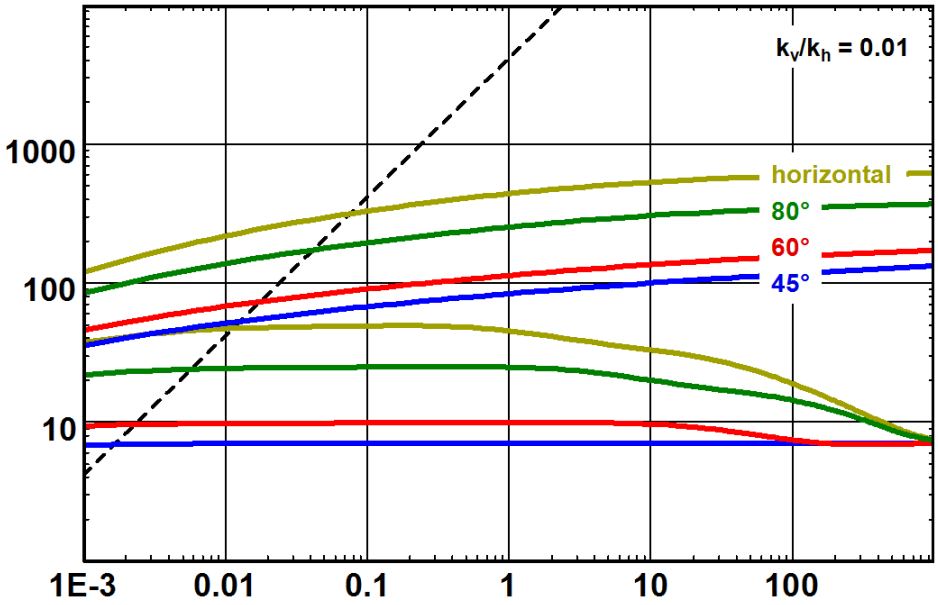


Fig. 6.I.5 – Slanted well, high permeability contrast

As the permeability contrast increases the efficiency of the well decreases. The figure below shows a slanted well with increasing permeability contrast.

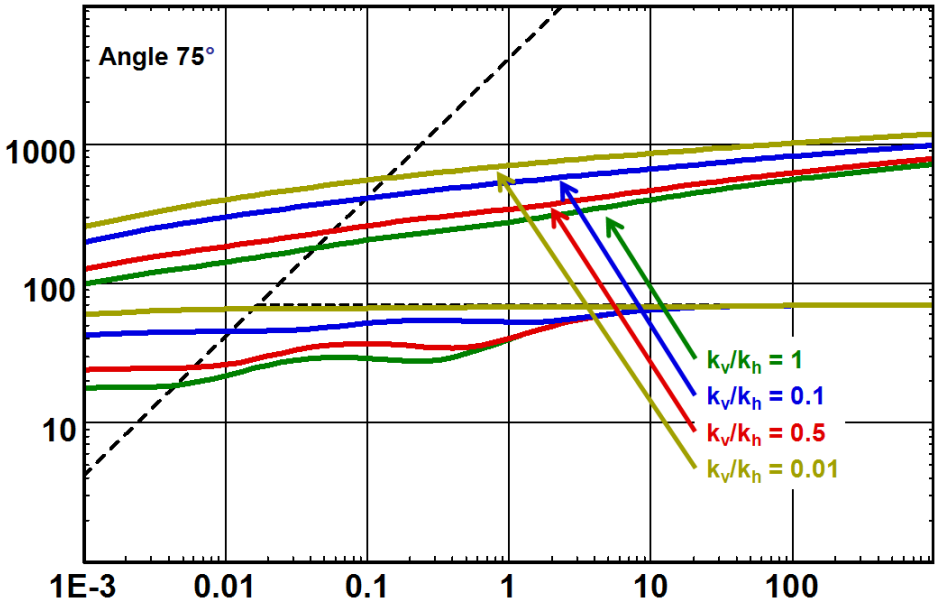


Fig. 6.I.6 – Slanted well, increasing permeability contrast

Finally we show a limited entry well with various inclinations, due to the anisotropy the vertical well is the best choice. Spherical flow develops in all the wells, and lasts longer as the inclination approaches the horizontal well.

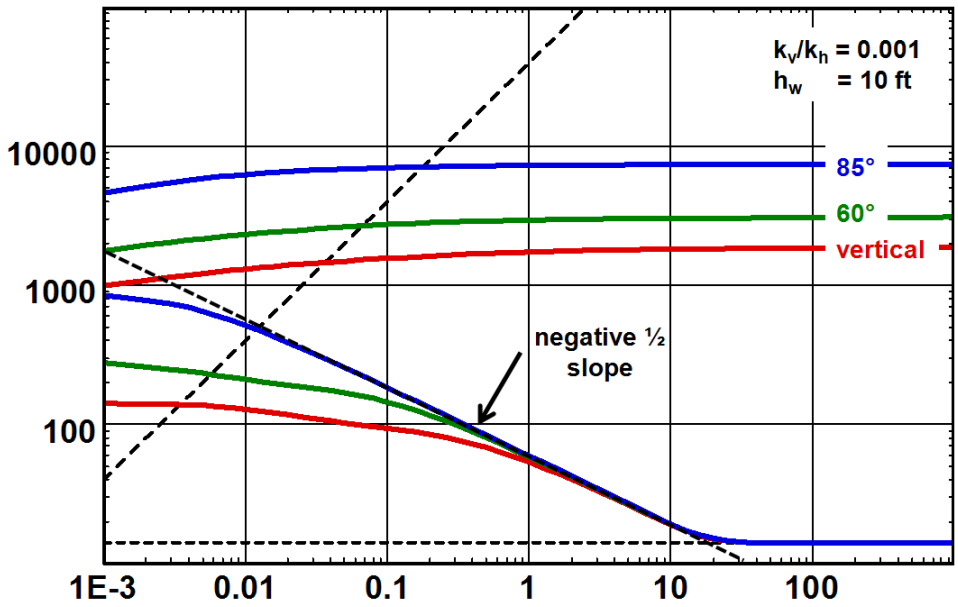


Fig. 6.I.7 – Limited entry well

6.I.3 Adding wellbore storage

Wellbore storage will affect the early time data and mask any 'early time' radial flow and the characteristic end effects of the slanted well. See the below figure.

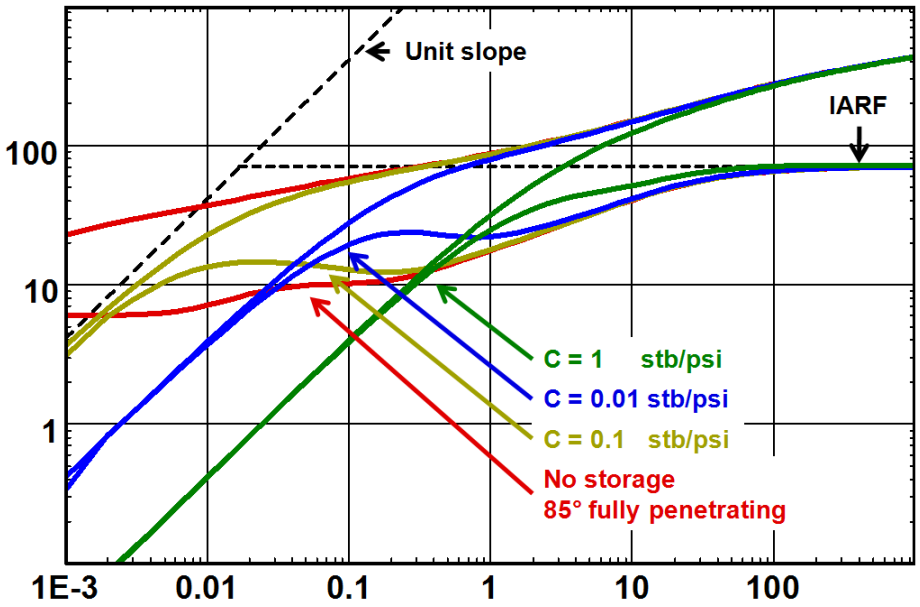


Fig. 6.I.8 – Wellbore storage influence

6.I.4 Skin

The skin has no effect on the derivative so none of the features (shapes) particular to the slanted well is lost. This is of course in practice not true as most wells will also be influenced by wellbore storage, and worse still changing wellbore storage and/or phase segregation in the wellbore.

Nevertheless, below is illustrated the effect of skin only on the slanted well.

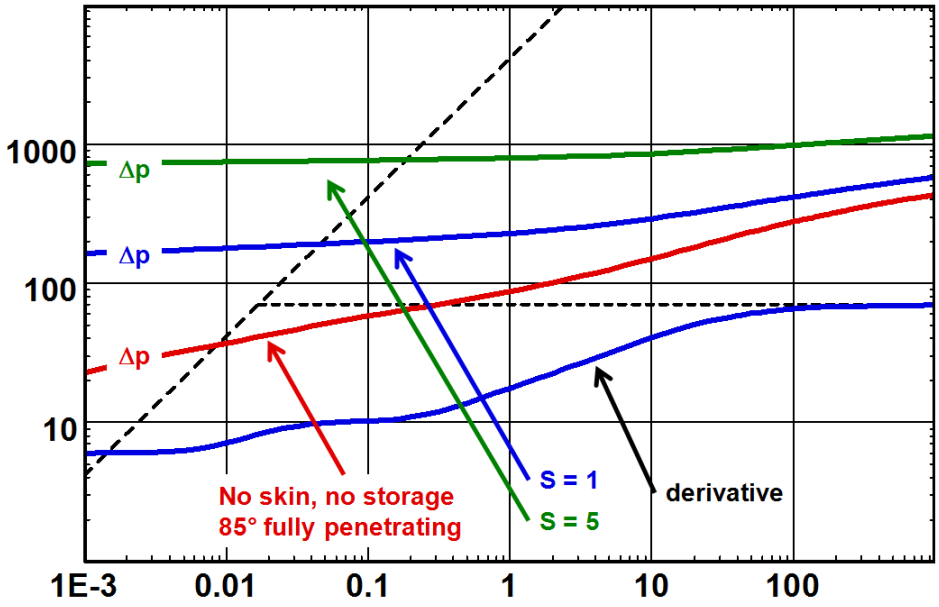


Fig. 6.I.9 – Influence of skin

6.I.5 Slanted well multilayer

6.I.5.a Hypothesis

The model simulates the behavior of a slanted well crossing multiple layers. The layers are strictly horizontal; however the model can easily predict the behavior of horizontal wells crossing slightly dipping layers.

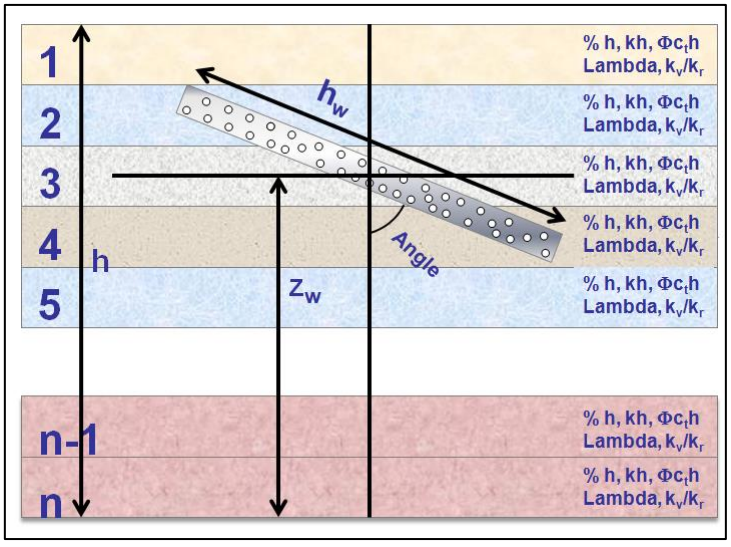


Fig. 6.I.10 – Slanted well multilayered

The individual layer parameters are defined by a fraction of the total thickness h, the permeability thickness product, kh and the storativity, $\Phi c_t h$. The anisotropy is also specified for each layer.

The interlayer crossflow is determined by the Lambda value, which can be automatically calculated.

Thus the model caters for layers with or without crossflow.

6.I.5.b Behavior

The following figure illustrates the classical behavior of the double permeability response but using this model (see the chapter on 'Reservoir models'). The fully penetrating slanted well model at 80° is compared to the vertical well. The longer slanted well is of course the best producer. The reservoir is isotropic.

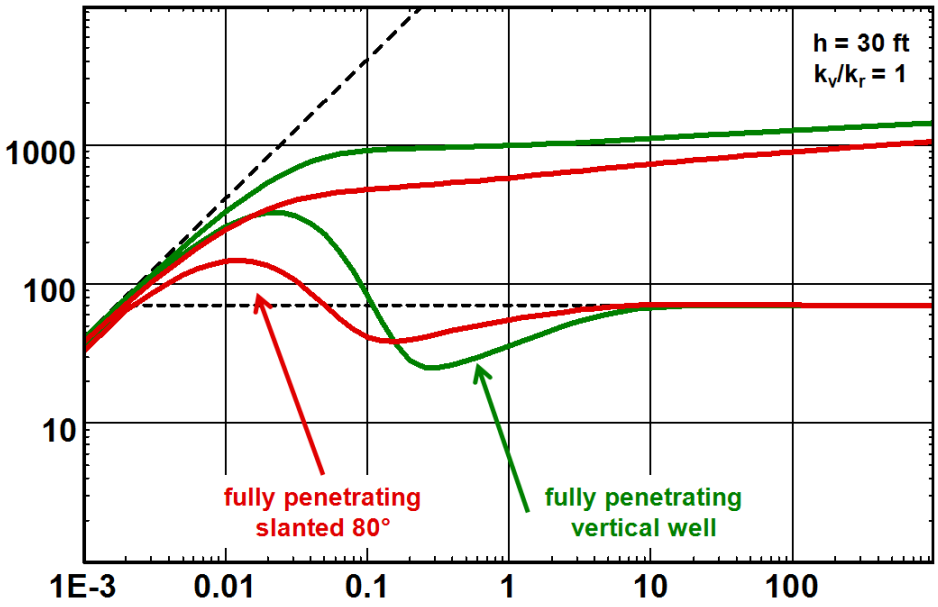


Fig. 6.I.11 – Slanted well, two layers with cross flow

The following figure illustrates the response of a three layered reservoir; the well is fully penetrating, vertical and slanted at 80°. The reservoir is isotropic. The double feature of the transition due to unequal heterogeneity parameters in the different layers can easily be seen in the fully penetrating vertical well. This is masked with the slanted well fully penetrating at 80°.

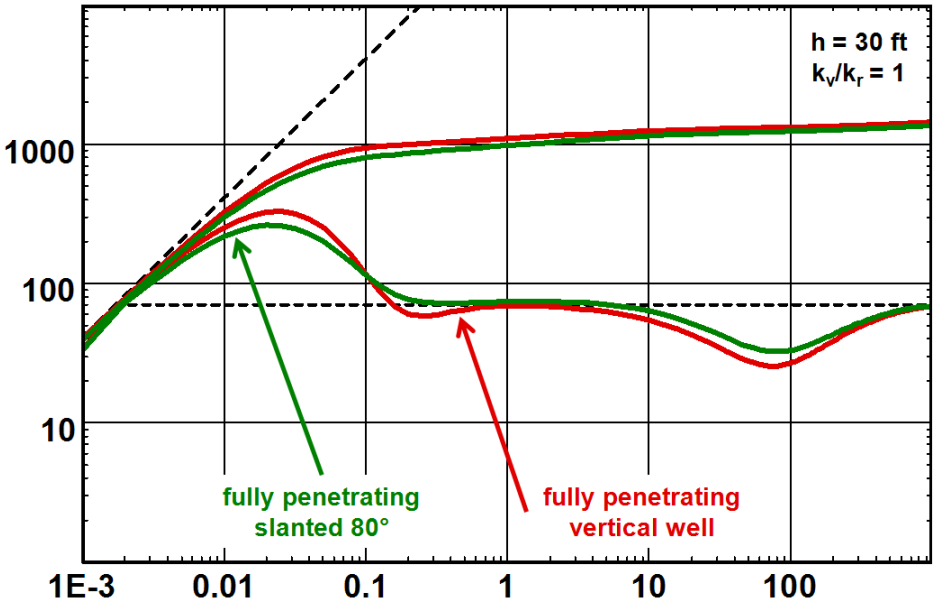


Fig. 6.I.12 – Slanted well, three layers, cross flow

The following figure show the responses with a horizontal well placed in a high permeably layer communicating with a low permeability layer and the well placed in the low permeability layer communicating with the high permeability layer. It is evident that placing the well in the high permeability layer is an advantage to the short term production.

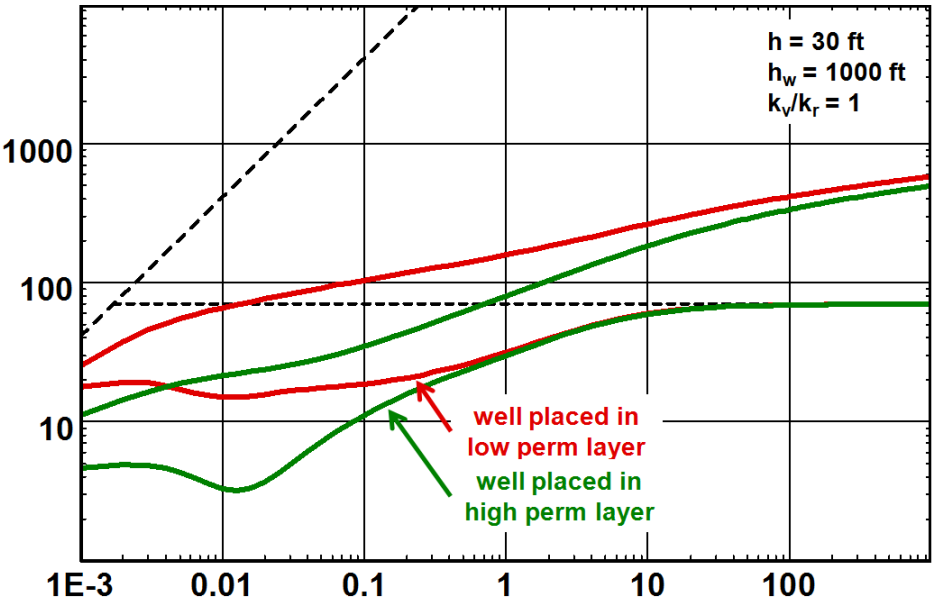


Fig. 6.I.13 – Well placement

We know that in general the horizontal wells are not strictly horizontal and in real life invariably the wells will cut through various layers on its way through the reservoir. This is just a fact of life and a problem the interpretation engineer is faced with constantly. Very often he will find to his dismay that the interpreted horizontal contributing length is much shorter than what had been predicted and even measured by production logging and that the anisotropy does not make any sense at all.

This could very well be caused by the fact that the well is in fact cutting through distinct layers and cannot be analyzed as if the horizontal well drained one single homogeneous medium.

To illustrate this we have generated the slanted well model traversing various no communicating layers. It can be easily seen from the below figure that if the response from several layers is interpreted using the classical horizontal well model draining one single layer, the interpreted contributing length (h_w) would be too small, and the anisotropy would probably show a vertical permeability larger than the horizontal.

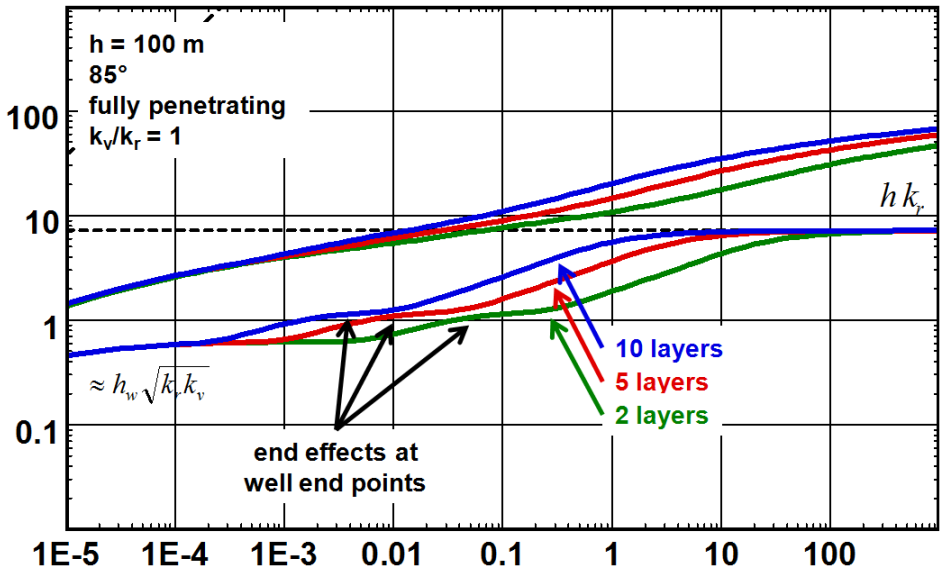


Fig. 6.I.14 – Influence number of layers

6.J Multilateral wells

6.J.1 Hypothesis

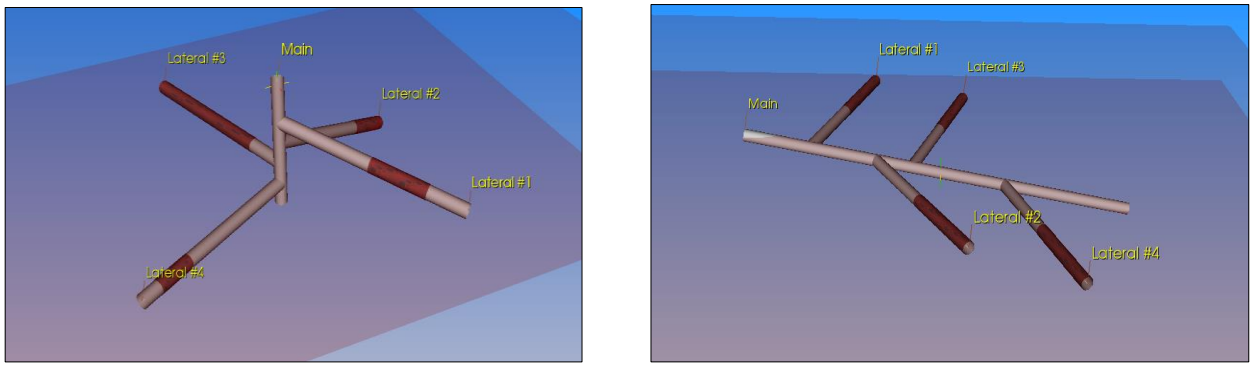


Fig. 6.J.1 – Multilateral wells schematics

Another answer to the quest for better productivity and sweep are the multilateral maximum reservoir contact wells. They consist of multiple drain holes, each drain can be aimed at a specific layer. For this purpose the drain holes may be drilled at different elevations and directions.

This is the production engineer's dream and the reservoir engineer's nightmare. If 'smart well completions' have not been installed only total well pressure is available, reflecting the 'average' behavior of all the drains/layers. The determination of the individual layer and drain characteristics is therefore impossible through a single information source.

6.J.2 The analytical multilateral well model

The latest analytical models have a very large flexibility and allow a wide range of geometry.

The main drain can be deviated from 0 to 90°.

There is not theoretical limit for the number of lateral drains and for each of them, it can be specified:

- The lateral drain radius and angle with the main drain
- The length and the perforation start and end
- The deviation with the vertical or the trajectory

6.J.3 The numerical multilateral well model

The numerical multilateral wells models have even less limits because they allow any geometry for the main and the lateral drain and multiple perforations intervals.

The perforation sets can even be equipped with Inflow Control Devices (see the following paragraph: 06-K).

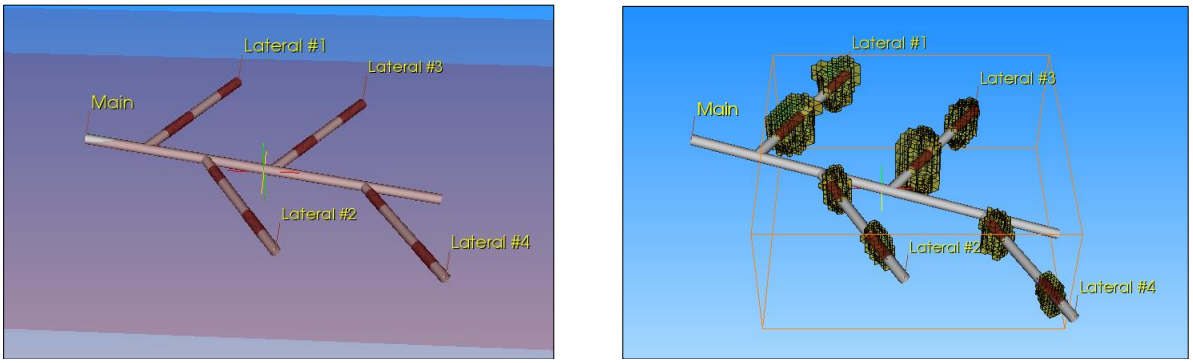


Fig. 6.J.2 – Numerical multilateral well models 3D view and its refined gridding

6.J.4 Behavior

Specific cases may allow analysis and the diagnostic of well-known behaviors. As an example; the pressure behavior of two lateral drains at 180° is similar to the behavior of a horizontal well of length equal to the sum of the two drains. The classical sequence (see horizontal wells) can be observed: infinite acting radial flow in the vertical plane, linear flow then, at late time horizontal radial flow.

The below figure illustrates the response of three different multilateral configurations.

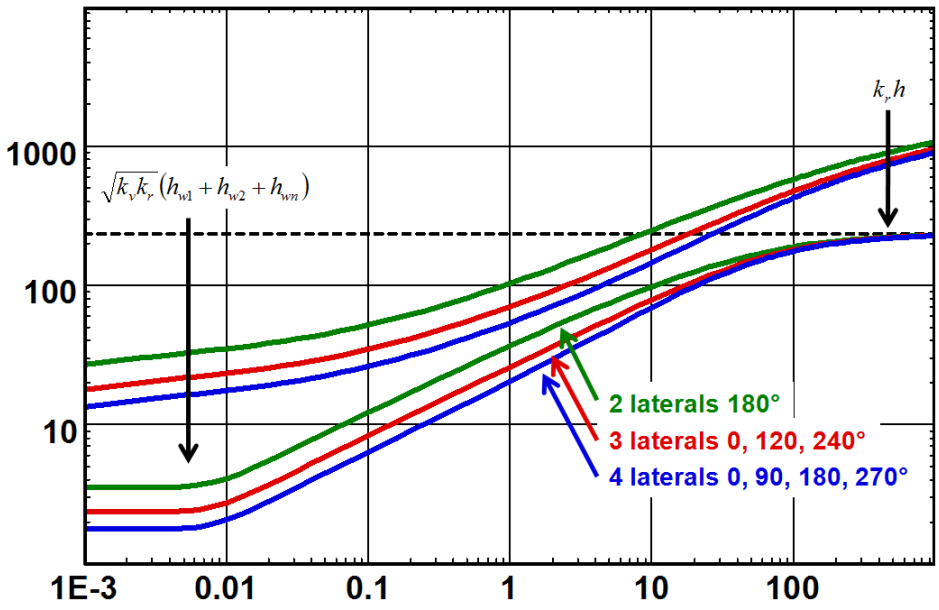


Fig. 6.J.3 – Multilateral well responses

In fact, the analytical model for multilateral wells simulates perfectly the sum of each drain behavior, but it does not permit a diagnostics that could be useful to understand detailed drain properties.

Testing lateral drains individually would permit the determination of individual drain properties. Aggregating this discrete information to simulate the global behavior is one possible approach.

6.K Inflow Control Device

6.K.1 Problems induced by a well completed in several formations

A well completed through several hydrocarbon bearing formations with different petrophysical properties drained non-uniformly the entire reservoir, therefore it can be not the most efficient producing system.

The diagram below shows how, a heterogeneous formation, in front of the rather uniform wellbore pressure, will be drained according to its properties:

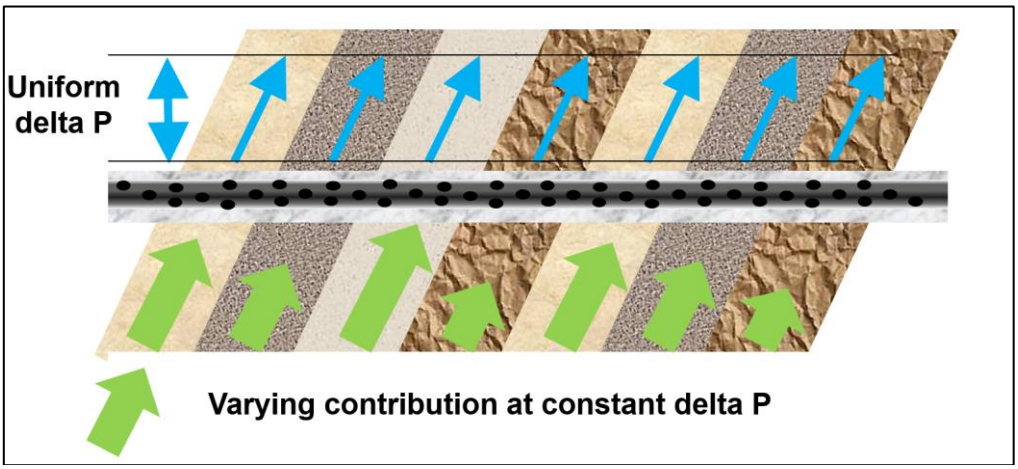


Fig. 6.K.1 – Production without Inflow Control Device

6.K.2 Solution proposed to optimize the drainage of the formation

The principle is to split the total length of the drain into multiple segments, according to the different layer that we detected, to separate them by means of packers and then to impose a restriction to the flow in the most producing segments, according to their individual contribution.

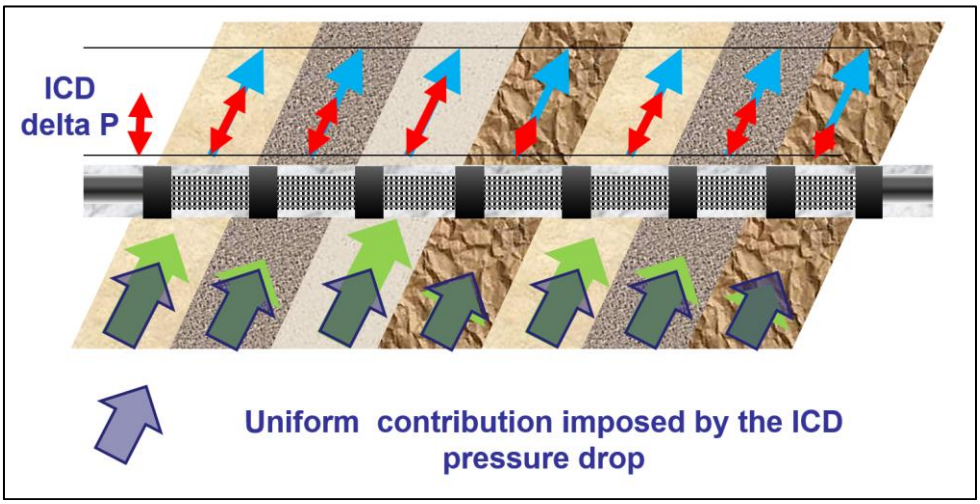


Fig. 6.K.2 – Production with Inflow Control Device

The reduction to the flow is created by devices sensitive to the flow rate and the average fluid density.

A layer producing originally a high rate will see the restriction automatically increased until the flow distribution becomes uniform in the drain.

6.K.3 ICD model principle

The principle of the model is to simply set the adequate restriction (rate and density dependent) between the reservoir and each one of the tubing segments.

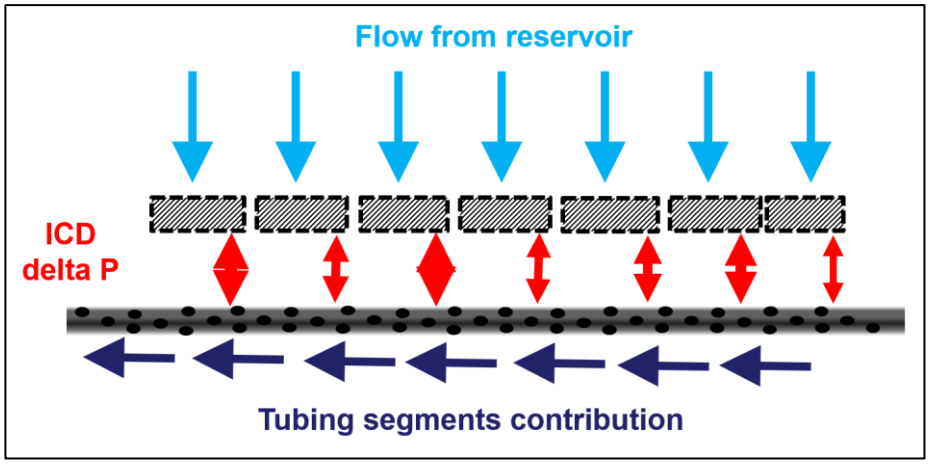


Fig. 6.K.3 – Inflow Control Device Schematic

The pressure drop between a reservoir cell and a well segment with an inflow control device (spiral type ICD) can be expressed as:

$$\delta P_{cons} = \gamma \cdot \left(S^2 \cdot u^2\right)$$

Where S is the production surface and u the local flow velocity of the mixture.

Spiral type ICD:

$$\gamma = \left(\frac{\rho_{Cal}}{\rho_{Mix}} \cdot \frac{\mu_{Mix}}{\mu_{Cal}}\right)^{1/4} \cdot \frac{\rho_{Mix}}{\rho_{Cal}} \cdot \frac{l_{ICD}^2}{h^2} \cdot a_{SICD}$$

Where l_{ICD} is the length of the ICD joint (12m?) and a_{SICD} is the ICD strength (see table 1).

Industrial "bar" rating	0.2	0.4	0.8	1.6	3.2
a_{SICD} $Pa/\left(m^3 s^{-1}\right)^2$	1.55 E12	3.09 E12	6.19 E12	12.38 E12	24.76 E12

Fig. 6.K.4 – Channel ICD strength (from Birchenko et al., 2011)

Nozzle/orifice type ICD:

$$\gamma = \frac{\rho_{Mix}}{2 \cdot C_v^2 \cdot A_c^2}$$

Where C_v is the dimensionless flow coefficient for the valve (typical values range between 0.6 and 0.68) and A_c is the cross-section area for flow in the constriction.

Comparison:

The main difference between the ICD nozzle and spiral type consists in the different sensitivity to the pressure and the fluid. Only the Spiral type is sensitive to the fluid viscosity, therefore it can be influenced by the WOR.

	Spiral	Nozzle
Physical mechanism	Frictional pressure loss	Venturi effect – constriction
Dependency	$f(\rho, \mu)$	$f(\rho)$
Advantages	Good resistance to erosion	Simple design / easy adjustment High viscosity insensitivity
Disadvantages	Viscosity sensitivity (might lead to preferential water flow if/when breaktrough occurs)	Small flow area: pluggin / erosion problems

We can observe in the comparative plots below the influence of the fluid specific gravity and viscosity on the ICD strength.

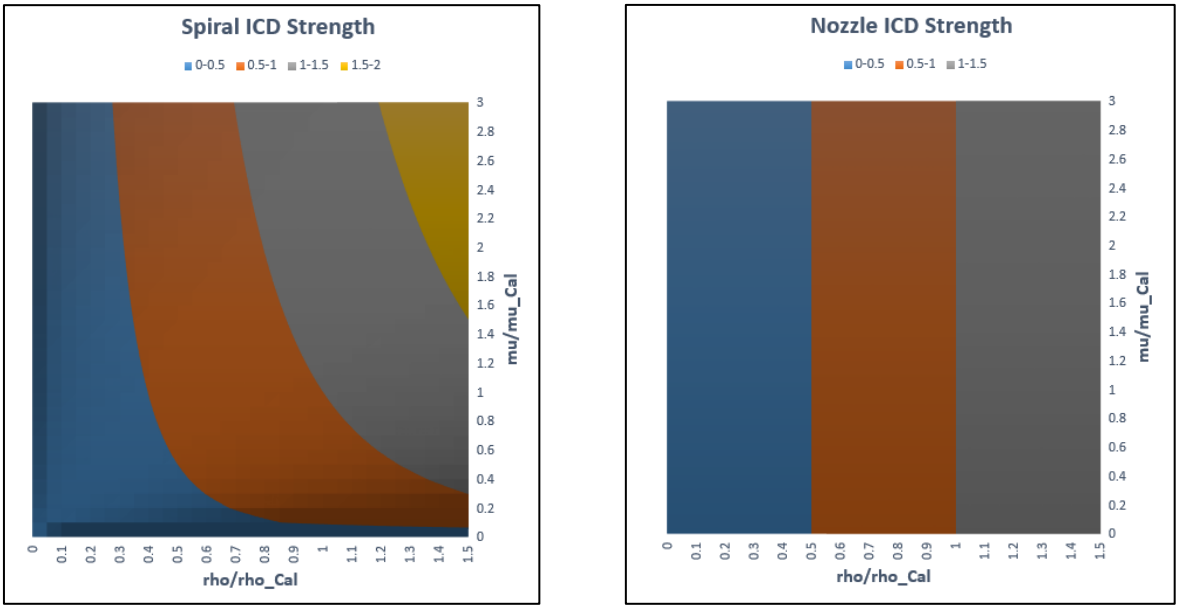


Fig. 6.K.5 – ICD strength sensitivity to μ and ρ

6.K.4 Behavior

The plots below show how the production can be more uniform by using the adequate ICD.

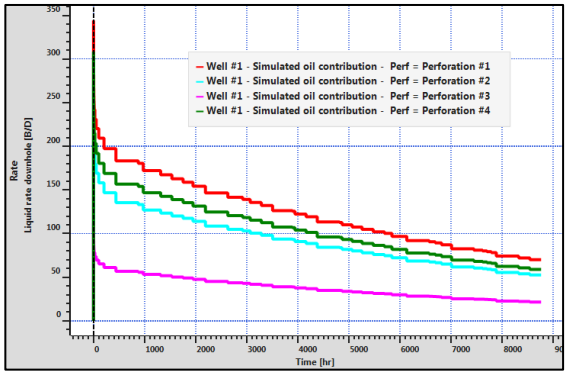


Fig. 6.K.6 – Layers contribution before ICD

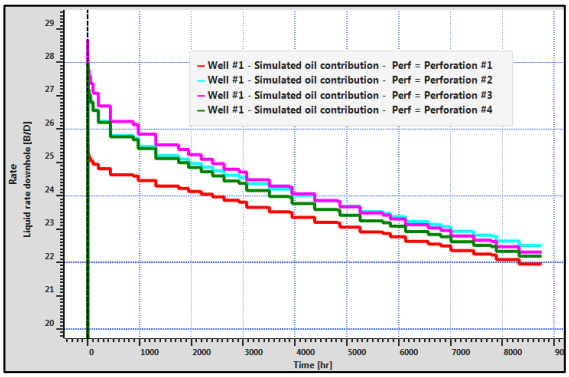


Fig. 6.K.7 – Layers contribution after ICD

6.K.5 Illustration

By imposing a more uniform pressure along a horizontal well close to a water contact, the possibility of water breakthrough due to coning can be delayed.

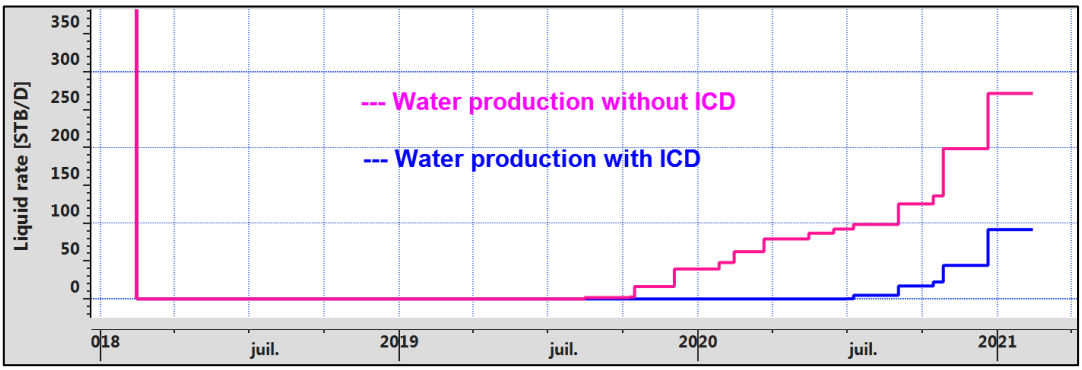


Fig. 6.K.8 – ICD effect on the water breakthrough

In terms of layer contribution the result is also very positive.

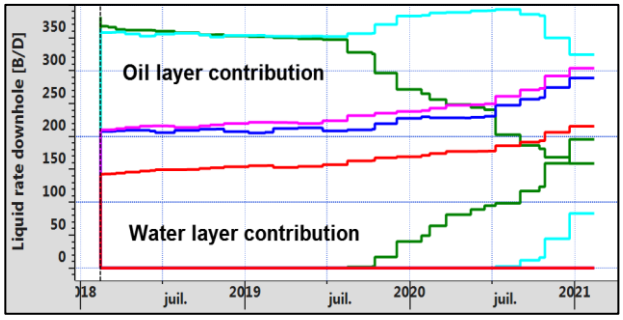


Fig. 6.K.9 – Without ICD

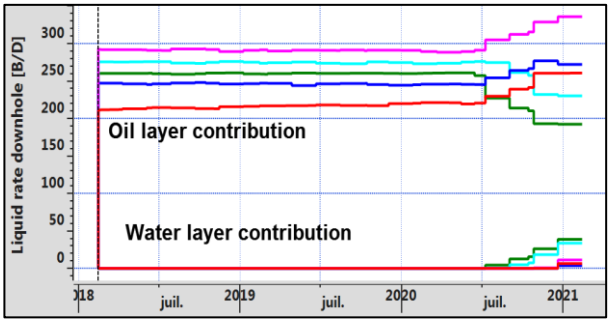


Fig. 6.K.10 – ICD effect layer contribution

7 – Reservoir models

OH – OSF – DV

7.A Introduction

In Pressure Transient Analysis (PTA), reservoir features are generally detected after wellbore effects and well behavior have ceased and before boundary effects are detected. This is what we might call an intermediate time response. In Rate Transient Analysis (RTA), reservoir behavior will be detected when a change in the production sequence is clear enough to produce transients before Pseudo-Steady State is reached. So for the production analyst, reservoir behavior will relatively be an early time effect that may or may not be seen.

The main parameter we are looking for is the mobility of the fluid in the reservoir, k/μ. When there is a doubt about the effective reservoir thickness, the parameter calculated is kh/μ. When the fluid viscosity is known and assumed to be constant we can calculate the permeability-thickness product kh. Whatever the variant, and whether we are performing pressure transient or rate transient analysis, this result will be quantified by the pressure match on the loglog (both PTA and RTA) and Blasingame (RTA) plots. This result will be common to all models described below, whether they are homogeneous or heterogeneous.

In PTA, some well configurations will allow reservoir characterization even at the early time of the pressure response. Early time behavior of limited entry wells will be a function of an equivalent spherical permeability that in turn will depend on the reservoir vertical anisotropy. Also the early time response of a horizontal well will involve an X-Z permeability which in turn also depends on the reservoir horizontal anisotropy. Fractured well early time behavior will depend on both fracture length and conductivity and so on.

The second factor will be the reservoir storativity $\phi c_t h$. Generally this parameter will be an input, but in the case of an interference test this will be a result of the interpretation process, generally giving the porosity and assuming the other two factors as 'known'.

Finally, one will want to characterize the reservoir heterogeneities by using and matching heterogeneous models. Such heterogeneities can be local, for example the double-porosity case, vertical as in layered reservoirs, or areal, in the case of composite systems and any combination of these. It is possible to input heterogeneities such as porosity, permeability and thickness maps into a numerical model, or generate and upscale a geostatistical model. In this case, quantifying the heterogeneities will be useful to correct our assessment of the long term reservoir potential.

7.B Homogeneous reservoir

The homogeneous reservoir is the simplest possible model assuming everywhere the same porosity, permeability and thickness. The permeability is assumed isotropic. That is, the same in all directions.

The governing parameters are:

kh Permeability-thickness product, given by the pressure match.

$\phi c_t h$ Reservoir storativity, input at the initialization of a standard test or as a result in interference tests.

S Skin

At early time the pressure response is dominated by the well models described in the chapter on 'Well models', the most common early time responses are thus:

Wellbore storage, linear flow (high conductivity fracture), bilinear flow (low conductivity fracture), spherical flow, horizontal well (linearity after early time radial flow). These regimes are coupled with a hump caused by the storativity and the skin.

In addition we have the line source well with no skin or wellbore storage used for the analysis of interference tests.

In fact, the reservoir response in a homogenous reservoir is simply the linearization of the pressure with respect to the logarithm of time, infinite acting radial flow (IARF) is established and the Bourdet derivative stabilizes and is flat at a level related to the permeability.

The below figure shows a schoolbook example of the response of a wellbore storage and skin homogeneous model in an infinite reservoir. If this was a common behavior the task of the PTA engineer would have been easy indeed.

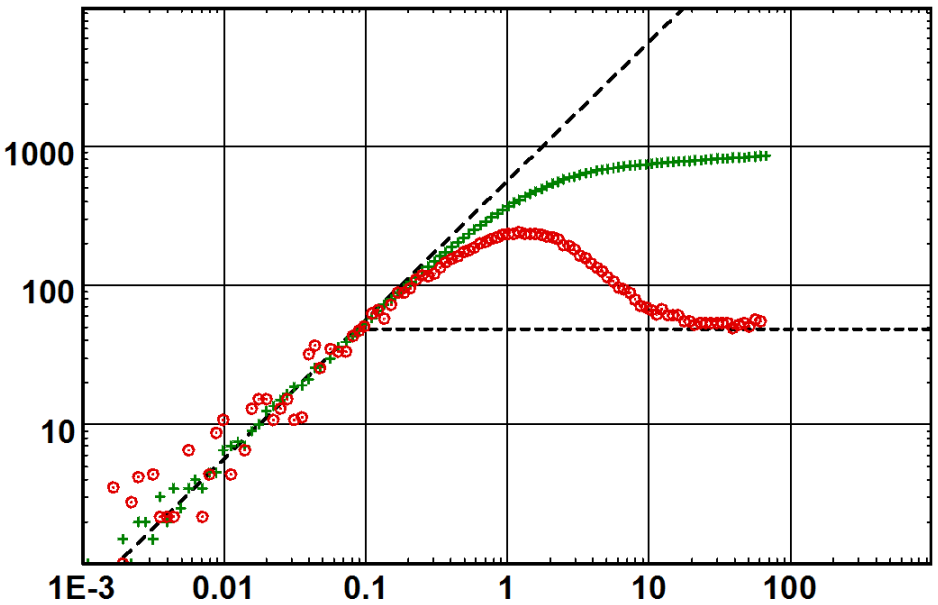


Fig. 7.B.1 - Schoolbook response

The below figures illustrates the various homogenous behaviors on a loglog plot commonly seen in pressure transient analysis. The line source solution is also shown.

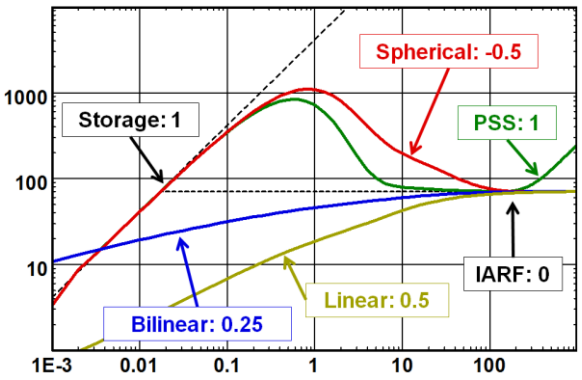


Fig. 7.B.2 – Homogeneous loglog plots

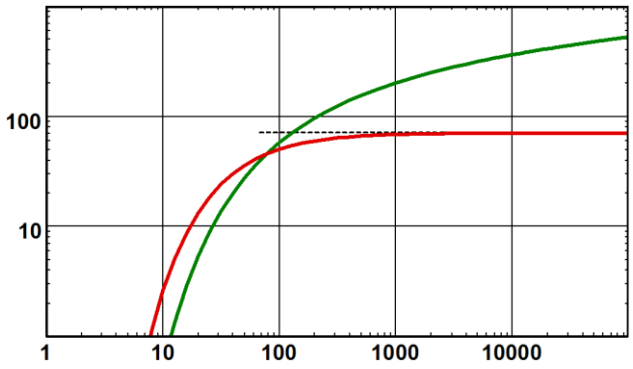


Fig. 7.B.3 – Line source

And following we illustrate the semilog behavior of wellbore storage and skin in a homogeneous reservoir.

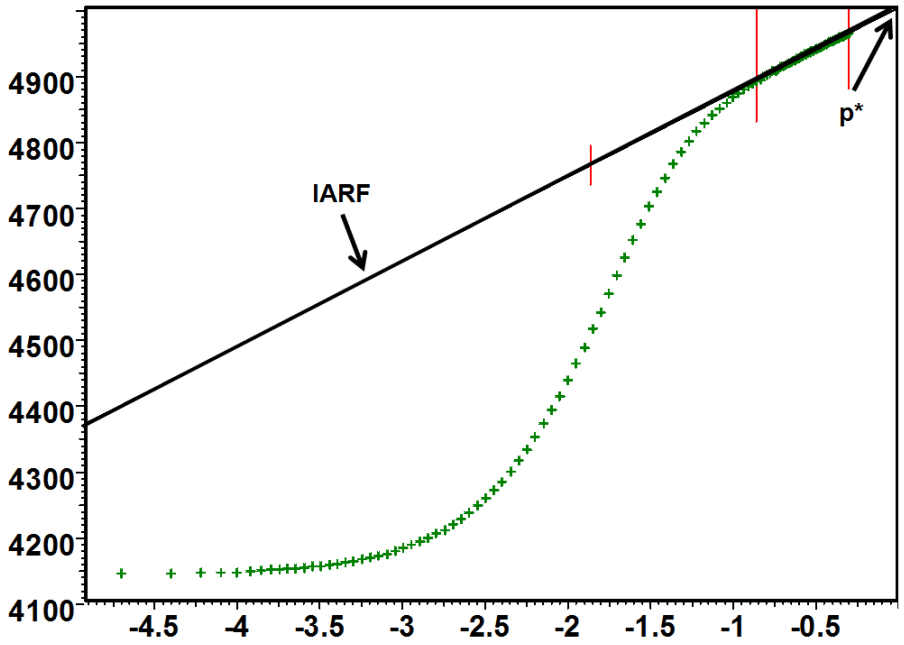


Fig. 7.B.4 – Homogeneous semilog plot

7.B.1 Homogeneous Sensitivity to parameters

7.B.1.a Skin

Below is shown the response with a variable skin. Values for skin are -3, 0, 2, 5 and 10.

Storage: Skin does not change the position of the early time unit slope (pure wellbore storage) but affects the amplitude of the hump. A larger skin will produce a larger hump, hence delaying the time at which Infinite Acting Radial Flow is reached.

IARF: Once IARF is reached, the skin has no effect on the vertical position of the derivative, but has a cumulative effect on the amplitude of the pressure.

PSS: Skin does not have an effect on the time at which PSS is reached or on the derivative response at the end. However the cumulative effect on the pressure remains and all responses 'bend' and remain parallel when PSS is reached (see history plot below).

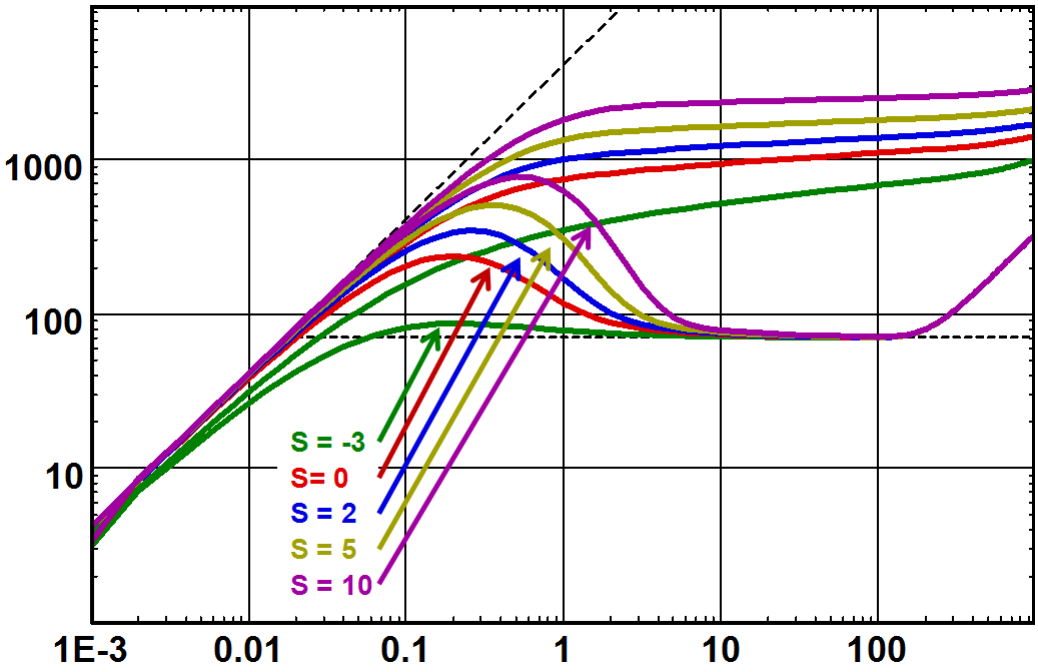


Fig. 7.B.5 – Effect of skin, loglog plot

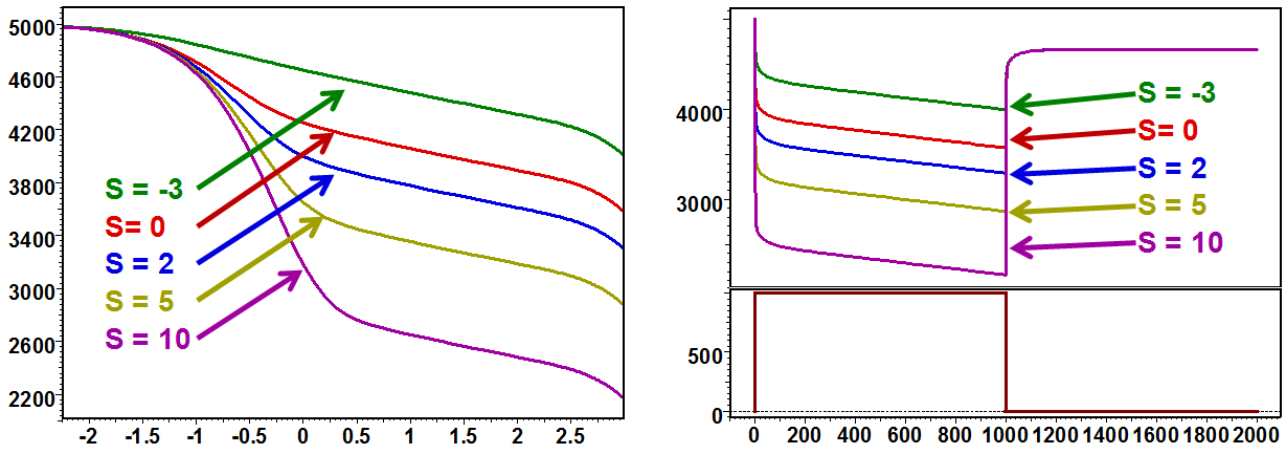


Fig. 7.B.6 – Effect of skin, semilog and history plot

7.B.1.b Permeability

The figure below presents the response with a variable permeability. Values for k are 2, 5, 10, 20 and 50 mD.

Storage and IARF: The derivative responses have the same shape but they are translated along the wellbore storage line of unit slope. When the permeability is higher, the reservoir reacts faster and deviates earlier from pure wellbore storage. The level of stabilization of the derivative, i.e. the slope of the semilog plot, is inversely proportional to k. For this reason the responses diverge on the semilog plot, the different slopes being inversely proportional to k.

PSS: At late time all derivative signals merge to a single unit slope. This is linked to the fact that permeability has no effect on the material balance equation.

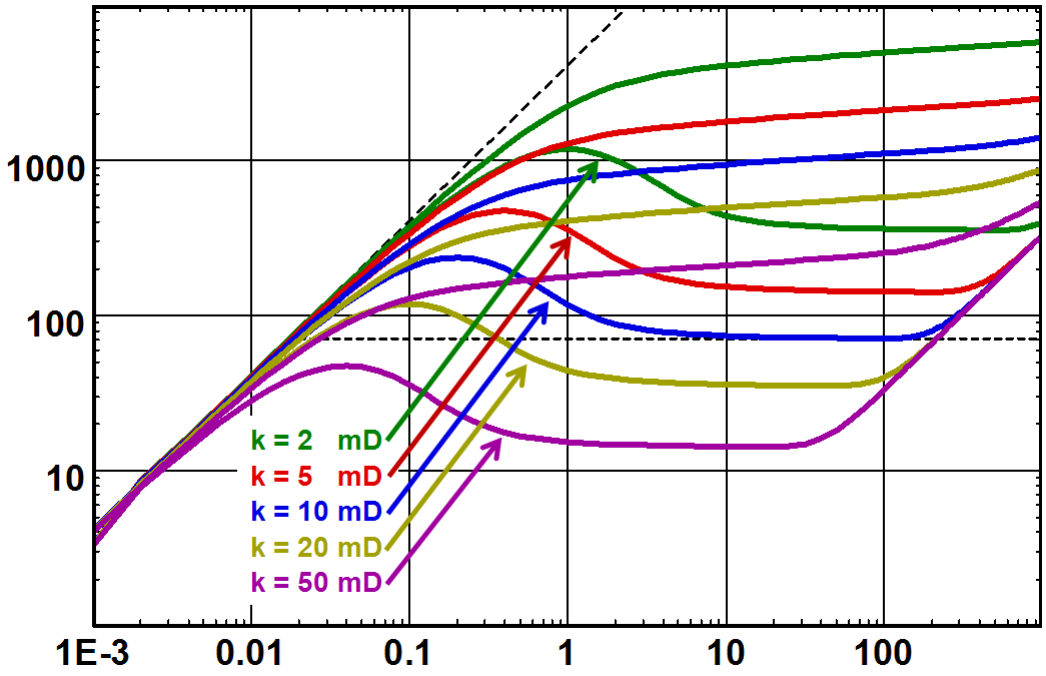


Fig. 7.B.7 – Influence of the reservoir permeability, loglog plot

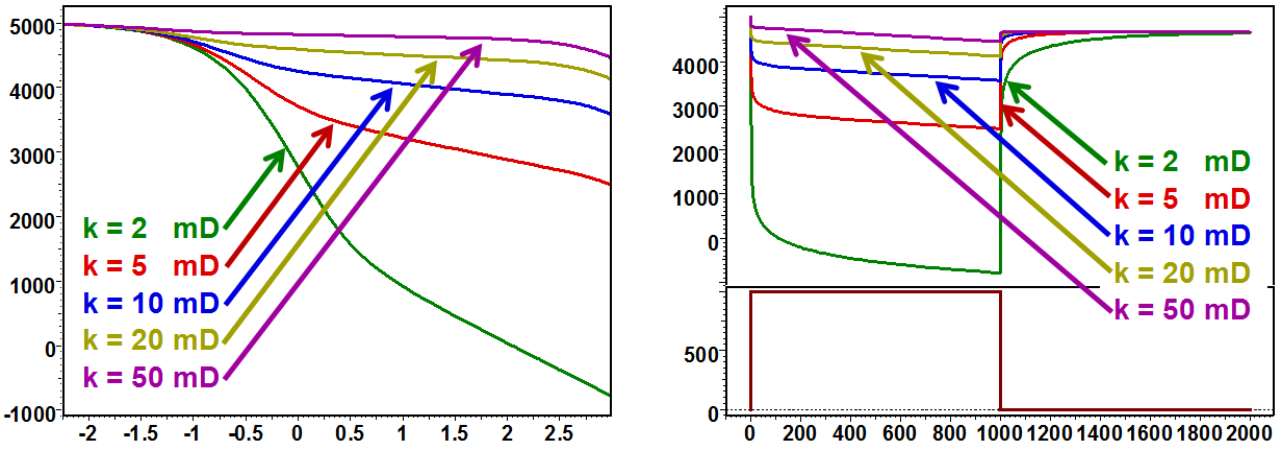


Fig. 7.B.8 – Influence of the reservoir permeability, semilog and history plot

7.B.1.c Wellbore radius

The response with varying wellbore radius is illustrated below. Values af r_w are 0.1, 0.3, 1 and 3 ft.

The effect of a change in the wellbore radius is strictly the same as the consequence of a skin change: Early time amplitude of the derivative hump, no middle time and late time effect on the derivative, but a shift in the pressure that stays constant once wellbore storage effects are over. The equivalence between wellbore radius and skin is hardly a surprise, as skin can also be defined with respect to an equivalent wellbore radius. The well response is in fact a function of the equivalent wellbore radius $r_{we} = r_w.e^{-Skin}$.

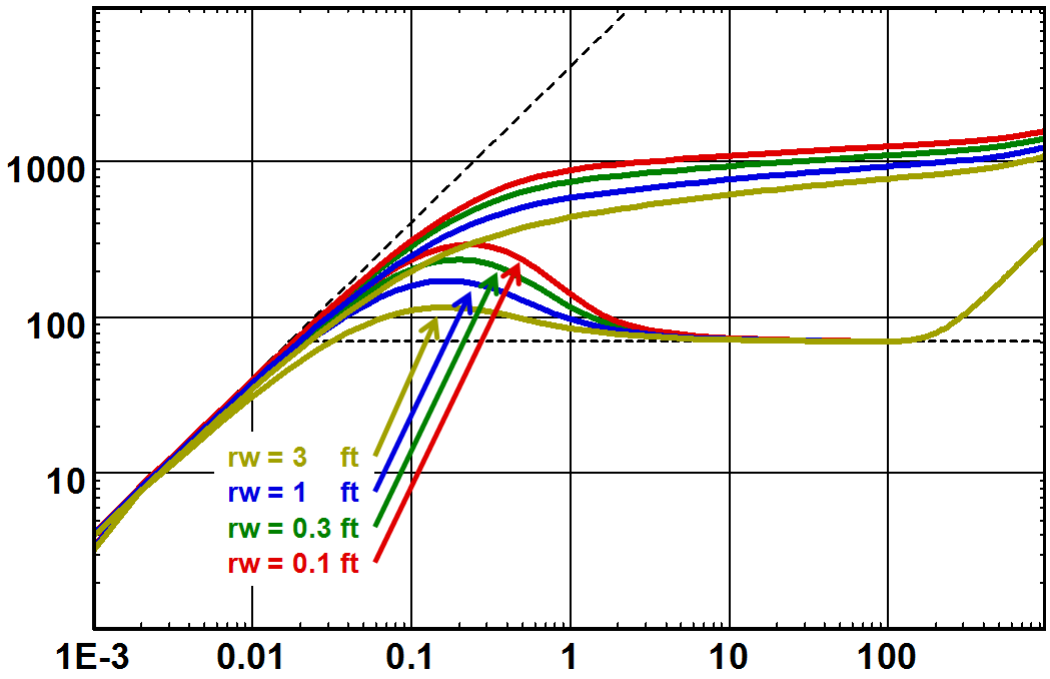


Fig. 7.B.9 – Effect of wellbore radius r_w, loglog plot

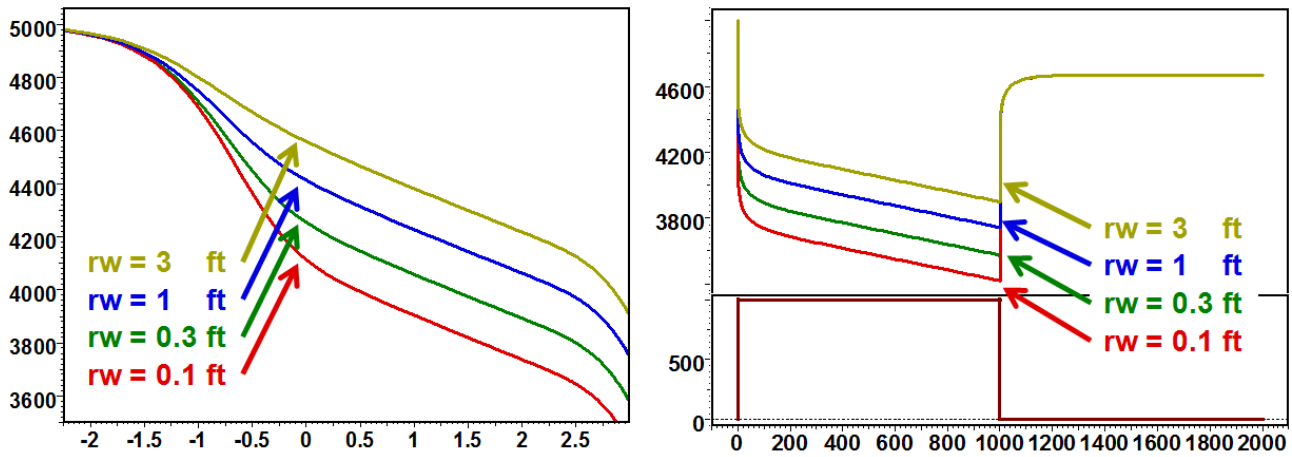


Fig. 7.B.10 – Effect of wellbore radius r_w, semilog and history plot

7.B.1.d Porosity

The figure below presents the response by varying the porosity. Values for ϕ are 3%, 10% and 30%.

Storage and IARF: Porosity behaves like the skin or the well radius. A smaller porosity produces a higher hump on the derivative but does not change the derivative IARF level. The equivalence between porosity and skin is used in two different areas. In Interference tests the Skin has a marginal influence, and the pressure amplitude is used to assess the porosity.

Hydrogeology: Hydrogeology will assess a value of skin (generally zero) and use the absolute value of the pressure change to assess the Storativity S, i.e. the porosity.

For a given reservoir size, the time for PSS is proportional to ϕ. Underestimating the porosity by 10% will provide an overestimation of the reservoir bulk volume of 10%, and therefore an overestimation of the boundary distance. The total pore volume will remain correct.

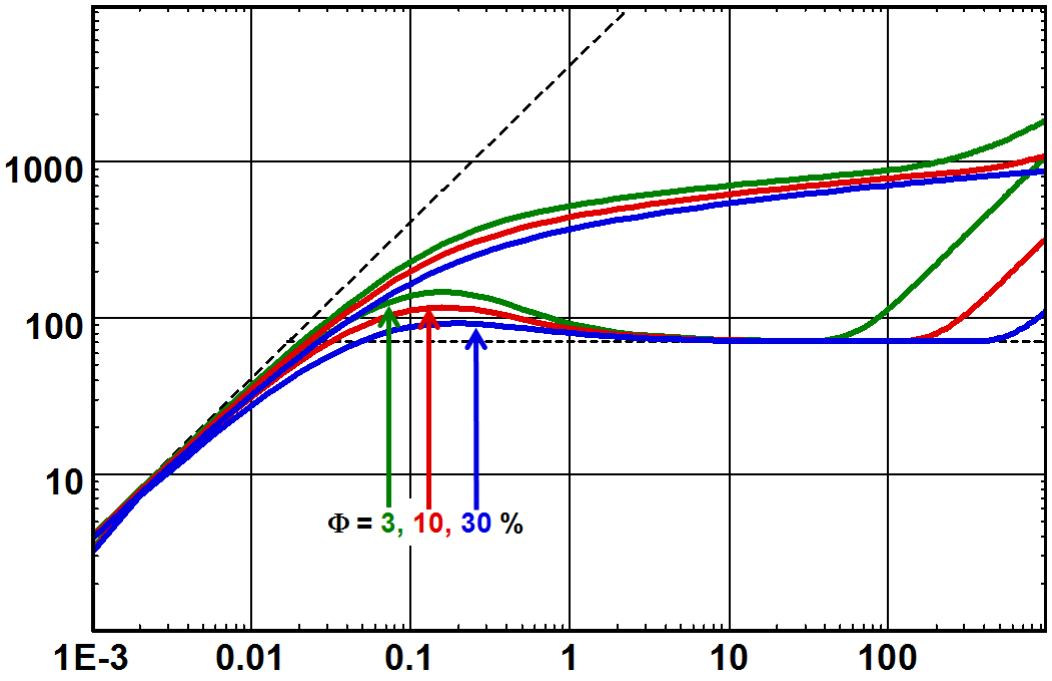


Fig. 7.B.11 – Effect of the reservoir porosity, loglog plot

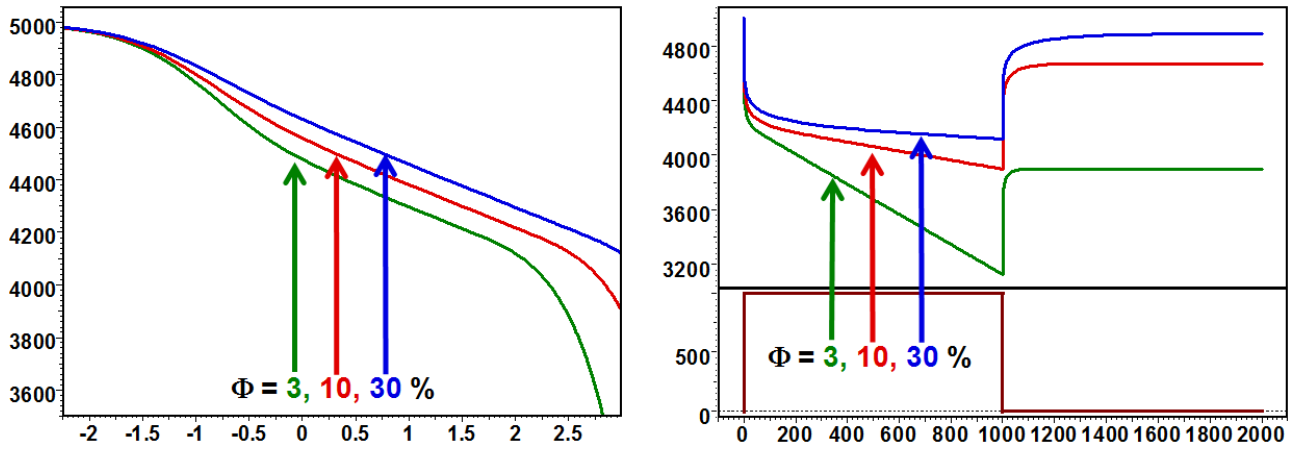


Fig. 7.B.12 – Effect of the reservoir porosity, semilog and history plot

7.B.1.e Total compressibility

Illustrated below is the response computed by varying the total compressibility. Values for c_t are 3.e-6, 1.e-5 and 3.e-5 psi-1. The sensitivities at Early Time (Storage), Middle time (IARF) and late time (PSS) are strictly the same as for the porosity: A smaller compressibility produces a higher hump of the early time derivative. Compressibility does not affect the derivative level when IARF is reached but has a cumulative effect on the pressure. At late time, compressibility affects the time at which the boundary is detected and the material balance equation. As for porosity, under-estimating c_t by 10% will provide an over-estimation of the reservoir size by 10%, and therefore an over-estimation of the boundary distance. In fact, on all parts of the response, the influence of porosity and compressibility will be a function of their product $\phi.c_t$.

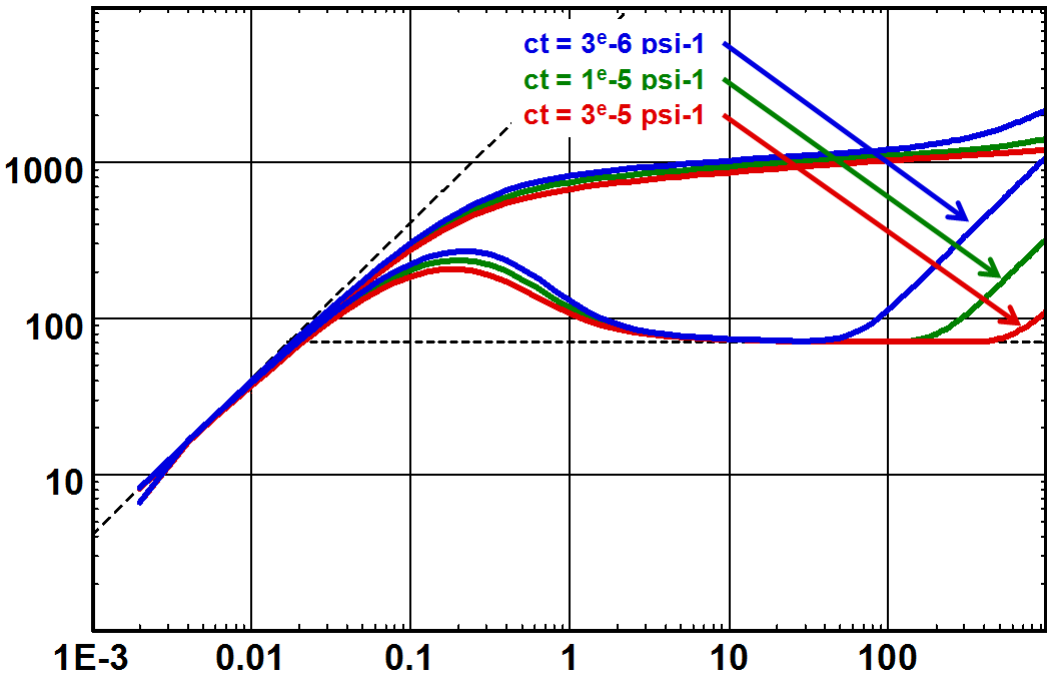


Fig. 7.B.13 – Effect of total compressibility, loglog plot

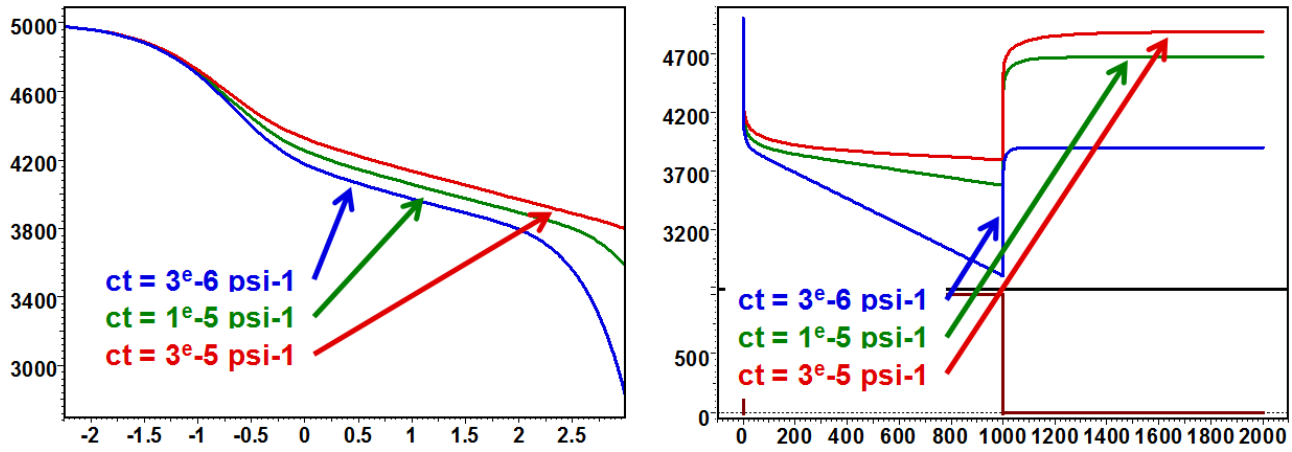


Fig. 7.B.14 – Effect of the total compressibility, semilog and history plot

7.B.1.f Viscosity

The next figure illustrates the response with variable fluid viscosity. Values for μ are 0.2, 0.5, 1, 2 and 5 cp. If we compare the response with the Fig. 2.H.8 illustrating the effect of a permeability change (above), we see that the sensitivity to viscosity is exactly opposite to the sensitivity to permeability. At early time (Storage) and middle time (IARF), the derivative responses have the same shape but translated along the wellbore storage line of unit slope. When the viscosity is lower, the reservoir reacts faster and deviates earlier from pure wellbore storage. The levels of stabilization of the derivative and the semilog slopes are proportional to μ. At late time all derivative signals merge to a single unit slope. In other words, the sensitivity on 1/μ is the same as the sensitivity to k on all parts of the response. This means that we have another governing group with k/μ, also called the mobility.

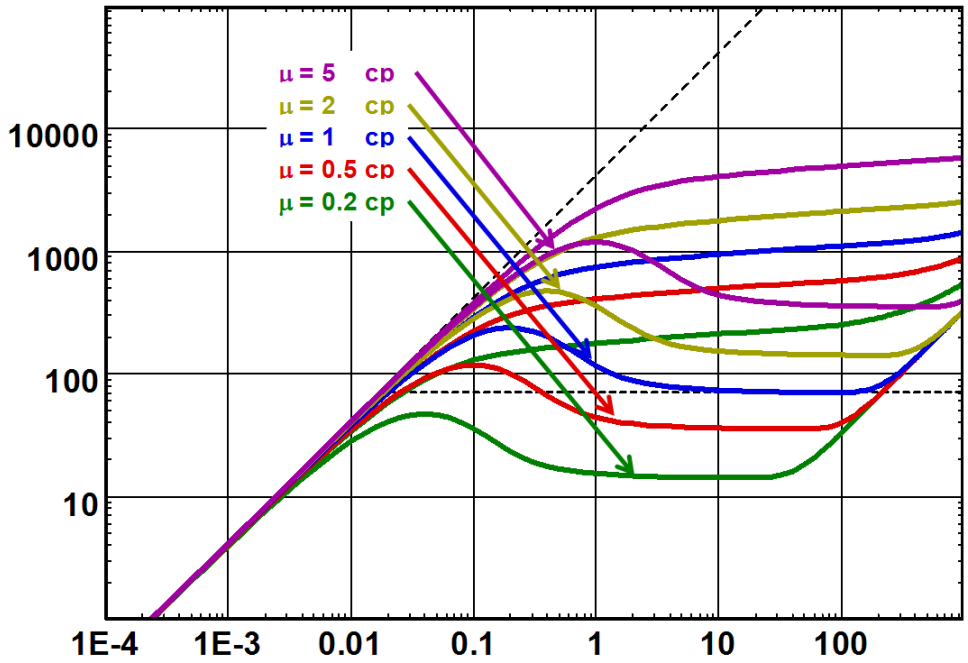


Fig. 7.B.15 – Effect of the fluid viscosity, loglog plot

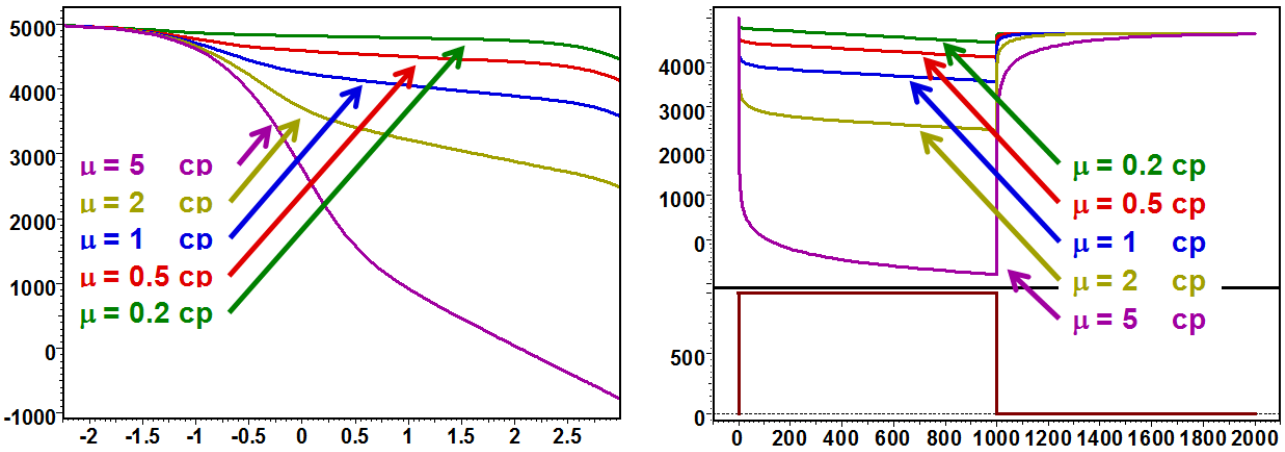


Fig. 7.B.16 – Effect of the fluid viscosity, semilog and history plot

7.B.1.g Thickness

Illustrated below is the response computed with a varying net drained thickness. Values for h are 20, 50, 100, 200 and 500 ft.

Storage and IARF: Changing the thickness has a similar effect to changing the permeability and an effect opposite to changing the viscosity. In other words, the governing group that defines the early time response, apart from wellbore storage and skin, is kh/μ.

PSS: Unlike permeability and viscosity, the reservoir thickness also has an effect on the late time material balance calculation. Also, the time at which the derivative deviates from IARF towards PSS does not change, and therefore the influence of the thickness on the position of the PSS straight line is similar to the sensitivity to the reservoir porosity or the compressibility.

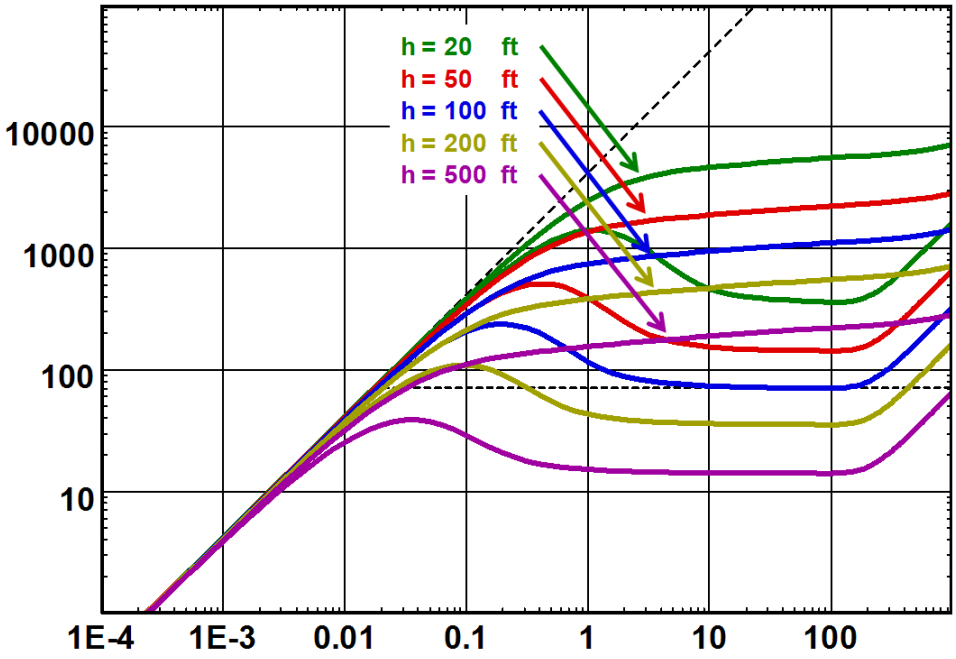


Fig. 7.B.17 – Effect of the reservoir thickness, loglog plot

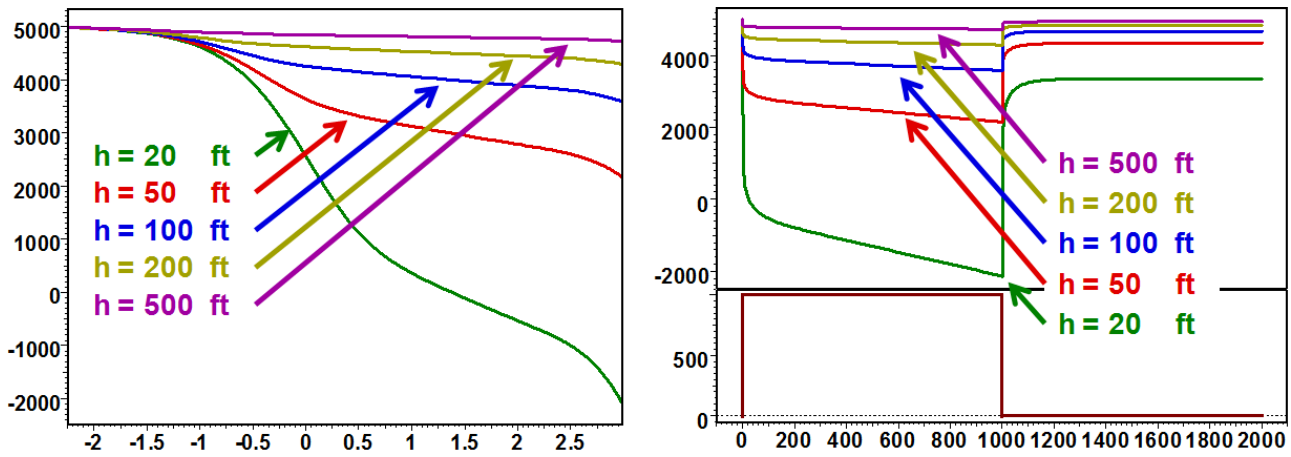


Fig. 7.B.18 – Effect of the reservoir thickness, semilog and history plot

7.B.1.h … and how about rates?

We are not referring to superposition effects, but to the plain value of the rate, i.e. the effect of a systematic error on the rate values and/or the formation volume factor B.

Fig. 7.B.20 below illustrates the response with a variable rate for each simulation. Values for q.B are 600, 800, 1000, 1200 and 1400 rb/d.

The result of varying q.B corresponds to a straight multiplication of the pressure change from pi. The loglog response is shifted vertically, and the semilog and history plots are vertically compressed or expanded, the fixed point being the initial pressure.

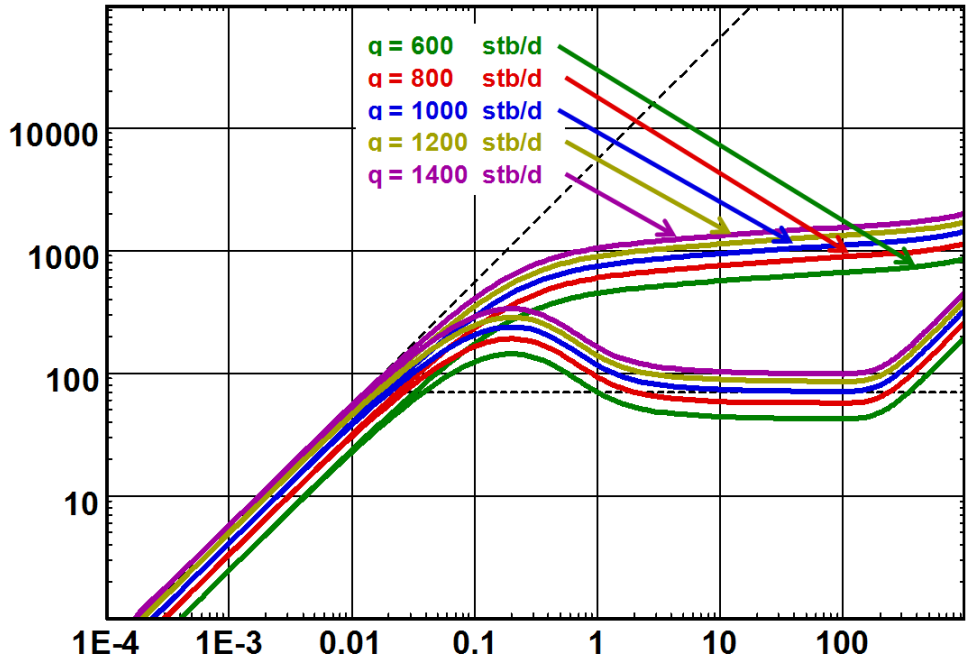


Fig. 7.B.19 – Effect of the rate – q.B, loglog plot

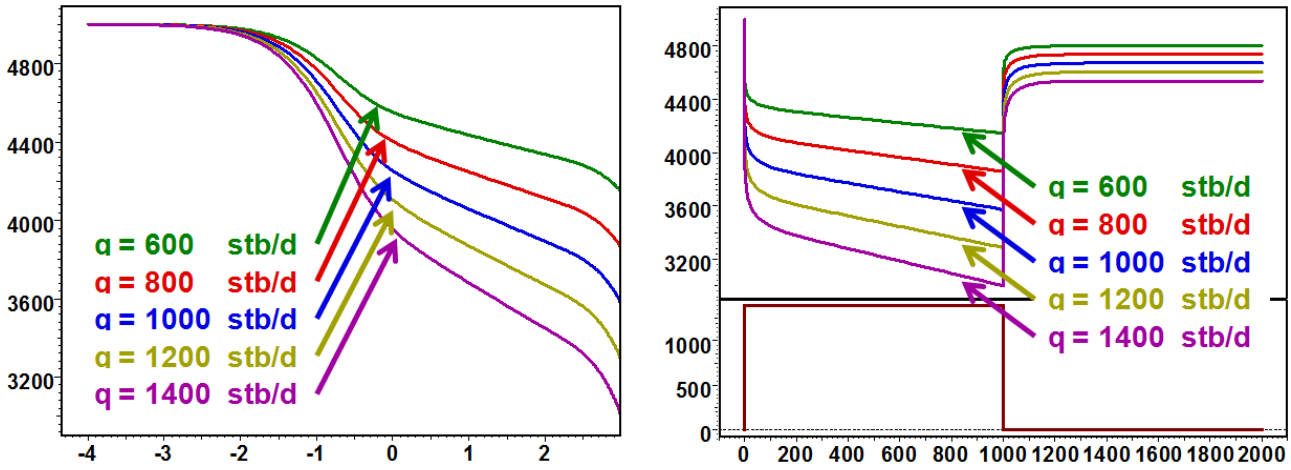


Fig. 7.B.20 – Effect of the rate – q.B, semilog and history plot

7.C Double-porosity reservoir

7.C.1 Hypothesis

The double-porosity (2Φ) models assume that the reservoir is not homogeneous, but made up of rock matrix blocks with high storativity and low permeability. The well is connected by natural fissures of low storativity and high permeability. The matrix blocks cannot flow to the well directly, so even though most of the hydrocarbon is stored in the matrix blocks it has to enter the fissure system in order to be produced.

The double-porosity model is described by two other variables in addition to the parameters defining the homogeneous model: ω is the storativity ratio, and is essentially the fraction of fluids stored in the fissure system (e.g. ω=0.05 means 5%).

ω, storativity ratio:

$$\omega = \frac{(V\Phi c_t)_f}{(V\Phi c_t)_m + (V\Phi c_t)_f}$$

λ is the interporosity flow coefficient that characterizes the ability of the matrix blocks to flow into the fissure system. It is dominated by the matrix/fissures permeability contrast, k_m/k_f.

λ, the interporosity flow parameter:

$$\lambda = \alpha r_w^2 \frac{k_m}{k_f}$$

The geometrical coefficient α is a function of the number "n" of families of fissure planes

$$\alpha = \frac{n(n+2)}{r_m^2} \qquad \text{With } r_m = n\frac{V}{A}$$

If the matrix blocks are spheres or cubes: $\alpha = \frac{15}{r_m^2}$

If the matrix blocks are cylinders: $\alpha = \frac{8}{r_m^2}$

When the well is first put on production, after any well dominated behavior, the first flow regime to develop is the fissure system radial flow, i.e. the fissure system is producing as if this system was there alone, and there is no change in the pressure inside the matrix blocks.

This first flow regime is typically over very quickly, and is frequently masked by wellbore storage. If not, it will develop as an IARF response and the pressure derivative will stabilize horizontally.

Once the fissure system has started to produce, a pressure differential is established between the matrix blocks and the fissures. The matrix is still at initial pressure p_i, and the fissure system has a pressure p_{wf} at the wellbore, the matrix blocks then start to produce into the fissure system, effectively providing pressure support, and the drawdown briefly slows down as this extra energy tends to stabilize the pressure, thus a transitional dip in the derivative is created.

The total system radial flow (IARF) is established when any pressure differential between the matrix blocks and the fissure system is no longer significant, and the equivalent homogeneous radial flow response is observed. A second IARF stabilization in the pressure derivative is therefore developed after the transitional dip, called by some the derivative valley. According to the mathematics, this takes place when the pressure inside the matrix blocks is the same as in the fissure system however; this can never be true at all points in the reservoir, as there would be no production into the fissure system.

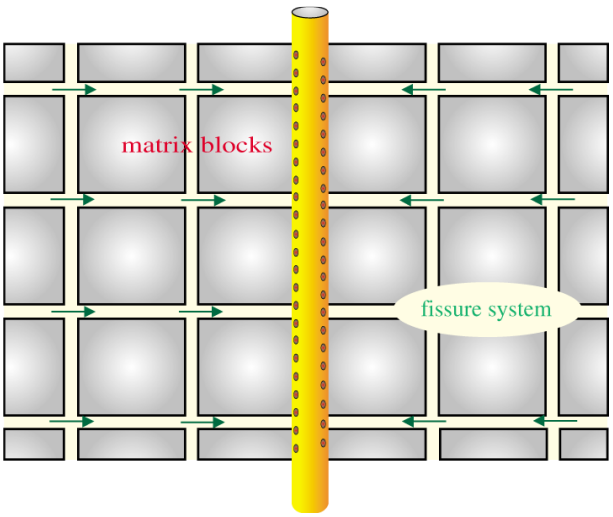


Fig. 7.C.1 – Fissure system production

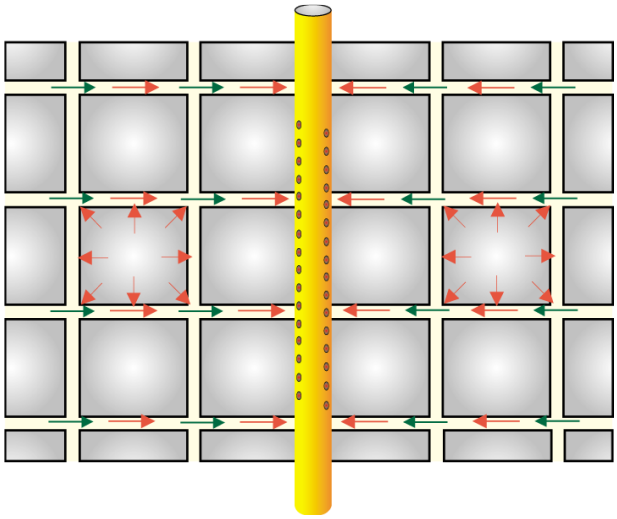


Fig. 7.C.2 – Total system production

7.C.2 Loglog behavior

Pseudo-Steady State (PSS) interporosity flow

In this case it is assumed that the pressure distribution in the matrix blocks is uniform, i.e. there is no pressure drop inside the matrix blocks. A physical explanation for this might be that the matrix blocks are small, so that any pressure drop inside them is insignificant compared to the pressure diffusion in the reservoir away from the wellbore. The entire pressure drop takes place at the surface of the blocks as a discontinuity, and the resulting pressure response gives a sharp dip during the transition.

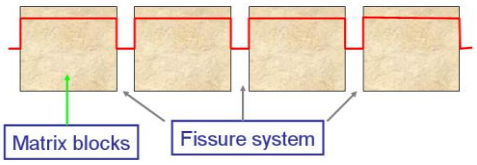


Fig. 7.C.3 – Pressure cross section

A real buildup from a double porosity reservoir is illustrated below.

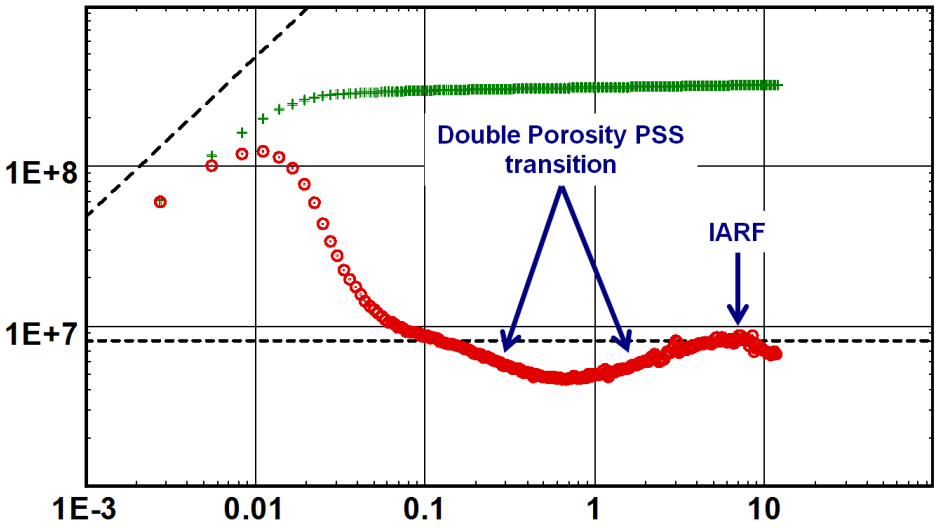


Fig. 7.C.4 – Double porosity loglog plot, PSS

ω is the fraction of interconnected pore volume occupied by the fissures. It determines the depth of the dip. For small ω values, corresponding to a very high proportion of the hydrocarbon stored in the matrix system, the support during the transition is substantial, and the dip is deeper and longer. The figure below illustrates the influence of the value of ω.

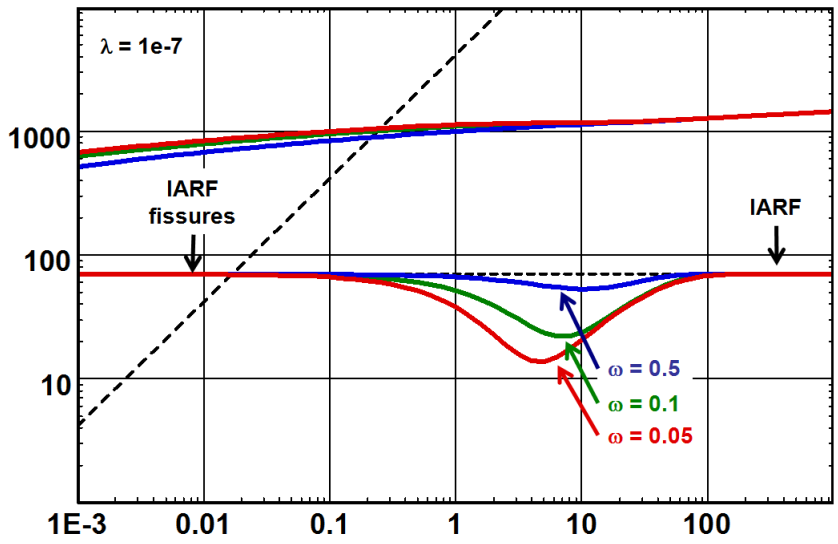


Fig. 7.C.5 – Influence of ω

λ describes the ability of the matrix to flow to the fissures, and is a function of the matrix block size and permeability. It determines the time of start of transition and controls the speed at which the matrix will react, therefore the total time of the transition. For a high λ, the matrix permeability is comparatively high, so it will start to give up its fluid almost as soon as the fissure system starts to produce. Conversely a low λ means a very tight matrix, and more drawdown will have to be established in the fissured system before the matrix blocks will appreciably give up any fluid, and the transition starts later? This is illustrated in the following figure.

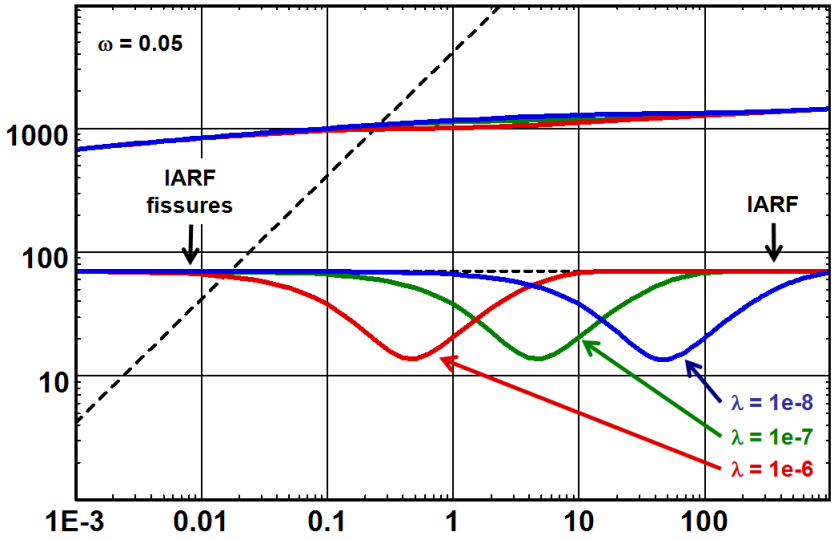


Fig. 7.C.6 – Influence of λ

Transient interporosity flow

This model assumes that there is a pressure gradient and therefore diffusivity, within the matrix blocks. If the pressure profile inside the blocks is significant, then the shape of the blocks has to be taken into consideration, and for this reason there are 2 models available, each corresponding to different matrix block geometries.

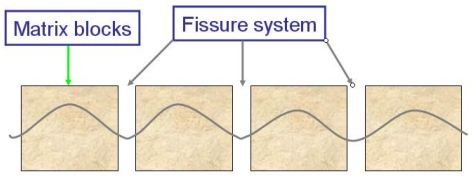


Fig. 7.C.7 – Pressure cross section

The 'slab' geometry model assumes rectangular matrix blocks, which is what we have been considering so far with the double-porosity PSS models. The 'spheres' model, physically realistic or not, represents another simple geometry with which to define the boundary conditions for the mathematical solution. It is difficult to visualize a reservoir consisting of spherical matrix blocks, but perhaps due to fluid movements over geological time the fissure network can become 'vuggy' and the edges of the matrix blocks rounded. Double-porosity data sets sometimes match the 'spheres' model better than any other. As before, our mathematical models may not be an accurate representation of what nature has provided in the reservoir, but the performance from these models is very close to the measured pressures from these wells. Below is a loglog plot of a buildup in a double porosity transient behavior reservoir. Unfortunately the test stopped in the middle of the transition.

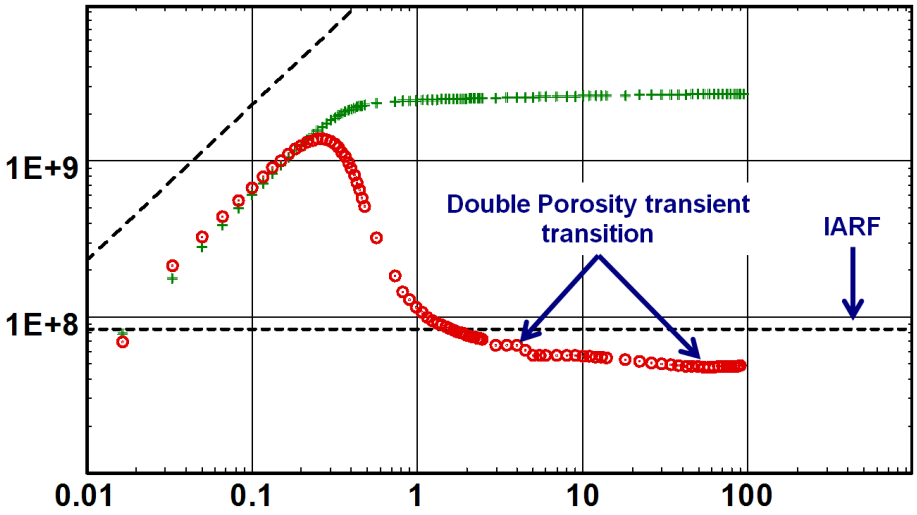


Fig. 7.C.8 – Double porosity transient behavior

The following figure illustrates the difference between the 'slab' and 'sphere' blocks, the difference is small.

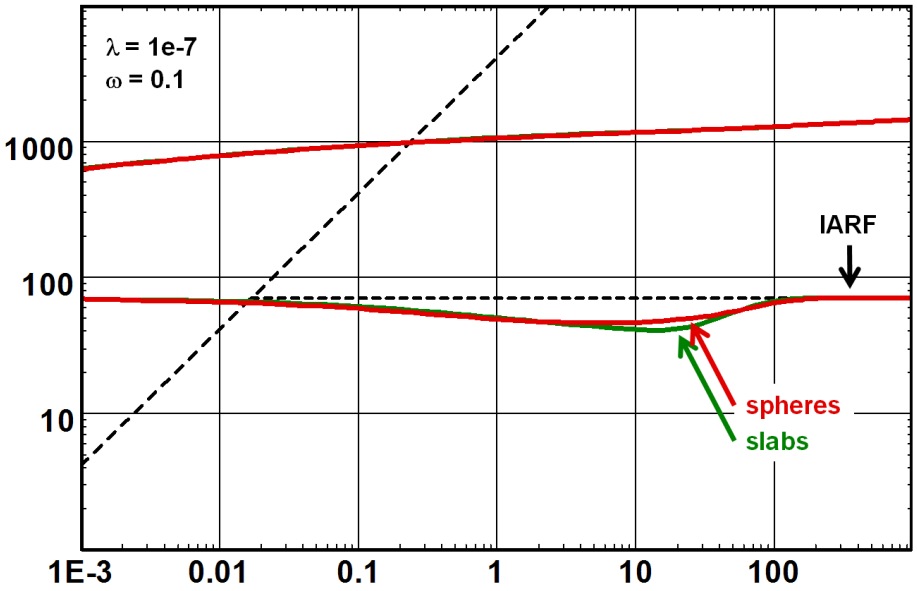


Fig. 7.C.9 – Slab/Sphere matrix blocks

As shown in the following plots, the fissure system radial flow is very short-lived, and in practice is not seen. At the deepest point in the transition, the semi-log slope/derivative value is half of the total system radial flow value. ω in this model has a more subtle effect on the shape of the derivative, and λ defines the time at which the response transitions to total system IARF.

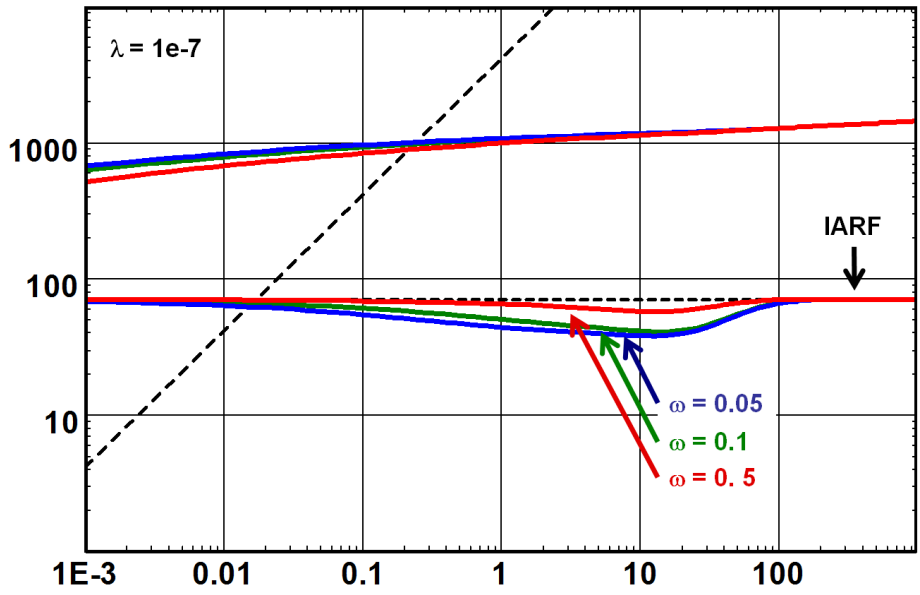


Fig. 7.C.10 – Slab matrix blocks influence of ω

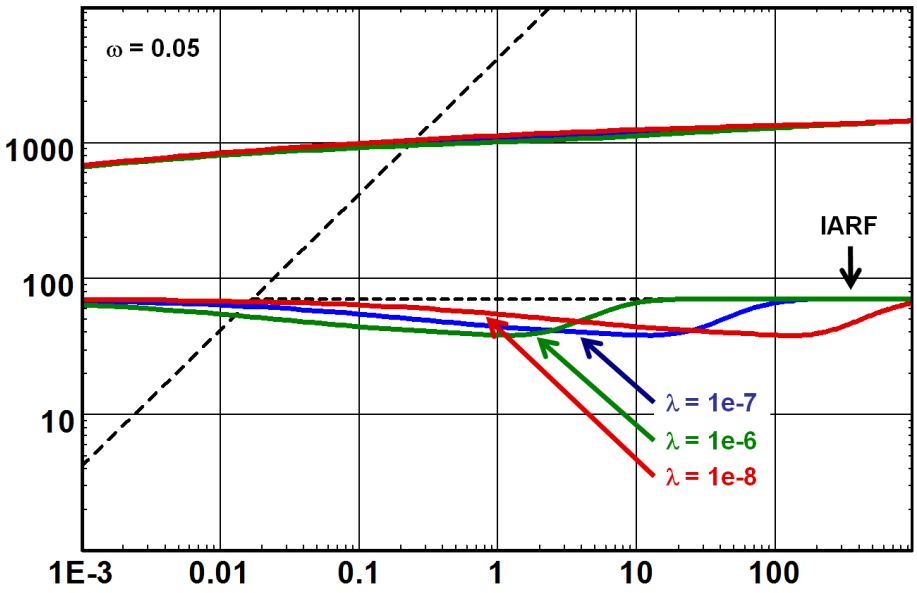


Fig. 7.C.11 – Slab matrix blocks influence of λ

7.C.3 Specialized analysis

There are theoretically two IARF stabilizations on the pressure derivative, hence two parallel straight lines on the semilog plot; the first is almost invariably obscured by wellbore storage.

If seen, the two lines would each correspond to $k_f h$, radial flow in the fissure system, as in the first case only the fissure system is producing. In the second case, although the total system is producing, any pressure differential between the matrix blocks and the fissure system is now negligible, and the only pressure drop in the system is in the fissures, as fluids flow to the wellbore. Imagine a droplet of oil in a matrix block 50 meters from the wellbore; it lazily travels a few centimeters to enter the fissure system, expelled by a negligible Δp, and then travels 50 meters through the fissure network, accelerating as it approaches the wellbore as the pressure gradient increases and flow area decreases. It is this pressure gradient, in the fissure system that creates the measured wellbore response.

In case the two straight lines *are* seen in the response, semilog specialized analysis can also yield information about ω and λ. ω is evaluated using the vertical separation of the two straight lines;

$$\omega = 10^{-\frac{\delta p}{m}}$$

and λ is evaluated using the time of the middle of the straight line through the transition;

$$\lambda = \frac{\omega \ln \frac{1}{\omega}}{0.000264k} \frac{\Phi \mu c_t r_w^{\ 2}}{\Delta t}$$

An example of this type of analysis, easily performed using Saphir, is illustrated below.

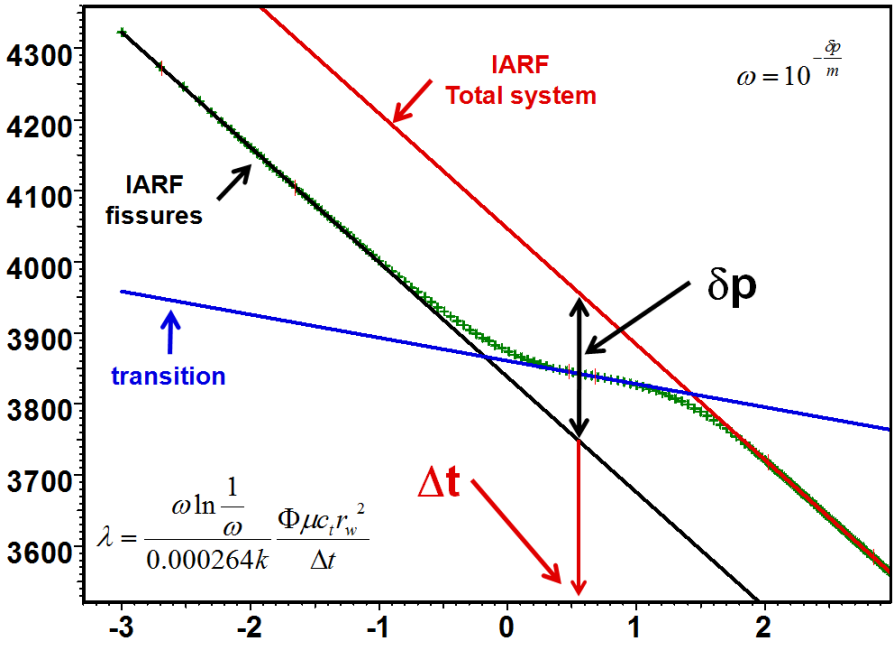


Fig. 7.C.12 – Double porosity PSS semilog analysis

7.C.4 Effect of wellbore storage

Wellbore storage will invariably mask the fissure response in the double porosity reservoir. The transition can thereby easily be misdiagnosed and the whole interpretation effort can be jeopardized. However, there are some lifelines that can save the day.

Typically there will be a negative skin associated with the double porosity reservoir where no negative skin was expected. The wellbore storage constant also tend to show a value which is unusually high and reflects the increase in the wellbore volume that the direct communication to the fissures and fractures sets up.

Illustrated below is a plot that demonstrates how the early time fissure response and transition is affected by an increasing wellbore storage coefficient. At higher wellbore storage coefficients even the whole transition period may be lost.

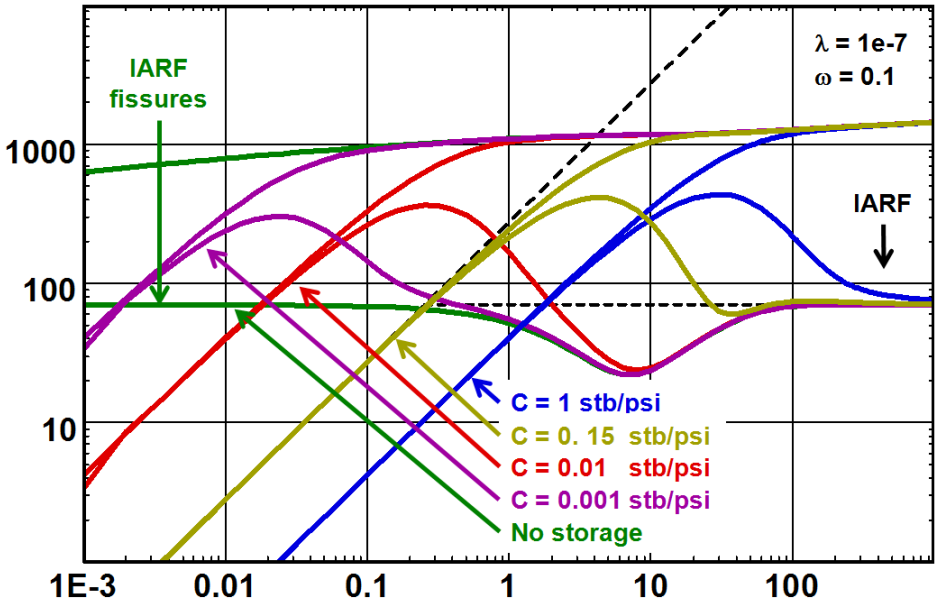


Fig. 7.C.13 – Double porosity PSS, influence of wellbore storage

7.C.5 Skin

Positive skin has no influence on the derivative and hence no influence on the transition thus no diagnostic feature is lost.

Highly negative skin will distort the early time response of both the derivative and the pressure change, the response approaches that of an infinite conductivity and linear flow can be seen to develop before the fissure system is in infinite acting radial flow.

See the below figure.

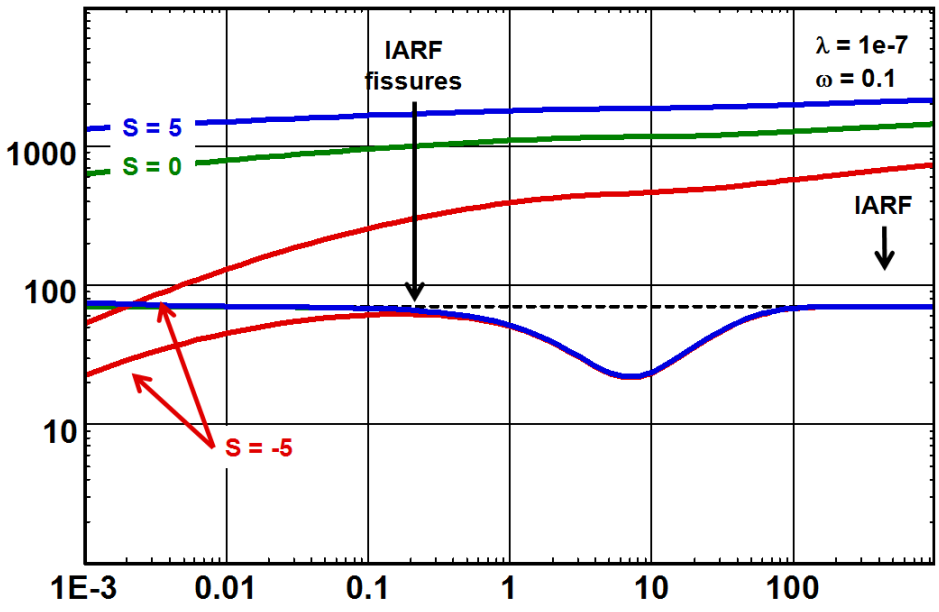


Fig. 7.C.14 – Double porosity, influence of skin

7.D Extensions of the double-porosity reservoir

7.D.1 Multiple porosities

The two families of double-porosity models are very different in behavior. The Pseudo-Steady state behavior starts with pure fissure flow, followed by an abrupt transition between the fissure and the total flow, characterized by a valley in the derivative response. The transient flow behavior (slab or sphere) will move immediately into transition, and this transition will be relatively smooth. In many cases, the behavior of naturally fractured formations, when seen, will be intermediate between the sharp and the smooth versions of these models. This is why several attempts were made to smooth the PSS model or sharpen the transient models.

7.D.2 Hypothesis

Pseudo-Steady State with multiple porosities

To extend the double porosity PSS solution one can consider matrix blocks of different sizes. In the following case we will consider only two different matrix blocks.

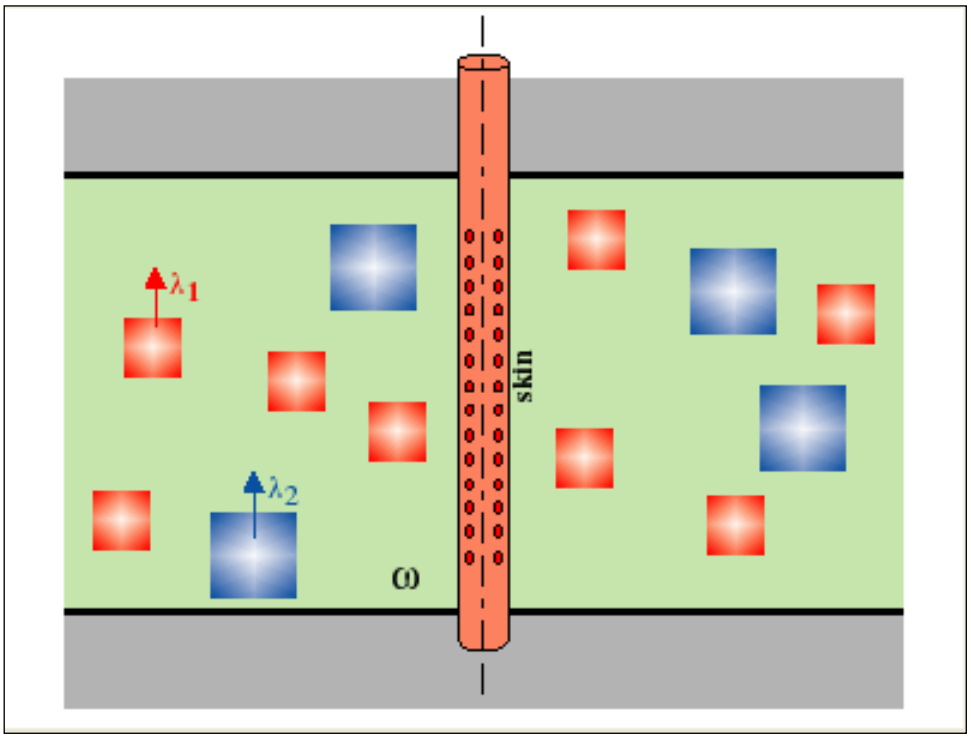


Fig. 7.D.1 – Triple porosity PSS

ω is still defined as the fraction of the interconnected pore volume occupied by the fissures. Each series of matrix blocks has its own value of λ (i.e. λ_1 and λ_2), corresponding to different transition times, and each subtype of blocks will occupy a different fraction of the total matrix pore space. We will define δ_1 the fraction of the matrix pore space occupied by the first series of blocks with respect to the total block storativity:

$$\delta_1 = \frac{(\Phi V c_t)_1}{(\Phi V c_t)_{1+2}} \quad \text{and} \quad \delta_2 = 1 - \delta_1$$

Transient double porosity with skin

An extension to the double porosity transient flow model is to add skin to the matrix face. The notion of spheres and slabs is still valid and ω and λ have the same definitions as before. The below figure illustrates the schematic of the model.

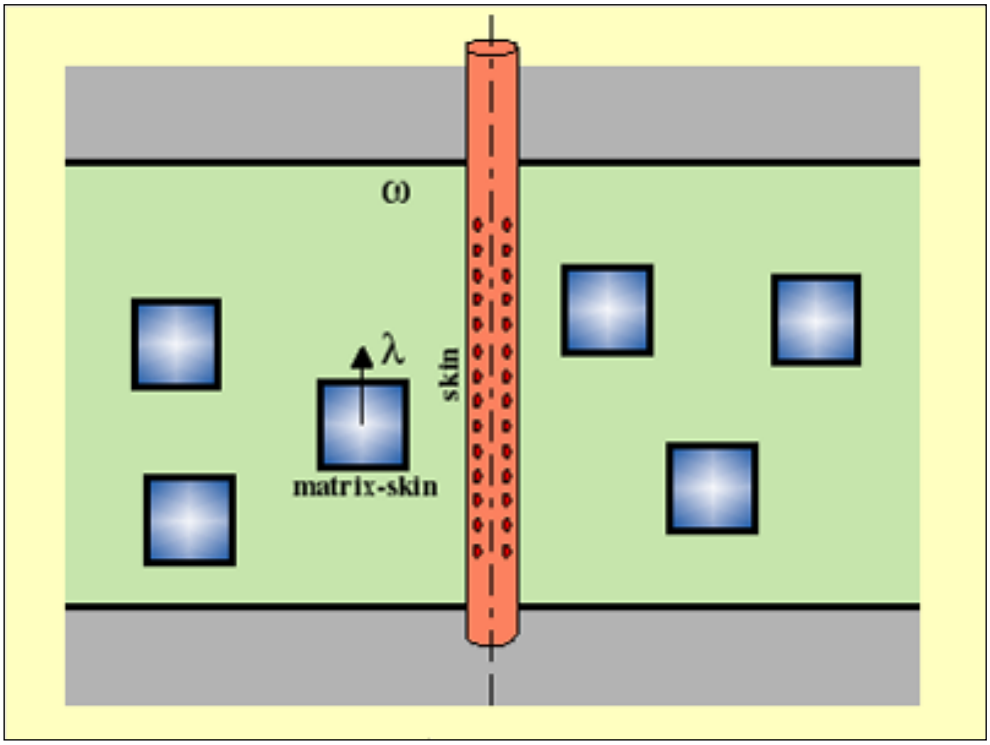


Fig. 7.D.2 – Transient model with matrix block skin

7.D.3 Loglog behavior

The following figure shows a typical response on the loglog plot. If an appropriate choice of the parameters and parameter ratios has been made it will allow the observation of a triple heterogeneous behavior. The first dip in the derivative is caused by the transition from the smaller sized block system to the fissures. The second dip in the derivative is only seen if the contrast of the interporosity flow coefficients of the two block systems is large enough.

For a constant ω value, the smaller the δ_1 value, the smaller the first dip and the greater the second.

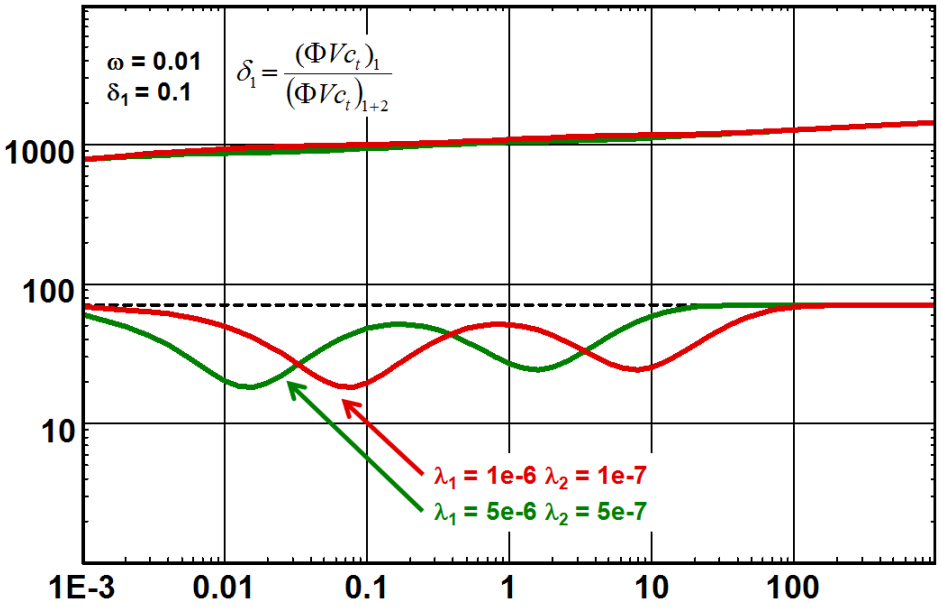


Fig. 7.D.3 – Triple porosity PSS response

Although this geological setting can easily be observed in real life the parameters governing this model is usually such that the two distinct transitions and valleys are not observed, in most cases only one transition valley is seen.

The following figure illustrates that adding skin to the matrix face the transient solution approaches that of the PSS double porosity response.

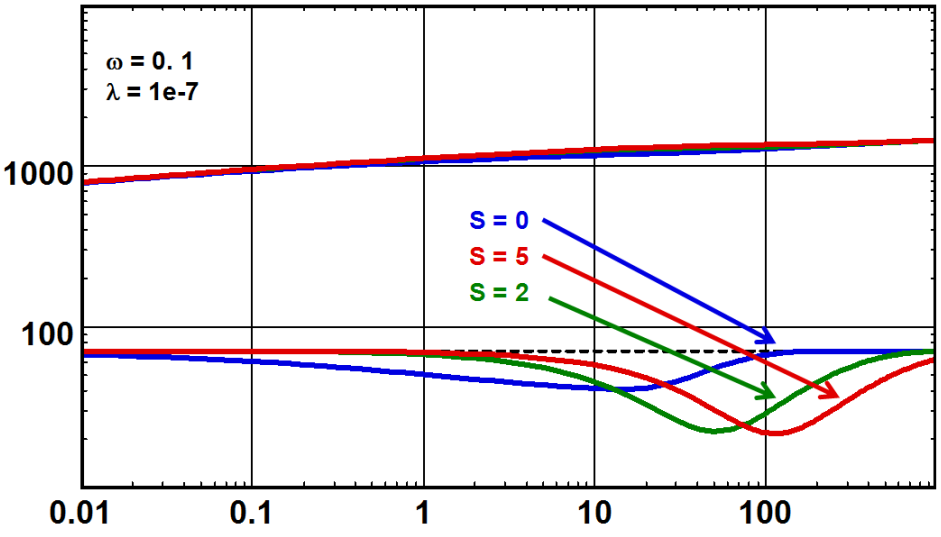


Fig. 7.D.4 – Transient double porosity, matrix blocks skin

7.D.4 Effect of wellbore storage

In the PSS model any wellbore storage will mask the first transition; as some wellbore storage is invariably present this means that in practice the first transition in such a system will very rarely be observed. See the following figure.

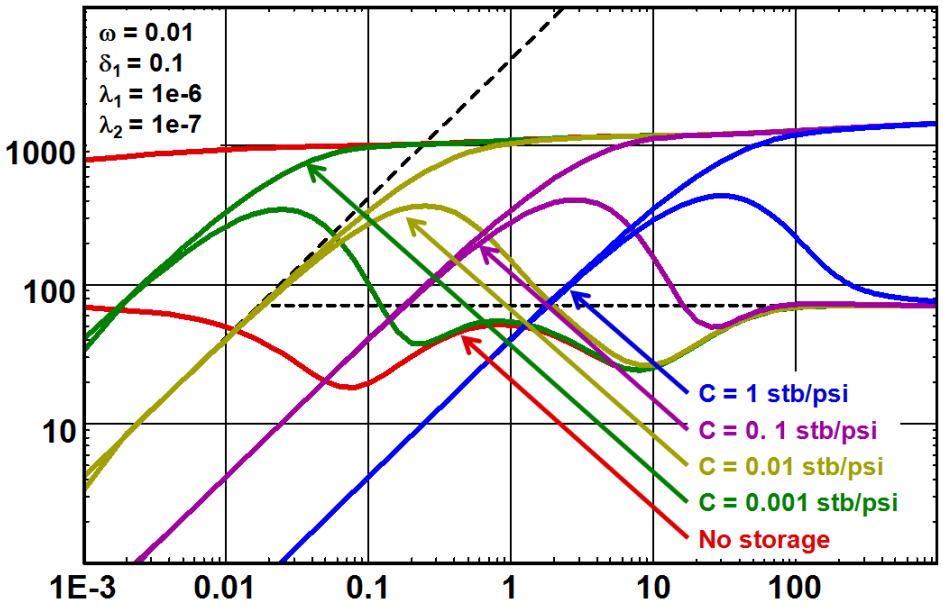


Fig. 7.D.5 – PSS influence of wellbore storage

The transient model with matrix skin will only be affected by significant wellbore storage which is illustrated by the following figure.

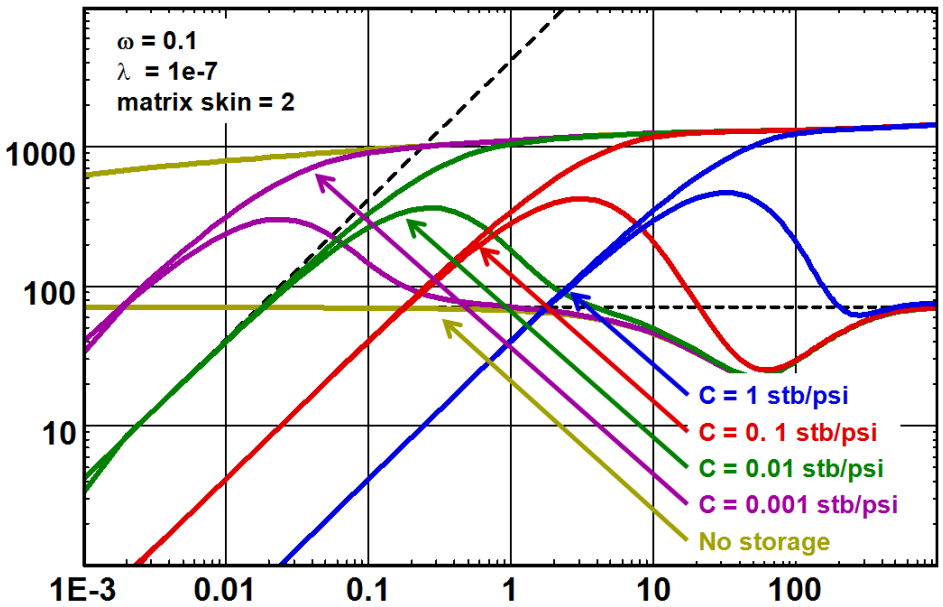


Fig. 7.D.6 – Transient, influence of wellbore storage

7.D.5 Effect of skin

The Bourdet derivative is not affected by the skin, except at very early time when the skin becomes very negative. In this case the behavior is similar to that of a fracture and linear flow in the fissure system may develop.

The below figure illustrates the model behavior with different skin values for the 'triple porosity' PSS reservoir.

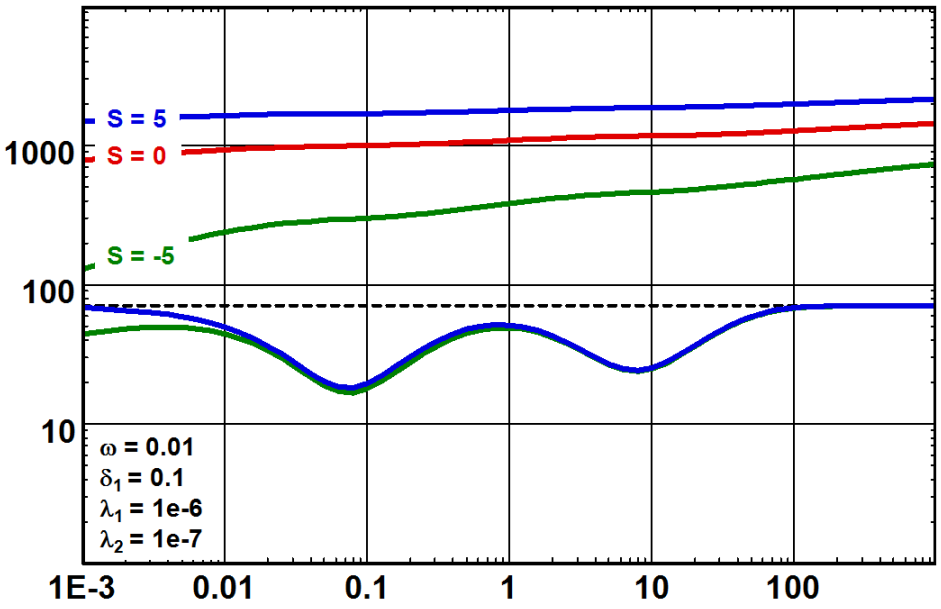


Fig. 7.D.7 – PSS influence of skin

Following we show the influence of the model skin (the skin acting between the well and the fissures) on the transient model with a constant matrix skin of 2 (the skin acting between the matrix blocks and the fissures).

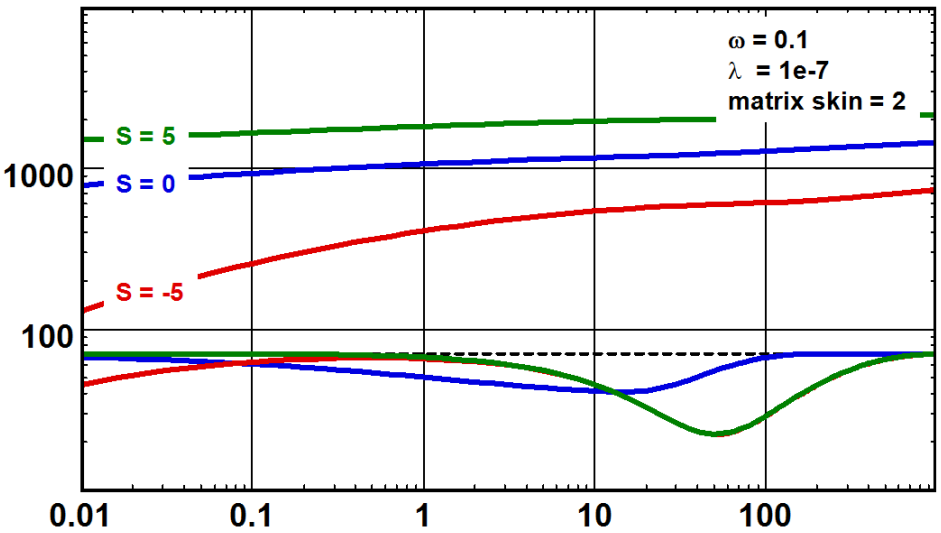


Fig. 7.D.8 – Transient, influence of skin

7.E Double-permeability reservoirs

7.E.1 Hypothesis

When is a layered reservoir not a layered reservoir? When each layer has the same properties, in which case the behavior of the system will be the equivalent behavior of the summed interval, it is homogeneous. However, the most pertinent question to ask is probably: "Does a homogeneous reservoir really exist? Just by the nature of the deposits would not most reservoirs be layered?".

Fortunately we know how to deal with layered systems.

In the double-permeability (2K) analytical model assumption the reservoir consists of two layers of different permeabilities, each of which may be perforated (contributing) or not. Crossflow between the layers is proportional to the pressure difference between them.

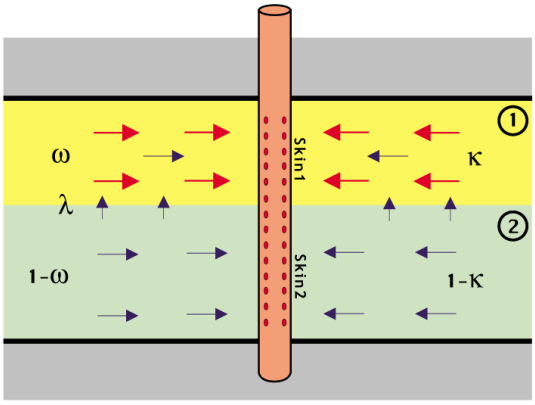


Fig. 7.E.1 – Double permeability reservoir

Making the comparison with the double-porosity PSS model, ω and λ have equivalent meanings. Adding one more leading parameter will describe the analytical model:

$$\omega = \frac{(V\Phi c_t)_1}{(V\Phi c_t)_1 + (V\Phi c_t)_2} \qquad \lambda = r_w^2 \frac{\alpha}{(kh)_1 + (kh)_2}$$

ω, layer storativity ratio, is the fraction of interconnected pore volume occupied by layer 1, and λ, inter-layer flow parameter, describes the ability of flow between the layers.

In addition another coefficient is introduced: κ is the ratio of the permeability-thickness product of the first layer to the total of both:

$$\kappa = \frac{(kh)_1}{(kh)_1 + (kh)_2}$$

Generally the high permeability layer is considered as layer 1, so κ will be close to 1. At early time there is no pressure difference between the layers and the system behaves as 2 comingled homogeneous layers without crossflow. As the most permeable layer produces more rapidly than the less permeable layer, a pressure difference develops between the layers and crossflow begins to occur. Usually the semi permeable wall hypothesis is applied and λ is

dependent upon the thickness of the wall, its vertical permeability and the individual vertical permeability of the layers:

$$\lambda = \frac{r_w^2}{kh} \frac{2}{2\frac{h'}{k_z'} + \frac{h_1}{k_{z1}} + \frac{h_2}{k_{z2}}}$$

Assuming that the vertical permeability in the layers is the same, if no semi permeable wall or skin is present then:

$$k_z = kh \frac{\lambda}{r_w^2} \frac{h}{2}$$

Eventually the system behaves again as a homogeneous reservoir, with the total kh and storativity of the 2 layers.

A transitional dip is governed by ω and λ, which have the same effect as in the double porosity models, and κ, which reduces the depth of the dip as κ decreases. If κ=1 then k_2=0 and the properties of the low permeability layer is equivalent to that of the matrix blocks of a double porosity system and can only be produced by cross flowing to the high-permeability layer, equivalent to the fissure system in the double porosity model PSS.

7.E.2 Loglog behavior

The below figure illustrates the response in a well tested in a two layered system.

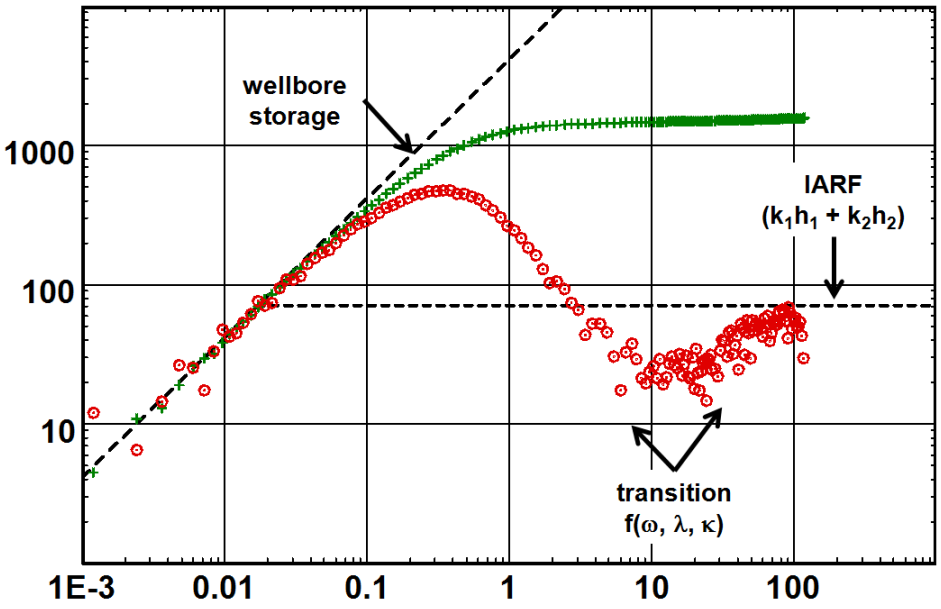


Fig. 7.E.2 – Loglog plot

The following figures illustrate the sensitivity to the parameters ω, λ and κ. Both layers are perforated and can produce to the well.

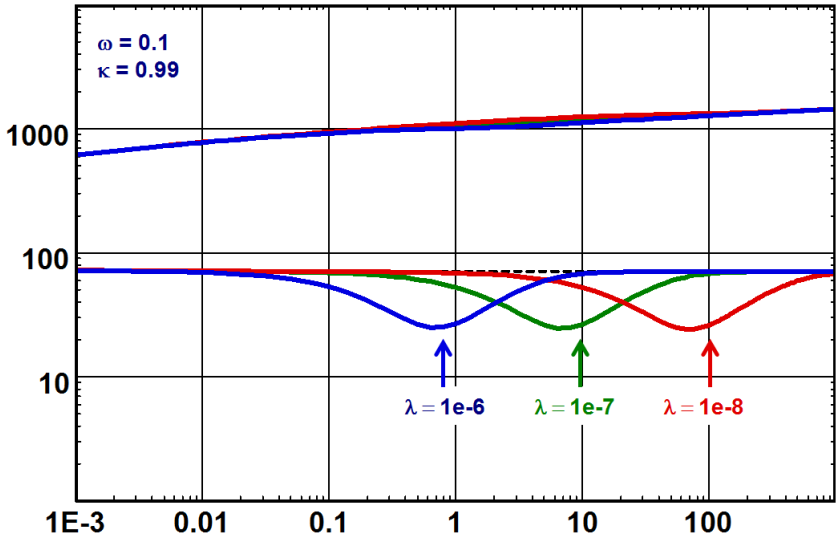


Fig. 7.E.3 – Influence of λ

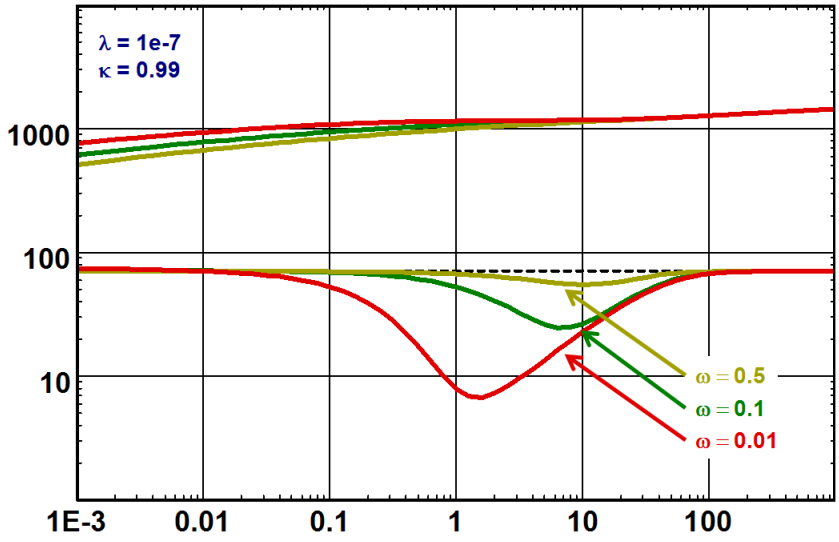


Fig. 7.E.4 – Influence of ω

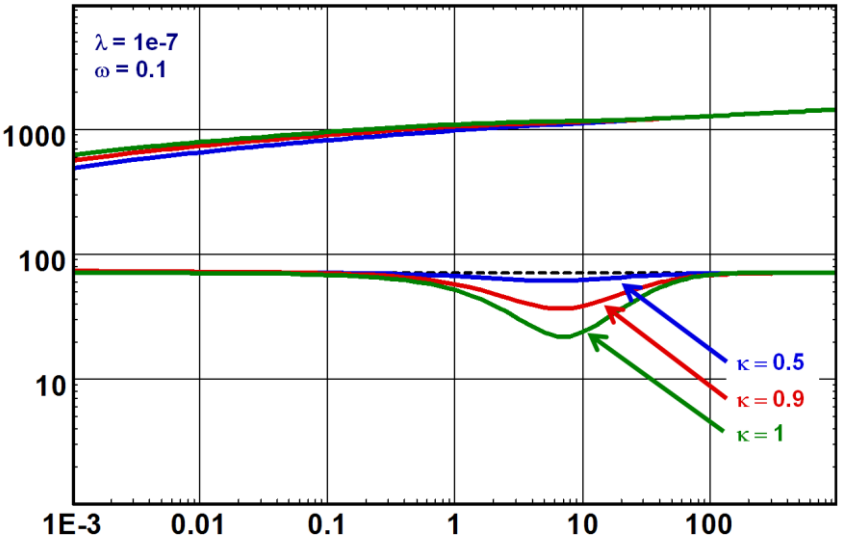


Fig. 7.E.5 – Influence of κ

7.E.3 Effect of wellbore storage

Wellbore storage will mask the transition. This is illustrated in the following figure.

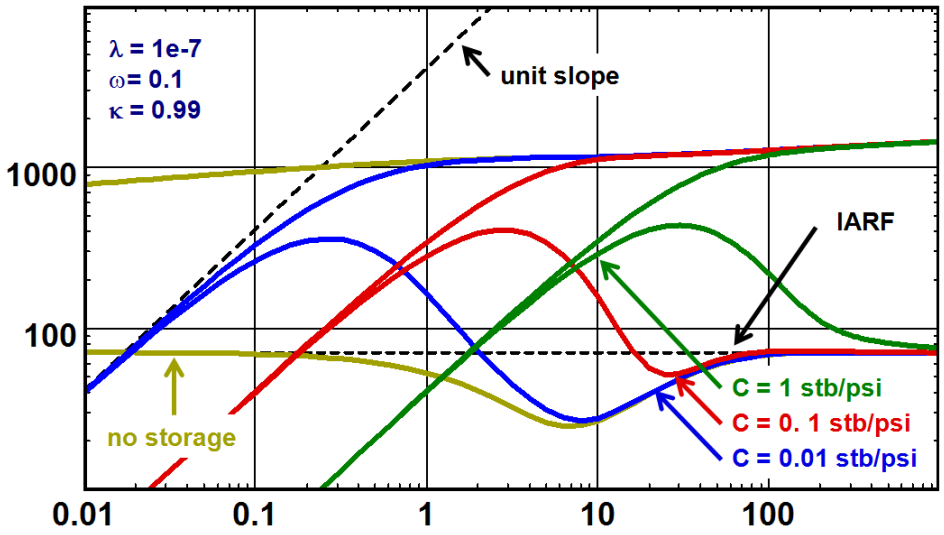


Fig. 7.E.6 – Influence of wellbore storage

7.E.4 Skin

Varying the skin in layer 2 has little or no impact on the model behavior as illustrated below.

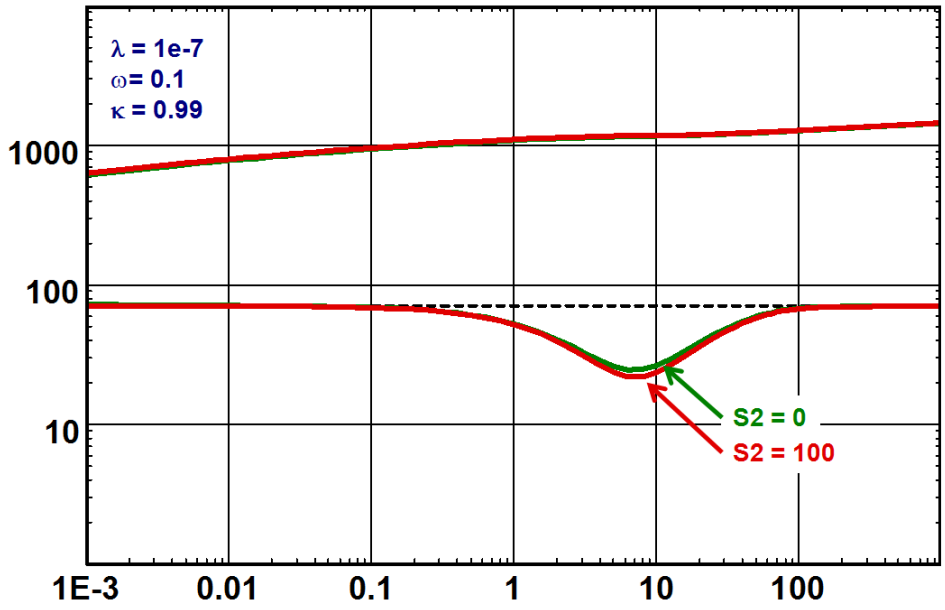


Fig. 7.E.7 – Influence of skin (S2)

However varying the skin in the high permeability layer sets up a totally different response and describes a different well configuration by using a reservoir model. The well could be perforated in the low permeability layer only or the high permeability layer could have been plugged at the well inducing a considerable skin. In this way the high permeability layer can only contribute to the production through reservoir cross flow to the lower permeability layer.

This is a scenario similar to that of limited entry or partial penetration, but in this case spherical flow will not quite develop. This well and reservoir configuration can easily be analyzed using the double permeability model by increasing the skin in layer 1 to simulate the high skin, plugging or non perforation of this layer. The below figure illustrates the behavior of the model as the skin in the high permeability layer increases.

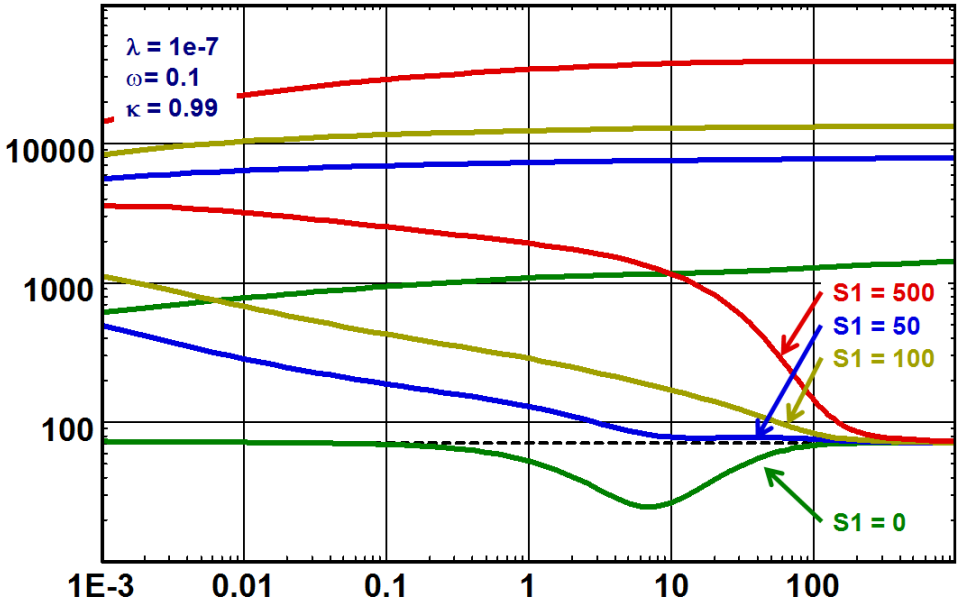


Fig. 7.E.8 – Influence of skin (S1)

7.E.5 Field examples

To illustrate two real examples and their model match we present a classical double permeability response and a real example where the higher permeability layer was plugged. Later this diagnostic was confirmed by a production log and remedial action was successfully taken.

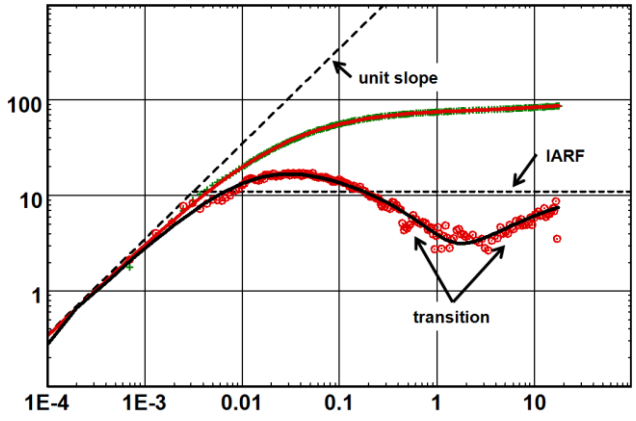


Fig. 7.E.9 – Classic double permeability

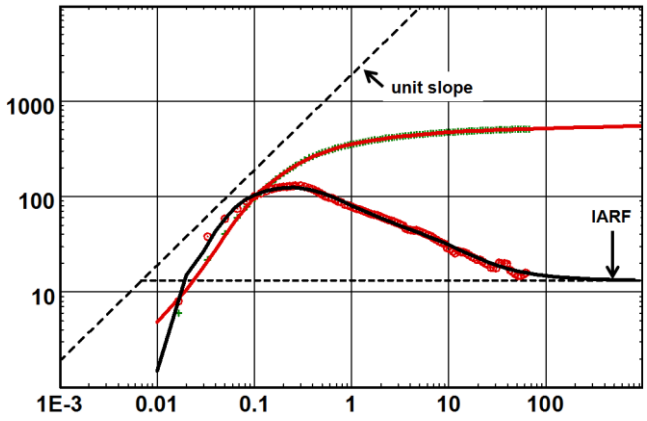


Fig. 7.E.10 – Double permeability layer 1 damaged

7.F Extension of double-permeability reservoirs

7.F.1 Multiple layers

The double permeability model can easily be extended to n-layers.

The two layer model can be applied to many cases in the measure that it is frequently possible to split a multilayer formation into two packs of layers and treat this as an equivalent two layer system. However, this may become an oversimplification and the use of more layers in the model can be necessary.

The same principle used in the double permeability solution can be directly extended to more than two layers.

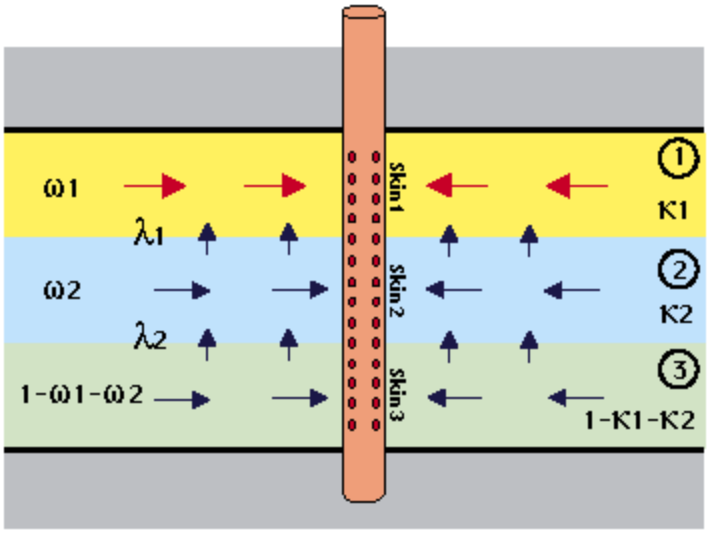


Fig. 7.F.1 – Three layers

The parameters already defined for the two layer case are extended to layer i:

ω_i, layer storativity ratio, is the fraction of interconnected pore volume occupied by layer (i) with respecti+1 to the total pore volume

$$\omega_i = \frac{(V\Phi c_t)_i}{\sum_j (V\Phi c_t)_j}$$

λ_i, inter-layer flow parameter, describes the ability of flow between the layer i and $i+1$:

$$\lambda_i = \alpha r_w^2 \frac{(kh)_i}{(kh)_i + (kh)_{i+1}}$$

κ_i is the ratio of the permeability-thickness product of the layer i to the total layers kh:

$$\kappa_i = \frac{(kh)_i}{\sum_j kh_j}$$

In this type of multi-permeability system one can expect to see as many heterogeneous responses as we have dual systems. This is as long as the parameters governing the heterogeneity are sufficiently different to not masked one another.

The below figure illustrates the behavior of a three layered model with cross flow. At early time, the layers are producing independently and the behavior corresponds to three layers producing without crossflow. When the first interlayer crossflow starts (interface with the greater λ value), a transition period is observed, shown by an inflection in the pressure response and a valley in the derivative.

After this first transition, the derivative comes back to its IARF stabilization and then exhibits a second transition. After all the transitions the reservoir acts as a homogeneous medium with total kh and storativity.

In the example only one parameter ω_2, changes the overall shape of the response as an increase in ω_2 implies a decrease in ω_3, therefore an inversion of contrast.

$$\omega_3 = (1-\omega_1-\omega_2) \; and \; \kappa_3 = (1-\kappa_1-\kappa_2)$$

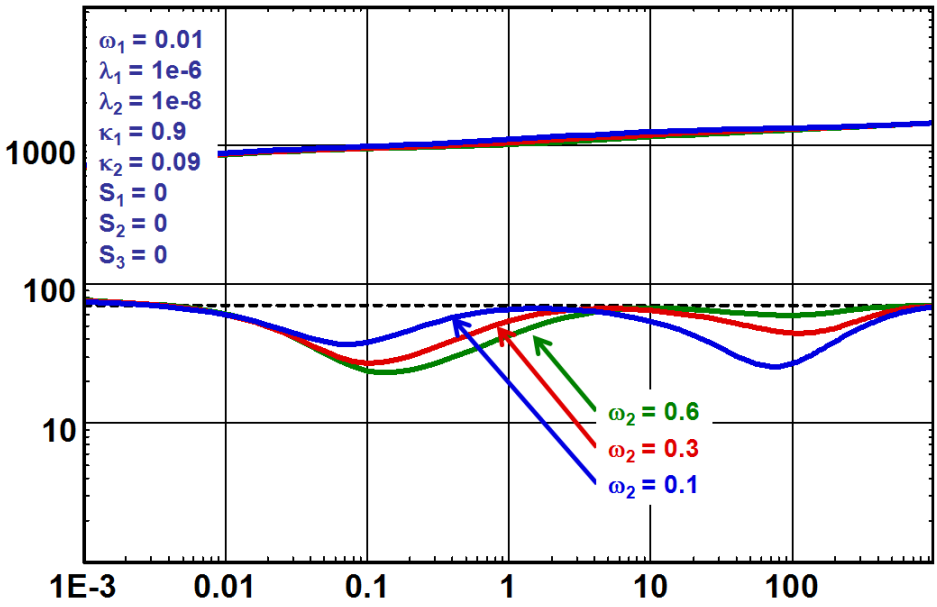


Fig. 7.F.2 – Three layers

The three layered model demonstrated here is part of the Saphir external model library. In this library also exists a 4 layered model with cross flow.

7.F.2 Numerical double permeability

The analytical double permeability model can easily be reproduced by a numerical multilayer model allowing cross flow. It suffices to define a leakage factor between the layers. The layers are isotropic and the vertical permeability is equivalent to the harmonic average of the layer permeabilities:

$$k_z = \frac{(h_1+h_2)}{\left(\frac{h_1}{k_{z1}}+\frac{h_2}{k_{z2}}\right)}$$

And the relationship with λ is:

$$k_z = kh\frac{\lambda}{r_w^2}\frac{h}{2}$$

The leakage factor has a value between 1 (full leakage) and 0 (no cross flow).

The use of numerical models to simulate complex layered formations is detailed in the chapter 'Multilayered models'.

Each layer can produce to the well or be completely blocked off thus only producing through cross flow.

The below figures illustrates the response of the numerical simulator with two layers with various leakage factors and the response when the high permeable layer has been selectively shut off (this is a feature of the numerical multilayered model, one can selectively shut off or open individual layers for flow to the well).

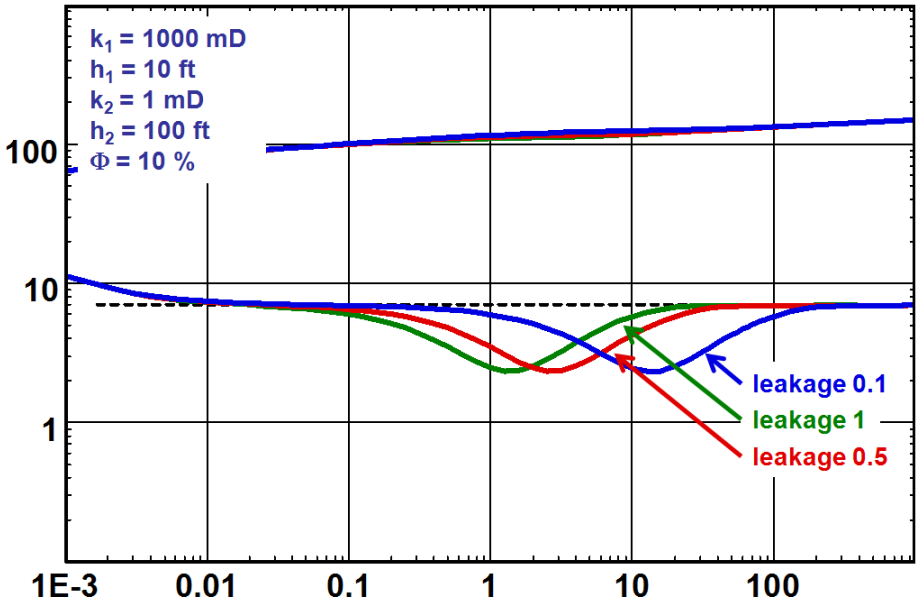


Fig. 7.F.3 – Numerical two layers both producing to the well

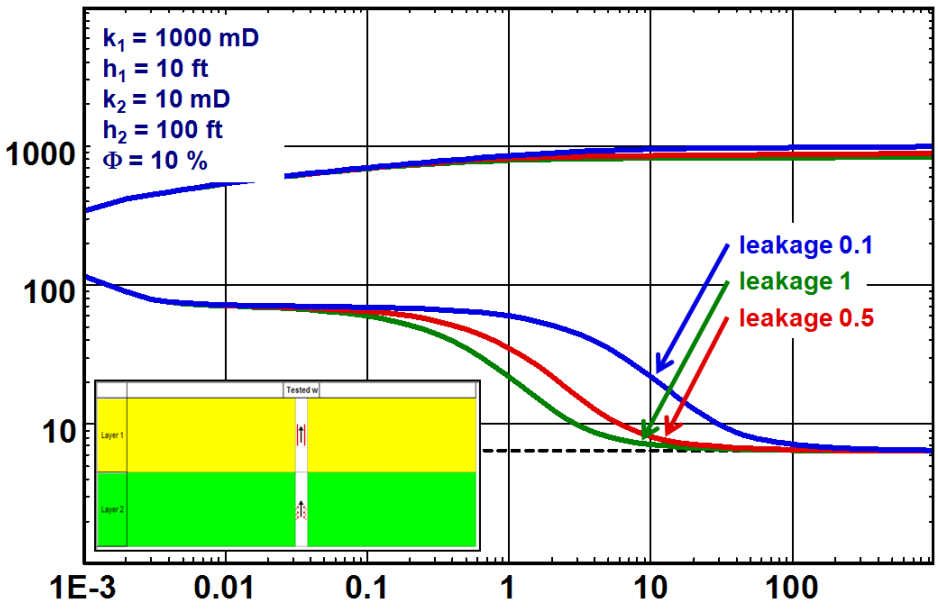


Fig. 7.F.4 – Numerical two layers, high permeability layer shut off

7.G Multilayered reservoirs

In this section we will present the multilayered analytical model and briefly describe the multilayer numerical solution available in the KAPPA suite of programs. As opposed to the double permeability solution presented earlier in this chapter, the multilayer analytical model assumes that the layers produces comingled to the well without any reservoir cross flow. This assumption is crucial and fundamental and leads us immediately to kill one of the biggest myths in well testing of multilayered reservoir:

If the layers are homogenous and infinite and even if the initial pressures of each layer is different we will not be able to differentiate the behavior of each layer in the common pressure response measure in the wellbore. The response measured at the pressure gauge is simply the global response.

Now, any text book with some respect for itself will invariably present a pressure response that wonderfully show the behavior of at least two and sometimes several layers. And this is possible if one or several of the layers are bounded. The boundaries are described in more detail in the chapter on 'Boundary models', however we show below the response of a two layered system where one layer is infinite and the other layer is just a small sand lens. And, yes, the first stabilization of the derivative corresponds to the total kh, the second level corresponds to the permeability thickness product of the infinite layer. The unit slope response in the middle of this buildup reflects the bounded layer and the distance (to the boundaries) can be deduced. This type of behavior can also easily be described by a composite model as it is a limiting case of the radial composite model, so the reader be aware.

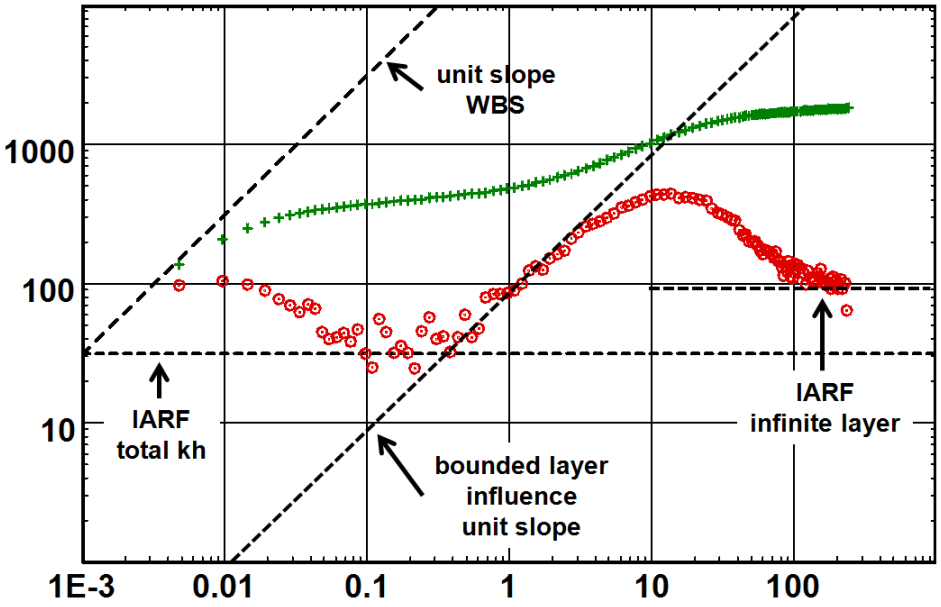


Fig. 7.G.1 – Two layers, one layer bounded the other infinite

To reiterate on the above observations, the behavior of any multilayered system as long as each layer is homogeneous and infinite acting, the model response will be an equivalent global response with early time wellbore storage and a global stabilization at the level of total kh;

$$(kh)_{total} = \sum_{i=1}^{n} k_i h_i$$

With total skin

$$S_T = \sum_{i=1}^{n} \frac{S_i k_i h_i}{(kh)_{total}}$$

7.G.1 Hypothesis

The reservoir has n layers; each layer can have a well model as the well models already described in the chapter on 'Well models'. The reservoir model of each layer can be any of the reservoir models already presented in this chapter and each layer can have boundary configurations as those presented in the chapter on 'Boundary models'. The initial pressure Pi can be different from layer to layer.

The analytical model does not allow any cross flow between the layers in the reservoir thus the production to the well is comingled. Cross flow between layers is allowed in well.

The total behavior of each model will be a superposition of each layer behavior, thus it is far too complex to generalize the model behavior in a similar manner compared to that done with the other reservoir models described elsewhere in this chapter.

The concept of pattern recognition and the identification of the different flowregimes during a flow period to be analyzed is no longer a straight forward task. The notion of solving the 'inverse' problem is no longer an issue. In order for the engineer to come up with a plausible answer to the problem he has to rely more heavily on other results and measurements done in the well. Open hole logging, cores and seismic are some of the data that will and has to influence the model choice and the final interpretation.

And finally, the layer contributions; this can be the individual rate of each layer or a combination of rates at different stations in the wellbore. Without the layer rates the engineer is faced with a task he can rarely win.

But we are the bearer of good news; the multilayer model can include the individual layer rates or a combination of different layer contributions. And the best news is that the layer rates or transient layer rates can be taken into account when optimizing the solution with non linear regression. In fact the only way to give a solution a proper chance is to include the layer rates in the object function thus optimizing with the layer rates becomes a part of the method for solving the multilayer transient test problem.

So, the bad news is that without production logging, PTA with the objective to assign individual reservoir characteristics and skin to each layer is virtually impossible with any confidence. Not knowing the layer contributions will open a 'Pandora box' that is so full of different models and leading parameters of which any combination can produce the same response, that it may become impossible to make a reasonable choice.

In fact the problem is expanded to what we are often up against with even simpler models; the solution is very far from unique.

As already stated the model response will be a superposition of the different well and reservoirs models assigned to each layer thus it is impossible to describe this in any detail over a few pages. The model response of the various well models is covered in the chapter on 'Well models', the reservoir responses are covered in this chapter, and the boundary responses are covered in the chapter on 'Boundary models'.

We will however, in the following section, describe how we build a multilayer model in the PTA (Saphir) or RTA (Topaze) KAPPA suite of programs.

7.G.2 How to build a multilayer model

The first task is to define the number of layers and their thickness. At the same time one can define if the layer rates or the layer contributions are reported at surface or downhole conditions. A word of advice here; in the KAPPA suite of software (Topaze and Saphir) the layer contribution is identical to the individual layer rate and layer rates are the rates measured at the top of each layer i. e. the depth cumulative rate.

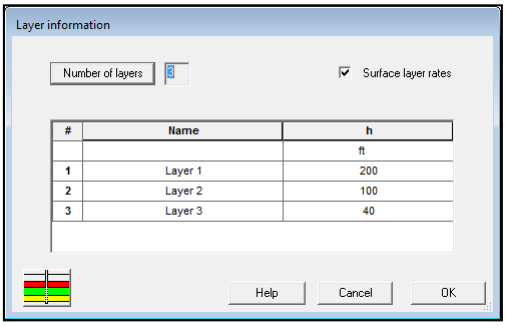


Fig. 7.G.2 – Defining the geometry and flowrate conditions

The layer rates will have to be loaded either as a compatible file, from Emeraude or by hand. The rate is usually measured during production logging and can be transient stationary rates versus time or is the result of a production log versus depth interpretation, such as provided using Emeraude.

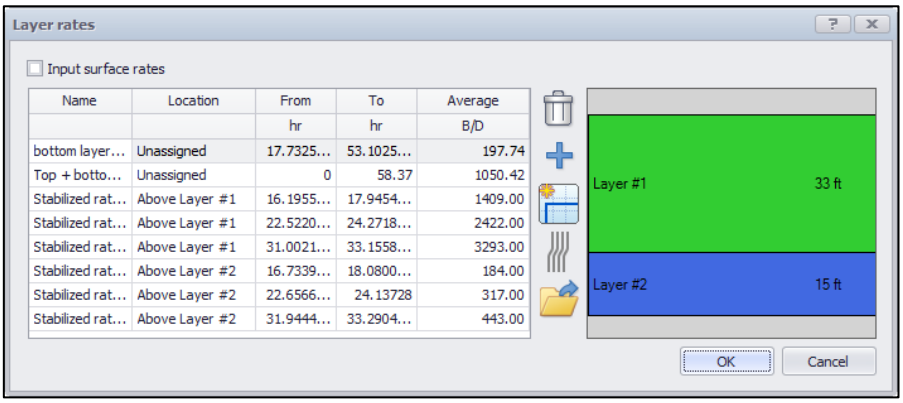


Fig. 7.G.3 – Defining the layer rates

The next step is to define the layer's well, reservoir and boundary model and the layer characteristics.

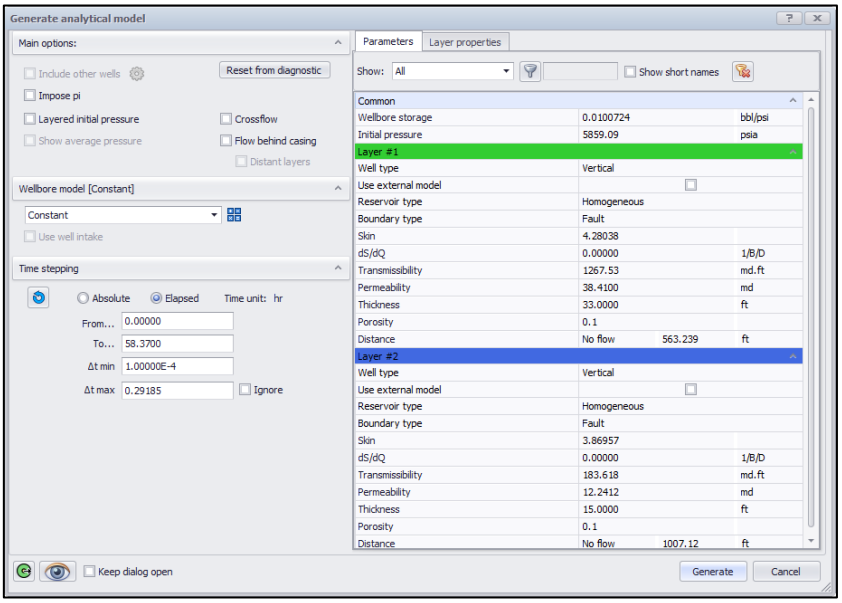
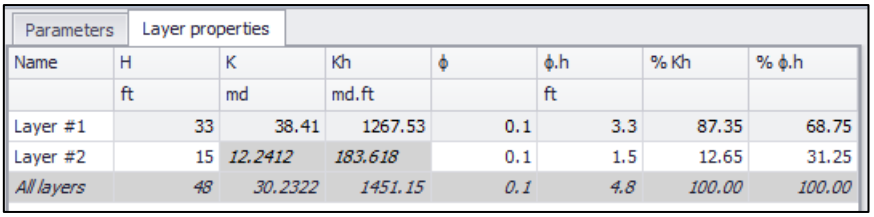


Fig. 7.G.4 – Defining the model and characteristics



Name	H	K	Kh	ϕ	ϕ.h	% Kh	% ϕ.h
	ft	md	md.ft		ft		
Layer #1	33	38.41	1267.53	0.1	3.3	87.35	68.75
Layer #2	15	*12.2412*	*183.618*	0.1	1.5	12.65	31.25
All layers	*48*	*30.2322*	*1451.15*	*0.1*	*4.8*	*100.00*	*100.00*

Fig. 7.G.5 – List of layer characteristics

Generate the model and adjust the parameters by hand or run the improve option. To add the layer rates in the objective function of the nonlinear regression the optimization is carried out on the history (simulation) plot.

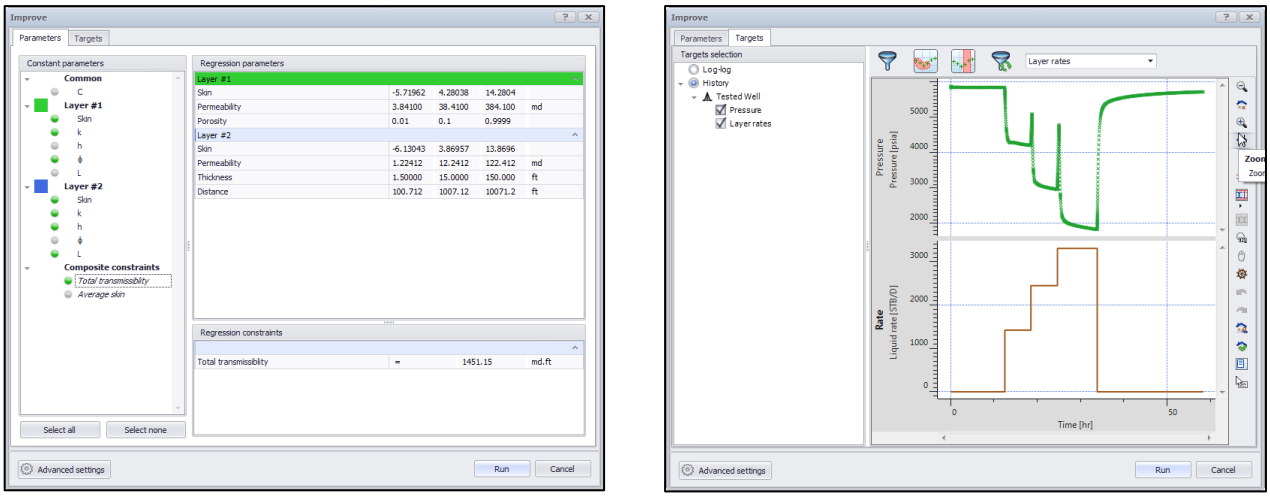


Fig. 7.G.6 – Improve settings for multilayer cases, including layer rate

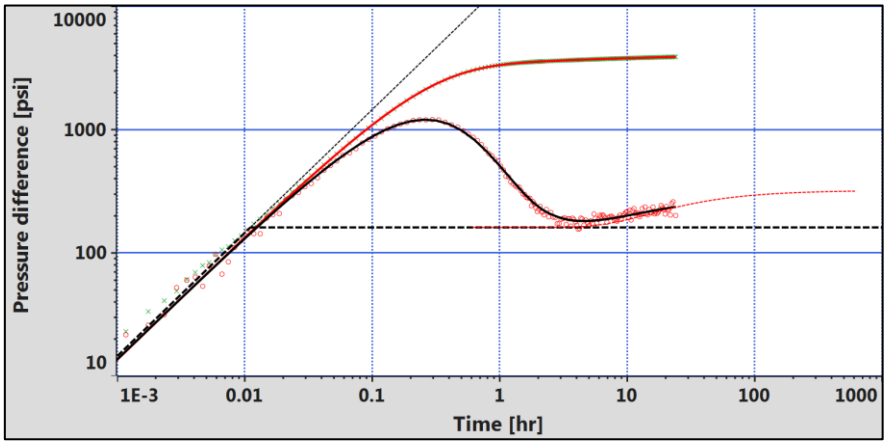


Fig. 7.G.7 – Multilayer model match

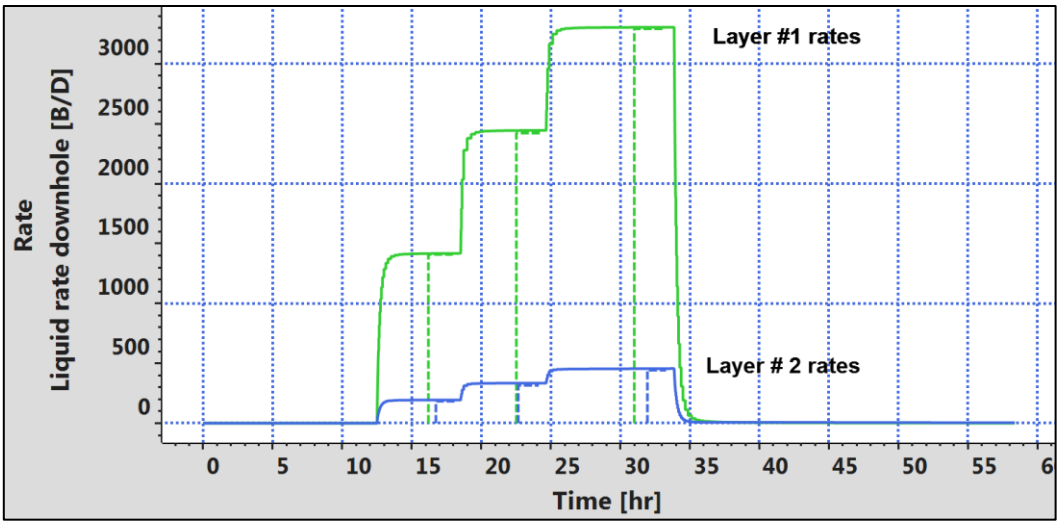


Fig. 7.G.8 – Layer rates match

A numerical multilayer model is also available. The numerical model is more flexible and allows cross flow in the reservoir. This is defined either as a leakage factor, an equivalent vertical permeability or the classical lambda coefficient of a double permeability reservoir. Each layer can also be specified as perforated (communicating with the well) or not.

There are various multilayer tests subject to pressure transient analysis; all of the tests involve in a form or another, the use of production logging tools to capture the production of the layers. These tests and their analysis approach is cover in the chapter on 'PTA – Special test operations'.

7.H Composite reservoirs

7.H.1 Hypothesis

Up to this point the models assumptions were uniform with constant saturations, mobility and effective permeability. In most cases this assumption is valid within the time limits of a well test and radius of investigation. However, in some cases it will be necessary to consider a variation in the mobility in the lateral direction.

The most common cases where one can observe a change in mobility in the reservoir area are:

- Injection of a fluid different to the reservoir fluid
- Change in saturation due to an aquifer
- Change in saturation due to a gas cap
- Change in lateral saturation due to production below bubble or dew point
- Compartmentalization
- Facies changes
- Actual changes in reservoir characteristics (k, Φ)

The analytical solutions which model these cases are called composite models. Their geometry is quite straightforward and they are governed by two simple parameters.

The most common analytical composite models are the radial and the linear composite. The radial composite geometry is centered at the well, and r_i is the radius of the inner compartment.

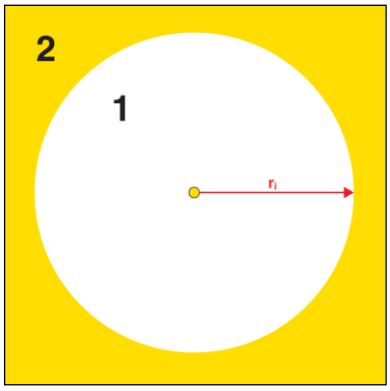


Fig. 7.H.1 – Radial composite reservoir

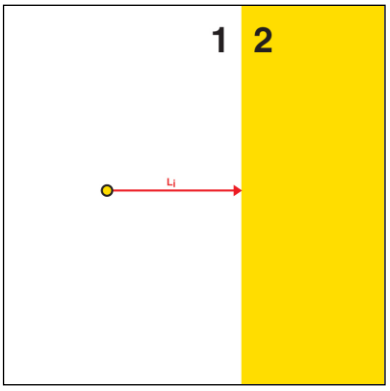


Fig. 7.H.2 – Linear composite reservoir

For the linear composite reservoir (of infinite extent), the corresponding parameter will be L_i, the distance from the well to the mobility change.

When one reference is chosen, the properties of the other compartment are calculated from the first using two parameters:

The mobility ratio $M = (k/\mu)_1 / (k/\mu)_2$

The diffusivity ratio $D = (k/\Phi\mu c_t)_1 / (k/\Phi\mu c_t)_2$.

It is interesting to introduce the ratio $M/D = (\Phi c_t)_1 / (\Phi c_t)_2$.

We see that the ratio M/D represents the compressibility ratio which is often taken, as a first approximation, equal to 1 when both fluids are of the same type.

Below we illustrate the pressure profile for a radial and a linear composite reservoir. At the composite interface, there is no pressure loss but a change in the pressure gradient. The flux on both sides is the same, but because the mobility is different Darcy's law will give two different pressure gradients.

At early time, the pressure will diffuse in compartment 1 only, and the behavior will be homogeneous. When the composite limit is detected, there will be a change of apparent mobility and diffusivity.

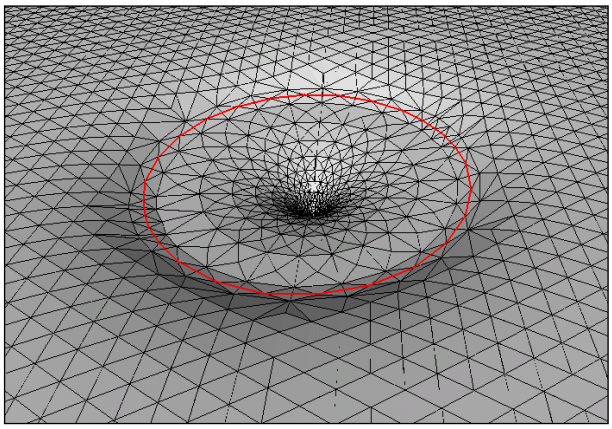


Fig. 7.H.3 – Radial composite pressure profile

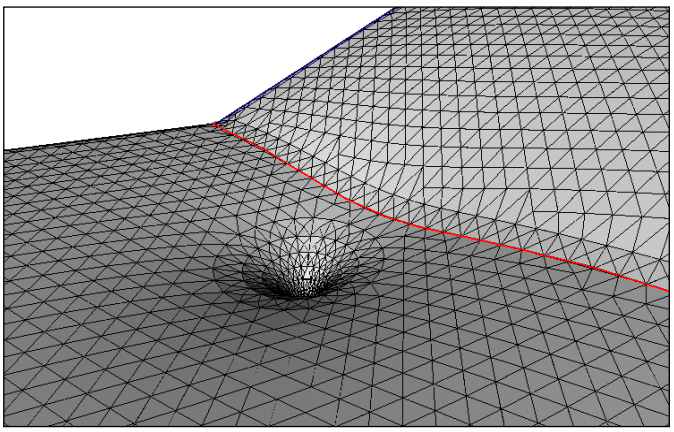


Fig. 7.H.4 – Linear composite pressure profile

With the radial composite reservoir, the apparent mobility and diffusivity will move from the inner values (compartment 1) to the outer values (compartment 2), the final mobility will be that or compartment 2. For the linear composite reservoir, after the transition, the final apparent mobility and diffusivity will be the average of compartments 1 and 2.

7.H.2 Loglog behavior

The following figure illustrates the response (buildup) of a typical well in a (radial) composite reservoir.

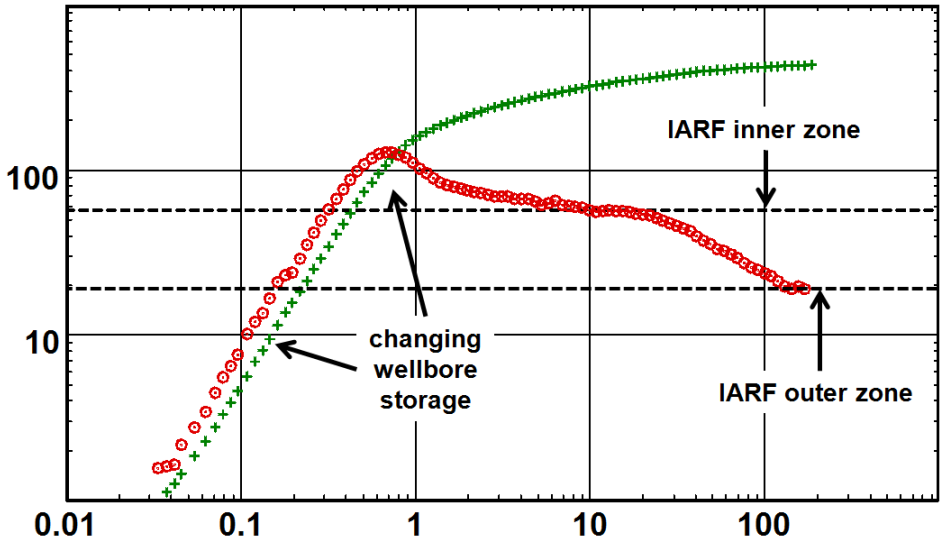


Fig. 7.H.5 – Radial composite buildup response

The following figures show the loglog response of a radial composite reservoir with constant distance to the interface and several values of M=D. The time at which the derivative deviates from the initial IARF (compartment 1) to the final IARF (compartment 2) is linked to r_i with the same relation as for a sealing or constant pressure boundary. The ratio between the final and initial derivative level will be that of the ratio between the initial and the final mobility, equal to M. When M=D=1, the response is obviously homogeneous.

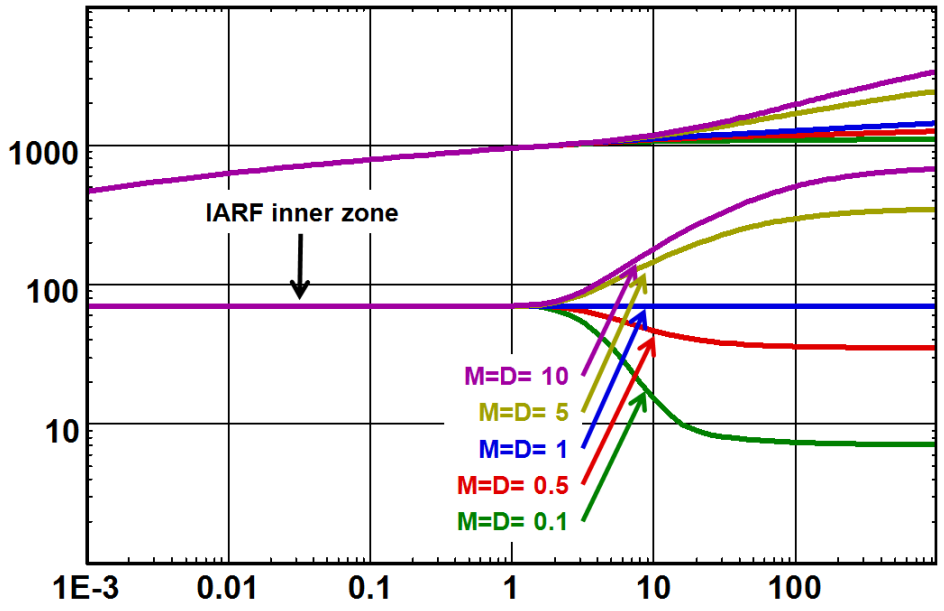


Fig. 7.H.6 – Loglog response, radial composite

Below is the loglog responses for the same parameters, but now in a linear composite reservoir. The final stabilization corresponding to the average of compartments 1 and 2, the transition will be smoother, and it is easy to show that the ratio between the final and initial derivative level will be 2M/(M+1).

When M tends to infinity, i.e. the permeability of the outer compartment tends to zero; this ratio will tend to 2. This corresponds to the particular case of a sealing fault. When M tends to zero, the permeability of the outer compartment tends to infinity and the pressure will be sustained at initial pressure at the boundary. This is the particular case of a constant pressure linear boundary.

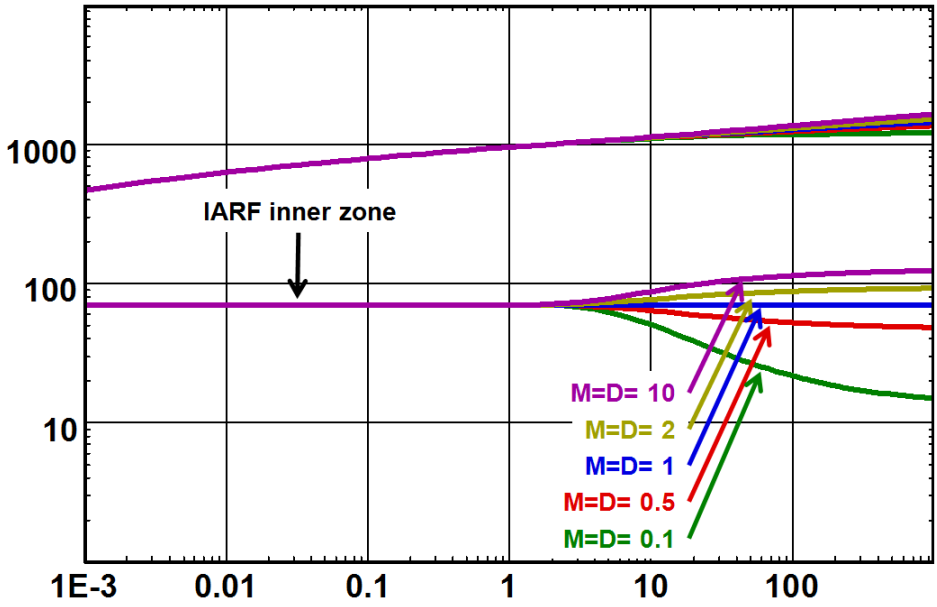


Fig. 7.H.7 – Loglog response, linear composite

To illustrate the behavior of the model when mobility and diffusivity is no longer equal we have generated the radial composite model under different scenarios.

Following is a figure where the mobility M is kept constant and varying the diffusivity ration D.

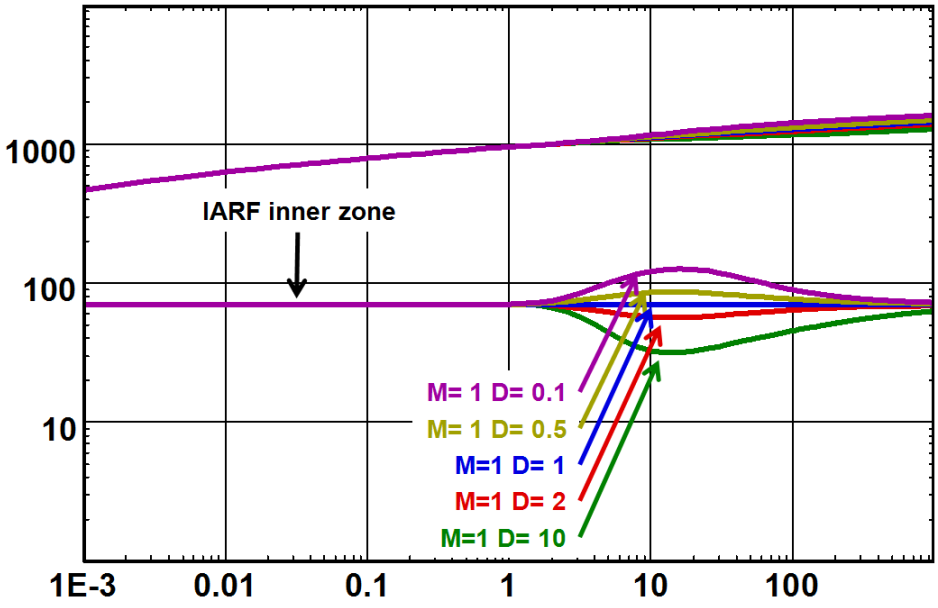


Fig. 7.H.8 – Loglog response, radial composite M≠D

Depending on the value of D, the derivative will deviate upwards (D<1) or downwards (D>1). The response with a valley is qualitatively close to a double-porosity behavior. The difference in shape comes from the fact that this change of storativity occurs in compartment 2 only, while in the double-porosity model it occurs everywhere.

In the general case where M and D are different, the derivative will go from the IARF level of the inner zone to the final level being a function of M only. There will be an upwards transition when D<M and a downwards transition when D>M.

7.H.3 Specialized analysis

Theoretically the semilog plot will exhibit two straight lines, the first line corresponds to the mobility in the inner zone, the second to the outer zone if the system is radial composite or the average of the two zones in the case of linear composite. The ratio of the slopes will give M (radial) or 2M/(M+1) (linear). For buildups the intercept of the second line can be extrapolated to p*, while the skin will be given by the first straight line (inner zone) analysis.

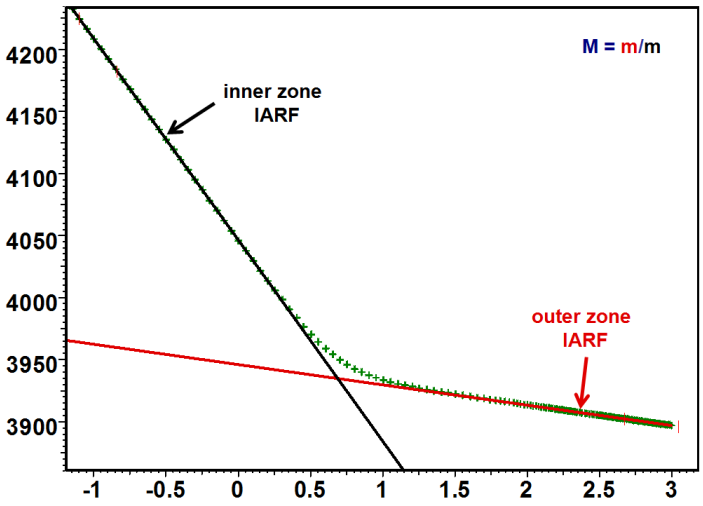


Fig. 7.H.9 – Semilog plot, radial composite

7.H.4 Effect of wellbore storage

Increasing the wellbore storage will mask the inner radial flow. The effect on the outer IARF is negligible as this is a flow regime that happens at relative late time. See the below illustrations.

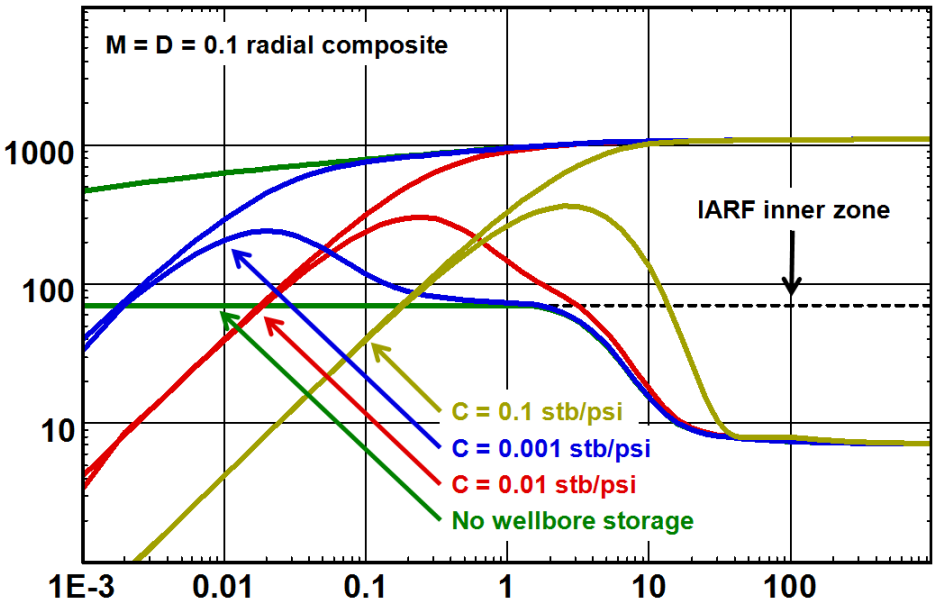


Fig. 7.H.10 – Influence of wellbore storage

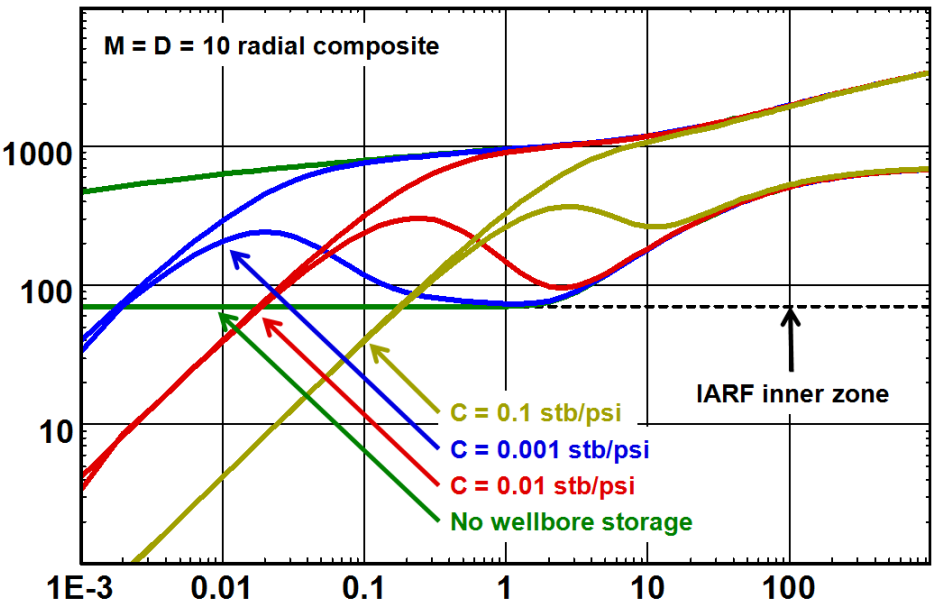


Fig. 7.H.11 – Influence of wellbore storage

7.H.5 Skin

The skin can be evaluated using the classical semilog methods. The 'inner zone' radial flow will give the well skin and the 'outer zone' radial flow will return a 'total skin'. This 'total skin' is defined by the two components:

$$S_T = \frac{1}{M} S_{(inner\ zone)} + \left(\frac{1}{M} - 1\right) \ln \frac{r_i}{r_w}$$

When M<1 we say that the mobility increases at some point further away from the well and often we consider that the inner zone as being damaged by invasion or other causes. This gives rise to the concept of a skin with 'dimensions'. The literature contains many examples of this behavior, whether due to actual damage or some other phenomena such as changes in fluids or geological facies. What the literature is missing is actual proof that remedial action can in fact connect the better mobility reservoir directly to the well thus bypassing the 'block' and increase the well performance. See the section in this chapter on "When should we use a composite model?".

The following figure illustrates the model behavior with a changing well skin with M<1. A positive skin has no influence on the Bourdet derivative. A negative skin will affect both the derivative and the pressure change as the early time behavior approached the behavior of a fracture.

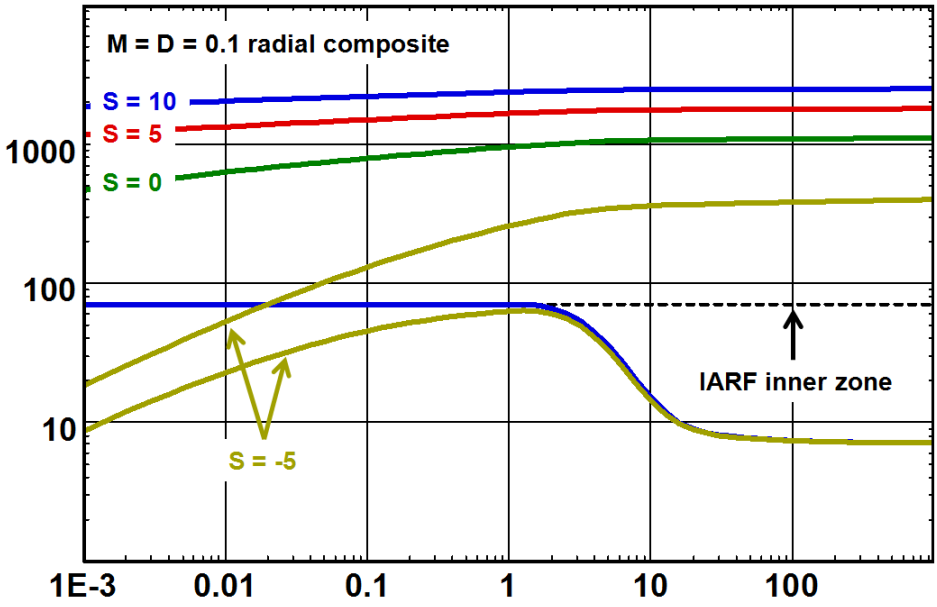


Fig. 7.H.12 – Influence of skin, M<1

Below we show the skin behavior when M>1.

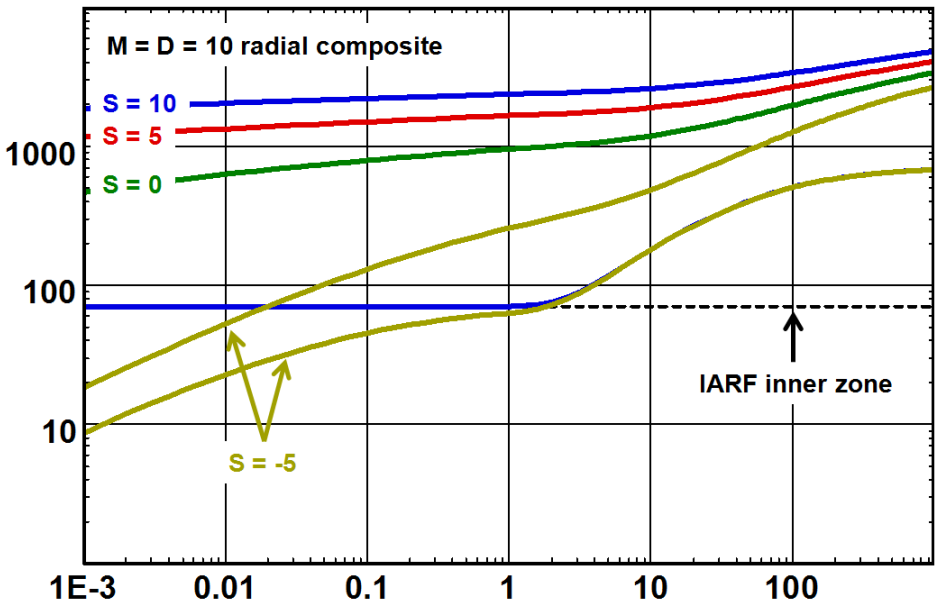


Fig. 7.H.13 – Influence of skin, M>1

7.H.6 Extensions of the composite reservoir

The above composite models are used as simplified approaches to simulate fluid saturation variations, facies changes and damage.

In some cases these assumptions may be too simplistic; e. g. when a producing well is surrounded by multiple fluid annuli, due to particular PVT characteristics creating gas blocking or condensate banks. There may be more than one distinct change in the facies properties. In these cases several condition changes can take place close to the well and will require a multiple radial change model.

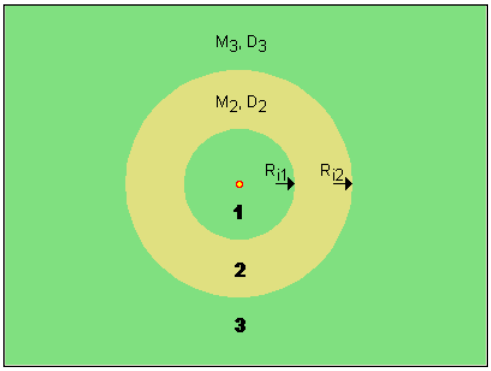


Fig. 7.H.14 – 3 zone radial composite

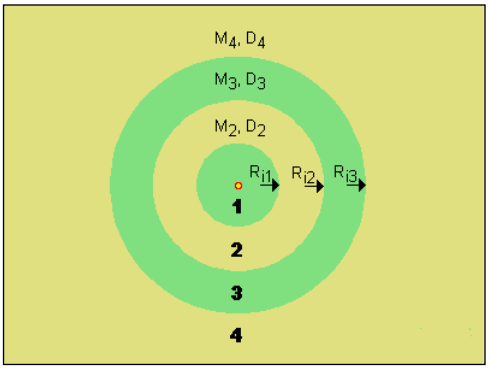


Fig. 7.H.15 – 4 zone radial composite

The parameters Mi and Di in the model have respectively the same definition as in the simple model described above. The below figure illustrates the response where a four zone radial composite model has been used.

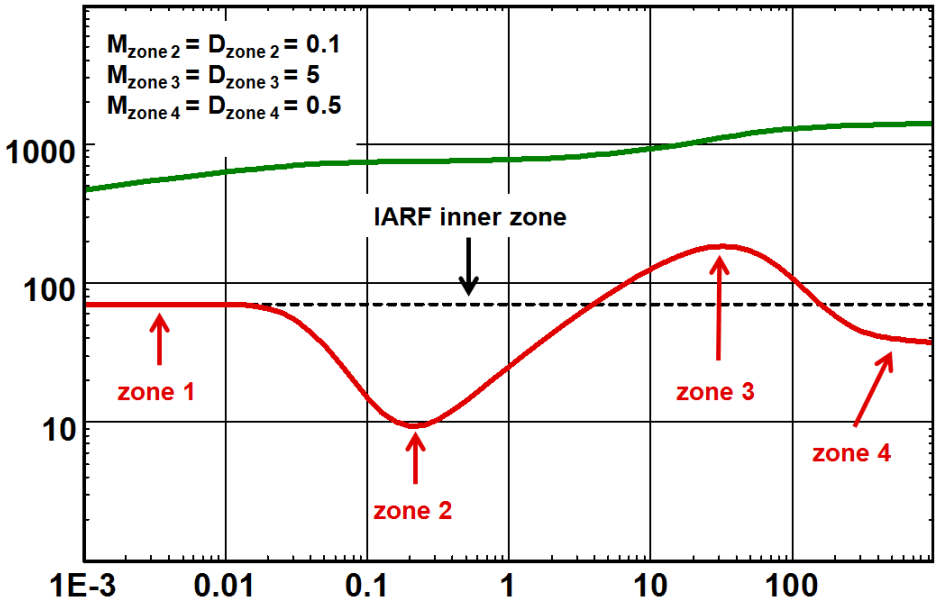


Fig. 7.H.16 – 4 zone radial composite

Now the question is, are these models really useful? Jumping forward and bearing in mind the paragraph on 'When should we use a composite model?' in this chapter, the answer is yes, but not in the hands of a novice interpreter. These models are certainly not to be used as a last resort just to obtain a match for the sake of making the match only and ignoring the physical implications that comes with the description of the model.

The obvious draw back that can make its use dubious is the fact that strictly speaking everything has to be perfectly radial which in real life is clearly not the case. However, we have to understand that when we use such models, and any analytical models for that matter, we are looking for an equivalent behavior. These models are particularly useful to describe changes in fluid banks close to the well. Production can be close to or below the bubble point pressure in a bubble point fluid and the gas saturation can vary radially away from the well. Thus there can be zones with both movable and immovable gas governed by the critical saturation. This can give rise to various zones of different mobilities and even gas blocking.

In a dew point type of fluid, different saturation fluid banks may build up around the well and again give rise to a variation of the mobility.

The physical properties may very well change and even gradually change as the distance increases from the well, thus a composite behavior is not only possible but common.

The below figures illustrates the changing mobility of a 'gas block' matched with a multiple zoned radial composite analytical model. The other figure illustrates the match of a response cause by condensate 'banking' around the well.

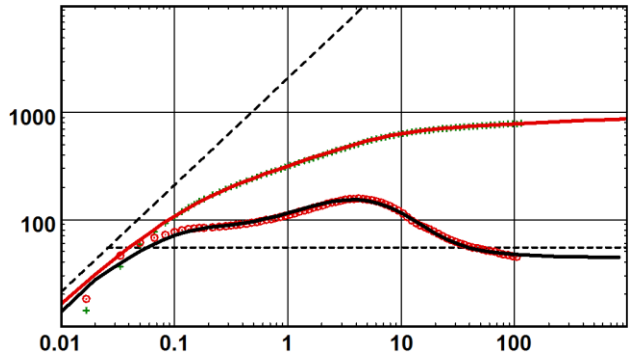


Fig. 7.H.17 – Gas blocking

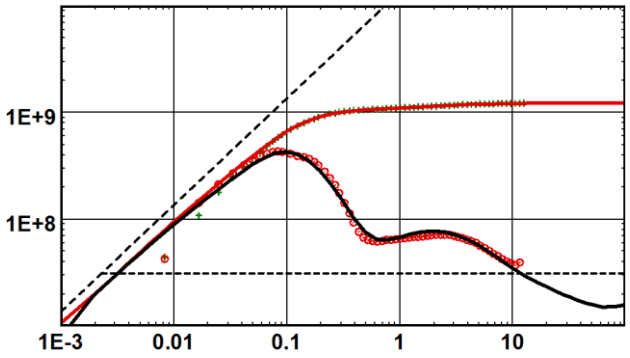


Fig. 7.H.18 – Condensate bank

7.H.7 Polymer injection Fall Off model

7.H.7.a Objective of the model

The objective of this model is to provide a simulation of the complex pressure behavior in case of fall off after a water/polymer mixture injection.

7.H.7.b Description of the model and assumptions

The main complexity is due to the coexistence of Newtonian and Non-Newtonian fluids.

This model not only takes into account the specific behavior of the injected polymer region but also the standard behavior of the Newtonian fluid flow in the external oil region.

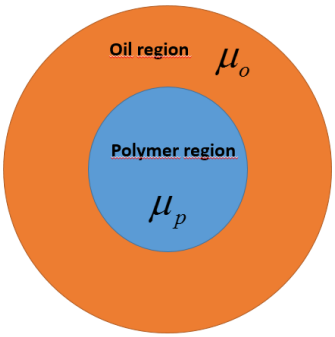


Fig. 7.H.19 – Model schematic

7.H.7.c Method used in the solution

In this model we keep the multi-composite reservoir approach but the viscosities are calculated in each region using the viscosity model from Meter (1964).

In the Meter's model the polymer viscosity depends on the exponent α, the Concentration Cp and the distance r, as indicated in the equations below:

$$\mu_p = \mu_w + \frac{\mu_p^o - \mu_w}{1 + \left(\frac{\dot{\gamma}}{\dot{\gamma}_{1/2}} \right)^{\alpha - 1}} \qquad \text{eq.(1)}$$

$$\mu_p^o = \mu_w \left(1 + a_1 C_p + a_2 C_p^2 + a_3 C_p^3\right) \quad \text{eq.(2)}$$

$$\dot{\gamma} = \frac{3.97}{\sqrt{k k_{rw} \phi S_w}} \frac{q}{2\pi h r} \quad \text{eq.(3)}$$

Where:

- α exponent in Meter's viscosity model
- C_p is the polymer weight concentration (%)
- $\dot{\gamma}_{1/2}$ is the reference shear rate
- $\dot{\gamma}$ is the shear rate calculated in the equation (3)
- r is the distance to the well

7.H.7.d Model input parameters

In addition to the relative permeability coefficients, the specific model parameters are:

- The weight concentration C_p of equation (2)
- Zero shear viscosity parameters a1, a2, a3 of the equation (2)
- Polymer viscosity exponent α of the equation (1)
- Reference shear rate $\dot{\gamma}_{1/2}$ of equation (1)
- Shear rate coefficient gamma-c, it is the constant 3.97 in the equation (3),

  The last constant is an input here because it can be treated as a variable in certain papers.

7.H.7.e Typical behavior

The loglog pressure and derivative plot shows the two typical behaviors corresponding at early time, to the polymer region, with an increasing viscosity, and later, to the original oil region.

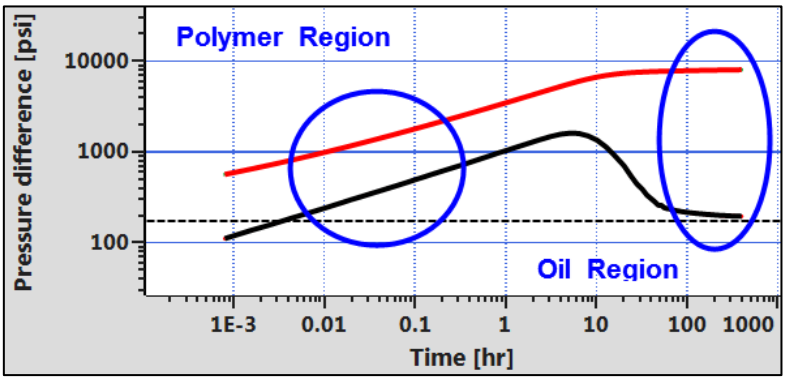


Fig. 7.H.20 – Typical model behavior

The interface detection time depends on the injected volume. The longer the injection, the further will be the interface and the later it will be observed.

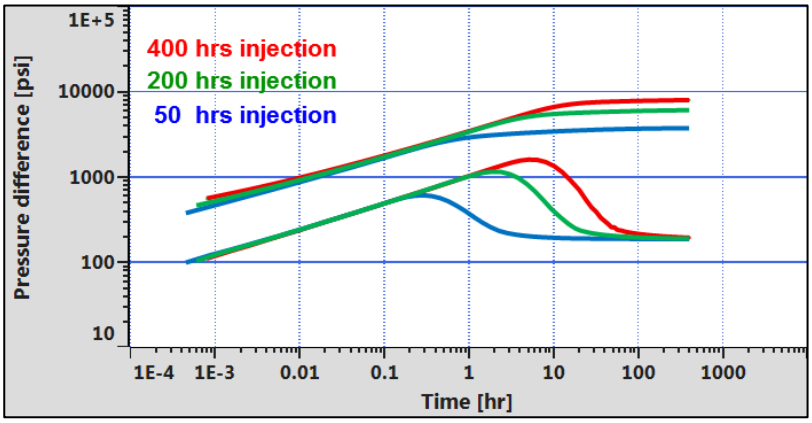


Fig. 7.H.21 – Sensitivity to the injection duration

7.H.7.e.i Sensitivity to the input model parameters

7.H.7.e.i.1 Sensitivity to the polymer concentration Cp:

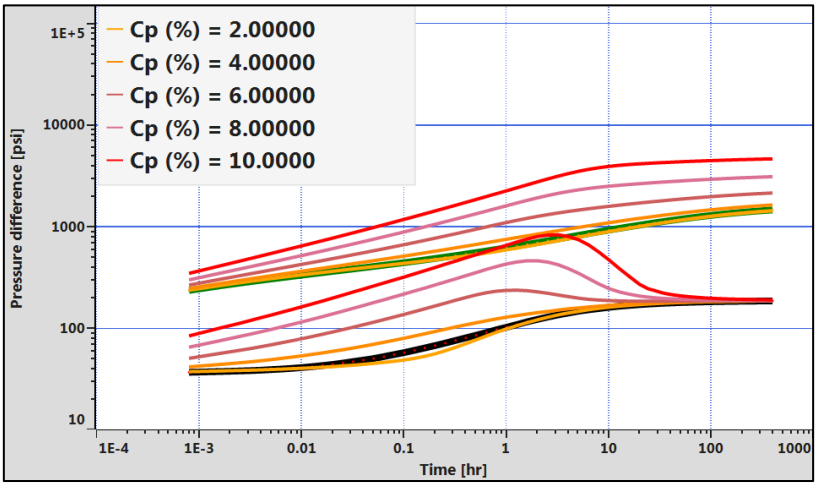


Fig. 7.H.22 – Sensitivity to the polymer concentration

For the same injected volume, the higher the polymer concentration, the higher will be the shear dependent viscosity and the oil sweeping efficiency.

In the above loglog plot the black derivative corresponds to 0% polymer: at early time the stabilization corresponds to the water mobility, 5 times higher than the oil mobility.

7.H.7.e.i.2 Sensitivity to the polymer viscosity coefficients a1, a2, a3

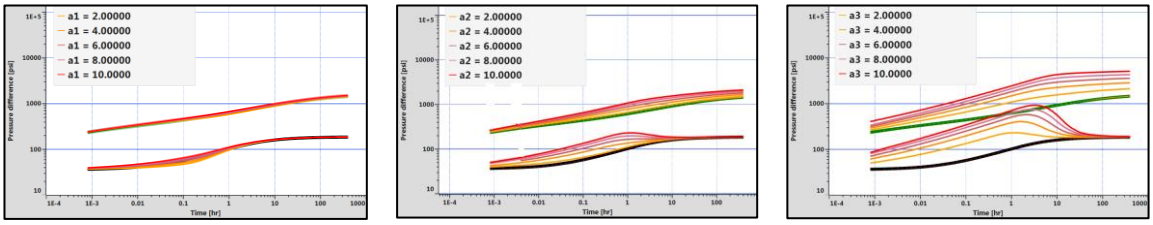


Fig. 7.H.23 – Sensitivity to the viscosity polynomial coefficients

The coefficients act directly on the viscosity function and the influence of each one depends of course on the exponent level.

7.H.7.e.i.3 Sensitivity to the Shear rate coefficient gamma-c

Note that this coefficient is taken constant and equal to 3.97 in the reference paper.

The sensitivity plot below show the impact of a change of the constant value. It is created with a constant value of $\dot{\gamma}_{1/2}$ set to 1

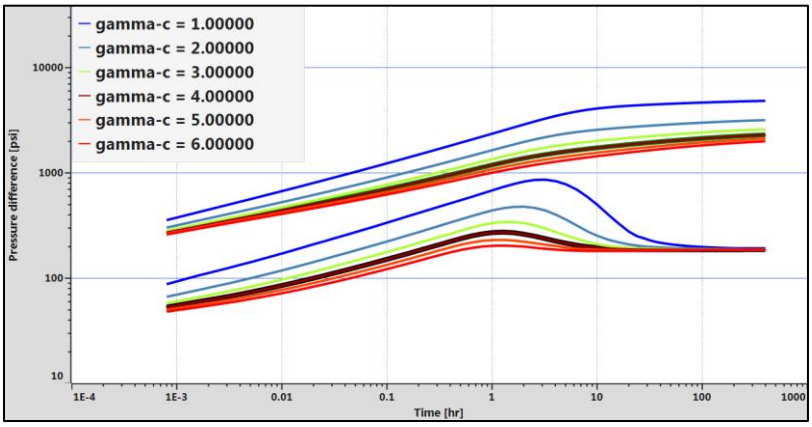


Fig. 7.H.24 – Sensitivity to the Shear rate coefficient

The higher the Shear rate coefficient gamma-c, the smaller is the Non-Newtonian viscosity increase with the distance.

Reference Paper: SPE-181472-MS : Use of Transient Tests to Monitor Progress of Flooding in IOP/EOR Operations. Medhet Kamal (Chevron), Chuan Tian (Stanford University), Suleen Suleen (Chevron).

7.H.8 Multiphase injection and fall off in a naturally fractured reservoir model

7.H.8.a Objectives of the model

This model simulates the pressure behavior during injection and fall off periods in a naturally fractured reservoir with pseudo-steady state interporosity flow.

7.H.8.b Definition and Assumptions

In this model we keep the multi-composite reservoir approach where the mobility changes due to diphasic conditions are considered in both fissures and matrix.

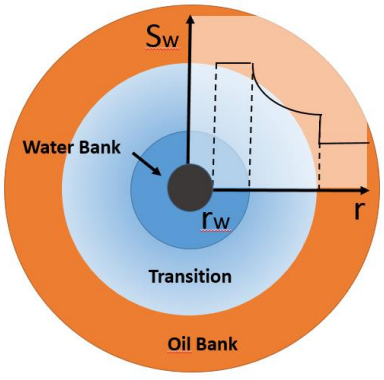


Fig. 7.H.25 – Schematic

The general case in a uniform and monophasic reservoir is governed by the two equations in dimensionless terms:

$$\frac{\partial^2 P_{Df}}{\partial r_D^2} + \frac{1}{r_D}\frac{\partial P_{Df}}{\partial r_D} = (1-\Omega)\frac{\partial P_{Dm}}{\partial t_D} + \Omega\frac{\partial P_{Df}}{\partial t_D}$$

And

$$(1-\Omega)\frac{\partial P_{Dm}}{\partial t_D} = \Lambda\left(P_{Df} - P_{Dm}\right)$$

Where

$$\Omega = \frac{\varphi_f c_{tf}}{\varphi_m c_{tm} + \varphi_f c_{tf}}$$

Is the storativity ratio and

$$\Lambda = \frac{\alpha\lambda_{tm} r_w^2}{\lambda_{tm}}$$

Is the interporosity flow coefficient, with model input parameter being the dimensionless shape factor αr_w^2.

The challenge of this model is to adapt the basic model to a case where the mobility changes due to diphasic conditions.

During the injection period the saturation profile changes in the fracture system as a function of time, as described by Buckley and Leverett.

In the model, it is assumed that the saturation profile does not change during the fall off test.

The saturation change with the distance is modeled by considering N banks.

The total mobility λ is defined as a function of the water saturation in both fracture and matrix system:

Fractures: $\lambda_{tf} = k_f\left(\frac{k_{ro}\left(S_{wf}\right)}{\mu_0} + \frac{k_{rw}\left(S_{wf}\right)}{\mu_w}\right)$

Matrix: $\lambda_{tm} = k_m\left(\frac{k_{ro}\left(S_{wm}\right)}{\mu_0} + \frac{k_{rw}\left(S_{wm}\right)}{\mu_w}\right)$

The same for the total compressibility:

Fractures: $c_{tf} = c_w S_{wf} + c_o\left(1-S_{wf}\right) + c_{ff}$

Matrix: $c_{tm} = c_w S_{wm} + c_o\left(1-S_{wm}\right) + c_{fm}$

Including the capillary pressure effect, the total flow from matrix to fracture is:

$$q_t = q_o + q_w = \alpha\left(\lambda_{tm}\left(p_m - p_f\right) - \lambda_{wm} p_{cow,m}\right)$$

The general solution in the Laplace space is:

$$\overline{P_{Df,j}}(r_D,z) = A_j K_0\left(r_D\sqrt{zf_j(z)}\right) + B_j I_0\left(r_D\sqrt{zf_j(z)}\right) - \frac{g_j(z)}{zf_j(z)}\,p_{cD,j} \qquad (1)$$

The inner and outer limit conditions are set and the pressure and flux at the interface of each annular ring (index j) are set as continuous from ring to ring:

$$P_{Df,j} = P_{Df,j+1} @ r_D = r_{Dj}$$

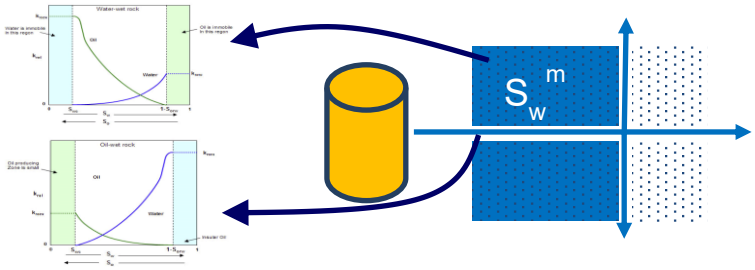
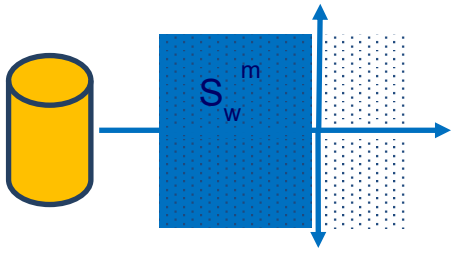
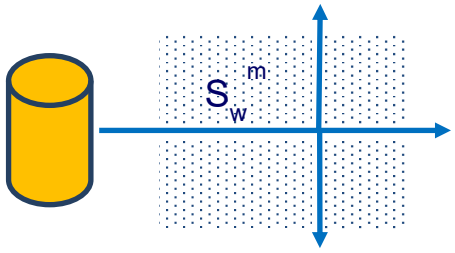
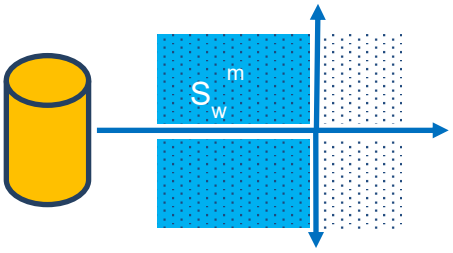
$$\lambda_{tf,j}\frac{\partial P_{Df,j}}{\partial r_D} = \lambda_{tf,j}\frac{\partial P_{Df,j+1}}{\partial r_D} @ r_D = r_{Dj}$$

Applying these conditions, with j varying between 1 and n, the Aj and Bj parameters of equation (1) can be determined by solving a (n,n) matrix, then the resulting equation is converted in the time domain using the Stehfest algorithm.

The description of the system is made in the most detailed and physical way, by the input of the specific properties of both fracture and matrix systems as indicated below.

7.H.8.c Model Parameters

- Equivalent Fracture Permeability
- Several frontal advance model options are available:

Fractures (matrix Sw = frac Sw), 	We consider the frontal advance in the fractures with the matrix Sw equal to the fracture Sw defined by Buckley and Leverett, but kept within the saturation limits of the matrix
Total system (matrix Sw = frac Sw) 	We consider the frontal advance in the total system with the matrix Sw equal to the fracture Sw defined by Buckley and Leverett with total porosity used instead of the fracture system porosity
Fractures (matrix Sw unchanged) 	We consider the frontal advance in the fractures with a constant matrix Sw at initial conditions.
Matrix split km/(kf+km) 	The frontal advance calculation is based on fracture properties with “injected volume” = (actual volume)*kf/(kf + km) = (actual volume)*(1-km/(kf + km))and the remainder, i.e., (actual volume)*km/(kf + km) going into the matrix. This is accomplished by imposing the same saturation changes in the fractures and matrix relative to the respective porosities and the km/(kf + km) split

- The fracture relative permeability parameters respectively for the fracture and the matrix systems
- The matrix Oil-water capillary pressure
- The dimensionless matrix shape factor Alpha
- Porosity of fractures and matrix
- Formation compressibility (fractures and matrix)

7.H.8.d Sensitivity to parameters and the injected volume

7.H.8.d.i Sensitivity to the mobility ratio

The basic behavior shows a first stabilization corresponding to the water zone IARF and a second one to the original oil zone IARF, they are separated by a heterogeneous transition on the derivative.

For the sensitivity to the mobility ratio, a contrast in the water and oil viscosity is used here to create the mobility ratio. We note that in this specific case, a longer injection shows a more stabilized IARF in the inner (water) zone.

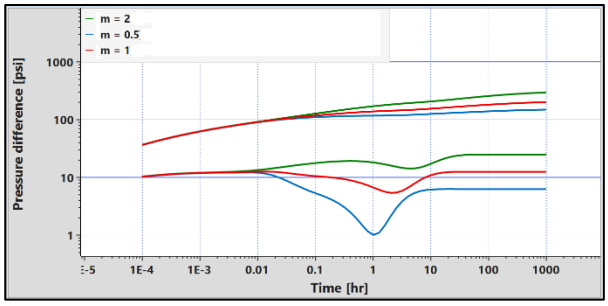


Fig. 7.H.26 – Sensitivity to the mobility ratio after 700h injection

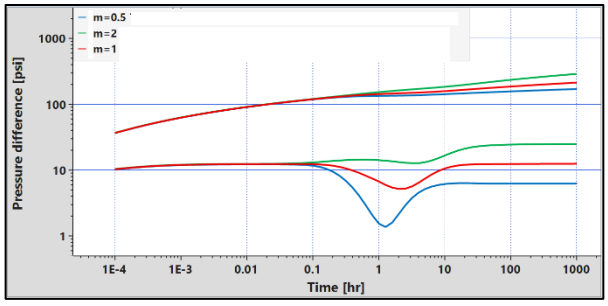


Fig. 7.H.27 – Sensitivity to the mobility ratio after 7000h injection

In fact, the complete behaviour can exhibit two heterogeneous transitions a first one in the water zone and a second one in the original oil zone. The position of the saturation transition zone being dependent on the injected water volume, the same reservoir can give different response according to the injection duration.

7.H.8.e Sensitivity to the fracture porosity

The smaller the fracture porosity, the deeper the transition, and the second transition is observed later after 7000 hrs of injection.

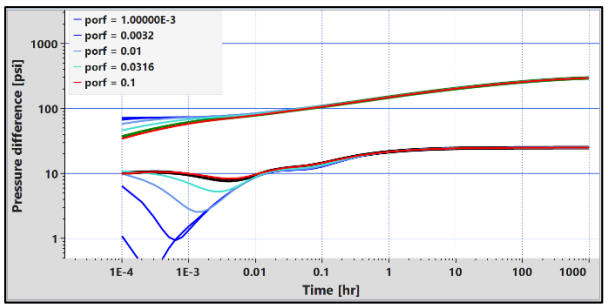


Fig. 7.H.28 – Sensitivity to the fracture porosity after 700h injection

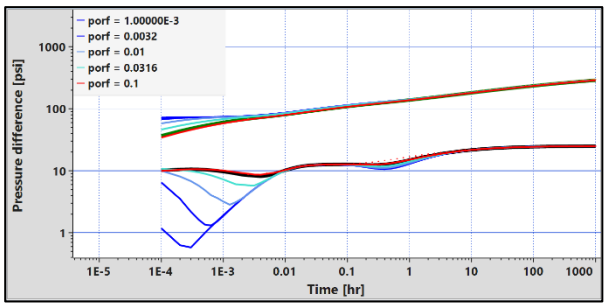


Fig. 7.H.29 – Sensitivity to the fracture porosity after 7000h injection

7.H.8.f Sensitivity to the matrix capillary pressure

The higher the capillary pressure, the deeper the transition, and the second transition is observed later after 7000 hrs of injection.

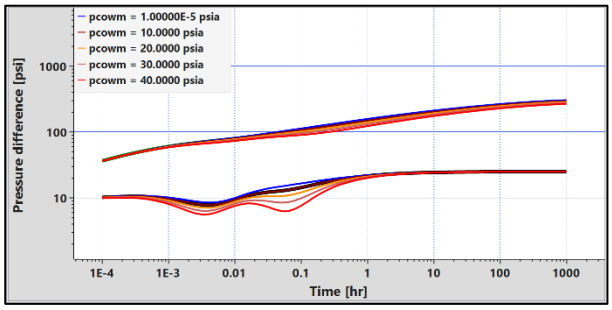


Fig. 7.H.30 – Sensitivity to the fracture porosity after 700h injection

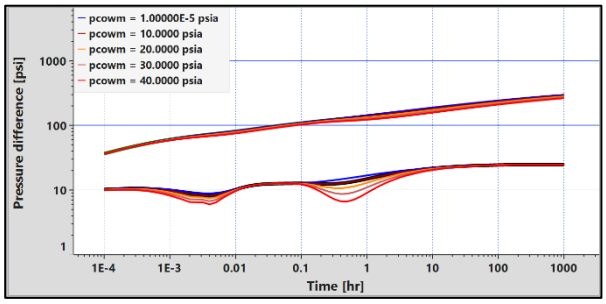


Fig. 7.H.31 – Sensitivity to the fracture porosity after 7000h injection

7.H.8.g Sensitivity to the matrix permeability

The smaller the matrix permeability, the later the transition, which is direct impact of the matrix permeability on the interporosity flow coefficient Λ. But here, the injection duration influences only the duration of the inner (water) IARF duration: it is observed longer time after 7000 hrs of injection.

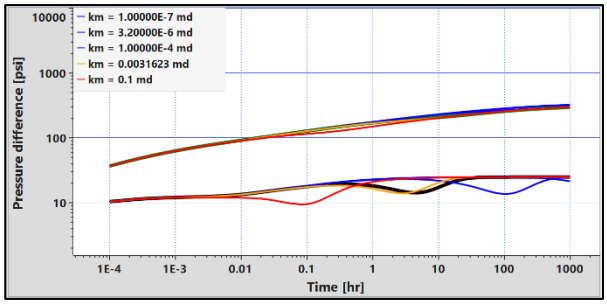


Fig. 7.H.32 – Sensitivity to the matrix permeability after 700h injection

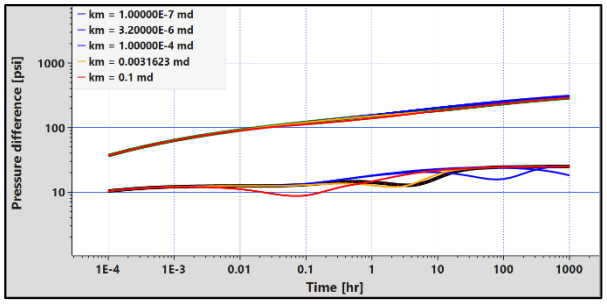


Fig. 7.H.33 – Sensitivity to the matrix permeability after 7000h injection

It results that this model offers a large number of parameters for a data/model matching, but most of them must be considered as input parameters and must be evaluated from the data and external information in order to remain with a minimum of adjustment variables.

Reference paper : SPE 190141 Falloff Testing Under Multiphase Flow Conditions in Naturally Fractured Reservoirs, A. Dastan & M.M. Kamal, Chevron Corporation; Y. Hwang, Texas A&M University; F. Suleen and S. Morsy Chevron Corporation

7.H.9 Numerical models

Composite numerical models can be built easily and will, in most cases, represent real life better than the analytical models. To many engineers the fact that a more real type of model is used is more convincing than using the composite analytical models. The use of numerical models to simulate complex composite reservoirs is detailed in the chapter on 'Numerical models'.Following we show a typical numerical model with an unstructured Voronoi grid. The colors indicate composite zones where the mobility ratio M, and diffusivity ratio D can be defined. The loglog response is also illustrated.

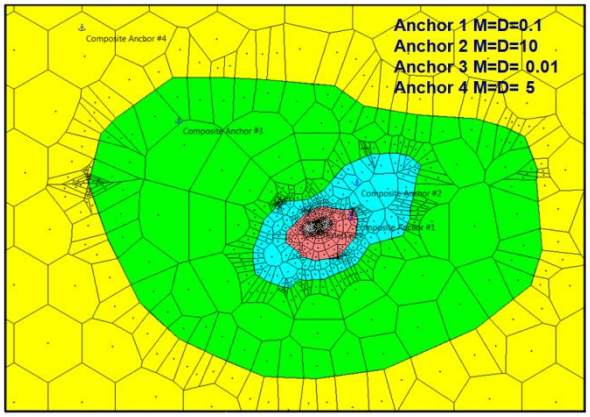


Fig. 7.H.34 – Numerical model

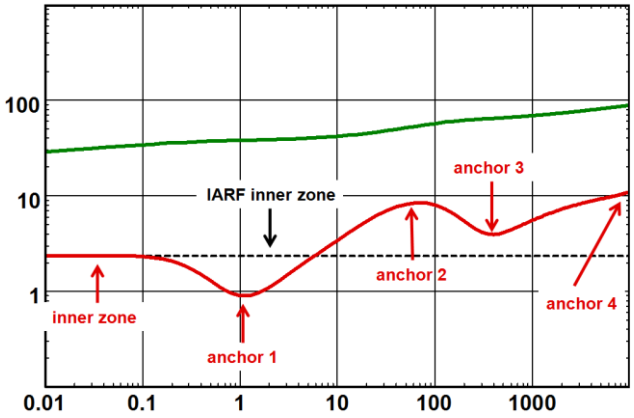


Fig. 7.H.35 – Response

7.H.10 When should we use a composite model?

7.H.10.a Changes of reservoir properties

In this case, the main physical changes are in the permeability and the porosity. M will reflect the permeability ratio, and D the porosity ratio. An example of such a model is the numerical simulation of the geological facies of the reservoir determined by geostatistics.

The use of the radial composite model can always be criticized as it is always highly unlikely that the well has been drilled smack in the middle of a circular reservoir.

7.H.10.b Fluid front

The simplest case is the water injector. When the well is shut-in the pressure response can behave as a radial composite reservoir, corresponding first, to the diffusion in water, then in the original reservoir fluid. M and D can be adjusted to the changes in relative effective permeability, viscosity and compressibility between water and the original fluid. The use of a radial composite model is valid during the shut-in phase, where the phase front is stable. During injection phases, the front is moving and the behavior will be different. The injection response will behave like a homogeneous reservoir with water only, i.e. the displacement of the phase front will mask the well from the original reservoir fluid.

7.H.10.c Gravel packs and the invaded zone

In such a scenario the classification of the composite model as a boundary effect is not proper, the inner zone can correspond to the packed zone or the gravel pack, while the outer zone represents the actual reservoir.

7.H.10.d Match any old weird response

Composite models are probably the most overused and misused models in the industry of well testing. Because of its remarkable flexibility in matching just about any derivative signature, the radial composite model, when combined with a changing wellbore storage model, is the ultimate weapon to get rid of any tough interpretation problem by generating the perfect match that will please everybody that knows nothing or too little about pressure transient analysis. Worse, multiple composite models, where changes in diffusivities and mobilities can be allocated at different distances, hence act at different times, gives no limit to our ability in matching any response. If this is the way the model is used it is nothing more than fudging and cheating. It just amounts to matching the transient well productivity index, and it is no better than doing this with a simple spline.

Composite models only make sense if all parameters such as the location of the interface, mobility change and diffusivity change are within acceptable ranges and can be explained. The decision to use these models is the knowledge of the actual real conditions where composite responses are expected, not that the data cannot be matched with other less flexible models.

7.I Reservoir anisotropies

In the past reservoir anisotropy was seldom considered in pressure transient analysis. As the inclusion of these limiting effects in the analytical model is relatively simple, today most analysis software have the option to include both horizontal and vertical anisotropy for applicable models.

During infinite acting radial flow (IARF) the slope of the semilog plot and the level of the pressure match in the loglog plot yields $h\sqrt{k_x k_y}$.

7.I.1 Vertical anisotropy

Vertical anisotropy typically comes into play in horizontal and limited entry wells. Vertical anisotropy also affects the behavior of multilayered systems with cross flow in the reservoir. Below is illustrated the sensitivity to the ratio of k_v/k_r in a limited entry, or partially penetrating, well. Following we show the sensitivity of horizontal well behavior to vertical anisotropy.

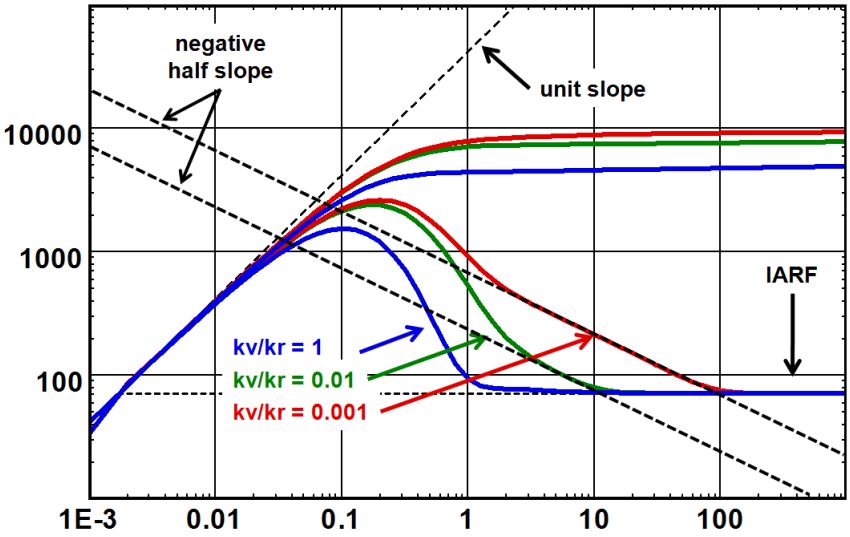


Fig. 7.I.1 – Limited entry well

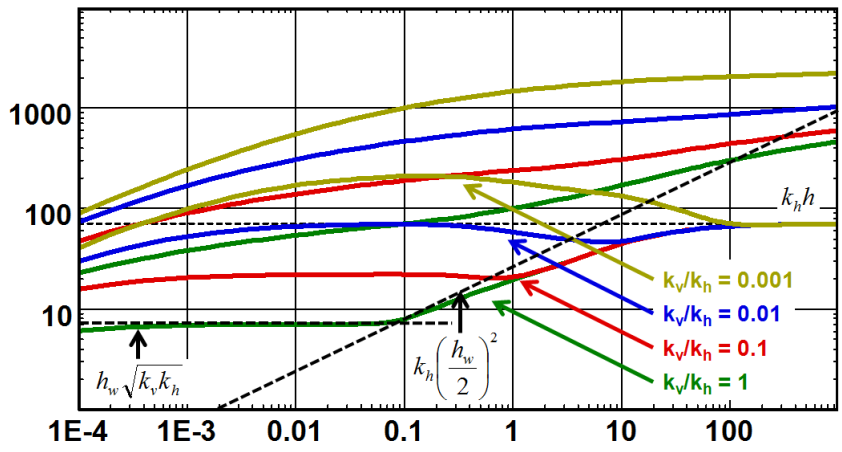


Fig. 7.I.2 – Horizontal well

7.I.2 Horizontal anisotropy

In a horizontal well the response will be dependent on the areal distribution of the permeability. The effect is illustrated below where it can be easily seen that the ideal permeability distribution is when the best permeability is perpendicular to the horizontal well. In this case the permeability in the x direction is along the well and the highest productivity is obtained when k_x/k_y <1.

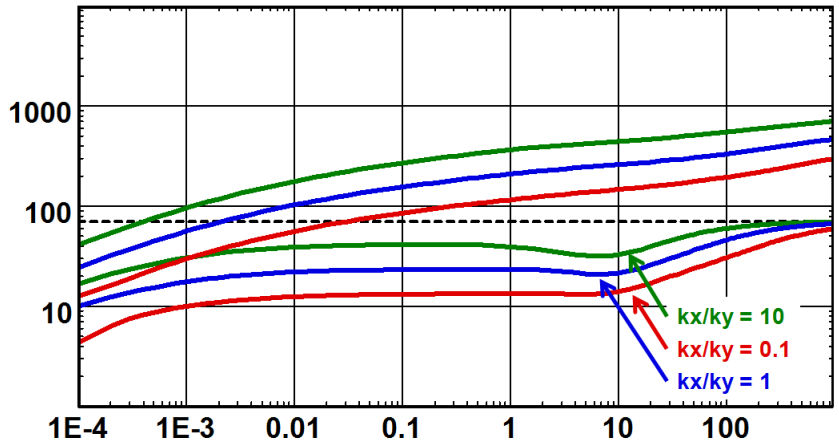


Fig. 7.I.3 – Horizontal well areal anisotropy

When the reservoir system is bounded, the time to 'see' a fault depends upon the directional permeability. In the below example the one single fault that is simulated, is by default parallel to the x direction in the reservoir (this default can be modified in the model dialog). An increase in the y direction permeability (decrease of the ration k_x/k_y) will decrease the 'time' necessary to 'see' the fault.

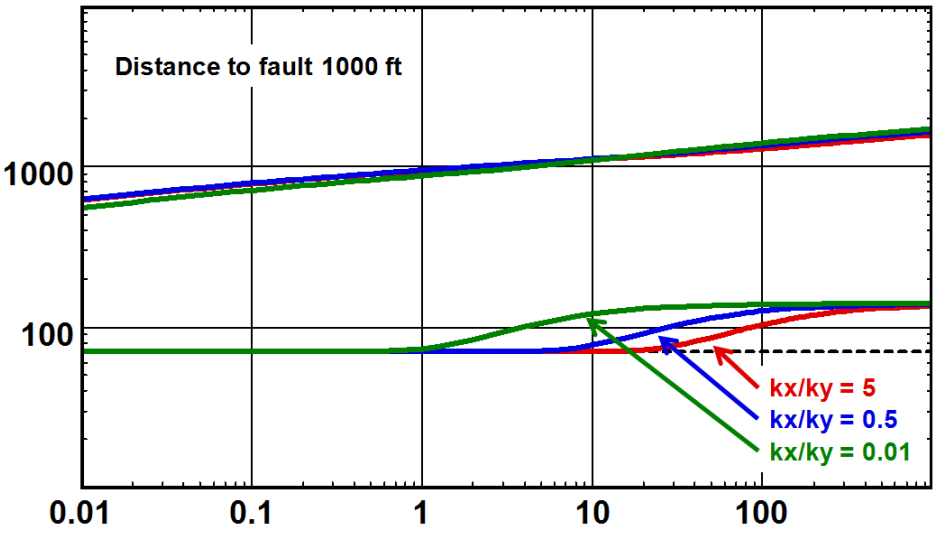


Fig. 7.I.4 – Model response single fault with horizontal anisotropy

7.J Analytical combinations of reservoir models

The heterogeneous models individually described in the previous sections can be combined in a single analytical model. Not surprisingly, the resulting behavior will be a combination of the individual behaviors, and may occur at completely different times if the parameters so dictate.

With respect to the KAPPA software suite, some model combinations were implemented as external DLL's that may be connected to the applications on a needed basis. The reasons that they were not made a part of the standard model catalog are summarized below.

- These are delicate models to use. They have so many leading parameters that, without paying attention to the physics it is possible to force a match to do anything. Delivering the solutions as external models allows client companies to control their distribution.
- The solutions are more complex and more rarely used and tested. They are therefore less stable than simpler models that are part of the built-in capabilities of the applications.

7.J.1 Double permeability radial composite

Below we show the schematic and an example of the behavior for the combination of two layers with cross flow in radial composite system. An example of the use of the model is a reservoir with two zones that are hydraulically separated at the level of the well but connected at a distance.

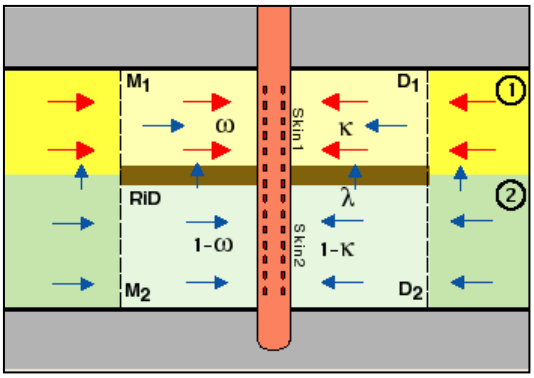


Fig. 7.J.1 – Double permeability radial composite

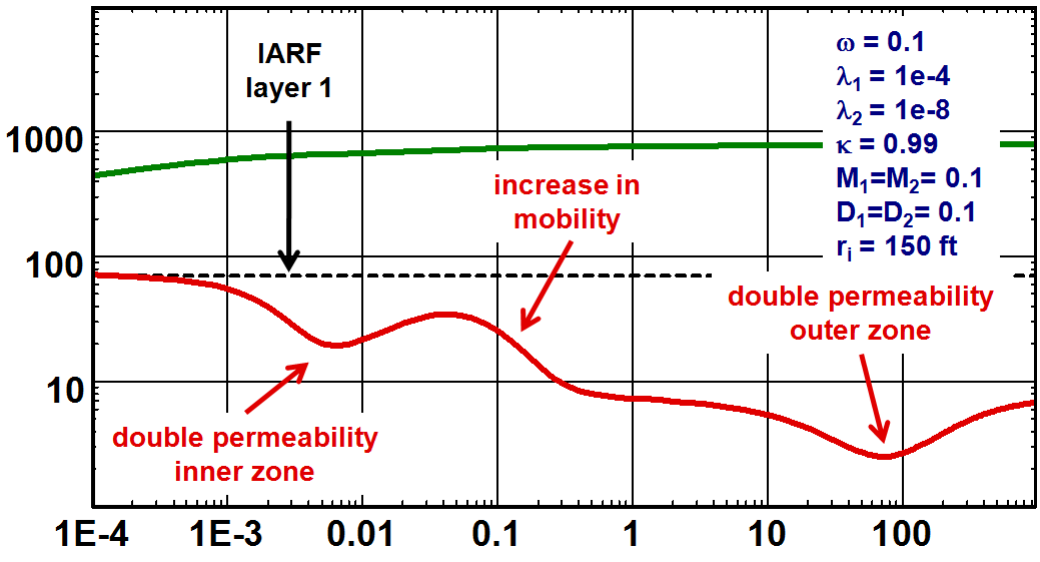


Fig. 7.J.2 – Double-permeability reservoir with radial composite zones

7.J.2 Double permeability double porosity layers

The below figure show the schematic of double-porosity layers in a double permeability reservoir, followed by the theoretical loglog response.

These models are only relevant if we know beforehand, from the petrophysics, that part or all of the layered and composite system is naturally fractured and fissured.

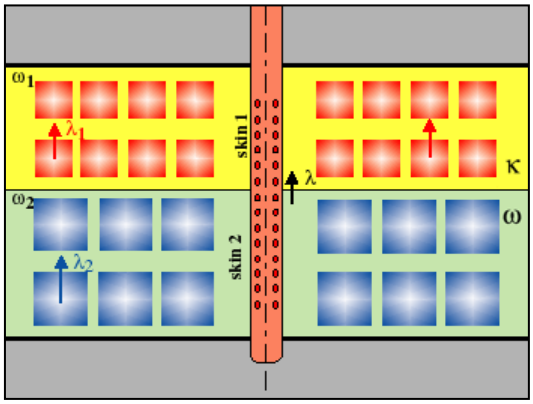


Fig. 7.J.3 – Double permeability double porosity

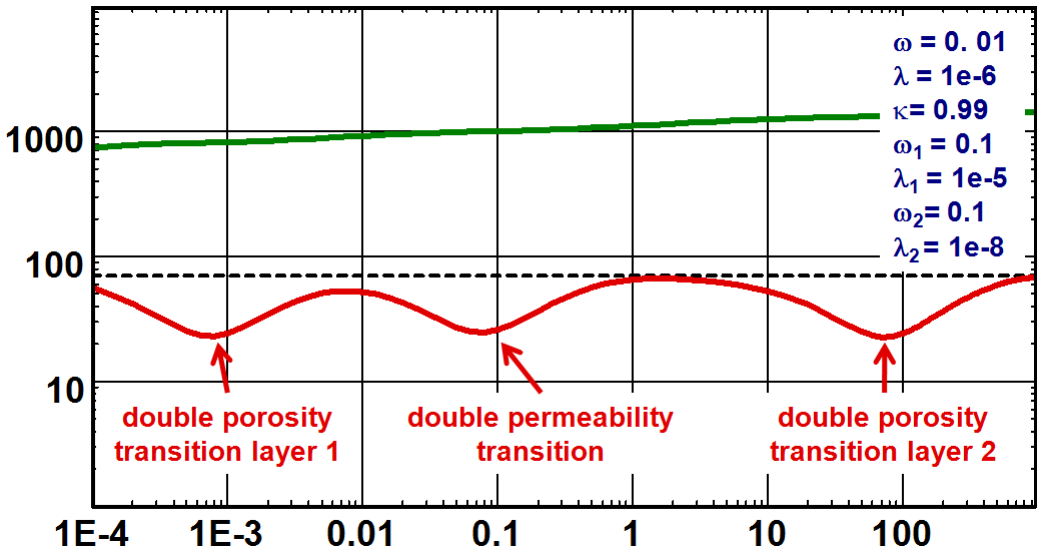


Fig. 7.J.4 – Double-permeability reservoir with double-porosity layers

7.J.3 Double porosity radial composite

The below figure show the schematic of the hypothesis and an example of a calculated response with the pressure change and the Bourdet derivative in the loglog plot.

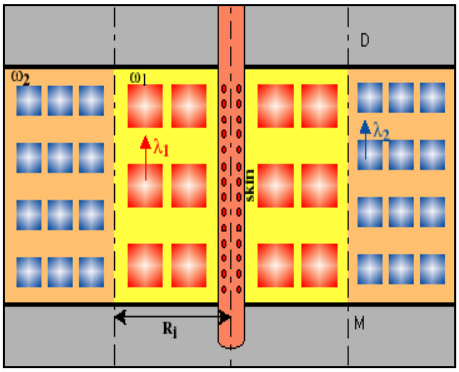


Fig. 7.J.5 – Radial composite double porosity

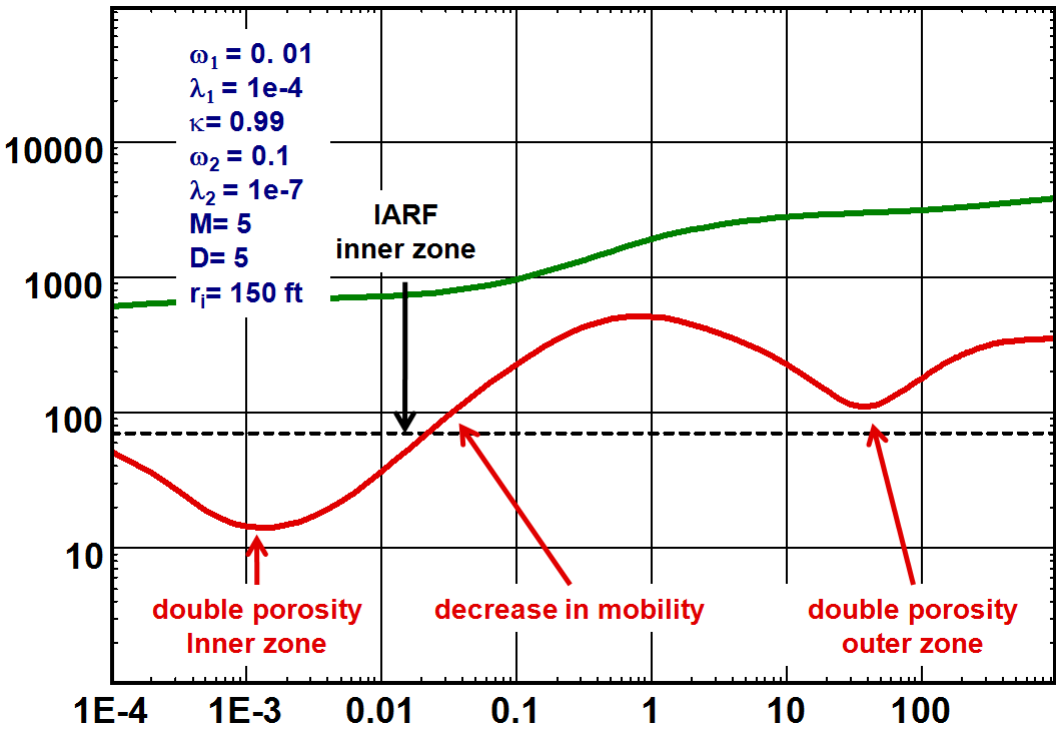


Fig. 7.J.6 – Radial composite reservoir with double-porosity

7.J.4 Just a comment on the above described models

Such models should never be used just for the sake of matching any strange looking response. There must be some evidence, some knowledge of the formation and fluids that would justify such a choice. One should also not forget that there are far too many leading parameters in the models so the concept of a solution to the 'inverse' problem is lost.

8 – Boundaries

OH – DV – OSF

8.A Introduction

In most well tests, and with most models used in pressure transient analysis, the first part of the pressure response is dominated by wellbore effects and flow diffusion immediately around the well. If the well is not fully penetrating the reservoir or not vertical, the early time response is also affected by vertical flow from the top and bottom parts of the producing interval. Then in most cases, but not always, the middle and/or late time pressure response will be dominated by Infinite Acting Radial Flow (IARF), characterized by a stabilization of the Bourdet derivative, where the average reservoir mobility (k/μ) and the global well productivity, total apparent Skin, may be assessed. In many well tests, the analysis will stop there and IARF will be the final detected behavior.

But, should the reservoir be small enough, and should the test be long enough boundary effects will be encountered during the test. This encounter may be accidental, deliberate, as in reservoir limit testing, or inevitable in the case of long term production data.

This chapter covers the different types of boundaries, their respective pressure and derivative behaviors and corresponding analysis methods. It also shows how apparent boundary effects may be, in fact, be something else.

We will only consider boundaries that produce deviations from IARF, and we will not consider the vertical limits of the producing interval. Physically this is a questionable option, as these are boundaries too but for our methodology it makes sense. Upper and lower boundaries will generally be considered in well models involving vertical flow, such as limited entry and horizontal wells, where the early time response will involve a vertical diffusion until these limits are reached. Paradoxically the analyses involving top and bottom boundaries is associated to well models and developed in the corresponding chapter.

We have also excluded composite limits. Though their detection and analysis process are similar to what is done for boundaries, they will be assimilated to reservoir heterogeneities, and treated in the chapter dedicated to reservoir models.

Finally we will also look at the way recent developments on the deconvolution allow boundaries to be assessed while not being detected in any individual build-ups.

8.B Different types of boundaries

8.B.1 Description of a boundary behavior

A boundary is a surface Σ located at a distance from the tested well where a change in the flowing property occurs. A typical boundary effect is shown below where the example used is a single sealing fault. We will start dealing with no flow boundaries.

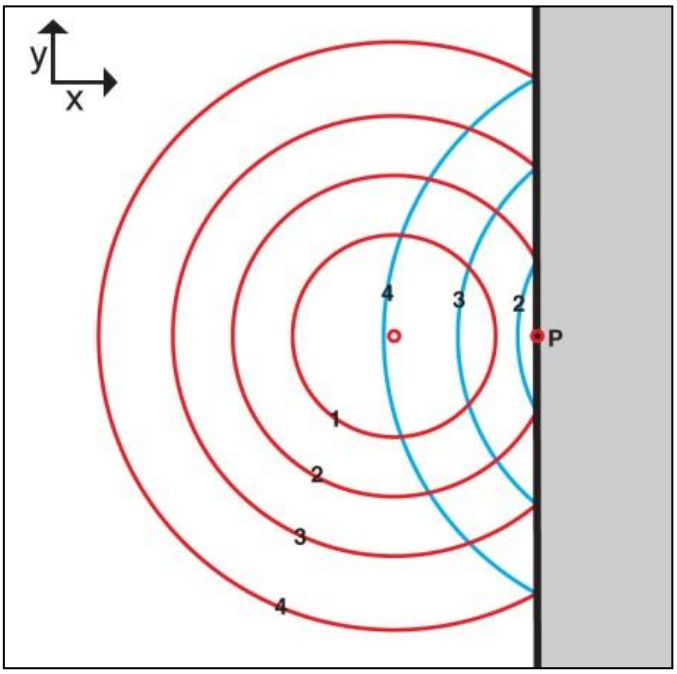


Fig. 8.B.1 – X-Y representation of the additional pressure drop (blue) due to a boundary (example of a sealing fault)

The figure above does not represent a 'wave' but the points at which the pressure drop reaches a given value (e.g. 1 psi) at different times (1, 2, 3, 4). The red circles represent the influence of the well production itself if it was producing in an infinite reservoir. The blue circles represent the additional pressure drop **due to the boundary** at the same times.

This requires a physical explanation: The well production creates a pressure drop around the well that diffuses within the reservoir. As long as the boundary influence is negligible the diffusion will be radial and the 'radius of investigation' (red circles) will be proportional to the square root of time.

When a boundary is present, there will be no pressure support beyond the boundary, and there will be an additional pressure drop compared to an infinite configuration. This pressure drop (blue circles) will affect the pressure profile and will also diffuse.

At a time the amplitude of this additional pressure drop will be picked up by the gauge in the well, and the boundary is detected. This will only occur if the test is long enough and the gauge is sufficiently sensitive to pick up the signal.

The pressure derivative deviates from IARF at the time when the influence of the closest boundary becomes noticeable. The derivative then takes a shape that will depend on the type and shape of the boundary, the flow period of interest, if it is a flow or shut-in, and in some cases the well production history.

We will consider four types of boundaries and their typical behavior, alone or combined with other boundaries. These are no flow, constant pressure, leaky and conductive.

8.B.2 No flow boundaries

No fluid will pass in any direction through a no flow boundary Σ. The mathematical formulation of this condition is given by Darcy's law, applied at zero rate at the boundary, in a direction orthogonal to this boundary:

$$\left[\frac{\partial p}{\partial \vec{n}}\right]_{\Sigma} = 0$$

This equation means that the pressure profile is flat when arriving orthogonally to the boundary. The vertical cross-section below shows the pressure profile from the well to the boundary.

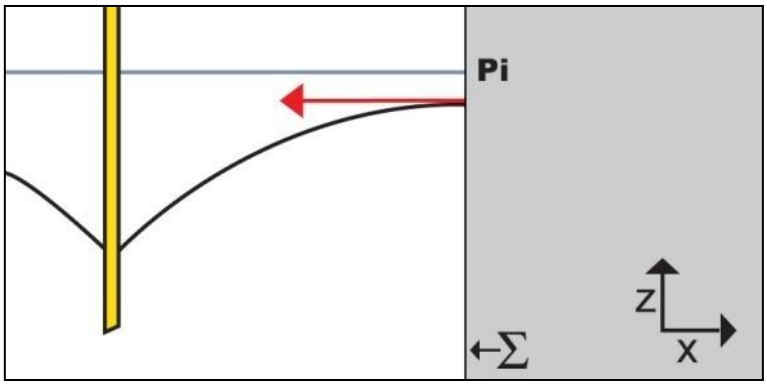


Fig. 8.B.2 – Profile near a no-flow boundary

The figure below is a 3D display of the pressure profile due to a well producing near a no-flow boundary. We are representing here a 2D problem, and the z axis represents the pressure. The pressure at the boundary is not uniform. The pressure change is larger at the point of the boundary than it is the closest to the well. But looking at every line orthogonal to the boundary it becomes flat at the boundary. This is simply Darcy's law for no flow in one direction.

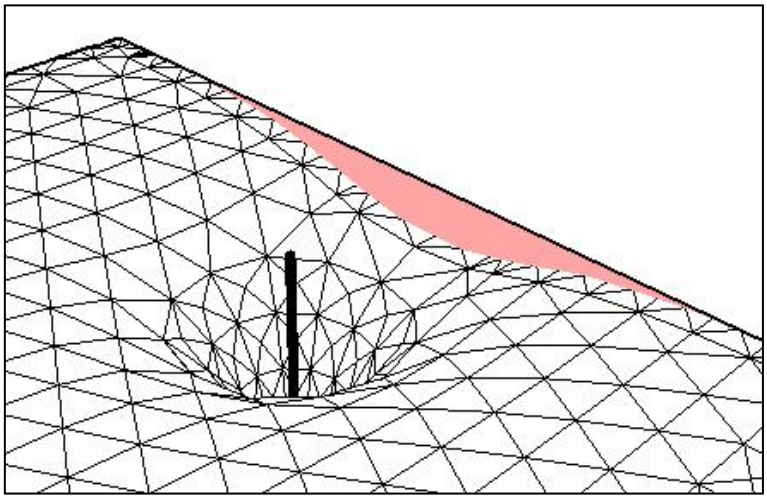


Fig. 8.B.3 – 3D representation of the pressure profile
Between a producer and a no-flow boundary
Pressure, in the z axis is a function of x and y

8.B.3 Constant pressure boundaries

A constant pressure boundary is a surface beyond which there is sufficient pressure support to keep the pressure at the boundary constant, generally at reservoir initial pressure:

$$[p]_{\Sigma} = p_i$$

The figure below shows a vertical cross-section of the pressure profile from the well to the boundary. The slope at the boundary will correspond to the fluid flux required to keep the pressure constant.

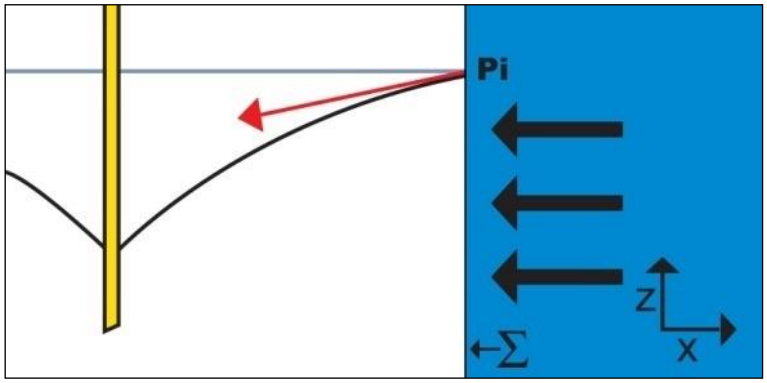


Fig. 8.B.4 – Profile near a constant pressure boundary

8.B.4 Aquifers

The constant pressure boundary above is the only pressure support model which can be easily modeled analytically, using the method of image wells. This implies that the pressure support is very strong and that multiphase flow effects can be neglected. This approximation works generally quite well for gas caps. In the case of water drives such approximation may not work, and aquifer models may be used.

Aquifers are generally modeled analytically. They require a choice of model, that will define the aquifer strength, and a relatively permeability table to model the sweeping of the hydrocarbon by the water phase.

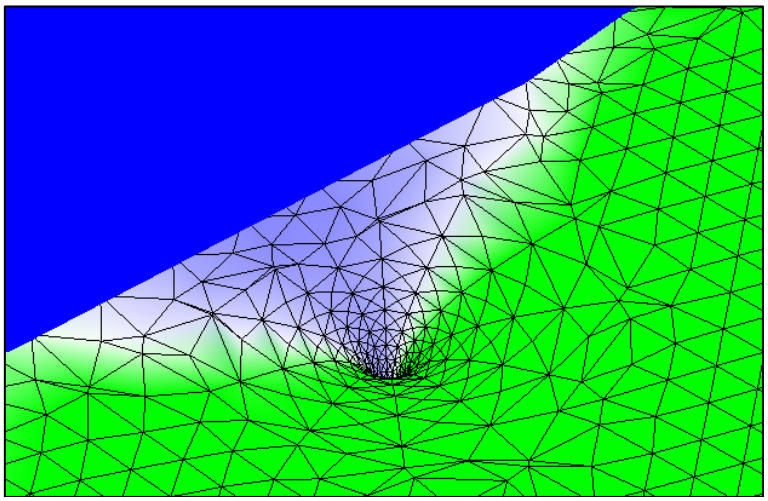


Fig. 8.B.5 – Numerical Aquifer

8.B.5 Leaky boundaries

A leaky boundary is a reservoir inner boundary through which a pressure drop occurs. As for a wellbore skin, the pressure drop at a point of the boundary will be, typically, proportional to the flux through the leaky fault at this point. The vertical cross-section below shows of the pressure profile from the well to the boundary.

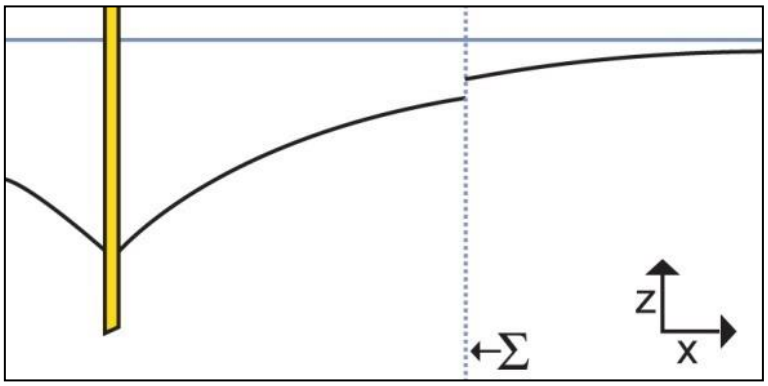


Fig. 8.B.6 – Profile near a leaky boundary

8.B.6 Conductive boundaries

Conductive faults (boundaries) can be modeled numerically or analytically. In this section we will use the analytical model which is part of the Saphir external model suite to illustrate its use and pressure response.

It solves for the pressure behavior at a well near a non-intersecting finite conductivity fault or fracture. The solution includes an altered zone around the fault across which it is possible to add Skin. The reservoir properties on either side of the fault can different.

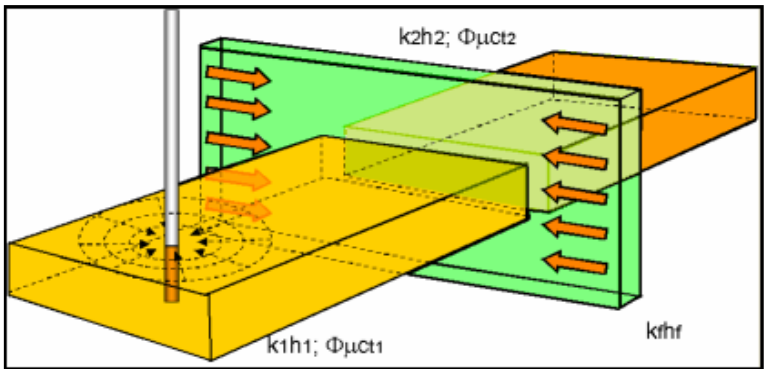


Fig. 8.B.7 – Conductive fault

8.C Single sealing fault

The simplest model for a no flow boundary is a single linear sealing fault of infinite extent. This configuration is easily modeled analytically using an image well (see the section 'Superposition in space of analytical models' in the 'Theory' chapter). The effect of a sealing fault is equivalent to adding a symmetric well with exactly the same production history. This will create an additional pressure drop that will assure that no flow occurs orthogonally to the fault.

In the case of more complex well models (fractures, horizontal wells, etc…), to ensure that the model is valid, one has to add an image well of the same geometry, the position being the symmetric to the real well. To enforce symmetry, wellbore storage must also be added. In some cases however it will be possible to get a good approximation of the response using a simple line source solution with no wellbore storage.

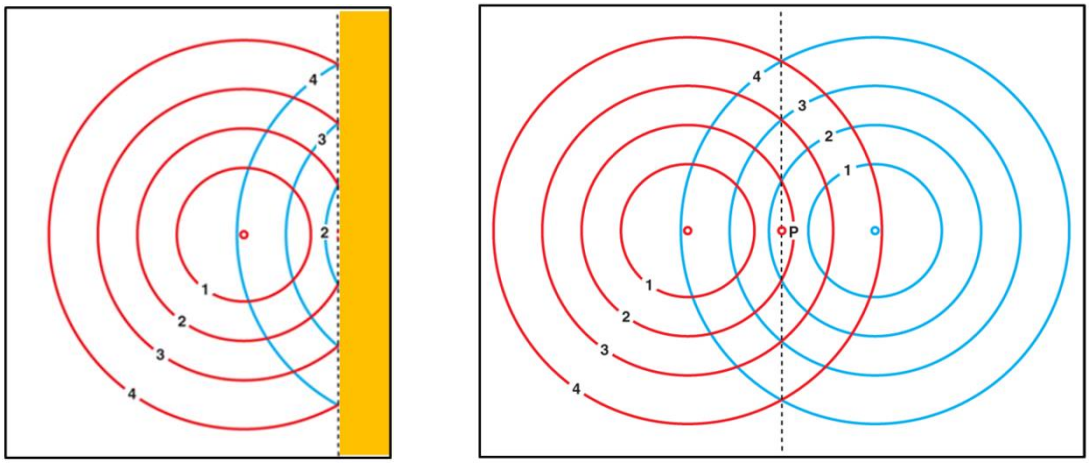


Fig. 8.C.1 – Single fault and equivalent image well.

8.C.1 Behavior

Before the additional pressure dropped due to the boundary is picked up by the pressure gauge, the system behaves as if the reservoir was of infinite extent in all directions.

When the boundary is detected, the response deviates from infinite acting radial flow until it doubles. If one considers the physical reservoir, the well has received the information that the reservoir is actually twice smaller than in the infinite case. After the sealing fault is detected, only half of the originally planned reservoir is now available, and therefore the speed of the pressure drop doubles. If one considers the equivalent image well, after the detection there are two wells producing instead of one, and for the same reason we have a doubling of the speed of the pressure drop.

8.C.2 Semilog analysis

The initial IARF is characterized by an apparent linearity on the semilog plot. Drawing the corresponding semilog straight line will give both kh and the total apparent Skin. A sealing fault will be characterized by a deviation from this initial straight line and a transition towards another semilog straight line with twice the original slope. From the time of intersection of the two straight lines, we can get the boundary distance:

Boundary distance:

$$L = 0.01217\sqrt{\frac{k\Delta t_{\text{int}}}{\phi\mu c_t}}$$

8.C.2.a Drawdown response

As for infinite reservoirs, the semilog plot of choice during a constant rate production will be the MDH plot. Starting from initial pressure, the pressure response will follow a first straight line when IARF is reached, and until the sealing fault is detected. The pressure response will then deviate before stabilizing towards a second straight line, that we call below 'half radial flow'. The slope of this line is twice the slope of the original IARF line.

As in the infinite case, the permeability and skin will be given using the slope of the IARF line. The time of intercept between the IARF line and the half radial flow line will give the boundary distance using the equation above.

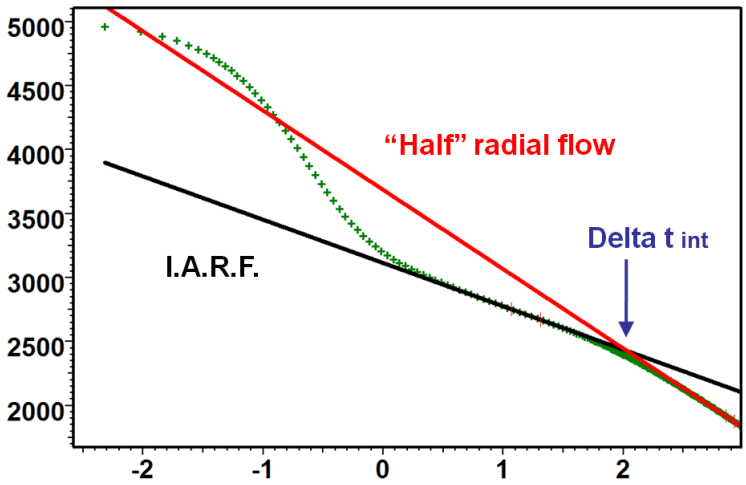


Fig. 8.C.2 – Semilog plot for a sealing fault

8.C.2.b Build-up response

In the case of a shut-in following a single production period, the MDH plot is replaced by the Horner plot. In the case of a more complex production history the semilog plot of choice will be the superposition plot, though the Horner plot is also used for complex shut-ins, provided that a sound value of production time is used.

The behavior is the same as for drawdowns, with an initial IARF line, a second line with twice the slope for half radial flow, and a boundary distance related to the time of intercept of these two straight lines. The only difference is that, in the case of shut-ins the intercept of the half radial flow line (and NOT the IARF line) will be the one used to calculate p*.

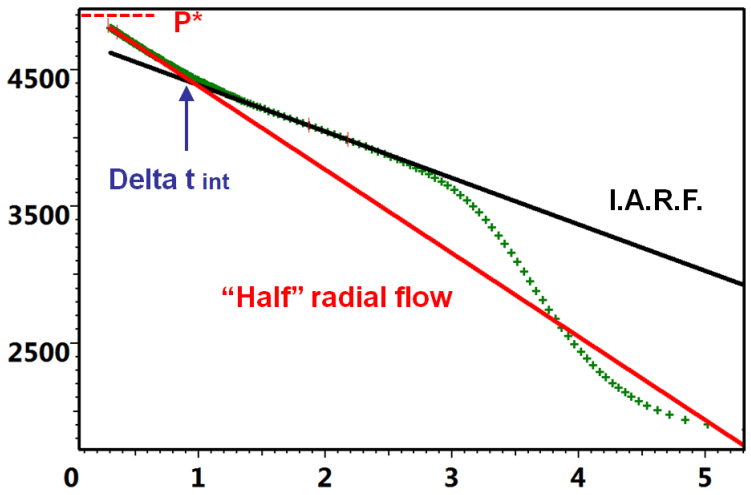


Fig. 8.C.3 – Horner plot or Superposition plot for a sealing fault

8.C.3 Loglog analysis

On a loglog plot, the derivative will initially follow an infinite response, and the derivative will stabilize to a level corresponding to IARF. When the boundary is detected the derivative will deviate upwards, then tend to stabilize again towards a level twice of the original IARF.

The easiest technique to match such response is to first focus on the early and middle part of the data, matching this par with an infinite model. This may include an initial nonlinear regression on all the points before the deviation from IARF. In the case of a vertical well in a homogeneous reservoir this will fix C, kh and Skin.

In a second stage the boundary effect is added, and the first estimation of the distance will be obtained from the semilog analysis or, preferably, an interactive Saphir / Topaze feature where the time of deviation is picked by the user. After initial simulation the parameters, especially the boundary distance, will be improved from nonlinear regression, this time on all data points.

In case of poor data quality, if the nonlinear regression fails it is possible to correct the boundary manually using the following rule of thumb: If we multiply the boundary distance by 2 we multiply the boundary time by 4. For small corrections, adding X% to the boundary distance will add 2*X% to the boundary time.

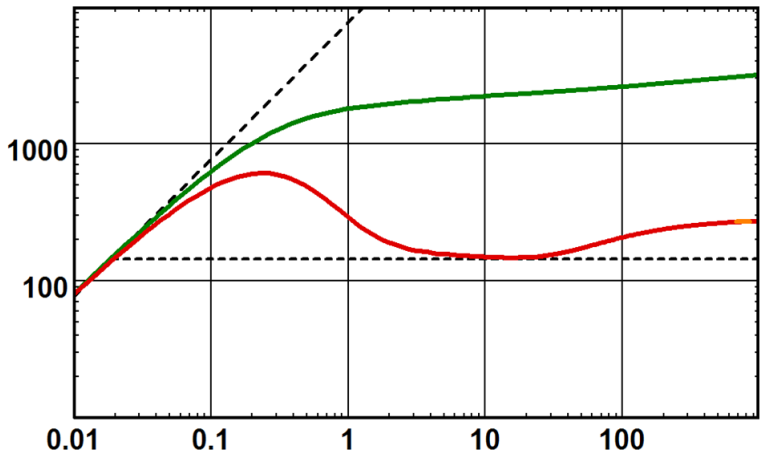


Fig. 8.C.4 – Loglog response for a sealing fault

8.C.4 Influence of the boundary distance

The figure below shows the sensitivity of the response to the boundary distance. As for any radial diffusion problem, the governing group is t/r^2. Doubling the boundary distance will multiply by four the time at which this boundary is detected. This relation is valid for all boundary models discussed in this chapter.

If the boundary is very close to the well (e.g. 100 ft in the example below), IARF may not develop before the fault is detected. For very nearby boundaries the pressure response could look like a homogeneous infinite response with an apparent kh equal to half the true kh.

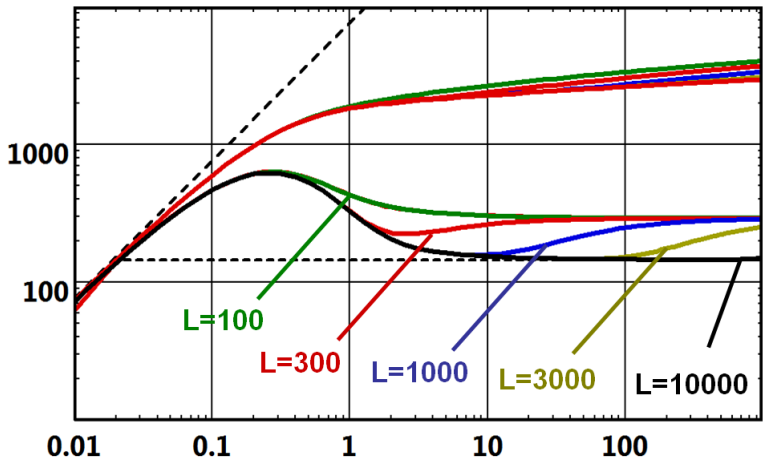


Fig. 8.C.5 – Influence of the boundary distance

8.C.5 The case of shut-ins after a short production time

The Bourdet derivative responses for single sealing faults are similar for drawdowns and shut-ins. In most cases the build-up response will actually match the drawdown response.

However the shape the Bourdet derivative may be distorted in the case of shut-ins following a very short production. In this case the initial effect of the boundary due to the opening of the well will be detected during the build-up, creating a temporary down trend before the effect of the shut-in on the same boundary is detected.

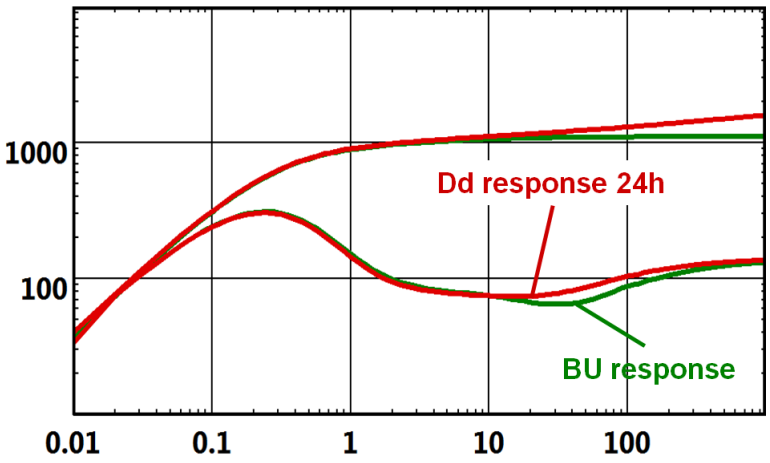


Fig. 8.C.6 – Shut-in after a short production time

8.C.6 Remarks on the sealing fault model

A full doubling of the slope is seldom seen on real data. It requires almost one and half log cycles in time after the initial deviation from IARF, i.e. over a period 30 times longer than what it took to initially detect the boundary. You are likely to see other boundaries before the doubling of the slope occurs. In addition, tests are rarely long enough to provide the opportunity for such a doubling to take place, and shutting the well in one or two more days will not be worth the additional information.

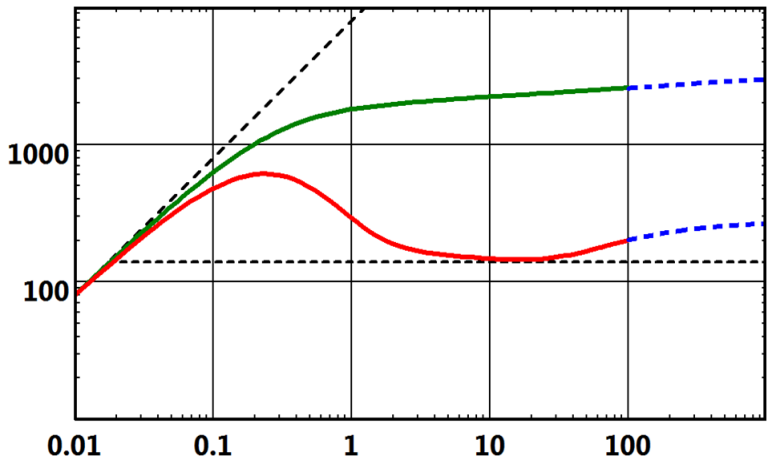


Fig. 8.C.7 – Loglog response for a sealing fault
Incomplete response with no doubling of the slope

The single fault model will be used when the slope is less than double because it is just the simplest boundary model that allows the association between a time and a distance. If we see a deviation from IARF, and IF we think this deviation is due to a boundary, the sealing fault model will provide a good estimate of the distance from the well to such boundary. From this distance we will decide if the hypothesis of a boundary is reasonable.

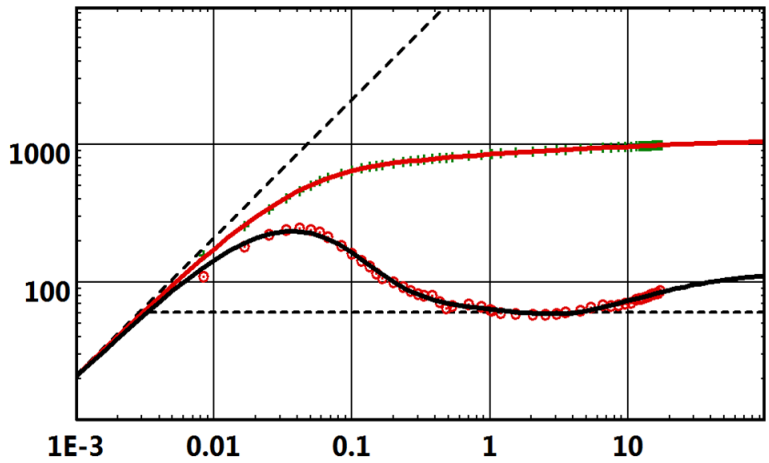


Fig. 8.C.8 – Example of sealing fault match

8.D Intersecting faults

8.D.1 Description

The simple single fault model described in the previous section is the simplest way to relate the time of detection of a boundary and its distance to the well. As stated above, it is rare to see a full doubling of the slope, as after a while the nonlinearity of the single fault, or other faults will be detected. Eventually the full extent of the reservoir is seen; see in 'Closed systems' section further. One of the main analytical models used to model these complex, but still open, systems is the intersecting faults model shown in figure below.

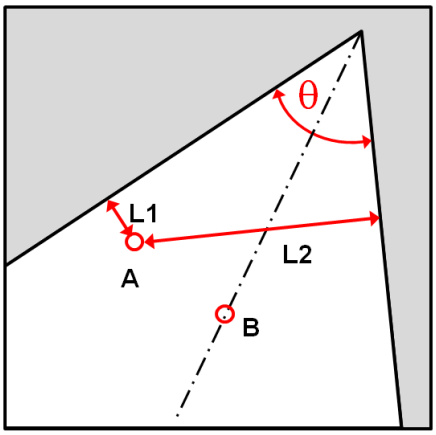


Fig. 8.D.1 – Schematic of intersecting faults
point A is closer to one fault, with point B at the bisector

The well is located between two intersecting linear boundaries of infinite extent. θ is the angle between the faults, L1 and L2 are the orthogonal distances between the well and the two faults. A particular case is when the well is located on the bisector of the faults (L1=L2).

8.D.2 Behavior

If the well is significantly closer to one of the boundaries (point A), the initial behavior is the same as for a single sealing fault. When the second fault is detected, the response enters its 'final' behavior. If the well is fairly equidistant from the two faults, the response goes straight from IARF into the 'final' behavior.

The 'final' behavior is semi-radial flow restricted to the quadrant delimited by the two faults. If θ is the angle between the two faults, the actual reservoir size is smaller than an infinite reservoir by a factor of $2\pi/\theta$; hence the pressure drop is $2\pi/\theta$ larger to produce the same fluid to the well.

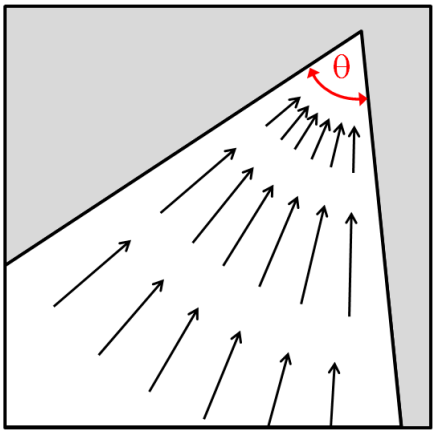


Fig. 8.D.2 – Schematic of intersecting faults wider view showing final semi radial flow

We use the term 'final' in parentheses as, clearly, there would be a time when further boundaries would be detected if the test was continued.

8.D.3 Semilog analysis

On a semilog plot, this will be characterized as a second straight line with a slope $2\pi/\theta$ greater than the initial IARF line slope. As for a single fault, kh and skin will be calculated from the first straight line. The angle θ between the faults, will be 2π / (m_{final} / $m_{initial}$).

8.D.3.a Drawdown response

As for infinite reservoirs, the semilog plot will be the MDH plot. Starting from initial pressure, the pressure response will follow a first straight line when IARF is reached, and until the faults are detected. The pressure response will then deviate before stabilizing towards a second straight line corresponding to the closest limit and eventually a third straight line that we call below 'final radial flow'. The slope of this last line is $2\pi/\theta$ the slope of the original IARF line.

In most of the cases the second straight line caused by the closest limit is very brief and masked by the effect of the second one.

As in the infinite case, the permeability and skin will be given using the slope of the IARF line. The time of intercept between the IARF line and the half radial flow line will give the boundary distance using the equation above.

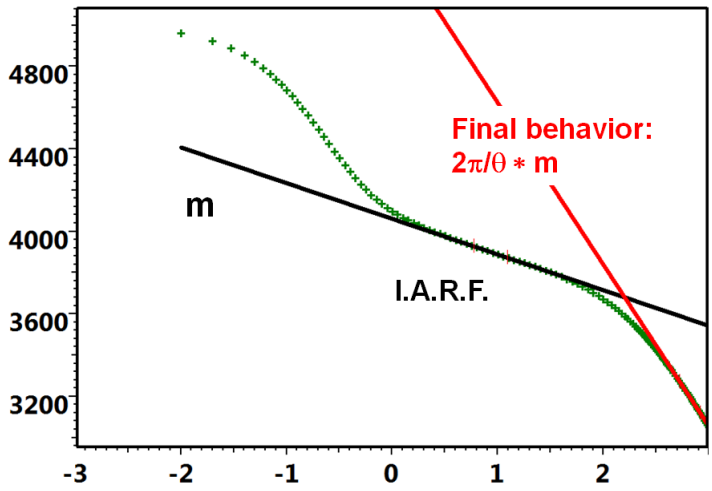


Fig. 8.D.3 – MDH plot for intersecting faults – point B

8.D.3.b Build-up response

As for a single limit, in the case of a shut-in following a single production period, the MDH plot is replaced by the Horner plot and the case of a more complex production history it is replaced by the superposition plot.

The behavior is the same as for drawdowns, with an initial IARF line, a second line with twice the slope for the first limit could be briefly seen then, when the second limit effect appears a third straight line called 'final radial flow' and the slope of this last line is $2\pi/\theta$ the slope of the original IARF line. The only difference is that, in the case of shut-ins the intercept of the 'final radial flow' line (and NOT the IARF line) will be the one used to calculate p*.

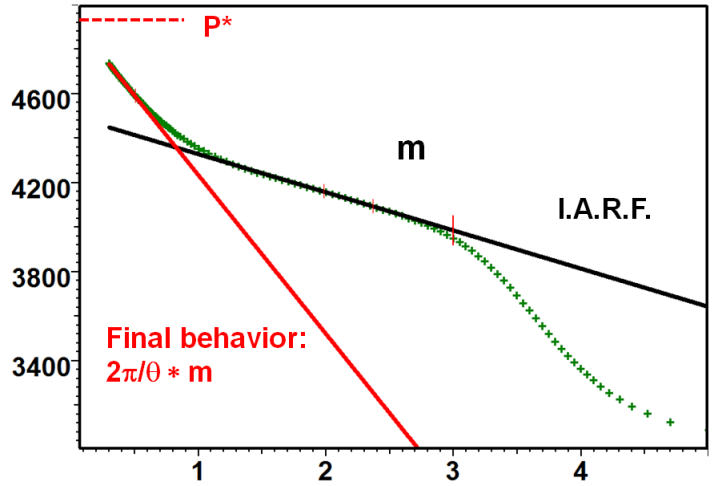


Fig. 8.D.4 – Horner plot for intersecting faults – point B

8.D.4 Loglog analysis

On a loglog plot, the response will be characterized by a final stabilization of the pressure derivative at a level $2\pi/\theta$ times above IARF. In other words, the stabilization level will provide an estimate of the fault angles, while the time at which the derivative levels off from IARF, and eventually (well A) levels off from the sealing fault line, will provide an estimate of the boundary distances.

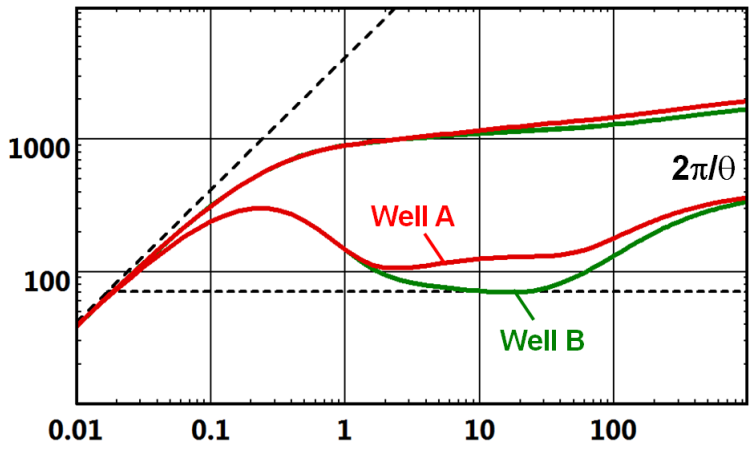


Fig. 8.D.5 – Loglog plot for intersecting faults – wells A & B

8.D.5 Remarks on the intersecting faults model

The single sealing fault is a particular case of intersecting faults where L1=L2=L and $\theta=\pi$

When intersecting faults are generated using image wells the interpreter has to choose the angle θ only within a discrete range of values, corresponding to integer fraction of π or 2π. Image wells are very easy to implement and very fast to calculate on a computer or a hand-calculator. But geometrically they require the angle to be an integer fraction of 2π if the well is situated on the bisector (well B), and an integer fraction of π if the well is located anywhere else (well A). The major limitation is that we will generally not match exactly the final stabilization level, and θ will not be accessible as a nonlinear regression parameter.

Conversely, methods using integral solutions will simulate the response for any angle at a higher, but now acceptable, CPU cost. These models will even allow θ to be higher than π, and go up to 2π. We then end up with a half fault that may be described later as an incomplete boundary. Integral solutions also allow regression on θ.

8.D.6 Example of intersecting faults match with field data

In spite of the acquisition noise, the diagnosis of intersecting limits is perfectly accessible:

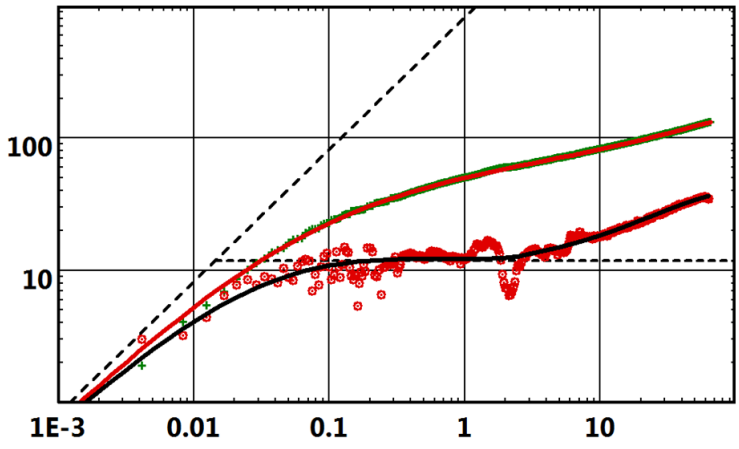


Fig. 8.D.6 – Example of intersecting faults match

8.E Two parallel faults

8.E.1 Description

This solution is also sometimes referred to as a channel reservoir. The well is located in a channel limited by two parallel sealing faults. We will call L1 and L2 the orthogonal distances between the well and the two boundaries. L = L1+L2 is the width of the channel. As was the case for intersecting faults, we will consider the situations where the well is much closer to one boundary or in the middle of the channel.

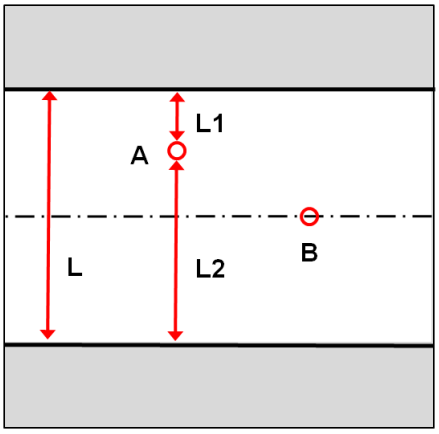


Fig. 8.E.1 – Schematic of parallel faults
A closer to one fault with B central

8.E.2 Behavior

If the well is significantly closer to one of the boundaries (well A), the initial behavior will be the same as a single sealing fault response. When the second fault is detected, the response will enter its 'final' behavior. If the well is at fairly equidistant from the two faults (well B), the response will go straight from IARF into the final behavior

The final behavior is linear flow along the channel. Again we should refer to the term 'final' in parentheses as, obviously, there will come a time when the last outer boundaries will be detected if we wait long enough.

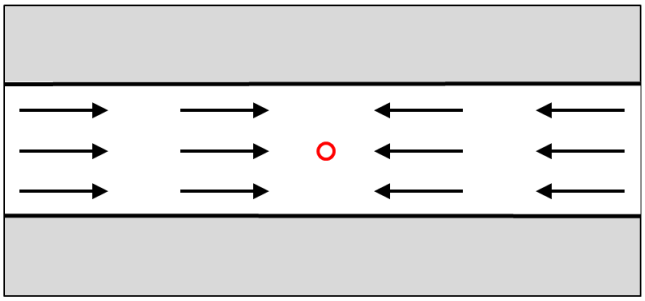


Fig. 8.E.2 – Schematic of parallel faults
wider view showing the 'final' linear flow

Linear flow, or more generally the flow of fluid though a constant cross-section, is encountered in several well test models, such as fractures at early time after storage, horizontal wells at intermediate times, after the top and lower boundaries have been reached (see 'Well models' chapter), and parallel faults at late time. In each case, the flow is characterized by linearity between the pressure change and the square root of the elapsed time:

$$\Delta p = A\sqrt{\Delta t} + B$$

$$\Delta p' = \Delta t.\frac{\partial \Delta p}{\partial \Delta t} = \frac{1}{2}A\sqrt{\Delta t}$$

8.E.3 Semilog analysis

Semilog plots are of little help in diagnosing or quantifying, parallel faults. After IARF, the pressure response will continuously increase.

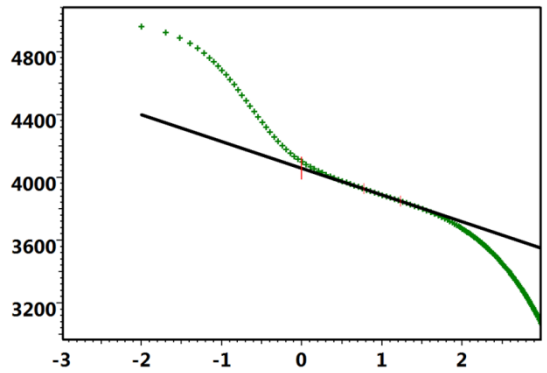


Fig. 8.E.3 – MDH plot for parallel faults

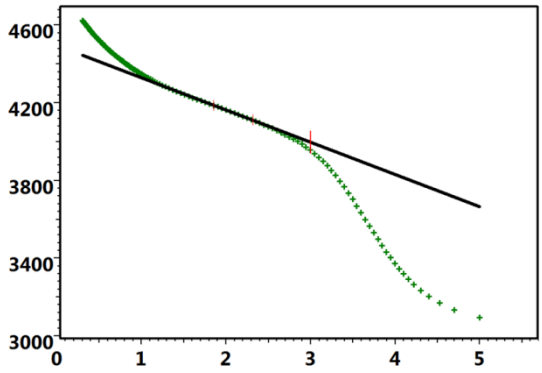


Fig. 8.E.4 – Horner plot for parallel faults

In case of build up the adequate plot would be the Horner plot or a Superposition plot, but in no case it could be used to extrapolate to a p* since the final pressure behavior do not reveal any straight line on a semilog plot.

8.E.4 Loglog analysis

We will first consider the case of a production phase. After a possible single fault response (point A), the response will reach linear flow. As soon as linear flow is reached, the pressure derivative will follow a half slope on the loglog plot, while the pressure change, because of the constant term B in the equation, will only tend to a half slope. If the pressure half slope is clearly established, there will be a ratio of two between the pressure and the derivative half slope lines.

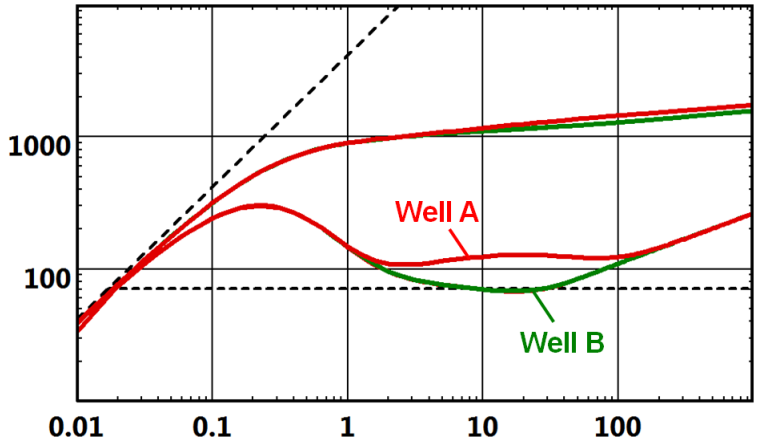


Fig. 8.E.5 – Loglog plot for parallel faults points A & B - drawdown only

The behavior above is only strictly valid for production. In the case of a build-up or complex production in theory, nothing guarantees that a specific behavior will occur on the loglog plot. In reality, the loglog plot is also usable for shut-ins.

Strictly speaking, only the derivative of the production period will follow a half slope. For any practical purpose, especially considering the noise of real data, all flow periods will show a derivative with a slope oscillating around 0.5. The pressure response itself will bend down during build-ups and will not show any specific behavior.

Practically, the interpretation engineer will require the program to generate the pressure response from the usual relation between mobility, time of departure from IARF and boundary distance. The model will be generated taking into account the well production. Any deviation from the strict half slope will also be simulated by the model. Then a nonlinear regression on the boundary distances will correct any initial error in the estimate of these boundary distances due to this superposition effect.

8.E.5 Specialized analysis

As an alternate to the model optimization method above, one can use a specialized analysis involving the square root of the time. For a drawdown, a plot of Δp vs $\sqrt{\Delta t}$ will exhibit linearity. The same plot will be used for the analysis of early time fractures, intermediate time horizontal well and late time channel responses. For parallel faults, the slope will provide an estimate of $k.L^2$, hence of L if the IARF has been clearly identified.

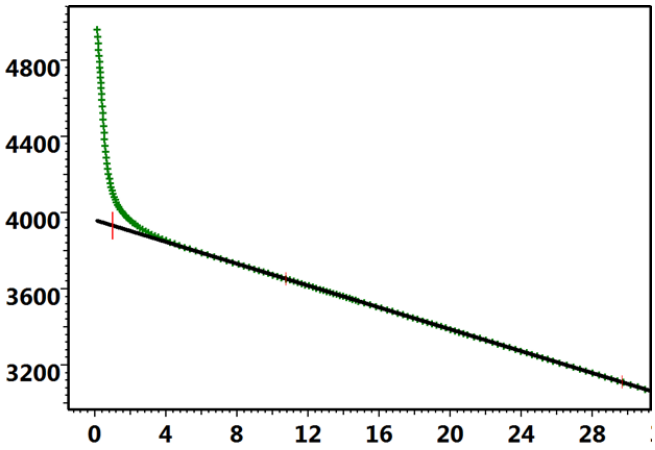


Fig. 8.E.6 – Square root plot for parallel faults point B - production period

For shut-ins and complex production histories, fracture, horizontal well and parallel faults will diverge in the choice of the superposition function. As the linear flow is the 'final' behavior of the channel response, if the considered shut-in has reached linear flow, all component functions used in the superposition will be in linear flow, and the time scale to use is the multirate superposition of the square-root.

For a simple build-up following a unique production, the tandem square root function $[\sqrt{(tp+\Delta t)}-\sqrt{(\Delta t)}]$ will be used. For more complex production, the superposition of the square root function will apply. For a shut-in, the extrapolated pressure corresponding to infinite shut-in time will be the right estimate of p*.

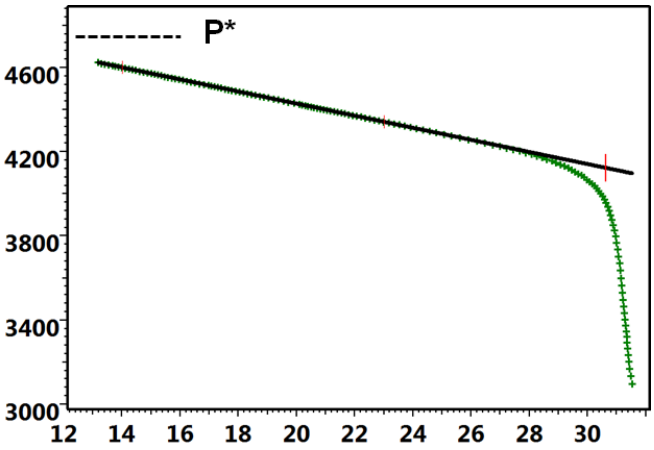


Fig. 8.E.7 – Tandem square root plot for parallel faults

8.E.6 U-Shape reservoir

The U-shape reservoir model, where parallel faults are limited on one side, exhibit at late time, a similar linear behavior to the above, but this time in only one direction.

The early time transient will depend on the distance between the well and the now three sealing faults. This will not be discussed in detail here, and we will only consider the case of a point at equidistant from the three boundaries. The solution is compared with the parallel fault solution, i.e. in the absence of the third boundary.

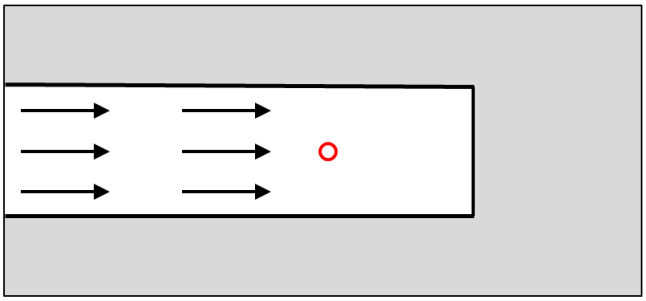


Fig. 8.E.8 – Schematic of a U-shape reservoir
Wide view showing the 'final' linear flow

The two responses are similar and the U-shape reservoir produces a late time half slope. Compared to the parallel fault solution, the final behavior is shifted upward by a factor of two on the loglog plot. This shift is coherent with the fact that the U-shape reservoir is half the size of the corresponding complete channel.

Specialized analysis will also provide an estimate of $k.L^2$. The software will need to know that it is a U-shape reservoir, in order to apply the correction by two in the line calculation.

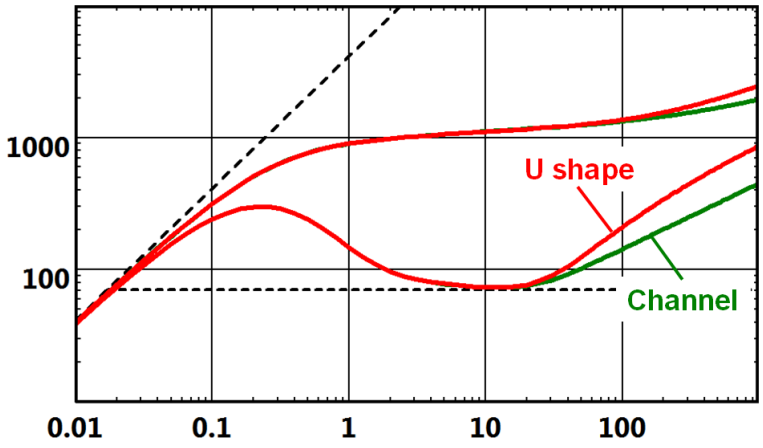


Fig. 8.E.9 – Parallel faults vs U-shape – loglog plot

8.E.7 Remarks on the parallel faults model

The response of the parallel fault model is not related to the fact that the boundaries are straight lines. A channel type reservoir, of any shape but of constant width, would have strictly the same response, as in the figure below. This is why this solution is also called a channel reservoir.

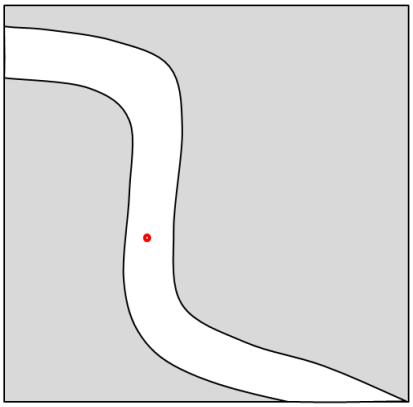


Fig. 8.E.10 – Channel reservoir

8.E.8 Field example

An analytical model for two parallel faults is used to match the field data below.

Even if the reality is not strictly two linear parallel faults but non regular limits close to to be parallel, this model gives a very satisfactory approach before going to more sophisiticated models.

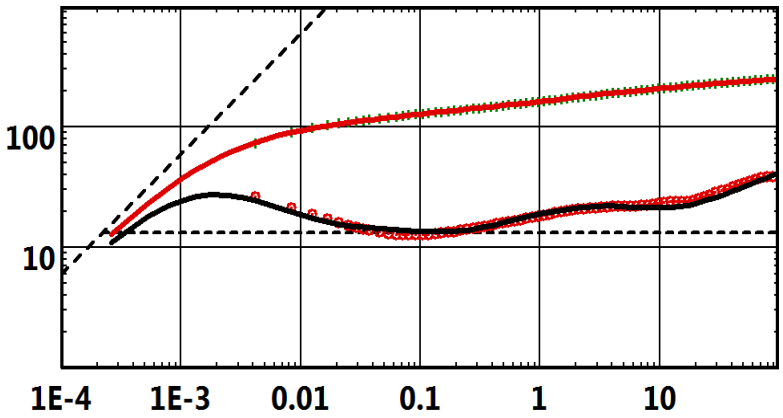


Fig. 8.E.11 – Example of parallel faults match

8.F Closed systems

In the previous sections, the reservoir was still considered to be of 'infinite volume'. What we mean by this is that, at least in one direction, the total extent was not detected during the pressure survey. As a result, the pressure would return to initial pressure at infinite shut-in time.

Conversely, a closed system will be modeled when the test is long enough, or the reservoir is small enough, to detect the whole extent of the reservoir. This will be characterized by at least one of the following behaviors: (1) during the production, we will see linear depletion, (2) at shut-in the pressure will stabilize at a pressure lower than the initial reservoir pressure.

8.F.1 Description

The most common and easiest way to model closed system is the circular model. It assumes that the tested well is located at the center of a reservoir of circular shape.

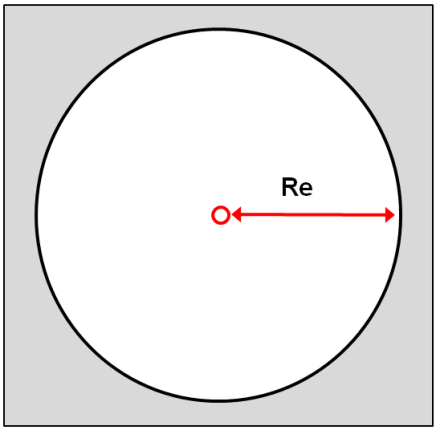


Fig. 8.F.1 – Circular reservoir

This model is unlikely to reflect the exact reservoir geometry and the well location. However it is useful and fast when depletion is detected. But the geometry is unknown and the response does not exhibit any intermediate boundary behavior.

The second most popular closed system model is the rectangular reservoir. Using the principle of image wells, this solution allows us to define an aspect ratio between the reservoir and the position of the well at any point in the rectangle. From the well point of view, it means that the four boundaries may be positioned at any distance. When all four distances are equal, the well is at the center of a square, which is practically identical in response to a circular solution with the same area.

Another advantage of this model is that it can easily be extended to multiwell solutions where contributions of interfering wells can be added. This possibility is critical to properly address material balance issues.

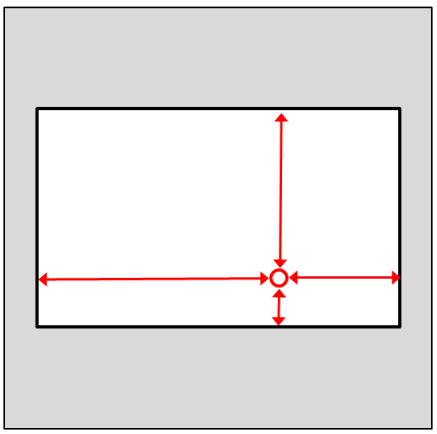


Fig. 8.F.2 – Rectangular reservoir

Numerous other models of closed systems have been published and used. Complex shapes can be modeled using boundary elements or numerical models, and can also be extended to multiple wells.

8.F.2 Behavior

In the illustrations below, we will show the response of a circular reservoir and a rectangle. The shape of the rectangle and the position of the well is illustrated in the figure above. Both rectangle and circle will have the same area.

Unlike the open systems described in the earlier sections, the behavior of closed systems is radically different between production, or injection, and shut-in periods.

During production, or injection, the pressure information will diffuse and reach boundaries sequentially. When the last boundary is reached, the pressure profile will stabilize and then drop uniformly. This particular phase of flow is called Pseudo-Steady State (see chapter 'Theory - Outer boundaries'). It is characterized by linearity between the pressure drop and the time.

$$\Delta p = A.\Delta t + B$$

$$\Delta p' = \Delta t.\frac{\partial \Delta p}{\partial \Delta t} = A.\Delta t$$

For the circle, the response will go straight from IARF to PSS. For the rectangle, closer boundaries will be detected beforehand.

When the well is shut-in, there will be a transfer of fluid back to the well zone, until the pressure stabilizes back to the average reservoir pressure.

8.F.3 Semilog analysis

As for the parallel faults, the semilog plot will not act as a tool to quantify the boundary effects. During the production, the semilog plot will deviate from IARF and tend to an infinite slope. For the shut-in, the pressure response will go horizontal, stabilizing at average reservoir pressure.

The figures below illustrate the stabilization, the model is closed circular.

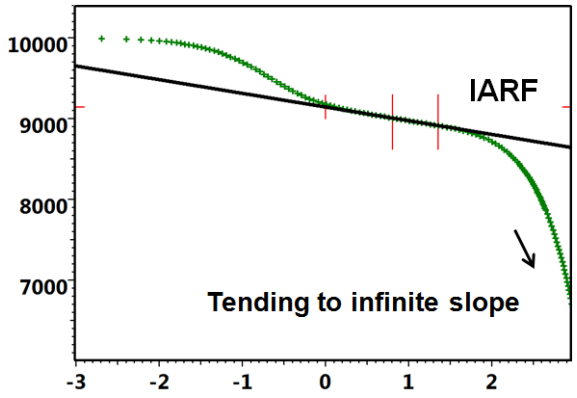


Fig. 8.F.3 – Production semilog plot, circular reservoir

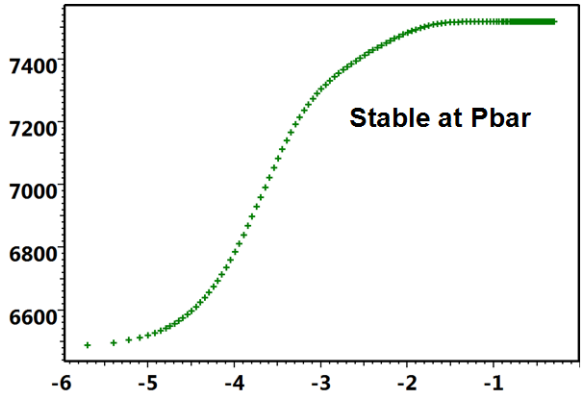


Fig. 8.F.4 – Build up semilog plot, circular reservoir

8.F.4 Loglog analysis

During the production or injection phase, PSS will be characterized by a late time unit slope, first on the derivative, then ultimately on the pressure response.

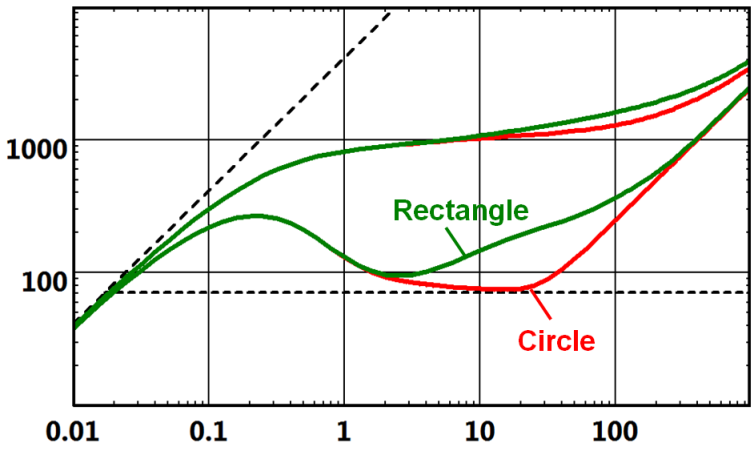


Fig. 8.F.5 – Circle and Rectangle solutions Production period, loglog plot

For the shut-in the pressure will stabilize at average reservoir pressure, the derivative will 'dive' towards zero. It would not be correct to imagine that because a system is closed, the shut in derivative will only behave this way and only 'dive'. For the rectangular model or any model with closer boundaries, intermediate boundary effects will be detected with the derivative going up before the final dive.

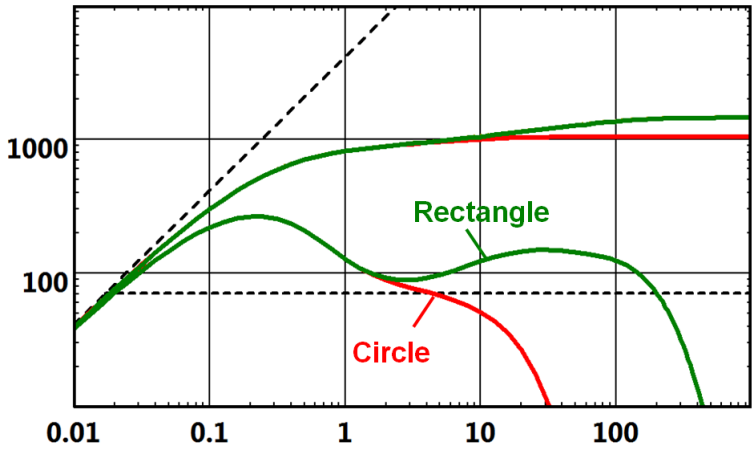


Fig. 8.F.6 – Circle and Rectangle solutions
Shut-in period, loglog plot

8.F.5 Specialized analysis

The PSS response will follow a straight line on a linear plot. The slope m will give the size of the reservoir. The intercept will be the cumulative effect of the well damage, ie: Skin factor and an additional pressure drop due to the transition between IARF and PSS. This pressure drop, linked to the shape of the reservoir and the position of the well, is generally linked to a parameter named the shape factor, CA. The higher the shape factor, the lower the pressure drop. The model with the highest shape factor is the circle, as there is a straight transition between IARF and PSS.

Today the contribution of the shape factor to the pressure drop at PSS is implicitly calculated by the model.

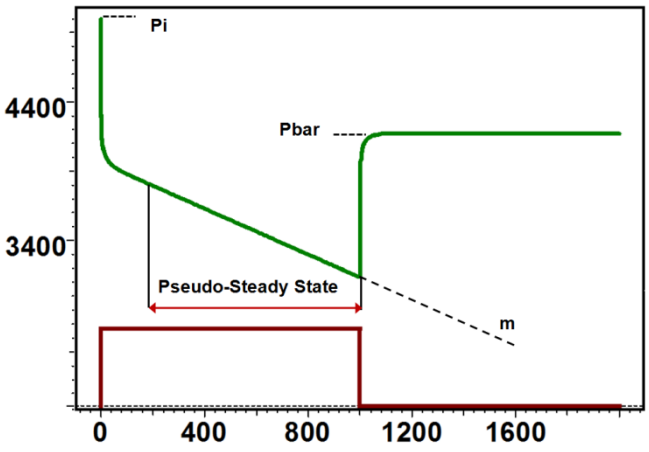


Fig. 8.F.7 – Linear plot of a closed system response

The slope of a linear plot of the flowing pressure versus time is:

$$m = 0.234 \frac{qB}{Ah\phi c_t}$$

8.F.6 Closed system versus drainage area

This is a subject of frequent confusion. In a producing field, when production is stable, the drainage area of a well will be the zone in which the fluid will flow towards this well rather than an offset well. It is not a physical but a mathematical boundary built from the equilibrium of production between the wells. In the absence of injectors, each drainage area will be limited by a curve where the pressure profile is flat. When a well production rate is changed, the limits will move and the drainage areas will change.

It is perfectly correct, over the production period, to work as if the drainage area was the limit of a small reservoir with one well only (left side figure below). This is what average pressure calculation, AOF and IPR curves are designed for. But the limit of a drainage area is in no way a hydraulic boundary as those described in this chapter and the analogy ceases as soon as we start dealing with a build-up. When the well is shut-in (central figure below), the drainage area will very quickly shrink, taken over by nearby wells. Ultimately another set of drainage areas will stabilize (right side figure). So a closed system model can NOT be used during a build-up.

We observe on the build-up the shut in effect superposed to the depletion effect due to the other wells production.

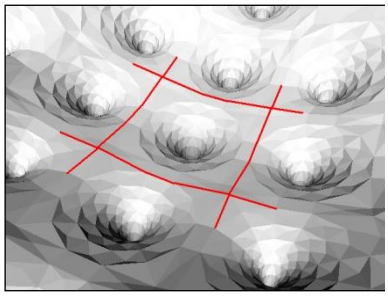


Fig. 8.F.8

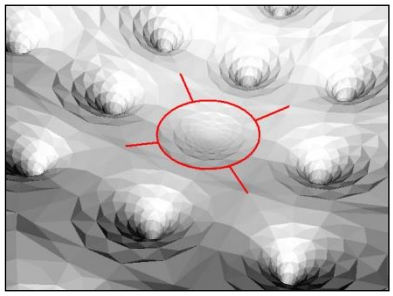


Fig. 8.F.9

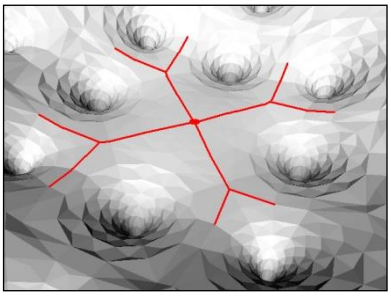


Fig. 8.F.10

Drainage area: Evolution when a well is shut in

8.F.7 Other remarks on the closed systems

One typical mistake with novice interpreters is the expectation that a build-up response in a closed system would follow a unit slope on the derivative. This is wrong, as this would mean that pressure potentially goes 'back' to infinity. But this triggers a question: why are drawdown and build-up responses so different while other models show equivalent derivative behaviors in both?

Actually, what is surprising is that most other models do show equivalent derivative behaviors during productions and shut-ins. We have already seen that it was not strictly true for parallel faults although close enough. The derivative is calculated with respect to superposition time, which itself was designed to handle one, and only one behavior; IARF. Calculations were done for the superposition derivative to stabilize when all components of the production history reach IARF. The wonderful surprise is that, indeed, the derivative carries the signature of numerous well, reservoir and boundary models, and in most cases these signatures survive the superposition process.

However there is no surprise with single faults and intersecting faults, because the long term behavior is IARF multiplied by a fixed factor. It just happens that, numerically, when the models are of infinite extent, i.e. the pressure returns to the initial pressure at infinite shut-in time, the derivative behavior is only marginally affected by the superposition.

But this is not the case for closed systems. When PSS is reached, we are no longer in the usual diffusion process. The reservoir behaves like a depleting tank, and all that survives from the diffusion is a steady pressure profile. When the well is shut-in, the diffusion process will regain its territory until, again, all boundaries are reached. Because the reservoir acts like a tank, as there is no longer any production, the pressure stays constant and uniform and at average reservoir level. This is why the behaviors are so different. On a large time scale, we have a straight material balance behavior, only perturbed by transient diffusion effects whenever rates are changed.

8.F.8 Example of matches with field data

On the production period data the derivative, after exhibiting the various limits effects, tend to a unit slope characteristics of the PSS.

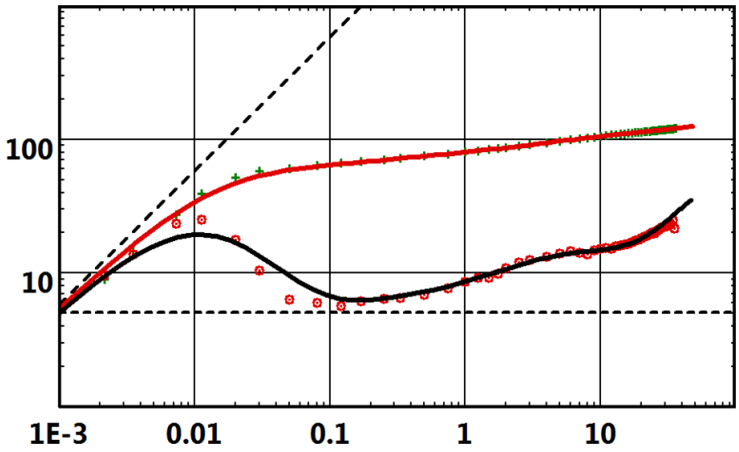


Fig. 8.F.11 – Match with the closed system, production field data

On the shut-in period data the derivative can also show the various limits effects but will drop down characterizing a stabilized pressure.

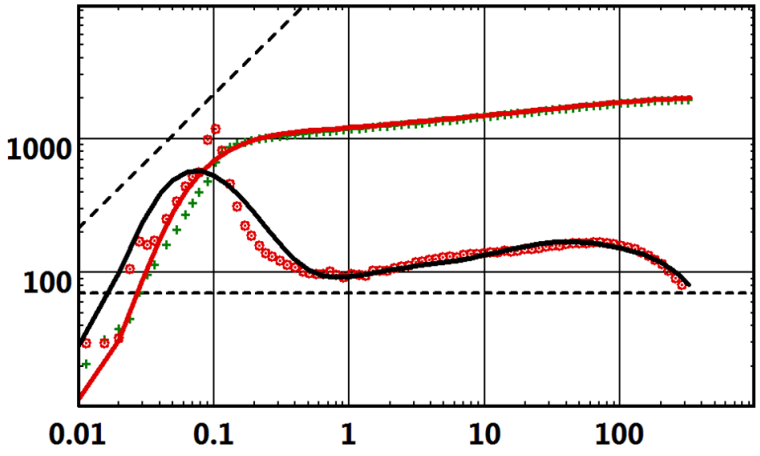


Fig. 8.F.12 – Match with the closed system, shut-in field data

8.G Constant pressure boundaries

8.G.1 Description

Constant pressure boundaries may be the only boundary effect in the model, or may be complemented by sealing boundaries. Most solutions involving boundaries account for sealing or constant pressure boundaries, and any combination when applicable.

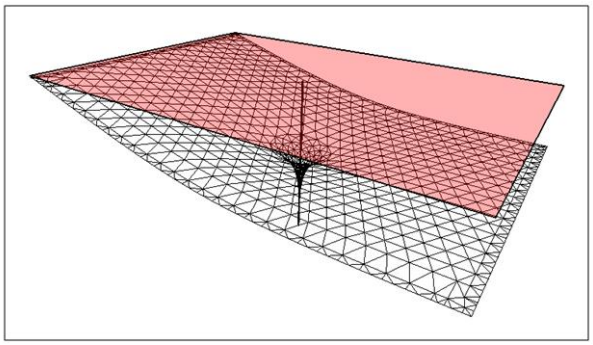


Fig. 8.G.1 – Flow profile in a rectangle with three sides sealing and one at constant pressure
In red the original pressure plan, in black the pressure plan after production

The combinations are potentially unlimited, but we will illustrate constant pressure behavior by the two simplest, pure, constant pressure boundaries using three examples. These are the linear, ie the constant pressure equivalent of the sealing fault, the circular; the constant pressure equivalent of the closed circle, and a rectangular model where one side is at constant pressure. We will use the geometry described below, and consider the west boundary to be at constant pressure.

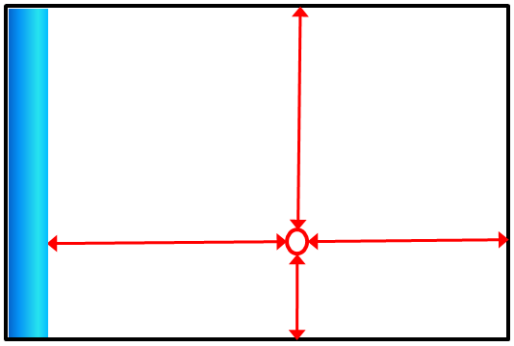


Fig. 8.G.2 – Rectangular reservoir, with a constant pressure west limit

8.G.2 Behavior

As soon as the constant pressure boundary is reached, it will provide the necessary volume of fluid to charge the boundary pressure to its original value to flow into the reservoir. The pressure will stabilize and the derivative will dip. The speed of this dip will depend on the boundary geometry.

8.G.3 Semilog analysis

As for the bounded reservoir models where the final behavior is not a radial flow, the semilog plot does not act as a tool to quantify the constant pressure boundary effect. During the production, the semilog plot will deviate from IARF and will tend to a constant flowing pressure line. For the shut-in, the pressure response will stabilize at average reservoir pressure.

The figures below illustrate this stabilization, the model is constant pressure circular.

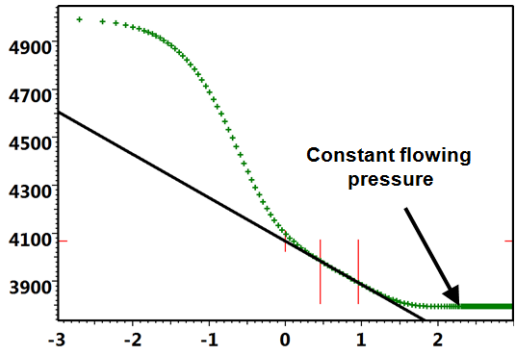


Fig. 8.G.3 – MDH for a production period

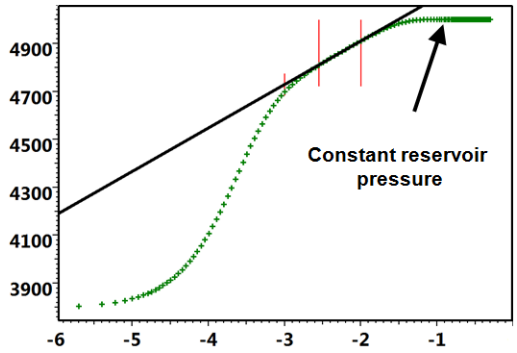


Fig. 8.G.4 – Horner for a Shut in period

8.G.4 Loglog analysis

8.G.4.a Drawdown response

Below, the response of a linear and a circular constant pressure boundaries, for a drawdown, is displayed and compared to their sealing counterpart. The circular boundary derivative response will exponentially dip down, while the response for a linear boundary will dip down with a negative unit slope.

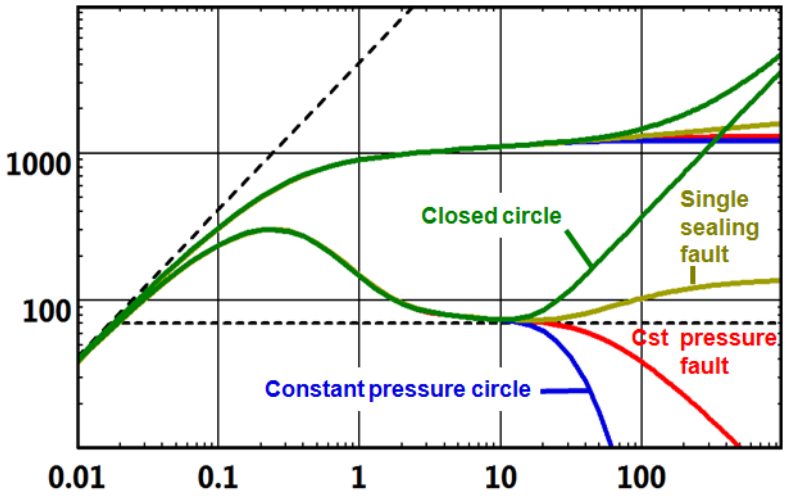


Fig. 8.G.5 – Ct pressure, flowing
Linear and Circular boundaries
Comparison with sealing equivalents

8.G.4.b Build up response

The same responses are shown below and compared for a build-up. In this example, both constant pressure models behave the same way as in the producing phase. This will not always be the case if the producing time is very short and the boundaries are not seen during the drawdown. Then transition effects will be seen during the build-up.

There may also be a slight difference in the shape of the response, due to the fact that the superposition time is used to calculate the derivative. In the case of constant pressure boundaries, it is preferable to use the drawdown derivative, and not the superposition derivative, to get a derivative response matching exactly the shape of the drawdown. But the difference is in, any case, small. And, if the model derivative is calculated the same way as for the data, either option in the derivative calculation will provide reliable and equivalent results after nonlinear regression.

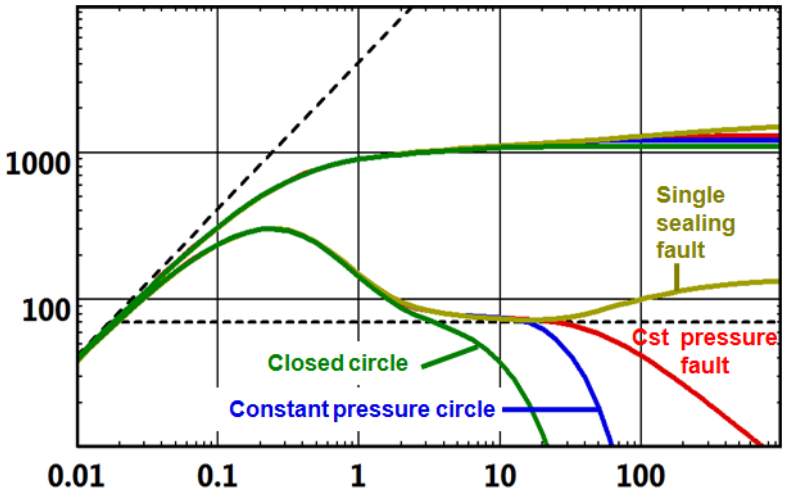


Fig. 8.G.6 – Ct pressure, shut-in
Linear and Circular boundaries
Comparison with sealing equivalents

In the figure below we see the response of the rectangular model during drawdown, with and without a constant pressure west boundary. Both responses match until this last boundary is seen. At this point, the closed system will reach PSS displaying unit slope of the derivative, while the derivative of the rectangle with a constant pressure boundary will go down and pressure will stabilize.

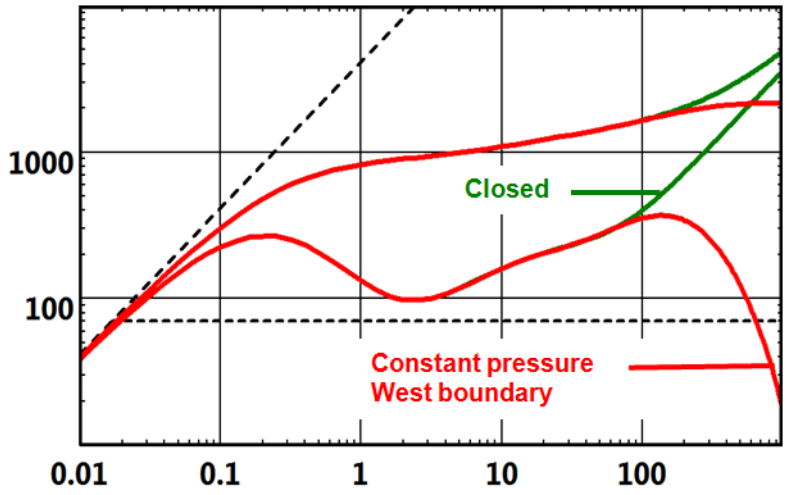


Fig. 8.G.7 – Rectangle, production
Last boundary sealing or constant pressure

Now, the same rectangular responses are compared for the shut-in. The closed system derivative response inverts its behavior and dives quickly, while the mixed boundary response show a very similar behavior. Again, this may not be strictly true if the production time is very short.

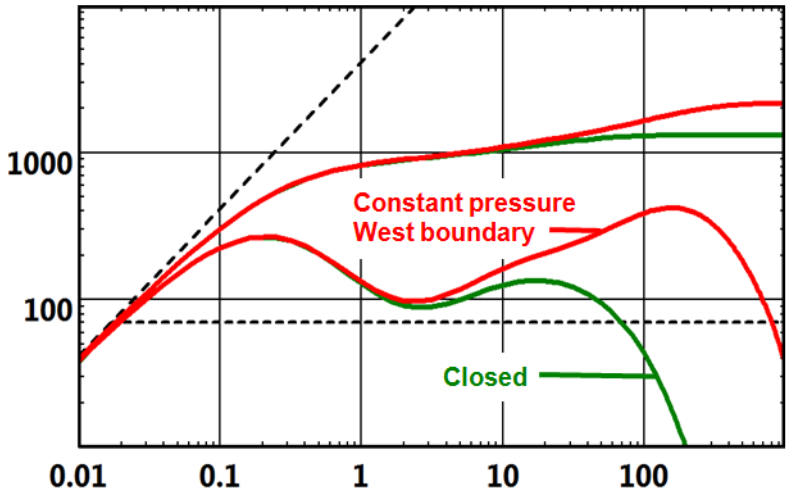


Fig. 8.G.8 – Rectangle, shut-in
Last boundary sealing or constant pressure

The figure below shows a field example, where the plunging derivative is interpreted as a constant pressure boundary. The same example as illustrated below can also be matched with a closed system model.

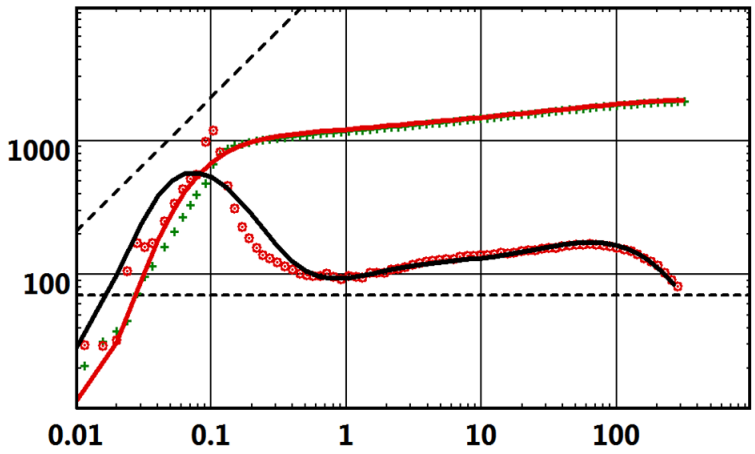


Fig. 8.G.9 – Closed system shut-in
Interpreted with a constant pressure boundary

8.G.5 Constant pressure vs. closed system

For production responses, there is a clear difference between sealing boundaries that will produce a rise of the derivative, and the constant pressure boundaries that will produce a stabilization of the pressure, hence a fall of the derivative. Unfortunately, for shut-in responses, both closed systems and constant pressure boundaries will show a fall of the pressure derivative. As an illustration the plots below show excellent matches of the same data, with these two very different models.

The loglog plot shows a comparison of this set of data, with two rectangular solutions, one with only sealing faults, one with combinations of sealing and constant pressure boundaries. Again, the quality of the match is excellent, and the slight differences alone would not permit us to discriminate between the choice of models.

There is no answer if all we have is the build-up response. But generally, the uncertainty will be lifted by looking at the rest of the well test, and in particular the starting pressure. When a constant pressure boundary is involved, the final shut-in pressure will invariably revert to the initial pressure.

For a closed system, the final shut-in pressure will be the average reservoir pressure, derived from the initial pressure with a straight material balance calculation. So the starting point of the simulation will be very different from one model to the other.

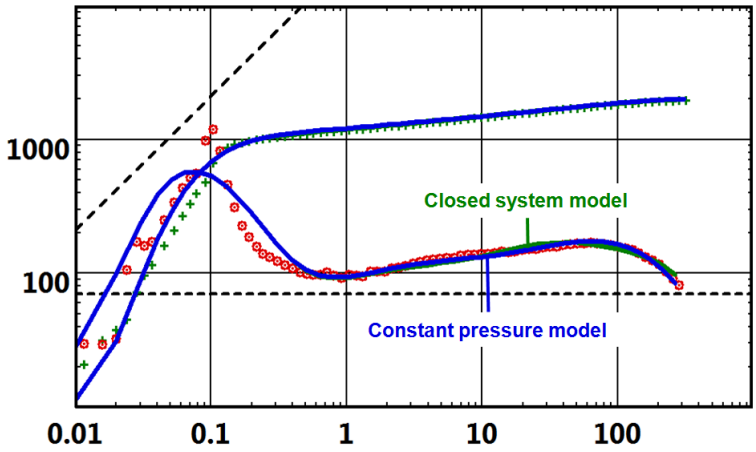


Fig. 8.G.10 – Loglog match of a shut-in
With both constant pressure and closed system models

The history plot below shows the comparison between the two options on the whole production history, showing that the constant pressure system model is absolutely not a realistic option, even if it perfectly matches the build-up response. Unfortunately, the choice is not always that simple.

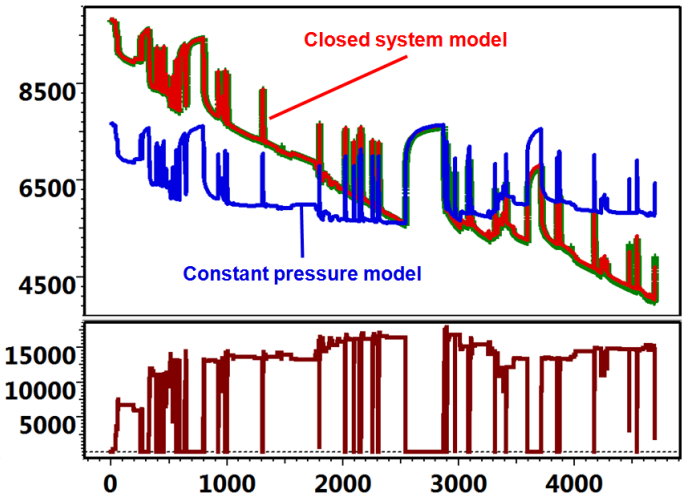


Fig. 8.G.11 – History match with both
constant pressure and closed system models

8.H Leaky and incomplete boundaries

Leaky and incomplete boundaries share similar behaviors, even though the assumptions are different.

Below, a leaky fault: the leakage allows some flow to pass through the fault.

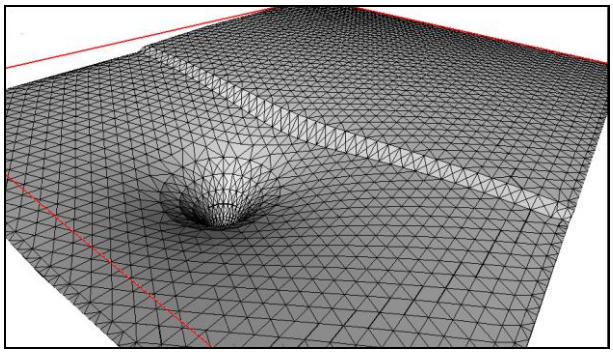


Fig. 8.H.1 – 3D pressure profile with a leaky fault
The red lines correspond to the level of pi

Here below, an incomplete fault: the flow will pass around it.

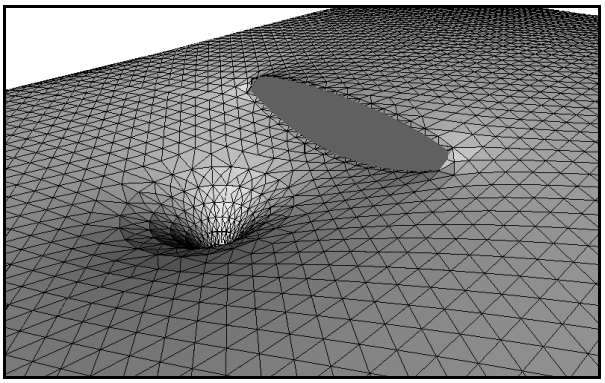


Fig. 8.H.2 – 3D pressure profile with an incomplete fault

In both cases, it is an obstacle that still allows the part of the reservoir beyond the boundary to contribute to the flow. The models will be characterized by a deviation from IARF, then a progressive return of the derivative to the same level.

8.H.1 Leaky fault

8.H.1.a Behavior

Leaky boundaries may be modeled numerically or analytically. We will illustrate the behavior of leaky boundaries with the simplest analytical model, i.e. a single leaky linear boundary of infinite extent. The compartment on the other side of the boundary may have different properties. In the following we will assume it is the same reservoir. If it is not, the behavior described below will have to be combined with a linear composite response.

The boundary property is defined by a leakage coefficient α, also called dimensionless transmissibility ratio:

$$\alpha = \frac{k_f / w_f}{k / L}$$

Where kf is the fault permeability, wf is the fault width, k the reservoir permeability and L the distance from the well to the fault.

α=0 will correspond to a sealing fault, an infinite value of α will correspond to an infinite reservoir (i.e. no boundary), nevertheless with α=1, the leaky fault effect is already hardly visible on the derivative.

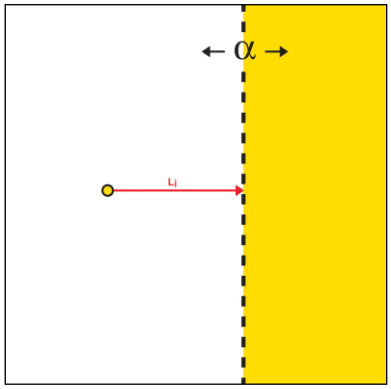


Fig. 8.H.3 – Schematic of a leaky fault

Note: in the numerical solution, the leakage factor α is a transmissibility multiplying factor varying between 1 (totally leaky) and 0 (sealing).

8.H.1.b Semilog analysis

The semilog plot exhibits a first straight line corresponding the IARF in well side of the reservoir then a drop, or increasing slope, describing the restriction to the flow, and finally the plot goes back to straight line parallel to the first one, because the reservoir is identical on the other side of the fault:

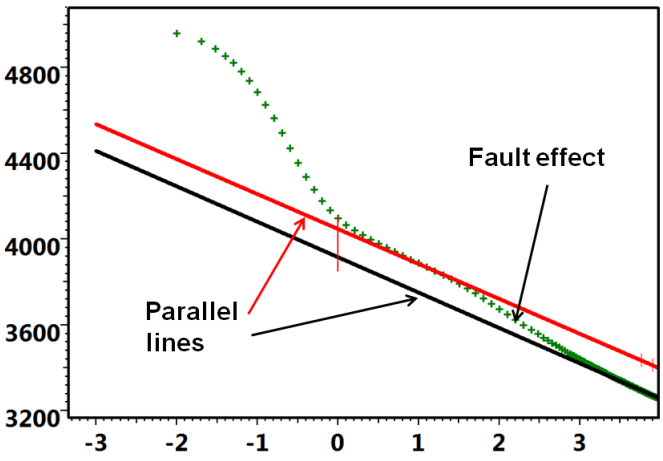


Fig. 8.H.4 – Semilog plot, leaky fault in a homogeneous reservoir

The amplitude of the drop, therefore the distance between the two straight lines depend on the α value. A very small value of α would make the drop to last longer and the distance between the lines to increase.

The behavior that we can observe on a Horner or a superposition plot for a build up is similar and, as mentioned before for other limit effects, the first line is used for the IARF calculation and it is the second one that is extrapolated to get the P*.

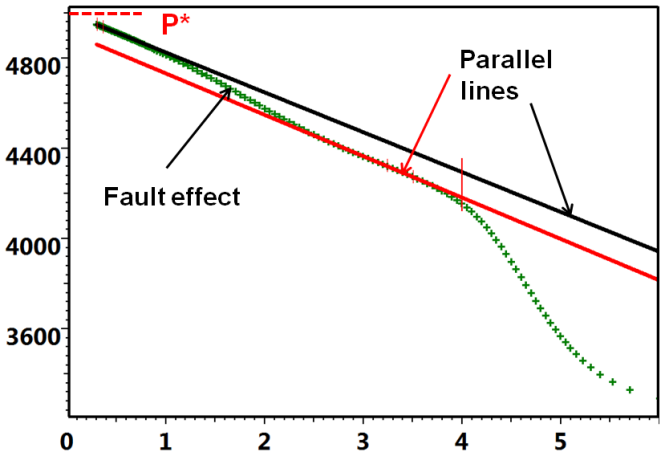


Fig. 8.H.5 – Horner plot, leaky fault, homogeneous reservoir

8.H.1.c Loglog analysis

The figure below shows the loglog response for several values of α. When the fault is detected, the derivative will deviate from IARF as for a sealing fault, albeit with a smoother behavior depending on the value of α. Then the pressure drop through the leaky fault will start to stabilize and the derivative will, progressively, return to IARF provided the reservoir has the same property on the other side of the fault.

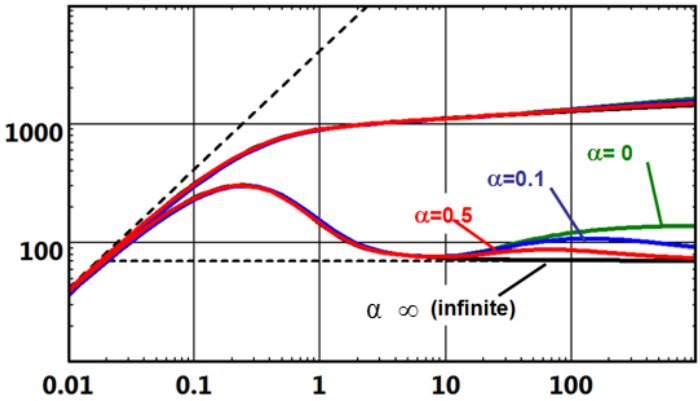


Fig. 8.H.6 – Loglog plot, leaky fault, homogeneous reservoir

It does not mean that when the derivative has returned to IARF the effect of the fault is over. In fact it is not IARF, and there is a cumulative effect on the pressure response, corresponding to the stabilized pressure drop through the fault as illustrated below on the isobar map generated with a numerical model:

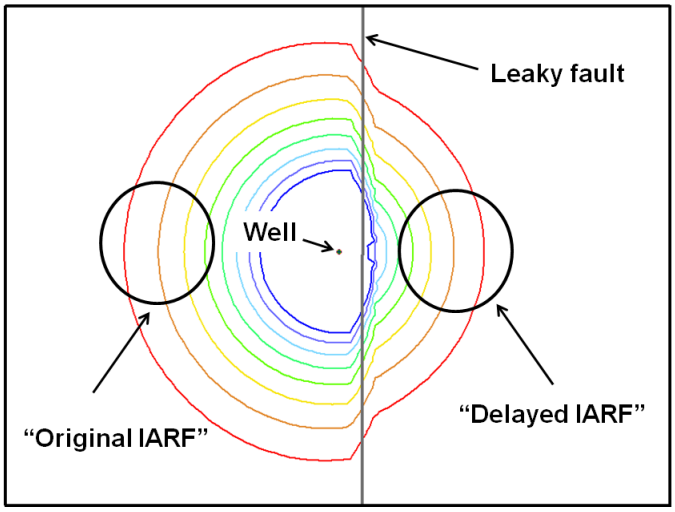


Fig. 8.H.7 – Isobar map showing the pressure drop at the fault

Each color line corresponds to a certain pressure value but it can also be interpreted as an investigation or influence zone at a certain time.

The blue represents the early time influence zone, the green to yellow the intermediate time and the red the late time.

We see on the map that the radial flow goes on the other side of the fault but with a certain delay. That corresponds to an additional pressure drop at the well compared to the infinite system.

8.H.2 Incomplete boundary

8.H.2.a Behavior

Incomplete boundaries are easily modeled numerically. To illustrate the behavior we will use an incomplete fault with various positions of its end with respect to the well as shown below.

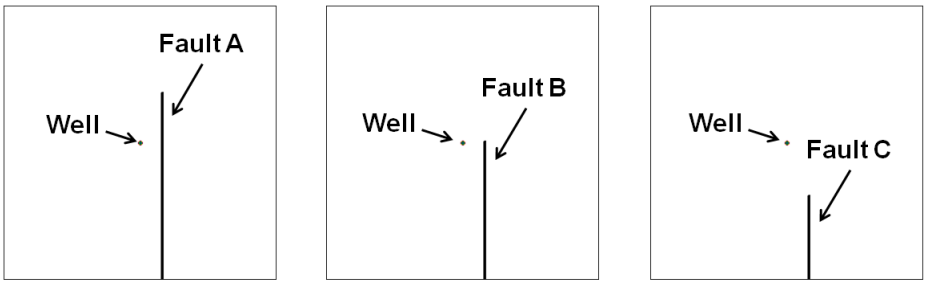


Fig. 8.H.8 – Half fault in positions A, B, C

The presence of the fault influence temporarily the pressure behavior, it creates a deviation from the IARF but when the pressure signal 'turns around' the fault, the complete reservoir contributes then to flow and the behavior goes back to IARF. It just remains a partial restriction to the drainage, creating an additional pressure loss.

The time when the fault effect is observed depends on the distance to the fault. Its amplitude depends on its position: the more the fault is in front of the well, the higher is the amplitude (case A).

8.H.2.b Semilog analysis

The semilog plot shows first an IARF straight line then a drop, or increasing slope, due to the obstacle created by the fault, then the plot show a second straight line parallel to the first one, corresponding to the complete drainage of the reservoir.

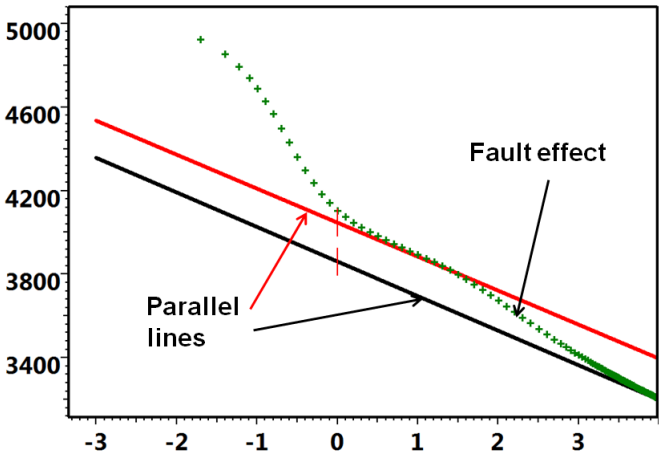


Fig. 8.H.9 – Semilog plot behavior for a incomplete fault

The build up behavior is identical. The first line is used for the IARF calculation and the second one to extrapolate to P*.

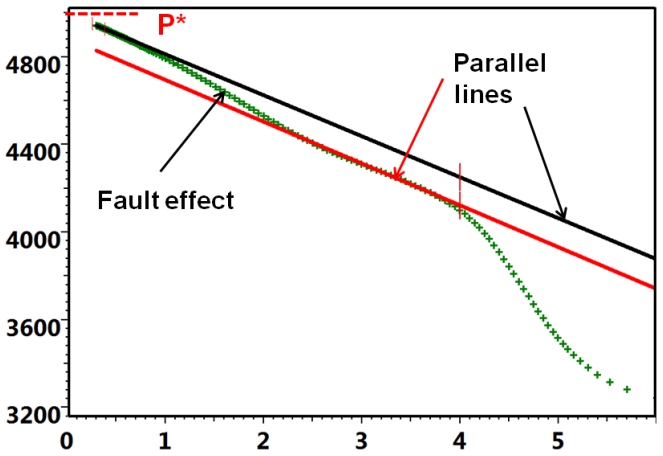


Fig. 8.H.10 – Horner plot, behavior for a incomplete fault

8.H.2.c Loglog analysis

The figure below shows the loglog behavior for these different cases. The response corresponding to the fault B is already very close to infinite behavior, and fault C case would show absolutely no boundary effect.

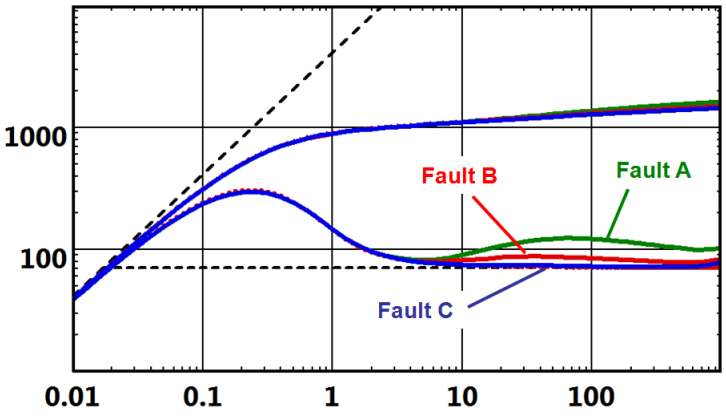


Fig. 8.H.11 – Loglog response of a incomplete fault in positions A, B, C

Below, the isobar maps plotted for a certain time of production illustrates very well the influence of the position of the incomplete fault on its effect on the pressure behavior.

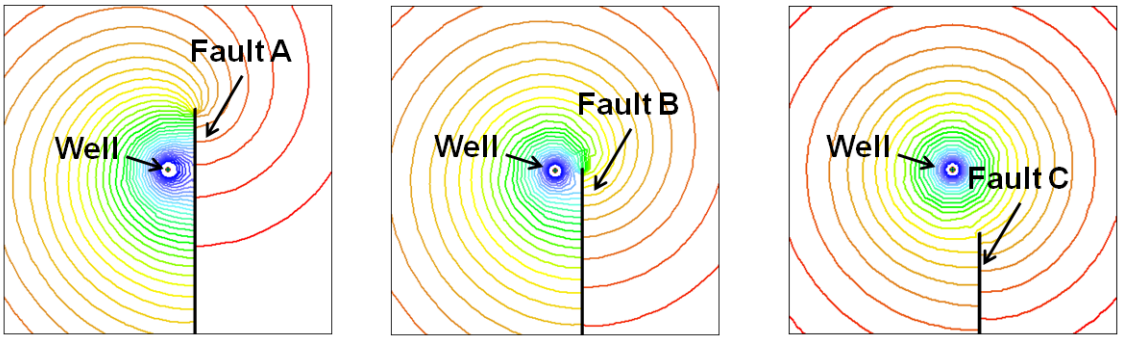


Fig. 8.H.12 – Isobar maps for three positions of an incomplete fault

For the fault B case, the early time and the intermediate time are influenced but the late time get very close to the classic circle of an Infinite Acting Radial Flow.

In the case C, the early and intermediate time are in infinite acting radial flow and the fault is hardly influencing the late time isobar lines.

8.I Conductive faults

Conductive faults can be modeled both numerically and analytically. In this section we will use the analytical model which is part of Saphir external models to illustrate its use and pressure response. We will use the numerical model for its display facilities.

This model solves for the pressure behavior at a well near a non-intersecting finite conductivity fault or fracture. The solution includes an altered zone around the fault with the possibility to add skin across it. The reservoir properties on either side of the fault can different.

3D schematic of the model:

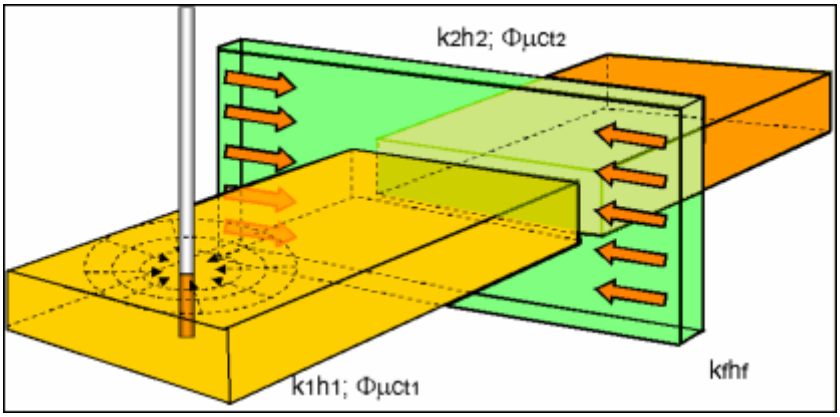


Fig. 8.I.1 – Conductive fault model schematic

The model needs the following parameters:

kh and skin of the well side, the distance to the fault or the fracture, the conductivity and skin of the same and the mobility, M and diffusivity, D ratios defined as the ratio of the well side parameters divided by the parameters of the reservoir on the other side of the fault or fracture:

Mobility ratio: $$M = \frac{(k/\mu)_{well\ side}}{(k/\mu)_{other\ side}}$$

Diffusivity ratio: $$D = \frac{(k/\Phi\mu c_t)_{well\ side}}{(k/\Phi\mu c_t)_{other\ side}}$$

8.I.1 Behavior

After wellbore storage, the next flow regime would be, typically, IARF reflecting the permeability and skin of the reservoir around the well. This would be followed by the influence of the fault seen as an increase in mobility, then by a linear flow corresponding to the drainage of the reservoir by a linear source. When the investigated reservoir area is large enough and the fracture flow is not anymore dominating a final IARF can be observed

An isobar map, generated after a certain of production can help to visualize the type of behavior due to a conductive fault.

Each color line corresponds to a certain pressure value but it can also be interpreted as an investigation or influence zone at a certain time.

The blue represents the early time influence zone, the green to yellow the intermediate time and the red the late time.

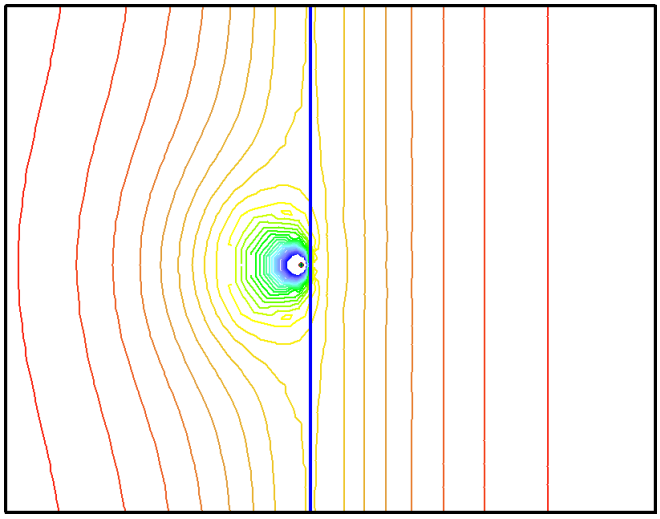


Fig. 8.I.2 – Isobar map conductive fault

We can observe in blue and green the early IARF before any fault effect.

At early time, on the well side, the radial flow is influenced by the uniform pressure imposed by the conductive fault while, that create the derivative dip.

On the other side of the fault, the parallel isobar lines characterize a linear flow which dominates at late time, until a larger zone is interested and a final radial flow is established.

8.I.2 Semilog analysis

The semilog plot can be used, when the fault is far enough and when the IARF can be observed before the conductive fault effect. The challenge is to detect the time interval where to draw the semilog straight line, it is recommended to determine it from the loglog derivative.

This limitation makes the semilog plot of not much interest in this case:

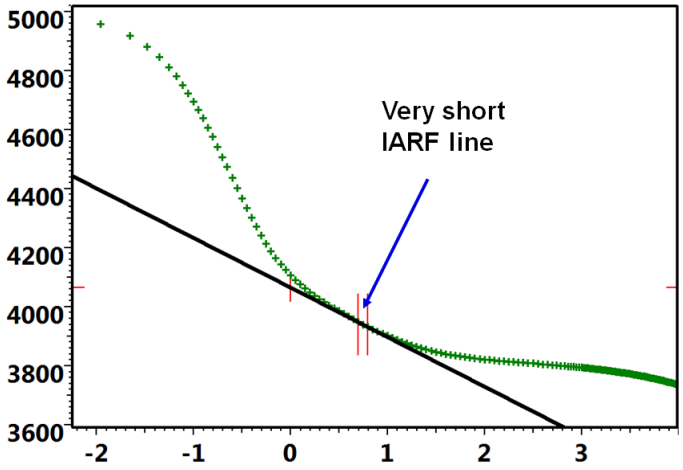


Fig. 8.I.3 – MDH plot for a conductive fault behavior

8.I.3 Loglog analysis

A first derivative stabilization corresponding to the initial IARF in the reservoir around the well can be observed before the fault effect. Then the derivative drops until bilinear/linear or linear flow develops in the fault (fracture) and the derivative follows a positive ¼ / ½ or ½ slope. The ¼ slope, or bilinear flow, is evidence of finite conductivity in the fault or the fracture, the ½ slope (linear flow) alone is a sign of infinite conductivity.

Finally a homogeneous global behavior should be observed with IARF stabilization at a level governed by the mobility ratio M.

The figure below illustrates the effect of the distance to a low conductivity fault or fracture (100 mDft). It can be seen that the transition through the fault ends with a ¼ slope (bilinear flow) before reaching the second IARF stabilization (M and D= 1). When the fault is far enough it can be observed an IARF on the well side before the fault effect.

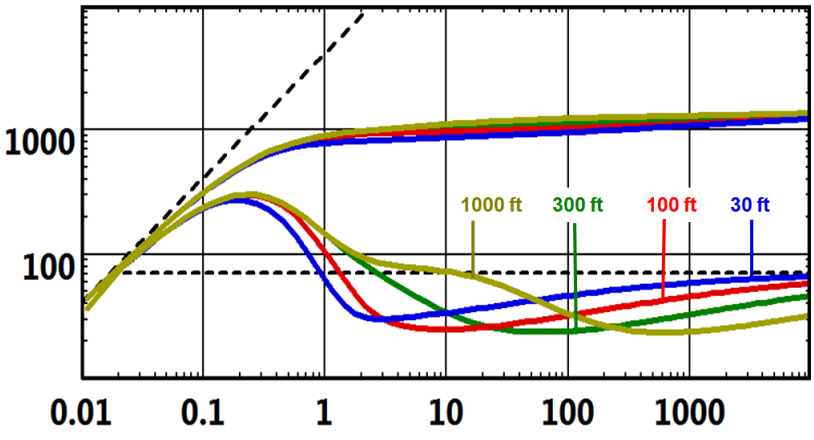


Fig. 8.I.4 – Effect of distance to fault

The figure below illustrates the effect of the distance to a high conductive fault (100000 mDft). In this case the transition through the fault is much deeper and ends with a ½ slope (linear flow) before reaching the second IARF stabilization (M and D= 1).

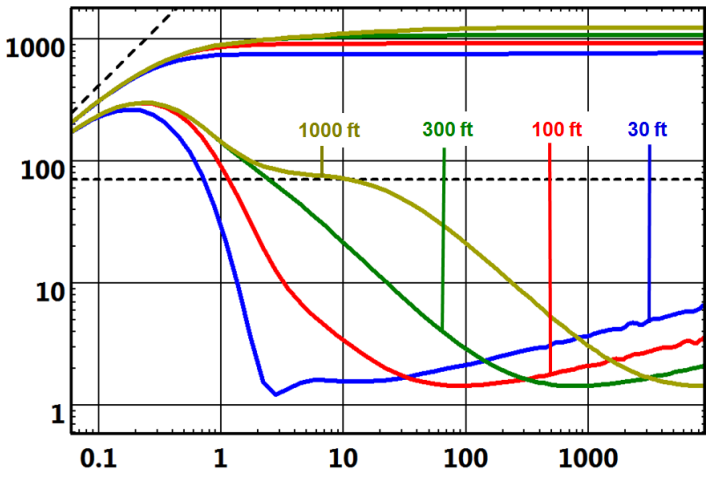


Fig. 8.I.5 – Effect of distance to fault

The figure below illustrates the effect of a change in the fault skin. The damage at the fault creates a hump on the derivative and the transition through the fault happens later as the skin increases. The distance to the fault is 1000 ft and the fault conductivity is 1.e5 mDft, M and D=1.

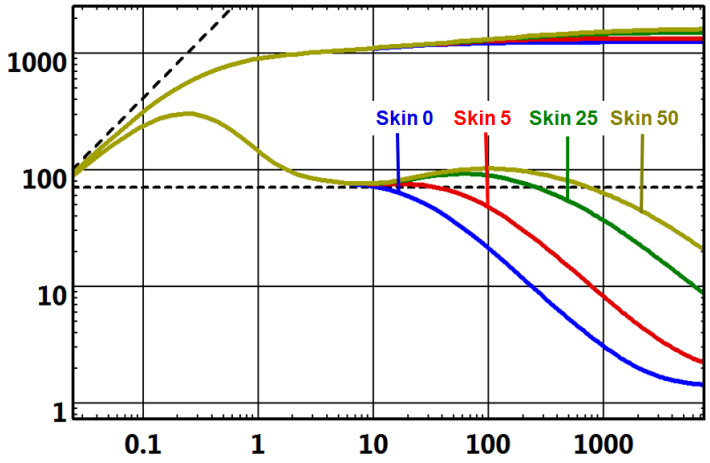


Fig. 8.I.6 – Effects fault skin

The below figure shows the influence of a change in mobility. The conductive fault has a permeability thickness product of 1000 mDft, the distance to the fault is 1000 ft, the fault skin is zero and the permeability thickness of the well side of the reservoir is 1000 mDft.

What is important to note here is that when the mobility increases the tell-tale bilinear and linear flow is largely masked.

The mobility ratio changes the level of the second level of IARF (final stabilization = first stabilization x 2/ (1+1/ M)).

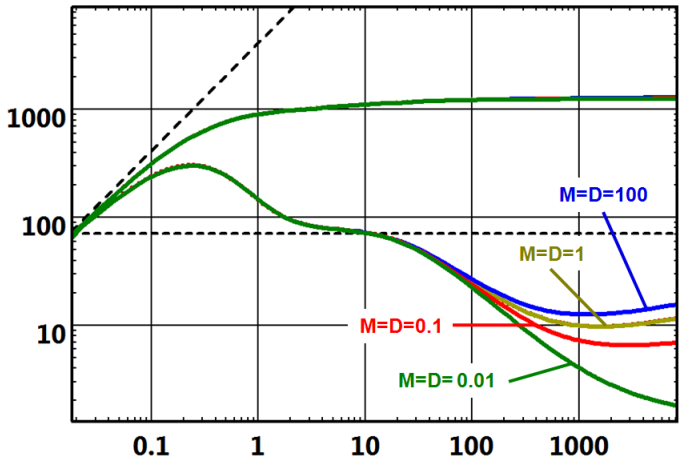


Fig. 8.I.7 – Effects of mobility changes

Note that when M tends to infinity (ie with no 'other side of the fault' conductivity) the second stabilization is twice that of the first IARF level; equivalent to a single sealing fault. Equally, when M tends to zero, the response is equivalent to a constant pressure fault. This is in line with the response of the linear composite reservoir model. However, for intermediate increases and decreases in mobility the conductive fault model retains the diagnostic sign of the presence of the fault or the fracture rather than the linear interface assumption used in the linear composite reservoir model. The figure below illustrates this.

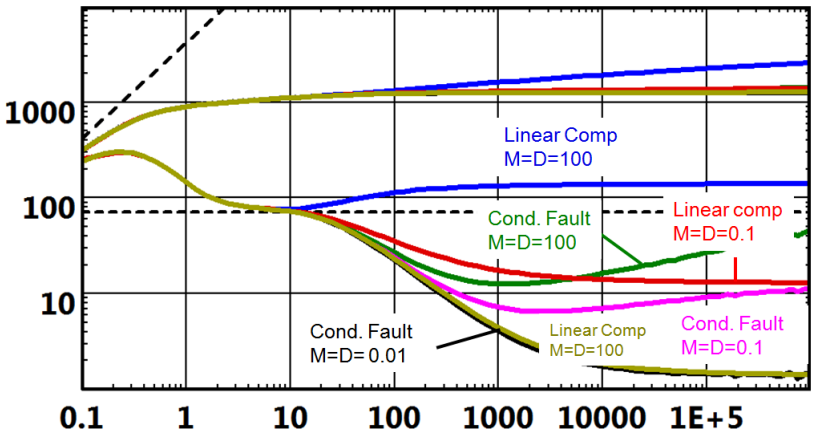


Fig. 8.I.8 – Comparison Conductive Fault and Linear Composite

8.J Combination with other reservoir and well models

All boundary models described above have been presented assuming a fully penetrating vertical well, with constant wellbore storage and skin, in a homogeneous reservoir. In real life, we will have to combine a wellbore, a well, a reservoir and boundary models, each of them having its own signature.

In an ideal world, one behavior will occur after the other, and logic dictates that we see first wellbore effects, then the well geometry, then IARF and/or reservoir heterogeneities, and then finally boundary effects. The figure below shows such a simulated combination. In this case, discriminating all behaviors would require six logarithmic cycles, provided that the parameters are such that one behavior starts exactly where the previous ends. In the case shown below, with IARF occurring after one hour, this means a test duration of 10,000 hours. So in real life this will not happen, and these different behaviors will often occur at the same time. Sometimes, and to make matters worse, they will not occur in their logical order, and a reservoir heterogeneity may, for instance, occur after the first boundary is seen.

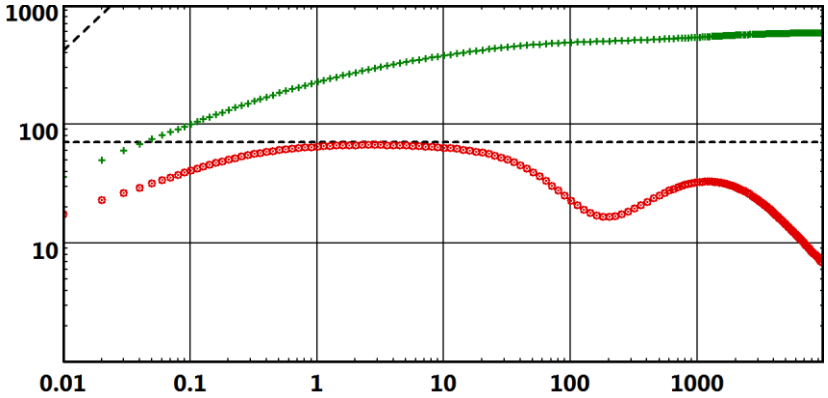


Fig. 8.J.1 – Fractured well in a double-porosity reservoir and a constant pressure linear boundary analytical simulation over six log cycles

The name of the game is common sense. In general, these behaviors will aggregate, or one will override the other. When the engineer has a good knowledge of how individual features will show up on the derivative, he/she will easily figure out, qualitatively at least, what the resulting combination may look like. But there may be 'numerical' surprises, and only the generation of the model will confirm this guess.

The above is a general comment. What is specific to boundaries is that they occur at late time and are numerically even more sensitive to errors and residual behaviors.

8.K Assessing boundary effects

In the previous sections we have described how the different boundary models will behave. Assuming that the boundary is the last behavior in the derivative response, the principle will be first to match the early and middle time behavior with the right wellbore / well / reservoir model, or alternatively in the situation where the data appears to be of poor quality, figure out why we cannot match the early time and at least get a fair estimate of the mobility, i.e. the pressure match, in order to gain a realistic relationship between the boundary distance and the time at which it is detected.

If this is done, the initial estimate of the boundary parameters will be relatively easy. The mobility and the identification of the time of deviation from IARF will give the distance(s), and various specialized analyses or interactive pick options will allow us to assess the other parameters. For example the angle between intersecting faults will be obtained by indicating the level of the second derivative stabilization by the click of the mouse.

After the initial model generation, and assuming that we think this is the right model, the principle will be to adjust the boundary parameters. This will be done manually and/or by nonlinear regression.

Manual improvements will be very effective to correct the initial gross mistakes, as the rules of thumb are pretty straightforward. For the distances, the basic rule is that for a given mobility the governing group is t/r^2. In other words, if we see that the model is showing the boundary behavior at the 'wrong' time, multiplying the boundary distance by two will multiply the time of occurrence by four. More realistically, for small multipliers $(1+\xi)$ where ξ is small, it means we get a time of occurrence ξ% longer, we will need to set a boundary distance $(\xi/2)$% further away. There are also software related 'tricks' that correct the boundary distance by sliding the match, but that will not be detailed here.

Using nonlinear regression to improve the boundary parameters will require a little more caution. Because the boundary effects are a late time behavior identified on a relatively small pressure change, the match will be very sensitive if the early time of the response has not been correctly matched. If one runs an optimization on all parameters; kh, skin and boundary distance, starting from an initial model where the infinite acting part is not matched, typically, the boundary distance will go bananas. Advanced software features, such as genetic algorithms, are improving the process, but these are not really needed if the engineer knows what he/she is doing.

The recommended procedure is to get a match first on the early part of the response. This will be done, for example, using an infinite model and optimizing all parameters on the part of the response that is not influenced by the boundary effect. Then, the boundary will be added, and generally the remaining work will be to regress on the boundary parameters, keeping the other parameters, especially the mobility, constant. Sometimes, adding the boundary will have a small effect on the match, and it might be necessary to allow the mobility to vary, or make a small correction to the mobility before running the regression.

The above is only valid if a good early time match is possible. Sometimes it will not be, because early time data is messy, or the combination of wellbore / well / reservoir / boundary models is just not available. It will still be possible to use optimization on the boundary distance if the following rule is followed. 'However nasty your early time match, the important thing is that the simulated pressure, at the time where the derivative deviates from IARF, is spot on'. This can be achieved by making a first optimization on skin only, the target being this particular point in time from which IARF will deviate. Then, if we keep all parameters not related to boundary, including the skin, constant, and if optimization is only performed on points after IARF, this will work.

Last but not least, there is information on boundary effects that may be obtained beyond the signature of the build-up derivative. This was already shown in section H, where the simulation match could discriminate between a no-flow and a constant pressure boundary. This is what we call the 'missing boundary'. If we consider a closed system, we may only assess one or two distances from the build-up response. The principle then is to add the missing boundaries at a distance large enough to be unnoticed in the build-up, and then run a nonlinear regression on the total production history, keeping all parameters that ensure the quality of the build-up match constant, in order to improve the objective function. This may not always work, but if there has been depletion during the production, matching the initial pressure will at least provide a rough estimate of the reservoir size, even if individual boundaries are not calculated.

8.L Radius of investigation vs minimum reserves

One of the most abused results in well test interpretation is the radius of investigation. By itself it is a harmless relation between time and distance for a given mobility. The most common definition of the radius of investigation is linked to the circular area where flow would reach PSS at a given time:

$$r_D = 0.029\sqrt{\frac{kt}{\Phi\mu c_t}}$$

This definition is harmless as long as it is not used. But the trouble starts when somebody else with no well test background takes this number, calculates the corresponding pore volume, assigns a recovery factor and uses this number to assess minimum proven reserves. This is, of course, completely erroneous, and for several reasons:

1. This definition assumes that the flow is radial homogeneous. This definition will lose its meaning when we are confronted by complex configurations that might include fractures, horizontal wells, lateral boundaries, composite zones and heterogeneous formations. So we should speak about area of investigation, or better still, the volume of investigation.
2. This definition does not take into account the gauge resolution and the overall quality and noise of the pressure response, which may or may not allow us to detect the boundary effect.
3. What time are we talking about? In the case of a build-up, is it the duration of the shut-in, or the duration of the test? After all, as shown in the previous section, it is possible to get some information from the history match.

   It is indeed possible to obtain a decent estimation of minimum reserves, but certainly not using the radius of investigation. This can be achieved using boundary models as follows:

1. If you have diagnosed a closed system and managed to identify all limits, the problem is over, and the reserve estimates will correspond to the pore volume of your reservoir times a recovery factor.
2. If you have not diagnosed a closed system, and even if you have only used an infinite model, the principle is to find the minimum size of the reservoir that is consistent with your well test response. If you have diagnosed an infinite reservoir you will take the same model and start with an arbitrarily large circular or square reservoir. If you have identified some, but not all, boundaries you will complement and close the system with additional, arbitrarily far boundaries. Then, in both cases, you shrink the reservoir model as much as you can, to get to a point where, if the reservoir was smaller, you would have detected and diagnosed the additional boundaries during the test. This is of course a much more subjective approach than a simple equation, but, from an engineering point of view, it is the only one that makes sense.

8.M Superposition effects

8.M.1 Can we see a fault in a build-up and not in the drawdown?

Theoretically, nothing prevents us from detecting the reflection of the pressure signal of the boundary after the well was shut-in, even if this was not detected during the drawdown. In practice, it is a matter of the amplitude of the signal, resolution of the gauges and background noise. More generally, if we consider a given production, the shut-in will be interpretable as long as the amplitude of the residual pressure signal is within the gauge capabilities, and the background noise does not jam this residual signal. Under these conditions, the initial duration of the production is not an absolute limit for the duration of an interpretable build-up. So it is possible, and routinely happens that we investigate during the build-up, a larger area than what was seen during the drawdown. The rules of thumb relating the production time and shut-in time were set at a time when the quality of the measurements was much lower. That said, they are not so bad, and should be overridden only after a careful test design.

There is even an extreme behavior that may be seen under exceptional conditions. In the case of a short production time, as mentioned in a previous paragraph, the reflection of the production information on the boundary may not have reached the boundary before the well was shut-in. So this information will reach the well after the shut-in, followed by the reflection of the shut-in itself. When the reflection of the production reaches the well, the derivative will go down, then back up when the shut-in information bounces back. The derivative will then look as below. It requires an exceptionally good signal and gauge, but it is seen from time to time. The presence of a slight valley in the derivative should not be, of course, systematically interpreted as such an effect, as the amplitude of the pressure signal is very small. But, in the case of a short production time, if the model also exhibits such transition behavior, this will be the explanation, and actually a sign of very good data quality.

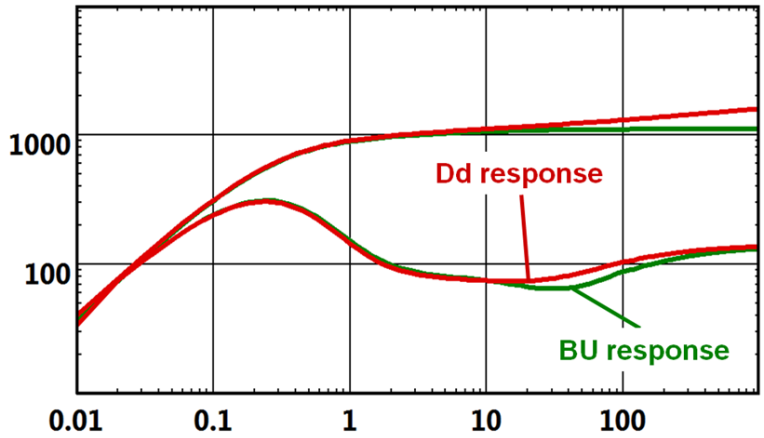


Fig. 8.M.1 – Loglog response for a sealing fault
Drawdown response vs. shut-in for a short production time

8.M.2 Superposition effect consequence on the boundaries diagnosis

The above signalled effect can be observed in case of multiple limits at different distances and therefore different times. i.e. A nearby fault can be observed during the production while a further limit could not have been detected but its effect will appear during the build up.

It results that the multiple limit behaviour observed on a build up can be quite different from the expected behaviour that was described for a production period.

It is a reason why the 'typical derivative behaviour' catalogs have a limited interest as long as they represent drawdown behaviour, excluding any superposition effects and we usually interpret build data.

The figures below show not only how the build up response can differ from the drawdown response but also how the same short production duration can have a different influence on different intersecting faults geometry.

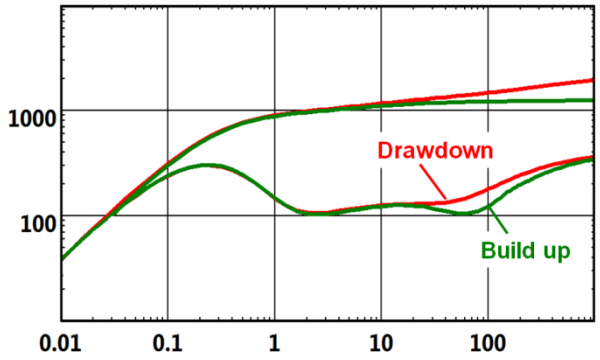


Fig. 8.M.2 – BU response after a short production on intersecting faults

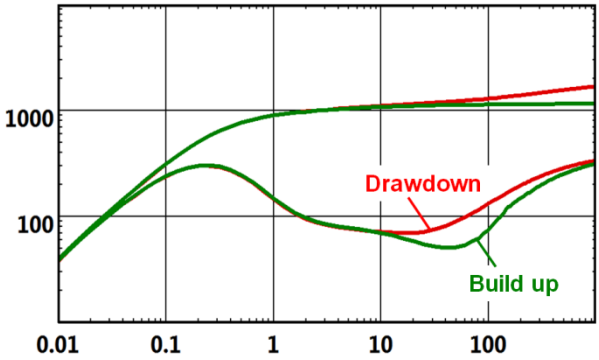


Fig. 8.M.3 – BU response after the same short production on different geometry intersecting faults

The same is observed in case of parallel faults: even the position of the half unit slope differs on the build up, that limits the quantitative result validity of the conventional '1/2 unit slope straight line' drawn on the derivative.

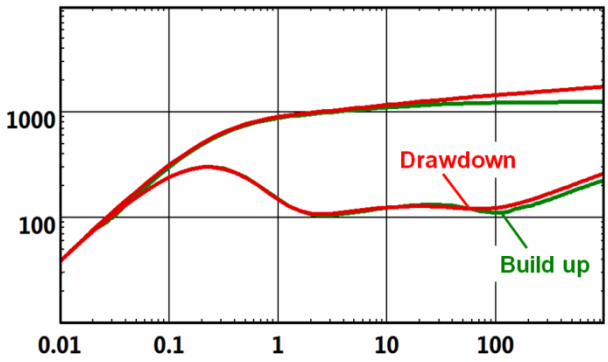


Fig. 8.M.4 – BU response after a short production on parallel faults

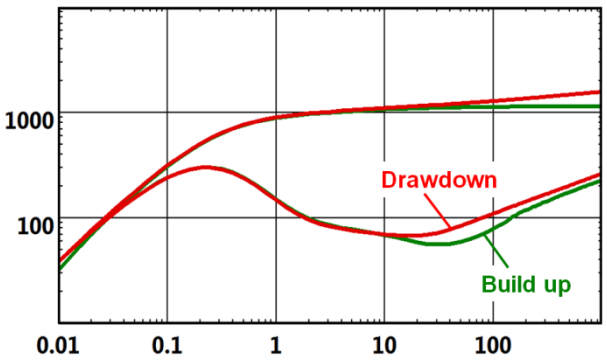


Fig. 8.M.5 – BU response after the same short production on different parallel faults

When dealing with a closed system the superposition and the build up effects cumulate and they become more crucial.

In the figure below we compare the drawdown derivative shape with two build ups after a long and a short production period.

It was already known that the drawdown and build up behaviour are systematically different in case of Pseudo Steady State but it also shows clearly that the two build up derivatives are also different and could lead to misinterpretation.

The long production duration build up derivative (in green) dips at the P.S.S.

The short production duration build up derivative (in blue) dips also but additionally it is subject to a deviation at intermediate time.

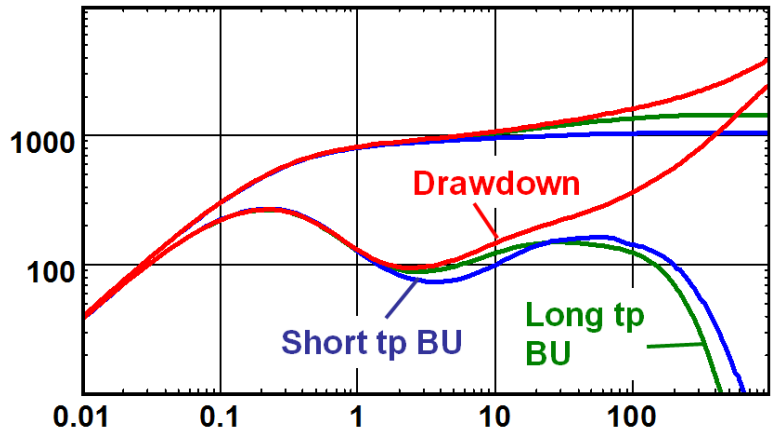


Fig. 8.M.6 – BU response after short and a long production on the same closed system

The diagnosis of multiple boundaries on build up data is not as straight forward as it appears if we only rely on the drawdown typical derivative behavior. The shape in highly influenced by the previous production history and only a model derivative taking into account the various superposition effects must be used for a final match with the data.

8.M.3 Conclusion

The only pure conventional boundaries effect can be observed on the production period data, assuming a constant production rate but the production period data are usually noisy due to rate instabilities.

The build up data, supposed to be more stable, are therefore classically used for analysis purpose, and their sensitivity to the superposition effect makes the diagnosis more difficult, it requires more experience and impose the used of software based on the model matching method.

A simpler answer could be brought if the build up data, victims of the superposition, could be 'de-superposed' in order to appear as a drawdown response to a constant rate, this is called the Deconvolution method and it will be developed in the next chapter.

8.N Typical errors diagnosing a boundary effect

Boundary effects are typically diagnosed from a derivative trend at the end of a build-up, when the pressure approaches stabilization. The derivative is a magnifying glass and a lot of importance is given to a signal of very small amplitude. The derivative may pick up a signal that has nothing to do with boundaries, or errors somewhere else may have an effect on the pressure, or on the superposition time from which the derivative is calculated. This may result in the improper diagnostic of a boundary effect. We will list below the most common mistakes.

8.N.1 Incorrect production history

This is certainly the most commonly known problem, but it is still, also, the main source of misinterpretations. The derivative calculation corrects the pressure scale in order to account for the details of the well production history. If this history is taken into account in the superposition time, the IARF behavior will result in a stabilized derivative. Conversely, if some relevant rates are not taken into account, or wrongly estimated, this will result in an artificial late-time trend in the derivative. Considering the wide range of models and behaviors described above, there will be no difficulty in finding several boundary models to match this trend.

In the figure below, on the left, a partial production history (last 60 hours well test data) was used to generate the loglog plot of a field data set. The derivative exhibits a clear 'boundary effect': it is actually the result of a false superposition calculation with a too short production time.

The right side plot shows the result when using the complete production history (adding 440 hours of previous production): no more boundary effect can be too 'easily' diagnosed.

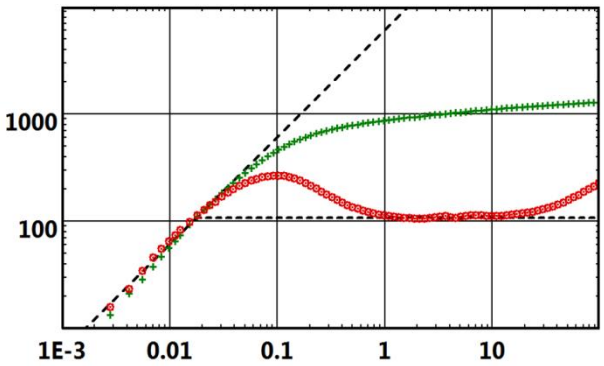


Fig. 8.N.1 – Loglog field data response with IARF using incomplete production duration

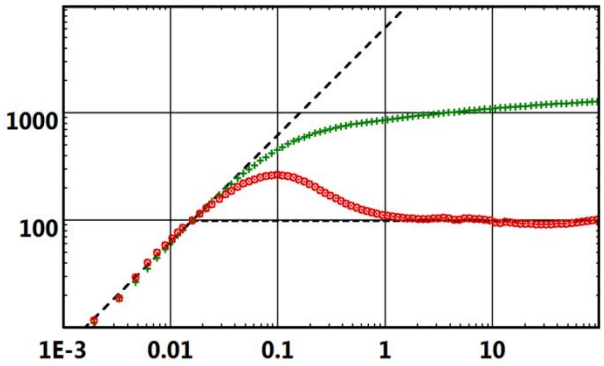


Fig. 8.N.2 – Loglog field data response with correct production history

Using a false too long production history (1000 hours more) can also have an incidence on the derivative shape. The resulting curve, below, does not really show a boundary effect, but the apparent mobility will be over-estimated. In other cases the response will display an artificial constant pressure boundary.

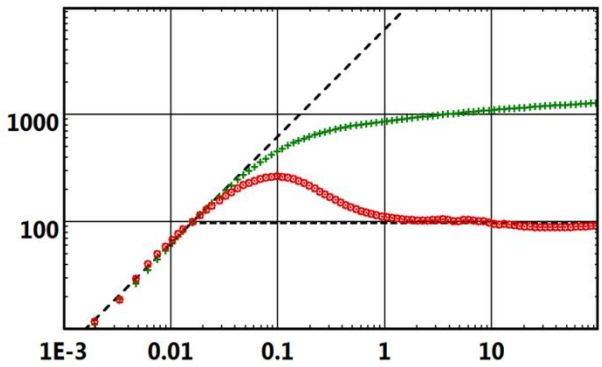


Fig. 8.N.3 – Loglog field data response
With over-estimated production time

Generally speaking, this rule of thumb works: when you under-estimate your production time you under-estimate your reservoir, i.e. your kh will be too low or you will see a no-flow boundary that does not exist. When you over-estimate your production your over-estimate your reservoir, i.e. your kh is too high or you will see a constant pressure boundary that does not exist.

8.N.2 End effect in the derivative calculation

The derivative, which is the slope of the semilog plot displayed on the loglog plot, is numerically calculated from the data. At a given point, the derivative generally comes from a 3-point central calculation process. The central point is the considered pressure point, the choice of the left and right points will depend on the smoothing.

Most algorithms take a superposition time window around the considered point, the smoothing being the distance between the point and each window limit. The program then selects, to the left and the right, the first points outside the window, and with these two additional points, makes a 3-point central calculation of the slope.

In the middle of the pressure response there is no problem. But, towards the end of the response the last point will be systematically used as the right point in the derivative calculations of all the data within the smoothing window. If this last point is wrong, and it may not even be displayed on the loglog plot, it will induce a trend in the smoothing that may be confused with a boundary effect.

Even if the way to calculate the derivative is different, an incorrect end point will generally create this sort of error.

The best way to avoid this problem is to properly set and synchronize the rate and pressure histories. But if this is overlooked, one way to check this sort of problem is to change the derivative smoothing. If the late time, boundary looking behavior changes with the smoothing, then the engineer will have to look for a possible erroneous point.

8.N.3 Gauge drift

If a gauge is drifting, it will add an artificial linear function of time to the pressure response, systematically creating a pseudo-boundary effect as soon as the slope of this drift becomes non-negligible compared to the effective change of pressure. The drift will affect the whole pressure response, but will only affect the shape of the derivative at the end of the response, hence creating this apparent boundary response.

When several gauges are run it is easy to identify drifting gauges if proper Quality Control is performed. If only one gauge is run, then one should select a type of gauge that will be unlikely to drift within the expected test duration.

The loglog plot below shows a comparison between two gauges used for the same test. Before deciding which gauge was correct, it was necessary to make a basic calibration check (i.e. at atmospheric pressure). In this case a 9 psi indicated pressure increase was found on the 'guilty' gauge, between before and after the measure.

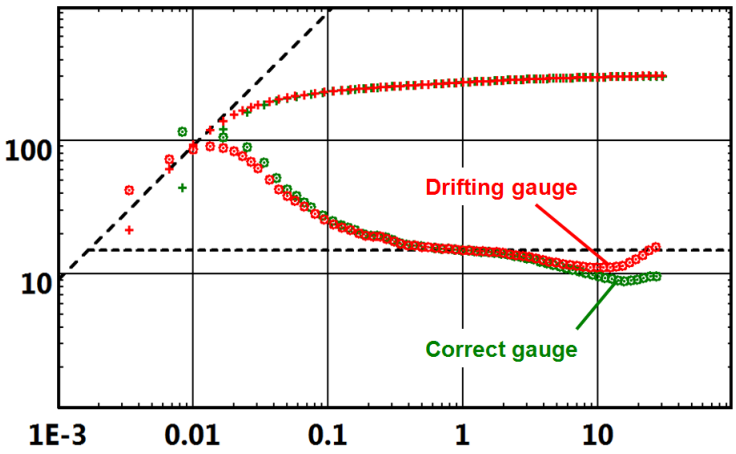


Fig. 8.N.4 – Gauge drift effect on the derivative shape

8.N.4 Reservoir trends

Reservoir trends will have the same effect as a drift. A producing reservoir may have a trend. For example, if an injection campaign was started recently the trend may be upward. Conversely the reservoir may have a depleting trend. When we run a well test we are applying a disturbance and observe the reaction to this disturbance. As the reservoir trend has nothing to do with this disturbance, it is perfectly justified to correct the pressure response by the observed trend. The principle is to run the gauge and monitor the pressure response for some time before starting anything related to the well test. The slope of this trend may then be used to correct the pressure data. We will then not interpret the pressure response but the corrected pressure, i.e. the pressure that would be, hopefully, observed if there was no reservoir trend.

8.N.5 Interference from other wells

If boundary effects can be modeled using virtual image wells, one can guess that the interference of real wells may induce virtual boundaries. The best example of a virtual boundary is the limit of the drainage area.

In a producing well, when you shut a well in and have not done anything recently on the nearby wells, the residual transient signal due to these wells will be negligible for the duration of the test. But for long term testing, or if the production of the nearby wells has changed, they may induce false boundary effects.

The author recalls an interpretation he had to do on a producing well on which a simple build-up survey was run. The response showed a constant pressure boundary that was making absolutely no sense. After (too) much time the author discovered that, in order to assure constant production, the production of the closest well had been temporarily increased simultaneously with the shut-in, hence creating an opposite image well, hence creating a ghost boundary at half the distance between the two wells.

When the engineer is in doubt about the influence of nearby wells, the best thing is to run a first interpretation without the wells, then run a second model adding the interference of nearby wells. If the difference between the two models is negligible, the engineer may return to the simpler interpretation and ignore the effect of interference.

That can be illustrated by a field example.

Below left is the pressure response acquired during the final build up of a well test, it can be adjusted with an analytical multilayer model. But if we compare this response with the one given during the previous build up it reveals an inconsistency see on right side plot.

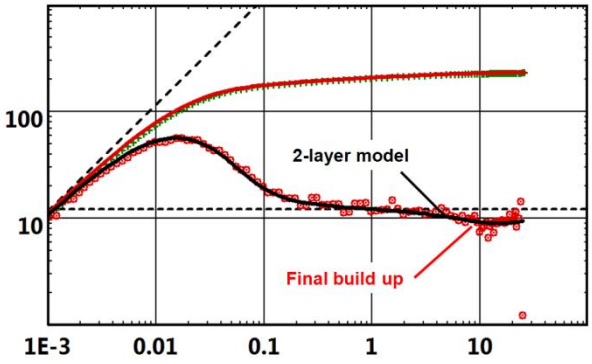


Fig. 8.N.5 – Build up raw data matched with a 2-layer model

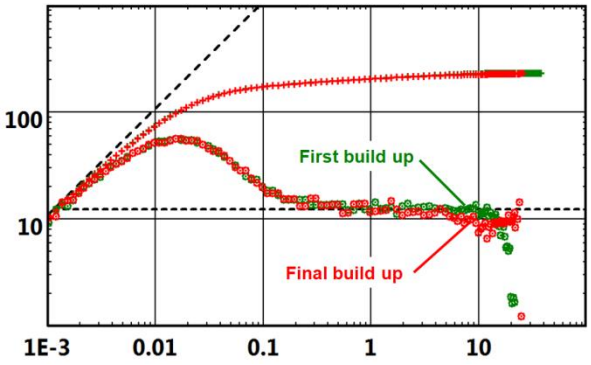


Fig. 8.N.6 – Comparison between two build ups Loglog plot response

In fact a nearby well (2200 ft distance) was opened for 50 hours and then closed during this test, creating interferences. Another well test performed in quiet conditions no other well was opened or closed but just left in their status reveals the truth, an homogeneous behavior:

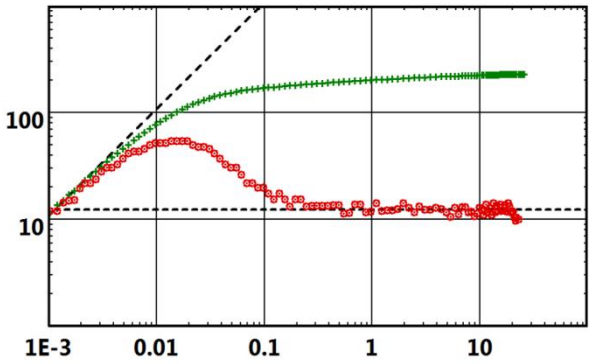


Fig. 8.N.7 – Pure build up response without any other well interference

8.O Deconvolution

As already mentioned above, the analyses are generally performed on the build up data for acquisition and stability reasons. Unfortunately these periods are limited in time and most of the information is contained in the 'noisy' production periods. Another fact, in addition to the short duration the build up data are subject to the superposition effect influences and the boundaries diagnosis become more difficult.

One solution is to get rid of the superposition effect and to take advantage of the long duration of the production periods. This solution passes through the technique called deconvolution: in few words it transform a limited duration build up into a drawdown pressure response with a duration equal to the considered production history, consequently, it makes possible to detect boundary effects in a test signal when the individual flow period was too short to detect said boundaries.

This approach is covered in detail in Chapter PTA.

A fied example illustrates the approach below.

We get a complete rate history but the pressure history data is poor and only the detailed acquisition for the last build allows an analysis:

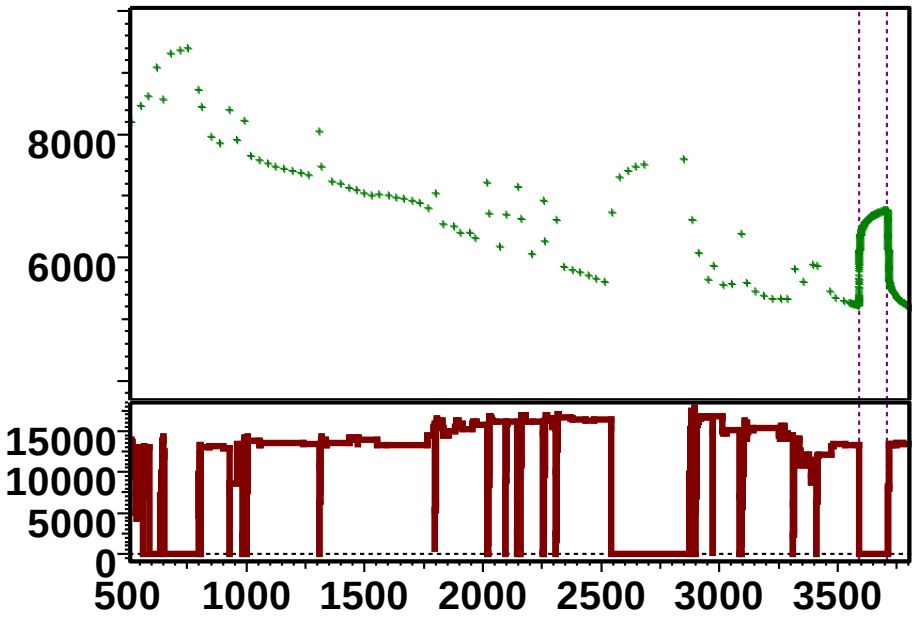


Fig. 8.O.1 – Production and rate history

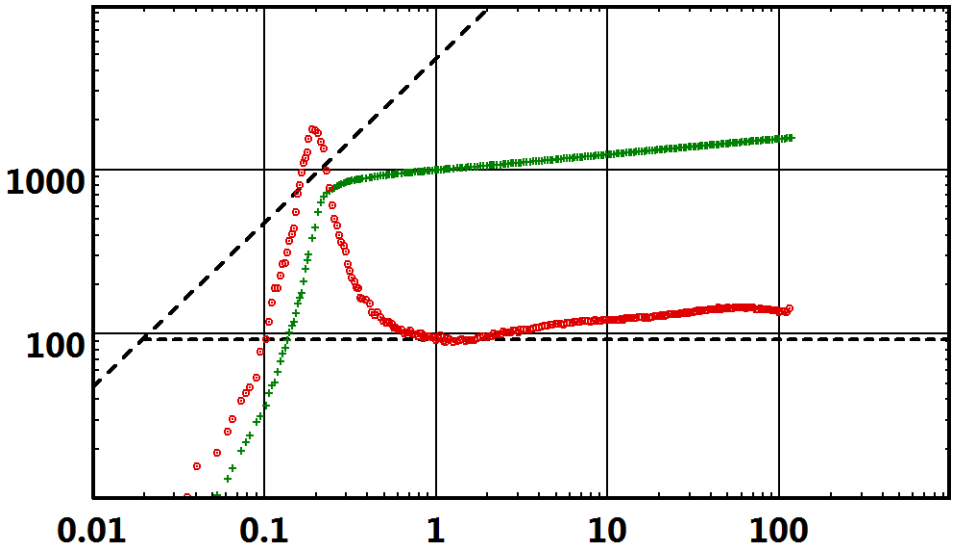


Fig. 8.O.2 – Single build up loglog plot

Although the build up data have a good quality, its relatively short duration (110 hours) limits the depth of the analysis to the observed boundaries.

If we use the build up pressure data and the complete previous production history for a deconvolution we get the loglog plot shown below:

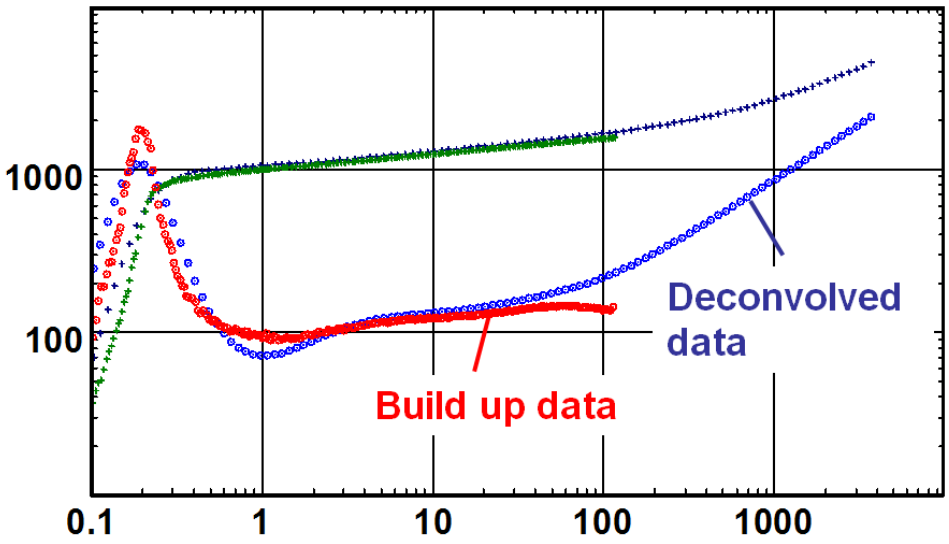


Fig. 8.O.3 – Loglog plot of build up and deconvolved data

Advantages:

- The deconvolved data exhibit the drawdown behavior shape.
- It makes the diagnosis easier, (i.e. making easy the distinction between closed system and constant pressure limit).
- Its duration corresponds to the total history length (3800 hours vs 110 hours).
- Consequently the investigation radius is increased (here it is multiplied by 5.8).

8.P Conclusion

Boundary effects are not systematically detected during a well test, but the identification of boundaries is one of the most important results of Pressure Transient Analysis. Such identification provides valuable information on proven volumes and reservoir geometry.

Even the lack of boundary effects is information by itself. The smallest closed system that can reproduce the infinite looking, or only partially sealing, response will produce a much more reliable estimate of the minimum reservoir size; far more reliable than using an equation of 'radius of investigation'.

The limits of the well drainage area may be reservoir boundaries or 'virtual' boundaries coming from the production equilibrium with other wells. They may be encountered in the producing phase of very long tests, or when using permanent downhole gauge (PDG) data. Rate Tansient Analysis is also a good candidate to interpret this data.

When analyzing a build-up, boundaries are generally detected at the end of the test by identifying deviations of the Bourdet derivative from Infinite Acting Radial Flow. A significant deviation of the derivative may correspond to a very small deviation of the original pressure signal. Numerous different causes, unrelated to reservoir limits, may incorrectly mimic the response of a boundary effect: for example, incorrect rate history, gauge drift, reservoir trends and interference from other wells.

Before rushing into the diagnostic of a reservoir limit, the pressure transient analyst must to check that there is no other explanation. The sensitivity to the well production history, and its integration in the calculation of the Bourdet derivative, is a critical point to consider. The boundary distances must also be compatible with prior knowledge of the reservoir. Talking to the geologist is a key to gaining confidence in the boundary diagnostic.

9 – PVT

OA – OH – OSF – DV - VA

9.A Introduction

Pressure-**V**olume-**T**emperature, PVT, is the study of the physical behavior of oilfield hydrocarbon systems. Information on fluid properties such as volumes and phases, and how they change with temperature and pressure, is essential to many aspects of Dynamic Data Analysis.

The need for valid PVT data cannot be over-stressed. Reservoir fluid sampling should be a major objective of any test, particularly during drill-stem testing, as PVT analysis should be performed as early as possible in the life of the field. Once production has started, it may never again be possible to obtain a sample of the original reservoir fluid, which may be continually changing thereafter.

For the PTA or RTA interpretation engineer, PVT will be used to:

- Assess which fluid phases are present at sandface and at surface
- Calculate fluid phase equilibrium and phase compressibility to correct produced volumes from surface to sandface
- Calculate fluid phase equilibrium and phase gravities to correct pressures to datum
- Calculate fluid viscosity to get from mobility to permeability
- Calculate pseudopressures and pseudotime to linearize the equations in order to use analytical models
- Input PVT properties in a numerical model

The present book is not aimed at teaching PVT, which is an ‘art’ in itself. However the validity of PTA / RTA diagnostics and results is largely dependent on the knowledge of the fluid PVT. It is difficult to assess where we should start this subject. So, we will assume nothing and start from scratch, with our humble apologies to those who have read this a hundred times before.

9.B Phase equilibrium

9.B.1 Single-component fluids

Hydrocarbon fluids can exist in two or more separate phases, typically gaseous and liquid, which have different properties. Water may also be present as a separate phase in the reservoir. Reservoir types are classified by their phase behavior, which depends upon the composition, the pressure and temperature. It is the phase behavior that determines the economic recovery in most cases, that makes fluid sampling difficult, and that can sometimes complicate Dynamic Data Analysis.

The simplest form of phase behavior is for a pure substance, such as methane or water, and it can be represented on a simple 2-dimensional graph of pressure versus temperature in the figure below:

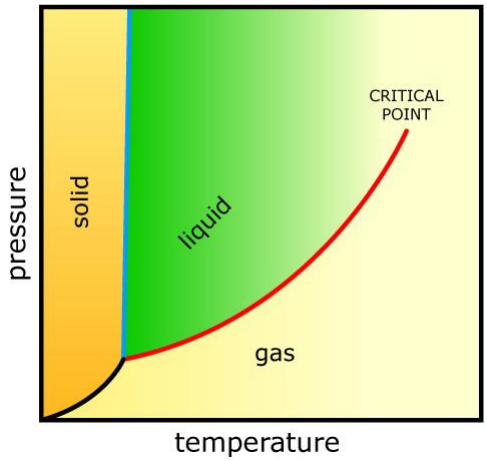


Fig. 9.B.1 – Pure component P-T behavior

The boundary lines between the solid, liquid and gas phases represent values of pressure and temperature at which two phases can exist in equilibrium. Crossing the liquid-gas curve from left to right at constant pressure, by increasing the temperature, corresponds to heating the liquid to its boiling point and boiling it off as gas or vapor.

If the gas is then cooled in the reverse process, it will condense at the same temperature. There is no upper limit to the solid-liquid equilibrium line, but the liquid-gas line or vapor pressure curve, terminates at the **critical point**. At pressures or temperatures above this point only one phase can exist, referred to only as fluid because it has properties similar to both gas and liquid close to the critical point.

For a pure component, the typical Pressure-Volume behavior at constant temperature is shown above. Starting in a single-phase liquid state, the volume is increased which causes a sharp pressure reduction due the low liquid compressibility. The point at which the first gas bubble appears is the **bubble point**. When the volume is further increased the pressure remains the same until the last drop of liquid disappears; this is the **dew point**. Past that point, only gas exists and as the volume increases, the pressure is reduced. By comparison not as quickly as with the single phase liquid, because of the higher compressibility. The following right figure brings together the P-V and P-T behaviors into a 3-dimensional surface.

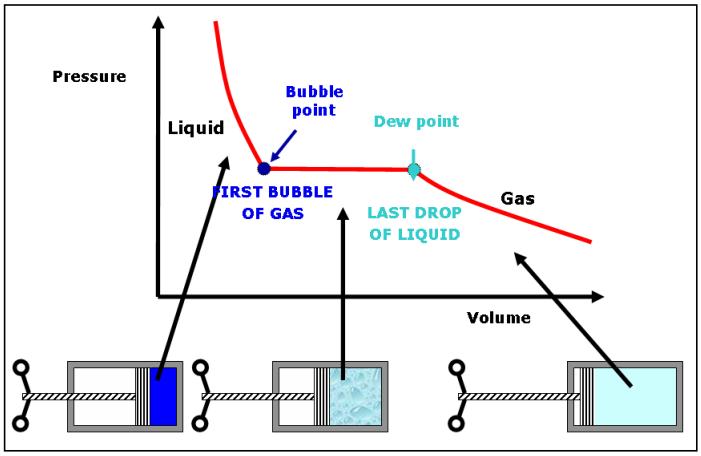


Fig. 9.B.2 – Single component P-V behavior

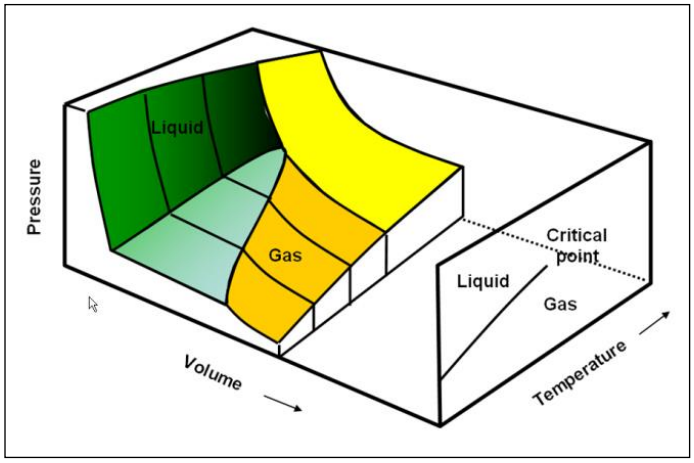


Fig. 9.B.3 – Single component P-V-T behavior

9.B.2 Multi-component fluids

As soon as a mixture of at least two components is considered, phase boundaries become areas rather than lines, due to the combination of the physical properties of two components with different compositions.

Instead of a single vapor pressure curve there are separate lines to represent the bubble points and dew points of the mixture. The two-phase boundary of the system can extend beyond the critical point, i.e. above the critical pressure or the critical temperature. The critical point lies at the intersection of the bubble and dew-point curves, and no longer serves to identify where the single phase region begins.

With most reservoir systems it is normal to concentrate only on the liquid-gas equilibrium behavior, although some hydrocarbons do exhibit solid phases, such as wax precipitation (solid-liquid) and gas hydrate formation (solid-gas). Natural hydrocarbon fluids can contain hundreds of different pure substances, and the multiple interactions may lead to a great number of phase loops where liquid and gas phases can exist in equilibrium over a wide range of pressures and temperatures.

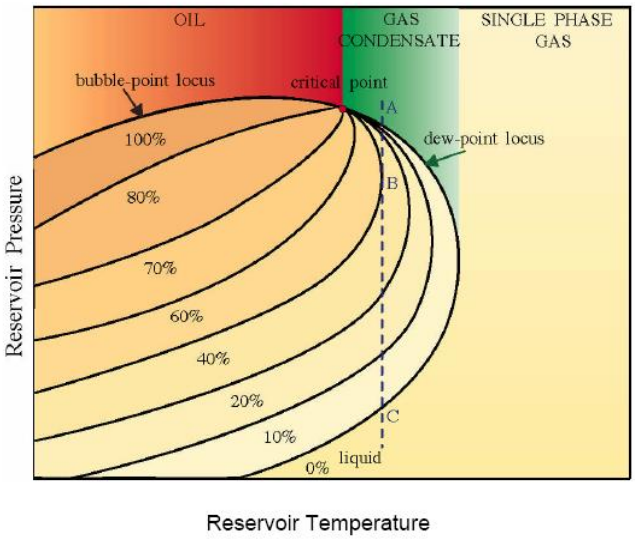


Fig. 9.B.4 – Generalized phase-diagram

The behavior of an oil reservoir with decreasing pressure would be as follows: At reservoir temperatures below the critical point, the two-phase region is entered via a bubble point, where there is initially 100% liquid. As pressure continues to fall, gas is liberated and the system reaches the 20% gas / 80% liquid line, and so on.

When it is above the bubble point, the oil is said to be **under-saturated**. At the bubble point, or anywhere in the two phase region, the oil is said to be **saturated**.

For a fluid above the critical point at 'A', pressure reduction will pass through a dew point with initially 0% liquid. Continued pressure reduction condenses more liquid through the 10% and 20% curves. It is this 'reverse' behavior, of pressure reduction condensing gas to liquid, which has led to the term retrograde. Below a maximum liquid percentage, at 'B', re-evaporation begins (normal gas-condensate behavior) and the system can go through a second dew-point at 'C', if the original fluid composition has not changed.

9.C Classification of reservoir fluids

The phase diagram is a function only of the reservoir fluid composition. The reservoir fluid behavior is determined by the shape of the phase diagram, in particular the position of the critical point, and the relative position of the reservoir temperature. It is actually possible to have the same fluid in two different reservoirs, and in one case it will be oil, while in the other, at higher temperature, it will be a gas. In rare cases this can happen even within a single reservoir, if it is near the critical temperature and has a significant temperature gradient. The main fluid types are:

- **Oil**: When the reservoir temperature is below the critical point, the fluid behaves as oil and shows a bubble point.
- **Retrograde gas condensate**: Between the critical temperature and the upper temperature limit of the two phase region, the fluid will be a retrograde gas condensate, and exhibit a dew-point.
- **Single phase gas**: If the reservoir temperature is above the upper temperature limit of the two phase region, the fluid will be a single phase gas.

The three main fluid types can be further subdivided:

- Oil reservoirs can be classified as **volatile** (high shrinkage) or **non-volatile** (low shrinkage).
- Retrograde gas condensates can be **rich** or **lean**.
- Single phase gas reservoirs can be **dry gas** or **wet gas**, depending on whether liquid is collected in surface separation facilities.

Divisions between the sub-types are not clearly defined, except in the case of single-phase gas, but usually give a good idea of the behavior of the fluid.

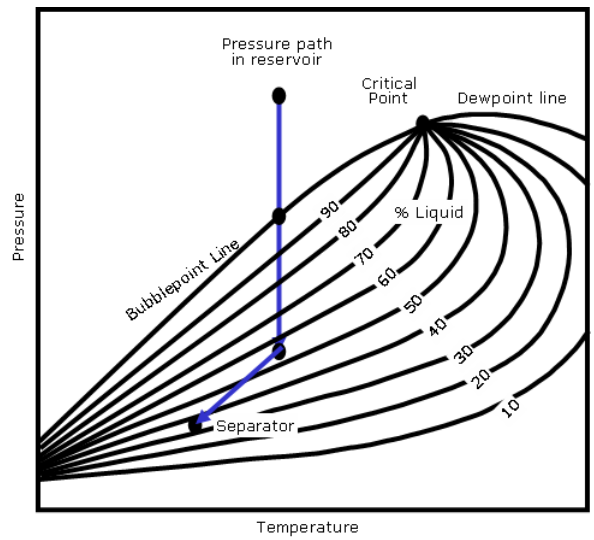


Fig. 9.C.1 – Non-volatile oil

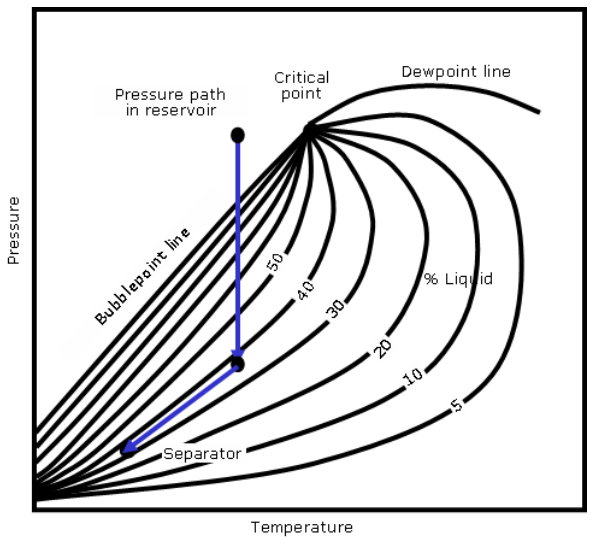
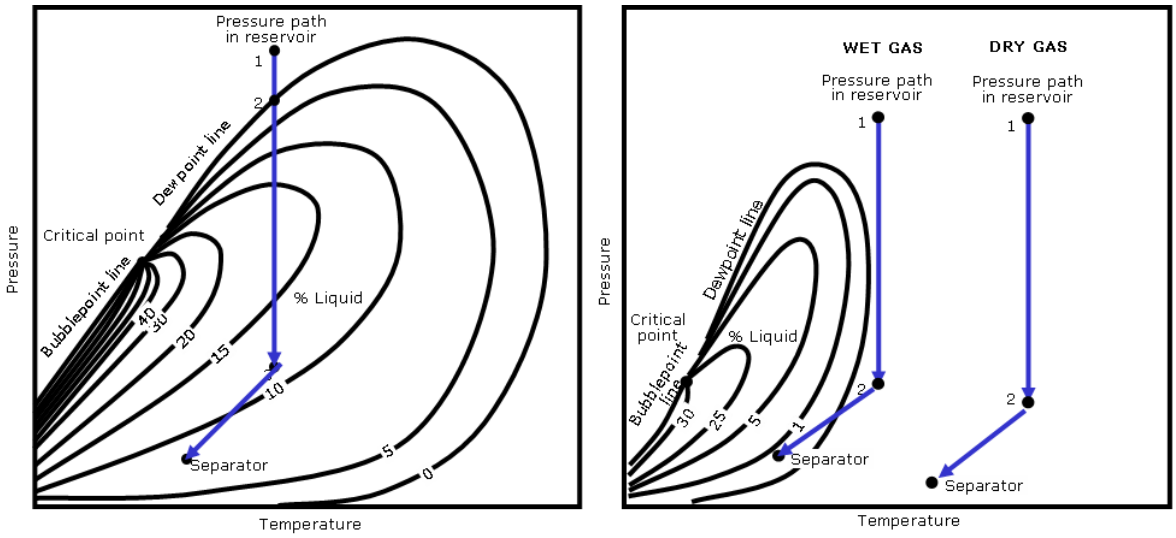


Fig. 9.C.2 – Volatile oil



Retrograde gas-condensate *Dry and wet gases*

Fig. 9.C.3 – The 5 reservoir fluid types

Field classification can be based on a few quantities:

- Initial Producing GLR = Initial producing Gas Liquid Ratio at surface conditions
- Initial oil API gravity; $^{\circ}API = \frac{141.5}{\gamma_o(60^{\circ}F)} - 131.5$
- Shrinkage @ Pb = reduction in the liquid volume from bubble point to surface

	Non Volatile Oil	Volatile Oil	Condensate	Wet Gas	Dry Gas
Initial producing GLR, scf/stb	< 2000	2000–3300	3300–50,000	> 50,000	> 100,000
Initial API	< 40	40-50	50-70	60-70	No liquid
Color	Very dark	Colored	Lightly colored	-	-
Shrinkage@ P_b	< 2	> 2	-	-	-

9.D Phase description

9.D.1 Oil - Classical Black-Oil (BO) formulation

The main assumption of the Black Oil formulation, sometimes referred to as the β-formulation, is that the reservoir fluid is made of two surface components resulting from the production process: stock-tank oil, and total surface gas. It is further assumed that the properties of the surface gas and stock-tank oil do not vary during reservoir depletion. The traditional BO properties characterize the volumetric behavior and the distribution of the surface components as a function of pressure.

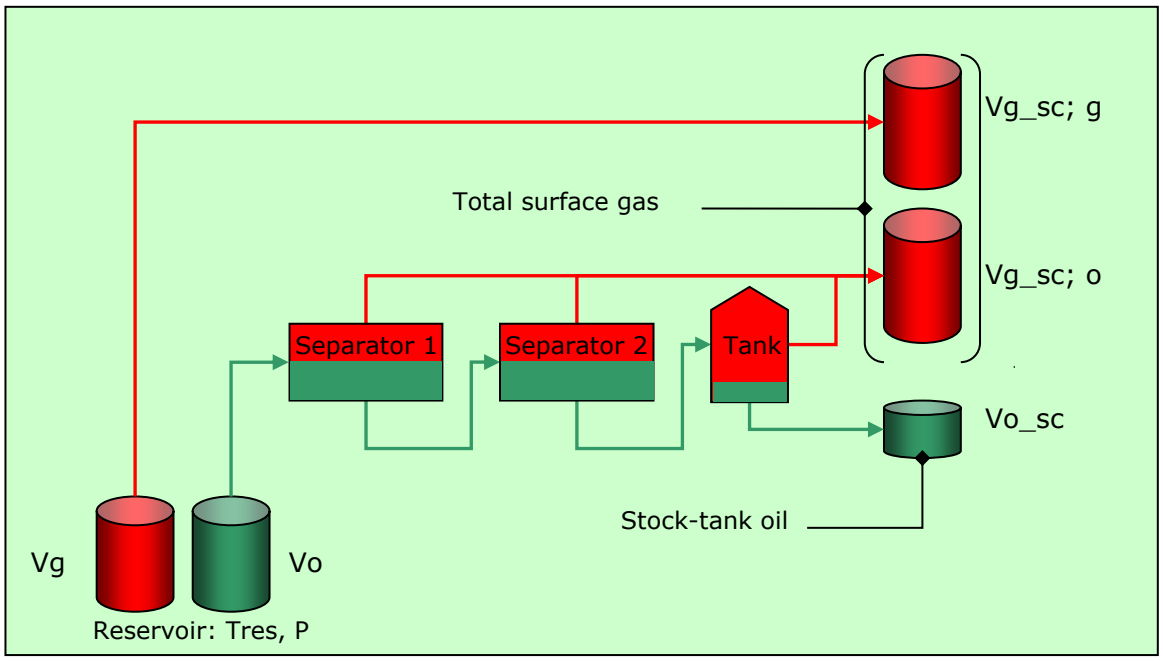


Fig. 9.D.1 – Black Oil volume definition

We consider the situation described above where reservoir gas and oil at some pressure P are brought to surface. The oil goes through a series of separation stages. The volumes are noted as follows:

- Vg = gas volume at reservoir conditions
- Vo = oil volume at reservoir conditions
- $Vg_sc;g$ = volume of surface gas produced from the reservoir gas
- $Vg_sc;o$ = volume of surface gas produced from the reservoir oil
- Vo_sc = volume of stock-tank oil

It is assumed that no liquid evolves from the gas when it is brought to surface; *the Modified Black-Oil accounts for this situation – see the Wet gas section*.

With the above definitions and assumptions the usual Bo properties are given:

- Solution Gas Oil Ratio, R_s: $$R_s = \frac{Vg_sc;o}{Vo_sc}$$
- Oil Formation Volume Factor, B_o: $$B_o = \frac{Vo}{Vo_sc}$$
- Gas Formation Volume Factor, B_g: $$Bg = \frac{Vg}{Vg_sc;g}$$

Entailing the following relation between surface and downhole volumes:

$$Vo_sc = \frac{V_o}{B_o}; \qquad Vg_sc = \frac{R_s \times V_o}{B_o} + \frac{V_g}{B_g}$$

B_o, B_g and R_s, are functions of pressure and temperature. They can be obtained from correlations or laboratory studies.

We write $R_{sb} = R_s(P_b)$, $B_{ob} = B_o(P_b)$. If we consider the separation process, it is important to realize that R_{sb} and B_{ob} do depend on the separator(s) conditions. A typical behavior is shown below with varying separator pressure.

The selected separator process should be the one providing the minimum R_{sb}.

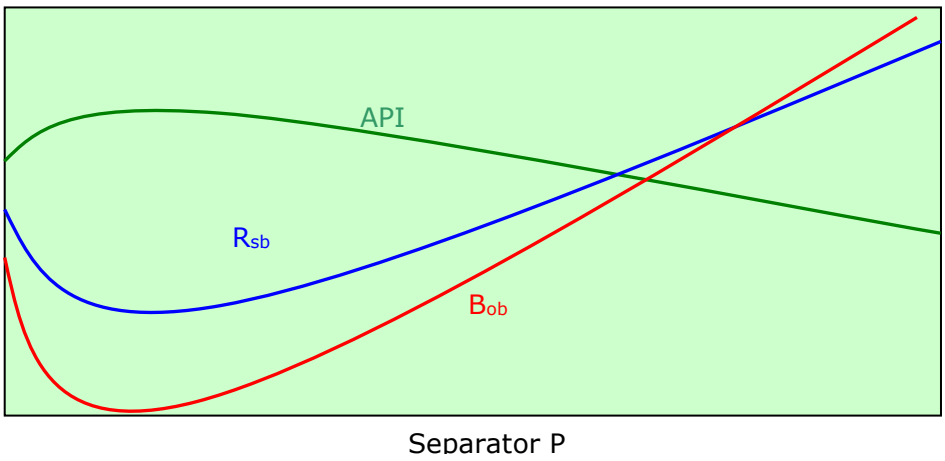


Fig. 9.D.2 – Influence of separation pressure

9.D.2 Wet gas

When dealing with wet gas it is common to calculate the reservoir gas gravity from the surface effluents. We assume that there is one separator stage before stock-tank conditions as pictured below:

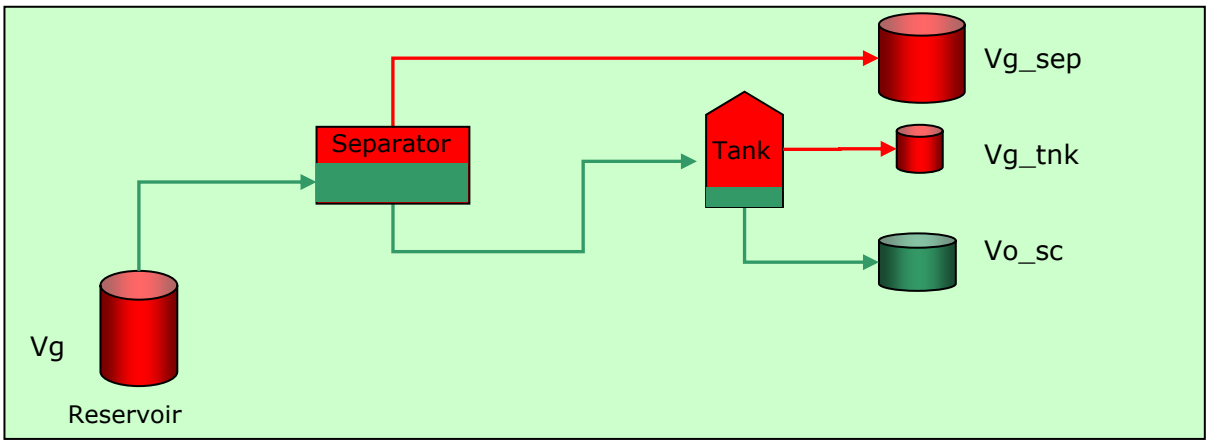


Fig. 9.D.3 – Wet gas production

The volume, at standard conditions, and the specific gravity of the gas produced at the separator and the tank are measured. The corresponding gas-oil-ratios, referenced to the stock tank oil volume are calculated:

$$R_{sep} = \frac{V_{g_sep}}{Vo_sc}\ ; \qquad R_{tnk} = \frac{V_{g_tnk}}{Vo_sc}\ ; \qquad \text{and the total gas-oil ratio is: } R = R_{sep} + R_{tnk}$$

9.D.3 Modified Black Oil (MBO) PVT Formulation

The modified formulation accounts for liquid condensation from the gas. The properties are defined from the volumes in the following schematic.

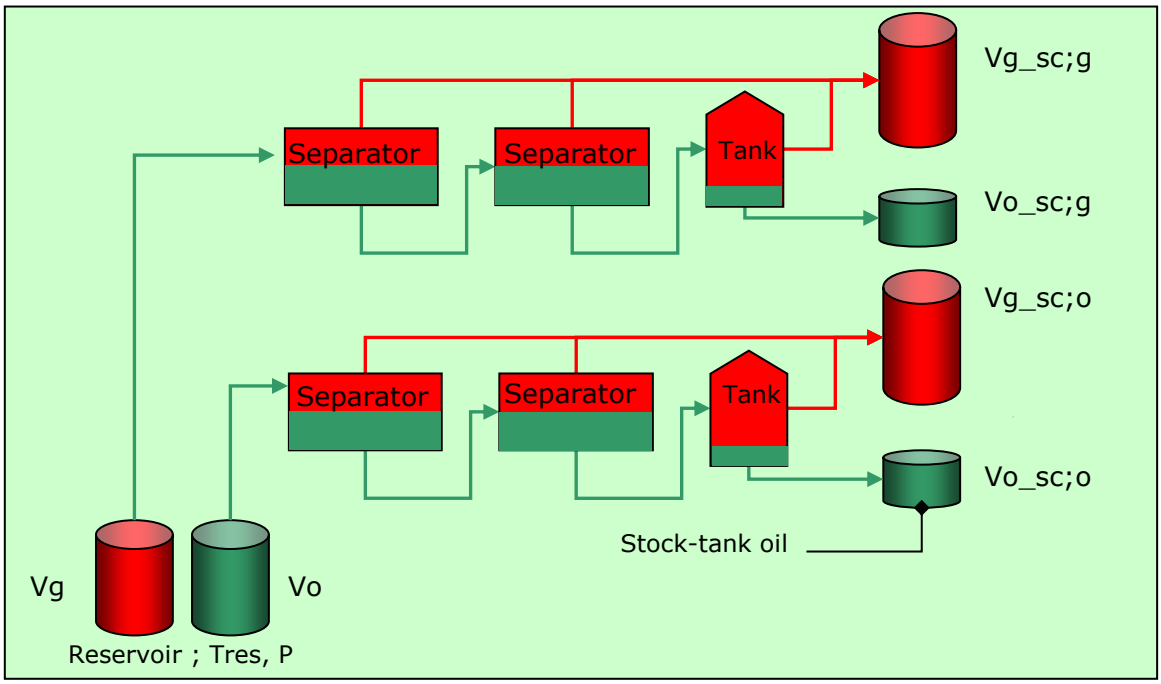


Fig. 9.D.4 – Modified Black Oil formulation: volume definition

The volumes are noted as follows:

- Vg = gas volume at reservoir conditions
- Vo = oil volume at reservoir conditions
- $Vg_sc;g$ = volume of surface gas produced from the reservoir gas
- $Vg_sc;o$ = volume of surface gas produced from the reservoir oil
- $Vo_sc;g$ = volume of surface oil produced from the reservoir gas
- $Vo_sc;o$ = volume of surface oil produced from the oil

The usual parameters are modified as follows:

- Solution Gas Oil Ratio, R_s: $$R_s = \frac{Vg_sc;o}{Vo_sc;o}$$
- Oil Formation Volume Factor, B_o: $$B_o = \frac{Vo}{Vo_sc;o}$$
- (Dry) Gas Formation Volume Factor, B_g: $$B_g = \frac{Vg}{Vg_sc;g}$$

A new parameter is added to quantify the oil produced from the gas:

- Solution Oil Gas Ratio, r_s: $$r_s = \frac{Vo_sc;g}{Vg_sc;g}$$

The relation between reservoir and surface volumes is thus expressed:

$$Vo_sc = \frac{V_o}{B_o} + \frac{V_g \times r_s}{B_g}; \qquad Vg_sc = \frac{R_s \times V_o}{B_o} + \frac{V_g}{B_g}$$

Most MBO formulations assume that all surface oils are the same. In other words the gravity of the oil produced from the reservoir oil and the one produced from the reservoir gas are assumed to be the same. A similar assumption is made for the surface gases.

9.D.4 Water production

In the case where the reservoir production includes water, an extension of the above definitions is made introducing a water formation volume factor B_w, and possibly water gas solubility, R_{sw}:

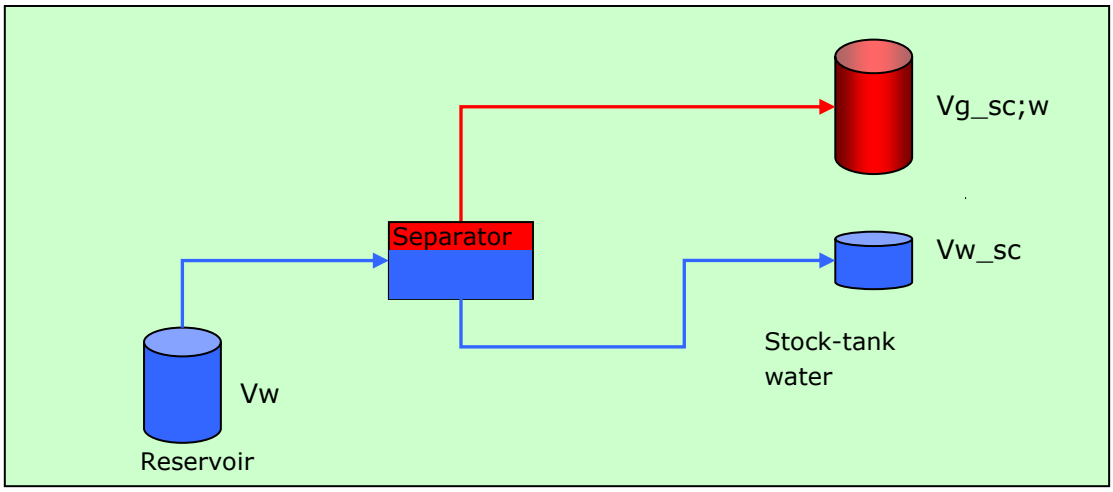


Fig. 9.D.5 – Black Oil property definitions for water

- $Vg_sc;w$ = surface gas produced from the reservoir water
- Vw_sc = surface water (produced from the reservoir water)
- Water gas solubility, R_{sw}: $$R_{sw} = \frac{Vg_sc;w}{Vw_sc}$$
- Water Formation Volume Factor, B_w: $$B_w = \frac{Vw}{Vw_sc}$$

9.E Fluid properties

In addition to the Black Oil properties described in Phase description section, the following are of interest to Dynamic Data Analysis: density, isothermal compressibility, viscosity, gas compressibility factor. This sections review them in detail for each phase. PVT studies, Correlations, and EOS are discussed later in their corresponding sections.

9.E.1 Gas properties

For Dry gas

Specific gravity: Ratio of the gas density at standard conditions, with air density at standard conditions.

$$\gamma_g = \frac{(\rho_g)_{sc}}{(\rho_{air})_{sc}}$$

Z factor: By definition of the real gas law $PV = ZnRT$

Can be obtained from a correlation or a PVT study, or from B_g if given from a PVT study.

Formation volume factor: relates the volume in the reservoir to the volume at standard conditions; defined by Z.

$$B_g = \frac{V_{res}}{V_{sc}} = \frac{Zp_{sc}T}{pT_{sc}}$$

Coefficient of isothermal compressibility: relative change in volume with pressure; given by Z.

$$c_g = -\frac{1}{V}\left(\frac{dV}{dP}\right)_T = -\frac{1}{B_g}\left(\frac{dB_g}{dp}\right)_T = \frac{1}{p} - \frac{1}{Z}\left(\frac{dZ}{dp}\right)_T$$

Gas viscosity: measure of the resistance to flow. Difficult to obtain from measurement, usually determined from correlations.

Gas density: given by Z.

$$\rho_g = (\rho_{air})_{sc} \times V_{sc} \times \frac{p\gamma_g}{ZRT}$$

where Vsc = volume of one gas mole at standard conditions: 379.4 scf

The plots below show some typical behaviors.

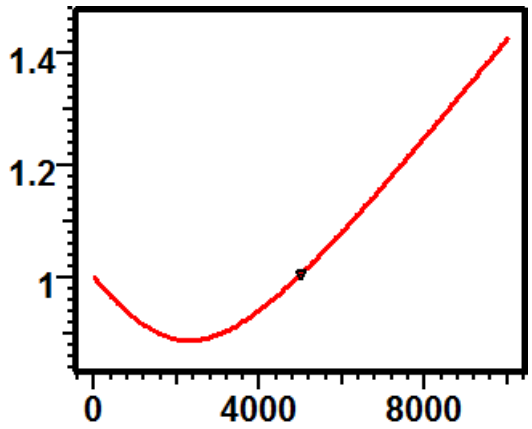


Fig. 9.E.1 – Z factor vs. p [psia]

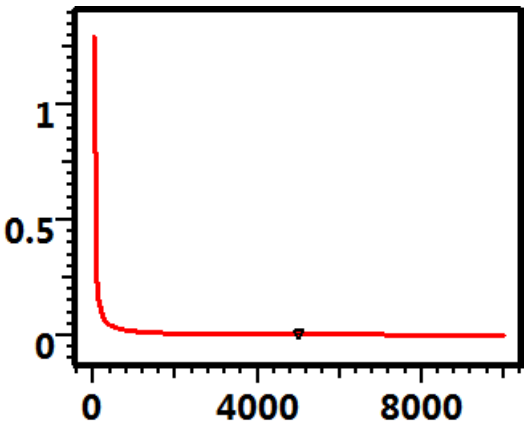


Fig. 9.E.2 – B_g [scf/rcf] vs. p [psia]

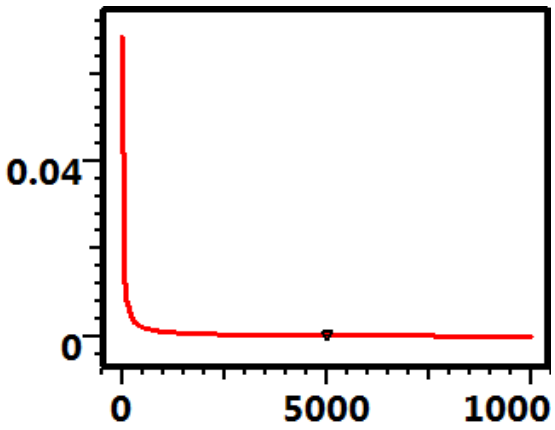


Fig. 9.E.3 – c_g [psi^{-1}] vs. p [psia]

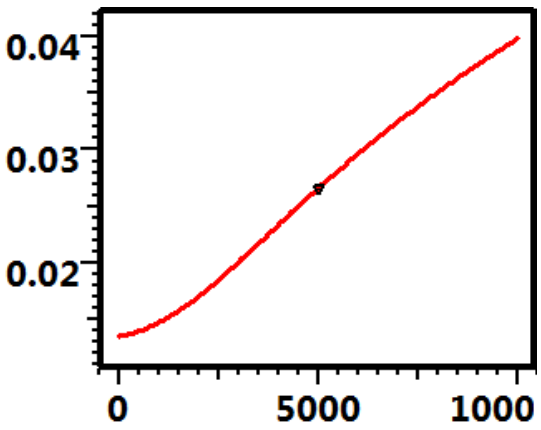


Fig. 9.E.4 – μ_g [cp] vs. p [psia]

For Wet gas

With the measurement of the two specific gravities γ_{g_sep} and γ_{g_tnk}, we define the average surface gas gravity as:

$$\gamma_g = \frac{R_{sep} \times \gamma_{g_sep} + R_{tnk} \times \gamma_{g_tnk}}{R}$$

And the specific gravity of the reservoir gas is then given by (R in scf/STB):

$$\gamma_{gr} = \frac{R \times \gamma_g + 4{,}600 \times \gamma_o}{R + 133{,}300\, \gamma_o / M}$$

With γ_o the stock tank oil gravity, Mo the condensate molecular weight.

This can be calculated from:

$$M_o = \frac{42.43\gamma_o}{1.008 - \gamma_o}$$

All reservoir gas properties are then estimated using the reservoir gas gravity.

9.E.2 Oil properties

Specific gravity: $$\gamma_o = \frac{(\rho_o)_{sc}}{(\rho_{water})_{sc}}$$

Recall also the definition of API gravity defined by $^\circ API = \frac{141.5}{\gamma_o(60^\circ F)} - 131.5$

Formation volume factor: Reservoir oil / surface oil. Obtained from lab study, or from a correlation.

Coefficient of isothermal compressibility: Calculated from B_o and R_s.

$$c_o = -\frac{1}{V}\left(\frac{dV}{dP}\right)_T ;$$

Above P_b: $c_o = -\frac{1}{B_o}\left(\frac{dBo}{dp}\right)_T$; Below P_b: $c_o = -\frac{1}{B_o}\left[\left(\frac{dBo}{dp}\right)_T - B_g\left(\frac{dR_s}{dp}\right)_T\right]$

Solution gas-oil ratio: gas dissolved in oil; lab study result or from correlation.

Viscosity: measured or from correlation.

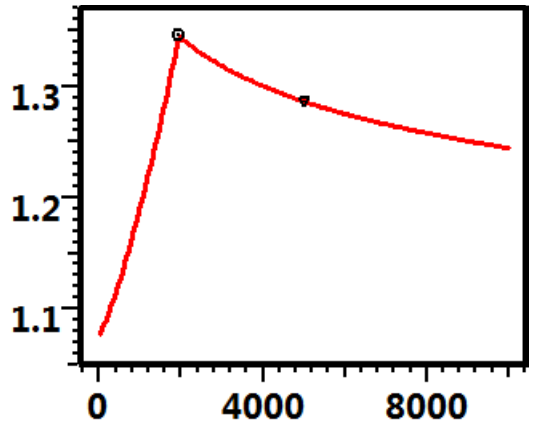


Fig. 9.E.5 – B_o [rb/STB] vs. p [psia]

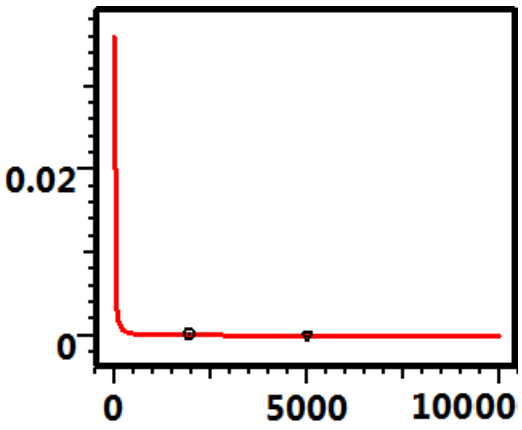


Fig. 9.E.6 – c_o [psi-1] vs. p [psia]

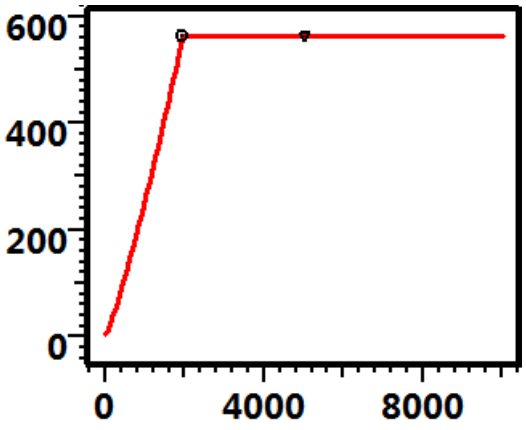


Fig. 9.E.7 – Rs [scf/STB] vs p [psia]

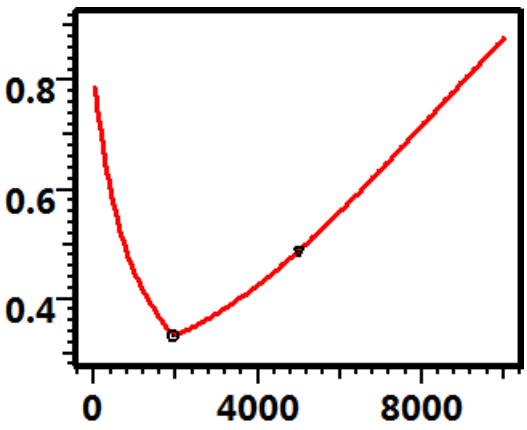


Fig. 9.E.8 – μo [cp] vs p [psia]

Oil density: calculated

$$\rho_o = \frac{(\rho_w)_{sc} \cdot \gamma_o + (\rho_{air})_{sc} \cdot \gamma_g \cdot R_s}{B_o}$$

9.E.3 Water properties

All formation water contains dissolved solids, primarily sodium chloride, NaCl. For this reason, the formation water is often called brine or salt water. The amount of dissolved solids in usually expressed in ppm; parts per million = grams of solids per million grams of brine. This is called water salinity and is a key input is estimating the water properties.

In addition, when gas is present, it may dissolve in the water leading to the consideration of R_{sw} Gas solubility.

Specific gravity: This is usually estimated from the measured salinity:

$$\gamma_w = 1 + 7.8216 \times 10^{-6} \times Salinity_ ppm$$

Density: The density at any condition is obtained by dividing the standard condition density by B_w. The effect of dissolved gas on the density is usually ignored.

$$\rho_w = \frac{(\rho_w)_{sc}}{B_w}$$

Formation volume factor: Reservoir water / surface water. Several effects are involved: evolution of dissolved gas from the brine as P and T change, the contraction of the brine. Obtained from correlation.

Gas-solubility: correlation value.

Coefficient of isothermal compressibility: calculated from B_w and R_{sw}.

$$c_w = -\frac{1}{V}\left(\frac{dV}{dP}\right)_T$$

Above P_b: $c_w = --\frac{1}{B_w}\left(\frac{dBw}{dp}\right)_T$; Below P_b: $c_w = --\frac{1}{B_w}\left[\left(\frac{dBw}{dp}\right)_T - B_g\left(\frac{dR_{sw}}{dp}\right)_T\right]$

Viscosity: correlation value.

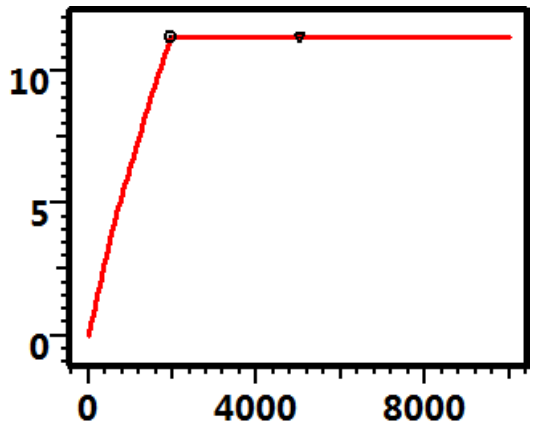


Fig. 9.E.9 – Rsw [scf/STB] vs. p [psia]

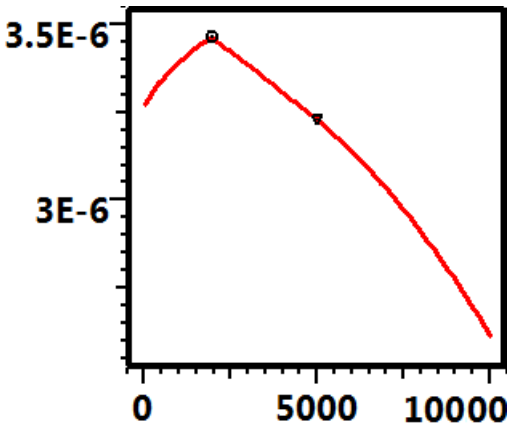


Fig. 9.E.10 – c_w [psi-1] vs. p [psia]

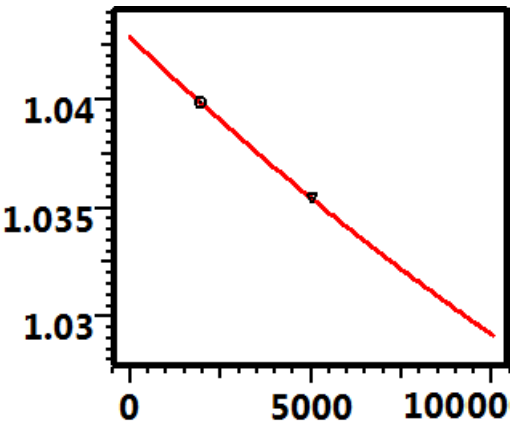


Fig. 9.E.11 – Bw [rb/STB] vs. p [psia]

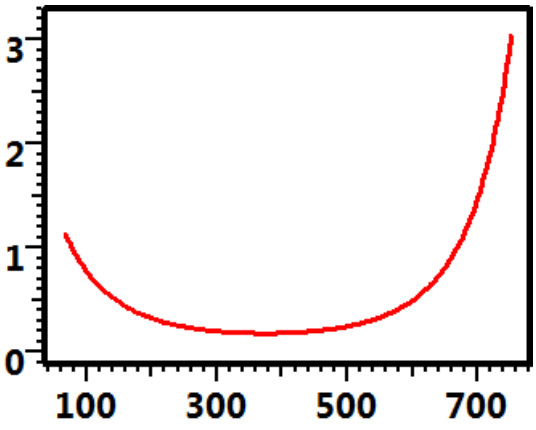


Fig. 9.E.12 – μw [cp] vs T [deg F]

9.F Use of PVT data in DDA (oil)

For historical and practical reasons, a significant part of DDA relies on using analytical solutions to a linearized diffusivity equation. To produce the required linearity, PVT properties are at times assumed constant, at other times encapsulated in a pseudo function that adequately transforms the problem. The various cases are covered here. An alternative to this approach is to solve the problem numerically. The complete PVT behavior is then required and non-linearities can be handled directly. A multiphase simulator can either use a Black Oil or compositional PVT. In the first case, we will see in the section 'Compositional' PVT from BO (and MBO) model how the problem can be formulated in terms of the mass fraction of the surface oil and gas in order to account for varying bubble point.

In a fully compositional simulator, the mass fractions of individual components such as methane, ethane, etc would be considered and PVT properties estimated using EOS.

Even though the problem is not different from what is done in other fields such a full-field reservoir simulation, a numerical model turns out to be inadequate to simulate short transients in a bubble point or dew point system. This is not linked to the PVT representation but rather to the way of estimating mobilities from average cell saturations. This aspect is not covered in this chapter. Instead we focus on the classical analytical approaches.

Oil reservoir treatment in DDA can be made in different ways: single phase oil, Perrine, or using an oil pseudo pressure.

9.F.1 Single-phase oil

The assumption is that only oil is flowing to surface, and the reservoir pressure is above the bubble point. The diffusivity equation introduced in the Chapter 'Theory' involves two PVT parameters: total compressibility ct, and oil viscosity. In addition, the surface volumes need to be converted to downhole conditions and this requires the knowledge of the oil formation volume factor Bo.

Total compressibility is defined as:

$$c_t = c_f + S_o c_o + S_w c_w + S_g c_g$$

Assuming no gas in the reservoir the last term can be removed. The influence of connate water may be considered.

In the simplest situation, DDA treats the three parameters ct, μo, and Bo as constants. They are estimated at the reservoir temperature and a given reservoir pressure.

9.F.2 Perrine

The Perrine method considers multiphase flow using a single mixture fluid downhole and treats this fluid as a liquid analogue. The PVT properties involved (FVF's, solution gas-oil ratio, etc), are estimated once and for all for the reservoir temperature and some given reservoir pressure.

The total downhole rate is calculated from surface rates as:

$$q_o \times B_o + q_w \times B_w + (q_g - q_o \times R_s) \times B_g$$

Internally a surface oil equivalent can be used, defined as the above expression divided by Bo.

$$q_t = \frac{q_o B + q_w B_w + (q_g - q_o R_s) B_g}{B_o}$$

This is the surface oil rate that would give the same downhole total rate.

In order to define the total compressibility, fluid saturations in the reservoir are needed, and they are assumed constant.

Total compressibility is calculated from:

$$c_t = c_f + S_o c_o + S_w c_w + S_g c_g$$

Then, a single phase liquid analysis is conducted, on the basis of total mobility:

$$\lambda_t = \frac{k_o}{\mu_o} + \frac{kw}{\mu_w} + \frac{k_g}{\mu_g}$$

In KAPPA-Workstation an oil equivalent permeability k_{o_equ} is defined, which is the total mobility, multiplied by the oil viscosity:

$$k_{o_equ} = \lambda_t \times \mu_o$$

The main assumption of the Perrine method is that the ratio of the fluid mobilities is equal to the ratio of the downhole productions. This can be used to express the effective permeabilities as follows:

$$\frac{k_o}{\mu_o} = \lambda_t \times \frac{q_o B_o}{q_t B_o} \quad ; \quad \frac{k_w}{\mu_w} = \lambda_t \times \frac{q_w B_w}{q_t B_o} \quad ; \quad \frac{k_g}{\mu_g} = \lambda_t \times \frac{(q_g - R_s q_o) B_g}{q_t B_o}$$

If the relative permeabilities are known the value of the absolute permeability can be calculated with:

$$k = \frac{k_o}{k_{ro}} = \frac{k_w}{k_{rw}} = \frac{k_g}{k_{rg}}$$

Two major assumptions of the Perrine's approach are that (1) reservoir saturations are constant (2) the ratios of mobilities are equal to the ratios of the downhole productions. By combination, those assumptions should entail that the production ratios are also constant. In fact, Perrine's method is usually applied on a given build-up, and only the last rates before this build-up are considered. The implementation in KAPPA-Workstation is an extension that should be used with care should the production ratios vary significantly.

9.G Use of PVT data in DDA - continued (oil)

9.G.1 Single phase oil pseudopressure

An alternative to the assumption that the PVT properties are constant with pressure is to replace P by a pseudopressure defined as:

$$m(P) = (B_o \mu_o)_{res} \int_0^P \frac{dP}{B_o \mu_o}$$

The integration of the viscosity and formation volume factor in the pseudo pressure permits a consistent analysis where the pressure and thus the PVT properties vary significantly over a period of time. This is provided that one considers periods where the pressures are above the bubble point. Typically a series of build-ups over a long history, each one being at pressure levels above the bubble point, will give consistent kh's. Note however that if the FVF and viscosity are assumed to vary, the change in compressibility is not captured by the pseudo pressure, so the pseudo pressure is only applicable for getting adequate permeability. Estimates of sizes, boundary distances with a varying PVT will not be reliable.

9.G.2 Multiphase pseudopressure

In order to linearize further in the case of multi-phase flow, pseudo functions have been proposed of the form below, for solution gas drive, as well as gas condensate reservoirs.

$$m(p) = \int_0^P \left(\frac{k_{ro}\rho_o}{\mu_o} + \frac{k_{rg}\rho_g}{\mu_g} + \frac{k_{rw}\rho_w}{\mu_w} \right) .dP$$

To evaluate the above expression a relation must be formulated between pressure and saturation. A common assumption is that of steady state, predicting that the sandface saturations can be calculated using the production ratio. More precisely, we can write the steady-state assumption here for oil / gas):

$$\frac{k_{ro}}{k_{rg}} = \frac{\rho_g \mu_o L}{\rho_o \mu_g V}$$

Where L and V are respectively the mole fractions of Liquid and Vapor.

If we know the relative permeabilities as a function of saturations, and if we have, or we can calculate, the quantities L and V from the PVT, then we can get the saturation corresponding to a given pressure and the full m(p) can then be obtained.

There are several potential problems with this approach. The relative permeabilities must be known and they will have a direct and important impact of the shape of the pseudo-pressures, and thus on the diagnostic made from looking at the response in terms of m(p). The necessary relation between saturation and pressure is typically based on a near wellbore behavior and this may not be valid elsewhere in the reservoir. For closed systems in particular, it has been shown that the pseudo-pressure will not provide an analogy with the liquid case in pseudo-steady state. Finally, in cases where the pressure in the reservoir varies significantly it is also necessary to worry about the variation of the total compressibility. Pseudo-time functions can be considered but again the saturations are part of the equations and this approach relies (as with m(p)) on the assumption of some relation between pressure and saturations, with the same potential dangers.

9.H Use of PVT data in DDA (gas)

Gas was covered in precedent chapters. As shown, the conventional approach is to try and linearize the diffusivity equation and to solve the gas problem as a liquid analogue. This is done replacing pressure and possibly time by pseudo functions.

9.H.1 Dry gas

Only gas is flowing to surface and inside the reservoir. The usual approach replaces pressure by the gas pseudo pressure, *see Chapter Theory - The case of dry gas.*

$$m(p) = 2\int_0^p \frac{p}{\mu Z} dp$$

Using pseudo-pressure alone assumes that the viscosity - compressibility product is constant. When this assumption is not valid, time may be replaced by a pseudo-time, see Chapter 'Theory – The case of dry gas'.

(Normalized version) $t_{ps}(t) = \int_0^t I(p_{wf}(\tau))d\tau$ where $I(p) = \frac{(\mu c_t)_{ref}}{\mu c_t}$

We saw also in precedent chapters that an equivalent function can be defined in order to correct for material balance, see Chapter 'Theory - The case of dry gas'.

9.H.2 Wet gas and condensate single phase analog

The approach is similar to that of dry gas, using the reservoir gas gravity, and correcting the rates. Recall from section Fluid Properties – Gas properties that the reservoir gas gravity is obtained from:

$$\gamma_{gr} = \frac{R \times \gamma_g + 4{,}600 \times \gamma_o}{R + 133{,}000\,\gamma_o / M}$$

Corrected rates qt are used in the analysis and defined as: $q_{geq} = q_g(1 + 133{,}000\frac{\gamma_o}{M_o.R})$

When dealing with gas-condensate, the same approach is often used even though the single phase m(p) is not strictly applicable within the reservoir. The formation of condensate within the reservoir will result in varying saturations and thus mobilities. This may be revealed on transient responses as radial composite reservoirs and analyzed as such. Some studies suggest that close to the well the fluid velocity may sweep the condensate more efficiently thereby causing a three mobility zones. Specific models have been developed for this situation.

9.I Use of PVT data in DDA - continued (gas)

9.I.1 Multiphase pseudopressures for condensate

The general form is the same as given earlier for oil:

$$m(p) = \int_0^P \left(\frac{k_{ro}\rho_o}{\mu_o} + \frac{k_{rg}\rho_g}{\mu_g} + \frac{k_{rw}\rho_w}{\mu_w} \right) .dP$$

And the same steady-state assumption relating production and saturations is usually made:

$$\frac{k_{ro}}{k_{rg}} = \frac{\rho_g \mu_o L}{\rho_o \mu_g V}$$

As stated before there are a number of potential problems with this approach, starting with the validity of the steady-state assumption. The pseudo pressure shows two distinct sections, below and above the dew point, with two distinct slopes. This change in slope which is supposed to correct the distortions due to the presence of condensate, and its effect on mobility, can produce such corrections that may create erroneous responses.

As in the oil case, pseudo pressure may work for the sake of a getting kh from a semilog analysis during a given flow period. Beyond that, their use is limited and dangerous.

9.J Getting properties from PVT studies

The objective of this section is to describe the main study types and to see in particular how their results relate to the usual Black-Oil properties. Apart from the compositional analysis, three main experiments are reviewed:

- Constant Composition Expansion (CCE)
- Differential Liberation Expansion (DLE)
- Separator Tests

In addition to measuring the physical properties of the reservoir fluid, PVT laboratories also determine the chemical composition. Because of the enormous number of individual components present in most hydrocarbons it is not possible to identify them all, and similar components are grouped together. Typically, individual measurements are given for the non-hydrocarbons; nitrogen, carbon dioxide and hydrogen sulphide, and for the hydrocarbon groups of primary paraffins, methanes to butanes. Heavier hydrocarbons are then grouped according to the number of carbon atoms, and a final fraction groups all the unidentified heavy components.

9.J.1 Constant Composition Expansion (CCE)

Also called Flash vaporization

In a CCE experiment, a reservoir sample is placed in a cell at a pressure greater than or equal to the reservoir pressure, and at reservoir temperature. Pressure is successively reduced by modifying the cell volume. The total hydrocarbon volume Vt is noted and plotted versus Pressure.

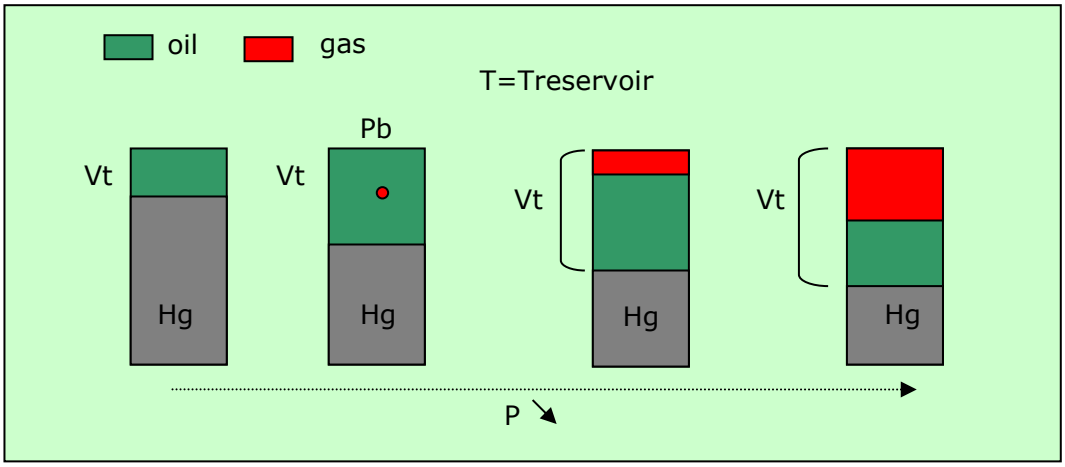


Fig. 9.J.1 – CCE schematic

With a fluid showing bubble point behavior, there is a dramatic change of slope as the first bubble of gas forms and the gas phase compressibility dominates the two-phase behavior.

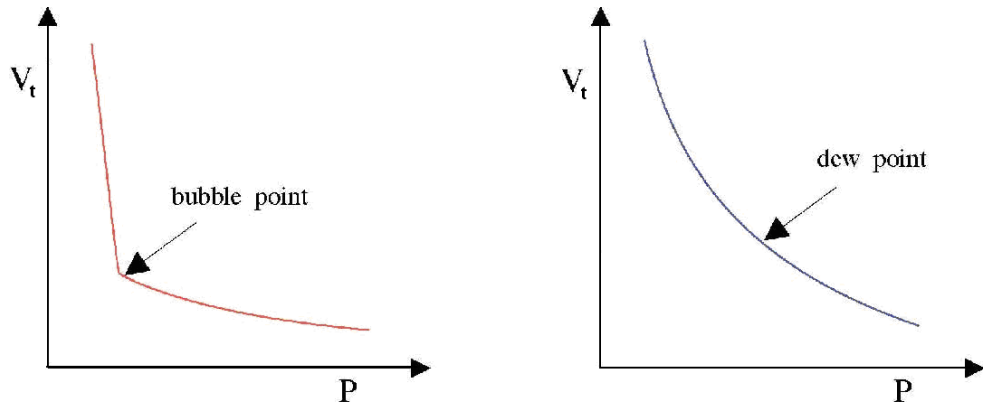


Fig. 9.J.2 – Total volume Vt versus P

In contrast, for gas condensates at the dew point pressure the first drop of liquid that forms has a negligible effect on the overall compressibility, and there is no identifiable change in slope. This curve will also be seen for single phase gases, and some volatile oil fluids near the critical point, where gas and oil phases have similar properties. In these cases laboratory studies are performed in a 'window cell', where the formation of a drop of liquid or a bubble of gas can be physically observed. This need for visual inspection is a major handicap in trying to identify samples at the wellsite.

9.J.2 Differential Liberation Expansion (DLE)

Also called Differential Vaporization.

The DLE experiment is designed to represent the depletion process within the reservoir. A sample of reservoir fluid is brought to reservoir T and bubble point pressure. The pressure is reduced by changing the cell volume. Gas is expelled while maintaining constant pressure. The gas volume ΔVg and gravity are measured, as well as the oil volume. The step is repeated until atmospheric pressure Psc is reached. The temperature is then reduced to 60°F and the residual oil volume is measured, Vor.

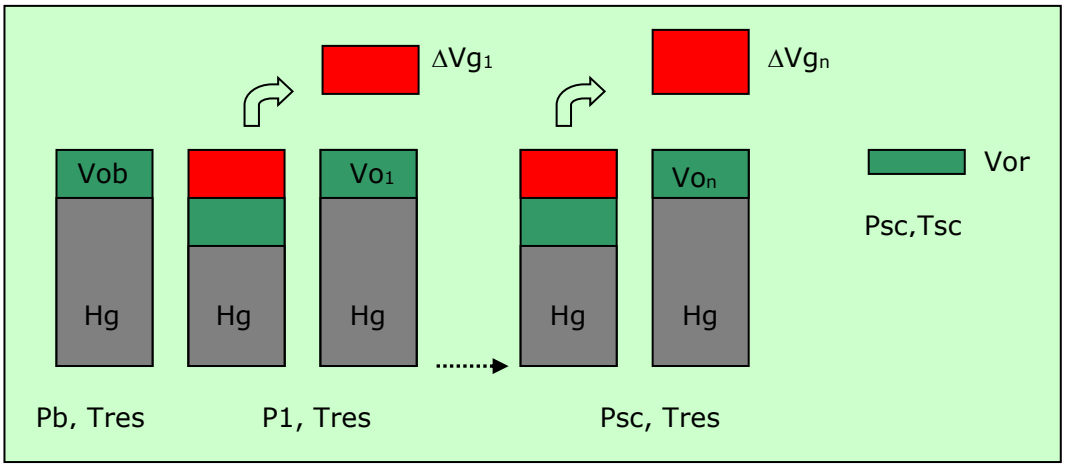


Fig. 9.J.3 – DLE schematic

The following quantities can be determined for the DLE experiment:

- Gas Z factor
- Differential solution gas-oil ratio R_{sD}
- Differential oil FVF B_{oD}

The Differential qualifier, and the 'D' trailing character on the properties, is introduced because the volumes determined in the DLE experiment are referenced to the residual oil volume Vor. This is different from the reference stock-tank oil volume obtained when going through different surface separator stages. The conversion of the DLE results to the usual BO properties is explained in section Converting Fluid Study Results.

At any step R_{sD} and B_{oD} are calculated from:

$$R_{sD}(P_k) = \frac{\sum_{i=k}^{n} \Delta Vg_i}{Vor} \; ; \quad B_{oD}(P_k) = \frac{Vo_k}{Vor} \; ;$$

9.J.3 Separator Tests

The main objective of the test is to obtain values to convert the DLE results from a residual oil to a stock-tank oil basis. A sample of reservoir fluid is initially set at reservoir temperature and bubble point pressure. It is then brought to the conditions of the first separator stage. The gas volume and gravity are measured. This is repeated until a last step to bring the sample to standard (stock tank) conditions.

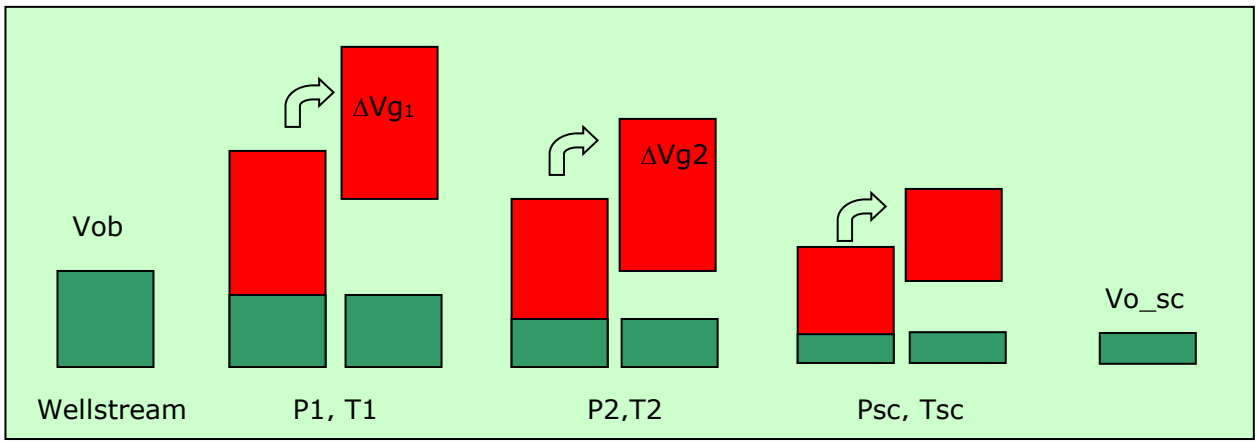


Fig. 9.J.4 – Separator test schematic

The following properties are obtained:

- R_{sSb} where the subscript 'S' indicates that this is from a separator test and 'b' indicates that the original sample pressure is bubble point pressure.
- Similarly a value of oil FVF is obtained: B_{oSb}.

The gas volumes expelled from the various separator stages are expressed at standard conditions. The above properties are then calculated as:

$$R_{sSb} = \frac{\sum_i \Delta Vg_i}{Vo_sc} \; ; \quad B_{oSb} = \frac{Vob}{Vo_sc}$$

9.J.4 Converting Fluid Study Results

Recall the results from the various tests:

- CCE: Vt = total (oil + gas) volume at P; and Vb = oil volume at P_b
- DLE: solution gas-oil ration $R_{sD}(P)$, oil FVF $B_{oD}(P)$
- Separator test: R_{sSb}, B_{oSb}

At pressures below the bubble point it is assumed that the process in the reservoir is represented by the DLE, and the process from bottomhole to the surface is represented by Separator Tests.

We note $R_{sDb} = R_{sD}(P_b)$ and $B_{oDb} = B_{oD}(P_b)$. The DLE values are corrected using the separator test values as follows:

$$P < P_b \;\Rightarrow\; B_o(P) = B_{oD}(P)\frac{B_{oSb}}{B_{oDb}} \; ; \; R_s(P) = R_{sSb} - (R_{sSb} - R_{sD}(P))\frac{B_{oSb}}{B_{oDb}}$$

<u>At pressures above the bubble point, properties are obtained from a combination of CCE and Separator tests.</u>

$$P > P_b \;\Rightarrow\; B_o(P) = \frac{Vt(P)}{Vb} \; ; \; R_s(P) = R_{sSb}$$

9.K Obtaining properties from PVT correlations

Correlations are empirical relationships between properties which have no simple inter-dependence, for which some apparent relationship has been identified. Charts and monographs have been in use in the oil industry for a long time, and have proved useful for providing values where measurements were not feasible, in extrapolating from measured values at different conditions, and for checking the consistency of measurements. Although most correlations are simple to use, they are often based upon data from limited geographical areas, especially those within North America. Also the precision of the correlation is rarely referred to, even in relation to the data on which it is based.

With the evolution of computers in the oil industry, many commonly-used correlations have been converted into equation form to facilitate their use. However, the equations are never a perfect fit to the original graphical relationship, so additional errors are incurred. For example, the Dranchuk and Abou-Kassem equations for the Standing-Katz Z chart add an average error of 0.3% to the values. Similarly, equations used to represent the Carr et al gas viscosity correlation introduce an average error of 0.4%. In most cases such additional errors are acceptable, but much larger than average errors do occur, particularly as the correlations can be used outside their acceptable range of application. Some more recent correlations have been developed directly in equation form, which avoids the additional fitting error.

Correlations are invaluable to the industry, but experimental data should be obtained wherever possible. If a choice between correlations has to be made, the ideal approach is to make comparisons with real PVT data on a number of similar fluids, to identify the most suitable correlation and to obtain an idea of the likely errors involved. If this is not possible, it is best to use the correlation derived from data of similar fluid type and geographical origin. It may also be advisable to compare results obtained from different correlations, to see if any key parameters are particularly sensitive to this choice. In the following sections we are providing some information that may be relevant in the selection.

9.K.1 Gas correlations

9.K.1.a Z factor

The existing correlations are representations of the Standing and Katz Z-factor chart, relating Z to reduced pressure and temperature.

The reduced pressure and temperature are defined as $P_r = \frac{P}{P_c}; T_r = \frac{T}{T_c}$; where P_c and T_c are the pseudo-critical pressure and temperature. Recall from the beginning of this chapter the definition of critical point for a pure component. The pseudo-critical properties are the mixture equivalent and they are obtained either by mixing rule or correlation.

A correlation by Standing gives the pseudo-critical properties from the gas specific gravity. A correction is required when sour gases are present (C02, N2, H2S), and this is based on a correlation by Wichert and Aziz.

Three classical representations of the Standing and Katz chart are:

- Dranchuk and Abou-Kassem
- Hall and Yarborough
- Beggs and Brill

The first two are the most accurate in representing the chart. Beggs and Brill is limited in range so the others should be preferred.

9.K.1.b Gas viscosity

As previously mentioned, gas viscosity is usually estimated from correlation since it is difficult to measure it in the PVT lab.

- Carr et al: gives a table for $\mu g(T,P)/\mu g_sc(T,P)$ and a way of obtaining the standard conditions viscosity from Tr,Pr, and the amount of sour gases.
- Lee et al: used by most PVT laboratories reporting gas viscosity, relates μg to molecular weight, density, and temperature.

These correlations predict gas viscosities with an error of about 3% in most cases. When the gas gravity increases about 1, i.e. with rich gas condensate, the error can increase to 20%.

9.K.2 Oil correlations

Oil correlations have been developed for bubble point pressure, Bo, solution GOR, viscosity, and compressibility. They predict properties from the surface oil and gas properties, and total solution gas-oil ratio.

9.K.2.a Pb and Rs

The correlations typically give a relation between bubble point pressure, solution gas-oil-ratio, oil and gas gravities. When using the total GOR as an input, the correlations provide Pb. Conversely, when using any pressure below Pb, they give $R_s(P)$. Below is the list of correlations used in KAPPA-Workstation.

- Standing (based on California crudes)
- Lasater (based on samples from Canada, US, and South America)
- Vasquez and Beggs (based on data from commercial laboratories)
- Glaso (based on North Sea samples)
- Petrosky and Farshad (based on samples from the Gulf of Mexico)
- Kuparuk
- South Brae

No significant difference should be expected between those correlations for most cases. Standing and Lasater correlations are recommended for general use. Correlations developed for a particular region should probably be used in that region.

9.K.2.b Oil FVF

The available correlations in KAPPA-Workstation are:

- Standing (based on California crudes)
- Vasquez and Beggs (based on data from commercial laboratories)
- Glaso (based on North Sea samples)
- Petrosky and Farshad (based on samples from the Gulf of Mexico)
- Kuparuk (based on Kuparuk River field samples)
- South Brae (based on South Brae field samples)

As for Pb and Rs, the estimates are based on total solution GOR, oil and gas gravities. The prediction of the above are in most situations fairly close.

9.K.2.c Oil viscosity

The determination of oil viscosity by correlation typically involves 3 successive steps:

1. Determination of the dead oil viscosity, μ_{oD} correlated in terms of gravity and temperature.
2. Correction of μ_{oD} based on Rs.
3. In the under-saturated section, correction (usually based on P alone).

There exist different correlations for those steps. In KAPPA-Workstation three methods are offered generically called 'Beal', 'Beggs and Robinson', and 'Glaso'. They correspond to the following combination:

- Beal: 1=Beal, 2=Chew and Connally, 3=Beal
- Beggs and Robinson: 1 = Beggs & Robinson, 2=Beggs & Robinson, 3=Vasquez and Beggs
- Glaso: 1=Glaso, 2=Chew and Connally, 3=Beal

  Other more specialized correlations are also available
- Kuparuk (based on Kuparuk River field samples)
- Andrade
- Petrosky
- Bergman-Sutton

The estimate of dead-oil viscosity by correlations is very unreliable. Lab values should be preferred whenever available.

9.K.2.d Oil isothermal compressibility

Oil compressibility can be calculated from the knowledge of Rs and Bo. Direct correlations exist. In KAPPA-Workstation the following is offered:

- Vasquez and Beggs: Actually combines a correlation by McCain below Pb and Vasquez and Beggs above Pb.
- Glaso: combination of McCain below Pb and Glaso above.
- Petrosky and Farshad: combination of McCain below Pb and Petrosky and Farshad above.

9.K.3 Water correlations

Following is the list of correlations available in KAPPA-Workstation.

9.K.3.a Water FVF

- Gould
- McCain
- Meehan and Ramey

9.K.3.b Water Compressibility

- Dodson and Standing
- Osif

9.K.3.c Gas solubility

- Katz
- Meehan and Ramey

9.K.3.d Water Viscosity

- Van-Wingen and Frick
- Helmoltz
- Meehan and Ramey

9.K.4 Correlation: feeding and matching

It is always desirable to adjust the prediction of fluid properties obtained from correlations. On-site measurements can be used for that purpose or else values resulting from PVT studies. In the latter case however if a full PVT study is available this should be used rather than the correlations. When correlations are applied with known values, the modification made to the properties is usually linear using a factor and a shift. The two fitting parameters can be obtained by running a non-linear regression on any number of constraint points. *For some properties, the modification is different as reference values must be preserved. This is the case for formation volume factors or gas Z-factor, with B(Psc)=1 and Z(Psc)=1.*

In the Black Oil model, we have seen that the oil and gas properties are obtained as a function of the surface component gravities, and the solution GOR. There is a one-to-one relation between total GOR and bubble point.

This can be considered as the definition of the fluid composition, as explained in the next section.

For given surface gravities, the effect of varying the GOR is shown below. The saturated sections up to the bubble points are the same, whereas a funnelling is seen above Pb.

The saturated section is therefore a function of the surface component gravity only, and the value of any property at a particular pressure requires only the additional knowledge of the GOR, or equivalent Pb.

When using match values, those values may characterize a fluid with a GOR different from the one under consideration. If this is the case then it may not be relevant to compare those values and the values predicted by the correlation. Only if the GOR is the same can values be compared for any pressure.

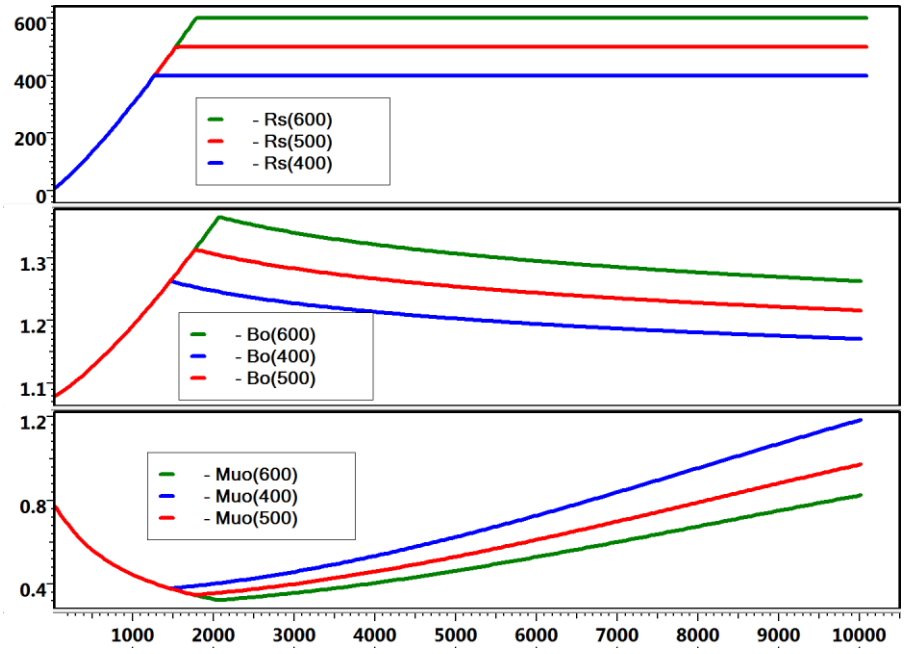


Fig. 9.K.1 – Effect of changing the total GOR

As a rule, the input to correlations should be the latest set of consistent production GOR, and surface oil and gas gravities. When constraining this PVT with values originating from lab studies of some initial fluid with GOR_i and Pb_i, beware that undersaturated values cannot be matched if the GOR has significantly evolved. For the saturated section, values can be matched only for pressures below min(Pb,Pb_i).

9.L 'Compositional' PVT from BO (and MBO) model

We consider as multi-component model, with three components named *water*, *oil* and *gas*. The *water* component exists only in the Water phase. The *gas* component exists in the Gas and Oil phases. The *oil* component exists only in the Oil phase for the BO model, and in both Oil and Gas phase for the MBO model. This can be summarized with the following tables.

BO	component		
phase	w	o	g
W	x		
O		x	x
G			x

MBO	component		
phase	w	o	g
W	x		
O		x	x
G		x	x

The *oil* and *gas* components are the stock tank oil and total separator gas, as defined in the previous sections. All reservoir fluids are a mixture of these components. The phases can be characterized by their composition, fraction of each component expressed in a conservative quantity, for instance the mass. So the phases are defined by their **mass composition** Co, Cg and Cw. We write C_p^k the fraction of component *k* in phase *p*. The compositions add up to unity: $\sum_k C_p^k = 1$.

9.L.1 2-Phase envelope

The phase envelope of the Gas-Oil equilibrium for a real mixture of two components similar to a reservoir sample can be plotted on a Pressure-composition plot as shown below. The plot considers a general MBO situation where oil can exist in both oil and gas phases, and similarly for gas.

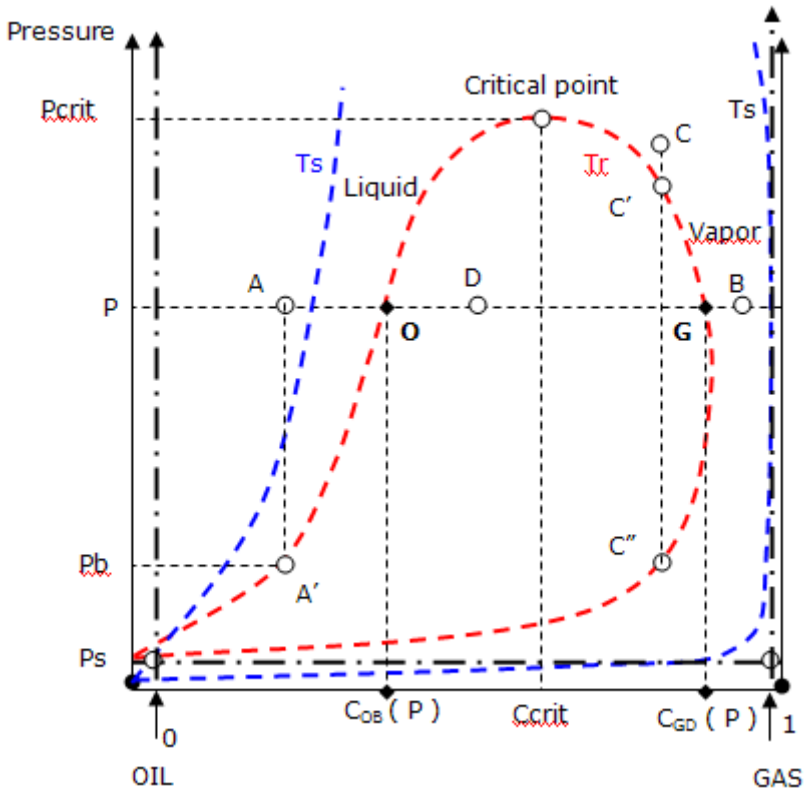


Fig. 9.L.1 – Pressure/Composition diagram of binary mixture

Two curves have been plotted: in red, for reservoir temperature Tr in blue for standard temperature Ts. Each mixture of known composition at a given pressure is represented by a point on this graph.

- The D mixture at pressure P is inside the envelope: it is the 2-phase region. The 2 phases are characterized by the points O and G, of compositions C_{OB} (P) and C_{GD}(P). The mass fraction of each component in each phase is given by:

For the oil phase, point (O):	For the gas phase, point (G):
- mass fraction of oil $C_O^o = (1 - C_{OB}(P))$	- mass fraction of oil $C_G^o = (1 - C_{GD}(P))$
- mass fraction of gas $C_O^g = C_{OB}(P)$	- mass fraction of gas $C_G^g = C_{GD}(P)$

- The A mixture is an undersaturated liquid, whose bubble point pressure Pb corresponds to the point A' of same composition on the Liquid curve.
- The C mixture is an undersaturated gas which has at reservoir temperature a retrograde dew point C', and a direct dew point C".
- The B mixture is a dry gas which has no dew point at reservoir temperature, but has 2 dew points at standard temperature Ts.

The critical pressure Pcrit at reservoir temperature is the maximum pressure where both phases can exist. The corresponding composition Ccrit is the critical composition at Tr. As we assume that the components are the phases at standard conditions, the components used in the model are the Oil phase in standard conditions, called **oil,** and the dryer gas phase at Ts, called **gas**.

The same diagram can be plotted in the ideal case for the BO and the MBO models. In the BO model, the gas phase always contains only gas.

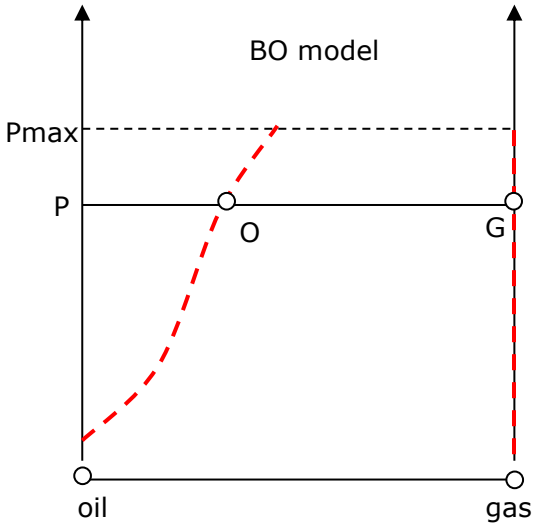


Fig. 9.L.2 – Pressure/Composition diagram of BO

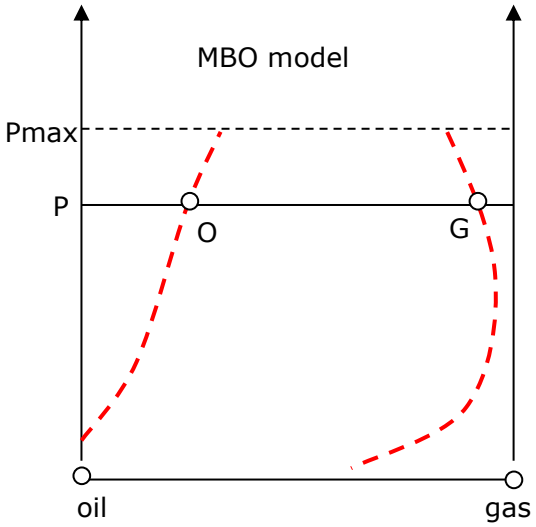


Fig. 9.L.3 – Pressure/Composition diagram of MBO

The composition at bubble point of the oil phase, and at dew point of the gas phases, can be obtained from the Black Oil properties and the oil and gas densities at standard conditions.

$$Rs(Pb) = \frac{C_O / \rho_g sc}{(1 - C_O) / \rho_o sc} \qquad \text{with } C_O = C_{OB}(P_b) \Rightarrow C_O = \frac{1}{1 + \frac{\rho_o sc}{R_s(P_b) \times \rho g sc}}$$

Similarly with the Modified Black Oil:

$$rs(Pd) = \frac{(1 - C_G) / \rho_o sc}{C_G / \rho_g sc} \qquad \text{with } C_G = C_{GD}(P_d) \Rightarrow C_G = \frac{1}{1 + \frac{\rho_o sc \times r_s(P_d)}{\rho g sc}}$$

As illustrated in the previous section, this indicates that once the surface gravities are known, the fluid is defined by the knowledge of the function Rs(Pb), which is the same as the under-saturated gas-oil ratio (and rs(Pd)). Visualizing the problem in terms of compositions makes it easier to consider mixture of varying compositions for which the bubble point and/or dew points can be readily obtained on the C_{OB} (P) or C_{GD}(P) curves. For other properties in the 2-phase region, all that is required is the knowledge of ρo(Pb) and μo(Pb) for the expected range of bubble points. In the single phase region (undersaturated case) an assumption can be made to estimate the properties. A common hypothesis is that of constant slope, ie the derivative of the particular property with pressure.

This is the basis for the multi-phase numerical model of KAPPA-Workstation. This model can be fed with a set of correlations, or may use tabulated properties resulting from a PVT study.

9.M Equations of State

Equations of State (EOS) are models predicting the phase behavior and properties from the fluid composition obtained from the laboratory analysis of the reservoir fluid. Most EOS have developed from early attempts to correct for behaviour of gases which deviated from the ideal gas law. The general form is a cubic equation usually expressed in terms of Z = PV/RT:

$$Z^3 + A_2 Z^2 + A_1 Z + A_{\square} = 0$$

Van der Waals proposed the equation:

$$P = \frac{RT}{V-b} - \frac{a}{V^2}$$

in which b represented the volume of individual molecules, and a was the inter-molecular attraction.

The two most common equations of state used in PVT calculations are:

- Soave-Redlich-Kwong (SRK): $P = \frac{RT}{V-b} - \frac{a}{V(V+b)}$

- Peng-Robinson (PR): $P = \frac{RT}{V-b} - \frac{a}{V^2 + 2bV - b^2}$

Equations of State are used in compositional simulators, as opposed to Black Oil, and they are a *sine qua none* condition for considering such problems as C02 flooding, mixture of several reservoir fluids, etc.

9.N Confined PVT

As mentioned in the chapter 10.B, this issue is unique to unconventional plays. When the size of the pores approaches the size of hydrocarbon molecules, the PVT behaviour in this confined environment may be considerably different from the phase behaviour obtained in a laboratory PVT cell.

This effect can be taken into account by adding an additional condition in the Equation of State that we use to define the PVT properties of the fluid in a numerical model.

9.N.1 Summary

The compositional flash algorithm is modified to account for capillary effects and critical property shift under confinement.

The simulation kernel is also modified to use this new flash. In particular, the pore radius of every cell are stored and accessed during the solution process. Also, the capillary pressure and gas fraction in all the cells are stored.

New flash derivatives accounting for the effect of P_{cap} are derived.

Simulation results with the Unconventional Resources model show a large impact of the critical property shift, but negligible impact of the capillary pressure.

9.N.2 Model description

Two methods can be applied:

- The correction of the flash calculation due to the capillary pressure in the pore.
- The shift of the component critical properties.

9.N.2.a Capillary pressure

For a given reservoir cell, if we assume a single pore size, the effect of capillary pressure can be incorporated in the conventional flash calculation algorithm.

Laplace's equation for vapor liquid equilibrium in porous media gives:

$$P_{cap} = P_g - P_l = \frac{2\sigma}{r} \quad (1)$$

where P_g is pressure of gas phase; P_l is pressure of liquid phase; P_{cap} is capillary pressure; σ is interfacial tension; r is radius of curvature for gas liquid interface.

When it is assumed that the solid surface is liquid wet, the contact angle is 0 degree,

$$r = \frac{r_p}{\cos\theta} = r_p \quad (2)$$

where r_p is the radius of the pore which is assumed to be cylindrical. And

$$P_g - P_l = P_{cap} = \frac{2\sigma}{r_p} \quad (3)$$

The interfacial tension σ can be obtained from the parachors by the MacLeod-Sugden formulation:

$$\sigma^{1/4} = \sum_{i=1}^{n_k} PCH_i \left(x_i \frac{\rho_L}{M_L} - y_i \frac{\rho_V}{M_V} \right) \quad (4)$$

where the PCH_i are the parachors of pure components, x_i and y_i are the molar compositions of liquid and gas phase respectively; ρ_L and ρ_V are the mass density of liquid and gas phase respectively; M_L and M_V are the molar mass of the liquid and gas phase respectively.

9.N.2.b Flash including capillary pressures

The model developed by Shapiro and Stenby, in 2001 takes into account liquid-gas pressure differences. It is used in the algorithms.

9.N.2.c Critical properties shift in nanopores

The Van der Waals theory is modified for a confined fluid in a nanopore with neutral walls (no fluid molecule-pore wall interactions).

$$P_{zz} = \frac{RT}{V-b} - \frac{a-2\left(\frac{c_1}{\sqrt{A_p}}\right)-2\left(\frac{c_2}{A_p}\right)}{V^2} \tag{8}$$

And the critical temperature and pressure shift (dimensionless) are defined as follows,

$$\Delta T_c = \frac{T_c - T_{cp}}{T_c} = 0.9409\frac{\sigma_{LJ}}{r_p} - 0.2415\left(\frac{\sigma_{LJ}}{r_p}\right)^2 \tag{9}$$

$$\Delta P_c = \frac{P_c - P_{cp}}{P_c} = 0.9409\frac{\sigma_{LJ}}{r_p} - 0.2415\left(\frac{\sigma_{LJ}}{r_p}\right)^2 \tag{10}$$

where T_c and P_c are critical temperature and pressure for bulk fluid respectively; T_{cp} and P_{cp} are critical temperature and pressure for confined fluid in pores respectively; σ_{LJ} is Lennard – Jones size parameter given in nm,

$$\sigma_{LJ} = 0.244\sqrt[3]{\frac{T_c}{P_c}} \tag{11}$$

where T_c and P_c are in K and atm respectively.

9.N.3 Results

The consequence of the confined conditions on the PVT behaviour are illustrated in the following examples:

9.N.3.a Influence on the phase envelope

Example 1:

We apply here the Confined PVT option on 2-component systems including 70% C1 and 30% C6, 50% C1 and 50% C6, 30% C1 and 70% C6.

The pore radius is 10 nm and the two approaches are used:

- "Pcap" indicates that Capillary pressure is considered.
- "Shift" indicates the shift to critical properties is considered.

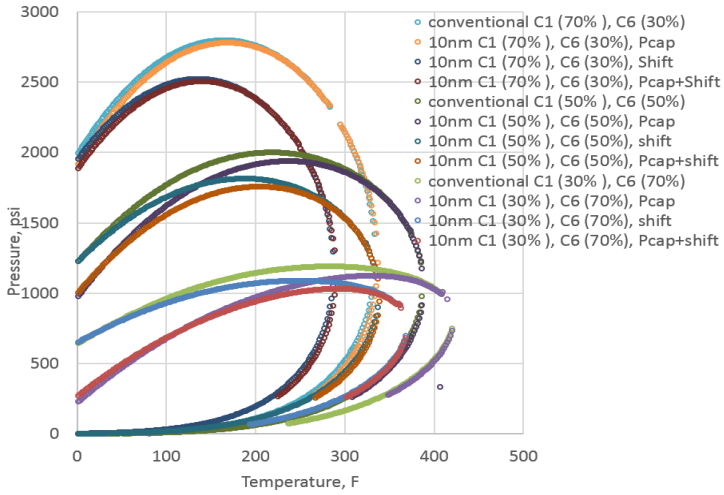


Fig. 9.N.1 – Phase envelopes for 2-component systems C1 and C6 with three different molar compositions.

Example 2:

We apply here the Confined PVT option on 3-component systems including 50% C1 and 30% C4, 20% C10.

The pore radius is 10 nm and the two methods are applied.

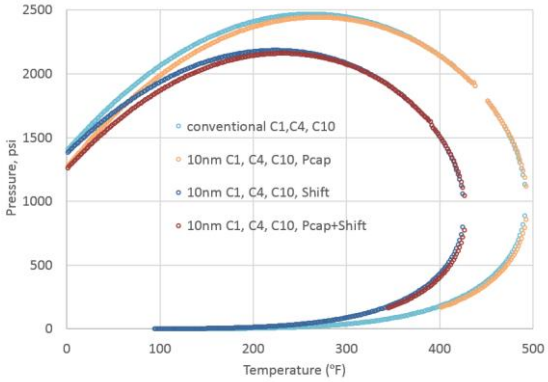


Fig. 9.N.2 – Phase envelopes for 3-component system 50% C1 and 30% C4, 20% C10.

Example 3:

We apply here the Confined PVT option on 4-component: C1 60%, C4: 20%, C6: 15%, C10, 5%.

The pore radius is 20 nm and the two methods results are compared.

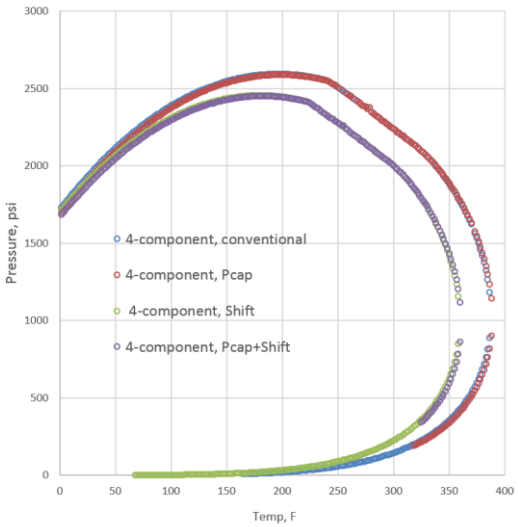


Fig. 9.N.3 – Phase envelopes for a 4-component fluid (C1 60%, C4: 20%, C6: 15%, C10, 5%).

9.N.3.b Influence on the PVT parameters; Density and Viscosity

When only capillary pressure is considered, the density and viscosity of oil may be different from those calculated by conventional PVT only in the saturated region. But with critical property shifts, they differ even in the undersaturated region. The liquid density and viscosity for Bakken oil (composition from SPE 159258 (Nojobaei et al 2012)) are plotted against pressure below.

The pore radius is 10 nm and the two methods are considered.

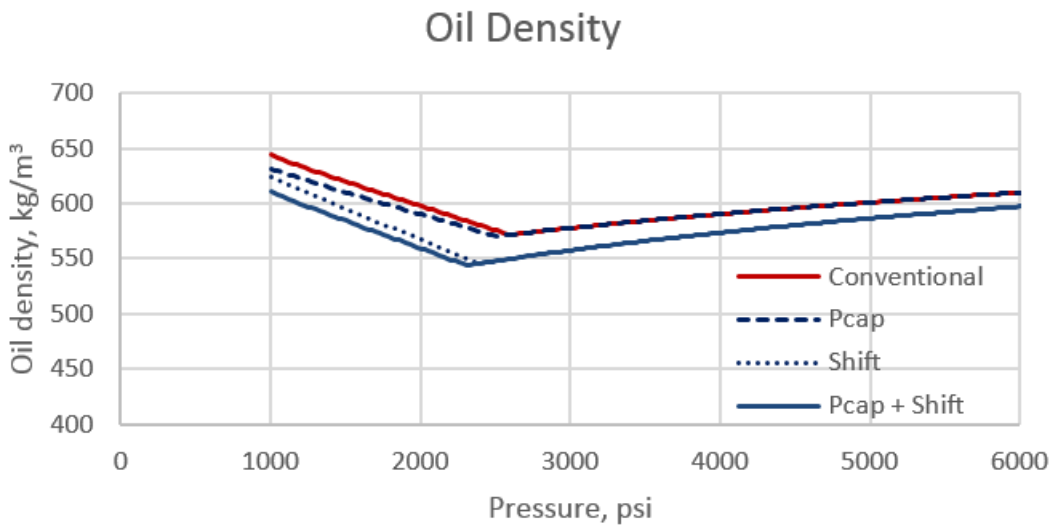


Fig. 9.N.4 – Liquid density for Bakken oil

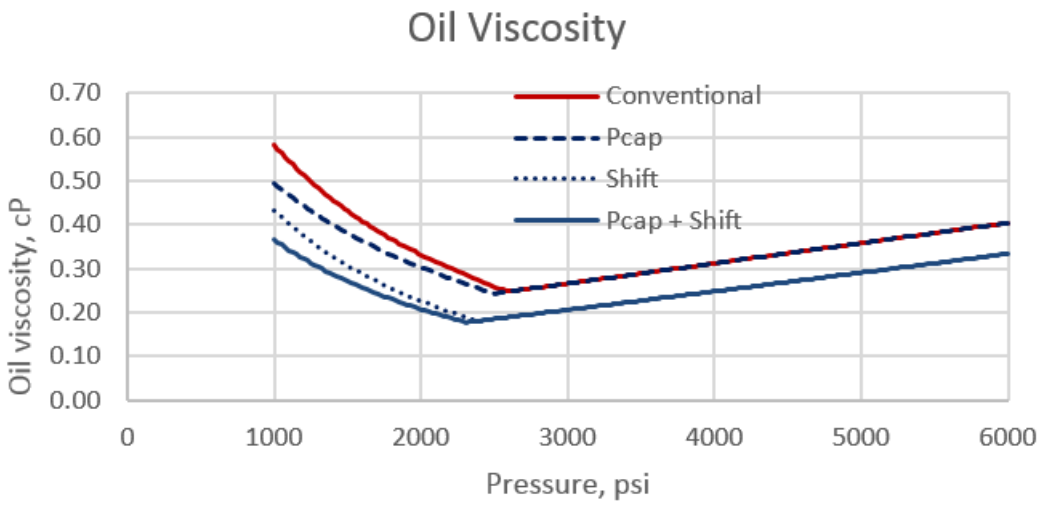


Fig. 9.N.5 – Liquid viscosity for Bakken oil

9.N.3.c Influence on the production simulations

The study is here made on a 3-component system contains 50% C1 and 30% C4, 20% C10. See Fig 9.N.2 for the phase envelopes.

The well model is a multiple fractured horizontal well with 2 fractures.

Reservoir parameters:

- Initial pressure and reservoir temperature: 4000 psi and 241 °F
- Bubble point pressure:
  - Conventional: 2462 psi; Pcap: 2431 psi;
  - Shift: 2179 psi; Pcap+Shift: 2159 psi.
- Bottom hole pressure: from 2000 psi to 1756 psi
- Permeability: 0.003 md
- Porosity: 6%

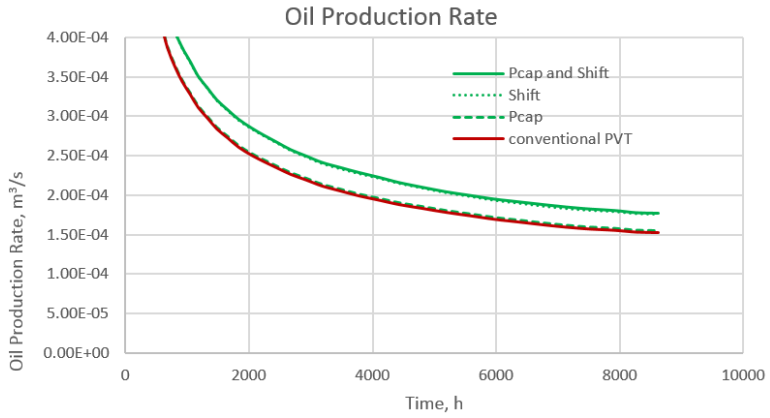


Fig. 9.N.6 – Oil production rate for a 3-component fluid with initial composition of 50% C1 and 30% C4, 20% C10.

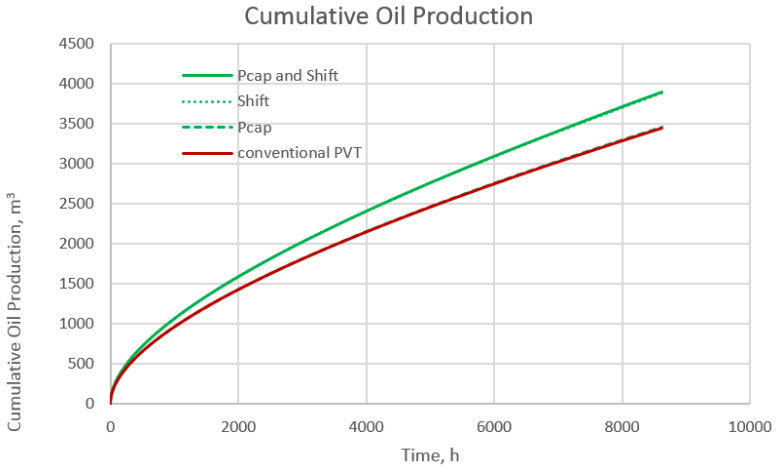


Fig. 9.N.7 – Cumulative oil production for a 3-component fluid with initial composition of 50% C1 and 30% C4, 20% C10.

9.N.4 References

Alharty, Nguyen, Teklu, *Multiphase Compositional Modeling in Small-Scale Pores of Unconventional Shale Reservoirs*, SPE 166306, SPE ATCE, New Orleans, Louisiana, 30 September – 2 October 2013.

Devegowda, Sapmanee, Civan, *Phase Behavior of Gas Condensates in Shales Due to Pore Proximity Effects: Implication for Transport, Reserves and Well Productivity*, SPE 160099, SPE ATCE, San Antonio, Texas, 8-10 October 2012.

Firincioglu, *Bubble Point Suppression Effect In Unconventional Liquids Rich Reservoirs And Its Impact On Oil Production*, PhD Thesis, Colorado School of Mines, 2012.

Firincioglu, Ozgen and Ozkan, An Excess-Bubble-Point-Suppression Correlation for Black Oil Simulation of Nano-Porous Unconventional Oil Reservoirs, SPE 166459, SPE ATCE, New Orleans, Louisiana, 30 September – 2 October 2013.

Nojabaei, Johns, Chu, Effectos of Capillary Pressure on Fluid Density and Phase Behavior in Tight Rocks and Shales. SPE 159258, SPE ATCE, San Antonio, Texas, 8 – 10 October 2012.

Teklu, Alharty, Kazemi, Yin, Graves and AlSumaiti, *Phase Behavior and Minimum Miscibility Pressures in Nanopores*, SPE Reservoir Evaluation and Engineering, 2014.

Shapiro and Stenby, *Thermodynamics of the Multicomponent Vapor-Liquid Equilibrium under Capillary Pressure Difference*, Fluid Phase Equilibria, 178 (1) 17-32, 2001.

Zarragoicoechea and Kuz, *Critical Shift of a Confined Fluid in a Nanopore*, Fluid Phase Equilibria, 220 (1) 7-9, 2004.

10 – Unconventional Resources

OH – DI – TBA – VA – DL – DV – ET – IK - DN

10.A Introduction and Definitions

The engineers already involved in the production of unconventional plays will not need to read and will certainly skip this section. However other readers come from regions where the production of these plays is new or non-existent. Hence this little introduction…

Hydrocarbons were generated in source rocks, where they stayed or migrated until they reached surface or were trapped by sealing rock barriers creating conventional reservoirs. Unconventional reservoirs are these source rocks where oil and/or gas remained in situ.

Knowledge of the presence of large amounts of hydrocarbons in these formations is not new. But they have a very low effective permeability and could not be produced because of technology limitations and prohibitive production costs.

Production has recently been made possible by creating multiple fractures along horizontal drains. This technique increases the order of magnitude of the contact area between the well and the formation, making the production economically viable.

Another way to introduce unconventional is to show the diagram below (Holditch), summarizing that the 'easy oil and gas' is coming to an end and unconventional formations represent a technological and economical challenge with the 'promise' of massive reserves.

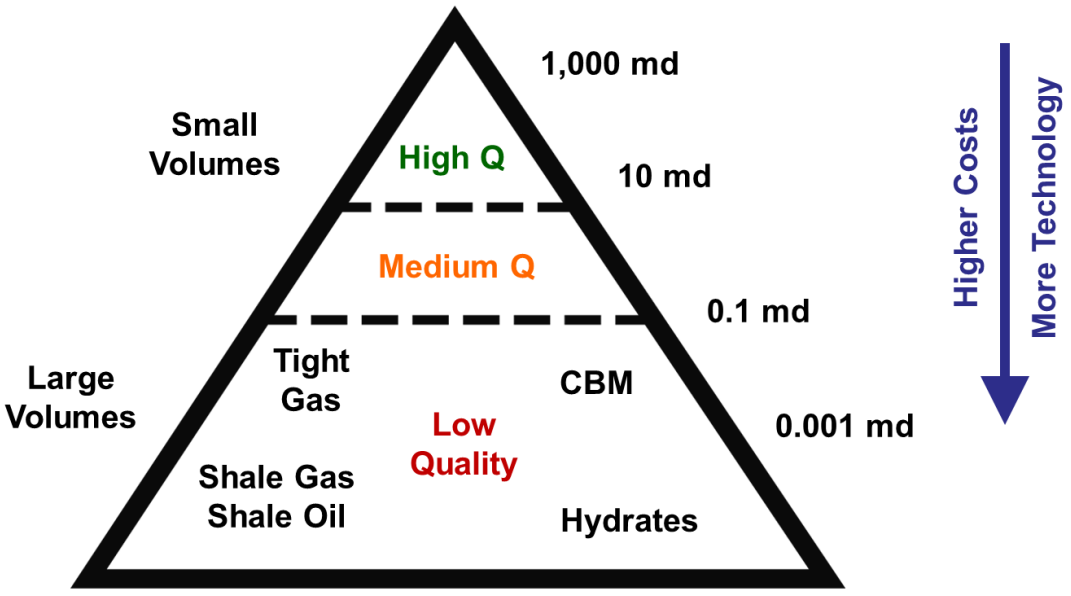


Fig. 10.A.1 – Resource triangle. (From Holditch, 2006)

It is the common understanding that the term 'unconventional' refers to shale gas, shale oil, coal seam gas, oil shale and methane hydrates. We will introduce all of them but in this chapter we will focus on shale oil and shale gas production.



Fig. 10.A.2 – North American shale plays. (From EIA, 2011)

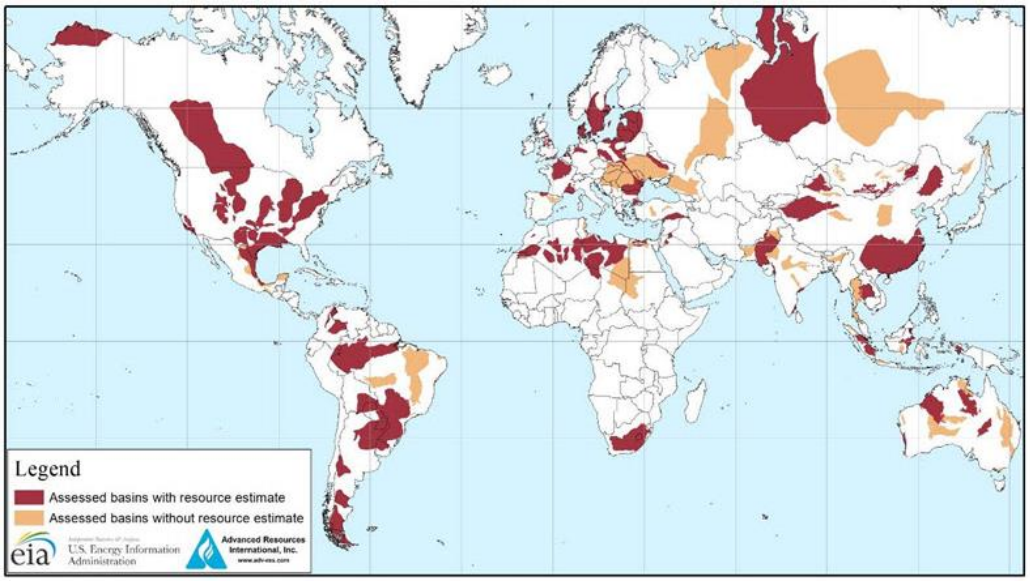


Fig. 10.A.3 – Global shale plays. (From EIA, 2011)

10.A.1 Shale gas

Shale gas is trapped within organic-rich sedimentary formations (usually 5-20% TOC) with a high proportion of fine-grained particles, such as shale (fissile), mudstone (non-fissile), siltstone, carbonates, and fine-grained sandstone interlaminated with shale or mudstone. Permeability in these source rocks typically range between $1x10^{-5}$ and $1x10^{-1}$ mD.

In 2013 the total technically recoverable shale resources was 7,300 trillion cubic feet, the main countries being China (1,100), Argentina (800), Algeria (700), the US (660), Canada (570), Mexico (540), Australia (440), South Africa (390), Russia (290) and Brazil (250) (From EIA, 2013). However the United States and Canada are by far the major shale gas producers.

According to the EIA (2012) the U.S. shale gas dry production was 25.7Bcf/d in 2012. Most of this production comes from nine formations, mainly from the Marcellus (West Virginia), the Haynesville (Louisiana) and the Barnett (Texas).

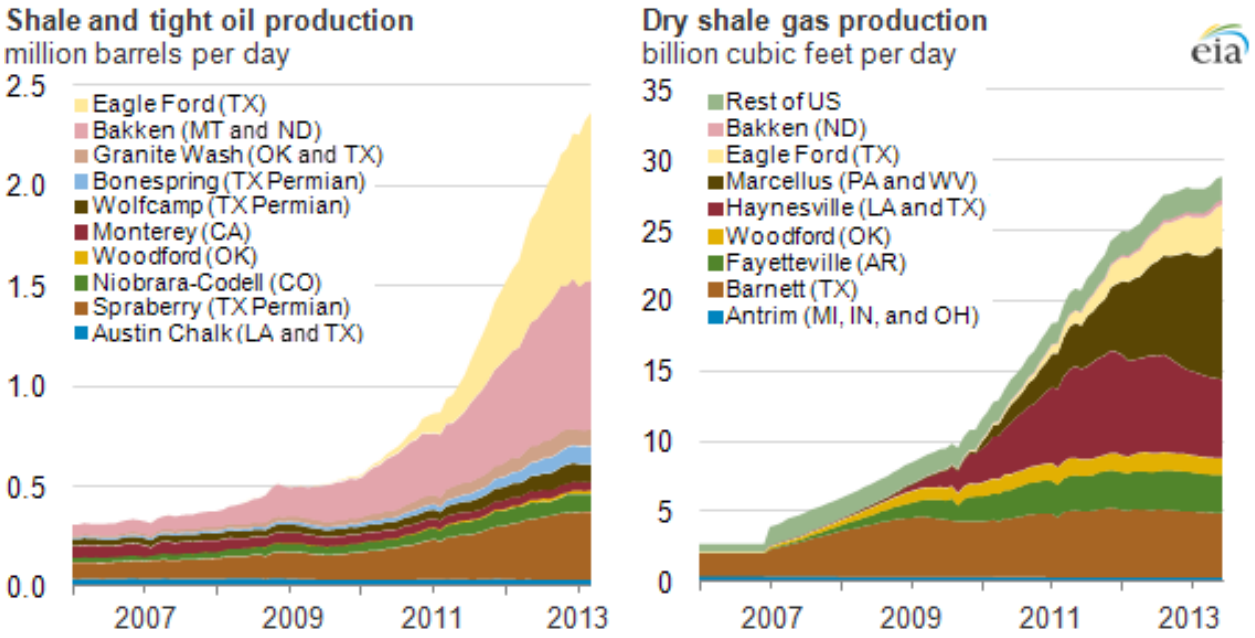


Fig. 10.A.4 – US shale/tight oil and dry shale gas production.
*(*From IAEE/AEA meeting, January 4, 2014, Philadelphia, PA*)*

In Canada, the two main formations produced are the Horn River (British Columbia) and the Montney in the Western Canadian Sedimentary Basin (British Columbia and Alberta), with about 2.0 Bcf/d in 2012, (From IAEE/AEA meeting, January 4, 2014, Philadelphia, PA).

Although China was ranked as the largest holder of technically recoverable shale gas resources by the EIA, commercial production is still very limited and concentrated in Sichuan Basin. In Central and South America, operations are essentially located in Argentina and Mexico (exploration). In Europe, exploration operations are underway (Poland, Romania, Germany, U.K., Austria, Denmark) without any real commercial production yet.

10.A.2 Shale oil

During the sedimentation and burial processes the temperature and pressure increase in these organic rich shale rocks. Chemical reactions break the kerogen down into various forms of hydrocarbon. Heavy, liquid hydrocarbons are generated in a lower temperature and pressure range 'the oil window', followed by lighter hydrocarbons at higher temperature and pressure in in 'the gas window'. The hydrocarbon content can hence vary depending on the maturation stage of the formation.

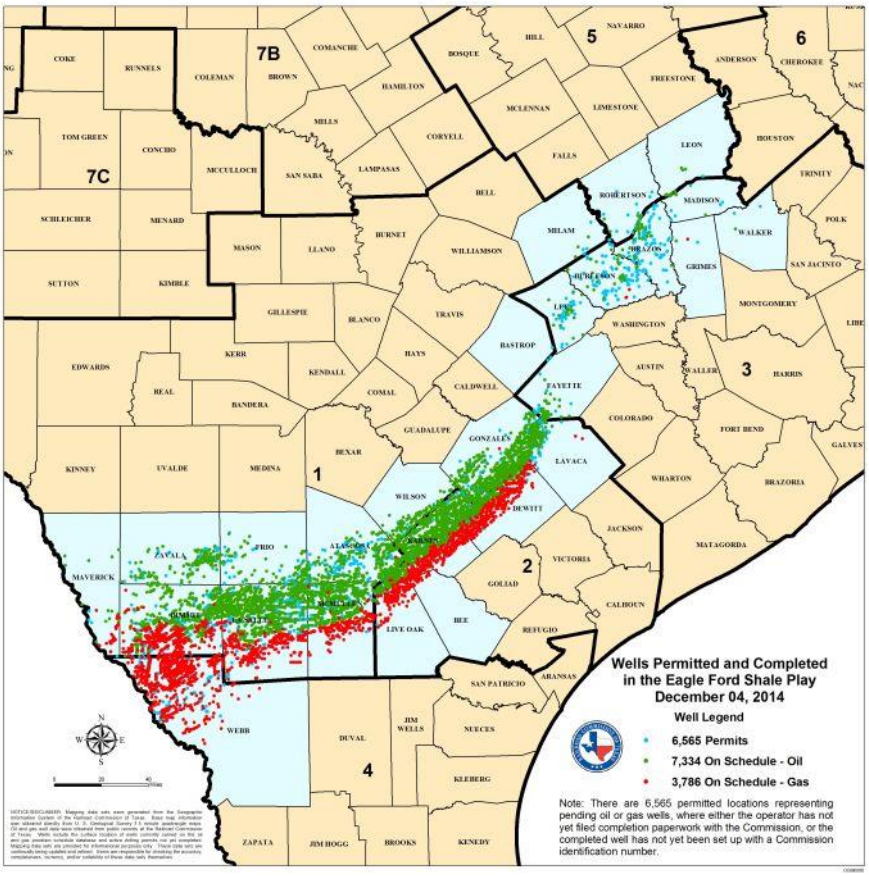


Fig. 10.A.5 – Eagle Ford shale play well permits and completions. (From TX RRC, 2014)

Initially, the production of shale plays was focused on gas windows, where the higher mobility enabled acceptable production despite the technical challenges. But technological advances in drilling and completion, as well as economic constraints (falling gas prices and relatively high oil prices) unlocked the production of source rock liquids. Hence production now tends to concentrate on the liquid-rich, condensate and oil windows.

In 2013 the total technically recoverable shale resources was 344 billion barrels, the main countries being Russia (75), the US (58), China (32), Argentina (27), Libya (26), Australia (18), Venezuela (13), Mexico (13), Pakistan (9) and Canada (9). (From EIA, 2013).

As for shale gas, the United States and Canada are so far the only major producers of shale oil. According to the EIA, the U.S. production of shale and tight oil averaged 3.22 MMbbl/d in 2013. Most of this production comes from two plays: the Eagle Ford (South Texas) and the Bakken Formation (North Dakota and Montana).

In Canada, the EIA estimated the shale and tight oil production to average 0.34 MMbbl/d in 2013, about 10% of the total Canadian crude oil production.

In Argentina, YPF is producing oil from the Vaca Muerta Shale in the Neuquén Basin. Exploration operations have also started in Australia, United Kingdom and China.

10.A.3 Coal seam gas (not covered in this chapter)

Coal Seam Gas, or CSG, was initially called Coalbed methane, or CBM, until the name became too unpopular and was changed. CSG refers to methane that is produced from coal beds.

It is generated during the conversion of plant material to coal through burial and heating (coalification). Most of the methane migrates to surface or into a reservoir rock, but a significant volume remains trapped within the coal itself. Hydraulic pressure, rather than a conventional pressure seal, is the major trapping force.

Two distinctive porosity systems characterize coal seams: (1) a network of natural fractures (cleats) which develop under shrinking or tectonic stress, and (2) matrix blocks of very low permeability and highly heterogeneous porous structure between the cleats.

With this structure, gas is stored in 4 different ways:

- free gas within the micropores and cleats;
- dissolved gas in water within the coal;
- adsorbed gas on the surfaces of micropores and cleats;
- adsorbed gas within the molecular structure of the coal molecules.

Some coals at shallow depths with good cleat development contain significant amounts of free and dissolved gas. But the proportion of adsorbed methane generally increases with the coal rank and pressure (depth). The surface area available for methane adsorption is extremely large (20-200 m^2/g). Coal is hence capable of adsorbing very large quantities of methane (from 100 to 800 scf of methane per ton of coal). Saturated coal seam gas reservoirs can have five times the volume of gas contained in a conventional sandstone gas reservoir of comparable size.

Most of the gas in coal beds is stored in the adsorbed form, which is one of the main differences with shale gas, where produced volumes essentially come from free gas storage in the micropores.

Another difference with shale gas is that coal seams are usually quite close to the surface, and surface aquifers, whilst shale gas is commonly found at depths below one kilometer. Cleats are then very often initially filled with water. When the reservoir is put into production very large volumes of water are first produced before gas can start desorbing from the matrix and flow through the cleats to the wellbore, leading to a characteristic production profile.

The cleat spacing is very uniform and ranges from the order of millimeters to centimeters. Face cleat is continuous throughout the reservoir, while the butt cleat is discontinuous and terminates at intersections with the face cleat. These cleat patterns are crucial for gas production because they allow for the release of adsorbed gas within coal beds and migration to the production well. The ratio of permeabilities in the face cleat direction over the butt cleat direction may range from 1:1 to over 10:1. Because of this anisotropic permeability, drainage areas around coal bed methane wells are often elliptical in shape.

Global CBM production totals 5.8 Bcfd from 15 basins in the USA, Australia, Canada, China, and India. Despite its unconventional nature and a lot of common features with shale oil and shale gas, CSG will not be developed further in this chapter but may be in a following update.

10.A.4 Oil shale *(not covered in this chapter)*

There is often confusion between Shale Oil, which will be treated in this chapter, and Oil Shales. To be honest they could have picked more distinct names…

Oil shales are sedimentary rocks with significant amounts of kerogen at early maturation stage. These deposits were formed by underwater deposition of silt and organic debris. This material is slowly transformed into shale oil by heat and pressure, but in the case of the oil shales the natural maturation process is still at a very early stage and may require millions of years to be completed.

Oil shales can generate oil when the rock is heated upon pyrolysis, either underground (in-situ upgrading for deep deposits) or at surface (retorting process for shallow deposits).

Modeling in-situ upgrading and production of oil shale is extremely challenging. A numerical simulation model is required, that involves a fully compositional formulation with chemical reactions and thermal effects. The solid phase must also be correctly modeled to account for the prechar resulting from the pyrolysis. Geomechanical effects and thermal wellbore effects may also need to be included in the model.

Total worldwide oil shale resources are estimated to be equivalent to 3 to 5 trillion barrels.

Despite their unconventional nature, oil shales are not considered further in this chapter.

10.A.5 Hydrates *(not covered in this chapter)*

Gas hydrate is a crystalline (ice) form of water trapping gas of low molecular weight, typically methane. A gas molecule is surrounded by stable 'cages' of water molecules. Each water cage encloses a space of a particular size, and only a gas molecule small enough to fit within this site can be hosted. These structures can store a significant amount of gas, typically 160 scf of methane for 1 cf of gas hydrate.

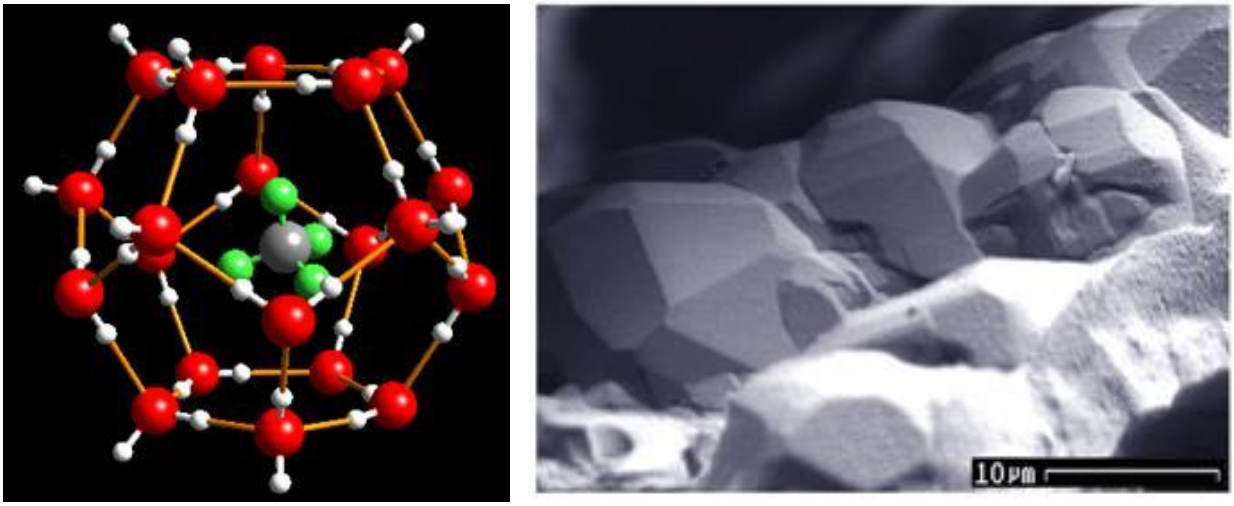


Fig. 10.A.6 – Water molecules around a methane molecule. (From USGS)

Gas hydrate occurs mostly in marine sediments of the continental shelf. In lesser quantities it also occurs in the onshore permafrost or offshore relic permafrost. Gas hydrate is stable at low temperature and high pressure. Hence, the gas can be released by depletion or heating. Injection of inhibitors is also possible.

Numerical simulation of these production processes is still at the research stage. It involves a fully-compositional formulation with chemical reactions and thermal effects.

The amount of methane sequestered globally in gas hydrate deposits is estimated to be between $1x10^5$ and $5x10^6$ trillion cubic feet. Only a fraction of this amount is likely to be commercially accessible. Despite their unconventional nature, gas hydrates are not considered further in this chapter.

10.B Specifics of shale plays

The most obvious difference between conventional and shale plays is the order of magnitude of the permeability. We are now speaking about micro and nano-Darcys. Without even considering the impact on the validity of the diffusion equations and unreasonably simple flow geometries, the low permeability alone will have a substantial impact;

- The flow is likely to be transient for most of the producing life of the wells.
- There are additional challenges to accurately model the system, either analytically or numerically.
- Because we are at the beginning of the life of these types of plays, we totally lack empirical knowledge of their long term production.

Then we have to question the diffusion equations we have been routinely using over the past century. A diffusion equation in a homogeneous context will be the combination of a pressure gradient law (e.g. Darcy), the principle of conservation of mass and a PVT correlation. For the gradient law the rock constant (e.g. permeability) may be sensitive to pressure and stress. Finally the reservoir may not be homogeneous and may require modeling using various networks of natural fractures and matrix blocks.

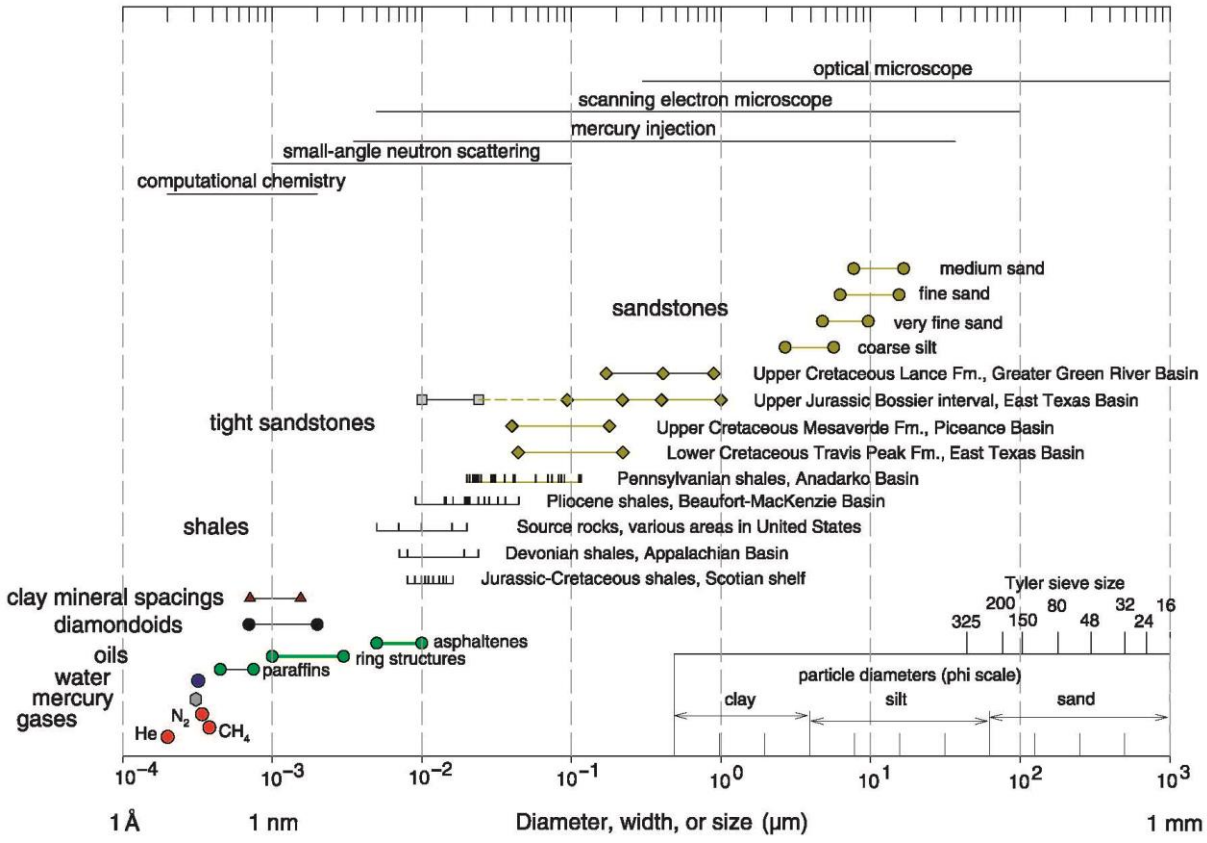


Fig. 10.B.1 – Sizes of molecules and pore throats in siliciclastic rocks. (From Nelson, USGS)

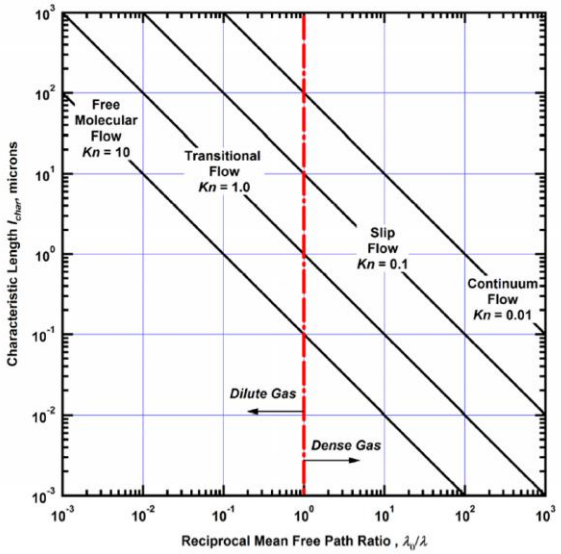


Fig. 10.B.2 – Limit of the different flow regimes (Florence, Texas A&M, 2007)

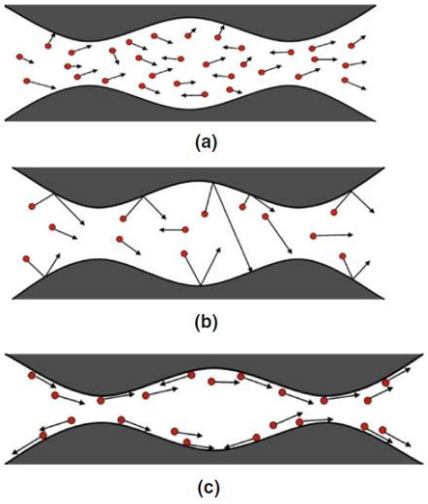


Fig. 10.B.3 – Schematic of cross section of a pore and gas molecule:

(a) Bulk diffusion
(b) Knudsen diffusion
(c) Surface diffusion

The diffusion equation resulting from these components will therefore be influenced by initial and boundary conditions. In a conventional play we will start, not unreasonably, with uniform pressures and saturations. Inner boundary conditions are mainly about the wells, using again a pressure gradient relationship such as Darcy's law. In a conventional well test the outer boundary conditions may be approximated to an infinite reservoir, but for longer term diffusion one will typically use pressure support (e.g. aquifers) or no-flow boundaries, either physical or coming from the definition of the well drainage area.

Compared to conventional plays, we might still believe in the conservation of mass but all the rest above can, and should be challenged:

- The diffusion equations are more complex, and it is accepted that one should consider at least three different scales of diffusion.
- Rock properties are highly dependent on stress.
- With pore size and molecule size converging dangerously, PVT correlations derived from lab experiments should be challenged.
- Initial producing conditions come after massive fracture jobs. Initial conditions should take into account important pressure and saturation gradients at production time zero.
- In order to compensate for the drop in permeability we increase the magnitude of the contact area between the well and the formation by the means of running multiple fractures along a drain that is generally horizontal. So the well models are much more complex, even assuming we exactly know the fractures geometries, which is seldom the case.
- The last and main challenge today is our lack of knowledge of the flow geometry in the reservoir, and the need (or not) to use discrete fracture networks (DFN).
- To add insult to injury, we typically lack quality data in shale plays.

The different specifics of unconventional plays are detailed below.

10.B.1 Impact of the low permeability

Transient behavior

In a conventional play, wellbore effects and the geometry of the flow around the well will dominate the system response for a few hours or a few days for long horizontal drains. In a matter of hours or days the reservoir will exhibit its average properties upon reaching infinite acting radial flow (or equivalent) regime. Eventually, after a few weeks, the first reservoir boundaries or nearby producing wells are detected. There is no strict rule and there are exceptions, but this is generally what you would expect.

Things are radically different in unconventional plays, because the drop in mobility dramatically increases the time scale of these behaviours. As a result the flow around the well, and more specifically orthogonally to the hydraulic fractures, will last months or years, and we may wait for centuries to eventually detect the equivalent of infinite acting radial flow. This is at least the case when we lump the reservoir into a homogeneous equivalent system.

As a result we may expect that the system will be in transient behaviour for most if not all the producing life of the well. Even the SRV flow, detailed later in this chapter, is strictly speaking a transient regime.

Lack of empirical knowledge

We have been actively producing these plays for only a few years. Considering that we are dealing with long transients, we do not yet have the experience of a complete production cycle. In the absence of such experience it is very courageous to extrapolate what we see today and predict what will happen in five or ten years. Using conventional analogs is hazardous, and we have seen this when early linear flow transients were extrapolated as if they were the final well regime, producing ridiculously high values of the 'b' decline factor.

Modeling issues

Even keeping the simplest diffusion assumptions, the modeling of extremely low permeability formations presents new challenges for both analytical and numerical models.

Analytical models are generally computed in dimensionless terms, in real or Laplace space. Even in Laplace space the model will be accurate to at least four significant figures and would not care less about the real value of permeability, whether it is a Pico-Darcy or a Giga-Darcy. However the accuracy issue arises when converting the solution to the real fluid pressure. Because the reservoir is of extremely low permeability the pressure gradients, in commercial production, will be very high in the vicinity of the sandface, and this is a direct effect on Darcy's law. Given this pressure gradient, it would be totally wrong to assume that the fluid is slightly compressible. The resulting compressibility gradient will not only require the use of pseudopressures, which is straightforward, but also the use of pseudotime functions. The problem with pseudotime is that it requires in turn, at each time step, a reference pressure that is supposed to be the average pressure in the zone affected by the well production.

This is obtained by a material balance in a moving volume constrained by the flow geometry. This is taken into account in the generalized pseudo function approach and the dynamic pseudo time method. See more details in the chapter "13.E - The use of pseudofunctions", paragraph 13.E.5.

Numerical models do not have this issue of pseudopressure or pseudotime, as the real PVT is used in each cell. However the numerical model is very sensitive to the permeability values and requires extremely refined grids in the places where the pressure gradients are the highest, i.e. in the vicinity of the well. So in turn the numerical model needs calibration.

Model calibration can be done, for the same geometry, by going back and forth between the analytical model and the numerical model:

- The first stage is to model a slightly compressible fluid diffusion for this geometry. If the fluid is slightly compressible, and even though we know it is not the case physically, the analytical solution, if derived properly, will be exact. If we enter the same slightly compressible fluid PVT in the numerical model we will be able to check if, for a given permeability, the gridding of the numerical model is suitable to match the analytical solution. In other words we calibrate the numerical model by the analytical model in the limit case of a slightly compressible fluid.
- Once we have done this we can be fairly confident in our numerical model and we have to continue with the real fluid diffusion. Except in extreme cases of multiphase flow the calibrated grid will be sufficient and we will be able to simulate the same case integrating the nonlinearities related to the compressibility gradients. This is the time then to try the analytical model using pseudopressure and pseudotime corrections. If the correction is sufficient to match the numerical results we have calibrated the analytical model and we can be fairly confident that the result will not be off. If the data is not matched it means that the nonlinearities cannot be corrected with pseudofunctions and that we may as well focus on the numerical model.
- We have noticed that some engineers are still using numerical models with a gridding that is not adapted to the low permeability and the high pressure gradients. In this case the simulation may be substantially wrong and the simulator itself is not to blame.

10.B.2 Diffusion equations

If we wanted to do the thing as correctly as we know how…

The accurate description of transport phenomena in unconventional formations is still an active research area, with wide and often contradictory literature.

Many different scales (up to 5 or 6) are involved, associated with a lot of different physical processes: molecular diffusion, desorption, Knudsen / Darcy / Forchheimer flow, PVT phase behavior, stress dependence, etc.

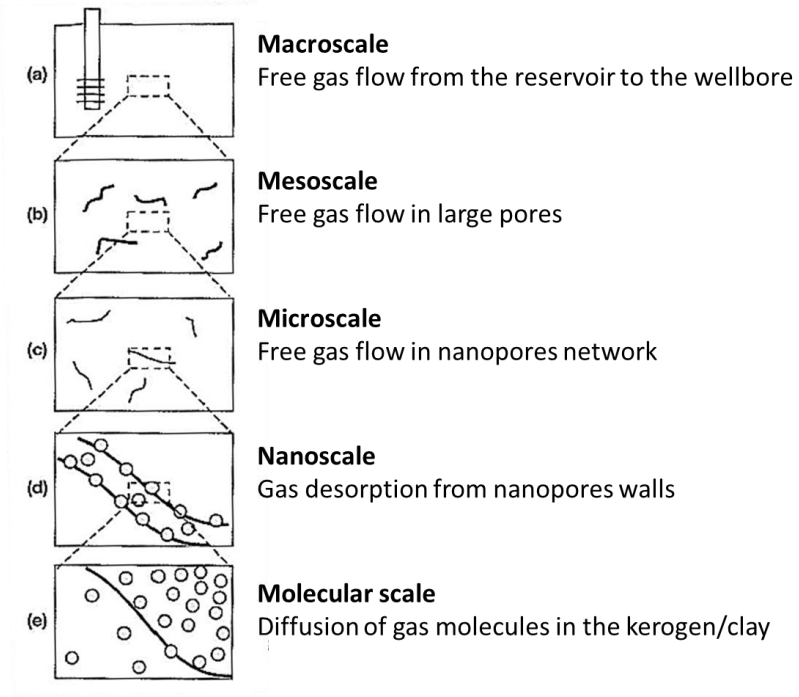


Fig. 10.B.4 – Storage and transport in shale gas sediments. (From Javadpour et al, 2007)

In order to achieve a practical model, some degree of simplification is necessary, and some scales have to be lumped together.

The general agreement is that one could consider three scales of diffusion in order to get an accurate picture of what is happening in unconventional plays: (1) At the level of micropores, (2) between micropores and (3) within the network of natural and hydraulic fractures leading to the well. For each of these scales, different storage mechanisms (solution, adsorption, free compressed fluid) and transport mechanisms (molecular diffusion, Darcy flow, etc…) may be considered. We also need to look at stress dependence and specific PVT issues.



Fig. 10.B.5 – Transport mechanisms in coal seam methane:
(a) Desorption from internal coal surface (b) Diffusion through the matrix and micropores and (c) Fluid flow in the natural fracture network. (From Reeves and Pekot, 2001)

10.B.2.a Desorption

Desorption occurs at the level of the micropores. In coals or organic shales, gas is stored by adsorption on the walls of the micropores in quantities that depend on temperature and pressure. When the pressure is reduced in the system by producing the free fluid, some molecules are desorbed from the walls and released into the micropores.

In practice, reservoir engineers use a model $V_{ads}(P)$ which gives the volume of adsorbed gas per unit mass of rock as a function of pressure:

$$V_{ads}(P) = V_S.\theta(P)$$

The quantity V_S is a reference volume of gas adsorbed per unit mass of rock material. $\theta(P)$ is called the adsorption isotherm. It is the coverage fraction of the surface available for adsorption (dimensionless). The most commonly used model is the Langmuir isotherm:

$$\theta(P) = \frac{P}{P_{half} + P}$$

Above, the P_{half} is the pressure for which the coverage factor is ½:

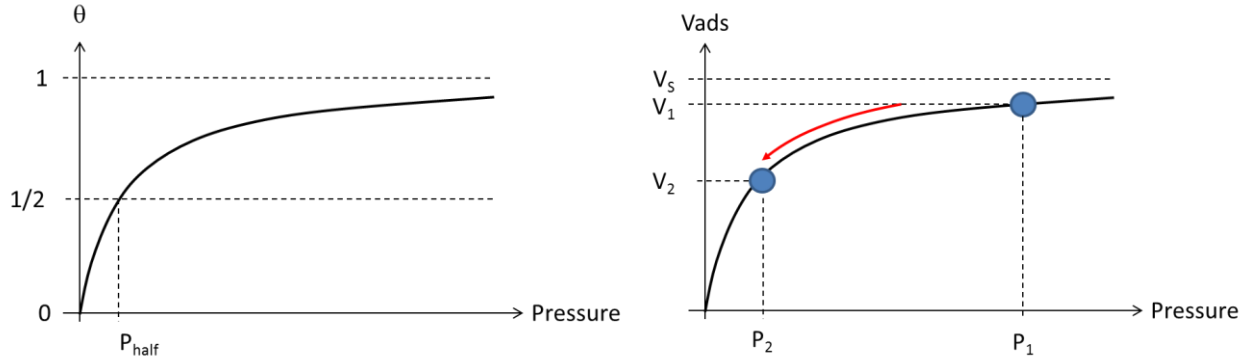


Fig. 10.B.6 – Langmuir isotherm. When the pressure is reduced from P1 to P2, the quantity desorbed in the system per unit mass of rock material is given by (V1-V2).

Although Langmuir's model is the most commonly used model in the industry, other θ functions can be found in the literature: Freundlich, Toth, Unilan, etc.

In coal seam gas, the pores are initially filled with water and the quantity of gas initially adsorbed in the system is actually lower than the prediction of the theoretical isotherm at P_i. In this case, the pressure in the pores will have to be decreased to the saturation pressure (also called critical desorption pressure) before gas can start to desorb. The quantity initially adsorbed corresponds to the value of the isotherm at this critical pressure P_{crit}. This situation is called undersaturated initial state.

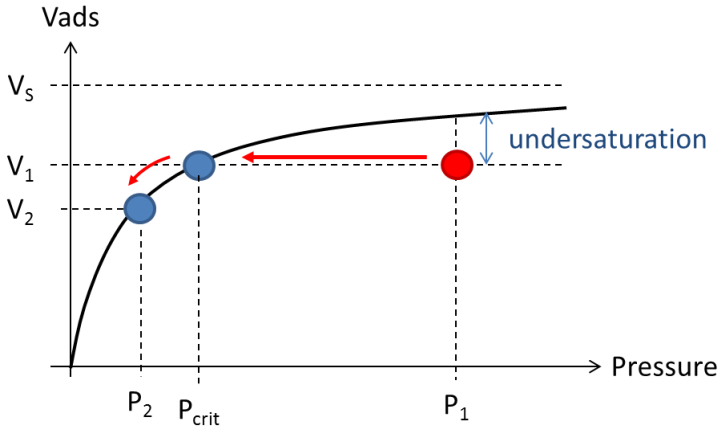


Fig. 10.B.7 – Langmuir isotherm. Gas starts to desorb when the pressure reaches the Pcrit, then, w the pressure is reduced from P1 to P2, the quantity desorbed in the system per unit mass of rock material is given by (V1-V2)

Isotherms used for volume estimations are typically obtained from laboratory measurements. When dealing with coal samples, two types are used for lab analysis and reporting:

- As received: the sample represents in-situ conditions, and can be used as is for in-situ volumes estimates.
- Dry and ash free: the sample is free from moisture and ash. The reference equation has to be corrected to account for the in situ moisture content f_m and the ash content f_a - in order to avoid overestimating the adsorbed quantity: $V_{ads}(P) = V_S.(1 - f_a - f_m).\theta(P)$

10.B.2.b Molecular diffusion and diffusion between micropores

Molecular diffusion: from desorption the concentration of the solution gas stored inside the kerogen changes between the surface and the bulk of the kerogen material. This induces a slow gas transfer by molecular diffusion inside the kerogen, following Fick's law:

$$J = -D.\nabla\emptyset$$

where J is the diffusive flux, D is the diffusion coefficient and ϕ is the gas concentration.

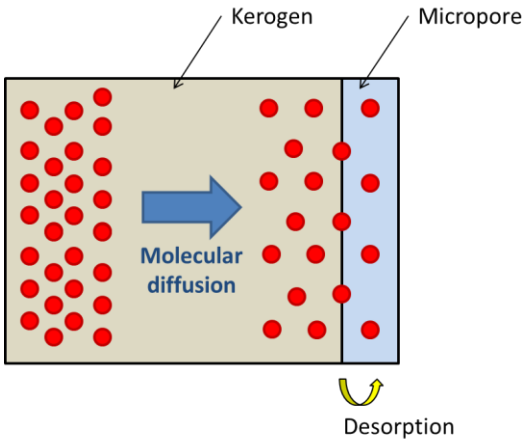


Fig. 10.B.8 – Gas diffusing from high gas concentration to low concentration.

Diffusion between micropores: This is usually modelled with continuum methods, using either Fick's diffusion (especially for coal seam methane) or a more classical diffusion based on the Darcy equation, with a very low effective permeability. However, given the size of pore throats in unconventional systems, the validity of continuum methods with no-slip conditions can be discussed.

The flow regime for a gas flowing in a micro-channel is given by the Knudsen number: $K_n = \frac{\lambda}{l_c}$, where λ is the mean free path of the gas molecules (distance between 2 consecutive collisions) and l_c is the channel radius. As long as the Knudsen number is small (ex: large pores in conventional formations), gas flows under no-slip condition, and average diffusion in the porous medium can hence be correctly described by Darcy's law using an intrinsic permeability value. But in nanoporous system, the pore size is not negligible compared to λ and the Knudsen number increases ($0.01 < K_n < 0.1$). In this case, gas molecules freely slip on the surface of the pores and collide with the wall or other molecules (slip flow conditions).

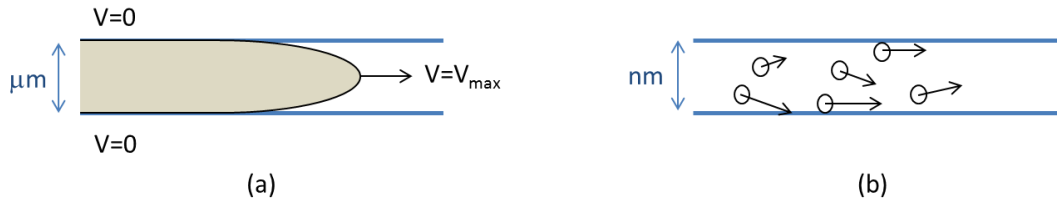


Fig. 10.B.9 – Gas flow in a pore under (a) no-slip condition with the characteristic Poiseuille velocity profile and (b) slip flow conditions. (From: Javadpour et al, Nanoscale gas flow in shale gas sediments, Canadian J. P. T. Oct 2007)

This induces an apparent increase of the effective permeability of the system, known as the Klinkenberg effect:

$$k = k_\infty \left(1 + \frac{b}{P}\right)$$

Above, k is the effective permeability, k_∞ is the reference permeability measured under no-slip conditions, and b is the gas slippage factor, which depends on the rock-gas couple.

An important consequence of this effect is that if we keep using the classical Darcy's law to match and forecast production data, the estimated effective permeability will actually not be an intrinsic property of the rock, but will also depend on the properties of the gas and on the production pressure. This aspect is also discussed in the PVT paragraph below.

10.B.2.c Fracture diffusion

Inside fractures, the classical Darcy's law is used, and the description does not fundamentally differ from conventional situations:

$$\boldsymbol{\nabla P = -\frac{\mu}{k}.\vec{u}}$$

When the gas velocity increases (ex: near the drain inside hydraulic fractures), significant inertial (non-Darcy) effects can occur. This induces an additional pressure drop in the hydraulic fractures in order to maintain the production rate, also modeled as a rate-dependent skin in pressure transient analysis. In this case, an additional term is simply added to the Darcy equation, involving the Forchheimer factor β:

$$\boldsymbol{\nabla P = -\frac{\mu}{k}.\vec{u} - \beta.\rho.|\vec{u}|.\vec{u}}$$

Darcy / Forchheimer equations may apply differently in hydraulic and natural fractures:

Hydraulic fractures are opened and propped during the injection process. Since their orientation and length have a major impact on production, they should always be explicitly included in the model.

For natural fractures two situations can be considered:

- They form a dense network of small, well-connected objects. The system behaves like a homogeneous equivalent medium with an effective large-scale permeability k*. The geometry of the natural network can be ignored. The fractured nature of the medium may then approximate to a double-porosity model.

  This is typically the case in coal seam methane, where the dense network of cleats is treated as a homogeneous equivalent medium, fed by diffusion inside the coal matrix.

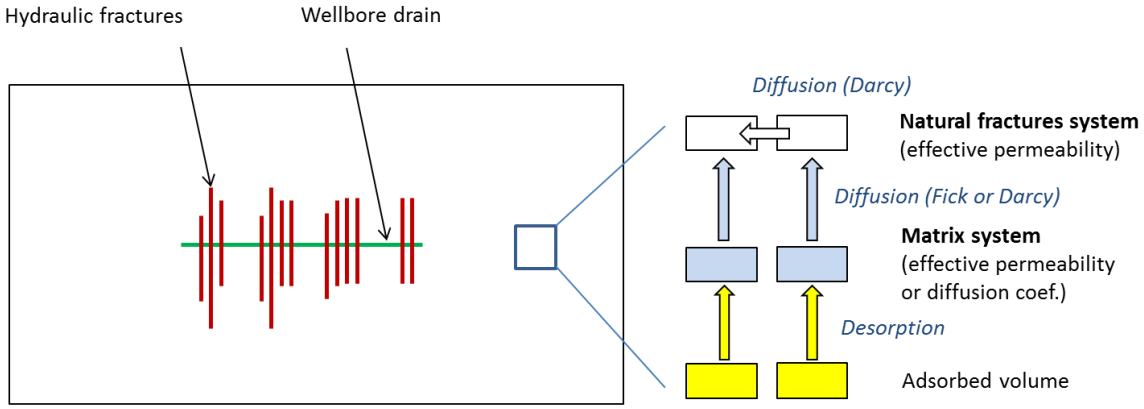


Fig. 10.B.10 – Natural fracture approximated with a double-porosity model

- The fractures are larger objects creating long-distance connections between the wells. They cannot be homogenized. The geometry of at least the main fractures is important and transport has to be described using Darcy's law. This large-scale fractures network is connected to a homogeneous micro-porous 'matrix' system. Smaller scale fractures may approximate to a double-porosity model.

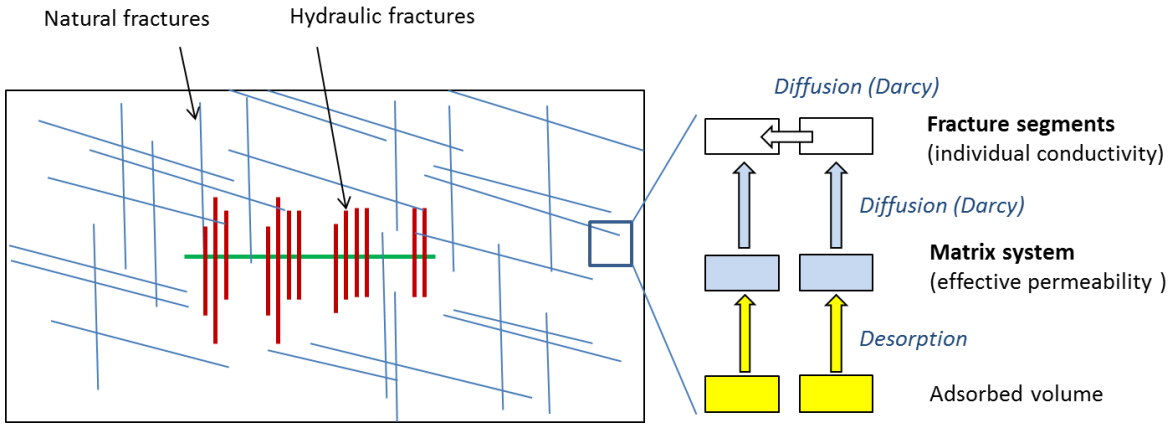


Fig. 10.B.11 – Natural fractures simulated by a fracture network connected to the matrix

10.B.2.d Stress and pressure-dependent properties

Modifications of the stress field (σ) during operations may have a significant impact:

- During the injection fractures propagate perpendicular to the minimum principal stress, which can change with location and time, depending on the operations schedule, as the stress field is modified while injecting and fracturing.
- During the injection pressuring of existing fractures reduces the effective stress across fracture planes (closure stress, σ-P). This opens the fractures, increasing their width and conductivity.
- As pressure decreases (fall-off and production) the closure stress increases again. Un-propped fractures and small fissures tend to close. Propped fractures remain open but the conductivity of the proppant may decrease.
- In the matrix, the effective permeability and porosity are also dependent on modifications of the stress field due to compaction.
- In extreme cases, proppant may get embedded into the matrix, dramatically reducing the conductivity of the hydraulic fracture.

One way to address this is by coupling the geomechanics and flow equations in the same the numerical model. A simpler approach is to add pressure dependence of the permeability and the porosity in the flow model. Three relations may be used:

- One for the matrix, used essentially to simulate the compaction and reduction of the effective permeability as pressure decreases.
- One for the natural fracture system, where the closing of fractures when pressure decreases can be captured by various models, ex: cubic, Ostensen's or Walsh's laws. For example, Walsh's law gives the variation of the fractures permeability vs. pressure:

$$\frac{k}{k_0} = \left[C.ln\left(\frac{\sigma_{ref}}{\sigma - P}\right)\right]^3$$

- One for the propped fractures, integrating the evolution of the conductivity as a function of the closure stress.

10.B.2.e PVT issues

There are PVT issues unique to unconventional plays. Conventionally, one may consider that methane is methane, and that the PVT behavior is therefore an independent block of the modeling process. This is unfortunately not the case when the size of the pores approaches the order of magnitude of the size of the hydrocarbon molecules. Lab experiments do not take this into account, and when we get to these extreme cases the fluid properties will not be the same under these conditions at a given pressure and temperature.

For instance, for a given composition of a hydrocarbon mixture, the phase behaviour obtained in a laboratory PVT cell may be considerably different from the behaviour in a confined environment: the phase envelope is shifted, leading to different values of the saturation pressure and an apparent bubble or dew point 'suppression effect'.

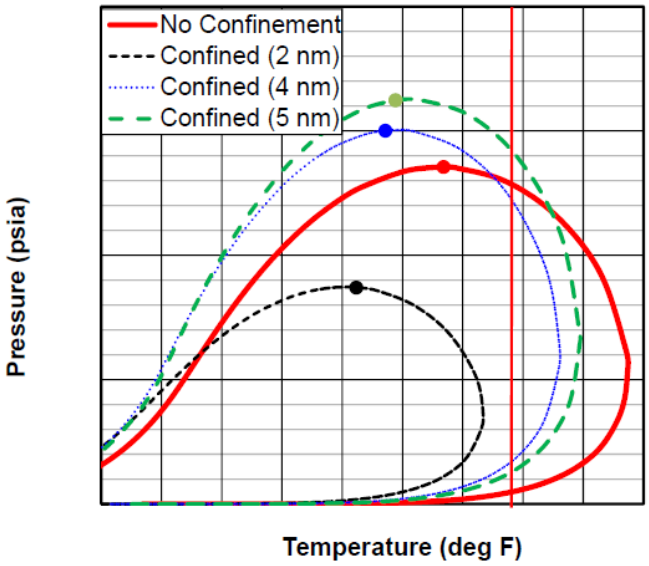


Fig. 10.B.12 – Phase diagrams of confined and unconfined gas-condensate fluid. (From Devegowda et al, 2012)

However, the agreement today is that this specific behaviour will only affect the estimation of the rock permeability in these particular areas. As we base our forecast on real production data, given our current knowledge, it should not dramatically affect the accuracy of our predictions. One way to approach problem is to consider that we have in the apparent permeability a component coming from the fluid and not the rock, and that all in all the errors are lumped and neutralized in the process of matching the production.

Another approach is to use a solution that takes into account the nanoporosity effects on the PVT properties.

10.B.2.e.i Confined PVT solution

One solution is proposed by adding an additional condition in the Equation of State that we use to define the PVT properties of the fluid in a numerical.

This option accounts for the phase envelope modification due to strong capillary pressure related to pore size.

In the approach used in the Kappa workflow, there are two methods for taking the effect of the confinement into account:

- To correct the flash calculation due to the capillary pressure in the pore.
- To shift the component critical properties.

More details are given in the paragraph 9.N Confined PVT.

What we do in practice

Often, despite the availability of data, for production analysis and forecasting purposes, engineers might use no model at all and just a decline model that may or may not account for a change in the apparent 'b' factor. This is the sad reality of our industry.

Even when engineers attempt to integrate some physics, in most flow models today the diffusion process is lumped into a homogeneous equivalent, with possibly the addition of double-porosity behaviour, pressure dependence of the permeability and a desorption equation. For analytical models these different correction parameters are integrated in pseudopressure and pseudotime functions, in addition to the usual PVT corrections.

Surprisingly the solution of these simplified diffusion equations seem to follow pretty well the first years of response we observe in these wells. This will be shown later in this chapter. The main question is whether these simplified models are sufficiently equipped to forecast longer term production, and whether or not they will be compatible with the productivity observed in future in-fill wells. Lumping the diffusion into a homogeneous equivalent has a substantial impact on our hypothesis for the extent of the Stimulated Reservoir Volume (SRV).

10.B.3 Fractured horizontal wells

As stated earlier the fractured horizontal wells are the only way we have found so far to make these plays commercial. If we look at Darcy's law and consider the term k·A, where A is the flow area, we try to get almost reasonable pressure gradients and compensate the low value of k by increasing dramatically the value of A.

The different levels of complexity of analytical and numerical tools used to model the behaviour of these wells will be detailed throughout this chapter. From operations we may have an estimate of the number of fractures, their lengths, directions and properties. Production logs and microseismics may also refine our understanding. However this information is not certain enough to consider it as a definitive input for the models to match the observed responses.

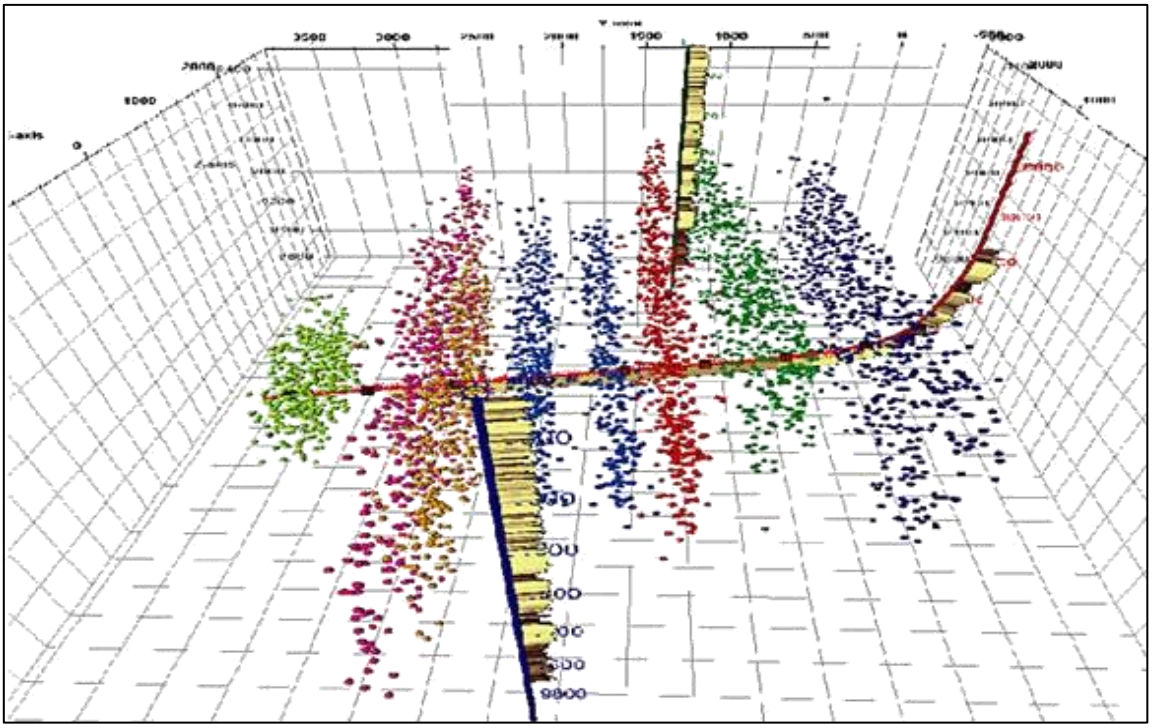


Fig. 10.B.13 – Microseismic events (Canada National Energy Board)

As a consequence we tend to simplify the hypotheses and lump the unknowns into a smaller number of parameters we will use to match the observed data. We are well past the illusion of a unique solution to the inverse problem. We are just looking for a proxy that is reasonably close to reality, and good enough to match observed data and forecast future production.

10.B.4 Initial state of the system

The well production starts after a substantial series of fracturing jobs. Typically this will involve the injection of Q_{inj} = 100,000 barrels of water, proppant and various chemicals. So we start with a system that is substantially disturbed in terms of pressures, saturations and stress.

There may be four different ways to model the initial state of the system:

- We ignore this and we consider an initial uniform pressure and saturation field. This may be acceptable for long term prediction and required when using analytical models. However it will unlikely match the early time response where substantial water flow back is expected.

- The "Static Method": we take a material balance approach and initiate a numerical model with a non-uniform initial water saturation field. 3 zones are defined: (1) the hydraulic fractures where the saturation is set to the S_{wmax} of the fractures relative permeability (S_{wmax}^{frac}), (2) a flooded zone surrounding the fractures, where the saturation is set to the S_{wmax} of the matrix relative permeability (S_{wmax}^{mat}), the extension of this zone derived such that its volume V_{tot} honors the material balance $Q_{inj} = V_{tot}.\emptyset.S_{wmax}^{mat} + V_{frac}.S_{wmax}^{frac}$ and (3) the remaining matrix volume, where the saturation remains unchanged at S_{wi}. This purely static approach is valid for long term predictions. It allows us to reproduce the water volumes corresponding to early time water flowback and capillary trapping, as well as the delay in gas production due to early-time dewatering. However, this is only an approximation since it does not account for the local pressure increase associated with injection, nor for any effective permeability or porosity variation due to modifications to the effective stress field during injection.

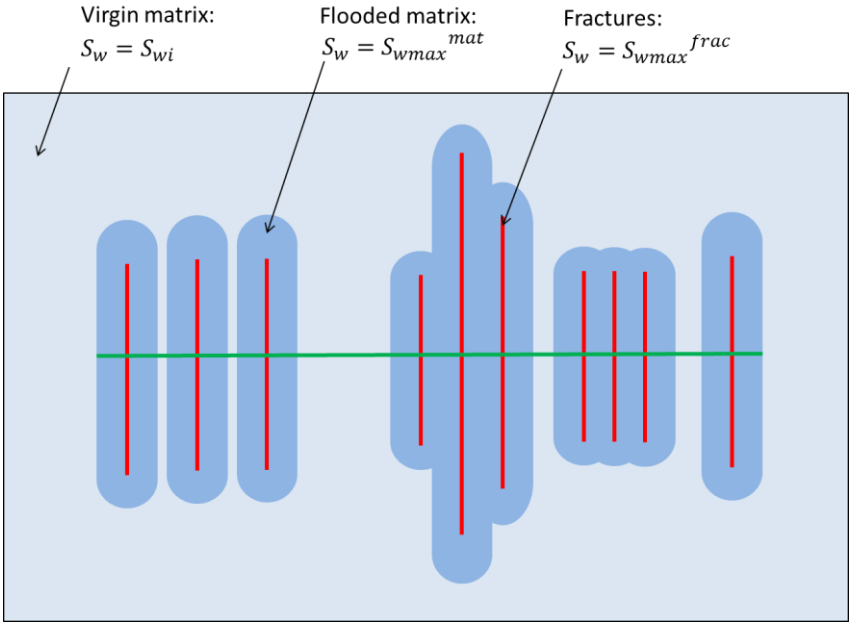


Fig. 10.B.14 – Initialization using the material balance static approach.

- The "Dynamic method": we simulate the injection in the final fractured system, as if the hydraulic / natural fracture system already existed… before the fracturing jobs. So we start with the geometry of the final system and simulate the increases of pressure and water saturation. This model is more rigorous than the previous one. It produces a non-uniform pressure field and a more realistic distribution of water. It requires a rather complex simulation and the exact injection history. Such a model could represent a good compromise in the perspective of simulating the initial state of the system before the production starts.

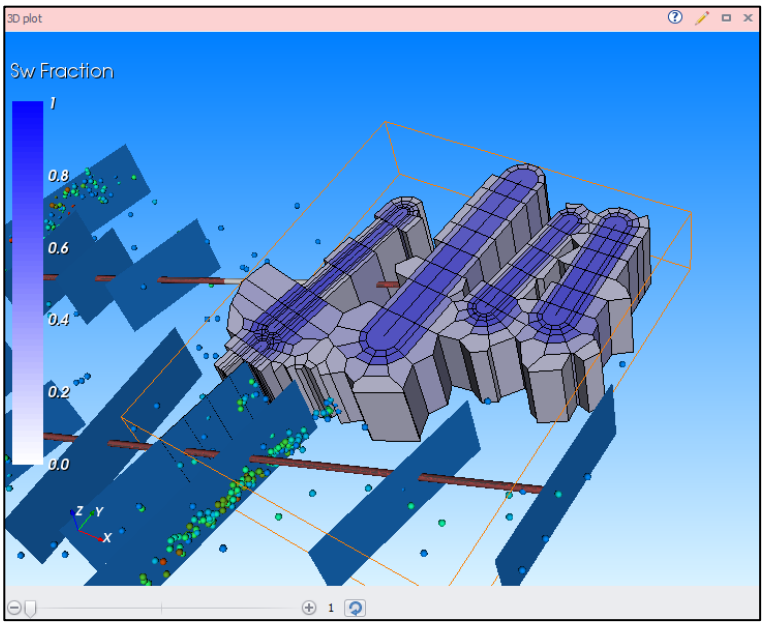


Fig. 10.B.15 – Initialization using the injection dynamic approach.

- The realistic approach: we simulate the exact fracturing job and use the resulting stress, pressure and saturation fields as the starting point for the production. This full-physics approach is the most rigorous one for detailed modeling/analysis of the water flowback. However, it requires a flow simulator fully coupled with a mechanic simulation engine, and a very large number of inputs (initial stress field, geomechanical properties of the rock, injection schedule, proppant properties, etc). KAPPA does not have yet the ability to simulate such a system.

More details are given in 10.H.3.

10.B.5 Heterogeneities and DFN

One of the big choices to make when trying to model unconventional plays is whether we consider a more or less complex diffusion at the micro-scale and extend it to the whole reservoir at the macro-scale, or if we need to consider macro-scale heterogeneities. Even if homogeneous models can, generally, pretty well explain single well production, they may quickly become insufficient to explain well interference.

Heterogeneities may have to be introduced at a point, even though it creates an even more under-defined problem. Discrete Fracture Network (DFN) models are for this reason becoming increasingly popular, whether they are generated numerically or approximated analytically.

10.B.6 Lack of quality data

The elements above point to very complex systems. The potential number of unknowns is much higher than for conventional formations, and with a total lack of empirical rules of thumb. If these formations constitute our 100-year future, one might have expected that substantial effort would be made on the metrology and, more generally, the acquisition of high quality data to mitigate the complexity of the problem.

The opposite was initially observed. There was a frenzy of drill & frac, and the paradigm was that we were creating a new mining industry. The reservoir and the well would be the same thing, no real reservoir engineering would be required because, in essence, the part of the reservoir of interest would be the famous SRV, i.e. more or less the bulk volume physically delimited by the set of hydraulic fractures. If for a given well the choice was to spend the same money on an additional fracture stage or a permanent downhole gauge, the immediate choice would be about fracking.

We have certainly passed this stage today, and companies are increasingly aware that proper reservoir engineering may be required in the long term. Most companies of a certain size are now running at least pilot developments where permanent gauges are installed and well interferences are being recorded and studied.

Still today most wells are poorly equipped, and most production databases contain allocated rates, with or without a pressure that is generally recorded at surface.

10.C Basic production behaviour of a shale well

In order to illustrate the basic production behaviour of a shale well, we first consider the simplest possible model using typical parameter values for a shale play. We ignore most of the complex elements described in the previous section and start with the following assumptions:

- Formation Conditions:
  - Assume a uniform initial pressure scenario for the reservoir.
  - No desorption or other chemical/thermodynamic effects are considered.
  - Single-phase flow only.
- Darcy's Law is Applicable:
  - Formation is homogeneous.
  - No micro- or nano-scale heterogeneous behaviour.
  - No macro-scale fracture network(s).
- Multi-Fractured Horizontal Well:
  - Fractures have the same length, width, and permeability.
  - Fractures are orthogonal to the horizontal well.
  - Fractures are placed evenly along the horizontal section.
- Well Placement:
  - The well is located in an infinite-acting reservoir, or
  - The well is located at the center of a bounded rectangular or square reservoir.
- Well Stimulation:
  - The fracturing process is not modelled.
  - Water invasion due to stimulation is not modelled.
  - Pressure and saturation gradients due to stimulation are not modelled.

In the following graphical representation and, although it integrates a large number of simplifications, this sort of model was more or less the state-of-the-art five years ago. For our purposes, we simulate production at a constant pressure for as long as it takes to observe the main flow regimes. We show the response on an RTA log-log plot.

Although the corresponding analytical model would qualitatively reproduce the same log-log response, we utilise the numerical model in order to visualize the pressure fields. This is critical in assessing the 'stimulated reservoir volume' (or SRV). For each case, on the left there is the log-log RTA plot and on the right, the pressure profile in the reservoir. A close-up of the same plot is integrated in the loglog area to show the pressure gradients at the well.

This is a theoretical exercise. To observe the final reservoir behaviour, such test would take several thousand years and the corresponding flowrates during very late times would approach infinitesimally small values. However this example will be quite useful for a reservoir engineer with a background in PTA to orient themselves to the various flow regimes and the state of the pressure distribution in the reservoir over time.

10.C.1 'Early' linear flow

The first series of plots shows the response after one month. At the start of the production the flow is orthogonal (linear) to the individual fractures and, because of the very low permeability, interference between the fractures is highly unlikely for a substantial period of time. In concept, the well behaves as a single equivalent fracture with an effective length equivalent to the sum of the individual fracture lengths.

This linear flow regime is characterized by a half slope on the log-log plot for both the normalized pressure and derivative functions, with a factor of 2 between the two curves. This response would also be characterized by a linear trend on a square root of time plot, similar to that used in PTA for a single hydraulic fracture.

If we were to construct a straight line on an Arps plot we would obtain a 'b' factor equal to 2.

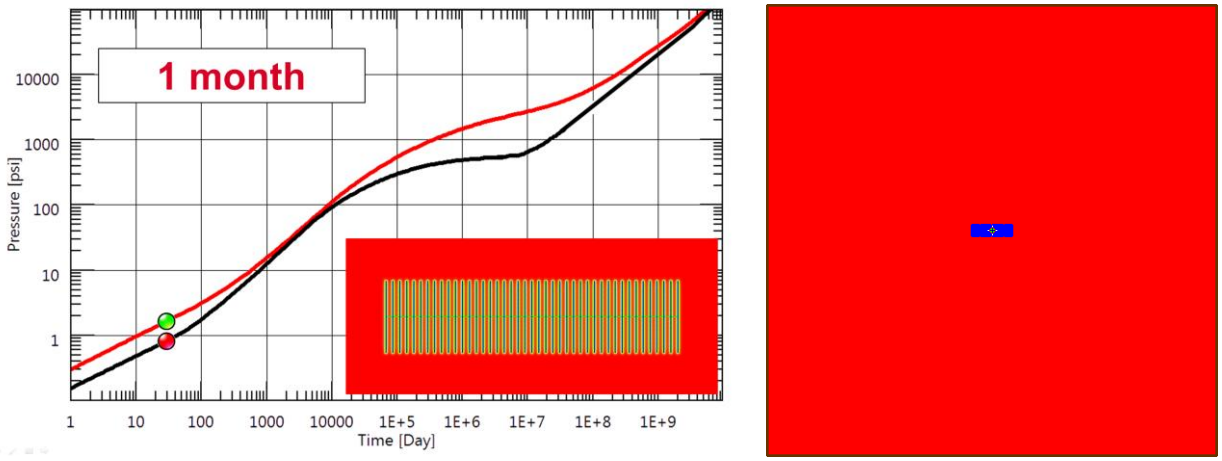


Fig. 10.C.1 – Linear flow behaviour

10.C.2 Transition from linear flow to SRV flow

After a certain period of production, the pressure distributions near the fractures begin to interfere. In this example, the next series of figures below show the response after three months. Both the normalized pressure and derivative begin to deviate (slightly) upwards from the expected linear flow half-slope trend where this represents a loss of productivity for the well.

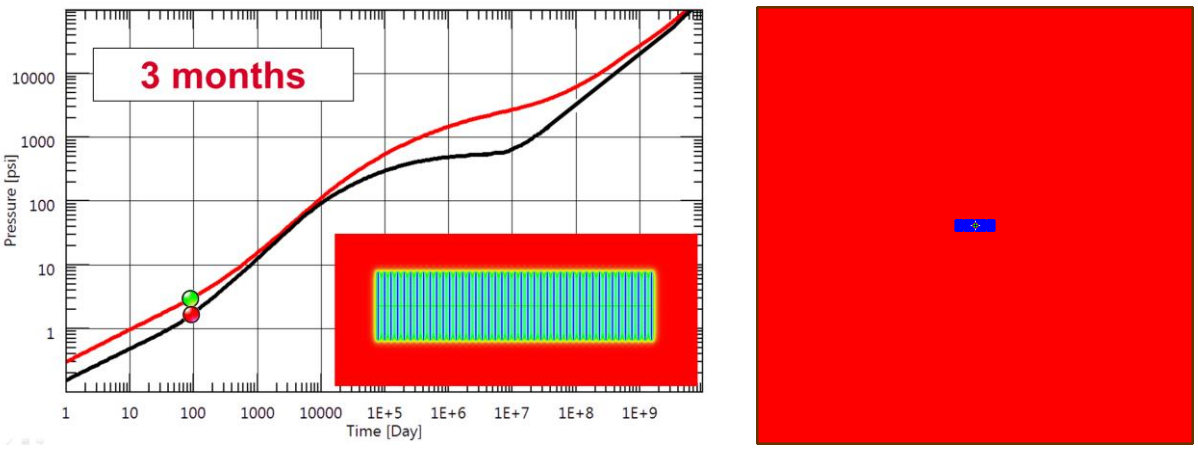


Fig. 10.C.2 – Start of interference between fractures

The next series of plots show the end of the transition from linear flow as both the normalized pressures and derivatives tend to merge onto a unit slope trend. During this transition period, the 'b' factor shown on the Arps plot continuously declines from the initial value of 2 (linear flow) the value of 0 (exponential decline).

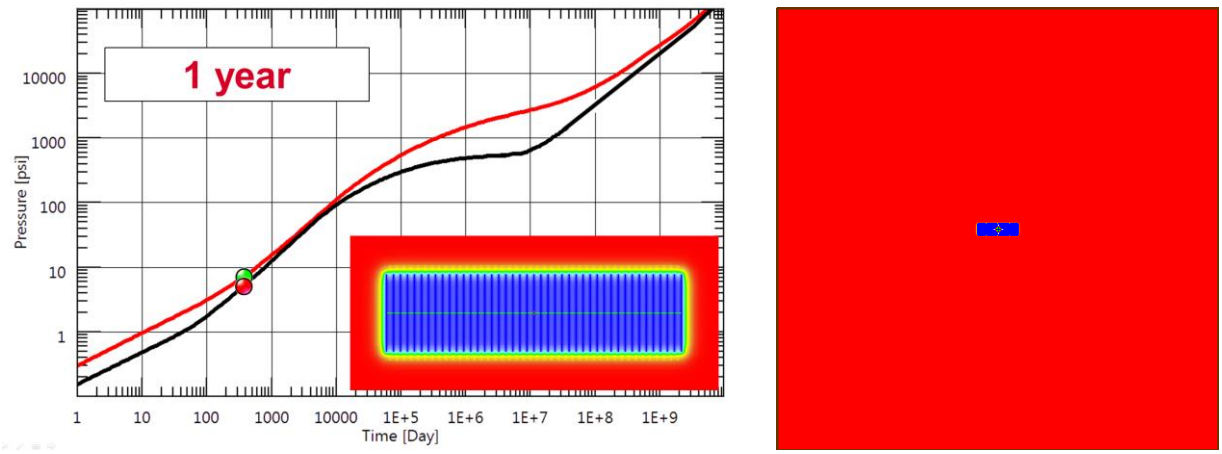


Fig. 10.C.3 – Transition period to SRV flow

10.C.3 SRV flow

We achieve a behaviour where both the normalized pressure and derivative functions have merged onto a unit slope, producing a regime that we will call the 'SRV flow regime' and this regime behaves exactly like the traditional Pseudo Steady state behaviour that we expect to encounter in conventional plays. The following plots show the system behaviour after five years.

The physical explanation is straightforward. During the early phase each fracture produced as if it was alone in the reservoir, so the diffusion is in all directions orthogonal to each fracture. Once the interference occurs we are taking the formation 'by surprise'. There is no diffusion expansion except at the outer face of the two extreme fractures and at the tips of all fractures. This suddenly decreases the area of contact between the well and the reservoir, and the only thing that is left to sustain the production is to deplete the volume already investigated, which we call the Stimulated Reservoir Volume, or SRV. It is not strictly Pseudo Steady state, because there is still diffusion going on at the limit of the SRV, but it will look very much like it. We could also call this flow Pseudo Pseudo Steady state.

On the right hand plot we start to see the diffusion (in yellow) at the very near border of the SRV.

During the SRV flow, the 'b' factor will be fractionally above zero.

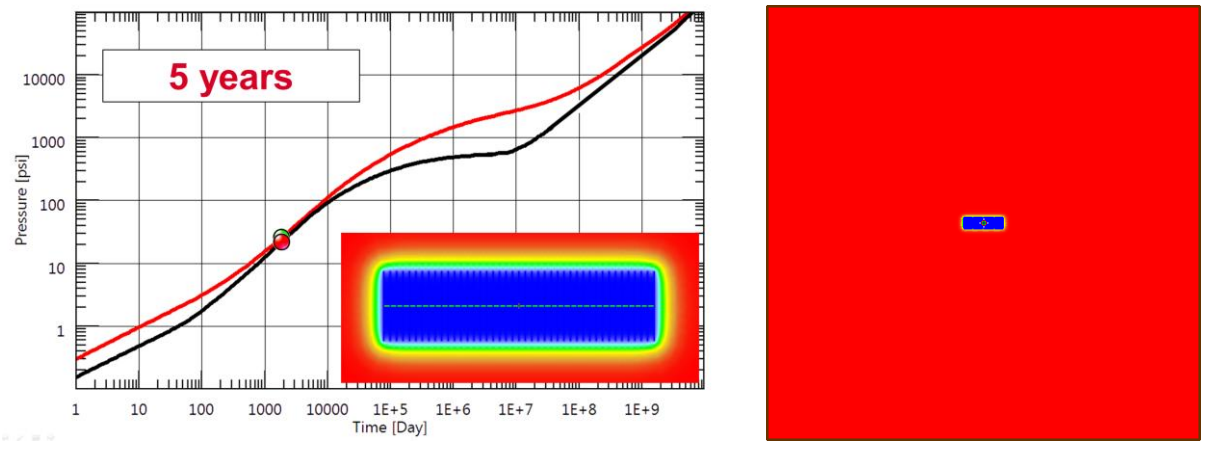


Fig. 10.C.4 – Established SRV flow

10.C.4 Beyond SRV

Depending on the reservoir parameters and the well-fractures system, one may see (or not) the response deviate from SRV flow once the contribution of the outer part of the SRV becomes non-negligible.

In theory, if we were to wait long enough, we could even see the system reach the more traditional Infinite Acting Radial Flow (IARF).

However this is very unlikely to happen as, by this time, the production would become infinitesimal and the well would be long abandoned. In addition, one would expect that other fractured horizontal wells would have been completed and produced in the meantime.

However, for the sake of the theoretical exercise you will find below in the three next series of plots the response of our example after 50 years, 500 years and 5,000 years, where in our case IARF is reached.

Just for fun, you can see in the fourth and last series the response after 50,000 years, where the system reaches the 'true', 'final' Pseudo Steady state response.

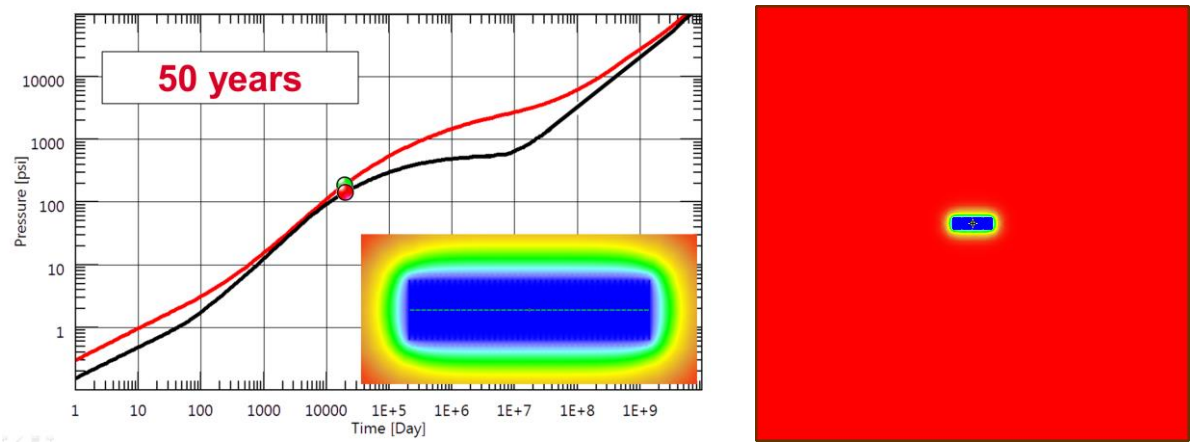


Fig. 10.C.5 – Deviation from the SRV flow

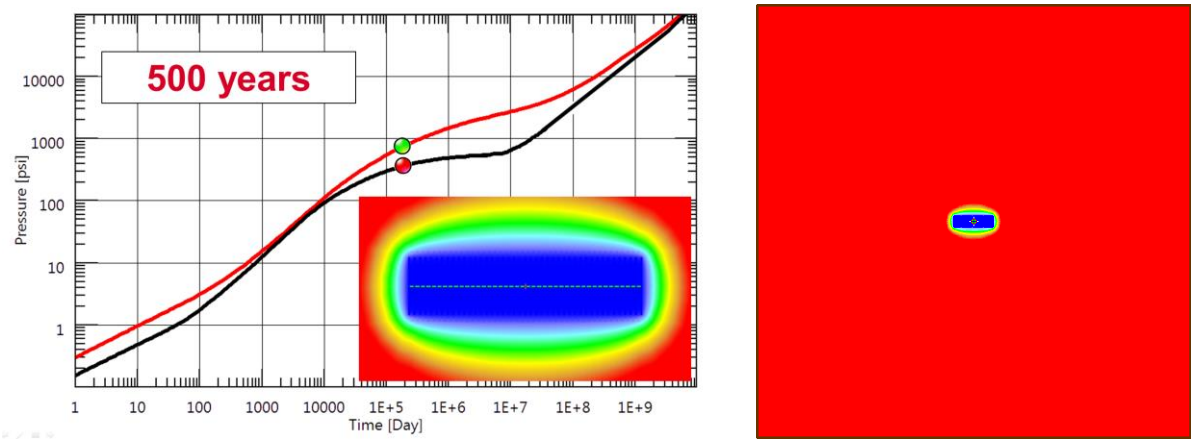


Fig. 10.C.6 – Effect of the formation out of SRV

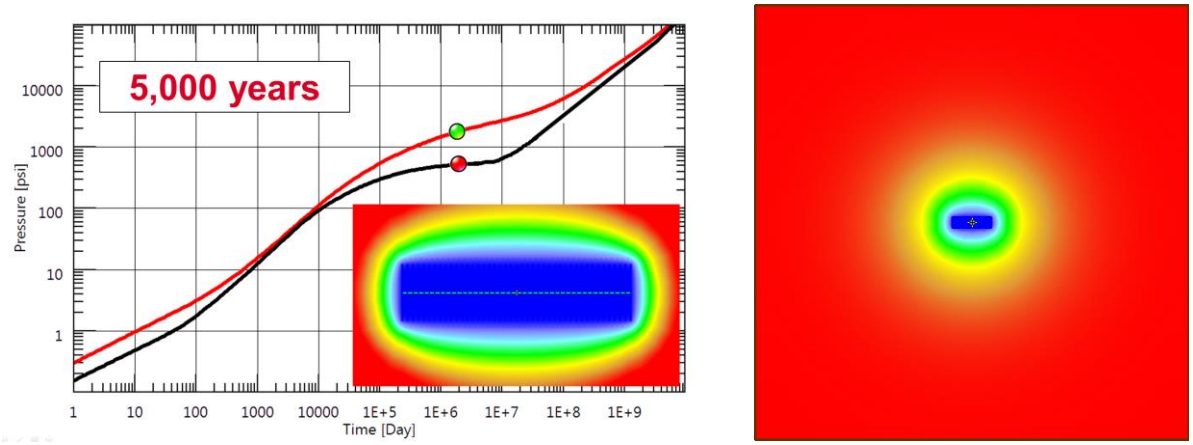


Fig. 10.C.7 – Possible IARF from the formation

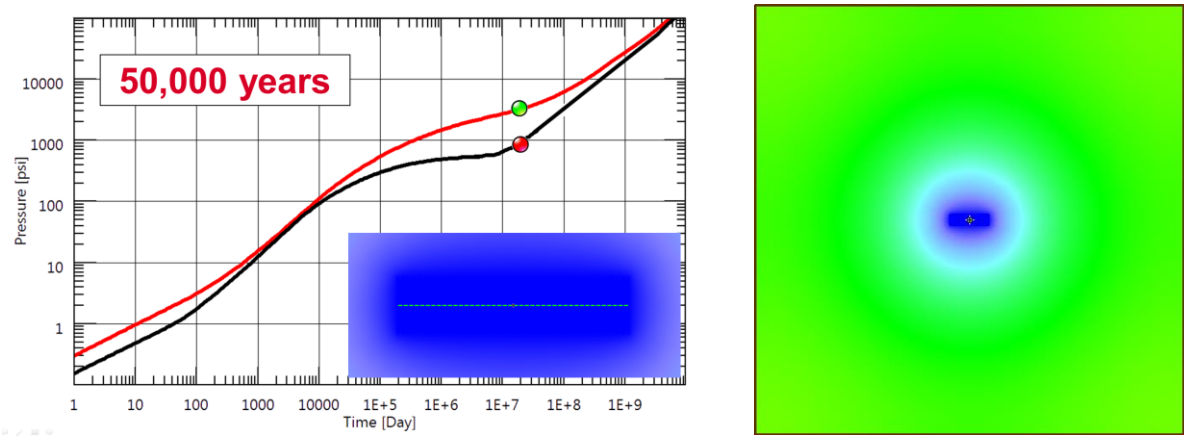


Fig. 10.C.8 – Very late final P.S.S.

Naturally all this is a theoretical exercise and there are four reasons not to get too much out of it: (1) 50,000 years may be a little long for a well test; (2) the whole idea of shale production today is to multiply the number of wells; (3) over long durations simplistic models just fail; (4) even for shorter durations we will see that a number of observations challenge this model.

If we believe this model and return to more realistic production times and abandonment rates, the conclusion is that the meaningful part of the response is constituted by the four first time log cycles (figure below). In the production life of such wells we would see the linear flow, some kind of transition towards the SRV flow, the SRV flow and, depending on the case, some late time deviation if it is not affected by the production of nearby wells.

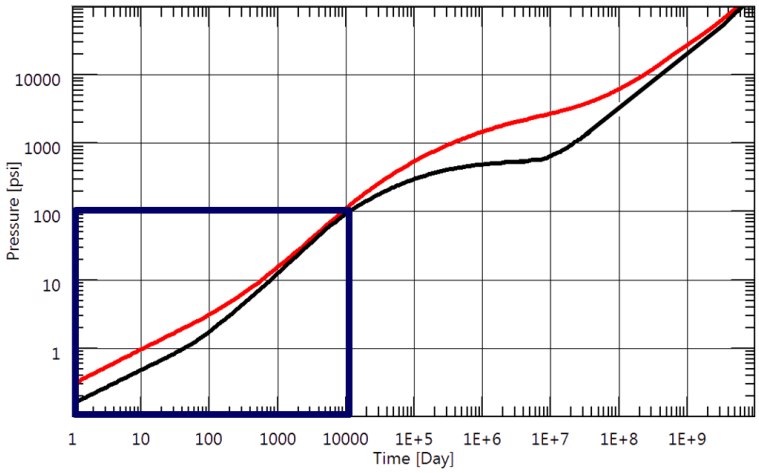


Fig. 10.C.9 – Realistic time range

This simulation reflects the state-of-the-art not so long ago. *Though an external analytical model was available in Saphir as long ago as 1999, these analytical and numerical models were integrated in Ecrin in 2009 and into Generation 5 Workstation in 2015.*

This model also represents the position of one of the main schools of thinking around these plays. Beyond the model itself, this school considers that the near totality of the production will come from an SRV that is indeed a slightly inflated version of the bulk volume determined by the series of hydraulic fractures.

This simple model is also the first occasion to introduce the difficulty of forecasting the production of these wells, as shown in the figure below. We have just started to produce these plays and we do not have yet any rule-of-thumb to anticipate these slow diffusion processes. So we only have a small number of data while the response starts with a long transient. Then we anticipate a transition and a long SRV flow. By the end of the production life we may see something else. The challenge is to use this little data and extrapolate it to get an estimate, or a probability function for EUR. The initial work that consisted of extrapolating the initial linear flow response has led to the issues we know.

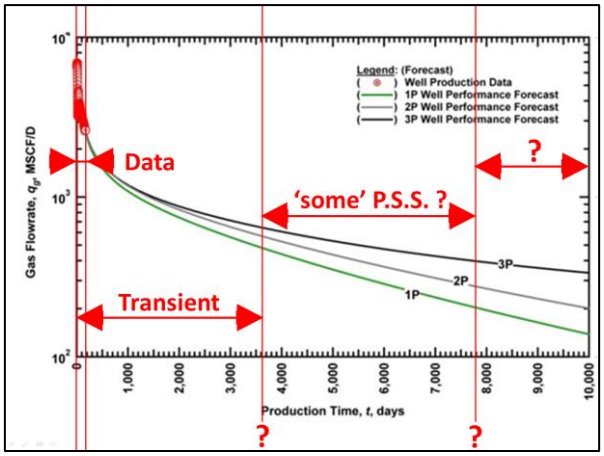


Fig. 10.C.10 – Forecast uncertainties

10.D Decline Curve Analysis (DCA) of unconventional plays

The application of Decline Curve Analysis (DCA) in unconventional plays could be problematic. A prerequisite to any discussion on DCA for unconventional plays is the understanding that no simplified time-rate model can accurately capture all elements of performance.

The analyst should be realistic and practical when attempting to characterize production performance of systems where permeability is in the order of the nano-Darcy. Although the hydraulic fractures enable the production performance, today we only have a basic understanding of the flow structure in the hydraulic and natural fracture systems.

From a historical perspective, DCA and production forecasting using Arps' exponential and hyperbolic relations have been the standard for evaluating Estimated Ultimate Recovery (EUR) in petroleum engineering. However, in unconventional plays such as shale gas, tight/shale oil reservoirs, these relations often yield ambiguous results due to invalid assumptions. The main assumptions which form the basis of traditional DCA can be summarized as:

- There is no significant change in operating conditions and field development during the producing life of the well
- The well is producing with a constant bottomhole flowing pressure
- There is a boundary-dominated flow regime and reservoir depletion was established
- In very-low permeability reservoir systems, it is common to observe basic violations of the assumptions related to traditional DCA, hence the misapplications of the Arps' relations to production data with significant overestimation of reserves, specifically when the hyperbolic relation is extrapolated with a *b*-exponent greater than one.
- In order to prevent overestimation of EUR, a hyperbolic trend may be coupled to an exponential decline at late time. However, this approach remains empirical and may be 'non-unique' in the hands of most users, yielding widely varying estimates of reserves.
- The issues with Arps' relations have led numerous authors [Ilk et al. (Power-law exponential, 2008), Valko (Stretched exponential, 2009), Clark et al. (Logistic growth model, 2011), and Duong (2011)] to propose various rate decline relations which attempt to model the time-rate behaviour observed in unconventional plays. Specifically these relations are focused on characterizing the early time transient and transitional flow behaviour. They are based on empirical observations of characteristic behaviours of certain plays. None of them are sufficient to forecast production for all unconventional plays. In other words, one equation may work for one play and perform poorly on another one. It is therefore important to understand the behaviour of each equation, and apply these relations appropriately for production forecasts.

This chapter presents the application of the decline curve equations. The results of time-rate analyses for each equation are presented and diagnostic plots to guide analysis are described.

10.D.1 Main plots used in Decline Curve Analysis

Diagnostic plots are very useful while performing decline curve analysis and provide direct insight into our understanding of decline behaviour. In particular, diagnostic plots can guide the analyst and are mainly used in an effort to understand data characteristics prior to performing decline curve analysis.

Our general procedure for decline curve analysis is to simultaneously use the diagnostic plots and calibrate the parameters of each model until a reasonable match is achieved. Regression may be used to refine the model parameters once diagnostic interpretation is complete. This procedure ensures consistency and may prevent non-uniqueness associated with matching multiple model parameters only on a single plot (e.g., time-rate plot).

Though many others may be used, the four following plots are recommended, and in most cases are considered sufficient for a proper DCA workflow:

1. [Semi-log]: (Log) Rate and Time
2. [Log-log]: (Log) D-parameter and (Log) Time
3. [Log-log]: (Log) b-parameter and (Log) Time
4. [Log-log]: (Log) Rate/Cumulative Production and (Log) Time

These plots may exhibit characteristic behaviours and validate the applicability of such or such decline equation. For example, by observing the D and b parameters, one can infer the b exponent to be used in the Arps' hyperbolic relation. For reference, D-parameter and b-parameter plots are derivative plots and their definition is tied to the term called the 'loss ratio' (Johnson and Bollens (1927)). For reference, these formulations are given as:

$$D(t) \equiv -\frac{1}{q(t)}\frac{dq(t)}{dt} \qquad \text{(}\textit{decline parameter}\text{)}$$

$$\frac{1}{D(t)} \equiv -\frac{q(t)}{dq(t)/dt} \qquad \text{(}\textit{loss-ratio}\text{)}$$

$$b(t) \equiv \frac{d}{dt}\left[\frac{1}{D(t)}\right] \equiv -\frac{d}{dt}\left[\frac{q(t)}{dq(t)/dt}\right] \qquad \text{(}\textit{derivative of the loss-ratio}\text{)}$$

The parameters are computed from the data using numerical differentiation. Such differentiation without smoothing results in noisy data. Proper editing of the time-rate data along with the Bourdet derivative are recommended.

The four plots to be used in decline curve analysis of a single well example are shown below (Figs. 1 to 4).

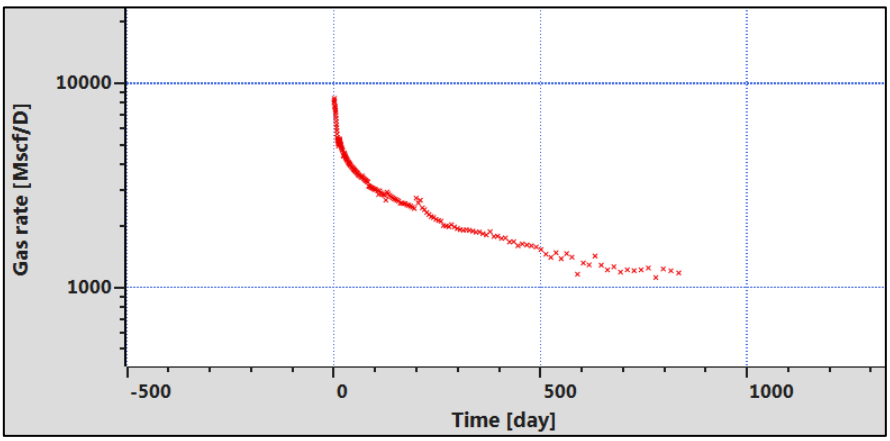


Fig. 10.D.1 – Rate and time plot.

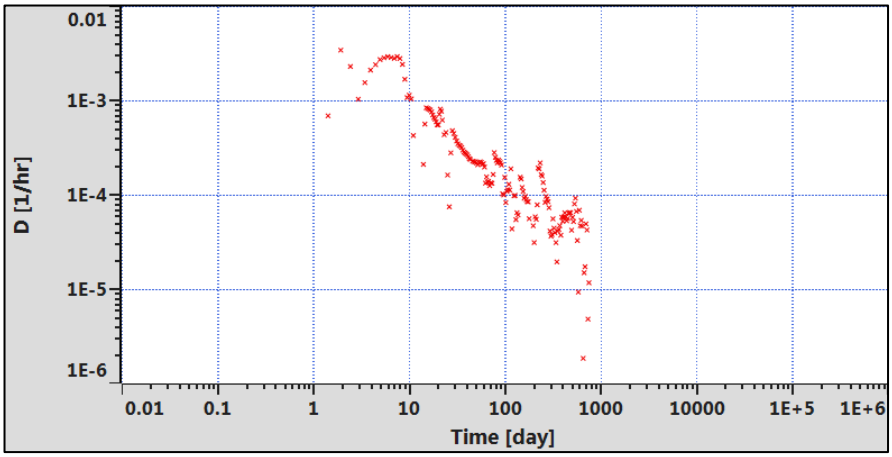


Fig. 10.D.2 – Computed D-parameter and time plot.

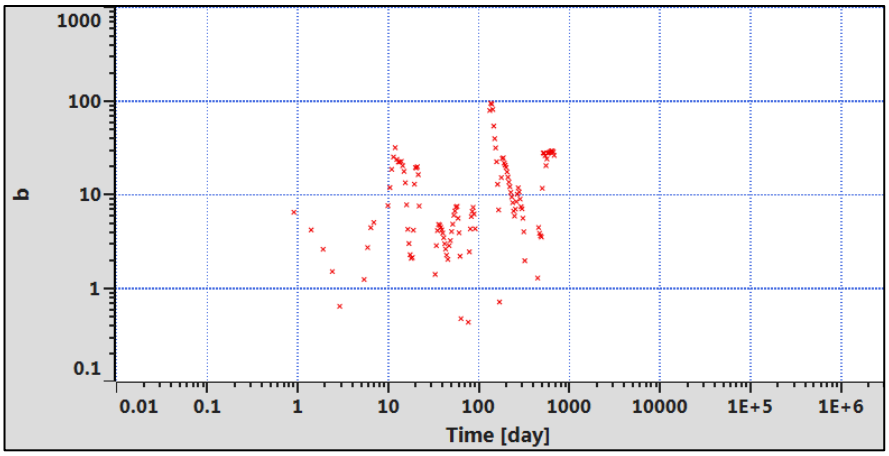


Fig. 10.D.3 – Computed b-parameter and time plot.

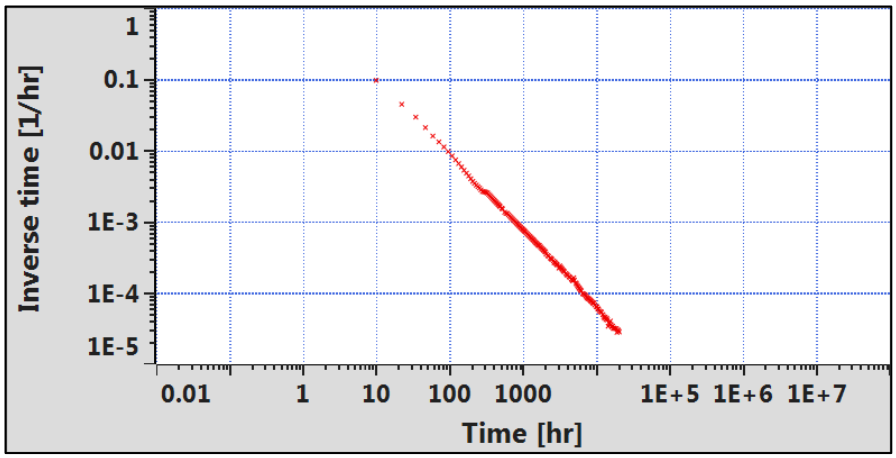


Fig. 10.D.4 – Rate/cumulative production and time plot.

10.D.2 The Arps equations

Arps' hyperbolic relations are widely used in DCA for production extrapolations and reserves estimations. The basis for the Arps' relations is empirical. The exponential decline corresponds to the Pseudo Steady State (PSS) flow in transient analysis. The hyperbolic relation does not have a transient equivalent. Gas flow during the boundary dominated flow regime can be approximated to a hyperbolic equation with b-values ranging between 0.4 and 0.6. For reference, exponential and hyperbolic relations are given as:

$$q(t) = q_i \exp[-D_i t] \qquad \text{(Exponential rate decline)}$$

$$q(t) = \frac{q_i}{(1 + bD_i t)^{1/b}} \qquad \text{(Hyperbolic rate decline)}$$

It is possible to infer exponential or hyperbolic behaviour by observing the D and b parameters. A constant D-parameter indicates exponential decline. A constant b-parameter indicates hyperbolic decline. For matching purposes, the user should first adjust b from the b-parameter plot, then match the D-parameter with a model. The initial rate (q_i) can be adjusted to complete the match and obtain the production forecast. It is possible to use a segmented hyperbolic if the user identifies multiple constant trends of the b-value.

Finally it is important to note that industry wide application of the Arps' hyperbolic relation in unconventional reservoirs includes a modification with the exponential decline at later times to prevent overestimation of reserves as the hyperbolic equation is unbounded for b-values greater than one (i.e. transient flow assumption for b-values greater than one). Hyperbolic decline is switched to an exponential decline once a certain yearly decline value is reached. This yearly decline value is set by the analyst and is called as the 'terminal decline' value. This protocol yields the 'modified' hyperbolic designation. Figs. 5 to 8 describe the application of the modified hyperbolic relation on a specific field example.

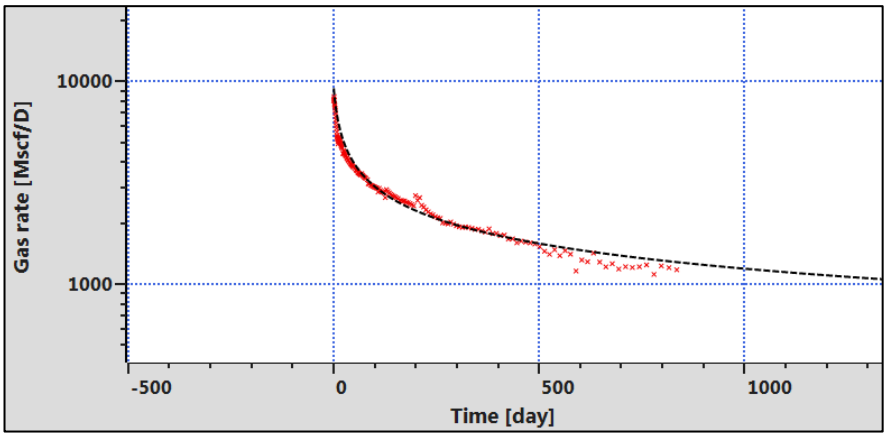


Fig. 10.D.5 – Rate and time plot (modified hyperbolic relation).

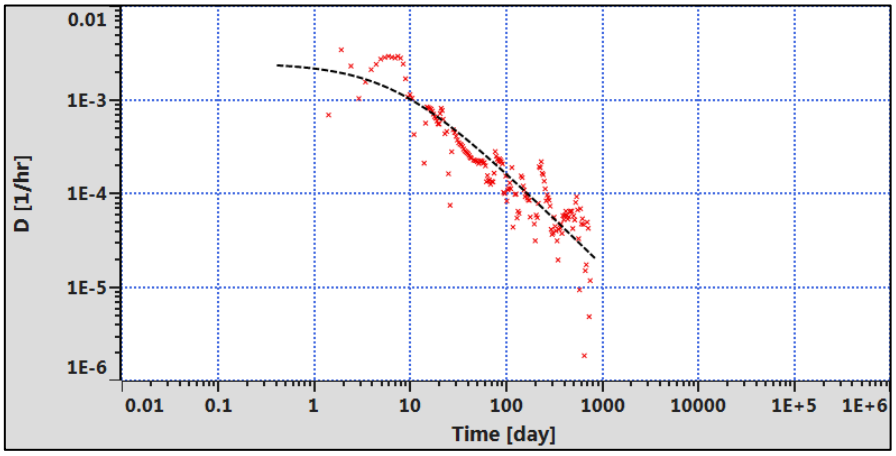


Fig. 10.D.6 – Computed D-parameter and time plot (modified hyperbolic relation).

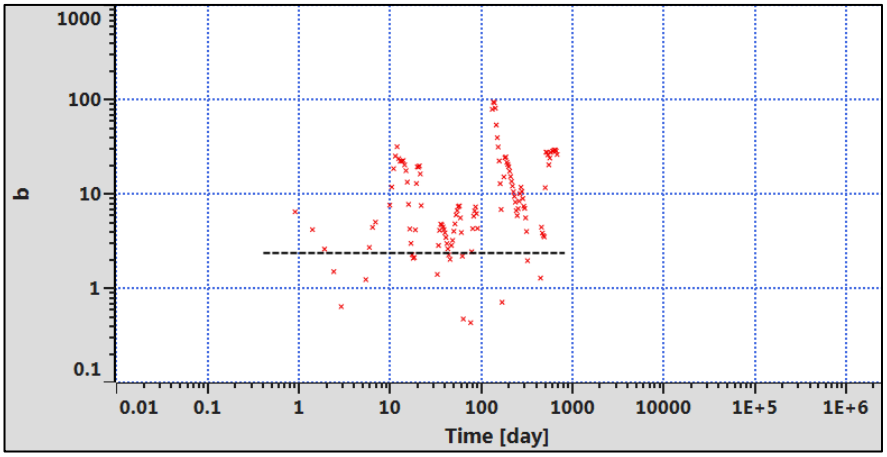


Fig. 10.D.7 – Computed b-parameter and time plot (modified hyperbolic relation). (From Ilk, 2014)

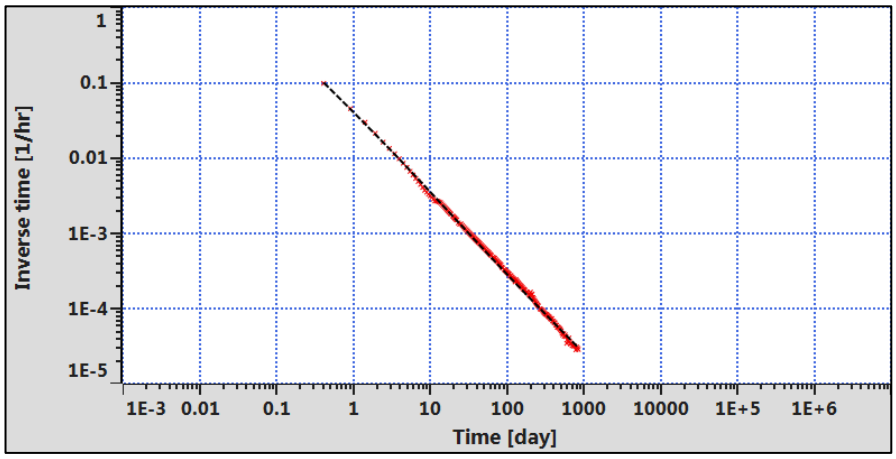


Fig. 10.D.8 – Rate/cumulative production and time plot (modified hyperbolic relation). (From Ilk, 2014)

10.D.3 Power-law exponential

The power-law exponential relation was derived exclusively from the observed behaviour of the D-parameter and b-parameter. Its primary assumption is that the D-parameter exhibits a straight line behaviour on a log-log scale, which essentially corresponds to a power-law model. If the D-parameter formulation (Eq. 1) is approximated to a power law model, the resulting differential equation yields the power-law exponential relation.

By introducing a constraining variable (D_∞), the D-parameter trend is constant at late times. This variable converts the power-law exponential equation to an exponential decline with a smooth transition. However, in almost all of the applications in unconventional reservoirs, D_∞ is not required since there has been no observation of the constant D-parameter trend and the nature of the power-law exponential relation is conservative as it models the b-parameter trend declining with time. Power-law exponential relation is given below:

$$q(t) = \hat{q}_i \exp\left[-\hat{D}_i t^n - D_\infty\right] \qquad \textit{(Power-law exponential relation)}$$

The application of the power-law exponential relation is centered on use of the D-parameter and time plot. Once the straight line is identified, slope and intercept values associated with the $\hat{D}_i$ and *n* parameters are obtained. The $\hat{q}_i$ parameter is adjusted to achieve the match on rate and time plot. Figs. 9-12 describe the application of the power-law exponential relation on a specific field example.

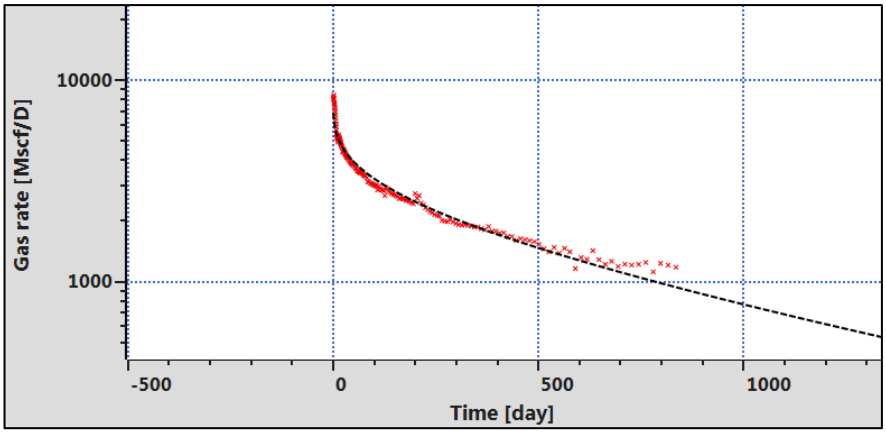


Fig. 10.D.9 – Rate and time plot (power-law exponential).

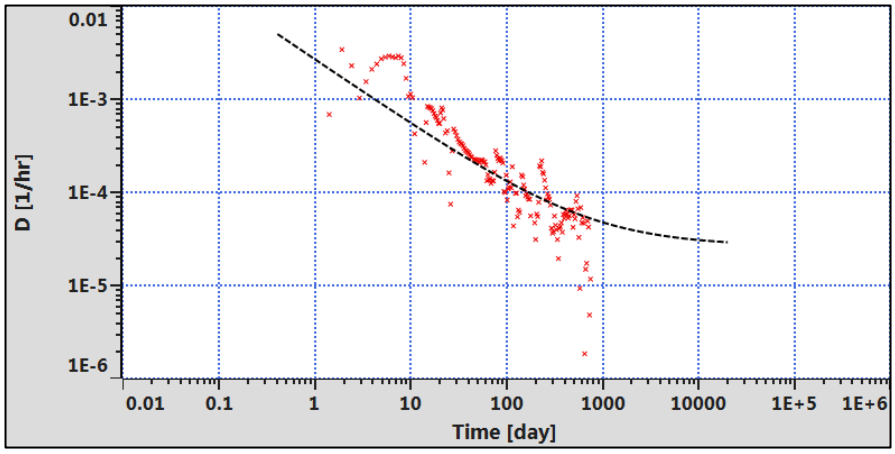


Fig. 10.D.10 – Computed D-parameter and time plot (power-law exponential relation).

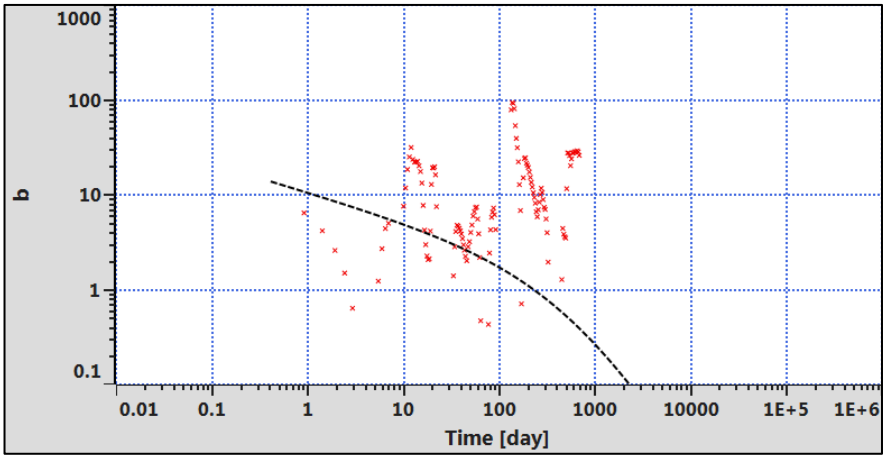


Fig. 10.D.11 – Computed b-parameter and time plot (power-law exponential relation).

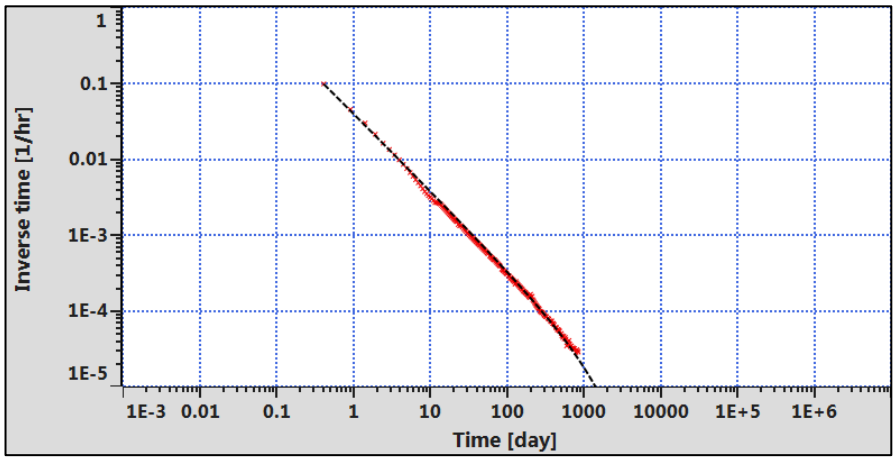


Fig. 10.D.12 – Rate/cumulative production and time plot (power-law exponential relation).

10.D.4 Stretched exponential function

The stretched exponential relation is essentially the same as the power-law exponential relation without the constraining variable (D_∞). Outside petroleum engineering, the stretched exponential relation has many applications such as in physics where numerous processes manifest this behaviour, as first described by Kohlrausch (1847), and then by various authors (Philips (1966)). In geophysics, the stretched exponential function is used to model aftershock decay rates (Kisslinger (1993)). In his seminal work (1945), Arps also provided the stretched exponential function, but no application was provided.

In general, the stretched exponential function is used to represent decays in randomly disordered, chaotic, heterogeneous systems. It can be suggested that the stretched exponential decay of a quantity is generated by a sum (superposition) of exponential decays with various time constants. This leads to the interpretation of heterogeneity where production decline in an unconventional reservoir system is determined by a great number of contributing individual volumes exhibiting exponential decays with a specific distribution of time constants. The stretched exponential function is given as (Valko (2009)):

$$q(t) = q_0 \exp[-(t/\tau)^n] \qquad \textit{(Stretched exponential relation)}$$

The stretched exponential relation can be applied in the same manner as the power-law exponential relation using diagnostic plots or alternatively the procedure described by Valko (2009) could be applied.

Figs. 13-16 describe the application of the stretched exponential relation on a specific field example.

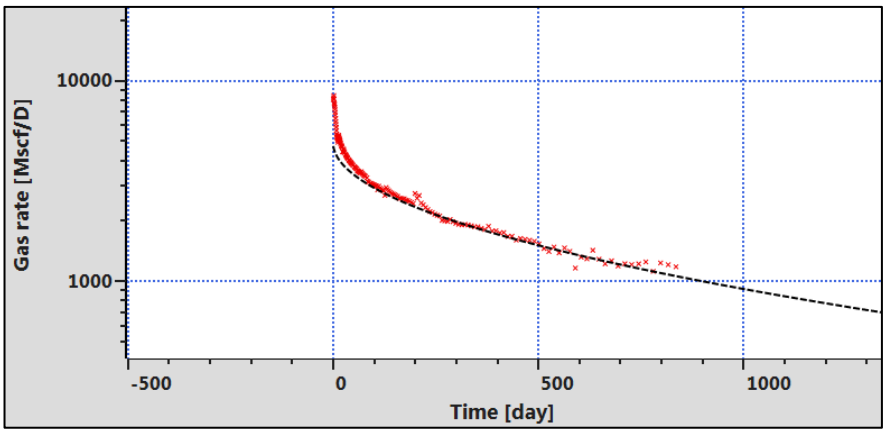


Fig. 10.D.13 – Rate and time plot (stretched exponential relation).

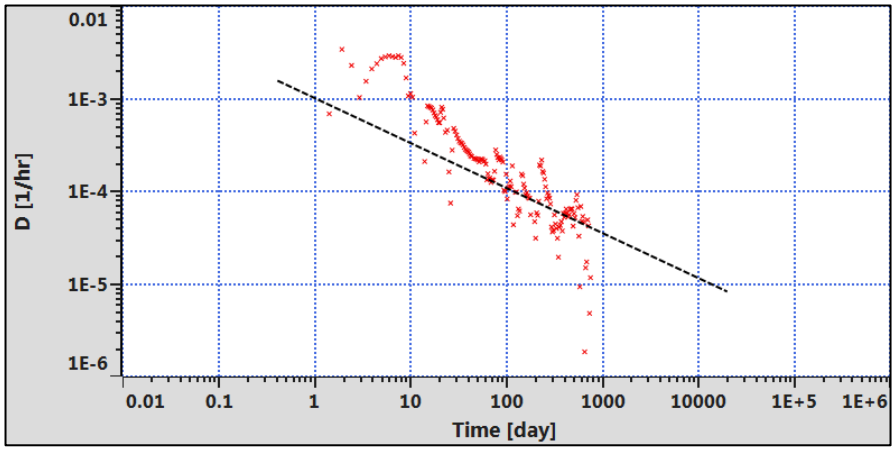


Fig. 10.D.14 – Computed D-parameter and time plot (stretched exponential relation).

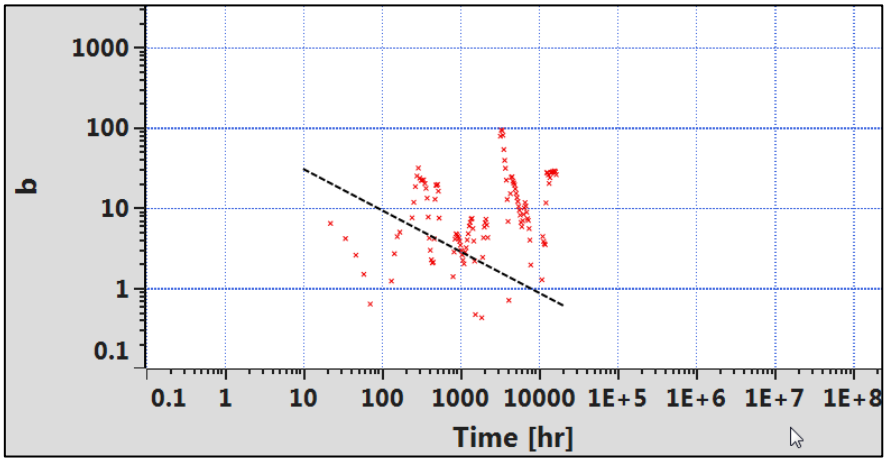


Fig. 10.D.15 – Computed b-parameter and time plot (stretched exponential relation).

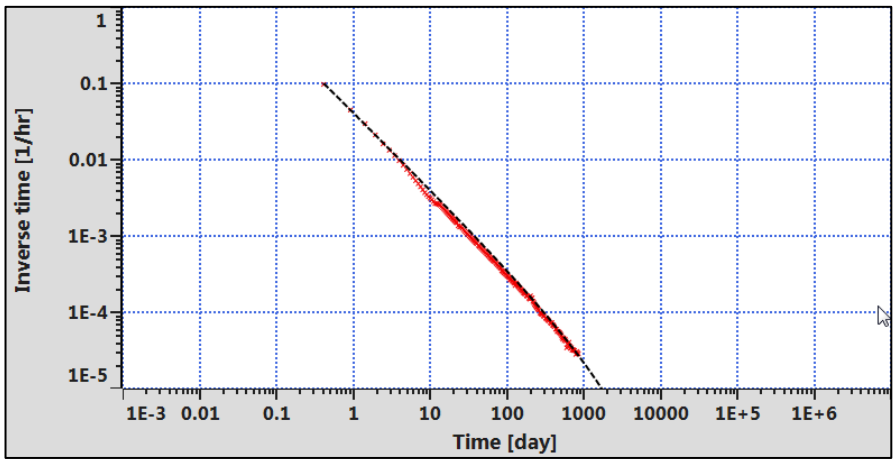


Fig. 10.D.16 – Rate/cumulative production and time plot (stretched exponential relation).

10.D.5 The Duong model

The Duong model is based on the assumption of dominant fracture flow and negligible matrix contribution. The fractured area increases with time and supports the fracture flow. Duong suggested that pressure depletion within fracture networks may reactivate existing faults or fractures. A log-log plot of rate and cumulative production vs. time yields a unit slope straight line regardless of the fracture type. Slopes greater than one may be due to flow regime changes and field operations. Time-rate relation can be calculated from the intercept and slope values of the log-log plot and an initial rate. The Duong's model is given as:

$$q(t) = q_1\, t^{-m_{Dng}} \exp\left[\frac{a_{Dng}}{(1-m_{Dng})}\,[t^{(1-m_{Dng})}-1]\right] \quad (\textit{Duong model})$$

Other models, such as the power-law exponential, the stretched exponential and the logistic growth, account for deviations at later times. Such deviations also occur when a terminal decline is imposed on the modified-hyperbolic relation. The EUR estimates from Duong's model are therefore higher unless a constraining variable is also imposed. The linear flow assumption of the Duong model may hold for some plays, but it will generally need modifications to deal with changes in flow regimes (i.e. transitional flow, depletion of SRV, interference, etc).

Figs. 17 to 20 illustrate the application of the model. An important step is to establish the slope (m_{DNG}) and intercept (a_{DNG}) values on the rate/cumulative production trend and then adjust the q_1 value to obtain the match.

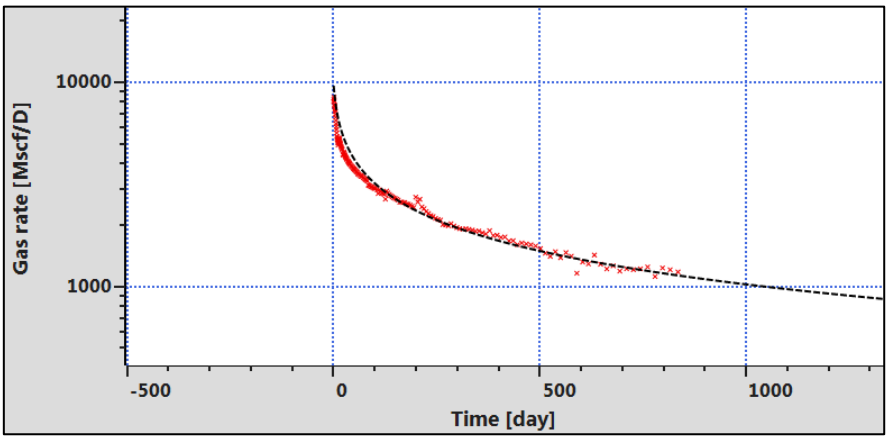


Fig. 10.D.17 – Rate and time plot (Duong model).

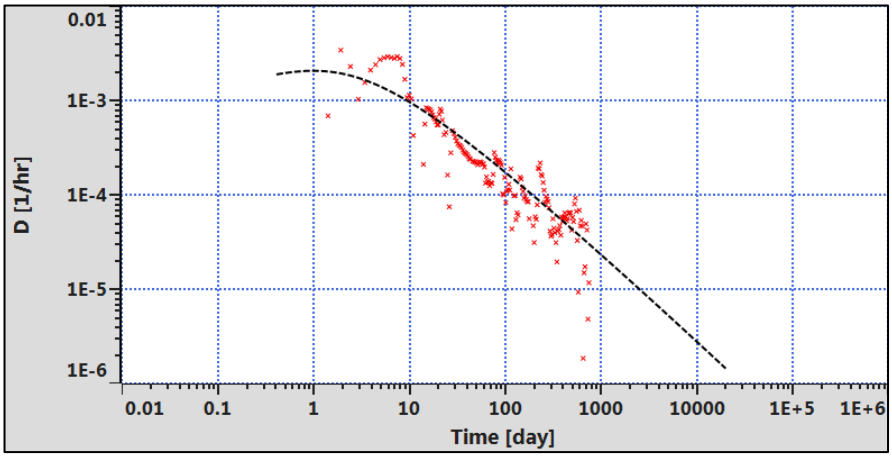


Fig. 10.D.18 – Computed D-parameter and time plot (Duong model).

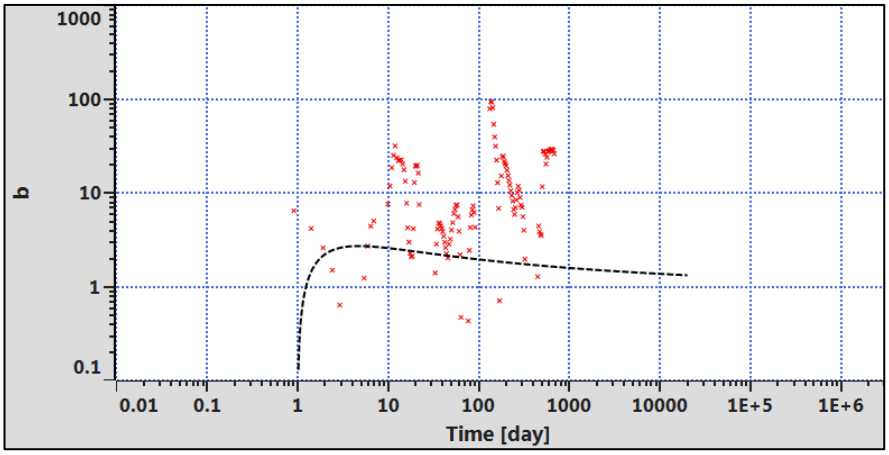


Fig. 10.D.19 – Computed b-parameter and time plot (Duong model).

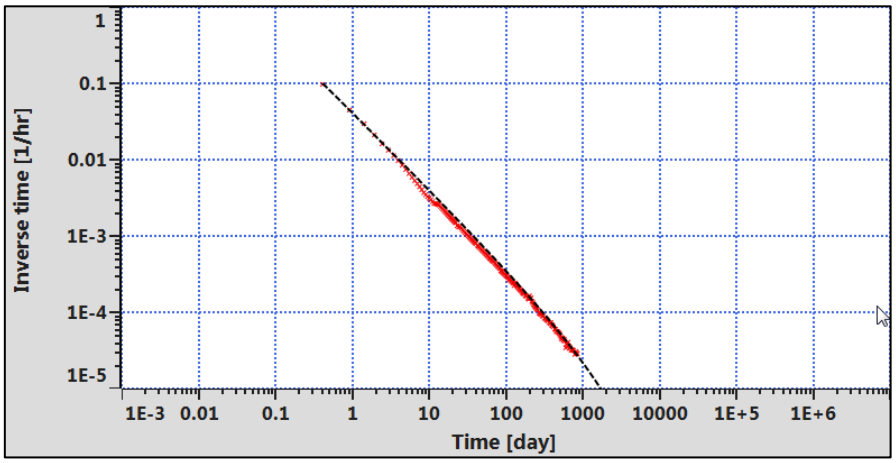


Fig. 10.D.20 – Rate/cumulative production and time plot (Duong model).

10.D.6 Logistic growth

Logistic growth curves are a family of mathematical models used to forecast growth (e.g., population growth, growth of agricultural products, regeneration of organs, market penetration of new products, etc.). Conceptually, logistic growth models assume that the growth variable increases then stabilizes. Logistic growth models have a term called the carrying capacity, which is the size at which the growth variable stabilizes and growth rate terminates.

Clark et al (2011) utilizes the logistic growth model for forecasting cumulative production of the wells in unconventional oil and gas reservoirs. The logistic growth model to describe cumulative production and rate is given below:

$$G_p(t) = \frac{K\, t^{n_{LGM}}}{[a_{LGM} + t^{n_{LGM}}]} \qquad \text{(Logistic growth model)}$$

$$q(t) = \frac{dG_p(t)}{dt} = \frac{K\, n_{LGM}\, a_{LGM}\, t^{(n_{LGM}-1)}}{[a_{LGM} + t^{n_{LGM}}]^2} \qquad \text{(Logistic growth model)}$$

The parameter *K* is the carrying capacity and referred to as the ultimate of oil and gas recovery from the well without any economic limits. This parameter is included in the model itself. Cumulative production will approach K while the rate tends to zero. The parameter *n* controls the decline. When *n* tends to one the decline becomes steeper. The parameter *a* controls the time at which half of the carrying capacity is reached. A high value of *a* indicates stable production. A low value of *a* points to a steeper decline.

Figs 21 to 24 show the application of the logistic growth model on a single well example.

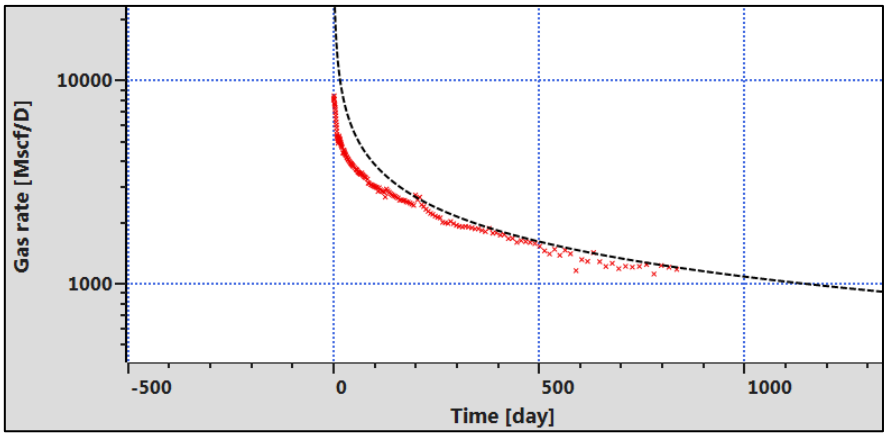


Fig. 10.D.21 – Rate and time plot (logistic growth model).

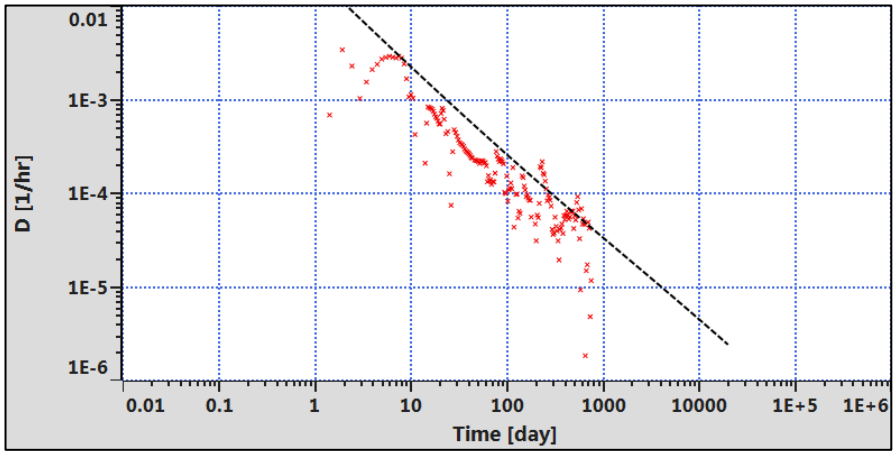


Fig. 10.D.22 – Computed D-parameter and time plot (logistic growth model).

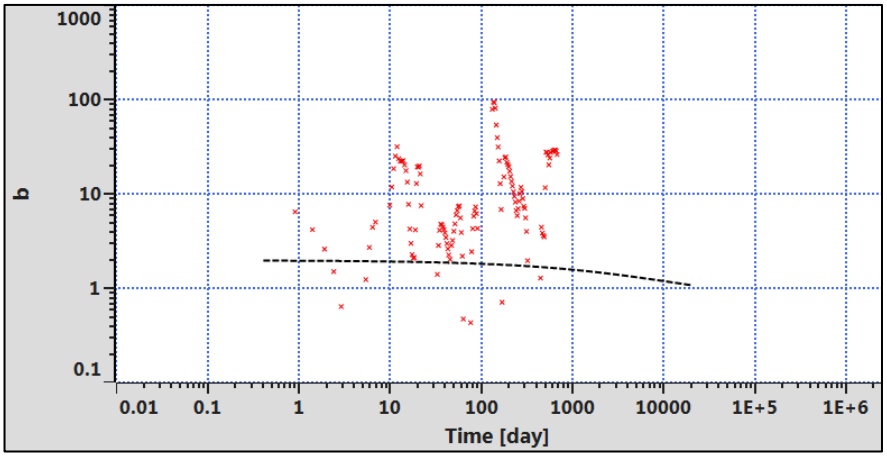


Fig. 10.D.23 – Computed b-parameter and time plot (logistic growth model).

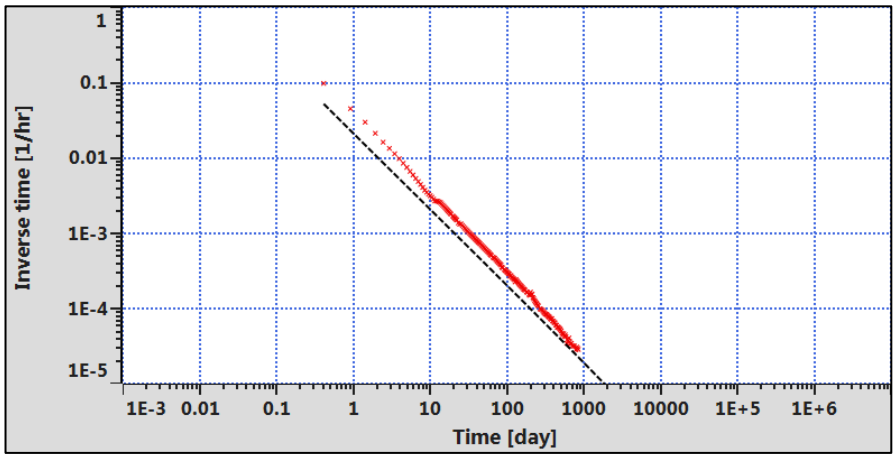


Fig. 10.D.24 – Rate/cumulative production and time plot (logistic growth model).

10.D.7 Stimulated Reservoir Volume Bounded decline curve

This decline curve includes the main Multi Fractured Horizontal Well flow regimes from the linear flow until the SRVB flow. The transition and the respective position of these two flow regimes are described by the three parameters:

- Initial rate *qi*
- The time of transition at the intersect of the ½ loglog slope straight line and of the unit loglog slope straight line.
- Pa, the rate normalized pressure value (a.k.a.reciprocal productivity index) at the intersect of the ½ loglog slope straight line and of the unit loglog slope straight line.
- τ (tau), which determines the beginning and the end of the transition and has an influence on the curvature of the transition

The advantage of using this Decline Curve is that an analytical MFHW model can be initialized from it. It is sufficient to confirm the well length and the permeability and the fracture length can be then estimated.

Figs 25 to 28 show the application of the SRVB model on a single well example.

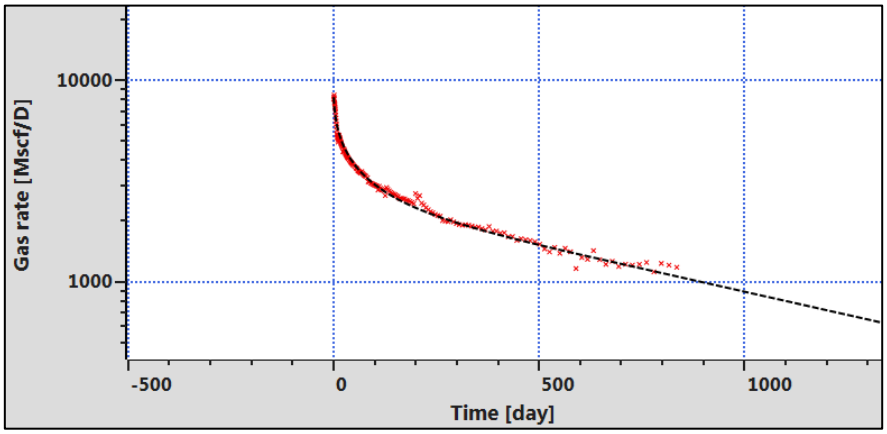


Fig. 10.D.25 – Rate and time plot (SVRB model).

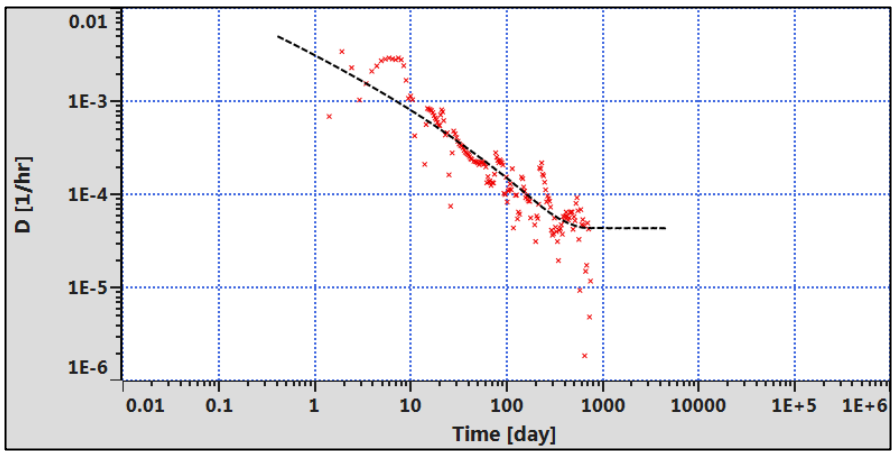


Fig. 10.D.26 – Computed D-parameter and time plot (SRVB model).

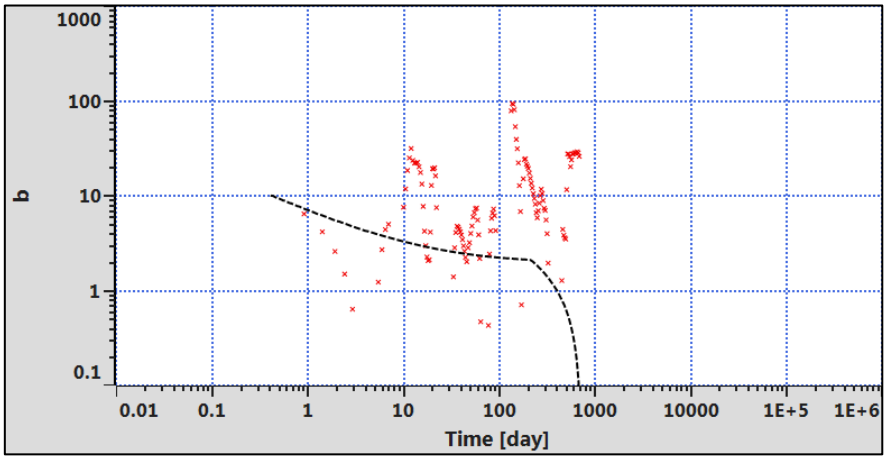


Fig. 10.D.27 – Computed b-parameter and time plot (SRVB model).

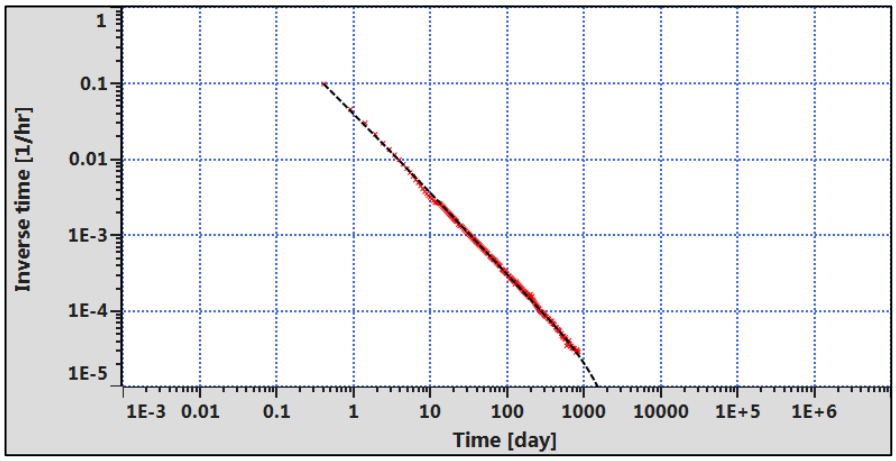


Fig. 10.D.28 – Rate/cumulative production and time plot (SRVB model).

10.D.8 Segmented DCA models

Long-term observation of the unconventional fields led many engineers to observe that the well behavior can exhibit not just a steady consistent power-law decline, but a sequence of them with changing parameters.

This can be due to changing production conditions, reservoir conditions or to changing reserves due to the drilling of other well in the vicinity.

For these reasons it can be perfectly reasonable and fruitful to split the history of the well production in to several segments, according to the observed behavior and to adjust different DCA model in order of study the evolution of the reserves with the time.

10.D.8.a Segmented Power Law Model

On the D parameter plot this is manifested as a sequence of straight lines with the same slope, separated from each other, and on the b parameter plot the model line would show several intervals with constant values (see Figure below). Each segment in this case corresponds to an individual power-law segment of the well behavior. There are a few attempts to connect this with a physical description of a well-reservoir fractured system (e.g. the multi-zone fractional dimension model).

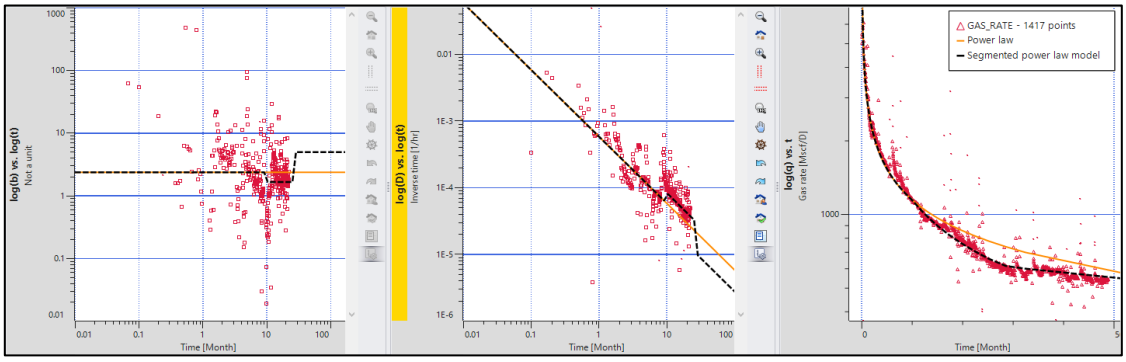


Fig. 10.D.29 – Segmented Power law model match

The model can also with the second (or latter) segment in the model forecast only to represent a situation when the expected future behavior of a well exhibits a different power-law decline from the historical one, e.g. when the production decline is sharper with stronger depletion.

10.D.8.b Segmented Hyperbolic DCA model

The Hyperbolic can also be used in a segmented model, it offers the possibility to adjust all the Hyperbolic DCA parameters in each segment.

The figure below shows an example of a Hyperbolic DCA model split into 5 segments and each segment automatically adjusted to the data in the interval.

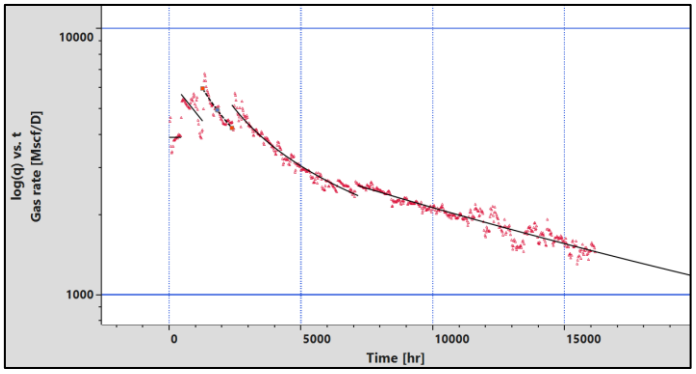


Fig. 10.D.30 – Segmented Hyperbolic DCA model match

The properties of each segment can be specified individually and several options allow the user to get the required match, for instance by imposing or not the continuity of the segments:

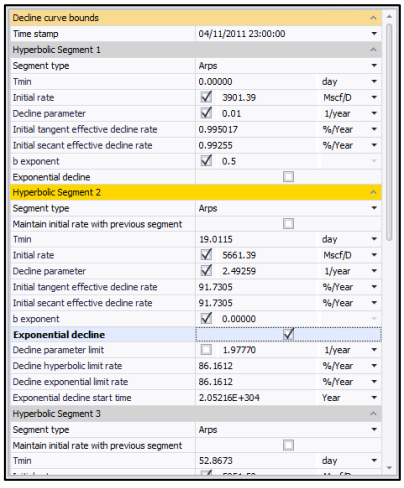


Fig. 10.D.31 – Parameter input table for Segmented model

10.D.9 Conclusions

DCA is a fast, sometimes efficient, yet empirical way to forecast production into the future under certain assumptions. All of the equations may produce good matches across the entire production and a EUR value can be estimated associated with each model. However, Fig. 29 presents an example where all decline curve relations (previously described) match the entire production data and differences are observed at late times due to specific model behaviour.

As mentioned earlier, none of these relations have a direct link to reservoir engineering theory other than analogy. At this point one must assume that each of these models can be considered as empirical in nature and generally center on a particular flow regime and/or characteristic data behaviour. A useful way to apply decline curve analysis is to apply all equations in tandem to obtain a range of outcomes rather than a single EUR value. This range of outcomes may be associated with the uncertainty related to the production forecast and can be evaluated as a function of time.

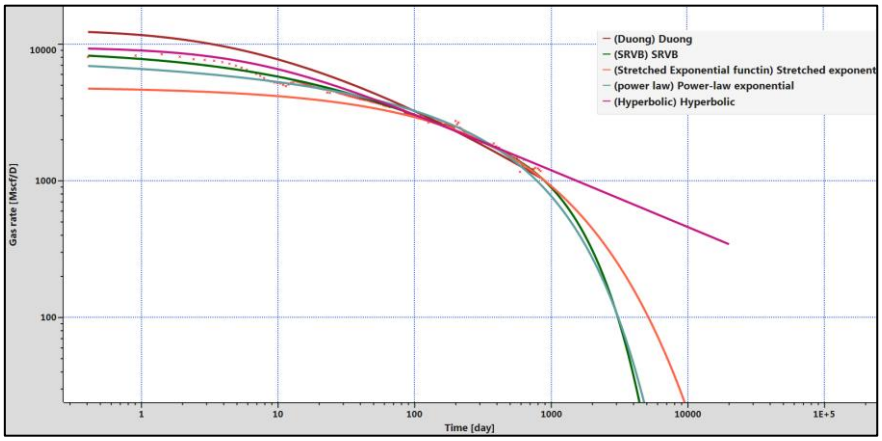


Fig. 10.D.32 – Rate and time plot (match with all models).

It is very optimistic to suggest that decline curve relations may approximate to, or match, model-based (time-pressure-rate) analysis profiles. These relations cannot capture all elements of the complexity of fluid flow behaviour in unconventional reservoirs modelled by reservoir solutions (analytically or numerically). However, the average trend can be used to approximate the behavior. Certain flow regimes can also be approximated by simpler models such as the power-law flow regime can be approximated with a constant b value in the hyperbolic model. Along these lines decline curve relations may also be used as proxies to represent model-based analysis (i.e. time-rate-pressure analysis) forecasts in economic software.

10.E Rate Transient Analysis (RTA) for unconventional plays

10.E.1 Linear flow diagnostics

The production behaviour for a fractured horizontal well exhibits the formation linear flow regime at early times, similar to the case for a single fracture. The analysis data obtained during this period gives us an estimate of the permeability-fracture half-length squared product (kX_{mf}^2), where X_{mf} is the aggregated length of the different fractures. For the case of a simple model with N_f fractures of equal half-length X_f, the value of X_{mf} will be $N_f X_f$.

For oil, in the case of a constant rate, we have:

$$\frac{p_i - p_{wf}}{q_{sc}} = \frac{4.06B}{h}\sqrt{\frac{\mu}{\phi c_t k X_{mf}^2}}\sqrt{t}$$

$$p_D = \sqrt{\pi\, t_{Dxf}}$$

$$t_{Dxf} = 0.0002637\ \frac{k}{\phi\mu c_t x_f^2} t \quad (t \text{ in days})$$

$$p_D = \frac{1}{141.2}\frac{kh}{qB\mu}(p_i - p_{wf})$$

$$\frac{1}{141.2}\frac{kh}{qB\mu}(p_i - p_{wf}) = \sqrt{\pi\, 0.0002637\frac{k}{\phi\mu c_t x_f^2}t}$$

$$(p_i - p_{wf}) = \frac{qB\mu}{kh}141.2\sqrt{\pi\, 0.0002637\frac{k}{\phi\mu c_t x_f^2}t}$$

$$\frac{(p_i - p_{wf})}{q} = (141.2\sqrt{\pi\, 0.0002637})\frac{B}{h}\sqrt{\frac{\mu^2}{k^2}\frac{k}{\phi\mu c_t x_f^2}t} = 4.0641\frac{B}{h}\sqrt{\frac{\mu}{\phi c_t k x_f^2}}\sqrt{t}$$

For gas we will have:

$$\frac{[m(p_i) - m(p_{wf})]}{q_{sc}} = 1447.8\frac{Tp_{SC}}{hT_{SC}}\sqrt{\frac{1}{\pi(\phi\mu c_t)_i k X_{mf}^2}}\sqrt{t}$$

Square-Root Time Plot

This relation is characterized by a linear trend on a square root plot of $\Delta p/q_{sc}$ (for oil) or $\Delta m/q_{sc}$ (for gas) versus $\sqrt{t}$. We can utilize the slope of this line (α) to estimate the kX_{mf}^2 product.

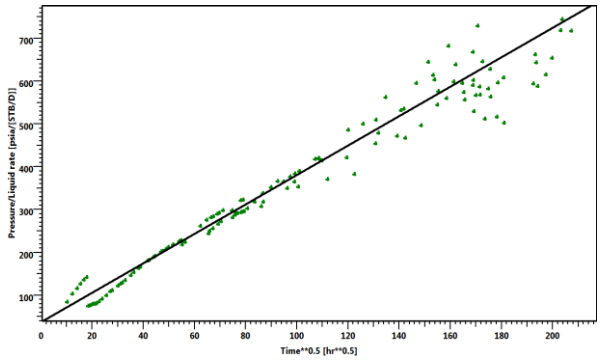


Fig. 10.E.1 – Square root plot for an oil case

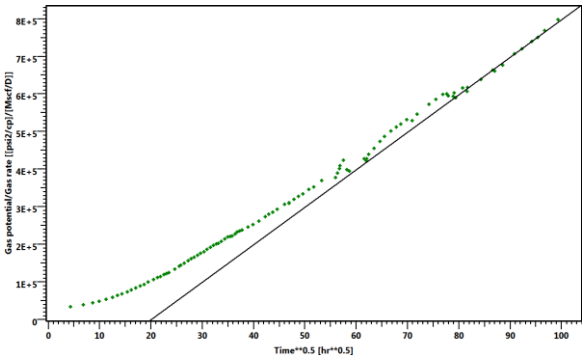


Fig. 10.E.2 – Square root plot for a gas case

For oil the slope is given by

$$\alpha = \frac{4.06\,B}{X_{mf}\,h}\sqrt{\frac{\mu}{k\phi c_t}}$$

The permeability-fracture half-length squared product (kX_{mf}^2) can be calculated from:

$$kX_{mf}^2 = \left(\frac{4.06\,B}{\alpha h}\right)^2 \frac{\mu}{\phi c_t}$$

For gas the slope is given as:

$$\alpha = \frac{Tp_{SC}}{hX_{mf}\sqrt{k}T_{SC}\sqrt{\pi(\phi\mu c_t)_i}}$$

The permeability-fracture half-length squared product (kX_{mf}^2) can be calculated from:

$$kX^2{}_{mf} = \left(\frac{Tp_{SC}}{\alpha h T_{SC}}\right)^2 \frac{1}{\pi(\phi\mu c_t)_i}$$

Loglog and Blasingame plots

The use of the half unit slope straight line on the Loglog plot provides an equivalent result. In the Topaze diagnosis plot, we have:

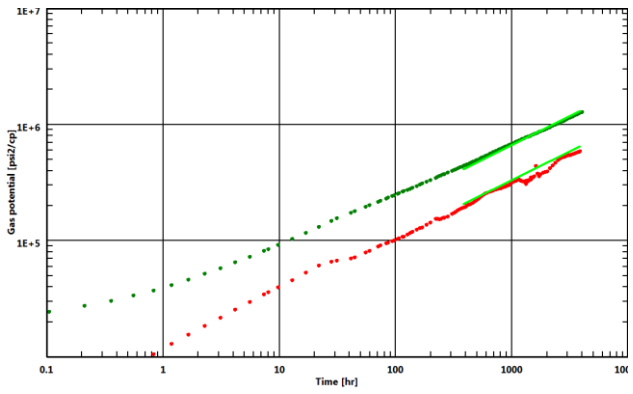


Fig. 10.E.3 – Loglog plot for production analysis

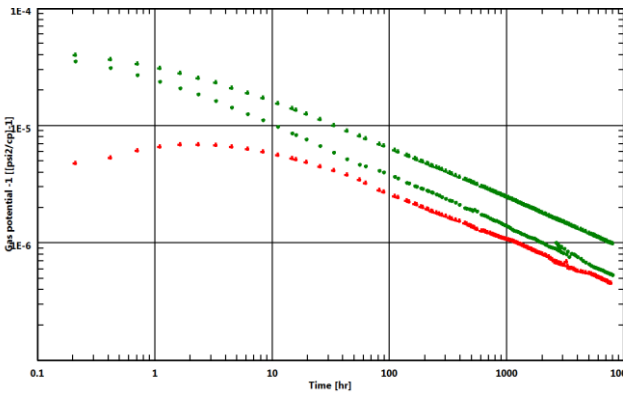


Fig. 10.E.4 – Blasingame plot for production analysis

10.E.2 Diagnostic of the SRV flow

The SRV flow regime is described in paragraph 10.C.3. The SRV flow regime exhibits behaviour similar to the traditional Pseudo Steady state (PSS) and the same diagnostics and analysis methods can be used. This flow regime has been called the 'Pseudo Pseudo Steady state'. The difference with conventional reservoirs is that for the unconventional reservoirs this flow does not describe the entire reservoir volume, but only from the SRV, which is thought to be the maximum practical volume for fluid production. The flow from beyond the SRV will be minor and will take from years to decades to manifest itself and will generally be ignored for any practical purpose.

In addition, the conventional Pseudo Steady state (or boundary-dominated flow) methods are only strictly valid when a distinct unit slope straight line is observed on a diagnostic Loglog or Blasingame plot.

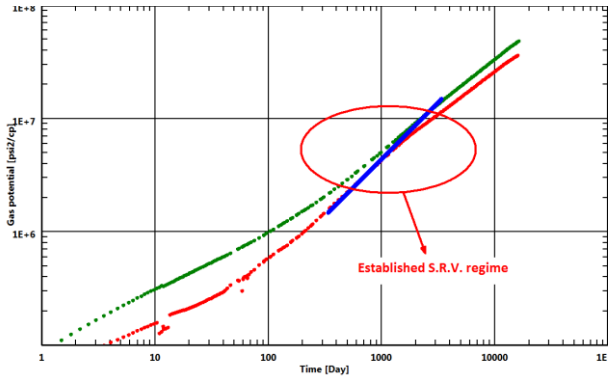


Fig. 10.E.5 – Loglog plot for production analysis

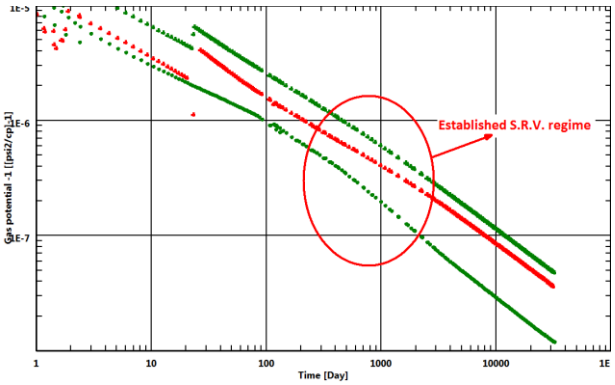


Fig. 10.E.6 – Blasingame plot for production analysis

Using the conventional PSS concepts, we can utilize a straight-line analysis on this portion of the data such that we can estimate a 'drainage area' (essentially the SRV). The governing relations are given as:

For oil, with the observation of a straight-line on a plot of $\Delta p/q$ vs. t_e, the slope is:

$$A = 3.36.10^6 \frac{qB\mu}{mh\phi c_t}$$

For gas, with the observation of a straight-line on a plot of $\Delta m/q_{sc}$ vs. t_e, the slope is:

$$A = 1.2.10^9 \frac{qTP_{sc}}{mh\phi\mu c_t T_{sc}}$$

Relating this value to the fractured region area, one can estimate the L X_f product.

In addition to plots of $\Delta p/q$ vs. t_e (oil) and $\Delta m/q_{sc}$ vs. t_e (gas), the material balance approach (using the Normalized Rate Cumulative plot) can also be used on the portion of the data exhibiting the SRV flow behaviour as shown in the figure below.

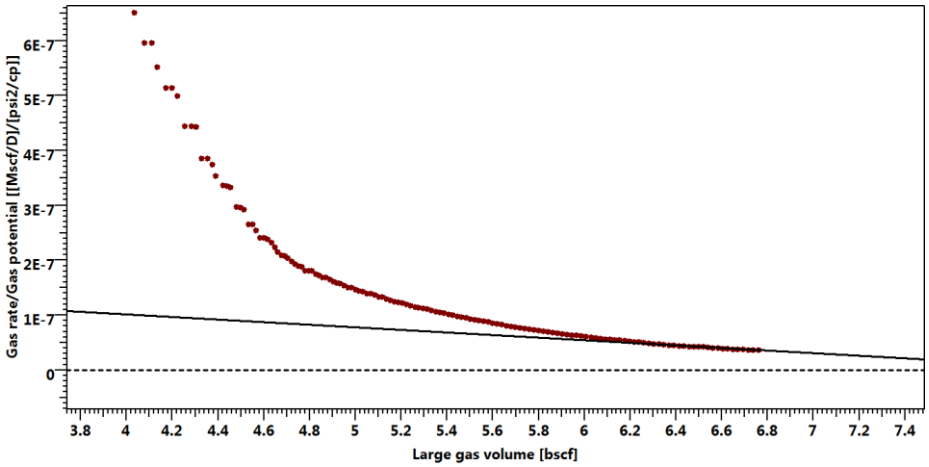


Fig. 10.E.7 – Normalized rate cumulative plot for an example gas case

10.E.3 Simultaneous diagnostic of several flow regimes

Loglog straight line diagnostics

We typically observe certain straight lines on the Loglog plot for conventional reservoirs (i.e., wellbore storage (unit slope), formation linear flow (half-slope), bilinear flow (quarter slope), and reservoir limits (unit slope)). There is also the special case of the 'zero-slope' trend which occurs for infinite-acting radial flow. The same principles apply for unconventional reservoirs, but it is unlikely that we will (ever) see certain flow regimes in the performance data for unconventional reservoirs. As guidance, we have:

- Very early time: unit slope governed by wellbore storage (material balance)
- Bilinear flow: 1/4 slope governed by fracture conductivity ($k_f w_f$)
- Linear flow: 1/2 slope governed by kX_{mf}^2
- SRV flow: unit slope governed by SRV drainage area (or volume)
- IARF: zero slope governed by k (*IARF regime is extremely unlikely in shales*)

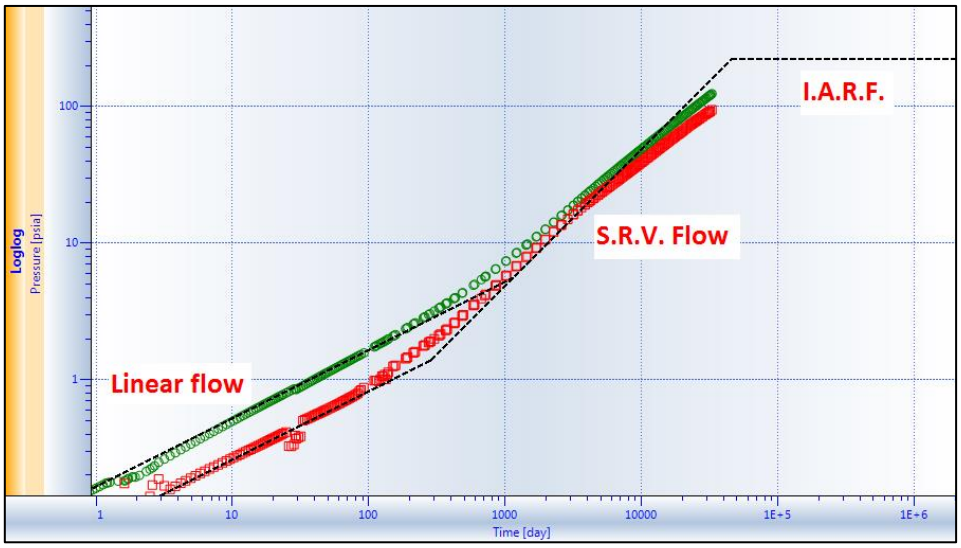


Fig. 10.E.8 – Multiple straight lines diagnostic plot

When we consider the case of the analytical multi-fracture horizontal well model (MFHW), we have the following primary unknowns:

- The horizontal well length (L) (this is typically treated as a 'known' or 'fixed' variable)
- The number of fractures (N_f)
- The fracture half-length (X_f)
- The fracture conductivity ($k_f w_f$)
- The formation permeability (k)

In most cases we can observe and analyze the linear flow and possibly the SRV flow. With them we can determine one or two of the unknowns, even assuming we know the L value.

- The Linear flow analysis provides a $k(NX_f)^2$ value
- The SRV flow analysis provides a LX_f value
- The IARF horizontal line which should provide a permeability k value

The 'ideal' workflow should be:

- Input the well length from completion records.
- Estimate permeability (k) using the IARF line.
- Use the permeability value in the linear flow analysis, estimate X_f.
- Using the results of the linear flow analysis, we compute the number of fractures (N_f).

Unfortunately, in practice, the IARF is never reached for unconventionals and k has to be estimated by other means, and is often found iteratively. Therefore, the 'practical' workflow is:

- Input the well length from completion records.
- Select a permeability value, maintain as constant for the given analysis cycle.
- Use the permeability value in the linear flow analysis to estimate X_f.
- Use the results of the linear flow analysis to compute the number of fractures (N_f).
- Make sensitivity estimates on each parameter, focus on relationship of k and X_f (i.e., hold one constant and vary the other).

Using the linear flow to SRV model

The transition period between Linear flow and SRV flow regime, as described in paragraph 10.C.2, represents a deviation from linear flow due to the interference of the pressure distributions between fractures. There is no simple (i.e., straight-line) model that can be used to match this transition behaviour.

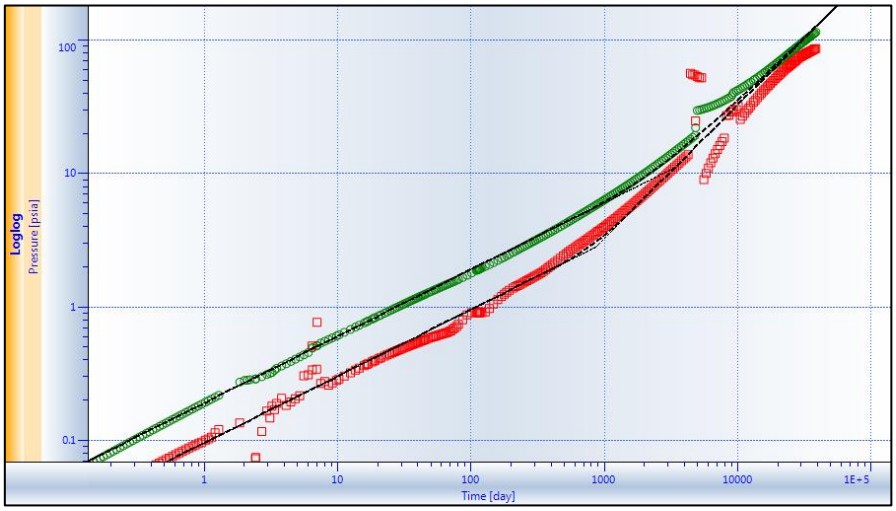


Fig. 10.E.9 – Loglog plot for production analysis (MFHW model)

Using the trilinear flow model

Another option is to consider the 'trilinear flow model'. This is analogous to the case for a single fracture where there three linear flow components: the flow inside the fracture, the flow into the fracture, and an 'external' flow component into the linear flow 'cell'. This model has gained extensive use because it is easier and quicker to model than the multi-fracture horizontal well and because it serves as a useful 'proxy' for SRV flow in the limiting case where a boundary is assumed. Although the characterization of the flow behaviour is an 'analog' when the trilinear flow model is used, this model does provide some diagnostic capability.

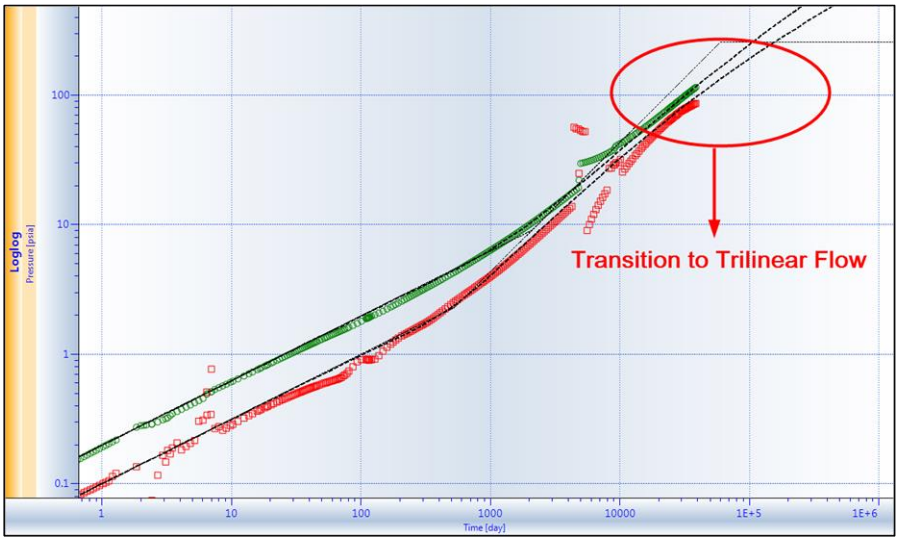


Fig. 10.E.10 – Loglog plot for production analysis (trilinear flow model)

10.E.4 Matching data with a model

The Loglog and Blasingame plots (see chapter 10.04.C) are designed to account for the non-constant flowing pressure and rate, generating an 'equivalent constant rate' response for comparison of data and model behaviour.

For the Blasingame plot (log-log plot) we have:

$$y = \frac{q(t)}{p_i - p_w(t)} \text{ and } y' = PI\ Int.Derivative = \frac{\partial(PI_{Int})}{\partial \ln(t_e)}$$

$$x = t_{cr} = \frac{Q(t)}{q(t)} \text{ (cumulative rate equivalent time).}$$

For the Loglog plot

$$y = \frac{p_i - p_w(t)}{q(t)} \text{ and } y' = \text{derivative or integral function of } \frac{p_i - p_w(t)}{q(t)}$$

$$x = t_{cr} = \frac{Q(t)}{q(t)} \text{ (cumulative rate equivalent time).}$$

These functions can be used for diagnostic purpose and also to adjust the match of the model compared to the measured data functions on log-log scales (see before and after adjustment plots below).

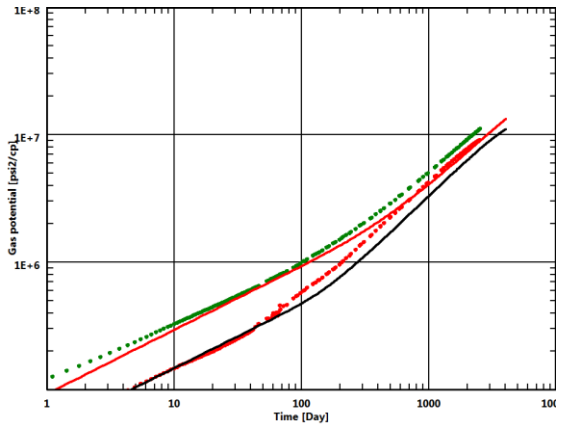


Fig. 10.E.11 – Loglog plot before adjustment.

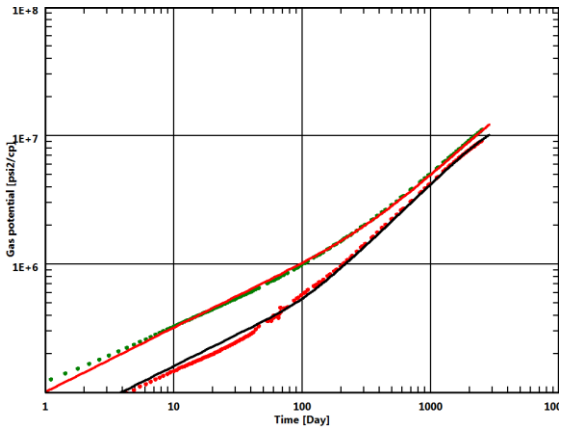


Fig. 10.E.12 – Loglog plot after adjustment.

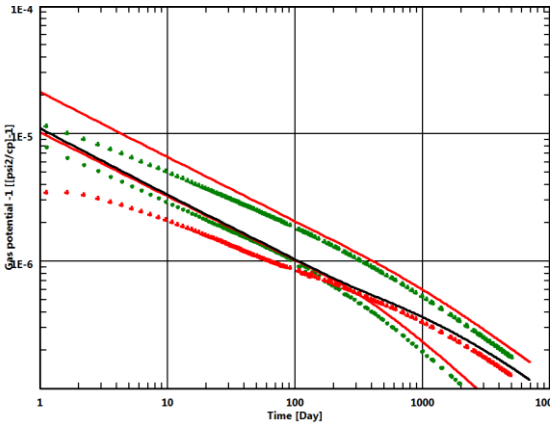


Fig. 10.E.13 – Blasingame plot before adjustment.

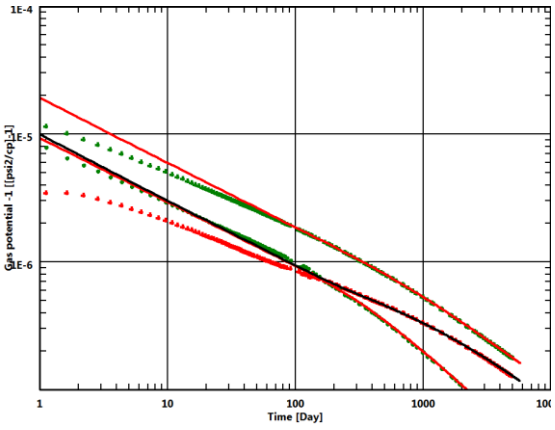


Fig. 10.E.14 – Blasingame plot after adjustment.

In the KAPPA formulation of the Loglog and Blasingame plots, the raw data functions can be compared to any model (analytical, semi-analytical, or numerical), the model parameters can be adjusted manually or using a regression model.

10.E.5 History matching

In addition to matching diagnostic functions for a specific flow regime, we utilize methods that permit automated and semi-automated matching of pressure and rate functions to a specified model using regressions methods. We acknowledge that the two classical plots (Loglog and Blasingame) are extremely well-suited for diagnostic purposes, but are less useful for matching time or pressure dependent parameters (i.e., quasi-linear and non-linear models).

In addition to the Loglog and Blasingame diagnostic plots, the history plots (q vs. t and P. vs t) are very convenient for observing the quality of a given model match. The 'history' plots shown below are perhaps the most effective presentation of model and data matches.

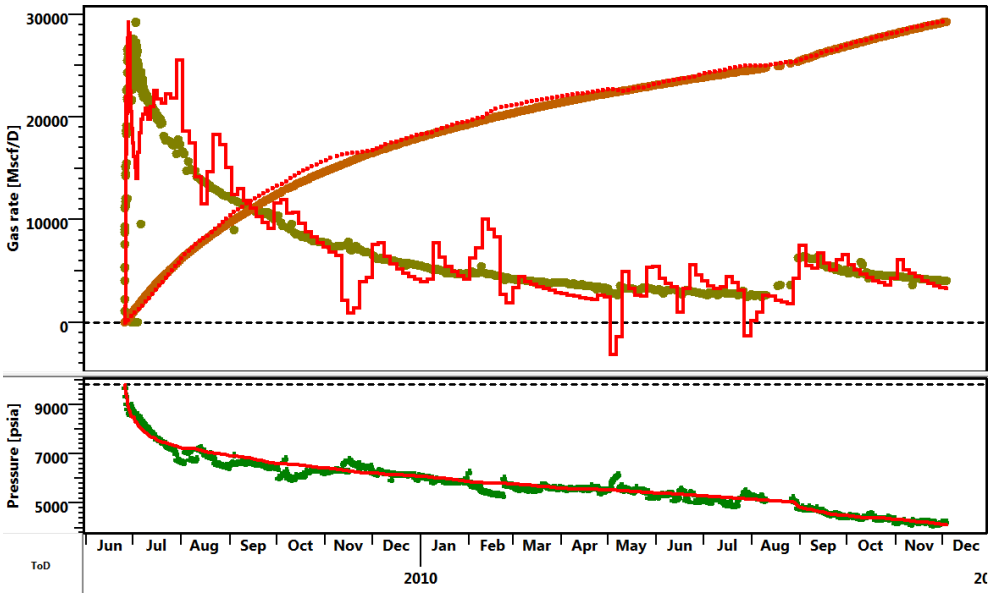


Fig. 10.E.15 – History plot for production analysis (rate, cumulative, and pressure vs. time).

Another valuable aspect of the 'history' plot is that changes in well behaviour as a function of time are more clearly visible than on the diagnostic plots. In the case shown below, a variable flowing condition can be observed (most likely a choke change, which is often seen in the surface pressures record). In such cases where a pressure-rate mismatch occurs, a time-dependent skin factor can be used to represent the changing well condition.

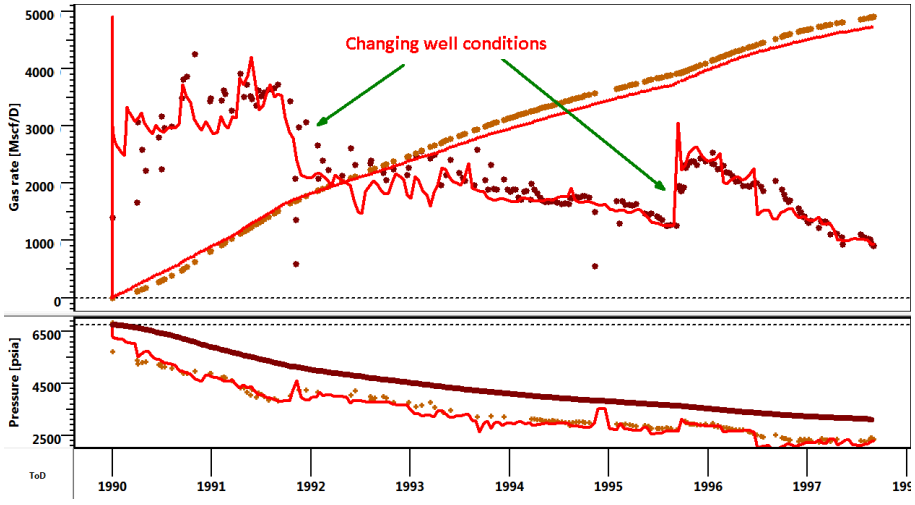


Fig. 10.E.16 – History matching with changing well conditions (analytical model).

The analytical models in Topaze include the detailed multi-fractured horizontal well (MFHW), but these analytical models are limited to the linear, liquid single phase, case. For the gas case, the pseudopressure function is used to compensate for non-linearities associated with pressure-dependent gas properties (i.e., z, μ_g, c_g)).

The numerical model implicitly allows essentially any non-linear condition such as:

- Non-Darcy flow,
- Pressure dependent permeability and porosity,
- Multiphase flow,
- Desorption,
- Compositional fluid behaviour, and
- Combinations of these effects.

These parameters and functions can be adjusted using regression. As seen in the example below, the dew point effect (condensate drop-out) has a dramatic influence on the production character.

Typically, the analytical model is used to address diagnostic features and the numerical model is used to account for the time-dependent production effects.

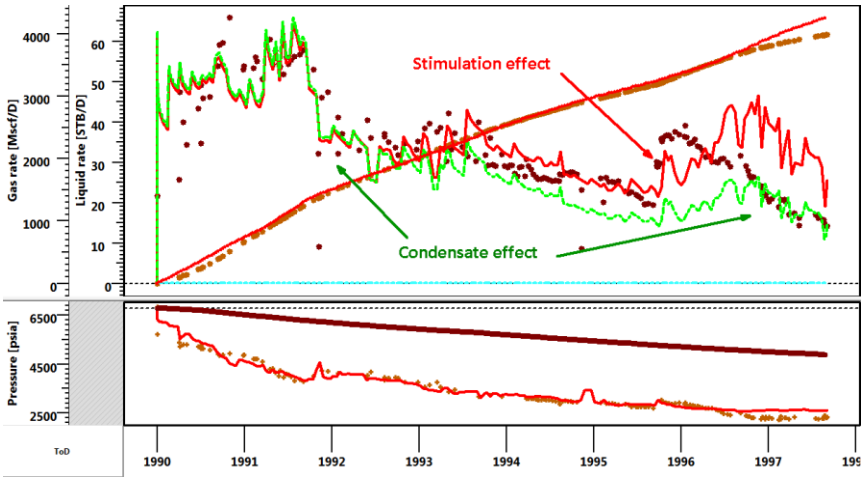


Fig. 10.E.17 – History matching with changing well conditions (numerical model).

In addition, history matching with a numerical model allows multi-well models which take into account interference from the well(s) in the immediate vicinity. The 'unconsolidated formation' option (i.e., pressure-dependent porosity and permeability) allows the user to differentiate between cases with and without the influence of pressure-dependent properties. The example below clearly indicates the need to include pressure-dependent effects.

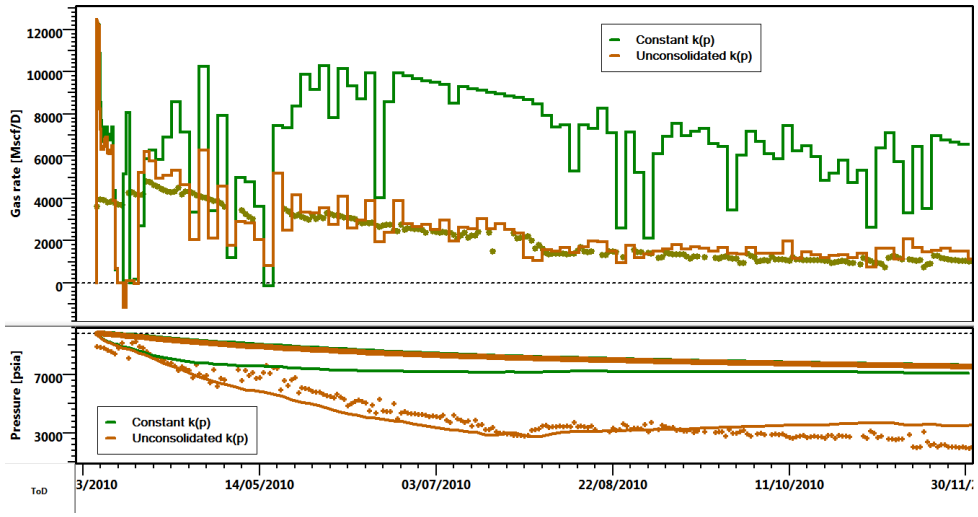


Fig. 10.E.18 – History matching – numerical model with k(p).

10.E.6 Production forecasting and EUR

Once an analytical or numerical model is tuned to a historical data set, this model can then be used to forecast long-term performance and estimate hydrocarbon recovery. Such forecasts are only reliable in the case where the producing conditions remain constant. The practical approach is to establish a history match then extrapolate rate performance assuming a constant pressure or a prescribed pressure decline profile. There exists some subjectivity in this approach, but model-based forecasts are still the most robust and reliable.

An example of production extrapolation is shown in the figure below, note that the pressure forecast is set to a constant value.

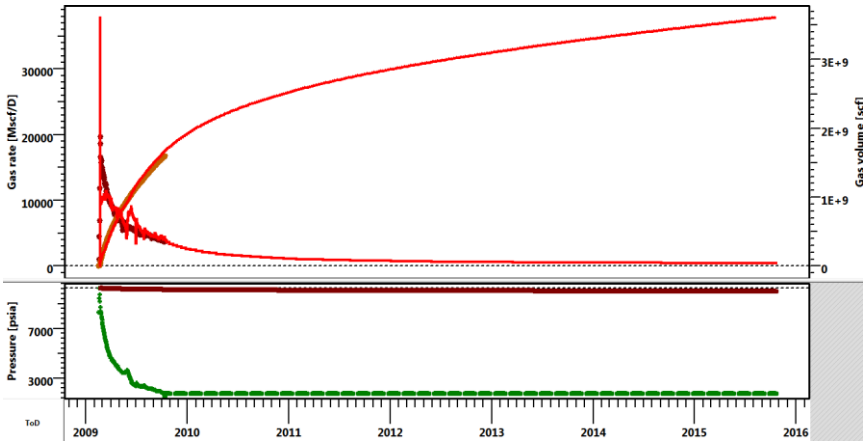


Fig. 10.E.19 – Performance extrapolation (extrapolated constant pressure profile).

Using a specified abandonment rate (or economic limit rate), the estimated ultimate recovery (EUR) can be established.

10.E.7 EUR statistics

In the the Rate Transient Analysis Topaze application there are two different modes for production forecasting: the 'standard' approach of imposing a rate or a pressure schedule (as described above), or the 'EUR mode'. In the latter, the simulation is run until a termination criteria is met (e.g., an abandonment rate, a maximum production time, or even limiting pressure).

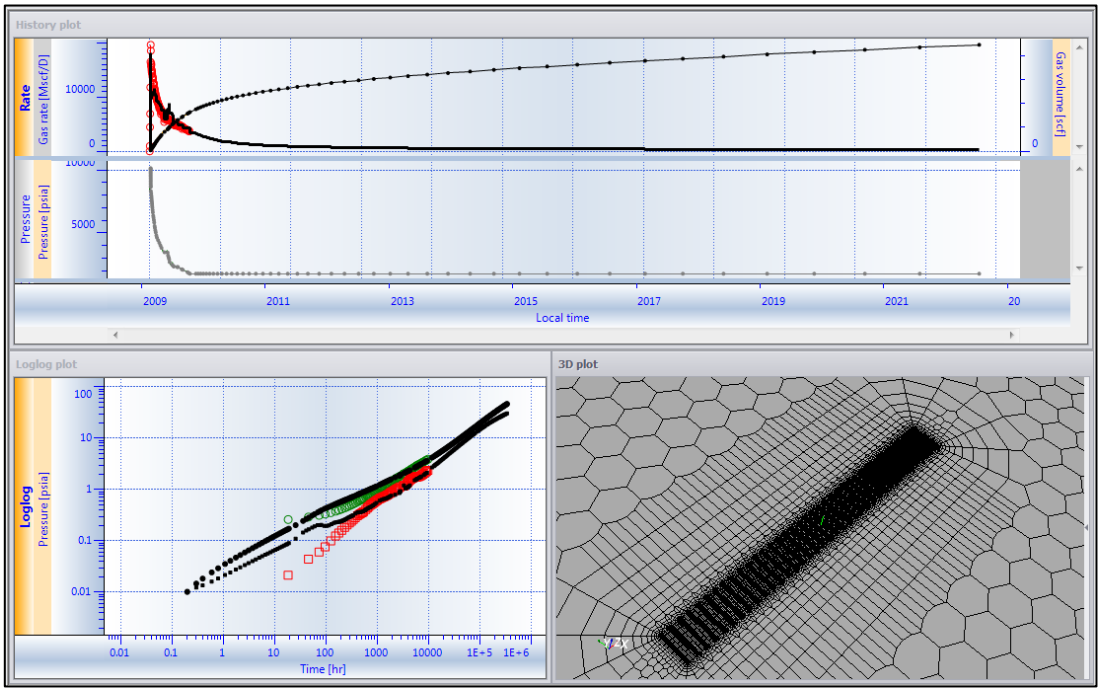


Fig. 10.E.20 – History match and performance extrapolation using a numerical model.

In our matching process we recognize the non-uniqueness of our parameter estimates, in particular the formation permeability, the fracture half-length, and on occasion, the fracture conductivity. These parameters are interdependent due to the ultra-low permeability nature of the formation and the strong influence of early-time flow regimes, in particular, linear flow. The most uncertain of these variables is formation permeability. But we accept this because, at least at present, there are no explicit model which can 'uncouple' the influence of early-time linear flow. One approach that is being used at present is to consider the effect of the distribution of various reservoir properties on the production forecasts and EUR predictions.

In the KW Rate Transient Analysis application, Monte Carlo simulation is run to randomly select parameter values from their probability distributions (most often these are permeability and fracture half-lengths) and then generate production forecasts and EUR predictions with the specified reservoir model. For reference, there are several different distribution profiles that can be used, and the user is able to select one they believe best represents a given parameter.

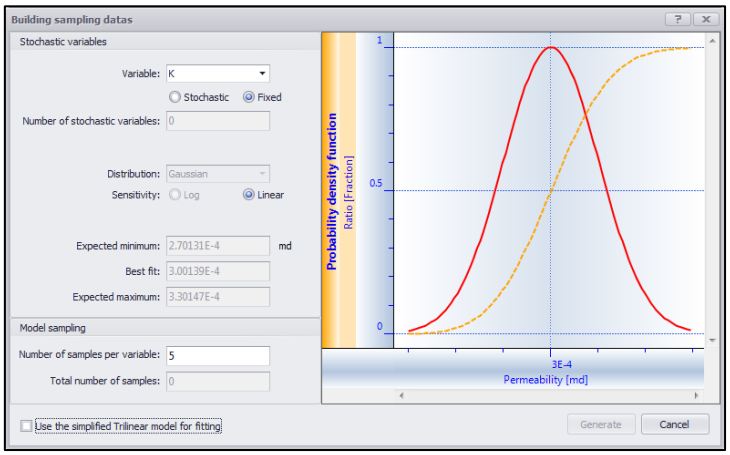


Fig. 10.E.21 – Permeability distribution plot.

As an example, we consider a case where permeability is being statistically sampled. The user specifies an appropriate number of samples, the model is generated for each permeability sample and a nonlinear regression is conducted on X_f and N to adjust the model for each permeability value and then a forecast is made to obtain the corresponding EUR values. The individual history matches and extrapolations are shown in the figure below.

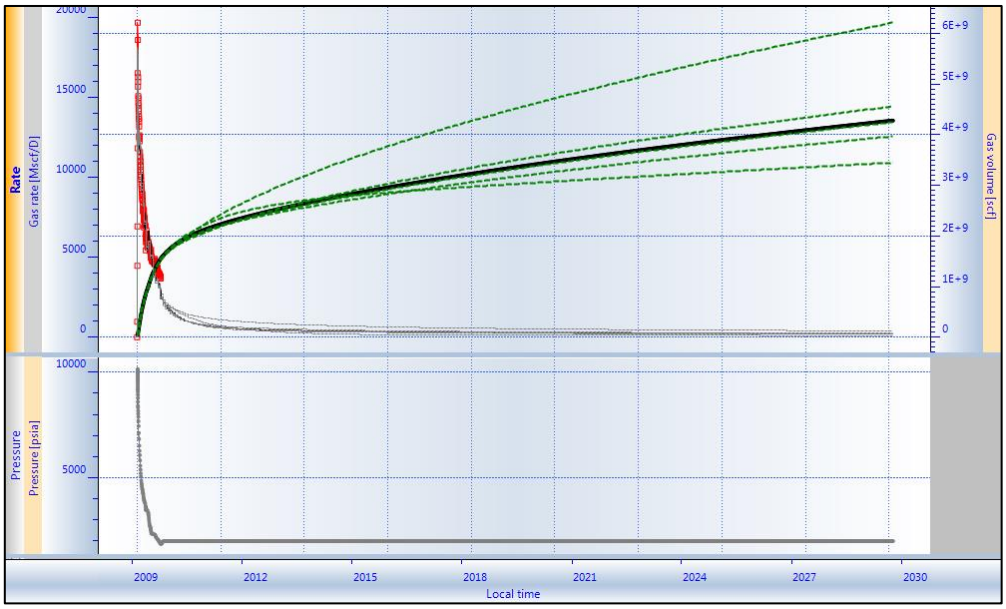


Fig. 10.E.22 – Multiple forecast plot.

Using these production extrapolations, the corresponding EUR values are then estimated based on the termination criteria specified by the user. The result is a probability distribution for the EUR and P10, P50 and P90 values can be estimated.

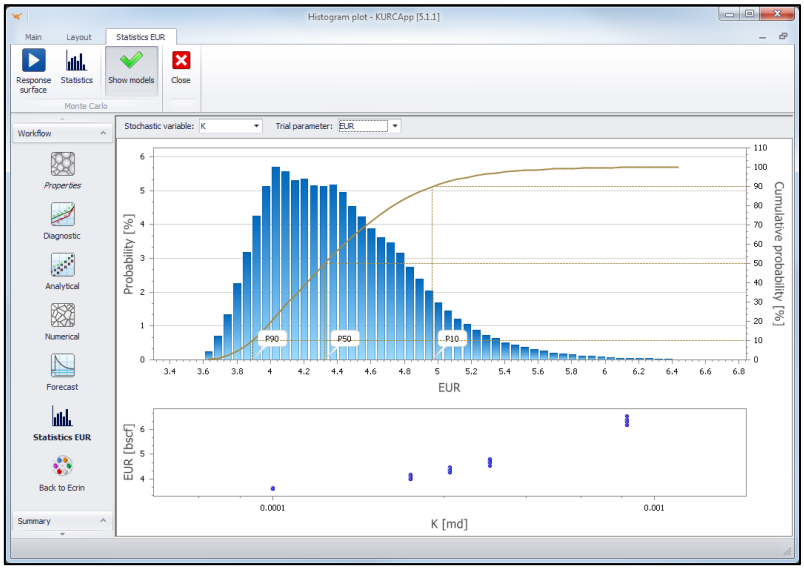


Fig. 10.E.23 – P10, P50 and P90 probability plot for EUR (as a function of permeability)

10.F Simple models

In this section we review the three most fundamental models that are used to represent the standard well design for unconventional reservoirs; the multi-fractured horizontal well (MFHW) case. These models can reproduce the flow regimes and rate and pressure performance as previously described in paragraph C. In the current versions of KAPPA software these models are available as either analytical or numerical models and are fully supported with a variety of options for either case.

These 'simple' models share the following assumptions:

- Reservoir:
  - The reservoir is homogeneous.
  - The traditional Darcy's law applies.
- Fractures:
  There are N_f fully penetrating fractures and they;
  - are orthogonal to the horizontal well.
  - are evenly distributed along the horizontal well.
  - intersect the horizontal well at their mid-point.
  - all have the same half-length X_f
  - all have the same fracture conductivity.

The models differ in terms of the boundary conditions and configurations.

10.F.1 'Classic' Multi-Fractured Horizontal Well (MFHW)

We assume the reservoir to be of infinite extent (analytical), or at least large enough for boundaries to be never seen during the producing life of the well (numerical). This classical model can also be combined with traditional simple boundary geometries such as a rectangle. This specific model was introduced in Topaze and Saphir more than ten years ago and was initially an 'external' analytical model. It was later fully integrated analytically and numerically as an 'internal' model.

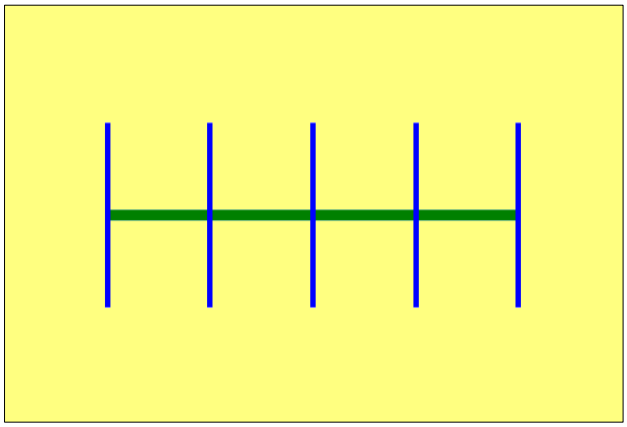


Fig. 10.F.1 – Schematic of the classic Multi-Fractured Horizontal Well (MFHW).

Analytical model

The typical behaviour of this model for an infinite reservoir is shown on the Loglog plot and a Blasingame plot below. One can observe the early-time (formation) linear flow, transition, and an SRV flow regime (also known as 'Pseudo Pseudo Steady state'), which, at unreasonably long times (years to decades depending on permeability) tends towards a hypothetical Infinite

Acting Radial Flow (IARF) regime. This model, as with all analytical models in the KAPPA software suite, can be used for gas cases using pseudopressure and pseudotime functions.

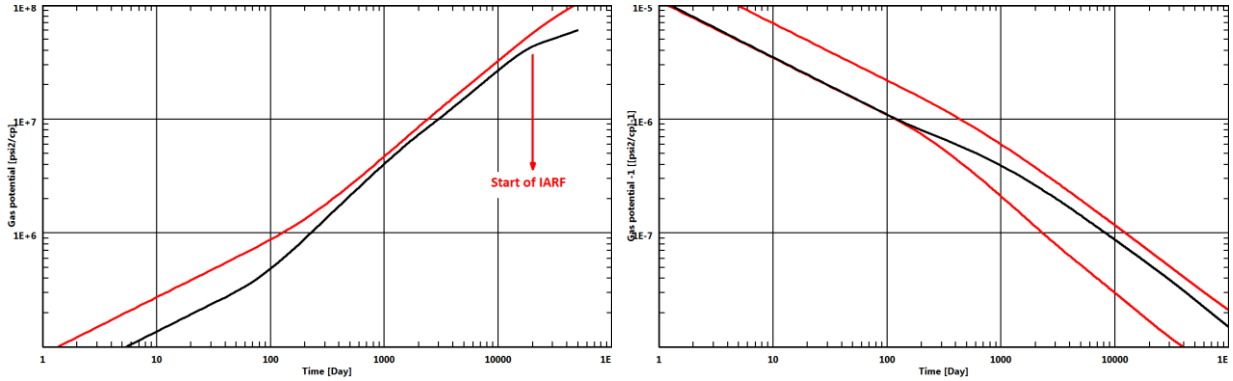


Fig. 10.F.2 – Classic MFHW — Loglog and Blasingame plots (analytical model).

Numerical model

The gridding used in the numerical version of this model is shown in the figure below. In each cell the system formally accounts for PVT (real gas compressibility, complex phase behaviour, etc.), pressure-dependent permeability and porosity, gas desorption, and complex diffusion if required (Forchheimer, Klinkenberg effect, Fickian diffusion, etc.).

In most situations, the horizontal well (i.e., the drain) is isolated and production is only coming from the fractures. If the fractures are fully penetrating the flow will be horizontal and this will be essentially a 2D problem, which is solved relatively fast. However, if we want to consider convergence of the flow towards the horizontal drain (which should be minimal), or if the fractures only partially penetrate the formation, this yields a full 3D problem which must be addressed by a fairly complex 3D grid.

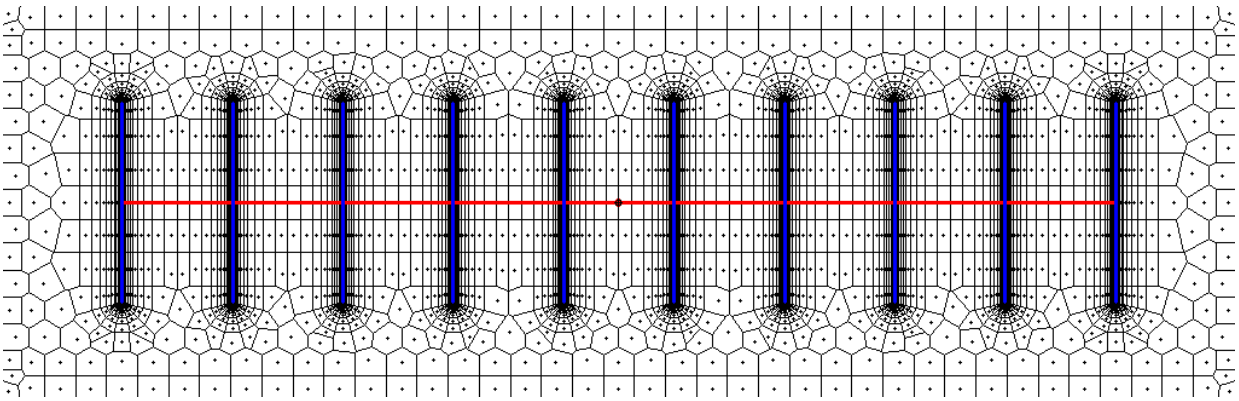


Fig. 10.F.3 – Gridding of the classic numerical model for MFHW.

Due to the high pressure gradients in the vicinity of the fractures, very fine-scale grid refinement is used to ensure that early-time pressure transients are properly represented. The size of the smallest cells connected to the fractures also depends on the fluid mobility. A large number of cells is also required when the fluid in place is a volatile oil or condensate gas, in order to accurately describe the evolution of the GOR.

10.F.2 SRV bounded model

The hypothesis for the SRV bounded model is that the reservoir is geometrically limited to the area defined by the series of fractures. The reservoir size along the horizontal drain is increased on each side by half of the fracture spacing to provide the same diffusion area for the fractures at the end of the well.

Because of the symmetry of the problem, each fracture has strictly the same contribution and a solution can be generated focusing on only one symmetry element corresponding to a quarter of the drainage volume of a given fracture (see below). By the use of the symmetry element, both analytical and numerical solutions are extremely fast, the speed not being dependent on the number of fractures. Once the elementary system has been simulated, the instantaneous rates are multiplied by $4 \cdot N_F$ to get the answer of the global SRV-bounded system.

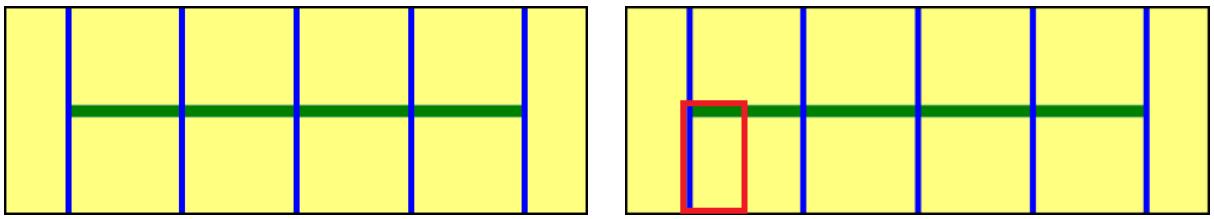


Fig. 10.F.4 – Schematic of the SRV bounded model (left), with basic symmetry element (right)

This simplistic model has been extensively used by other technical groups as their reference analytical model. It does not account for diffusion beyond the SRV, which is generally acceptable during the first years of production. Understandably, for a given well the EUR will be conservative.

Analytical model

The typical behaviour of this model is shown below on the Loglog and Blasingame plots. As one may expect the early behaviour is linear, characterized by a half slope on the loglog plot, and after a transition the final behaviour is the SRV flow (actual Pseudo Steady state in this case), characterized by a unit slope.

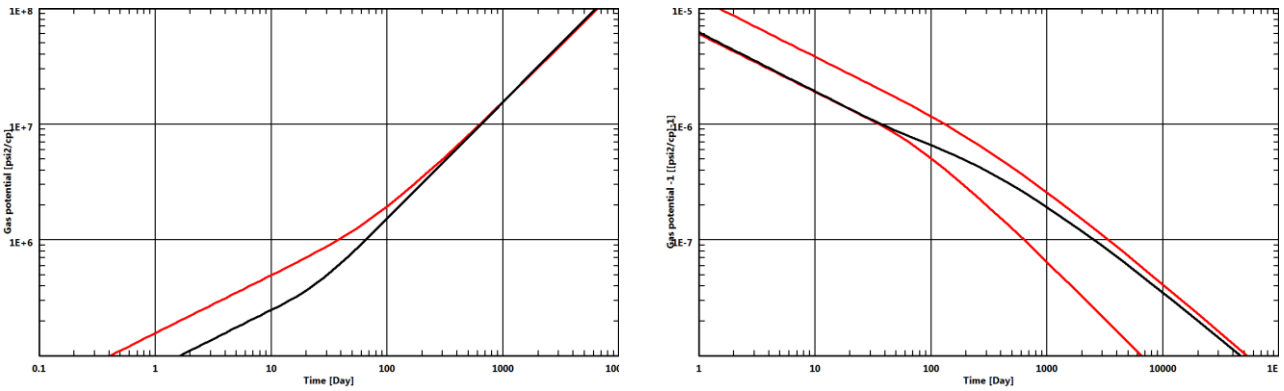


Fig. 10.F.5 – SRV model: Loglog and Blasingame plots.

The speed of the analytical model allowed us, in the KAPPA Workstation, to use it as an instantaneous, interactive 'glorified' straight line. A simple adjustment of the data allows a simultaneous match of the linear and the SRV flow regimes, providing instant parameters estimates.

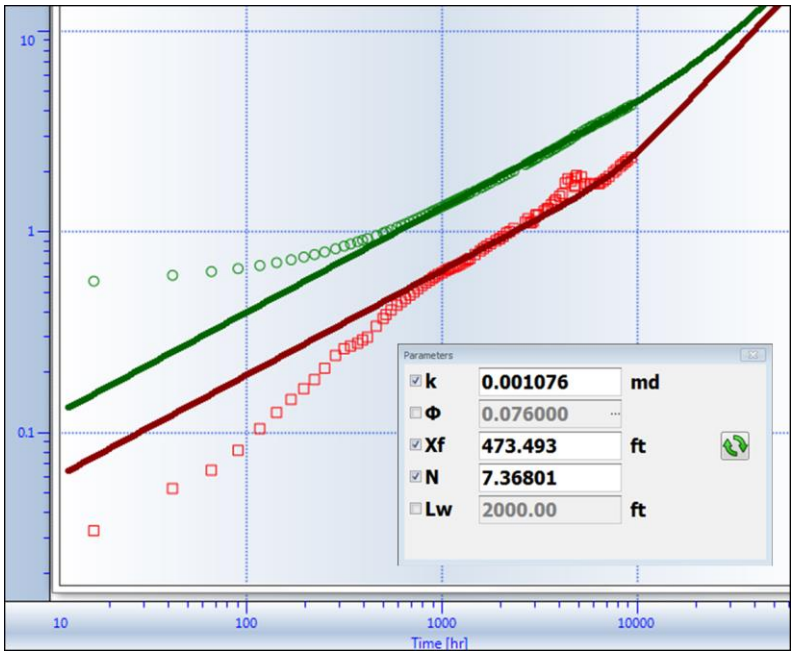


Fig. 10.F.6 – Using the SRV model as a diagnostic tool .

Numerical model

The SRV bounded model can be generated using the same symmetry element as for the analytical model. The result, in terms of speed, is even more spectacular. This problem is simulated by filling the symmetry element with a geometric 1-D grid (see below). As a result the numerical model is even faster than an analytical model. The behaviour is qualitatively the same as for the analytical model for the simplest diffusion cases.

This remarkable speed can be precious to test complex diffusion effects. Rather than running cases on the classic model, one can use the SRV model to assess the sensitivity of the system to complex hypotheses related to the diffusion equations, compositional PVT, stress dependence, etc. This model is even fast enough to run a nonlinear regression on the most complex diffusion hypotheses.

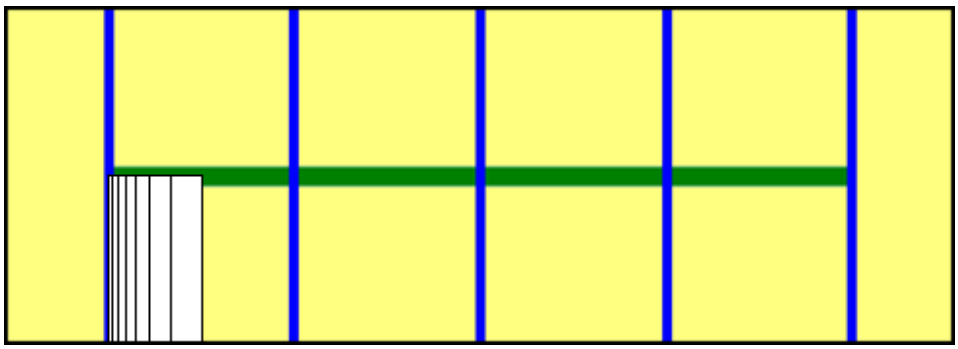


Fig. 10.F.7 – SRV Model — gridding of the symmetry element.

10.F.3 Trilinear model

This is an extension of the SRV-bounded model to which a linear flow was added from the outer unstimulated, reservoir matrix zone toward the inner SRV zone. Petrophysical properties (permeability, porosity, rock compressibility…) may be different in the two zones. Because of the influx from the outer zone, this model may be considered an intermediate between the SRV model and the 'classic' model.

As for the SRV model, the trilinear problem can be solved by focusing on a single symmetry element (see below) corresponding to a quarter of the drainage area of a given fracture. In both analytical and numerical cases, the speed is very high and not dependent on the number of fractures.

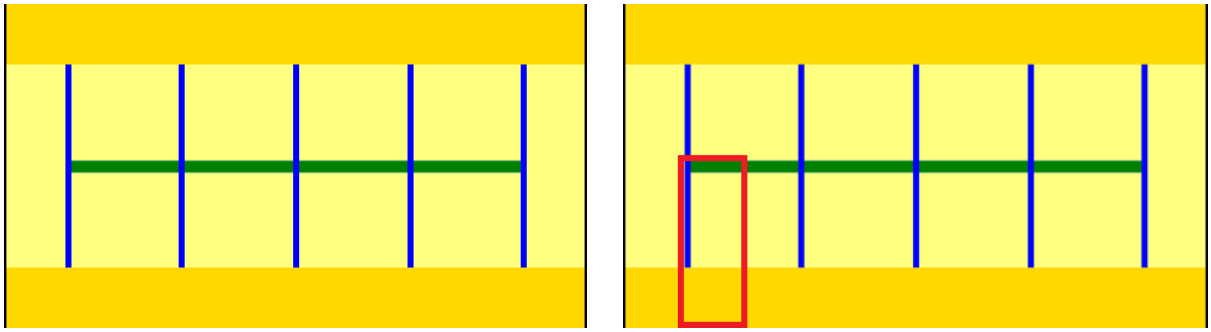


Fig. 10.F.8 – Schematic of the trilinear bounded model (left), with basic symmetry component (right).

Analytical model

The typical behaviour of this model is shown below on the loglog plot and Blasingame plots. It starts with an initial linear flow, followed by the transition to the SRV flow, but it deviates at late times when the impact of the outer zone is felt. Because the final flow regime is the linear diffusion from the outer zone, the late time behaviour may once again exhibit a half slope on the Loglog plot. The position of this straight line depends on the well length and external reservoir permeability.

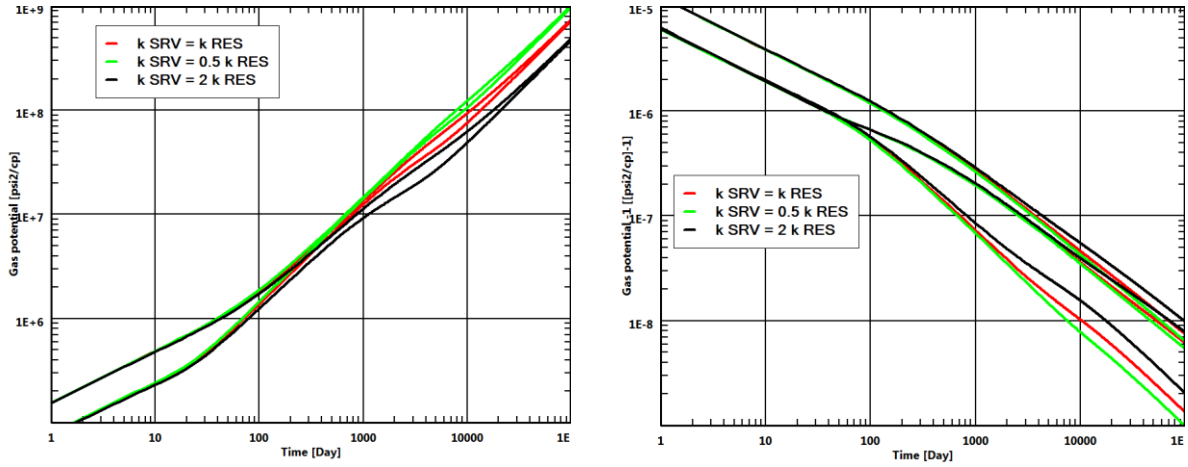


Fig. 10.F.9 – Trilinear model — Loglog and Blasingame plots.

Numerical model

The numerical model is generated using the same symmetry element. To the 1D-grid of the SRV model, a second 1D grid is added to simulate the linear flow in the outer zone. The resulting solution is also extremely fast.

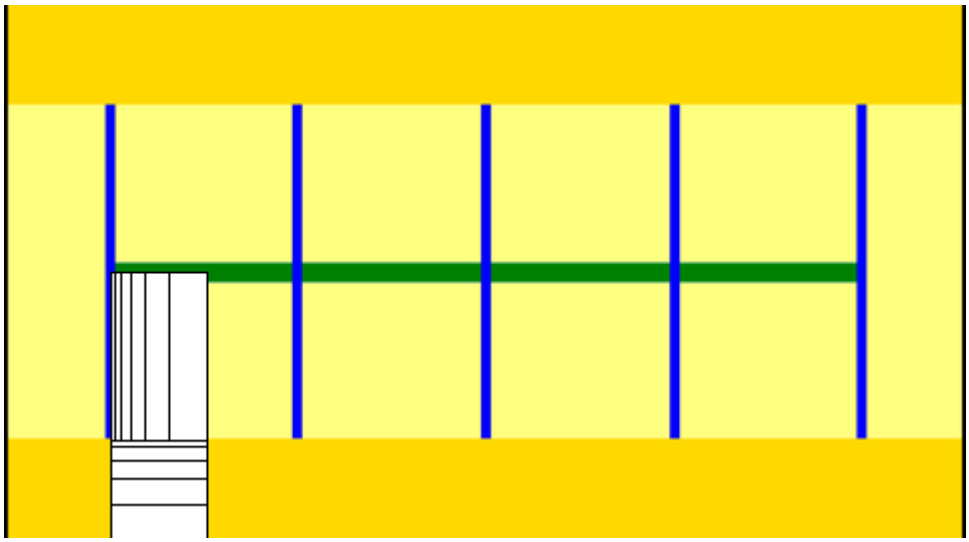


Fig. 10.F.10 – Trilinear model — gridding of the symmetry element.

To be totally honest, at KAPPA we are not very fond of this model, for three reasons:

- The existence of a composite zone outside the SRV is subject to discussion
- Because you have one more parameter related to the outer zone it is a flexible model that can match virtually anything. It is to RTA in unconventional plays what the radial composite model is to PTA in conventional formations. This model is too often selected for its flexibility rather than for its physical relevance.
- Because the final regime is linear we are back to the magic of b=2. It is as if this model had been designed to retroactively justify the unreasonably high values of b carelessly calculated from the initial linear flow.

As often in this case the trilinear model can have a valid usage if and only if its assumptions are validated by physical evidence, and not just the outcome of a regression process.

10.G Field example – Demonstration of simple models

To illustrate the basic concepts presented in the previous section we will show the summary of a study done in 2010 with the tools that were then available. We will not get into the details of the analysis and we will just scan through the main phases and main conclusions. Though some parameters are given in the next paragraph the results will not be discussed here.

This horizontal gas well had a length of around 3,900 ft, and 42 hydraulic fractures were expected to be present with an average half-length of around 300 ft. Expected permeability was in the order of 10^{-4} md, water saturation of 25%, pay zone of 100 ft, temperature of 305 °F, initial pressure of 11,300 psia. Desorption data were available. The well was initially produced from casing, then production was switched to the tubing.

We were initially given 8 month of production data, with both rates and surface pressure. Water flow back was noted during the clean-up and the first hundred hours of production. A series of analyses were done using the different tools available at the time. All these tools history matched the data and forecasts were done assuming a constant final flowing pressure. The three forecasts, matching the same data, gave different forecasts and EUR.

A year later we were given 10 more months of data. We used the results of the three previous interpretations and ran a simulation, but now using the effective 10 months of pressure data. These simulations were compared to the effective 10 months of production to see how these different models behaved in this double-blind process.

10.G.1 First eight months of production

Rates and surface pressure were provided for the first months of data as shown on the history plot below. Pressure were available at surface and they had to be corrected to sandface.

This correction has to take into account the fact that the well was first produced through the casing, then after completion, through the tubing. The lift curves used to apply this correction correspond to the two different conditions. Extracting the production we get the loglog plot and the Blasingame plot. Both plots indicate that, after the initial water flow back that dominated for around 100 hours, the main regime during these first months was the linear flow orthogonal to the fractures.

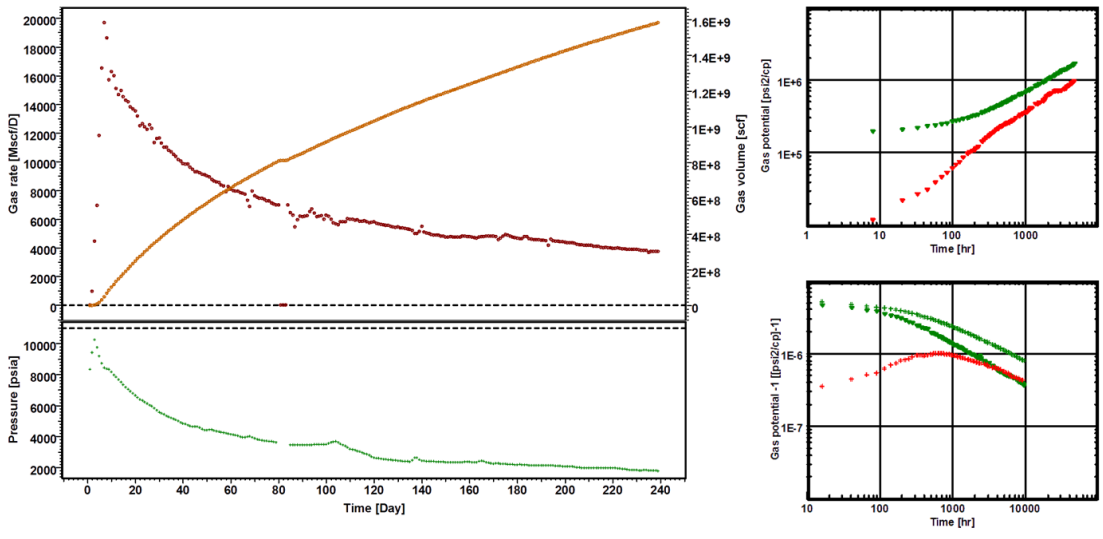


Fig. 10.G.1 – History, Loglog and Blasingame plots for 240 days of production.

10.G.2 Linear flow model

We started focusing on the linear flow. A square root plot would exhibit a linear behaviour during this period, allowing an early estimation of $k\cdot(N\cdot X_f)^2$, where N is the effective number of fractures, k is the matrix permeability and X_f the average fracture half-length.

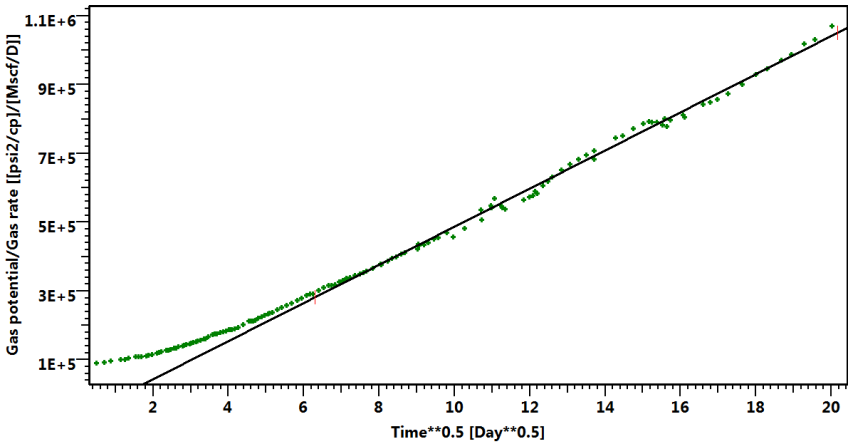


Fig. 10.G.2 – Square-root time plot.

In order to implement superposition and forecast in the model, we simulated this linear flow using the analytical model of a single infinite conductivity fracture in a homogeneous reservoir.

The indefinite linear flow from this model was ensured by setting the permeability to an arbitrarily low value. The fracture half-length was then adjusted to match the observed linear flow in the data. A nonlinear regression was then the resulting loglog match and history match are shown below. A production forecast was then calculated and is shown in the paragraph G.5.

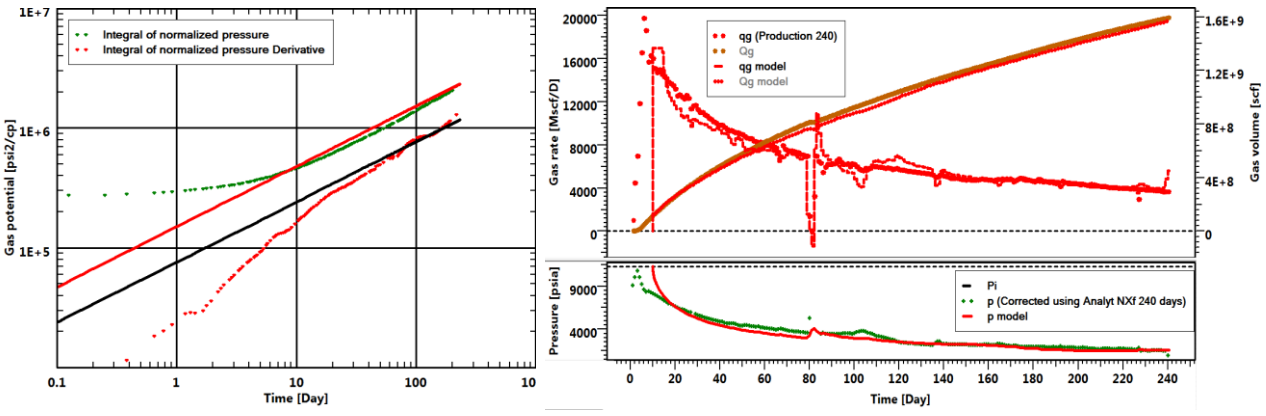


Fig. 10.G.3 – Match with a single fracture model on the Loglog and history plots.

10.G.3 Analytical Multi Fractures Horizontal Well (MFHW)

The analytical multi-fracture horizontal well model is described in the paragraph 1.B.3. This model has the advantage over the equivalent single fracture model of accounting for the real geometry of the system, and in particular the interference between the different fractures.

This time the permeability was set to a realistic value, as well as the number of fractures and the fracture half-length corresponding to the total length calculated above divided by the number of fractures. After nonlinear regression the loglog and history matches were calculated and shown below. Even though it was not clear on the data the model would tend to show that the interference between the fractures would start to occur after 8 months. A production forecast was then calculated and is shown in the paragraph G.5 below.

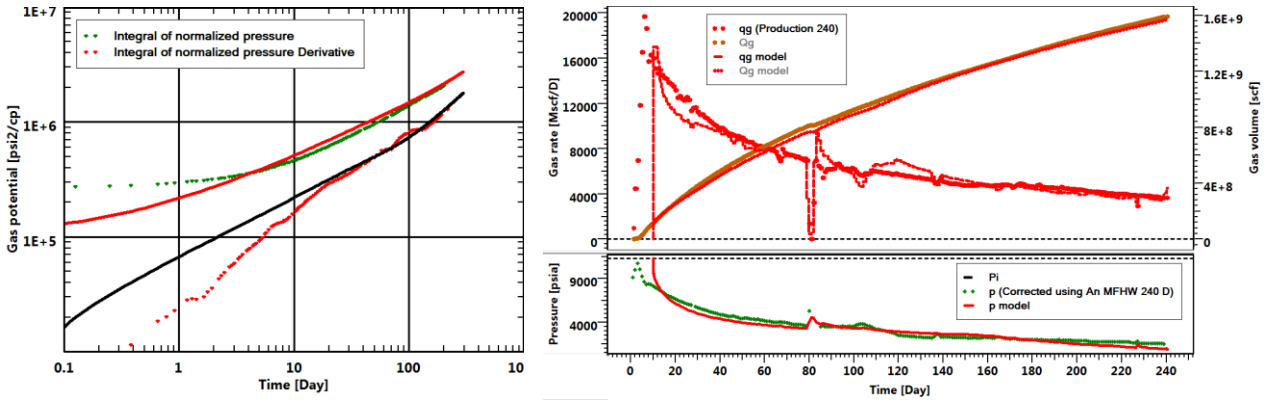


Fig. 10.G.4 – Analytical match on the Loglog and history plots.

10.G.4 Numerical MFHW

Again, and in a process similar to what was done with the analytical model, a numerical model was initiated and simulated. The figures below show the main grid, together with a zoom on the pressure profile around a few fractures after 1 month and 8 months. As we can see in the last representation, interference between the fractures started to be felt after 8 months.

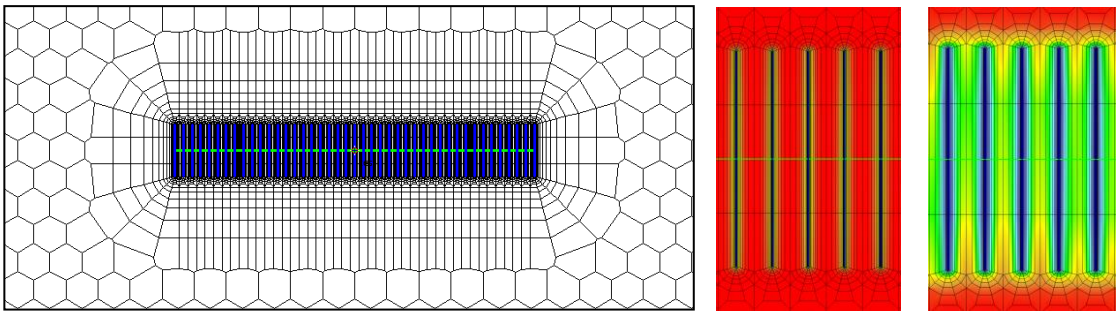


Fig. 10.G.5 – Numerical MFHW grid with a zoom on pressures after 1 month and 8 months.

The data was history matched and the resulting loglog and history plots are shown in the next page. This exercise was done with and without the integration of desorption in the model.

Note on material balance time and models: the apparent noise in the numerical model on the loglog plot comes from the material balance time function and not the model itself. In the previous section the analytical model was smooth because it was displayed as an equivalent constant pressure solution. This is not possible with numerical models. As for the other models a production forecast was then calculated, with and without the desorption effect (the paragraph G.5 below).

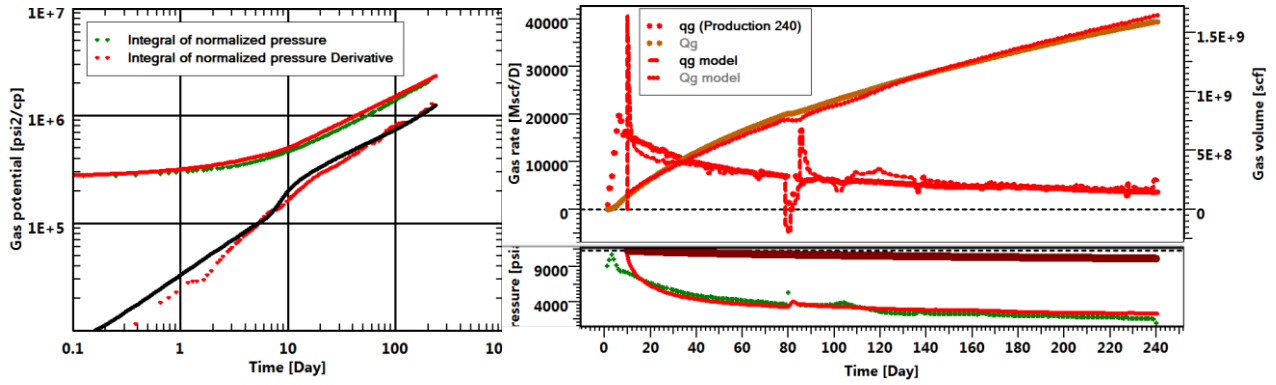


Fig. 10.G.6 – History match using the numerical model

10.G.5 Comparing production forecasts

The three models described above were all matching pretty well the production data, given that they were allowed to converge with different parameters. However, because the underlying assumptions are substantially different they are bound to provide very different long term production forecasts and EUR. In the plot below the linear model, the analytical model and the numerical model with and without desorption are compared with a 10-year forecast using a constant pressure taking the last flowing value.

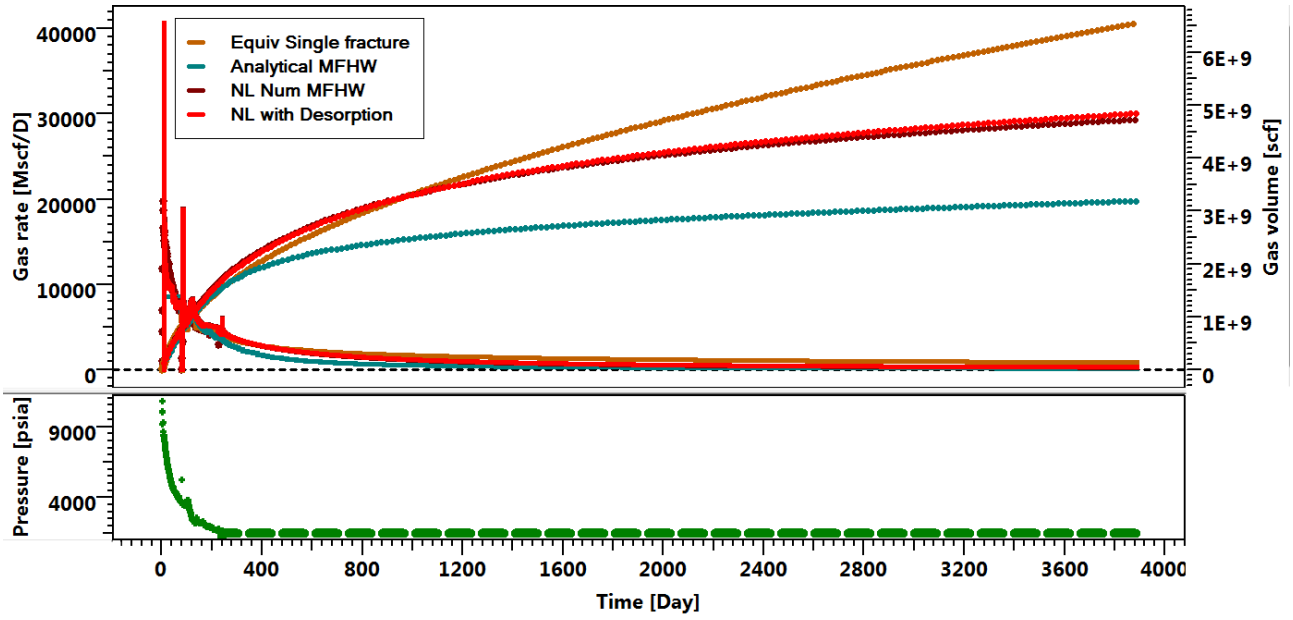


Fig. 10.G.7 – 10-year forecast – analytical and numerical (with and without desorption) models.

The equivalent single fracture model, with indefinite linear flow is definitely the most optimistic, as it does not take into account the inevitable interference between the fractures.

The analytical model is the most pessimistic. It takes into account the bad news that fractures will interfere, but it does not take into account the fact that compressibility of the fluid will improve when pressure is depleted. To be fair to this solution, at the time this study was done the pseudotime correction was not applied. With pseudotime correction the simulation would be much closer to the result of the numerical model.

The numerical model is a priori the most realistic. It takes into account all our hypotheses, if these hypotheses are correct. The numerical model with desorption is a little more optimistic as it adds the additional desorption observed after eight months. The numerical model without desorption matched the eight first months of data, hence the result of the initial desorption. So the difference between the two models is only marginal.

The loglog plot below shows the 10-year forecast of the numerical model, the pressure profile after 10 years of production is also shown.

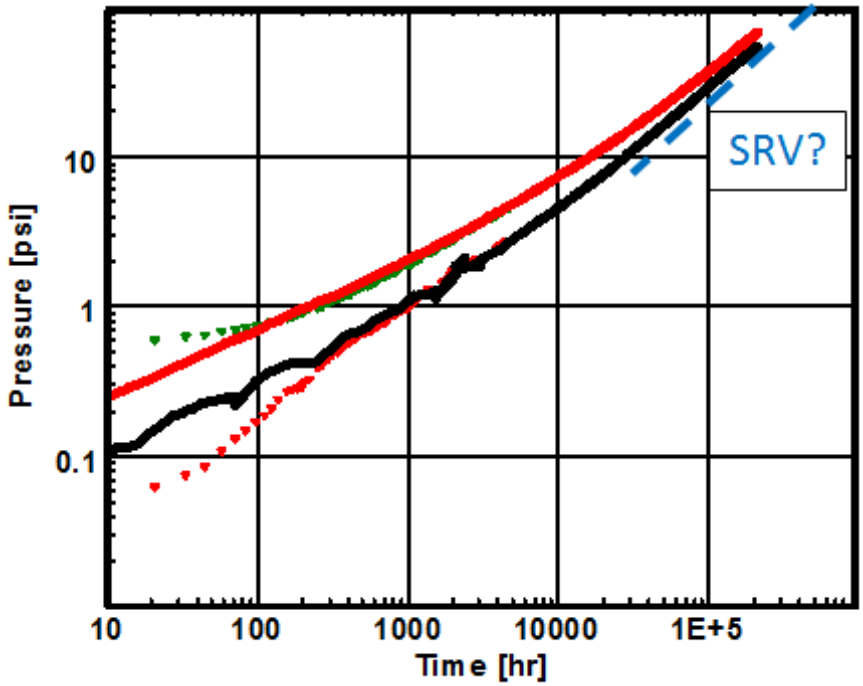


Fig. 10.G.8 – Long-term SRV flow.

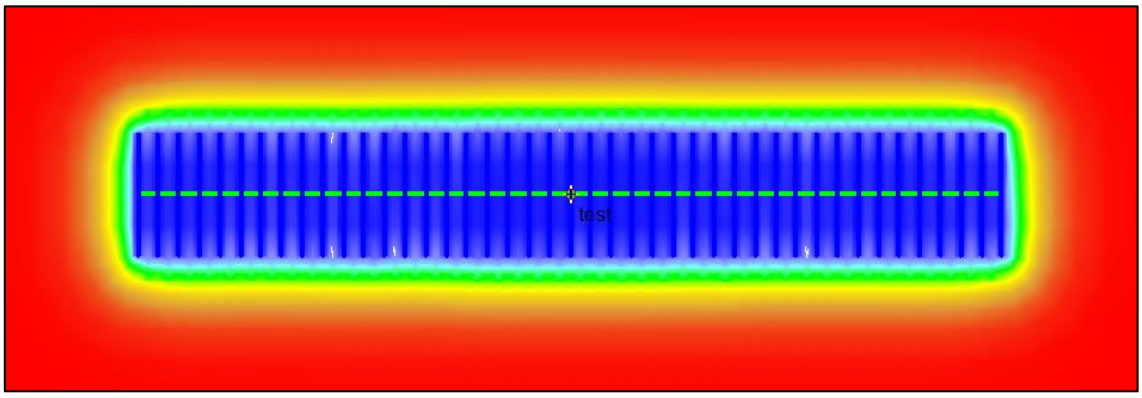


Fig. 10.G.9 – Pressure profile after 10 years of production.

10.G.6 Receiving ten more months of production data

One year after our initial interpretation shown in the five previous sections, we received 10 more months of data and it was the occasion to check how our initial forecast matched the observed behaviour.

The data was extracted again on a loglog plot and the three models re-generated with the same parameters. The main difference with the initial forecast of paragraph G.5 was that the real producing pressure was used instead of the constant pressure of the previous exercise.

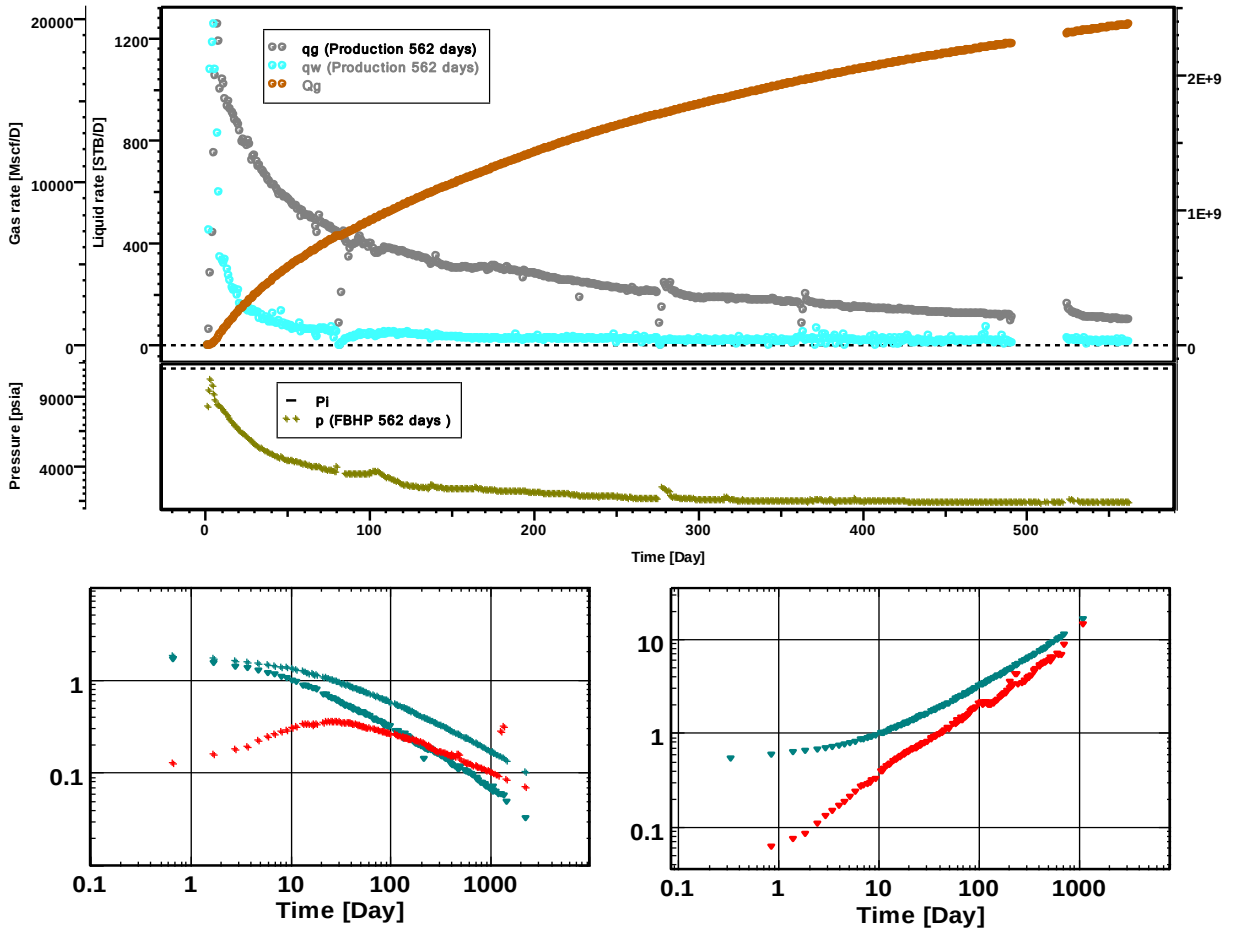


Fig. 10.G.10 – 10 more months of data on the history, Blasingame and Loglog plots.

The three loglog plots below show how the three models match the observed response:

- As expected the single fracture model stayed on its initial trend while the observed data deviates due to the interference between the fractures. The model, which corresponds to a 'b' factor remaining at 2, is naturally over-optimistic.
- As expected again the analytical model, without pseudotime correction, deviates towards SRV flow without taking into account the improvement of the permeability. It is therefore over-pessimistic;
- Finally and although the numerical model does not match the data exactly, it is pretty close.

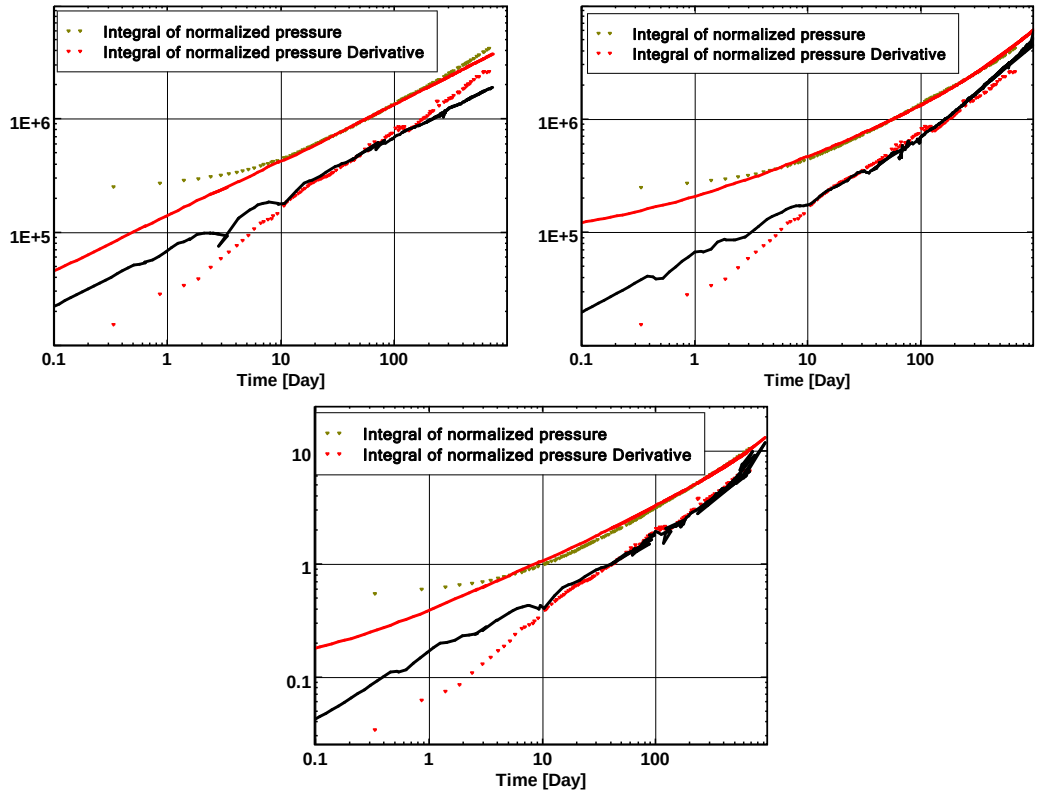


Fig. 10.G.11 – Loglog match with the linear, analytical, and numerical models.

A direct comparison is made on the history match plot, which shows how close the numerical model is to the observed behaviour.

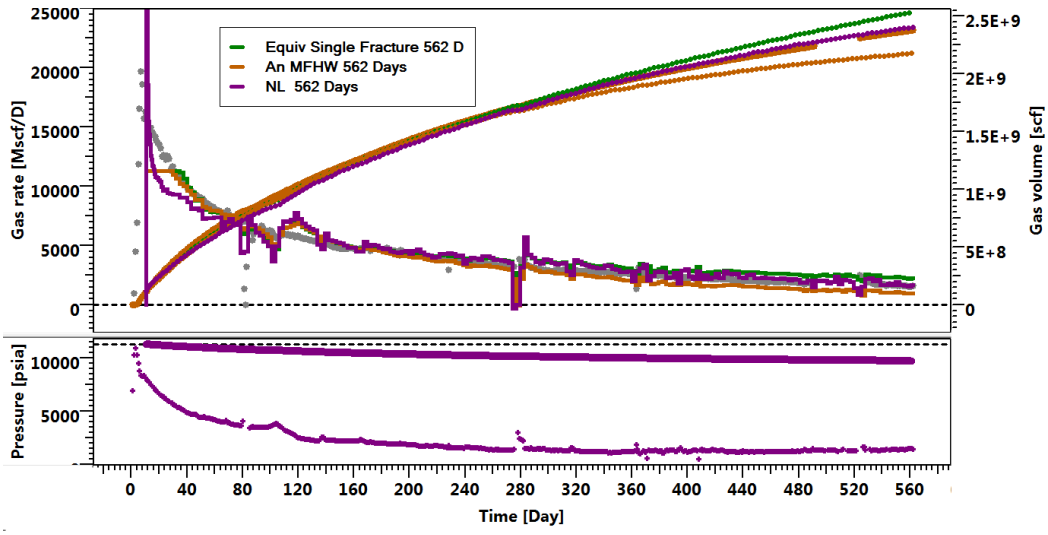


Fig. 10.G.12 – History plot with comparison of the 10-year forecasts.

10.G.7 Discussion

The example of this section was published in 2011. It is in no way a smoking gun proving that the numerical model used at this time is a long term solution to all our problems.

However, we can see from these examples that a relatively simple numerical model carrying the basic assumptions of diffusion and PVT can match pretty well, in some cases, the early years of responses of these wells.

Extrapolating this relatively satisfactory result to long term multiwell production would certainly be an excessive leap of faith. There are actually a lot of mitigating factors:

- Poor data: recorded pressures were at surface. It is a shame considering the cost of these wells, but this is the way the industry operates on these fields. In the absence of permanent downhole gauges, sandface pressures had to be calculated using a flow model. To add insult to injury the change of production mode from casing to tubing implied a change of model. Some truth may have gone in these cracks.
- Later operational issues: Data received on this same well, several years later, were not that brilliant. In the absence of PDG it was very difficult to exploit this data. The well head pressure data had to be corrected for depth, but the changing flowing conditions made the correction uncertain. The later forecast deviated from the initial numerical models, but data was so poor that it was nearly impossible to explain it either by the changing well conditons or by the uncertain BHP calculation.
- Other elements, such as well interference, well damage, the contribution of natural fractures, a geometric reality much more complex than these simplified models, clearly highlight the limitations of these simplistic models, even if they are already a challenge to properly model.

As a result it became clear that these simplified proxies, whether analytical or numerical, could not constitute a satisfactory answer to our long term needs. Several technical groups in the industry have been working on more sophisticated models. In the case of KAPPA the efforts were made in the framework of KURC, i.e. KAPPA Unconventional Resources Consortium.

10.H Advanced models

The simple models described in paragraph F assume that all hydraulic fractures share common features: same length, same conductivity, evenly spaced and orthogonal to the horizontal drain. This allows models, whether analytical or numerical, to be determined using a limited number of parameters: number of fractures, fracture half-length and conductivity. Given the poor level of data we have this is already enough to make the problem under-defined.

However, there are cases where one has other information, or sometimes the simple models just do not explain the observed behaviour. In such cases you may need to simulate more complex models, probably closer to reality, but with the risk of having insufficient data to nail the problem down.

Part of the work in the KAPPA Unconventional Resources Consortium was to develop such analytical and numerical models.

10.H.1 Complex geometries (analytical + numerical)

The first way to refine the models is to keep the same assumptions related to global homogeneous diffusion equations, but refine the geometry of the hydraulic fractures. We want here to substantially increase the range of possible geometries, analytically if we can, numerically if we must.

So the basic model, beyond the even more simplified SRV and bilinear models described in the paragraph F, assumes a homogeneous infinite reservoir with the simplest case of fractured horizontal well. All fractures have the same length, they are centered on the well drain, orthogonal to this drain and evenly spaced. In 2014 this model was available analytically and numerically in the standard KAPPA suite (Saphir, Topaze and Rubis).

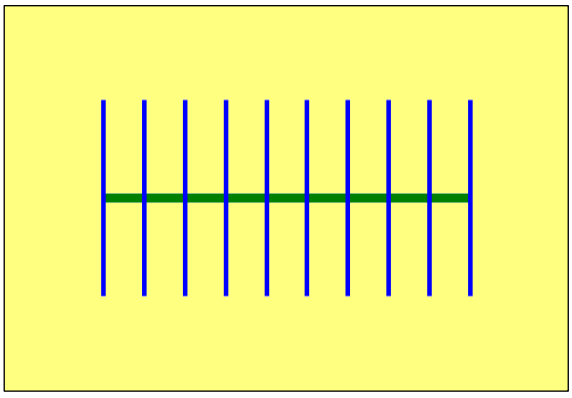
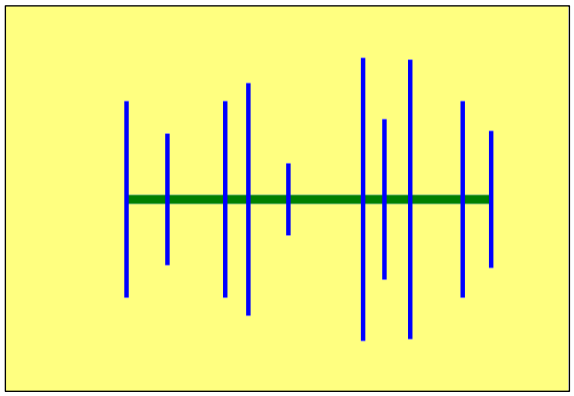


Fig. 10.H.1 – Standard model (analytical and numerical).

The first step towards a more complex geometry is to allow the fractures to have individual lengths and individual intersection with the well drain. They are still orthogonal to the well and their intersection is at the center of the fracture. This is shown in the next figure, right. In complement we can apply a global angle between the well and the set of fractures. This is shown in the next figure, left. Since 2014, and in the KAPPA Workstation since 2016, both analytically and numerically.



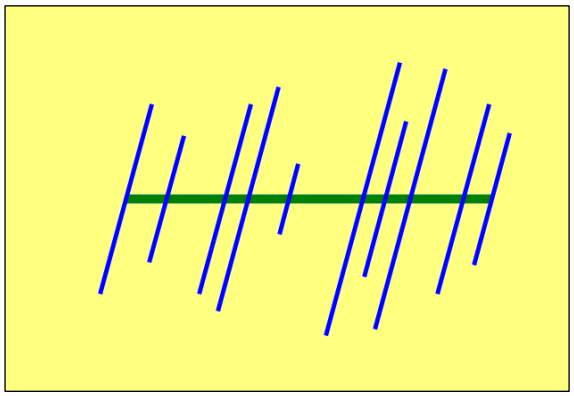
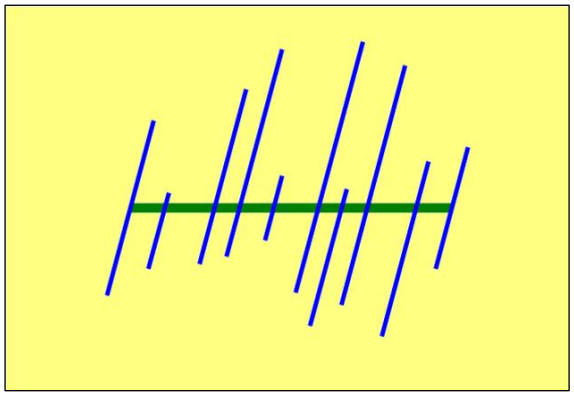


Fig. 10.H.2 – Left: Fractures (individual lengths) + uneven spacing along the well.
Fig. 10.H.3 – Right: Fractures + uniform fracture angles.
(analytical and numerical)

Apart from rigorously accounting for nonlinearities, numerical models allow us to simulate almost any type of geometry, as long as a suitable grid can be designed. For this reason numerical models can get one step closer to reality in terms of flexibility, allowing fractures to have their own angle and an intersection with the horizontal drain that is off-centered.



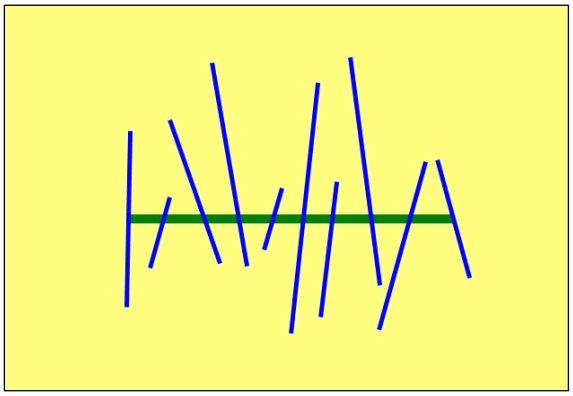
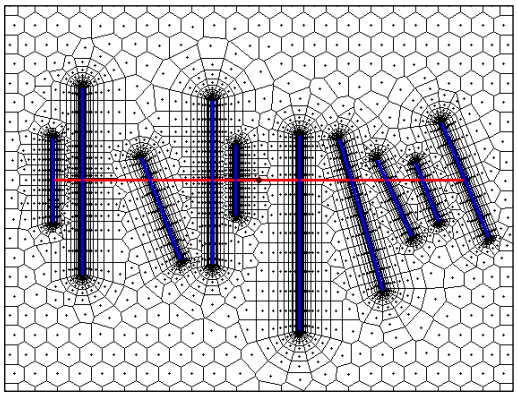


Fig. 10.H.4 – Left: Off-center fractures (individual lengths) + uneven spacing along the well.
Fig. 10.H.5 – Right: Off-center fractures + arbitrary fracture angles.
(numerical only)

Since we are working with unstructured grids, the problem consists of rigorously constraining the grid to the direction of the fractures, while ensuring we do not lose the continuous refinements specifically made to capture transients, and without creating too much distortion.

This is a complex yet manageable task, as long as we deal with (1) planar vertical fractures (2) that do not intersect and (3) a cased wellbore. These 3 restrictions being defined, our model is fully flexible: fractures can be non-uniformly distributed along the drain, have different half-lengths and be intercepted by the drain with any (individual) angle or offset.

Fractures can also be partially penetrating, with individual penetration. In this case, a 3D grid is built around each fracture to ensure that we properly simulate the radial flow from the matrix toward the fracture plane. The drain can intercept the fractures at any depth.



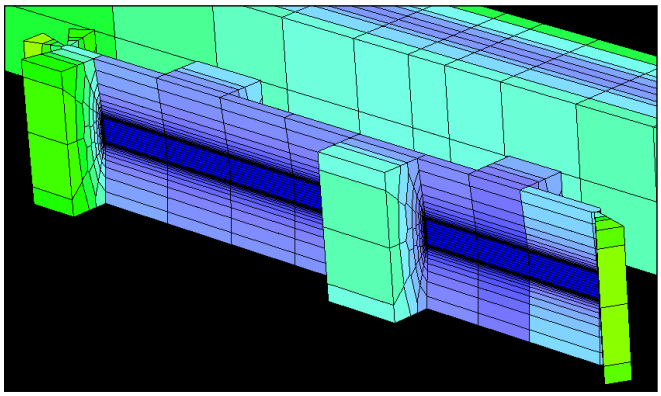


Fig. 10.H.6 – Left: previous complexity, representation of the grid pattern.
Fig. 10.H.7 – Right: 3D refinement for partially penetrating fractures (both numerical only).

The conductivity, the width and/or the porosity can be redefined for each fracture. Relative permeability curves and pressure-dependent properties (k/k_0 and ϕ/ϕ_0) can be different for the fractures and the matrix, but they are identical for all the fractures.

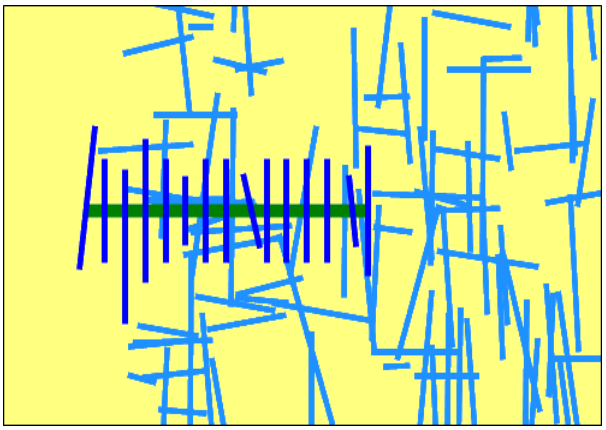
10.H.2 DFN models (numerical + analytical)

The next level of complexity is to challenge the assumption that we can model the reservoir response using a more or less complex diffusion equation that would be applied in a homogeneous way. The Discrete Fracture Network (DFN) model considers a network of pre-existing natural fractures that may have been stimulated, or even simply produced after the stimulation jobs. DFN can be combined with the complex hydraulic fracture geometries of the previous sections. Given the complexity of the problem and the probable stochastic nature of its definition, the numerical model is the natural way to go, though we will see at the end of this section that a first analytical pass can be run to narrow the problem.

10.H.2.a Numerical DFN

When various objects (e.g. hydraulic or natural fractures, boundaries…) intersect each other, the problem of constraining the Voronoi grid becomes fairly complex.

This is precisely the case when one wants to simulate the effect of the natural network of fractures by connecting the multiple fractures horizontal well model to a DFN.



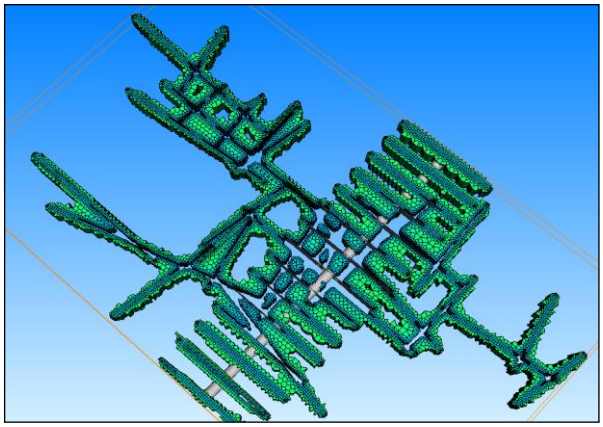


Fig. 10.H.8 – 2D (left) and 3D (right) representation of a numerical DFN.

A specific algorithm was developed for this situation, with the assumption that:

- All the fractures (hydraulic and natural) are made of individual, vertical planes.
- All the fractures (hydraulic and natural) fully penetrate the pay thickness.
- The wellbore is cased, i.e. it only connects hydraulic fractures (not the matrix).

With these assumptions, we can limit ourselves to a 2D or a 2.5D background Voronoi grid, which is iteratively refined in the vicinity of the fractures, so that transients in the matrix are properly captured. The grid portions in contact with the fractures are rigorously constrained to the geometry of the network, so that we do not create nor lose any intersection.

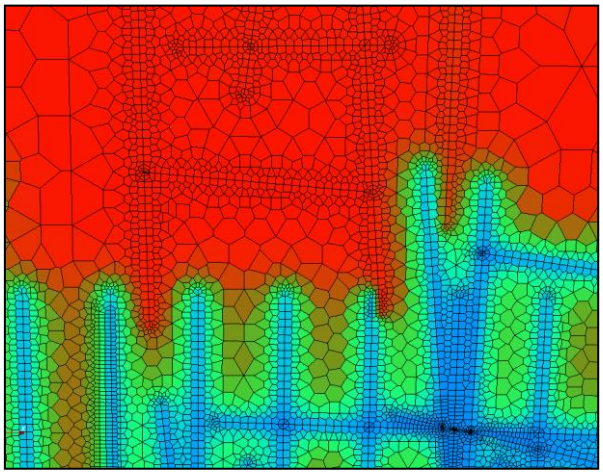


Fig. 10.H.9 – Pressure fields in a numerical DFN.

The various fracture segments can take any direction or length. This means the numerical model can handle the two regular patterns offered by the analytical option, but also simulate more complex, stochastically generated networks.

The conductivity, the width and/or the porosity can be redefined for each natural or hydraulic fracture. Also, three groups of relative permeability curves and pressure-dependent properties (k/k_0 and ϕ/ϕ_0) can be defined for the:

- matrix.
- hydraulic fractures.
- natural fractures.

Although in theory, an individual redefinition of these curves at the level of each fracture could be handled by the simulator.

For networks of finite conductivity, the transmissibilities at fracture intersections are derived using a specific algorithm which ensures that fluxes within the network are properly derived, even when multiple segments intersect at the same location.

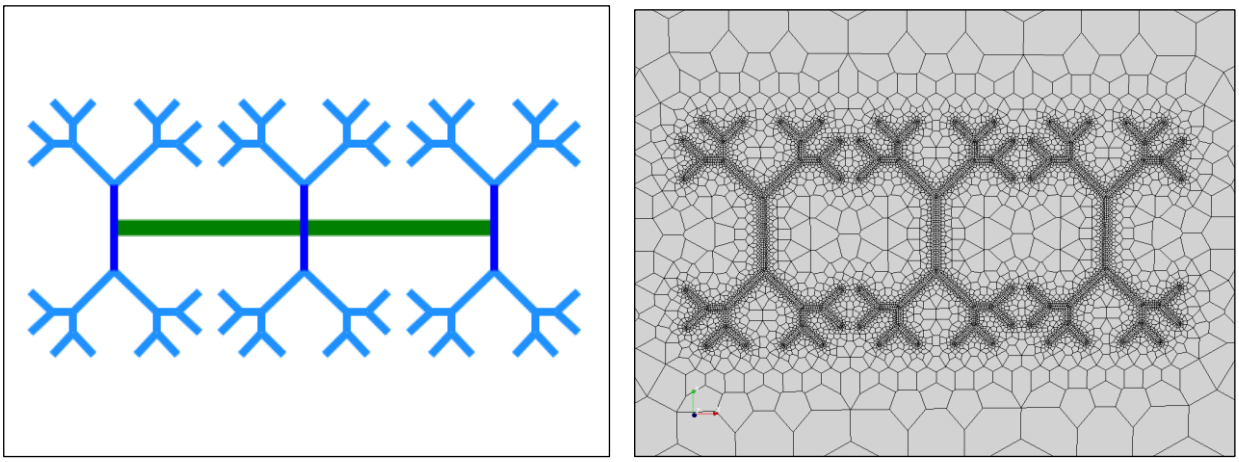


Fig. 10.H.10 – Fractal type variations of a numerical DFN.

10.H.2.b Stochastic DFN

Considering the natural origin of this fracture network it is totally logical to think about the description, then the generation of the DFN according to a random algorithm but in the same time constrained by certain aspects and information.

The principle is set a total number of expected natural fractures, then to define several families of natural fractures and to specify for each one the following characteristics:

- Fraction: percentage of each family in the final DFN
- Minimum, maximum fissure lengths
- Power: controls the fracture lengths distribution (power law)
- Strike angle: "average" fracture angle
- K strike: K parameter for the Fisher law angle distribution (dimensionless number)

The position of the region where we want to generate this DFN in the map can be set with respect to the well(s).

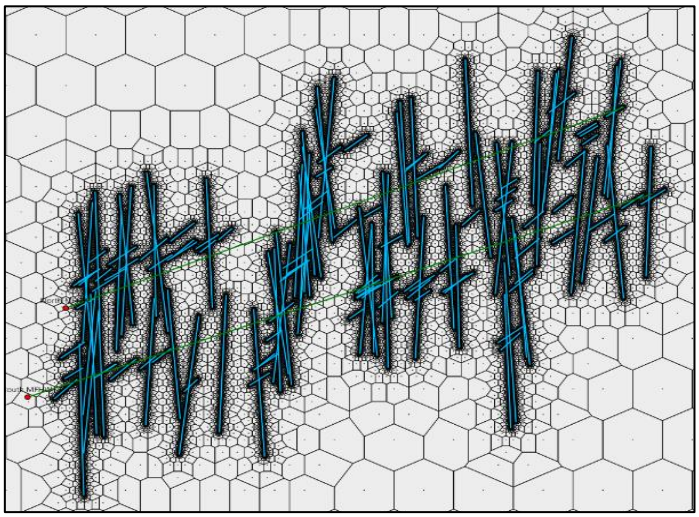


Fig. 10.H.11 – Stochastic distribution of DFN with two families crossed by two wells

The fractures can be connected or not to the well and to possible artificial fractures:

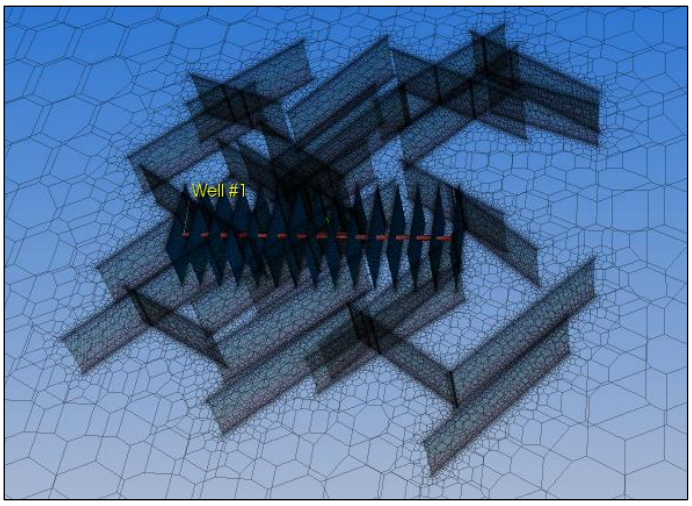


Fig. 10.H.12 – Stochastic DFN connected to a multiple fractured horizontal well

If microseismic events are available they can be used as a constraint on the DFN generation:

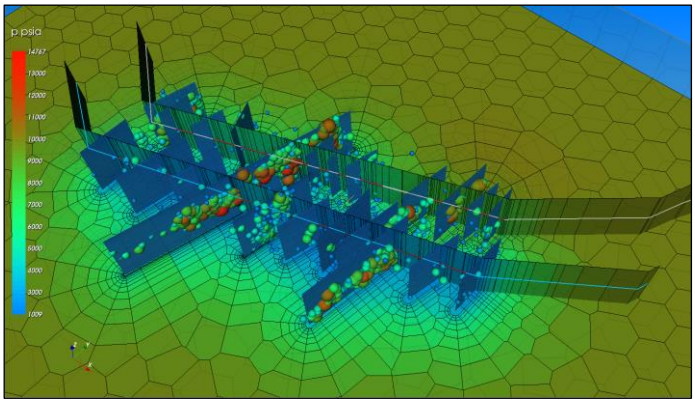


Fig. 10.H.13 – DFN constrained by seismic events

When the fracture network is crossed by two horizontal wells and that an interference test has been performed, the stochastic DFN generator can be connected to an optimization algorithm (called Fast Marching Method) in order to select the stochastic DFN realizations compatible with the observed interference time.

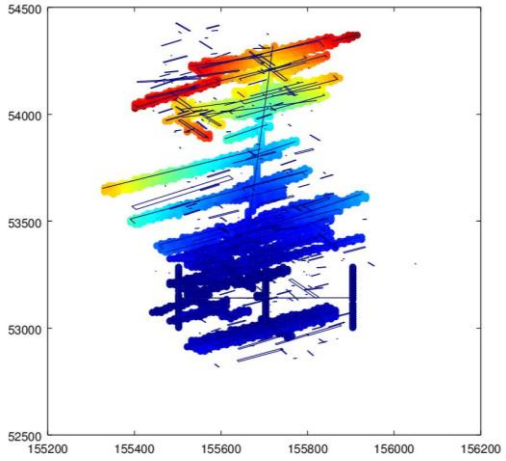


Fig. 10.H.14 – DFN selected by the FMM from the interference test information

10.H.2.c Analytical DFN

Analytical models are certainly insufficient to model a DFN, but they may be used to arrive at a first estimate of the parameters (density, orientation, etc) that may be used as a seed to simulate the numerical DFN. In order to achieve this one may use a model such as the conjugate fractures. This model complements the hydraulic fractures with a set of evenly spaced natural fractures orthogonal to them, hence parallel to the horizontal drain. These fractures may be totally connected (left) or of insufficient length to directly connect the hydraulic fractures (right).

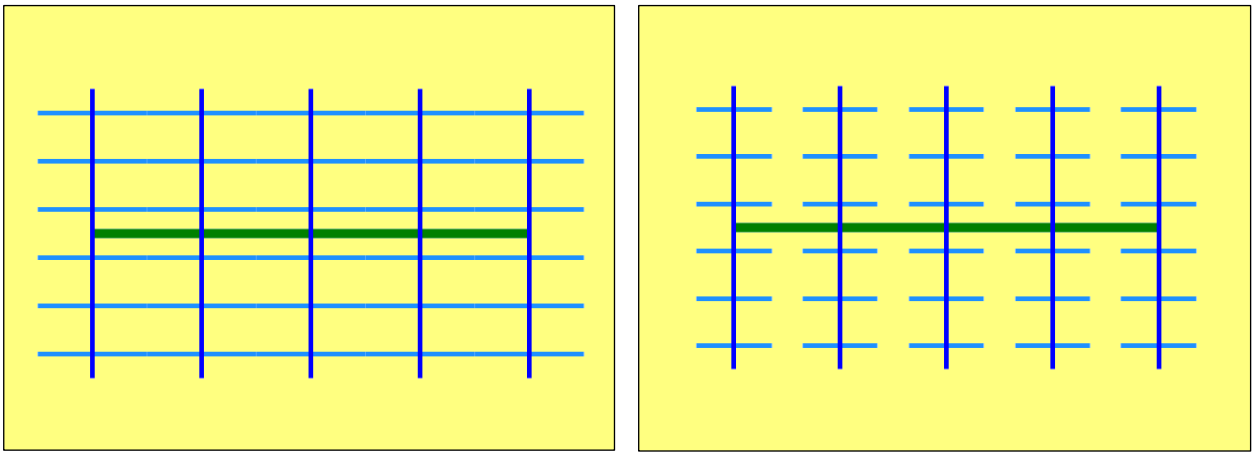


Fig. 10.H.15 – Analytical approximations of a DFN.

10.H.3 Modeling water flowback (numerical)

Fracturing jobs involve the injection of massive volumes of water, combined with proppant and chemicals. When the well is put on production large quantities of water are produced during the clean-up phase. If the associated rates and pressures have been recorded, this may provide valuable information for reservoir characterization.

Furthermore, since very often only a fraction of the injected water flows back during production, one may want to evaluate the various scenarios to explain the volume difference and figure out how the missing water may impact the gas flow.

The first issue for the simulation of water flowback is in starting with a perturbed initial state, in order to account for the presence of injected fluids in the reservoir. We chose to use the material balance approach described in a previous section, i.e to initiate the numerical model for flowback with a non-uniform initial water saturation field. The initial pressure field is uniform at P_i.

As indicated in 10.B.4 two methods are available, the Static and the Dynamic methods.

10.H.3.a Static initialization

When the "Static method" is used for initialization, the volume of the flooded zone is derived so that the total amount of water added to the system (i.e. in excess to S_{wi}) is equal to the volume of water pumped during fracturing operations.

Fractures and matrix can be associated to different relative permeability curves, hence they can be initialized with different values of water saturation in the flooded areas (S_{wmax}).

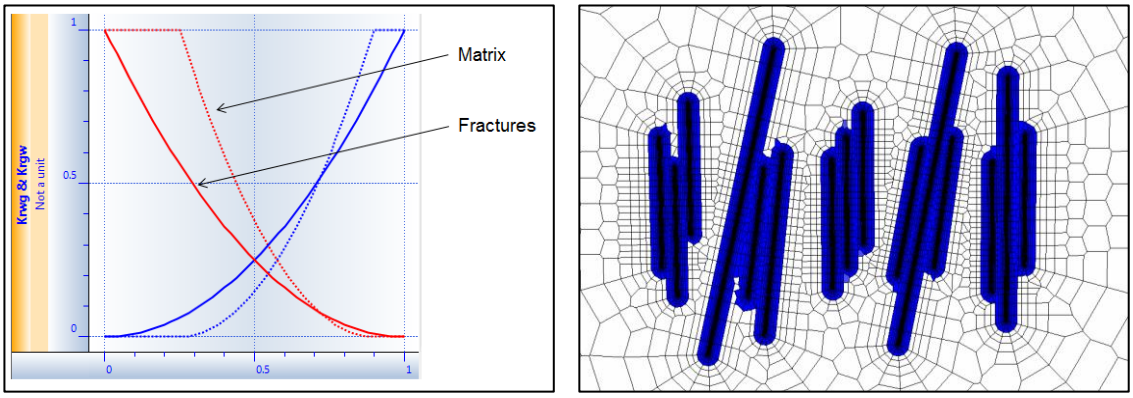


Fig. 10.H.16 – Relative permeability curves and simplified initial water saturation state.

Three different zones are defined:

- The background system, with cells initialized at S_{wi}
- Hydraulic fractures, where cells are assigned S_{wmax}^{HF}.
- A flooded zone in the matrix, where cells are assigned S_{wmax}^{matrix}.

This purely static approach allows us to represent the delay in gas production due to early-time dewatering of the system:

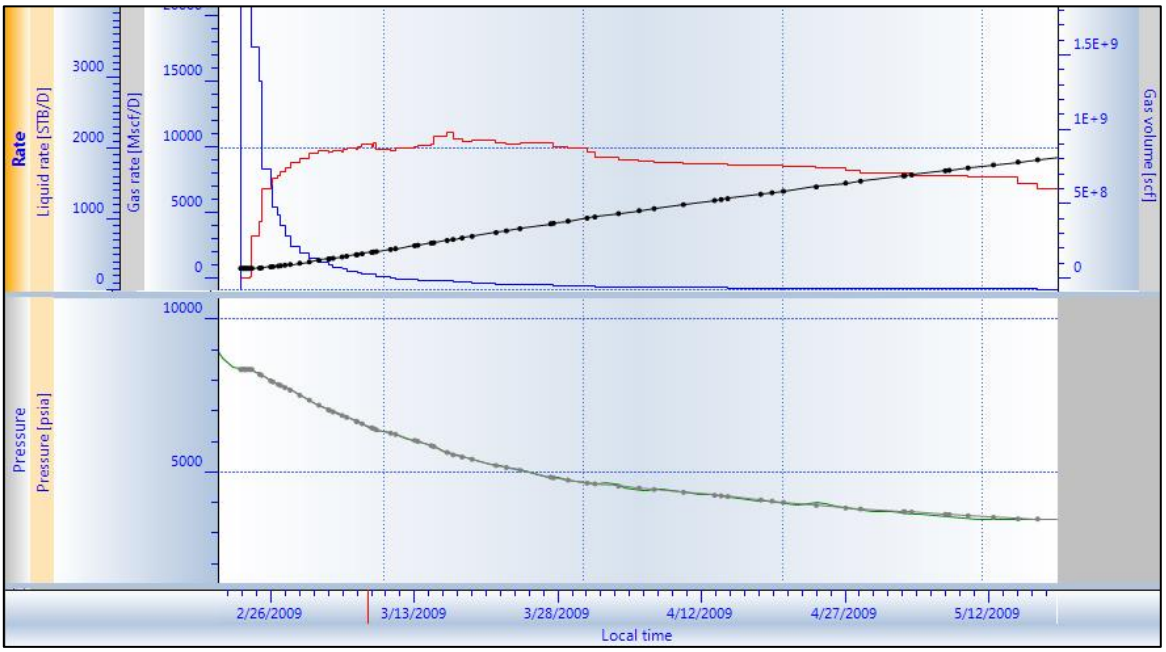


Fig. 10.H.17 – Example of simulated water and gas production.

This approach also captures some of the water trapping in the matrix. In a given cell, the volume of water added to represent the initial 'flood' is:

$$V_{wi}^{added} = V_i . \emptyset_i . (S_w^{max} - S_{wi})$$

As a consequence, if the original initial water saturation is lower than the residual water saturation, $S_{wi} < S_{wr}$, some water will be capillary trapped in this cell after some production time. The volume of trapped 'injection water' in the cell will be:

$$V_{wi}^{trapped} = V_i . \emptyset_i . (S_{wr} - S_{wi})$$

This allows us to take into account capillary trapping and representing lost volumes without strictly modeling injection and KrPc hysteresis. Gravity trapping within the fractures can be simulated with vertical subdivisions of the simulation grid.

For the DFN model, the procedure is almost the same:

- A fast run (steady state) is conducted to identify the parts of the DFN that are effectively connected to the hydraulic fractures
- The total system is initialized at S_{wi}
- Water is added inside the hydraulic fractures (S_{wmax}^{HF})
- Water is added inside the connected part of the DFN (S_{wmax}^{DFN})
- The remaining water is added in the matrix (S_{wmax}^{matrix}), so that the total volume flooded honors the total amount of injected water

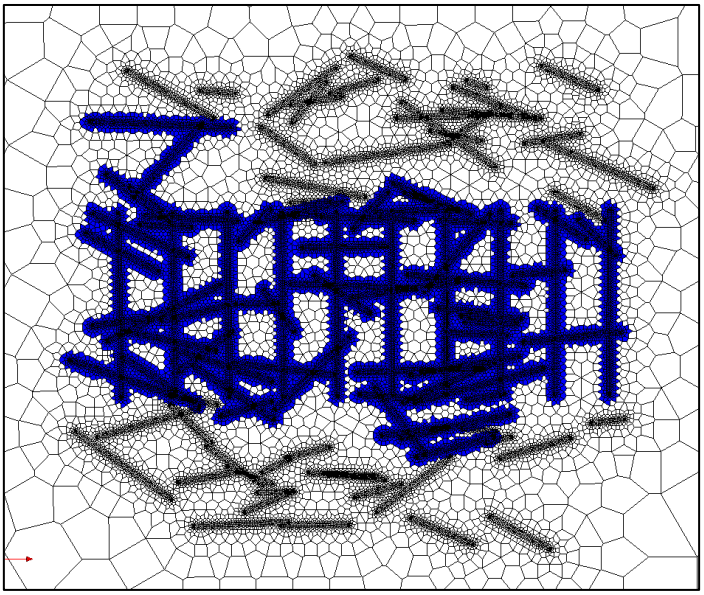


Fig. 10.H.18 – Initial water saturation profile in a DFN.

10.H.3.b Dynamic initialization

As presented in the paragraph 10.B.4, in the "Dynamic method" initialization, we simulate the injection in the hydraulic/natural fractured system.

The resulting water distribution is more rigorous because it corresponds to the ability of the various fractures and matrix to store water. It results also a non-uniform pressure field which corresponds to a realistic consequence of an injection.

It requires a rather complex simulation and the exact injection history.

Even though this approach does not model the opening of the fractures nor the stress reorientations, using the k and phi pressure dependent option, the volume of water stored in the fractures can be simulated.

The saturation distribution and the pressure map are realistic and synchronized:

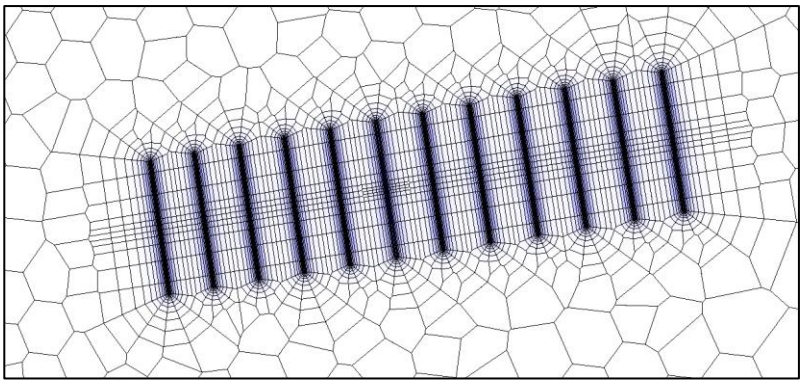


Fig. 10.H.19 – Initial water saturation after dynamic initialization

The static and the dynamic methods give rather different results. In particular, since the shape of the water bank is not very realistic with the static method (too much water at the tip of the fractures because of the assumed stadium shape), the static method predicts less gas being produced – since a lot of water remains trapped at the tip of the fractures and slightly impairs production.

NB - Spontaneous imbibition, osmosis phenomena, etc. that may participate in the trapping of injected water are still considered as research areas and are not covered in this chapter.

10.H.4 Refrac jobs modeling

Additional fracturing jobs can be performed after the well was put on production, either to create new fractures or to increase the existing fracture performances.

This option is only available for fractured horizontal wells and finite conductivity fractures. It is restricted to a delayed opening of fractures, limiting the input to a single time of opening.

The refract possibility is compatible with special reservoir conditions like:

- Specific unconsolidation laws (k(p), ϕ(p)) in the fractures.
- Specific relative permeability laws in the fractures.
- Stimulated zones around fractures option.

The principle is to act on the transmissibility of the fractures and on the well index, starting with a zero value at start, then setting them to the adequate value at the "refract time" in order to activate the selected fractures.

10.H.4.a Features for simple fracture system

When the fractures properties are globally defined, two global parameters are required:

- The re-fracturation time which corresponds to the time when the fracture system will be modified.
- The re-fracturation ratio R_f, expressed as a positive number equal or greater than 1, is the ratio between the initial and the final number of fractures.

The number of fractures N_f represents the well geometry after refrac, implying that the simulation will start with INT(N_f / R_f), evenly distributed along the well.

In all cases, the user interface does not distinct between the fractures opened at simulation start and the refrac ones.

When INT(N_f/R_f) is equal to 1, we consider that the whole well is an infill well and is entirely fractured at the refrac time.

For instance, in the case of a refracturation ratio set at 2 with an initial number of fracture of 4, it leads to a final total number of 10.

In this case, the initial grid includes 10 fractures but only 4 will be active, 6 more will be activated at the fracturation time, set here to 3000 hours for a total simulation duration of 6000 hours.

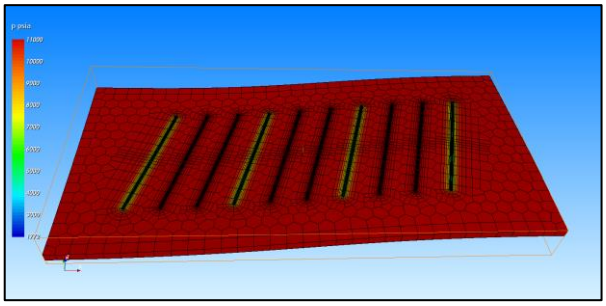


Fig. 10.H.20 - Pressure map before re-frac job

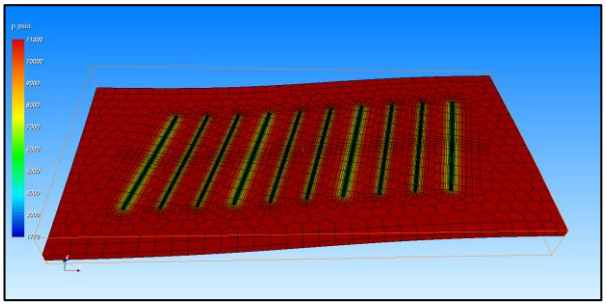


Fig. 10.H.21 - Pressure map after re-frac job

The effect of the refract can be easily observed on the pressure and rate history plot:

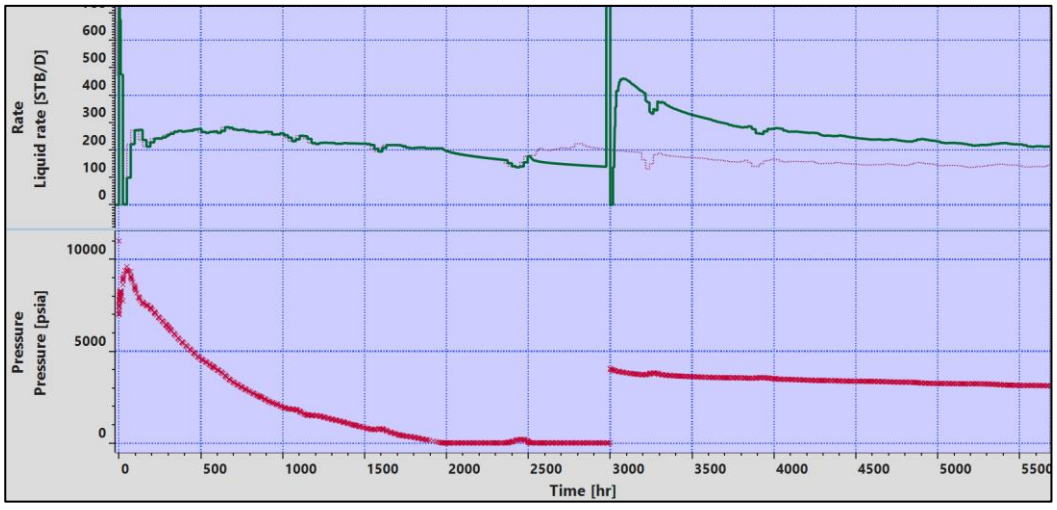


Fig. 10.H.22 - Pressure and rate history with two refrac jobs

10.H.4.b Features for complex fracture system

When the well fractures modelling type is complex and when the "Individual properties" can be input, the individual properties, the "fracture opening time", can be specified for each fracture.

In this case, the initial grid includes all the fractures and they are activated according to the "opening time" attributed to each one.

For instance in the following case the fracture no 6 opens after 3000 hours and the fracture no 8 after 5000 hours:

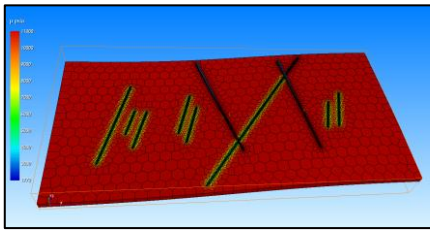


Fig. 10.H.23 - Pressure map before re-frac job

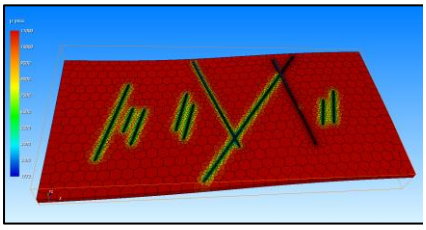


Fig. 10.H.24 - Pressure map after 3000 hr, refrac of "fracture 6"

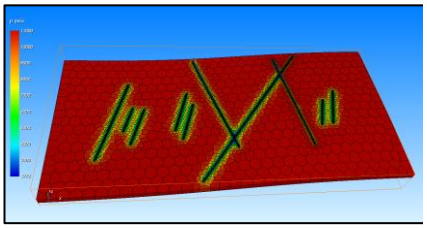


Fig. 10.H.25 - Pressure map after 5000 hr, refrac of "fracture 8"

The effect of the multiple refrac jobs can be observed on the pressure and rate history:

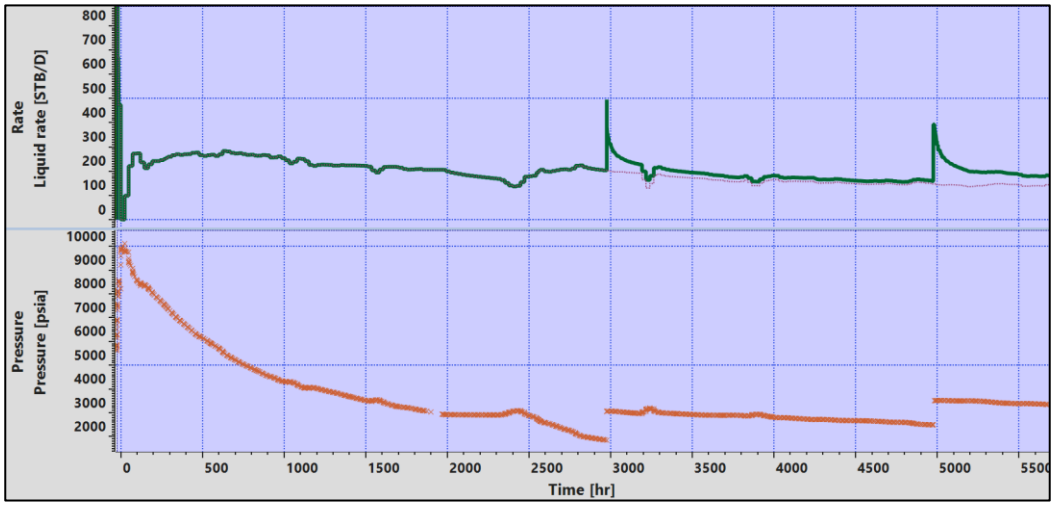


Fig. 10.H.26 - Pressure and rate history with two refrac jobs

10.H.5 Multi-Zone Fractional Dimension

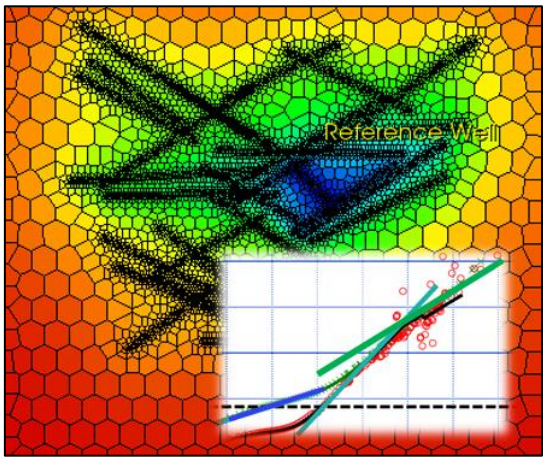


Fig. 10.H.5.27 - Multi-Zone Fractional model schematic

This approach presents a way to analytically model transient behavior of a complex fracture network.

The method presented by Acuña (2016) allows interpreting pressure and flow rate behaviors observed in unconventional wells that do not exhibit linear flow regime. The method suggests a way to diagnose multiple flow regimes (sub-linear, linear, sub-radial) on the standard loglog plot.

A multi-fractured horizontal well in a fractured formation can be compared to a fractured well (with the fracture length equal to the sum to all initially connected high conductivity fractures) that drains a reservoir with a flowing area A, that is perpendicular to the flow and changes with distance according to the power law:

$$A = X_f h r_D^{2\delta-1}$$

Where:

X_f is the half flow area width,

$r_D = \frac{r}{r^*}$

r is the distance and r^* is taken as the half fracture length.

δ is the half flow dimension

Note that in the case of $\delta = 0.5$ the flow regime is linear and the flowing area becomes constant with respect to the distance to the fracture area, i.e. the case reduces to the channel geometry. Also the case of $\delta = 1$ is a classical radial flow, and $\delta = 0$ corresponds to the PSS.

This generalised model is versatile as it includes the cases with:

- The flow area A decreasing with the distance from the fracture (sub-linear flow, values of $0 < \delta < 0.5$, Fig. 1),
  and
- The flow area A increasing with the distance from the fracture (sub-radial flow, values of $0.5 < \delta < 1$, Fig. 2).

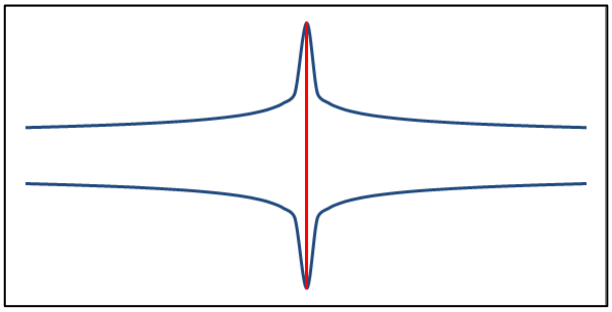


Fig. 10.H.5.28 - Sub-linear flow with $\delta = 0.375$

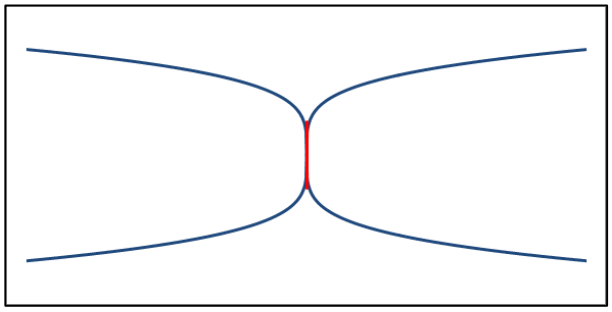


Fig. 10.H.5.29 - Sub-radial flow with $\delta = 0.75$

The dimensionless pressure is shown to have the following form:

$$p_D = \frac{(4t_D)^{1-\delta}}{2\Gamma(\delta)(1-\delta)}$$

And its log pressure derivative can be written as follows:

$$t_D \frac{dp_D}{dt_D} = \frac{(4t_D)^{1-\delta}}{2\Gamma(\delta)}$$

Hence during this flow regime the pressure and the derivative are functions of the time raised to the power $(1-\delta)$, which can be reliably diagnosed on a loglog plot by two parallel straight lines with a slope $(1-\delta)$, which provides directly the fractional dimension value δ and gives an insight into the nature of the fractures network geometry.

The production of a Discrete Fracture Network system with its complex geometry can lead to a sequence of different flow regimes, depending on the drained and investigated area.

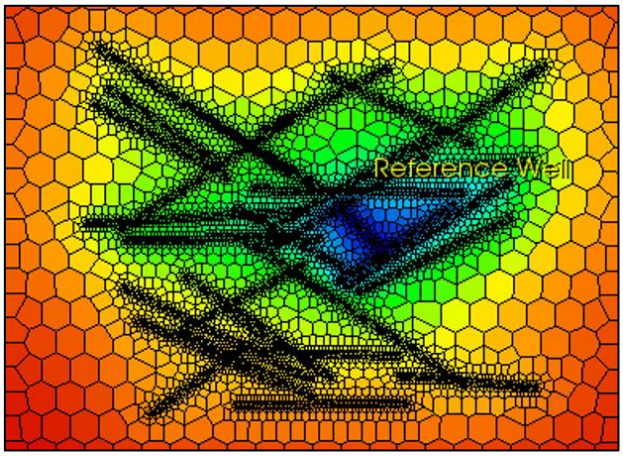


Fig. 10.H.5.30 - Investigation areas

The sub-linear case might represent a MFHW in a densly fractured reservoir, when the areas drained by earch fracture reduce with distance because of fractures interference. On the other hand, the sub-radial case might correspond to a network of fractures of both high and low conductivity, the latter having drainage area that increases with distance in a more pronounced way.

Also the presence of fractures of different conductivity and their geometrical closeness can result in a system that exhibits a sequence of linear, sub-linear, radial, sub-radial flow regimes. This is illustrated below in terms of reservoir model geometry and corresponding δ versus distance from the fractured area.

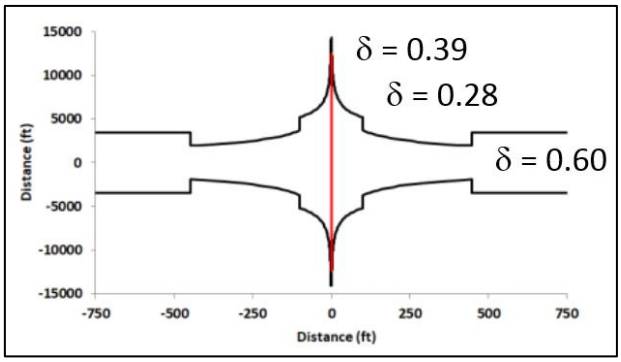


Fig. 10.H.5.31 - Model flow area geometry

This type of geometry gives a sequence of straight lines on the loglog plot.

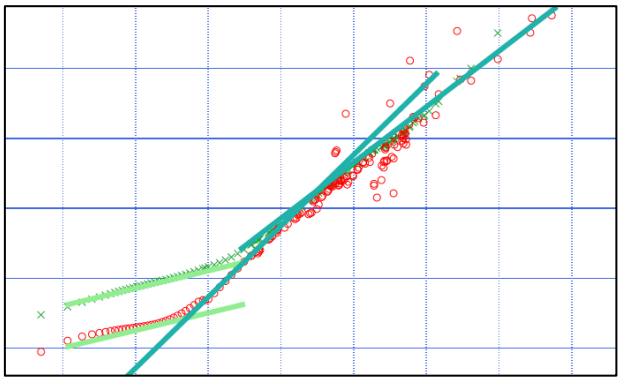


Fig. 10.H.5.32 - Pressure and derivative loglog plot

The multi-zone fractional dimensional model concept presents an extension of the described model to n zones characterized by their individual δ parameters and sizes. The outer boundary of the last zone can be defined as infinite, no-flow or constant pressure.

References

Analytical Pressure and Rate Transient Models for Analysis of Complex Fracture Networks in Tight Reservoirs. Jorge A. Acuña*, SPE, Chevron U.S.A. Inc. URTeC: 2429710, 2016.

Pressure and Rate Transient Analysis in Fracture Networks in Tight Reservoirs Using Characteristic Flow Volume. Jorge A. Acuña*, SPE, Chevron U.S.A. Inc. URTeC: 2667753, 2017.

Alternative Production Mechanisms in Unconventional Reservoirs. Jorge A. Acuña*, Shugang Wang and David Forand, SPE, Chevron U.S.A. Inc. URTeC: 2896802, 2018.

Straightforward Representative Fluid Flow Models for Complex Fracture Networks in Unconventional Reservoirs. Jorge A. Acuña. SPE, Chevron U.S.A. Inc. URTeC: 2876208, 2018.

10.H.6 Anomalous Diffusion in a Tri-linear model

10.H.6.a Description and assumptions

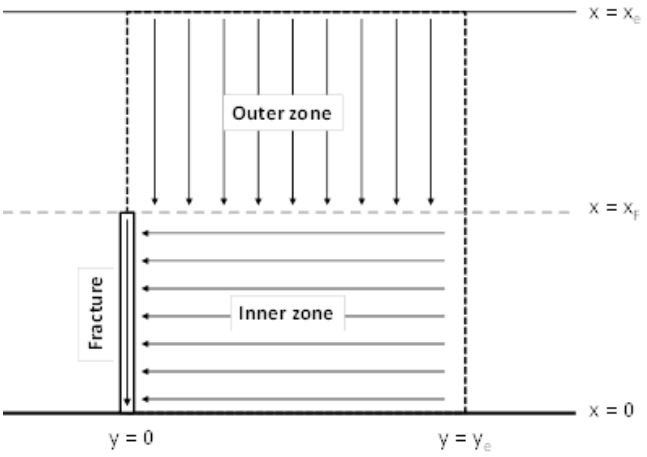


Fig. 10.H.6.33 - Tri-linear model basic component

This model considers transient flow under a possible anomalous diffusion (also called Space-Time Fractional Diffusion) toward a horizontal well that produces a reservoir through multiple fractures. The objective of this modelling approach is to address the effects of the magnitude of heterogeneities in both the fissure and matrix systems by considering non Gaussian distributions governing rock properties. This model, is a simplified composite 3-zone linear model that is normally called a trilinear model.

As mentioned in the chapter "Theory" paragraph 2.A.3, the "normal" diffusion equation for a linear flow is:

$$\lambda \frac{\partial^2 p(x,t)}{\partial x^2} = \phi c_t \frac{\partial\ p(x,t)}{\partial t}$$

We consider a diffusion as "Anomalous" when the relationship between the time and the displacement is governed by:

$$\frac{\partial}{\partial x}\left[\lambda_{\alpha,\beta} \frac{\partial^\beta p(x,t)}{\partial x^\beta}\right] = \phi c_t \frac{\partial^\alpha p(x,t)}{\partial t^\alpha}$$

Where the diffusion exponents α and β are ≤ 1.

With $\alpha = \beta = 1$ we get normal diffusion corresponding to Darcy's Law with ordinary permeability

Note that if the super-diffusion exponent $\beta = 1$and the sub-diffusion exponent $\alpha < 1$, then, we have a case with pure sub-diffusion.

Among the anomalous diffusions, the sub-diffusion is an appropriate model for situations that reflect internal structure with numerous scales and existence of cracks, cervices & obstacles.

In the model used in this chapter, the reservoir can be either homogeneous or double porosity.

In case of Dual Porosity the sub-diffusion exponent are considered in both the fissures (α_f) and the matrix (α_m). Note that for classical diffusion, $\alpha_f = 1$ and $\alpha_m = 1$.

When double porosity is considered, the flow from matrix to fissures can be either pseudo steady state or transient. For transient double porosity consideration, the configuration of matrix elements can be slab, sphere or cylinders. The reservoir can be infinite or a rectangular reservoir.

The hydraulic fractures can be either infinite conductivity, uniform flux or considering incompressible or compressible fluid in fractures.

The hydraulic fracture properties are assumed to be identical.

Note: in the reference papers, dealing more with sub-diffusion, the exponent β is considered equal to 1.

10.H.6.b Model features and parameters

The inner and the outer zone model can be either:

- homogeneous
- double porosity pseudo steady state
- double porosity transient, slabs matrix
- double porosity transient, sphere matrix
- double porosity transient, cylinder matrix

The fracture model can be: Uniform Flux, Infinite Conductivity, Finite Conductivity, Incompressible or Finite Conductivity Compressible.

The relative zone properties are defined by the composite ratio parameters:

The mobility ratio

$$M = \left(k/\mu\right)_{outer} / \left(k/\mu\right)_{inner}$$

and the diffusivity ratio

$$D = \left(k/\Phi\mu c_t\right)_{outer} / \left(k/\Phi\mu c_t\right)_{inner}$$

10.H.6.c General Anomalous Diffusion Behaviour

In a first step it is convenient to describe briefly and simply the physical meaning and consequences of the two diffusion exponents α and β.

Globally, the sub-diffusion exponent $\alpha < 1$ will induce a lower equivalent diffusivity, and the super-diffusion exponent $\beta < 1$ will induce a higher equivalent mobility.

This can be illustrated by using a simple version of the model, where the well model in a 8000ft horizontal drain with 40 fractures of 200ft half-length and where the two regions of the reservoir are initially defined as identically homogeneous, with the sub-diffusion exponent α and a super-diffusion exponent β are equal to 1 to simulated a normal diffusion.

It results a sequence of two linear flows corresponding to the flow from reservoir to the fractures, then from the reservoir to the SRV:

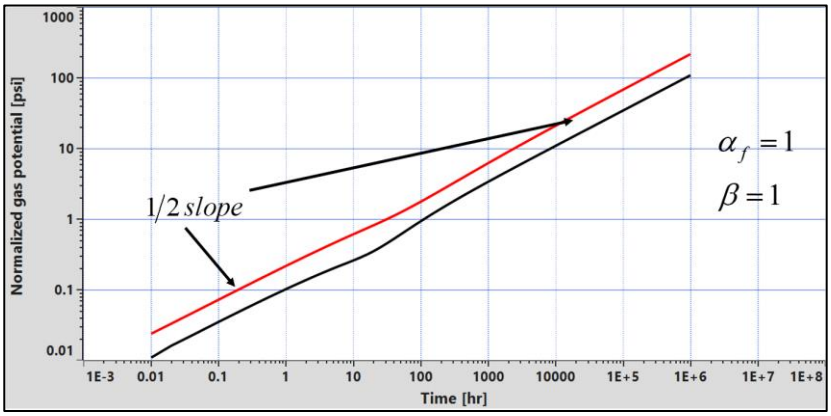


Fig. 10.H.6.34 - Reference case: 2 equal homogeneous regions, Infinite outer zone

Now, let's consider the influence of the exponents α and β in the inner zone:

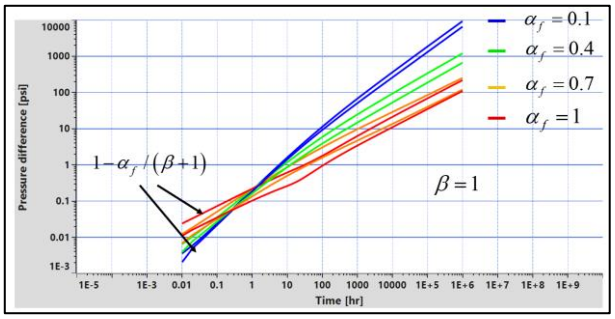


Fig. 10.H.6.35 - Influence of the inner zone α (constant $\beta = 1$)

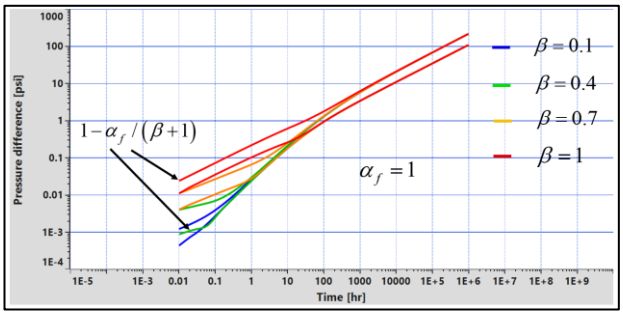


Fig. 10.H.6.36 - Influence of the inner zone β (constant $\alpha = 1$)

An inner α smaller than 1 leads to as lower diffusion in the inner zone, it decreases the fractures efficiency thus increases the early time behavior slope, as a "pseudo skin" it increases the pressure drop at late time.

An inner β smaller than 1 leads to as higher mobility in the inner zone, it imposes a very early time slope smaller than ½, it has not impact on the late time behavior.

The influences of the exponents α and β in the outer zone are even more characterized:

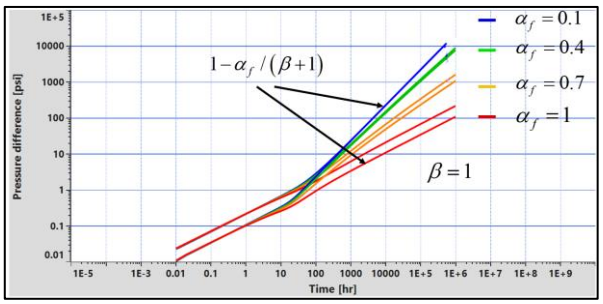


Fig. 10.H.6.37 - Influence of the outer zone α (constant $\beta = 1$)

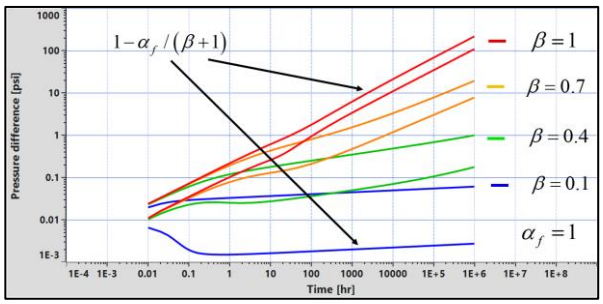


Fig. 10.H.6.38 - Influence of the outer zone β (constant $\alpha = 1$)

An outer α smaller than 1 leads to as lower diffusion in the outer zone, a small α value can lead the model to show a slope close to the unit, close to Pseudo Steady State created by a very low diffusion surrounding area.

An outer β smaller than 1 leads to as higher mobility in the outer zone, a small β value reduces drastically the slope value.

Conjugated influences of the exponents α and β: the α effect on the behavior can vary according to the β value, it can almost hide the α influence.

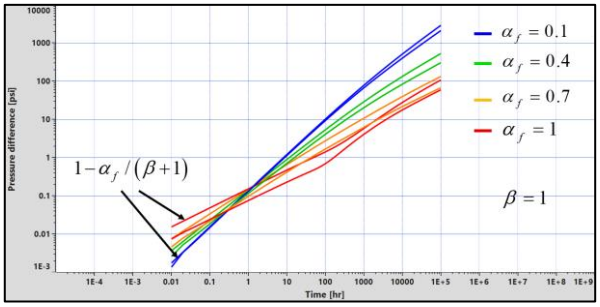


Fig. *10.H.6.39 - Influence of the inner zone α (with β =1)*

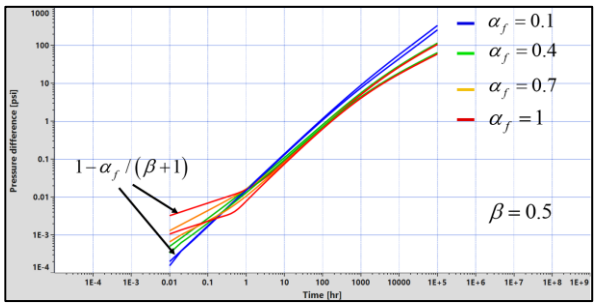


Fig. 10.H.6.40 - Influence of the inner zone α (with β =0.5)

The two figures below show that the effect of the inner α on the late time is extremely reduced by a value of β=0.5, all other parameters remaining equal.

In a similar way, the outer exponents α and β interact one on each other:

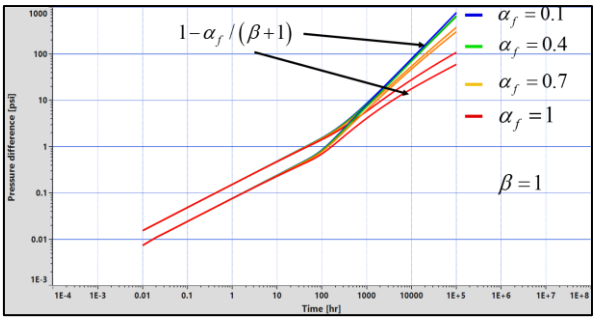


Fig. 10.H.6.41 - Influence of the outer zone α (with β =1)

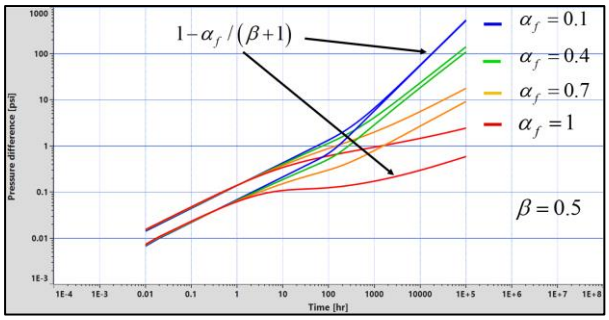


Fig. 10.H.6.42 - Influence of the outer zone α (with β =0.5)

The two following figures show that while a small value of the outer α (0.1) makes the model to tend to a P.S.S. effect, a value of β=0.5 will leave the (α=0.1) effect identical but will modify the behavior for α values close to 1, widening consequently the α effect.

When the system is considered as closed, it will be mainly the outer zone β and α diffusion exponents that will affect the pressure behavior.

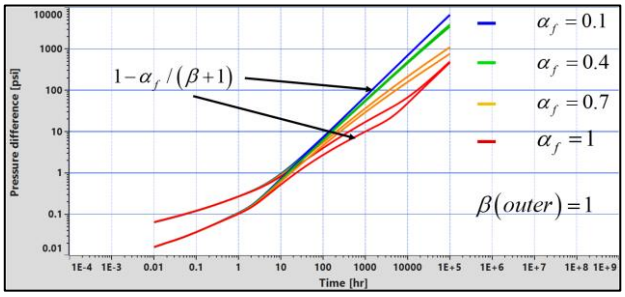


Fig. 10.H.6.43 - Closed outer zone, influence of α (with β =1)

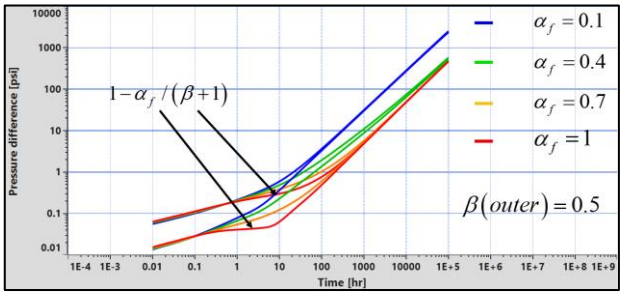


Fig. 10.H.6.44 - Closed outer zone, influence of α (with β =0.5)

The above figures show that the P.S.S. final unit slope is always observed, but smaller values of α make the diffusivity smaller, therefore a latter P.S.S.. But values of β smaller than one increase the equivalent mobility and make the α effect to appear earlier.

10.H.6.d The anomalous diffusion applied to a heterogeneous reservoir

Composite reservoirs parameter impact

The effects of the two composite ratios:

The mobility ratio

$$M = (k/\mu)_{outer} / (k/\mu)_{inner}$$

and the diffusivity ratio

$$D = (k/\Phi\mu c_t)_{outer} / (k/\Phi\mu c_t)_{inner}$$

Are classical and well known, as shown in the two following figures:

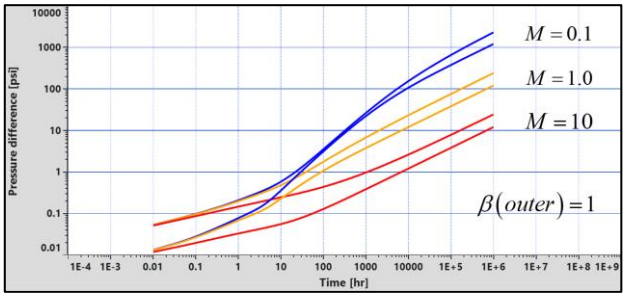


Fig. 10.H.6.45 - Infinite outer zone, influence of mobility ratio with β =1

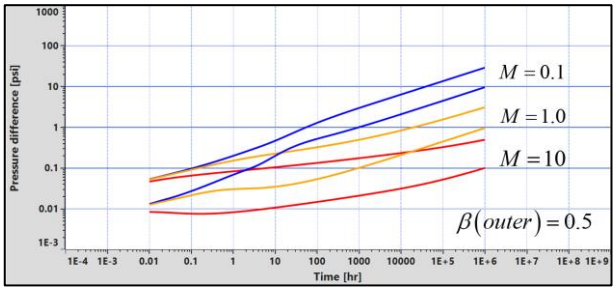


Fig. 10.H.6.46 - Infinite outer zone, influence of mobility ratio with β =0.5

The smaller the M, the smaller will be the external mobility therefore the higher will be final pressure response, but a β value smaller that one, will compensate this effect by increasing the outer resulting mobility.

In case of closed outer region, in addition to the observed final P.S.S. unit slope, the same M effect is observed:

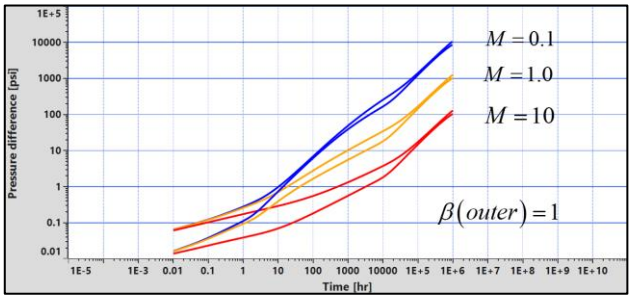


Fig. 10.H.6.47 - Closed outer zone, influence of mobility ratio with β =1

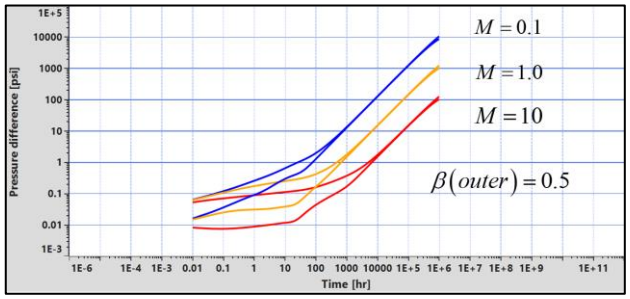


Fig. 10.H.6.48 - Closed outer zone, influence of mobility ratio with β =0.5

Once more a β value smaller than 1 makes the external conditions to be observed earlier because of the increase equivalent mobility.

The diffusivity ratio D has a similar effect: for a constant M value, the smaller the D value, the larger is the storativity product Φc_t , then the latter the depletion effect:

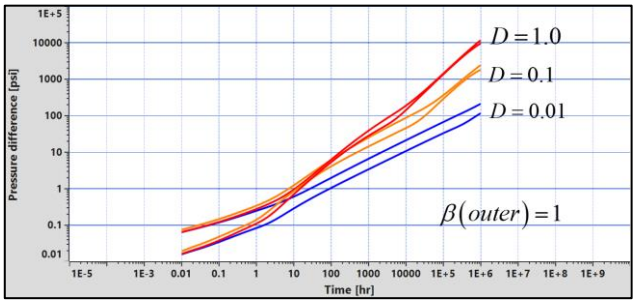


Fig. 10.H.6.49 - Closed outer zone, influence of diffusivity ratio with β =1

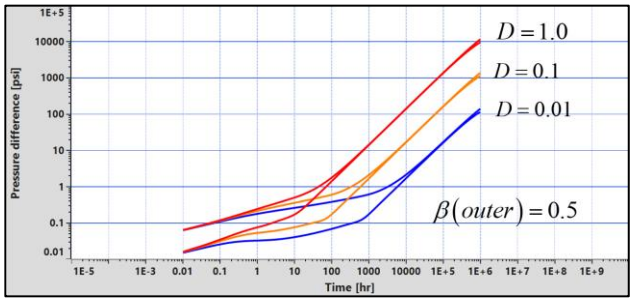


Fig. 10.H.6.50 - Closed outer zone, influence of diffusivity ratio with β =0.5

In the same time, a β value smaller than 1 makes the P.S.S. to be observed earlier because of the increase equivalent mobility.

The Sub-diffusion in a composite heterogeneous reservoir.

In the following, we are going to consider only the case of sub-diffusion setting the β exponent equal to one and the α exponent in both fracture system (α_f) and matrix system (α_m).

Even if the homogeneous reservoir or the pseudo steady state double porosity options are available, the transient double porosity option probably is the best model option to describe the unconventional plays.

For the transient-flow double porosity model, five types flow regimes could be considered:

Flow Regime	Fissure System	Matrix System
FR 1	Infinite-acting	No influence
FR 2	Infinite-acting	Infinite-acting
FR 3	Infinite-acting	Pseudosteady
FR 4	Pseudosteady	Infinite-acting
FR 5	*Pseudosteady*	*Pseudosteady*

Fig. 10.H.6.51 - Table 1 Flow regimes summary

In the current case, we have to go beyond the regimes noted above because of the need to consider fractured wells; many sub-flow-regimes may exist depending on fracture conductivity, $k_F w_F$, and length, x_F, (single or multiple fractures) and fracture spacing (multiple fractures).

Flow Regimes of the model

There are two major paths can happen depending on existence of flow regime 3.

Path A is from FR 1 → FR 2 → FR 4 → FR 5

Path B is FR1 → FR 3 → FR 5.

Note that flow regime 3 is the condition of the Warren and Root model. In reality, the path in unconventional most probably is Path A without FR 5, i.e. FR 1 → FR 2 → FR 4.

As the general behaviour of the subdiffusive consideration is the power-law behavior, the well responses in many cases may be represented by the expressions of the form

$$\frac{\Delta p(t)}{q} = At^a, \qquad (1)$$

for production at a constant rate or by

$$\frac{\Delta p}{q(t)} = At^a \qquad (2)$$

for production at a constant pressure.

The exponent a for many typical situations is noted in Table 2.

	Exponent
FR1, Linear Flow	$(2-\alpha_f)/2$
FR 1, Bilinear Flow	$(2-\alpha_f)/4$
FR 2, Linear Flow	$(4-2\alpha_f-\alpha_m)/4$
FR 2, Bilinear Flow	$(4-2\alpha_f-\alpha_m)/8$
FR 4	$(2-\alpha_m)/2$
FR 5, Constant Rate	1
FR 5, Const.Pressure	$1/(1+\alpha_f)$

Fig. 10.H.6.52 - *Table 2: Exponents of the flow regimes*

Flow Regime 3 is not listed in Table 1 as responses do not follow the form suggested in Eq. 1.

During flow regime 3, $\Delta p(t) \sim \frac{1}{2}\frac{1}{\Gamma(2-\alpha_f)} t^{(1-\alpha_f)} * \ln t^{\frac{(\alpha_f-\alpha_m)}{2}}$.

It is worth to note that the exponential decline only happens during pseudo steady state when the well is produced under constant rate production. It is power-law behavior during pseudo steady state when the well is produced under constant pressure production. It is also reasonable to expect that the late time performance would be flow regime 4 and the heterogeneity in the matrix system dominates the behavior as the exponent of flow regime 4 is $(2-\alpha_m)/2$.

The production rate, q, during hyperbolic decline, according to the Arps (1945) model is given by

$$\frac{q(t)}{q_i} = \frac{1}{(1+bD_it)^{1/b}}, \quad (3)$$

where q_i is the rate at any point in time following the onset of the decline period, D_i is the corresponding loss ratio, and b $(0 \le b \le 1)$ is the exponent of the decline curve. During Flow Regime 4, the expression for b is $2/(2-\alpha_m)$. Again, this implies that the matrix heterogeneity dominates the late time performance.

It is also important to note that the permeability in the model input is the apparent fissure permeability instead of the intrinsic fissure permeability.

It is convenient to apply the CPG (Chow Pressure Group) to check the slopes for power-law behaviors. Let Δp_c be the CPG, Δp be pressure difference, $\Delta p'$ be the logarithmic derivative of Δp , and a be the exponent of the straight line, the CPG is defined as

$$\Delta p_c = \frac{\Delta p}{2\Delta p'} = \frac{1}{2a}. \quad (4)$$

On the log-log plots in Saphir and Topaze, users can right click on the plot to choose the Chow Pressure Group to check the exponent on the plots directly. In the following two plots, the CPG curves are also displayed.

Global pressure behaviour and parameters influence

The double porosity parameters, λ interporosity flow coefficient and ω storativity ratio can be specified for both inner and outer regions.

The inner interporosity flow coefficient has only and influence on the early time and acts on the time of the transition that can be observed on the derivative

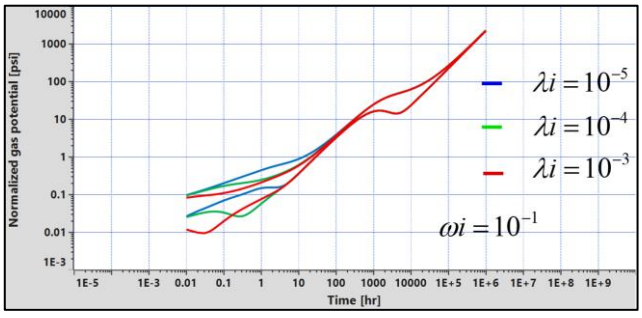


Fig. 10.H.6.53 - Closed outer zone, influence of interporosity flow coefficient with $\omega = 0.1$

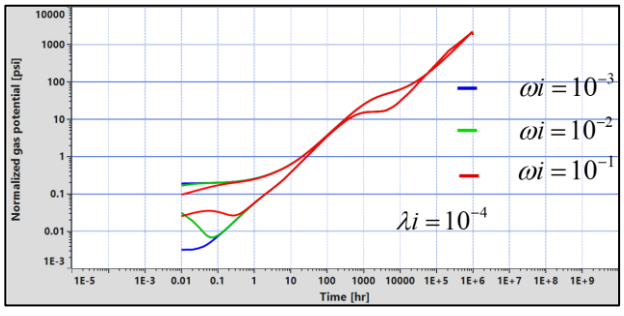


Fig. 10.H.6.54 - Closed outer zone, storativity ratio with $\lambda = 0.0001$

The smaller is λ, the latter is the transition and the smaller is ω the deeper the transition but this effect affects only the early time in the inner region.
Because it is acting in total system behaviour, the inner condition does not influence the outer region behaviour.

Conversely, the dual porosity outer parameters values affect only the late behaviour of the outer region.

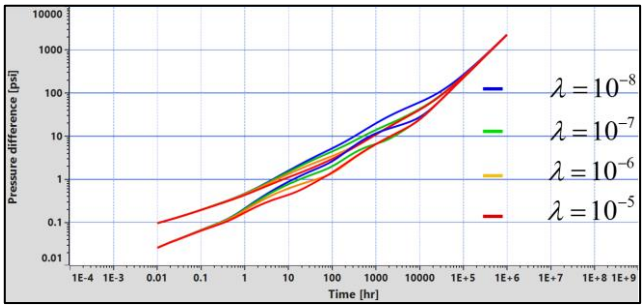


Fig. 10.H.6.55 - Closed outer zone, influence of interporosity flow coefficient with $\omega = 0.1$

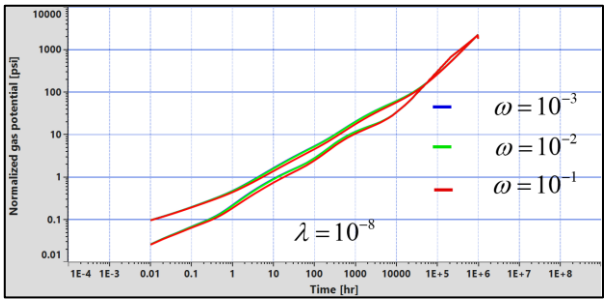


Fig. 10.H.6.56 - Closed outer zone, storativity ratio

While the effect of the outer lambda determines the time of transition, the effect of the omega is not significant because it occurs at intermediate time, masked by the multiple flow behaviours.

The late P.S.S. remains unchanged because it occurs after the transition, therefore during the global system behaviour.

We have seen that we can set specific sub-diffusion exponent in the fissure and in the matrix system. The result is not much different in the P.S.S. part since is acts mainly of the diffusion parameter.

References

Raghavan and Chen, "Addressing the Influence of a Heterogeneous Matrix on Well Performance in Fractured Rocks", March 2017, Transport of Porous Media, Volume 117, No. 1

Raghavan and Chen, "A Conceptual Structure to Evaluate Wells Producing Fractured Rocks of the Permian Basin", SPE 191484, 2018

10.I KAPPA recommended workflow (2020)

In the early days of the production of unconventional plays the workflow seemed to be limited to decline curve analysis using Arps hyperbolic equations. Due to early time linear flow it was very likely to arrive at high 'b' values which would most likely overestimate reserves without proper constraints. Recently it became common to see the incorporation of analytical and numerical solutions into the workflows for well performance analysis and forecasting.

However, a lot of work has been completed in terms of understanding complex PVT and interference between wells we still have to go deeper with flow phenomena at the nanoscale, geomechanics, etc... For this reason the workflow recommended in this section is dated (2020) because it will be in continuous evolution and this is for several reasons:

- We are still on the learning curve for advanced technologies.
- The data available today is still poor, considering what is at stake. Metrology, although it improved, is still, on average, below what we could expect. These plays are strategic and complex, but despite that we seldom get proper rates and downhole pressures. The best case scenario is to get daily wellhead pressure and rate data for analysis.
- The processing software tools (from KAPPA and others) are still a work in progress.

So we position the workflow described in this section as the best, or least bad thing we can do today with the tools we have at hands. For KAPPA this means Citrine, Topaze and Rubis. Other technical groups will offer alternatives.

10.I.1 Accessing data

Production data are typically stored in public or proprietary databases and historians. One may sometimes have to dig and find the necessary information (e.g., well completion data) in flat files and printed reports. The retrieval of this data in a proper state is sometimes far from a trivial task and may involve a lot of wasted time.

Whenever there is a structured way to store this data, commercial software applications will typically provide flexible means to access and load the data, either built-in or using specific plug-ins that will allow this data to be loaded with a minimum effort from the engineer.

The amount and quality of data may be unequal from one play to the next and from one company to the next. The workflow presented in this section implies that sufficient quality data is available. This is in no way guaranteed. Public data sources generally lack key information (e.g. continuous pressure data, completion information) that would be required for proper processing. The main data used are listed below:

Well information: The basic request will be the position/location of the well and its trajectory, well completion data (i.e. number of fracture stages, number of perforation clusters, well length) and wellbore data which will be used to correct pressure to datum when needed. When the completion changes, or when the flow path changes (e.g. casing production followed by tubing production) such information related to those events will have to be known to the engineers. In addition, petrophysical data (e.g., formation thickness, initial water saturation, porosity) and PVT data are required for analysis. Public data sources generally do not include such completion and reservoir data.

Production data (rate-time data): This data we will always have and, unfortunately, sometimes it will be the only available data. In this case analysis will be reduced to standard decline techniques. Statistical analyses may be performed based on the results of decline curve analyses.

Surface pressures: The surface pressure data is generally measured at the wellhead continuously by most of the operators. However, public data sources do not provide this data. It is, however, critical to have at least surface pressure data to be able to perform rate transient analysis/model-based analysis for production forecasting. In particular, rate transient analysis is very useful for forecasting when there is no apparent decline behavior due to varying pressures/choke management.

PDG data: Unfortunately, PDG data are still rarely acquired in unconventional reservoirs, although having access to downhole pressure data can provide critical information.

Surface pressures require lift curve corrections i.e. converting surface pressure data to bottomhole pressures, which are a potential source of error, especially when the producing systems and the phases in the wellbore change. Having the bottomhole pressure data directly eliminates the problem.

PDG data also record incidental shut-ins. Shut-in data may be very useful in some instances such as when, even with limited linear flow regime data, it might carry information on the well productivity (k, x_f^2k), skin and its evolution. Shut-ins are also ideal occasions to 'listen' to the reservoir, sometimes even detecting well to well interference.

Microseismics: Monitoring microseismic events during hydraulic fracturing is increasingly popular, though it still represents only a small percentage of fracturing operations in North America. Raw signals are recorded by the array of geophones. Interpreted data include, for each microseismic event: (1) the event time, (2) its location, and (3) some attributes, especially its magnitude and amplitude.

The distribution of events can help characterize the limits of the possible fracture network induced by the fracturing operations. The interpretation process is delicate and results should not be taken for granted. Since the microseismic events are not necessarily correlated with production, it is not trivial to insert the microseismic data in a flow model. At the very least the interpretation of microseismic can qualitatively give an idea about the possible drainage area.

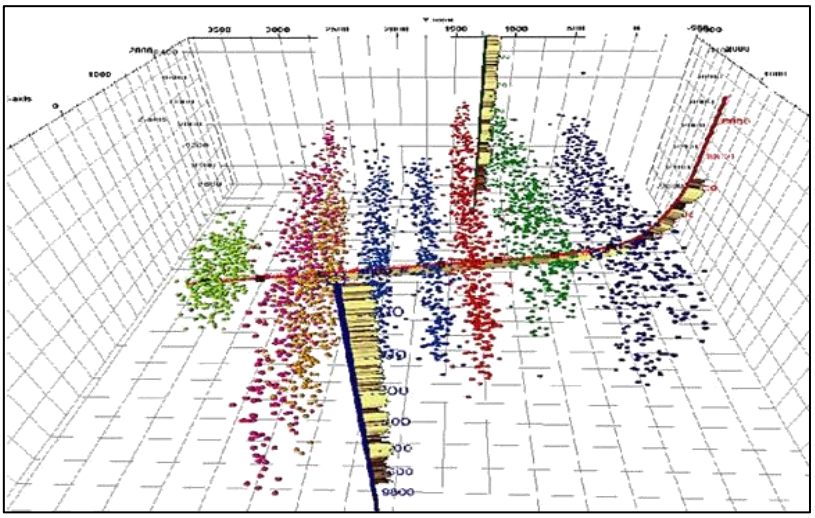


Fig. 10.I.1 – Microseismic events (Canada National Energy Board)

Fracture related data:

- Minifrac (also called DFIT: Diagnostic Fracture Injection Test) analyses can be conducted before the actual hydraulic fracturing operations to estimate a number of parameters such as permeability, formation pressure, leakoff coefficient, closure stress, providing critical information to design the hydraulic fracturing job. Results of DFIT data interpretation (particularly permeability, formation pressure) may help to calibrate production analysis, although the interpretation of DFIT data is oftentimes challenging.

10.I.2 Quality control (Citrine)

Quality control of data is critical to assess rate-time and pressure-rate-time data consistency and quality. It is generally preferable to start by reviewing available pressure-rate-time data for quality assurance and detection of correlations between pressure and rate data. Data without correlation will not provide any diagnostic value, and is thus meaningless for analysis. A diagnostic plot should highlight if there is something wrong with the data and identify the causes and deviations from the data plot.

One can also detect features or events which could be filtered or discarded prior to the analysis. For example, off-trend data can be removed from log-log plots used for flow regime diagnosis. A visual inspection may reveal obvious events or inconsistencies, such as well-completion changes, liquid loading, offset well fracture hits, etc. It is generally common to observe data inconsistencies and issues throughout the quality control process. Failure to identify and address these issues likely results in analysis of artefacts unrelated to actual well/reservoir behavior.

10.I.3 Diagnostic analysis, well grouping and selecting representative wells (Citrine)

It is usually not desirable to perform a diagnostic analysis on a very large group of wells. Many of the data features are difficult to distinguish and it is often difficult to establish characteristic performance trends due to differing completion practices and reservoir heterogeneities, to name a few. Using Citrine's well selection feature, working sets or groups may be defined.

These subsets of wells may be established according to differing fluid type, completion practice, completion horizon, start of production. The following order is preferred for grouping the wells: (1) similar location/geology, (2) similar fluid properties, (3) similar completion practices. In addition, metrics can be defined via normalizations and parameter plots which could indicate certain well groupings. A special plot referred to as Probit, which is used to plot the distribution of a well parameter across all wells, can also help in visual identification of well groups.

Once the groups are identified, production diagnostics can be performed. We can either perform diagnostics on a single well to identify characteristic flow regimes or on multiple wells to compare flow efficiencies, completion effectiveness, and characteristic reservoir signal. The identification of flow regimes is a primary objective of production diagnostics.

The Log-log plot is a particularly useful tool to detect these flow regimes. On the Y scale one will display the flow rate, preferably normalized by the pressure drop. On the X scale one can use standard time or, preferably, Material Balance Time, i.e. the instantaneous cumulative production divided by the instantaneous rate.

Such a plot is particularly useful to identify flow regimes. Some commonly used slope values are listed below:

- Quarter slope → bi-linear flow (finite conductivity fracture)
- Half slope → linear flow (infinite conductivity fracture)
- Unit slope → depletion type flow (or productivity loss) [material balance time plot]

The following figure illustrates an example of a single well plotted on a log-log rate and material balance time plot with a half slope (linear flow) identified by an annotation. This exercise is performed for the other wells of the group to make sure each well exhibits the same behavior.

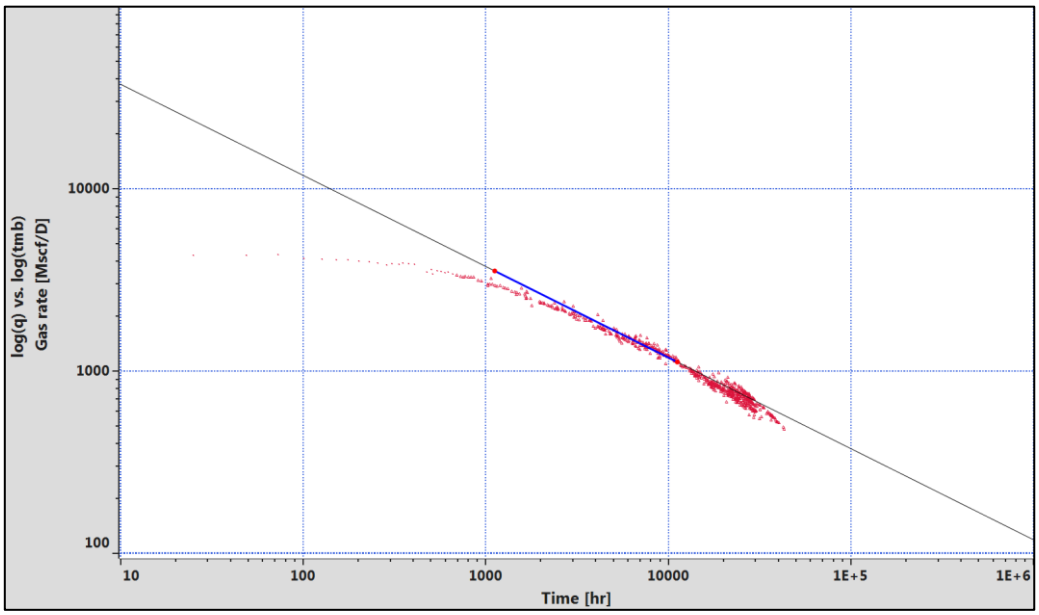


Fig. 10.I.2 – Log-log plot of rate versus material balance time with a negative half slope

In addition to analyzing individual well behavior, we will investigate the possibility of characterizing flow regimes for an entire group of wells. For instance, on the left hand side of the figure below all of the wells from the well group are plotted on the same rate versus material balance time plot as before.

It is immediately noted that while the well responses seem to exhibit a similar shape, there are marked differences between the wells in the vertical direction. These vertical separations can be thought of as differences in productivity due to reservoir heterogeneity, completion practices, or operational issues to name a few. Normalizations can be used to pinpoint the cause of the shifts.

For instance, the right hand side of the figure below shows each of the wells in the well group normalized by six month cumulative production for each well.

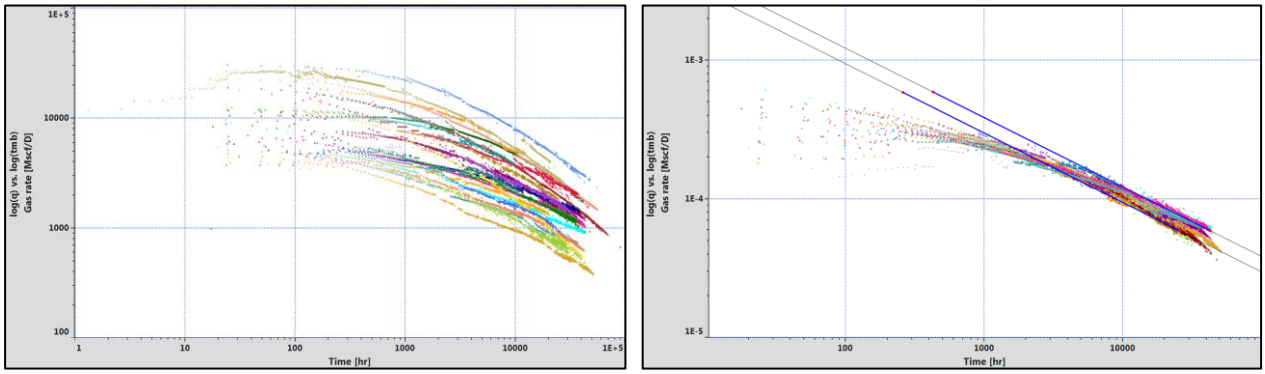


Fig. 10.I.3 – Normalization application for a group of wells

The six month cumulative production could serve as a 'proxy parameter' for local differences in reservoir quality and completions that might drive production behavior. With normalization, most wells exhibit linear flow at early times and then transition towards a unit slope at late times. This interpretation serves as a basis for choosing an appropriate model for the group of wells.

One may use qualitative and quantitative production metrics to compare wells within and across groups. For instance, the slope of the initial data trend on a reciprocal rate (or rate normalized pressure drop) versus the square root of time plot may serve as a proxy for a 'lump parameter' integrating the number of fractures, average effective fracture half-length and permeability (a.k.a. the linear flow parameter). This information can be used to handle non-uniqueness in model based production analysis, keeping different parameter combinations consistent with the diagnostic.

The following figure presents rate normalized pressure drop and square root of time plot and straight lines drawn to identify the slope values corresponding to each well. Note that it is possible in Citrine to attach a straight line to each of the wells in a particular well group, with individual line slopes found as a best fit to the data from an individual well.

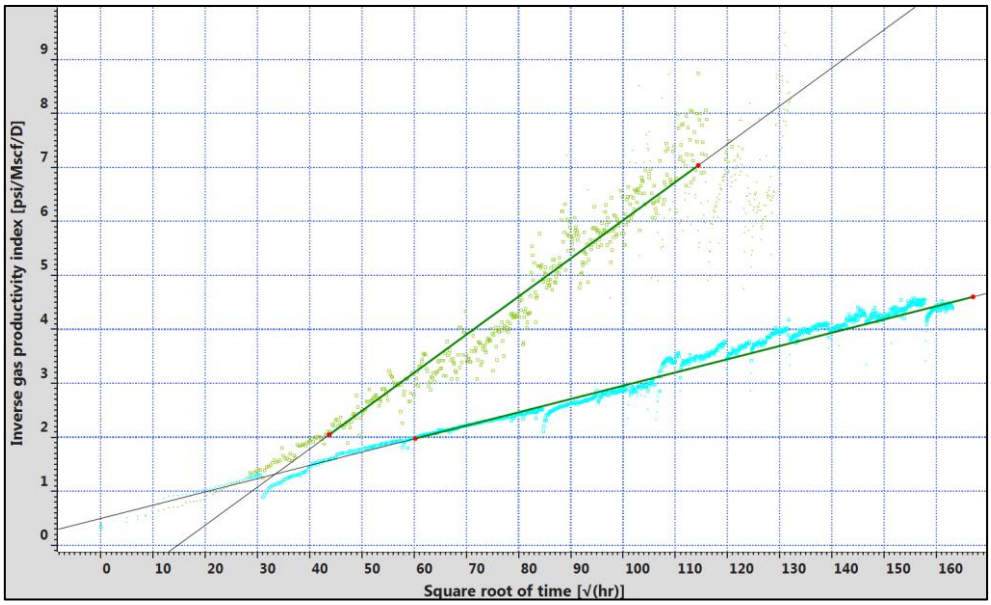


Fig. 10.I.4 – Rate normalized pressure drop versus square root of production time (Cartesian scale for linear flow)

Recalling the simple linear flow equation, m_{sqrt} is a lump parameter, which is inversely related to the slope of the straight line drawn on data. The lump parameter term contains the product of cross sectional area perpendicular to the flow (effective fracture half-length times fracture (or formation) height and the square root of permeability.

The slope values can be used as a guide for the rate transient analysis of the wells. For example, if one assumes the same permeability for these two wells, slope values may yield effective fracture half-length. The well with the shallower slope may indicate a better completion efficiency compared to the well with the steeper slope. This type of observation can be used to filter well groupings more accurately and/or compare completion types between similarly drilled and fractured wells in the same reservoir.

The Y-intercept on this plot is an indication of fracture conductivity. A well with a slope directly through the origin is said to be flowing into an infinitely conductive fracture from the well's stimulated or matrix regions. Wells with positive intercepts may have an associated skin around their fractures due to non-darcy flow, proppant embedment, or fracture fluid not breaking down properly. It should be mentioned that negative intercepts may be an indication of a well being supercharged by the high pressures during fracturing and flowback. These pressures may need to be filtered prior to rate transient modeling.

Other plots can be used to identify additional performance metrics. For example, straight line extrapolations on a semi-log rate or pressure drop normalized rate vs. cumulative production might give a rudimentary estimation of total recovery, or the stimulated region volume. These values may serve as a performance metric for the recovery of each well.

Similarly, these values can be mapped on a cross-plot versus another parameters like completion properties to identify high and low productive areas.

To conclude, various diagnostic plots will be useful to serve for the purposes mentioned earlier. The following four plots are found to be applicable and relevant in many cases and are recommended to start diagnostic interpretation:

1. [Log-log] rate (or pressure drop normalized rate) and time for flow regime identification
2. [Log-log] rate (or pressure drop normalized rate) and material balance time for flow regime identification (Blasingame plot)
3. [Cartesian] reciprocal rate (or rate normalized pressure drop) and square root of time for well productivity assessment (metrics)
4. [Semilog] rate (or pressure drop normalized rate) and cumulative production for production

More diagnostic plots, which the analyst may find useful, can be created and used to accomplish diagnostic interpretation. These additional plots may be different for each play or field. However, it is strongly recommended that the four plots above are created for diagnostic interpretation.

10.I.4 Selection of representative wells (Citrine/Topaze)

Following production diagnostics, the next step is to carry out rigorous modeling for one or more wells within a group. These wells are called the 'representative wells' and show the characteristic behavior of the group. When choosing a representative well it is critical that the chosen well has consistent rate and pressure data. The additional data required for analysis and modeling, namely PVT and well/reservoir properties along with completion data must also be considered. Once the representative well is selected, it can be sent to Topaze (RTA) for analysis and forecast.

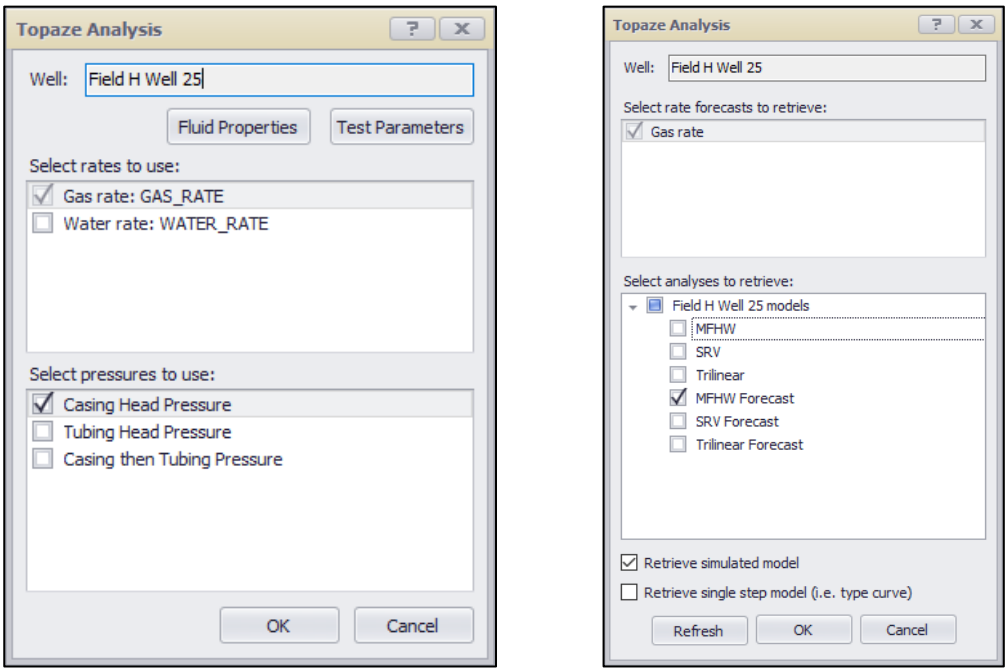


Fig. 10.I.5 – Import/export dialog of connection between Citrine and Topaze

10.I.5 Single well Rate Transient Analysis (Topaze)

Single well rate transient analysis of the representative well is performed using the workflow described earlier in the document. For this example uncertainties were considered on the contacted drainage area and three almost identical history matches were obtained using SRV bounded, trilinear, and infinite-acting multi-frac horizontal well models.

Other uncertainties (e.g., contribution from fracture stages, contacted drainage area, formation properties, etc.) can also be considered for history matching. Eventually, this process will transform into a probabilistic forecast through experimental design / Monte Carlo simulation.

Each of the cases provides virtually the same match of the historic well production; however, each of the models has different assumptions, and therefore each history match was obtained with different model parameters (e.g., effective fracture half-length). Therefore, using the model parameters obtained from three different history matches will translate into a range of production forecasts.

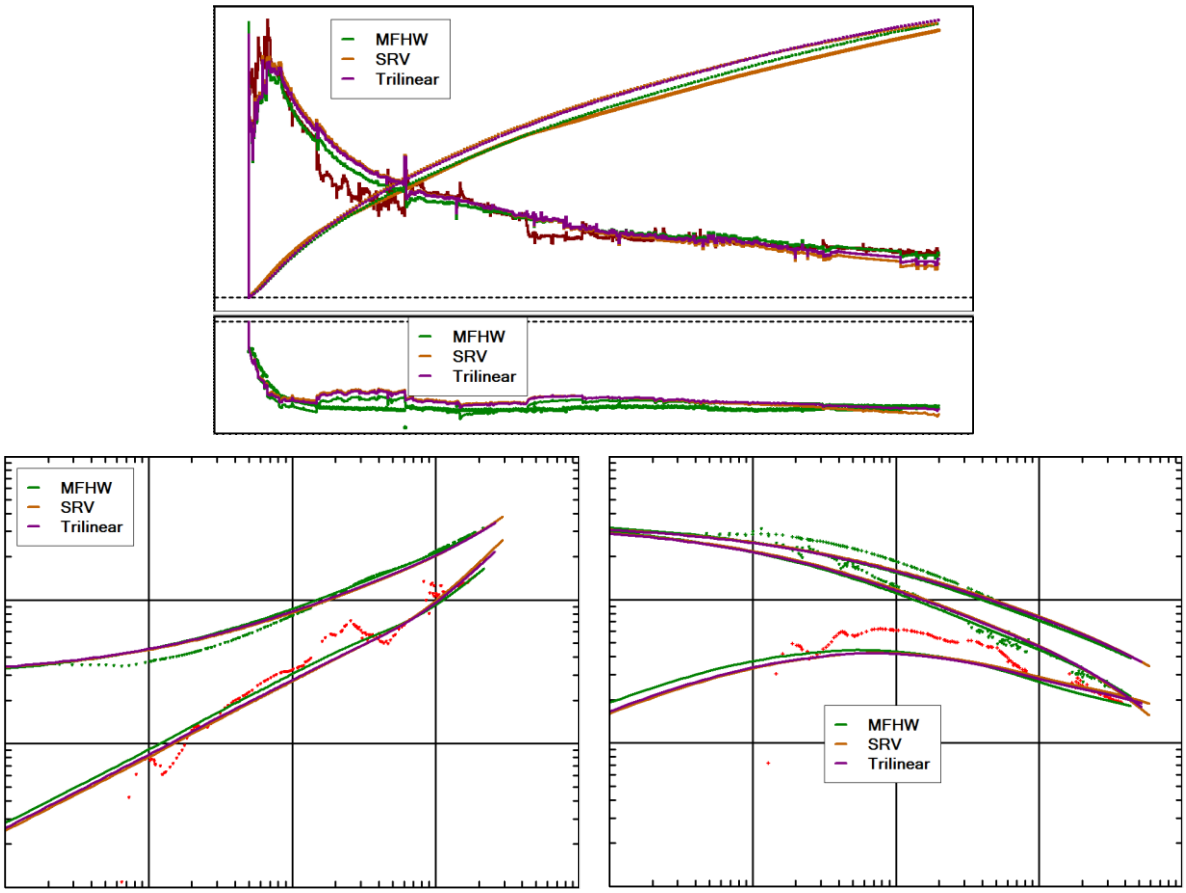


Fig. 10.I.6 – Comparison of three different rate, pressure, and diagnostic matches for the representative well

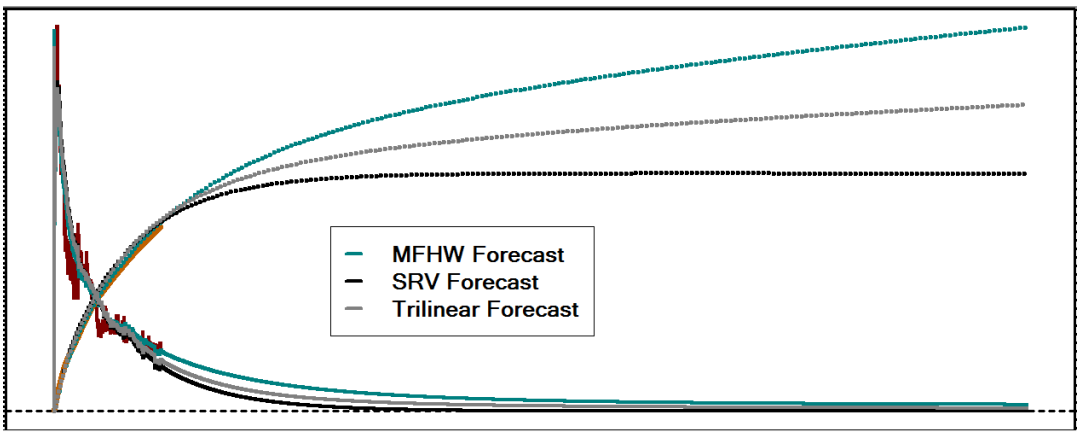


Fig. 10.I.7 – Production forecasts of the representative well based on three different models

10.I.6 Extension of the representative well model forecast to other wells

Once the history match of the representative well is established, production can be forecast based on a future pressure constraint. Uncertainties on model parameters can be considered to yield probabilistic forecasts. The main question at this point becomes how to extend these forecasts to other wells. In order to answer this question, it is critical to make sure that well groups consisting of similarly performing wells are established correctly.

Model forecasts in Topaze are retrieved in Citrine and can be extended to other wells in Citrine's Analysis mode using the n-Well (a.k.a. Multi-well) option. As different wells might have different early clean-up times, it is possible to fit the reference model to the other wells' data starting after their corresponding peak rates, or select a particular time interval for fitting the trend.

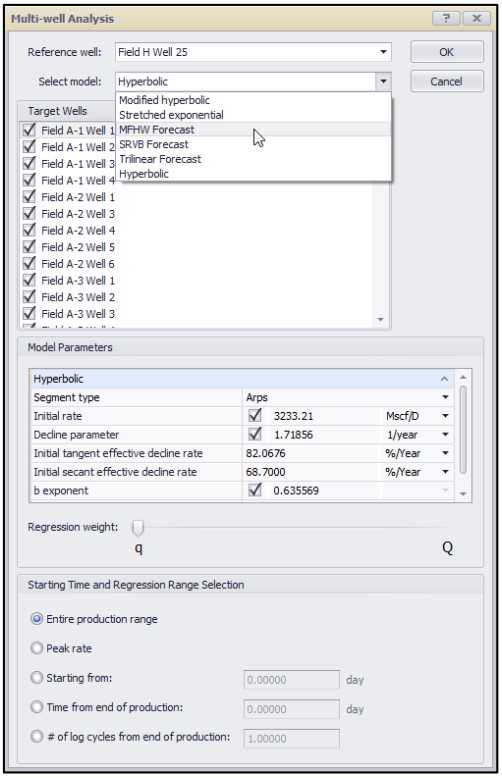


Fig. 10.I.8 – Initialization of Topaze type curve for other wells analysis in Citrine

In Citrine, '(Sim)' is added to the Topaze model forecast for the representative well and can only be applied to the well which was chosen to be modeled in Topaze. Once this forecast is imported into Citrine, the model match can be visualized across all selected plots.

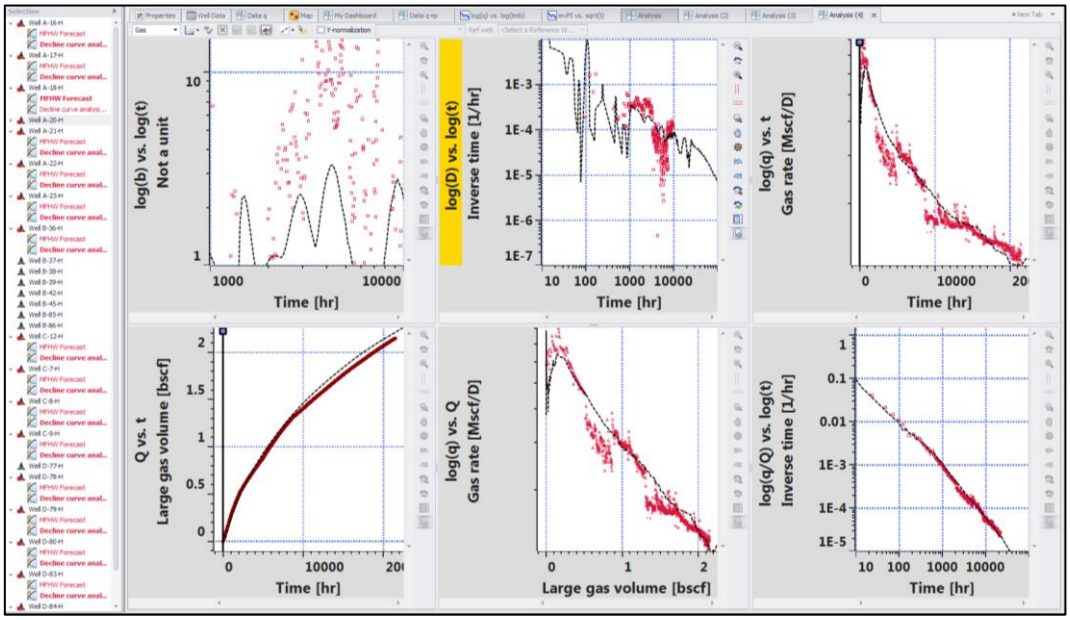


Fig. 10.I.9 – Imported Topaze model response for the representative well

A response of the same model to a single step response is also simulated in Topaze and is brought into Citrine as a Type Curve, hence an addition '(TC)' to its name, and it can be transferred to other wells through X and Y factors found automatically to history match and forecast well performance for each well in the group.

If the working sets, or groups of similar wells, were chosen correctly, we might find that some of the wells that were not modelled will almost behave like the representative well. Other times, however, we will find that there is a degree of separation between the model matches and the other wells in the group. This separation that was discussed earlier could be due to the differences in completion and reservoir characteristics. If the well groups are properly chosen, then utilizing X and Y factors as 'shifting' parameters on the $\log(q)$ vs. $\log(t)$ plot could be used for extending Topaze models to other wells within a particular working set.

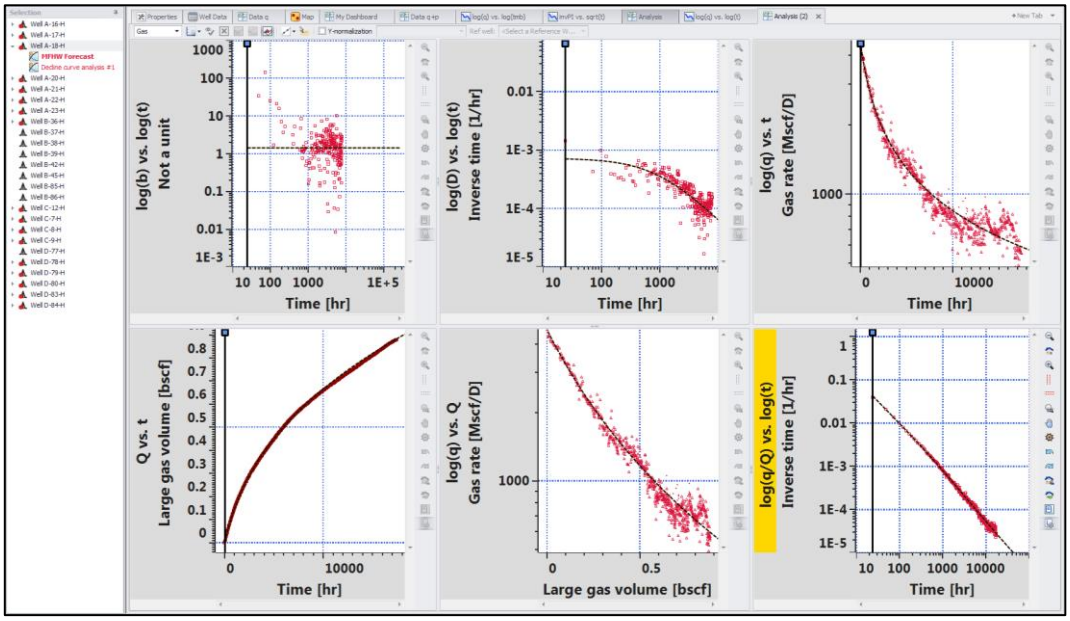


Fig. 10.I.10 – Type curve from Topaze adjusted for the other well in the working set

Once each of the wells in a group has a forecast associated with it, statistical curves can be applied to the model values to show the average/percentile forecast curves. Note that these would be different from fitting a model to the percentile wells that were created based on wells' data only, so it might prove an interesting exercise to compare the two.

In case when multiple single step curves are imported from Topaze, it is possible to forecast wells production as a combination of these forecasts using machine learning algorithms. The essential idea behind the workflow is that the single-step models represent and encompass the important physical processes that occur during production, and by combining them one can match other wells behaviour and perform forecasting. Iterating over each well, Model Mining first employs superposition to condition the type curves to the individual well pressures, and then employs regression to match the superposed type curves to the well production. The advantage of using this method is that the Model Mining procedure automatically creates a data-driven, physics-based forecast. The diagram below provides a visual description of the workflow.

For the detailed description and information on how to use this option please refer to additional documentation on the Citrine section of KAPPA website. Please note that the Model Mining option is provided as an Experimental module.

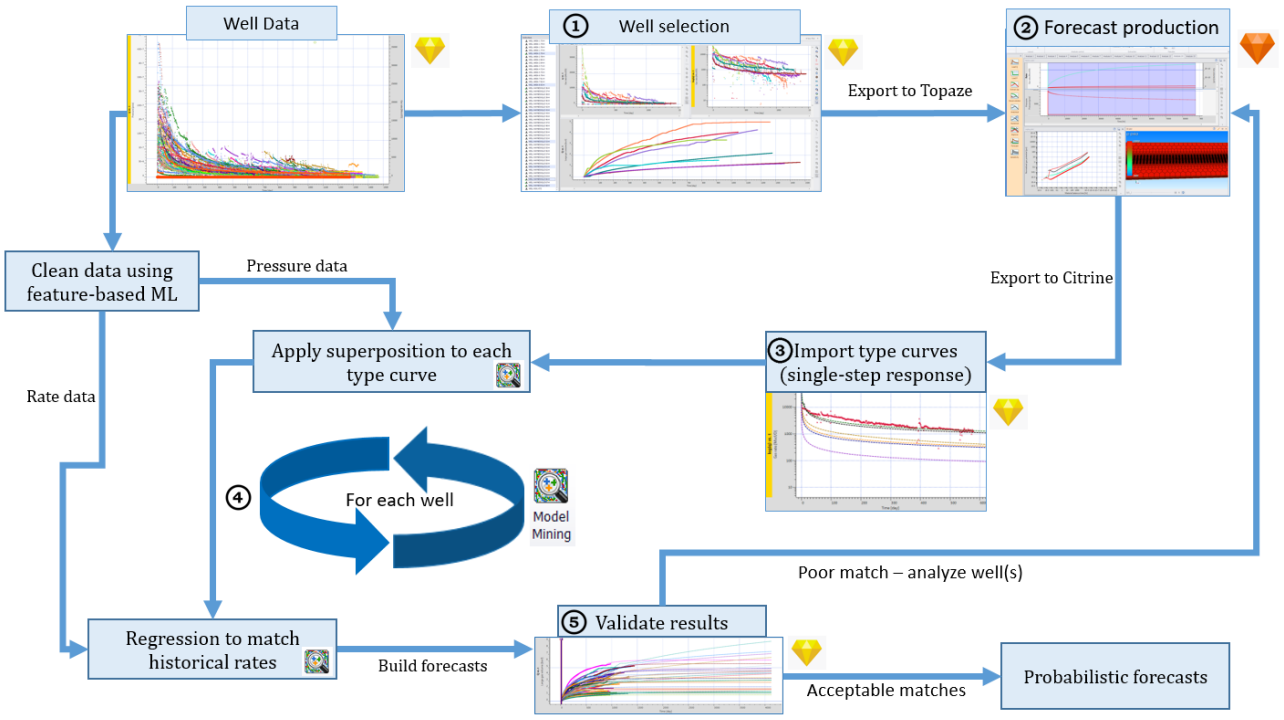


Fig. 10.I.11 – Diagram of the Model Mining workflow

Once all the forecasts are calculated, being the result of DCA, Topaze modeling, or Model Mining, a consolidated forecast for the group of well or the entire field can be calculated in Citrine, so that the historical (data) and future (forecast) production are rolled up into a channel of the total production for the selected wells. The reference forecasts for all the wells can also be exported in bulk in a spreadsheet for further reporting purposes, or converted into a required format to be re-imported into third party economical evaluation and planning packages.

11 – Formation Tests
OH – OSF – DV – JCNF – DB

11.A Introduction

When looking at the pressure response at the producing probe or packer, a formation test (FT) can be interpreted as a standard test using a very specific well geometry. The methodology is strictly the same. When using multi-probe tools one has to integrate the standard pressure response of the producing probe and the vertical / lateral interference observed at the other probes. The methodology then becomes more specific.

The first formation testers developed in the 1950's were designed for fluid sampling. The next generation included the measurement of formation pressure. When conditions were favorable permeability from pressure transients could also be determined.

The latest generation of formation testers records pressure at different depths in a single wireline operation. This operation is generally carried out after running the openhole logs. Logging While Drilling (LWD) was developed in recent years to characterize the formation during drilling operations.

Data acquired from formation tests is time dependent. It is especially dependent on the stage of development of the reservoir. In virgin reservoirs (with gravity-capillary equilibrium) different parameters can be determined to improve the reservoir characterization: original fluid contact, reserves, heterogeneities, fluid density, productivity, etc. In developed reservoirs, formation test results may be used to monitor and improve the reservoir performance.

11.B What is Formation Testing (FT) used for?

FT operations can be run at any stage in the life of a field. They are commonly carried out during the appraisal phase, but they also have a role in the field development phase.

During the exploration and appraisal phase the FT objectives encompass:

- Initial reservoir pressure
- Fluid density and gradients
- Fluid contacts
- Initial estimation of minimum reserves
- Formation fluid samples
- Local mobility / permeability (kh, kv)
- Vertical and lateral compartmentalization
- Initial state for reservoir simulation

During the development phase FT objectives include:

- Vertical communication between layers
- Evolution of fluid contacts
- Pressure profile deviation from initial state
- Hydraulic communication between wells

Formation tests are a partial alternative to conventional well tests. They require far less surface equipment and they do not require flow to surface. They complement conventional well testing by providing information with a finer vertical resolution. They do not, however, meet all the objectives of standard tests.

In this section we will detail the three main objectives in running an FT tool: pressure profiling, sampling, and permeability determination.

11.B.1 Pressure profiling

Modern FT tools allow unlimited pressure measurements along the wellbore during a single trip. High accuracy, high resolution gauges have increased the confidence in pressure readings to build a pressure profile.

The pressure is recorded from the pretest. These pretests comprise short (seconds) production periods followed by short (minutes) shut-ins. The pressure is determined during the buildup. It is plotted versus true vertical depth (TVD) to define straight lines corresponding to fluid trends (gas, oil and water) and contacts as shown in the figure below.

Under static conditions, the pressure change is a function of the fluid density in the formation. In field units the pressure gradient is given by:

$\gamma_f = 0.433 * \rho_f$, where γ_f is the fluid gradient (psi/ft) and ρ_f is the formation fluid density (g/cc)

If the pressure is measured at different depth levels, a gradient line for each fluid can be built and fluid contacts can be identified. Additionally, the mud density can be calculated using wellbore pressure gradients:

$\gamma_m = 0.052 * \rho_m$ where γ_m is the mud gradient (psi/ft) and ρ_f is the mud density (lbm/gal)

In the following figure, the track on the right shows a common behavior of fluid gradients where a gas cap can be identified as well as the oil water contact (OWC). The track on the left illustrates the mud pressure for each of the FT stations. The hydrostatic gradient can be obtained from the mud pressure.

Gradient calculations are influenced by different parameters that may bring confusion: gauge resolution, formation thickness, number of stations (pressure points), depth measurement accuracy, supercharging effects, mud filtrate invasion, capillary pressure effects, etc.

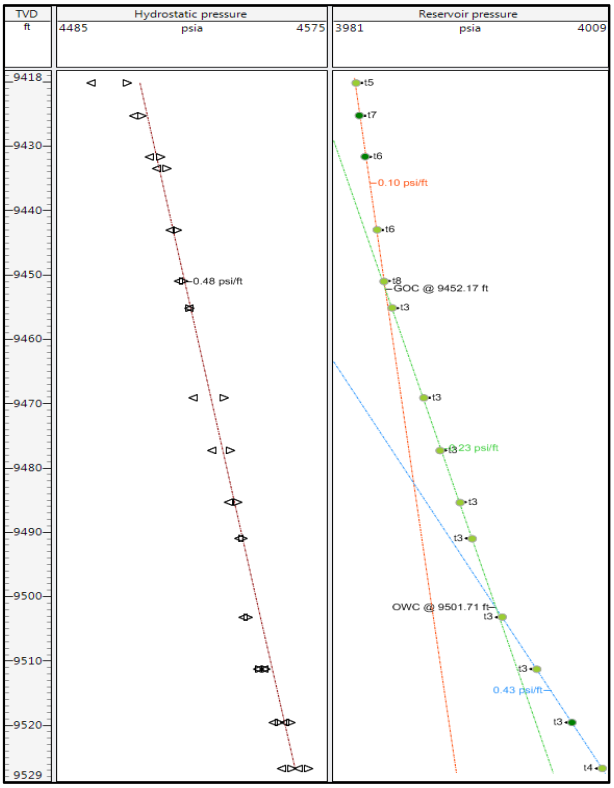


Fig. 11.B.1 – Pressure Profile

In thin layers, the gauge resolution and depth control will play a key role in the measurements as the pressure may have small variations along the formation.

The use of pressure points may help in the identification of vertical flow barriers. In virgin reservoirs vertical connection must be considered carefully: having different points located on the same gradient trend possibly infers that they are in the same hydraulically connected unit. When points fall on different trends it is possible to come to the conclusion there is no communication. In developed reservoirs, vertical connectivity such as connected, partially connected or sealed, may be easier to deduce based upon the comparison of pressure trends.

The next figure illustrates this example where the track on the left represents the pressure trend during the appraisal stage. The track on the right is shown after some production time in the lower formation.

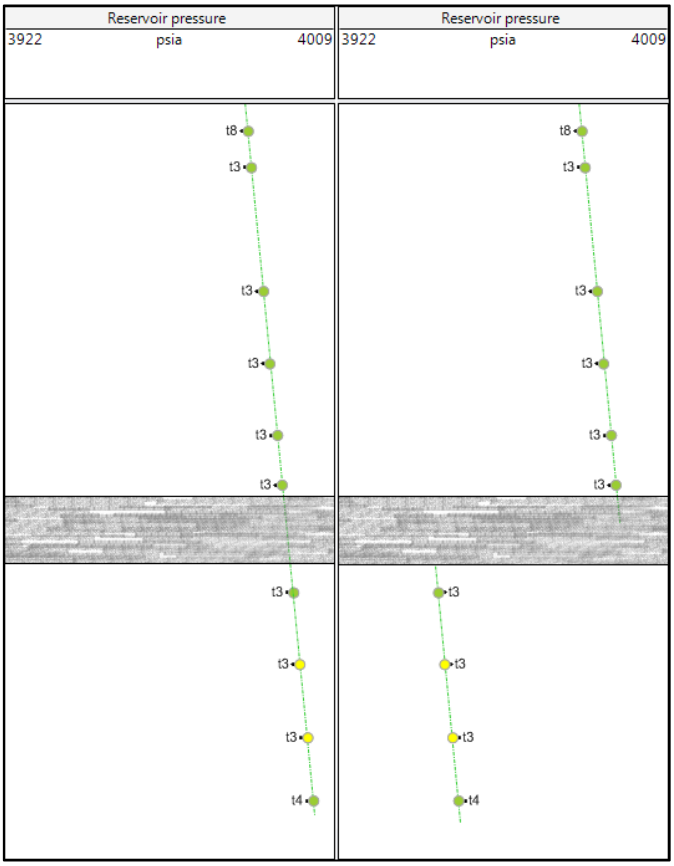


Fig. 11.B.2 – Two flow units separated by a thin barrier

FT results from different wells may indicate horizontal flow communication. In virgin reservoirs, FT data from different wells may lead to a better understanding of the reservoir if they are complemented by petrophysics, geophysics and geological data. The figure below shows how different pressure data trends from several wells can change the interpretation from log data.

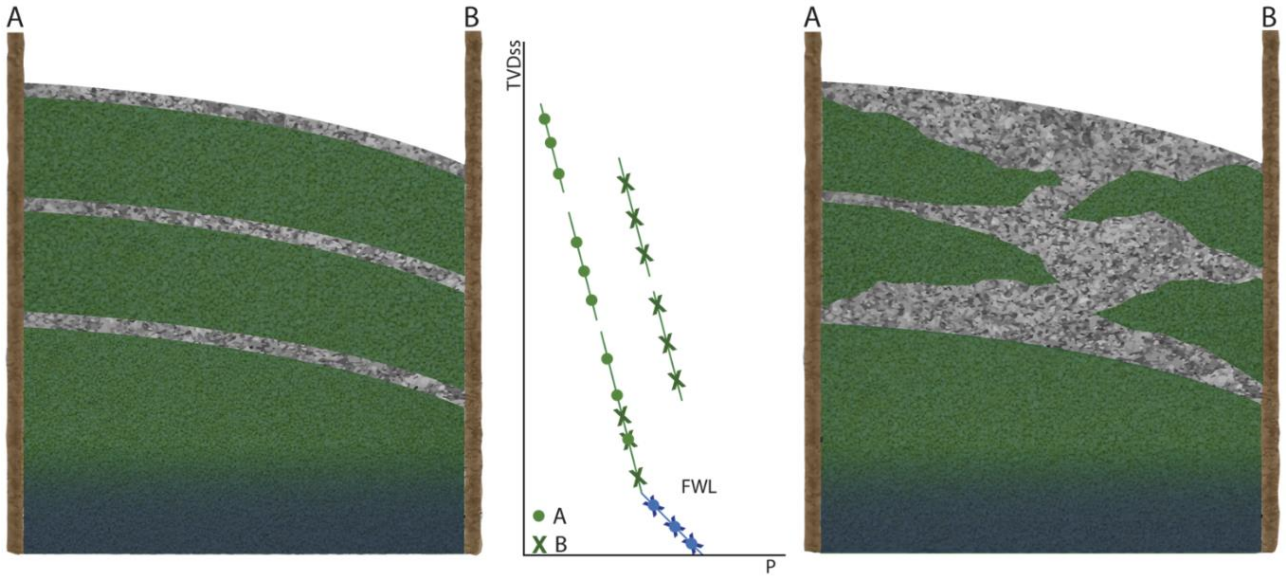


Fig. 11.B.3 – Pressure profile from different wells

Reservoir fluid gradients

Pressure vs. depth plots establish formation fluid gradients and identify fluid contacts in the reservoir. The table below lists densities and fluid gradients for common reservoir fluids. Confidence in fluid identification from the gradient is highest when there is a large contrast between fluid densities. The density of heavy oil is close to the density of fresh water so there will be more uncertainty in fluid type based on gradient in a heavy oil reservoir. Fluid sampling or downhole fluid analysis should be used to support gradient analysis when fluid densities are similar. Thicker sands are also needed to establish gradients with confidence.

Compositional fluid gradients in the reservoir create curved gradient profiles. Extrapolation far up or down dip must only be done if it can be proven that lateral and vertical flow continuity exist, and that the fluid model in use is applicable throughout the reservoir volume of interest, and there is ample independent corroborating data to suggest such communication. Analysis of pressure data should always be done in conjunction with logs because in the analysis of pressure data, the context is just as important as the data itself.

Changes in layer pressure in produced reservoirs can mask changes in fluid density but offsets in the gradient lines is a good indication of pressure isolation so the data is still valuable.

Azurite software will automatically fit gradients to classify fluid type and project gradient lines to locate fluid contacts. The results can be modified by the analyst.

Variable	Density Range (g/cc)		API Gravity (deg API)	Initial GOR (scf/bbl)	Gradient Range (psi/ft)		Gradient Range (kPa/m)	
Wet & Dry Gas	0.03	0.34	50+	100,000+	0.01	0.15	0.28	3.34
Gas cond	0.23	0.35	45–60	3500 – 50,000	0.10	0.15	2.27	3.39
Volatile oil	0.46	0.60	42–55	900 – 3500	0.20	0.26	4.52	5.89
Black oil	0.72	0.88	15–45	200 – 900	0.31	0.38	7.06	8.63
Heavy oil	0.83	1.00	5–15	0 – 200	0.36	0.43	8.14	9.81
Water/brine	0.95	1.17			0.41	0.51	9.32	11.44
Drilling Mud	1.00	2.00			0.43	0.87	9.81	19.67

Fluid density data from Petroleum Engineer Handbook, Volume V(b), pg V-897, Table 9-1,

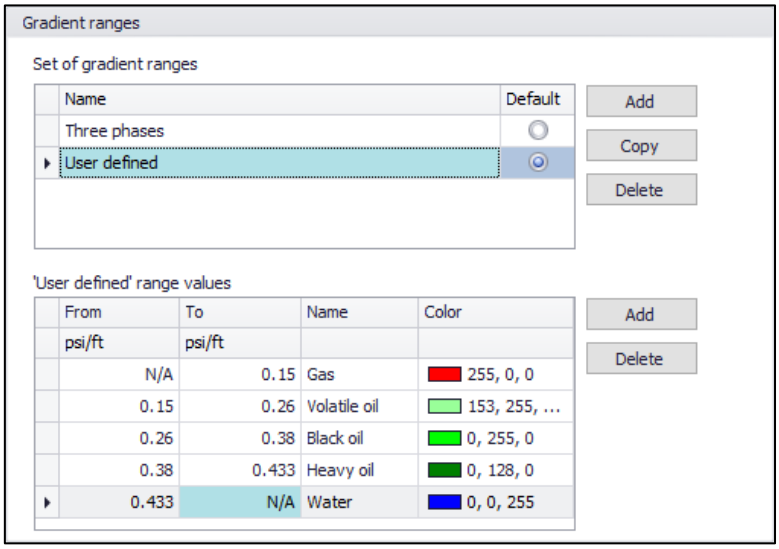


Fig. 11.B.4 – Fluid density reference values (top table) and Azurite gradient ranges used for automatic fluid detection in Azurite

Gradient Uncertainty

The figure shows how depth uncertainty and pressure uncertainty impact gradient uncertainty. Gradient uncertainty is dominated by interval thickness, interval density, and the number of pressure points recorded. It is highest in thin reservoir intervals with low fluid density.

Actions that can be taken to minimize gradient uncertainty include:

- Following all depth control best practices
- Filter low quality pressure points that are supercharged or have short build
- Record sufficient data points to constrain the gradient answer

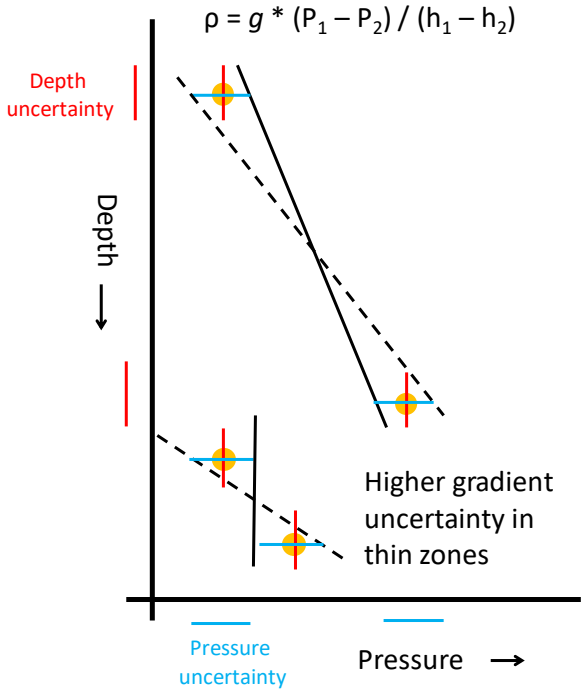


Fig. 11.B.5 – Impact of depth and pressure uncertainty on gradient uncertainty

Influence of capillary pressure effects (FWL vs OWC)

Capillary Pressure is defined as the pressure difference between two immiscible fluids. This phenomenon becomes manifest due to the interfacial tension of the fluids and also depends on pore size distribution, fluids saturation, and rock wettability.

In a water wet reservoir, the capillary pressure value is given by:

$$P_c = P_{oil} - P_{water}$$

Or more generally:

$$P_c = P_{nw} - P_w = \frac{2\sigma cos\theta}{r} = (\rho_w - \rho_{nw})gh$$

Where σ is the interfacial tension between the two fluids, θ represents the wettability of the capillary tube (pore throat), r is the radius of the capillary tube (pore throat). P_w, P_{nw} are the pressures of the wetting and non-wetting phases, respectively, and ρ_w and ρ_{nw} are the wetting and non-wetting phase densities, respectively. Lower permeability rock (small pore throat

radius r) will have longer transition zones for a given fluid system (oil/water or gas/oil, gas/water). Low density contrast between the wetting and non-wetting phase also cause longer transition zones.

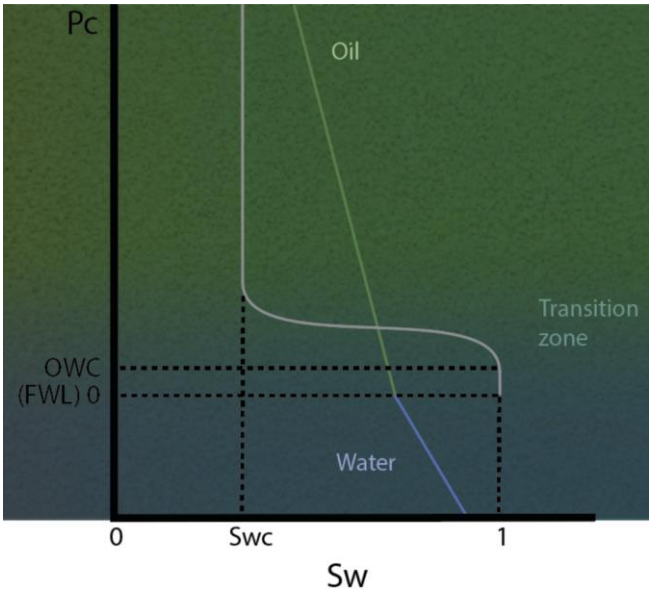


Fig. 11.B.6 – Fluid gradient (green line) and Capillary pressure in an Oil-Water system

The figure above shows the pressure gradient curves (in an oil-water system). In this example the reservoir is water wet. The plot also illustrates the capillary pressure as a function of water saturation.

The intersection of the pressure gradient curves is the depth of the Free Water Level (FWL). At this depth, both fluids have the same pressure, so the capillary pressure is nil. At the FWL, the reservoir saturation is 100% water. The lowest level where oil can be detected is known as Oil-Water Contact (OWC). The FWL and the OWC can have different depth due to capillary effects of the rock pores. The water column may rise above the free water level, so the reservoir will be 100% saturated by water up to the OWC. Generally, this level is detected by well logs.

Between the OWC and the FWL, capillary effects are active; this interaction results on the displacement pressure (Pd). The displacement pressure is the minimum pressure required for the non-wetting phase to displace the wetting phase from the largest pores.

Above the OWC the oil saturation starts to increase. Along the transition zone, capillary pressure difference will exist due to the presence of the two fluids. In the transition zone, the capillary pressure can be computed as the difference between the oil and water pressure gradients.

In the oil zone, there is still water in the system but at connate saturation (Swc). At this point, the water is immobile and discontinuous. The water cannot be displaced by increasing the oil pressure, so the capillary pressure curve becomes almost vertical as shown in the figure above.

The capillary pressure curve shape depends on pore geometry and size and the densities of the reservoir fluids . In well sorted grains and large pores (high permeability), the capillary transition zone will be quite short (Fig. 11.B.7). A poor grain and size distribution (low permeability) will impact the extension of the transition zone. The Pc curve presents higher slope as shown in the figure below.

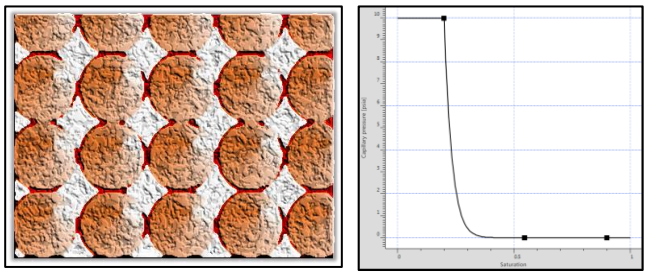


Fig. 11.B.7 – Capillary pressure in well sort grains

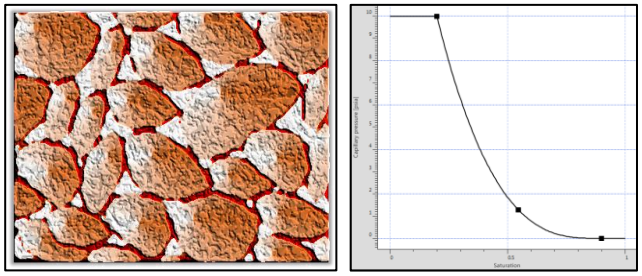


Fig. 11.B.8 – Capillary pressure in low permeability rock

Supercharging impact on pressure analysis

During (and after) the construction phase of a well, mud is used to maintain optimal conditions of the wellbore. In general, drilling operations are carried out in overbalance (hydrostatic pressure higher than formation pressure) which causes the mud to invade permeable zones. Another objective of the drilling fluid is to create a mud cake avoiding high rate of fluid loss (filtrate) to the formations.

The FT tool measures the pressure at the sandface (P_s); in tight formation this can be problematic because the invading fluid increases the pressure around the wellbore. Pressue dissipation is slow in low permeability formations which can cause unrealistically high pressure results during FT measurements (usually hours after the drilling operation). This phenomenon is known as supercharging, and it shifts the pressure results to the right (P_r vs TVD plot). Supercharging is a function of mud fluid loss rate (during drilling operation and in static conditions) and the ratio between formation permeability (k_r) and mud cake permeability (k_{mc}). High supercharge effect is observed if $k_{mc}>>>k_r$.

In high permeability formations supercharging is insignificant, the pressures measured in virgin reservoirs display small deviation from fluid gradients.

The next figure depicts the pressure behavior in the well-reservoir system. The wellbore is at hydrostatic pressure (P_{hyd}), then the pressure starts to decrease across the mudcake to finally approach reservoir pressure (P_r). The pressure measured by the FT tool is just behind the mudcake (sandface).

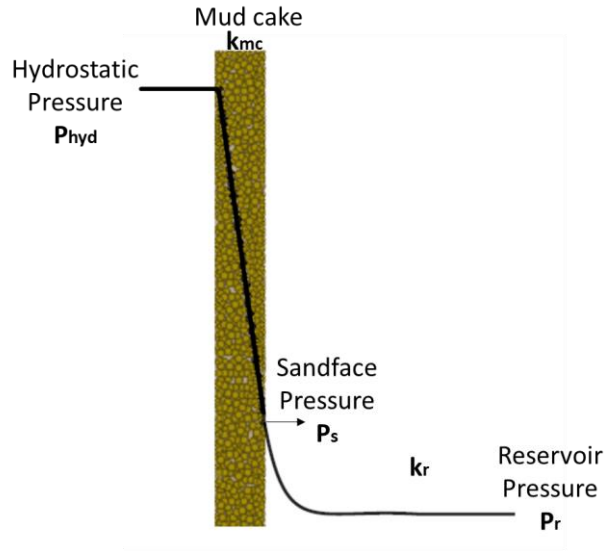


Fig. 11.B.9 – Pressure drop of mud filtrate near wellbore

The figure below illustrates the impact of supercharging on the fluid gradient definition.

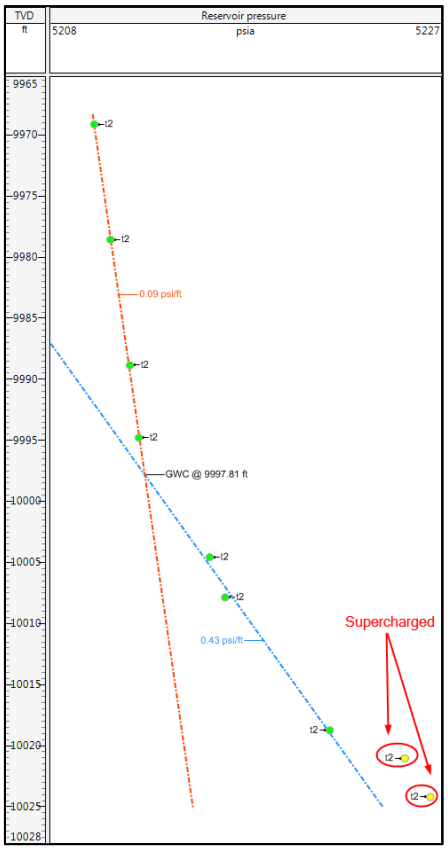


Fig. 11.B.10 – Effect of supercharging on fluid gradient determination

It is important to consider the supercharging effect in order to reduce its impact on the pressure results. In case of virgin reservoirs, it is known that the pressure measurements should follow the hydrostatic gradients. Also, it is recommended to carry out several pretest at a station to relieve any supercharging and verify repeatability. The effects of supercharging may be reduced in moderate permeability reservoirs if the FT operation is run several hours after circulating the well to give time to the dissipation of the pressure in the sandface caused by dynamic losses.

Quality control using gradient statistics

Filtering outlier data will help reduce the uncertainty reservoir fluid contacts and fluid densities determined from pressure gradient FT data. Azurite software captures gradient statistics for the measured data and compares it to expected uncertainty from Monte-Carlo simulations that account for density, gauge uncertainty, and depth uncertainty. Outliers can be identified where the measure pressure residual uncertainty (blue in the figure below) is greater than the theoretical uncertainty form Monte-Carlo simulation (red). If the measured uncertainty is greater than the theoretical uncertainty then reviewing the pretest data, filtering outliers (such as supercharged points), or recording more stations during a job can improve precision of the interpreted results. In this example the uncertainty of the measured data is below the theoretical uncertainty.

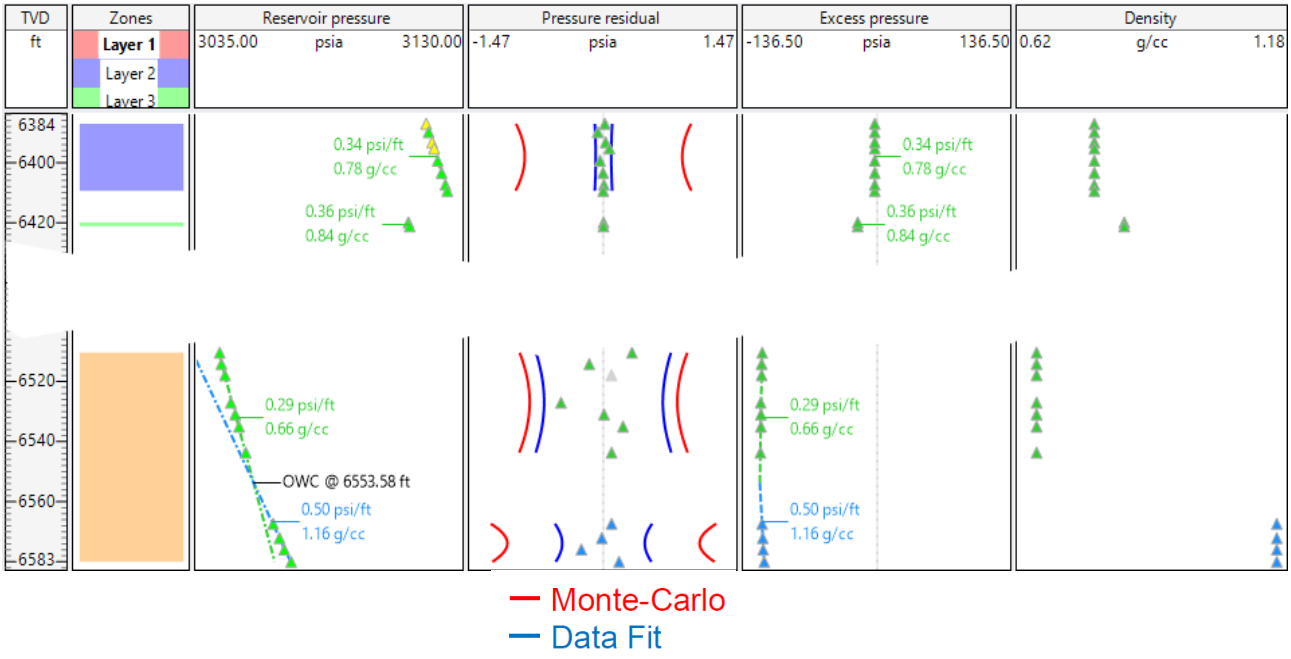


Fig. 11.B.11 – Gradient statistics

11.B.2 Sampling

The analysis of reservoir fluids is key during the appraisal phase of a field. Fluid behavior in response to pressure and temperature changes impacts the design of the completion and surface facilities. Taking representative samples using the FT tool has become one of the main objectives for running this operation and decreases costs during the exploitation stage.

One of the main concerns whilst fluid sampling with FT tools is the contamination due to the invasion by the drilling mud filtrate. Modern FT tools allow real time monitoring of the fluid being withdrawn. During the sampling operation the fluid is monitored using resistivity measurements. These sensors are part of the probe module and provide a means to discriminate between the filtrate and the reservoir fluids. If oil based muds have been used during drilling operations an optical analyzer is used to differentiate the mud filtrate and the formation fluids. Fluid density, pH and viscosity sensors are also available.

An optical analyzer can be attached to the FT tool string. It identifies the fluid type, which is very helpful when capturing representative samples. A pump-out module is used to flow contaminated fluid into the wellbore until representative formation fluid has being identified.

The fluid is then diverted to the sample chamber and stored. The configuration of the FT string allows multisampling in different chambers during a single trip. The optical analyzer, and the sample and multisample modules, are optional and can be assembled in different locations in the tool string depending on operational conditions. The figure in the tool description section shows such a configuration using different tool modules.

11.B.3 Permeability determination

Transient formation test pressures are increasingly used to assess reservoir parameters, mainly permeability. Early permeability estimates promote greater confidence in the design, or decision, to proceed with traditional tests.

Using in-situ measurement, FT provides a rapid, local permeability profile estimate along the wellbore. In turn this gives a good indication of the expected well productivity and helps in the design of the completion and recovery mechanisms.

This information is however mainly qualitative due to the uncertainty associated with this method, although in certain cases the permeability from FT can be compared with those derived from core and well test analysis.

The nature of a pretest is such that only invasion filtrate fluid is withdrawn and spherical flow, a combination of horizontal and vertical flow, is induced. The general form of permeability during this flow period is:

$$k_s = \sqrt[3]{k_v(k_h)^2}$$

where:

k_s: spherical permeability (mD)

k_h: horizontal permeability (mD)

k_v: vertical permeability (mD)

The effective permeability corresponds to the mud filtrate. Additionally, in the near wellbore zone, the formation parameters may have changed due to drilling fluid invasion. Moreover, the setting procedure of the probe into the rock may create additional formation damage that will impact the permeability determination.

During a pretest, the probe is set and sealed into the formation. Fluid flows and a spherical flow pattern is created. The flow regime analysis for the pretest will be discussed in next sections. The drawdown pressure will depend on the permeability of the formation. After the drawdown stage there is a shut-in and the pressure is measured during buildup and stabilization. The time required for the pressure to stabilize is a function of reservoir permeability. Using pressure transient analysis it is possible to determine permeability either from the drawdown or from the shut-in period. While the latter is similar in principle to a PTA analysis with a dedicated model, the permeability (or mobility) determination in the drawdown is usually based on a steady state spherical flow assumption and equation. This equation is discussed in section 11.F.4.

The main limitations of a pretest for permeability determination are:

- The drawdown pressure may be very small in formations with very high permeability with low fluid viscosity causing the signal-to-noise ratio to be small.
- In very low permeability formations the drawdown can reach very high values that may cause the saturation pressure to be reached. In modern tools, the drawdown rate can be controlled from surface setting a maximum drawdown pressure to avoid this.
- The radius of investigation is quite small, so the permeability measured is probably from the invaded zone, which is not a complete representation of the formation permeability.
- The mud cake may block the probe and, in addition, setting the probe may cause further formation damage.

Anisotropy

Anisotropy is defined as the ratio between vertical and horizontal permeability (k_v/k_h). FT tools allow calculation of anisotropy. One of the main operational procedures for determining anisotropy is the Vertical Interference Test (VIT). The FT tool is configured with a combination of probes and/or packers, allowing the open hole to be tested and monitored at several points on the tool. The calculation of vertical and horizontal permeability can then be carried out.

11.C Tool description

Most modern FT tools are modular. This means that the tool string can be configured according to the test objectives. One of the simplest configurations of the FT tool is used to measure formation pressure, assembling the single probe module with the hydraulic module and the electric power module that also provides telemtry. Permeability and anisotropy can be addressed with more than one probe or a dual packer. Fluid sampling requires chambers, fluid analyzers and pump out modules, among others.

The modular nature of the string allows a multi-tool assembly to be run in hole with the advantages of saving rig costs, accurate measurements of temperature and pressure, identification of fluid type in real time, multisampling in a single trip and surface-controlled rate.

The following is a brief description of these modules.

- The **electric power module** provides power for the FT tool, converting AC power from surface to DC at the tool. It also establishes communication with the surface logging unit. This is the default module that is mounted at the top of the FT string used in all string configurations.

- The **hydraulic power unit** converts electrical power to hydraulic power for the probe module. An electric motor drives a fixed-displacement pump and, by counting the motor revolutions, the pumped fluid volume can be quantified.

- The **single probe module** allows the pressure and fluid communication between the FT tool string and the formation. It is coupled to the hydraulic power module.

  The probe is surrounded by a rubber packer. The tool is set by activating the hydraulic module which pushes the probe through the mudcake to make a seal with the formation. Backup piston push against the opposite side of the wellbore and support the tool in the hole. Modern tools are equipped with two different pressure gauges; a strain gauge and a

highly accurate and fast dynamic response quartz gauge. Once the communication between the formation and the tool has been made the formation pressure is measured using both. Additionally, this module, using temperature and resistivity sensors, provides differentiation between water and hydrocarbon, which is very helpful if a sampling operation is planned.
Depending on the reservoir and fluid properties, different type of probes can be used. From Darcy's law it is known that the rate is proportional to the imposed delta pressure, the cross sectional area and permeability, and inversely proportional to the viscosity:

$$\frac{\delta P}{\delta x} = -887.2\,\frac{q_x \mu}{k_x A}$$

For tight formations or very viscous fluids, the pressure drop imposed by the hydraulic module may not be sufficient to obtain a significant rate needed for pressure testing or sampling. Therefore, the two possible solutions are either to increase the hydraulic capacity or increase the flow area through a larger probe. Some of the available probes on the market are described below:

- Standard probe: The smallest of the probes. Useful for consolidated and moderate to high permeability formations.
- Large diameter probe: Used in good hole conditions with low permeability formations as well as unconsolidated formations.
- Large area packer: features an area more than 20 times larger than the standard probe, with good results in tight formations.
- Extra-large diameter probe: reduces drawdown and allows pumping at higher rates. Improved flow conditions compared to the large-diameter probe.
- Oval probe: features an area 60 times larger than the standard probe.

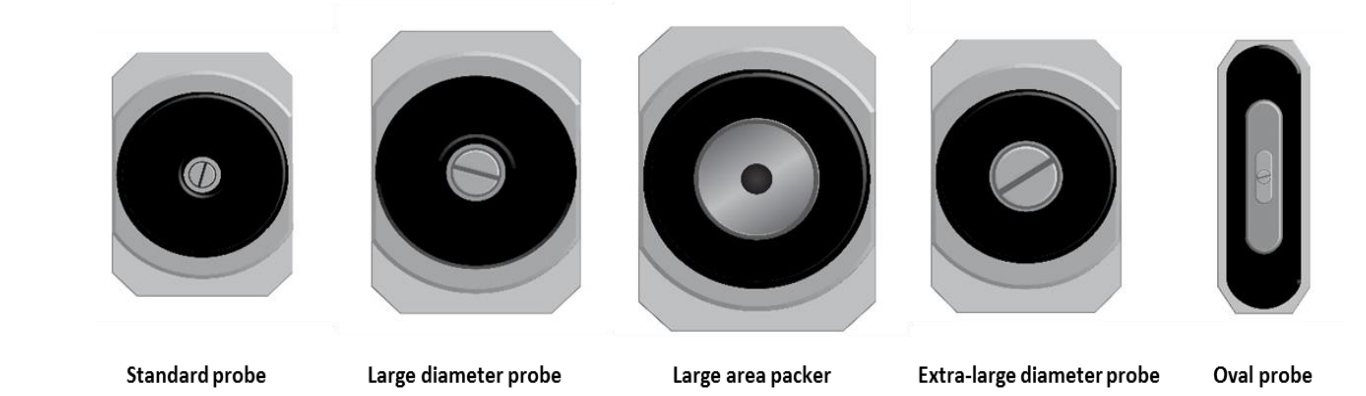


Fig. 11.C.1 – Formation tester Probes

- If a representative formation fluid sample is one of the objectives of the test, the **sample chamber module** may be assembled in the tool string allowing communication between the probe module and the sample bottles. The volume allowable, as well as the number of chambers, will depend on the service provider, weight and length considerations. The standard chamber can handle between 1 to 6 gallons.

- The **multisample module** can be used with or without the sample chambers. This module comprises several chambers (approx. 0.12 gallons each), the number and volume of bottles vary with the service provider. These samples are suitable for PVT analysis. The main advantage of this module is that each sample is stored in individual bottles, pressure compensated or otherwise, which can be safely transported without needing fluid transfer.

- The **pump-out module** drives formation fluid from the tool back to the wellbore with no volume limitation. During sampling operations, this module pumps the contaminated fluid (e.g. invasion filtrate) to avoid taking unrepresentative formation samples. It is common practice to run the optical fluid analyzer to monitor the fluid being withdrawal. This module can work either pumping fluid from the formation to the borehole or pumping mud fluid through the tool e.g. to inflate the packers, or to the formation e.g. to carry out a minifrac job, or within the tool.

- If anisotropy identification is one of the main objectives of the FT job, the **multiprobe module** allows the assembly of a sink source (probe or double packer) and several observation probes. The sink source creates a disturbance in the formation and the observation probes identify barriers and allow the calculation of vertical and horizontal permeability.

- The **dual packer module** controls the isolation of a larger area of the formation. The advantage of this module is that it provides a greater flow rate with lower pressure drop increasing the depth of investigation to several meters. This module should be assembled with the pump-out module due to the need to inflate and deflate the packers. They can replace the conventional probes for testing and/or sampling, or can be operated in tandem for a vertical interference test.

- The **optical analyzer** is an optional module that can be attached to the FT tool string to identify fluid type. This sensor is helpful if representative samples are required for PVT analysis. In general practice this module is attached below the probe module but its location will depend on operational conditions. The principle of the optical analyzer varies by manufacturer. Some sensors use absorption spectroscopy to detect liquid and reflection measurements to detect gas. In other sensors, photometric recognition is used to observe an optical spectrum measuring the intensity of light passing through the fluid, identifying hydrocarbons and their components.

The figure below shows a FT diagram using the modules described above. The configuration and order of the modules will depend on operational conditions during the FT job.

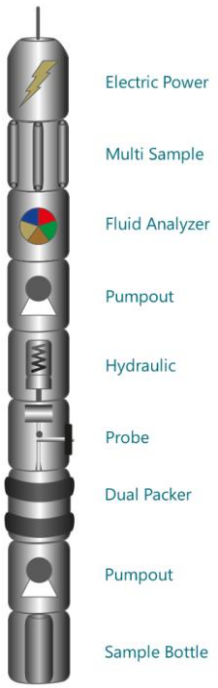


Fig. 11.C.2 – FT tool with different modules

11.D Typical FT job sequence

Before starting an FT sequence, it is common to identify the reservoir zones and fluid contacts using wireline logs such as gamma ray, resistivity, caliper, image logs, density, neutron-porosity, etc. This provides good definition of the required depth of measurements and samples.

After selection of the pressure points, the service company will run and set the FT tool in hole taking the measurements from the shallowest to the deepest point in the sequence.

When positioned, the tool is activated and the probe packer sets against the formation. An effective seal between the packer and the formation is achieved using hydraulically operated rear arms which push the probe packer with sufficient force against the wellbore wall. The probe emerges from the tool, and a small volume of invasion filtrate fluid is withdrawn from the reservoir. Depending on the service provider, the tools are equipped with a pretest chamber with a piston displacing between 0.1 to 100cc, the rate is controlled at surface.

There are a number of stages during the operation that can be identified in the pressure sequence versus time as is shown in the figure below. Before the tool is set, the pressure gauge measures mud hydrostatic pressure. Once the tool is set, a slight increase in pressure is observed due to mudcake compression. The pressure then starts to decrease during depressurization of the flow lines of the tool. The extraction of fluid stage is known as the drawdown and in normal conditions the pressure will drop. The duration of the period is quite short (seconds). The drawdown pressure will depend on the flow rate and permeability of the formation. Once the production stops, the pressure starts building-up, this is the shut-in stage which is again quite short (minutes). The Drawdown – Buildup sequence can be repeated as many times as required, depending on operational conditions. The objective of the pretest is to verify packer seal integrity and to obtain an initial formation pressure. Once the last Build-up is recorded, the tool is unseated, this stage is known as the retract cycle. Then the tool can be moved to a new, lower depth allowing the construction of the pressure profile versus TVD. A similar sequence will be noticed using the double packer module, but the duration of the operation will vary depending on the objectives (e.g. sampling).

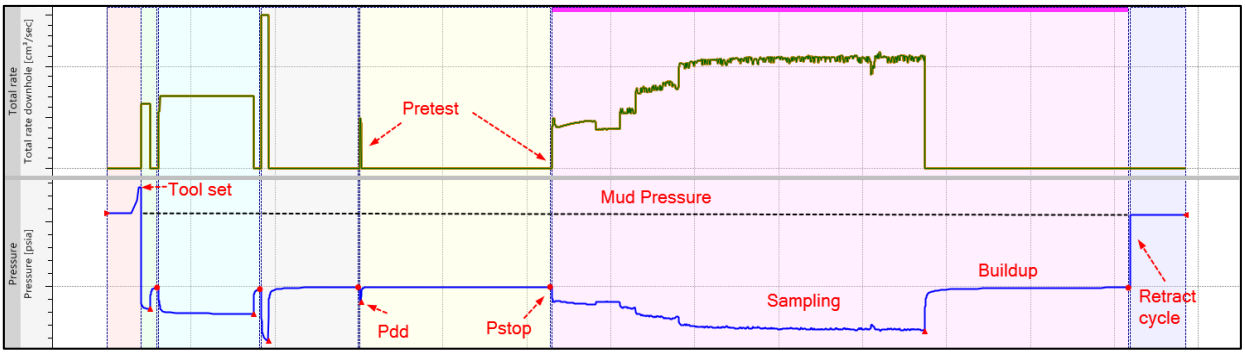


Fig. 11.D.1 – FT job sequence

It is important to recognize the different pressure behavior periods types and to separate them in order to use them adequately in the analysis.

Certain criteria can be used for a possible automated detection of these periods:

- **Tool set**: the observed pressure after the probe/pad or the packers is set can be less or greater than the hydrostatic pressure of the fluid in the well, depending on the model of tool used.
- **Pretest** is the pressure period recorded after setting the tool (Drawdown - Buildup sequence).
- **Sampling**: the pressure recorded as the fluid of the formation is allowed to flow or is being pumped to or through the tool.
- **Retract cycle**: the pressure returns to the hydrostatic mud pressure in the well when the tool is unset.
- **Vertical Interference Test**: The observed pressure is due to the pumped out volume at the distant probe, or inter-packer interval.
- A **mini DST** is an operation performed with a single probe or a dual packer, after the sampling period. It includes pumping periods and pressure buildup.
- A **minifrac** is an operation performed before a frac-job for determining the minimum *in situ* total stress. The pressure is observed during the injection and fall off periods.

11.E Data quality control

It is essential to check the reliability of the data before analyzing them to evaluate the pressure and the mobility.

The pretest consists of a very short duration drawdown of several seconds and a short buildup of several minutes. The main result is the value of the formation pressure before any production, but they also give the user the means to check data quality.

The drawdown/buildup sequence can be repeated two or three times to improve the reliability.

A quality control table can be generated with the rating and comments made from the pretests for each station.

11.F Pressure Analysis

As discussed in previous sections, FT data allow building a pressure profile along the formations. This is a combination of time and depth related data giving the advantage of a detailed characterization of the reservoirs. In the next sections a general workflow to interpret these data is described.

11.F.1 Data formats, data loading

The complete interpretation of a FT data set considers versus depth and versus time data. The time related data is displayed in Fig. 11.F.1, while the depth data in Fig. 11.F.2.

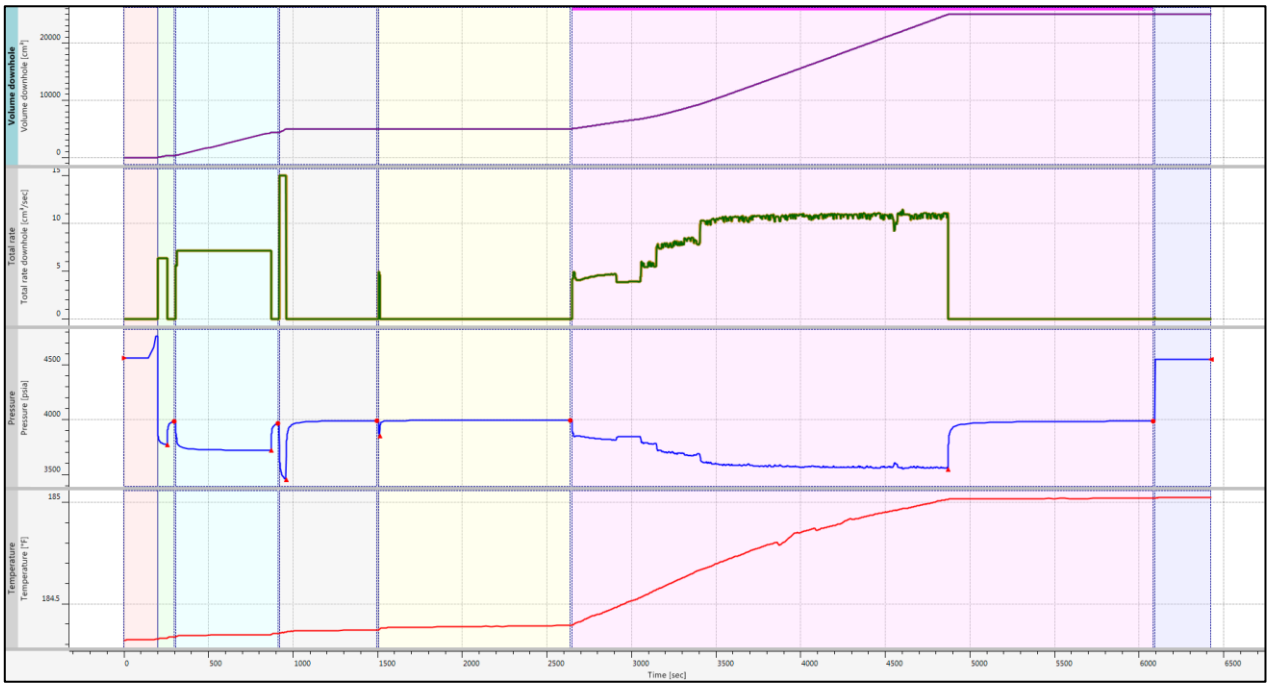


Fig. 11.F.1 – Versus time data in Azurite

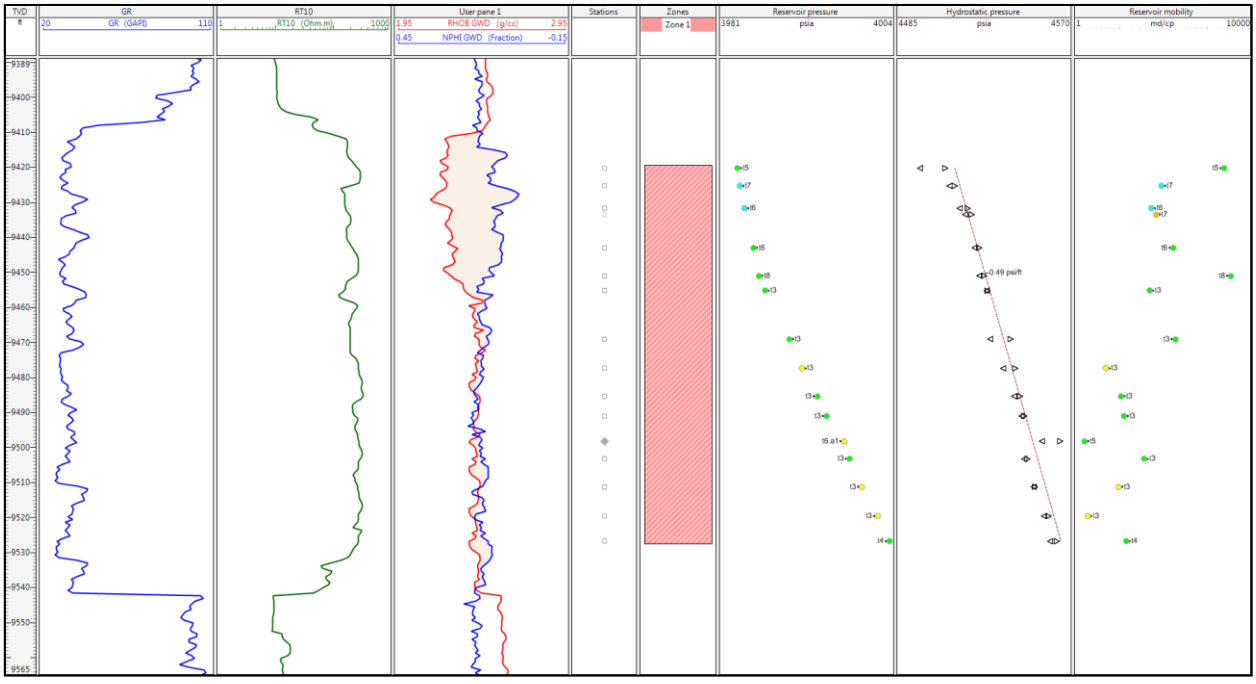


Fig. 11.F.2 – Versus depth data in Azurite

In general, the data comes in LAS, LIS, DLIS, ASCII, xls (Excel) formats. In Azurite, the load option automatically recognizes the file format and decodes as appropriate. The recognition is based on a built-in list associating mnemonics with data types (Mnemonic catalog) to which user defined associations can be added.

11.F.2 Automatic determination of tests

Depending on the input data, different calculations can be carried out automatically. These calculations require that reference data (pressure, temperature) be selected. The main workflow leads to the identification of the tests, and the determination of the final stabilized buildup pressure for each valid test. Assuming steady state hemispherical flow, the mobility is calculated as well. The reservoir pressure and the reservoir mobility tracks are generated and displayed on the depth plot (Fig. 11.F.3). This assumes that the choice of the preferred test for each station is also automated, and this can be driven by automated quality rating – see below.

The hydrostatic pressure is calculated considering mud pressure at start and end of each station. All downhole rate data (if available) are summed up to calculate a single rate channel, otherwise, the Compute Q calculation is launched on the station volume in order to get the total rate (QTT). Searching Drawdown - Buildup sequences on each station, the tests are identified and based on a built-in logic, they are qualified as Tool set, Pretest, Mini DST, or Retract cycle. Once the Pretests or MiniDST are identified, the drawdown pressures (P_{dd}) and the stop pressures (P_{stop}) are computed, as well as the drawdown mobilities. The reservoir pressure and mobility, to be displayed on the depth plot, will depend on the test quality (calculated from the buildup pressure and temperature stability, pressure standard deviation, and the drawdown mobility), these results allow to calculate fluid gradients.

The automatic calculation uses different default parameters to carry out the identification of tests and quality ratings.

11.F.3 Computation of rates from volumes

All downhole rate data are summed up and aggregated into a single total downhole rate channel, with mnemonic QTT. If no rate data are found, the Compute Q calculation is launched on the station volumes (total volume, VTT) in order to finally get total rate (QTT).

Most of the FT tools currently in use measure pumped volumes (usually expressed in cm^3), and the flow rate must be indirectly calculated from those measurements; service companies do not usually provide those calculated rates. Considering the importance in having reliable rate values for the following analysis steps, the Compute Q step can be quite sensitive. However, for the sake of the automatic test identification process, in Azurite this option is launched automatically on data sources with no rate data defined (only volumes). The total volume is calculated by summing all volume data found in the station, and the total rate is computed from this total volume. As a consequence, it is of primary importance, that the rates automatically calculated are carefully controlled before going further into the data analysis process. By default, in Azurite, QTT is computed by simple three point derivative.

In the Compute Q dialog shown below, the upper part of the plot displays the loaded cumulative volume gauge (cm^3), whereas the bottom part shows the resulting computed rate (cm^3/sec). Rate values are also displayed in the left-hand table.

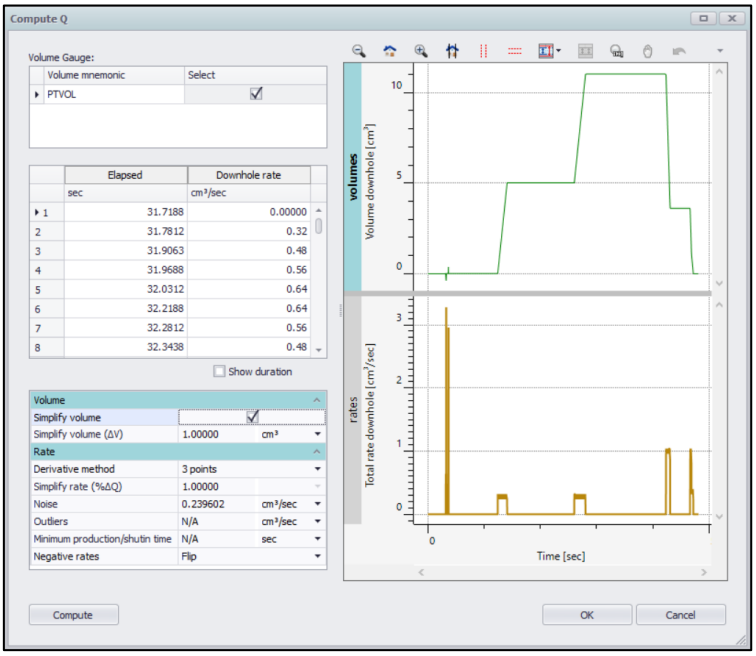


Fig. 11.F.3 – Compute Q from volumes in Azurite

- **Volume gauge**: VTT is the total volume, built by adding selected volume gauges from the station). Any individual volume gauge in the station can be used to compute Q. If volume data is missing in any station, Azurite will automatically fill gaps to calculate VTT retaining the last value before the absent values.
- **Simplify volume**: When checked, volume steps that differ by a specified value (1 cc by default) are merged together while conserving the overall cumulative. The value can be changed by the user.
- **Three point derivative**: QTT can be computed by simple point-to-point derivative. This straightforward computation is appropriate when the volume measurements carry a good precision.
- **Two point derivative**: it is the first order derivative y' = (y1-y2)/(x1-x2).
- **Simplify rate**: Rate values within the define percentage value of each other are merged together.
- **Noise threshold**: whatever value is lower than this value is considered as noise, and simply discarded from the final result.
- **Outlier(s)**: the rate data are truncated to this value, and whatever is above is redistributed on the whole rate history.
- **Minimum production/shutin time**: Any volume change/rate duration under this value is ignored
- **Flip negative rates**: makes negative rates positive. Although the volume is decreasing, this option makes the rate positives.
- **Ignore negative rates**: makes negative rates nil.

It is important to notice that the rate reconstruction algorithm ensures that the total measured cumulative volume is constrained to the measured data at the end of every flowing phase. This is achieved by eventually re-scaling the computed rate history.

11.F.4 Pretest calculations (P_{dd}, P_{stop}, drawdown mobility)

After the identification of tests, the automatic workflow defines the drawdown pressure (P_{dd}), stop pressure (P_{stop}), and drawdown mobility (M_{dd}) for each pretest or mini DST identified.

P_{dd}: The drawdown pressure. By default, it is the minimum pressure of the last half of the production sequence.

P_{stop}: The stop pressure (reservoir pressure). By default, it is the last pressure of the test, read on a line obtained by regression over the last 60 seconds of the buildup.

The figure below illustrates the identification of P_{dd} and P_{stop} for a pretest.

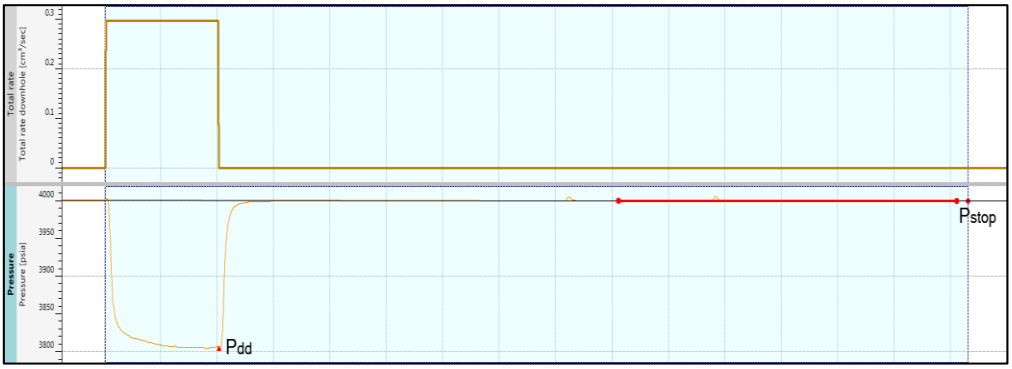


Fig. 11.F.4 – P_{dd} and P_{stop} from pressure channel

Drawdown mobility:

The general equation for flow to a point in an unbounded 3D homogeneous and isotropic porous medium can be expressed in the form

$$\frac{1}{R^2}\frac{\partial}{\partial R}\left(R^2\frac{\partial P}{\partial R}\right)=\frac{\varphi\mu c_t}{k}\frac{\partial P}{\partial t}$$

where R is the only spherical coordinate affecting the pressure solution.

Under steady-state conditions this flow equation can be solved to obtain:

$$P_i - P(R) = \frac{q\mu}{4\pi kR}$$

This can be rearranged to give:

$$M_{dd} = \frac{k}{\mu} = \frac{460.42}{R_p}\frac{q}{\Delta P_{dd}}$$

to determine the mobility from the drawdown at the spherical distance R_p from a point source (or point sink).

where:

R_p: spherical source radius, inches

q: average rate during Drawdown period, cm^3/s

$\Delta P = P_{stop} - P_{dd}$, psi

M_{dd}: spherical drawdown mobility, md/cp

k: permeability, md

μ: viscosity, cp

A spherical probe is not realistic, but it does give us an upper bound in terms of efficiency. For any realistic circular probe it follows that the drawdown must be higher and therefore the coefficient must also be higher.

As a realistic model, what we need is a solution for flow to a point or circular opening on a cylindrical wellbore. A general solution for 3D flow to a point on a no-flow cylindrical surface was presented by Goode and Thambynayagam (SPEFE, Dec. 1992). With standard dimensionless variables (used for radial flow) the solution can be expressed in the form

$$P_D(t_D, r_D = 1, \theta, z_D) = \frac{h_D}{4\sqrt{\pi}} \int_0^{t_D} \frac{e^{-z_D^2/4\beta}}{\beta^{3/2}} G(\theta, \beta) d\beta$$

Solving the above equation, with the necessary boundary conditions and variable transformations gives us:

$$M_{dd} = \frac{460.42}{r_{pe}} \left(1 + \sigma(r_{peD})\right) \frac{q}{\Delta P_{dd}}$$

The term in blue in the equation above can be replaced by a single term:

$$M_{dd} = C_{pf} \frac{q}{\Delta P_{dd}}$$

C_{pf} is denoted as the 'Probe flow coefficient' and it captures the unit conversions and the effect of:

- The actual sink probe (or probes) geometry
- The presence of the wellbore
- The anisotropy (often not considered)

Note that extensions of this equation are also possible for a straddle packer configuration.

The literature presents some equations for C_{pf} but they are not ready for generalization or extension to other situations. Starting from a general formulation of the diffusivity problem, KAPPA has developed general transient models to address all the possible geometries in anisotropic formations. The limiting form of those models provides the means to compute C_{pf} in all situations.

It should be noted that there are other methods to evaluate permeability/mobility for the pretests.

Alternative methods included in Azurite include the Flow Rate Analysis (FRA) technique from Baker, the Exact Method from Halliburton, and the Area Under method from Schlumberger. These "tight-zone" analysis methods have been developed to use more of the early and mid-time data to improve the accuracy of the calculated mobility when permeability is less than 1 md. In normal conditions they should provide mobility similar values when mobility (within the resolution of the pressure and rate measurement).

The 'Flow Rate Analysis' technique (or FRA) is derived from Darcy's law and splits the piston rate into the actual formation rate and the rate resulting from tool storage.

A plot of P(t) vs. formation rate should approach a straight line with negative slope and intercept P* at the P(t) axis and mobility calculated from the slope.

The FRA plot should yield identical slopes for both buildup and drawdown if there was constant compressibility.

$$P(t) = P^* - \frac{\mu}{kG_o r_i}\,(q_f)$$

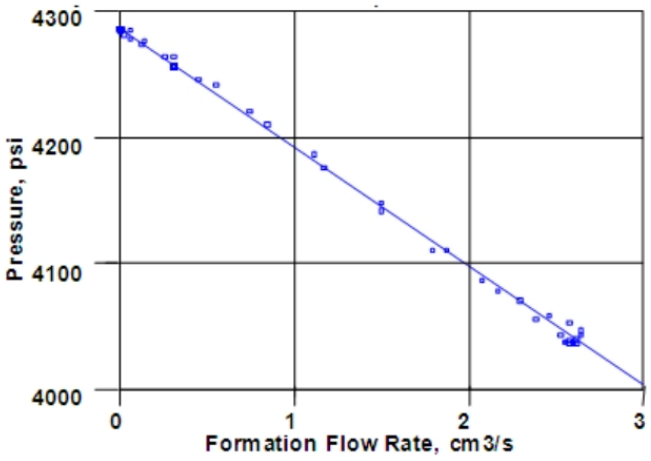


Fig. 11.F.5 – Formation Rate Analysis Method (courtesy from Baker)

The Exact Method presented by Halliburton (Proett et al.-SPE 39768 and SPE 64650), is a closed-form, analytical spherical solution that includes flowline storage to predict the dynamic pressure behavior of formation tests more fully. The exact solution applies for all times and does not require substantial numerical evaluation. It allows accurate formation evaluation with only early- and intermediate-time data and is usually applied in low mobility reservoirs. It is based on fitting a line to the natural logarithm of the buildup data time derivative.

$$\ln\left(\frac{dP_{bu}}{dt}\right) = \ln\left(\frac{\beta}{\alpha}\right) - \frac{t'}{\alpha}$$

$$\text{Slope} => \alpha \qquad M_{dd} = \frac{C_{pf}}{\beta}\left(1 - e^{\frac{t_{dd}}{\alpha}}\right)$$

$$\text{Intercept} => \beta \qquad P_f = P_{dd} - \beta$$

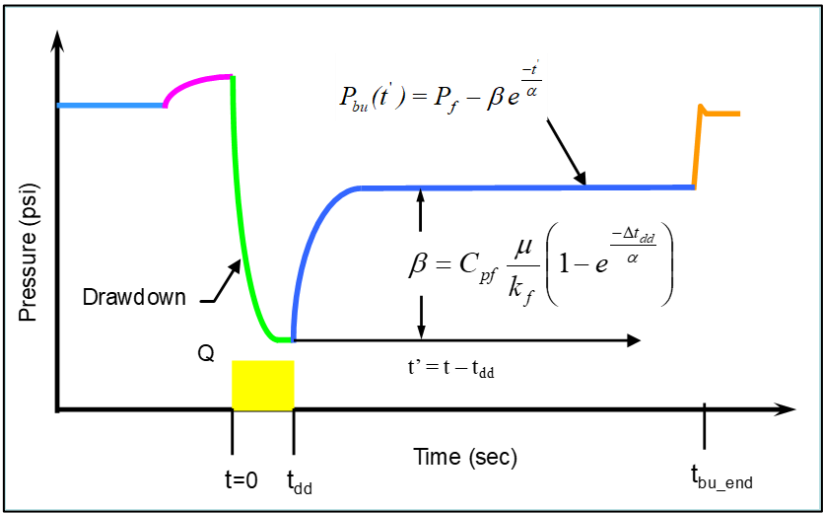


Fig. 11.F.6 – Halliburton Exact pretest analysis method

In low mobility formations where steady-state conditions are difficult to reach, the area-under method can be applied. This method uses the integral form:

$$M_{dd} = C_{pf} \frac{V}{\int_0^{td} \Delta P(t).dt}$$

Where the pressure integral considers the part of the pressure below P_{stop} as shown in figure below. V is the volume after decompression of the flowline (i.e. after the pressure crosses P_{stop}).

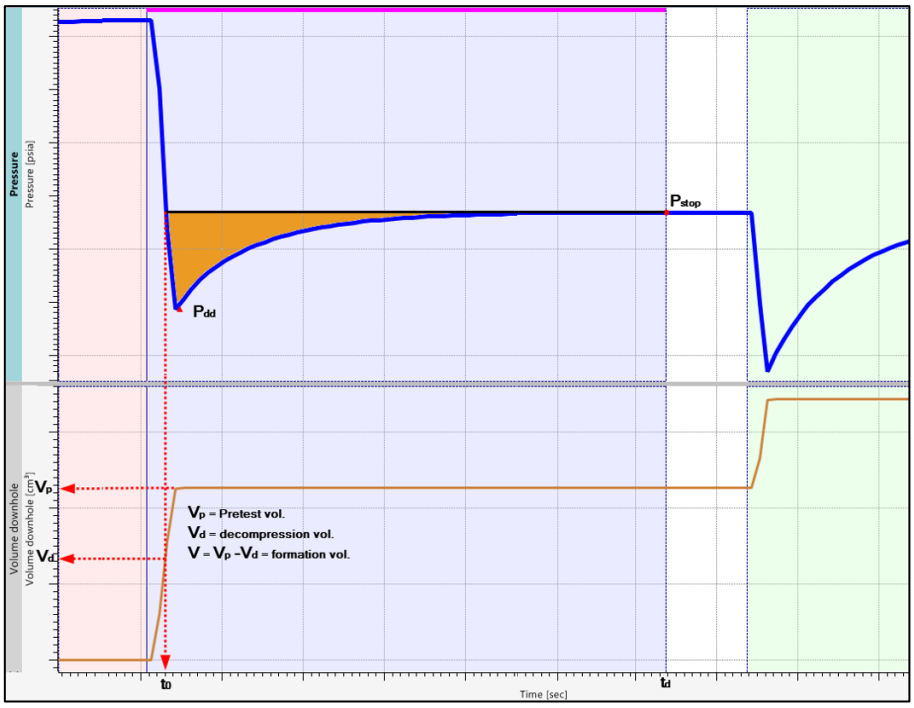


Fig. 11.F.7 – Area-under method

11.F.5 Pretest quality assessment and rating

The test quality is calculated from the pressure standard deviation, the buildup pressure stability, the buildup temperature stability, and the drawdown mobility. A rating in quality is carried out based on this final score as illustrated in the figure below. The maximum score is 4 which corresponds to a High quality test (Excellent), while the minimum score (0) corresponds to a Low quality test. Each quality score has a color code (light blue- excellent, light green - good, yellow - satisfactory, orange - fair, red - low quality, gray - unknown).

Data Quality			User Inputs				Ratings & Comments										Norm.
			Setting		Range	Weight											
Criterion		Units	Valid		>1	0-1	Excellent		Good		Satisfactory		Fair		Low Quality		%
Buildup Stability	Std dev.	psia	≤	0.5	10	0.5	≤	0.088914	≤	0.281171	≤	0.88914	≤	2.811707	≥	2.811707	17.9%
	Pressure	psia/min	≤	0.1	100	1	≤	0.003162	≤	0.031623	≤	0.316228	≤	3.162278	≥	3.162278	35.7%
	Temp	F/min	≤	0.01	5	0.5	≤	0.002991	≤	0.006687	≤	0.014953	≤	0.033437	≥	0.033437	17.9%
Mobilities	Mdd	md/cp	≥	1	100	0.8	≥	31.62278	≥	3.162278	≥	0.316228	≥	0.031623	≤	0.031623	28.6%
Test Quality	**Score**	**4-0**		**2**			≥	**3.5**	≥	**2.5**	≥	**1.5**	≥	**0.5**	≤	**0.5**	100.0%

Fig. 11.F.8 – Quality assessment and rating

- Setting: defines if the parameter is valid or not (e.g. by default, the pressure standard deviation is considered valid if it is less than or equal to 0.5 psia).
- Range: geometric factor that scales the valid entry for the lower and upper limits of the rating.
- Weight: determines the relative weight for each parameter in the final rating score.

Then, knowing the Pretest/MiniDST test quality, Azurite automatically selects, for each station, the formation pressure (P_{stop}) and the mobility (M_{dd}) of the Pretest/MiniDST with the best quality, and shows it into dedicated tracks into the Logs tab.

11.G Standard pressure transient analysis

In view of the probe configuration, which is relatively small and in the majority of cases also very small compared to the effective bed thickness (that can be up to several meters), depending on the distribution of vertical permeability seals, the pressure behavior will invariably show spherical flow before the possible onset of classical infinite acting radial flow.

11.G.1 Common features

Spherical flow

During this flow regime a straight line of slope –½ (negative half slope) will develop on the Bourdet derivative (corresponding to spherical or hemi-spherical flow). The pressure during that flow regime is proportional to $^{1}/_{\sqrt{\Delta t}}$.

The exact relation between the pressure change and the 'one over the square root' of the elapsed time is:

$$\Delta p = \frac{70.6qB\mu}{k_s r_s} - \frac{2453qB\mu\sqrt{\emptyset\mu c_t}}{{k_s}^{3/2}} \frac{1}{\sqrt{\Delta t}}$$

With: $k_s = (k_r^2\, k_v)^{1/3}$

That can be expressed:

$$\Delta p = a - m\frac{1}{\sqrt{\Delta t}} \quad where \quad m = \frac{2453qB\mu\sqrt{\emptyset\mu c_t}}{{k_s}^{3/2}} \quad and \quad a = \frac{70.6qB\mu}{k_s r_s}$$

The Bourdet derivative then becomes:

$$\Delta p' \approx \frac{d\Delta p}{dln(\Delta t)} = \Delta t\frac{d\Delta p}{d\Delta t} = \Delta t\frac{m}{2\Delta t^{3/2}} = \frac{1}{2}m\frac{1}{\sqrt{\Delta t}} = \frac{1}{2}(a - \Delta p)$$

and thus will show a -1/2 slope.

From this flow regime it is possible to determine spherical permeability (k_s). If k_r is known, anisotropy $^{k_v}/_{k_r}$ can be determined.

Radial flow

Chapter 2 and 7.B can be referenced for the development of this flow regime.

The figure below illustrates the flow regimes that are commonly found in an FT operation.

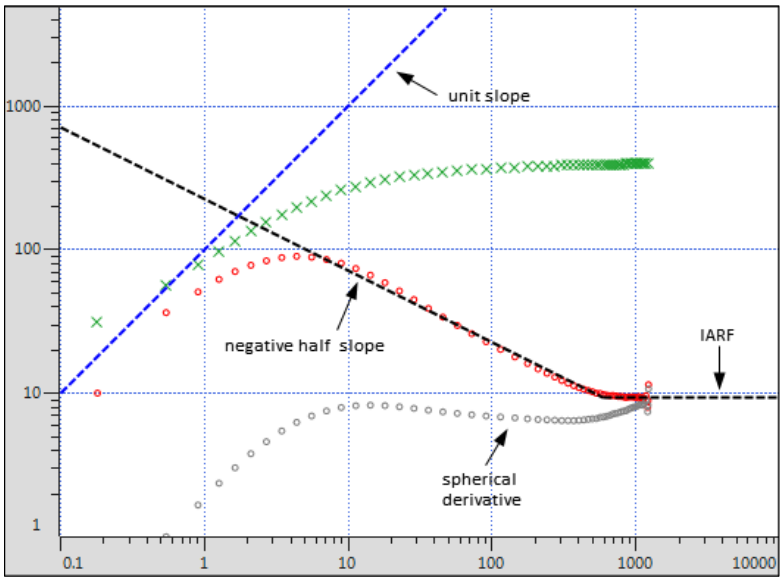


Fig. 11.G.1– Loglog plot of Mini-DST

11.G.2 Analytical model matching

Once the diagnostic tools are used to evaluate the spherical and the radial mobilities, more detailed and adequate models can be generated which take into account the tool geometry and specification and the reservoir main features.

The analytical models must be created in order to cover the widest possible range of cases.

- The main type of probes, single or multiple:

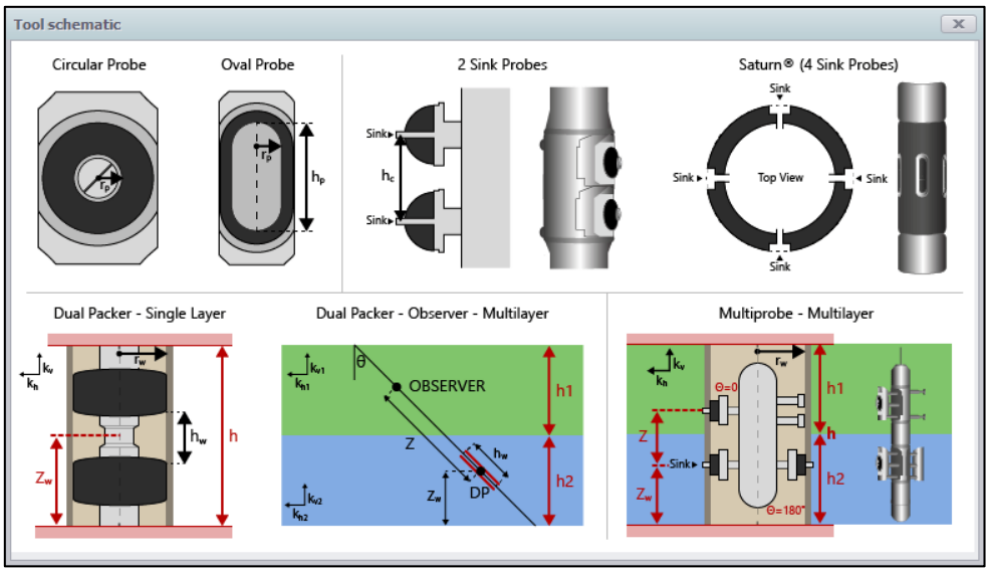


Fig. 11.G.2 – Different type of probes and geometries covers by the analytical models

- Several type of reservoirs can be considered, including the possibility of multiprobe tools:

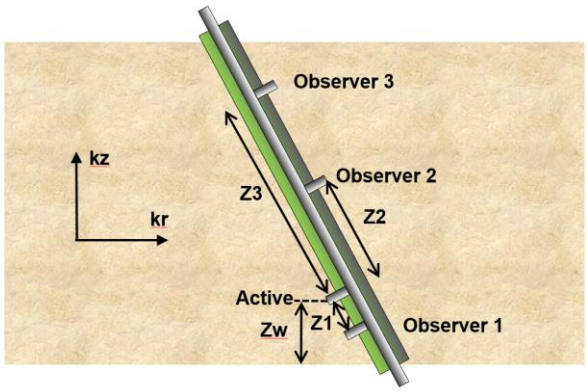


Fig. 11.G.3 – single layer multiprobe

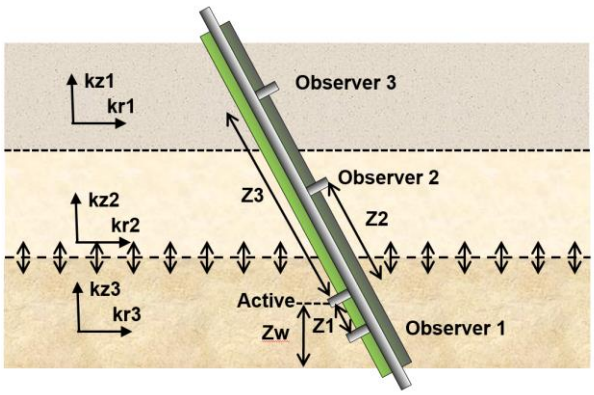


Fig. 11.G.4 – multilayer multiprobe

The table below illustrates the possible combinations of models available currently in Azurite.

Model / Probe	SINGLE LAYER							
	Anisotropy		Deviation		Orientation		Multi-probe	
	A	N	A	N	A	N	A	N
Circular	✓	✓	✓	✓	✓	✓	✓	✓
Dual Packer	✓	✓	✓	✓	-	-	✓	✓
Oval	✓	×	✓	×	✓	×	✓	×
Dual	✓	×	✓	×	✓	×	✓	×
Saturn	✓	×	✓	×	-	-	✓	×

Model / Probe	MULTI-LAYER							
	Anisotropy		Deviation		Orientation		Multi-probe	
	A	N	A	N	A	N	A	N
Circular	✓	✓	✓	✓	×	✓	✓	✓
Dual Packer	✓	✓	✓	✓	-	-	✓	✓
Oval	✓	×	✓	×	×	×	✓	×
Dual	✓	×	✓	×	×	×	✓	×
Saturn	✓	×	✓	×	-	-	✓	×

Model / Layers (s)	Reservoir type				Boundary											
	Homogeneous		Dual porosity		Infinite		Single fault		Channel		Intersecting fault		Rectangle			
	A	N	A	N	A	N	A	N	A	N	A	N	A	N	A	N
Single-layer	✓	✓	✓	✓	✓	-	✓	✓	✓	✓	✓	✓	✓	✓	✓	✓
Multi-layer	✓	✓	×	✓	×	-	×	✓	×	✓	×	✓	×	✓	×	✓

A: Analytical model
N: Numerical model
Multiple probe: Circular as observer
-: Not applicable

Fig. 11.G.5 – Current model catalog

The analytical models are created using the general Goode and Thambynayagam solution already mentioned above:

$$P_D(t_D, r_D = 1, \theta, z_D) = \frac{h_D}{4\sqrt{\pi}} \int_0^{t_D} \frac{e^{-z_D^2/4\beta}}{\beta^{3/2}} G(\theta, \beta) d\beta$$

The geometry function G is used to add the effect of the wellbore shape:

$$G(\theta, \beta) = \frac{8}{\pi^2} \sum_{n=-\infty}^{\infty} \int_0^{\infty} \frac{\cos(n\theta)\beta e^{-\alpha^2\beta}}{\alpha\left[J_n'(\alpha)^2 + Y_n'(\alpha)^2\right]} d\alpha$$

These equations are solved under the several conditions:

- For the probe geometry (i.e. a line source is used for oval probe)
- For the wellbore surface corrections:

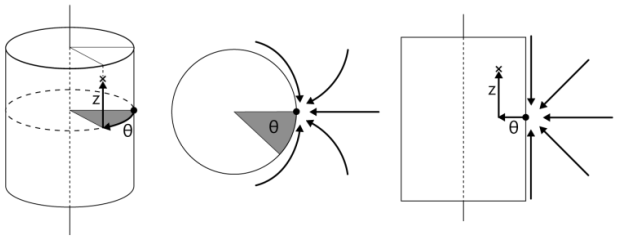


Fig. 11.G.6 – Probe wellbore geometry

- The anisotropy cases are converted to isotropic cases by coordinate change

The Probe Flow Coefficients Cpf, used to take the probe geometry into account in the steady state drawdown analysis are deduced from these solutions:

For circular probe it is:

$$C_{pf} = \frac{460.42}{r_{pe}}\left[1+\sigma(r_{peD})\right]$$

Where

- rpe represents the effective probe dimension and distance to pressure points,
- rpe = rp / sqrt(2) for circular probes.

The sigma function is used to correct for the effect of the wellbore:

$$\sigma(z_D) = \frac{2}{\sqrt{\pi}}\int_0^{\infty} e^{-(x^2+0.42 z_D/x)}dx$$

For oval probe it is:

$$C_{pf} = \frac{460.42}{L_{pe}}\left[ln\left(1+\frac{L_{pe}}{r_{pe}}\right)+\sigma_{LS}(r_{peD},L_{peD})\right]$$

Where:

- rpe and Lpe represent the effective probe dimension and distance to pressure points,
- The parameters are numerically determined for oval probes.

The sigma function, used to correct for the effect of the wellbore, is:

$$\sigma_{LS}(r_{peD},L_{peD}) = \int_0^{\infty}\left[\mathrm{erf}\left(\frac{L_{peD}+r_{peD}}{2}x\right)-\mathrm{erf}\left(\frac{r_{peD}}{2}x\right)\right]e^{-0.84/x}\frac{dx}{x}$$

It is the description of the tool, of its probes and of the geometry which makes the selection of the adequate analytical solution.

Once the proper model is selected, the model matching optimization allows to adjust the unknown reservoir and well parameters.

The main features of the various models are described in more details below.

11.G.3 Tool types, solutions and sensitivity

11.G.3.a Single circular active probe

The pressure behavior is modeled with the point source solution in a no-flow cylindrical surface.

The probes can be placed in 'side' or 'up/down' position depending on the type of well as illustrated below.

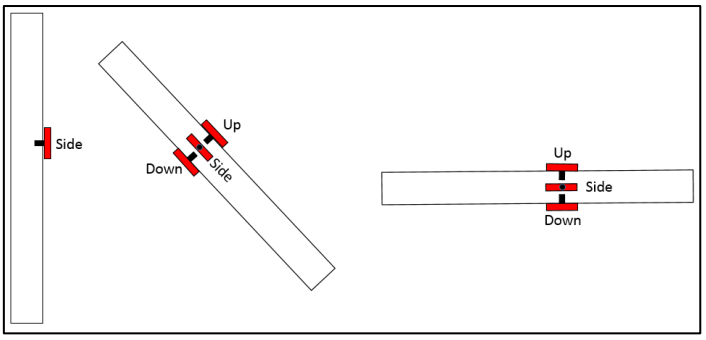


Fig. 11.G.7 – Probe position and orientation

Due to its configuration, there will be horizontal and vertical contribution to flow and consequently the spherical flow (1) will develop differently depending on the probe orientation.

If the test is long enough and upper and lower vertical flow boundaries have been reached then a classical radial flow (2), IARF, could be observed in the reservoir.

The figure below illustrates the configuration of the probe and the flow regimes associated.

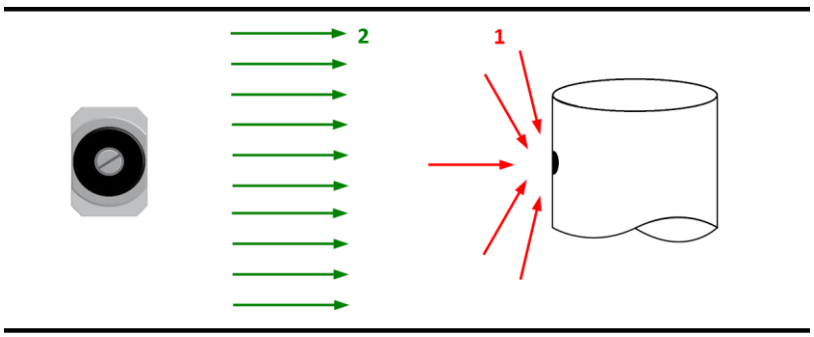


Fig. 11.G.8 – Circular probe flow regime

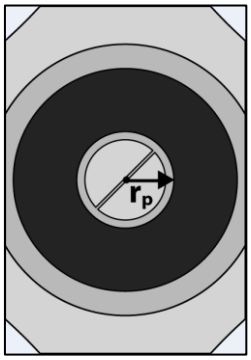


Fig. 11.G.9 – Single Probe

In the following example oil is used as the reference fluid, single phase, PVT parameters are default:

Parameter	Value
r_w (in)	3.6
h (ft)	30
z_w (ft)	15
k_r (mD)	33.33
r_p (in)	1.0
Φ (%)	10
p_i (psia)	5000
q (cm^3/s)	6

Fig. 11.G.10 – Parameters values

The following plot is the extraction of the simulated buildup with a duration of 1 hour. This duration might not be practical in a FT environment as the chances of hydrostatic differential sticking will be higher so station time would be much shorter and chances of seeing anything but spherical flow is high as the radial permeability decreases.

There is no effect caused by the deviation of the well since the reservoir is isotropic.

The three models (vertical, horizontal and slanted at 45 °) overlay perfectly because the spherical and radial permeabilities are equal.

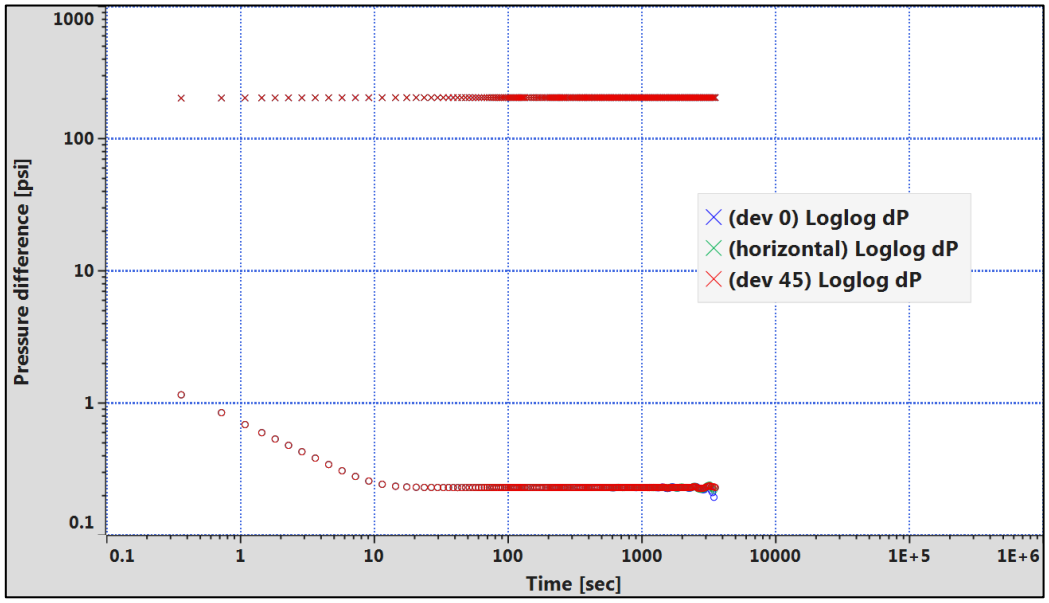


Fig. 11.G.11 – Sensitivity to the well deviation in isotropic formation

The next plot shows the comparison of the responses from a vertical, slanted (45°) and horizontal well with the probe placed on the 'side' with an anisotropy of kz/kr=0.001.

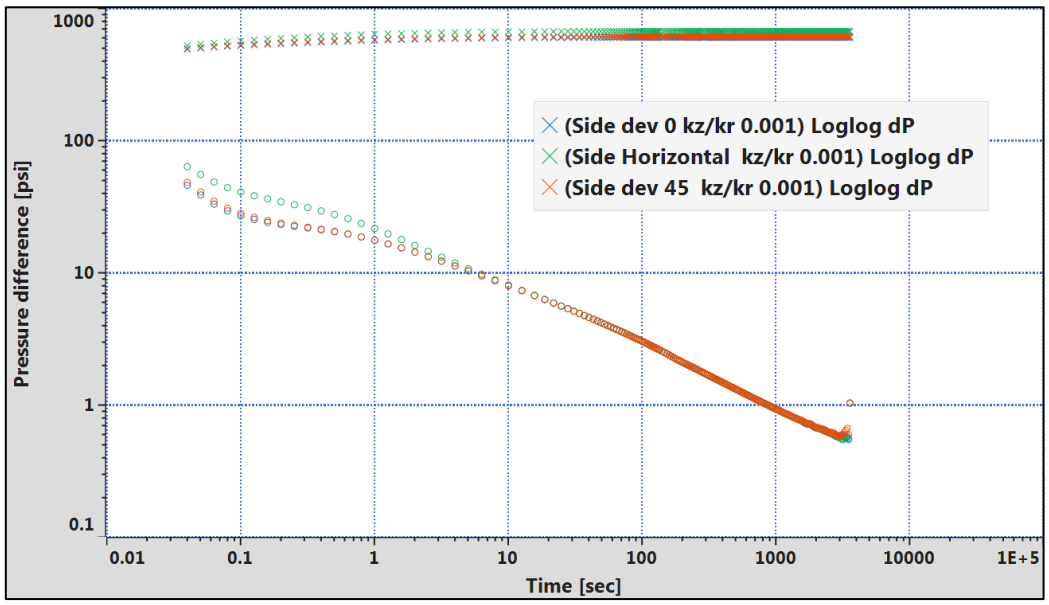


Fig. 11.G.12 – Sensitivity to the well deviation with anisotropy

The initial spherical flow is more exposed to the vertical permeability in case of side probe in a horizontal well, the pressure drop is greater than the deviated and vertical wells.

The following plot illustrates the difference of the placement of the probe in a horizontal well.

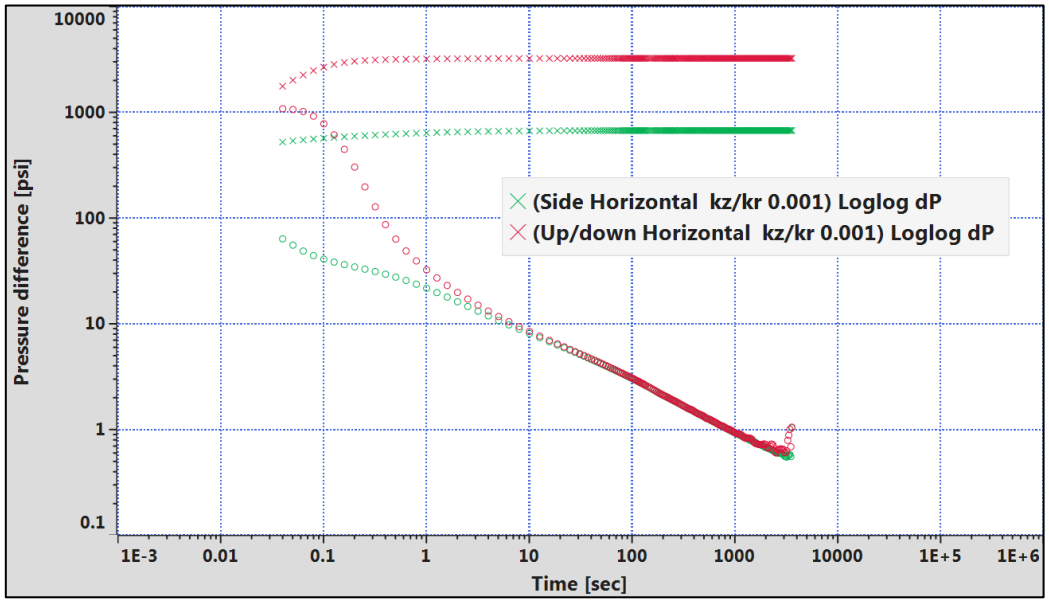


Fig. 11.G.13 – Sensitivity to the probe placement in a horizontal well

The early time pseudo linear flow (pre-spherical flow) is directly exposed to the vertical permeability in case of up/down probes. The low vertical permeability induces a low quality transmissibility between the well and the formation, therefore a larger pressure drop.

The below figure illustrates the difference made by the placement of the probe in the deviated well (45°).

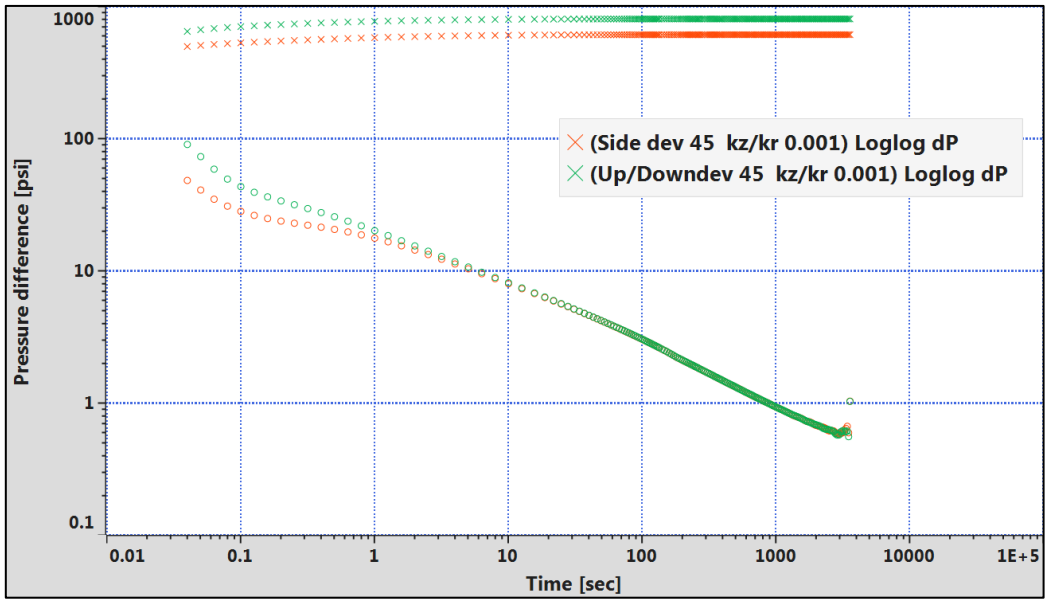


Fig. 11.G.14 – Sensitivity to the probe placement in a slanted well

As for the horizontal well case, the up/down probe is more exposed to the low vertical permeability than the side probe but induces a smaller difference than in the case of horizontal well.

11.G.3.b Single oval active probe

The oval probe solution is modeled by considering a line source sink on the side of a no-flow cylindrical surface.

The probe can be placed in 'side' or 'up/down' position depending on the type of well.

Due to its configuration, there will be horizontal and vertical contribution to flow and consequently the spherical flow (1) will develop differently depending on the probe orientation.

Depending on the reservoir parameters and the storage effect, an early radial flow (1) may be observed. As with circular probes, there is a vertical contribution to flow and the spherical regime (2) will develop. The spherical flow is defined with straight line of slope –½ (negative half slope) in the Bourdet derivative as is shown later on. If vertical borders are reach IARF (3) is observed.

The next figure shows a schematic for the tool description and a schematic for the flow regimes.

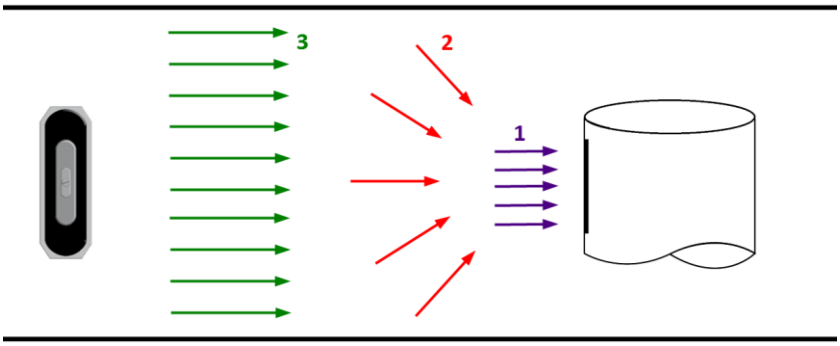


Fig. 11.G.15 – Oval Probe flow regime

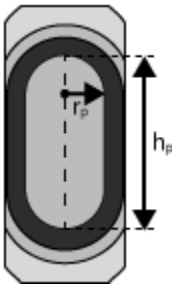


Fig. 11.G.16 – Oval Probe parameters

In the following example oil is used as the reference fluid, single phase, PVT parameters are default:

Parameter	Value
r_w (in)	3.6
h (ft)	30
z_w (ft)	15
k_r (mD)	33.33
r_p (in)	1.0
h_p (in)	3.84
A (in^2)	6.83
Φ (%)	10
p_i (psia)	5000
q (cm^3/s)	6

Fig. 11.G.17 – Table of parameters values

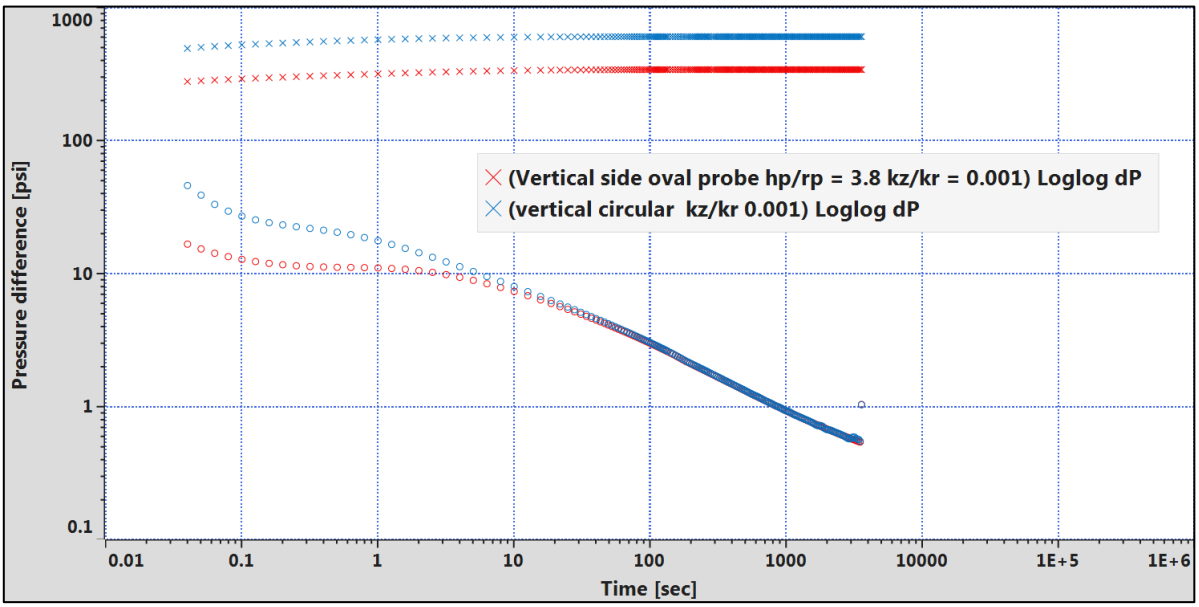


Fig. 11.G.18 – Comparison between Circular and Oval probes

The flow area influences directly the pressure drop observed for the same rate, the larger oval flow area induces a smaller pressure drop.

The sensitivity of the flow area of the oval probe is illustrated below, the well is vertical, kz/kr=0.001. The ratio hp/rp from top to bottom varies from 1 to 6.8.

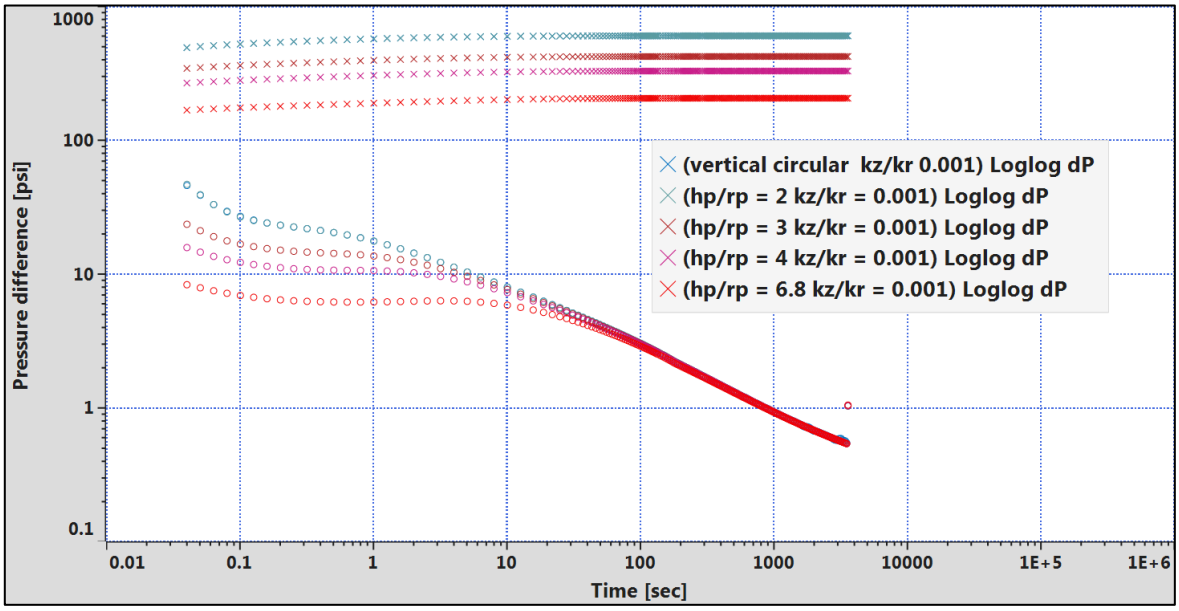


Fig. 11.G.19 – Sensitivity to the probe area

It can be seen as hp goes towards 2 x rp (from oval to circular) the oval probe response get close to the pure circular.

The figure below illustrates the difference of an oval side probe in a 45° Slanted, a Horizontal and a Vertical well with kz/kr=0.001:

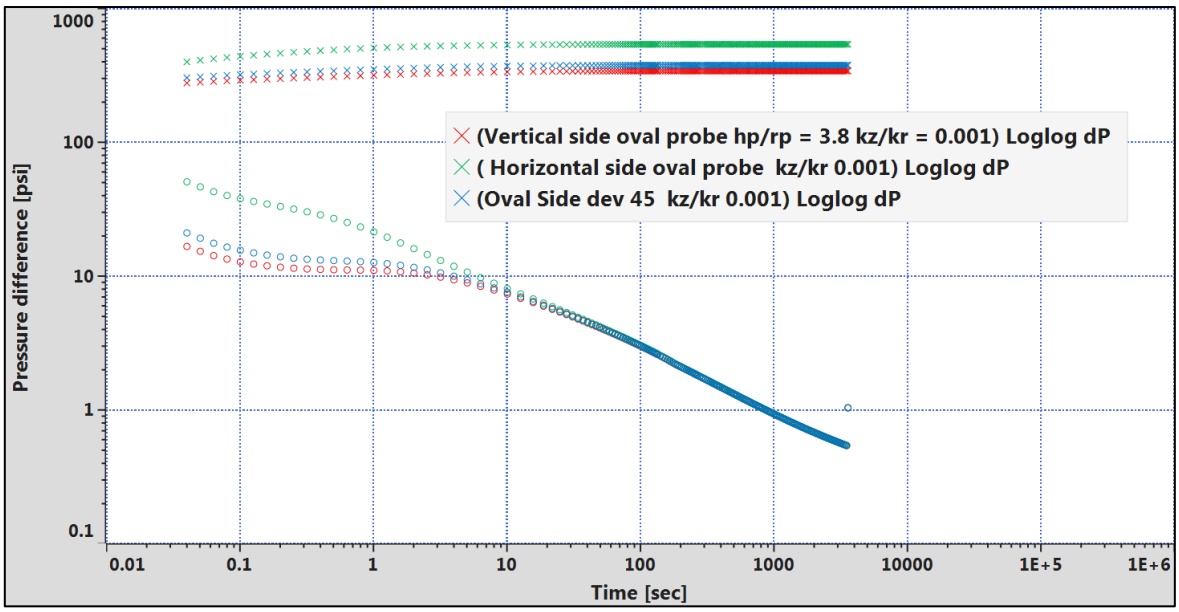


Fig. 11.G.20 – Influence of the well deviation

Due to the shape of the oval probe, the early pseudo elliptic flow transmissivity is more sensitive to the vertical permeability in case of horizontal well.

The following plot illustrates the difference of the placement of the probe in a horizontal well (kz/kr=0.001).

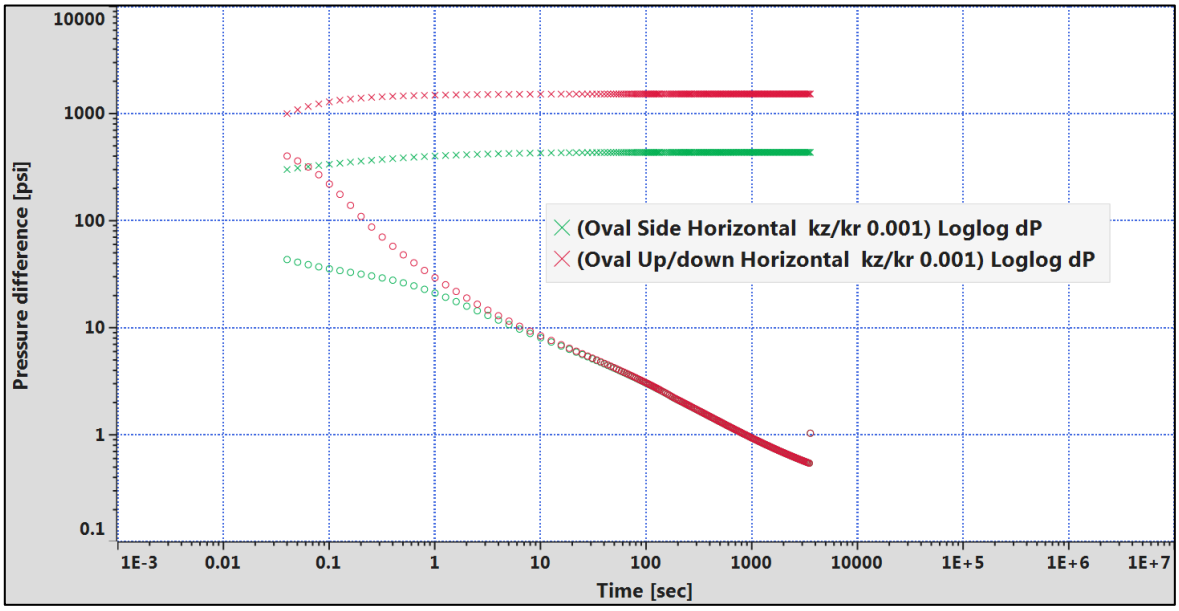


Fig. 11.G.21 – Influence of the Oval Probe position in a horizontal well

For the same geometrical reason, the early flow is more exposed to the low vertical permeability in case of up/down probe.

11.G.3.c Two sink probes (dual circular)

The dual probe module consists of two in-line circular probes (lined up along the wellbore). The solution is an extension of the single circular probe model treating the effect of the additional probe handled as interference.

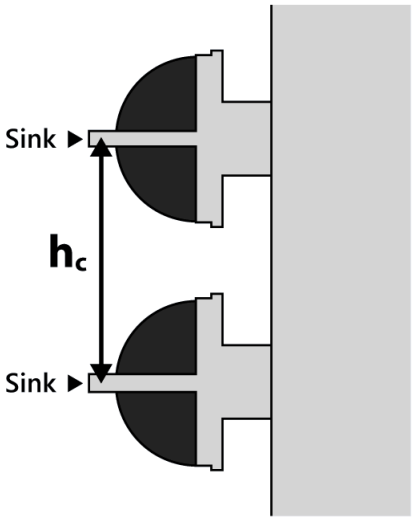


Fig. 11.G.22 – Dual probe geometry

A separate strain gauge measures the pressure response of each probe. The pressure used by the analyst is the pressure measured by a quartz gauge some 8 ft below the top sink and some 7.5 ft from sink two, hydraulically connected to both probes. The advantage of such a configuration is backup purposes, if one probe fails to seal, hopefully the other probe will hold and the individual strain gauge can be used.

The following input parameters were used to run the sensitivity study of the probe configurations in a vertical, slanted at 45° and horizontal well.

Parameter	Value
r_w (in)	3.6
h (ft)	30
z_w (ft)	15
k_r (mD)	33.33
r_p (in)	1.0
h_c (in)	7.25
Φ (%)	10
p_i (psia)	5000
q (cm^3/s)	6
k_z/k_r	0.001

Fig. 11.G.23 – Table of parameters values

Comparison between the single circular, oval and dual sink probes all with the same flow area of A=6.28 in^2. The placement at the side in a vertical well. Both the oval and circular responses overlay, the dual sink probe is slightly different at early time due to the separation of the two probes creating a double spherical flow before going to a single spherical flow with an equivalent total flow area.

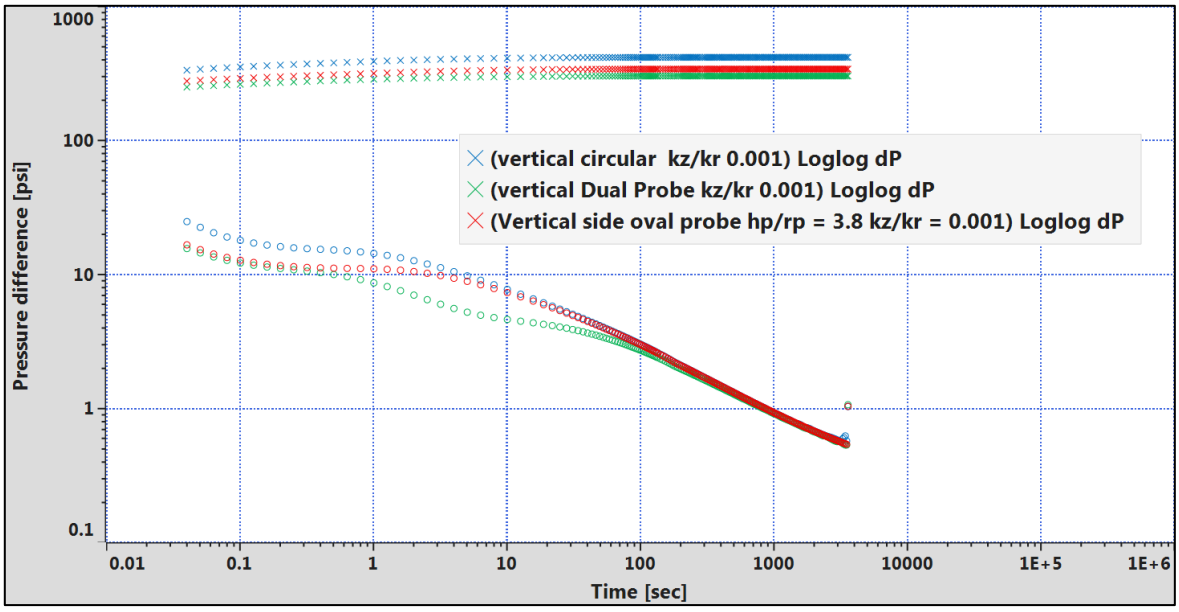


Fig. 11.G.24 – Comparison between Dual probe and single probe

Influence on distance between probes: Current model h_c 7.2”, varying from 3.6” to 14.5” vertical well probe position to the side.

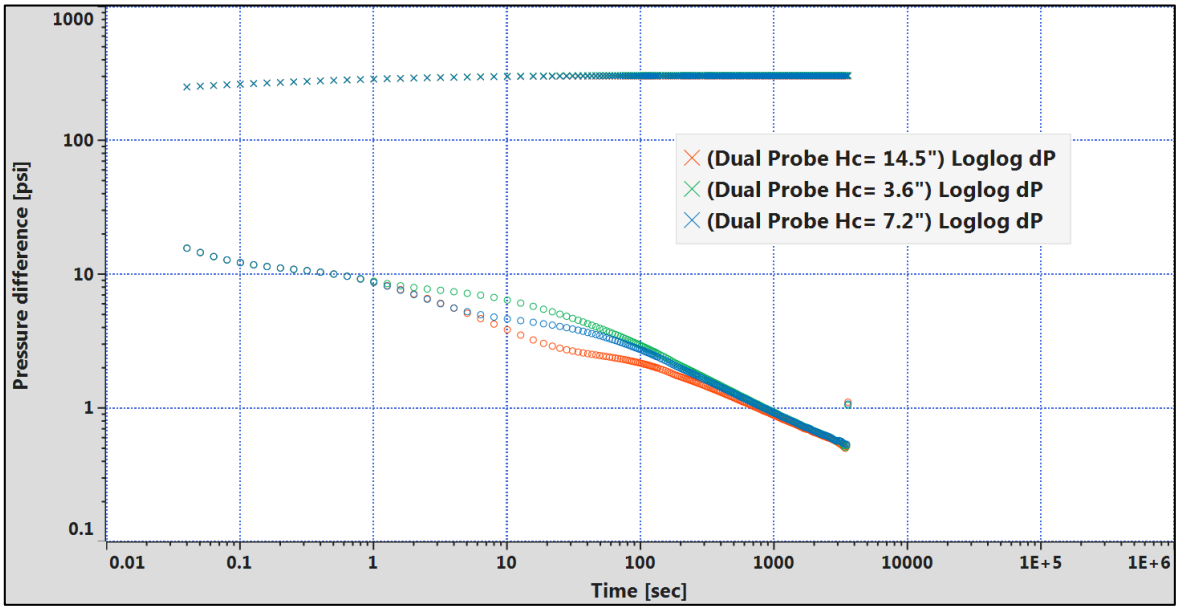


Fig. 11.G.25 – Influence of the distance between probes

The larger the spacing between the two sinks, the later the transition between the "dual source spherical flow" and the final "single source spherical flow" is observed.

The following illustrate a dual sink probe tool, side mounted, vertical, slanted at 60° and horizontal well:

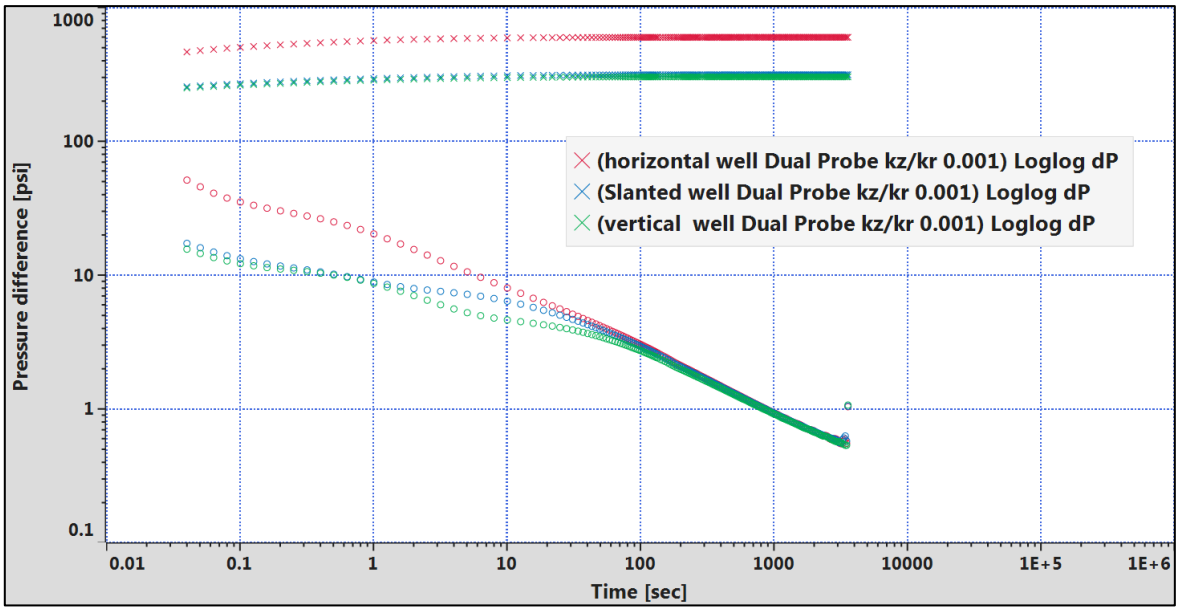


Fig. 11.G.26 – Influence of the well orientation on dual probe response

The horizontal well results are more influenced by the vertical anisotropy effect on the initial spherical flow.

The following plot illustrates the difference of the placement of the probes in a horizontal well (kz/kr=0.001).

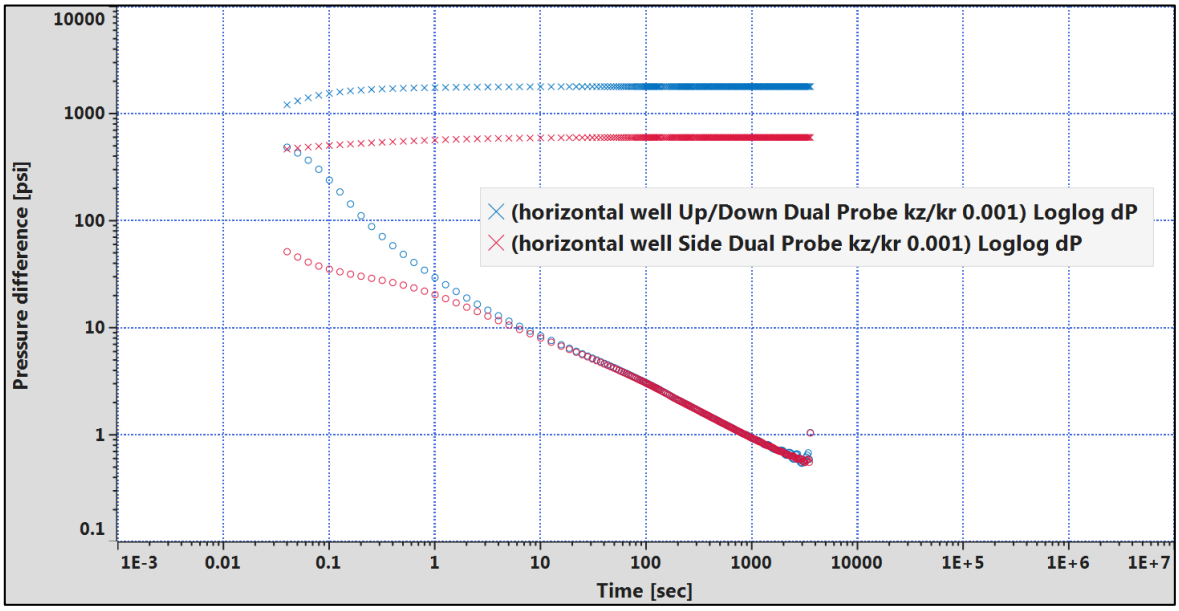


Fig. 11.G.27 – Influence of the probe position in a horizontal well

The initial spherical flow if even more influenced by the vertical anisotropy in case of up/down position of the probe.

11.G.3.d Four oval probes – Schlumberger Saturn™

This case is handled as an extension of the single oval probe using the superposition (interference) of the additional probes.

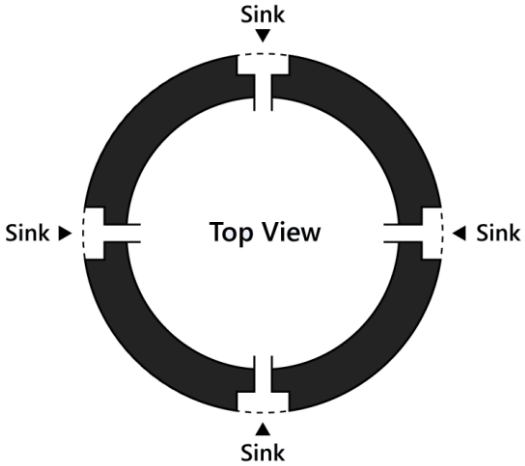


Fig. 11.G.28 – Four sink oval probes – Top view

Parameter	Value
r_w (in)	3.6
h (ft)	30
z_w (ft)	15
k_r (mD)	33.33
r_p (in)	1.457
h_p (in)	7.402
Φ (%)	10
p_i (psia)	5000
q (cm^3/s)	6
k_z/k_r	0.001

Fig. 11.G.29 – Four sink oval probes – Parameters table

The drain (pump) time is 10 minutes (3.6 liters) with a shutin time of 1 hour for sensitivity purposes only.

The 3D probe has 4 oval probes set at 90° angles. It provides a total flow area of some 79 in^2 thus and r_p of some 1.457 in.

The interest of this kind of geometry is that the measurement is no longer dependant on the probe orientation (side or up/down) and eliminates the possible local anisotropy.

The figure below illustrates the vertical well with variable anisotropy from kz/kr=0.001 to 1. kz/kr=1 is the current model. The measurement is purely influenced by the vertical anisotropy.

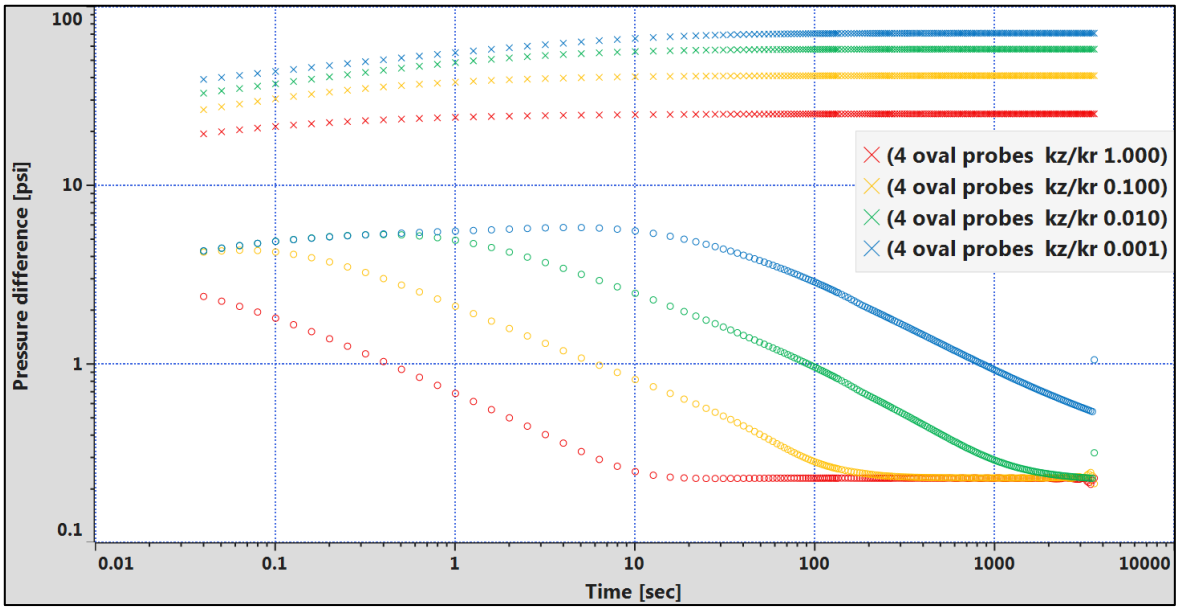


Fig. 11.G.30 – Influence of the vertical anisotropy

In the following graph is illustrated the influence of the well deviation between a vertical, slanted at 60° and horizontal well with kz/kr=0.001.

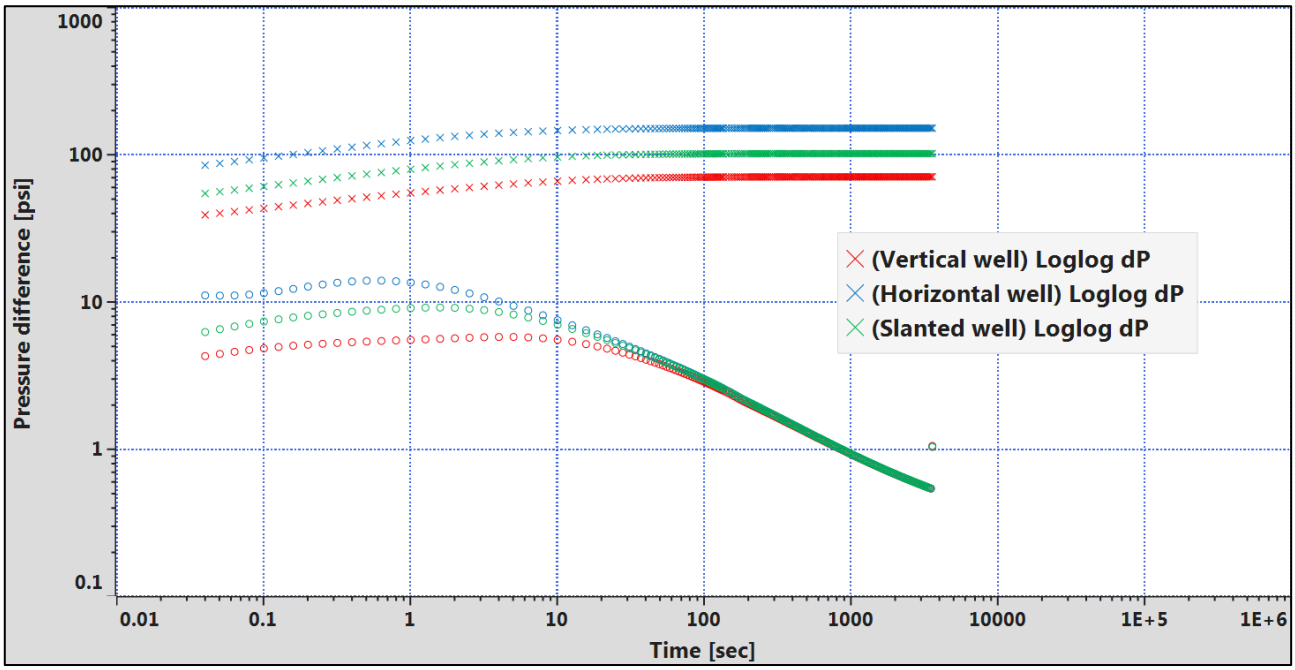


Fig. 11.G.31 – Influence of the well orientation with a fixed anisotropy

The highest total skin is observed in the horizontal well and is due to the low transmissivity during the early "pre-spherical" flow imposed at the top and bottom probes by the small vertical permeability.

Dual packer

The pressure behavior is modeled with the classical limited entry well solution. There are several studies in the well test literature that have clearly shown that in most practical cases the use of this model gives satisfactory results and thus eliminates the old straight-line analysis developed before such analytical models became available.

An early radial flow (1) may be observed if anisotropy is quite high (low k_v/k_r ratio) and wellbore storage does not impact the early pressure behavior. As shown below, there is vertical contribution to flow in the second regime corresponding to spherical or hemi-spherical flow (2).

The characteristic flow regime is spherical flow until upper and lower vertical flow boundaries have been reached and then followed by classical radial flow (3) in the reservoir.

A schematic of the theoretical flow regimes is illustrated in the figure below:

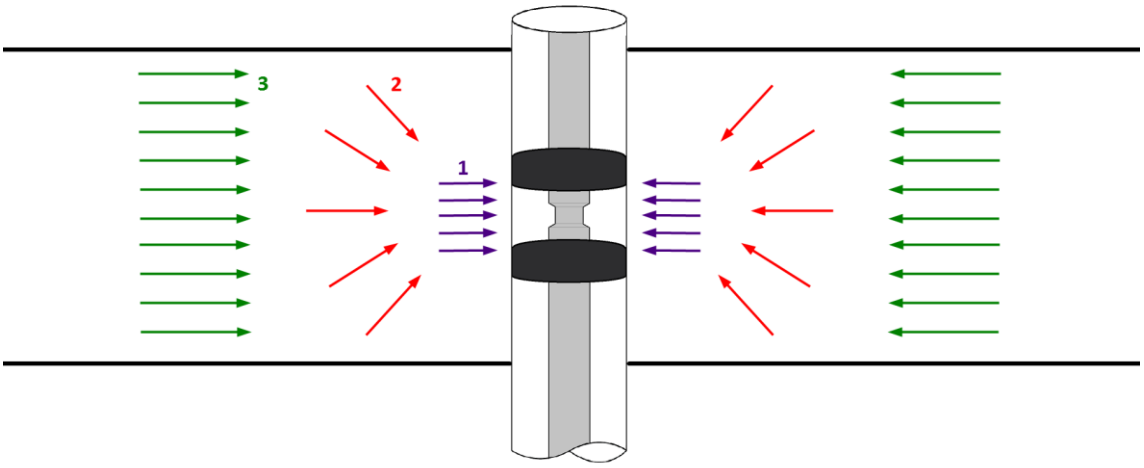


Fig. 11.G.32 – Limited entry flow regimes

11.G.4 Comparison of Behavior

In the next figure the pressure response using the five probe configurations described above (with their typical geometries) is illustrated on a typical example. It is evident that the lowest pressure drop is perceived with the dual packer module having the higher contact area with the formation, while the single circular probe has the lowest area giving the highest Δp (same rate).

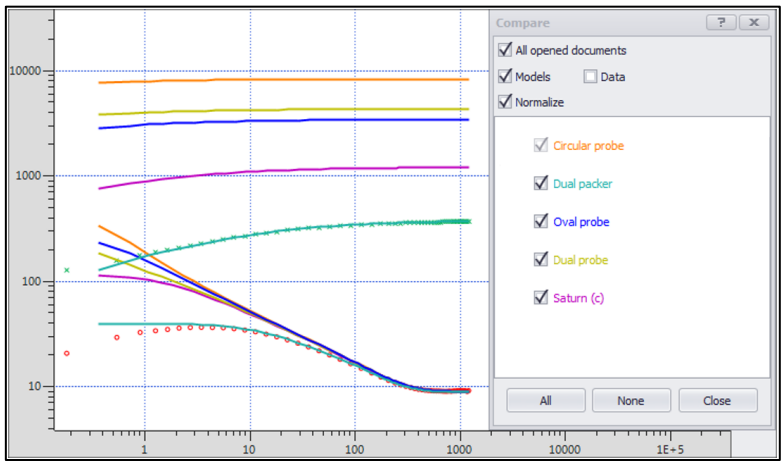


Fig. 11.G.33 – Loglog plot with different probe types

11.H Specific FT analysis

11.H.1 Vertical Interference Tests

FT tools allow to carry out vertical interference tests (VIT) by the inclusion of one or several observation probes in the tool and the measurement of the pressure at those additional probes.

The tool can be assembled by combining any of the tools described above as sink (active) probe with circular probes as observers. The observation probes can be located at the same depth or at any distance above/below the active probe.

Multilayer analysis can be carried out using any of the probes available.

The pressure response in this model is a transition between the behavior observed at a producing point (spherical then radial flow) and the interference response observed at a distant point. This combination depends on the distance and the horizontal angle between the active and the observation probes.

The horizontal angle has a significant influence when the vertical distance between the observation probe and the active probe is small (here they are at the same depth).

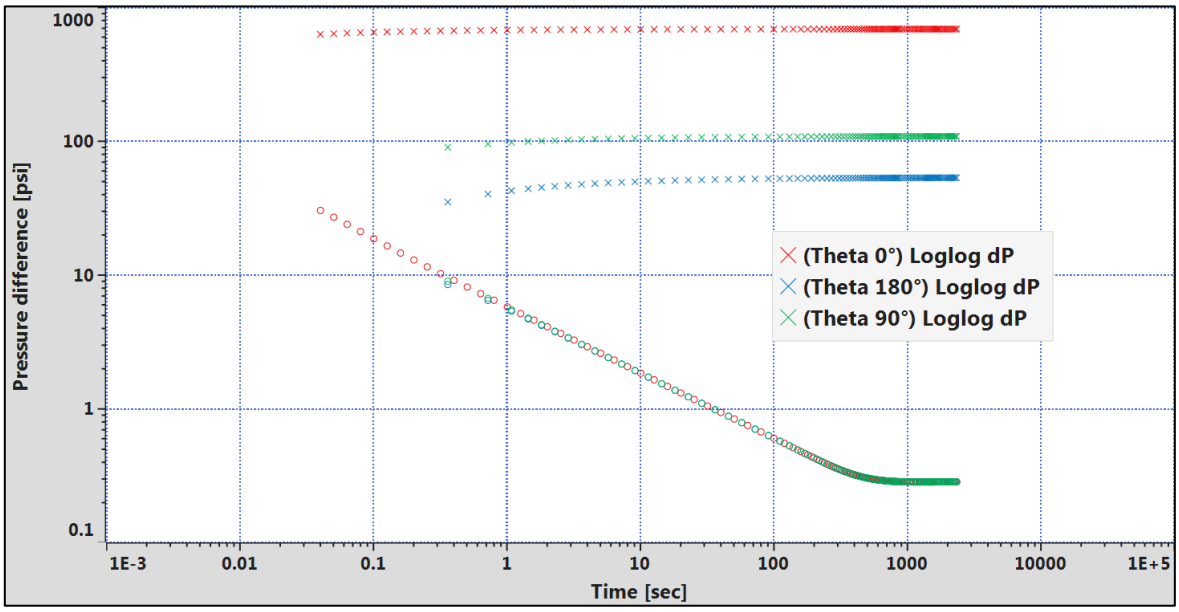


Fig. 11.H.1 – Horizontal observation probes at same depth as active

The angle influence decreases when the vertical distance increases. It can become undetectable, after a certain vertical distance which depends on the radius of the well (rw). The greater is rw, the further is the influence of the angle. The figure below shows that the pressure response is practically the same with an rw = 0.25 ft and a distance of 3ft.

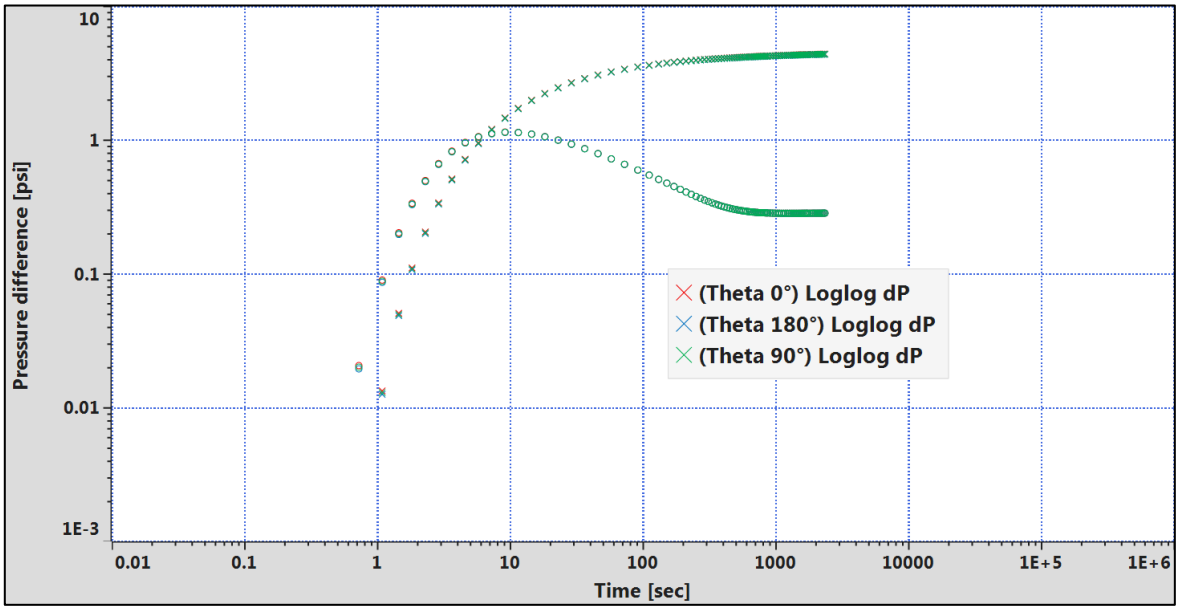


Fig. 11.H.2 – Horizontal observation probes at 3 ft above active - rw = 0.5ft

The radius has to be increased up to rw = 1 ft to detect the angle influence at a distance of 3ft as shown below.

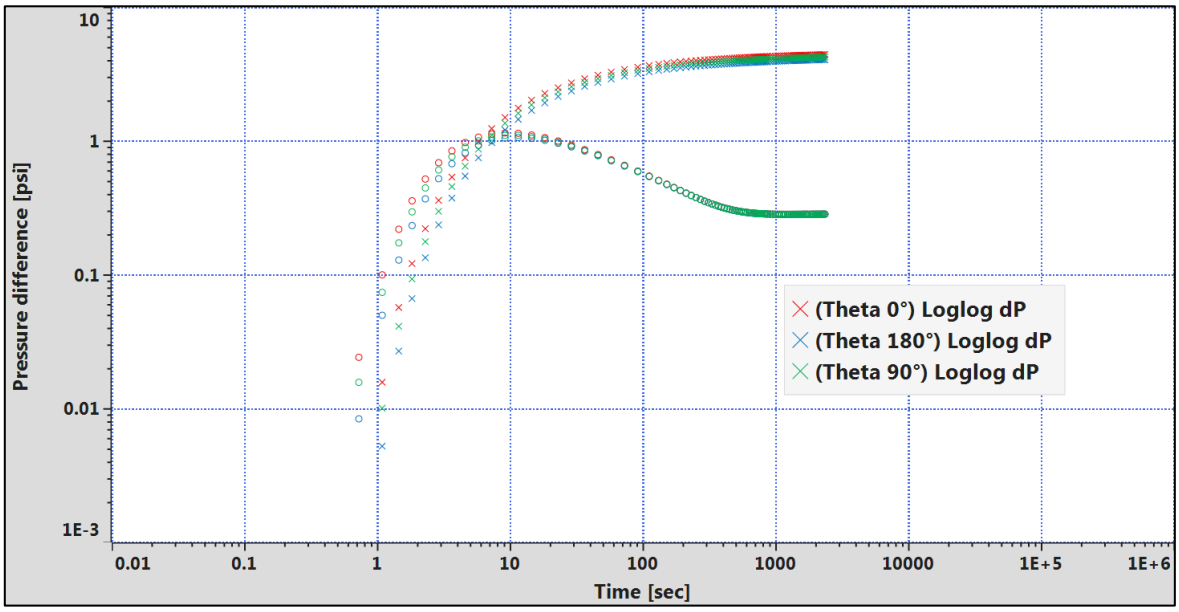


Fig. 11.H.3 – Horizontal observation probes at 3 ft above active - rw =1ft

The vertical permeability, defined by the k_v/k_r ratio, influences the pressure response (it delays the observation of the response).

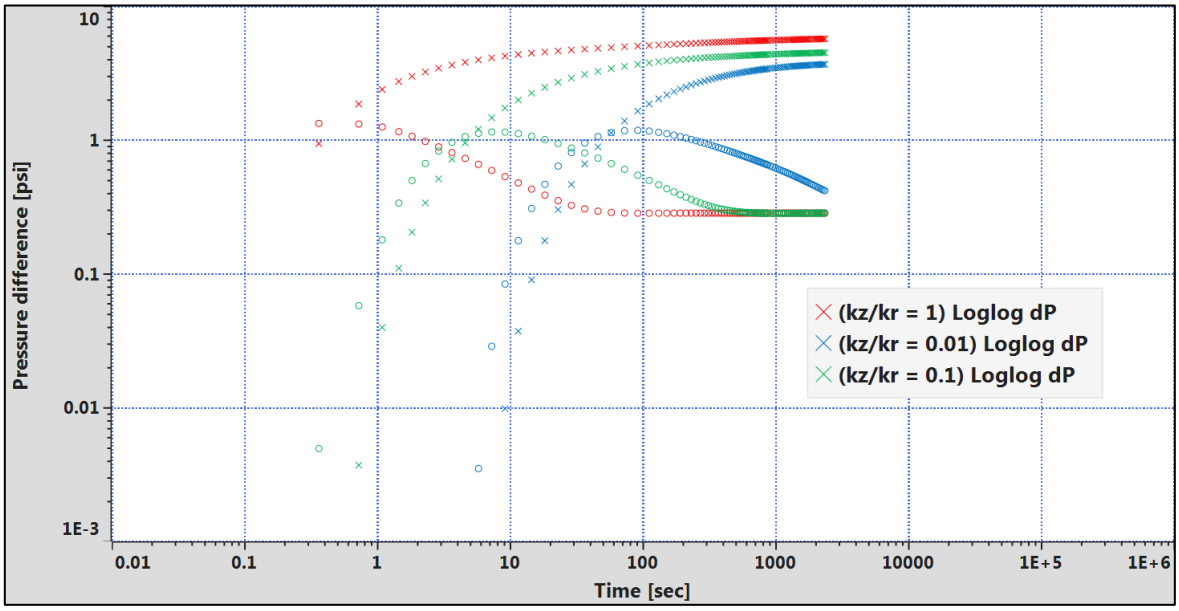


Fig. 11.H.4 – Vertical observation probe at 3 ft with different anisotropy

The loglog plot below is for a build-up with one sink probe and 3 observation probes. We see that the active probe and all the observers appear to have a common stabilization at later time thus indicating common kh. The active and the nearest observer probes have largely a common derivative behavior indicating no vertical changes of the reservoir characteristics. The observer probe furthest away from the active probe is recording close to its gauge resolution.

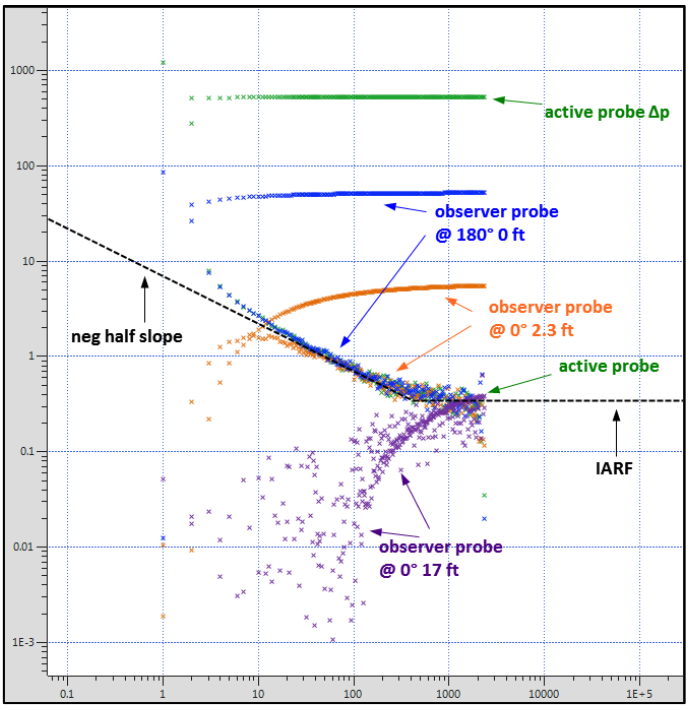


Fig. 11.H.5 – Loglog plot of 4 FT probes

Below we illustrate the final model match with the FT probe model.

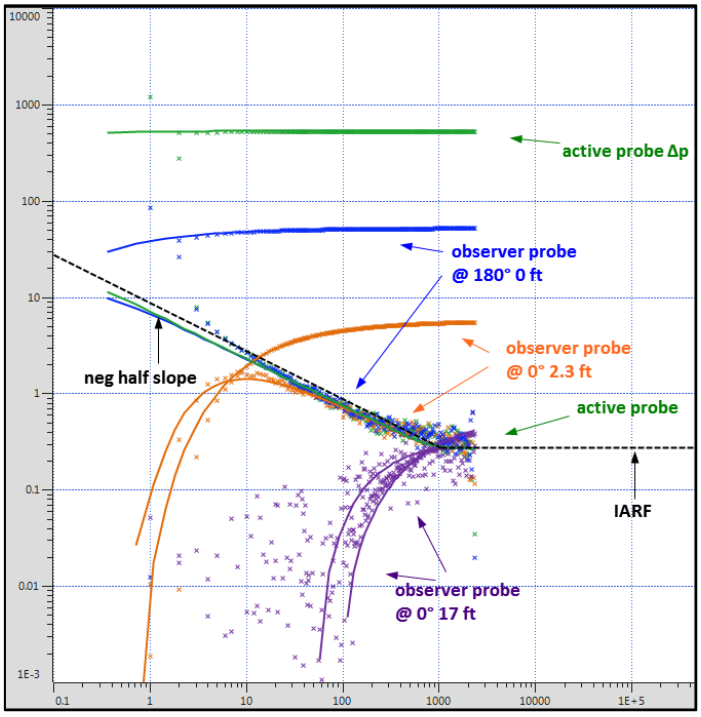


Fig. 11.H.6 – FT model match

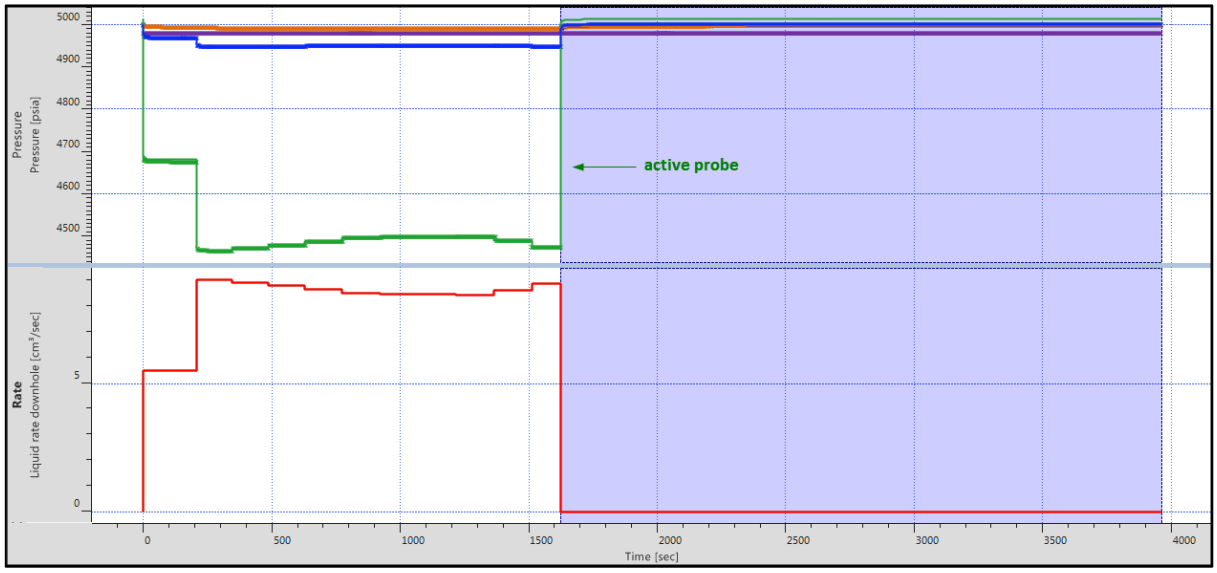


Fig. 11.H.7 – FT History match

11.H.2 Formation Tester in Multilayers

11.H.2.a Model description

The configuration of the analytical multilayer model incorporated in Azurite is similar to the single layer multi probe solution. The active probe is assumed to be on the side of the well, and the observer probes can be turned to any angle with respect to the active probe.

There can be n layers communicating or not with any homogeneous reservoir characteristics.

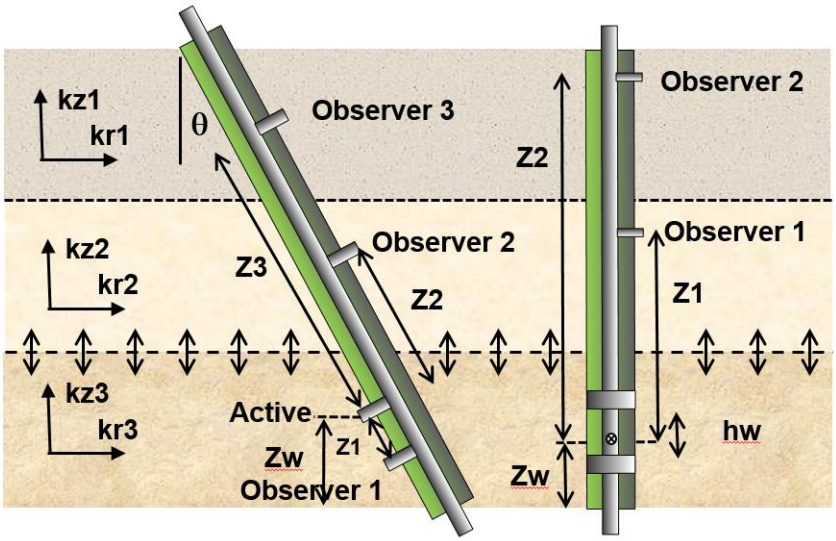


Fig. 11.H.8 – Model Schematic

Reference paper where the model is described: SPE-183791-MS

Analyzing Pressure Transient and Steady State Drawdown Data From Current Formation Tester Tools in Vertical and Deviated Wells With a Consistent Approach

Leif Larsen, KAPPA Engineering and University in Stavanger, Olivier Allain, KAPPA Engineering

11.H.2.b Heterogeneous behavior

If a two-layered system is selected the model describing the response of the active probe will be the similar to the double permeability model where the interlayer communication can be described either by the parameters Lambda, Omega and Kappa, or by a leakage factor or by an equivalent vertical permeability kze.

The crossflow between layers is controlled by the harmonic average vertical permeability:

$$k_{z_{avg}} = (h_1 + h_2) \Big/ \left(\frac{h_1}{k_{z1}} + \frac{h_2}{k_{z2}} \right)$$

The leakage factor is a multiplying factor of this permeability.

Several figures below show the classical derivative transition period that characterizes a two layered system with cross flow. This transition corresponds to a pressure stabilization of the active layer, when the pressure drop reaches the necessary value to allow the second (passive) layer to contribute to the production by crossflow. We imagine perfectly that the interlayer leakage, the vertical permeability and the storativity of the second layer govern directly the crossflow effect amplitude and time.

By placing an observer probe in the middle of the Layer 2 (the lower layer) the response at the observation point allows to evaluate by model matching the interlayer cross flow parameters (Lambda, Leakage or kze).

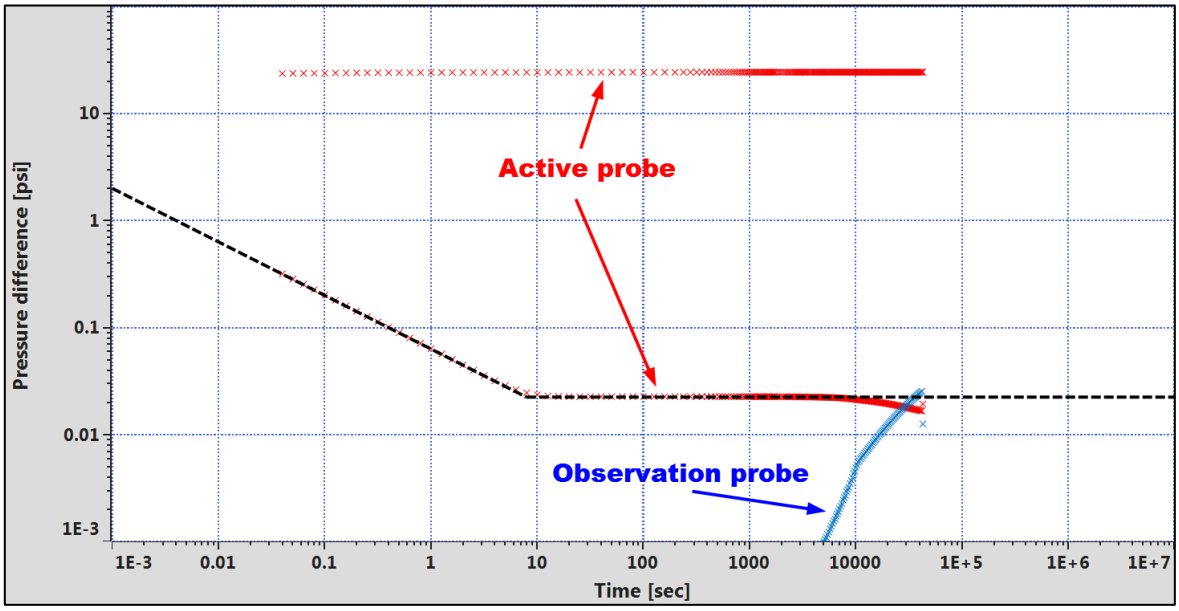


Fig. 11.H.9 – Pressure response at active and observation probes with a low vertical crossflow (kz/kr = 0.01 Leakage = 0.03)

11.H.2.c Observation of the crossflow

In order to better demonstrate the effect of the crossflow on the active probe a case with a long shut-in was simulated, such a shut-in would be normally not be seen in 'real life' thus the evidence that cross flow and vertical communication exists will be seen on the observation probe only.

The active circular probe is in the middle of the bottom layer of k= 1 D, the observer is in the middle of the upper layer of k=10 mD.

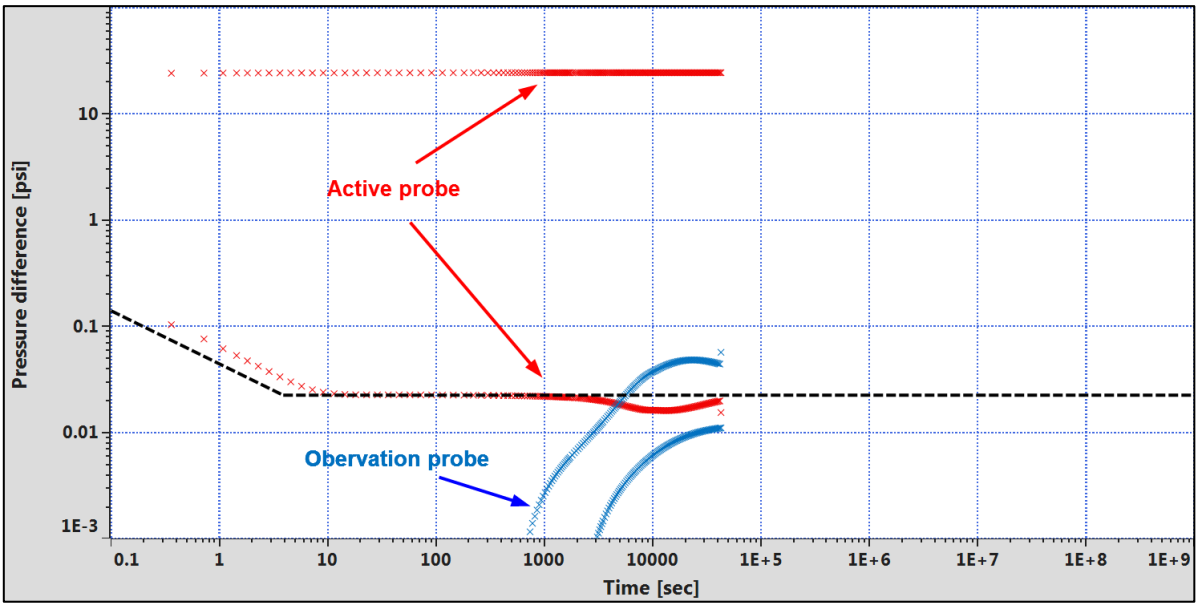


Fig. 11.H.10 – Crossflow effect observed at late time on the active probe pressure response

The above figure was generated using an anisotropy of kz/kr=0.01 but a leakage of 0.2.

By reducing the anisotropy, with a kz/kz close to 1.0, the crossflow event happens earlier and is more pronounced. The response at the observer starts earlier and although small, more pronounced than in the previous example.

Below is shown the sensitivity to the observation layer anisotropy: the lower is the vertical permeability, the later is observed the signal and the crossflow transition.

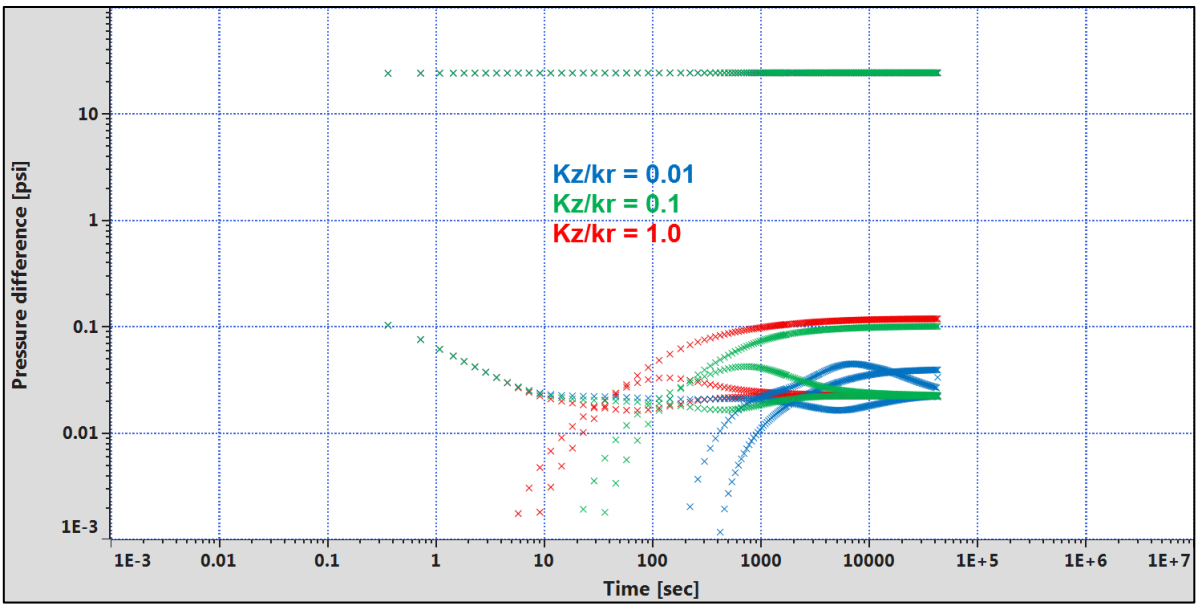


Fig. 11.H.11 – Influence of the observation layer anisotropy on the crossflow event time

The smaller the kz/kr, the later the cross flow effect and the signal reception.

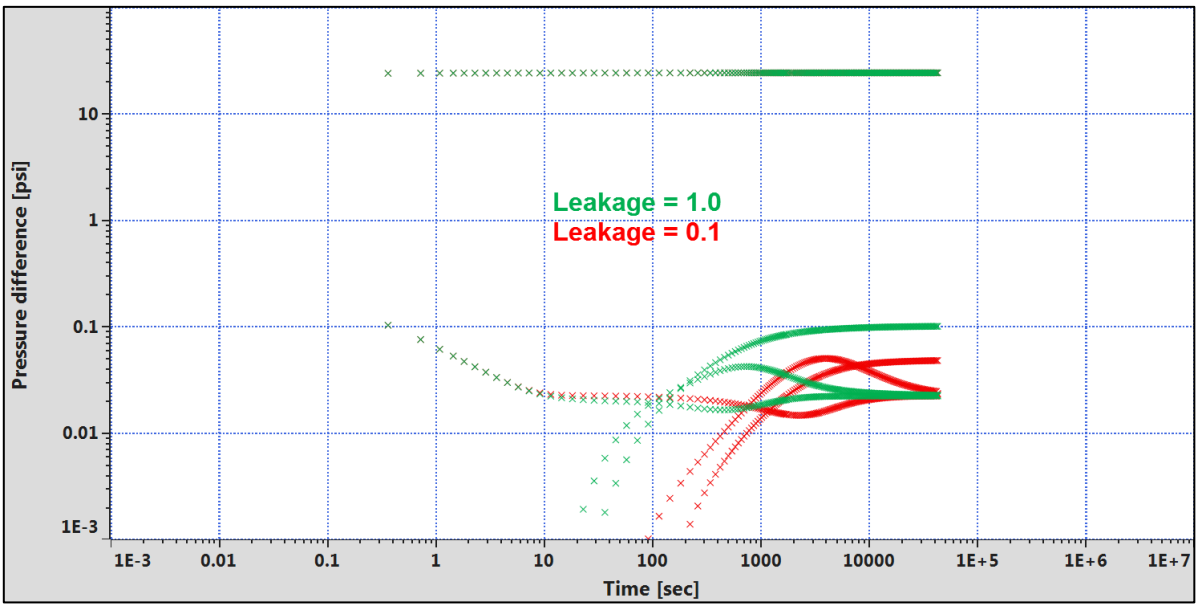


Fig. 11.H.12 – Influence of the leakage factor on the crossflow event time

The smaller the leakage, the later the cross flow effect and the signal reception.

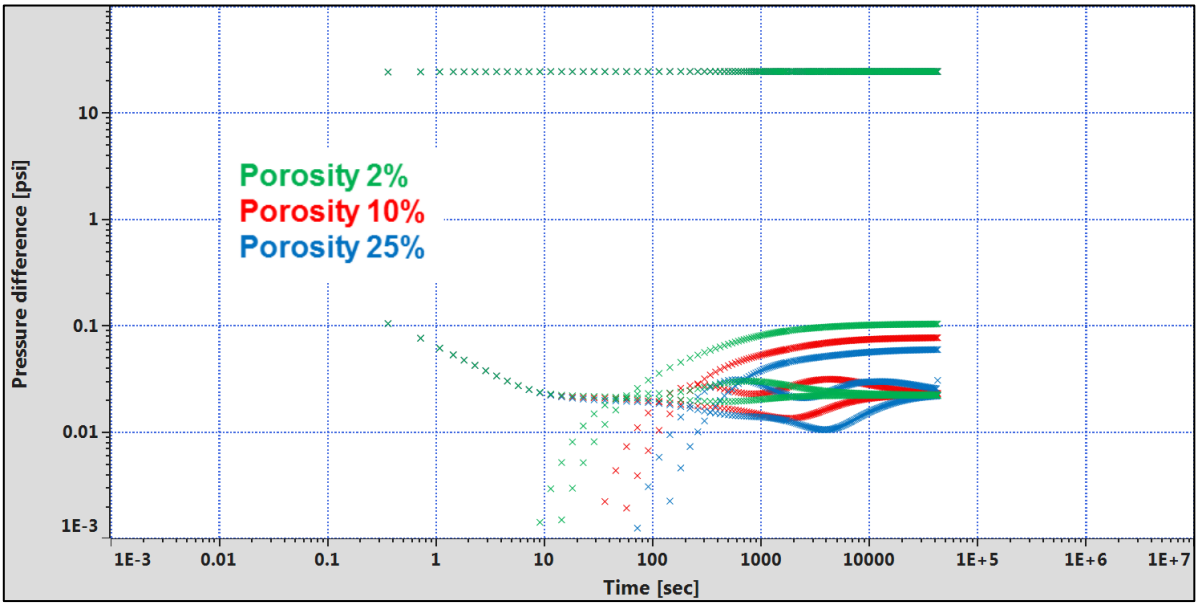


Fig. 11.H.13 – Influence of the observation layer porosity on the crossflow event time

The larger the porous volume in the "passive layer", the later and the stronger the crossflow effect will be observed at the active probe because a larger porous volume of the observation layer induces a larger fluid contribution, therefore creates a larger pressure stabilization effect.

11.H.2.d Effect of deviation

The effect of the deviation on the permeability has been commented in the paragraphes above and we use the same combination of the permeability tensor according with the deviation to allow to calculate the longitudinal and perpendicular permeabilities from the vertical and horizontal permeabilites.

In the case of vertical interference, it is the impact of the deviation on the geometry, thus on the distances, that will influence more the observed pressure signal.

The figure below describes the geometry of the example used to illustrate the deviation impact on the observed pressure.

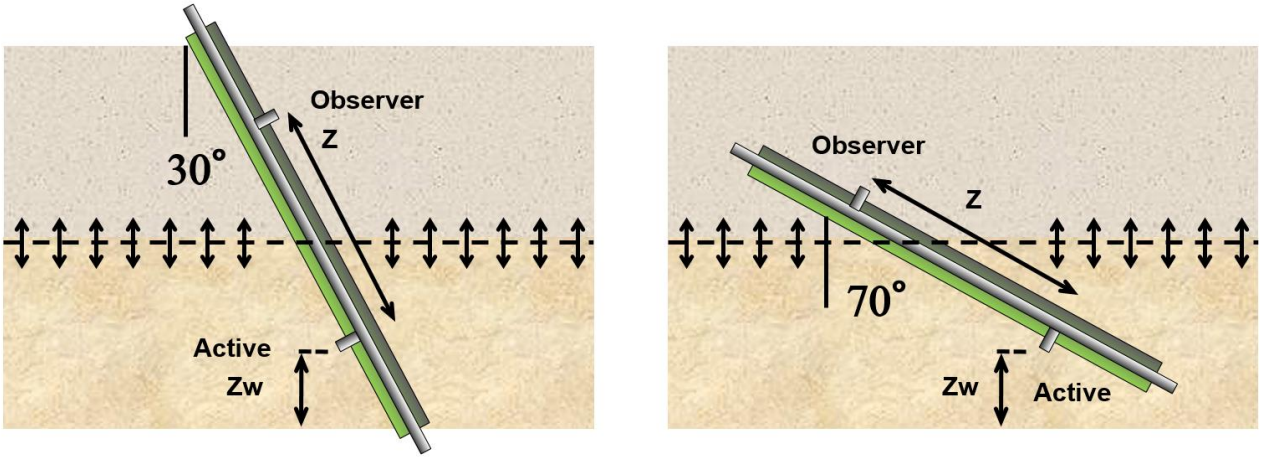


Fig. 11.H.14 – Evolution of the geometry with the well deviation at constant Zw

The figure below illustrates the response of the active circular probe (rp=1.0”) placed in the middle of the lower layer of 15 ft., the observation probe is placed in the middle of the upper level (15 ft). kz/kr=0.01 in both layers and the leakage between layer is set to 1.0.

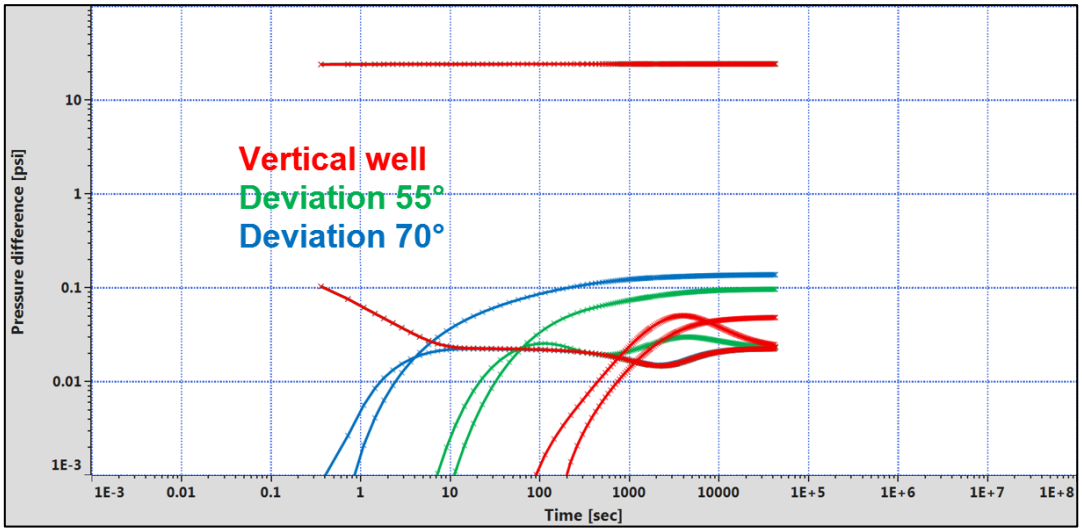


Fig. 11.H.15 – Pressure response of a 2-layer system in a deviated well with a leakage of 1.0

The tool geometry being constant, the observation probe gets closer to the interlayer when the deviation increases, therefore the signal arrives earlier.

12 – PTA: Special test operations

OH – OSF – DV

12.A Introduction

In a *standard test* we put the well in production and we monitor the pressure build-up. We use the single total production rate in the same well to correct the pressure model by superposition. As long as we neglect the difference of fluids, injection / fall off tests can also be considered standard tests. *Special tests* are just whatever is not standard. In this version of the book we will detail four different types of special tests.

Slug tests

A slug tests corresponds to a production resulting of a rising liquid level in an initially empty production string above a bottom hole shut-in device, followed or not by a build-up.

It can consist in the initial flow of a Drill Stem Test (DST) but it can be also deliberately designed when no production is allowed or possible at surface.

'Slug' pressures vs. time will be used to quantify the sandface production, which then can be used as the input rate history for the build-up analysis. However there are some techniques that allow the transient pressure response of the slug to be analysed independently. This specific processing will be demonstrated in this chapter.

Multilayer tests

One will perform a standard test in a multilayer formation if we produce the whole reservoir and just acquire the pressure and total producing rates. There are analytical models in Saphir / Topaze which will account for layering, such as the double-permeability model. We will call a multilayer test an operation where we will adjust the test sequence or add measurements to discriminate the different layer contributions. This can be done by producing the layers successively or in different combinations, or by adding production log measurements.

Interference tests

In any test we can add the interference of the other wells in the Saphir analytical and numerical models. Despite this model refinement we will still consider that we are in a standard test if the reference production history and the pressure are taken at the same well. In a proper interference test the pressure that we interpret was acquired in an observation well, i.e. not in the well from which the reference rates were recorded. This will generally imply that the observation well is not producing and that most of the amplitude of the observed pressure change is, precisely, this interference.

12.B Slug Tests

A slug tests corresponds to a production resulting of a rising liquid level in an initially empty production string above a bottom hole shut-in device, followed or not by a build-up.

It can consist in the initial flow of a Drill Stem Test (DST) but it can be also deliberately designed when no production is allowed or possible at surface.

This period can be used to define the flow rates in order to analyse the following build-up, or it can be analysed by itself using the method presented in this section.

12.B.1 Test sequence in a DST

We will not explain what a DST is, the types of tools that are run downhole, etc. There are plenty of other places to learn this. We describe the DST from the point of view of the analyst.

The downhole pressure recording of a typical DST is shown in the figure below. During this operation the well is open and closed with a downhole valve. The pressure sensor is positioned below the downhole valve to follow the reservoir pressure when the well is shut in.

We start at initial pressure p_i. Before the well is open downhole an initial static column of fluid, typically a cushion of diesel or water, may or may not be placed above the downhole valve.

During this operation the surface valves remain open to flow to bleed the air.

The test starts by opening the downhole valve. The pressure instantaneously switches from p_i to the initial static pressure p_0. If the well is not flowing the pressure will remain stable or will change very little, and the test will be over.

If we have a producer and if p_0 is less than p_i the fluid starts to flow from the reservoir to the well, the static column rises and so does the pressure. This is the beginning of the slug test. It will last until the fluid eventually reaches surface. The well is shut in and we have our first build-up. While the well is shut-in the static column will remain stable, but it will not be recorded by the pressure gauge which is on the other side of the valve.

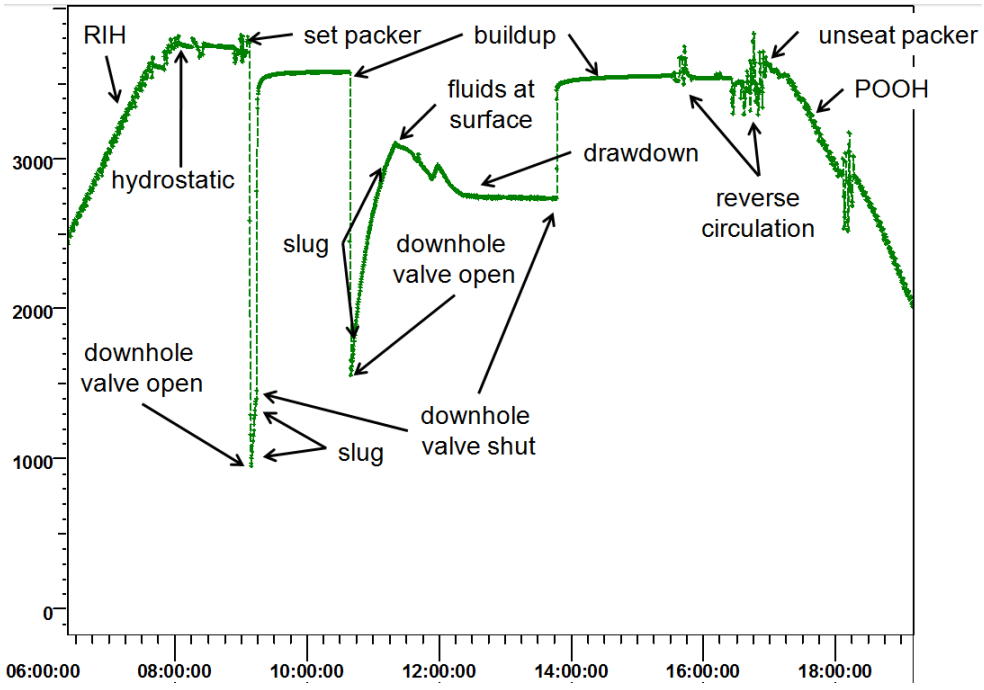


Fig. 12.B.1 – Conventional DST

When we open the well again we restart at the previous level of the static column and the slug resumes. At this stage several scenarios can happen:

- The system does not have enough energy and the slug dies. Throughout the test there is no flow to surface.

- The system has enough energy and the fluid breaks at surface. At this stage the pressure starts to decrease again and we are back to the conditions of a standard test. After stabilization the fluid is flowed through the separator, surface rates and samples are taken until a final build-up is run. This standard scenario is the one shown in the figure above.

12.B.2 Build-up analysis using slug rates

Before we go into the specifics of the slug analysis we will look at the 'standard' analysis of the build-up data following the slug. To analyse this build-up we need to know the flow rates before shut-in. As no separator measurements were possible at this stage we use the fact that the recorded downhole pressure reflects the rise of the static column. From this rise we can assess the volume of fluid produced at sandface, hence the rate.

If we cut the slug sequence into a discrete series of intervals we get the following equations:

Slug rates from slug pressures:

$$q(t_i) = C \times \frac{p(t_i) - p(t_{i-1})}{t_i - t_{i-1}} = 80.5 \frac{r_w^2}{\rho} \times \frac{p(t_i) - p(t_{i-1})}{t_i - t_{i-1}}$$

The rates are calculated using the internal diameter of the effective well and the fluid density to obtain a wellbore storage coefficient that is then used to calculate the rates.

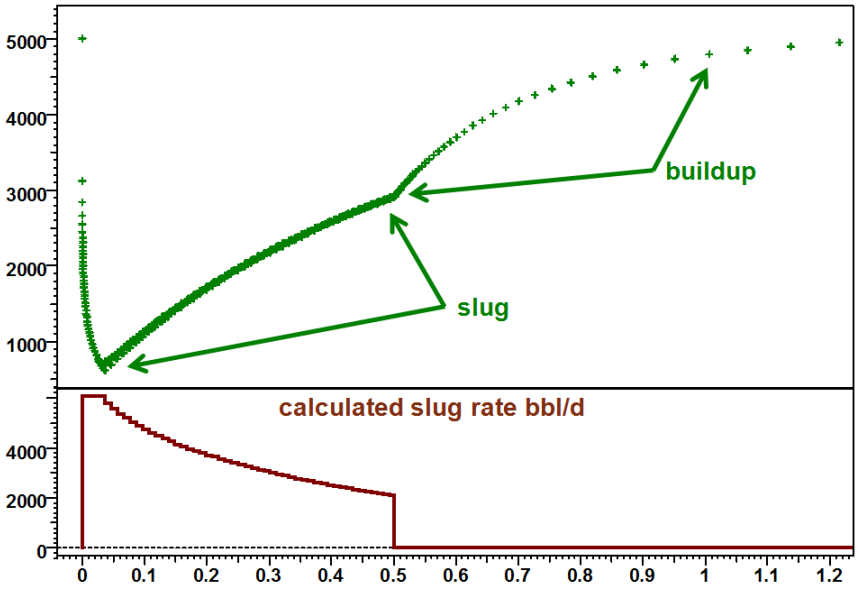


Fig. 12.B.2 – History plot

The figures below show the build-up loglog and history match. The trick here is to use a changing well model and the changing wellbore storage option. There are two statuses; the first during the slug will have a wellbore storage of 0 and the build-up whatever is appropriate.

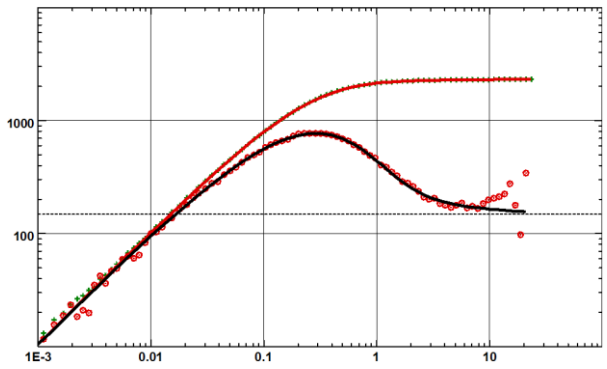


Fig. 12.B.3 – Build-up loglog match

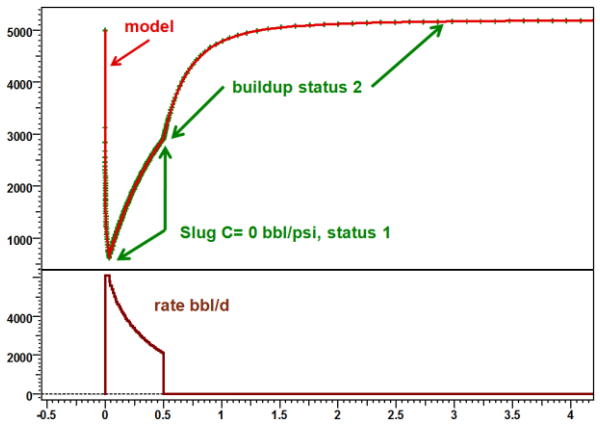


Fig. 12.B.4 – History match

12.B.3 Slug test analysis

In the previous section we have used the pressures recorded during the rise of the static column to build a rate history and analyse the following build-up in a standard way. The Slug test analysis is about considering the rise of the column itself, independently of the build-up.

In a standard test we have two separate sets of data: the rates and the pressures. In PTA one will try to interpret the pressure response using the rate history to correct for the superposition effects. In Rate Transient Analysis it will do more or less the opposite. What is puzzling at first glance in slug test analysis is that the pressure, by differentiation, also gives the rate. So here we have a single transient signal that is supposed to give all information at the same time, and from which we are expected to make an analysis. How come?

Mathematically, a slug is the answer to an instantaneous production with wellbore storage. The volume of the instantaneous production corresponds to the initial static column, i.e. the internal cross-section of the tubing at the liquid interface multiplied by the height of the difference between the initial static column ($p_{sf}=p_0$) and a virtual stabilized static column ($p_{sf}=p_i$). This is virtual as the height of the stabilized column could exceed the internal volume of the completion if the well / reservoir system has enough energy to flow to surface.

So to make a parallel with a standard test the pressure remains the pressure but the rate is replaced by the value of this virtual volume.

The slug test is mathematically equivalent to a close chamber test, even if the volumes are calculated differently. The hydro-geologists have been doing this sort of test for a long time. In the very low permeability formations for nuclear waste disposals, they pressure up a fixed volume of water and watch the relaxation. They call these tests impulse tests, which should not be confused with the trademarked impulse test by Schlumberger.

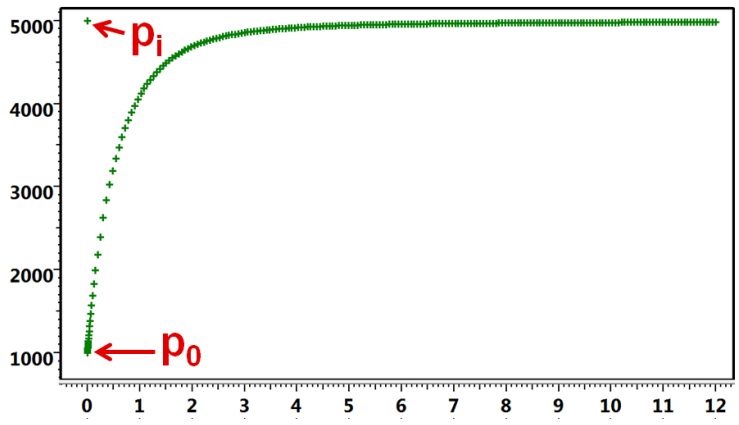


Fig. 12.B.5 – Slug schematic

In 1975 Ramey et al published a set of loglog type-curves showing the slug test responses, in dimensionless terms, for various values of the usual dimensionless parameter CDe2S. These type-curves were starting with a horizontal behavior and finish with a negative unit slope. The pressure data would be matched on the type-curve after the following transformation

Ramey's slug transform: $$p_D(t) = \frac{(p_i - p(t))}{(p_i - p_0)}$$

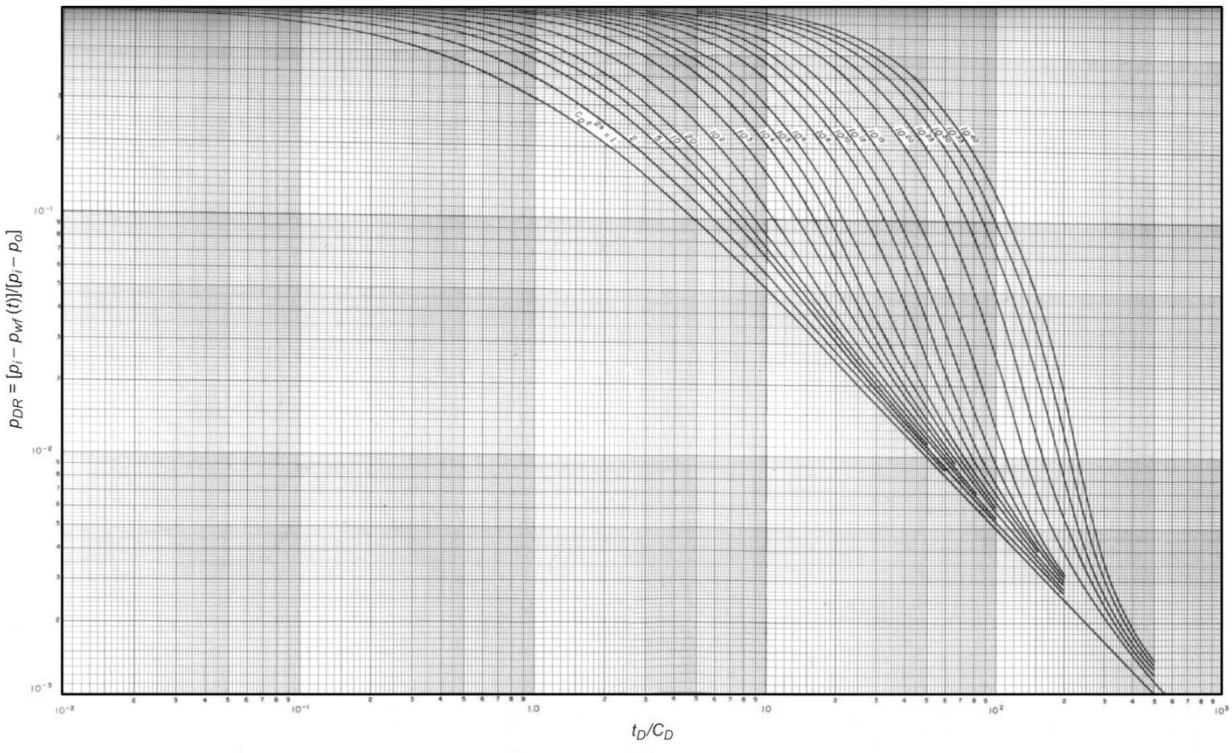


Fig. 12.B.6 – Ramey's type-curves

In 1995 Houzé and Allain had to adapt Saphir for ANDRA (French nuclear wastes agency) in order to implement hydro-geologist's impulse tests for very low permeability formations. This is when they realized that multiplying the 1975 Ramey's type-curves by Δt we would get… the dimensionless derivatives (in red below) in the 1983 Bourdet derivative type-curves.

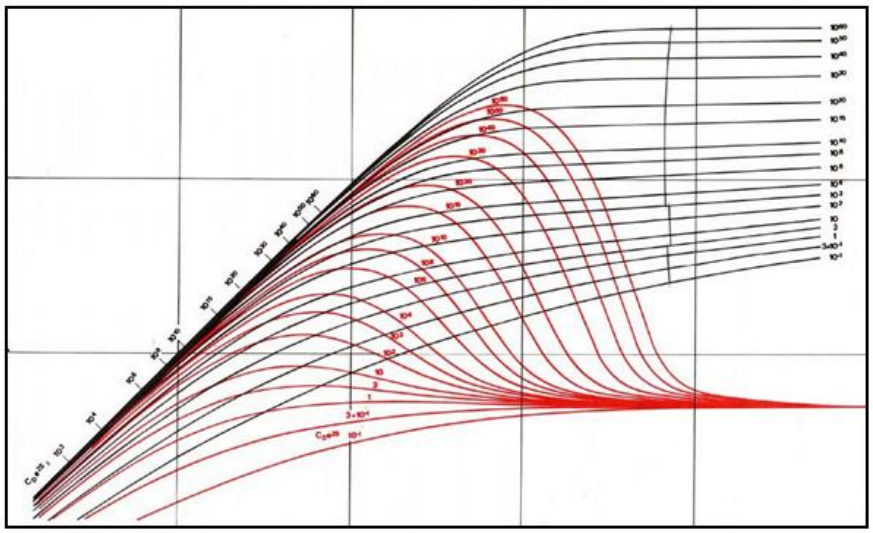


Fig. 12.B.7 – Bourdet derivative type-curve

So, in order to match the analytical models the modified Ramey transform will be:

Modified Ramey transform $$\frac{(p_i - p)}{(p_i - p_0)}\Delta t = \frac{3389C\mu}{kh} p'_D\,(Tmatch \times \Delta t)$$

Where p'_D is the Bourdet derivative of the corresponding dimensionless model. Another way to present this (initially surprising) observation is that:

After the modified Ramey transform, the pressure response to an instantaneous (Dirac) production matches the derivative of the constant rate response for the same system.

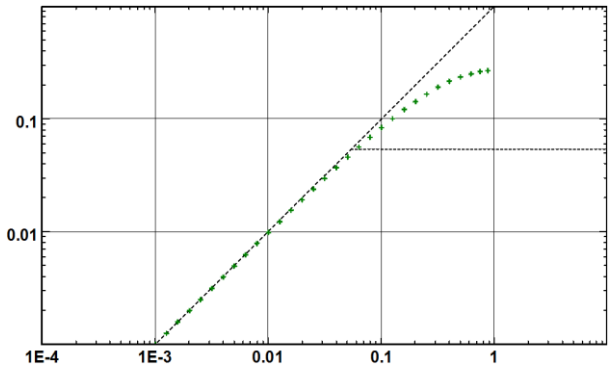


Fig. 12.B.8 – Typical duration Slug: Loglog plot

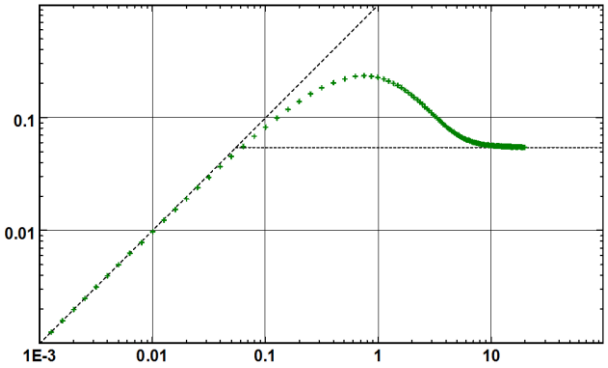


Fig. 12.B.9 – Extended duration Slug: Loglog plot

To perform the analysis the values of p_i and p_0 must be input. The wellbore storage coefficient can be calculated from the tubing diameter and the wellbore fluid density. It is assumed that the inner diameter is constant. If changes occur there will be a corresponding change in the wellbore storage coefficient.

With a fixed storage and a loglog response like the one displayed above on the left one can see immediately that it is not possible to get both skin and kh with any confidence from the analysis. This is illustrated in the figures below with two different diagnostics. In the fist we have the skin set to 0, in the second the skin is set to 10. A regression was run on kh for each case and the values are respectively 1740 and 4610 mDft.

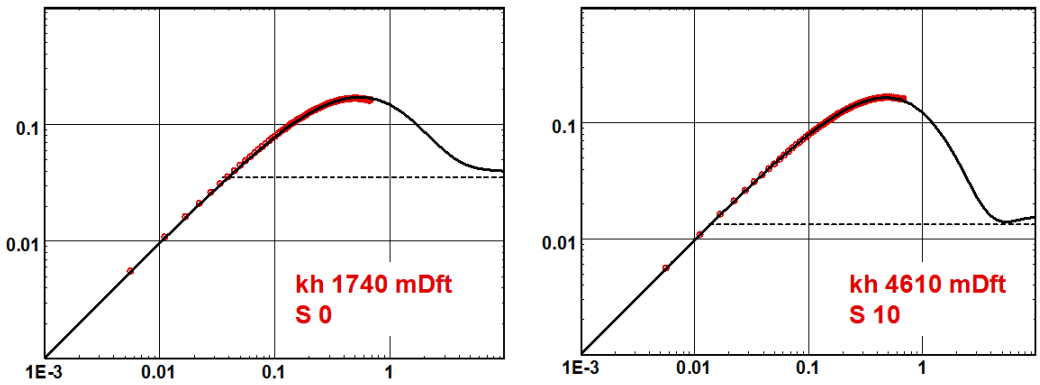


Fig. 12.B.10 – Slug Loglog matches

In the worst case we can only establish a relationship between the permeability and skin.

However, in the oil industry most slug tests are followed by a downhole shut-in. The pressure slug can also be used to calculate the downhole flowrate as we have illustrated in a previous section, as long as we have a reasonable idea of the fluid density. It goes without saying that we know the hardware we have put in the well, so we know dimensions such as internal diameter and if there are any diameter changes in the well. We also know what fluid has been put in the pipe above the tester valve, so P_0 is known and acts as a check.

The figures below show the slug match versus the build-up match. Due to the length of the build-up, the pressure and time match becomes 'unique' with high confidence in analysis results.

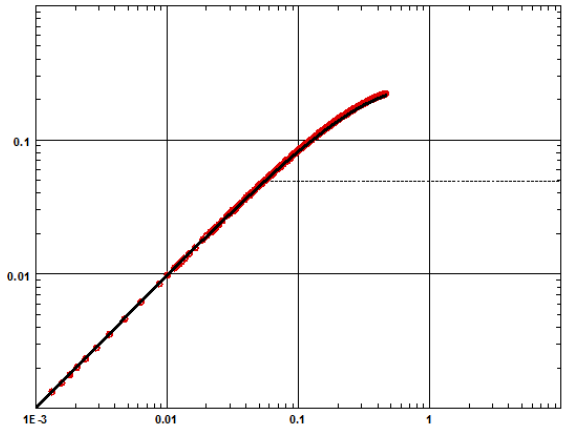


Fig. 12.B.11 – Slug match

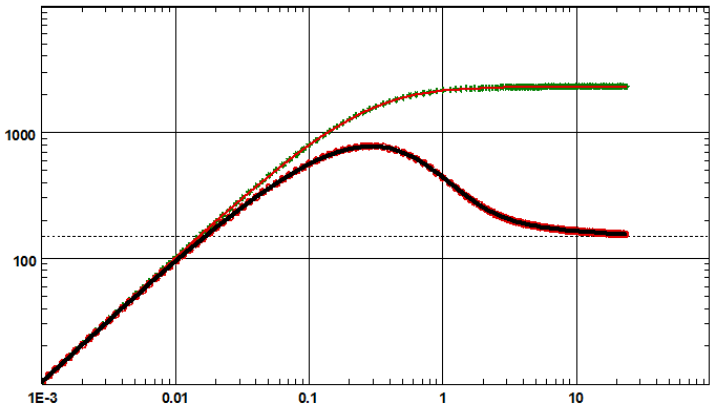


Fig. 12.B.12 – Build-up match

12.C Multilayer tests

12.C.1 Introduction

Most reservoirs have a commingled production from multiple zones. These zones may or may not be from the same geological formations, and they may or may not be communicating at the level of the formation. In most cases we perform a Pressure Transient Analysis considering the reservoir as a single global contributor.

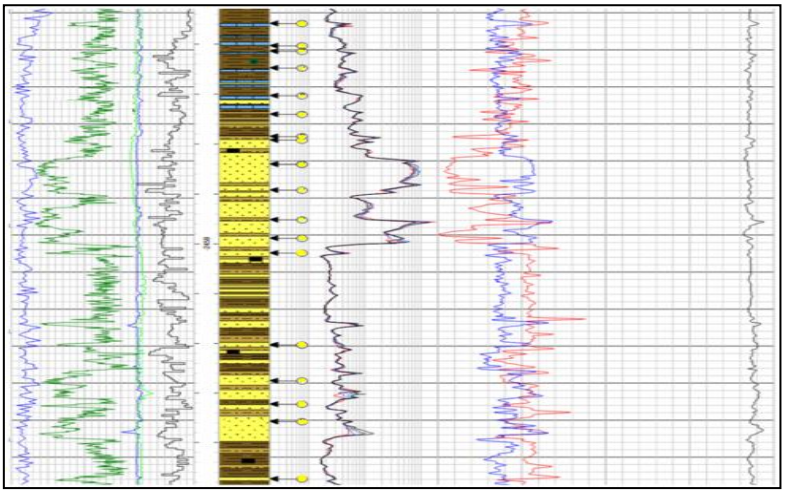


Fig. 12.C.1 – Log of a multi-layer formation

However we want to get a better understanding of the vertical distribution of the production, hence the contribution and characteristics of individual layers, or selected groups of layers. We will execute a multilayer test and perform a multilayer analysis. The challenge is to see if we can discriminate the layers with the standard information we have, or to add measurements and/or specific test sequences to allow this discrimination.

Analyzing a multilayer reservoir may be eased if there is a 'multilayer behavior' and the pressure response that cannot be matched with a homogeneous model. However this is not required. Even multilayer formations showing a global homogeneous behavior in terms of pressure-rate response can be subject to multilayer tests and analyses if we decide to add measurements or adjust the test sequences in order to isolate individual contributions.

12.C.2 Available models

In order to simulate multilayer responses modern software offer 3 types of models. All these models are able to provide the global pressure response and individual layer rates:

- **Analytical models**: The first and most common model is the double-permeability reservoir, which has now been around for thirty years. It has been extended to three, four and more layers, and recent developments can model the response of complex slanted and multilateral wells, all allowing crossflow between the layers.

- **Analytical commingled multilayer models**: A mathematical trick allows the simulation of the pressure and rate response for any number of layers, provided that there is no reservoir crossflow between these layers. Each such layer may correspond to any analytical model, including the multilayer analytical models presented before.

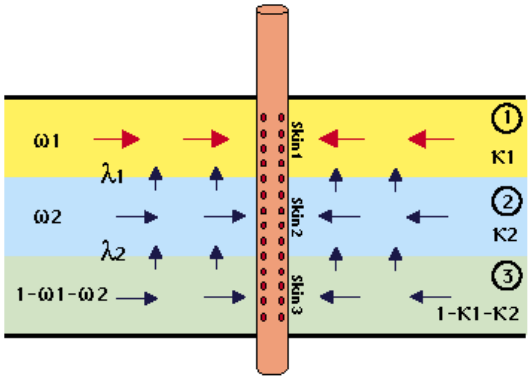


Fig. 12.C.2 – Schematics of a 3-permeability model

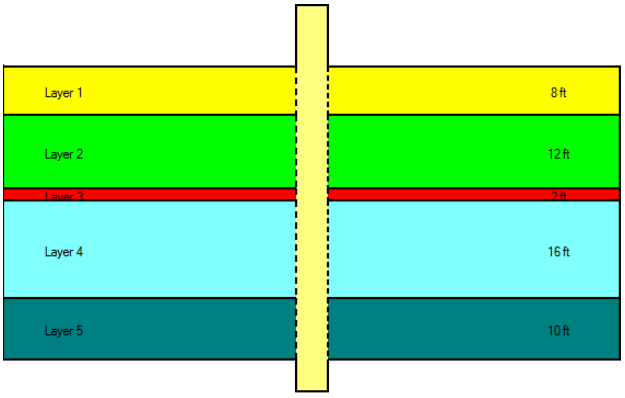


Fig. 12.C.3 – Schematic of a generic multilayer analytical model

- **Numerical models**: A multilayer numerical model with cross flow in the reservoir can be easily built by defining vertical leakage governing the flow at the interface between each layer. The anisotropy defined here is not the anisotropy of the layers but of the semi-permeable wall between the layers.

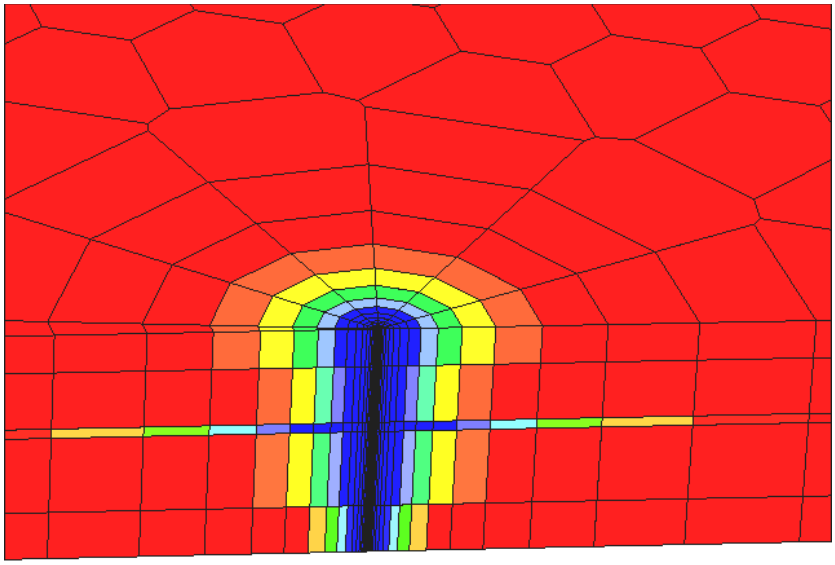


Fig. 12.C.4 – Multilayer numerical model

12.C.3 Standard tests

A standard well testing acquisition provides only the total production rates and bottom hole pressure channel; they represent the global behavior and cannot give direct access to individual layer properties. So the layered nature of the formation will be characterized only if the Bourdet derivative exhibits a heterogeneous behavior.

The typical analytical model used to perform such standard analysis is the double-permeability model, which assumes that the reservoir is constituted by two layers that may or may not be producing to the well, and that may or may not be communicating at the level of the reservoir.

The simplest homogeneous reservoir model will have 3 parameters: C, kh and skin. The double-permeability model will have 7: C, total kh, skin to layer 1, skin to layer 2, ω (porosity ratio), λ (cross-flow connectivity) and κ (permeability ratio). This is described in details in the Reservoir Models chapter.

Incidentally the name of KAPPA Engineering comes from the parameter κ.

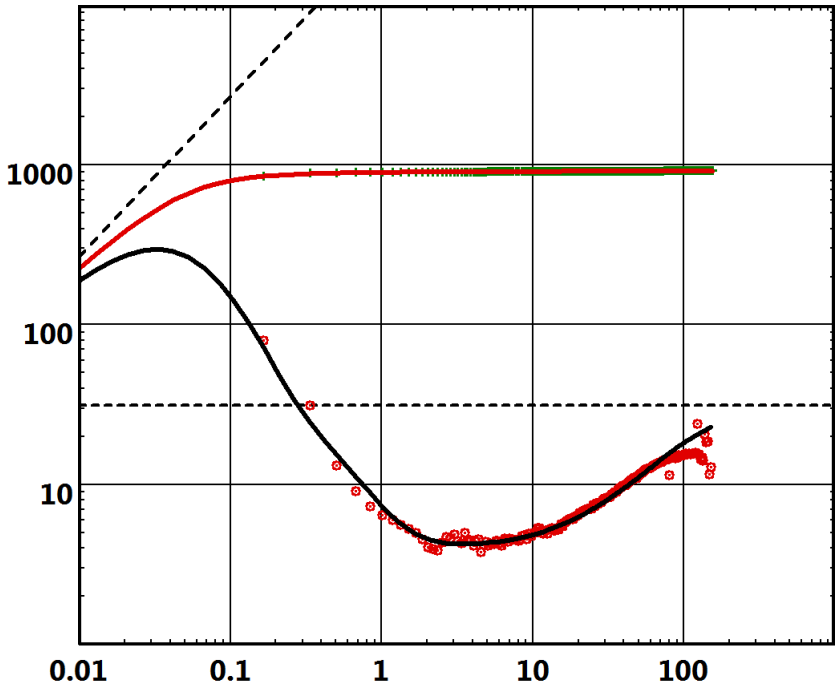


Fig. 12.C.5 – Loglog match with a double-permeability model

There are more complex analytical models available that model layered formations: three layers, four layers, and generic models allowing the combination of as many comingled layers as we want with separate well, reservoir and boundary models. However in a standard test we match models on a single, global Bourdet derivative response. Matching and identifying the seven parameters of the double-permeability model is already an act of faith, and will already require strong contrast between layer properties to show any specific behavior. Matching even more complex models without any strong information to constrain them is simply ridiculous.

So if we want to go further we need to change the test sequence or acquire additional information.

12.C.4 Using Production Logs

12.C.4.a Stabilized rate acquisition

The pressure and fluid velocity and density measurements are performed under stabilized rate conditions during runs up and down at several constant cable speeds.

The production logging data analysis can give access to rate versus depth logs, therefore to the individual layer rate and contribution.

It is necessary information for the determination of certain layer properties.

- The layer static pressure: using selective inflow performance analysis.
- The respective layer permeability by using the adequate multilayer model which calculates the individual layer contribution.

Note: We shall call in the following pages:

- Layer rate: the production rate measured above a layer, it is the sum of the production of all the layers below.
- Layer contribution: the individual production of a single layer.

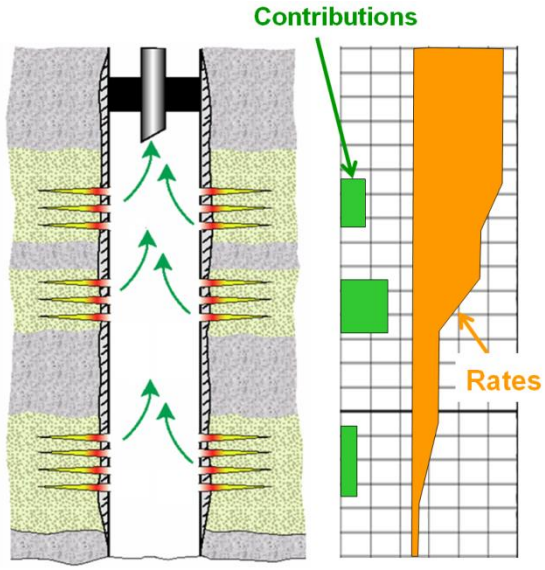


Fig. 12.C.6 – Layer rates and contributions

12.C.4.b Transient rate acquisition

The pressure and fluid velocity and density measurements can also be made versus time at constant depth and during the transient behavior due to a production rate change.

The objective is to acquire and observe the transient behavior of the layer rate, and then to intent to analyze it to get the individual properties by:

Either, analyzing globally the layer system and describing it in detail with a multilayer model matching

Or processing the data in order to extract the individual behavior and then to analyze separately the various layers using a classical single layer model.

12.C.5 Designing a multilayer test

We have seen above, that various types of measurement can be performed. Each type of acquisition provides different class of data that will be used in the adequate analysis.

The objective of a Multilayer Test is to gather the maximum information in a single well test therefore the design must offer all necessary circumstances to a complete acquisition.

The base of a multilayer test design is a multirate test, and the sequence of PLT operations allows the acquisition of both Static measurements of transient rate versus time and measurement of stabilized pressure.

A first step is to define the possible Static survey points, according to the openhole logs and/or the perforation. At this level logic and realism are the key points for a necessary simplification:

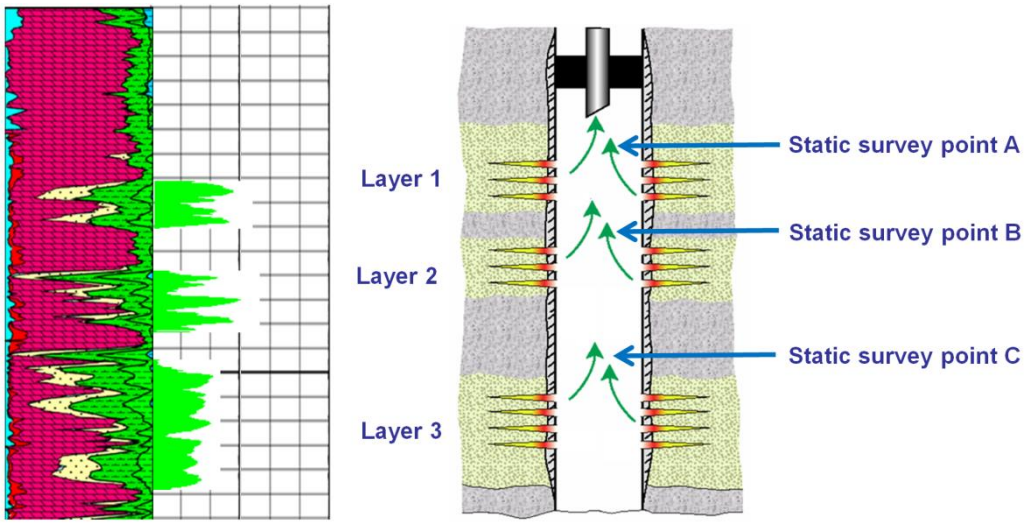


Fig. 12.C.7 – Survey location determination: simplification of the reality

Then to program the operation to acquire static and versus depth measurements, i.e.:

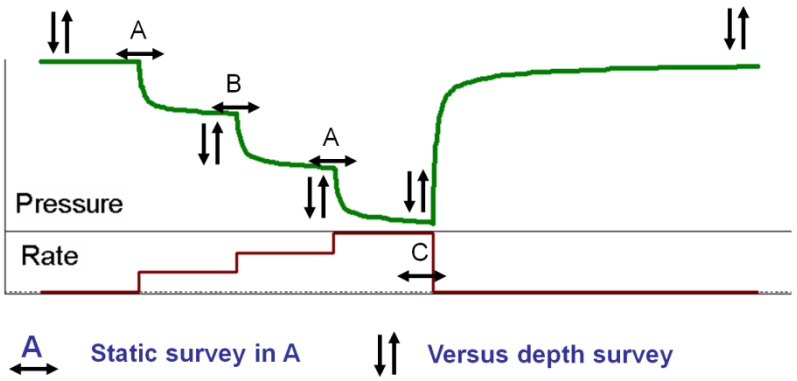


Fig. 12.C.8 – Example of testing sequence of events

This sequence includes the stabilized rate versus depth acquisition under various flowing and shut in conditions and also the transient rate static acquisition at the key points under various rate changes.

12.C.6 Multilayer analysis workflow

The method is based on the model matching, but not only the measured pressure but also the individual measured rate using the adequate analytical or numerical multilayer models.

Both versus depth and versus time acquisition can be used, but each one presents its own interest and provides certain information with more or less success:

- The rate versus time acquisition measures the transient rate behavior, its analysis gives better information on early time behavior (well conditions) and for late time behavior (limit conditions). Its weakness: it is easily subject to the noisy acquisition conditions.
- The rate versus depth acquisition measures the stabilized rate. It is more adequate for the IARF period (permeability and skin determination). Its weakness: it is a constant value ignoring any unstable behavior.

The model optimization is global and aims the adjustment of the complete set of parameters. This method, compared to other methods, sequential and iterative, presents the advantage not to accumulate the uncertainty at each step: when analyzing layer 1, then 1+2, then 1+2+3...

These methods show their limits above three layers.

The field data analysis presents several difficulties and pitfalls that can be avoided by following an adequate work flow.

12.C.6.a Preparation of the data

- The layer geometry must be simplified and clearly defined:

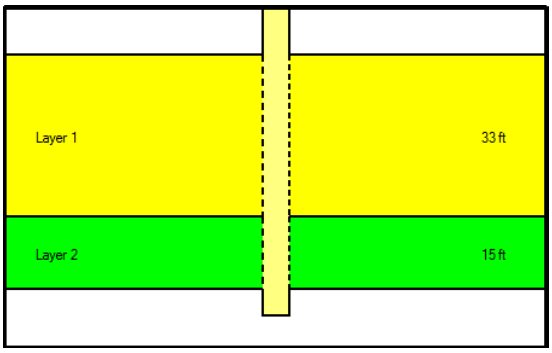


Fig. 12.C.9 – Layers geometry

- The pressure data must be first corrected at the same depth when the transient behavior was recorded at several depths.

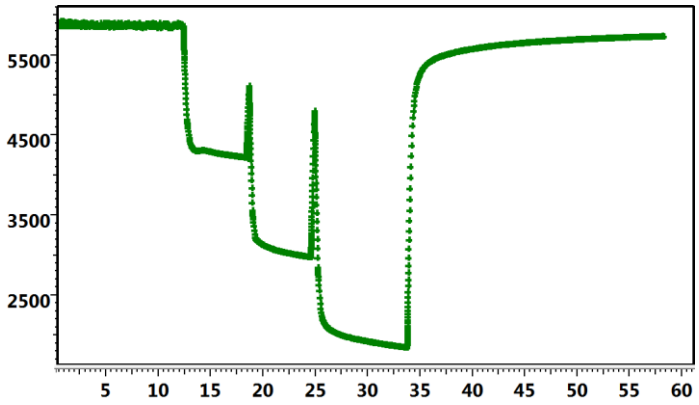


Fig. 12.C.10 – Pressure history

- The stabilized rate and/or contribution data must be calculated with the adequate software from the Production Logging measurements.
- The transient rate data must be extracted and set in a proper format files then synchronized with the pressure data.

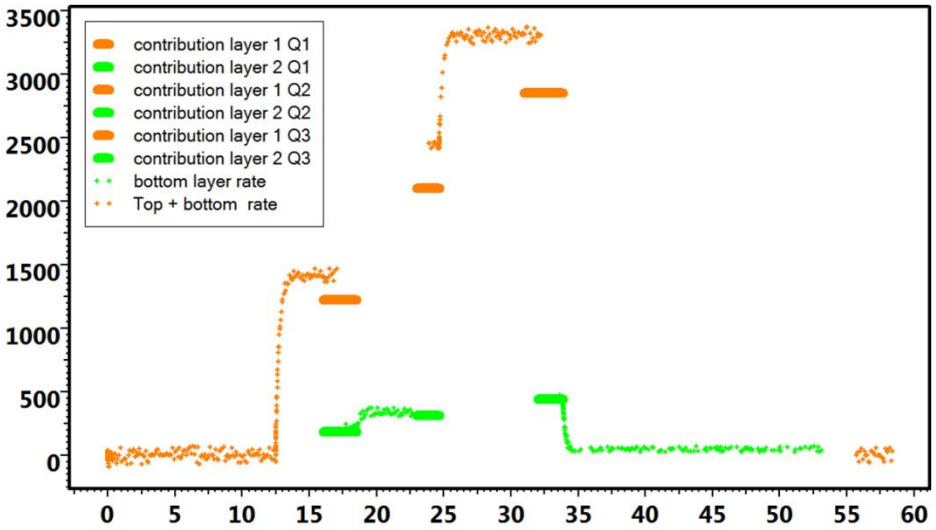


Fig. 12.C.11 – Rate and contribution history

Note: the pressure and rate model matching method used for this multilayer analysis does not requires specifically the rate data to be under the 'rate' or the 'contribution' format since, the model is able to provide the simulated individual production under any format.

12.C.6.b Getting the global results

In order to get a starting point for the model definition, it is necessary to perform first a standard analysis of the multirate test data. That provides the main parameter values for the global behavior: total permeability-thickness product, global skin, limit effect diagnosis.

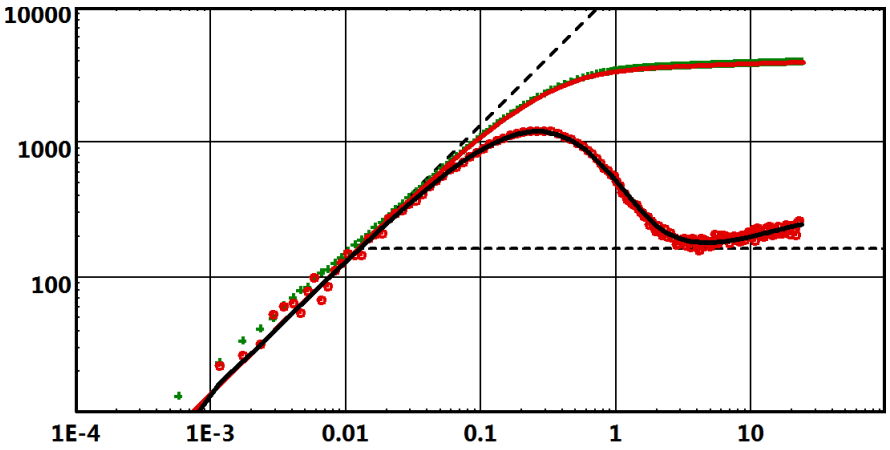


Fig. 12.C.12 – Single layer global match

- The total kh value will be kept in the rest of the analysis as a constraint for the global regression.
- The static pressure, found at 5869 psia will be also kept in the continuation of the analysis as a constraint as long as no 'layered pressure' hypothesis is considered.
- The wellbore storage value will also be kept since it is a well characteristic.
- The limit diagnosis is here a single fault at around 500 ft.

12.C.6.c Multilayer model building and first run

The layer geometry is defined, then, the layer rates and contribution are input.

The first multilayer model parameter definition is, by default uniform permeability, equal skin and boundaries conditions are taken identical to the standard analysis results.

Parameter	Value	Unit
Layer 1		
Skin	2.5	
k	26.017	md
h	33	ft
Phi	0.1	
L No flow	500	ft
Layer 2		
Skin	2.5	
k	26.017	md
h	15	ft
Phi	0.1	
L No flow	500	ft
Wellbore & other reservoir parameters		
Pi	5869	psia
C	0.00933634	bbl/psi

Fig. 12.C.13 – Initial multilayer parameters table

The result of this first run confirms the global pressure behavior:

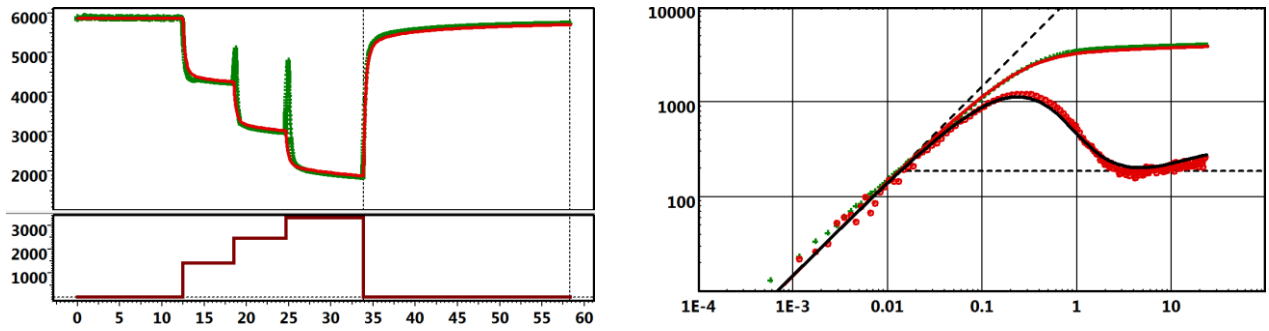


Fig. 12.C.14 – Initial history and log log match

But the non-matching simulated layer rates and contribution reveals clearly the permeability contrast consequence on the individual contributions:

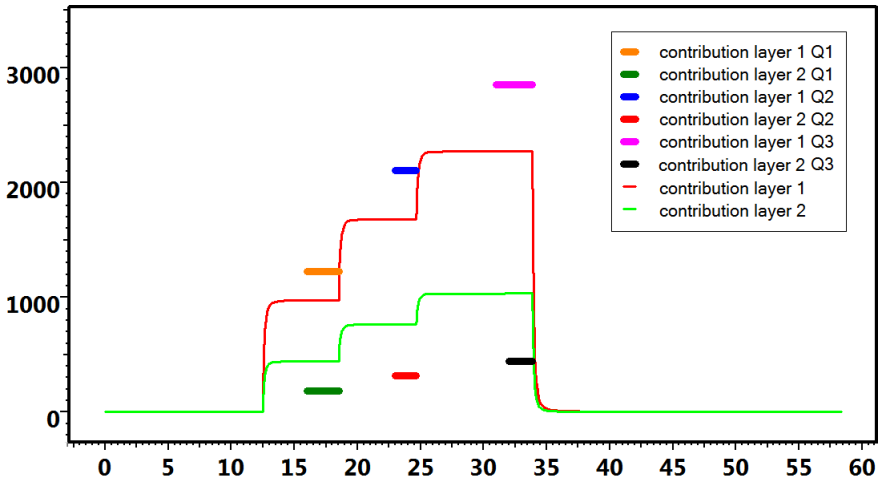


Fig. 12.C.15 – Initial layer rate match

12.C.6.d First improve of the model

The individual permeability values will be adjusted by performing a nonlinear regression on the pressure and rate values with only the permeability and the skin as adjustment parameters. The constant total kh has to be set as constraint.

This has to be done on the complete pressure history and by selecting the stabilized rate values adjustment as objectives.

For the sake of the efficiency it is absolutely compulsory to select the most adequate regression point on the history plot, taking care to eliminate the 'abnormal' pressure behavior like phase segregation effects or operational errors, i.e.:

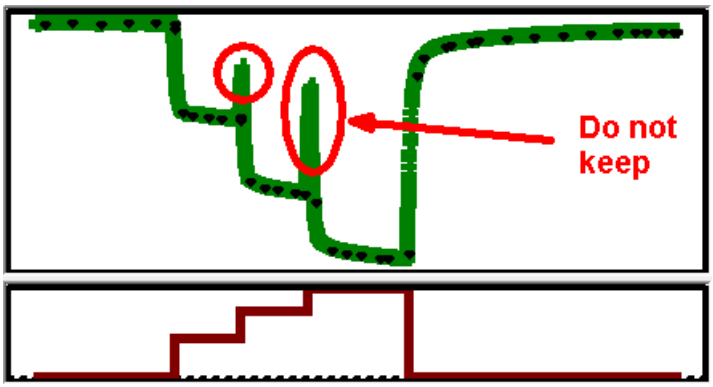


Fig. 12.C.16 – Regression point selection

The effect of the nonlinear regression on the contribution and rate matching is immediate:

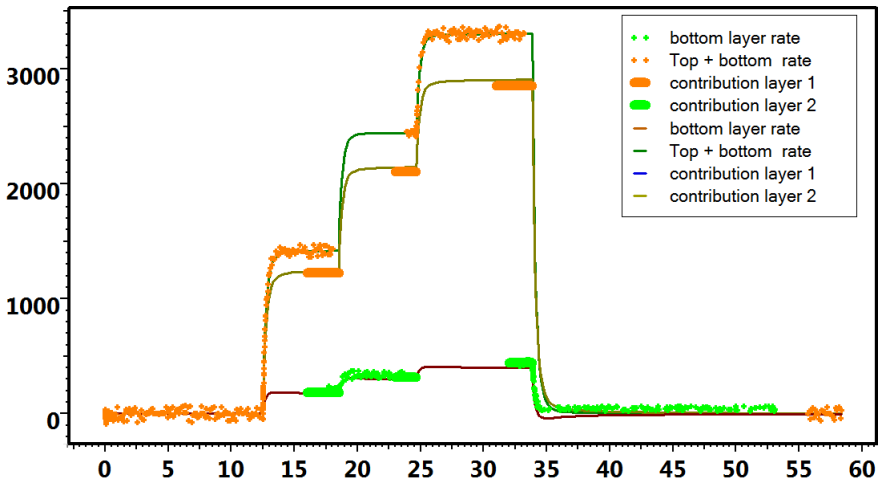


Fig. 12.C.17 – Layer rate match after regression

It is the result of the adjusted permeability and skin values:

Layer 1			
Skin		4.2	
k		38.5067	md
h		33	ft
Phi		0.1	
L	No flow	500	ft
Layer 2			
Skin		3.1	
k		11.4146	md
h		15	ft
Phi		0.1	
L	No flow	500	ft
Wellbore & other reservoir parameters			
Pi		5869	psia
C		0.010468	bbl/psi

Fig. 12.C.18 – Multilayer parameters table after regression

The quality of the pressure match on the loglog and history plot is maintained:

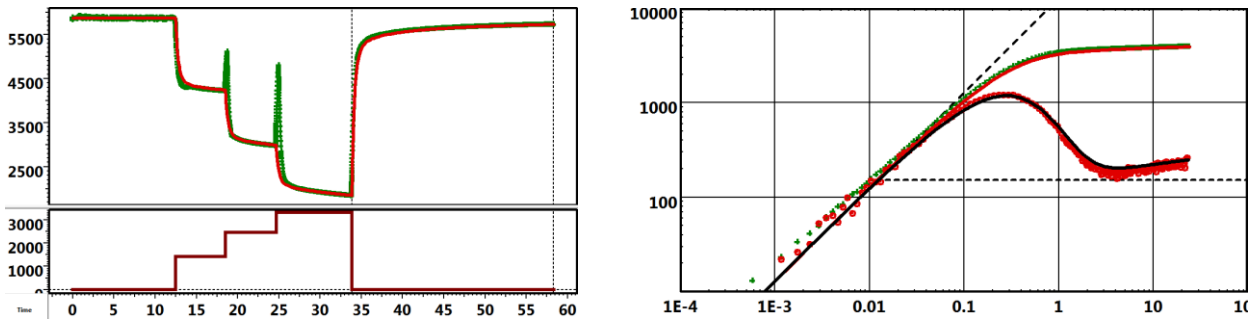


Fig. 12.C.19 – History and log log match after regression

12.C.6.e Final model adjustment

Once the main parameters are determined and considered as reliable, the additional parameters, like the boundary geometry, can be then adjusted.

The same process is used, with the nonlinear regression, to adjust the limit distance:

- The permeability, the skin, the wellbore storage and the initial pressure values are removed from the regression parameters list.
- More weight is given to the transient rate measurement matching.

The final model parameters values:

Layer 1		
Skin	4.2	
k	38.5067	md
h	33	ft
Phi	0.1	
L No flow	626.97	ft
Layer 2		
Skin	3.1	
k	11.4146	md
h	15	ft
Phi	0.1	
L No flow	1657.61	ft
Wellbore & other reservoir parameters		
Pi	5869	psia
C	0.010468	bbl/psi

Fig. 12.C.20 – Final multilayer parameters table

Provide a match satisfying:

1) Pressure history matching:

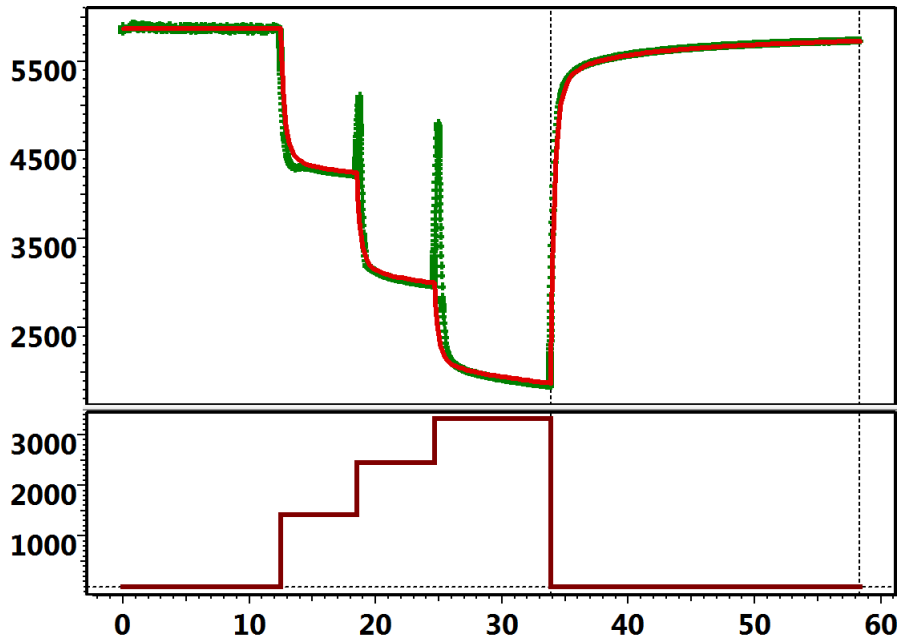


Fig. 12.C.21 – Final pressure history matching

2) Pressure and derivative loglog:

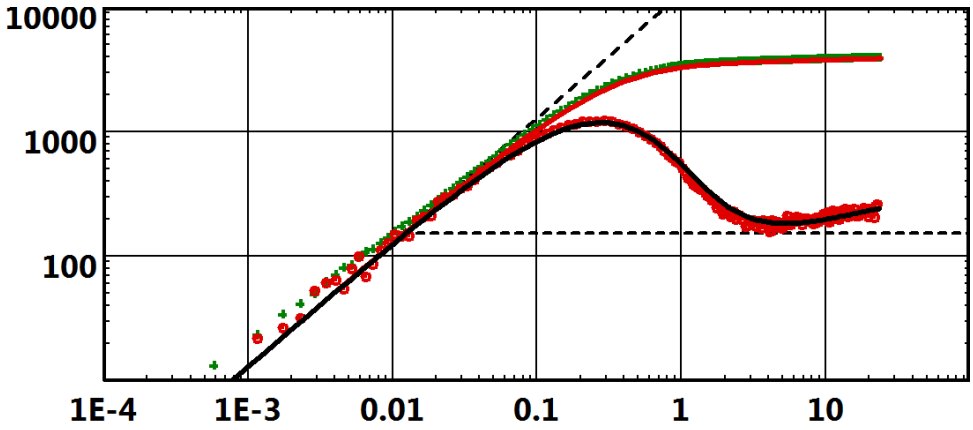


Fig. 12.C.22 – Final pressure and derivative loglog

3) The production rate and contribution:

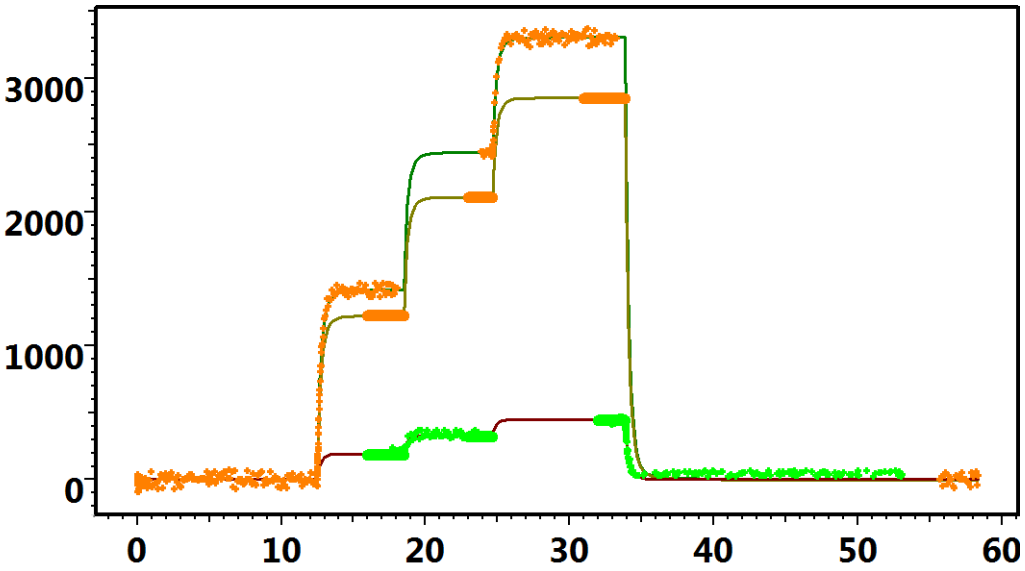


Fig. 12.C.23 – Final production rate and contribution match

12.C.6.f The solution uniqueness

We are dealing here, in this specific case, with a 12-parameter system to be adjusted to match three data channels, one pressure and two layer production rates.

It would be presumptuous to pretend that this solution is unique since we are looking for the minimum of three values (the average distance between simulated and measured pressure and rates) in a 12 dimensions space. This complex space certainly contains multiple areas where the searched minimum is approached (local minimum), and a unique one which is the absolute minimum.

It is certain that other sets of slightly different parameters could give equivalent satisfaction in term of pressure and rate matching, but any result has to be guided and eventually chosen according to other external information coming from geology, geophysics or just the logic.

This method remains, by its principle and its flexibility, a perfectly adequate tool to help us in this search and to check the validity of the results.

12.D Interference Tests

Under the umbrella of multiple well, well testing comes the classic and theoretically simplest (and oldest) of all pressure transient tests, the interference test. Pulse testing is just another variety of the interference test that was devised to avoid the long disruption of production that a typical interference test sometimes was causing. It was also devised to avoid natural phenomena such as tide effects and reservoir noise that could sometimes make the interference test difficult to analyse.

C. V. Theis developed the interference test for hydrogeology (1935). Johnson, Greenkorn and Woods devised the pulse test and Kamal and Brigham perfected and developed a special analysis procedure using type curves to facilitate the analysis by hand. None of the old analysis techniques are relevant today, thus we will not repeat what is already abundant in the old literature on well testing but concentrate on the modern methods of analytical and numerical modelling.

Interference testing involves at least two wells but the test can easily be extended and analysed today with any number of wells present in the interference test scenario. Simply put, the interference test involves the withdrawal or injection of (reservoir) fluids from/into one well while measuring the resulting response in another. So we have the concept of an "Active well" and an 'Observation well'. It is the well response in the 'Observation' well that is subject to analysis and since this well is (hopefully) at static conditions the concept of skin and wellbore storage is eliminated. Thus, in the majority of cases, the Line source solution (or the Theis' solution) as presented in the chapter on 'Theory' can be used directly to analyse the observation well pressure response.

The solution, at any point and time, for a Line Source well producing a homogeneous infinite reservoir, is given by the following:

$$p(r,t) = p_i - \frac{70.6qB\mu}{kh}\left[-E_i\left(-\frac{948.1\Phi\mu c_t r^2}{kt}\right)\right]$$

A typical line source response is displayed in the figures below, on loglog (with the Bourdet derivative) and semilog scale.

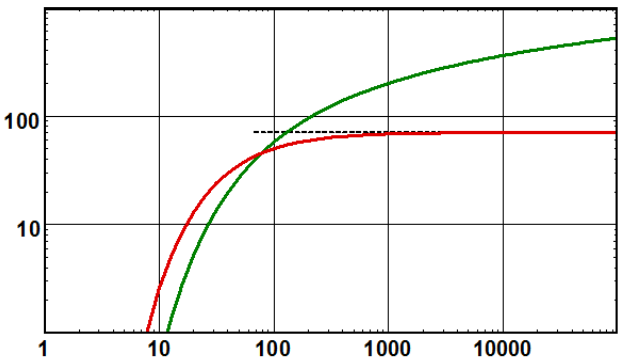


Fig. 12.D.1 – Line source loglog plot

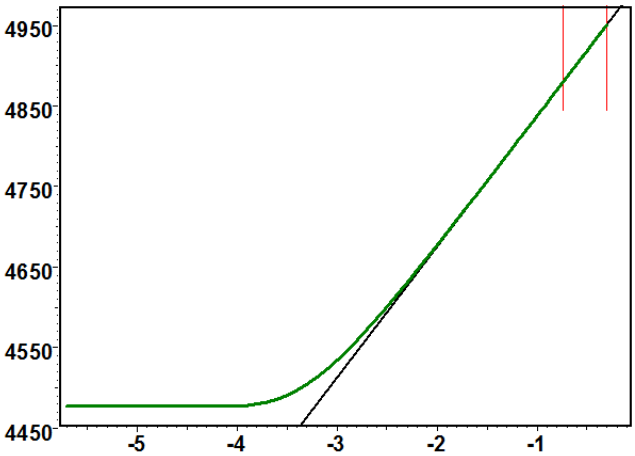


Fig. 12.D.2 – Line source semilog plot

As demonstrated in the chapter on 'Theory', there is a value of time above which the Line Source Solution reaches a 'regime' where one can use an approximation of the highest interest to the well test interpretation engineer. It is the semilog approximation and this regime is called **Infinite Acting Radial Flow**, or **IARF**.

IARF: For $t \geq \frac{379200\Phi\mu c_t r_w^2}{k}$ $\quad p(t) \approx p_i - \frac{162.6q\mu}{kh}\left[\log(t) + \log\left(\frac{k}{\Phi\mu c_t r_w^2}\right) - 3.228\right]$

The workflow involved in the analysis of the observation well pressure response is thus largely the same has that of conventional well testing. Both loglog and semilog analysis is used and can be valid, and the Line source and wellbore storage and skin models are available to analyse and model the response.

Heterogeneities such as layering, double porosity and permeability and outer boundaries can also be applied analytically.

The figure below illustrates the response in an observation well at static conditions resulting from a simple constant rate production of the active well.

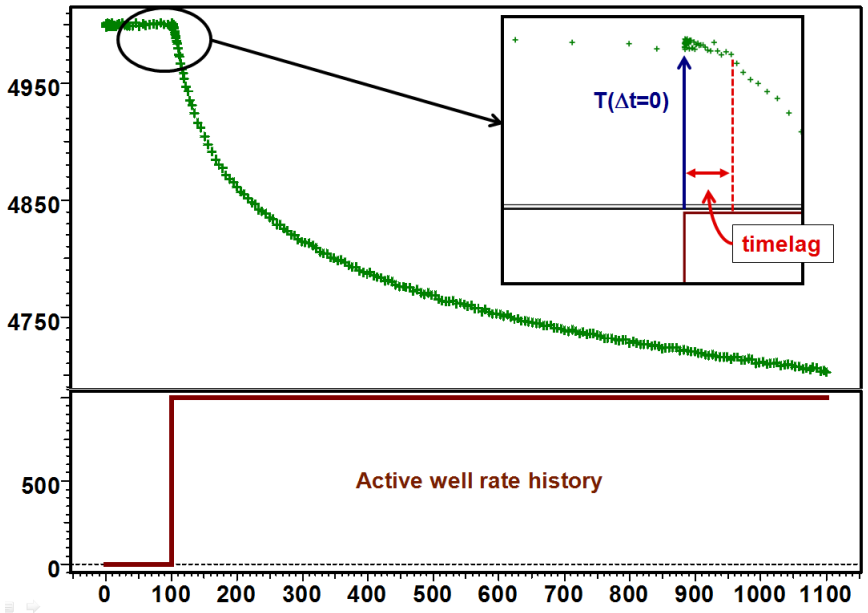


Fig. 12.D.3 – Interference response

As illustrated in the figure above there is a delay (time lag) before the pressure gauge can start to see the response in the observation well. The loglog plot below is constructed as the pressure change from time T(Δt=0) thus it can be seen that the first points before there is an actual detectable response in the pressure signal has to be ignored.

Below is the response plotted in loglog coordinates as the pressure change and the Bourdet derivative.

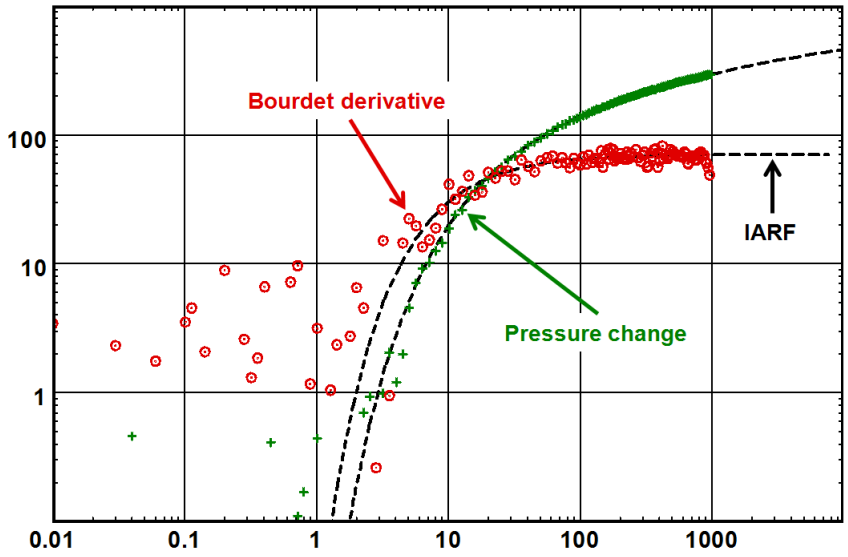


Fig. 12.D.4 – Loglog plot of observation well response

12.D.1 Homogeneous, sensitivity to parameters

The governing parameters are:

kh Permeability-thickness product.

$\phi c_t h$ Reservoir storativity.

Both are results from the analysis. It is said that the only way to get a reliable value for rock compressibility is through an interference test. Of course this assumes that you know the fluid saturations, and the individual fluids compressibility and the porosity. Normally, however, it is the ϕc_t product that is posted as the result with the permeability vector k.

The following figures illustrate the sensitivity to the porosity Φ.

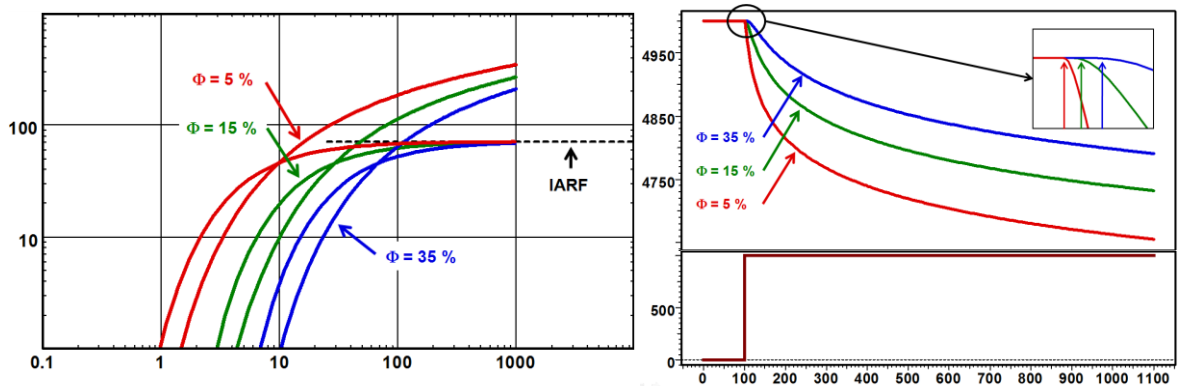


Fig. 12.D.5 – Sensitivity to the porosity, Φ

And below we illustrate the sensitivity to the permeability thickness product, kh.

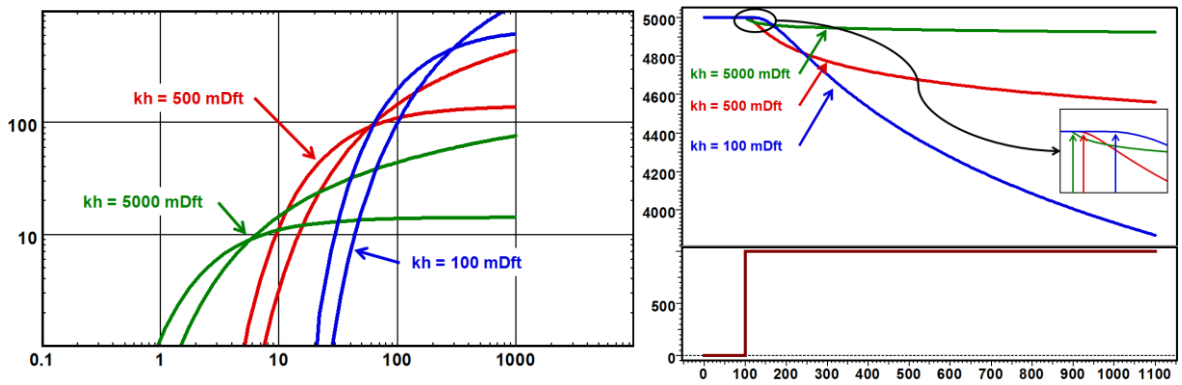


Fig. 12.D.6 – Sensitivity to permeability, kh

Not surprisingly, we observe that the lower the porosity and higher the permeability, the disturbance caused by the active well travels faster to the observation well. The lower the permeability and the porosity the higher is the response amplitude in the observation well.

Actually the original leading parameters can be seen in the line source equation and the exponential function argument:

$$p(r,t) = p_i - \frac{70.6qB\mu}{kh}\left[-E_i\left(-\frac{948.1\Phi\mu c_t r^2}{kt}\right)\right]$$

On the time scale, determining the time lag, it is the diffusivity group: $\frac{\Phi\mu c_t}{k}$

On the pressure scale, determining the pressure amplitude, it is the transmissivity group: $\frac{kh}{\mu}$

12.D.2 Influence of wellbore storage and skin

Ignoring wellbore storage in the active well can lead to underestimation of kh and an over estimation of the porosity Φ. Wellbore storage and skin will increase the time lag and decrease the amplitude in the observation well, it acts as a delaying effect at the active well and this effect is increased by the skin damage.

Below we have illustrated the response in the loglog plot of two different cases of wellbore storage and skin and compared this to the line source solution. The figure to the right illustrates the increase in time lag and the decrease in the amplitude of the response.

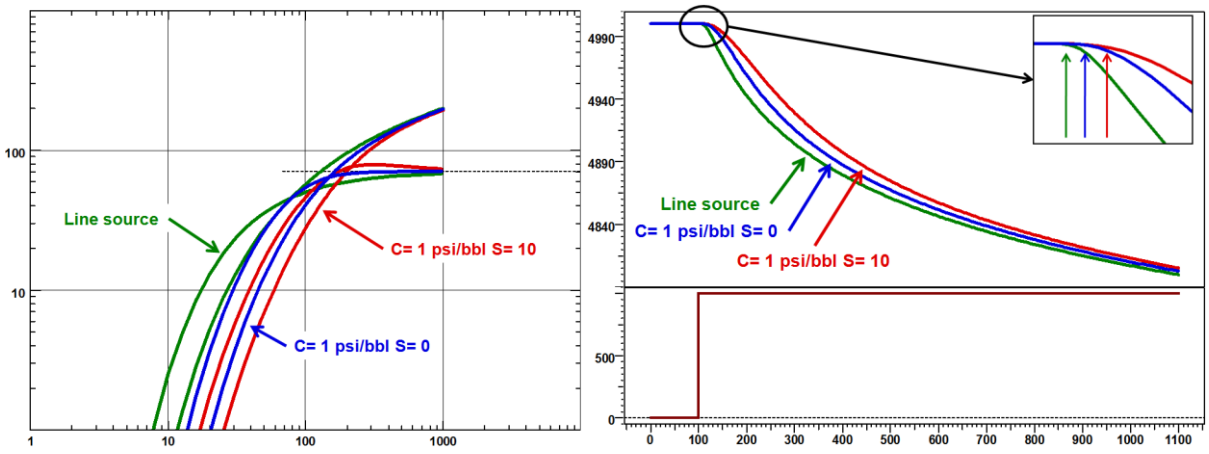


Fig. 12.D.7 – Sensitivity to wellbore storage and skin

Note that the wellbore storage coefficient value used in this simulation is taken very large to make the effect more visible. It is certain that a normal wellbore storage value would have a lot less effect.

12.D.3 Multilayer numerical: An overview

The interference problem can easily be solved numerically with any number of layers, with or without cross flow. It would be beyond the scope of this document to present all possible scenarios in a multilayer situation so we are just presenting an appetizer of what can be done using a numerical linear solution to the problem. It would be up to you, the user, to apply what is outlined here to your own particular problems.

In order to keep it simple and in line with what was discussed in the foregoing section on double permeability, we will only consider a system of two layers with cross flow.

The figure below illustrates the simulated loglog response of a two layered system with the following characteristics matched with the analytical double permeability model for comparison.

Layer name	h	k	kh	Phi	Phi.Ct.h	% k.h	% Phi.Ct.h
	ft	md	md.ft		ft.psi-1		
Layer 1	15	66	990	0.017	7.65E-7	99	10.1796
Layer 2	15	0.66666	9.9999	0.15	6.75E-6	0.99999	89.8204
All Layers	*(total)*	*(average)*	*(total)*	*(average)*	*(total)*	*(total)*	*(total)*
	30	*33.3333*	*1000*	*0.0835*	*7.515E-6*	*100*	*100*



Fig. 12.D.8 – Numerical layer properties

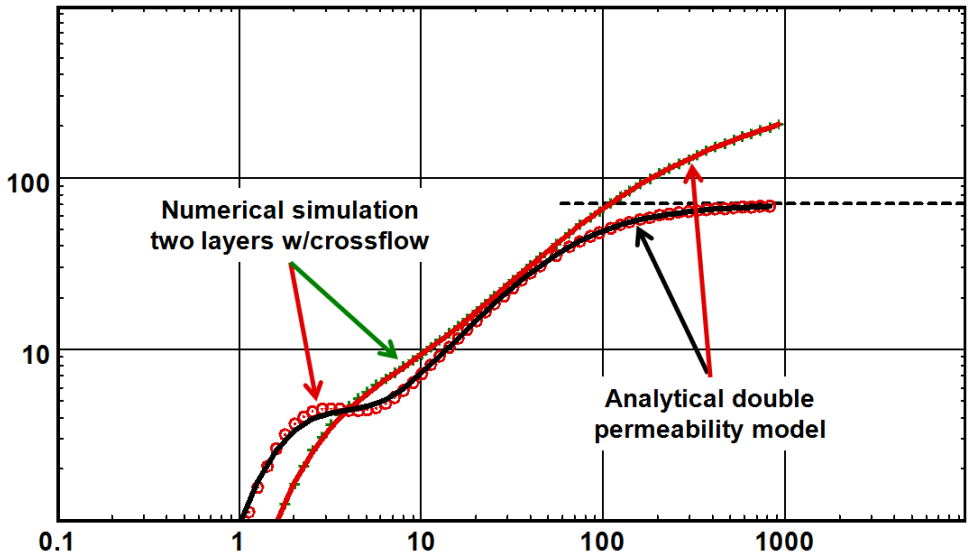


Fig. 12.D.9 – Simulated numerical and analytical model match

One can also open and close perforations of the layers in the observation well of the example. If the high permeability and low storativity layer is turned off the pressure gauge in the observation well will only record the pressure interference through the lower low permeability layer. One can see the comparison of the response in the observation well with the upper layer closed and the response with both layers open. One can indeed conclude that the effect of the active well will induce cross flow from the lower to the upper layer in the observation well. See the figure below.

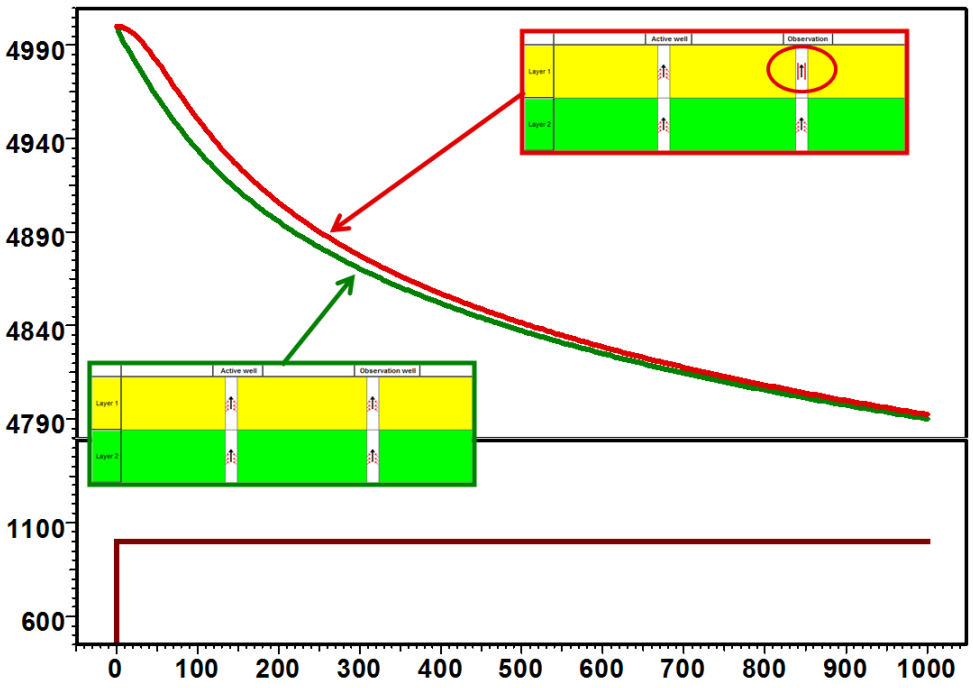


Fig. 12.D.10 – Comparison of response with dominating interfering layer closed off

12.D.4 Other application of the numerical model

The analytical models are limited with respect to the well models of the active well. However, using the numerical model the active (and the observation) well can be any type of well. Naturally fractured (infinite conductivity), induced finite conductivity fracture, limited entry, slanted and horizontal wells. Horizontal fractured wells can also be defined. The well model of the active well can and will in some cases have a direct influence upon the response measured in the observation well thus it makes sense to take this into account in any analysis or design work carried out.

The figure below illustrates the response in a vertical observation well caused by production of a vertical, and two differently configured horizontal wells. The horizontal well at 0° has the toe pointing to the active well in the X direction and the well at 90° has the heel and toe parallel to the Y direction.

Not surprisingly, one observes that the response caused by the horizontal active well with the tip pointing towards the observer is 'seen' by the observer earlier than the interference caused by the horizontal well which points in the Y direction.

Another interesting observation is that the response amplitude caused by the vertical active well is higher than the horizontal well at 90°, and the amplitude caused by the horizontal well placed in the X direction, pointing towards the observer is causing the highest delta p.

From this follows naturally, the fact that it should be possible from these observations to identify areal anisotropy that can also be used in the numerical models.

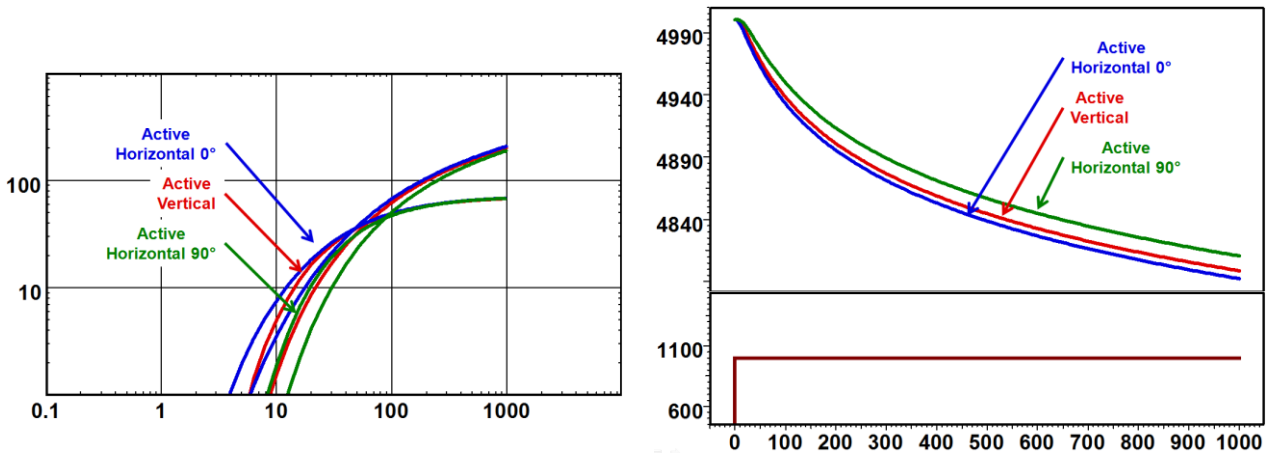


Fig. 12.D.11 – Vertical observer horizontal active well: Loglog and history plot

The numerical model will also take care of reservoirs that are not handled analytically. Composite reservoirs can easily be modelled using the numerical model. Variable data fields such as thickness, porosity and permeability can be modelled.

Below we illustrate the use of the numerical model on fake reservoir with variable permeability. The distance between the observation and the active well is some 12500 ft as the 'crow flies', however the actual distance the diffusion has to travel before a response is seen in the observation well is a lot more tortuous because of the faults. The active well is producing for a month followed by a two months shut-in of the active well. The observation well is at static conditions throughout the interference test. It is possible to extract both the production and the shut-in and display the derivative and the pressure change in the loglog plot. However it can be immediately be seen in the simulated pressure history that even after two months of shut-in the effect has not yet been detected in the observation well thus the loglog plot will be empty and no diagnostics can be done. In fact in this case the diagnostic plot becomes the history plot and the interpreter will thus just try to match a model to the history response. See the next section on 'Interference testing and real life'.

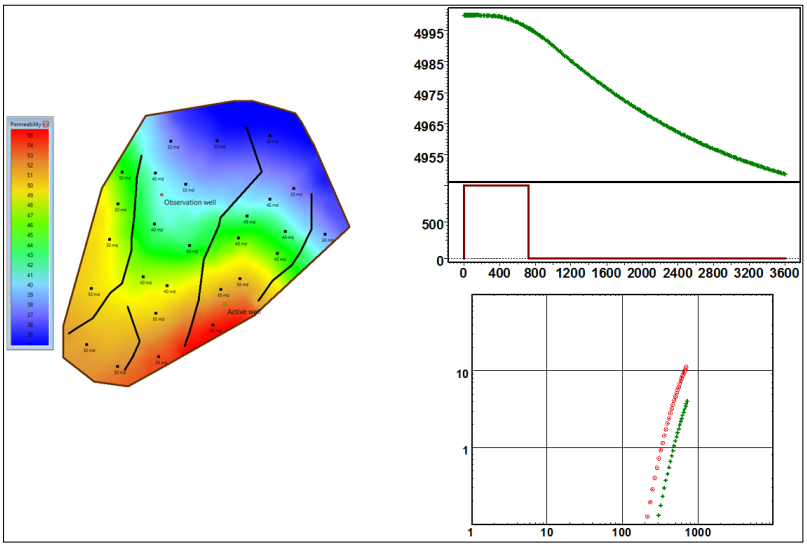


Fig. 12.D.12 – Simulated numerical interference response

12.D.5 Interference testing and real life

12.D.5.a The signal

In an interference test we measure a signal in one or several wells caused by a change in conditions in one or more active wells. The pressure signal can have a short term changing amplitude with a certain value or the pressure signal is the result of more long term and larger changes. It is important to realize that a signal can only become detectable by the pressure gauge in the observation well(s) if it induces a break in the latent response that may already be present due to natural or other foreign causes.

The signal in itself must be measurable by the pressure instrument, thus the resolution of the tool is an issue that cannot be overlooked. This was in particular critical in the past when the quality of the measuring tools was average and the best pressure gauges were not readily available, and when they were, at an exuberant price. This is no longer an issue as most pressure and temperature sensor, at least those based on quartz technology, are readily available and at an affordable price. Even permanent downhole gauges are today of such a quality that they can easily be used for interference testing were only minute pressure changes is necessary in order to detect a signal through the reservoir.

The most common natural signal present in static pressure measurement is the Tide; the combined effect of the gravitational forces exerted by the Moon, the Sun and the rotation of the earth. This effect is not only seen in pressure measurements in offshore fields, but is also common in the middle of the desert or in the middle of a rain forest. To enable the detection of a manmade signal it must therefore be possible to distinguish this signal from the tide signal. A pulse test would never be designed in such a way that the pulse period would correspond to the natural tide period.

The below figure illustrates the tides signal measured in a static observation well during a long term interference test in some part of the world.

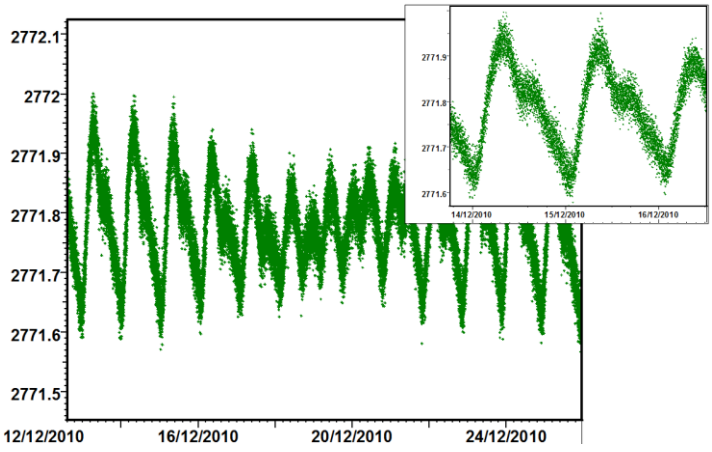


Fig. 12.D.13 – Tides

There is no response in the signal other than the tide effect so there is no other external influence on the measurements. We are 'seeing' no interference i. e. there is no 'break' in the signal. To illustrate that we have indeed a 'break' we are looking at the same signal but some three months later on in the history of the measurements. There is definite a 'break' that can be explained by the interference from a nearby injector.

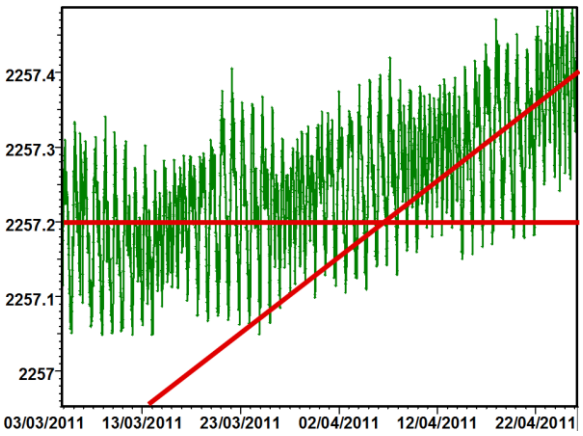


Fig. 12.D.14 – 'Break' detected

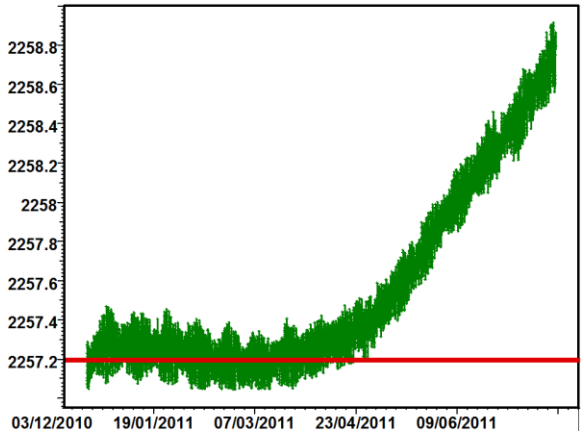


Fig. 12.D.15 – The whole story

Although the 'break' is small to start with we can definitely see that there is an interference response in the well which was caused by a nearby injector when we look at the 'whole' story.

The tide signal oscillates with a delta p of about 0.3 psi, the 'break' is achieved by a total delta p of about 1.5 psi.

The following figure illustrates the response in a well where the pressure rises linearly over time; in this pressure response there is no 'break' thus no interference response. In fact the pressure gauge is 'drifting' with a drift of about 0.03 psi/day.

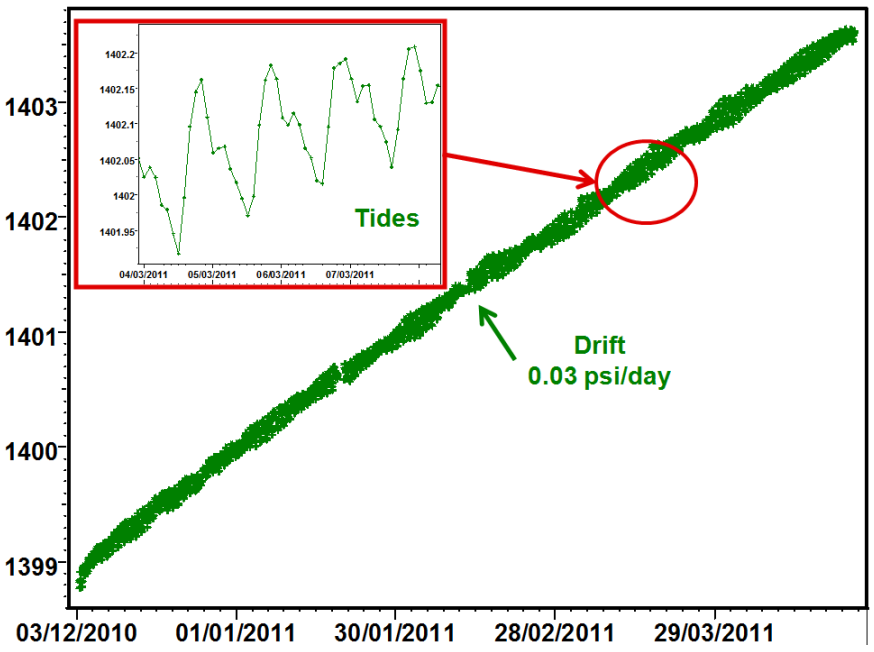


Fig. 12.D.16 – No interference response, drifting gauge

12.D.5.b The tests

One of the pitfalls with interference and pulse testing is that they are so easy to design using the relatively simple theory. This will sometimes backfire and become a problem. The theory can in most cases show that whatever scenario you choose with as many wells that you select as observers or active wells, the theory says that you will get a detectable response every time (as long as you're not testing tombstone and the distance between the wells is not too big). You can even have producers or injectors as the observer wells, the theory will show that this works. Experience shows us that this is more often than not a myth in real life.

The workflow is based upon the same principle as conventional PTA where a diagnostic plot is generated and plotted in loglog coordinates with the pressure change and the Bourdet derivative plotted versus the elapsed time. If the workflow is adhered to it is an easy task to differentiate the shapes and thus the different reservoir and boundary models and deduce all pertinent parameter associated with this and that model. Therefore the requirement is that some 'clean' periods are built into the test design. By clean periods we mean periods of constant flowrate, be it shutin, injection or production periods.

Unfortunately experience show that although these 'clean' periods may have been built into the design, they are often too short so there is not sufficient time to see in the pressure response the actual influence of these 'clean' periods, thus any extraction to the loglog plot is not possible. In real life the production or injection is never totally stable, and the flowrate is variable, and on top of this, may not have any 'built-in' clean periods at all, so the interpreter is left with an empty loglog plot and is reduced to the task of blindly matching a pressure history.

The below figure illustrates a typical long term interference test where the active well is just following the normal operation of production of the active well with all the day to day incidents that always happens to disturb the this production, such as unscheduled shutins, changes in rate, perturbations due to normal and daily operation etc. In fact the interference design here is just the ramp-up of production at the end of November 2001 which we can see has little noticeable effect on the pressure response in the observation well.

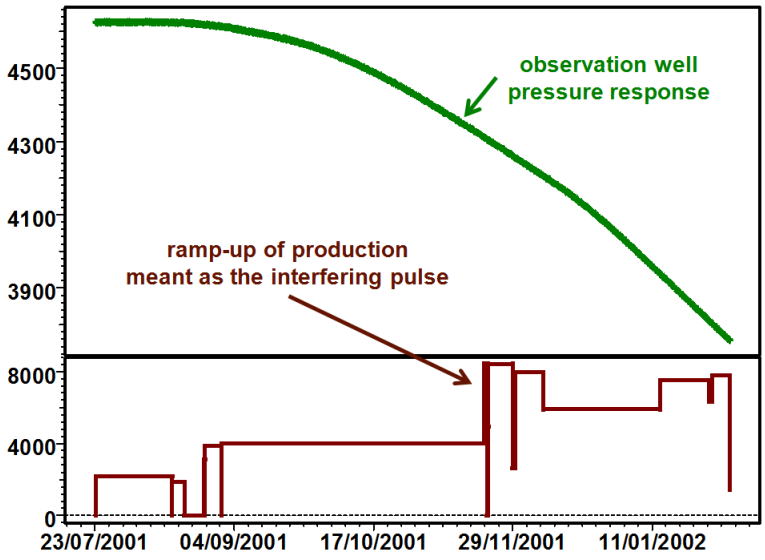


Fig. 12.D.17 – Interference test

We lose the diagnostic power of the loglog plot.

By artificially adding a clean period to the production history of the previous example, a shutin at the end, and generating the model to 5000 hrs shutin time (some 200 days) we can easily observe that the period of buildup has to be a minimum of some 100 days long to give a reasonable response at the observation well and allow the extraction of a loglog plot for diagnostic purposes. Not an easy task to sell to the management. See the illustration below.

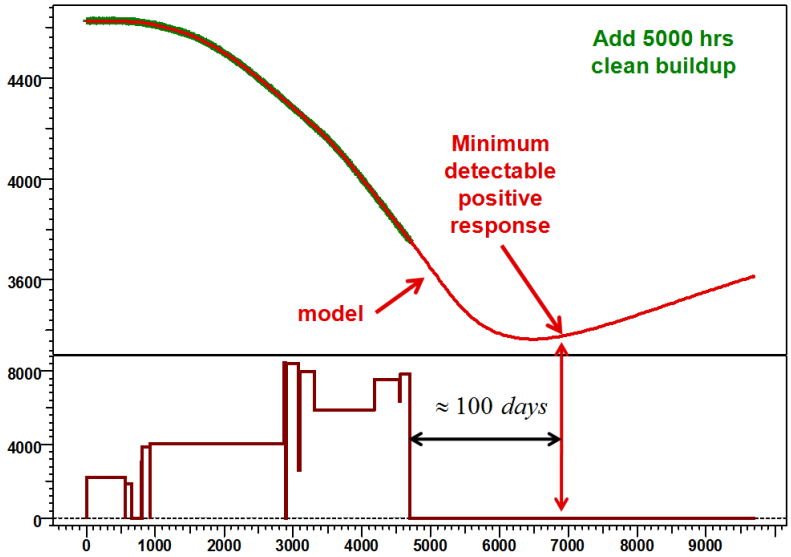


Fig. 12.D.18 – Clean period design

The only diagnostic we can exercise here is to blatantly state that, yes, there is a response in the observation well and the reservoir in between the wells is in communication. Using the history and the simple homogeneous model will (hopefully) give a match, thus a value for permeability kh, and the storativity product Φc_t. Assigning any parameters to heterogeneities would be pure speculation.

Very often we are actually only looking for a yes or a no answer. If no communication is detected this is also valuable information to the practicing reservoir engineer.

Interference testing in producing fields is possible and can be very successful. The times it does not work it is usually due to the under design of the desired minimum pulse amplitude and the lack of the induction of 'breaks' that can be recognized and distinguished from the background noise and trend in the observers.

The ideal interference test is of course carried out in a reservoir that is at rest, but we all know that this would be a costly affair in a producing field....

12.D.6 Pulse tests

The pulse test was first developed when the first high sensitive mechanical pressure gauges became available in the 1960-70's. Since these gauges could measure a small pressure change the pulse test was designed so that the active well flowrate rate was alternating between short flow or injection periods and equally timed shut-in periods. The idea was to be able to shorten the traditionally long duration of an interference tests.

As high sensitive pressure gauges were both expensive and not readily available, they were often reserved for this kind of test.

Later high accuracy electronic gauges became common and cheaper and consequently the argument of the pulse test to enable the shortening of the classical interference test did no longer hold.

However, the pulse test still has an application when the background trend and noise in the reservoir is such that a small response of the interference test can be difficult to detect and find in the pressure history. It is easier to recognize the pulsing behaviour resulting from a pulse test and is not easily lost when the time lag of the response is long.

If one is planning and programming a pulse test one should be aware that there is a phenomenon that can easily perturb the results. Many reservoirs are under the influence of tide effects which overall resembles the response from a pulse test. Therefore it is important to remember the tide influence on the background trends and noise and we need to know the tide amplitude and frequency. The pulse test must be programmed to be 'out of phase' with the tides and the response amplitude must be such that the two signals can be differentiated.

The early studies of the pulse tests proposed methods for manual analysis. At the time the proposed method turned out to be the best advantage of the pulse test compared to conventional interference testing. The method was based on the 'tangent method' and is illustrated in the below figure.

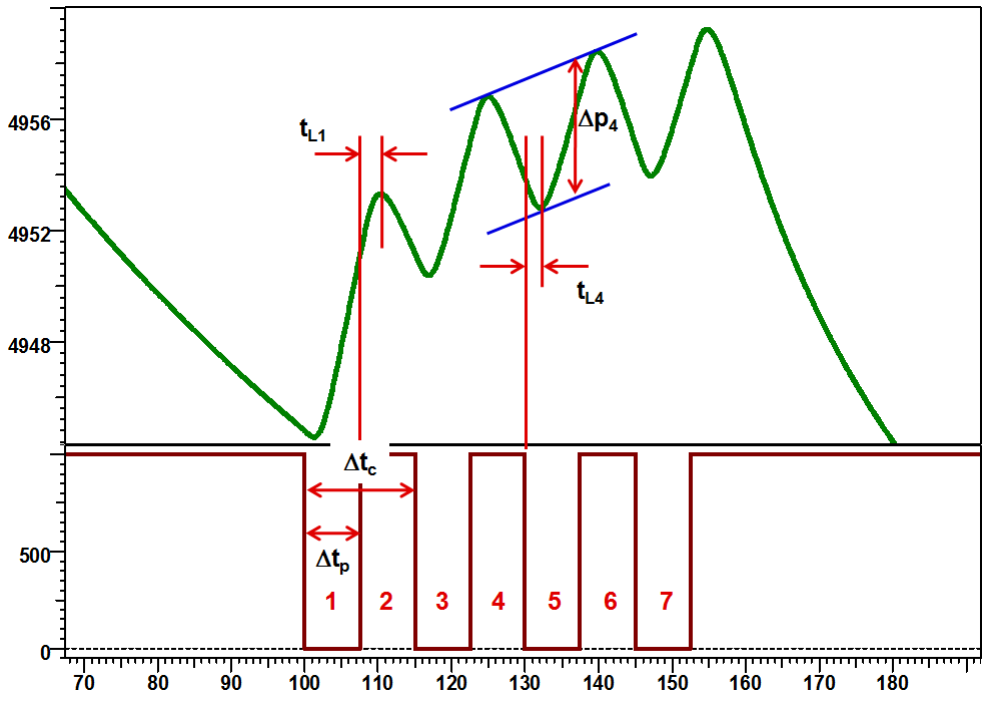


Fig. 12.D.19 – Pulse test tangent method

12.D.6.a The old stuff

Kamal and Brigham presented correlation curves for the manual analysis of pulse tests (1976); these were later modified by Al-Khalifa (1985). The pulses were split between odd and even pulses. The curves for the first even and odd pulse are different, for all other even and odd pulses the correlation charts are the same.

The correlation charts were developed for a homogeneous infinite reservoir with line source wells.

The leading parameters in the correlation charts based on the parameters defined in the 'tangent' approach as defined above:

$F' = \frac{\Delta t_p}{\Delta t_c}$ cycle time divided by pulse time

$(t_L)_D = \frac{t_L}{\Delta t_c}$ dimensionless time lag

$(\Delta t_c)_D = \frac{k\Delta t_c}{948.3\mu r^2 \Phi c_t}$ dimensionless cycle time

$\Delta p_D = \frac{kh}{70.6qB\mu}\Delta p$ dimensionless pressure

The correlation charts are not shown in this book as these charts are seldom used nowadays as these methods have been replaced by a new modern approach (the right stuff). However, older textbooks on pressure transient analysis will carry these charts so they are readily available to the users.

12.D.6.b The right stuff

Today the manual approach has been replaced by proper modelling of the pressure history using available analytical and numerical models. Due to the lack of an appropriate diagnostic plot the problem is often reduced to matching the pressure history of the observation well. Thus, in most cases the analysis is obtained through non linear regression and seeking interpretation results that are in line and consistent with data from other sources.

The example below illustrates a history match of a pulse test where the pressure response is influenced by tide effect.

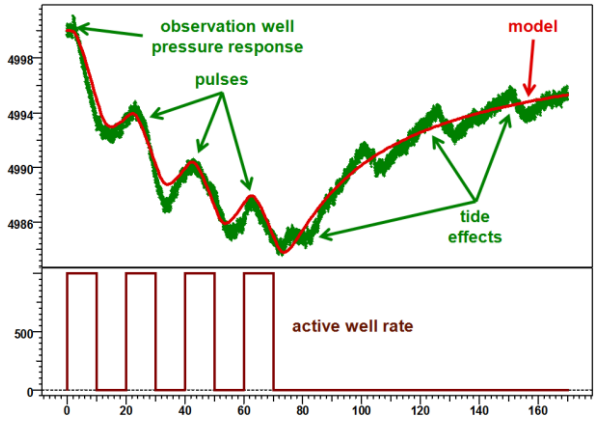


Fig. 12.D.20 – Pulse test

12.D.7 Vertical interference tests

The vertical interference or pulse test is designed to determine the vertical communication in the reservoir or simply to prove that vertical barriers exist to flow.

The figure below illustrates the typical geometric scenario of a vertical interference test.

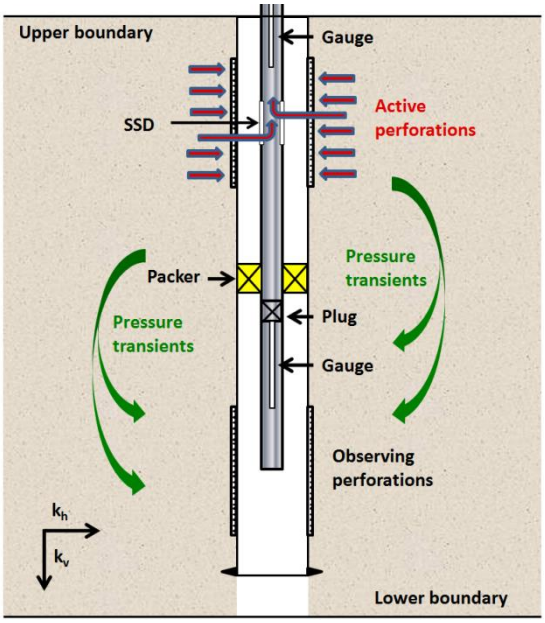


Fig. 12.D.21 – Vertical interference test

Type curves were developed to allow conventional analysis by hand in the 1980's (Kamal). The curves had to be developed for a number of geometrical situations as both the active and observer perforations have to be identified and appropriately placed with respect to each other and the upper and lower boundary. Using the type curves it was possible to estimate both horizontal and vertical permeability.

Today we use modelling as the analysis method. We can apply directly the models developed for the formation tester tools and can thus determine all the pertinent parameters of the reservoir including the vertical permeability.

Below is illustrated the model match of a vertical interference test in a homogeneous infinite reservoir with vertical anisotropy. The response and the model match of the active and observer perforations are shown in the same graphic.

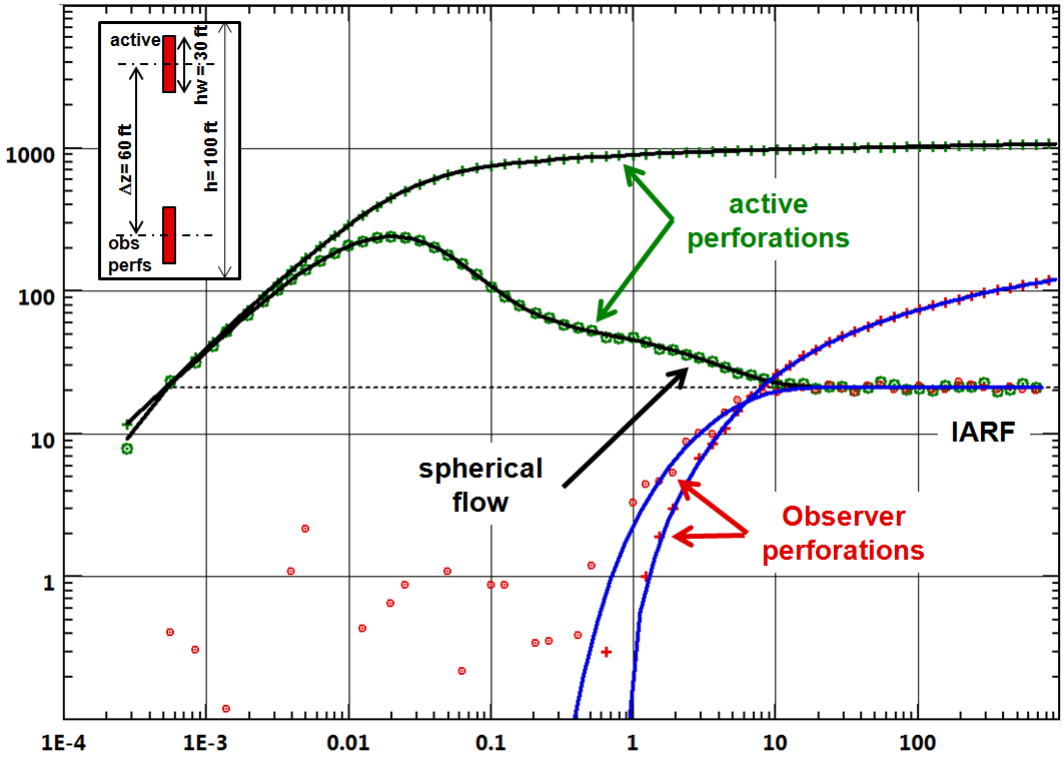


Fig. 12.D.22 – Vertical interference test

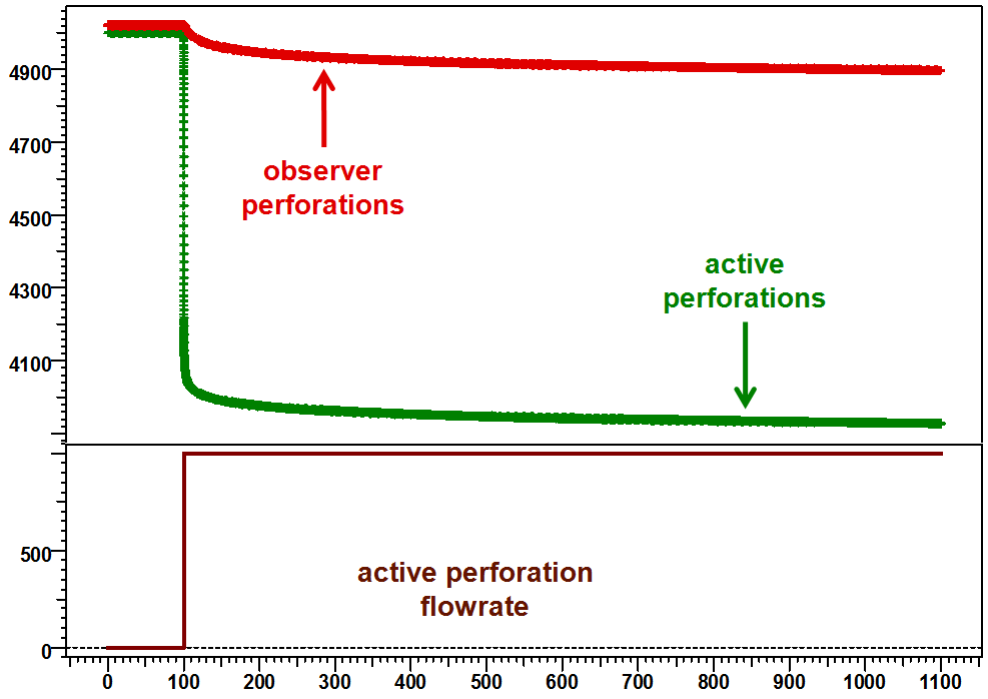


Fig. 12.D.23 – Vertical interference test history plot

12.D.8 Permeability tensor determination from multiple interference

A method has been developed to estimate the value and the direction of a possible horizontal anisotropy from interference data acquired in a multiple observators interference test.

It requires the result in term of permeability of three observation well tests.

If *A* is the active well, and the three observation wells *Oi, i =1, 2, 3*, the analysis of each individual interference test *[A, Oi]* gives:

$$TM_i = \frac{k_i}{\phi_i \mu c_t r_i^2} = \frac{1}{\phi \mu c_t} \frac{k_{eff}}{k_x y_i^2 + k_y x_i^2 - 2k_{xy} x_i y_i}$$

With the definition of effective permeability:

$$k_{eff} = \sqrt{k_{xx}.k_{yy} - k_{xy}^2} = k_{min}.k_{max}$$

The 4 equations can be solved to get: k_x, k_y, k_{xy}, ϕ. Finally the procedure concludes with the determination of:

$$k_{min} = \frac{1}{2}\left(k_x + k_y - \sqrt{(k_x - k_y)^2 + 4k_{xy}^2}\right)$$

$$k_{max} = \frac{1}{2}\left(k_x + k_y + \sqrt{(k_x - k_y)^2 + 4k_{xy}^2}\right)$$

$$\theta = \tan^{-1}\left(\frac{k_{max} - k_x}{k_{xy}}\right)$$

The results are given in the following dialog:

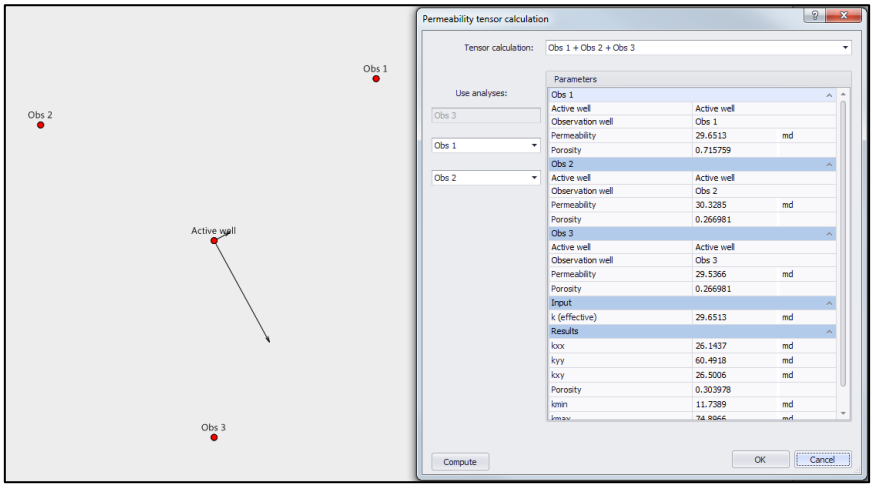


Fig. 12.D.24 – Tensor determination results

<u>Reference:</u> Field-wide Determination of Directional Permeabilities Using Transient Well Testing; Yan Pan, Medha Kamal, and Wayne Narr, SPE181437.

12.E Minifrac test analysis introduction

The Minifrac, Pre-frac injection test, analyses provide information necessary to the fracture job design and also post fractures reservoir characteristics.

A Minifrac operation pressure data set includes several flow regimes and pressure behaviours that have to be analysed with the adequate method. It is necessary to use all available existing techniques and to insure the consistency between the various methods results.

The standard Minifrac test design consists in an injection period of very short duration compared to the fall off duration, consequently, the classical analysis based on the pressure and superposition derivative cannot be used because the superposition principle does not apply.

12.E.1 Minifrac analysis overview

Several flow regime and pressure behavior can be observed during a Minifrac fall off data acquisition:

- Pseudo bilinear flow with leak-off before the fracture closure
- Pseudo linear flow with leak-off before the fracture closure
- Pseudo bilinear flow after the fracture closure
- Pseudo linear flow after the fracture closure
- Pseudo radial flow after the fracture closure

The available analysis and plot type to extract the information are:

- The G-function plot, which is used to analyze the post shut-in period, before fracture closure. It allows for the determination of the closure parameters (time, pressure and G-value).
- The square root of time plot, used to check the closure point obtained from the first plot.
- The After Closure Analysis (A.C.A.) plot, which allows for after closure flow identification and characterization in order to obtain initial reservoir pressure and far field transmissibility.
- The loglog plot which allows the diagnosis of the linear and radial flow in order to deduce the fracture length and the formation transmissibility.

12.E.2 The G-Function analysis plot

The plot uses Cartesian coordinates and contains the following curves:

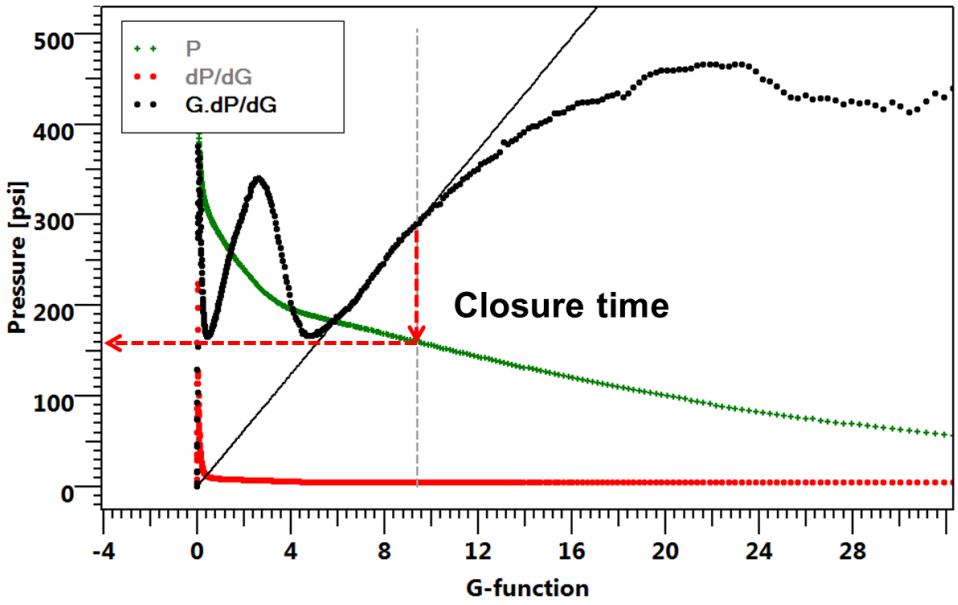


Fig. 12.E.1 – G-Function plot

(1) The bottomhole pressure as a function of the G function;
(2) The direct derivative of the above;
(3) The semi-log derivative (G.dp/dG) of the above.

The 'G-function' definition is developed later in 'G-Function background' paragraph.

The main analysis steps consist in:

- Fitting a straight line going through the origin over the semi-log derivative curve.
- Defining the closure time by setting the vertical line (red arrow in the sketch above) in the correct position on the data.

The main analysis results are:

- The closure time (from shut-in).
- The closure pressure.
- The corresponding G-function value at closure.
- The straight line slope.
- The Instantaneous Shut-In Pressure (ISIP).
- The fracture fluid efficiency η .
- A Farfield permeability estimate.

The ISIP is necessary for the injected fracture proppant design is the intersection of the tangent to the pressure curve at the closure time with the pressure axis. It can be considered as the initial pressure if the flow would have been only linear.

12.E.3 The square root of time analysis plot

This plot is similar to the G-function plot but uses the square root of time instead of the G-function. It is used to confirm the closure point by checking that it corresponds to a local maximum of the pressure derivative.

The analysis procedure is to set the closure vertical line through a local pressure derivative maximum.

The main analysis results are:

- The closure time (from shut-in).
- The closure pressure.

12.E.4 After Closure Analysis plot (A.C.A.)

The After Closure Analysis (A.C.A.) plot is a specialized plot showing either

- The pressure difference and the semi-log pressure derivative versus the square linear flow function

or

- The pressure versus linear flow function or radial flow function as described in the section "Additional analysis plot"

When the plot type selected is square linear, the plot is shown as a Log-Log plot and displays pressure difference and semi-log derivative. In this mode, the analysis steps consist in:

- Fitting a specialized straight line (slope 1 for pseudo-radial flow regime and/or ½ for pseudo-linear one) over the semi-log derivative curve.
- Moving the vertical lines that defined start of linear flow, end of linear flow and start of radial flow.

Once the time ranges of the flow periods are defined, the plot type can be changed to either linear or radial. For these types, the pressure is displayed in a Cartesian plot versus the linear or radial flow function. The analysis steps consist in fitting a straight line over the pressure curve in the corresponding time interval. The initial reservoir pressure is then updated (together with the far-field permeability in radial mode) and one can go back to the square linear type to check pressure difference behaviour with the specialized lines (see section D2 ACA analysis for a more detailed description).

The main analysis results are:

- The start of pseudo-linear flow time (from shut-in).
- The end of pseudo-linear flow time (from shut-in).
- The start of pseudo-radial flow time (from shut-in).
- Reservoir initial pressure.
- Far-field permeability (if a straight line has been defined in the pseudo radial flow period).

12.E.5 G-function Interpretation

The interpretation is done by plotting the pressure P, its derivative $\partial P / \partial G$ and the semi-log derivative $G \cdot \partial P / \partial G$ versus G. The analysis allows identifying the leak-off type among four known types:

a) Normal Leak-off:

- Fracture stops propagating at shut-in.
- Fracture area is constant after shut-in.
- Homogeneous rock matrix.

This type is identified by the semi-log derivative falling on a straight line passing through the origin.

Deviation from the straight line identifies the *fracture closure*.

b) Pressure Dependent Leak-off (PDL):

- Secondary fractures.

It is identified by a characteristic hump in the semi-log derivative above the extrapolated straight line through the origin.

The end of the hump identifies the **fissure opening pressure** while the subsequent deviation from the straight line identifies the *fracture closure*.

c) Fracture Height Recession (FHR):

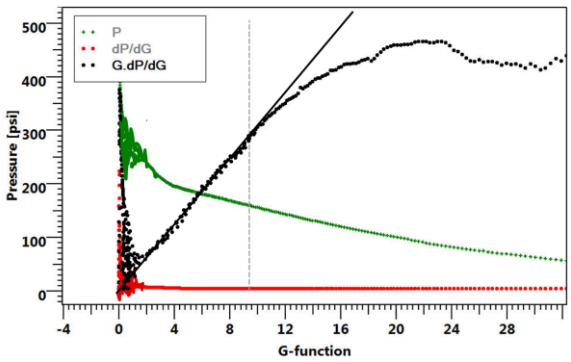
It is identified by a characteristic hump in the semi-log derivative below the extrapolated straight line through the origin.

Deviation from the straight line identifies the *fracture closure*.

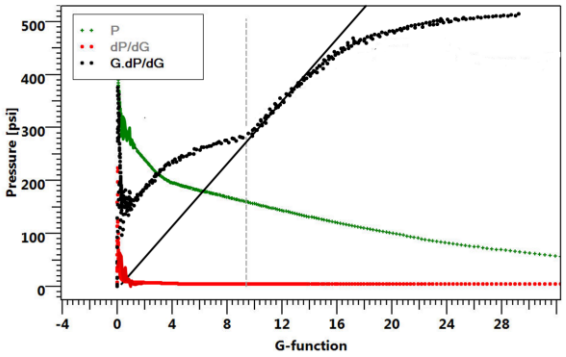
d) Fracture Tip Extension (FTE):

- Fracture continues to grow after shut-in.
- Fracture closure is not observed.

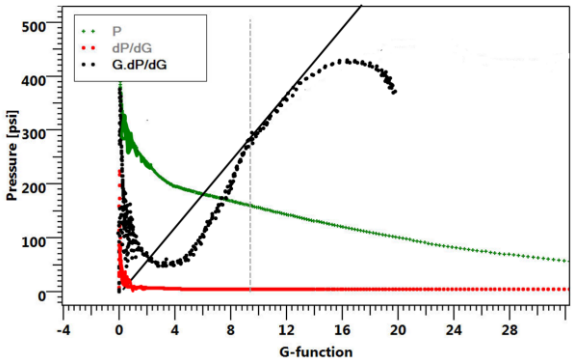
It is identified by the semi-log derivative lying along a straight line that extrapolates above the origin.



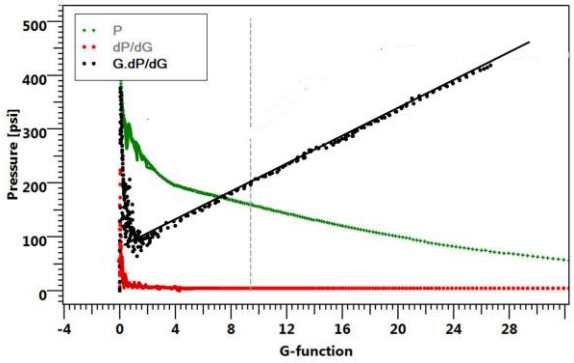
(a) Normal leak-off



(b) Pressure Dependant Leak-off



(c) Fracture Height Recession



(d) Fracture Tip Extension

Fig. 12.E.2 – Typical G-function plots

12.E.6 Additional analysis plot

The G-function plot can be complemented by several plots to either confirm data obtained from the G-function plot or to infer additional information.

12.E.6.a Square root plot

The square root plot is a plot similar to the G-function plot where the G-function is replaced by the square root of time $\sqrt{t}$. It is commonly used to validate results obtained from the G-function plot.

As for the G-function plot, the pressure, the pressure derivative and the semi-log derivative are plotted together.

A common mistake is to pick the closure as the departure of the pressure from the straight line trend. This is incorrect and leads to a later closure and lower closure pressure. The correct way is to pick the closure (or confirm it if it has already been evaluated using the G-function) as the maximum of the pressure derivative. At closure, the semi-log derivative should as well depart from the straight line trend.

This plot should be used to **confirm the closure** point obtained from the G-function analysis.

12.E.6.b ACA analysis: Linear, Radial and Square linear plots

After closure analysis (A.C.A.) requires the identification of fully developed pseudo-linear and/or pseudo-radial flow regimes. These regimes can be identified by characteristic slopes on a log-log plot of falloff pressure minus reservoir pressure $(P-P_i)$ and the semi-log derivative of pressure versus the square linear flow function (F_L^2). Note that the reservoir pressure P_i seriously impacts the shape of the pressure difference function; it does not affect the semi-log derivative however.

In the pseudo-linear flow regime the slope of the semi-log derivative should be ½. The pressure difference function should as well behave with a ½ slope and its magnitude should be twice that of the semi-log derivative.

In the pseudo-radial flow regime both slopes should be 1 and the curves should coincide.

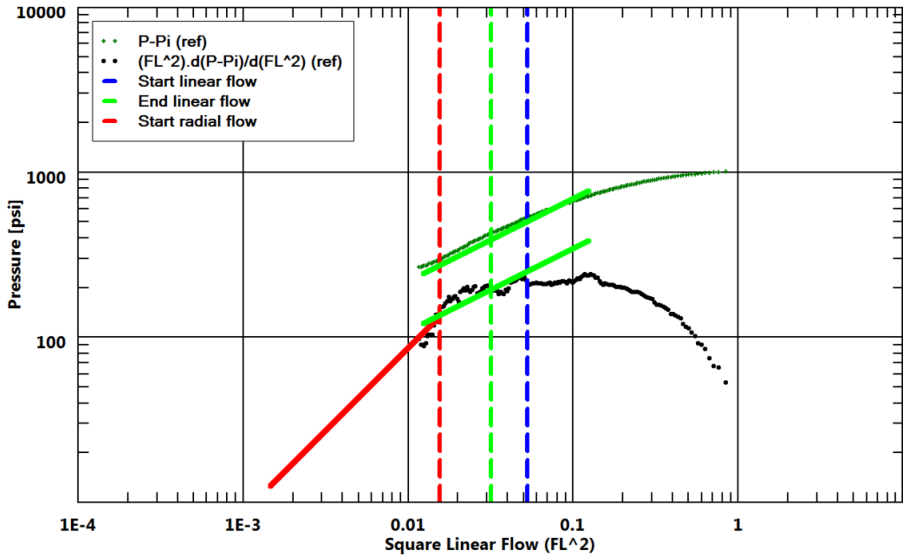


Fig. 12.E.3 – ACA analysis plots

If a linear regime is identified then a Cartesian plot of pressure versus F_L (for pseudo-linear flow regime):

$$F_L(t) = \frac{2}{\pi} \cdot \sin^{-1} \sqrt{\frac{t_c}{t}}$$

For the radial flow regime, then it should be a Cartesian plot of the pressure versus F_R (for pseudo-radial flow regime):

$$F_R(t) = \frac{1}{4} \cdot \ln\left(1 + \frac{16 \cdot t_c / \pi^2}{t - t_c}\right)$$

This last plot yields a straight line with intercept equal to the reservoir pressure Pi. In the case of pseudo-radial flow regime the slope m_R of the fit line can be additionally used to infer the far-field reservoir transmissibility:

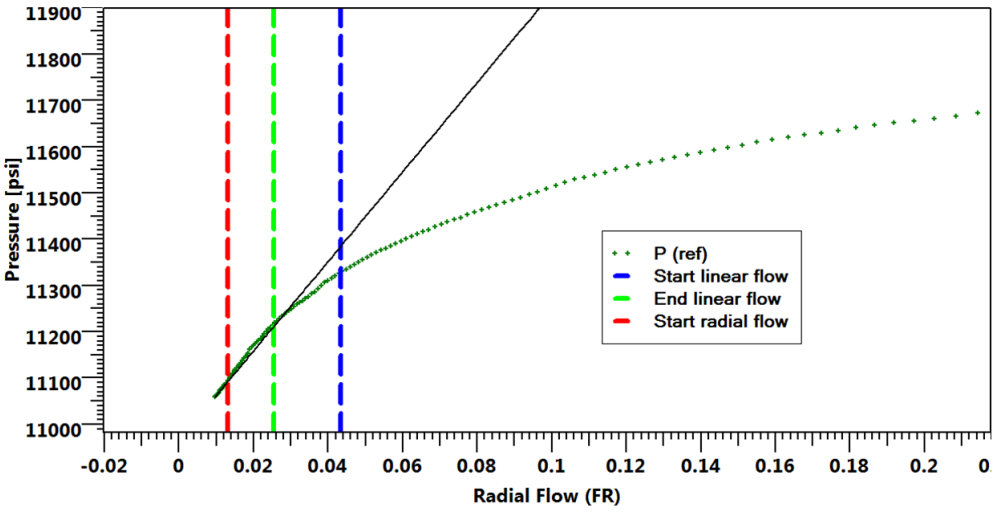


Fig. 12.E.4 – ACA analysis Radial flow plot

This Pi value is used then as correct value and going back to the Square linear plot after this Pi adjustment, the aspect reveals the validity of the radial flow diagnosis and, in this specific case that the linear flow diagnosis was not correct.

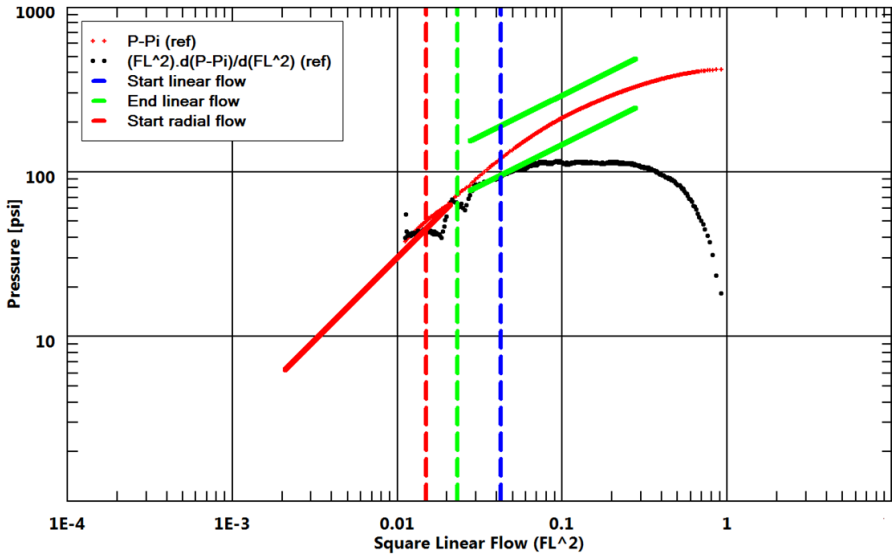


Fig. 12.E.5 – ACA analysis square linear flow plot

Procedure summary, it requires a two steps procedure:

1- From a first guess of reservoir pressure one can match the flow regime lines based mainly on the semi-log derivative slope, identify the regime periods,

2- Then perform a straight line match on the corresponding Cartesian plot to correct the reservoir pressure.

3- Switching back to the square linear plot should yield the correct pressure difference behavior.

12.E.6.c LogLog Plot

The loglog plot displays three data curves:

Pressure curve: $\Delta P vs \Delta t$

Drawdown derivative curve: $d\Delta P / d(\ln(\Delta t) vs \Delta t$

Build up derivative curve: $d\Delta P / d(\ln((t_p + \Delta t)/\Delta t) vs \Delta t$

Note that the standard superposition derivative:

$$\Delta P' = d\Delta P / d(\ln(Sup(\Delta t))$$

is not used for the simple reason that the superposition is not applicable here because of the very short duration of the injection period.

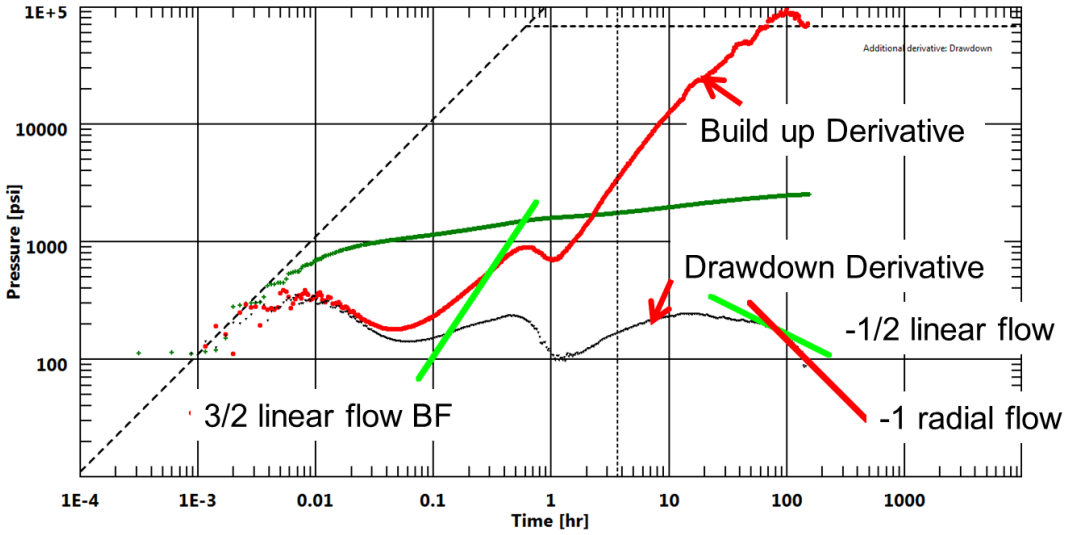


Fig. 12.E.6 – Loglog analysis plot

The procedure is to detect the various flow regimes according to the slope that the derivatives exhibit, then to draw the adequate straight lines and to deduce the corresponding parameter values.

The parameter values resulting from the linear flow analysis is the product kxf^2 or xf and from the radial flow the product kh.

12.E.6.d Loglog specialized lines

Starting from the pressure equation corresponding to the three classical flow regimes, Bilinear, Pseudolinear and Pseudoradial, we can calculate the drawdown and build up derivatives to deduce the exponent of the time function, therefore the slope of the straight lines on the log-log plot:

Before closure:

Flow regime	Solution	Drawdown derivative $d\Delta P / d(\ln(\Delta t)$	Build up derivative $d\Delta P / d(\ln((t_p + \Delta t)/\Delta t)$
Linear	$\Delta P = m_2\sqrt{\Delta t}$	$\Delta P'_{Dd} = \frac{1}{2} m_2 \sqrt{\Delta t}$	$\Delta P'_{BU} = \frac{1}{2} m_2 \frac{\sqrt{\Delta t}}{t_p}(t_p + \Delta t)$

After closure:

Flow regime	Impulse solution	Drawdown derivative $d\Delta P / d(\ln(\Delta t)$	Build up derivative $d\Delta P / d(\ln((t_p + \Delta t)/\Delta t)$
Bilinear	$\Delta P = m_1 /(t_p + \Delta t)^{\frac{3}{4}}$	$\Delta P'_{Dd} = m_1 \frac{3}{4(t_p + \Delta t)^{\frac{3}{4}}}$	$\Delta P'_{BU} = m_1 \frac{3(t_p + \Delta t)^{\frac{1}{4}}}{4}$
Pseudolinear	$\Delta P = \frac{m_2}{2} \frac{1}{\sqrt{t_p + \Delta t}}$	$\Delta P'_{Dd} = \frac{1}{4} m_2 \frac{\Delta t}{(t_p + \Delta t)^{\frac{3}{2}}}$	$\Delta P'_{BU} = \frac{1}{4} m_2 \frac{\Delta t}{t_p} \frac{1}{\sqrt{t_p + \Delta t}}$
Pseudoradial	$\Delta P = m \ln((t_p + \Delta t)/\Delta t)$	$\Delta P'_{Dd} = m \frac{\Delta t}{(t_p + \Delta t)^2}$	$\Delta P'_{BU} = m \frac{1}{t_p} \frac{\Delta t}{(t_p + \Delta t)}$

It results the straight line slopes that can be expected:

	Before Closure (BC)		After Closure (AC)		
	(Bilinear)	Linear	Bilinear	Pseudo-Linear	Pseudo-Radial
Drawdown derivative $d\Delta P / d(\ln(\Delta t) vs \Delta t$	(1/4)	1/2	-3/4	**-1/2**	**-1**
Build-up derivative $d\Delta P / d(\ln((t_p + \Delta t)/\Delta t) vs \Delta t$	(5/4)	**3/2**	1/4	1/2	**0**

- Between parentheses are the flow regimes which are rarely observed.
- In bold are the flow regimes which are the most frequently observed.

12.E.7 Parameters identification

12.E.7.a G-Function and A.C.A. plot results

X-Axis Function	G-Function	$\sqrt{t}$	F_L^2	F_L	F_R
Plot type	Cartesian	Cartesian	Log-Log	Cartesian	Cartesian
Results					
Closure time and pressure	Time, pressure and G-function value Gc and slope m_G at closure.	Time, pressure at closure.			
Fracture fluid efficiency η					
I.S.I.P. Frac. Area Permeability estimate					
Flow time limits			Specialized line diagnosis.		
P_i				Straight line intercept.	Straight line intercept.
Farfield mobility					Straight line slope.

12.E.7.b Results equations

ISIP

The Instantaneous Shut-In Pressure (ISIP) is given directly by

$$ISIP = G_c \cdot m_G + P_c$$

It is the intersect of the tangent straight line at the closure time, it can be interpreted as the initial pressure if the flow would been always linear.

Fracture fluid efficiency

The fracture fluid efficiency η is the ratio of volume of fluid in the fracture at shut-in over the total pumped volume. Assuming no spurt loss:

$$\eta = \frac{G_c}{2 + G_c}$$

Leak-off coefficient

The leak-off coefficient is given as $C_L = \frac{2}{\pi} \cdot \frac{m_G}{r_p \cdot \sqrt{t_p} \cdot S_f}$. Depending on the fracture model,

$$C_L = \frac{m_G}{r_p \cdot \sqrt{t_p} \cdot E'} \cdot \beta \cdot \begin{cases} h_f, & PKN \\ 2L_f, & GDK \\ (32R_f)/3\pi^2, & Radial \end{cases}$$

$r_p = \frac{h_p}{h_f}$ is the ratio of permeable to gross height and β is a geometry-dependent factor given by:

$$\beta = \begin{cases} (2n+2)/(2n+3+a), & PKN \\ 0.9, & GDK \\ 3\pi^2/32, & Radial \end{cases}$$

Where n is the power law exponent of the fluid and a is a variable describing how constant the viscosity of the fracture fluid is in the fracture (usually taken equal to 1).

Fracture dimensions

The area of the fracture wing is:

$$A_f = \frac{(1-\eta) \cdot V_i}{2 \cdot g(0,\alpha,1/2) \cdot C_L \cdot r_p \cdot \sqrt{t_p}} = \begin{cases} 2L_f \cdot h_f, & PKN \\ 2L_f \cdot h_f, & GDK \\ \pi \cdot R_f^2, & Radial \end{cases}$$

Average fracture width can also be obtained:

$$\overline{w}_f = \frac{2 \cdot g(0,\alpha,1/2) \cdot C_L \cdot r_p \cdot \sqrt{t_p} \cdot \eta}{(1-\eta)}$$

G-Function permeability estimate

Empirical formulation derived from numerical simulations:

$$k = \frac{0.0086 \mu_f \sqrt{0.01(P_{ISIP} - P_c)}}{\Phi c_t \left(G_c \cdot E \cdot r_p / 0.038\right)^{1.96}}$$

Units: mu[cp], P[psi], phi.ct[psi-1],E[Mpsi], k[md]

The reservoir fluid and its residual saturation in the invaded region will have some effect on the leakoff fluid mobility, hence as a general rule, an assumed injected fluid viscosity of 1 cp is used to incorporate the effects of reservoir temperature and relative permeability in the invaded zone.

E is the Young module.

The storage ratio r_p is equal to 1 for normal and PDL leak-off type and represents the amount of excess fluid that needs to be leaked off to reach fracture closure when the fracture geometry deviates from the assumed constant-height planar fracture.

In practice, the storage ratio is calculated as the area under the G-function semilog derivative up until closure divided by the area of the triangle defined by the straight-line tangent to the semilog derivative at closure. For transverse storage and fracture height recession signature it is some value lower than unity, else it is 1.

Note: when the rp is not equal to zero, the closure time used in the ACA analysis is multiplied by the storage ratio for permeability and transmissibility estimates to account for the delay caused by this excess fluid volume in the fracture.

Far-field Transmissibility

In the case of pseudo radial flow:

$$\boxed{\frac{kh}{\mu} = \frac{\pi}{16} \cdot \frac{V_i}{m_R \cdot t_c}}$$

The permeability can as well be estimated for pseudo linear flow:

$$\frac{k \cdot \Phi \cdot c_t}{\mu} = \pi \cdot \frac{C_L^2}{m_L^2}$$

Where C_t denotes total compressibility.

Note that in these equations the viscosity refers to the far-field viscosity.

12.E.8 G-Function: Theoretical background

Once the fracture is initiated its growth is defined throughout its areal evolution by

$$A(\tau) = A(t) \cdot (\tau / t)^{\alpha}$$

where α is **the fracture area growth exponent**.

Carter (1957) developed an equation for fluid loss rate across the fracture surface which can be generalized. For a differential surface element ∂A of a fracture that is exposed to the fracturing fluid at time $\tau(A)$, the leak-off rate is given by:

$$\partial q_L = 2 \cdot \partial A \cdot C_L / (t - \tau)^{1-\theta} \partial t$$

where C_L is the **fluid loss coefficient** and where θ is the **fluid loss exponent.**

The integration of the fluid loss rate over the leak-off surface over the whole injection period gives:

$$VL_p = 2 \cdot \int_0^{A_p} \int_{\tau}^{t_p} C_L / (t - \tau(A))^{1-\theta} \partial A \partial t$$

Using the fact that $\tau / t_p = (A_{ND})^{1/\alpha}$, with $A_{ND} = A / A_p$, $t_{ND} = t / t_p$ we have

$$VL_p = 2 \cdot A_p \cdot t_p^{\theta} \cdot \int_0^1 \int_{A_{ND}^{1/\alpha}}^1 C_L / \left(t_{ND} - A_{ND}^{1/\alpha}\right)^{1-\theta} \partial t_{ND} \partial A_{ND}$$

Following Nolte (1979) and assuming that the fracture area remains constant after shut-in prior to fracture closure, we can introduce $\Delta t = t - t_p / t_p$ and perform a similar integration over this added period to get

$$VL_p(t_p + \Delta t) = 2 \cdot A_p \cdot t_p^{\theta} \cdot \int_0^1 \int_{A_{ND}^{1/\alpha}}^{1+\Delta t} C_L / \left(t_{ND} - A_{ND}^{1/\alpha}\right)^{1-\theta} \partial t_{ND} \partial A_{ND}$$

Integration over ∂t_{ND} gives:

$$VL_p(t_p + \Delta t) = 2 \cdot A_p \cdot t_p^{\theta} \cdot C_L \cdot g(\Delta t, \alpha, \theta)$$

$$\boxed{g(\Delta t, \alpha, \theta) = \frac{1}{\theta} \cdot \int_0^1 \left(1 + \Delta t - A_{ND}^{1/\alpha}\right)^{\theta} \partial A_{ND}}$$

The material balance can hence be used to relate volumes and pressures (Nolte, 1979) as:

$$\frac{\partial V}{\partial t} = \frac{A_f}{S_f} \cdot \frac{\partial P_n}{\partial t}$$

where P_n is the **fracture net pressure** and where S_f is the **Fracture stiffness**, given depending on the two-dimensional fracture model used as:

$$S_f = \frac{2E'}{\pi} \cdot \begin{cases} 1/h_f, & \textit{Vertical Plane Strain (PKN)} \\ 1/(2L_f), & \textit{Horizontal Plane Strain (GDK)} \\ 3\pi^2/(32R_f), & \textit{Radial} \end{cases}$$

With E', the plain strain modulus.

Finally the net pressure difference can be expressed as:

$$\boxed{\Delta P_n = \frac{\pi}{2} \cdot r_p \cdot S_f \cdot C_L \cdot t_p^{\theta} \cdot \left\{ \frac{4}{\pi} \left[g(\Delta t, \alpha, \theta) - g(0, \alpha, \theta) \right] \right\} = \frac{\pi}{2} \cdot r_p \cdot S_f \cdot C_L \cdot t_p^{\theta} \cdot G(\Delta t, \alpha, \theta)}$$

With $r_p = h_p / h_f$, ratio of permeable height to gross height.

Note that Nolte (1979) and Castillo (1987) consider an extra corrective term by multiplying S_f by β_s, where β_s is the ratio of average net pressure in the fracture to the wellbore net pressure at shut-in. It is given by Nolte for vertical fractures and by Castillo for horizontal and radial fracture geometries in terms of fracturing fluid rheological behaviour and Nolte's viscosity degradation correction.

12.E.8.a Fluid type assumption

The fluid loss exponent θ is linked to the nature of the filtrate fluid, if the flow behaviour index of the power law fluid model of the fracturing fluid is given by n:

$$\theta = \frac{n}{n+1}$$

Filtrate fluid type	n	θ
Newtonian fluid	$n=1$	$\theta=1/2$
Pseudoplastic non-Newtonian	$n<1$	$\theta<1/2$
Viscoelastic	$n\approx 10-15$	$\theta\approx 1$

Most authors assume a Newtonian fluid ($\theta=1/2$).

12.E.8.b G-function simplification

For a Newtonian fluid, Valkó & Economides (1995) found an analytical expression for the g function on the form:

$$g(\Delta t,\alpha,1/2)=\frac{4\alpha\sqrt{\Delta t}+2\sqrt{1+\Delta t}\cdot F(1/2;\alpha;1+\alpha;(1+\Delta t)^{-1})}{1+2\alpha},$$

where $F(a;b;c;z)$ is the hypergeometric function (polynomial approximation can be derived for specific values of α (Valkó & Economides, 1995)).

The exponent α has been related to the type of fracture model, to the efficiency at the end of the pumping and to the rheological behaviour of the fluid.

It is bounded by the interval $[\alpha_L \quad \alpha_U]$ (itself bounded between ½ and 1), where the bounds are given depending on the flow behaviour index and on the fracture geometrical model in the following table:

Model	α_L	α_U	α_L Newtonian	α_U Newtonian
PKN	$1-\frac{n}{n+1}$	$\frac{2n+2}{2n+3}$	1/2	4/5
GDK	$1-\frac{n}{n+1}$	$\frac{n+1}{n+2}$	1/2	2/3
Radial	$1-\frac{n}{n+1}$	$\frac{4n+4}{3n+6}$	1/2	8/9

α -bound values for various geometrical fracture model for power law fluids and Newtonian fluids

The G function can then be evaluated by integrating it with α values taken as each of these bounds and using simple interpolation to obtain the G function for any other value of α (linear interpolation):

$$\boxed{g(\Delta t,\alpha,\theta)=g(\Delta t,0.5,\theta)+(2\alpha-1)\cdot\left[g(\Delta t,1,\theta)-g(\Delta t,0.5,\theta)\right]}$$

If unknown, the α value can be calculated by interpolating between lower and upper bound using the fracture treatment efficiency:

$$\alpha=\alpha_L+\eta(\alpha_U-\alpha_L),$$

where the treatment efficiency $\eta=\frac{G(\Delta t_c,1,0.5)}{2\kappa+G(\Delta t_c,1,0.5)}$ with κ, spurt factor.

For a Newtonian fluid the G function bounds are given as:

	$g(0,\alpha,1/2)$	$G(\Delta t,\alpha,1/2)$
$\alpha=1/2$	$\frac{\pi}{2}$	$G_L(\Delta t)=\frac{4}{\pi}\cdot\left((1+\Delta t)\cdot\sin^{-1}(1+\Delta t)^{-1/2}+\Delta t^{1/2}-\frac{\pi}{2}\right)$
$\alpha=1$	$\frac{4}{3}$	$G_U(\Delta t)=\frac{4}{\pi}\cdot\left(\frac{4}{3}\left[(1+\Delta t)^{3/2}-\Delta t^{3/2}\right]-\frac{4}{3}\right)$

A more straightforward strategy consists in taking the function at one bound (or the average function over the two bounds). Nolte's derivation was made using the upper bound ($G=G_U$) based on the fact that these two bounds are surprisingly close to each other (less than 10 percent differences have been reported by Nolte and others).

It seems to be of common use to consider the upper bound function in place of G.

Recommendation: It is recommended to consider a Newtonian fluid and to use either:

a) The upper bound function for the considered fracture geometrical model (use polynomial approximation of the hypergeometric function as given by Valko et al.).

b) The analytical upper bound function for $\alpha = 1$.

References

Carter, R.D. 1957. Appendix to '*Optimum fluid characteristics for fracture extension*' by G.C. Howard and C.R. Fast. Drilling and Production Practice, API 261-270.

Castillo, J.L. 1987, '*Modified Fracture Pressure Decline Analysis Including Pressure-Dependent Leakoff.*' Paper SPE 16417.

Nolte, K.G. 1979. '*Determination of Fracture Parameters from Fracture Pressure Decline.'* SPE 8341 presented at the 1979 SPE Annual Technical Conference and Exhibition, Dallas. Texas, 23-25 September.

Valkó, P. and Economides, M.J. 1995. 'Hydraulic Fracture Mechanics.' Wiley, Chichester, England.

R.D. Barree, V.L.Barree, D.P. Craig 2009, SPE 107877 'Holistic Fracture Diagnotics: Consistent Interpretation of Prefrac Injection Tests Using Multiple Analysis Methods'.

13 – Analytical models

OH – ET – LL

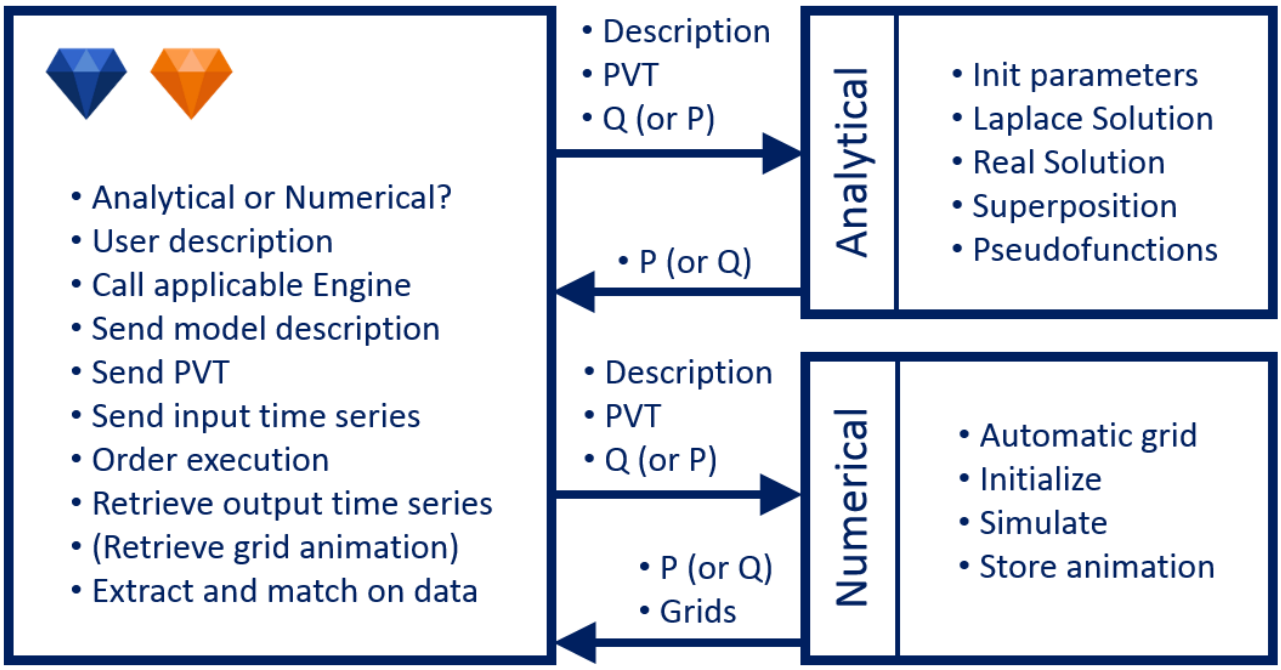
13.A Introduction

Until the 2015 version (v4.30) of the DDA book the general theory section (chapter 2) integrated both general methodology tools and theoretical items related to the generation of analytical models. This was done for historical reasons. Most of the modern PTA and RTA tools were initially developed using analytical models and there was no real reason to differentiate the methodology theory and the theory used to generate these analytical models.

Today the situation is very different. Numerical models have gained momentum in the last fifteen years. Analysis software such as Saphir (PTA) and Topaze (RTA) treat analytical models and numerical models the same way. The physical description of the problem is sent to an analytical engine or a numerical engine, and the post-processing is essentially the same.

The analytical engine will superpose dimensionless solutions while the numerical engines will just simulate the response using the input time series as a constraint. Both analytical and numerical engines return to Saphir / Topaze the required time series. The programs then extract the time series, calculate its derivative as if it was data, and superposes both data and models, with their Bourdet derivatives, on all relevant plots.

The diagram below shows the exchange of information between the analysis software and the analytical and numerical engines.



While Chapter 2 is about the methodology tools developed in PTA and RTA software, this chapter focuses on the technical content of the analytical engines, while the following chapter 14 will focus on the technical content of the numerical engine.

13.B Dimensionless problems

Analytical models are developed by mathematically solving the different diffusion and limit condition equations. A first stage is to eliminate physical parameters by changing variables to solve the problem only once even when properties vary. The resulting variables are generally dimensionless, and the corresponding problem is called the dimensionless problem.

As an illustration we consider the simplest problem we can find: the diffusion in a homogeneous infinite reservoir, starting at initial uniform pressure p_i, produced by a vertical line source well. The basic equations were presented in Chapter 2.

13.B.1 Derivation

The complete real problem is described with the four following equations:

Homogeneous radial diffusion: $$\frac{\partial p}{\partial t} = 0.0002637 \frac{k}{\Phi \mu c_t} \frac{1}{r} \left[\frac{\partial}{\partial r} \left(r \frac{\partial p}{\partial r} \right) \right]$$

Uniform initial pressure: $$p(t = 0, r) = p_i$$

Infinite reservoir: $$\lim \left[p(r,t) \right]_{r \to \infty} = p_i$$

Line source well: $$\lim \left[r \frac{\partial p}{\partial r} \right]_{r \to 0, t} = 141.2 \frac{qB\mu}{kh}$$

The problem is simplified by introducing dimensionless variables that will integrate all other parameters and end up with a unique set of equations that we will solve analytically once and for all. These dimensionless parameters are not only useful to solve the problem. They have a historic importance, as they were at the origin of the method of type-curve matching (see the 'old stuff' in the PTA Chapter). Though it does not look like it, there are not so many ways to simplify the complete set of equations. The dimensionless parameters are defined as:

Dimensionless radius: $$r_D = \frac{r}{r_w}$$

Dimensionless time: $$t_D = 0.0002637 \frac{kt}{\Phi \mu c_t r_w^2}$$

Dimensionless pressure: $$p_D = \frac{kh}{141.2 qB\mu} (p_i - p)$$

It is not strictly necessary to introduce the dimensionless radius to solve the problem. However we will approximate the solution at the well by taking the line source solution at $r=r_w$. The same definition of r_D is also used to exactly solve the finite radius problem. Injecting the dimensionless terms in the physical problem brings us to the dimensionless problem:

Homogeneous radial diffusion: $$\frac{\partial p_D}{\partial t_D} = \frac{1}{r_D} \left[\frac{\partial}{\partial r_D} \left(r_D \frac{\partial p_D}{\partial r_D} \right) \right]$$

Uniform initial pressure: $$p_D(t_D = 0, r_D) = 0$$

Infinite reservoir: $$\lim \left[p_D(r_D, t_D) \right] = 0$$

Line source well: $$\lim \left[r_D \frac{\partial p_D}{\partial r_D} \right]_{r_D \to 0, t_D} = -1$$

The dimensionless equation can be further simplified by moving the problem into Fourier space (Joseph Fourier, France, 1822) or Laplace space (Pierre-Simon de Laplace, France, 1820). We will use here the Laplace transform, under which the diffusion equation, combined with the initial condition becomes:

Laplace Transform: $$\bar{p}_D(u,r_D)=\int_{t_D=0}^{\infty} p_D(t_D,r_D)\exp(-ut_D)dt_D$$

Diffusion Equation in Laplace space: $$u\bar{p}_D=\frac{1}{r_D}\left[\frac{\partial}{\partial r_D}\left(r_D\frac{\partial \bar{p}_D}{\partial r_D}\right)\right]$$

This equation is known to be a modified Bessel equation (Wilhem Bessel, Germany, 1824), the generic form of the solution uses modified Bessel functions:

Generic Modified Bessel solution: $$\bar{p}_D(u,r_D)=A(u)K_0(r_D\sqrt{u})+B(u)I_0(r_D\sqrt{u})$$

K_0 and I_0 are the modified Bessel functions of order zero. The unknown functions A and B are taken from the inner and outer boundary conditions. This gives:

From the outer boundary condition: $$B(u)=0$$

From the inner boundary condition: $$A(u)=\frac{1}{u}$$

Line source solution in Laplace space: $$\bar{p}_D(u,r_D)=\frac{1}{u}K_0(r_D\sqrt{u})$$

The real dimensionless solution is the inverse Laplace transform of this function. Generally, the inverse Laplace transform is numerically obtained using the Stehfest algorithm (Harald Stehfest, Germany, 1970). In this particular case we know the inverse transform. It is called the Exponential Integral function and it can be written:

Exponential Integral solution: $$p_D(r_D,t_D)=-\frac{1}{2}E_i\left(-\frac{r_D^2}{4t_D}\right)$$

Before we return to the physical world, let us notice an interesting property of the Exponential Integral: for small negative arguments, it has a logarithmic approximation that will be the basis of 'Infinite Acting Radial Flow'. It can be written:

for $t_D \geq 100\,r_D^2$ $$p_D(r_D,t_D)\approx\frac{1}{2}\left[\ln\frac{t_D}{r_D^2}+0.80907\right]$$

To get the physical solution, the dimensionless parameters are replaced by their real values. The solution is then given by the following:

Line Source Solution: $$p(r,t)=p_i-\frac{70.6qB\mu}{kh}\left[-E_i\left(-\frac{948.1\Phi\mu c_t r^2}{kt}\right)\right]$$

13.C Superposition in time

13.C.1 The principle of superposition

Derivations as shown before assumed a constant rate production. Analytical models are used to solve more complex flow histories. This is done using the principle of superposition. We generate the solution of a complex problem as the linear combination and superposition, in time of simpler constant-rate components.

For any problem involving a linear diffusion equation, the main superposition principles are:

- Linear combinations of solutions honoring the diffusion equation also honor this equation.
- At any flux point (well, boundary), the flux resulting from the linear combination of solutions will be the same linear combination of the corresponding fluxes.
- If a linear combination of solutions honors the diffusion equation and the different flux and boundary conditions at any time, then it is THE solution of the problem.

From these principles it is easy to build the following series of rules for superposition in time:

- The pressure change due to the production q of a given system is q times the unit rate solution of the same system. This extends to injections using a negative rate.
- To simulate the sequence of a constant rate q_1 from time zero to time t_1, followed by the production q_2 from time t_1 to infinity, you can superpose the production at rate q_1 from time zero to infinity and a production of rate (q_2- q_1) from time t_1 to infinity.
- As a particular case, to simulate a constant production q of duration t_p, followed by a shut-in, you can superpose the production of q from time zero and an injection of q from time t_p.
- This is then easily extends to more complex production sequences.

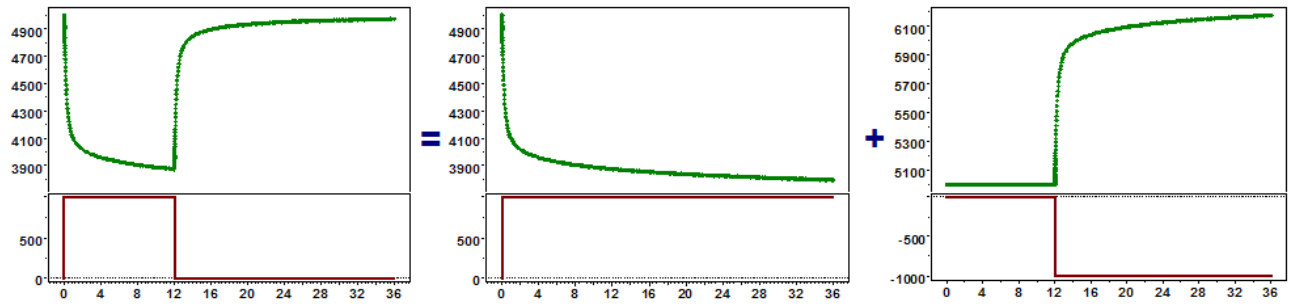


Fig. 13.C.1 – Graphical illustration of simple superposition

13.C.2 Build-up superposition

$\Delta p_{unit}(\Delta t)$ is the solution of a problem for a constant production of unit rate. We also consider $\Delta p_{DD}(\Delta t)$, solution of a given problem in the case of a constant production at rate q. We have:

Drawdown solution: $$\Delta p_{DD}(\Delta t) = q\Delta p_{unit}(\Delta t)$$

We now consider a production at rate q of duration t_p, followed by a shut-in:

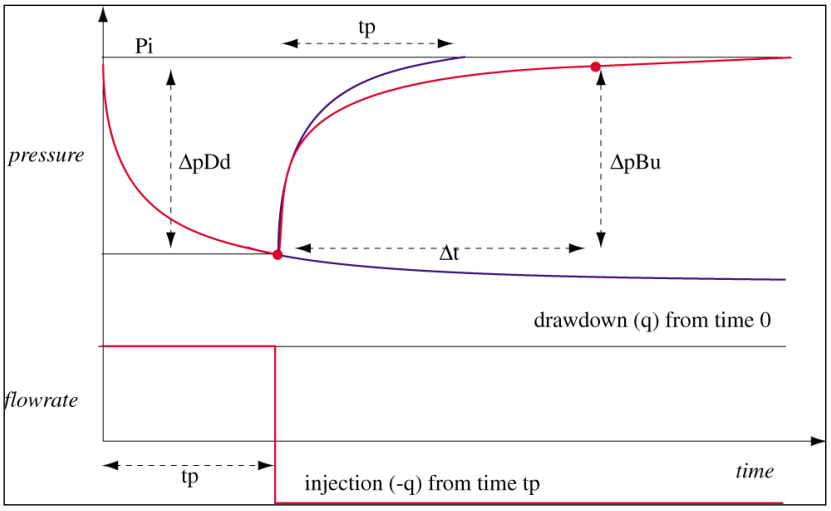


Fig. 13.C.2 – Build-up superposition

During the initial production phase, the pressure will be given by:

Production phase: $$p_{DD}(t) = p_i - \Delta p_{DD}(t) = p_i - q\Delta p_{unit}(t)$$

The pressure change during the build-up is the superposition of the pressure change due to the production of q from time 0 and an injection of q starting at time tp. This will be written:

Build-up pressure: $$p_{BU}(t) = p_{BU}(t_p + \Delta t) = p_i - q\Delta p_{unit}(t_p + \Delta t) + q\Delta p_{unit}(\Delta t)$$

or: $$p_{BU}(t_p + \Delta t) = p_i - \Delta p_{DD}(t_p + \Delta t) + \Delta p_{DD}(\Delta t)$$

The initial pressure may not be known at this stage. We generally start from the pressure change observed during the shut-in, i.e. starting from the last flowing pressure before shut-in:

Build-up pressure change: $$\Delta p_{BU}(\Delta t) = p_{BU}(t_p + \Delta t) - p_{BU}(\Delta t = 0) = p_{BU}(t_p + \Delta t) - p_{DD}(t_p)$$

Replacing, we get: $$\Delta p_{BU}(\Delta t) = \left[p_i - \Delta p_{DD}(t_p + \Delta t) + \Delta p_{DD}(\Delta t)\right] - \left[p_i - \Delta p_{DD}(t_p)\right]$$

And we get the build-up superposition relationship: The pressure change during a build-up, i.e. the difference between the current pressure and the last flowing pressure, can be calculated as the simple superposition of elementary drawdown solutions:

Build-up superposition: $$\Delta p_{BU}(\Delta t) = \Delta p_{DD}(t_p) + \Delta p_{DD}(\Delta t) - \Delta p_{DD}(t_p + \Delta t)$$

13.C.3 Multirate superposition

Multi-rate superposition is the natural extension of the build-up superposition to any type of production history. A sequence of rates q_1, q_2, …, q_n, of respective durations T_1, T_2, ... T_n, with respective starting times $t_1=0$, t_2, ... t_n.

We calculate the pressure at any time t during the period of flow q_n. In the diagram below, we have $q_n=0$. For Pressure Transient Analysis we often deal with shut-in pressures after more or less complex production histories. However the following equations are valid for any rates.

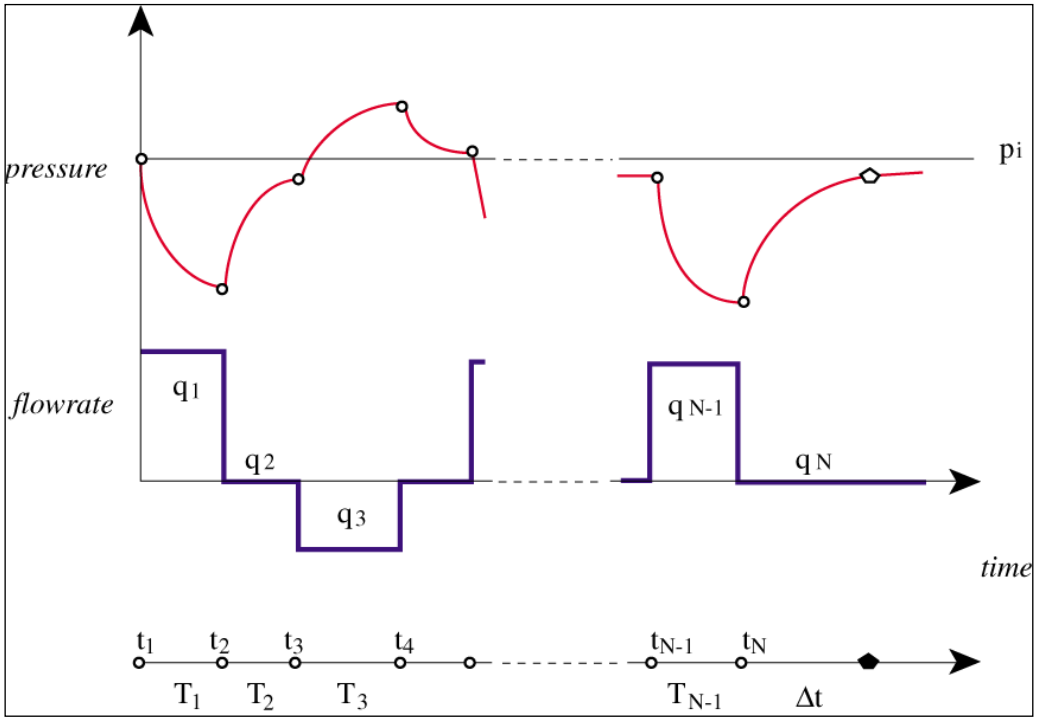


Fig. 13.C.3 – Multirate superposition

Using the principle of superposition we calculate the pressure change by superposing drawdown responses, starting from the beginning of each flow period to the current time, and of respective rates q_1-q_0, q_2-q_1, ... q_n-q_{n-1} (with $q_0=0$).

Multirate superposition: $$p(t) = p_i - \sum_{i=1}^{n} (q_i - q_{i-1}) \Delta p_{unit}(t - t_i)$$

If the period of interest is a producing period, or multi-rate drawdown, the pressure change of interest will correspond to the above formula. In case of a shut-in after a multi-rate production, the interpretation engineer will, as for a simple build-up, consider the pressure change since the well was shut-in.

Multirate shut-in: $$\Delta p_{BU}(\Delta t) = p(t_n + \Delta t) - p(t_n)$$

From superposition: $$\Delta p_{BU}(\Delta t) = \sum_{i=1}^{n-1} (q_i - q_{i-1}) \Delta p_{unit}(t_n - t_i) - \sum_{i=1}^{n} (q_i - q_{i-1}) \Delta p_{unit}(t_n + \Delta t - t_i)$$

13.D Superposition in space

The three models presented so far were solved analytically. Analytical models are fast and accurate. Unfortunately a lot of problems are too complicated to be directly solved analytically. This section presents the main tools used in the industry to provide such solutions.

13.D.1 Superposition in space of analytical models (image wells)

In a way similar to the superposition in time introduced in the previous section, superposition in space tells us that if two or more solutions honor the diffusion equation, for example two line sources coming from different wells, any linear combination of these solutions will honor the diffusion equation. The resulting inner and outer boundary conditions will be the same linear combination of the conditions generated by the individual solutions.

Using this principle, the method of image wells consists of superposing individual mirrored infinite solutions to create a pseudo-boundary. In the case of a single sealing fault of infinite extent, we will add two pressure changes: (1) the pressure change due to the well response in an infinite reservoir, and (2) the interference solution of an image well, symmetric to the well with respect to the fault.

The sum of these two pressure changes, at any point of our half plane reservoir, will honor the diffusion equation (superposition in space). Because the response will be symmetric with respect to the fault, the continuous pressure gradient orthogonal to the fault will have to be zero, and the no flow boundary condition will be honored. All other conditions, initial and well, being honored, we have built the exact solution to our problem.

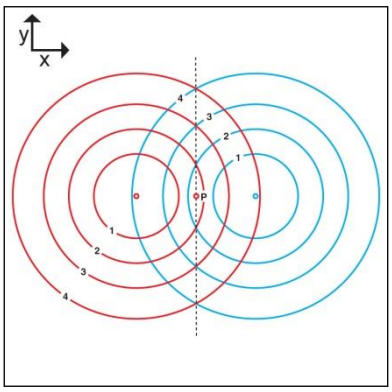


Fig. 13.D.1 – X-Y representation of an image well.
The pressure drop of a fixed value is shown at different times.
Effective pressure drop is the sum of these two signals

Strictly speaking, the interference solution has to be the exact interference solution from the image well. For instance, the time delay due to wellbore storage may need to be taken into account. In the case of a fracture with a sealing fault this will involve an image fracture properly positioned. In most cases the difference between the proper interference solution and a line source will be negligible, but not always.

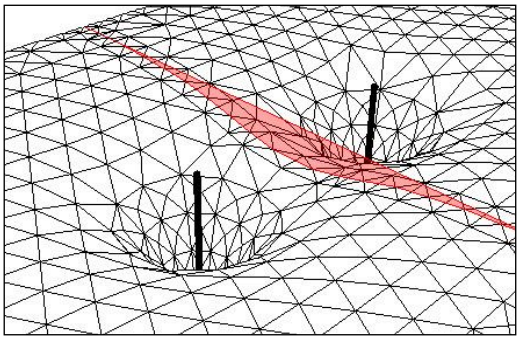


Fig. 13.D.2 – 3D representation of the pressure profile in a 2D plane, with an image well

Note: in case of multiple faults, if the number of image wells is limited (sealing faults, intersecting faults for some angles) the sum of the image solutions constitute the exact analytical model. Conversely, when the sum is infinite the resulting solution could be classified as a semi-analytical solution.

13.D.2 Semi-analytical solutions

When a complex problem cannot be solved rigorously i.e. with a simple closed form solution, it has to be approximated by cutting the solution into steps, either time steps or bits and pieces of boundary / well segment / fracture segment. Then the solution will show an integral function or a time-by-time matrix inversion. Such a solution is called semi-analytical, because some components are calculated analytically but put together numerically.

Integral solutions are generally computationally slower than closed form solutions, and the difficulty is to re-formulate the integrals, optimize the components and use extrapolation whenever feasible, in order to reduce the calculation time to a level acceptable to the end user. This is especially so in the case of nonlinear regression. As an example, the equation below is the solution in Laplace space for a horizontal well in a closed circle.

$$\overline{p_D}(u)=\frac{\tilde{q}\mu}{2\pi k h_D u}\left\{\begin{array}{l}\displaystyle\int_{-\tilde{L}_h}^{\tilde{L}_h}\left[K_0\left(\tilde{r}_D\sqrt{u}\right)+\frac{(-1)^{s+1}I_0\left(\tilde{r}_D\sqrt{u}\right)K_s\left(r_{eD}\sqrt{u}\right)}{I_s\left(r_{eD}\sqrt{u}\right)}\right]d\alpha \\ \displaystyle+2\sum_{n=1}^{\infty}\cos\frac{n\pi z}{h}\cos\frac{n\pi z_w}{h}\int_{-\tilde{L}_h}^{\tilde{L}_h}F_n(\alpha)d\alpha\end{array}\right\}$$

$$where\quad F_n(\alpha)=K_0\left(\tilde{r}_D\varepsilon_n\right)+\frac{(-1)^{s+1}I_0\left(\tilde{r}_D\varepsilon_n\right)K_s\left(r_{eD}\varepsilon_n\right)}{I_s\left(r_{eD}\varepsilon_n\right)}$$

Application: linear composite, leaky faults, combinations of linear and radial geometries.

13.E The use of pseudo functions

13.E.1 Definitions of the gas pseudo pressure and pseudo time

Analytical models have been extensively used for decades in Pressure Transient Analysis (PTA). They have also been increasingly popular in Rate Transient Analysis (RTA) in the past decade. These models are the simplest and fastest way to take into account some physics of the problem by substituting the real system with a simplified description (geometry, diffusion) which is mathematically solved. The limitations of analytical models lay in these simplifications, both geometrically and in terms of diffusion process.

For diffusion the problem is that the real diffusion is generally nonlinear and analytical models strictly work when the slightly compressible approximation (see Chapter 2) is valid. This generally applies, though not always, to single phase oil and to water.

For gas, multiphase fluids, and more generally fluids which compressibility and viscosity change when pressure drops, we may reduce the errors related to this nonlinearity of the diffusion equation by replacing the pressure and the time by new variables (pseudo pressure and pseudo time) which integrate some of the nonlinearities.

For the derivation of these pseudo functions we will consider the case of real gas. The process to introduce pseudo functions for multiphase flow, or to integrate other phenomena such as desorption and stress, are qualitatively the same.

We have seen in Chapter 2 that the diffusion equation for gas can be written:

Gas diffusion equation:
$$\frac{p}{\mu Z}\frac{\partial p}{\partial t} = 0.0002637\frac{k_x}{\phi \mu c_t}\frac{\partial}{\partial x}\left[\frac{p}{\mu Z}\frac{\partial p}{\partial x}\right]$$

We introduce the pseudo pressure in order to eliminate the additional terms in the gas diffusion equation (there is an historic factor 2 in this equation):

Gas pseudo pressure:
$$m(p) = 2\int_0^p \frac{p}{\mu Z}dp$$

Taking the partial differential:
$$\frac{\partial m(p)}{\partial t} = \frac{\partial m(p)}{\partial p}\frac{\partial p}{\partial t} = \frac{2p}{\mu Z}\frac{\partial p}{\partial t}$$

And, the same way:
$$\frac{\partial m(p)}{\partial x} = \frac{\partial m(p)}{\partial p}\frac{\partial p}{\partial x} = \frac{2p}{\mu Z}\frac{\partial p}{\partial x}$$

The gas diffusion equation becomes:
$$\frac{\partial m(p)}{\partial t} = 0.0002637\frac{k_x}{\phi \mu c_t}\frac{\partial^2 m(p)}{\partial x^2}$$

Extending to x, y, z directions:
$$\frac{\partial m(p)}{\partial t} = 0.0002637\frac{k}{\Phi \mu c_t}\nabla^2 m(p)$$

We now get the same formulation as the case of a slightly compressible fluid. In a lot of cases the introduction of pseudo pressure will be sufficient to linearize the case. However, one may notice that in the right hand part of the equation we have the viscosity and the compressibility, which are pressure dependent.

For tight gas the high pressure gradients induce a gradient of compressibility. Also, for long term production, the average compressibility in the reservoir will increase when the pressure drops. In these two cases, if we want to keep on using analytical models, we have to integrate these properties in the time variable, introducing the pseudo time.

We introduce the pseudo time integrand $$I(p) = \frac{1}{\mu(p) c_t(p)}$$

And the pseudo time by: $$t_{ps}(t) = \int_0^t I\left(p(\tau)\right) d\tau$$

… which, by derivation gives: $$dt_{ps} = I\left(p(t)\right) dt$$

Replacing in the diffusion equation we get: $$\frac{\partial m(p)}{\partial t_{ps}} = 0.0002637 \frac{k}{\Phi} \nabla^2 m(p)$$

We now have a linear diffusion equation but there are three major flows:

- viscosity and compressibility terms are missing
- the new variables have completely different dimensions and units than what they replace

The problem can be solved by using normalized pseudo pressure and pseudo time. This requires the use of a reference pressure p_{ref} that will be used for this normalization. A common choice for p_{ref} is the reservoir initial pressure p_i when we know it.

Because the time is only present on one side of the diffusion equation, the normalized pseudo time can be used to re-establish the viscosity and porosity in the diffusion equation:

Normalized pseudo time: $$\tilde{t}_{ps}(t) = \mu(p_{ref}) c_t(p_{ref})\, t_{ps}(t) = \mu_{ref} c_{tref} \int_0^t I\left(p(\tau)\right) d\tau$$

The diffusion equation becomes $$\frac{\partial m(p)}{\partial \tilde{t}_{ps}} = 0.0002637 \frac{k}{\Phi \mu_{ref} c_{tref}} \nabla^2 m(p)$$

In Saphir and Topaze v4.30 and before, we used standard pseudo pressures and normalized pseudo time, and the equation above was the one applicable.

Whatever the normalization we take on m(p), because the pseudo pressure is on both sides of the equation, so the equation itself will not be modified by the change in variable. The main interest of normalized pseudo pressure is to reset the dimension to pressure. It is simply done by applying a factor in order for the normalized pseudo pressure to coincide to pressure for a certain value p_{ref}.

Normalized pseudo pressure condition $$\tilde{m}(p) = m(p) \frac{p_{ref}}{m(p_{ref})} = p_{ref} \frac{\int_0^p \frac{p}{\mu Z} dp}{\int_0^{p_{ref}} \frac{p}{\mu Z} dp}$$

The diffusion equation remains $$\frac{\partial \tilde{m}(p)}{\partial \tilde{t}_{ps}} = 0.0002637 \frac{k}{\Phi \mu_{ref} c_{tref}} \nabla^2 \tilde{m}(p)$$

But the dimension is pressure and we have $$\tilde{m}(p_{ref}) = p_{ref}$$

To summarize…

For real gas, standard pseudo pressures, introduced by Al-Hussainy and Ramey in 1966, are the ones currently used in Saphir and are defined by the equation below:

$$m(p) = 2\int_0^p \frac{p}{\mu Z}\, dp$$

The field unit for pseudo pressures is psi²/cp, and the order of magnitude is 10^9, which makes them unintuitive to manipulate. An alternative is to use normalized pseudo pressures, which apply a factor related to a reference pressure at which the normalized pseudo pressure equals the pressure. This normalized pseudo pressure has the dimension of pressure, its field unit is psi, and it is given by

$$\tilde{m}(p) = m(p)\frac{p_{ref}}{m(p_{ref})} \quad \Rightarrow \quad \tilde{m}(p_{ref}) = p_{ref}$$

Either pseudo pressure definition integrates nonlinearities and produces a diffusion equation similar to one of a slightly compressible fluid:

$$\frac{\partial m(p)}{\partial t} = 0.0002637\frac{k}{\Phi \mu c_t}\nabla^2 m(p)$$

However there are cases where the diffusion factor, which includes pressure dependent variables such as the fluid viscosity and (mainly) the compressibility, varies in a way that cannot be ignored. This is particularly the case for tight formations, where high pressure gradients induce high gradients of compressibility and changing wellbore storage, or for long term production where the drop of the average pressure requires a correction. In either case we introduce normalized pseudo time:

$$\tilde{t}_{ps}(t) = \mu_{ref} c_{tref} \int_0^t I\big(p(\tau)\big)\, d\tau \qquad \text{where} \qquad I(p) = \frac{1}{\mu(p) c_t(p)}$$

However this transformation implies that we assign a pressure at a given time while the pressure field is not uniform. The choice of this pressure is critical and related to the nonlinearity we want to integrate. The remaining inaccuracy of the analytical mode will reside in this choice. This change of variable integrates the variations of viscosity and compressibility and end up with a diffusion equation which a constant term.

$$\frac{\partial \tilde{m}(p)}{\partial \tilde{t}_{ps}} = 0.0002637\frac{k}{\Phi \mu_{ref} c_{tref}}\nabla^2 \tilde{m}(p)$$

13.E.2 Behavior and usage of Pseudo pressures

A typical m(p) behavior with respect to the pressure is shown in the plot below:

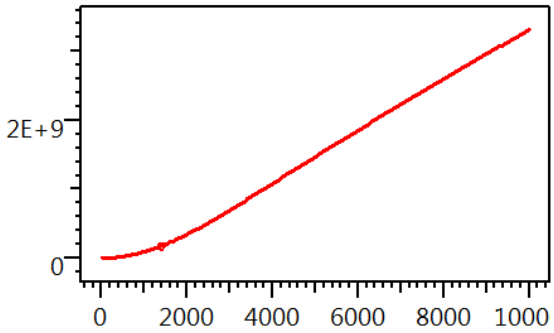


Fig. 13.E.1 – m(p) [psi²/cp] vs p [psia)

The principle for using the Pseudo pressure is to convert first the pressure history into a Pseudo pressure history then to proceed normally with the analysis, applying, of course, the adequate equations parameters.

For a model matching, the model is calculated in dimensionless terms, then converted into pseudo pressure using the proper pressure match formulation:

$$P_{match}^{m(p)} = \frac{T_{sc}}{P_{sc}} \frac{kh}{5.03x10^{4} Tq}$$

If a history matching is required, the simulation calculated in terms of m(p) can be converted back into a simulated pressure history by using the table m(p) vs p.

The only drawback remains in the order of magnitude of the loglog pseudo pressure axis:

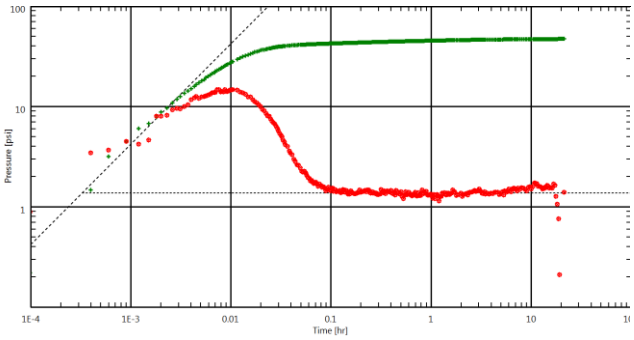


Fig. 13.E.2 – Original Δp vs Δt log plot

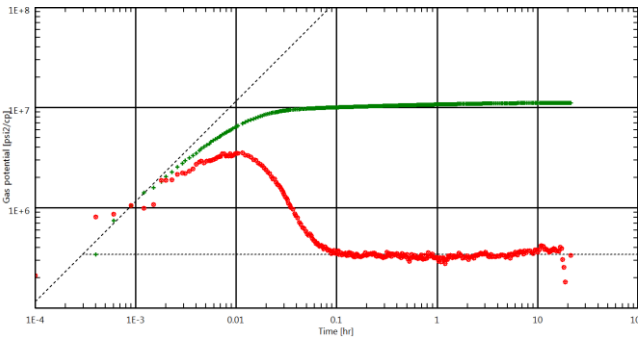


Fig. 13.E.3 – Δ m(p) vs Δt log plot

Using the normalized pseudo pressure allows to correct the non-linearity and to get order of magnitude and units similar to the one used with the pressure.

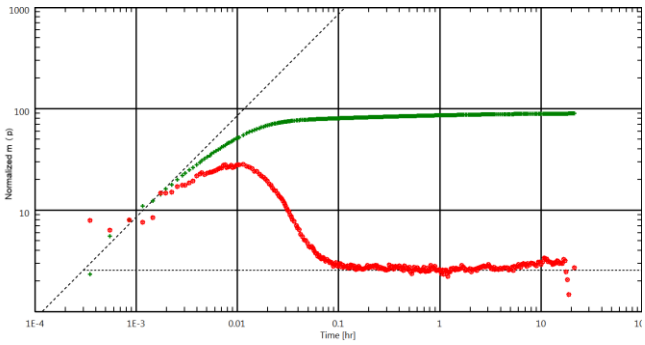


Fig. 13.E.4 – Δ(normalized m(p)) vs Δt log plot

Approximation

There is a possible approximation of the pseudo pressure at low pressure. Considering a typical behavior of the product μz with respect to the pressure.

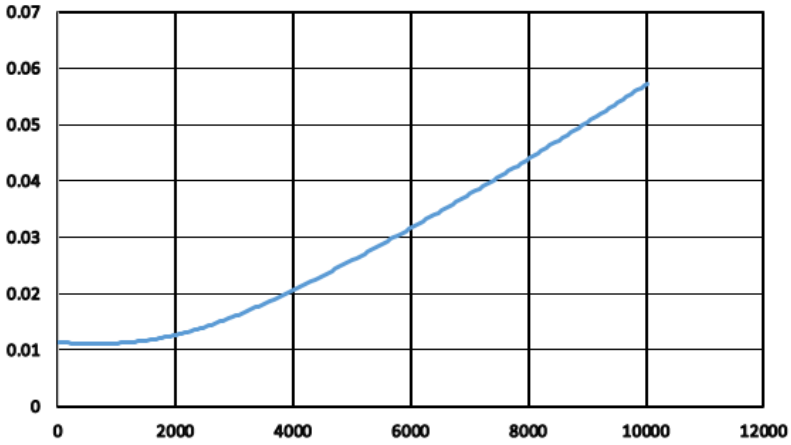


Fig. 13.E.5 – μz vs p [psia)

We see that it is rather constant below 2000 psia.

We can consider:

$$\mu z = \mu_i z_i$$

Therefore,

$$m(p) = 2\int_{p_0}^{p} \frac{p}{\mu z} dp$$

can be approximated by:

$$m(p) = \frac{2}{\mu_i z_i}(p^2 - p_0^2)$$

Below 2000 psia, the pressure square can be used to approximate the pseudo pressure.

In the same way, above 3000 psia:

$$\mu z/p = \mu_i z_i/p_{i=} \text{ Cst}$$

Therefore, the pseudo pressure can be approximated by:

$$m(p) = \frac{2p_i}{\mu_i z_i}(p \quad - p_0)$$

13.E.3 Pseudo time for early time wellbore storage correction

The Pseudo-time is defined by:

$$t_{ps}(t) = \int_0^t I\left(p_{wf}(\tau)\right) d\tau \qquad \text{where} \qquad I(p) = \frac{1}{\mu(p) c_t(p)}$$

Note : the flowing pressure pwf is used here.

The I(p) behavior with respect to the pressure is shown in the plot below:

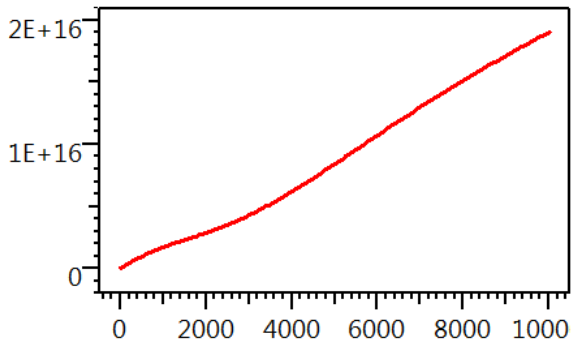


Fig. 13.E.6 – I(p) [hr-1] vs p [psia]

The following figures show a loglog response at early time before and after pseudo time correction.

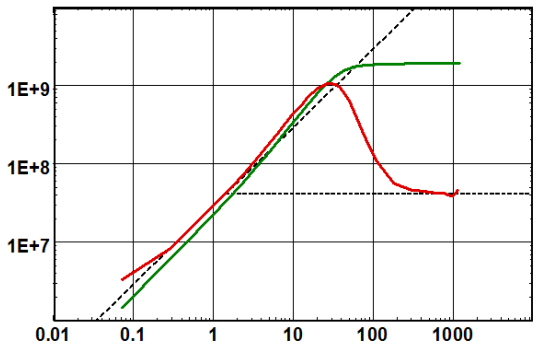


Fig. 13.E.7 – Without pseudo-time

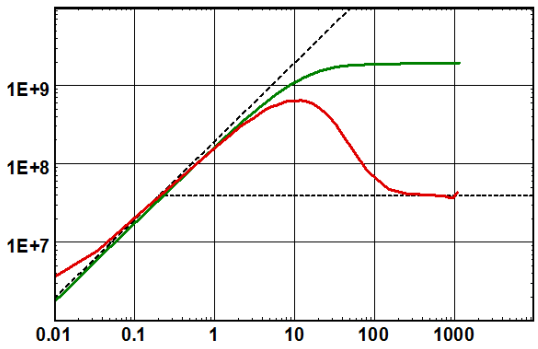


Fig. 13.E.8 – With pseudo-time

There are two drawbacks to this approach:

- This method modifies, once and for all, the data to match the model, and not the opposite. This excludes, for example, the possibility of comparing several PVT models on the same data. The method was the only one available at the time of type-curve matching, where models were limited to a set of fixed drawdown type-curves.
- In order to calculate the pseudo time function one needs the complete pressure history. When there are holes in the data, or if the pressure is only acquired during the shut-in, it will not be possible to calculate the pseudo time from the acquired pressure. There is a workaround to this: use the pressures simulated by the model, and not the real pressures. This amounts to the same thing once the model has matched the data, and there is no hole. However it is a bit more complicated for the calculation, as the pressure at a considered time requires the pseudo time function, and vice versa.

13.E.4 Pseudo time for late time material balance correction

In case of long production and large depletion, the average pressure therefore the average product μc_t can widely vary and the diffusion equation is not anymore linear:

$$\frac{\partial m(p)}{\partial t} = 0.0002637 \frac{k}{\Phi \mu c_t} \nabla^2 m(p)$$

Ignoring this effect would lead to consider a constant compressibility when, in the reality, the decreasing pressure induces an increasing compressibility, it can result a "pessimistic" deviation of the simulated pressure compared to long term data:

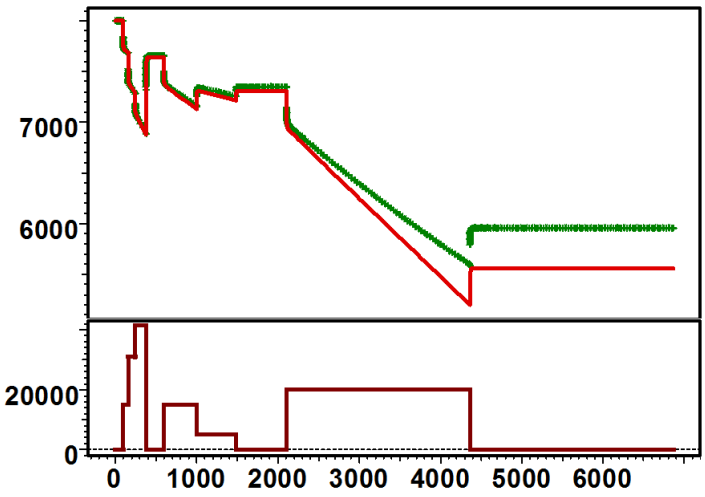


Fig. 13.E.9 – Match (red line) without a material balance correction

The same principle as for the changing wellbore storage can be used, but this time the pressure from which the pseudo time function is calculated will be the reservoir, or drainage area, average pressure:

- The process starts from an initial estimate of the reservoir initial pressure and volume. These two parameters are required to calculate the initial gas in place G_i.
- At each time step, the cumulative production is calculated and subtracted from the initial gas in place. A standard p/Z calculation is used to estimate the reservoir average pressure at this time, to be used to calculate the pseudo time integral, and then the pseudo time. This pseudo time is used on the loglog plot, and the data is therefore expanded to the right, allowing the match with a classic closed system type-curve.

This method was useful at the time when one only had type-curves as models. Today computers can do much better and faster. The main shortcoming was that the initial estimate of the volume and the initial pressure was made before the model was matched. The model would give a value of initial pressure and volume, which might not be the same as the initial guess, hence requiring another modification of the data, another match, and so on. The process would however, converge quickly.

We consider the total gas in place at initial pressure. V_{res} is the pore volume occupied by the gas. T_{res} is the fluid temperature at reservoir conditions. G_i is the initial gas in place at standard conditions.

Real gas equation at initial pressure: $$p_i V_{res} = Z_i nRT_{res}$$

Same amount of fluid at standard conditions: $$p_{sc} G_i = nRT_{sc}$$

So we get immediately G_i: $$G_i = \frac{p_i}{Z_i} \cdot \frac{V_{res} T_{sc}}{p_{sc} T_{res}}$$

We now consider, at time t, the same situation after a total cumulative production of Q(t). We now want to calculate the average reservoir pressure:

Real gas equation at initial pressure: $$\bar{p} V_{res} = \bar{Z} n(t) RT_{res}$$

Same amount of fluid at standard conditions: $$p_{sc}\left(G_i - Q(t)\right) = n(t) RT_{sc}$$

So we get immediately G_i: $$G_i - Q(t) = \frac{\bar{p}}{\bar{Z}} \cdot \frac{V_{res} T_{sc}}{p_{sc} T_{res}}$$

We calculate the average pressure from: $$\frac{\bar{p}}{\bar{Z}} = \frac{p_{sc} T_{res}}{V_{res} T_{sc}} \left(G_i - Q(t)\right)$$

When we apply this method to a long term pressure measurement and simulation the deviation is easily corrected:

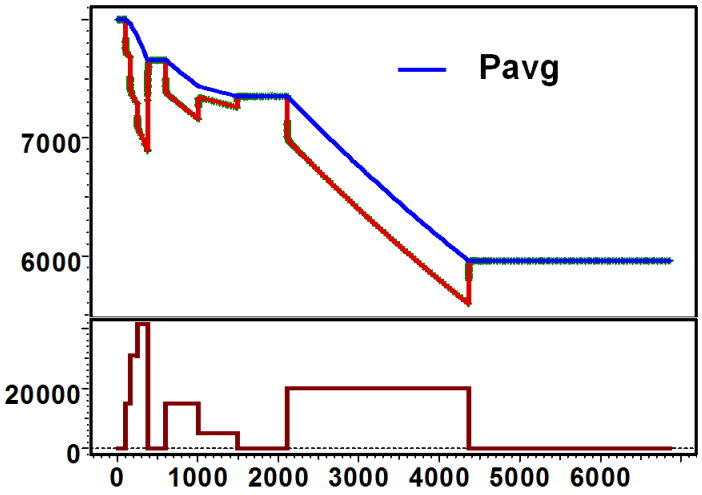


Fig. 13.E.10 – Match with a material balance correction

13.E.5 The case of unconventional formations

This is particularly the case of unconventional formations, where the large pressure gradients produce, among other things, a large gradient of compressibility. In this case, and for 35 years (Agarwal, 1979) we have been using pseudo time with an integral term is given by:

$$t_{pseudo} = \mu_i c_{t_i} \int_0^t \frac{dt}{\mu[p^*(t)]c_t[p^*(t)]}$$

The integral term used in unconventional formations may be more complex, as it may integrate such effects as desorption and the relation between reservoir parameters and pressure.

13.E.5.a Generalized Pseudo functions

For the solution of Shale Gas cases, we have to think about a general form that would account for:

- Large pressure gradients and their effect of the viscosity-compressibility product
- Pressure dependent properties (k(p), ϕ(p))
- Desorption

The approach is introduce a general expression for permeability, porosity, compressibility and viscosity:

$$\phi(p) = \phi_{ref} \cdot f_\phi(p) \; ; k(p) = k_{ref} \cdot f_k(p); \; c_t(p) = c_{tref} \cdot f_\phi(p) \; ; \; \mu(p) = \mu_{ref} \cdot f_\phi(p)$$

We re-write the equation:

$$\frac{p}{\mu Z}\frac{\partial p}{\partial t} = 0.0002637 \frac{k}{\phi \mu c_t} \vec{\nabla}\left[\frac{p}{\mu Z}\vec{\nabla} p\right]$$

using the general expression for k:

$$\frac{f_k p}{\mu Z}\frac{\partial p}{\partial t} = 0.0002637 \frac{k}{\phi \mu c_t} \vec{\nabla}\left[\frac{f_k p}{\mu Z}\vec{\nabla} p\right]$$

This last expression of the diffusion equation allows us to deduce pseudo pressure that accounts for pressure dependent permeability:

$$m(p) = 2\int_0^p \frac{f_k p}{\mu Z} dp$$

And to introduce a pseudo time:

$$t_a(t) = \int_0^t \frac{f_k}{f_\Phi f_\mu f_{c_t}} dt$$

The equation becomes then:

$$\frac{\partial m(p)}{\partial t_a} = 0.0002637 \frac{k_{ref}}{\Phi_{ref}\mu_{ref}c_{tref}} \nabla^2 m(p)$$

13.E.5.b Taking into account the desorption effect

The problem of shale gas cannot be properly described if the desorption phenomenon is not taken into account.

The desorption effect, more developed in the chapter Unconventional Resources, paragraph 10.B.2, is governed by the Langmuir equation:

$$p_E = \frac{V_L\, p}{p_L + p}$$

The desorption contribution appears as an additional source term in the raw diffusion equation:

$$\frac{\partial \rho \phi}{\partial t} + \rho_{sc} \frac{\partial V_E}{\partial t} = \vec{\nabla}\left[\frac{k\rho}{\mu} \vec{\nabla}\, p \right]$$

Developing the left side of the equation we get:

$$\frac{\partial p}{\partial t}\left[\rho\phi\left(c + c_f\right) + \rho_{sc} \frac{\partial V_E}{\partial t} \right] = \vec{\nabla}\left[\frac{k\rho}{\mu} \vec{\nabla}\, p \right]$$

Which leads to:

$$\frac{\partial p}{\partial t}\left[\rho\phi\left(c + c_f\right) + \rho_{sc} \frac{\partial V_L p_L}{\left(p_L + p\right)^2} \right] = \vec{\nabla}\left[\frac{k\rho}{\mu} \vec{\nabla}\, p \right]$$

The desorption term can be seen as a contribution to the total compressibility ct

If we define an effective compressibility c_t^* as:

$$c_t^* = c + c_f + c_d$$

Where c_d can be seen as a "desorption compressibility":

$$c_d = \rho_{sc} \frac{\partial V_L p_L}{\left(p_L + p\right)^2}$$

The desorption effect is then included in the diffusion coefficient and doesn't appear in the pseudo-pressure definition.

References

Al-Hussainy R. et al.,"The flow of real gases in porous media". J. Pet. Tech., 1972.

F. Samaniego V. et al.,"An investigation by numerical methods of the effect of pressure-dependent rock and fluid properties on well flow tests". SPE 2617, 1972.

F. Samaniego V. et al., "An investigation of transient ow of reservoir fluid considering pressure-dependent rock and fluid properties". SPE 5593, 1977.

Bumb A. C. and McKee C. R., "Gas-well testing in the presence of desorption for coalbed methane and Devonian shale". SPE Formation Evaluation, 1988.

13.E.5.c Pseudo time calculation

The challenge of pseudo time is to choose, at a given time, the right pressure to calculate the integral. As there is a pressure gradient the choice is generally related to the flow regime. From experience the best choice for a fractured horizontal well would be, during the linear flow regime:

$$p^*(t) = \frac{p_i + p_{wf}(t)}{2}$$

But the above expression would not apply anymore in Shale Gas case, during SRV dominated flow, not to mention late time radial flow.

In practice, the way we internally compute p^* in analytical models is from a material balance performed on the depleted pore volume, at each computed time step. We end up with a specific pseudo time definition based the following calculations:

(a) at every model time step, we approximate the depleted pore
(b) we compute p^* using mass balance equations on this volume
(c) we use this average pressure to compute gas properties, which in turn are used to update the corresponding pseudo time.

This method is obviously an approximation because none of the three steps described above is fully valid: the investigation radius calculation is weakened because we are not dealing with radial flow, the average pressure calculation is questionable because transient flow applies, not to mention that using this pressure to calculate average gas properties is in itself questionable.

13.E.5.d Dynamic Pseudo time

The objective of this approach is to determine as accurately as possible the reservoir volume and the average pressure in it that will be taken into account in the pseudo time calculation.

The idea is to compute the average pressure from the Gi, gas initially in place, which is estimated at each step. The improvement consist in an advanced way to calculate the investigated area.

It is not based on an IARF investigation radius, not applicable in shale gas case, but on the estimate of an elliptic investigation area around each fracture, growing with the time and interfering on each other one.

The size of the ellipse is governed by the square root of time:

$$r = \alpha\sqrt{(t)}$$

Where α is a constant fixed experimentally by comparison with Non Linear numerical model simulations.

The evolution of the investigated area with the time in a complex case is shown in the figure below:

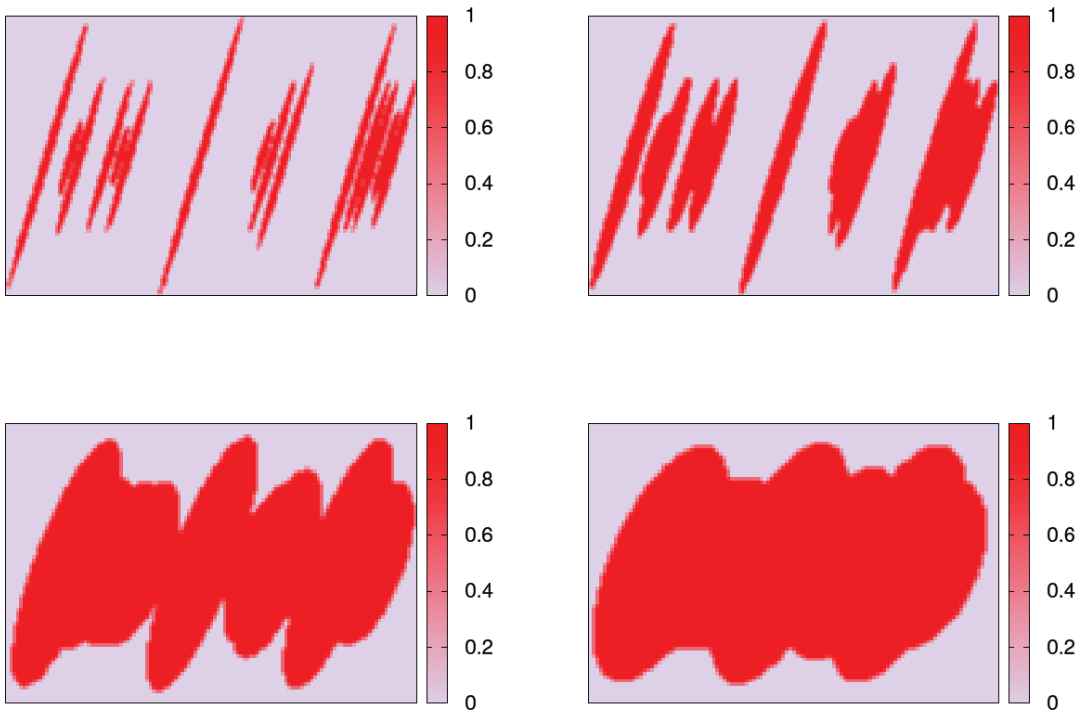


Fig. 13.E.11 – Match with a material balance correction

This method is more successful in reducing the gap between analytical and numerical models in shale gas, hence allowing a smoother transition in the analysis workflow.

As a conclusion, beyond the usual corrections brought by pseudo pressure and pseudo time in conventional plays, pseudo functions in shale plays allow the following extensions:

- Rock dependent properties (permeability and porosity as functions of pressure)
- Gas desorption

Ultimately, dealing with large scale approximations of nonlinearities can only be treated rigorously in numerical models. The intention is 'only' to narrow the gap between analytical and numerical models in order to use the results of the former as an initial guess for the latter.

13.E.5.e Clarkson Dynamic drainage area Workflow

The Clarkson Dynamic Drainage Area Workflow facilitates the inclusion of nonlinearities (such as pressure-dependent fluid and rock properties and two-phase flow of gas and oil/condensate) into RTA of the transient linear flow period exhibited by multi-fractured horizontal wells in tight/shale systems. The generalized pseudo pressures already take single phase unconsolidation into account. This workflow, thus, extends the use of the linear flow plot to multiphase cases – taking the secondary phase (gas or oil) into account in addition to the main hydrocarbon (oil or gas) whenever both productions are available, through the use of specific pseudo pressure functions.

Governing Equations

The main governing equations for the analysis are summarized in the table below, in oilfield units.

1	pseudo-pressures, oil and gas:	$$m_o(P) = \int_{P_0}^{P} \left\{ \frac{f_k(\hat{P}) k_{ro}(S_o) \hat{P}}{\mu_{oD}(\hat{P}) B_{oD}(\hat{P})} \right\} d\hat{P}$$ $$m_g(P) = \int_{P_0}^{P} \left\{ \frac{2 f_k(\hat{P}) k_{rg}(S_o) \hat{P}}{k_i \mu_g(\hat{P}) Z_g(\hat{P})} \frac{B_g(\hat{P})}{B_{gd}(\hat{P})} \right\} d\hat{P}$$
2	Linear flow equation, oil	$$\frac{m_o(\bar{P}_{inv}) - m_o(P_{wf})}{q_o} \sqrt{\frac{\mu_{oD}(\bar{P}_{inv}) \varphi_D(\bar{P}_{inv}) c_{tD}(\bar{P}_{inv})}{f_k(\bar{P}_{inv})}} = \frac{57.16 B_{oi}}{A_c \sqrt{k_i}} \sqrt{\frac{\mu_{oi}}{\varphi_i c_{ti}}} \sqrt{t}$$
3	Linear flow equation, gas	$$\frac{m_g(\bar{P}_{inv}) - m_g(P_{wf})}{q_g} \sqrt{\frac{\mu_{gD}(\bar{P}_{inv}) \varphi_D(\bar{P}_{inv}) c_{tD}(\bar{P}_{inv})}{f_k(\bar{P}_{inv})}} = \frac{576.59 T}{A_c \sqrt{k_i}} \sqrt{\frac{1}{\varphi_i \mu_{gi} c_{ti}}} \sqrt{t}$$
4	Material balance, oil	$$N_p = 4 x_{ft} y_{inv} h \left(\frac{\varphi_i S_{oi}}{5.615 B_{oi}} + R_{vi} \frac{\varphi_i S_{gi}}{10^6 B_{gDi}} - \frac{\varphi(\bar{P}_{inv}) \bar{S}_{o,inv}}{5.615 B_o(\bar{P}_{inv})} - R_v(\bar{P}_{inv}) \frac{\varphi(\bar{P}_{inv}) \bar{S}_{g,inv}}{10^6 B_{gD}(\bar{P}_{inv})} \right)$$
5	Material balance, gas	$$G_p = \frac{4 x_{ft} y_{inv} h}{1000} \left(\frac{\varphi_i S_{gi}}{B_{gDi}} + R_{si} \frac{\varphi_i S_{oi}}{5.615 B_{oi}} - \frac{\varphi(\bar{P}_{inv}) \bar{S}_{g,inv}}{B_{gD}(\bar{P}_{inv})} - R_s(\bar{P}_{inv}) \frac{\varphi(\bar{P}_{inv}) \bar{S}_{o,inv}}{5.615 B_o(\bar{P}_{inv})} \right)$$
6	Radius of investigation (α = 0.159)	$$y_{inv} = \text{Min} \left\{ \propto \sqrt{\frac{k_i t}{\varphi_i \mu_i c_{ti}}}, y_e \right\}$$
7	Oil saturation	$$S_o(P) = \begin{cases} 1 - \dfrac{S_{g,base}(P)}{1 + \left(\dfrac{dk_{rg}}{dP} \right)_{S_{g,base}(P)}} \text{ ... black oil} \\ \dfrac{S_{o,base}(P) P_i Z_g(P_d)}{1 + (k_{ro})_{S_{o,base}(P)} P_d Z_{gi} \text{erfc}^{-1} \left[\dfrac{P_i - P_d}{P_i} \right]} \text{ ... gas condensate} \end{cases}$$
		$$S_{o,base}(P) = \begin{cases} \dfrac{5.615 B_o(P)}{5.615 B_o(P) + B_g(P)[R_{sb} - R_s(P)]} \text{ ... black oil} \\ 5.615 \left(\dfrac{R_{v,dew} - R_v(P)}{10^6 - R_s(P) R_v(P)} \right) \dfrac{B_o(P)}{B_{gd,dew}(P)} \text{ ... gas condensate} \end{cases}$$

The point is naturally to come up with an estimate of k.Xmf2. In essence, all equations are assuming two-phase flow – oil and gas, water being considered as immobile. Some additional (and relatively weak and empirical) assumptions are taken to come up with the evaluation of average oil and gas saturations in the SRV. Let's summarize the different equations (in oil field units, we will have to convert them to SI) before to precise the mechanism:

All in all, the mechanism assumes the following iterative steps:

a) $k.X_{mf}^2$ is assumed.
b) This estimate is used to compute average pressure (vs time) using (4) or (5).
c) Data are plotted on a linear flow plot using (1).
d) A straight line is drawn on the plot to give a new estimate of $k.X_{mf}^2$, using (2) or (3).
e) Back to (a) until convergence is reached.

The iterative workflow is summarized in the schematic below*:

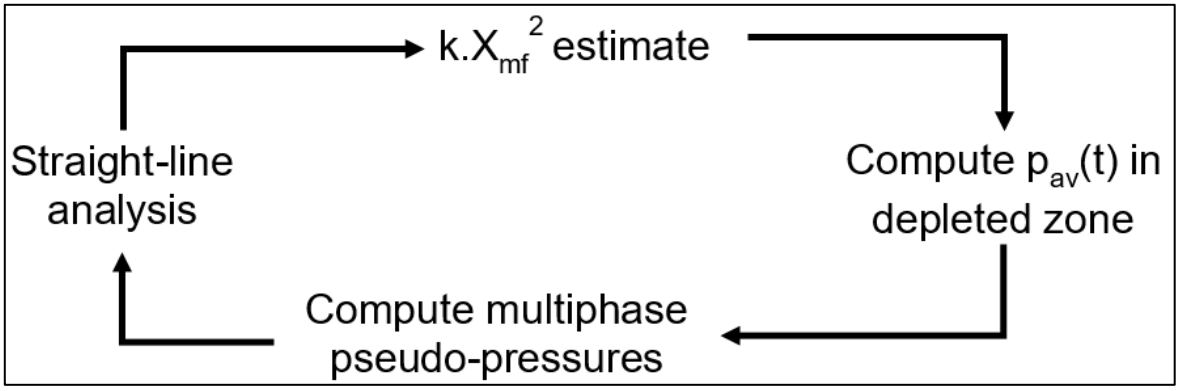


Fig. 13.E.12 – Clarkson DDA iterative workflow

1. "Semi-analytical model for matching flowback and early-time production of multi-fractured horizontal tight oil wells", Clarkson, C. R., Qanbari, F. and Williams-Kovacs, J. D., J. Unconventional Oil and Gas Resources, 15 (2016), 134-145.
2. "Rate-transient analysis of liquid-rich tight/shale reservoirs using the dynamic drainage area concept: Examples from North American Reservoirs", Qanbari, F. and Clarkson, C. R., J. Natural Gas Sci. and Eng., 35 (2016), 224-236

14 – Numerical models
OH – ET – OSF – DV

14.A Introduction

Numerical models are becoming increasingly popular in well test analysis, mainly because they address problems far beyond the reach of analytical and semi-analytical models. The two main areas of usage of numerical models are nonlinearities, such as multiphase or non-Darcy flow, and complex reservoir or well geometries. Numerical models can also be used to replace rate by pressure constraints when the well flowing pressure goes below a certain point, hence avoiding the embarrassing negative pressures often generated by analytical models.

The first attempts at numerical well testing were done ad hoc across the industry by engineers using standard reservoir simulators with local grid refinement. In the early 1990's, the first industrial project involved pre-conditioning of an industry standard simulator using PEBI gridding. Since then, several technical groups have been working on numerical projects dedicated to transient analysis.

In recent years, improvements in automatic unstructured grids and the use of faster computers have allowed such models to be generated in a time that is acceptable to the end user. The change has been dramatic, the time required to calculate the solution has decreased from days to hours, then to minutes, and now, for linear diffusion problems, to seconds. Using gradient methods even nonlinear regression is possible, and improved well-to-cell models allow simulation on a logarithmic time scale with little or no numerical side effects. Last, but not least, automatic gridding methods allow such models to be used without the need for the user to have a strong background in simulation.

The main goal of numerical models is to address complex boundary configurations, but this part of the work is actually easily done by any simulator. The problem is to also address what is easily done by analytical models, i.e. the early time response and the logarithmic sampling of the time scale. This requires, one way or the other, to get more grid cells close to the well, and this has been done using three possible means: local grid refinement of cartesian grids, unstructured (Voronoi, PEBI) gridding, or finite elements. These different options, shown below, have their pros and cons that are beyond the scope of this book.

14.B Principles of Voronoi, PEBI and CPG grids

14.B.1 Building complex geometries

To start a bitmap (BMP, JPG, etc) representing the reservoir is loaded (Figure below). The engineer first defines the scale by using a known distance between two points. Once these dimensions are known, the tested well is positioned and the reservoir outer limits described as a closed polygon.

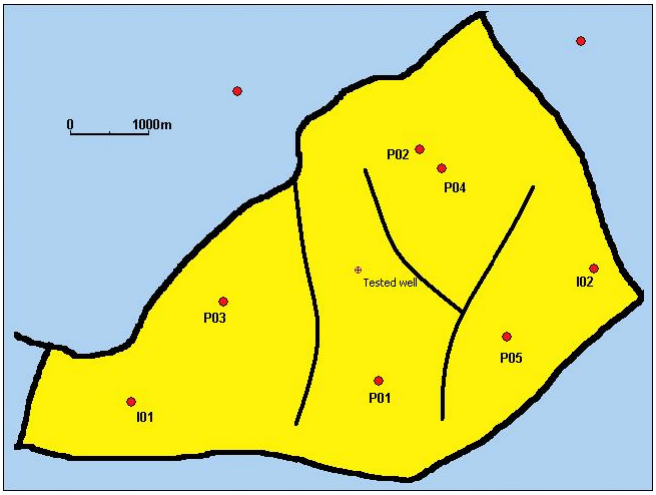


Fig. 14.B.1 – Bitmap of field

Any segment of this polygon may be set as a sealing or constant pressure boundary. If inner boundaries are present, any number of polyline faults may be drawn with control of individual fault transmissibility. Individual wells (vertical, horizontal and/or fractured) may be created and positioned, and their corresponding production history entered. Later, when the model is defined, vertical and fractured wells may be individually specified as fully penetrating or of limited entry. Once the geometry of the problem is defined, the display of the original bitmap is turned off and the 2D Map displays a vector description of the problem:

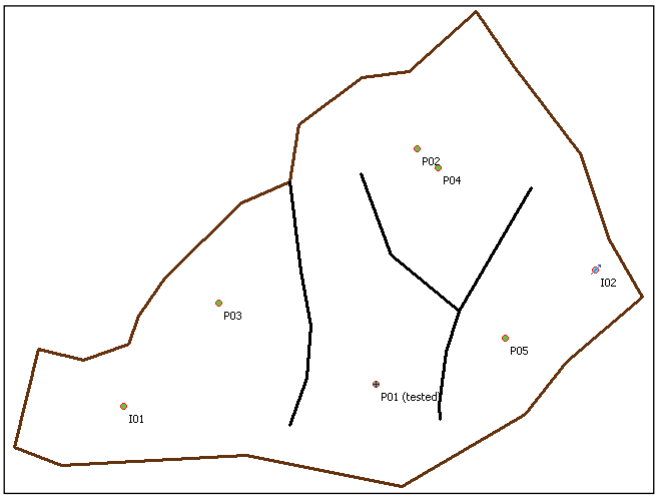


Fig. 14.B.2 – Vector description of the problem

Fault polylines may also be used to delimit composite zones where separate mobilities and diffusivities may be defined. Additional composite zones may also be added around each well, the figure below illustrates this with two radial composite wells and a different western reservoir compartment.

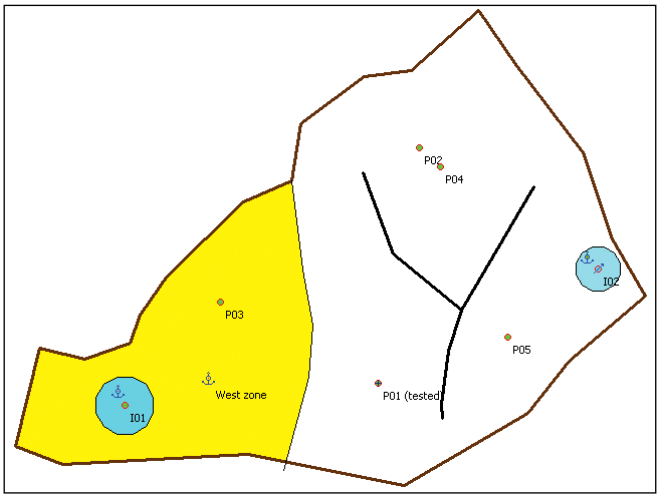


Fig. 14.B.3 – Composite zones added

Porosity, thickness or permeability fields may also be defined, either interactively or by importing an ASCII file. Kriging and other interpolation / extrapolation algorithms are used to populate these properties at each cell:

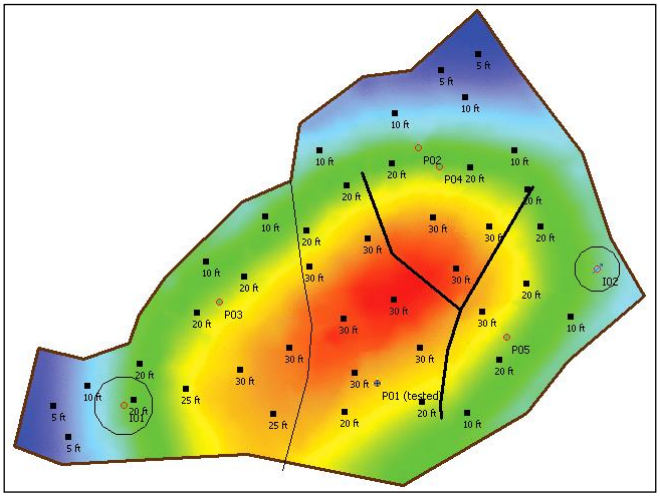


Fig. 14.B.4 – Thickness map

The model can display the automatic gridding, adapted to honor the reservoir contour, inner faults and wells:

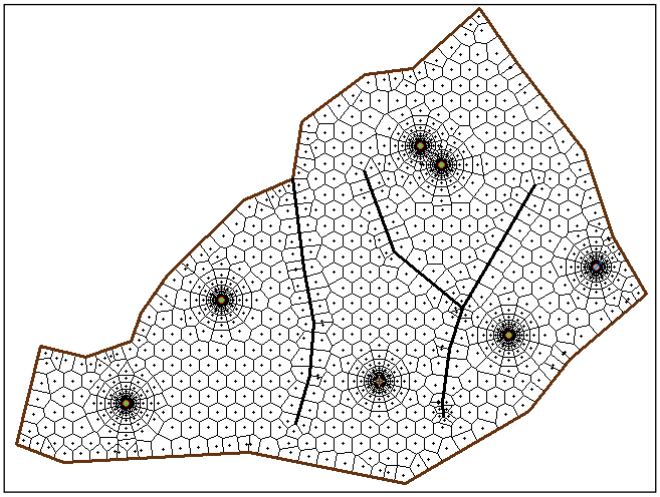


Fig. 14.B.5 – Unstructured Voronoi grid

The default is recommended but specialists may modify the basic grid geometry, size, main directions, and the local grid refinement around each well:

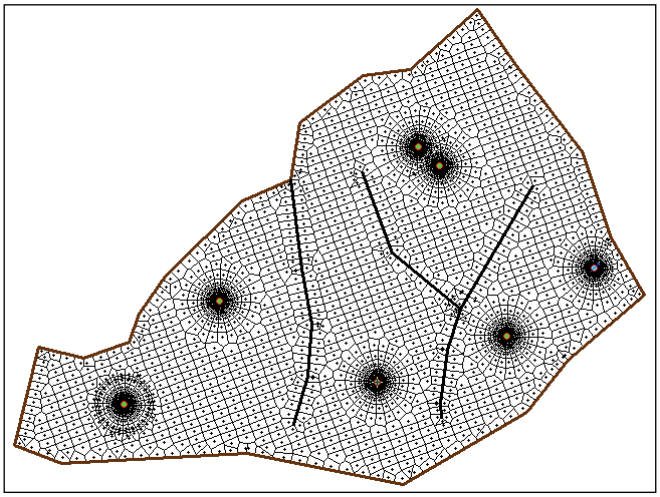


Fig. 14.B.6 – Customized grid

14.B.2 What is a Voronoi grid

The basis of Voronoi gridding is to generate a series of carefully located points called 'grid nodes'. Individual grid nodes can be specified anywhere inside the domain regardless of the position of any other node. It is therefore impossible to identify a grid by a series of indices (i,j) in 2-D and (i,j,k) in 3-D. This is why a Voronoi grid is qualified as 'unstructured'.

A Voronoi cell is defined as the region of space that is closer to its grid node than to any other grid node. A key property of the Voronoi grid is that the contact segment (also called contact face) between two neighboring cells is the bisector of the segment linking the cell nodes.

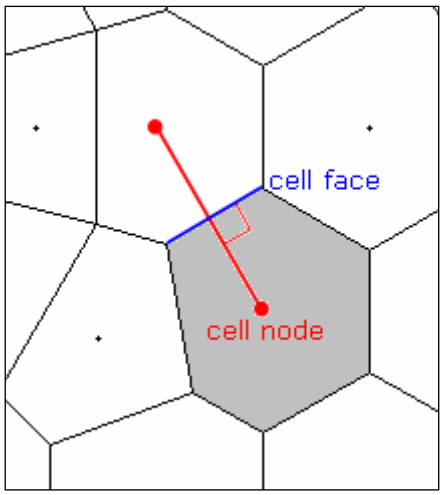


Fig. 14.B.7 – Property of Voronoi grid

The Voronoi grid is closely related to the Delaunay triangulation. In fact the Delaunay facets are obtained by linking the Voronoi cell nodes together. The most important geometrical property of the Delaunay triangulation is that each triangle verifies the empty circle condition, i.e. each triangle's circumcircle does not enclose any other point of the point set:

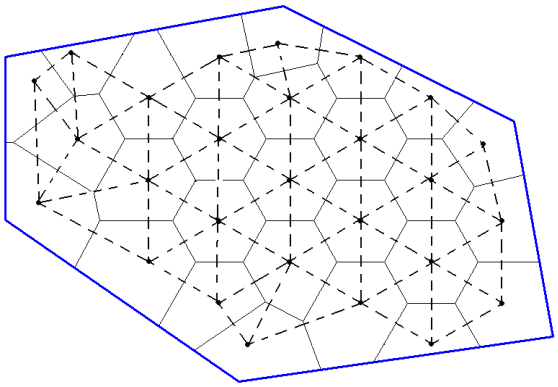


Fig. 14.B.8 – Voronoi grid and Delaunay triangulation (broken lines)

14.B.3 Building the Voronoi grid

The grid is built by superposition of simple modules. A module is a set of sites associated to a reservoir element. The main module types are presented in the three figures below:

- Base, or background, modules, which may be rectangular of hexagonal.
- Segment module introduced in order to respect constraint lines such as the reservoir contour and faults.
- Corner modules introduced at corners of the constraint lines.
- Well modules, which are radial for vertical wells but present more complex shapes for fractured (2-D), horizontal and limited entry wells (3-D).

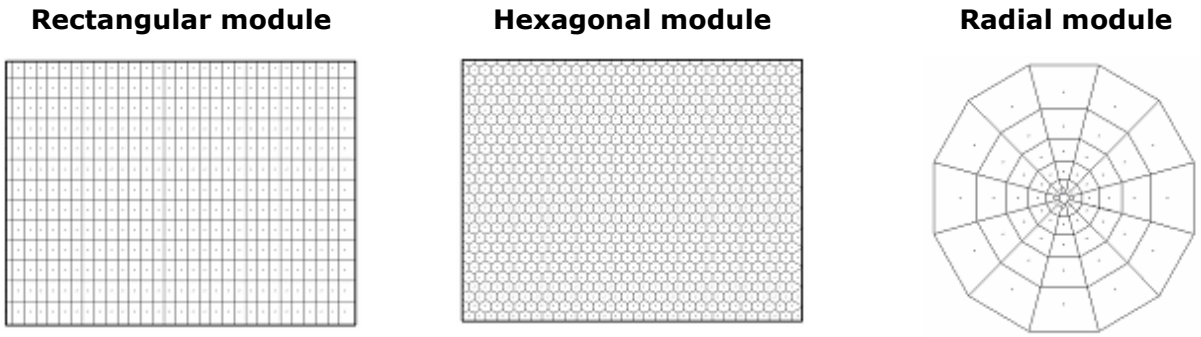


Fig. 14.B.9 – Base modules used in the Voronoi grid construction

A short description of how to build a complete Voronoi grid is presented below. We will however not detail here all steps that are necessary to do so. In particular we will skip the somewhat tedious treatment of interference between modules.

Everything starts with a vector representation of the problem and particularly with a contour, wells and inner boundaries:

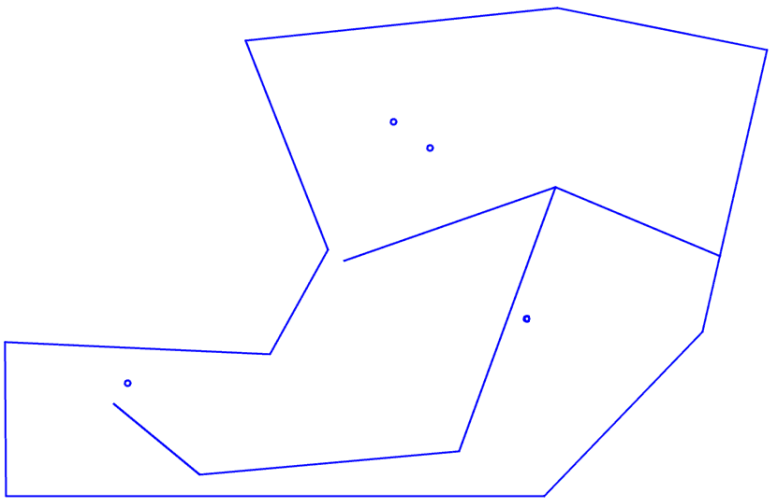


Fig. 14.B.10 – Vector representation of the problem: contour, faults, vertical wells

The base module is built as in the figure below. In this figure the points that would be overlapping with other modules have already been removed.

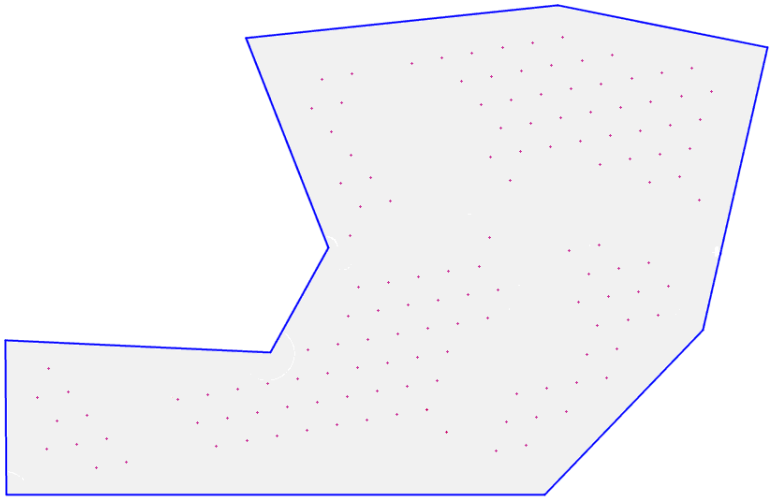


Fig. 14.B.11 – Base module nodes for a hexagonal grid

The radial modules are built around the wells. *Fig. 14.B.12* shows the new modules truncated by interference and the nodes remaining after processing:

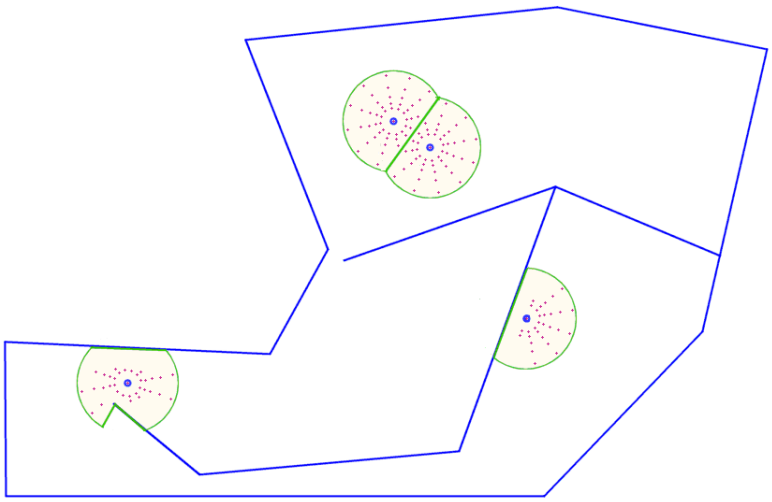


Fig. 14.B.12 – Radial modules around wells

The segment modules are built around the faults and the contour. In the diagram below the corresponding nodes remaining after processing:

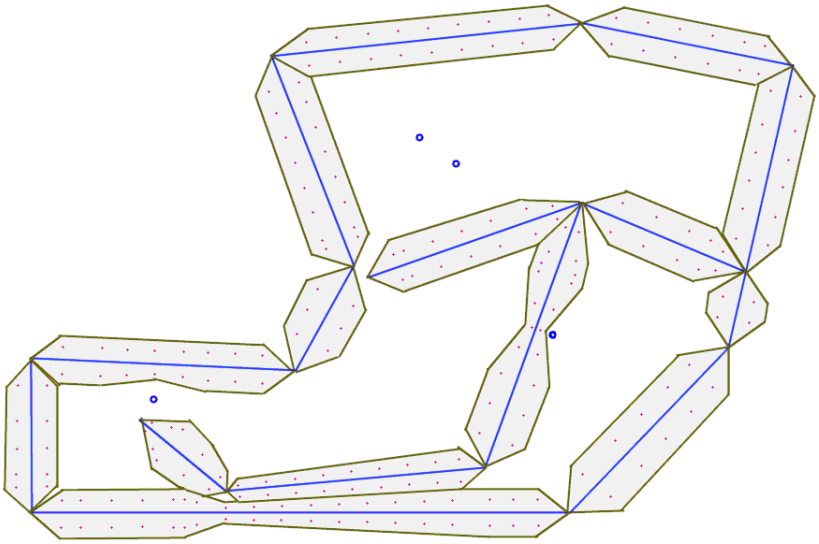


Fig. 14.B.13 – Segments modules around faults and contour

The corner modules are built. They constitute a local refinement that ensures that the shape of the Voronoi grid will exactly follow the angles of the contour and inner fault polylines.

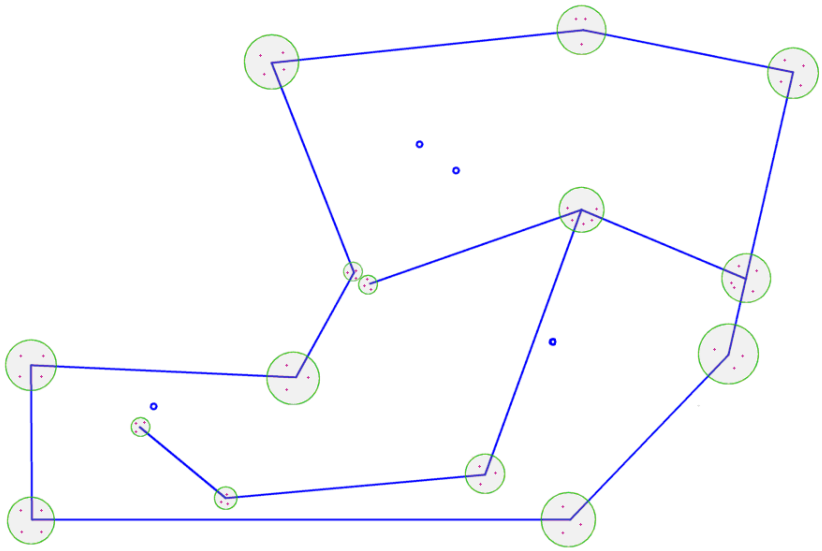


Fig. 14.B.14 – Corners modules around faults and contour angles

The figure here shows the final superposition of all modules leads to the representation below, in which the main interferences are indicated (S=segment, R=radial, C=corner):

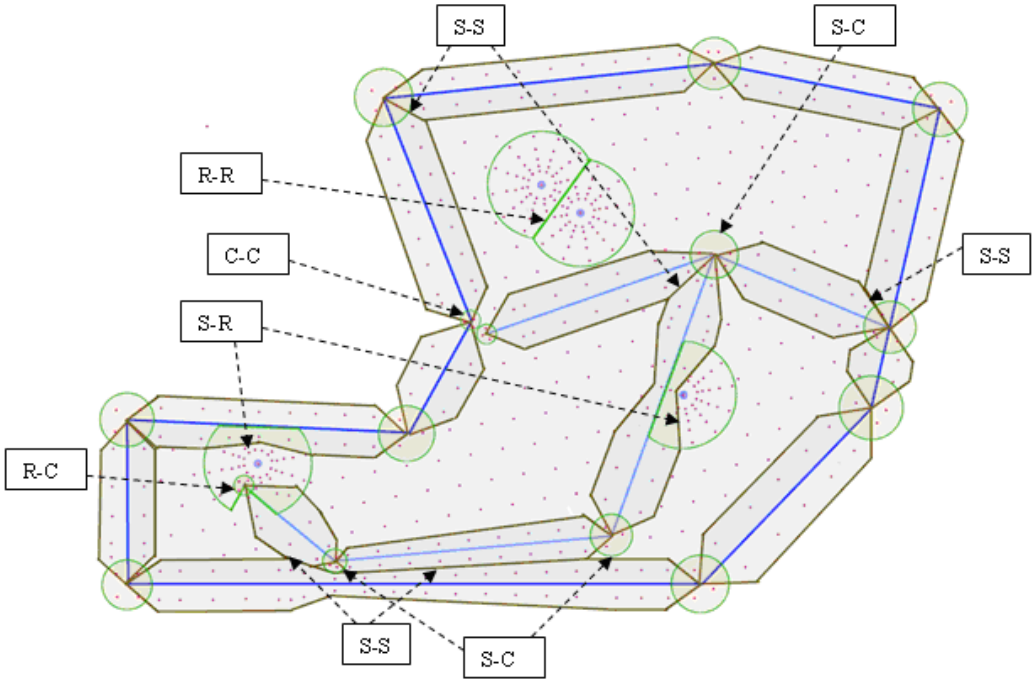


Fig. 14.B.15 – Final superposition

Finally, the triangulation is performed and the resulting Voronoi grid is shown here:

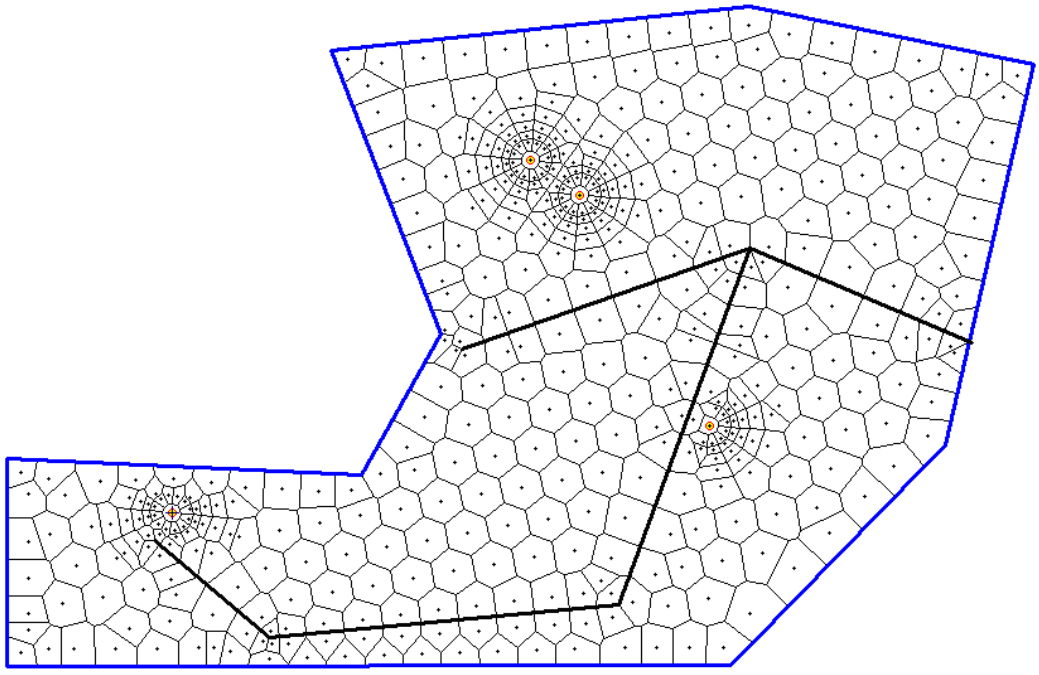


Fig. 14.B.16 – Final Voronoi grid

This result is to be compared with the composite image below showing the specific influence of each module on the final result:

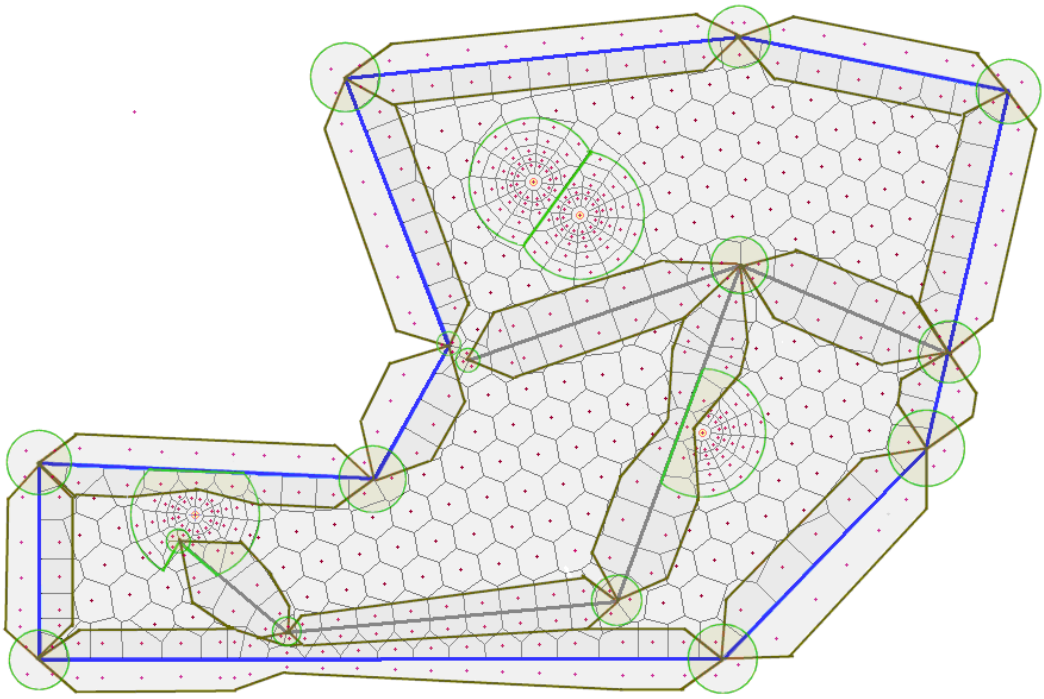


Fig. 14.B.17 – Final Voronoi grid and modules areas of influence

14.B.4 Local 3D refinement for specific well geometries

The example detailed in the previous paragraph addresses only vertical fully penetrating wells, but beyond those simple well geometries the numerical module should also account for fractured, partially penetrating, limited entry fracture and horizontal wells. Whenever needed the 2D reservoir module around the well is replaced by a 3D unstructured grid refinement.

14.B.4.a Vertical wells

Because the well is vertical and fully penetrating a 2D gridding module is sufficient to capture the radial flow. Circular rings are constructed following a geometric series. The other well gridding controls are the bounding radiuses of the module (R_{min}, R_{max}) and the number of sectors (12 here below).

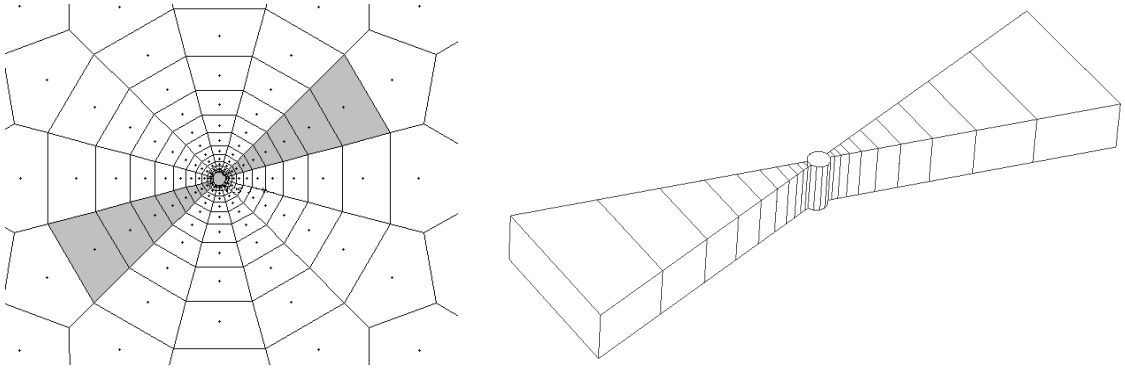


Fig. 14.B.18 – Vertical well gridding: 2D view and 3D display of the highlighted (gray) sectors

14.B.4.b Fractured (fully penetrating) wells

As before, a two-dimensional grid is sufficient because both well and fracture are fully penetrating. As a result fluid flow towards the wellbore is two-dimensional. The gridding module must be designed to follow the fluid flow characteristics in such a case: linear flow at early time, followed by radial flow at later time. The fracture itself has a grid constructed when it presents finite conductivity behavior. In addition to the number of sectors and the bounded radii the module is characterized by the number of linear segments (N_{dx}) used to grid the fracture – reservoir interface (10 segments in the example below).

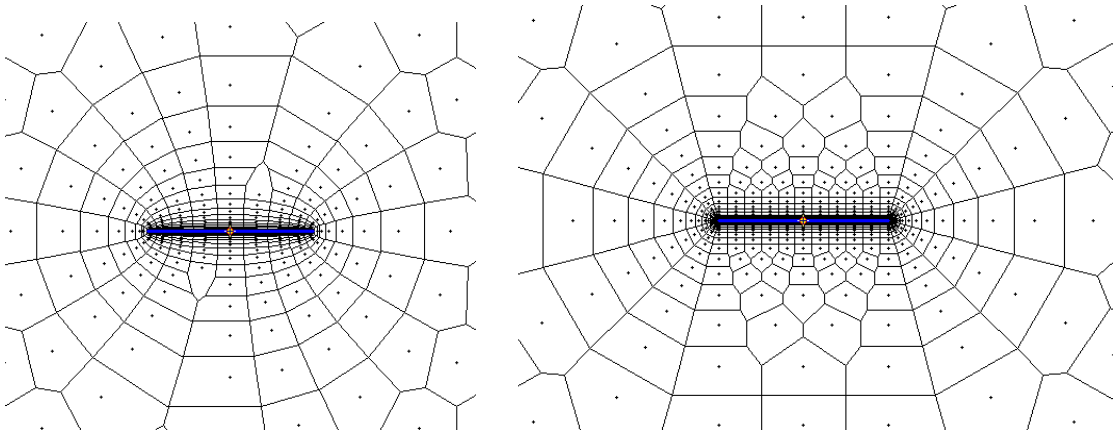


Fig. 14.B.19 – Two possible gridding modules for a fractured well: elliptic (left) and pseudo-radial (right).

14.B.4.c Limited entry wells

The well gridding must be tri-dimensional because of the necessity to reproduce early time hemispherical flow. A 3D Voronoi unstructured module is inserted in the 2D background grid. This module may be distorted by vertical anisotropy as necessary. The number of vertical cells N_z and 10 in the example below, now appear as an additional gridding parameter.

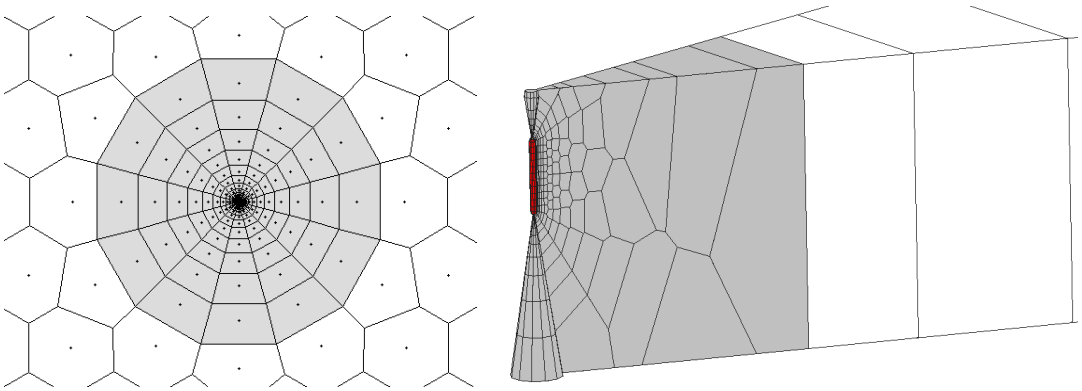


Fig. 14.B.20 – Limited entry gridding module: 2D display (the 3D module is highlighted in gray) and 3D view (the well is highlighted in red).

14.B.4.d Limited entry fractured wells

As before, the well module must be tri-dimensional. The resulting unstructured 3D module is obtained by combining the limited entry with the fully penetrating fracture module. Hence, the defining parameters are now: R_{min}, R_{max}, number of sectors, N_{dx} and N_z.

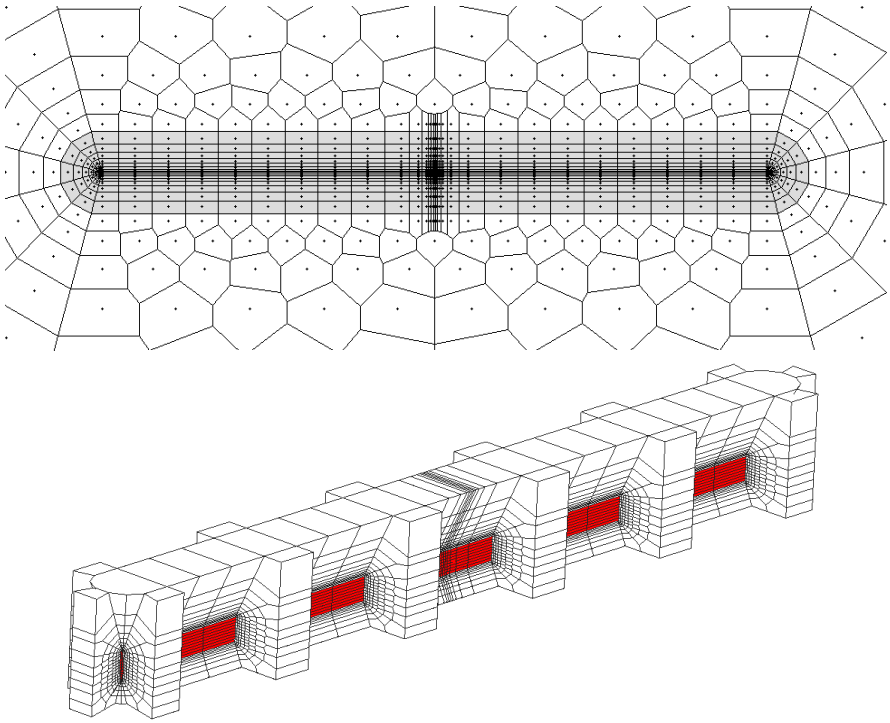


Fig. 14.B.21 – Limited entry fracture gridding module: 2D display (the 3D module is highlighted in gray) and 3D view (the fracture is highlighted in red).

14.B.4.e Horizontal wells

The well module is 3D in order to capture early time spherical and vertical radial flows. The resulting 3D unstructured module may be distorted if vertical anisotropy is introduced. It is controlled by the following parameters: R_{min}, R_{max}, number of sectors and N_{dx}.

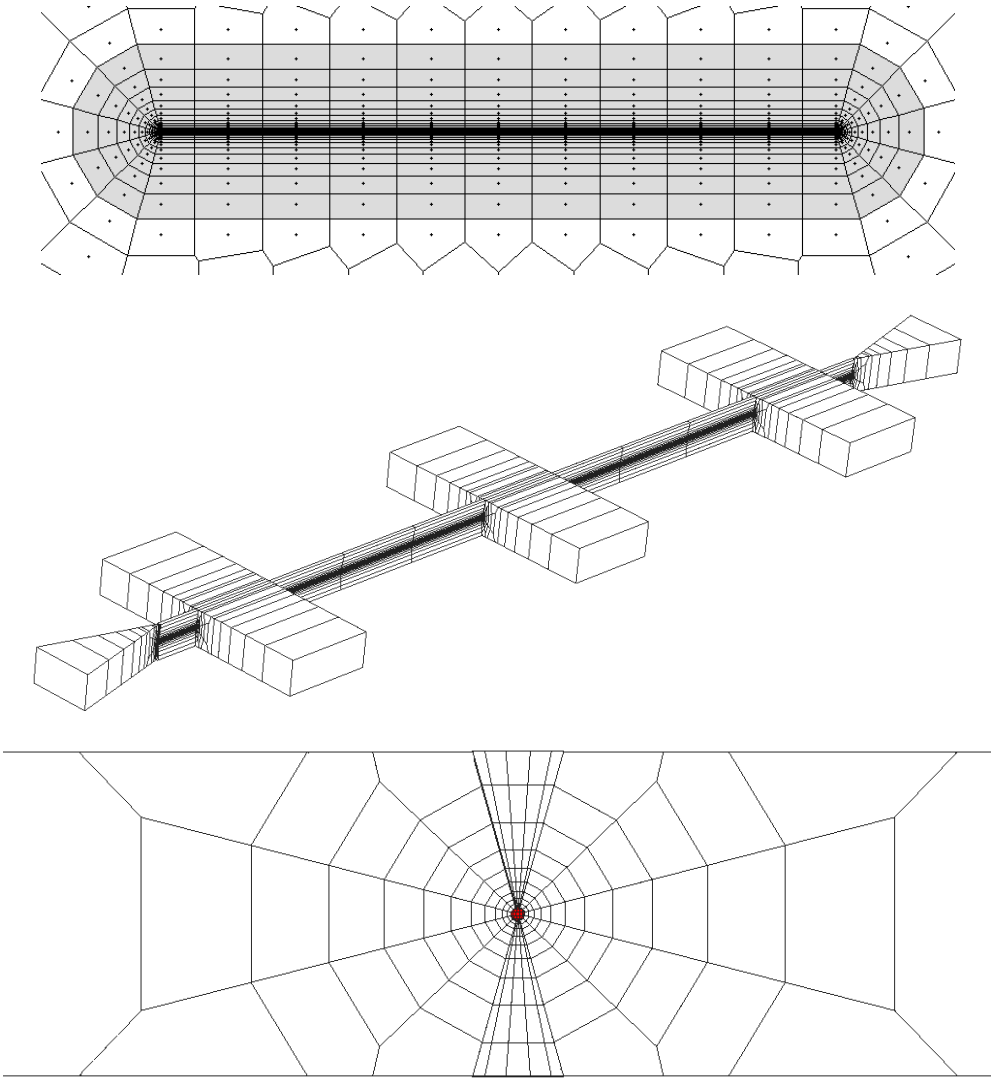


Fig. 14.B.22 – Horizontal well module: 2D display (the 3D module is highlighted in gray), 3D view and vertical cross-section (the well is highlighted in red).

14.B.4.f Complex well

When horizontal wells were introduced some 30 years ago the well test analyst suddenly had a problem. There was no analytical model available. This was quickly remedied and a simple horizontal analytical well model was introduced, however it was strictly horizontal and was not able to cut through different horizons, thus any layers where also strictly horizontal. The reservoir was homogeneous, double porosity, or composite and could be bounded by a circle, rectangle or any shape using the 2D Map (analytical or numerical). The well could not extend from one zone into another and the first numerical equivalent wells followed the stratigraphy of the zone where the well started.

An analytical multilayered slanted well was later introduced, however the layers were still strictly horizontal. This model is described in chapter 6 (6.I.5) of this document.

This enables the modeling of slanted wells, fully or partially penetrating the formation, and with multiple perforations in single or multi-layer reservoirs.

Thus it is possible now model a real horizontal well and use the actually trajectory of the well as input to the model or model arbitrary geometrical trajectories.

To achieve the desired goal it has to comply with the constraint of precise simulations at all-time scales (from pressure transient analysis to history matching) using a 'reasonable' amount of grid cells.

The most satisfying results were obtained with a Voronoi solution, combined with the use of generalized transmissibility corrections.

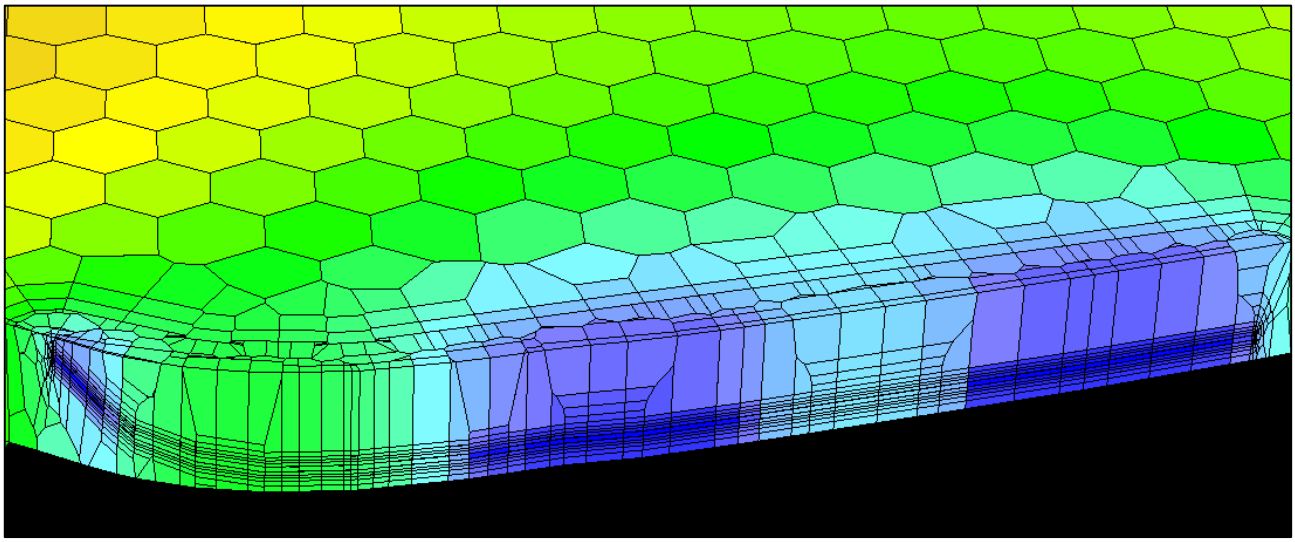


Fig. 14.B.23 – Cross section of a complex well grid

This method, developed internally, consists in carefully defining a set of points around the wellbore. A purely 3D Voronoi grid is then generated using this set of points. Sub-grids are next generated for each layer with additional constraints on the horizons. The background grid is then merged with all the sub-grids to generate a final 3D grid that respects the horizons. This strategy has the advantage of being fast and results in a grid with a relatively limited number of cells; it is however not conformal to a pure 3D Voronoi grid anymore and therefore requires proper transmissibility corrections.

We will come back to the generalized transmissibility corrections in a few pages, but let us insist at this stage that combining those corrections with this new gridding strategy enables us to account for x-y-z anisotropy in a seamless manner.

14.B.5 Near-well upscaling

14.B.5.a Adjusting the grid resolution

As previously described, the grid incorporates 3D "well modules" following the wellbore geometry and allowing the accurate capture of radial effects during flow simulation. The size of the cells inside a well module follows a geometrical progression with the distance to the well block. The length of the first, smallest cell in a fine well module may be about several centimeters (depending on the size of the wellbore diameter or the width of the fracture), while the typical length for a back grid cell varies between ten and a hundred meters. Such refined near-well grids are specifically designed for very precise, transient flow simulations, i.e.: well tests analysis.

When the transient period can be ignored, a variety of coarser well modules can be build for longer-term simulations. This allows to create 3D simulation grids of smaller size, for which the transients may be lost but where the long term response is accurately captured, at a fraction of the CPU cost required with a fine resolution grid.

Only the resolution (or the corresponding "upscaling level" *u*) of the well module itself is changed from the finest resolution (*u=0*) to the coarsest grid (*u=1*), so the back grid remains unchanged. Due to the very detailed discretization of the fine grid, the local upscaling ratio can be very large, especially for horizontal wells, for which more than a thousand fine cells can typically be included into a single coarse cell.

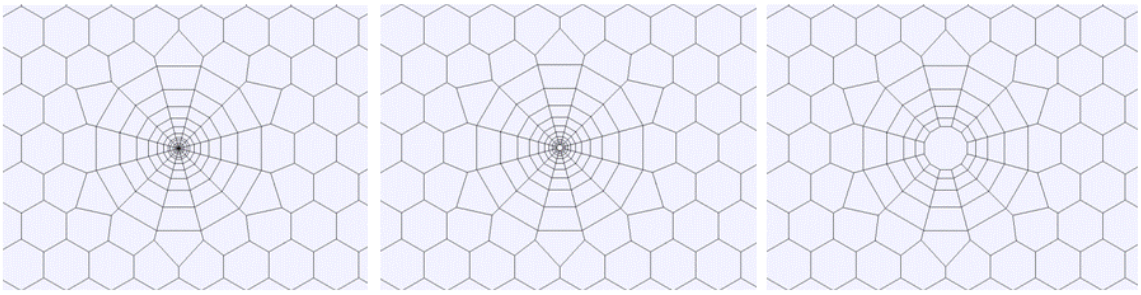


Fig. 14.B.24 – Fine (u=0), intermediate (u=0.6) and coarse (u=1) grids for a vertical well. Top view.

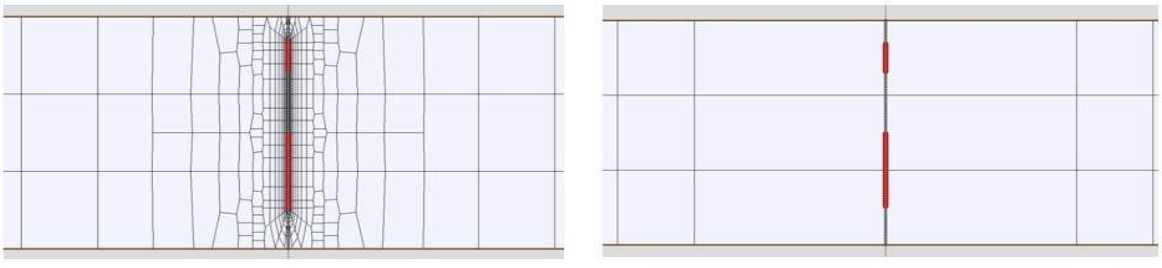


Fig. 14.B.25 – Fine and coarse grids for a vertical well in three layers with two perforations (in red lines). Vertical cross-section

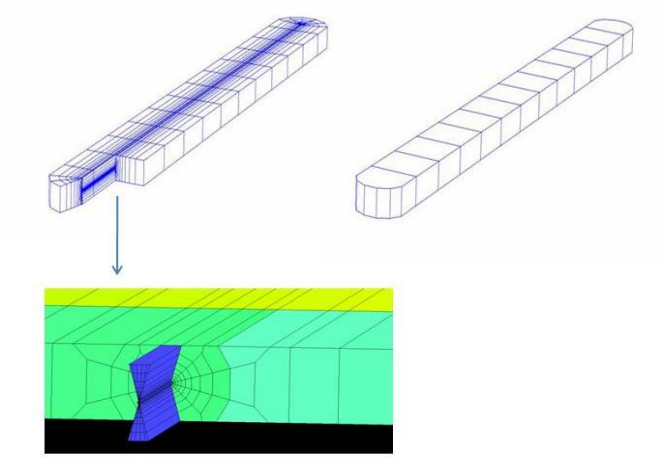


Fig. 14.B.26 – Fine and coarse well modules for a horizontal well

In order to ensure accurate long-term results despite the lower resolution, the well index and transmissibility values of the coarse well modules are calibrated from a local, steady state simulation performed on the fine scale well module, following a "numerical upscaling" procedure detailed in paragraph [14.B.5.b].

Let us consider a 1300ft-long deviated well in a 3 layers reservoir, producing for 1000hr at a constant oil rate of 1000stb/day (Figure [14.B.28]). The pressure fields obtained after 1000hr of production on the corresponding "fine" (*u=0*) and "coarse" (*u=1*) grids are shown on Figure [14.B.27]. The fine, high-resolution 3D-Voronoi grid contains 5259 cells, while the coarse 2.5D-Voronoi grid contains only 1524 cells. The simulation on the fine grid is performed using a minimum time step of 0.1hr, while the minimum time step for the coarse simulation is set to 1hr. The history and log-log plots showing the fine and the coarse simulation results are presented figures [14.B.28] and [14.B.29]. As can be seen, the coarse model is able to very nicely reproduce the long-term results of the 3D fine-scale results, at a much smaller computational cost. Note that the early time (transient) response is, of course, being lost in the procedure.

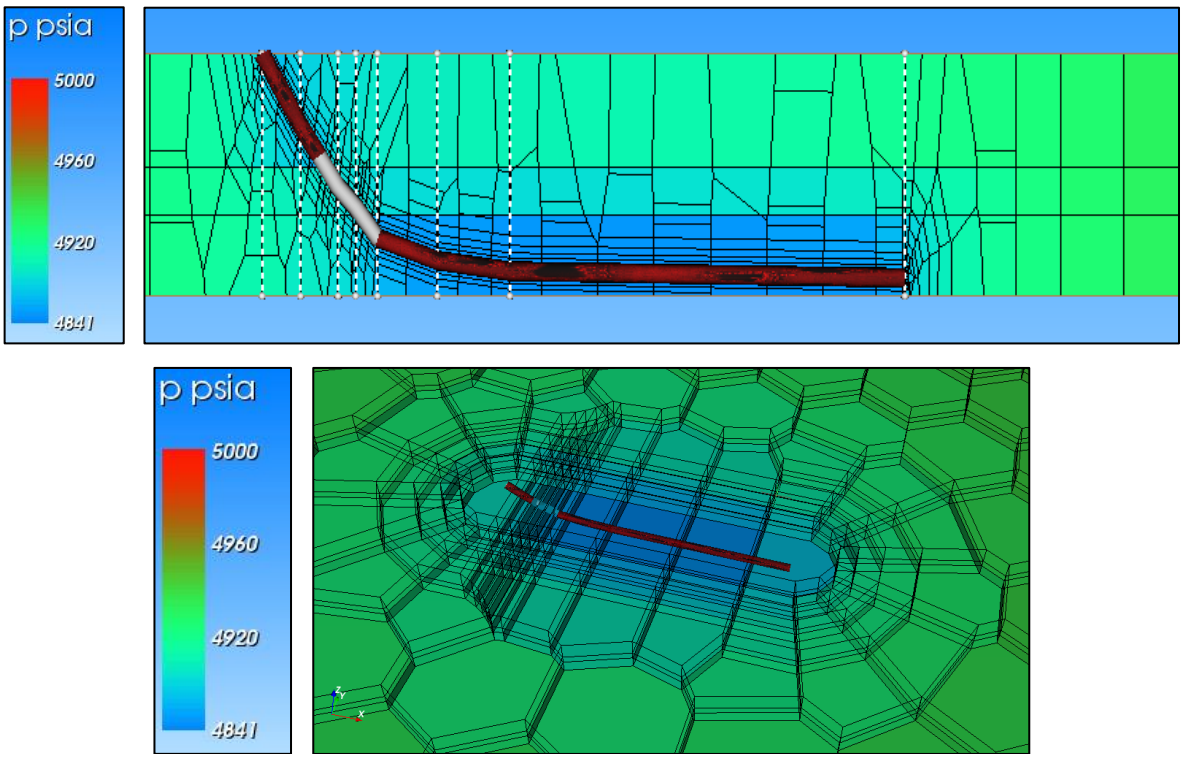


Fig. 14.B.27 – Comparison of the coarse and fine pressure fields after 1000hr

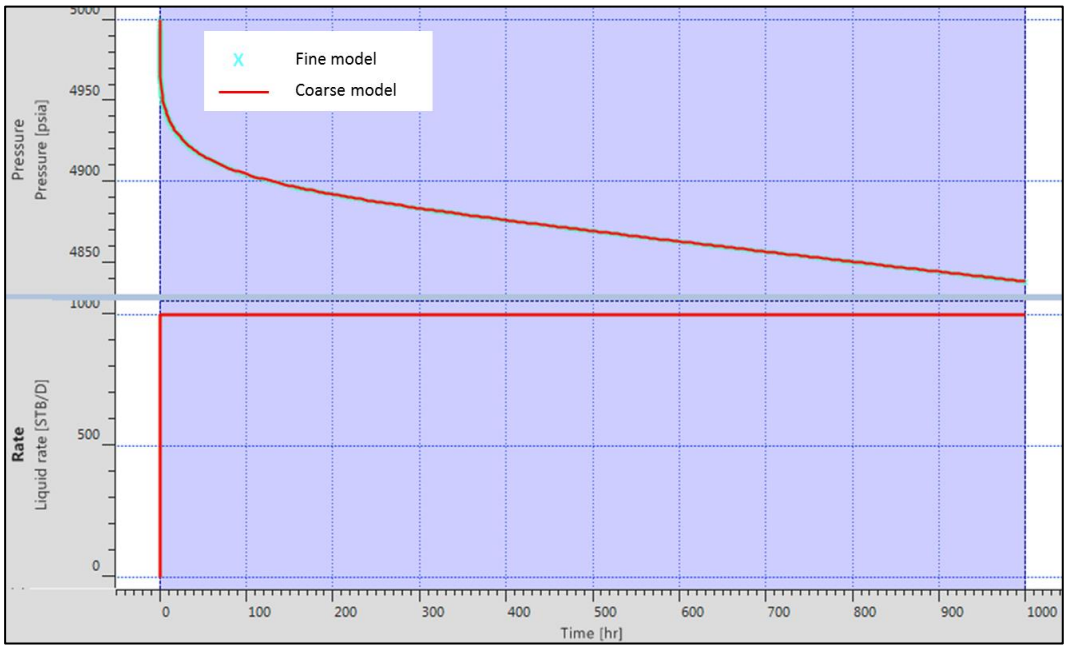


Fig. 14.B.28 – History plot: comparison of the results obtained with the fine and coarse grids

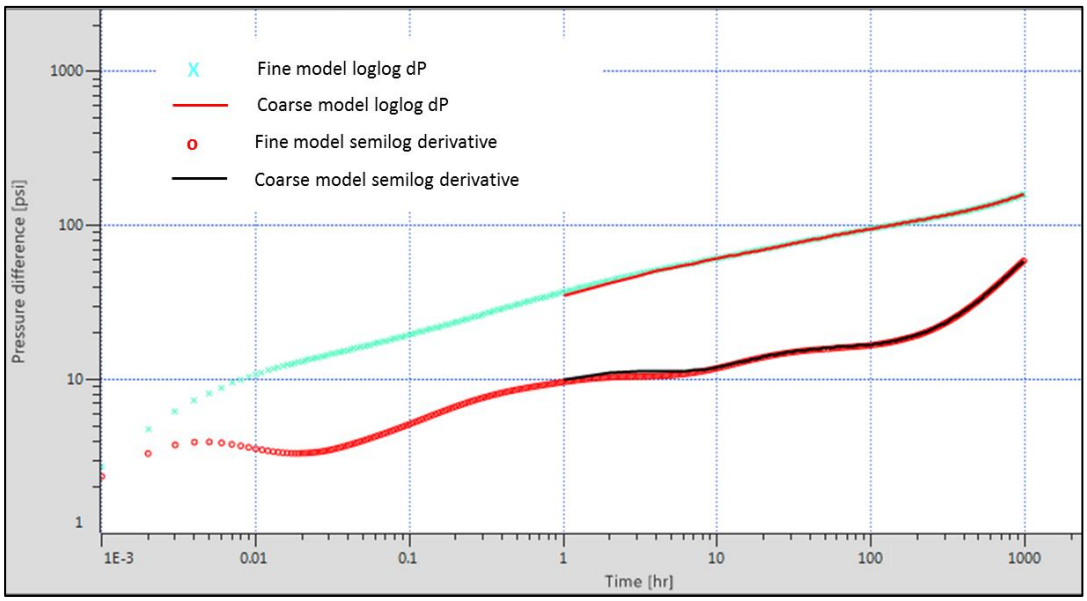


Fig. 14.B.29 – Log-log plot: comparison of the results obtained with the fine and the coarse grids

14.B.5.b Numerical upscaling procedure

The numerical near-well upscaling procedure is based on the solution of a single-phase, well driven flow problem, from which the equivalent near-well transmissibility values between coarse gridblocks are computed. This accounts for radial flow and boundary conditions controlled by the presence of the well, and have been shown to greatly improve coarse-scale simulations results, in comparison with standard, linear conditions.

The derivation of coarse transmissibilities is based on the 4 following steps:

1 - A near-well zone is extracted on the fine grid, defined as the well module plus a ring of back grid cells around the module. Constant pressure conditions are assigned along the wellbore and on the lateral boundaries of the selected zone. No flow conditions are assigned on the top and bottom.

2 - With the conditions described above, a single phase, steady-state problem a solved on the (fine) extracted grid. This provides the fine near-well pressure and rate solution, which satisfies, for each link l and corresponding transmissibility T_l:

$$T_l \Delta P_l = Q_l$$

3 – Based on the results of the fine simulation, the equivalent pressure P_I of each coarse gridblock *I* and the equivalent fluxes Q_L for each coarse link *L* can be derived:

$$Q_L = \sum_{l \in \Omega_l} Q_l$$

$$P_I = \left(\sum_{i \in \Omega_i} V_i \right)^{-1} \sum_{i \in \Omega_i} V_i P_i$$

where Ω_I is the ensemble of fine cells i located in the coarse cell I.

4 – The effective coarse transmissibility between two coarse blocks *I* and *J* of a coarse link *L* can hence be derived and assigned to the coarse grid:

$$\Delta P_L = \left(P_I - P_J \right)$$

$$T_L = -\frac{Q_L}{\Delta P_L}$$

The numerical well index T_{wi} relates the well flow rate (from well block i to well w) to the well block pressure P_i and the wellbore pressure P_w:

$$Q = T_{wi} \cdot \left(P_i - P_w \right)$$

Following the same procedure as the one described above, the average coarse well block pressure P_I, the total well flow rate Q in all the segments connected by this block, and the coarse wellbore segment pressure P_S are derived from the fine resolution. The coarse segment index is hence determined by identification with:

$$T_{SI} = \frac{Q}{P_I - P_S}$$

14.B.5.c Optimum upscaling factor

For pressure or rate transient analysis, numerical models must accurately capture the early time response. The flow regimes occurring in the first minutes of a production or shut-in phase should be reproduced, and the required resolution in time is much finer than for a standard full-field simulation.

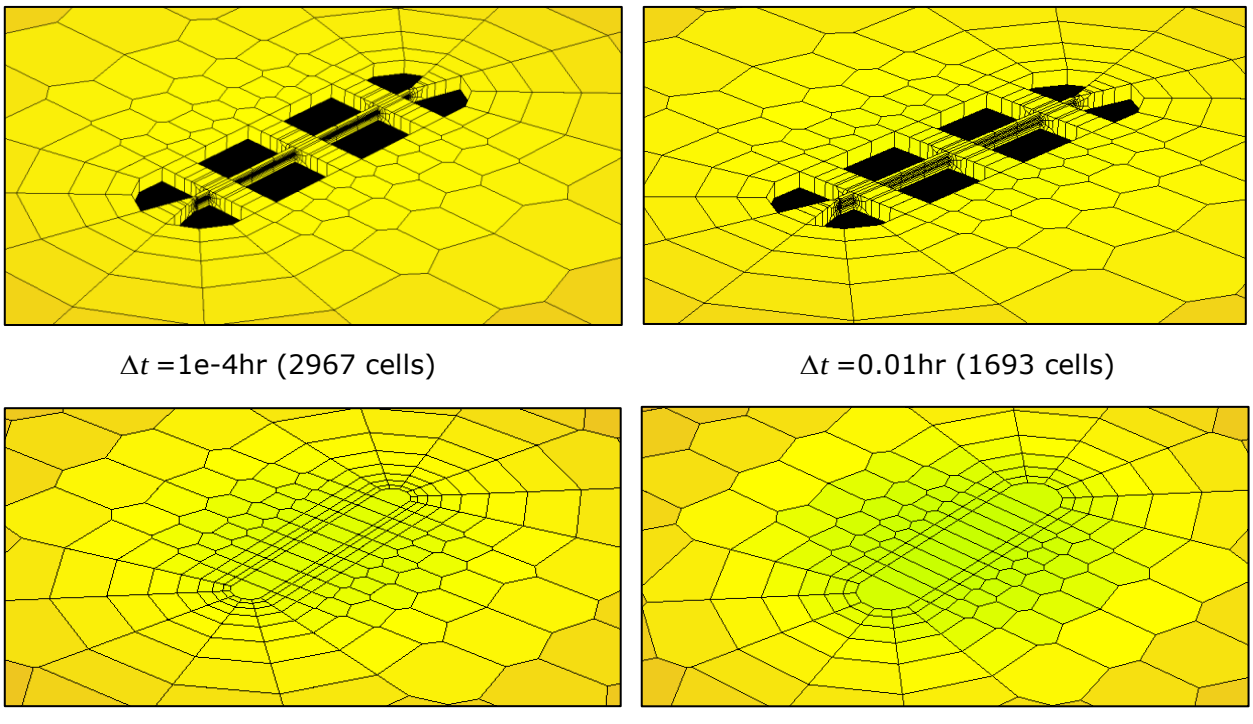
The geometrical resolution of the grid (cell sizes) should automatically be adapted to this time resolution. Note that this resolution is not necessarily the smallest simulation time step. It is related to the time for a given flow regime to develop and be accurately reproduced. One has to determine the optimum resolution required by the grid in order to properly capture the transient effects when needed (i.e.: a buildup analysis in Saphir), while keeping a relatively small number of cells when a lower resolution can be used (i.e.: long term simulation in Rubis).

A simple grid refinement control was developed, which automatically computes the size of the well cells as a simple function of the 'investigation' radius *r* related to the desired time resolution:

$$r = \sqrt{\frac{k}{\phi \cdot \mu \cdot ct} \Delta t}$$

where ϕ and k are the porosity and permeability of the formation, μ is the fluid viscosity and c_t is the total compressibility of the system. In practice, the well cell size is set to half of this investigation radius.

Once the desired resolution time is known, a 3D grid with the corresponding optimum well cell size can be derived. The well index and transmissibility values of this simulation grid are being automatically calibrated from a grid of finer resolution (*u=0*), via the numerical upscaling previously described. This procedure ensures that, beyond the time solution, the same results as for the fine grid are obtained. Earlier transients are naturally being lost.



Δt =1e-4hr (2967 cells) Δt =0.01hr (1693 cells)

Δt =1.0hr (741 cells) Δt =5.0hr (677 cells)

Fig. 14.B.30 – Grid dependence to the time resolution criterion

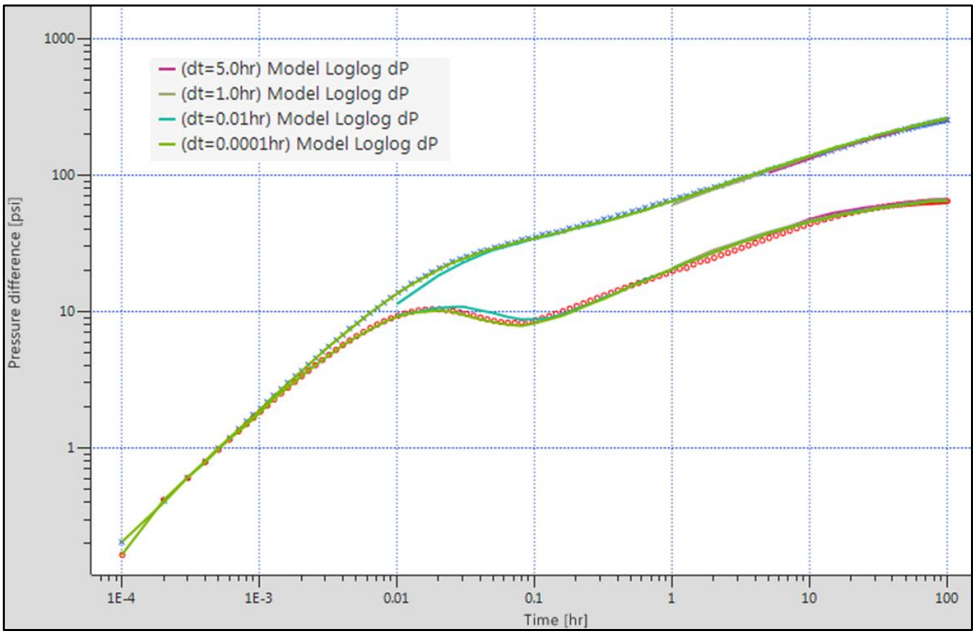


Fig. 14.B.31 –Simulation results for different values of the time resolution criterion

The procedure described above is theoretically only valid in the context of a linear PVT (oil with constant properties). However, it is quite robust and the results remain qualitatively acceptable in the context of real (nonlinear) gas PVT produced with a large pressure drop (i.e.: simulation of unconventional reservoirs).

14.C Formulation

14.C.1 Formulation

The numerical resolution of the partial differential equations ruling fluid flow in reservoirs consists in replacing those equations by difference equations where space and time are discretized. We have seen in the previous paragraphs how space is discretized into grid cells and grid nodes. Time discretization implies that the simulator will not provide a continuous solution (As, say, the cylindrical source solution computed analytically for a vertical well in an infinite reservoir), but will instead provide a discrete series of pressures P at given time steps $\{t_1, \ldots, t_N\}$.

The single phase incompressible flow through a homogeneous porous media is described by Darcy's law and the mass conservation law:

$$\vec{v} = -\frac{k}{\mu}\nabla P$$

$$\frac{\partial(\rho\varphi)}{\partial t} + \nabla\left(\rho\vec{v}\right) = 0$$

where k and φ are the reservoir permeability and porosity. These can be uniform (homogeneous reservoir), or follow a heterogeneous distribution. They can be constant in time or pressure-dependent (ex: rock compressibility, unconsolidation). The fluid properties are the viscosity μ and the density ρ. At any simulation time and location, these can be evaluated via the PVT module, as functions of the local pressure value.

We follow a finite volume, fully implicit discretization approach for the resolution of the above system. Considering the gridding of the reservoir, and a given cell i of reference volume V_i, the mass conservation equation is integrated over the cell volume as:

$$V_i \frac{\partial}{\partial t}(\varphi\rho)_i + \int_{V_i} \nabla \cdot (\rho \cdot \vec{v}) dV = 0$$

Switching from a volume integration to a surface integration over the cell boundary, we obtain:

$$V_i \frac{\partial}{\partial t}(\varphi_i \rho_i) + \int_{\partial V_i} \rho \vec{v} d\vec{S} = 0$$

Let us note J_i, W_i and B_i the sets of cells, wells and reservoir bounds connected to the considered cell i. Discretizing in time between t^n and t^{n+1}, we finally get:

$$V_i \frac{\varphi_i^{n+1}\rho_i^{n+1} - \varphi_i^n \rho_i^n}{\Delta t} + \sum_{j \in J_i, W_i, B_i} q_{ij}^{n+1} = 0$$

The first term corresponds to the accumulation of mass in the cell during the time step (with the corresponding variation of fluid density, ρ_i). The other term is the sum of all the mass fluxes q_{ij} between the considered cell i and its connected neighbor cells, bounds or well segments j. The expression of q_{ij} is detailed in the next paragraph.

In the compositional context, the same approach can be followed, with the mass balance equation now applying to each component *k* of the system. The primary unknowns at any time and location become the pressure *P* and, for each phase *p* and each component *k*, the phase saturation S_p and the phase composition C_p^k. The discretization procedure described above then leads to the following equation for each cell *i* and component *k*:

$$\frac{V_i}{\Delta t}\sum_p\left(\varphi_i^{n+1}S_{p,i}^{n+1}\rho_{p,i}^{n+1}C_{p,i}^{k,n+1}-\varphi_i^{n}S_{p,i}^{n}\rho_{p,i}^{n}C_{p,i}^{k,n}\right)+\sum_{j\in J_i,W_i,B_i}\left(\sum_p q_{p,ij}^{k,n+1}\right)=0$$

Here again, the first term corresponds to the mass accumulation of component *k* in the cell during the time step (with the corresponding variation of phase densities, $\rho_{p,i}$). The other term is the sum of all the mass fluxes $q_{p,ij}^k$ of this component between the considered cell i and its neighbor cells, bounds or well segments j. Note that even when the selected PVT context is Black-Oil (volatile oil) or modified Black-Oil (gas condensate), our internal formulation remains compositional, with a number of hydrocarbon components being reduced to two ("oil" and "gas").

For every phase *p*, the main fluid properties are the viscosity μ_p and the density ρ_p. At any simulation time and any location, they can be evaluated via the PVT module, as functions of the pressure value and global compositions at this particular time and location.

14.C.2 Flux terms

Transmissibility

The flow velocity through a homogeneous porous media is described by Darcy's law:

$$\vec{v}=-\frac{k}{\mu}\nabla P$$

Let us consider two adjacent reservoir cells i and j.

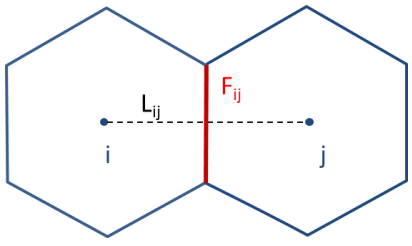


Fig. 14.C.1 – Adjacent cells

The mass flux q_{ij} between these two cells is classically written as a function of the local pressure drop, through the use of a constant "transmissibility" T_{ij}:

$$q_{ij}=\frac{\rho_{ij}}{\mu_{ij}}T_{ij}\left(P_i-P_j\right)$$

where P_i and P_j is the average pressure of each cell, and where fluid properties μ_{ij} and ρ_{ij} are being evaluated at the pressure of the "upstream" cell, i.e. $\mu_{ij}=\mu(P_i)$ if $P_i>P_j$, otherwise $\mu_{ij}=\mu(P_j)$.

When the pressure field between the two cells is assumed to be linear, a relatively simple integration of Darcy's law leads to the classical expression of the transmissibility T_{ij} in terms of the reservoir permeability, the distance between the cell centers L_{ij}, and the contact surface F_{ij}.

$$T_{ij} = \left(\frac{L_i}{k_i S_{ij}} + \frac{L_j}{k_j S_{ij}} \right)^{-1}$$

This expression leads to rigorous results as long as the grid is k-orthogonal and the pressure distribution is locally close to linear. However, when one of these conditions is not valid (ex: in the vicinity of a source term), the transmissibility have to be corrected, as described in the next paragraph 14.C.3.

Note that when the permeability depends on pressure, the transmissibility T_{ij} is not constant anymore, and the flux term needs to be dynamically corrected at every iteration.

Well index

The flux q_{iw} between a cell i and a well w located in this cell follows a similar expression, and is classically written as a function of the local pressure drop via the use of a "well index" T_{wi}:

$$q_{iw} = \frac{1}{\mu_{iw}} T_{wi} \left(P_i - P_w \right)$$

where P_i is the average pressure in the cell and P_w is the pressure of the contacted well segment. When the wellbore is centered in the cell, and when the pressure field can be assumed to follow a radial convergence toward the well, a relatively simple integration of Darcy's law leads to the standard Peaceman's expression of the well index, in terms of the reservoir permeability, the cell geometry, and the well skin. For more complex situations (ex: off-centered, slanted well), a more general expression can be achieved via local analytical solutions, as described in the next paragraph 14.C.3.

The well index is usually constant. But when the permeability depends on pressure, or when the skin changes (time-dependent skin or rate-dependent skin), T_{wi} is not constant anymore, and the flux term needs to be dynamically corrected at every iteration.

Multiphase

In the multiphase, compositional context, the flux of a given phase p is also computed using the same transmissibility and well index values as for the single phase context. However, the expression of the flux must account for relative permeability and capillary effects:

$$q_{p,ij} = \frac{\rho_{p,ij}}{\mu_{p,ij}} T_{ij} \cdot k_r \left(S_{p,ij} \right) \cdot \left[P_i + P_c \left(S_{p,i} \right) - P_j - P_c \left(S_{p,j} \right) \right]$$

As for the single phase context, an upstream scheme is followed to evaluate the fluid properties $\rho_{p,ij}$ and $\mu_{p,ij}$, as well as the relative permeability term. The composition of the upstream cell is also used to evaluate the compositional flux for the considered phase p:

$$q^k_{p,ij} = q_{p,ij} \cdot C^k_{p,ij}$$

The above reasoning is limited to a Darcy flow, the extension of it to non-darcy flow is presented later in the paragraph 14.E.1 Non Darcy flow.

14.C.3 Generalized transmissibility corrections (Saphir–Topaze–Rubis)

This option is actually fulfilling two roles:

(a) It is automatically used in the slanted / complex well gridding scheme context, where it allows to obtain accurate models while keeping the number of cells (relatively) low.

(b) In the particular case of fractures flowing in shales (let them be connected to a vertical well or to a multi-fractured horizontal well), the high transient pressure gradient in the immediate vicinity of the fracture(s) would drive our existing gridding algorithm to its limits. In essence, linear numerical simulations would show irreducible discrepancies with the corresponding analytical models. Those discrepancies are not huge by any means (< 3% in the most extreme situations), but they do exist.

The introduction of generalized transmissibility corrections addresses those two issues. This computation is described at length in a paper posted on KAPPA website (see references), but we will attempt to summarize it in a few sentences.

We have seen previously how the flux between two adjacent cells is classically written as a function of the local pressure drop through the use of a constant transmissibility T_{ij}:

$$q_{ij} = \frac{1}{\mu_{ij}} T_{ij} \left(P_i - P_j \right)$$

The standard expression for T_{ij} given in the previous paragraph is valid as long as the grid is k-orthogonal and the pressure distribution is locally close to linear. The problem is that these assumptions can be proven wrong, such as in the extreme cases mentioned above (vicinity of deviated wells, complex gridding schemes, low permeability in the vicinity of hydraulic fractures…). Then, we have no other means but to rely on some external ways to calculate the overall pressure field, in order to integrate it in space and obtain the desired T_{ij} value:

$$T_{ij} = -k \frac{\iint_{Fij} \nabla P \cdot d\vec{S}}{1/v_i \cdot \iiint_{Ci} P dv - 1/v_j \cdot \iiint_{Cj} P dv}$$

We found that using an analytical pseudo-steady state solution based on Green's function representation is, indeed, providing good calculation results. Here is for instance the analytical potential field calculated around a limited entry slanted well which can be used as a base for the computation of generalized transmissibility's in that case:



Fig. 14.C.2 – Potential field around a limited entry slanted well

Of course, all this comes with a price: a CPU overhead which, even though it does not significantly impact the overall simulation time, is noticeable enough not to use it systematically – read: even in (most) situations where it does not bring any additional added value.

In KAPPA Workstation, the generalized transmissibility corrections are systematically used whenever a slanted / complex well is simulated. They are also available as an option as soon as a fractured well (or multi-fractured horizontal well) is being simulated. You may access this option in the numerical run settings dialogs.

14.C.4 Solvers

Nonlinear and linear solvers

Let us assume that we know the pressure distribution [P^n], and let us recall the discretized material balance equation in the cell *i* over the time interval $\left[t^n, t^{n+1}\right]$, obtained above:

$$e_i^{n+1} = V_i \frac{\varphi_i^{n+1}\rho_i^{n+1} - \varphi_i^n \rho_i^n}{\Delta t} + \sum_{j \in J_i, W_i, B_i} q_{ij}^{n+1}$$

The unknown of our problem is the vector [P^{n+1}] describing the new pressure distribution in all the cells at t^{n+1}. Ideally, when the exact pressure field [P^{n+1}] is found, the corresponding residual e_i^{n+1} becomes equal to zero for every cell.

The above system $F(P) = 0$ is usually non-linear, because the components in the e_i^{n+1} term depend on pressure. We have no other choice but to iteratively linearize this system within a non-linear root finding algorithm - the "non-linear solver". The iterative Newton-Raphson method is broadly used in this situation. In this approach, a linearized approximation of the solution for each non-linear iteration is written $F^{l+1} = F^l + J.\Delta P$, where $J = \left[\frac{\partial F}{\partial P}\right]$ is the Jacobian matrix, and $\Delta P = \left(P^{l+1} - P^l\right)$. For every nonlinear iteration, a linearized system

$P^{l+1} = P^l - J^{-1}.F^l$ is then solved, using a classical "linear solver", and the pressure vector is updated. A few options are available for the linear solver, as described further below.

At each time step, the Newton-Raphson algorithm iterates (hence updates the pressure vector) several times, until an acceptable minimum of the residuals is obtained. In this process, we see that the number of nonlinear iterations (hence the CPU time) clearly depends on the precision sought. In other words, the average number of nonlinear iterations per time step increases when the input "nonlinear solver residual" criterion is decreased for higher precision.

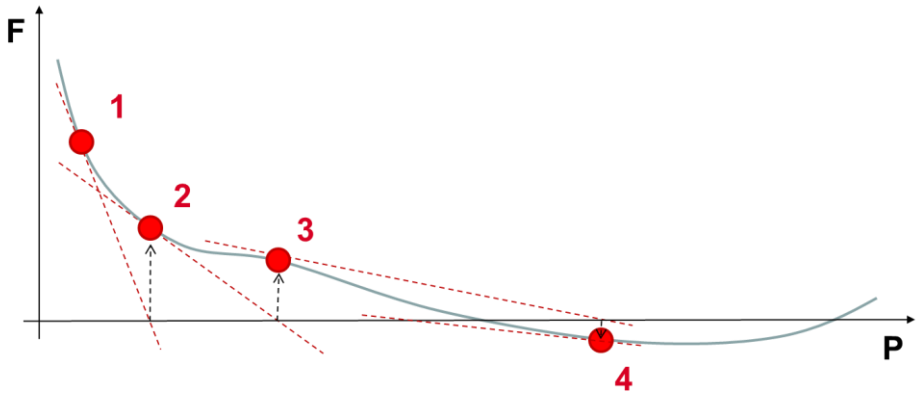


Fig. 14.C.3 – Illustration of the Newton-Raphson iterative procedure

When the number of non-linear iterations reaches an (input) maximum value and the residuals are still too high, the current Newton-Raphson procedure is abandoned, and the process is repeated with a smaller time step size.

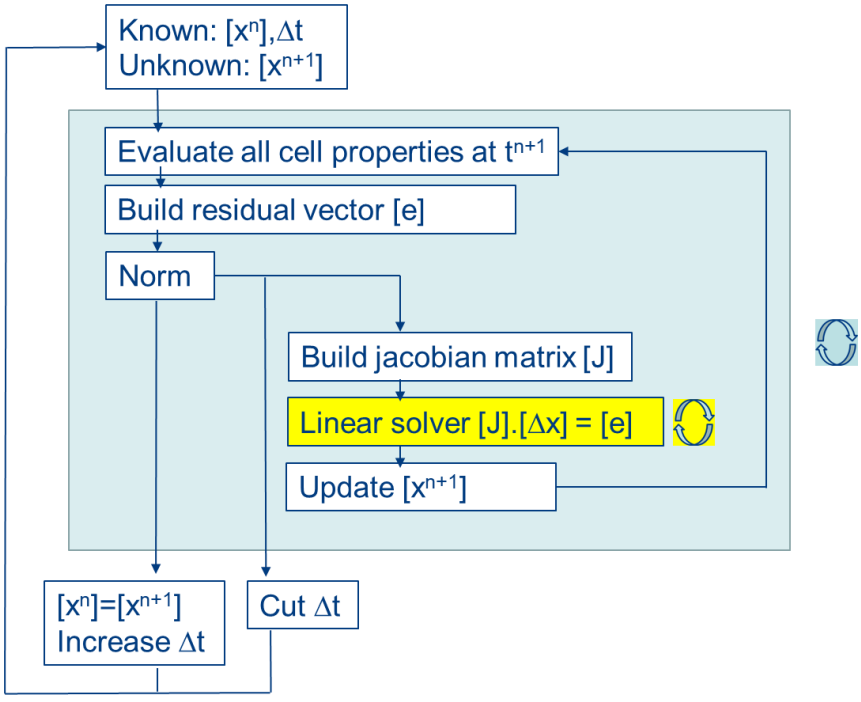


Fig. 14.C.4 – Nonlinear solver

The description above is for a single phase case, so the vector [P] representing the pressure in all the cells is the sole unknown. In the compositional context, this is generalized to a vector [X] also implying the compositions. The size N of this vector [X] is then proportional to the number of components, multiplied by the number of cells. The size of the corresponding Jacobian [J] is then (NxN). We see that the size of the linear system to be solved for each iteration of the non-linear solver (i.e. multiple times for each simulation time step) then increases very quickly with the complexity of the problem to be solved – hence the associated CPU cost.

Linear solvers library

We have seen above that every iteration of the nonlinear solver is associated to the resolution of a linearized system, $\boldsymbol{P}^{l+1} = \boldsymbol{P}^{l} - \boldsymbol{J}^{-1}.\boldsymbol{F}^{l}$, via the use of a "linear solver" (Fig. 14.C.4). Since this happens for every nonlinear iteration of every time step, we see that the total number of calls to the linear solver during a whole simulation can be eventually be very large. The total time spent in this procedure can then quickly become predominant when the number of cells and/or components increase.

Several iterative solver methods (BiCGStab, GMRES, SAMG), coupled with various matrix pre-conditioners (ILU, SSOR, etc…) are available to solve the linear system, in serial and parallel versions.

The default solver in KAPPA workstation is a serial version of BiCGStab, which is the optimum choice as long as the size of system remains relatively small (moderate number of cells, a few components). Parallel versions of the linear solvers can be chosen, in which case the operations will be distributed over several threads working in parallel. However, the corresponding speedup is balanced by the cost of this distribution, so the effective speedup is not directly proportional to the selected number of threads. In practice, the advantage of using a parallel version becomes noticeable only for very large systems (ex: compositional simulations, DFN cases…). SAMG seems to be performing particularly well for large systems with high heterogeneity (typically DFN cases).

Linear cases

In the specific context when these reservoir (k, ϕ) and fluid (μ, ρ) parameters are independent on pressure and constant in time, the problem becomes linear.

The nonlinear iterative procedure described above (Fig. 14.C.4) is not needed anymore and is replaced by a single call to the linear solver. This simplification reduces quite considerably the complexity and CPU time needed to numerically solve a given problem, bringing it closer to the resolution speed of analytical models.

References: https://www.kappaeng.com/papers

Transmissibility Corrections and Grid Control for Shale Gas Numerical Simulation Vincent Artus (KAPPA) ; Dorian Fructus (KAPPA)

14.D Handling Linear Problems

14.D.1 A 'super-analytical model'

When solving linear diffusion problems, we may consider the numerical simulator as a super type-curve generator.

One typical application of this is numerical solutions for gas flow in which pressure dependence of the gas properties is, in part, handled by the classical pseudo-pressures. In which case the numerical simulator is solving its system of equations for m(P), instead of P. This approach allows us to easily obtain solutions that would be out of reach to analytical solutions (the two figures below). Even more important, in some situations the numerical (linear) simulator provides a solution faster than analytical solutions on equivalent geometries, considering its simplicity and the somewhat complex form that the later can take.

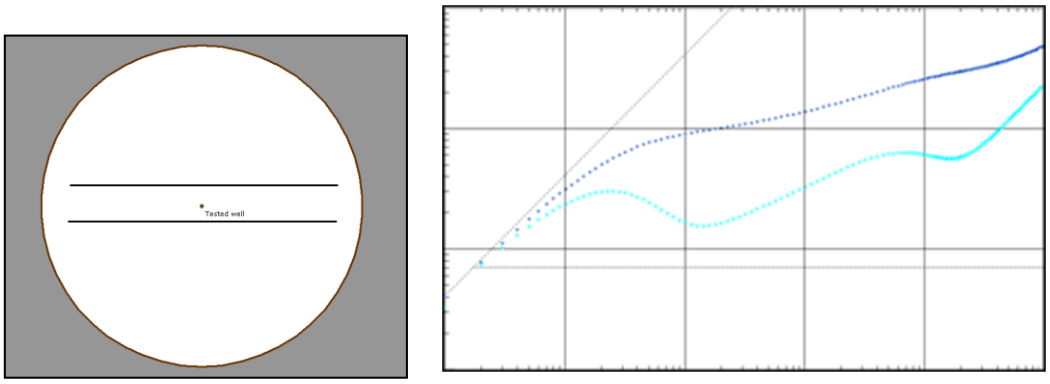


Fig. 14.D.1 – Circular reservoir with two parallel faults, and its corresponding numerical type curve. One can see the transition from linear flow, due to the faults, to pseudo-steady state flow that is due to the circular boundary.

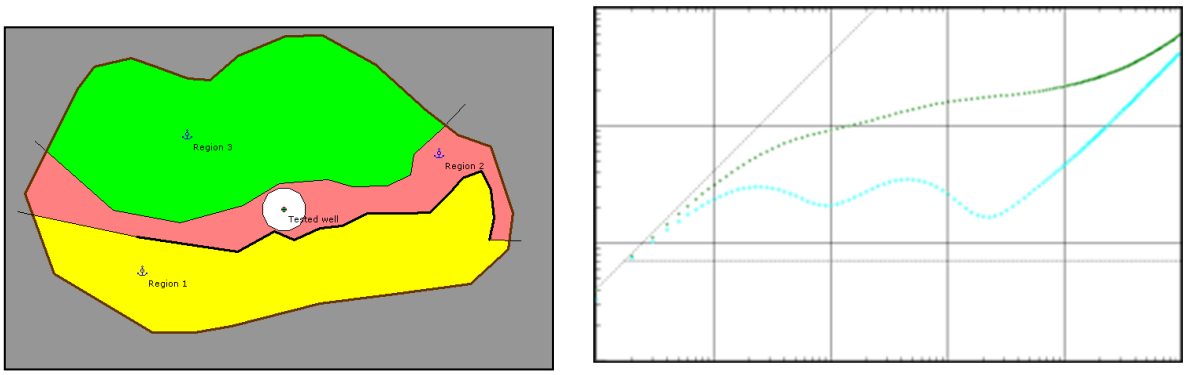


Fig. 14.D.2 – Complex composite reservoir (3 zones)

Naturally, in this application the solution obtained numerically is based on the usual assumptions and limitations for analytical solutions: single phase flow of a slightly compressible fluid, constant rock properties, etc. Hence it will lead to the same approximations and possibly the same errors:

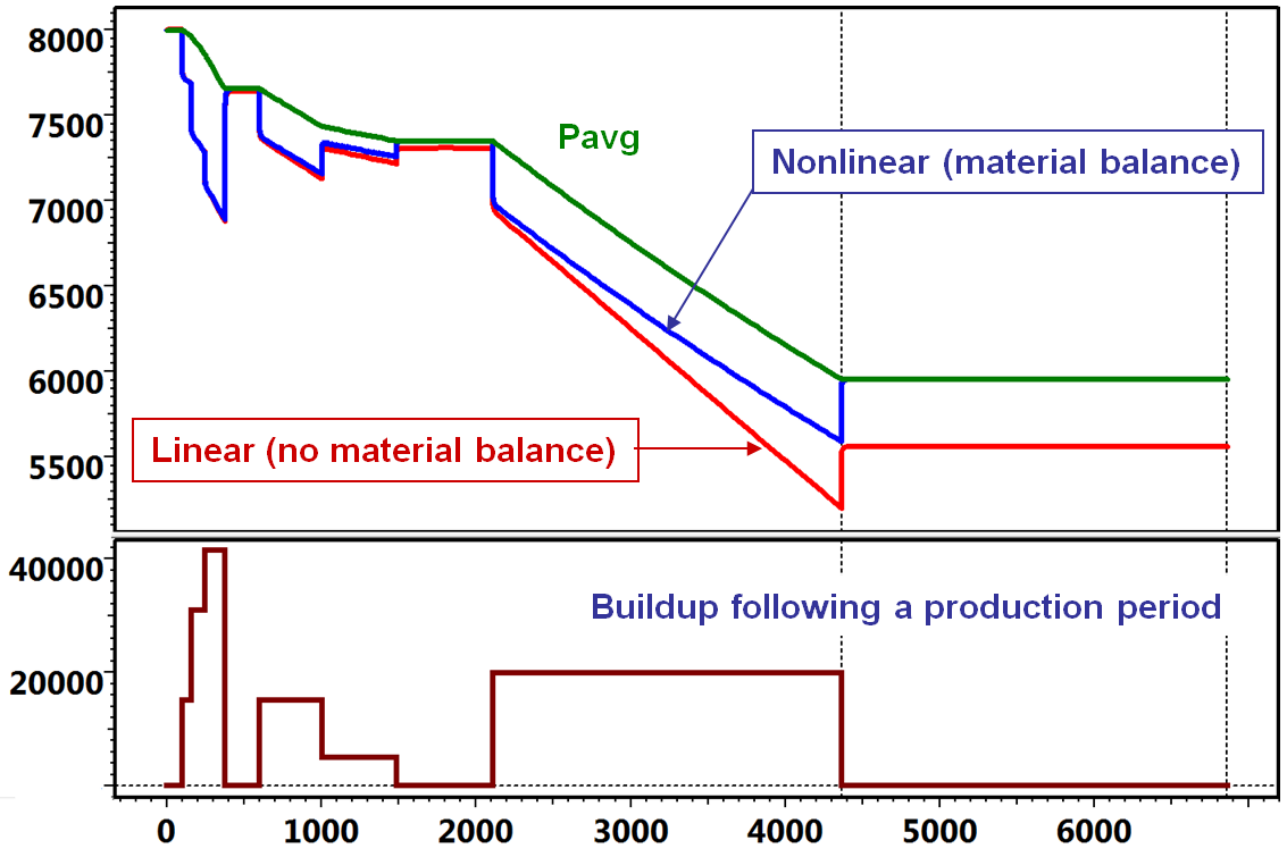


Fig. 14.D.3 – Buildup following a production period. Both solutions are numerical, but the linear curve (in red) does not take gas material balance into account, whereas the full nonlinear solution (in blue) does so: it is in agreement with the average pressure (in green).

14.D.2 Modeling composite zones

Linear numerical models are not limited to the treatment of complex boundaries and faults. It is possible to define regions of enhanced or reduced mobility and/or storativity without a penalty in CPU time, since in any case the simulator computes transmissivities at every grid node. Hence it is possible to reproduce analytical solutions for composite systems (see below) – and to compute some solutions on composite systems that are not so easy to obtain analytically (2nd figure below).

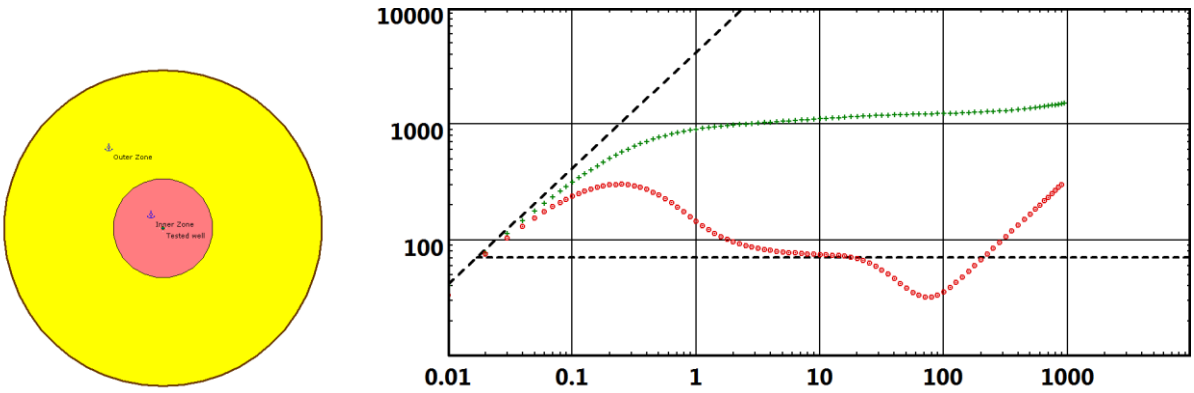


Fig. 14.D.4 – Numerical solution for a radial composite system in a closed circular reservoir. The outer zone (in yellow) presents a higher mobility.

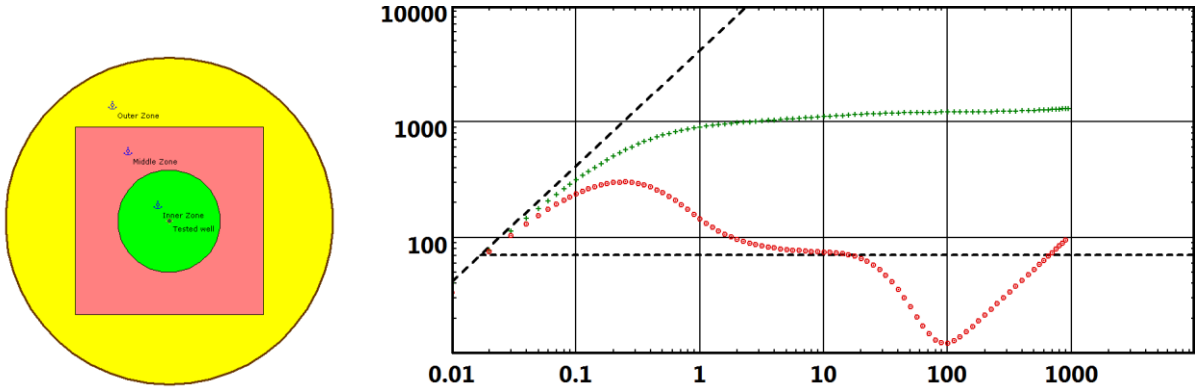


Fig. 14.D.5 – There is now one more composite zone, for which there is no simple analytical solution for this (unrealistic) geometry.

Composite zones are particularly useful to model a transition between fluids such as water around an injector. But from the simulator point of view it is just a matter of different rock properties assigned to the grid cells.

14.D.3 Using field data

It is of course possible to go one step beyond and to define specific rock properties for each cell. For instance it may be possible to make a numerical simulation based on permeability and porosity maps, as shown below.

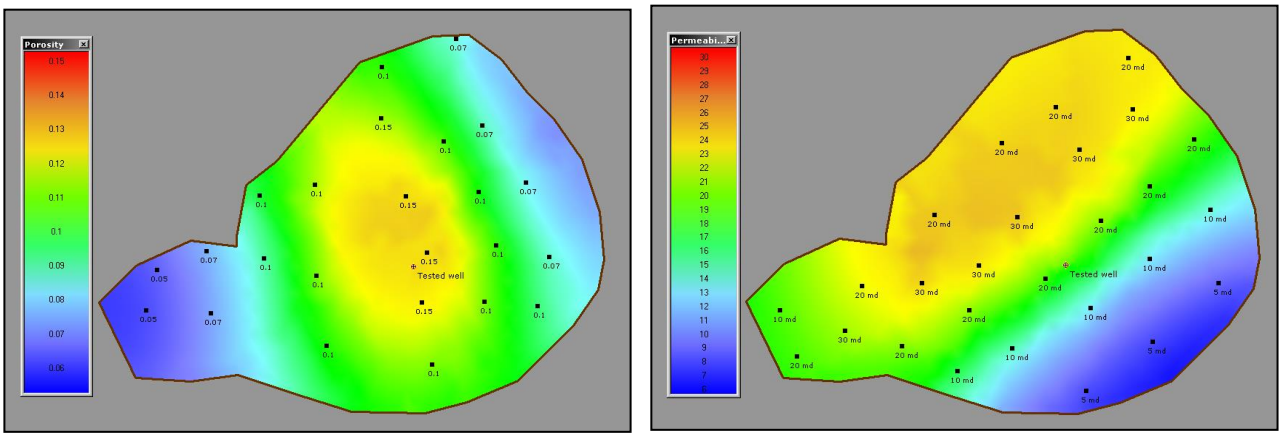


Fig. 14.D.6 – Interpolated porosity (left) and permeability (right), and the point data used to generate their corresponding maps.

The representation of petrophysical properties displayed in the above figure is the final result of a two-dimensional interpolation of input data which are represented by the black data points.

Three interpolation algorithms are available in KAPPA-Workstation:

- Inverse distance weighting, where the power parameter n (typically, n=2) is the power to which each distance is elevated in the weighting process. The smaller n, the smoother the final interpolated surface.
- Linear interpolation, where the surface is assumed to be linear by parts. In this case the interpolation is performed on the Delaunay triangulation.
- Kriging, where the interpolated surface is obtained from a variogram (inverted covariance) fit on the data points.

The three options along with their leading parameters permit a wide spectrum of possible interpolation results, illustrated here:

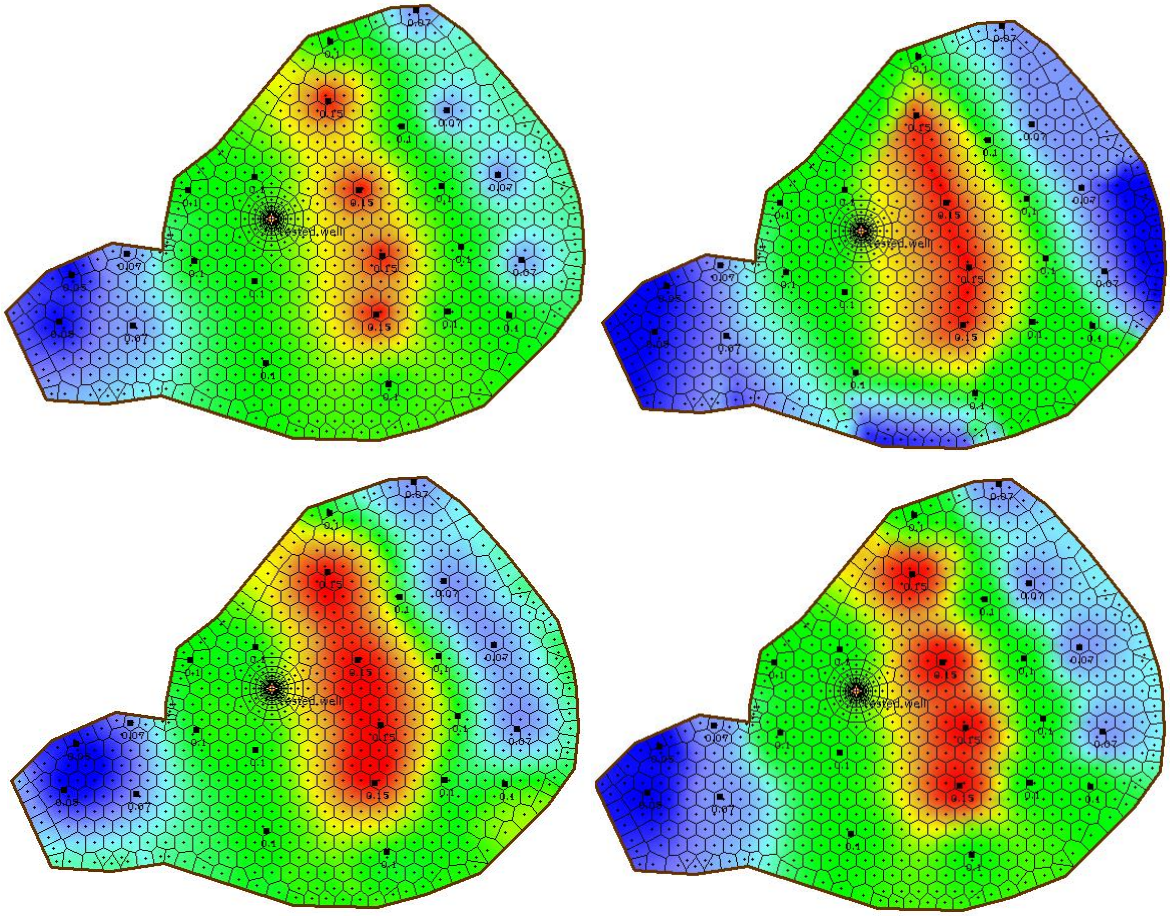


Fig. 14.D.7 – Four different interpolated fields obtained from the same input (porosity) data. From top-left to bottom-right: inverse distance weighting (n=2), linear interpolation, kriging with a range of 1500 ft, kriging with a smaller range of 750 ft.

The data subject to interpolation may be classified into two categories: the data that affects the reservoir geometry such as horizons and thickness. And the data describing the fluid and rock properties. Concerning the reservoir geometry, only the layer thickness presents a significant importance in well test analysis, since gravity effects are usually neglected. With the fluid and rock properties, the main data of interest are usually porosity and permeability. The interpolated fields for the two last parameters are radically different in one respect: the average reservoir porosity can be easily calculated from the interpolated field values, however there exists no rigorous approach to compute the average permeability equivalent to a permeability field such as the one shown in the figure below.

In fact, the best approximation consists in evaluating the effective average permeability as a result of the numerical simulation. In such a case the pressure match line on the loglog plot is no longer an input but a simulation result. This match line may still be moved up and down if one introduces a 'fudge factor' k/k_{field}, i.e. a global multiplier applied to the entire interpolated permeability field when a simulation is performed.

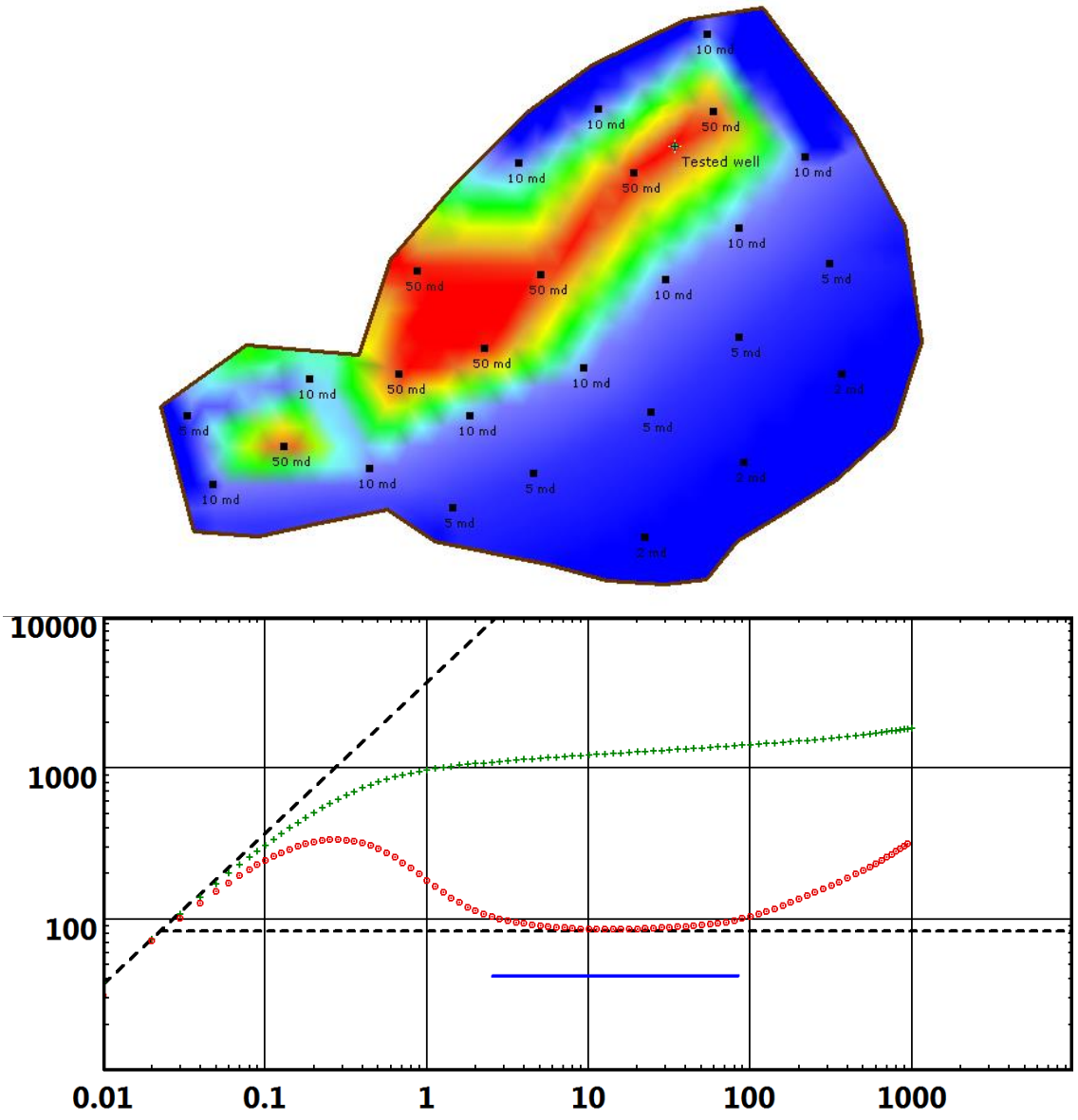


Fig. 14.D.8 – Permeability field and corresponding simulation: although the tested well is in a 50 mD 'channel' (the red zone in top figure), the effective simulation permeability is more than 40% lower (when comparing the pressure match line to the 50 mD blue IARF line).

14.D.4 Double-porosity reservoirs

The numerical model can simulate a double porosity medium by splitting each grid cell into two: the first half represents the fissure and the second the matrix. Each sub-cell will occupy the same geometrical volume and the same location. Hence the gridding is not affected. In the simulation, the pore volume and the transmissivity of each fissure and matrix sub-cell is computed using the model storativity ratio (ω) and interporosity flow parameter (λ). Furthermore, the matrix sub-cell is only connected to its corresponding fissure sub-cell. In other words, the model input permeability k is the fissure permeability.

The reservoir cell characterized by a pore volume *V* and a permeability *k* is split into a fissure sub-cell *f* with a pore volume V_f and a matrix sub-cell *m* with a pore volume V_m. V_f and V_m are computed from the storativity ratio ω:

$$V_f = V.\phi.\omega$$
$$V_m = V.\phi.(1-\omega)$$

Where ϕ is the porosity. The transmissivity T_{fm} between the fissure and the matrix sub-cells is defined using the interporosity flow parameter λ:

$$T_{fm} = k.\lambda.\frac{V}{r^2}$$

Where *r* is a characteristic length of the matrix-fissure interface.

To sum-up, double-porosity reservoirs in numerical models may be described with identical parameters as for analytical solutions. We may use the same basic procedures to graphically estimate ω and λ as in the analytical case, as shown in here:

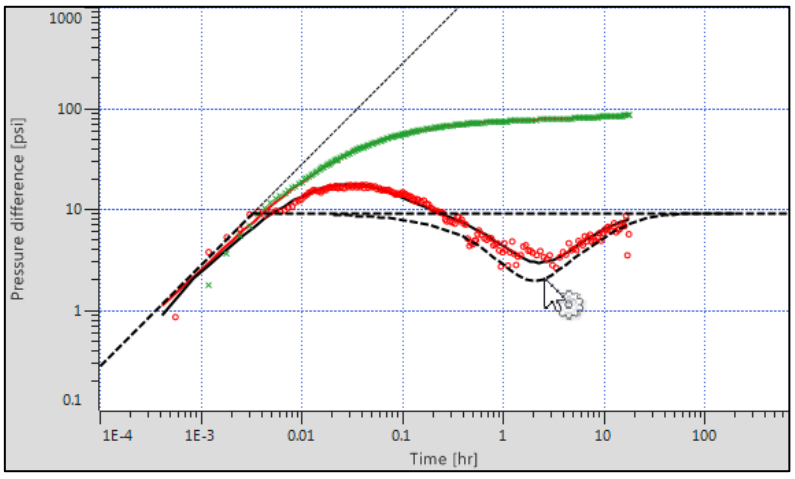


Fig. 14.D.9 – Estimating ω and λ by pick in the definition of a double porosity numerical model.

The numerical simulation of double porosity behavior may be combined with more complex geometries and heterogeneities, hence providing far more flexibility in terms of problem definition than can be found in analytical solutions. It is even possible to consider the combination of different defined double porosity within different composite zones, as shown in here:

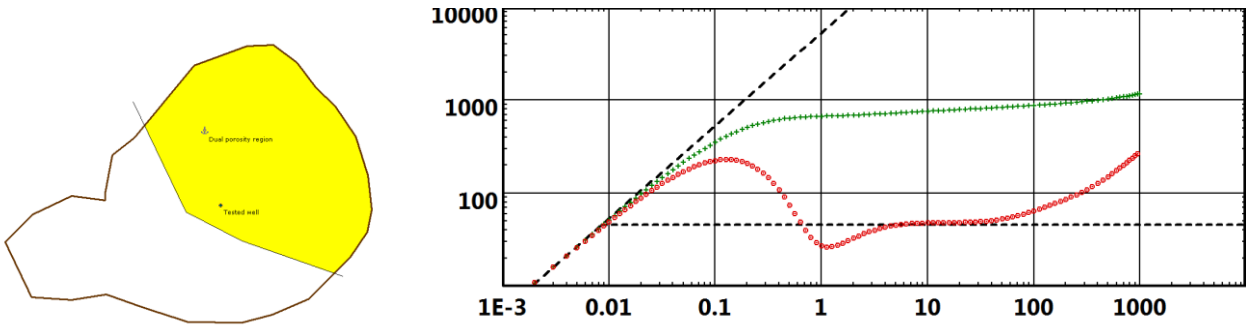


Fig. 14.D.10 – Yellow zone only defined as double porosity.

14.D.5 Modeling permeability anisotropy

When an horizontal permeability anisotropy is defined the Voronoi grid is internally deformed (figure just below). However, the deformed grid is no longer a Voronoi grid, as it does not respect the orthogonal condition between node segments and cell faces. In fact, the problem is solved on an equivalent isotropic grid displayed in the second figure below. Similar situations and grid deformations are encountered in the case of vertical anisotropy and 3D gridding modules.

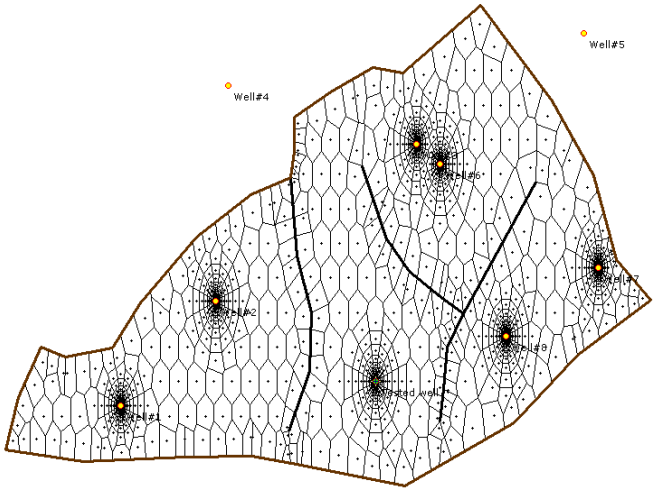


Fig. 14.D.11 – 'Voronoi' grid for an anisotropic reservoir (k_x/k_y=0.2)

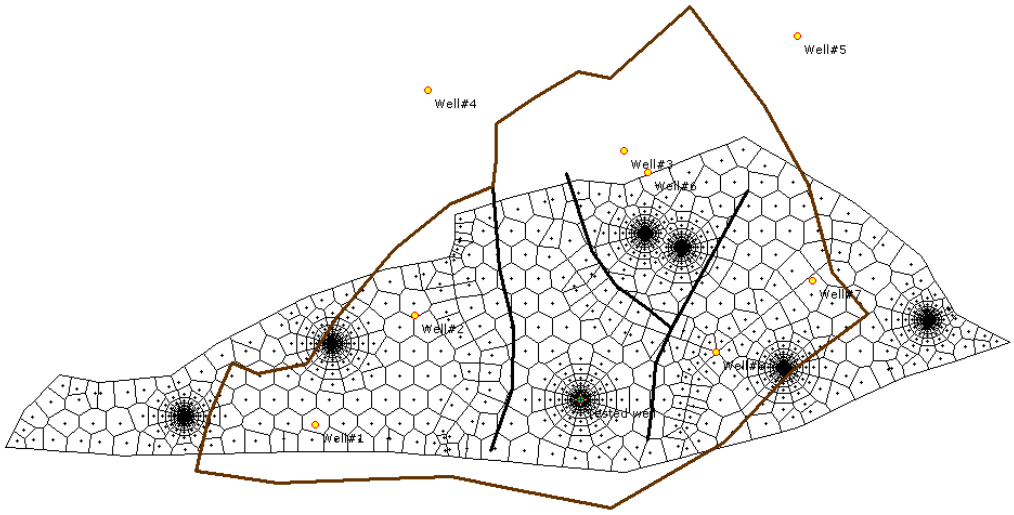


Fig. 14.D.12 – Equivalent Voronoi grid for an anisotropic reservoir (k_x/k_y=0.2)

To sum up, horizontal and vertical anisotropies affect the grid construction phase but the other simulation steps such as the matrix system to be solved, are not affected. This simple treatment is only possible when the anisotropy is constant, that is, when the grid may be entirely deformed using a unique anisotropy tensor.

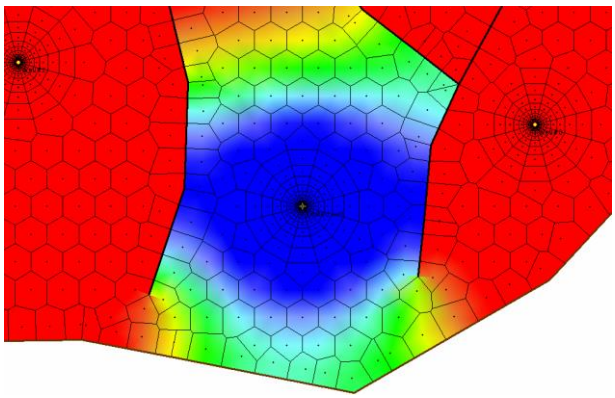


Fig. 14.D.13 – Pressure field around producer, isotropic reservoir

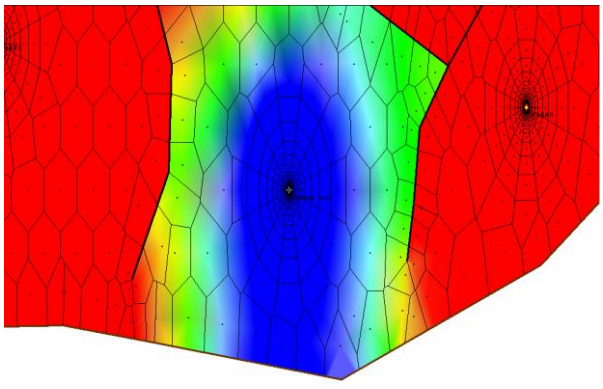


Fig. 14.D.14 – With anisotropy ratio k_x/k_y of 1/5.
Obviously the faults are seen much later than in the isotropic case.

14.D.6 Modeling multi-layer reservoirs (with or without cross-flow)

Extending the numerical model to multi-layer reservoirs can be made in a very simple way if we limit ourselves to vertical wells and if the contour / faults are handled as vertical walls intersecting all layers identically. In this case the 2D single layer grid merely needs to be replicated *n* times for *n* layers, as shown here:

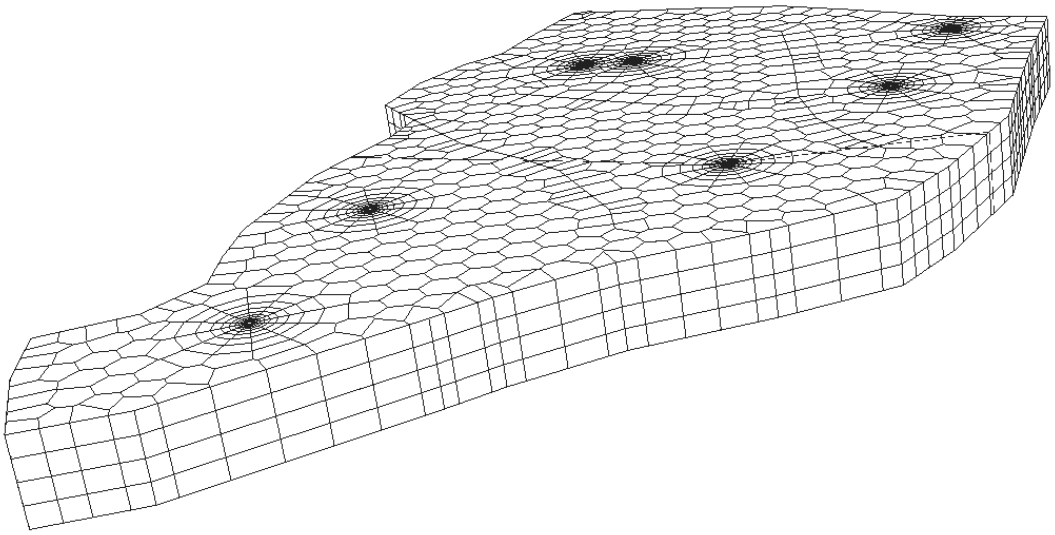


Fig. 14.D.15 – 2D grid piled up to simulate a 4 layer system

The reservoir geometry is somewhat restricted with this configuration: the layers cannot be disconnected and the layer horizons are constant. In fact this limitation is acceptable as long as single phase flow without gravity effects is simulated. Other than that, the layered system may be commingled with no hydraulic communication between layers, or there may be some crossflow between layers, as shown below:

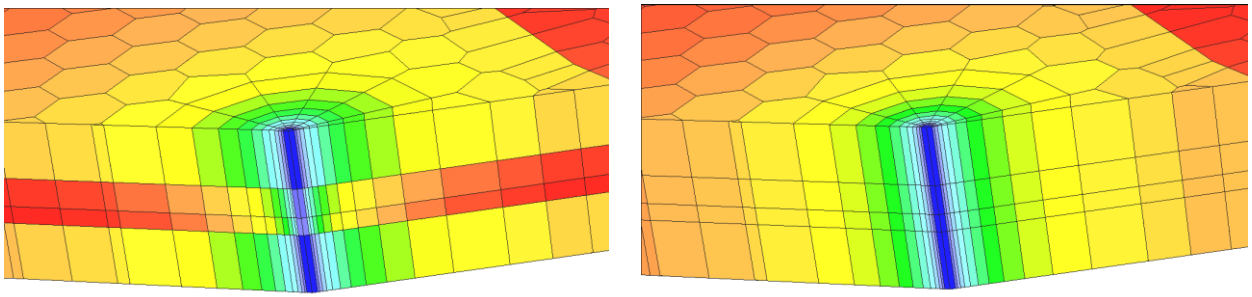


Fig. 14.D.16 – Pressure field around a well producing in a four layer system, without and with vertical crossflow between layers. (left and right respectively). The top and bottom layer have been defined with equal permeability. Middle layers with lower permeability.

Multi-layered systems give more degrees of freedom concerning the well perforations. Instead of perforating the well over the complete reservoir it is possible to open individual perforations of each layer (figure below). Note however, that with the 2 ½ D gridding used the early time spherical flow that should theoretically appear due to the partial completion does not do so, as the specified vertical permeability in the model only applies at the interface between the layers. The layers themselves are isotropic.

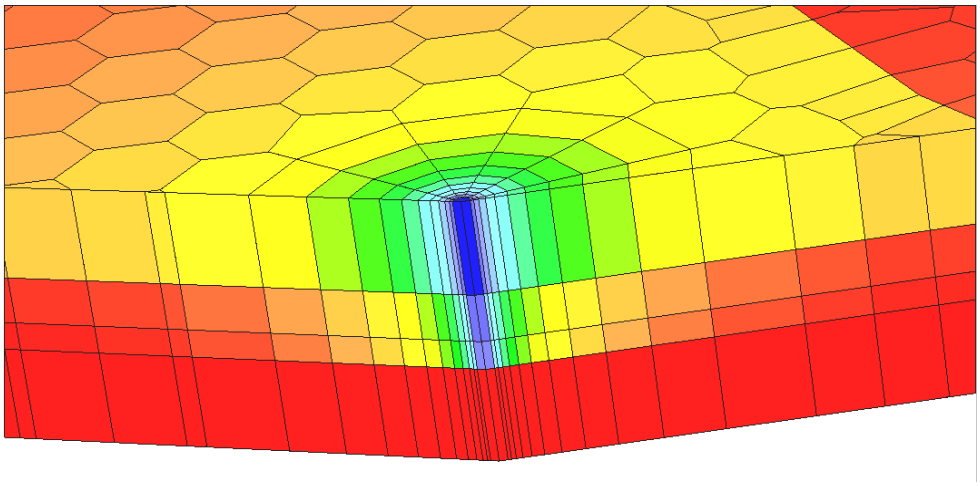


Fig. 14.D.17 – Pressure field around a well producer in a (commingled) four layer system. The bottom layer is not perforated (compare with Fig. 14.D.16).

In multilayer simulations it is also possible to compute and output layer rates at the wellbore, i.e. individual layer, bottom hole, contributions. This output facility is particularly useful in identifying potential crossflow in the wellbore during shut-in periods, as displayed below.

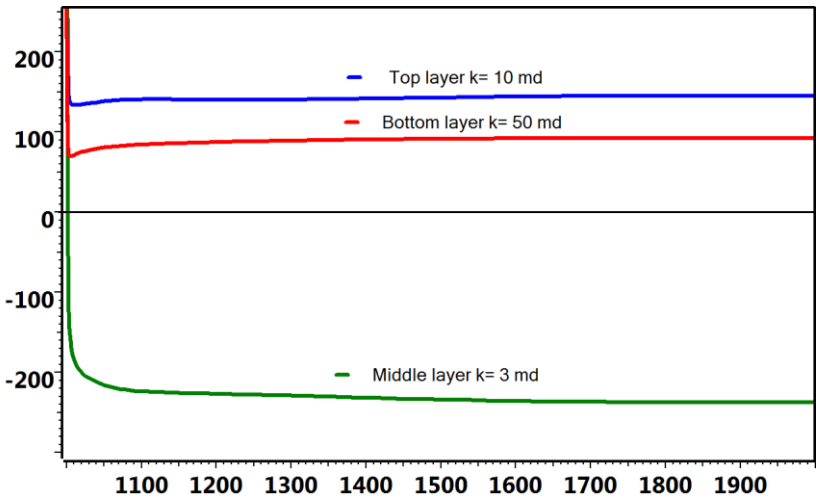


Fig. 14.D.18 – Three layer system, layer contributions simulated at the well during a build-up following a production period. Because the pressure drop is less important in the middle, high permeability, layer at the end of the production, crossflow occurs in the wellbore until the pressure reaches equilibrium.

14.E Handling nonlinear problems

In situations where the pressure, hence time dependency of the reservoir and fluid parameters, can no longer be ignored, the numerical problem to be solved becomes non-linear. We have no other choice but to iteratively linearize this non-linear system within a non-linear root finding algorithm. The Newton-Raphson technique is broadly used in this situation.

If we recall the discretized material balance equation in the cell (i) over the time interval $\Delta t = \left[t^n, t^{n+1}\right]$ obtained in section Handling Linear Problems (Basic):

$$e_i^{n+1} = \sum_{j \in Ji} T_{ij} . \lambda_{ij}^{n+1} \left(P_j^{n+1} - P_i^{n+1}\right) - \frac{V_i}{\Delta t}\left[\left(\frac{\Phi_i}{B_i}\right)^{n+1} - \left(\frac{\Phi_i}{B_i}\right)^{n}\right] - q_i^{n+1}$$

The system $F(P) = 0$ is now non-linear because the components in the e_i^{n+1} term depend on pressure. It can be solved with an iterative Newton-Raphson method, in which a linearized approximation of the solution for the non-linear iteration can be written:

$F^{l+1} = F^l + J.\Delta P$ where $J = \left[\frac{\partial F}{\partial P}\right]$ is the Jacobian matrix and $\Delta P = \left(P^{l+1} - P^l\right)$.

The linearized system $P^{l+1} = P^l - J^{-1}.F^l$ can now be solved for P^{l+1}, using the same techniques as in the linear case.

At each time step, the Newton-Raphson algorithm iterates until an acceptable minimum is obtained. This will happen until the next iteration point gets too close to the current solution. In this process the CPU time clearly depends on the precision sought, as can be seen in the table below.

	Number of linear iterations/time step	Material balance error (%)	CPU ratio
Linearized problem (m(p))	14	--	0.9
Nonlinear, residual=1E-3	14.5	5.0E-12	1
NL, residual=1E-5	15.5	1.8E-12	1
NL, residual=1E-8	30	1.1E-12	3
NL, residual=5E-9	102	1.5E-14	13.4

The above numbers were obtained simulating a single gas well producer in a rectangular, homogeneous reservoir. Various runs were compared; a linear case where the simulator solves a problem made linear after the introduction of pseudo-pressures, and four non-linear cases with increasing restrictions on the non-linear loop convergence criterion (the 'residual'). The non-linear loop introduces only a small overhead in this example because the problem remains only slightly non-linear. More so because the dependency of the gas PVT on the pressure variable remains relatively smooth. It will be shown in the sections below that the additional CPU time can be far more important when strong non-linearities are introduced. It can also be demonstrated that forcing the convergence criterion to very small values is particularly useless. The only effect being to make the CPU time explode, for a slight gain in precision before reaching the limit of the machine.

14.E.1 Non-Darcy flow

See also section of dry gas considerations for PTA.

Darcy's equation is only valid for laminar flow but in some situations fluid flow in the reservoir can become turbulent. For example, in a reservoir in the vicinity of high rate gas producers. In fluid mechanics the transition from laminar to turbulent flow is characterized by the Reynolds number Re:

$$\mathrm{Re} = \frac{\rho v L}{\mu} = \frac{Inertial\ forces}{Viscous\ forces}$$

Laminar flow occurs at low Reynolds numbers (Re<2000-3000), in which case fluid flow is a constant and smooth fluid motion. When inertial forces (Re>4000) dominate fluid flow becomes turbulent, producing random vortices and other fluctuations.

Because turbulence usually occurs in the vicinity of the wells a classical way to handle this involves introducing a pseudo-skin parameter D so that the total skin S' becomes: $S' = S_0 + Dq$, where q is the well flowrate. This simplified approach can of course be used as-is in numerical simulations. However numerical simulation makes it possible to incorporate the non-Darcy flow effects at an upper level, through the introduction of the Forchheimer factor β in a generalized Darcy's equation.

The classical Darcy's law:

$$-\nabla P = \frac{\mu}{k} \cdot \vec{u}$$

is replaced by its generalized form:

$$-\nabla P = \frac{\mu}{k} \cdot \vec{u} + \beta \cdot \rho \cdot \left|\vec{u}\right| \cdot \vec{u}$$

In which β is the Forchheimer factor. β has the dimension L^{-1}, that is m^{-1} in SI system. If we introduce the notions of Darcy velocity u^D (grossly speaking, the velocity given by laminar flow) and non-Darcy velocity u, we can obtain the following relationship:

$$u = f^{ND} u^D \qquad \text{with} \qquad f^{ND} = \frac{2}{1 + \sqrt{1 + 4 \cdot \beta \cdot k \cdot \lambda \cdot u^D}}$$

Where k is the permeability, and $\lambda = \rho/\mu$ is the inverse of the kinematic fluid viscosity.

In fact it can be shown that both approaches (pseudo-skin and Forchheimer factor) are equivalent when the kinematic fluid viscosity (μ/ρ) is held constant. In practice, both approaches provide results that are comparable:

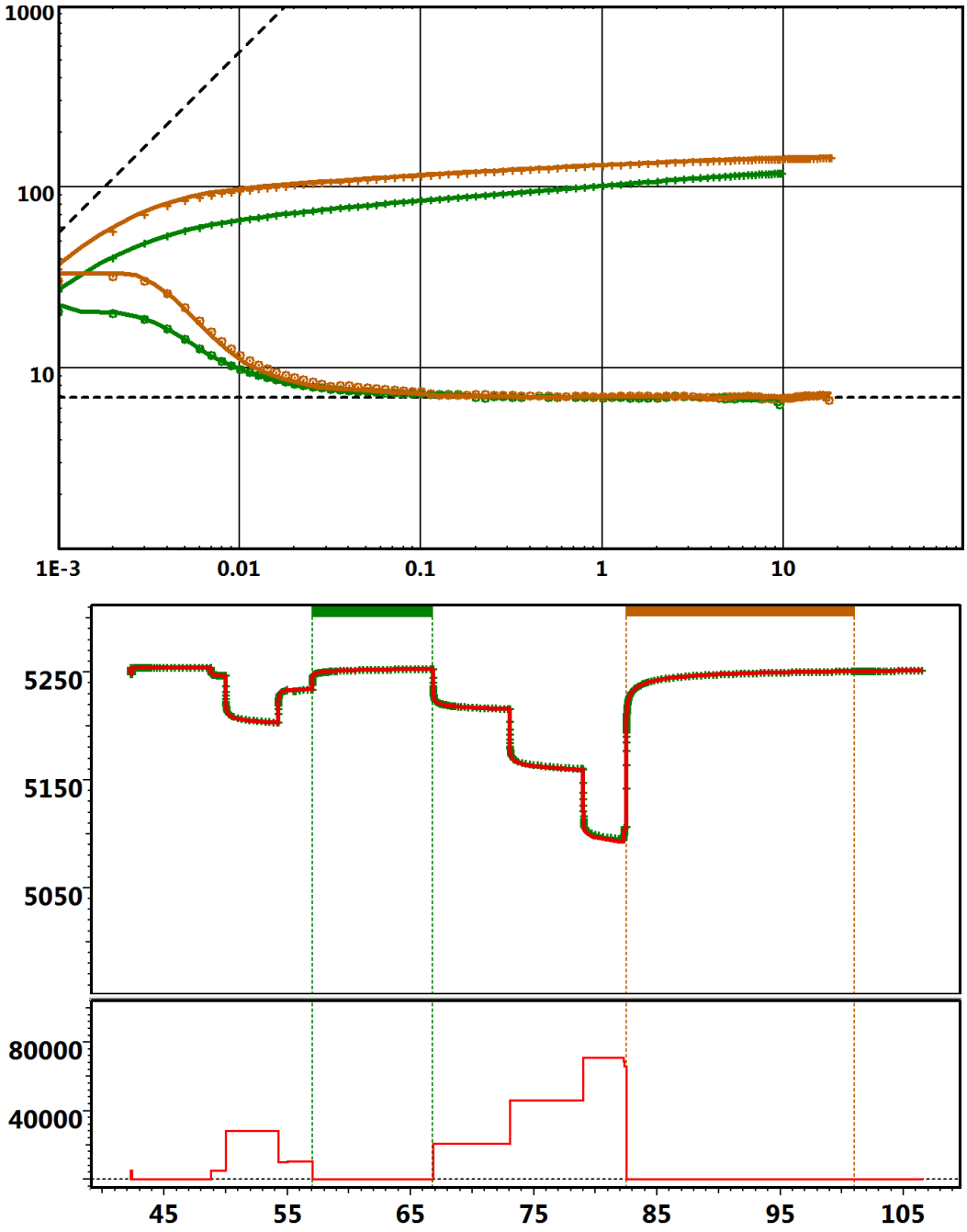


Fig. 14.E.1 – Non-Darcy flow around a gas producer, successive buildups following constant, and increasing, rate production periods. The crosses and dots are simulated using the Forchheimer equation, whereas the plain curve is obtained using an equivalent pseudo-skin factor D.

However there are situations in which the pseudo-skin factor D leads to a somewhat incomplete modeling of the problem and it is better to replace this by the generalized Darcy equation.

14.E.2 Flow with Water and Hydrocarbons (Oil OR Gas)

The numerical simulator is not limited to single phase flow. We will consider dead oil + water and dry gas + water, situations without phase exchange between the components, no dissolved gas in the oil phase, no vaporized oil in the gas phase. Capillary pressures are neglected.

In that case relative permeabilities must be introduced and total mobility becomes:

$$\left(\frac{k}{\mu}\right)_t = \left(\frac{k_p}{\mu_p}\right) + \left(\frac{k_w}{\mu_w}\right) = k.\left(\frac{k_{rp}(S_w)}{\mu_p} + \frac{k_{rw}(S_w)}{\mu_w}\right)$$

Where *p* refers to oil or gas and S_w is the water saturation. Contrary to the assumptions that have to be made in analytical methods (Perrine), the water saturation is not held constant in time or in space. Relative permeability curves define regions of phase mobility, as shown in the figure below.

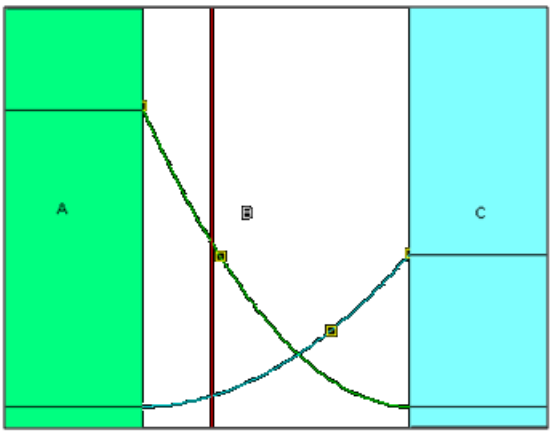


Fig. 14.E.2 – oil (green) and water (blue) relative permeability curves. In the saturation region (A) water is not mobile and maximum oil relative permeability is reached. In region (C) oil is not mobile.

Hence, the stabilization of the derivative on the loglog plot depends not only on the bulk permeability, but also on the dynamic phase mobilities induced by the distribution of fluid saturations.

Let us consider the example of a water injector in an oil reservoir (following figure):

- During the injection phase the pressure match line is based on the total mobility with maximum water saturation since we inject only water.
- The fall-off however sees different effective permeabilities induced by varying water saturation. This is at a maximum close to the well and a minimum further away in the reservoir.
- The effective two-phase mobility can take values in the range of 'minimum water saturation (the green line)' and 'maximum water saturation (the blue line)'.

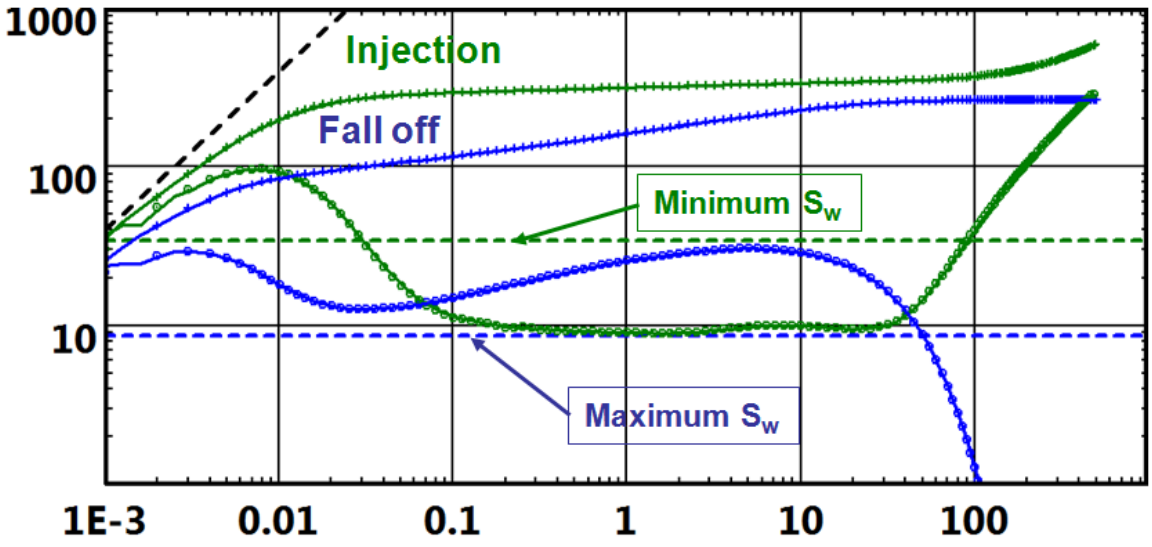


Fig. 14.E.3 - Fall-off following a water injection in an oil reservoir

14.E.3 Unconsolidated formations

In unconsolidated formations porosity and permeability depend on the internal stress of the formation. When there is no overburden isostatic pressure, this stress is directly related to the difference between external and internal fluid pressure, so we may model porosity and permeability as decreasing functions of the pressure drop (P_i-P) occurring in the reservoir. That is the porosity and permeability decrease as the reservoir deplete:

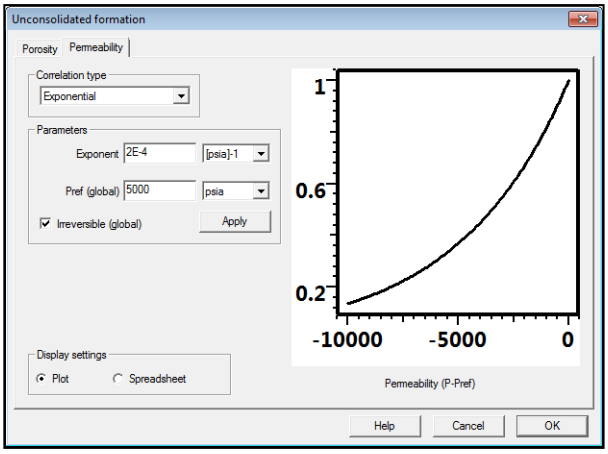


Fig. 14.E.4 – Defining the k(P-P_i) function for an unconsolidated formation

In an isotropic, linear, elastic reservoir we model the rock deformation through a relationship between porosity, permeability and the average internal stress σ_m:

$$\phi = \phi_0.(1 - a\sigma_m)$$

$$k = \begin{cases} k_0.(1 - b\sigma_m) & (1) \\ k_0.\exp(-b\sigma_m) & (2) \\ k_0.\left(\frac{\phi}{\phi_0}\right)^n & (3) \end{cases}$$

Where k is defined by the equation (1), (2) or (3) depending on the rock type. In the absence of overburden isostatic pressure, we introduce the following relationship between σ_m and the pressure drop P_i-P:

$$\sigma_m \equiv \frac{1}{3}(\sigma_x + \sigma_y + \sigma_z) = (P_i - P)$$

Hence, k and ϕ are directly related to the pressure drop P_i-P.

Porosity and permeability reduction may or may not be irreversible, in the sense that the model can authorize (or not) the model parameter to recover its initial value when the pressure drop decreases (see figures below). The effective permeability is lower here during the two production phases (blue and red), and reverting to its initial value during the build-ups, as the model permeability is reversible.

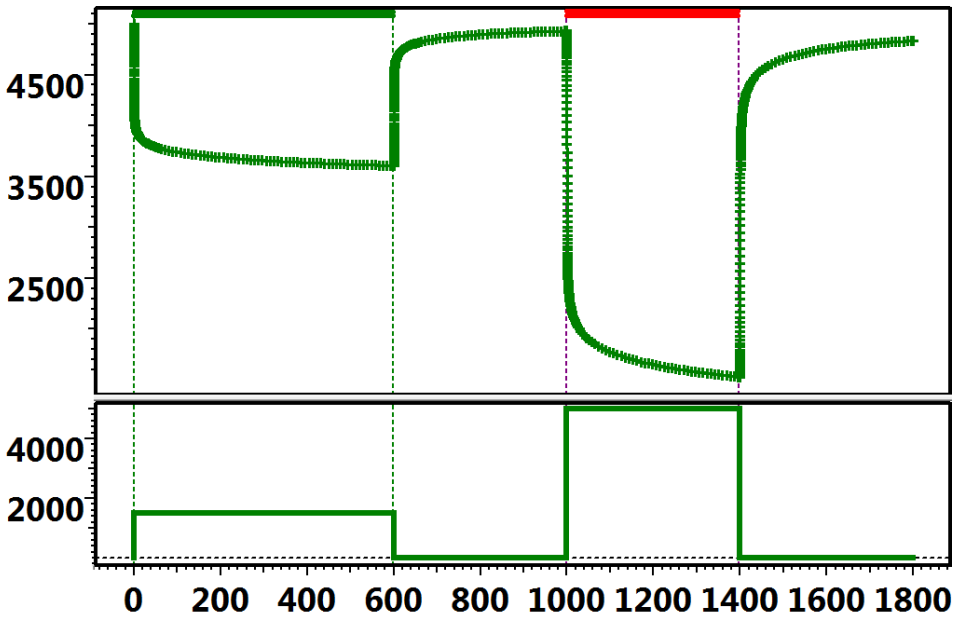


Fig. 14.E.5 – Simulation of two production and build-up sequences in an unconsolidated reservoir: History plot

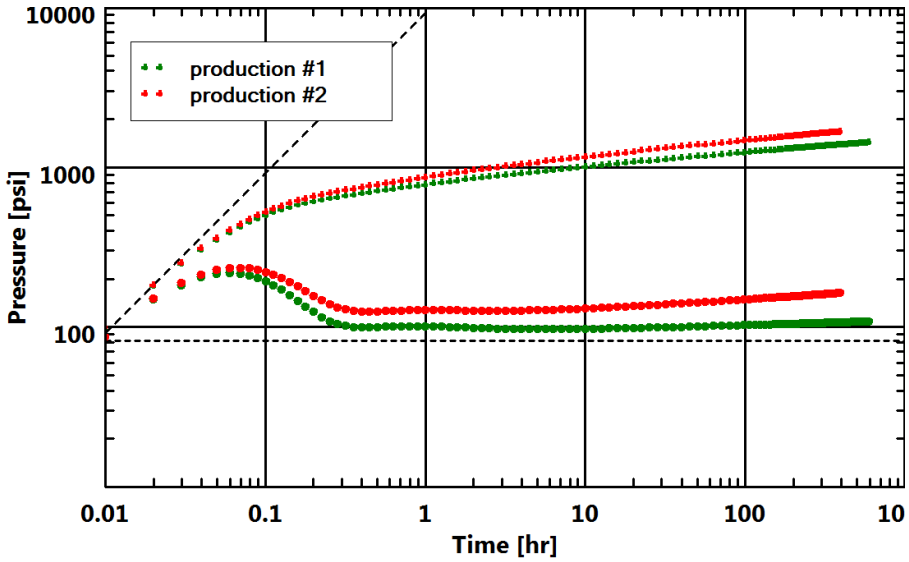


Fig. 14.E.6 – Simulation of two production and build-up sequences in an unconsolidated reservoir: Loglog plot

Introducing pressure dependency on porosity and permeability renders the problem highly nonlinear. This makes it awkward to use and to interpret considering the difficulty in gathering valid data to build the $\phi(\Delta P)$ and $k(\Delta P)$ curves, and the strong dependency of the simulated pressure to these curves. A 5% error on $k(\Delta P)$ can easily induce a 50% error on the simulated pressure.

14.E.4 How about three-phase flow?

Numerical simulation applied to well test analysis is almost identical to 'classical' reservoir simulators, except that the models have to be simulated on a much smaller time-scale that is minutes and seconds instead of days. They also have to be viewed on a loglog plot; to be examined through the Bourdet derivative 'magnifying glass'.

With the simulation of three-phase flow problems we reach the limits of our current capabilities in terms of numerical well test modeling. The ruling equations and the solution methodologies are well known and in essence three-phase flow is merely an extension of the dead oil and water or dry gas and water problems we have already described. Unfortunately one unexpected problem arises, as can be seen in the figure below.

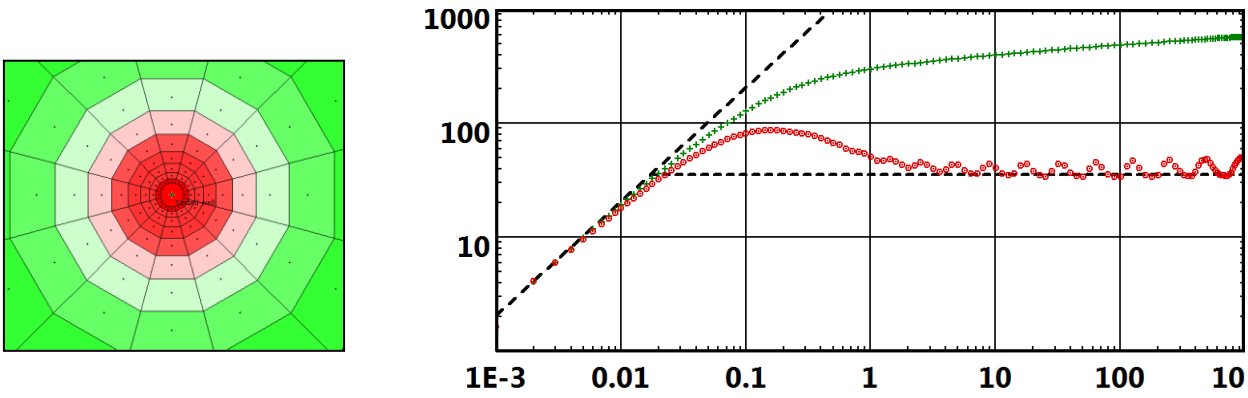


Fig. 14.E.7 – Simulation of a producer in a saturated oil reservoir: left: the gas saturation at the end of the production, right: the resulting simulation on a loglog plot.

In the illustrated example, the erratic behavior of the semilog derivative is due to the successive appearance of free gas, cell ring by cell ring, around the well as the depletion occurs and the cell pressure drops below the fluid bubble point.

This appearance is not controlled by the relative permeabilities (free gas can appear before it reaches a saturation high enough to be mobile) but by thermodynamic equilibrium. Successive cell rings can be flooded by free gas within a few time steps, hence changing considerably the effective permeability, and thence inducing the erratic behavior on the loglog plot.

Unfortunately, changing the grid cell size is not sufficient to get rid of the problems. This just changes the frequency of the humps and bumps on the loglog plot.

14.E.5 Thermal modelling

The specific case where the thermal effects are taken into account is developed in detail in the chapter 18 - Thermal Analysis and Simulation.

14.F Numerical settings

14.F.1 Changing well controls

With numerical modeling combining constant rate and constant pressure well controls becomes relatively straightforward. It is possible to impose a pressure constraint in addition to the rate target. This constraint takes the form of a pressure interval within which the simulated well sandface pressure must remain, as shown in the figure below. The pressure interval lower limit may be reached by producing wells, whereas the upper limit may be reached by injectors.

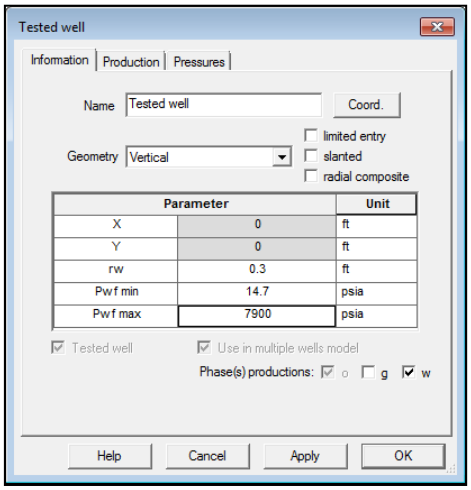


Fig. 14.F.1 – Throughout its production history the well pressure must remain above 14.7 psia ('pwf min') and below 7900 psia ('pwf max').

When the bounding pressure values are reached, the well is switched from rate-controlled to pressure-controlled production. It may switch back again to rate-controlled production when the simulated pressure re-enters the permitted limits. Such a case is shown in *Fig. 14.F.2*: during the first production phase the well pressure reaches a minimum and switches to constant pressure production. Later it reverts back to variable rate production.

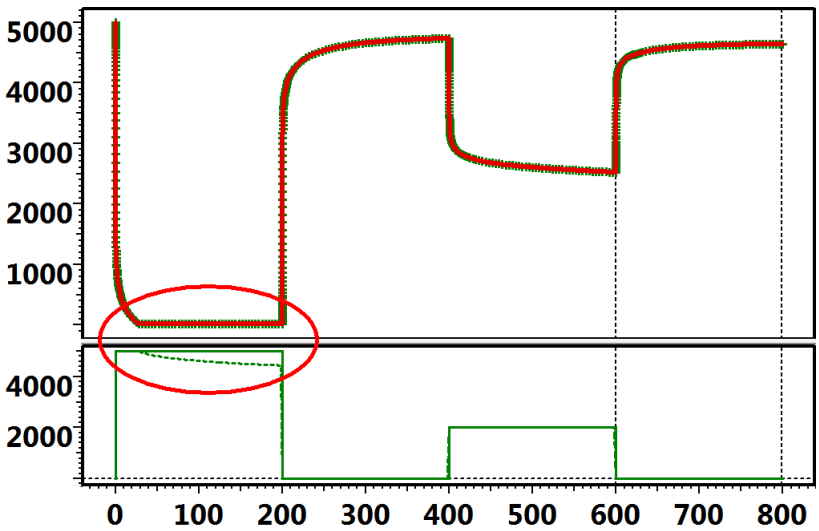


Fig. 14.F.2 – The minimum bounding pressure is reached during the first production

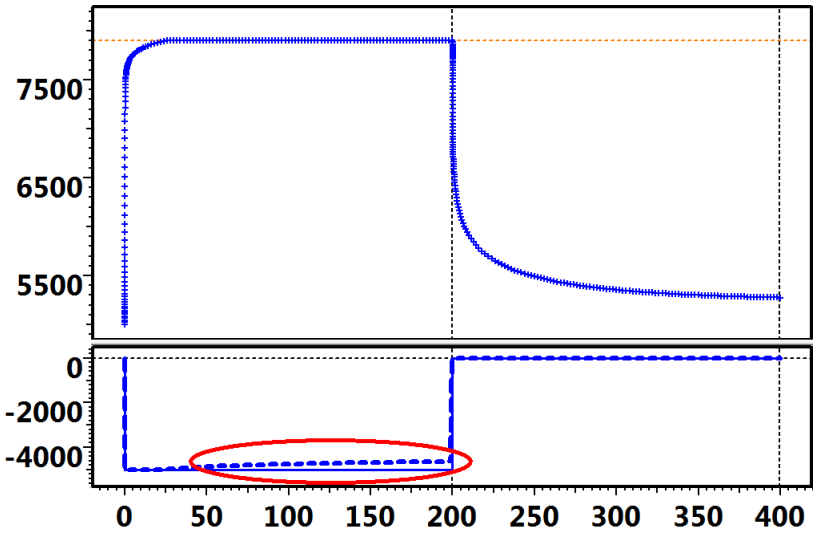


Fig. 14.F.3 – This water injector reaches its maximum pressure (orange dotted line) and is then switched to constant pressure injection. Later, the injection target rate is lowered and the well can switch back to constant rate injection.

14.F.2 Change in time stepping for numerical models

Many improvements have progressively been brought in the numerical system and in the non-linear loop, in order to stabilize and speed-up simulations. Among the main changes, we may cite:

(a) Numerical precision has been modified to better handle absent phases (e.g., water defined in the PVT but S_w=0). This improves convergence and speeds-up simulations with absent phases.
(b) System variables - unknowns - have been reorganized. This improves each linear system resolution in a multiphase context.
(c) Depending on the application, the default value of the 'time step ratio' can be adjusted in the numerical settings dialog in order to optimize the number of iterations per constraint step.
(d) For a well constraint in steps, constraint values may now be relaxed when time steps drop below the input 'minimum' value. This intends to reduce the number of restarts at very small time steps for problematic cases.
(e) Several internal thresholds regarding time step growth or restarts have been modified, further reducing the overall number of iterations per simulation.
(f) The well constraint gauges can be 'in points' or 'in steps', the nature of a gauge is systematically honored, with very important consequences in terms of time stepping, as detailed below.
(g) An option was introduced to force the numerical simulation stepping to follow the gauge stepping. In this case, the 'time step ratio' setting is completely ignored, and only the minimum number of time steps is performed.

Among these modifications, points (f) and (g) have the most important consequences and will be detailed in this section.

Let us consider a simple history with 3 constraint steps (either pressure or rate).

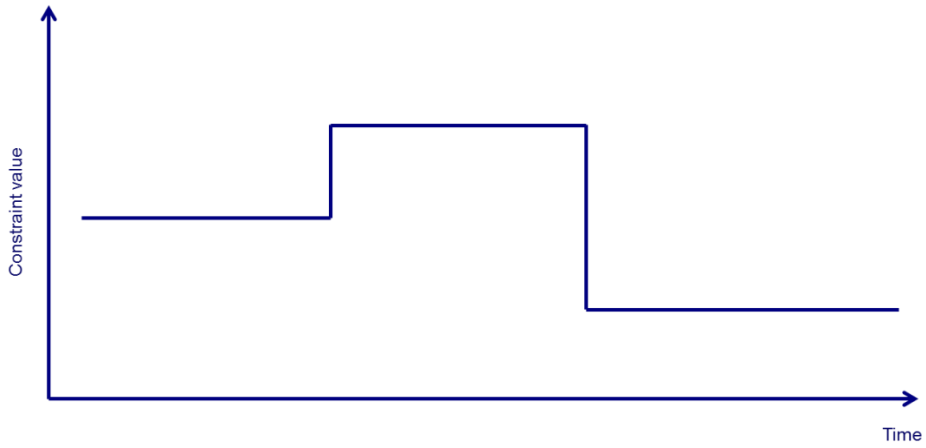


Fig. 14.F.4 – Simple history with 3 constraint steps

In order to honor the 'in steps' nature of the constraint, time stepping in the numerical kernel is handled as follows:

- At the beginning of each new constraint step, the time step is reduced to a small value ('dt new' in the figure below). This value is referred to as the 'Δt min' in the interface of KAPPA-Workstation.
- After each converged simulation step, the duration of the next time step is increased, following the input 'time step ratio'. Note that this growth is limited by the maximum allowed variations of pressure and saturations in the reservoir during a time step.
- The end of the current constraint step is strictly honored.

As a consequence, the simulation typically follows the path below:

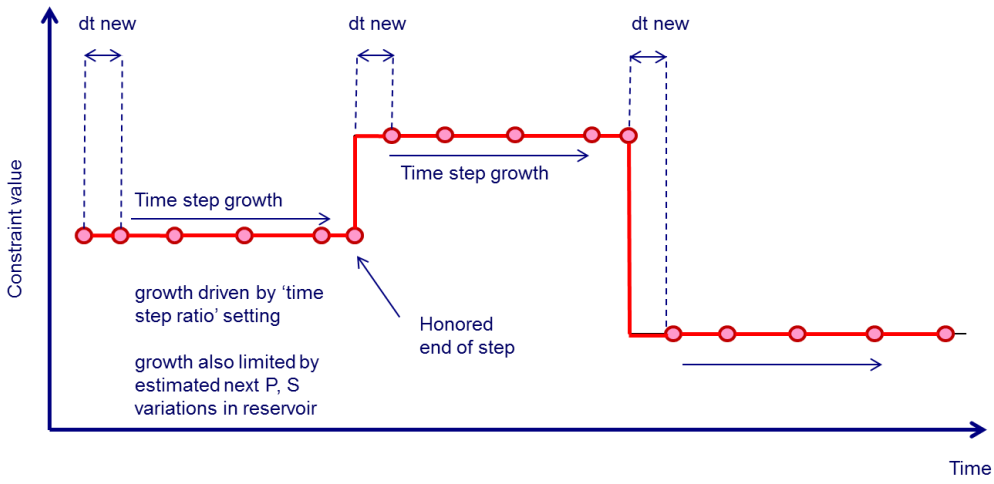


Fig. 14.F.5 – Steps followed by the simulation

Note that for each constraint step, many actual *simulation* steps may be required.

Let us now consider a more complex history, where the well constraint is a pressure gauge in points. This gauge contains 172 points (with, in average, one point every 180hr):

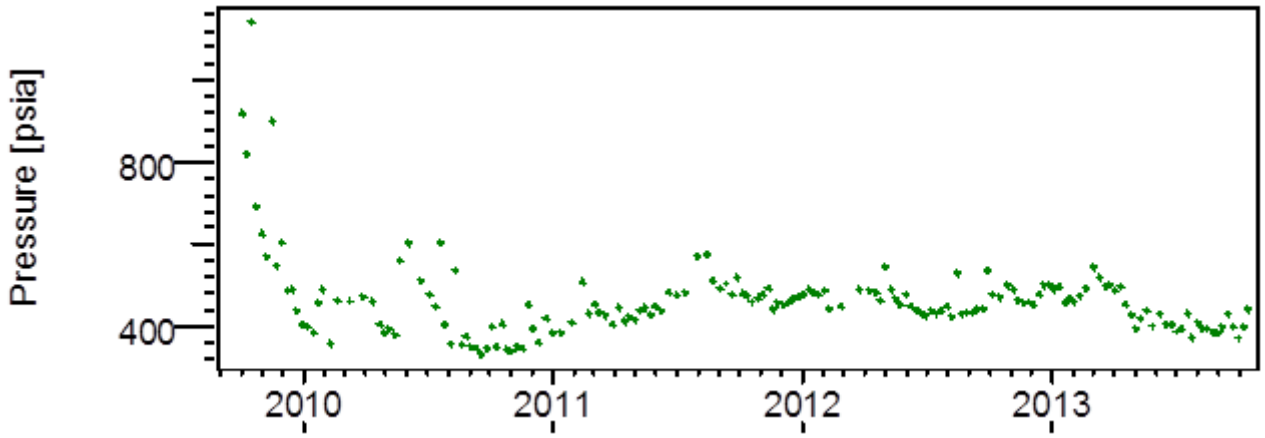


Fig. 14.F.6 – Pressure history

If such a constraint gauge 'in points' was treated as a gauge 'in steps', each step being centered on the corresponding original point the actual simulated history would be:

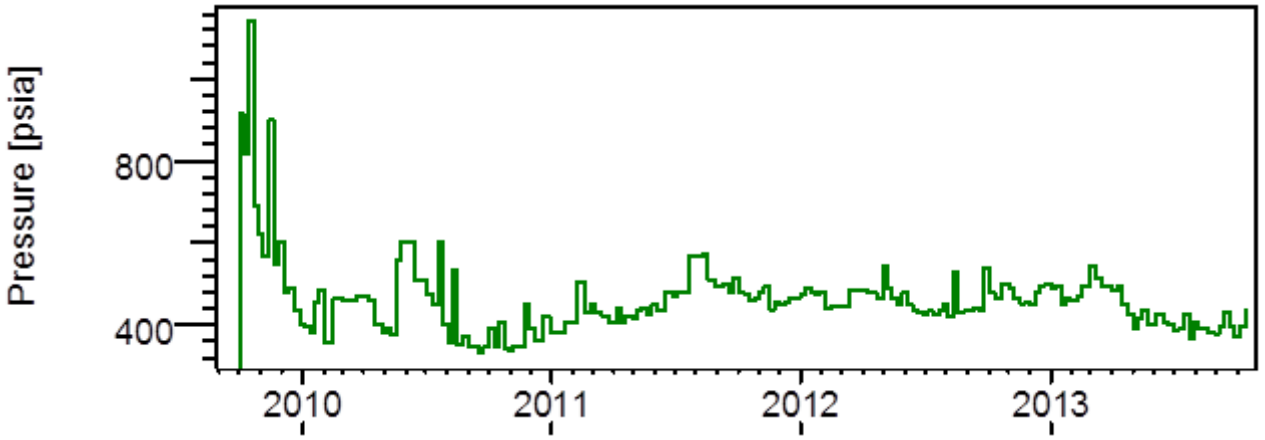


Fig. 14.F.7 – Simulated pressure history

If this history 'in steps' was simulated using the algorithm described above, many numerical time steps would be required per constrain data. For this particular example, we would end up with 1709 numerical time steps, for a total simulation time of 16 seconds.

The time stepping algorithm is also implemented to honor the 'in points' nature of the constraint gauges. To illustrate this approach, let us consider a simple history with 13 constraint points (either pressure or rate):

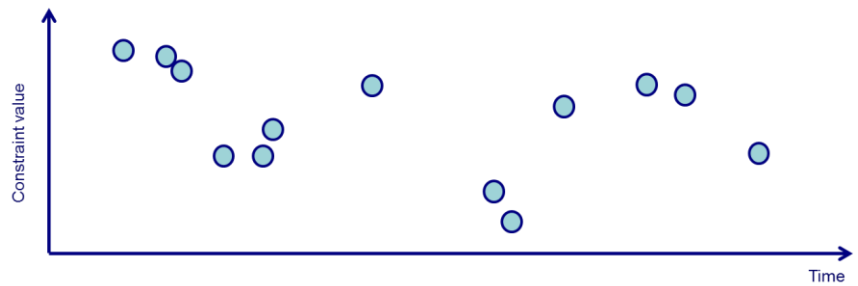


Fig. 14.F.8 – Simple history with 13 constraint steps

The new algorithm proceeds as follows:

- Only the first time step of the simulation is set to 'Δt min'.
- The time step growth is driven by the input 'time step ratio'.
- This growth is limited by gauge points (that are actually simulated).
- This growth is also limited by the maximum allowed variations of pressure and saturations in the reservoir during a time step.
- Constraint values are linearly interpolated between two gauge points.

As a consequence, the simulation typically follows the path below:

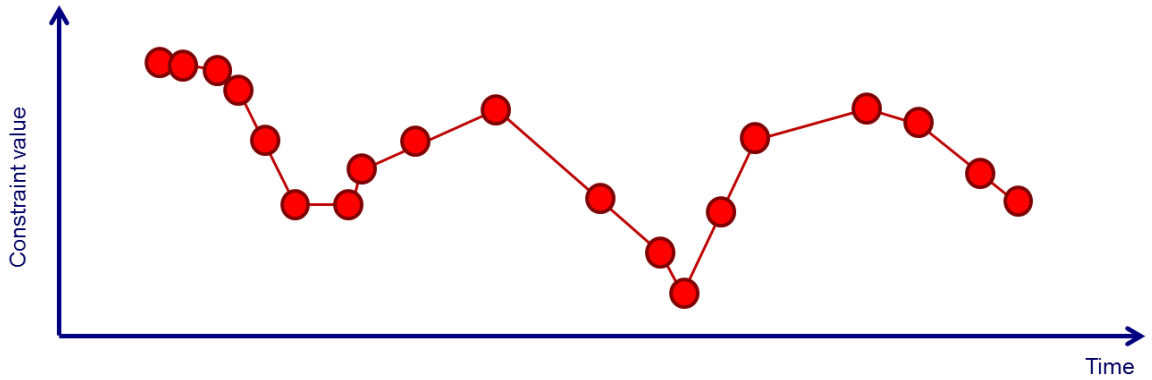


Fig. 14.F.9 – Path followed by the simulation

We see that this algorithm requires much less time steps than the former 'by steps' approach, since we do not come back to the smallest time step duration after each constraint gauge point.

Using this approach on the previous example (with the 172 points pressure gauge), we end up now with only 310 numerical time steps, for a simulation time of 8 seconds. This corresponds to an x2 acceleration compared to the previous one. CPU improvements by a factor of 5 can easily be observed for larger gauges.

Further CPU reduction can even be achieved, by using the option 'follow gauge' in the time settings of the model.

When this option is checked, the time step ratio is simply ignored and the simulator tries to go through gauge points only (provided numerical convergence is achieved). This further reduces the total number of simulated time steps when the gauge sampling is irregular.

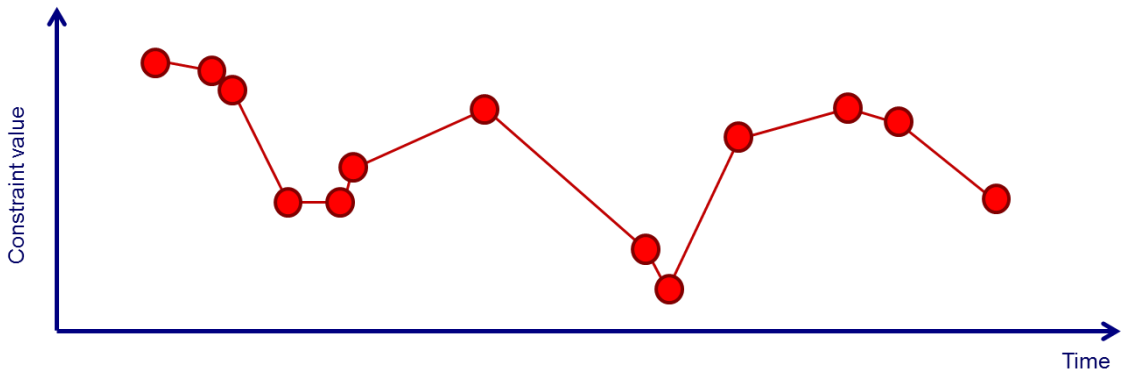


Fig. 14.F.10 – Simplified path followed by the simulation

15 – Nodal Analysis

OH – OSF – DV

15.A Introduction

The objective of any dynamic data analysis is the best possible understanding of the system 'Reservoir / Well'. To achieve that, it is absolutely necessary to dissociate the respective influences of the reservoir side and of the well side. Not only the performance of the system depends on both, but also the analysis of the reservoir requires being able to correct the data for the wellbore effect in order to extract the pure reservoir response.

The following paragraph will deals with the 'well modeling', necessary to correct the pressure data for depth and to include the wellbore effects in the reservoir analysis.

15.B Inflow Performance Relationship and A.O.F.

The goal of an Inflow Performance Relationship (IPR) is to establish a relation between the flowing pressure and the flowing rate. The Absolute Open Flow (AOF) uses this IPR in order to estimate the maximum possible rate when the flowing pressure is as low as possible, i.e. at atmospheric pressure.

Objection: Needless to say the idea of IPR and AOF is an anathema to the purist Pressure Transient Analyst. Everyone knows that, even in the optimistic case of an infinite reservoir, the pressure will continue drawing down when we are at constant rate, and the rate will keep declining when we are at constant flowing pressure. So, from a well testing point of view, this makes as little sense as the notion of a productivity index.

Objection to objection: Of course this objection is not completely correct. There is a regime where there is such a relationship and that is Pseudo-Steady State. When PSS is reached the shape of the pressure profile stabilizes and moves downwards. A relation between the production and the difference between the average pressure and the flowing pressure can be established.

Objection to objection to objection: Unfortunately we generally do not wait for PSS to be reached before performing an IPR, and the conditions under which the data is acquired are, generally, transient. We therefore look for changes that become small enough to be ignored. This complete process is therefore not strictly correct.

Objection to objection to objection to objection: This will not be too far out and, in any case, it has proven to work relatively well in the past, especially for gas reservoirs. In addition, IPR from PSS models are the best we have to simulate production networks and input in reservoir simulators where the details of the transient responses are not this important. IPR / AOF are useful because they give accurate ideas of the performance of the wells, and they are really the least bad thing to use when we optimize reservoir production.

15.B.1 The IPR types

Any available method is based on an equation which links the rate and the flowing pressure drawdown values.

These equation parameters can either be determined by adjusting the IPR curve to measured well test data set or they can be calculated using empirical equations.

15.B.1.a Straight line Constant IPR:

The constant productivity index (P.I.), only used in oil wells, was during a long time the only approach to oil IPR. Nowadays this is applicable to undersaturated oil only.

It is the simplest inflow performance relationship where the inflow is directly proportional to the drawdown.

$$PI = \frac{Q}{P_r - P_{wf}}$$

Where:

Pwf	flowing wellbore pressure	Pr	reservoir average pressure
Q	liquid flow rate		

It just requires a minimum of two measured rate and pressure values under flowing conditions.

15.B.1.b Darcy Equation

The Darcy IPR describes a linear relationship, where the parameters are calculated from the reservoir properties. Its equation results directly from the solution of a radial flow around a well within a circular drainage area of constant external boundary pressure, assuming a laminar flow.

It requires the knowledge of the well and reservoir drainage area parameters.

Oil case

$$P_r - P_{ws} = Q141.2B\mu\left(\left(\ln re/rw\right) - 0.75 + sCA + s \right)/\left(kh\right)$$

Where:

Q	liquid flow rate	k	permeability
h	net formation drained thickness	rw	wellbore radius
S	skin	m	viscosity
Pws	flowing sandface pressure	Pr	reservoir average pressure
sCa	shape skin	s	mechanical skin

Gas case

The equation is expressed in terms of Pseudo pressure m(p):

$$m(P_r) - m(P_{ws}) = ((1.42248e+6)TQ(\ln(re/rw) - 0.75 + sCA + s) + QDg)/kh$$

Where:

Q	gas flow rate	m(p)	pseudo pressure
sCa	shape skin	Dg	Drainage area factor
k	permeability	hw	perforated interval
h	net formation drained thickness	A	drainage area
rw	wellbore radius	gg	gas specific gravity
S	skin	m	viscosity
T	reservoir absolute temperature (° R)		

15.B.1.c C&n IPR

Several approaches were made to add the turbulent or the diphasic flow influences, among which is the C&n approach.

It was first used in gas cases, where the turbulent flow cannot be ignored or neglected, then it was extended to oil cases.

The measured production rates and their corresponding flowing pressure values are used to determine the C & n coefficients values.

Gas case

In 1936, Rawlins and Shellhardt published the IPR equation:

$$q = C\left(\bar{p}^2 - p_{wf}^2\right)^n$$

Where:

C is the performance coefficient

n the turbulent flow exponent, equal to 0.5 for fully turbulent flow and equal to 1 for laminar flow.

Oil Case

In 1973 Fetkovich demonstrates that the same can be used for oil wells.

The effect of the reservoir turbulences can be modeled with the use of the back pressure equation:

$$Q = C\left(\bar{p}^2 - p_{wf}{}^2\right)^n$$

Where:

Q main phase $\bar{p}$ average drainage area pressure

p_{wf} well flowing pressure

15.B.1.d Gas LIT IPR

The LIT (Laminar Inertial Turbulent) IPR equation, deduced from the Houpeurt or Forchheimer equation, also includes the turbulence effects:

$$m(\bar{p}) - m(p) = aq + bq^2$$

Where:

a = laminar flow coefficient b = turbulent flow coefficient

The method consists in getting from a multirate well test the pressure values corresponding to the production rate and to determine graphically the equation coefficients values, respectively C&n or a&b, then, eventually to calculate the Absolute Open Flow.

Another approach is to evaluate the a&b values from empirical equations using the well and reservoir parameters values as input (i.e. Jones method below).

15.B.1.e Vogel Oil IPR for Solution gas drive reservoir

This Vogel relationship can be regarded as a general equation for solution gas-drive reservoir producing below the bubble point.

The rate is governed by:

$$\frac{Q}{Q_{\max}} = 1.0 - 0.2\left[\frac{Pwf}{\Pr}\right] - 0.8\left[\frac{Pwf}{\Pr}\right]^2$$

If the reservoir pressure is above bubble point, the Vogel IPR is only valid when the well flowing pressure is below the bubble point pressure.

In this case, the combination of Vogel and other IPR method is recommended.

Above Pb it is a Darcy equation or a constant PI.

Below Pb it is the Vogel relationship:

$$Q = \frac{PI.P_b}{1.8}\left(1.0 - 0.2\left[\frac{Pwf}{Pb}\right] - 0.8\left[\frac{Pwf}{Pb}\right]^2\right) + Q_b$$

With:

$$Q_{\max} = Q_b + \frac{PI \times P_b}{1.8}$$

Where:

Q	Total liquid rate flow rate	Qmax	Maximum flowrate
Qb	Rate at bubble point pressure	Pr	Average reservoir pressure
Pwf	Bottom hole flowing pressure		

The method consists in using pressure and production data to determine the Pi, then the Qmax value.

15.B.2 Different types of multirate tests

The IPR equations assume stabilized rate and flowing pressure conditions, the most basic multirate test design is the back pressure test also called the flow after flow test which is a sequence of flow periods long enough to reach stabilized conditions originally proposed by Rawlins et al in 1936.

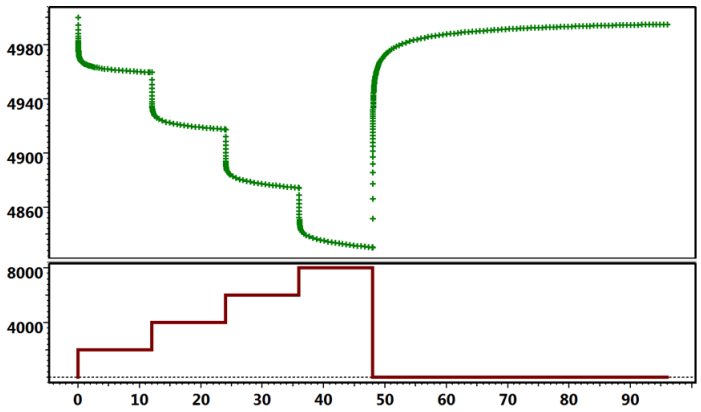


Fig. 15.B.1 – Back pressure (Flow after Flow) test

A second approach is based on the fact that only the laminar coefficient of the equations depends on the flow duration, the NonDarcy coefficient remains independent.

The test design includes short flow periods of equal duration, not necessarily stabilized, at various rates followed by shut-ins of equal duration until stabilization which are not necessarily the same duration as the drawdowns. The resulting values are used to determine the NonDarcy flow coefficient.

An extended flow period until stabilization allows determining the correct laminar coefficient.

This is the isochronal test proposed by Cullender in 1955.

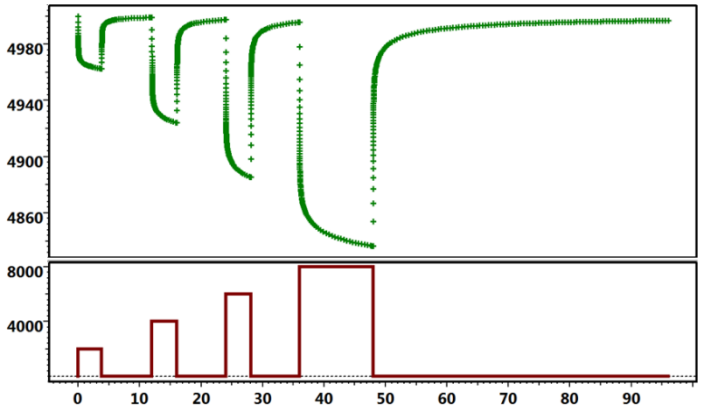


Fig. 15.B.2 – Isochronal test

The flowing pressure drawdown values are calculated from the initial average pressure.

The modified isochronal test, proposed by Katz et al in 1959, is characterized by short shut-ins between production periods, of equal duration, with neither of the periods necessarily stabilized. The final flow to stabilization is followed by a final long shut-in.

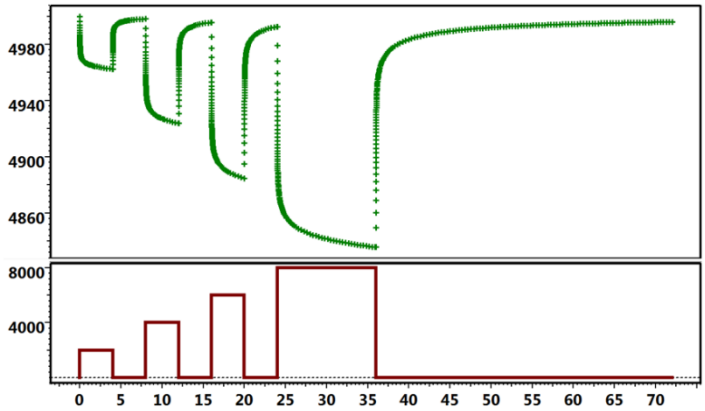


Fig. 15.B.3 – Modified isochronal test

The flowing pressure drawdown values are calculated from the previous last shut in pressure.

15.B.3 Different IPR/AOF calculation methods

15.B.3.a The Rawlins and Shellhardt method (C&n)

It can use either the p^2 valid for Oil or Gas:

$$q = C\left(\overline{p}^2 - p_{wf}^2\right)^n$$

Or, for gas only, the pseudo pressure m(p):

$$q = C\left(m(\bar{p}) - m\left(p_{wf}\right)\right)^n$$

The pressure and rate data are plotted on a log-log scale:

$$\log\left(\bar{p}^2 - p_{wf}^2\right) versus \log(q)$$

Or

$$\log\left(m(\bar{p}) - m\left(p_{wf}\right)\right) versus \log(q)$$

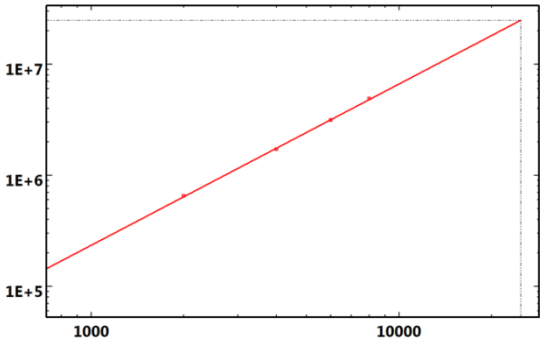


Fig. 15.B.4 – Back pressure test

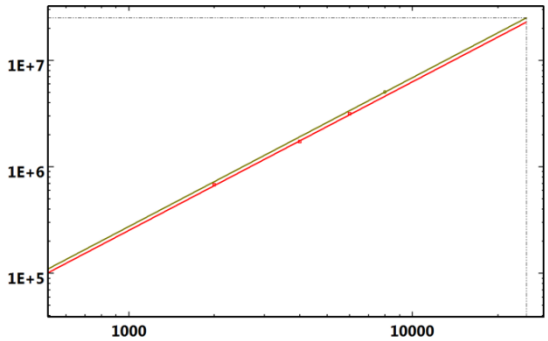


Fig. 15.B.5 – Isochronal test

The n value is calculated from the slope, C from the line intersect.

Then: $$AOF = C\left(\bar{p}^2 - (p_{atm})^2\right)^n$$

Or $$AOF = C\left(m(\bar{p}) - m(p_{atm})\right)^n$$

15.B.3.b The LIT Method

Developed specifically for gas, it is based on the equation:

$$m(\bar{p}) - m(p) = aq + bq^2$$

The pressure and rate data are plotted:

$$\frac{m(\bar{p}) - m(p_{wf})}{q} versus(q)$$

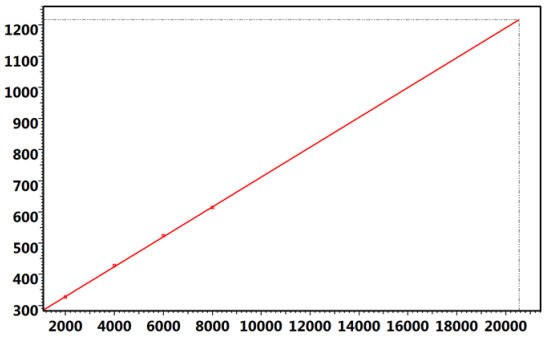


Fig. 15.B.6 – Back Pressure test

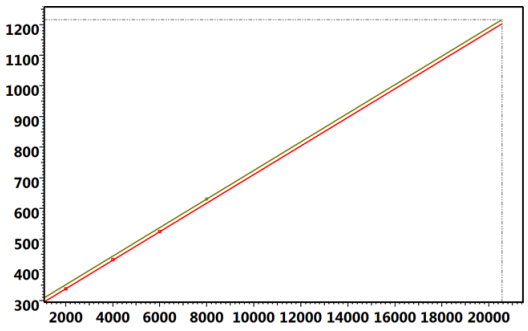


Fig. 15.B.7 – Isochronal test

The b value is calculated from the line slope and the a value from the intersect:

The AOF is then:

$$AOF = \frac{-a + \sqrt{a^2 + 4b\left[m(\bar{p}) - m(p_{atm})\right]}}{2b}$$

15.B.3.c Jones method

The method is also based on the equation suggested by Jones, Blount and Glaze in 1976 to account for turbulences in a producing oil well:

$$\Pr - Pwf = aQ + bQ^2$$

Where a and b parameters are calculated from empirical equations:

Oil case

The equation:

$$\Pr - Pwf = aQ + bQ^2$$

With:

$$a = (141.2B\mu(\ln(re/rw) - 0.75 + sCA + s)/kh$$

$$b = \frac{1.4352 \times 10^{-12}\gamma_l \beta B^2 \left(\frac{1}{r_w} - \frac{1}{r_e}\right)}{hw^2}$$

SCA	Shape skin (from Dietz shape factor)	k	permeability
hw	perforated interval	B	formation volume factor
γ_l	liquid specific gravity	β	turbulence coefficient
h	net formation drained thickness	re	drainage radius
rw	wellbore radius	S	skin
μ	viscosity		

Gas Case

The same principle equation, using m(p) is:

$$m(\bar{p}) - m(p) = aq + bq^2$$

But the parameters a and b are estimated from the following empirical equations:

$$a = \frac{1495.6T\left(\log\frac{A}{r_w^2} + \log\left[\frac{2.2458}{C_A}\right] - 0.87s\right)}{kh}$$

$$b = \frac{1299.15TD}{kh}$$

$$D = \frac{0.00003gg}{\mu h r_w k^{0.333}}$$

Where:

Ca	Dietz shape factor	D	Turbulence factor (1/ft)
k	permeability	hw	perforated interval
h	net formation drained thickness	A	drainage area
rw	wellbore radius	gg	gas specific gravity
S	skin	μ	viscosity
T	reservoir temperature (deg R)		

Other similar methods exist for various well geometries, the difference remains in the empirical equations.

15.C Intake models in PTA and RTA

15.C.1 Classic pressure correction

The fact that the pressure gauges sensing points are seldom at the level of the sandface is most often overlooked by the interpretation engineer.

Classically, the static pressure (pi, p*, p bar, final build-up pressure) are corrected:

- from the gauge depth to the sandface using the well static gradient.
- from the sandface to a common reservoir datum using the reservoir gradient taking into account any gradient changes if it is necessary to move through a fluid contact in the reservoir.

This correction is usually done manually and is essential to establish reservoir pressure trends, declines and depletion rates.

The resulting corrected static pressure maps can be used to study:

- The effectiveness of artificial or natural pressure maintenance.
- It can also reveal reservoir compartmentalization.

It is an essential part of material balance studies and full field simulations.

Little attention has been put on the correction of flowing pressures and the fact that the skin calculation returned by Pressure Transient Analysis is in fact at the gauge level, therefore it includes the pressure loss due to friction between the sandface and the gauge.

In that way, the skin, and specially the rate dependant skin, can be considerably over evaluated. We are only interested in sandface values but this problem has largely been ignored by the well test community until recently.

Most Pressure Transient and Rate Transient Analysis software packages include such corrections. This can be a correction of the model to simulate the pressure at a given depth, or to correct, a priori, the pressure history from the gauge depth to sandface.

15.C.2 Correction methods

It is necessary to evaluate the pressure profile and lift curve of the well under flowing and shut-in conditions.

The pressure profile is defined by:

- A temperature profile;
- A flow correlation or a lift curve;
- PVT definitions;
- The completion configuration including deviation.

The below figure shows a ‘Vertical intake curve’; pressure vs. rate at a selected well depth using a fixed GOR and water cut.

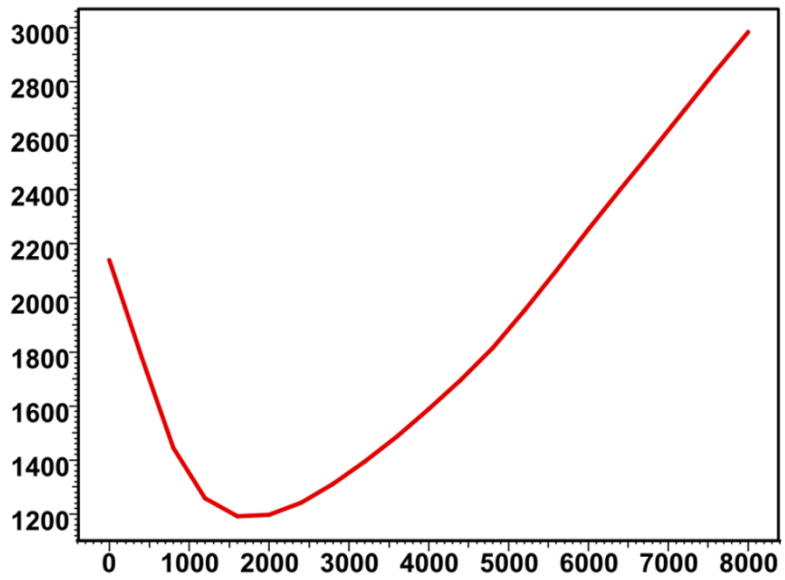


Fig. 15.C.1 – Vertical intake curve, flowing pressure vs. rate

15.C.3 Flow models and correlations

The slippage effect, non-equal phase velocities, is determining in the calculation of pressure drop versus phase rates. In general the behavior of the slippage velocity strongly depends on the nature of the flow regime encountered. Whereas a water-oil mixture moving upward can often be considered in bubble flow, liquid-gas mixtures will give rise to much more complex regimes, as illustrated below with one of the classical empirical correlations by Duns and Ross.

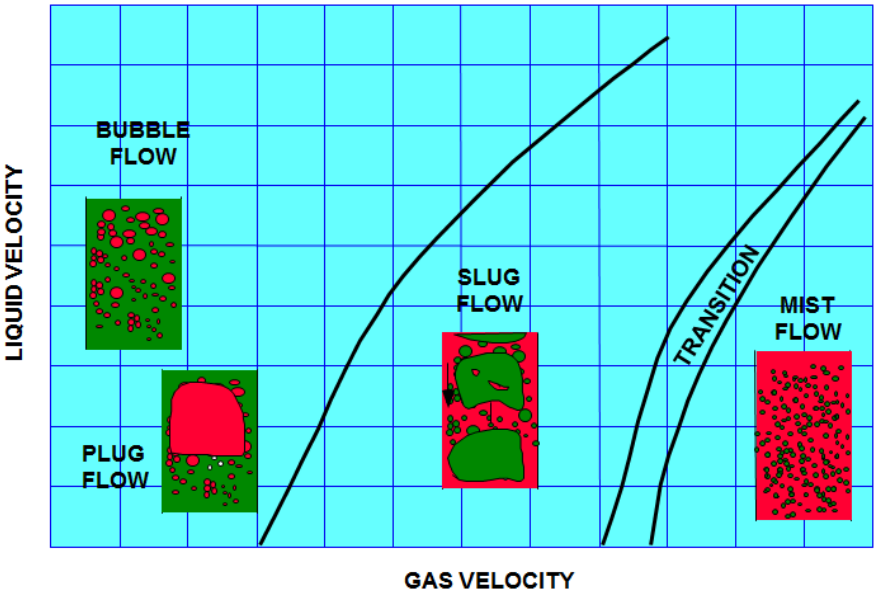


Fig. 15.C.2 – Duns and Ross flow map

Slippage correlations have been derived for a number of situations either empirically, or by solving the general momentum balance equation ('mechanistic' correlation).

In each regime, a specific slippage correlation will be applicable with extreme cases like Mist flow, where no slip exists between the two phases. Many correlations will start with a determination of the flow regime using a flow map, and continue with the application of the corresponding slippage equation. Slippage correlations can be organized in three categories.

15.C.3.a Flow correlations for Liquid-Liquid

This category gathers bubble flow correlations (e.g. Choquette), correlations developed for stratified flow (e.g. Brauner) and combinations of those.

15.C.3.b Flow correlations for Liquid-Gas

This is by far the largest population with many empirical correlations. Most of those correlations have been primarily designed for representing wellbore pressure drops in the context of well performance analysis.

Duns-Ross: The result of laboratory work where liquid holdup and flow regimes were observed. This utilizes a flow pattern map to determine the slip velocity, and consequently liquid holdup, and friction factor. This correlation is recommended for wells where high GLRs and flow velocities have induced flow regime behavior.

Orkiszewski: Developed using work from both Duns & Ross and Hagedorn & Brown. It uses the Griffith and Wallis method for bubble flow, a new method for slug flow, and Duns and Ross for transition and mist flow.

Hagedorn-Brown: Developed experimentally using a 1500ft test well with 1”, 1.25”, and 1.5” tubing. The correlation is used extensively throughout the industry and is recommended in wells with minimal flow regime effects.

Beggs-Brill: This correlation was developed experimentally using 1” and 1.5” pipe, inclined at several angles. Correlations were made to account for the inclined flow. The correlation is recommended for deviated or horizontal wells.

Mukherjee-Brill: Developed experimentally using 1.5” steel pipe inclined at several angles. This includes downhill flow as a flow regime. This is recommended for inclined or horizontal wells.

Dukler-Eaton: Based on 2600 laboratory and field tests to generate an expression for frictional pressure losses along pipelines. It can be used for horizontal flow.

15.C.3.c Flow correlations for dry gas

Cullender & Smith: This correlation is based on gas properties as defined by the PVT, and a general friction factor calculated using the Colebrook and White equation. Note that when handling a condensate case with equivalent gas gravity and total rates, the proper gradient and rates are used in Cullender and Smith to account for the presence of condensate. The presence of water can be accommodated, based on a constant water to gas production ratio.

15.C.3.d Flow correlations for Three phase

There are very few such correlations and when they exist they are for a very specific situation, e.g. stratified 3-phase flow (Zhang). In practice, three-phase slippage / holdup prediction from rates are done using two 2-phase models, typically for the gas-liquid mixture on one hand and the water-oil mixture on the other hand.

15.C.3.e Lift curves

The interpretation engineer can input lift curves generated by third party programs such Amethyste, Eclipse and Prosper. The lift curves are usually imported in Eclipse format.

Lift curves usually provide the pressure drop between the well head and lift curve depth. However, it can happen that they correspond to a pressure drop between a given depth that is different from the well head and the lift curve depth.

External lift curves are discrete data. When using them the pressure drop calculations are performed by interpolations in the lift curve table in each of the required dimensions. Therefore it is recommended to provide as many lift curves as possible to cover the widest possible range of situations such as varying rates, phase ratios and well head pressures.

15.C.4 General calculation method

In vertical multiphase flow calculations the pipe is divided into small depth increments. The pressure loss in each increment is determined in a reiterative process using average pressure and temperature values to calculate fluid properties. This is necessary as flow regimes and subsequent fluid and flow properties continually change through the pipe. As a result, a computer solution is almost mandatory.

Multiphase cases are treated using multiphase flow correlations. In the event that the interpreter has identified more than one phase rate, Perrine's method is usually used and the phase ratios are calculated at each step from the loaded measured multiphase rates and used in the intake calculator for the pressure depth correction.

If a non-linear numerical model is used the numerical model output will provide sandface phase rates. The phase ratios are calculated at each step from the simulated multiphase rates and used in the intake calculator for the pressure depth correction.

Pressure drop correlations are valid under dynamic conditions only, not during build-ups or fall-offs. To ensure continuity of the corrected pressure, the limit of the pressure drop when the flowrate tends to zero is used during shut-ins. With the flow correlations, this amounts to dividing the tubing into small segments where each contains phase rates corresponding to the amount given by the flash PVT, and consequently the deduced holdups.

15.C.5 Correcting gauge data vs. correcting model

Correcting the data: In production analysis, Topaze, when the intake pressure model has been defined, the interpretation engineer will decide during extraction to make the pressure correction to whatever depth is desired. There is an option to create a new pressure gauge with the corrected pressure. In Saphir it is possible to transform the pressure data to whatever depth at any time.

Correcting the model: In Saphir, when the intake pressure model has been defined, the interpretation engineer will decide that when generating the model the model response will be corrected to gauge depth.

In both situations, for wells undergoing artificial lift by means of an electrical submersible pump (ESP) or gas lift, the intake pressure model can account for the time evolution of the pressure support conditions (motor operating frequency, free gas vented fraction…).

The downhole rates are calculated by the model and will therefore incorporate wellbore storage effects. This ensures that, with significant friction, there will be no discontinuity in the corrected model when the surface rate changes.

The model match will now return results at sandface.

15.C.6 Well intake in multilateral wells

The case of multilateral well can be handles in detail by defining the individual well intake curve for each branch.

It is sufficient to check the option "Individual layer definition" in the Well Intake definition dialog, then a drop list allows to select the branch we want to describe:

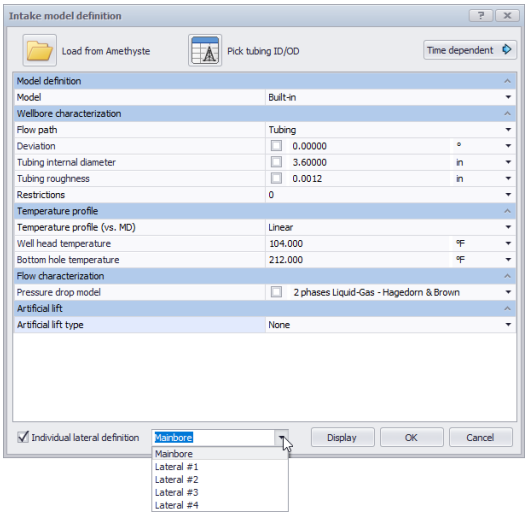


Fig. 15.C.3 – Specification of the individual well intakes

Then all the features are available for each lateral branch.

16 – Permanent Gauges & Intelligent Fields
OH – OSF – DV

16.A What PDG data can bring

Historically the pioneers in the deployment of PDG were large operators wishing to implement real time reservoir surveillance on a few high profile wells or field development projects. The use of PDG is increasing constantly. By 2010, however, the spread was still very unequal from one country to another and from one operating company to the next.

However the trend seems irreversible. Unit prices are falling, and reliability is increasing, and the installation cost for a permanent gauge in a new development well is now marginal compared to the overall cost of a brand new well.

When they are placed in the hole, PDG have already been sold for the sake of reservoir surveillance and the wish to know what is happening in real time. Any additional use of this data, as presented in this chapter, can be considered as the icing on the cake, although there are some additional steps to take in the acquisition, storage and retrieval of the data in order to properly fit our needs.

The interest in PDG data goes beyond the simple knowledge of pressure and temperature at any given time. The combination of the well production, when known, and this pressure data is a good candidate for mainly two types of analyses and for real time rate allocation. Fig. 16.A.1 shows a typical set of permanent downhole pressure data. The period covered is approximately three months. With an acquisition rate of one point every five seconds, this corresponds to around 1,500,000 raw data points.



Fig. 16.A.1 – Example of permanent pressure gauge data three months of data - downhole pressure vs. time

This data carries two types of information:

Each peak in the data is a shut-in. The following figure shows an expanded version of one of these peaks. If we have a fair idea of the producing rates, and this may in itself be an issue, each peak is a good candidate for Pressure Transient Analysis (PTA). It is potentially the equivalent of a free, but not designed well test. In addition, comparing these successive build-ups in time will provide information on how the well and the reservoir within the well drainage area have evolved between these build-ups.

In order to get a reliable last flowing pressure and analyse the early time of each build-up we will use the smallest time steps, i.e. the highest frequency we can get, on repeated but relatively short time ranges.

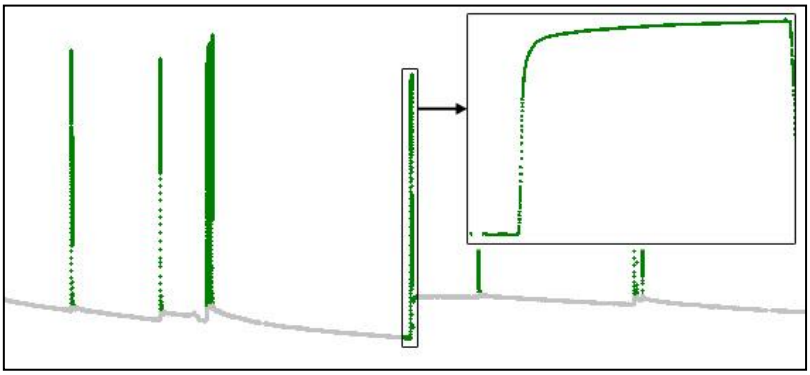


Fig. 16.A.2 – Example of permanent pressure gauge data
High frequency signal for Pressure Transient Analysis

On the other hand, in the following figure we have ignored the peaks and focussed on the producing pressures, as a low frequency signal over the whole time range of the permanent gauge survey. These pressures, combined with the production rates, may be used for Rate Transient Analysis (RTA) if, again, we have some idea of the well production.

In order to use these data, we need a low frequency extraction of the producing pressures over a relatively large time range.

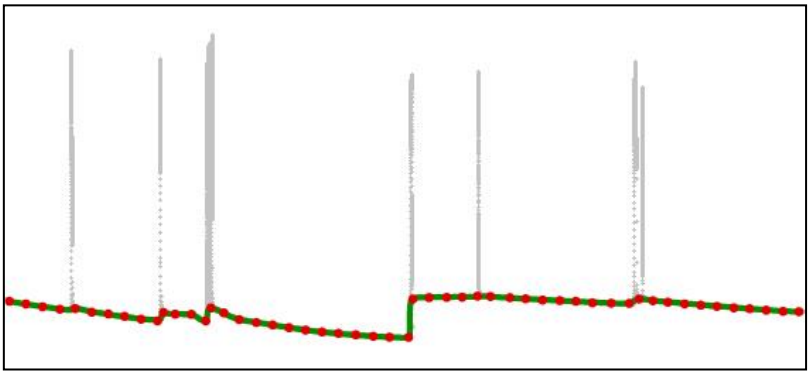


Fig. 16.A.3 – Example of permanent pressure gauge data
Low frequency signal for Rate Transient Analysis

16.B Challenges of PDG data

The main challenge with continuous information is the enormous mass of data that is involved.

The usage of permanent gauge data presented in the previous section and developed later in this chapter is possible only because we are getting data at a high acquisition rate AND over a large time interval. If we multiply high frequency by large durations, crudely, we end up with a huge number of data points.

For an acquisition rate of every 5 seconds over a period of 3 years, we get 20 million data points per channel. Acquisition rates and durations vary, but 20 million is a reasonable geometric average, with a range typically between tens of millions and a few hundred million data points per gauge channel, sometimes referred to as **tags** in the storage databases. And with the life expectancy of the permanent installations increasing all the time, this number just grows to mind-boggling values.

16.B.1 Storage and access

When visiting operating companies, the following questions often generate embarrassed answers, or no answer at all. Sometimes, a fight breaks out:

- Where is your PDG data stored?
- What is stored? (acquisition rate, storage duration, interpolation, filtration, etc)
- How can I access this data right now and from here?

Answering these questions is generally half of the work. Historically, storage and access options would be decided by the people that purchased the gauges and essentially 'just' saw them as a real time surveillance tool. Getting back to ALL the raw data from the beginning of the acquisition was not really top of the agenda. But we will see in the following that this is precisely what is needed; ALL data, since the beginning, with NO prior editing.

16.B.2 Smart reduction

We need to have access to ALL the data in order to ensure that no processing has been done that could reduce the value of this data in the analysis processes. However it does not mean that we need all data for such analysis; it is the analyst that decides what data to use:

- Low frequency data (RTA): Considering that rates are typically given daily, 1 pressure point per hour is more than enough. For a 10-year survey, we need less than 100,000 points.
- High frequency data (PTA): Considering we will typically find 100 or less relevant build-ups, and considering that 1,000 points extracted on a logarithmic time scale will be suitable for analysis, we need another, albeit different, 100,000 points.

So even for the largest data sets 200,000 points are sufficient to satisfy our processing needs. This is around 100 times less than the median size of a raw data set. Unlike the number of raw data, this reduced number is also well within the memory and processing capability of today's PCs.

The challenge is how to get to this reduced number of *relevant* points. The answer lies in applying a 'smart' filter that picks and selectively reduces both low and high frequency data. Then we need to be able to transfer the filtered data to the different analysis modules. The work flow is shown in the following figure.

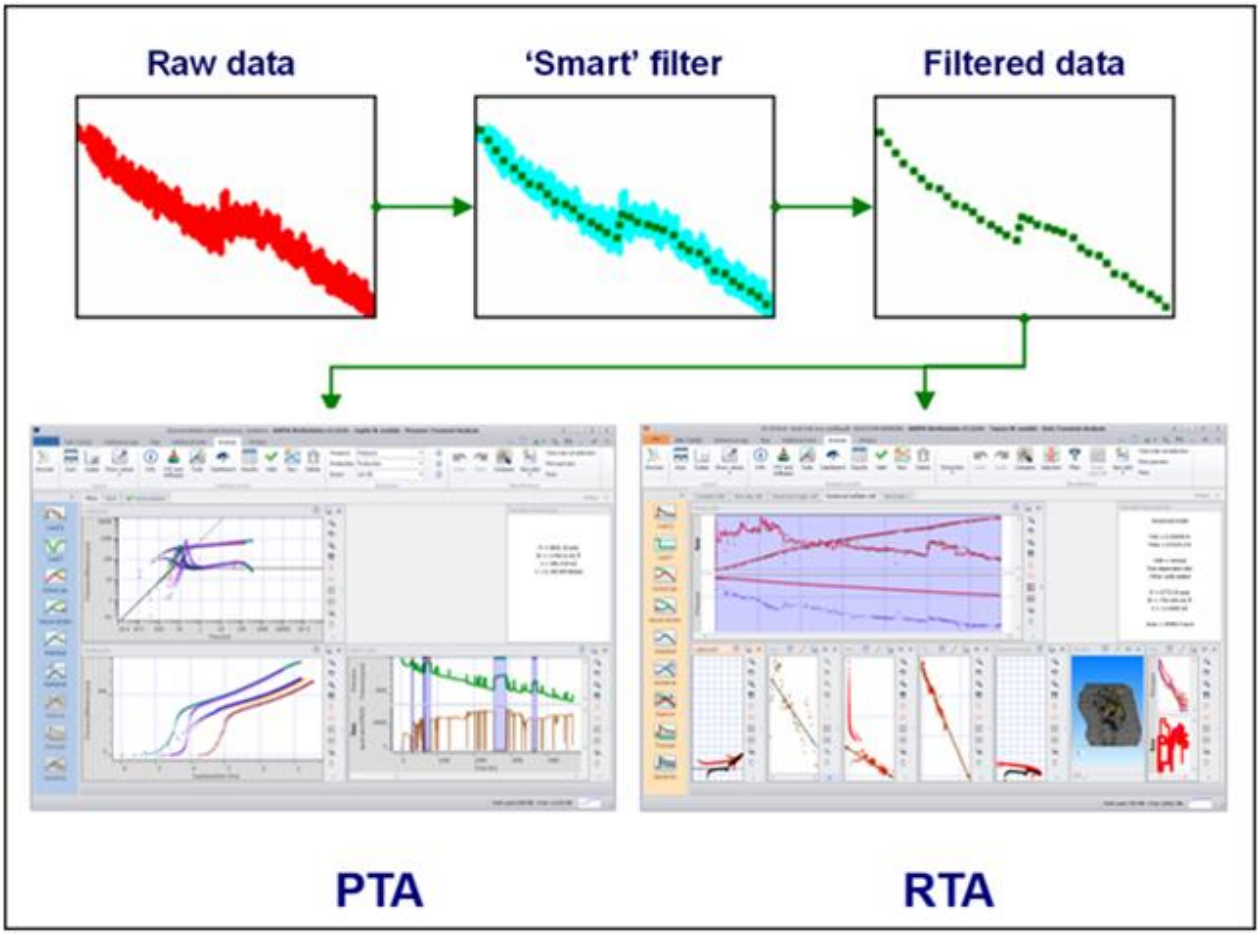


Fig. 16.B.1 – Permanent gauge data: storage, filtering and access

16.C Wavelet filtration – an overview

The main challenge in the processing of permanent gauge data was to implement a 'smart' filter that would drastically reduce the number of data points without losing either high frequency or low frequency data.

Permanent gauge data is naturally noisy. For the low frequency information, i.e. the production period, an efficient reduction requires some de-noising before the reduction in number of points. This is the typical task of a low pass filter.

The problem is the opposite when we want to keep the high frequency data. Whenever we have a shut-in, we do not want the break in the pressure response to be masked by a low pass filter. At the time of the shut-in, we want a high pass filter.

So, depending on the part of the information we are interested in, we need a low pass filter or a high pass filter. The 'magic' solution would be a filter that identifies the relevant break of high frequency data, acts as a high pass filter on these breaks to keep them intact, but acts as a low pass filter anywhere else, in order to smooth producing phase responses and allow an efficient data reduction. This must be done based on the pressure data only, without knowing, a priori, the well producing history.

This specification is successfully met by wavelet algorithms. For the engineer it acts as a filter with a threshold. Any noise below a certain level is considered as noise and is filtered out. This will be, hopefully, the case for most noisy signals during the producing phase. On the other hand, any noise above a certain level of threshold will be considered as a representative break in the data and will be preserved. This will be, hopefully, whenever the well is shut in. The break in the pressure data will act as local, high level noise.

Before we get into the (optional) theory of the next section, the below figure shows the different steps of the wavelet filtration process, from the 'user's point of view.

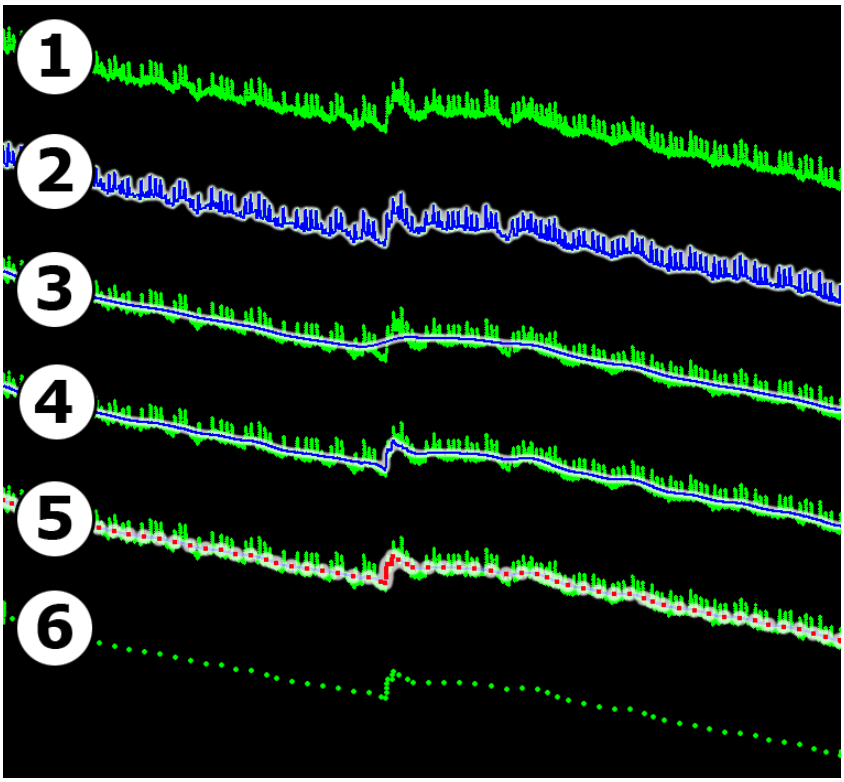


Fig. 16.C.1 – The steps of wavelet filtration

Curve 1 shows a set of raw data corresponding to 12,000 points over a period of 5 days. The noise level is high, and we see that a change in the trend occurs in the middle of the display window.

Curve 2 shows the wavelet filtered signal with a low threshold. With such a setting the significant break and a lot of noise is considered significant.

Curve 3 shows, conversely, the result with a very high threshold. All features in the response, including the break, are below threshold, and the wavelet acts as a standard low pass filter.

Curve 4 shows the result for an intermediate value of threshold that clears most of the noise but keeps the break intact. We will use this setting.

Once the correct threshold is set, we still have the same number of points but it is now possible to reduce them using simple post-filtration, which is typically a combination of time intervals and maximum pressure change.

Curve 5 in Figure above shows the suggested result of this post-filtration.

Curve 6 shows the filtered data, with only 70 points remaining.

16.D Wavelet filtration - Theory

16.D.1 Wavelet and scaling functions

Wavelet algorithms are multi-frequency processes. We will start by showing what happens on one given frequency, corresponding to a time period 'a'.

We use two basic tools: a normalized **scaling function** ϕ used to define a low pass filter, and a corresponding **wavelet function** ψ used to define a high pass filter. These functions must respect the following conditions:

$$\int_{-\infty}^{\infty} \phi(x)dx = 1 \quad \text{and} \quad \int_{-\infty}^{\infty} \psi(x)dx = 0$$

A simple example for functions ϕ and ψ is shown in the following figure. In reality the functions are a little more complex in order to avoid numerical effects, we will see this in a later section discussing wavelet processing.

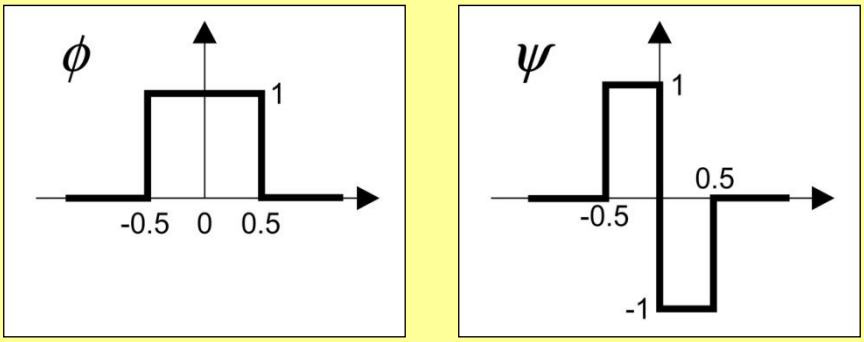


Fig. 16.D.1 – Simplest example of scaling and wavelet functions

These functions are used to decompose a given signal (our original data or some transformed data) into two component signals: the complementary transform C_a and the wavelet transform W_a, by respective convolution of the original data with the scaling and wavelet functions.

$$C_a(t) = \frac{1}{a}\int_{-\infty}^{\infty} f(x)\phi(\frac{x-t}{a})dx$$

$$W_a(t) = \frac{1}{a}\int_{-\infty}^{\infty} f(x)\psi(\frac{x-t}{a})dx$$

If we consider our example functions, the complementary transform $C_a(t)$ is the average of the signal f on the segment $[t-a/2,t+a/2]$. This is our 'low pass' filter.

Understanding the wavelet transform $W_a(t)$ is less immediate:

- If the signal is constant or slowly changing over the interval $[t-a/2,t+a/2]$, the wavelet transform is zero, or very close to zero.
- If the signal is random, or oscillating at a much higher frequency, the wavelet transform will also be very close to zero.
- It is only if substantial variations occur at the scale of a, for example, if the signal has a shape like ψ over this interval, then the wavelet transform will be positive or negative.
- If there is a break of the signal at time t, one can expect that the wavelet transform, whatever the considered frequency, is likely to be strongly positive (break downwards) or negative (break upwards).

One remarkable property of these transforms is that there is a numerical way to make these transformations reversible. If we decompose a signal into a wavelet transform and a complementary transform, we will be able to re-create the original signal from these two transforms by a reverse operation. So this dual transforms act as a 'projection' of the signal into two complementary spaces. This is only possible because the operators ϕ and ψ have been carefully chosen. One operator ϕ will correspond to one operator ψ, and reverse.

16.D.2 Wavelet filtration with a single frequency

The process for a single frequency is schematized in the following figure. The numerical implementation of this algorithm requires that original data are evenly sampled in time, the time interval being *a*.

Important: Original raw data is generally not evenly sampled. The required initial interpolation may have a large impact on the process, as any information in the raw data lost in this initial interpolation will be lost for good. This is why the frequency choice is important.

The transforms given in the equations above are replaced by numerical algorithms on discrete, regularly sampled data sets. They will not be detailed here.

The function $W_a(t)$ depends on the level of noise of frequency *1/a* around time t. If the noise is high, or if there is a break in the data at time t, the value of $W_a(t)$ will be strongly negative or positive. We select a threshold value *THR*, which defines the value of W_a above which we consider the signal should be kept. We define then a modified wavelet function:

$$|W_a(t)| > THR \quad \Rightarrow \quad W'_a(t) = W_a(t)$$
$$|W_a(t)| \leq THR \quad \Rightarrow \quad W'_a(t) = 0$$

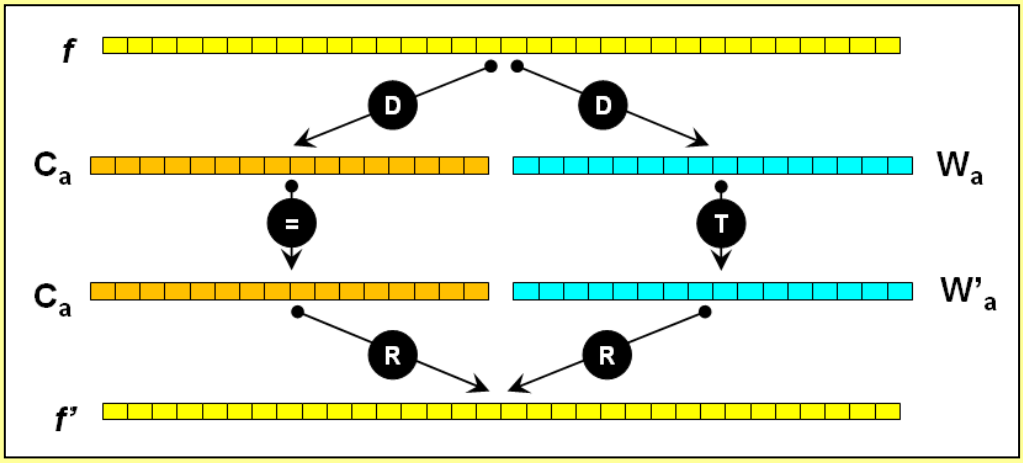


Fig. 16.D.2 – Schematic of a single frequency wavelet algorithm
D = Decomposition ; T = Threshold ; R = Recombination

Instead of recombining $C_a(t)$ with the original wavelet transform $W_a(t)$ and arriving back at the original signal, we recombine $C_a(t)$ with the **modified** wavelet transform $W_a'(t)$.

When the noise level corresponding to the frequency *1/a* is small, i.e. when the wavelet transform is **below threshold**, the function $W_a'(t)$ is set to zero, and after recomposition the data will have been smoothed out. When the wavelet transform is **above threshold**, the function $W_a'(t)$ is not truncated, and after recomposition the noise/break is kept.

If we had N evenly sampled data points on the original signal f, after decomposition we now have N/2 evenly sampled data points in each of the transforms. The total number of points remains N, but as we have two signals the time interval is now *2a*.

16.D.3 Wavelet filtration with multiple frequencies

Comprehensive wavelet de-noising is a multiple frequency process as shown in the following figure. In this example there are four such frequencies. This is a parameter that will be controlled in the filtering application.

The process must first interpolate (I) the raw data to start with a set of points C_a with a uniform time spacing *a*. The choice of *a* is discussed in a later section.

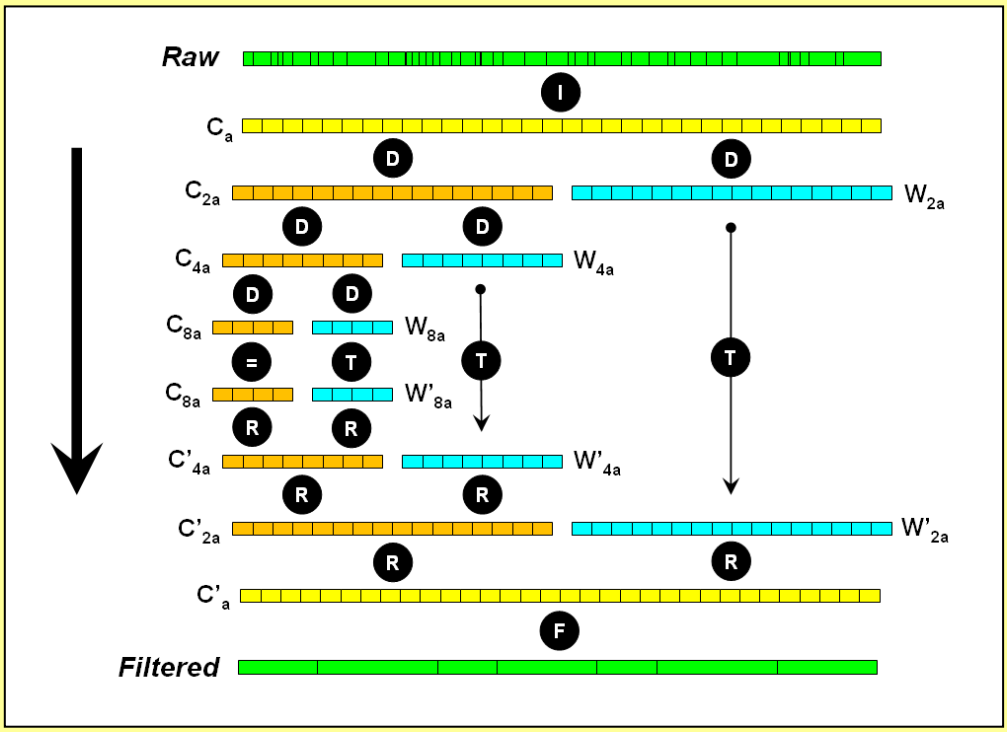


Fig. 16.D.3 – Schematic of complete wavelet algorithm
(I) = Interpolation; (D) = Decomposition; (T) = Threshold
(R) = Recombination; (F) = Post-Filtration

The filter will not interpolate and process ALL raw data in a single run. This would be far beyond the computing power of most of the usual computers. The idea is to take windows of typically 100,000 to 1 million data points, and work successively on overlapping windows in order to avoid end effects.

The signal C_a is decomposed (D) into a complementary transform C_{2a} and a wavelet transform W_{2a}. The total number of points remains the same, half with C_{2a} and half with W_{2a}. The time spacing for each of these series is $2a$, and the frequency is now half the original. The signal C_{2a} is in turn decomposed into C_{4a} and W_{4a}, C_{4a} is decomposed into C_{8a} and W_{8a}, until the desired number of decomposition levels is reached. Here we will stop at C_{8a}.

At this stage, the original interpolated signal C_a was decomposed into four series: C_{8a}, W_{8a}, W_{4a} and W_{2a}, representing the same total number of points as C_a. If we were recombining these components in the reverse process, we would return to our original signal C_a.

The data is de-noised by applying the Threshold (T) to the different wavelet transforms. The new signal C_a' will be created by successively recombining (R) C_{8a} with the modified wavelet transforms W_{8a}', then recombining the resulting C_{4a}' with W_{4a}', and finally recombining the resulting C_{2a}' with W_{2a}'.

We now end up with the same number of points, but this time large sections of the data, the producing part, will be smoothed, and this will allow data elimination with simple post-Filtration (F).

In order to avoid any fatal improvement due to the filtration, the process will typically store the break points, i.e. the points at which the wavelet functions had exceeded the threshold, and instruct the filtration process to keep them no matter what.

On a typical set of permanent gauge data, the ratio between the number of raw data points and the number of filtered points will range between 100 and 1000.

16.D.4 Parameters controlling wavelet processing

The functions ϕ and ψ presented in Fig. 16.D.1 are the simplest case and were presented to illustrate the process. Functions used on real data are smoother in order to avoid numerical effects. The following figure shows another set of functions, more likely to be used on real life data. Similarly, the threshold algorithm presented in the wavelet function is too abrupt. Threshold filters used in real life are continuous.

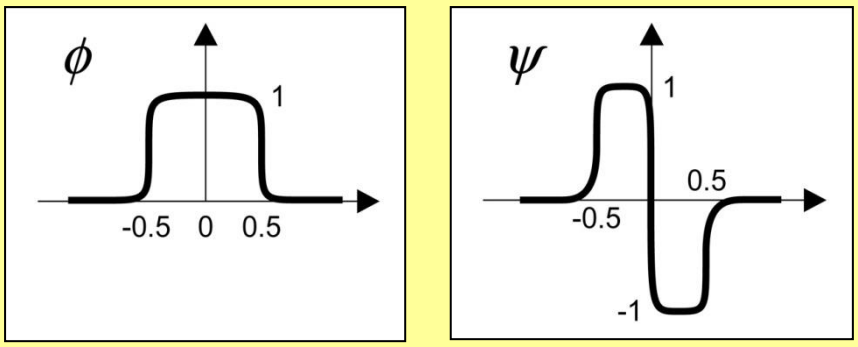


Fig. 16.D.4 – Real scaling and wavelet functions

The parameters that define the wavelet process may be automatically set or controlled by the engineer performing the filtration. In the following list we specify the parameters that will generally be automatic or controlled, and the following sections will describe the influence of the controlled parameters.

- Scaling and wavelet functions ϕ and ψ (automatic)
- Starting data frequency *1/a* (controlled)
- Number of decomposition levels (automatic)
- Choice of threshold function (controlled)
- Threshold value (controlled)
- Post-filtration parameters (controlled)

16.D.5 Selection of the initial time step / frequency

The initial time spacing *a* is very important. *1/a* will be the highest frequency handled by the wavelet algorithm, and behaviour with a higher frequency will be lost in the initial interpolation.

Selecting the smallest time interval between consecutive raw data is not a solution as acquisition times are not regular, and it will not guarantee that the raw data points are taken.

The highest possible frequency, i.e. the smallest possible *a*, (e.g. the resolution of the time information) does not work either as the amount of interpolated data would be unmanageable.

Filtration with an initial interpolation sampling of one tenth of a second would guarantee that we will not miss anything, but it would involve one or several billion points.

Furthermore, starting with a very high frequency has a major drawback. For each additional level of decomposition there is only a doubling of the time stepping. As the number of these decomposition layers is limited, we might miss the frequency of the real noise.

The solution is to select an initial time stepping that fits the engineer's needs. A time stepping of 1 second will work but will involve CPU demands that may not be worth it, and the de-noising of the production data may be insufficient. If the interest is not at all in high frequency data, a time step of one minute will be more than enough and very fast. When one wants to pick the high frequency at a reasonable expense, a time step of 10 to 20 seconds will be a good compromise. The exact point of shut-in may not be spotted exactly, but still the data will be usable for pressure transient analysis, and it will be possible to return to the raw data and selectively reload specific sections of interest.

16.E Wavelet filtration - Practice

The following wavelet filtration work flow is presented as it is implemented in KAPPA-Server; the KAPPA workstation and client / server solutions dedicated to the processing of PDG data. At this stage we do not focus on where the raw data comes from, how it is accessed and where the filtered data is stored. We only focus on the filtration itself and the kind of interface required for the engineer to properly control this process.

The first thing that one has to do when 'connecting' to a PDG data tag is to have an idea of what the data looks like globally. Having a quick preview of the data seems to be an obvious task, but this is not the case when one has to connect to 300,000,000 data points on a slow server. To do this, the process will request, when possible, the total number of data points and request to send one data every n (typically 1,000 to 10,000) in order to get a fast preview of a few thousand points. Such a preview is shown below.

This may be the time for a surprise. In many cases the data were stored and never looked at again. Here are some of the typical, irreversible problems that may be encountered at this stage:

- No data! Data was stored over time, never checked and we only have zeros.
- Buffered data! Only the last, say, three months are present. The data historian was programmed to only buffer the data for so long. Data older than the buffer were irreversibly erased or massively decimated.
- Bad data! Data are very noisy and scattered and hardly usable.
- Massaged or pre-filtered data! In the interest of saving storage or data transmission bandwidth the data has been filtered from one per second to one every fifteen minutes.

Other issues may be detected and addressed:

- Slow access! The time to get this initial preview takes forever. One may analyse the process to get the data or improve the bandwidth between the machine and the data historian. There may also be too many simultaneous accesses to the same historian. This problem will generally be addressed by mirroring the data from the historian to the dedicated server (KAPPA-Server).
- Apparently buffered data! On the face of it this is the same symptom as the buffered data, except that fortunately, in this case, the data is stored. The problem is that the setting of the data historian is such that older data is not accessible to the client unless the historian setting is changed.
- Partly irrelevant data! For whatever reason there were some times when the gauge failed, or was turned off, or for whatever reason gave irrelevant readings. The engineer may then wish to graphically select a data range out of which data will just be ignored.

After the preview, and unless an irreversible problem was detected, the engineer may proceed to set the wavelet filter and post-filtration. At load time the wavelet will be applied on consecutive packs of data of a given buffer size. The first pack of points, within the load range, is loaded and displayed. The typical size of a buffer will be 100,000 points but this can be changed by the engineer. 100,000 points corresponds to six days of data stored once every five seconds.

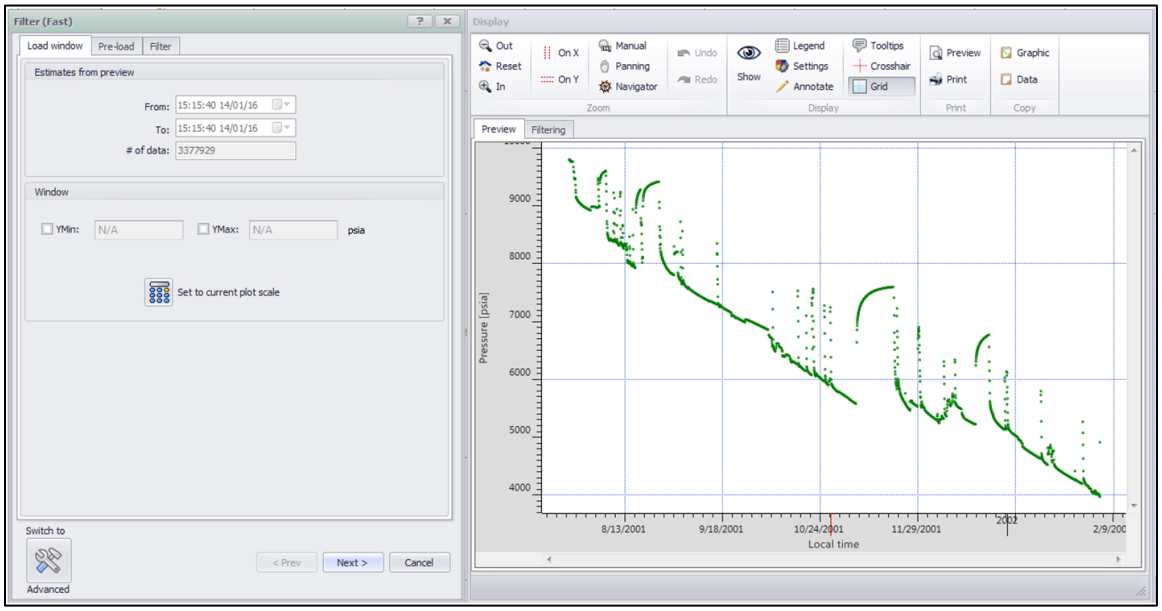


Fig. 16.E.1 – Data preview and selecting the first buffer of points

The engineer will then specify the wavelet and the post filtration. At this stage it is the engineer's decision to set the different parameters, zoom on some parts of the data (shut-ins, noisy sequences, etc) in order to ensure that the data reduction does not affect the information we want to keep in the de-noised signal. An example of wavelet setting is shown below. The process will also show the difference between the original data and the de-noised signal.

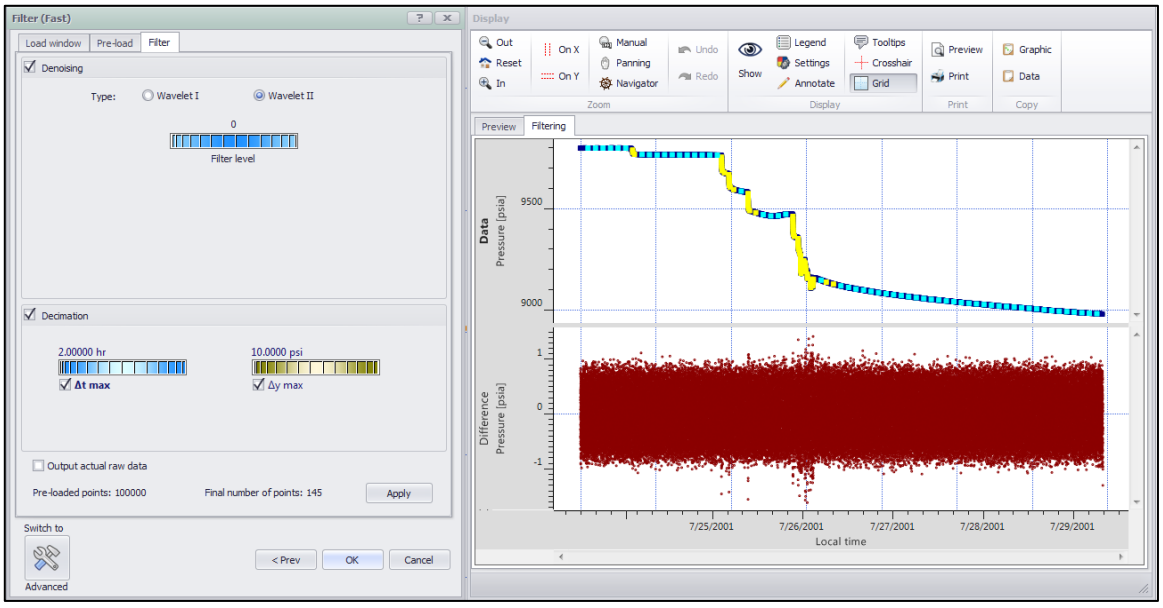


Fig. 16.E.2 – Setting the wavelet filtration and display of the extracted noise

Once the engineer is satisfied by the filter the real load can start. The process takes raw data by packs corresponding to the size of the buffer. In order to avoid tail end effects, the different packs will overlap and the first / last de-noised points will be systematically ignored. The process will typically show the global load, i.e. where the current buffer stands in the overall data history and a local view of the buffered data with both raw and de-noised data. At this stage the engineer may stay and watch. If the data is locally mirrored, the process takes around one second of CPU per buffer of 100,000 points.

During the load the engineer may realize that the filter setting is incorrect. The load can be interrupted and the settings modified and tried. Once the setting is modified the load can be restarted again, or the new setting may take over the old setting from a time selected by the engineer.

Once the load is over, i.e. when all data currently stored in the data historian have been treated, the process stops and statistics are displayed.

At this stage, the application has maintained a persistent link with the data historian and will know how to get the new incoming data. With a time set by the engineer, typically one week, or on the engineer's direct request, the same process will re-establish connection to the data historian, get the new raw data and apply the wavelet filter to this new data to increment the filtered data set. At this stage the engineer probably has better things to be getting on with as the refreshing and updating of data becomes an automatic process.

16.F Pressure Transient Analysis of PDG data

The figure below shows PDG pressure and flowrates data coupled over several months of production, after filtration in KAPPA-Server. The rate history originates from another permanent measurement and was simplified. Buildup periods were defined using the automatic buildup detection functionality available in KAPPA-Server.

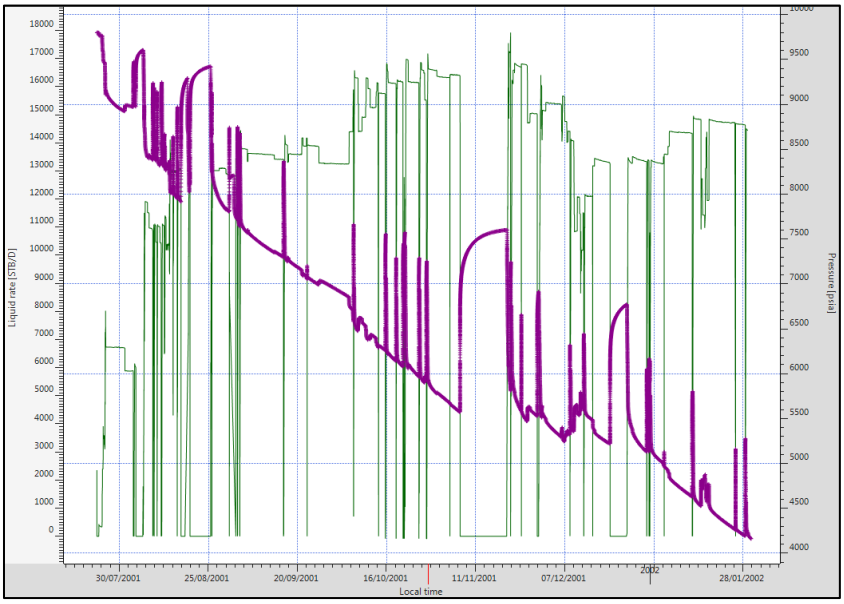


Fig. 16.F.1 – Several months of PDG data - 20 build-ups

Most aspects of Pressure Transient Analysis developed in this document are relevant to interpret buildups recorded by PDG i.e.: there is nothing specific in the methodology itself.

However, the process will have to be adapted to the origin of the data, its volume and its signature. The main differences with a standard well test are the following:

- In most cases, the rate information is the daily reallocated production. Rates are generally not synchronized with pressures. Though it will not be detailed here, with rare exceptions the creation of the rate history will be the main source of trouble after the link with the data historian and the filtration is established. Furthermore, it is now possible to perform the synchronization automatically using KAPPA-Server, in case that this might be an issue.
- There are not one or two shut-ins, but typically 20, 50 or more. Because no engineer will have a spare three months to interpret this data, productivity tools have been developed to process all the buildups in a single work flow.
- Many of these shut-ins are 'free', however they are rarely designed on purpose: they can come from unscheduled automatic safety shut-downs of the wells, well operations or well maintenance. Some of the shut-ins will be too short to carry any relevant information, or they will follow a production phase that may not be stabilized and for which we may not have any rate value. As a consequence, only part of the recorded build-ups will be valid and useable.

- The shut-ins are spread over the life of the well, and one cannot assume that the well model, or at least the skin factor, will be constant throughout PDG recordings. However, the succession of buildups will be an opportunity to study the evolution with time of the well productivity, in particular the skin.

The loaded data is sent from the data module (KAPPA-Server) to the PTA module (Saphir) by drag-and-drop or transferred seamlessly by a click of the mouse. All build-ups are extracted and shown on the loglog plot. Typically, an option will allow the engineer to select only build-ups of a certain minimum duration. The resulting history and loglog plots are illustrated below.

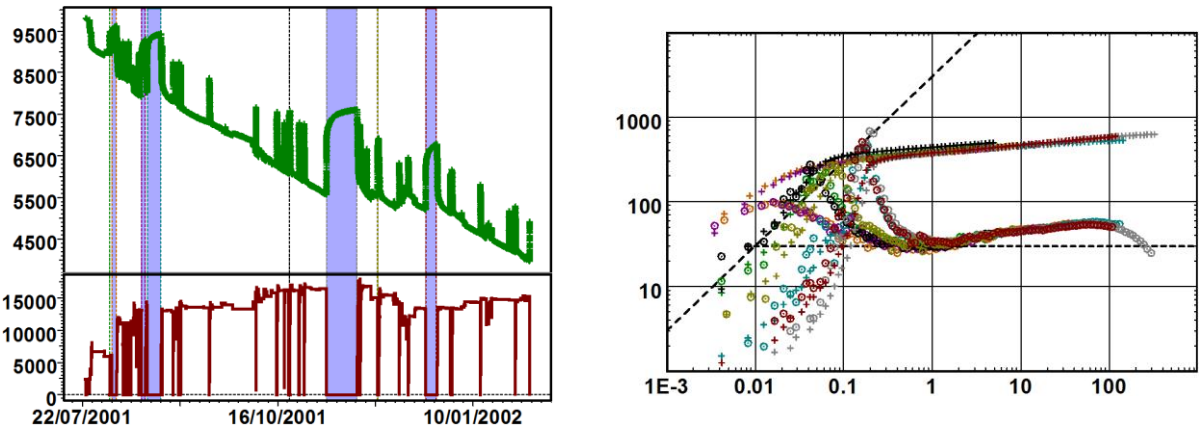


Fig. 16.F.2 – Transfer to PTA software and extraction of the build-ups

The main problem when obtaining 20 to 100 build-ups, is that we certainly do not want to extract and interpret all of them, one after the other. In order to face this problem (too much data!) we need to use productivity tools that will run statistics and qualify the build-ups on which we are ready to spend some time.

One 'low tech' way to do this is to return to IARF (yes, the old stuff). An example of this method is, on the loglog plot, to select the time of stabilization of the majority of the derivatives and draw a series of semilog straight lines from this. An option could be to set a vertical range of acceptable permeabilities, only keep the build-ups which calculated k within this range, then run a global regression where the unknown is one single value of k and one skin value per build-up. The resulting straight lines and evolution of skin in time is shown below.

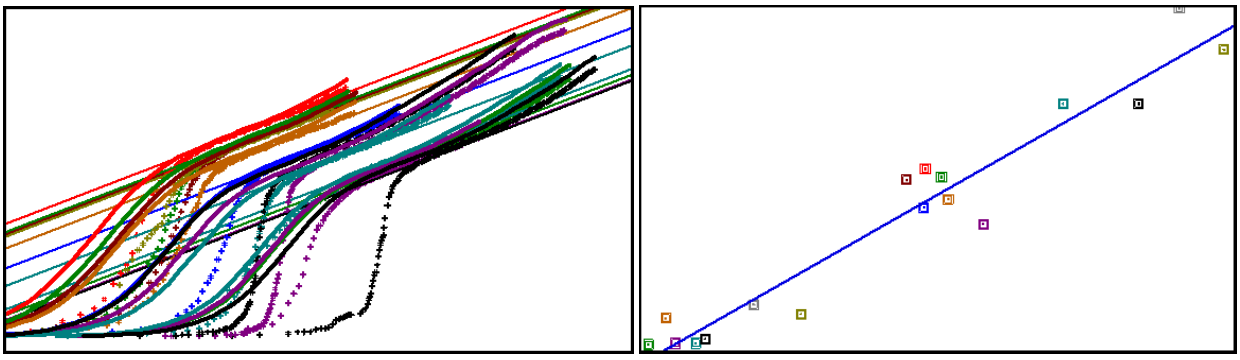


Fig. 16.F.3 – Multiple line analysis with the same k (left) and plot of skin vs. time (right)

Another way to use this information is to select consecutive quality build-ups that tell, more or less, the same story. We can then use recent work on deconvolution to end up with a response that will be longer and may provide more information on the reservoir boundaries and/or the drainage area of the well. This tool must however be used with care. The extracted build-ups and deconvolved responses are shown below.

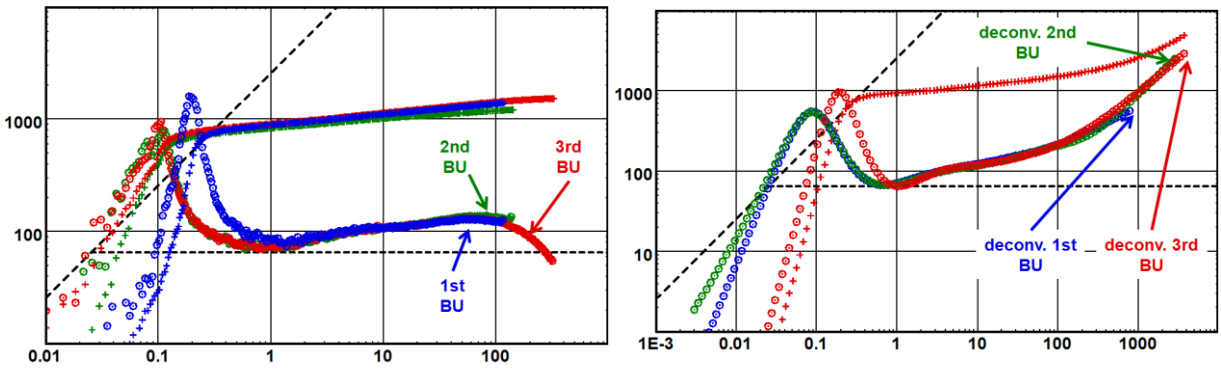


Fig. 16.F.4 – Extraction of three build-ups and simultaneous deconvolution

Once the engineer has focussed on a few build-ups of interest, it may be wise to return to the raw data and reload some of these. After all, what we have loaded so far is the result of a careful but not fool proof filtration. Because the data module (KAPPA-Server) maintains the link with the data historian, it may be possible to re-visit this raw data and, for the time range, corresponding to the build-ups of interest, reload the raw data with a different filter or none at all. The originally filtered data will be replaced by the reloaded data on this time range only. New data will still be loaded with the default wavelet setting.

The original filtered data and the reloaded data are compared in the figures below. In most cases, the wavelet filtration will not have affected the response and could have been used for analysis, but the advantage of the reload is that we are now absolutely sure the signature was maintained.

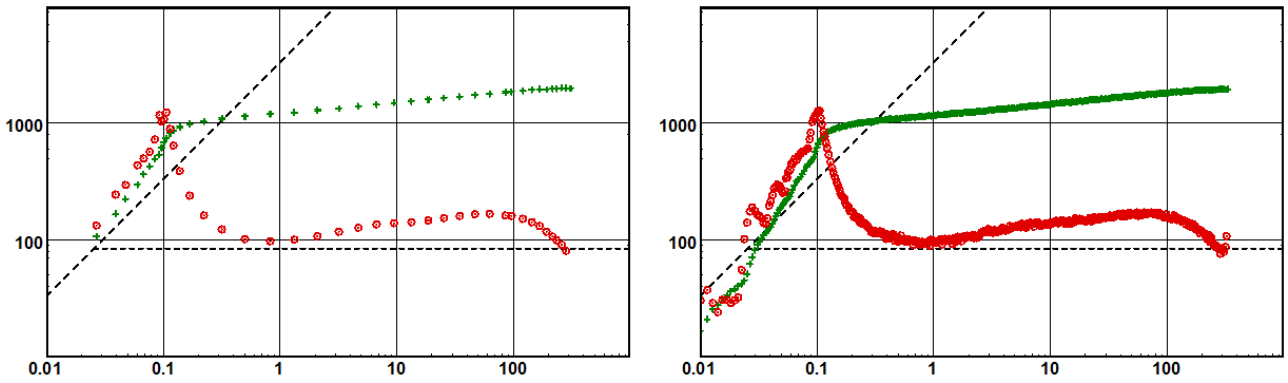


Fig. 16.F.5 – Partial reload to repopulate a build-up with original data

16.G Rate Transient Analysis of PDG data

The data presented in the section on 'Pressure Transient Analysis of PDG data' can also be transferred to the RTA module (Topaze) in order to perform Rate Transient Analysis. The result of this drag-and-drop is shown below. When the producing rates are transferred, the cumulative production is also calculated.

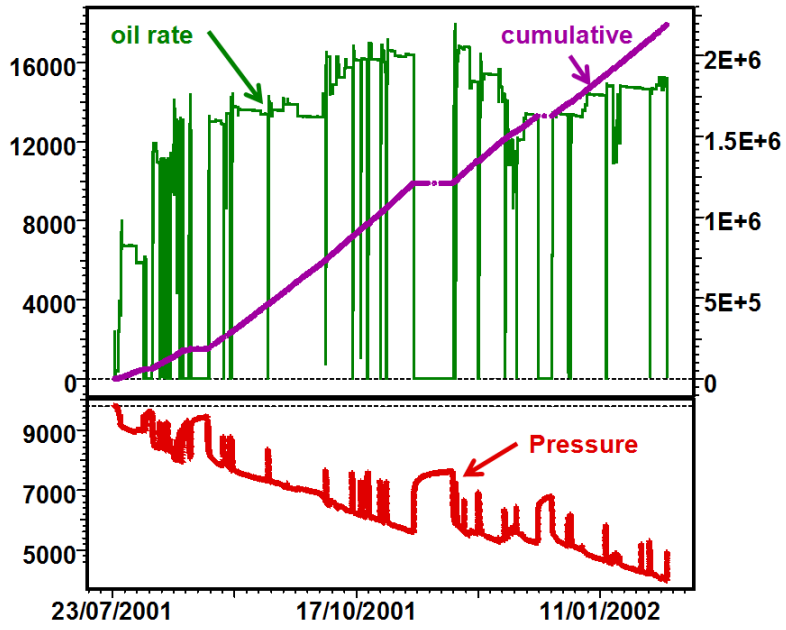


Fig. 16.G.1 – Rate Transient Analysis history plot

Traditional analysis techniques, using type-curves (e.g. Fetkovich) or straight lines (e.g. Arps) are based on the assumption of a constant pressure production. This is the 'old stuff' described in the chapter Rate Transient Analysis. Just looking at the above figure it is clear that the constant pressure assumption is rarely valid; for any practical purpose the traditional (old) methods are not very useful. There is no way to select a reliable curve match in the Fetkovich type curve plot or draw a reliable decline in the Arps plot (there is no decline).

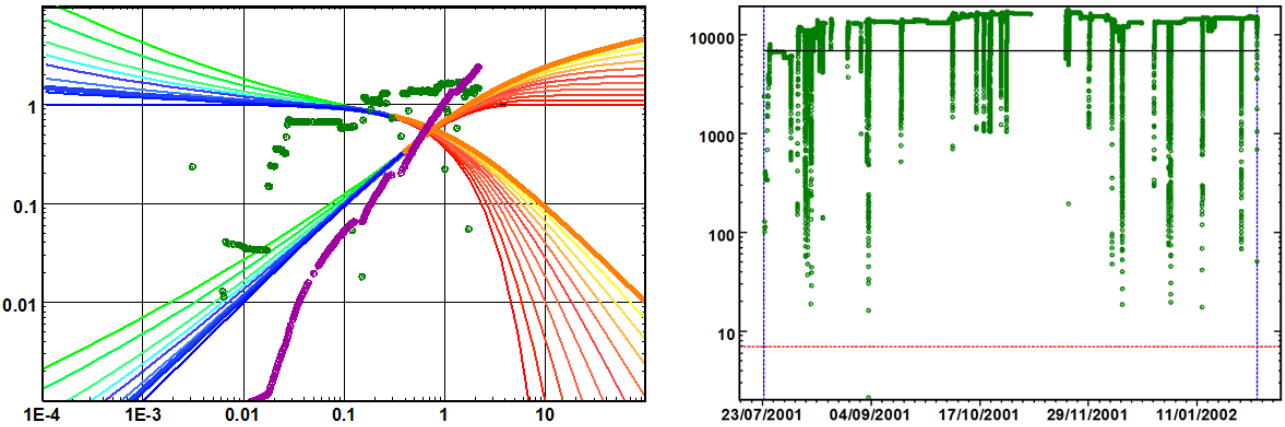


Fig. 16.G.2 – Fetkovich type-curve and Arps plot

The next step in Rate Transient Analysis is the use the modern tools that also takes into account the pressure history. The loglog plot, showing rate normalized pressure, and the Blasingame plot, which plots the productivity index, can be highly scattered as they plot against material balance time, see illustrations below. The models, which are plotted as continuous lines, will jump back and forth when the rate changes. The diagnostic capability is limited as we are essentially matching a cloud of measured points against a cloud of simulated points.

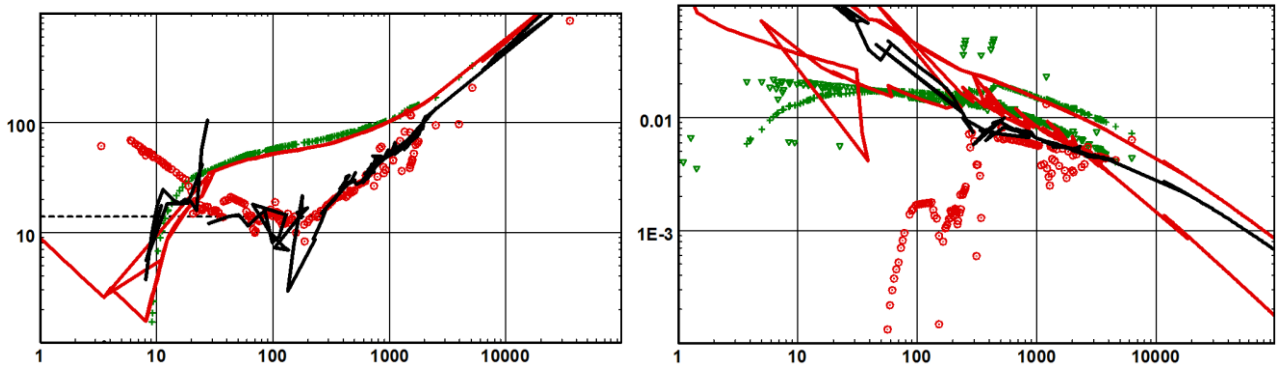


Fig. 16.G.3 – Loglog and Blasingame plots with model 'matching'

Therefore, in the majority of cases the only diagnostic tool will be the history plot, and the goal will be to globally history match the data (see below). Forecasting of the well performance from an anticipated producing pressure is also illustrated below. To improve confidence in the process it is always recommended to use the models found in the PTA of the buildups and constrain the RTA model with that model, eventually integrating the evolution of skin with time.

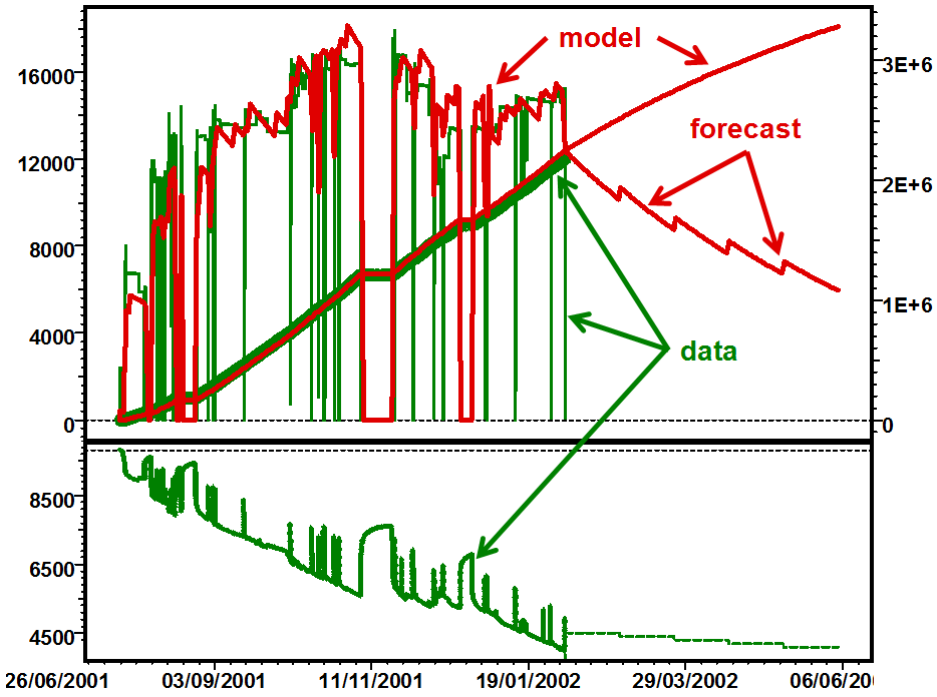


Fig. 16.G.4 – History match and forecast

16.H Applications and data flow

This section is very software related. However, even if you are not a KAPPA-Workstation user it has generic interest as it describes the problem our technical group encountered in implementing PDG data processing. This integration takes place in a single environment (KAPPA-Workstation). This groups three components: a PDG module (KAPPA-Server), a PTA module (Saphir) and a RTA module (Topaze). The goal of this integrated environment is to get together the three aspects of the PDG data processing described in this chapter.

Now, the PDG process is performed by the user through the Kappa Server Client, on a dedicated machine in a shared environment where is installed KAPPA-Server.

In the integrated environment, filtered data are transferred between the PDG and the PTA/RTA modules by single drag-and-drop or using various other internal options. In the next session we will refer to PDG, PTA and RTA processes / modules in order to avoid repetition of commercial software product names.

When this integrated environment was released and tested on a few pilot sites, there was one bit of good news and two bad. The good news was that this process was exactly what operators needed to face the challenge brought by PDG data. However we quickly faced two major issues: the poor access to the data historian and the lack of sharing of this process within a workgroup.

16.H.1 Accessing the historian, Client/Server solution

The historian databases in which PDG data are stored are not designed to provide fast access to, typically, 30 million data points. Even sequential access is poor. It is even worse when a process needs to navigate 'randomly' within the data.

The wavelet processing and filtering can handle 100,000 data points per second. The ability of a data historian to deliver the points will be typically 100 to 1,000 times less.

One of the first feature of our workflow is a mirroring of the raw data. This is sequential and is done, once for all, with only incremental loads on a daily or weekly basis. The data is mirrored using a storage option in order to have fast and random access to the raw data, using a direct binary access format sped up by an indexing that have immediate access to the first data of every calendar day.

The workflow is described in the following figure. There are distinct processes:

- Data mirroring: The engineer connects to the right tag and the mirroring starts as a background process. Because there may be several gauges involved, the mirroring will cycle in an infinite loop on the different gauges until the end of the tags is reached. When the end is reached for a given tag, the mirroring process will re-connect and update the mirror on a timing controlled by the engineer.
- Data filtering: When there is enough data in the mirror to start working on it, typically 100,000 points, the engineer may define the wavelet algorithm and post-filtering according to the process described in section Wavelet filtration - practice. The filtering is executed until the end of the mirror is reached. Once this is done the process will return to the mirror on a timing controlled by the engineer (typically it will require 100,000 more points) and filter the next pack of data.
- PTA and RTA: By drag and drop, or using internal options, the filtered data is sent from KAPPA-Server to the Saphir and Topaze modules for analysis.

- Partial reload: When a build-up is selected, the engineer can, from KAPPA-Server, return to the mirrored data and replace a range of filtered points by the original points, or filtered data with a more refined setting.
- Storage: While mirrored data are stored in the dedicated BLI files, all the rest, including the serialization, is stored in a dedicated KAPPA Server file.

The solution runs on a dedicated server that is continuously mirroring and filtering the data. Export to a third party database allows filtered data to be permanently shared and accessible to third party applications. Filtered data and other objects are stored in a local database and are accessible and may be shared by all engineers. Mirroring is done only once for each gauge. A given gauge may be subject to several filtering options, but the result is also shared.

The workflow is described in the following figure.

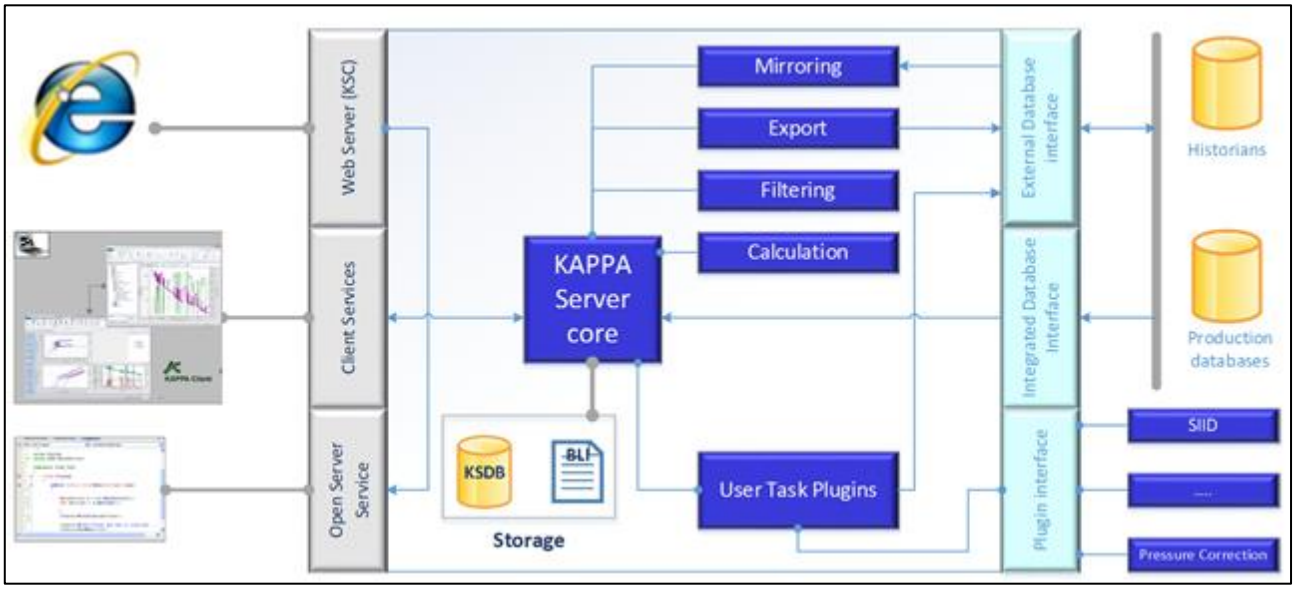


Fig. 16.H.1 – KAPPA Server Client organization of the PDG work flow

Some engineers, given the privilege, may be entitled to mirror tags and create new filters. Others will just take the result of the filtration and drag-and-drop into their analysis applications.

17 – Production logging

OA – OH – NK

17.A Introduction

This chapter is not an exhaustive manual on the interpretation of Production Logs (PL). It does not go into the detail as done for PTA and RTA. However, it summarizes pretty well the history and current status of the methodology, and how PL Interpretation integrates into the analysis of Dynamic Data.

The first production logs were temperature surveys run in the 1930's. The first spinner based flowmeters appeared in the 1940's. They were complemented by fluid density and capacitance tools in the 1950's. Together with some PVT correlations and Flow Models, these were the elements required to perform what we will call today a 'classical' multiphase interpretation.

The first probe tools were introduced in the 1980's. Although they acquired local measurements at discrete points across the borehole cross section, the initial objective was to reduce the local measurements to a normal pipe averaged value. In the late 1990's, these probes were packaged into complex tools that began to measure the velocity and holdup distributions across the pipe in order to address the challenges of understanding the flow in complex, horizontal and near horizontal wells.

PL interpretation was long overlooked by the Industry. Typically, it is not part of the standard Petroleum Engineering course. To our knowledge, few universities include a PL module in the curriculum. With a few noticeable exceptions, most oil companies used to consider that PL was a simple process of measuring downhole rates. Specialized interpretation software was developed and used by Service Companies to process the data, either on-site or in a computing center. This situation changed in the mid-90's, when commercial PL software became more accessible within in the industry, and oil companies began to realize that PL Interpretation was, indeed, an interpretation process and not just data processing.

PL is an in-well logging operation designed to describe the nature and the behavior of fluids in, or around, the borehole during production, injection or shut-in conditions. We want to know, at a given time, phase by phase and zone by zone, how much fluid is coming out of or going into the formation. To do this the service company engineer runs a string of dedicated tools.



Fig. 17.A.1 – An example of tool string

PL may be run for different purposes: monitoring and controlling the reservoir, analyzing dynamic well performance, assessing the productivity or injectivity of individual zones, diagnosing well problems and monitoring the results of a well operation (stimulation, completion, etc.). In some companies the definition of PL extends to what we call Cased Hole Logging, including other logs such as Cement Bond Logs (CBL), Pulse Neutron Capture Logs (PNL), Carbon/Oxygen Logs (C/O), Corrosion Logs, Radioactive Tracer Logs and Noise Logs. In this chapter we will focus on Production Logging per se and explain the main methods in interpreting classical and multiple probe Production Logs.

17.B What Production Logging is used for

PL can be used at all stages of the well life, during the natural production of the well, at the time of secondary or tertiary recovery, or in injection wells.

It is the authors' recommendation that PL be run at an early stage in the life of the well in order to establish a baseline that can be subsequently used when things go wrong. This is generally done when PL is identified as a necessary reservoir engineering tool (for example in extremely layered formations), otherwise it can be a hard sell to Management.

Too often Production Logs are run when 'something' has gone wrong…

At the end of a successful interpretation, the PL engineer will have a good understanding of the phase-by-phase zonal contributions. When multiple probe tools (MPT) are used, this will be complemented by very good looking tracks describing the areal flow.

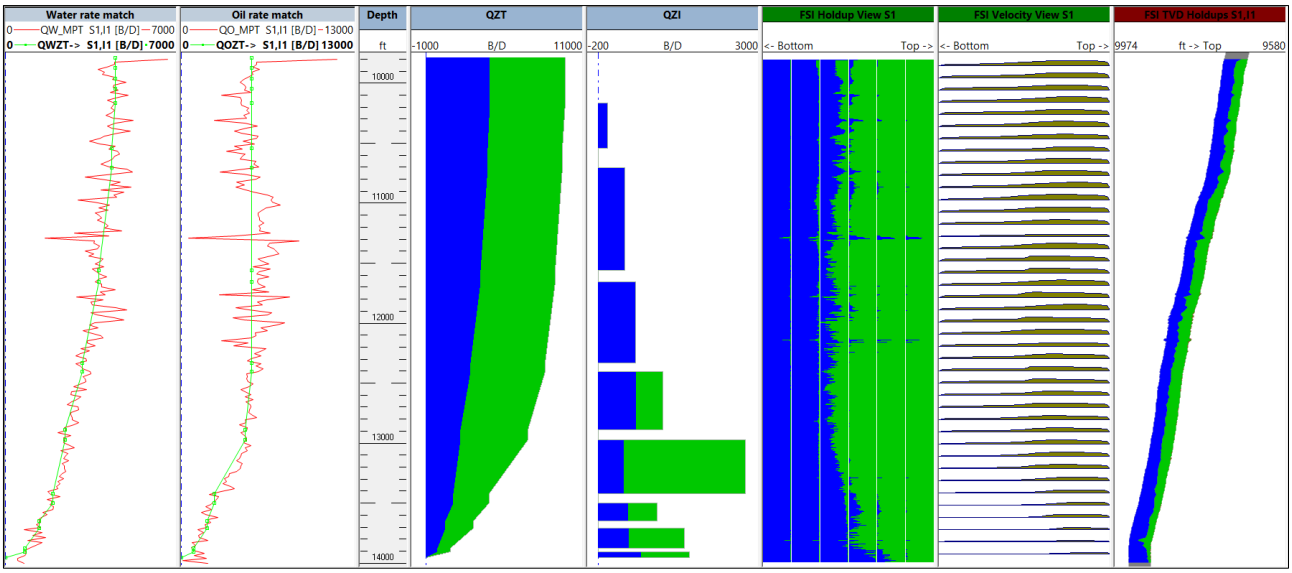


Fig. 17.B.1 – MPT interpretations in Emeraude (FSI)

PL allows the qualification and /or the quantification of a certain number of operational issues: Formation crossflow, channeling of undesired phases via poor cement, gas and water coning, casing leaks, corrosion, non-flowing perforations, etc.

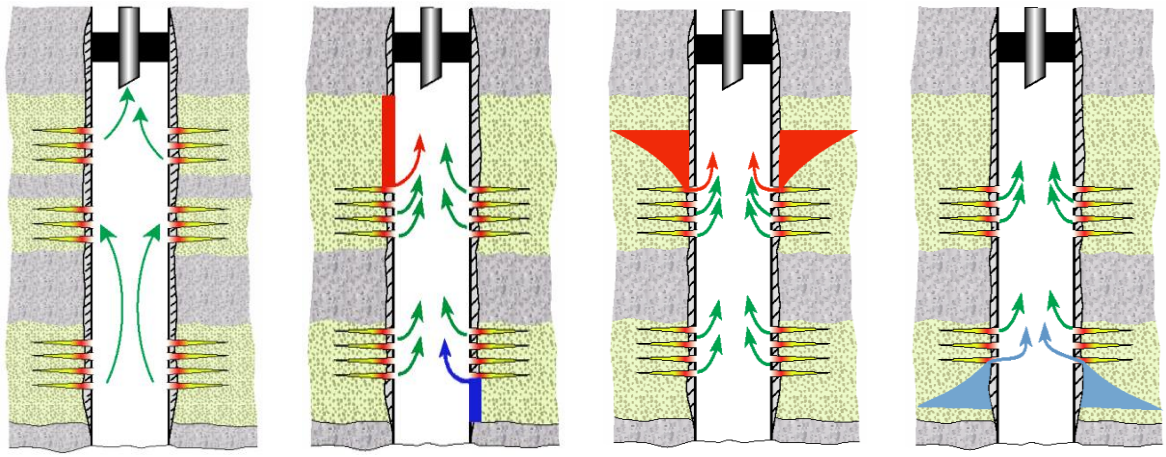


Fig. 17.B.2 – Examples of usage: Crossflow, Channeling, Gas Coning and Water Coning

Production Logging can also be used to identify fracture production and early gas or water breakthrough via high permeability layers. During shut-ins the movement of a water or oil column can also be identified.

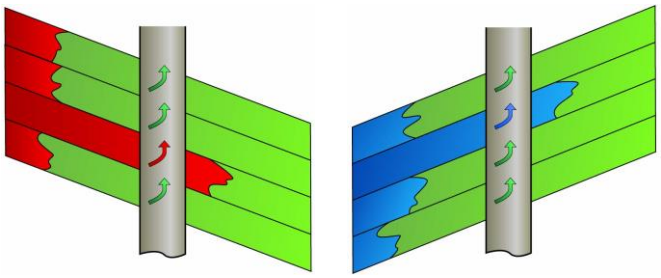


Fig. 17.B.3 – Early gas or water breakthrough

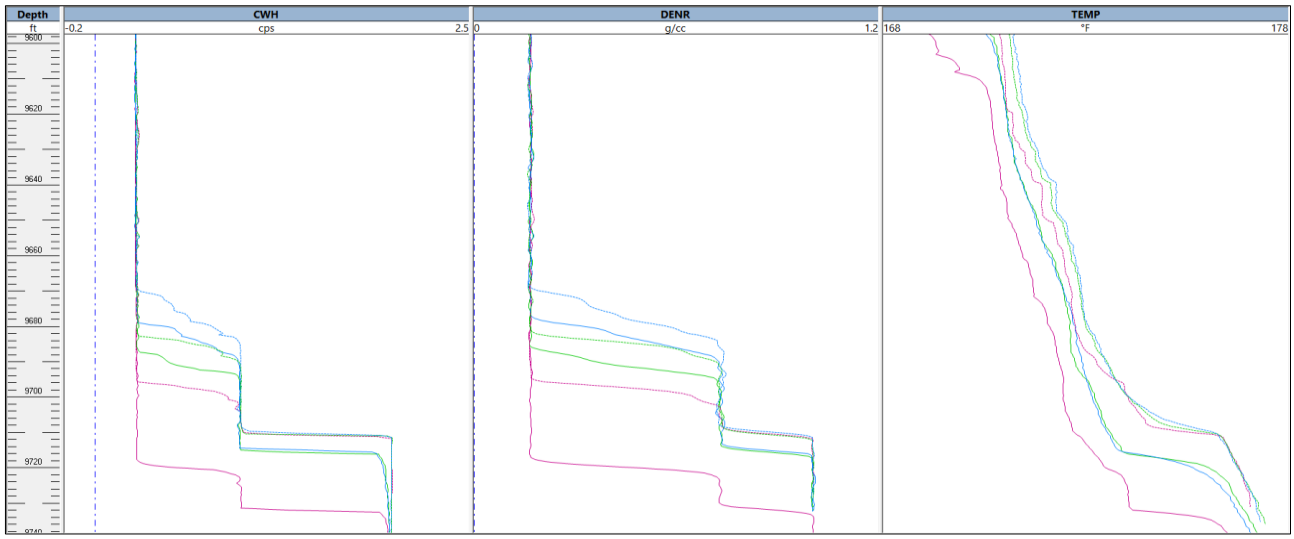


Fig. 17.B.4 – Rise of a water column during a shut-in

17.C Classical Production Logging Tools

The schematic of a typical PL job is shown in the figure below, left. During a stabilized flow period (production, injection or shut-in) the production logging tool string, hanging on a cable controlled by a logging unit, is run up and down in front of the contributing zones at different speeds. There are also static transient surveys, referred to as 'stations', where the tool is immobilized at different depths. From these runs the PL interpretation engineer will calibrate the tools, then calculate a flow profile.

PL tool strings may be run with surface read-out, using a mono-conductor cable, or on slickline. Surface read-out allows a real time quality control of the data at surface. The logging program can then be adjusted depending on the results. The slickline option is less expensive and easier to run. However, it is a blind process, as data are stored in the tool memory. There is no way to check the data before the string is retrieved. Power requirement also limits the range of tools that can be run on slickline.

A typical, classical tool string is shown in the figure below, right. Sensors are not located at the same measure point of the string. As measurements are presented versus depth, they are not synchronized for a given depth, and this may become a serious issue when flow conditions are not stabilized. In some cases, one may have to stop the tool and check for the transients in order to discriminate noisy tools and real effects. Conversely, when running stationary surveys tools are not recorded at the same depth. This issue of time versus depth is the reason why compact tools are recommended to minimize errors due to this limitation.

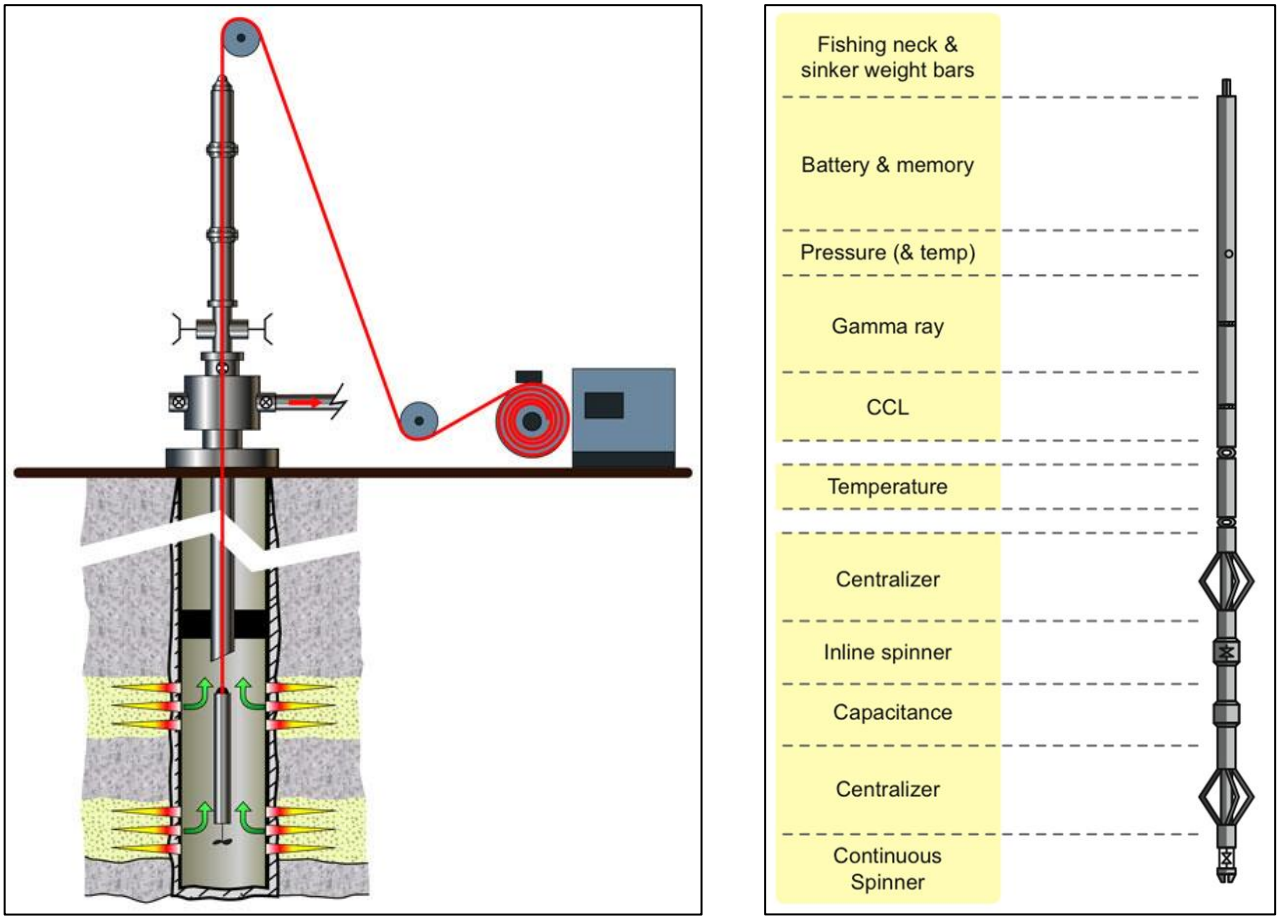


Fig. 17.C.1 – Schematics of PL operations and PL tool string

17.C.1 Flowmeters (spinners)

These are THE tools naturally associated to Production Logging. Despite numerous attempts to use other technologies, the spinner based tools remain the primary way to assess fluid velocities. Even the latest multiple probe tools use micro-spinners placed at strategic points in the wellbore cross-section.

Spinners are of various types, material and shapes, depending on usage. They turn with as little friction as possible, and include internally located magnets which will activate powered Hall effect switches, generating a pulse several times per revolution. If the magnets are asymmetric they provide a way for the tool to detect the direction of the rotation.

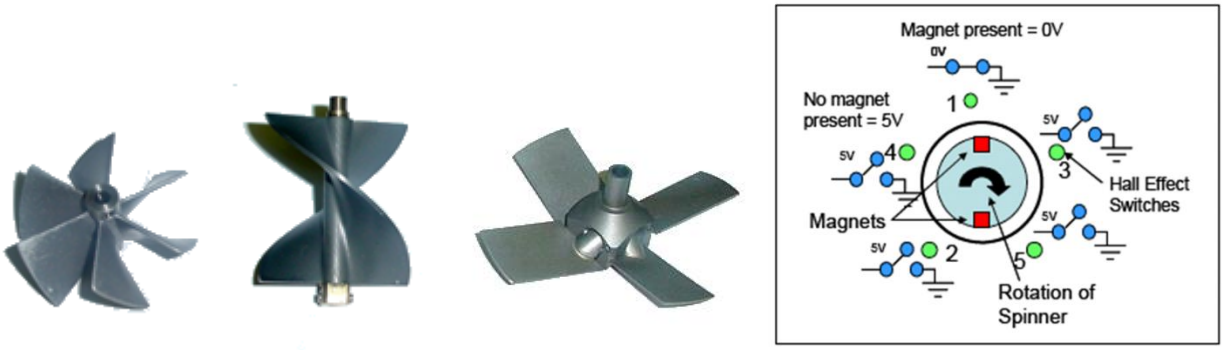


Fig. 17.C.2 – Various types of spinners – Schematic of the Hall effect – Courtesy Sondex

The spinners are packaged in several types of tools. There are three main types of flowmeters: Inline, Fullbore and Petal Basket. Other types are not described here.



Fig. 17.C.3 – Inline, Fullbore and Petal Basket flowmeters – Courtesy Sondex

Inline flowmeters have small diameters and can be used to log in completions with restricted diameters (tubing, scaled up wells, etc.). Conversely they have a lower sensitivity and must be selected to log high rates / high velocity wells. Because of the small spinner size, good centralization of the tool is required.

Fullbore flowmeters have larger blades that are exposed to a greater part of the flow cross-section. The blades collapse in order to pass through tubing and other restrictions. They expand and start turning when the cross-section becomes sufficiently large. Fullbore flowmeters have good sensitivity and can be run for a wide range of flow rates and velocities. There may be issues with injectors where the blades may collapse when the flow coming from above is too great. Many tools (see below) combine the fullbore spinner with an X-Y caliper that will protect the blade and expand / collapse the tool. Such a set-up combining two tools in one, creates a more compact tool string.



Fig. 17.C.4 – PFCS Fullbore flowmeter with built-in X-Y caliper – Courtesy Schlumberger

Petal Basket flowmeters concentrate the flow towards a relatively small spinner. They are highly efficient at low flowrates. However, they are not sufficiently rugged to withstand logging passes and are really only designed for stationary measurements. The tool shape often affects the flow regime.

It is important to realize that spinner-based flowmeters do not measure rates. They do not even calculate the fluid velocity. The output of a spinner based flowmeter is a spinner rotation in RPS (or CPS for some tools). The process of converting RPS to apparent velocity, then average velocity and ultimately rates, is the essence of Production Logging Interpretation and requires additional measurements and assumptions. This is described later in the Chapter.

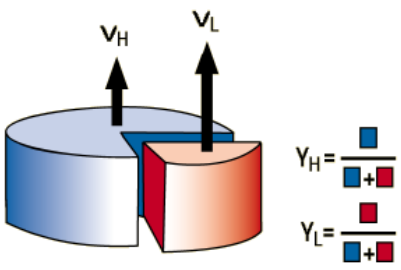
17.C.2 Fluid identification tools

In single-phase environments spinner measurements may deliver flow rates. However, when several phases flow at the same time, the problem becomes under-defined and one needs additional measurements in order to discriminate possible solutions. For generic two-phase flow, the light and heavy phase rates at any depth are given by:

$$q_l = v_l A Y_l$$

$$q_h = v_h A Y_h$$

Where v_l and v_h are the light and heavy phase velocities, and Y_l and Y_h are the light and heavy phase holdups.



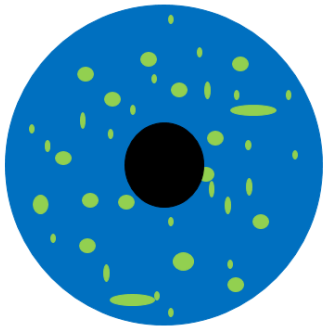
The holdup of a phase at any given depth, is the volume fraction occupied by that phase. The figure opposite shows a heavy (blue) and light (red) phase and indicates the corresponding holdups.

Holdups add up to 1 by definition.

Fig. 17.C.5 – Definition of holdup

For a two-phase interpretation we need at least one fluid identification tool that allows us to make the split of the total rate into light and heavy phases. For three phase flow, an additional independent fluid identification tool is needed. If there are more tools than necessary, one will not be able to match all measurements exactly at the same time, because of the nature of the calculations. More on this later.

The holdups can be measured in two ways: either by direct measurements based on a physical property of the fluids (resistivity, refractive index, dielectric constant), or can be derived from density measurements. We will focus on the latter first.



For two phase flow, the cross-sectional mixture density at any depth is given by:

$$\rho_m = Y_l \rho_l + Y_h \rho_h$$

From this, the heavy phase holdup can be calculated as:

$$Y_h = \frac{\rho_m - \rho_l}{\rho_h - \rho_l}$$

Fig. 17.C.6 – Centerline tool in well mixed fluid

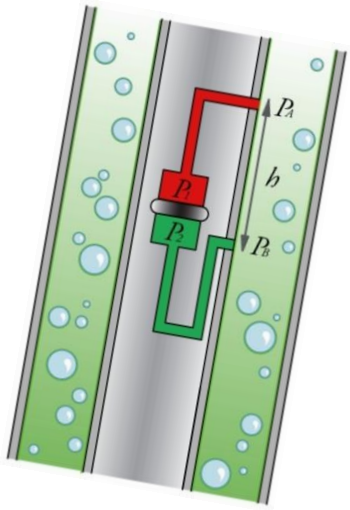
It can be seen that a tool that measures a representative cross-sectional mixture density will allow us to estimate the holdups. The validity of the measurements is largely dictated by the flow regime. In the image above, where the flow is well mixed, a single point measurement can provide a good average mixture density, regardless if the tool is well-centered or not.

It can also be seen that the density-derived holdups require the knowledge of the in-situ light and heavy phase densities. Therefore, a good knowledge of the PVT system is required.

There are four main tools that may give a fluid density: gradiomanometers, nuclear density tools, tuning fork density tools (TFD) and pressure gauges after differentiation.

17.C.2.a Gradiomanometers

The tools measure the pressure difference between either side of a differential pressure transducer. The direct calculation (P_2-P_1) must be corrected for the hydrostatic pressure of the internal column of silicon oil in order to get the effective pressure (P_B-P_A). This pressure then has to be corrected for deviation and friction effects in order to get a corrected density.



$$\rho_{fluid} = \frac{\left[P_2 - P_1\right] - \Delta p_{fric} - \Delta p_{acc}}{gh\cos(\theta)} + \rho_{so}$$

The acceleration term is generally ignored. For a given surface the friction gradient is a function of the friction factor (f, calculated from the Reynolds number and the surface roughness) the density, the relative velocity, the friction surface and the flow area:

Fig. 17.C.7 – Gradiomanometer

$$\left[\frac{dP}{dZ}\right]_{friction} = \frac{f\rho V^2}{8} \times \frac{S}{A}$$

We generally split the friction into tool friction and pipe friction:

$$\left[\frac{dP}{dZ}\right]_{friction} = \left[\frac{dP}{dZ}\right]_{pipe} + \left[\frac{dP}{dZ}\right]_{tool} = \frac{f_p \rho V^2}{2} \times \frac{D}{(D^2 - d^2)} + \frac{f_t \rho V_t^2}{2} \times \frac{d}{(D^2 - d^2)}$$

Even though the tool outputs a mixture density measurement, this is not the final corrected density that is used in the multiphase calculations. Since the friction correction is a function of the fluid velocity and mixture density itself, which are unknown, then the corrected density is calculated as part of an error minimization process and only available at the end of the interpretation.

17.C.2.b Nuclear density tool



This tool contains a gamma ray source and detector, located either side of a chamber with well fluid access. The gamma rays reaching the detectors are attenuated as a function of the electronic density of the fluid, which is in turn related to the volumetric density.

The tool does not require deviation or friction corrections. However, for segregated or stratified flows, typical of high deviations, the fluid filling the chamber may not be representative of the cross-sectional fluid mixture at that depth. The existence of a radioactive source is also an issue.

Fig. 17.C.8 – Nuclear density tool (Courtesy – Sondex)

17.C.2.c Tuning Fork Density (TFD)



The fluid inside the chamber affects the vibration frequency of the resonant fork. The denser the fluid, the lower the resonant frequency. The tool calibration also accounts for the fluid temperature.

As for nuclear density tools there is no need to correct for friction and deviation.

Fig. 17.C.9 –Tuning fork density (Courtesy – Sondex)

17.C.2.d Pseudo-density from pressure

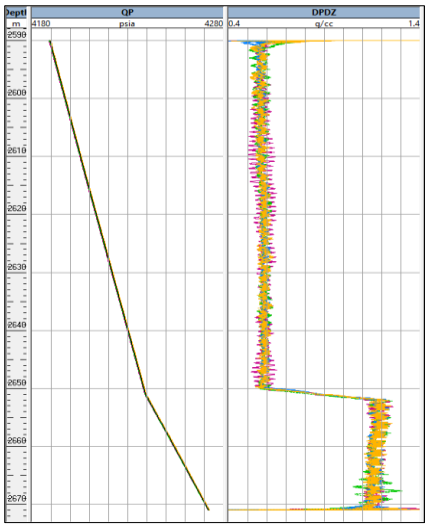


Fig. 17.C.10 – Pseudo-density

The pressure derivative, also called 'pseudo-density', gives an instantaneous picture of the fluid density. The pressure gradient in a flowing well is a function of the hydrostatic, frictional and acceleration components. Therefore, the pseudo-density needs to be corrected for these components. Also, since the derivative is created with respect to measured depth, in deviated wells it is also necessary to enter the deviation survey to account for real vertical depth variations.

Clearly, if the well is unstable, the pressure derivative will exacerbate the pressure variations and it will not be of sufficient quality for quantitative purposes.

17.C.2.e Capacitance tools for water holdup

The dielectric constant of the water and hydrocarbons is around 78 and 4 times the vacuum permittivity respectively. The way to find the dielectric constant of a substance is to put it between the plates of a capacitor This is the principle of the Capacitance tool.

Each tool includes a calibration chart, which relates the capacitance measurements (typically a frequency) to the water holdup. The measurements are typically valid up to 40% water holdup since above this value the conductive water becomes the continuous phase and the capacitor is short-circuited.

This tool is also subject to delays in the response by filming (down passes) and wetting effects (up passes), hence the risk of misinterpretation of the fluid contact.



Fig. 17.C.11 – Capacitance tool Courtesy Weatherford

17.C.2.f Gas holdup tools (GHT)

This tool is designed to calculate the gas volume fraction in the fluid. A transmitter emits gamma rays; the measurement discriminates the gas based on the amount of back scatter, knowing that the gas has a low electron density and a low back scatter.

The tool gives a measurement across the wellbore with no influence from the formation behind the casing. It is not sensitive to deviation and requires no friction correction.

The negative is that it uses a short half-life radioactive source and must be run centralized. Raw counts have to be corrected by the pipe ID, prior knowledge of certain PVT properties and results may be affected by scale.



Fig.17.C.12 – Gas holdup tool Courtesy Sondex

17.C.3 Pressure and Temperature sensors

Pressure and Temperature measurements are used directly or indirectly and they constitute two very important components of any PL string.

Pressure is required for PVT calculations; it can be used as an indication of the production stability; it can supplement a missing / faulty density measurement when differentiated; it provides one of the key information sets required for Selective Inflow Performance (SIP).

Pressure gauges can be divided into Strain or Quartz gauges. With strain gauges, the mechanical distortion caused by the applied pressure is the primary measuring principle. There are several sensor types based on Bourdon tubes, thin-film resistors, sapphire crystals, etc.

In Quartz gauges, a quartz sensor oscillates at its resonate frequency. This frequency is directly affected by the applied pressure.

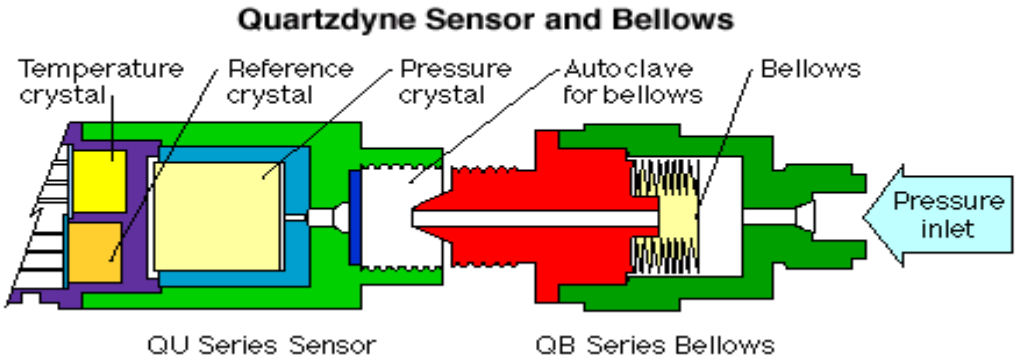


Fig. 17.C.13 – Quartz sensor example (Courtesy Quartzdyne)

As with pressure, temperature is used in PVT calculations. It can also reveal flow outside the wellbore because of a cement channeling leak for instance. The temperature can be used quantitatively, provided an adequate forward model for calculations is available. Chapter 18 presents a comprehensive description of temperature measurements and its qualitative and quantitative application.

17.C.4 Depth and ID devices

17.C.4.a Depth measurement

When the cable exits the drum, it goes through dual tangential measuring wheels of known radius. Integrating the number of turns allow us to determine the length of the cable passing through. The depth measurement does not consider possible stretch of the cable or conversely slack due to, for instance, deviation or restrictions. Tension measurement can be used to spot such cases. As previously mentioned, the log data needs to be offset in time to be displayed at the same depth. This is because the various sensor measurement points are at different depths.

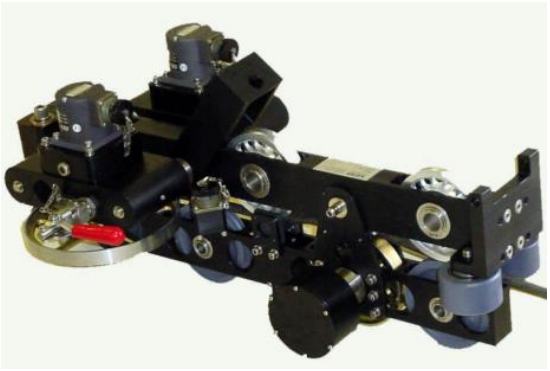


Fig. 17.C.14 – Depth measuring device Courtesy NOV ELMAR

17.C.4.b Depth correction: Open Hole Gamma Ray

The tool 'zero' is set at surface when the log is run. The first task in the data QAQC is to set the log data consistently with the other available information: completion, perforations, etc. This can be achieved by loading a reference Open-Hole Gamma Ray and shifting the acquired data so that the PL and Open-Hole curves overlay. The presence of naturally occurring radioactive minerals and scale can be detected by this measurement. In these cases, it is normally not possible to compare the PL GR with the OH GR for correlation purposes.

17.C.4.c Depth correction: Cased Hole CCL

The CCL contains two permanent magnets with a coil between them. Variations in metal thickness will lead to a change in the magnetic field, which in turn generates a voltage change (Faraday's law of induction). Therefore, the CCL can detect the presence of collars, packers and other metal thickness variations.

17.C.4.d Depth correction: Cased Hole MML

The Magnetic Marker Locator (MML) is a magnetic field measurement. The presence of the different completion elements will lead to anomalies on the measured earth magnetic field. Similar to the CCL, the MML can detect the presence of different completion elements, even though the signature of these two measurements in not necessarily similar.

17.C.4.e ID calculation: Calipers

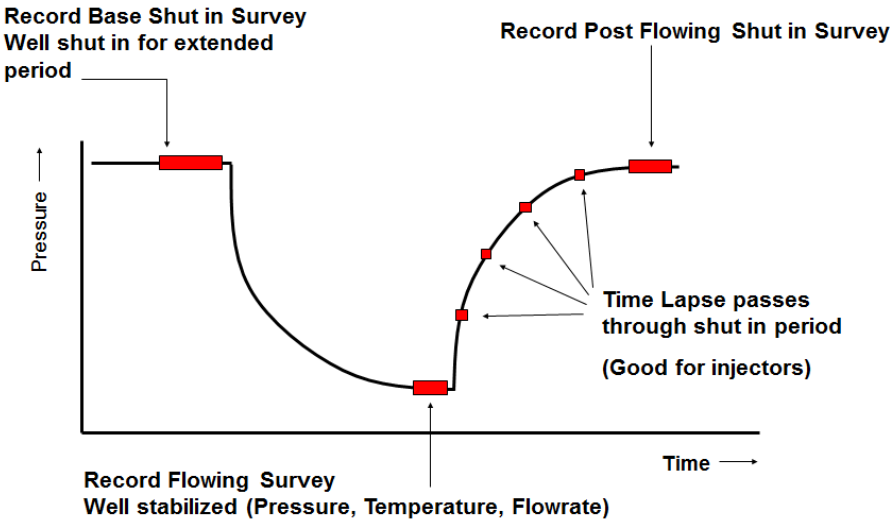
Calipers are mechanical devices used to calculate the cross-section of the wellbore. They are critical since the cross-section must be known to convert velocities to flowrates. Even in cased holes, a completion diagram may not reflect the reality. Calipers can be integrated in the spinner tool or as a separate device. They usually measure the diameter in two orthogonal directions; in this case they are referred to as X-Y calipers. For such calipers, the ID at every depth is calculated as: $\sqrt{(X^2 + Y^2)}$. These measurements can also give information about different integrity issues, such as pipe ovalisation, deposition, leaks, etc.



Fig. 17.C.15 – Independent X-Y caliper; X-Y caliper combined with fullbore spinner
Courtesy Sondex and Schlumberger

17.D A typical PL job sequence

The basic assumption in Production Logging is that the well is in steady state. It is therefore important that the well be stabilized before running the tools. A typical job will consist of several surveys corresponding to different surface conditions. Shut-in surveys are also recorded with the goal being to calibrate the tools in an environment where the phases are segregated. Shut-ins can also reveal crossflow due to differential depletions; they provide a reference gradient in shut-ins; they provide a baseline for a number of measurements in flowing conditions, e.g. temperature.

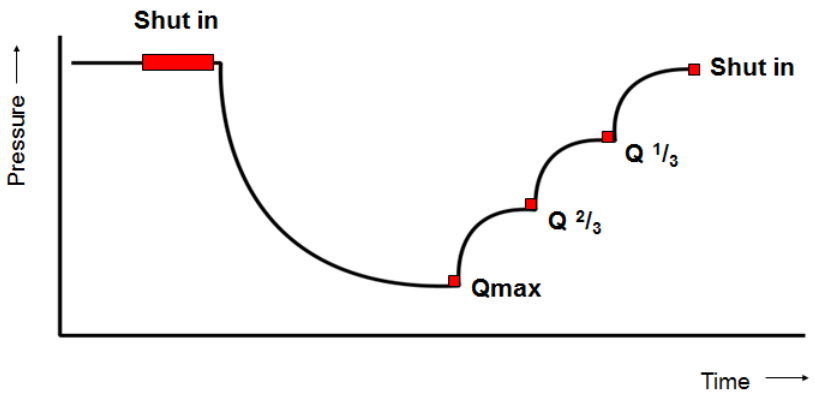


Part of the job planning is to account for the time it will take for the well to stabilize. The notion of stability is defined as a pressure variation over time since we know from welltest that the flowing pressure will usually not be strictly constant. Time lapsed passes will be interesting to record evolution with time, for instance, the warmback following an injection period.

The job sequence is also determined by operational constraints. For example, some liquid-loaded gas wells cannot be shut-in since the well would be immediately killed. On the other hand, in some locations it is mandatory to shut-in the well before rigging up the tool and lubricator.

Multirate PL and SIP

In order to get Selective Inflow Performance (or SIP) it is necessary to achieve more than one rate. Typically, 3 rates and a shut-in are recorded, as illustrated below. The SIP methodology is presented in Section 17.M.



17.E Typical job

In a single-phase situation, a typical tool string will comprise temperature and pressure, spinner, and caliper. No further information is required, assuming of course that the flow conditions are indeed single-phase. It is not uncommon to encounter fluids downhole that are not produced at surface. If in doubt, it is always better to add a fluid identification tool in the string, such as density or holdup, before running the job.

In a multiphase situation, there are n-1 additional unknowns, n being the number of phases. So, in two-phase flow, a density or holdup is required, and in 3-phase, two such independent measurements are required.

For all tools, except the spinner, one pass could be sufficient for calculation. However, comparing several passes for other tools is a way of judging the well stability. Having multiple passes also provides a better chance of having a representative measurement if the data is bad on some section of some passes.

The spinner calibration, which is explained next, requires several passes at various logging speed. A typical job will comprise 3-4 down and 3-4 up passes, as illustrated below. Passes are normally numbered by increasing speed, and the slow passes are recorded first. This means that Down 1 is normally the first and slowest pass in the well.

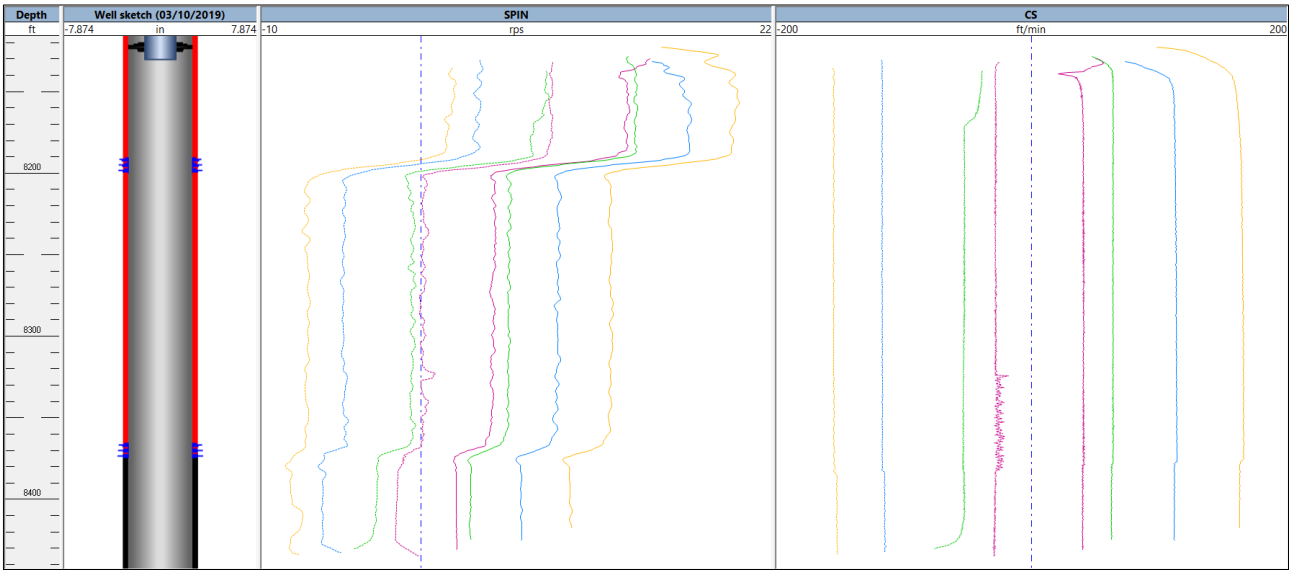


Fig. 17.E.1 – Spinner and cable speed for an 8-passes job

Stations may be recorded for certain tools that require it. In addition, the ability to display the measurement of a station versus time is a further indication of well stability or instability.

17.F Data loading, QA/QC, and reference channels

The first task after the job is run is to load and review the log data for QAQC. The following is a list of checks and possible actions.

Data editing - general: telemetry errors can introduce spikes on data which in turn will upset the scaling and make the QAQC difficult. De-spiking should be achieved beforehand to avoid this problem using, for instance, a median filter. Some tool responses, such as nuclear, may also be noisy and will usually require processing with a low-pass filter.

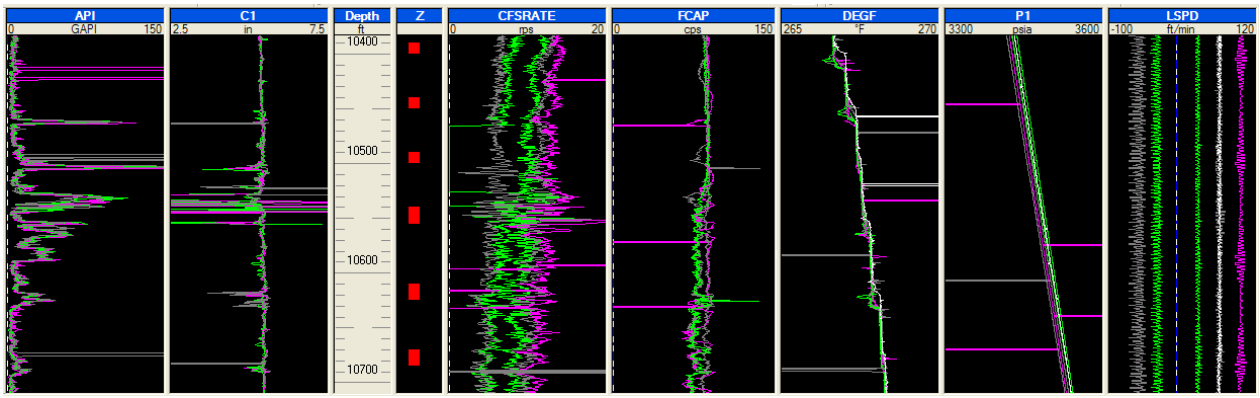


Fig. 17.F.1 – Example of telemetry spikes

Data editing – spinner / cable speed: when starting fast passes 'yoyo' effects may be seen. Similarly, oscillations may appear on the flowmeter as a result of the cable sticking/slipping along the length of the completion. These can be edited out with sliding window averaging.

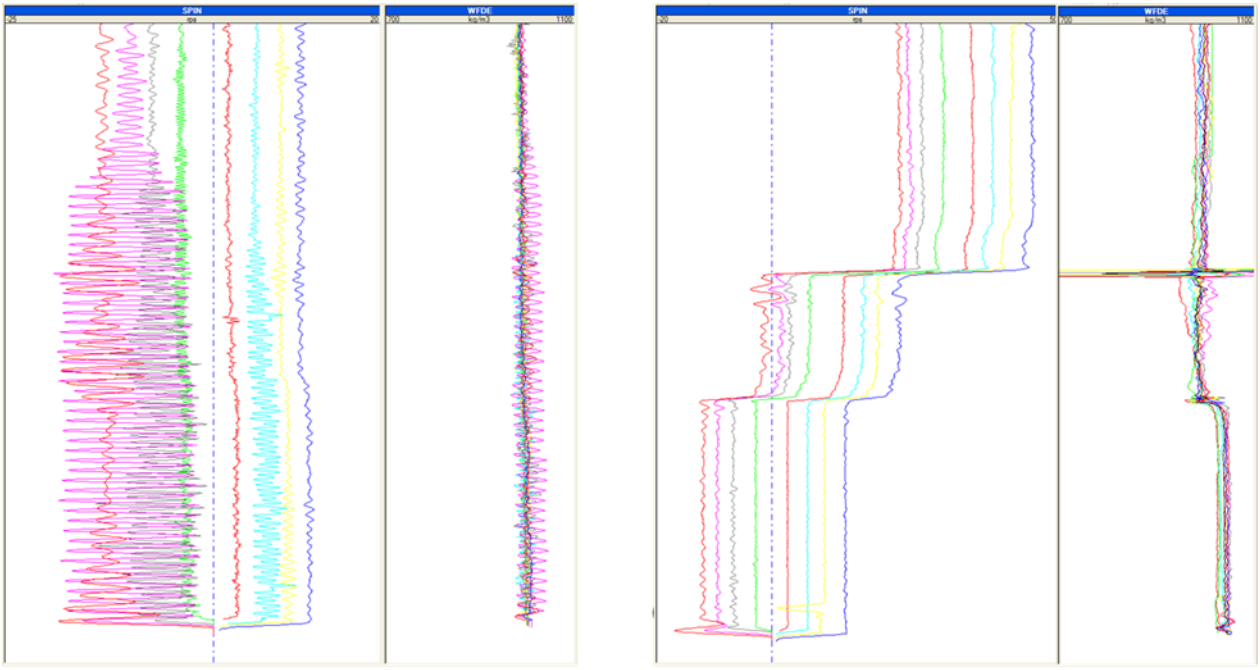


Fig. 17.F.2 – Stick & slip (left) and yo-yo at start of passes (right)

Unsigned spinners will need to be corrected before processing, on Up passes in producers and Down passes on injectors.

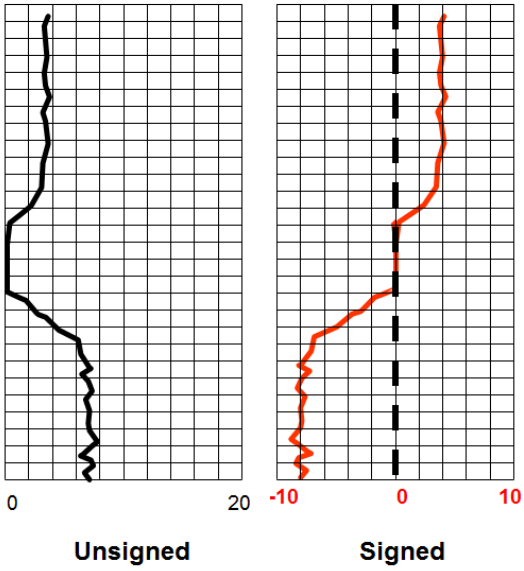


Fig. 17.F.3 – Comparison of unsigned/signed responses

Depth matching: using the Gamma Ray or CLL all the available data should be set with coherent depth. Sometimes the depth correction may require more than a shift.

Repeatability: the repeatability of readings from one pass to another will be an indication of the well stability. Some tool readings are affected by the cable speed when the fluid mixture changes drastically (density, temperature for instance) and this should be noted as it will orient the choice of reference channels for the calculations.

Consistency: a first consistency check between sensors can be done at this stage. Beware that some tools will need corrections before they can provide a quantitative answer (e.g. a pseudo density – dP/dZ - in a deviated well). Some tools react to what happens behind the tubing or casing (e.g. the temperature) and will behave differently from the spinner.

Qualitative analysis: once all data have been cleaned, most of the questions can be answered qualitatively but there are some pitfalls, such as mistaking a change in spinner response to an inflow/outflow when it is in fact due to a change in ID.

Reference channels: for any measurement that will be used quantitatively in the interpretation, a single curve must be selected or built. Most of the time this curve will be the slowest down pass but some editing or averaging may be necessary. This procedure will not apply to the spinner that needs to be calibrated first, in order to calculate velocities, before we can define or build the reference velocity channel.

17.G Spinner calibration and apparent velocity calculation

To conduct a quantitative interpretation, the spinner output in RPS needs to be converted into velocity. The relation between RPS and velocity depends on, amongst other things, the fluid property and, for this reason, an in-situ calibration is required.

17.G.1 Spinner response

The spinner rotation depends on the fluid velocity relative to the spinner; this is a function of the fluid and the tool velocities. The usual sign conventions consider that the tool velocity is positive going down and negative coming up. Similarly, the spinner rotation is counted positive when the fluid is seen by the spinner as coming from below, and negative when it is seen as coming from above. With these conventions, the spinner rotation is relative to the sum: Cable Speed + Fluid Velocity.

The response of an ideal spinner run in a static fluid would be as plotted below, with 2 distinct response lines for Up passes (negative CS) and Down passes (positive CS).

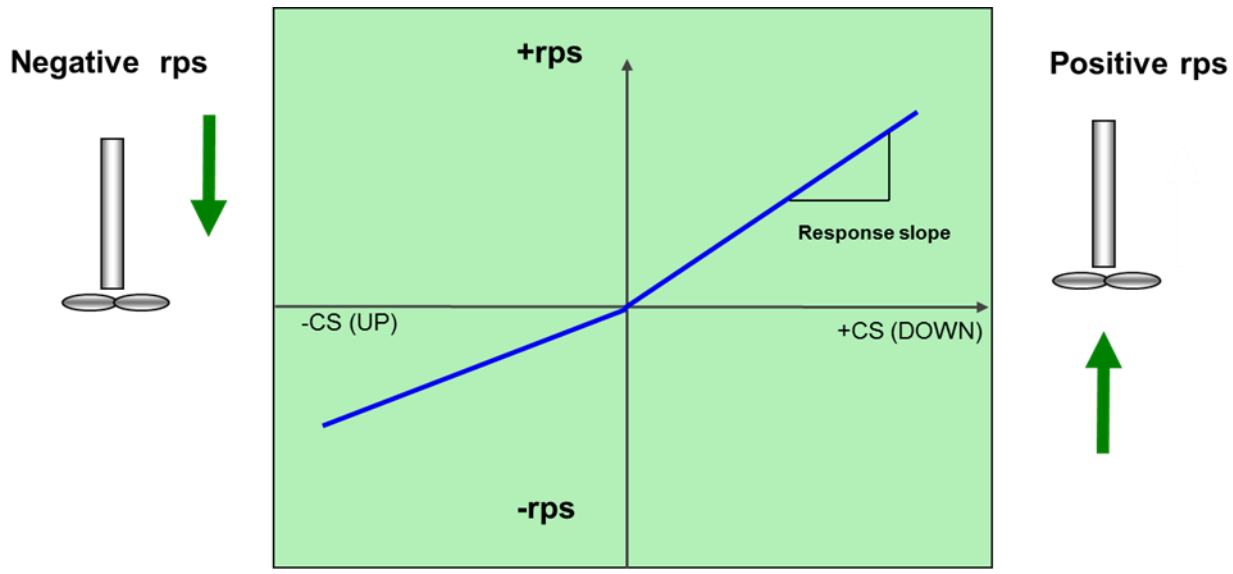


Fig. 17.G.1 – Ideal spinner response (in a no-flow zone)

(1) The rps value is a linear function of the velocity; the response slope depends on the spinner pitch; i.e. its geometry only.

(2) The spinner rotates with the slightest movement of the tool, i.e. the slightest movement of fluid relative to the tool.

(3) The negative slope is lower, typically as the tool body acts as a shield; this is not the case with a symmetrical tool like an in-line spinner.

In reality, the response is affected by the fluid properties as well as the bearing friction. The equation below is a possible representation (SPE Monograph Vol. 14; Hill A.D.):

$$rps = aV_{fs} - \frac{b}{\rho V_{fs}} - c\sqrt{\frac{\mu}{\rho V_{fs}}}$$

For PL interpretation we will consider that the calibration is still a straight line. Since this line is approximating a non-linear function, it may vary with the encountered fluid. In addition, the tool response is shifted by a threshold velocity, the minimum velocity required for the spinner to rotate. This threshold velocity will depend on the fluid; typical numbers for a fullbore spinner are 3 to 6 ft/mn in oil, 10 to 20 ft/mn for gas.

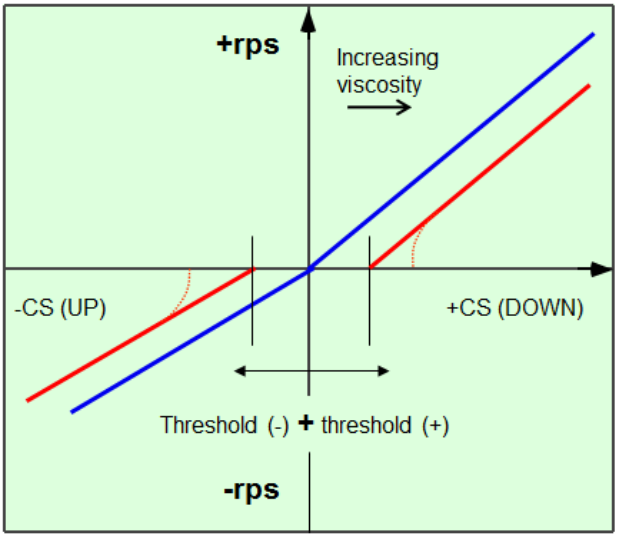


Fig. 17.G.2 – Real spinner response (in a no-flow zone)

The plot above represents the spinner response in a no-flow zone as a function of the cable speed. If the fluid is moving at some velocity V_{fluid}, the tool response will be the same, but shifted to the left by V_{fluid} as shown below. The reason behind the shift is that since the spinner reacts to the sum of (V_{fluid} + Cable Speed), the rps value for a CS value 'X' in V_{fluid}, is the response to a CS value of (X+ V_{fluid}) in the no-flow zone.

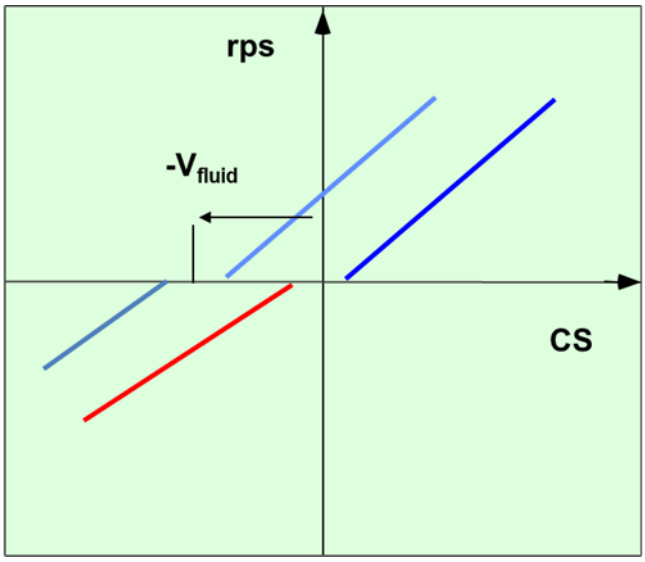


Fig. 17.G.3 – Real spinner response in a no-flow zone, and a zone with production

17.G.2 Spinner in-situ calibration

In practice the objective is to build the calibration response in-situ to take into account the changing fluid properties and their effect on the spinner calibration. The image below shows the spinner RPS, cable speed and density. Three different fluids can be identified, and therefore it is necessary to obtain three sets of calibration parameters since the spinner will respond differently to the changing fluid properties. Zones in yellow represent the spinner calibration zones, whilst zones in red represent the perforations

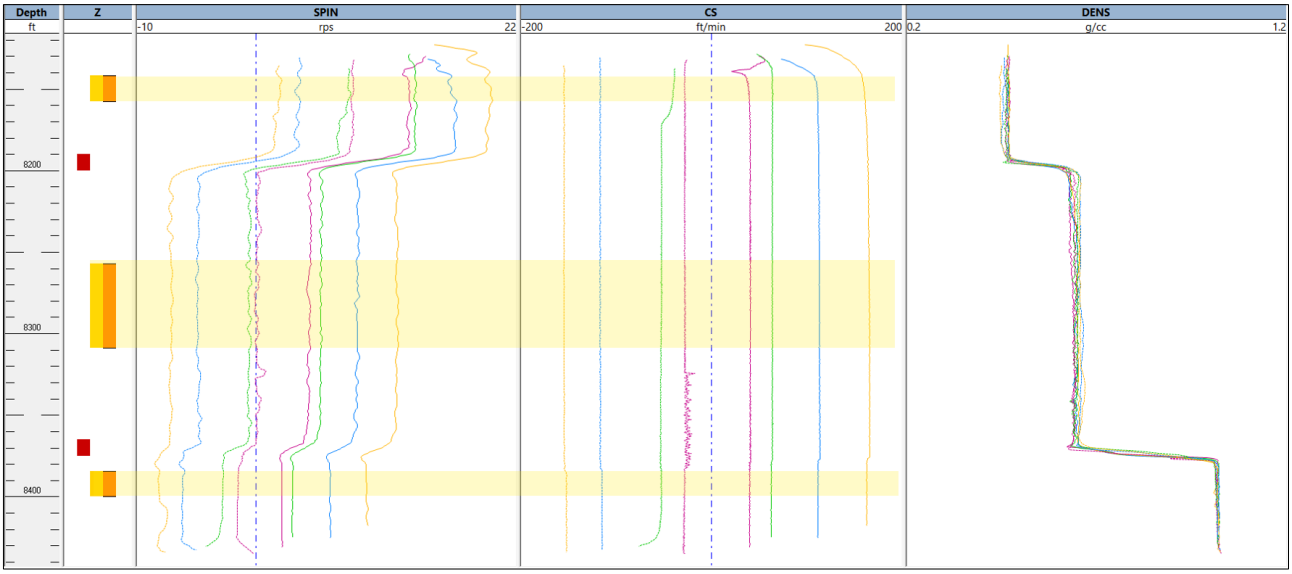


Fig. 17.G.4 – Spinner calibration zones

For each spinner calibration zone, the average spinner RPS and cable speed are plotted in the calibration cross plot. The lines are drawn by linear regression:

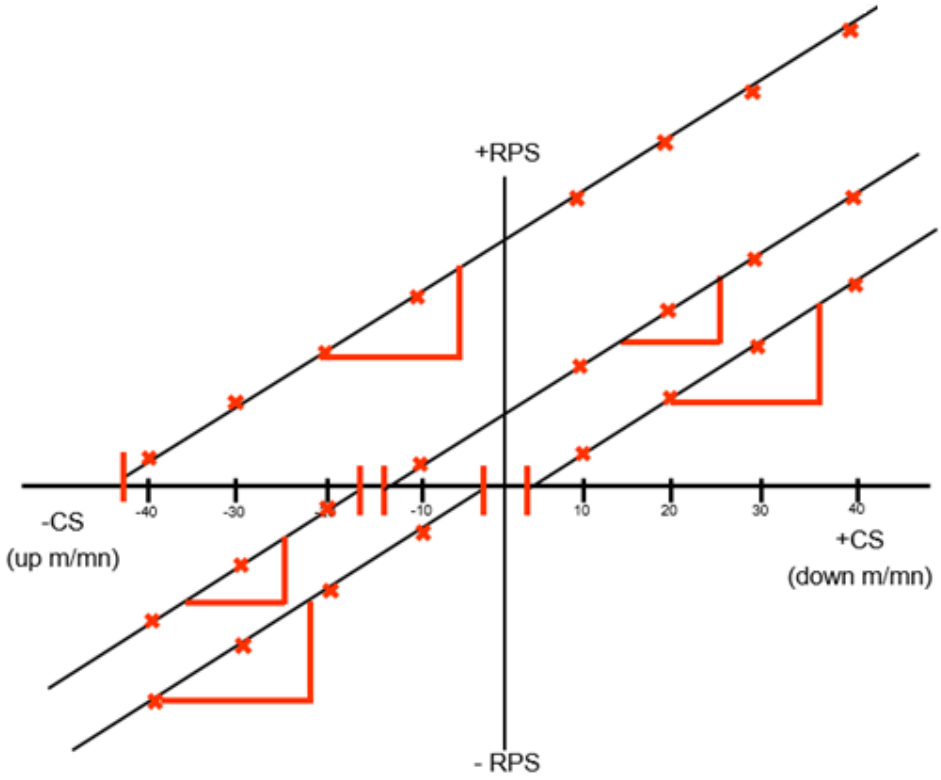


Fig. 17.G.5 – In-situ calibration for the case above

Historically when doing hand calculations, the usual method was to consider a spinner calibration zone in stable regions in-between every perforation, as above. The velocity was then calculated directly from the cross-plot for every zone. Today's idea is that you only put in spinner calibration zones because you think there has been a change of slope or threshold, (usually due to a change of fluid type). In theory a single phase well only needs one spinner calibration zone. In reality, having multiple zones, as long as they are stable, ensures that any change is properly captured.

17.G.2.a Spinner Calibration application zones

In situations such as in Figure 17.A.4, where more than one set of calibration parameters are calculated, it is necessary to establish what parameters are used where. The Z track shows three orange zones called Spinner calibration application zones. By default, these are of the same size as the spinner calibration zones. Three options to control the transitions are offered in Emeraude:

- Interpolation: between the spinner calibration zones the slopes and thresholds are interpolated using a distance-weighted approach. This is the default transition method.
- Sharp: the spinner calibration application zones are in contact, and therefore a single transition depth is defined between two zones.
- Free: The length of the zones is typically adjusted to encompass one fluid. In the gaps between two zones, a linear interpolation of the calibration parameters will be applied.

17.G.3 Velocity from calibration: threshold handling and Vapparent

The calibration does not give the fluid velocity directly and some calculation or assumptions remain to be done. If the response of the various sections were strictly parallel, we know from the previous discussion that the fluid velocity could be obtained by estimating the horizontal translation between, say, the positive line of a given zone and the positive line of the no-flow zone. This method is fine for manual analysis, but it is quite limited. A general approach needs a systematic way of handling slope and threshold variations.

17.G.3.a Threshold options

Below are the options given in Emeraude.

Unique value of (+) and (-) thresholds for all zones

The apparent velocity for a point on a positive line is calculated based on the slope of that line and the common positive threshold. The apparent velocity for a point on a negative line is calculated based on the slope of that line and the common negative threshold. This mode is suitable in case of single-phase fluid.

Distinct thresholds, unique ratio threshold(-)/[Intercept(-) – Intercept(+)]

This ratio is equal by default to **7/12** = **0.583** but can be set from the value of a no-flow zone. Obviously, this can be used only on zones with both positive and negative intercepts.

Independent Thresholds

This mode allows different thresholds for each calibration zone and is the most general. Note that the only problem with this mode is that on a zone where there is fluid movement, at best we can get the sum of the thresholds. Deciding the positive and the negative can be done bluntly (i.e. halving the sum) or based on the split on the no-flow zone.

17.G.3.b Apparent Velocity

No matter what method is used, we will end up with a measurement of velocity that represents the fluid velocity seen by the spinner. This value is the average velocity in the cross-section covered by the spinner and it is different from the actual fluid average velocity. For this reason, it is referred to as apparent velocity, noted Vapparent or V_{APP}.

17.G.4 Apparent velocity log

After the calibration is complete and the transitions between zones are defined, the goal is to obtain a continuous apparent velocity curve representing the velocity at every depth. This can be calculated based on the following equation:

$$Vapp = \frac{RPS}{slope} - CS + Th$$

Where RPS and CS are taken from the logs, and the slope and threshold are calculated from the spinner calibration for each zone.

This can be done graphically for each depth, by plotting the pairs RPS-CS, extrapolating to zero RPS using the slope and correcting by thresholds.

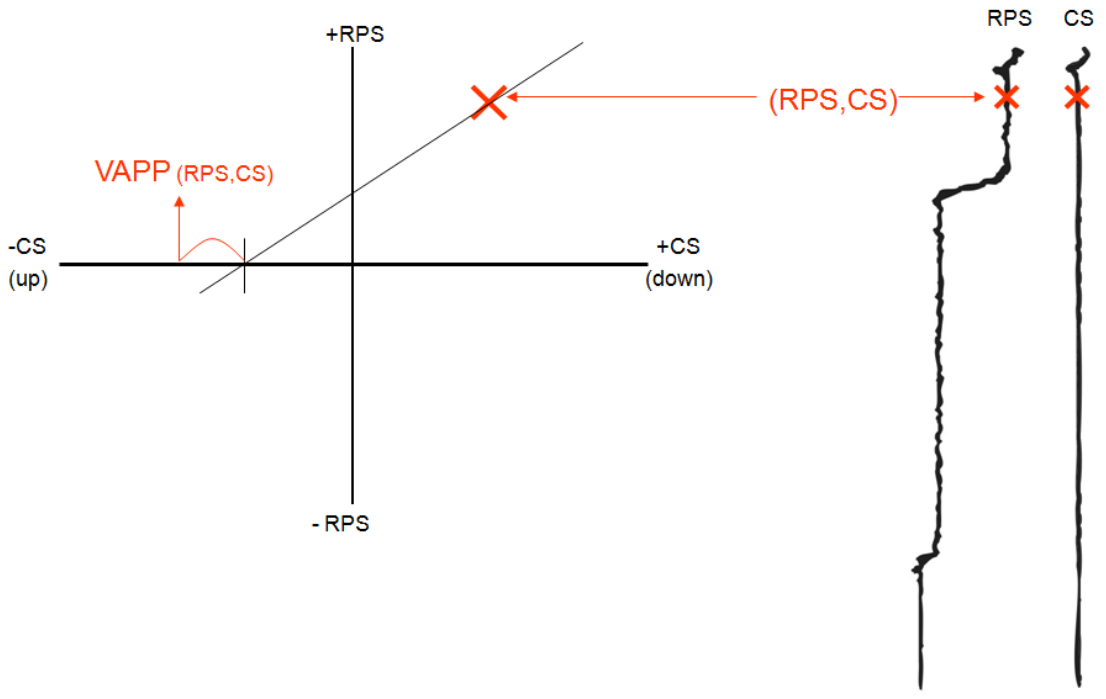


Fig. 17.G.6 – From spinner calibration to apparent velocity

It can be seen that once the calibration parameters are defined, then it would suffice with a single pass in order to obtain the apparent velocity. However, producing one apparent velocity channel per pass allows an overlay and is a further check of the well stability and the calibration adequacy. When this check has been made, the multiple apparent velocity curves are typically replaced with a single average value (median stack or lateral average). This single apparent velocity curve is the sole information required for quantitative analysis.

17.H Single phase interpretation

Rate calculations may be performed on each depth frame or averaged on calculation zones of interest. Such calculation zones could be the calibration zones or the top of each perforation zone. But in most cases the engineer will define where the rate calculations are most relevant.

The spinner calibration allows us to get the apparent velocity, V_{APP}, everywhere there is a measurement.

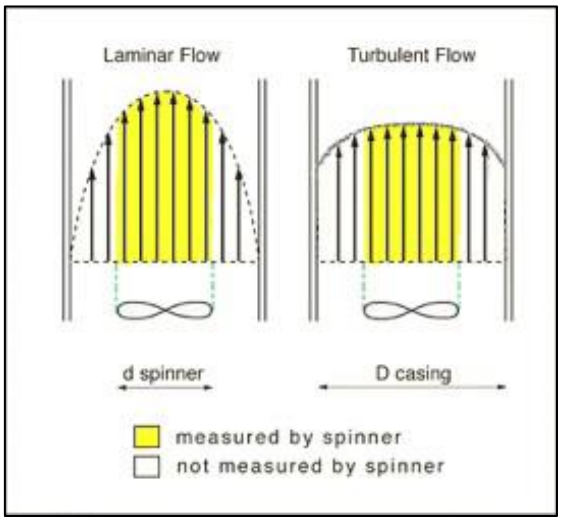


Fig. 17.H.1 – Velocity profiles and spinner sampling section

The previous image shows that in single phase, a well-centered spinner is located in the region of maximum fluid velocity. To get a single phase rate we need the total average flow velocity, which can be expressed from V_{APP} with some correction factor usually noted VPCF:

$$V_M = V_{APP}\, VPCF$$

17.H.1 Velocity profile correction factor

Historically, and at least for any manual interpretation, VPCF is taken as 0.83. More generally this factor can be calculated from the Reynolds number and the ratio of blade diameter to pipe diameter using the correlation illustrated in the figure below.

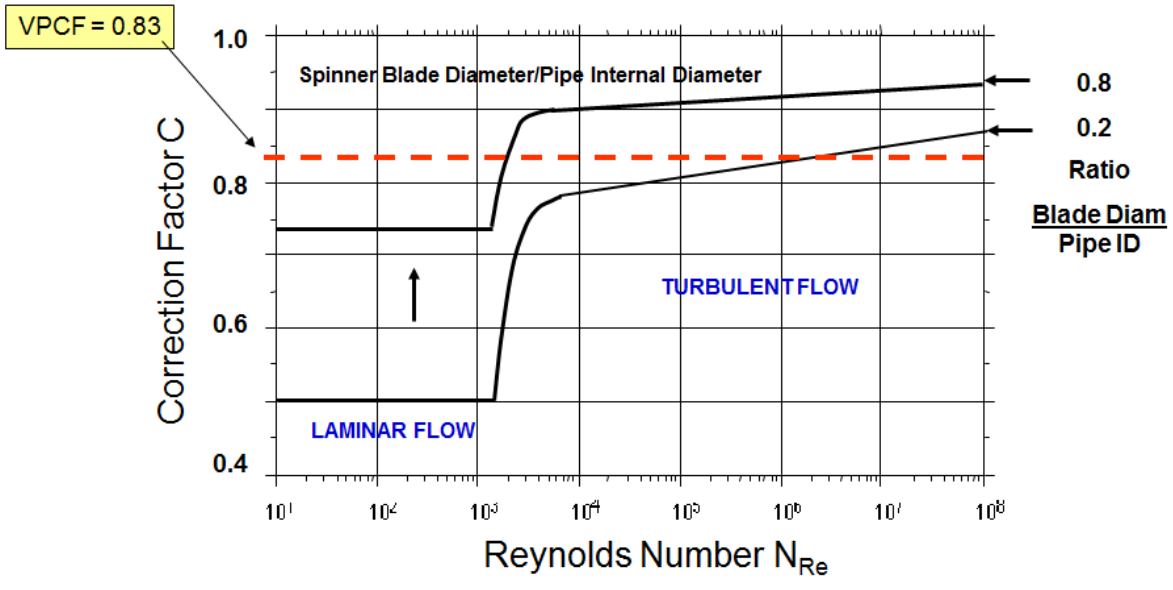


Fig. 17.H.2 – VPCF vs. Reynolds number for different ID ratios

Under a value of 2000 for the Reynolds number the flow is laminar with a parabolic velocity profile. In this situation, the maximum velocity is twice the average leading to VPCF of 0.5 for a small blade diameter. When the Reynolds number increases, the correction factor increases from 0.5 and its value tends asymptotically to 1. Also, as the blade diameter tends to the pipe ID, the correction factor moves towards 1.

The Reynolds number is expressed below for fluid density ρ in g/cc, diameter D in inches, velocity in ft/sec and viscosity in cp:

$$N_{Re} = 7.742\ 10^3\ \frac{\rho\ D\ v}{\mu}$$

Obviously, the value we are seeking, the fluid velocity, is part of the equation, meaning that an iterative solution is required.

The classical solution is to assume a value of velocity, typically based on a VPCF of 0.83, then calculate the Reynolds number, from which a new value of VPCF would be calculated, hence a corrected estimation of the flow velocity.

The process would go on until the solution eventually converges.

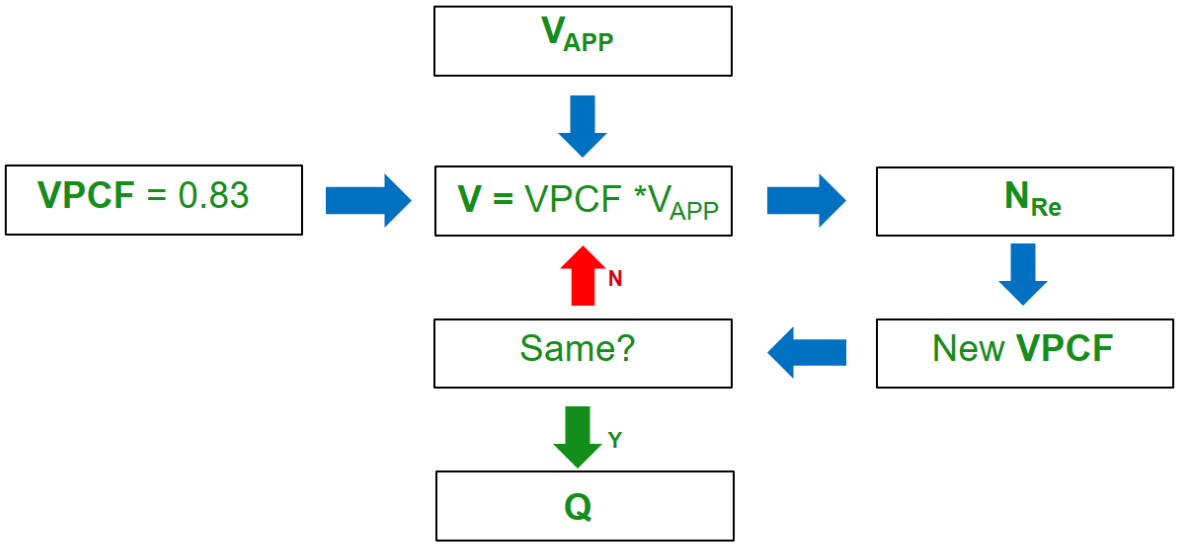


Fig. 17.H.3 – Single phase interpretation workflow

In modern software, this has been replaced by a regression algorithm, and the single-phase calculation is only a specific case of what is done for much more complicated processes such as multiphase rate calculations or the processing of multiple probe tools.

The principle of the nonlinear regression process is that we take as unknowns the results we wish to get, here the single-phase downhole rate Q.

The target will generally be the observed tool measurement.

In the case of a single phase calculation the target is the apparent velocity calculated after the spinner calibration.

From any value of Q in the regression process, we calculate the velocity, hence the Reynolds number, hence the VPCF, hence a simulated apparent velocity.

This allows the creation of a function VAPP = f(Q). We then solve for Q by minimizing the standard deviation between the simulated apparent velocity and the measured apparent velocity.

$$Q \rightarrow v \rightarrow N_{\mathrm{Re}} \rightarrow VPCF \rightarrow V_{APP}$$

$$Simulated\ Apparent\ Velocity: \quad V_{APP} = f(Q)$$

$$Measured\ Apparent\ Velocity: \quad V_{APP}^{*}$$

$$Minimize\ Error\ Function: \quad Err = \left(V_{APP} - V_{APP}^{*}\right)^{2}$$

17.H.2 Single phase interpretation results

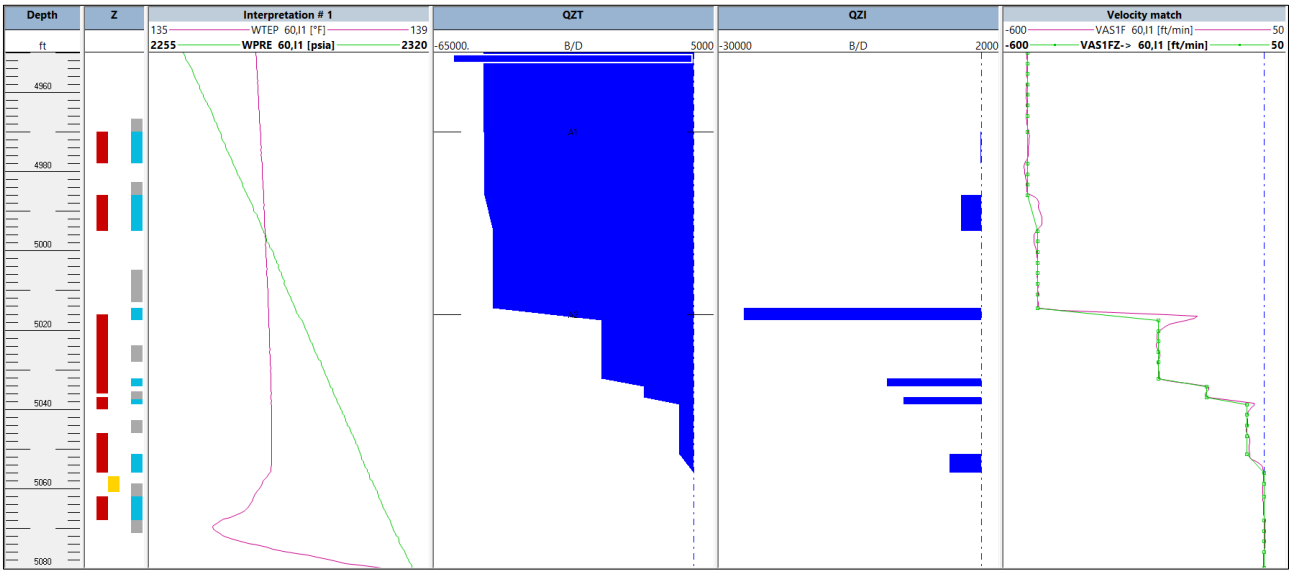


Fig. 17.H.4 – Typical log presentation for a single-phase interpretation

The previous figure is a typical presentation of results. In this water injector, eight different calculation zones (grey) were selected to isolate the contributions.

The non-linear regression described previously was executed on all of them to get Q.

The results are summarized by the QZT track where the value of a given calculation zone is extended up to the inflow zone above and down to the inflow below.

Inflow zones (blue) can be distinct from the perforations (red) simply to capture the fact that not all the perforation interval may produce or in this case, take fluid.

The QZI track represents contributions or injections and they are obtained by the difference of the rate above and below an inflow.

The last rate track, noted Q, represents the application of the non-linear regression at every depth, the point being to obtain a continuous log everywhere faithful to the log data. Having this log provides, in particular, a guide to refining the position of calculation zones.

In the complete log (Q) or for the zone rates (QZT), the calculation of the rate at Depth 1 is independent of the calculation at Depth 2. As a result, those rates may entail contributions of a sign or amplitude that is not physically justified.

We can address this potential inconsistency in a global regression process described later in this document.

The final track above shows the target V_{APP} and the simulated equivalent in green. Note that we arbitrarily decided to take the apparent velocity as the target function, rather than the real tool response in RPS.

We could have integrated the spinner calibration in the regression process and matched the RPS measurements for the different selected passes.

The simulated (green) curves and the QZT logs are referred to as schematics in Emeraude.

17.H.3 Matching surface conditions

It is possible to apply a global gain on the rate calculations. In single phase a multiplier on the VPCF is applied. In multiphase, a multiplier on the slippage velocities is also applied, in order to modify the proportions of the different fluids.

Before forcing a surface match, it is worth reviewing the quality of all the different factors that may lead to a discrepancy between the surface and PL rates: quality of the surface measurements, selection of the multiphase correlations, PVT description, spinner calibration, etc. Blindly forcing a surface match does not improve the validity of the interpretation.

17.I Multiphase interpretation

In single phase interpretation the spinner alone provides the answer, even if the determination of the correction factor needs a good grasp of the downhole conditions to have a representative density and viscosity. In multiphase flow there are at least as many unknowns as we have phases, i.e. one rate per phase. Actually due to the fact that different phases do not flow at the same velocities the number of unknowns is larger, including not only rates but also holdups.

17.I.1 Definitions

17.I.1.a Holdups

This definition was given before but it is repeated for clarity. The holdup of a phase is the volume fraction occupied by that phase. The Fig. opposite shows a heavy (blue) and light (red) phase and indicates the corresponding holdups.

The holdups are usually noted 'Y'; they add up to 1 by definition.

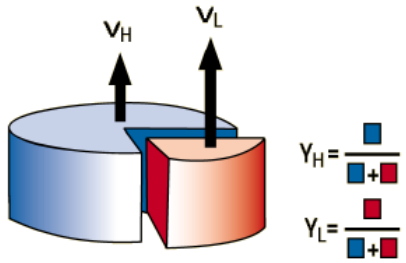


Fig. 17.I.1 – Definition of holdup

In two phases with a heavy ('H') and a light phase ('L'): $Y_H + Y_L = 1$

In three phases with water ('w') oil ('o') and gas ('g'): $Y_w + Y_o + Y_g = 1$

17.I.1.b Phase velocities

The average velocity of a particular phase is obtained from the rate of that phase, its holdup, and the cross sectional area by: $V_P = \frac{Q_P}{A\,Y_P}$

17.I.1.c Slippage velocity

As mentioned before, to quantify a two phase rate we should be able to solve at any depth:

$$q_l = v_l\, A\, Y_l$$

$$q_h = v_h\, A\, Y_h$$

Fluid identification tools, to measure or estimate the holdups, were presented in Section 17.C.2. The phase velocities still remain an unknown since, from the flowmeter, we will be able to compute the mixture velocity (Vapp*VPCF). An extra input is needed, and this comes from the concept of slippage velocity.

The slippage velocity is the difference between the velocities of two distinct phases. When light and heavy phases are considered, the slippage velocity is usually defined as the difference between the light phase velocity and the heavy phase velocity, namely:

$$V_s = V_L - V_H$$

When going uphill, the light phase will move faster and Vs will be positive. The opposite situation will be encountered when going downhill where the heavy phase will go faster. The

slippage velocity is not something the PL tool measures, nor are the phase rates (at least with conventional tools). Getting the rate values will only be possible if we can estimate the slippage value using a correlation. There are many correlations available in the literature, empirical or more rigorously based. For the time being let us simply assume that such correlation will be available to us if we need it.

17.I.2 Starting with 2-phase…

For 2-phase flow, the alternatives will be water-oil, water-gas and oil-gas. Even though the general approach that we advocate is using non-linear regression, we describe here a deterministic approach whose value is to explain the concepts in a simple situation, and to introduce the basic notions / presentations that will be used in the general case. Recalling the definitions above and using the subscript 'H' for heavy and 'L' for light we can write:

$$Y_H + Y_L = 1 \qquad Q_H + Q_L = Q_T$$

$$V_S = V_L - V_H = \frac{Q_L}{A\,Y_L} - \frac{Q_H}{A\,Y_H} = \frac{Q_T - Q_H}{A\,(1 - Y_H)} - \frac{Q_H}{A\,Y_H}$$

Solving for Q_H gives: $Q_H = Y_H\,[Q_T - (1 - Y_H)\,V_S\,A]$

And to finish: $Q_L = Q_T - Q_H$

Holdup is a quantity we can measure directly, or infer from density. If we measure mixture density and know the individual phase densities downhole, holdup can be obtained as shown below:

$$\rho = \rho_H\,Y_H + \rho_L\,Y_L \qquad \rightarrow \qquad Y_H = \frac{\rho - \rho_L}{\rho_H - \rho_L}$$

Note that when density is measured with a gradio the reading needs to be corrected for friction. This correction requires knowledge of velocity and the fluid properties so, as in single phase case, such a calculation will necessitate an iterative solution scheme.

Since we know how to calculate the total rate from the single phase equivalent, all we need is a way of determining the slippage velocity. In the simplest situations, this could be done manually. The chart below shows the Choquette correlation, representative of bubble flow in vertical well for an oil-water mixture.

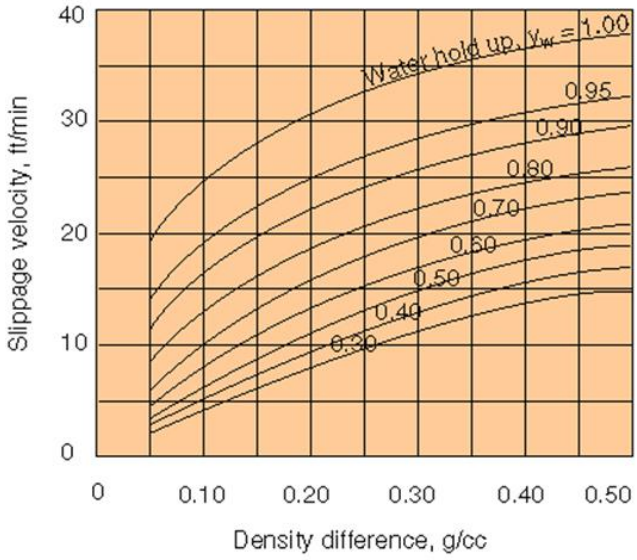


Fig. 17.I.2 – Choquette bubble flow chart

With such a chart, the slippage is obtained from the holdup and density difference. With a spinner and a density measurement, the steps of a manual deterministic approach would be straightforward:

(1) Estimate Q_T from V_{APP} and VPCF = 0.83

(2) Estimate Y_H from ρ and ρ_H and ρ_L. Iterate for frictions and VPCF as desired

(3) Get Vs from the Choquette chart

(4) Estimate Q_H and thus Q_L

In a general situation, the slippage velocity is given as a function of the rates, the fluid properties (densities, viscosity, surface tensions, etc.). The manual approach must be modified.

17.I.3 General solution using non-linear regression

The suggested workflow, as in single phase, relies on using non-linear regression to find the rates that minimize an objective function defined by the error between the target measurements and the simulated equivalent. In the case above for instance, all we need is a forward model that from an assumption of the rates Q_H and Q_L that calculates the simulated V_{APP} and density. In a general situation, the steps are as follows:

(1) From the rates, the fluid and the local geometry, get the slip velocities

(2) From the slip velocities and the rates get the holdups

(3) From the holdups calculate the fluid mixture properties

(4) Calculate the simulated tool response using the relevant model (eg VPCF, friction equations, etc).

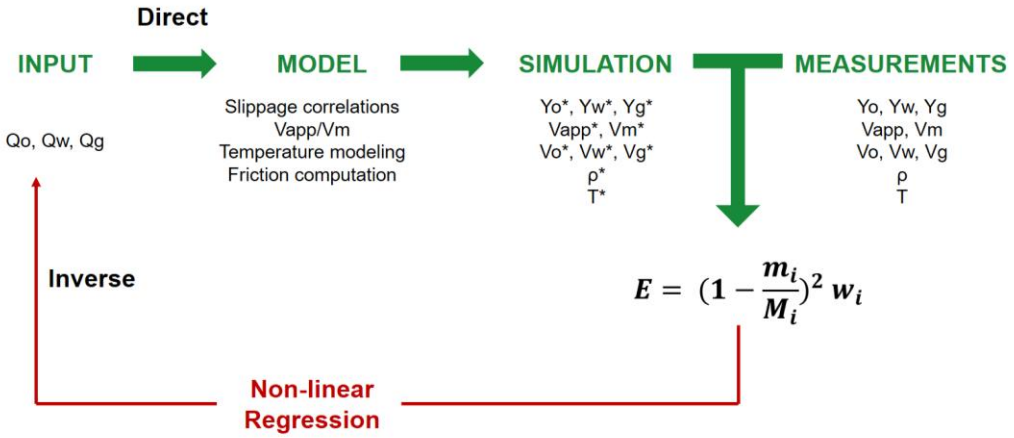


Fig. 17.I.3 – Methodology using non-linear regression

The interest of such an approach is that any number and type of measurements can be chosen as targets provided that they are sufficient and the problem is not undetermined (insufficient measurements for the number of unknowns). Having redundant measurement is also possible where the regression will try and find a compromise based on the confidence assigned by the user to the different measurements.

It is important to realize in the above procedure that slippage correlations are a necessary evil to relate the rates to holdups because holdups are the quantities we are best at measuring. When PL can measure phase rates or phase velocities directly, which is the Holy Grail of Production Logging, the procedure can do away with slippage correlations.

17.I.4 Flow models and correlations

Slippage correlations have been derived for a number of situations either empirically, or by solving the general momentum balance equation, in which case the correlation is said to be 'mechanistic'. In general, the behaviour of the slippage velocity will strongly depend on the nature of the flow regime encountered. Whereas a water-oil mixture moving upward can often be considered in bubble flow, liquid-gas mixtures will give rise to much more complex regimes as illustrated below with one of the classical empirical correlations by Duns and Ross.

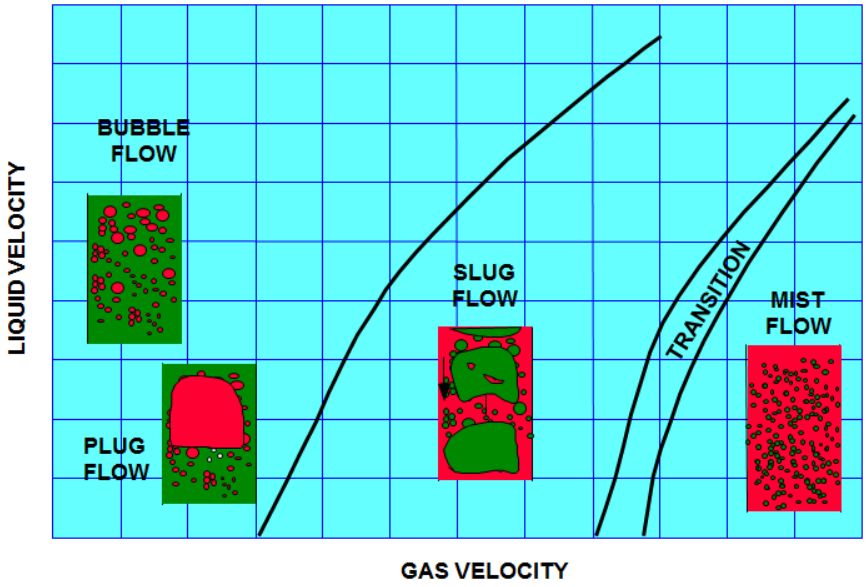


Fig. 17.I.4 – Duns and Ross flow map

In each regime, a specific slippage correlation will be applicable with extreme cases like mist flow, where no slip exists between the two phases. Many correlations will start with a determination of the flow regime using a flow map and continue with the application of the corresponding slippage equation. Slippage correlations can be organized in the following categories:

Liquid-Liquid: This category gathers bubble flow correlations (e.g. Choquette), correlations developed for stratified flow (e.g. Brauner) and combinations of those.

Liquid-Gas: This is by far the largest population with many empirical correlations (Duns and Ross, Hagedorn & Brown, Orkiszewksi, etc) and mechanistic models (Dukler, Kaya, Hassan & Kabir, Petalas & Aziz, etc). Most of those correlations have been primarily designed for representing wellbore pressure drops in the context of well performance analysis.

Three phase: There are very few such correlations and when they exist they are for a very specific situation, e.g. stratified 3-phase flow (Zhang). In practice, three-phase slippage / holdup prediction from rates are done using two 2-phase models, typically for the gas-liquid mixture on one hand and the water-oil mixture on the other hand.

17.I.5 Graphical presentation

A graphical presentation, albeit based on a 2-phase analogy, can help understand some previous concepts and provides a means of comparing different correlations.

For a given mixture rate Q, we consider the possible mixture and plot the corresponding mixture density. The X axis value range from 0 (100% Light phase) to Q (100 % Heavy phase). The density at those end points is the relevant single phase density. The equation derived previously for Q_H is now used to express Y_H:

$$Y_H = \frac{Q_H}{[Q_T - (1 - Y_H)\, V_S\, A]}$$

This equation shows that without slippage, the heavy phase holdup would be equal to the heavy phase cut. This situation is represented by the red line on the plot below. With slippage velocity on the other hand, Vs is positive uphill hence the equation above tells us that Y_H should be higher than the cut. The curve representing the case with slippage is thus above the no-slip line. An opposite situation would be expected downhill.

Another way of considering the plot below is to realize that for a given cut, the higher the slippage, the heavier will be the mixture. This is because the light phase is going faster and therefore occupies less volume in the pipe. The light phase is 'holding up' the heavy phase, leading to more heavy phase present at any depth than there would be with no slippage. For a given solution with slippage, the density will read heavier than if there is no slip.

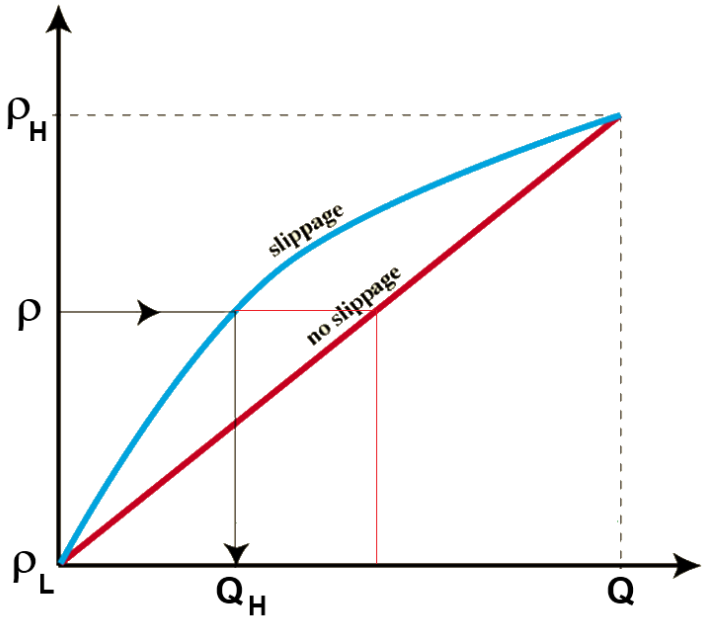


Fig. 17.I.5 – Density vs. heavy phase rate with and without slippage

We can look at this plot from a last perspective. If we have a measurement of density, the solution we should find (or that the non-linear regression will find) is seen graphically by interpolating the relevant curve for this density value.

17.I.6 Emeraude Zoned approach and the Zone Rates plot

The simplest interpretation method in Emeraude, called the Zoned approach, amounts to using the regression described previously on a set of user defined calculation zones. As in single phase, the zones are selected in the stable intervals above and below the inflow zones.

For each zone, a non-linear regression is performed and the result of this regression presented graphically in the Zone Rates plot. The Y-scale can display density or holdups as relevant. Below is an illustration in a 2-phase oil-gas situation with spinner and density. The dashed line represents the measured density. The current solution is such that for the selected correlation (Dukler) the predicted density value (horizontal dotted line) is similar to the measured one (horizontal dashed line).

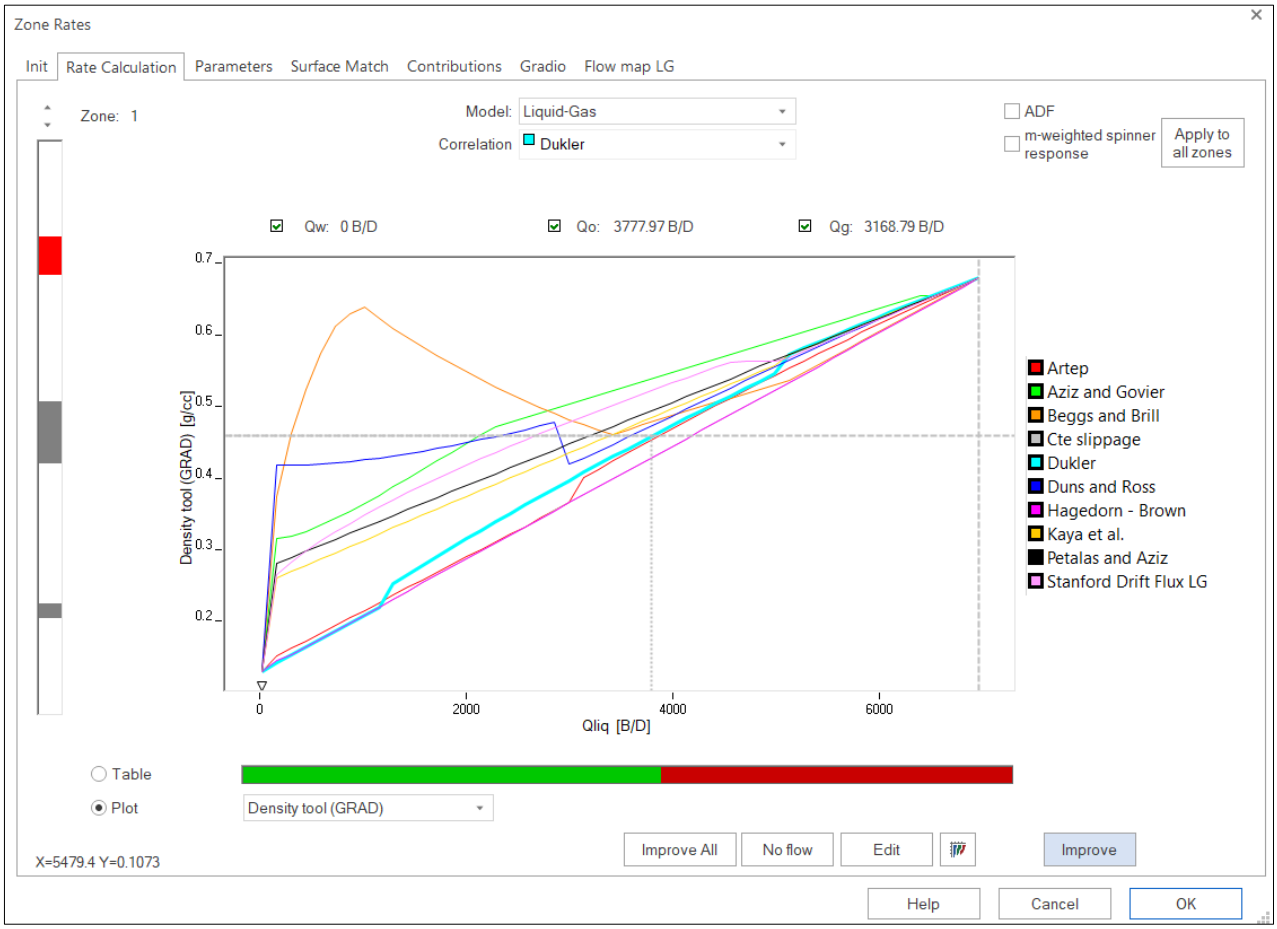


Fig. 17.I.6 – Emeraude Zone Rates dialog

Each colored line represents a different correlation. As we did previously, one way to look at this graph is to consider how different the rate solution will be depending on the selected correlation. The rationale behind a proper selection is to start by ruling out the correlations developed for situations not applicable to the particular test. Beyond this first elimination, it is possible to check which correlation is the most consistent with additional information, surface rates in particular. This selection is a very important step of the analysis, and at least should be noted and justified. Software defaults will not be a sufficient excuse.

17.I.7 Multiphase interpretation results

Below is a typical presentation in Emeraude. In this vertical oil-gas producer, three different (grey) calculation zones were selected to isolate the contributions of the two (red) perforations. The non-linear regression described previously was executed on all three calculation zones to get Qo, and Qg. Actually on the bottom zone, the rate was set to 0 and water holdup to 1. On other zones we have only two measurements (spinner, and density) and we imposed Qw=0, so the regression solved only for Qo and Qg. The results are summarized by the QZT track where the value of a given calculation zone are extended up to the inflow zone above and down to the inflow below.

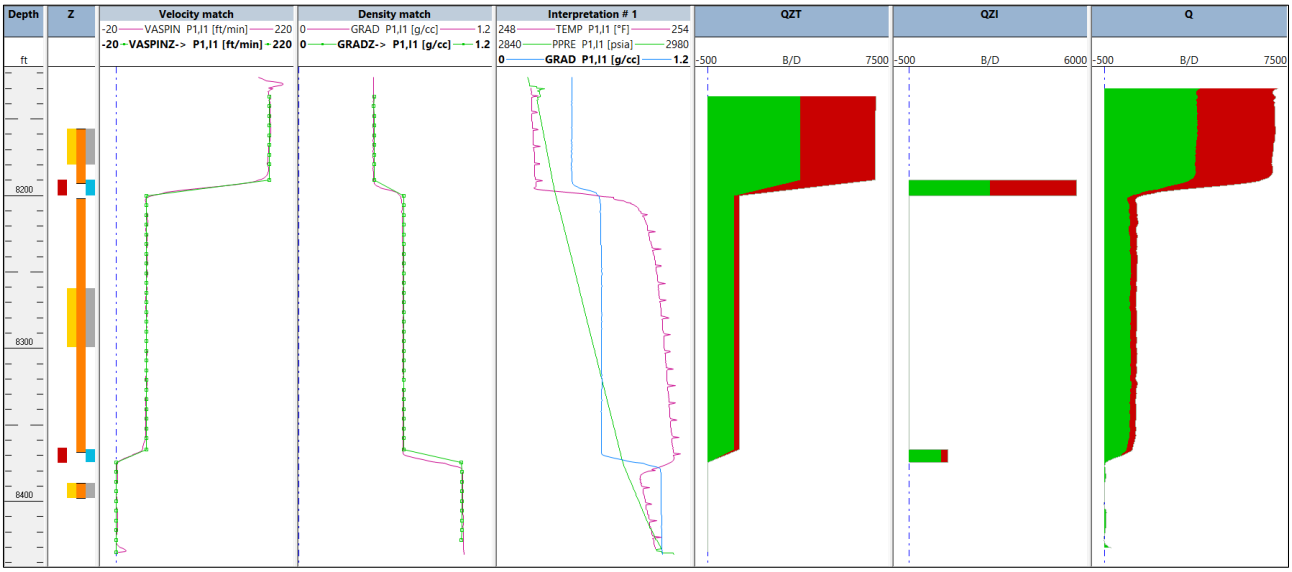


Fig. 17.I.7 – Typical multiphase result; Zoned approach

The QZI track represents contributions or injections and they are obtained basically by the difference in the rates above and below an inflow. The Q track represents the application of the non-linear regression at every depth frame.

The two match views show the comparison between the target (red) and simulated (green) measurements. The simulated curves are obtained by feeding at every depth the known rates into the forward model including, in particular, the slip correlation. The simulated curves and the QZT logs are referred to as schematics in Emeraude.

17.I.8 Zoned Approach and Global Regression

The calculation method explained previously is known as Zoned Approach. Here, for each rate calculation zone a non-linear regression is executed and the rates are calculated in these intervals only. The contributions per inflow zone are then obtained by taking the difference of the rates above and below for each zone. A mass balance is applied by default, in order to account for possible volume changes between zones (expansion or compression). By proceeding this way there is no guarantee that in the end the contributions of a given zone will be of the same sign. For example, the image below shows the contributions for a number of inflow zones, obtained by the Zoned approach. For the top perforation, water is injected while oil and gas is produced. These 'downhole separators' are clearly not physically possible, and are a result of the calculation method:

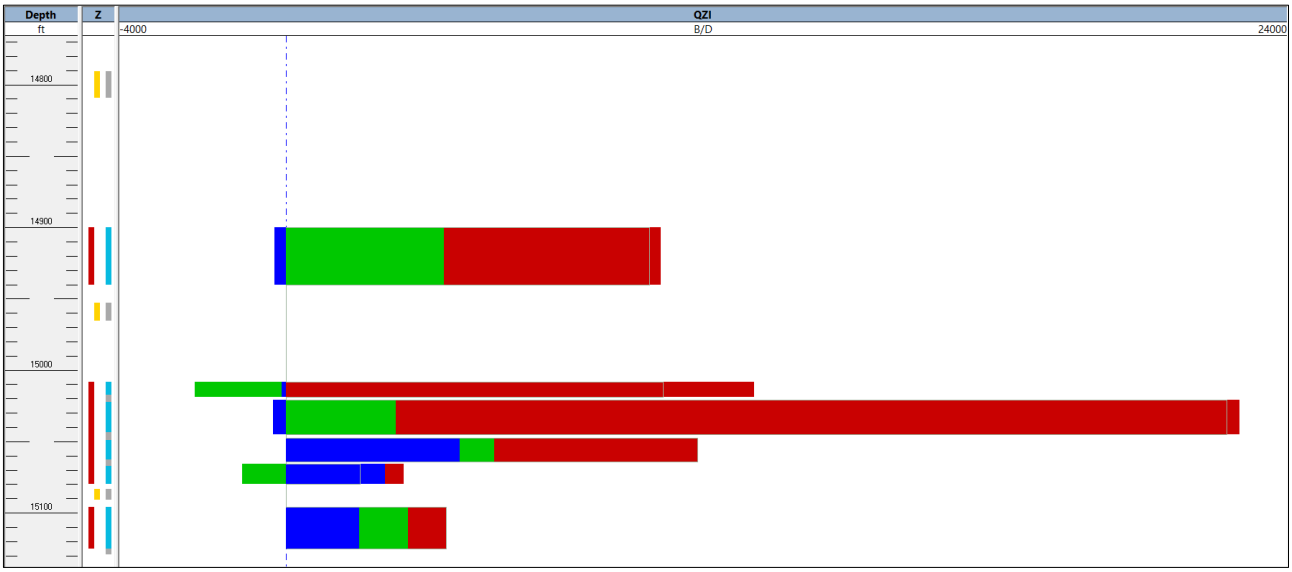


Fig. 17.I.8 – Typical multiphase result; Zoned approach

To avoid this, it is possible to solve for the entire well at once with a single global regression, where the unknowns are the zone contributions, dQ's. Since the contributions are the direct unknowns we can impose some sign constraints upfront. For each iteration the assumption of the dQ's translates into a series of Q's on the calculation zones, which can be injected into the forward model to calculate the objective function. Here again the objective function is evaluated on the calculation zones only; and to this error, other components might be added such as a constraint using the surface rates.



Fig. 17.I.9 – Local vs. global regression

Note that whether the regression is local or global the end result is only influenced by the solution on the few user defined calculation zones. This is why we call this approach the 'Zoned' approach.

17.I.8.a Slippage compliance and Zoned method

In multiphase calculations using the Zoned Approach, the simulated holdups will be derived from the local rates and the selected slippage correlations. Two different treatments are offered in Emeraude when using the Zoned method:

- Strict compliance: The error is minimized between the simulation and measurements. The simulated holdups come directly from the slippage correlations.
- Loose compliance: The holdups can depart from the slippage correlation prediction in order to be closer to the measurements. This is done by adding the slippage velocity as an extra term in the error minimization process (more on this in the next section).

It is up to the user to select the slip compliance approach to be applied in a particular interpretation. The decision will be based, among other reasons, on the confidence in a given correlation to predict the expected holdups in a particular flow regime.

17.I.9 The Continuous approach

The clear advantage of the Zoned approach is speed, since only a few points are required to get an answer, even if the Global regression is finally run. Its main drawback is that the results are driven by the choice of calculation zones. A way to remove this dependency is to run a Global regression with the errors evaluated *everywhere* on the logs, and not only at a few points. We could, for instance, seek to minimize the difference between the data and the simulated measurement logs (the schematics) everywhere. When we look at match views however, we see that the schematics are very square in shape. This is because, between inflow zones, the mass rate does not change and, if using strict slippage compliance, there are little variations in holdups and deduced properties.

The only way to account for the changes seen on the data is to let the holdups differ from the model prediction, as described previously for the loose slip compliance. With the Continuous approach the Global regression can be modified as follows:

- The **main regression loop** is still **on the contributions** but the objective function considers an error on the log points.
- At each depth, the simulated log values are evaluated by running a second **regression on the holdups** to minimize an error made on the difference between simulated and measured values and, at the same time, a new constraint using the slip model holdup predictions. In cases where one can do without the slip model, this new constraint is obviously not included.

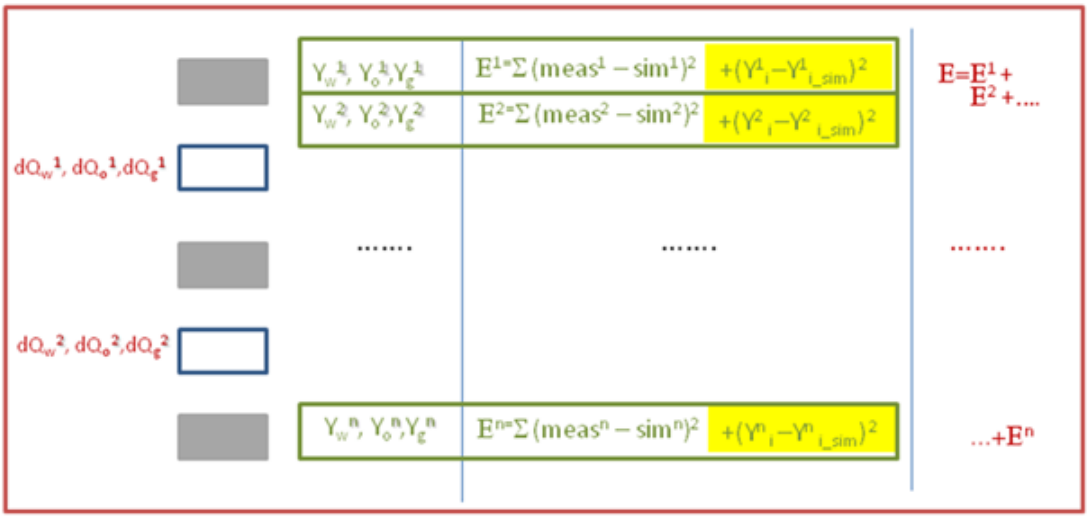


Fig. 17.I.10 – Global regression in Continuous mode

17.I.9.a Illustration with a 3-Phase example

The Fig. below shows the result of the Zoned approach on a 3-phase example. The calculation zones (grey) were defined. See how the second perforation has been split. Local regressions have been run, followed by a Global regression with the constraint that all contributions are ≥ 0. Without running the Global regression, the contributions would look like Figure 17.I.8.

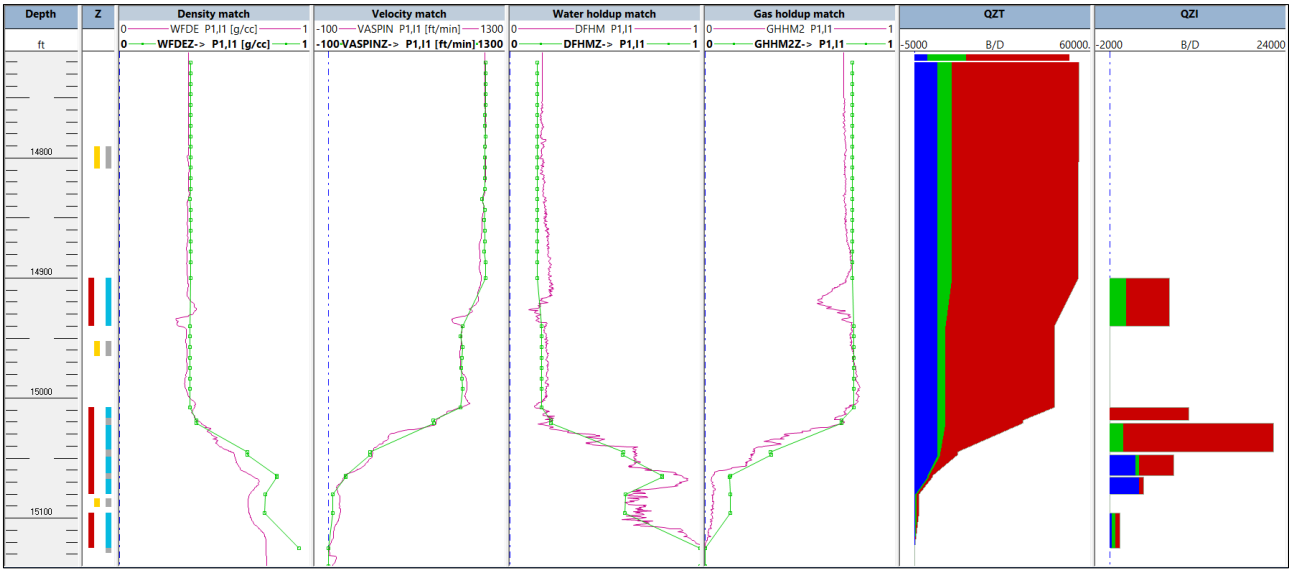


Fig. 17.I.11 – Example of zoned approach result in Emeraude

This example is now interpreted with the continuous approach and the Global regression rerun. In the end, there are certain differences. The match looks better overall, but at the expense of not honoring the slip models. The deviation from the slip models is indicated in the rightmost track (line=model, markers=solution). *Note that the number of depth samples on the logs is user defined.*

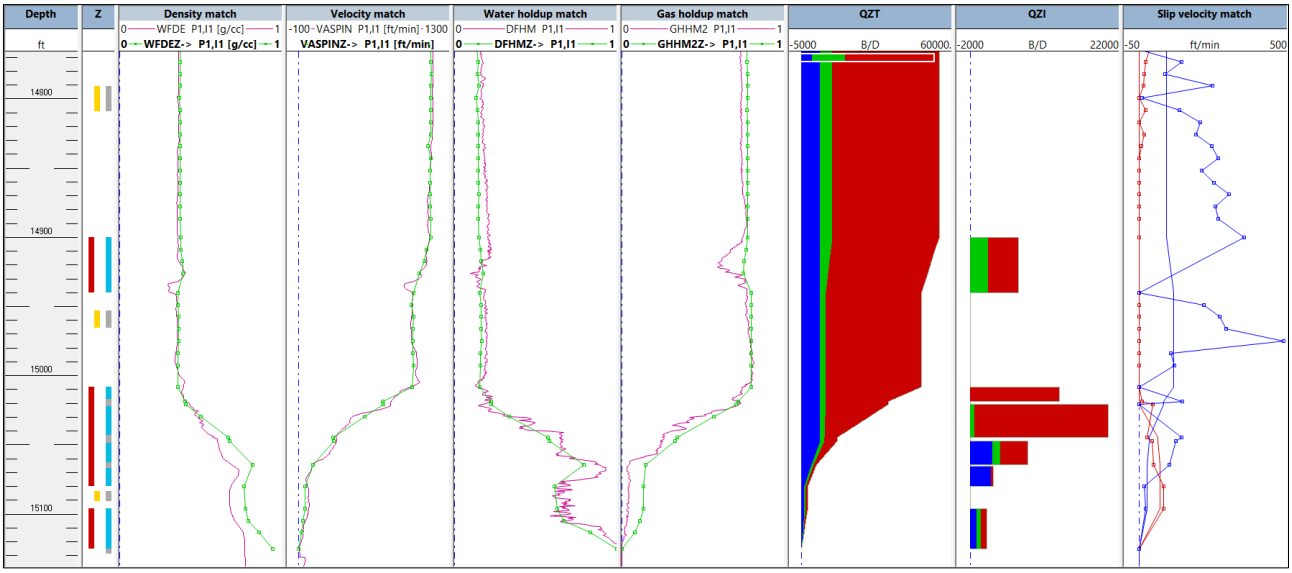


Fig. 17.I.12 – Example of continuous approach result in Emeraude

17.I.9.b So?

In the above example there is no drastic benefit to use the Continuous method. But there are cases where the reverse will apply. For instance, when the data is unstable between contribution intervals. In this case, the location of the calculation zones may dangerously impact the Zoned method results. Note however, that the continuous method is also influenced by the location of the calculation zones *inside the inflows,* since the way the inflows are split has a direct influence on the shape of the simulated logs over the inflows. Another situation where the Continuous method might provide a better answer is with temperature as the temperature is essentially an integral response. In Emeraude the two methods, Zoned and Continuous, are offered in parallel and you can switch from one to the other at any stage.

It is important to stress that a nice looking match does not necessarily mean a right answer. It all comes down, at some stage, to the interpreter's judgment. Also, any regression is biased by the weights assigned to the various components of the objective function. Different weights will lead to different answers. The starting point will also be critical as a complex objective function will admit local minima. So, the Continuous approach is not a magical answer, and more complex does not necessarily mean better. The Continuous approach is more computing intensive and a bit of a black box.

17.J Slanted and Horizontal wells

Even though the solutions presented up to now are in principle applicable to any well geometry, things get terribly complex in deviated or horizontal wells. The response of a conventional tool in these environments can be unrepresentative of the flow behavior. In addition, even if the tool responses can be trusted, the slippage models can turn out to be inadequate.

17.J.1 Apparent down flow

In a slanted well with significant water holdup, the water phase tends to circulate around whilst the light phase is going up. As the light phase occupies a small section of the pipe, the spinner will mostly see the water going down and a straight analysis will come up with a negative water rate.

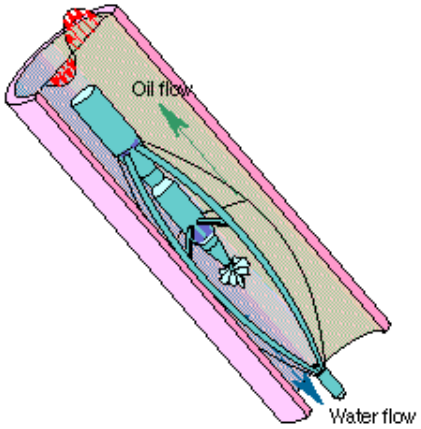


Fig. 17.J.1 – Flow recirculation

The heavy phase is not limited to water and could also be oil.

One way to deal with this situation is to use a dedicated model considering that the heavy phase is essentially static whilst the light phase moves up at a speed proportional to the slippage velocity. In this case the spinner measurements are completely disregarded. A valid cross-sectional holdup is required. Note that some centered fluid identification tools (nuclear density, tuning fork, capacitance) may not provide a representative value in segregated conditions. The slippage velocity comes from the correlation selection.

Another possible way of dealing with this situation is to use the temperature quantitatively as one of the target measurements. This obviously requires a forward temperature model representing the necessary thermal exchanges between the fluid, the reservoir and the well.

17.J.2 Horizontal wells

The first problem in horizontal well logging is that the tools do not go down by gravity. Dedicated conveyance systems are required, mainly coiled tubing, tractors and carbon rods.

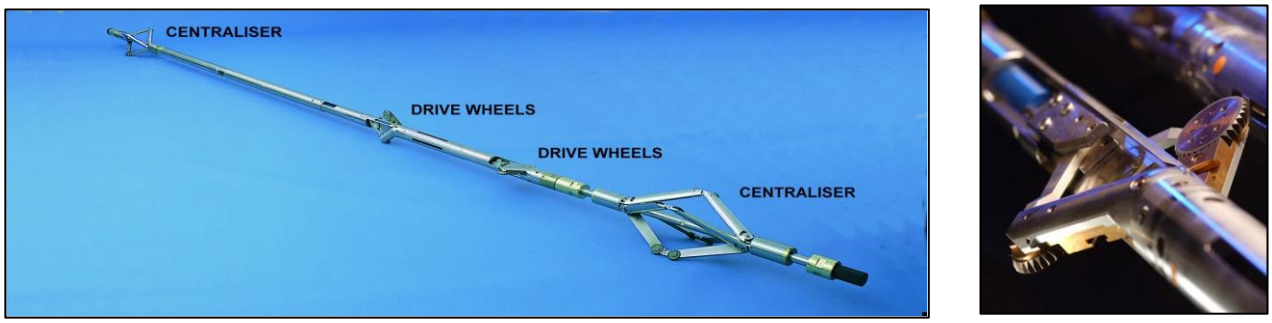


Fig. 17.J.2 – Tractor example; Courtesy Sondex

The conveyance may affect the measurements as, for instance, the presence of the coiled tubing in a small ID pipe can increase the frictional pressure drop towards the toe of the well, decreasing the driving force for production (drawdown). Also, swabbing and surging effects will affect the production profile of the well. For example, in the image below it can be seen that for the down pass (blue) the deepest inflow is detected nearly one thousand feet above the up pass:

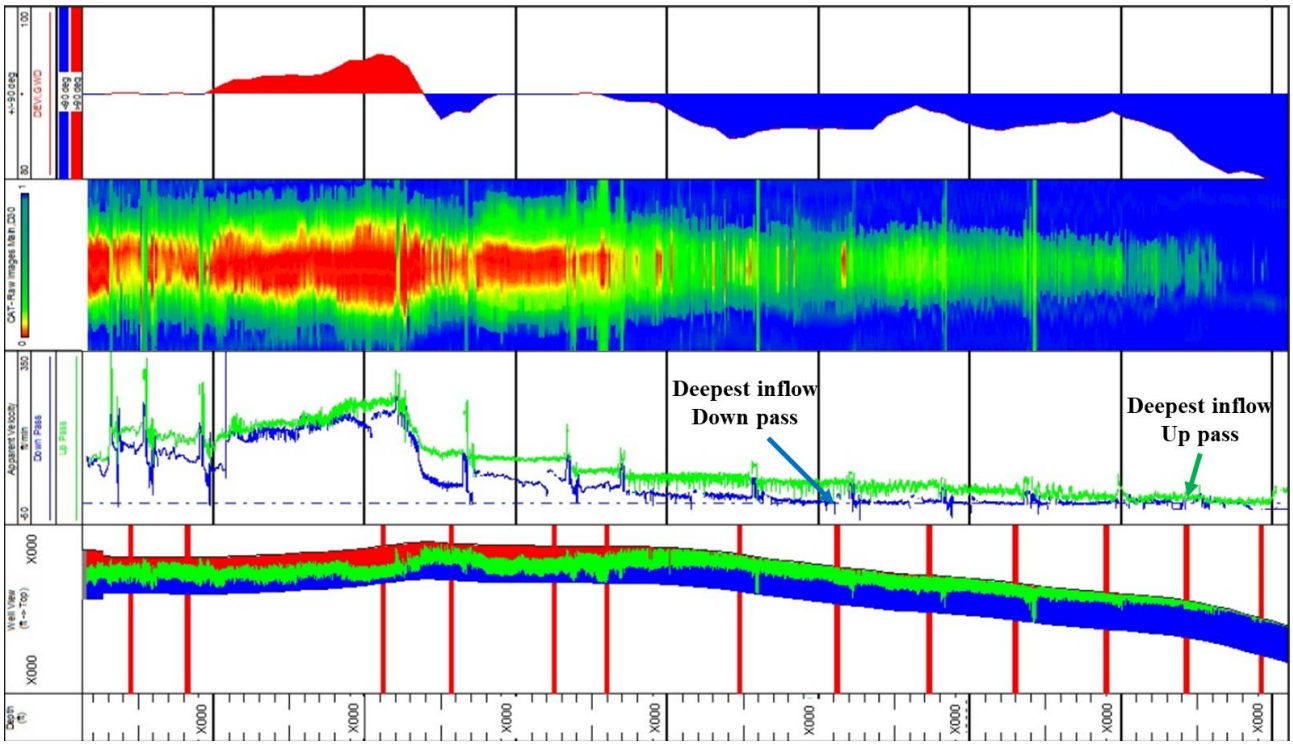


Fig. 17.J.3 –Effect of the conveyance method and deviation

As seen in the previous Figure, Horizontal wells are rarely strictly horizontal and unfortunately, slippage velocities, hence holdups are very sensitive to slight changes of deviation from the horizontal. The bottom track shows the well trajectory vs. TVD and the top track shows the well deviation around 90 degrees. For deviations greater than 90°, gravity causes the heavy phase to move faster, which leads to a decrease in holdup (if there are no change in rate). On the other hand, for deviations less than 90° the light phase will move faster, leading to a reduced holdup. This is observed in the holdup image (second track from the top). While the flow seems to be stratified, the repeated variations in deviation can give rise to transitional flow regimes, such as waves or slugs. The undulation of the wellbore will also create natural traps for heavy fluids in the lows and light fluid in the highs. Those trapped fluids will act as blocks and impact the tool responses when they occur.

The pictures below, taken in the Schlumberger Cambridge Research flow loop, show this dependence. A 50-50 mixture water and oil is flowed. A blue dye is injected in the water and at the same time a red dye in the oil. At 90° both phases move at the same speed and the holdups are each 50%. At 88° i.e. going uphill by only 2 degrees, the oil flows much faster and its holdup decreases significantly. Conversely, going downhill by 2° at 92°, the situation is reversed with the water going faster.

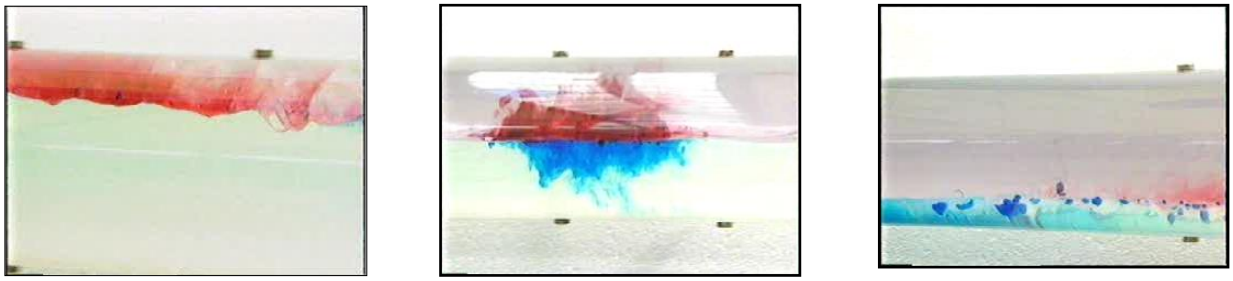


Fig. 17.J.4 – Slippage dependence around the horizontal; Courtesy Schlumberger

The methodology for multiphase profiling using correlations and conventional tools was presented previously. We must be able to provide average fluid velocities and holdups (or density), which can be obtained by centerline tools for well-mixed flow (vertical, slightly deviated, bubble, mist, etc.). As the deviation increases, and depending on the fluid velocities, segregation will occur and the centerline measurements will not provide the necessary inputs of mixture holdups and velocity. For a horizontal well, the response of conventional tools will be, for most of the time, useless. Even if they were reliable, slippage models that capture the physical behaviors in this situation are few.

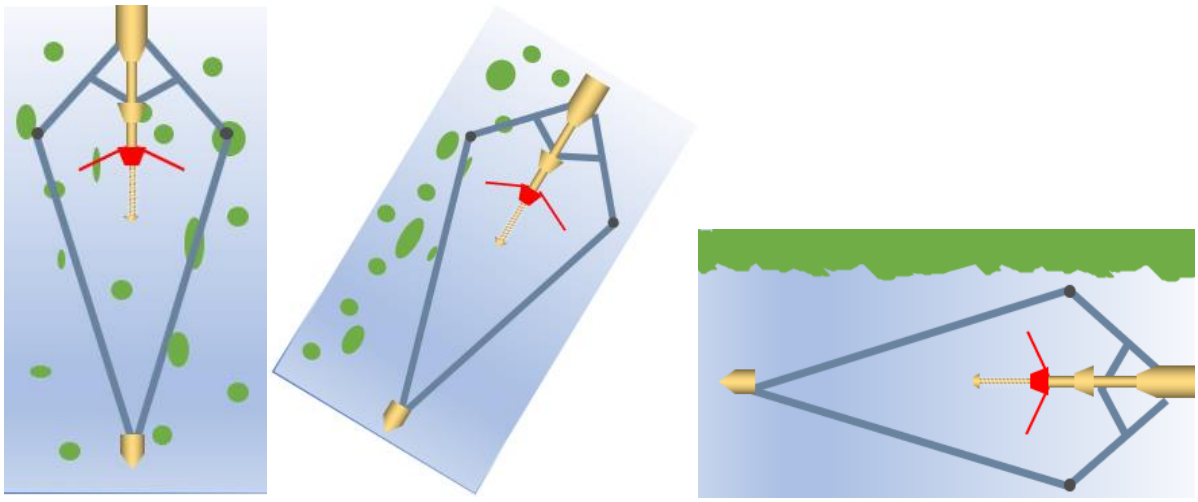


Fig. 17.J.5 – Effect of the deviation on the flow and the influence on centered measurements

For all the above reasons, specific tools were developed, called Multiple Probe Tools, or MPT. The goal with these tools is to replace a single value response with a series of discrete points in order to better characterize the flow behavior and ultimately to remove the need for slippage models.

17.K Multiple Probe Tools (MPT), or Array Tools

17.K.1 Schlumberger FloView – *Courtesy Schlumberger*

The FloView is a generic name that includes the PFCS and the DEFT. The tools include 4 or 6 water holdup probes that use the electrical conductivity of water to distinguish between the presence of water and hydrocarbons.

In a water continuous phase, current is emitted from the probe tip and returns to the tool body. A droplet of oil or gas has only to land on the probe tip to break the circuit and be registered.

In a continuous oil phase, a droplet of water touching the probe tip will not provide an electrical circuit. Instead, the water droplet must connect the electrical probe to the earth wire. This requires a larger droplet than is needed for gas or oil detection in a continuous water phase.



Fig. 17.K.1 – DEFT

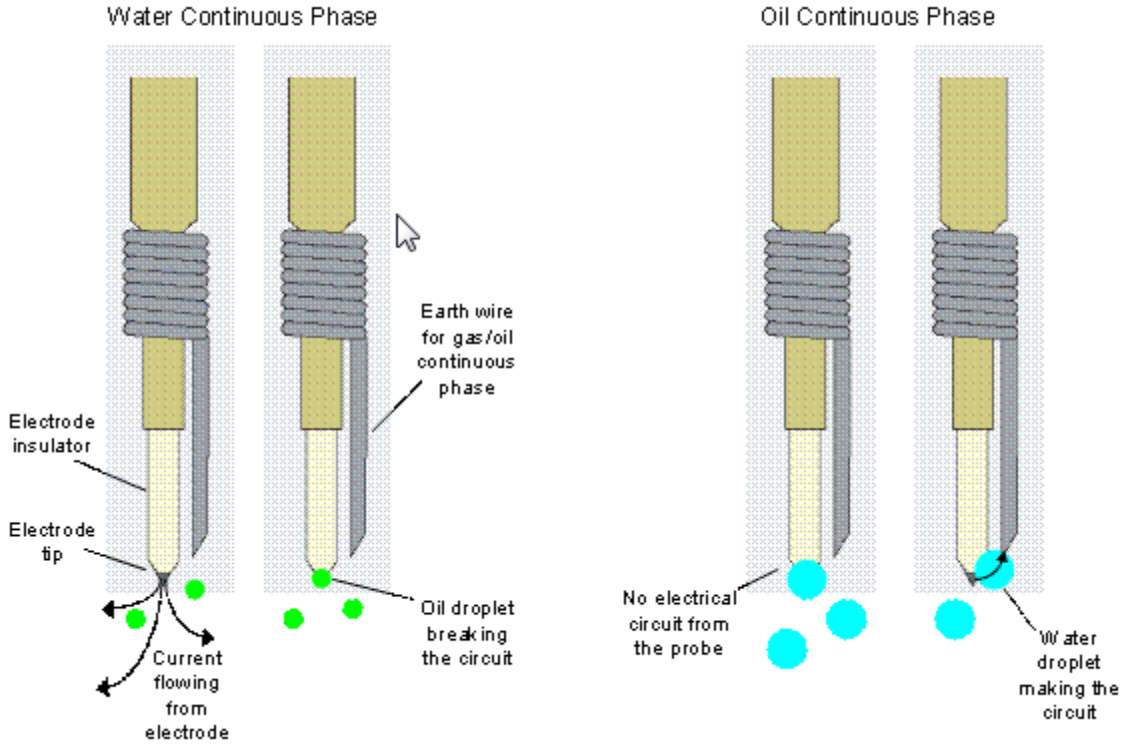


Fig. 17.K.2 – Theory of FloView Probe Operation, Courtesy Schlumberger

The signal from the FloView probe lies between two baselines, the continuous water-phase and the continuous hydrocarbon-phase responses. To capture small transient bubble readings a dynamic threshold is adjusted close to the continuous phase and then compared with the probe waveform. A binary water holdup signal results which, when averaged over time, becomes the probe holdup. The number of times the waveform crosses the threshold is counted and divided by 2 to deliver a probe bubble count.

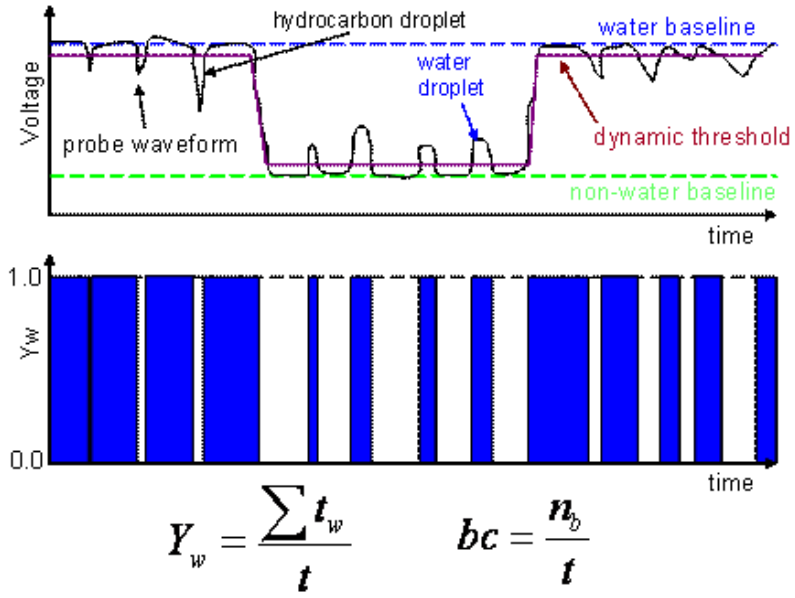


Fig. 17.K.3 – FloView Probe Waveform Processing, Courtesy Schlumberger

17.K.2 Schlumberger GHOST – *Courtesy Schlumberger*

The GHOST comprises 4 gas holdup probes. The probes use the refractive indices of gas, oil and water to distinguish between the presence of gas and liquid.

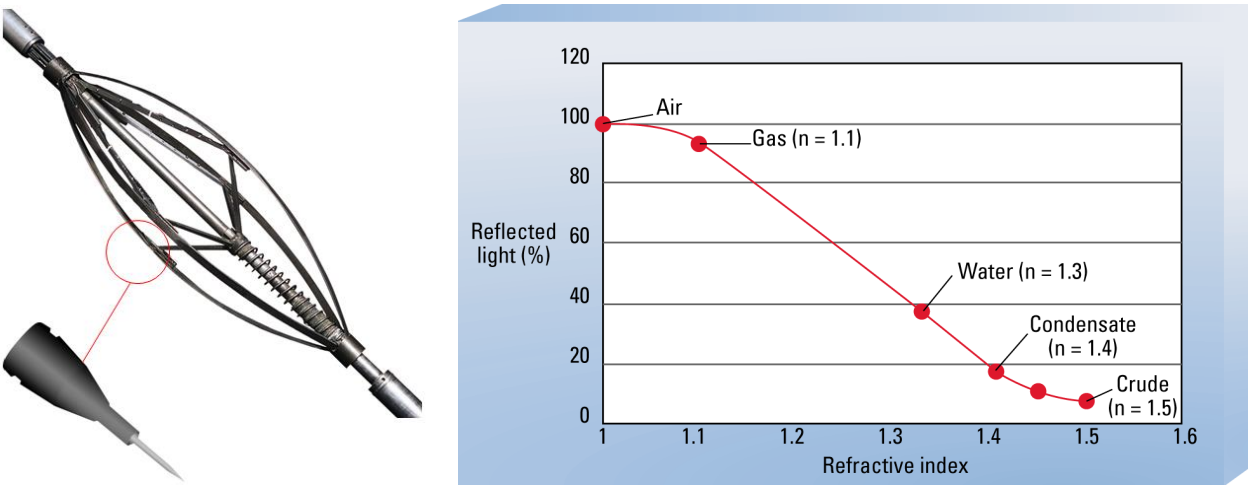


Fig. 17.K.4 – Reflected Light versus Refractive Index, Courtesy Schlumberger

Light emitted at a suitable frequency is fed down an optical fiber through a Y-coupler and finally to an optical probe made from synthetic sapphire crystal. Light that does not escape is returned via the Y-coupler to a photodiode and is converted to a voltage.

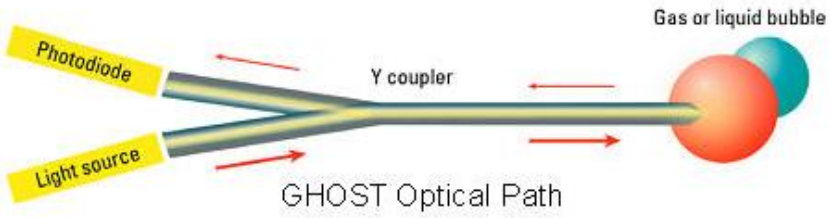


Fig. 17.K.5 – Sensor Optical Path, Courtesy Schlumberger

The signal from the optical probe is at or below the gas baseline and at or above the oil baseline. To capture small transient bubble readings a dynamic threshold is adjusted close to the continuous gas phase and close to the continuous liquid phase. The threshold is then compared with the probe waveform to deliver a binary gas holdup signal, which is averaged over time. The number of times the waveform crosses the threshold is counted and divided by 2 to deliver a probe bubble count.

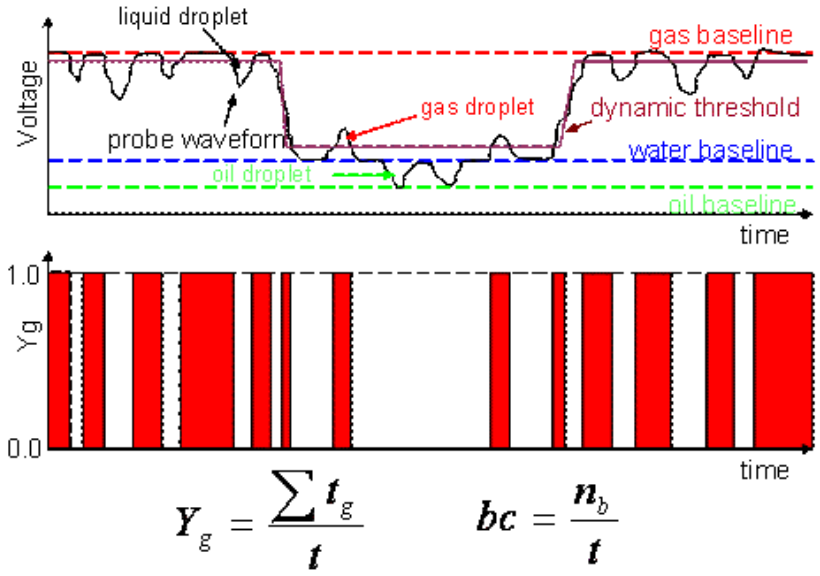


Fig. 17.K.6 – Optical Probe Waveform Processing, Courtesy Schlumberger

17.K.3 Schlumberger FloScanner (FSI) – *Courtesy Schlumberger*

The FSI combines 5 micro-spinners (MS) with 6 FloView probes (Electrical - Ep) and 6 GHOST probes (Optical - Op). The tool is designed to sit on the low side of the pipe by gravity, hence providing water holdup, gas holdup, and velocity profiles on a vertical axis.

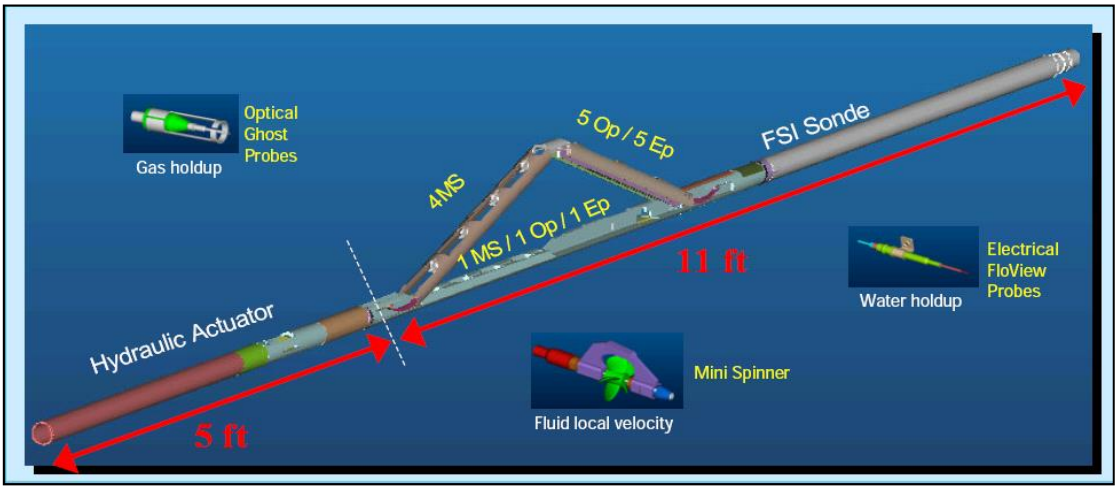


Fig. 17.K.7 – FSI tool geometry; Courtesy Schlumberger

The operation principle of the holdup sensors is the one explained in the previous sections. The calibration of the individual FSI spinners is pretty straightforward, as the spinners are supposed to be in the same vertical location from one pass to the other.

17.K.4 Baker Hughes-Sondex MAPS and PAI

MAPS tools were originally developed by Sondex, and in Emeraude they are still refered as Sondex tools, even though now they are part of Baker Hughes.

17.K.4.a CAT: Capacitance Array Tool

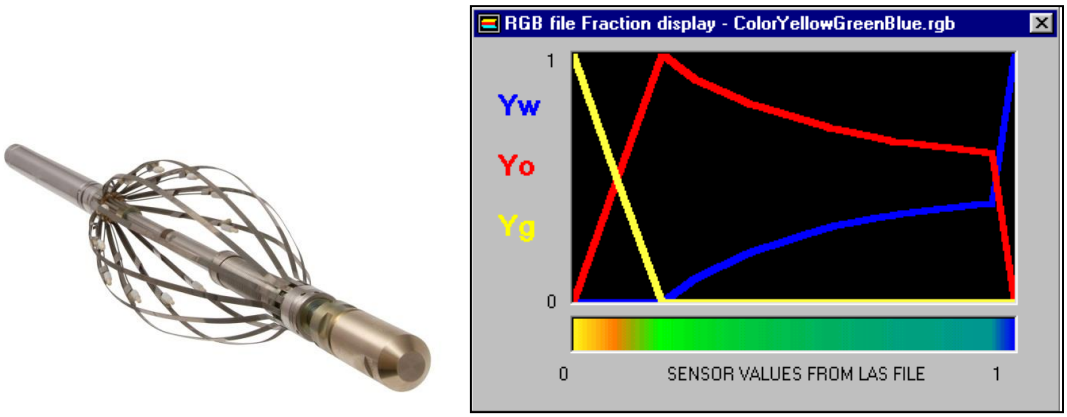


Fig. 17.K.8 – CAT tool (left) - Normalized values in [Gas-Oil] then [Oil-Water] mixtures (right). Courtesy Sondex

The CAT uses 12 capacitance probes distributed on a circumference. As with any capacitance sensor, the CAT probes discriminate mostly between water and hydrocarbons. The contrast in dielectric values for oil and gas may however be used to differentiate the two fluids.

In a stratified environment the probe response can be used to get holdup values using 2 two-phase calibrations as represented on the graph above. When the probe normalized response is between 0 and 0.2 a gas-oil system is considered, and from 0.2 to 1, an oil-water system. To

solve in three phase without any assumption about the local holdups, a 3-phase response can be used as shown below. This response is an extension of the previous graph that constitutes the intersection of the surface with the side walls.

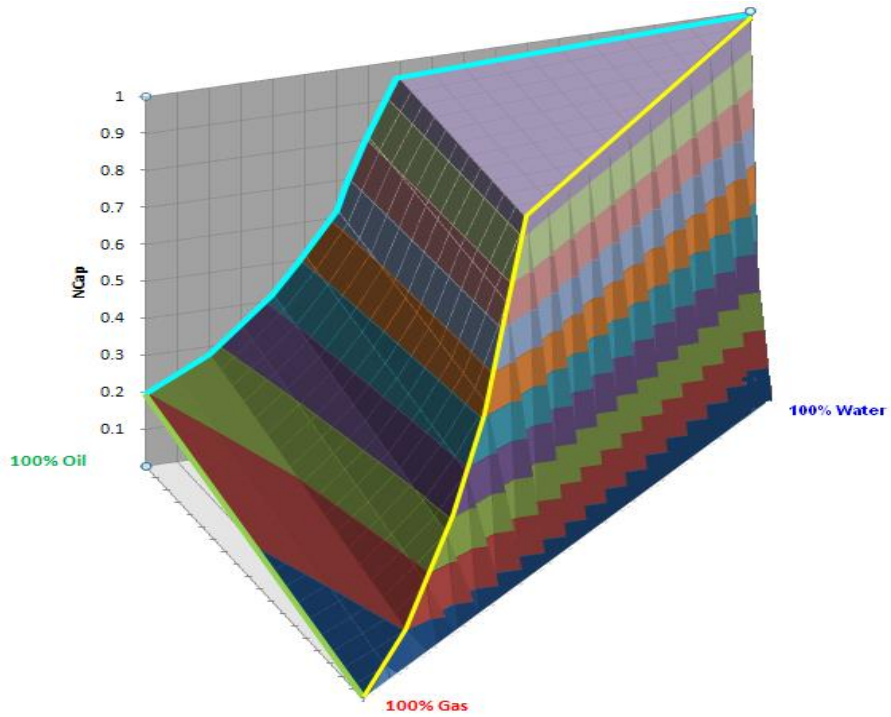


Fig. 17.K.9 – 3-Phase CAT response - Note the 2-phase segments:
Oil-Gas Oil-Water Gas-Water

17.K.4.b RAT: Resistance Array Tool

The tool incorporates 12 sensors arranged on a circumference. The sensor mechanics comprise (1) a probe tip that ultimately connects to the sensor electronics input and (2) a reference contact, typically at earth potential.

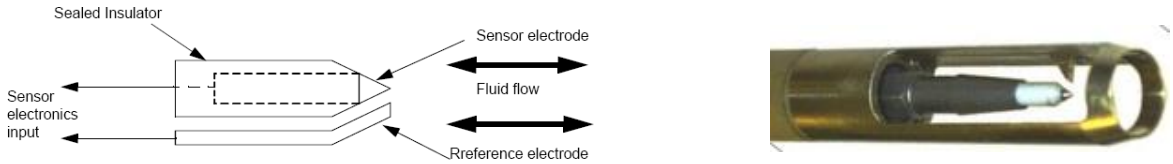


Fig. 17.K.10 – RAT, and RAT probes. Courtesy Sondex

Resistance measurements are made between the probe tips, and result in a number that is proportional to the logarithm of the resistance detected between the electrodes, and therefore the fluid resistivity. The field outputs include a mean resistivity and a standard deviation over a small time window, as well as histograms. The usual processing is based on the mean resistivity, R, considered to be a linear function of the conductive water resistivity Rc and the insulating hydrocarbon resistivity Ri.

The water holdup is thus obtained directly as: $Y_w = \frac{R - R_i}{R_c - R_i}$

17.K.4.c SAT: Spinner Array Tool



Fig. 17.K.11 – SAT, and SAT probes

Courtesy Sondex

The SAT uses 6 micro spinners distributed again on a circumference. One of the complexities of the SAT is that the MAPS tool string can usually freely rotate, hence a SAT spinner will typically be at a different position in the pipe at a given depth for distinct passes. This makes the spinner calibration in flowing conditions problematic.

17.K.4.d PAI

PAI is a 6 arms tool, which includes in each arm a SAT spinner, RAT (water holdup) and an optical gas hold-up sensor (GAT). The tool body incorporates a relative bearing measurement and deviation. The maximum tool opening is 9'' and each arm can be restricted independently of the other arms.

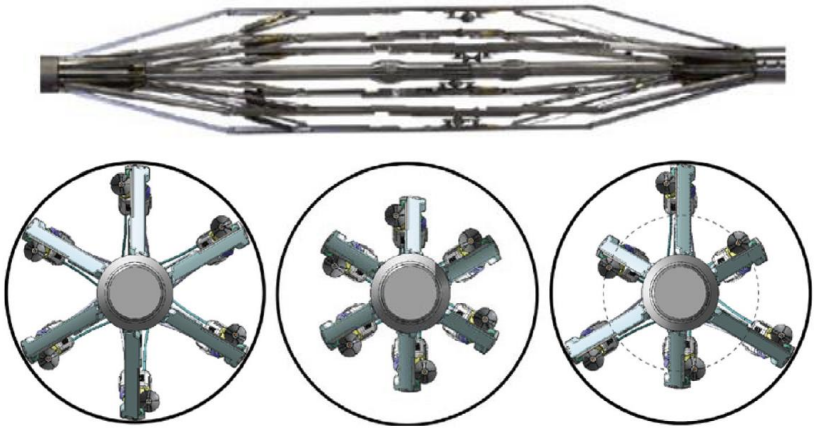


Fig. 17.K.12 – PAI tool. Courtesy Baker Hughes

Multiple PAI tools can be combined in a single toolstring with an angular offset in order to increase the cross sectional coverage of the pipe. The tool is also combinable with centered measurements (GR, spinner, CCL, etc.).

17.K.5 OpenField FAST

The Flow Array Sensing Tool (FAST) is a 3 foot-long tool with four arms. Each arm includes two sensor positions, and the type and number of probes can be addapted to the specifics of the job. The sensors can be 3-phase optical, electrical, minispinners, doppler flowmeters, sand detection, etc. As shown in the image below, a number of measurements are included in the tool body, such as temperature, pressure, relative bearing, MML and ultrasonic doppler transducers.

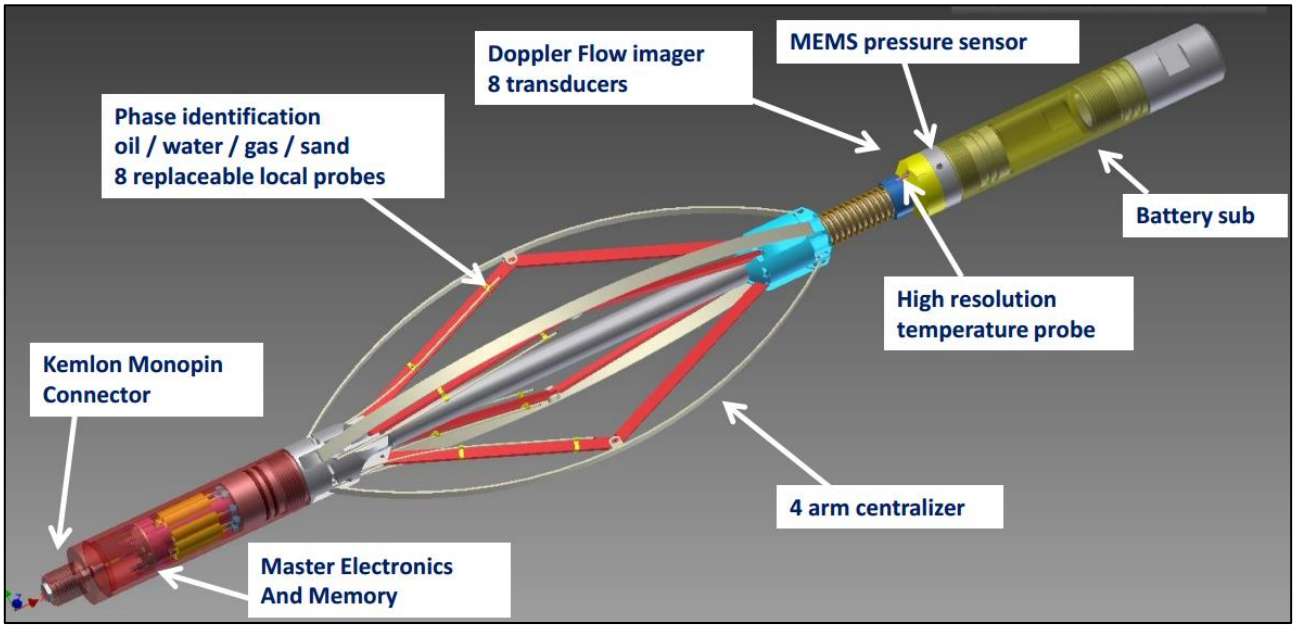
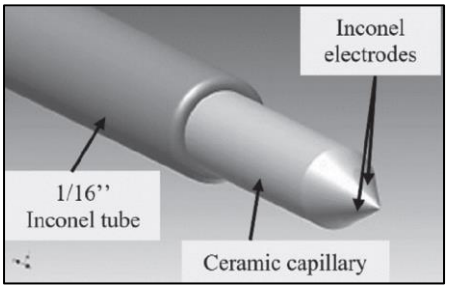


Fig. 17.K.13 – FAST v2 tool. Courtesy OpenField



The Electrical probes for water holdup determination works on the principle of a digital switch between the conductive water and insulating hydrocarbon. Compared to the previously presented water hold-up sensors, both electrodes are contained on the tip of the probe. The sensor outputs the Average conductivity, Majority, Maximum and Minimum. Using dynamic thresholds, the holdups are computed downhole.

Fig. 17.K.14 – FAST Electrical probe. Courtesy OpenField

The OpenField optical probes measure the refractive index in a range from 1 to 1.6 (see Fig 17.K.4), which allows the discrimination of oil, gas and water. The tip of the probe contains a sapphire needle. Similar to the Electrical probes, the waveform is represented by its Average, Majority, Minimum and Maximum values. By setting three dynamic thresholds, each sensor computes the 3-phase holdups.

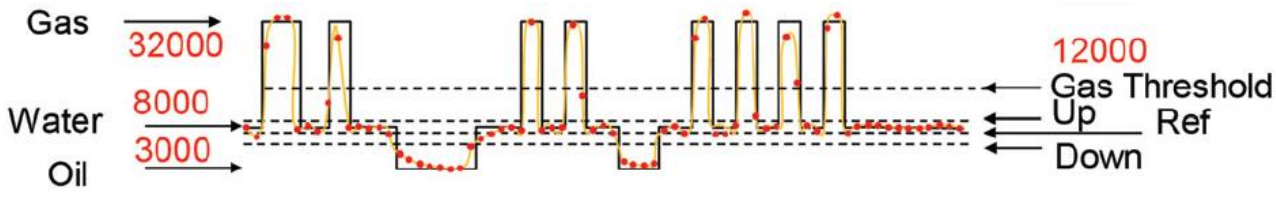


Fig. 17.K.15 – FAST 3-phase optical probe

FAST tool also incoporates ultrasonic transducers for Doppler effect-based flow metering. An ultrasonic wave is emitted through the fluid and scatters back from inhomogeneities such as bubbles, droplets or solid particles carried by the flow. An FFT spectra computation is embedded in the tool electronics. The Doppler effect shifts the reflected beam that can be related to the flow speed using the Doppler equation. At the time of writing (2019), the methodology to go from the different frequency extractions to fluid velocity is still under development since these are a function of the flow direction, flow regime, cable speed, etc.

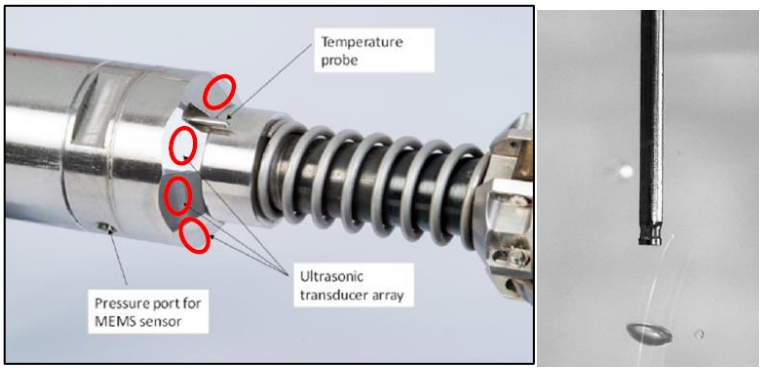


Fig. 17.K.16 – FAST Electrical probe. Courtesy OpenField

17.L MPT Processing

The objective of the MPT Processing is to obtain, at every depth, an average value of phase holdups and rates, based on local velocities and holdups measurements.

For any MPT tool, the exact position of the probes at a given depth is determined from the tool geometry, the local diameter, and the tool bearing which is part of the acquired measurements. The logged interval is 'spliced' in a number of cross sections. For each depth, the measurements are mapped, in order to move from the discrete values, to a 2D representation. Having this 2D representation will then serve two purposes:

(1) Integration of the individual properties to have representative average.

(2) Combination of the local properties to get phase rates and integration.

Imagine for instance that we know holdups and velocity everywhere. Locally we can assume that there is no slippage and at every location in the cross-section, calculate the phase rates as the local velocity multiplied by the local holdup. By integrating the phase rates, we can get average phase rates directly, and therefore produce a final result without the need for slippage models.

17.L.1 Mapping models

Most mapping models assume horizontal stratification. Therefore, the 2D mapping results in a 1D interpolation, as there are no lateral changes. However, a real 2D mapping algorithm is also available, that accounts for the areal variations of velocity and holdups.

17.L.1.a Linear model

The linear model defines the measurement of interest by a number of variables representing the values of that measurement along the local vertical axis. There are as many variables as there are distinct valid projections of probe readings on this axis. The values are then extended laterally. Without further constraints, this model will perform a linear interpolation through the discrete projected values. The figure below (left) illustrates this for a CAT cross section. The colored 2D map of the water holdup (water = blue, oil = green, gas = red) shows segregation but at different depths seems to be layers of water between oil, which is not physically possible. This may be the result of a bad calibration or an arm not fully extended.

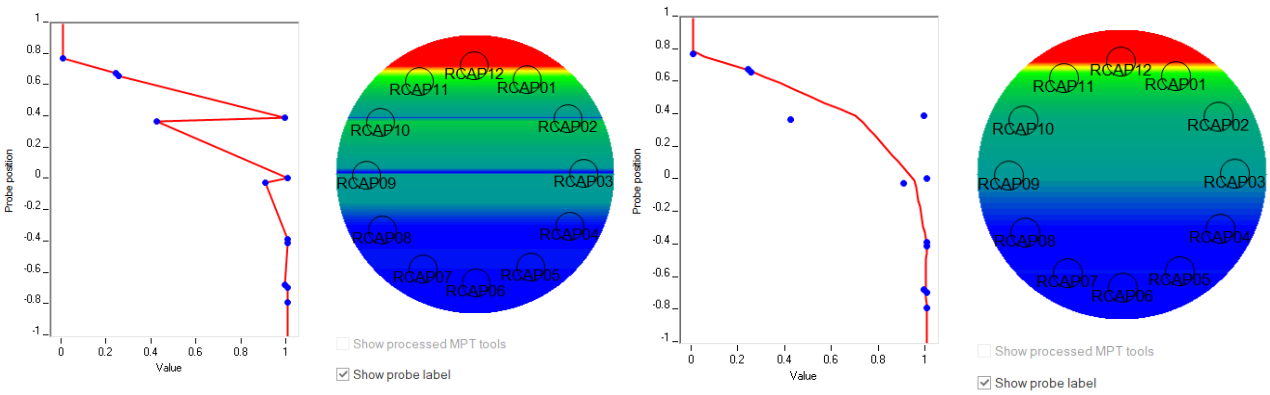


Fig. 17.L.1 – Linear CAT mapping. Without (left) and with (right) segregation constraint

To correct the previous situation, it is possible to alter the linear model using gravity segregation constraints, i.e. imposing that water hold-up decreases from bottom to top, or gas holdup increases from bottom to top. This is shown in the Figure above on the right.

A non-linear regression can be used to try and match the values and satisfy the constraints at the same time. The result is shown below.

The linear interpolation model can be applied to holdup and velocity data.

17.L.1.b Polynomial model

A polynomial interpolation is offered for the velocity model. By default, the velocity goes to zero at the pipe wall, using both the linear or polynomic. The latter fits the velocity with a grade 3 function and uses a rounding factor close to the pipe wall. The image below shows the difference between linear (left) and polynomial (right) models applied to SAT data:

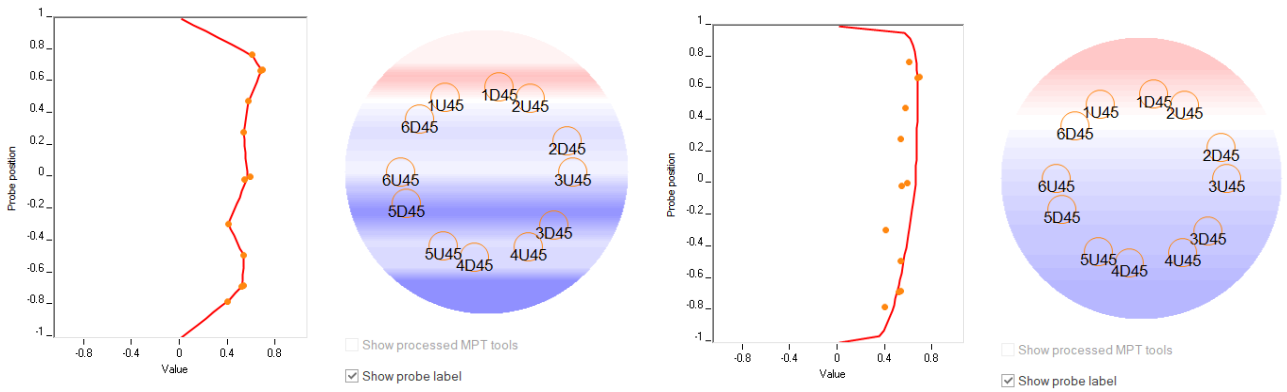


Fig. 17.L.2 – SAT mapping with the linear (left) and polynomial (right) models

This image also shows that it is possible to stack or combine *n* passes in order to create an equivalent pass with *n*-times the number of probes. In this case, 2 SAT (6 minispinners) are combined to form an equivalent 12 measurements cross-section. Before combining passes, it is necessary to check that the tool and well conditions remain constant throughout the survey.

17.L.1.c MapFlo holdup model

This model is restricted to Schlumberger holdup measurements. It can be used with PFCS, DEFT, GHOST, FSI or even combinations. All the model tries to match, like the linear model, is the projection of the measurements on the vertical axis. The MapFlo model is based on 2 parameters and produces the typical shapes/responses shown below.

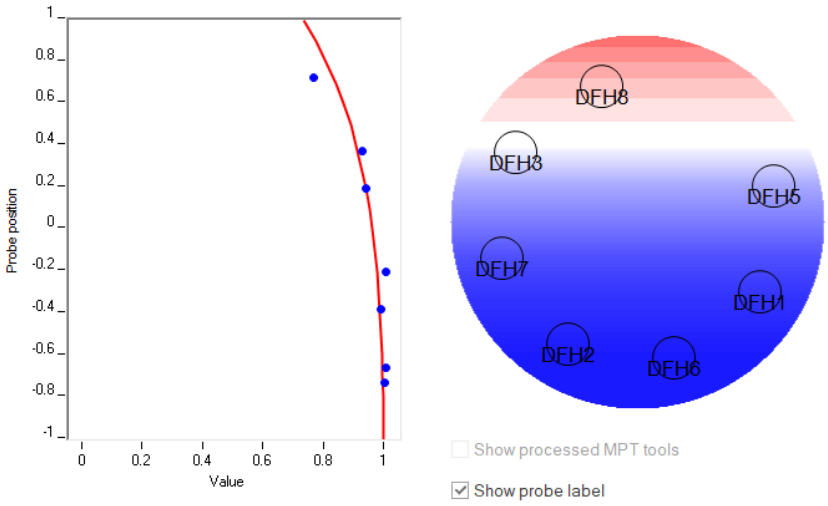


Fig. 17.L.3 – Dual-PFCS mapping with the MapFlo model

This image shows that one probe is missing (30° from the vertical). At QAQC stage of the data it might be decided to ignore *n* number of probes during the mapping process.

17.L.1.d Prandtl velocity model

This model can be used for the FSI velocity mapping.

Like MapFlo it is driven by 2 parameters. The main idea behind this model is to obtain the velocity profile by applying a linear transformation of the holdup profile and then rounding the profile near the pipe walls. More precisely, the velocity profile is obtained with the equation below, regressing on α and β to match the velocity projections.

$$\left[\left(Y_w - Y_g\right) \times \alpha + \beta\right] \times \left(1 - \left|\frac{z}{r}\right|\right)^{1/7}$$

The next Figure shows how the vertical holdup and velocity profiles were obtained on an FSI example with MapFlo and Prandtl combined. The gas holdup is everywhere zero; the water holdup profile is shown in blue (see the Yw scale at the top). The velocity profile is displayed with the yellow curve. The squares represent the discrete measurements (blue=Yw, red=Yg, yellow=V).

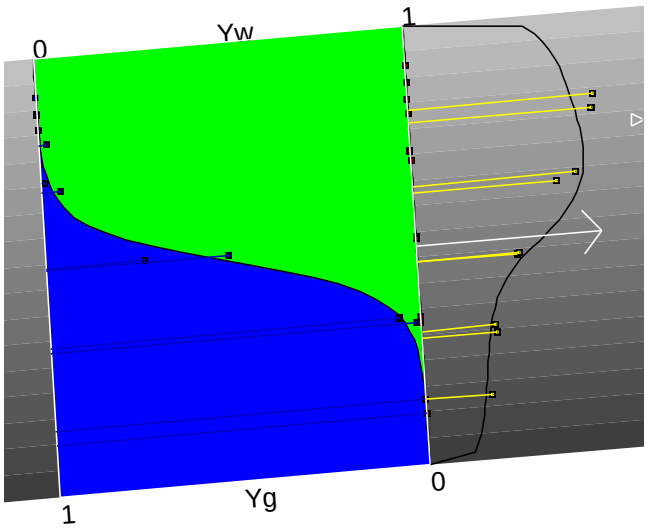


Fig. 17.L.4 – FSI mapping in a deviated well with MapFlo and Prandtl

It should be noted that the Prandtl model rounds the edge of the velocity on the entire circumference and not just at the top and bottom.

A typical 3D velocity profile is shown in the following figure.

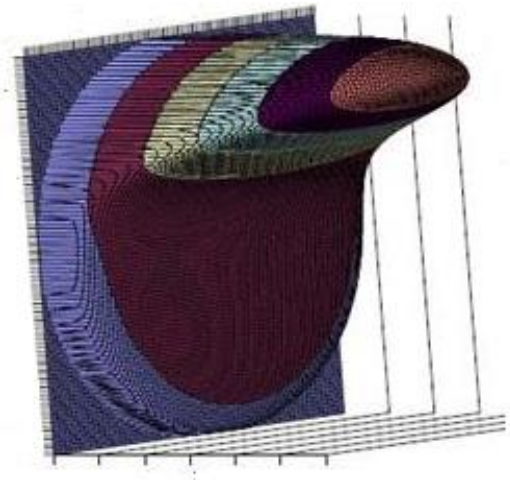


Fig. 17.L.5 – A typical Prandtl Velocity Profile; Courtesy Schlumberger

17.L.1.e 2D interpolation model

Instead of assuming local segregation, this approach is based on 2D interpolation algorithms, sometimes used to map petrophysical data: Kriging, linear triangulation, etc. If applicable, central measurements (capacitance, density, spinner) can be used as extra constraints on the model. The image below shows the results of 2D mapping in CAT and SAT data.

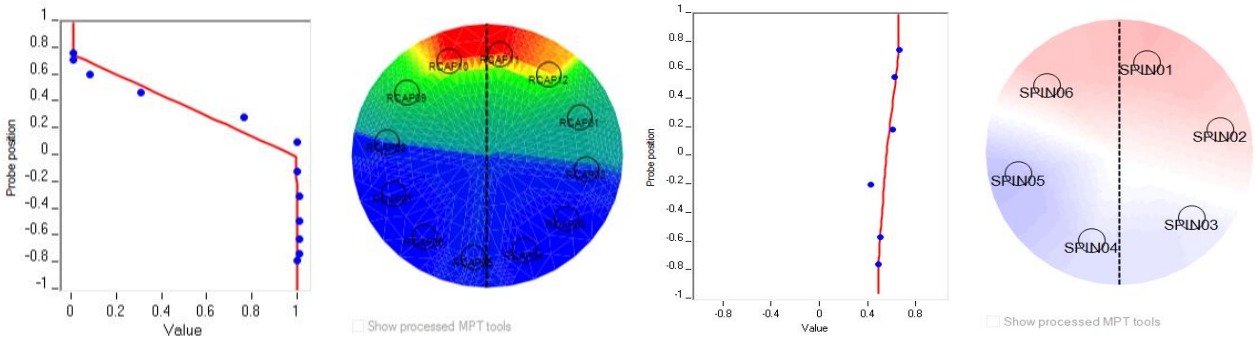


Fig. 17.L.6 – 2D interpolation in CAT (left) and SAT (right) data

17.L.2 Integration

The mapping allows integration over the cross-section at every depth in order to get average values.

$$Y_w = \frac{\int_S Y_w \times dS}{S} \; ; \; Y_g = \frac{\int_S Y_g \times dS}{S} ; \; Y_o = \frac{\int_S Y_o \times dS}{S} ; \; V = \frac{\int_S V \times dS}{S}$$

As explained earlier, with the assumption of no local slippage, we can use the local velocity and holdups to obtain phase rates.

$$Q_w = \frac{\int_S Y_w \times V \times dS}{S} \; ; \; Q_o = \frac{\int_S Y_o \times V \times dS}{S} ; \; Q_g = \frac{\int_S Y_g \times V \times dS}{S}$$

17.L.3 Interpretation

The interpretation is conducted using the process outputs: holdups, phase rates, total velocity together with any additional tool available. Even though the answers we are seeking are in essence already provided (we have the phase rates everywhere) the interpretation is still a required step to come up with actual zone contributions, possibly honouring additional constraints such as sign and surface rates.

Using a loose slip compliance or the Continuous method is the best choice as it contains a built-in mechanism to by-pass any slippage model on the recognition that enough information is supplied. Below is a typical output example for an FSI job.

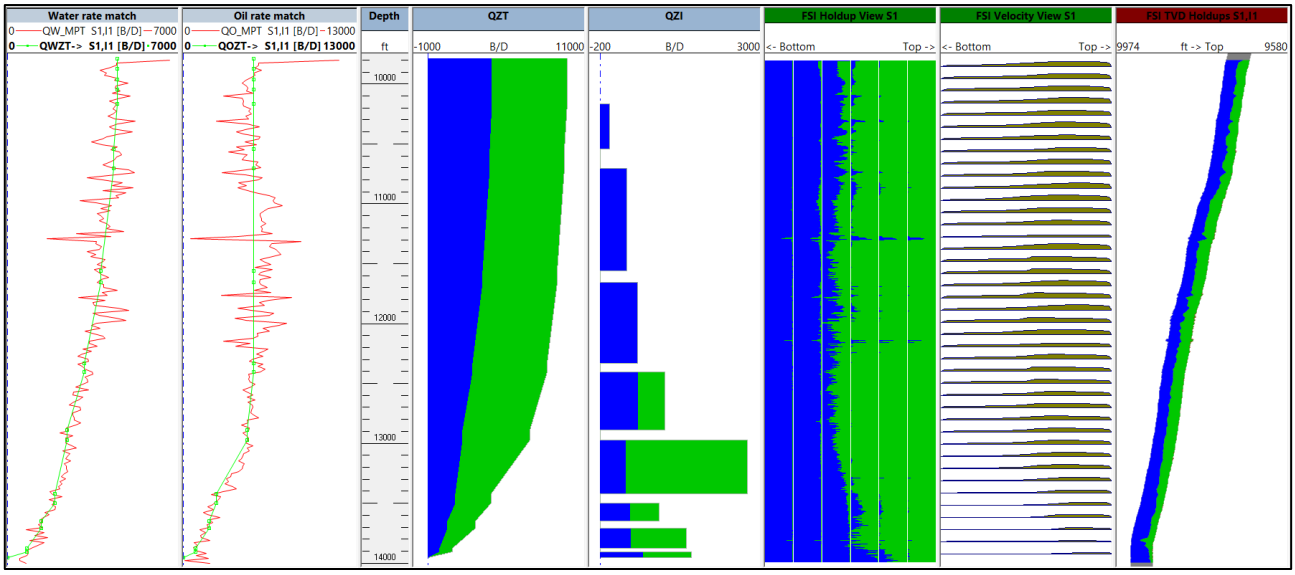


Fig. 17.L.7 – FSI Interpretation

17.M SIP

Selective Inflow Performance (SIP) provides a mean of establishing the steady state inflow relationship for each producing layer.

The well is flowed at several different stabilized surface rates and for each rate, a production log is run across the entire producing interval to record simultaneous profiles of downhole flow rates and flowing pressure (see Section 1.7.D). Measured in-situ rates can be converted to surface conditions using PVT data.

The SIP theory is strictly valid for single-phase.

To each reservoir zone corresponds, for each survey/interpretation, a couple [rate, pressure] used in the SIP calculation. For the pressure, the interpretation reference channel is interpolated at the top of the zone.

For the rate, the value used in the SIP is the contribution. It is calculated for a given reservoir zone as the difference between the values interpolated on the schematic at the top and the bottom of that zone.

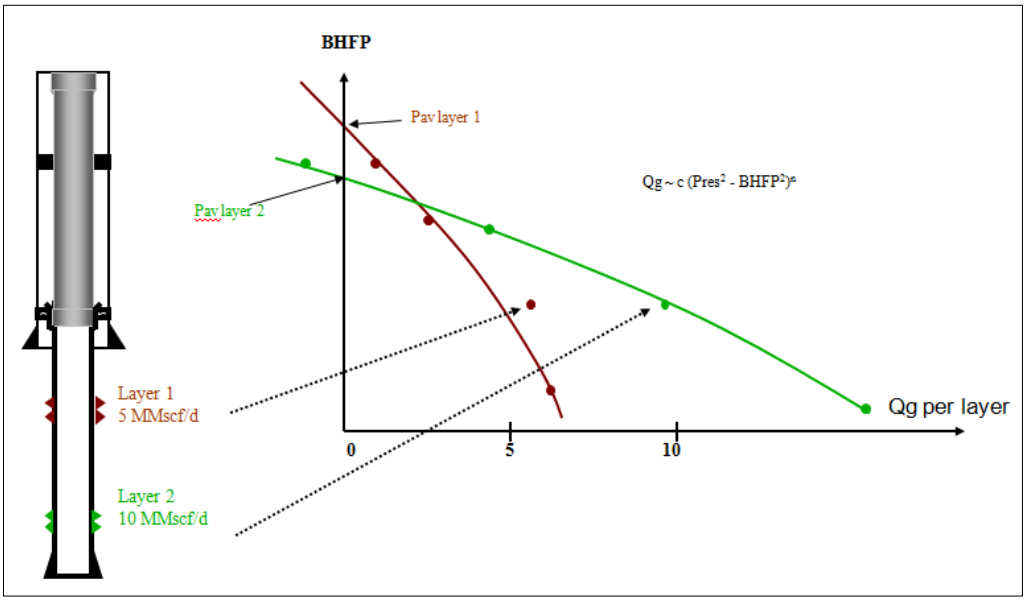


Fig. 17.M.1 – SIP example with 2 layers, 3 rates and a shut-in survey

17.M.1 IPR Type

Different IPR equations can be used: Straight line, C&n, and LIT relations. In the case of a gas well, the pseudo pressure m(p) can be used instead of the pressure p to estimate the gas potential.

Straight line (Darcy): $Q = PI \times (\bar{p} - p)$

LIT (Jones, a & b): $\bar{p}^2 - p^2 = a \times Q + b \times Q^2$

or $m(\bar{p}) - m(p) = a \times Q + b \times Q^2$

Fetkovitch or C&n: $Q = C \times (\bar{p}^2 - p^2)^n$

or $Q = C \times (m(\bar{p}) - m(p))^n$

It is possible to generate the SIP after correcting the pressures to a common datum. This is typically done using the shut-in pressure profile for the estimation of the hydrostatic head between layers. A pressure corrected SIP highlights the eventual crossflow between layers.

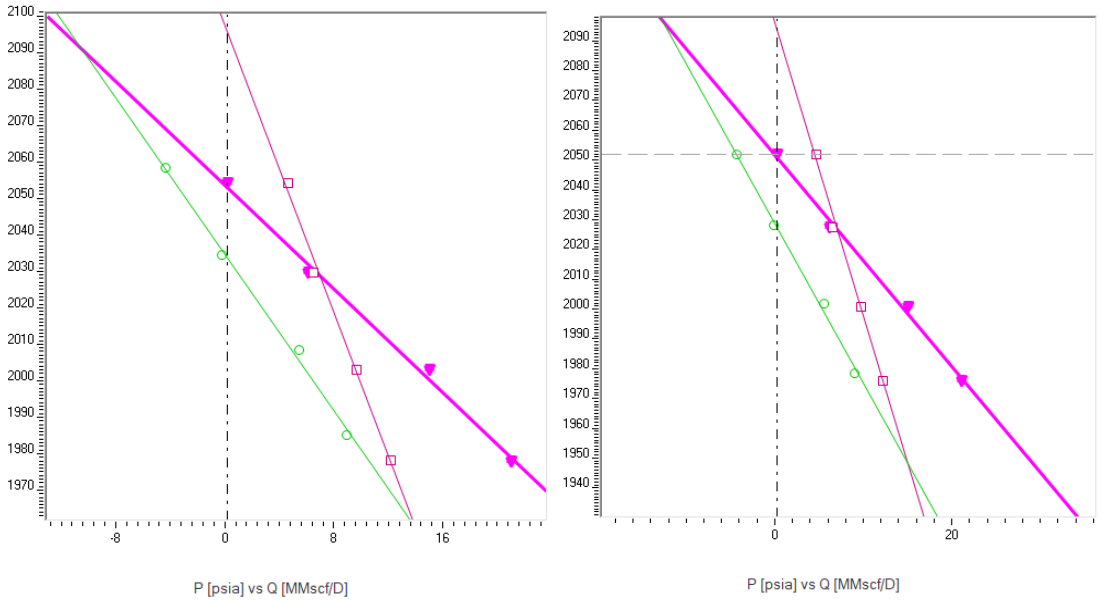


Fig. 17.M.2 – SIP example without and with datum correction

18 – Thermal Analysis and Simulation

NK – VA

18.A Introduction

Temperature data is a remarkable source of reservoir and well information and complements the Dynamic Data Analysis (DDA) workflow. There is a wide range of applications for this data including, but not limited to, qualitative indications of flow, completion integrity, assessment of valve operation, quantitative production and injection profiling.

Temperature logging started in the 30's with methods for temperature-based flow profiling developed shortly after. Latterly, temperature has been recorded as part of production log surveys. Although often considered as a secondary measurement used for PVT calculations and qualitative indications of flow when flowmeter measurements fail, temperature can, with some limitations, prove valuable for quantitative computing of the flow profile. More recently, Distributed Temperature Sensing (DTS) systems based on fibre optics have gained considerable traction as permanent installations as part of the completion, or temporary deployment as part of an intervention. DTS has provided massive, high resolution, data gathering of temperature versus depth at rates up to every 10 seconds.

Similar to permanent downhole pressure gauges (PDG), the ever growing volume of data generated has presented its own challenge. Typically, massive data is required for time stepped qualitative purposes, whilst quantitative interpretation requires relatively very few data points.

This chapter starts by exploring the different applications of temperature data, followed by a summary of the key theoretical concepts on thermodynamics and heat transfer that must be considered to make educated clicks. The different thermal methods offered by KAPPA are also described: for Emeraude, the Energy model, Water Injection Fall-off and different options for forward modeling. For Rubis, the coupled wellbore-reservoir fully transient 3D simulator.

The non-unique nature of the thermal interpretations is emphasised by presenting sensitivity analysis for all available models.

18.B What information can be extracted from Temperature data?

In wells with permanent temperature monitoring installations (DTS, fixed gauges, discrete distributed measurements, etc.) it is possible to extract a variety of information throughout the life of the well. When running temperature acquisition surveys (wireline or slickline) the gauges are typically combined with other sensors (acoustic, calipers, flowmeters, etc.) to facilitate the interpretation. In either case the data that can be extracted includes:

Completion and integrity evaluation

Right from the beginning of the life of the well, permanent installations of fibre optics can help to monitor and extract information about the cementing and stimulations operations. The image below shows a temperature map during the cementing. The onset of the exothermic curing reaction is clearly seen, together with the top of the cement:

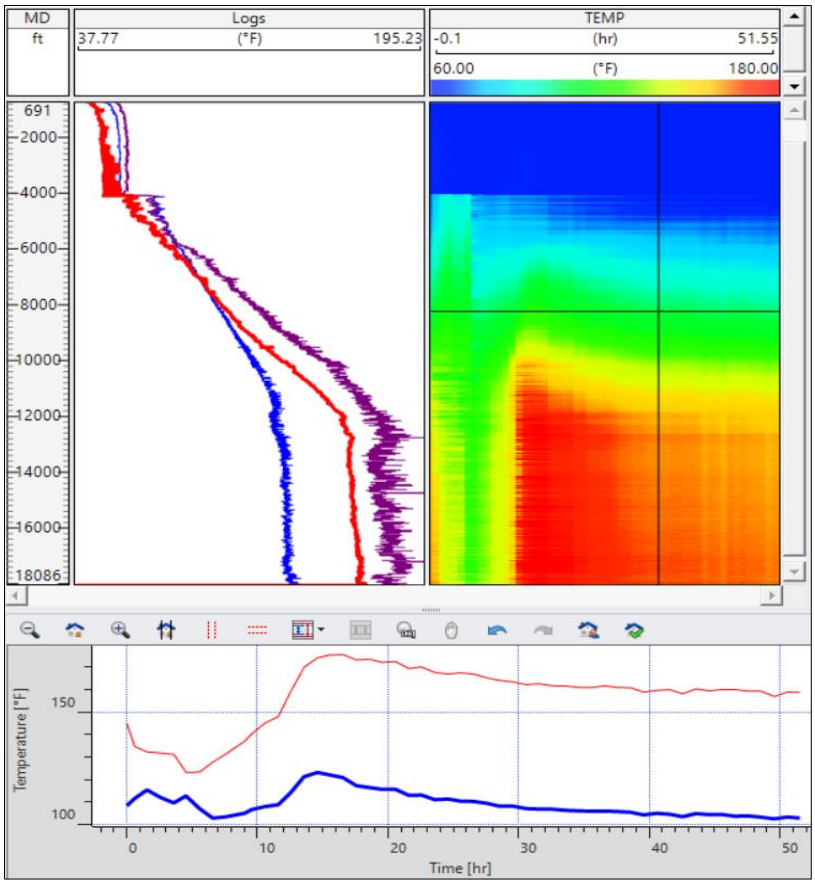


Fig. 18.B.1 – Temperature map during a cementing operation

In hydraulic fracturing operations the water injected typically cools the formation, and this can be observed as local temperature variations around the perforations or sleeves that received water. Also the exothermic reaction as a consequence of minerals dissolution while acidizing can be observed by temperature measurements. This can help to understand the effectiveness and location of the different stimulation treatment.

With the well in production, qualitative information about gas lift valves, packer isolation, cement channelling, producing intervals, leaks, etc. can be extracted. The image below shows a well that had been closed a number of days. The well was put in production and is clear that the Gas Lift Valve 2 is injecting. The producing interval shows cooling from some perforations, while others do not seem to undergo any change. The operation of the ICVs can also be understood from this picture:

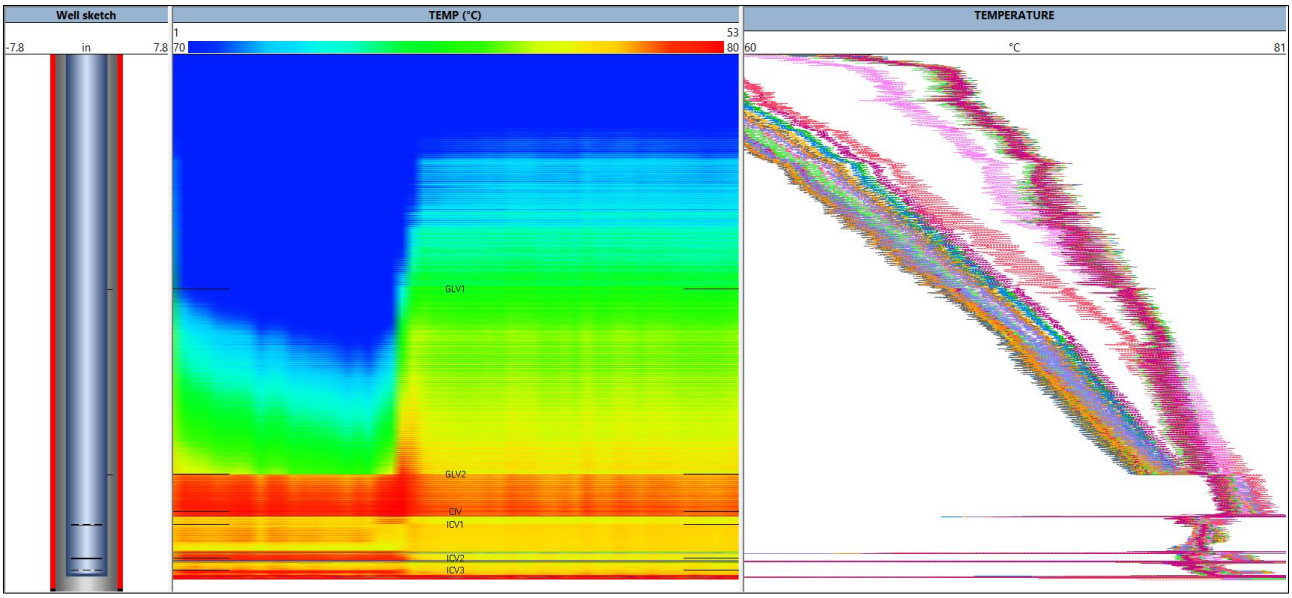


Fig. 18.B.2 – Start-up sequence of a gas-lifted well

Flow profiling

The implementation of the thermal models in Emeraude dates from 2001, where a "Segmented" model (Ramey equation and enthalpy balance) was introduced. Later in 2010 the Energy model was also implemented in Emeraude. Being a PL interpretation software, the early use of these models was in general intended to replace the use of the spinner as main fluid velocity source, when due to the sensor condition (clogged, broken) or the flow regime challenges (recirculation, segregation), the flowmeter measurements did not provide a representative velocity.

The image below show a PL acquisition were, below the tubing, the Fullbore spinner indicates downwards moving flow. At the same time, the capacitance and density tools show that this interval is filled with water. What the spinner is actually measuring is the recirculating water, flowing down on the low side of the pipe while the light phase flows upwards on the high side of the pipe. A temperature measurement can be used as a replacement of the spinner in the interval where this indicates downwards flow to quantify the production profile. Other sensors contained in the PL toolstring can be added in the interpretation.

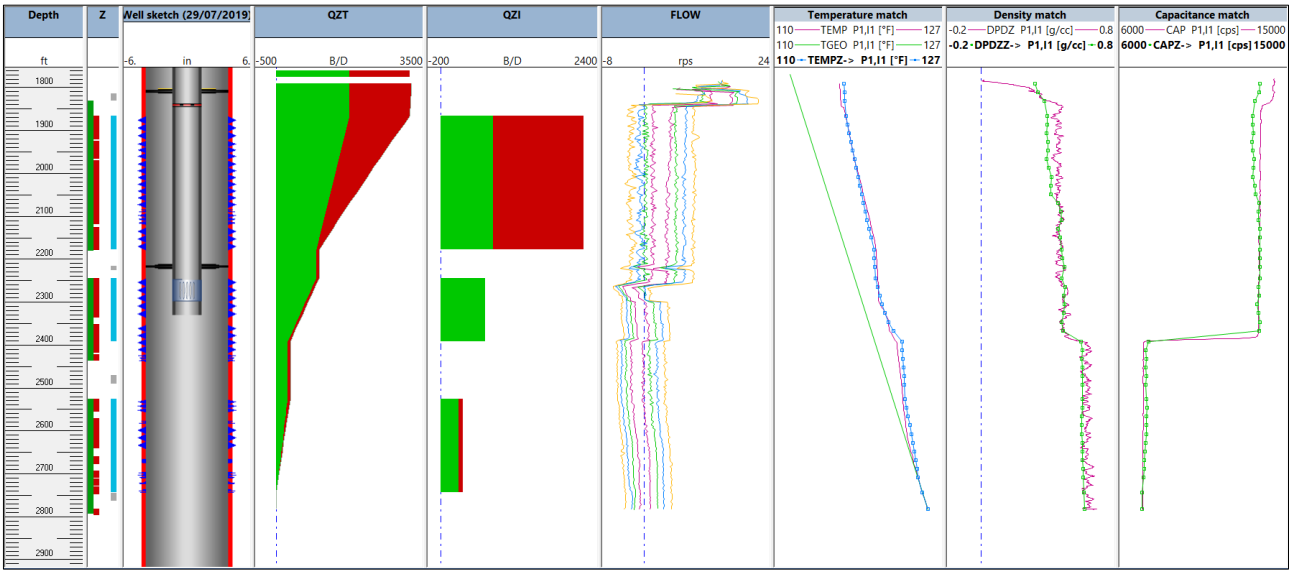


Fig. 18.B.3 – Temperature-based multiphase flow profiling

Water injection profiling

In typical water injection conditions, the water temperature is considerably lower than the formation temperature. While injecting the temperature changes due to the different outflows are in general very small and difficult to be quantified. However, the measured temperature during shut-in conditions after a period of water injection will reflect the volume of injected water that each layer received previously. This can be used for quantifying the injection profile, using a method called Water Injection Fall-off. The image below shows an injection profile using DTS temperature data only.

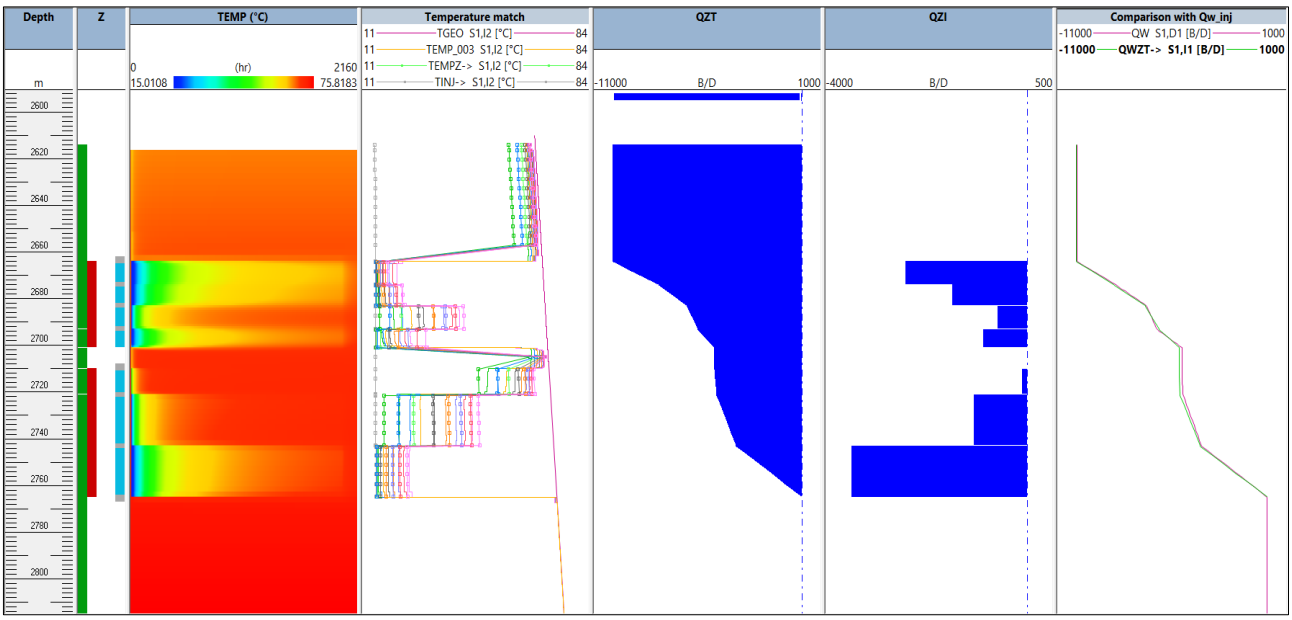


Fig. 18.B.4 – Injection profiling from DTS

Reservoir response

Apart from the single well applications described above, the thermal analysis of a sector of a field might bring interesting insights about different reservoir aspects: interference between wells, connection between producing and injecting wells, high permeability streaks, faults, etc. This type of analysis is on the ground of numerical modelling, where the field model is gridded and the flow and thermal equations are solved for each cell. Rubis incorporates a coupled reservoir-wellbore fully transient, 3D, 3-phase simulator.

The image below shows the interaction between a producer and injector. The temperature simulations can be displayed as production logs and gauges at any depth (surface, sandface, etc.) facilitating the comparison against measured data. Also the temperature maps are shown in 2D or 3D maps.

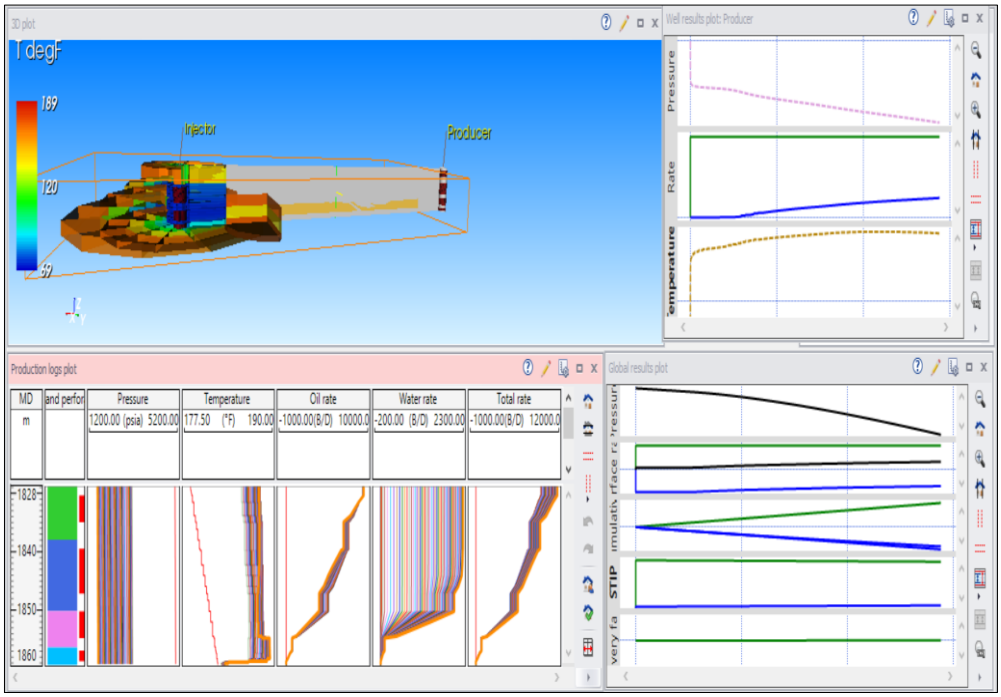


Fig. 18.B.5 – Thermal numerical simulation in Rubis

18.C Temperature Measurements

A brief review of the different technologies on downhole temperature measurements is presented below.

18.C.1 Distributed Temperature Sensing (DTS)

When a monochromatic light interacts with a material like silicon dioxide (SiO_2), the scattered light shows a wavelength shift compared to the incident light. This phenomenon is called Raman Scattering. The molecular vibrations of the SiO_2 lattice structure can gain or lose energy as a result of the interaction with the light's photons. If the material absorbs energy, the backscattered wavelength increases (lower frequency) compared to the incident light. This reflection is called Raman Stokes. On the other hand, if the material loses energy, the wavelength of the backscattered light decreases (higher energy). This is the Raman anti-Stokes peak, and interestingly it has a strong dependency on the temperature of the material. This is the principle of fibre optics temperature measurements.

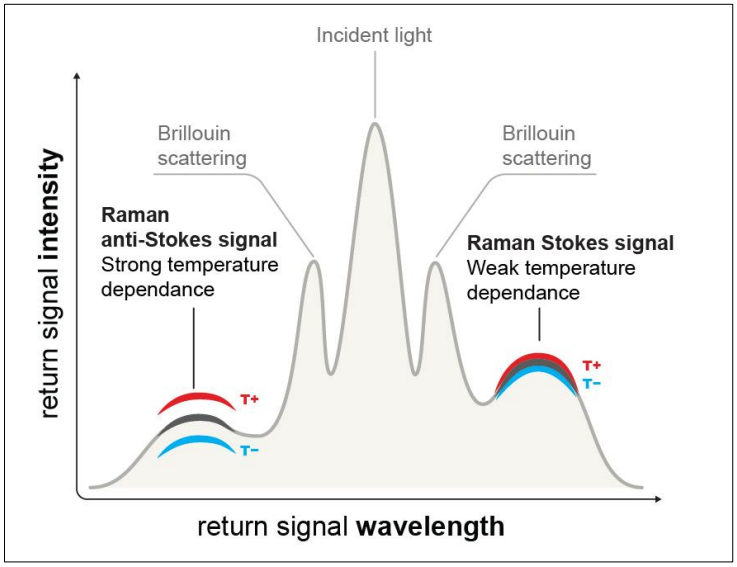


Fig. 18.C.1 – Wavelength spectrum of the backscattered light (Courtesy: AP Sensing)

Distributed Temperature Sensing (DTS) systems couple two main components: a surface opto-electronic interrogator and a fibre optic deployed in the well. The interrogator sends pulses of laser light of short duration (nanoseconds) into the optical fibre. At each depth the photons will interact with the fibre, and the backscattered energy spectrum is analysed at surface. As explained before, the ratio of the Raman Anti-Stokes and Stokes counts is a function of the temperature of the fibre. Assuming that the speed of light through the fibre optic is constant, the location of the backscattered light returning to the surface can be established. This allows obtaining a continuous temperature vs. depth measurements.

The counts received at surface for the different peaks may be small and subject to statistical variation, so a single temperature profile typically results from the computation of multiple laser-fibre interactions. Depending on the acquisition settings, the DTS system can output a temperature trace as few as every couple of seconds or minutes.

The counts per second decrease with depth, reducing the dynamic range between the Stokes and Anti-Stokes counts with the light loss. This can be assessed and corrected by using double ended fibre optics (injecting light through both ends). Otherwise, in single ended fibre optics, a correction factor is applied.

In terms of the metrology of the DTS measurements, the vertical resolution is a function of the length of the pulse, but values down to 0.125 m are reported. Also, a minimum resolution of 0.01 °C is reported, comparable with conventional temperature gauges. To increase the accuracy, temperature is measured independently at the interrogator.

The core glass of the fibre is made of fused silica, typically around 50 µm. This core is surrounded by a glass cladding of lower refractive index than the core, to ensure total reflection and the light staying in the fibre. Multiple optical fibres can be deployed at the same time, and are normally contained in a ruggedized cable (metal or plastic). The picture below shows the different options of fibre optics for downhole applications, contained in a cable and in a rod:

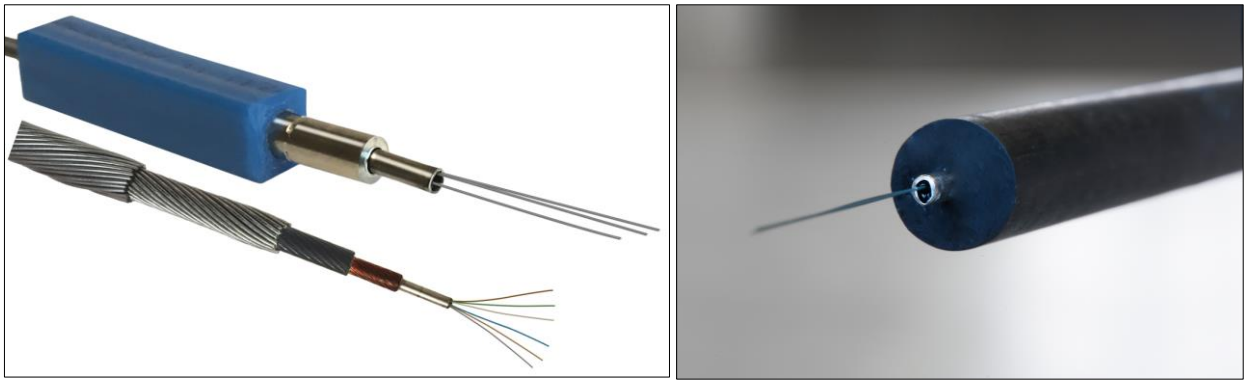


Fig. 18.C.2 – Left Image: Permanent and wireline Fibre Optics (Courtesy: Silixa). Right Image: Carbon rod with fibre optics (Courtesy: Ziebel)

The most typical deployment options are:

- Permanent: strapped on the casing and cemented in place
- Semi-permanent: strapped on the tubing
- Intervention-based: deployed through tubing for a specific acquisition program

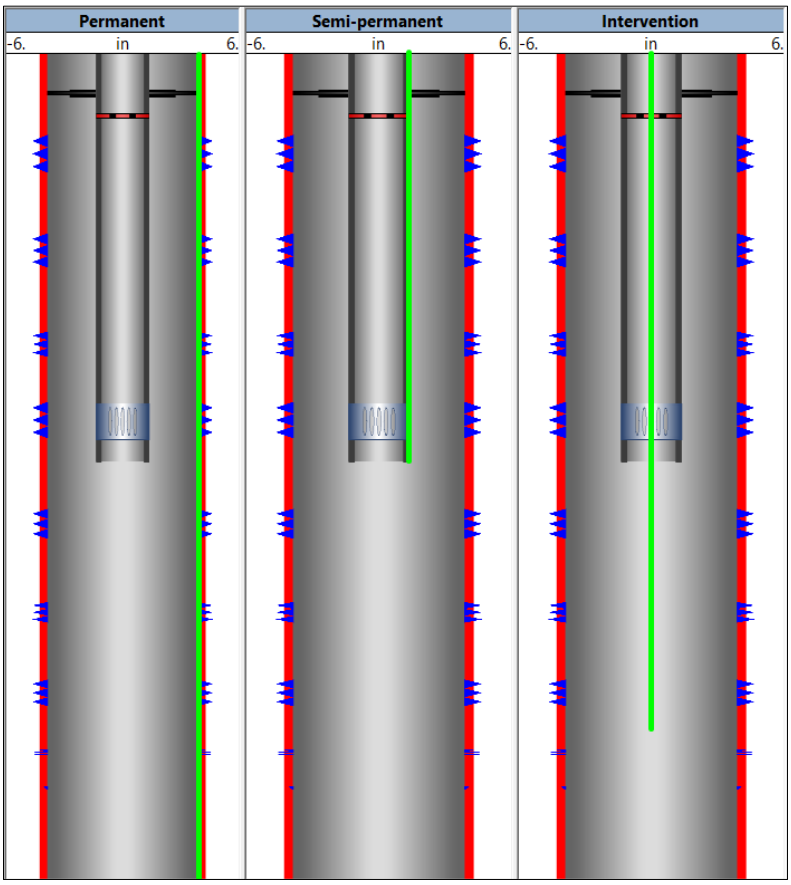


Fig. 18.C.3 – DTS deployment options

Among the advantages of DTS it can be mentioned that there is no need of downhole electronics, that may be prone to degrade with harsh environments. Permanent fibre installations do not require (neither allow) maintenance, but the surface interrogator may be replaced if needed.

18.C.2 Discrete Temperature Sensors

A different technology able to provide a continuous temperature vs. depth profile at different times consist on arrays of discrete temperature sensors. These are clamped onto TCP guns, DST assembly and some completion elements, like sand screens.

The sensors can be very closely spaced, down to 0.2 m, which gives similar vertical resolution than the DTS systems. The sensors require energy, which is provided by batteries. Depending on the duration of the acquisition program, a single battery that lasts up to 30 days may be used, or extended battery packs may be added allowing years of measurements.

The data transmission to surface is wireless, which adds flexibility on the type of completion or tool where this array may be installed.

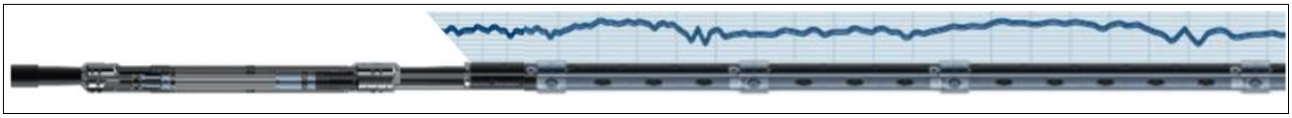


Fig. 18.C.4 – Discrete Temperature Sensors (Courtesy: Metrol – PRO-LOG®)

18.C.3 Temperature gauges

Temperature gauges can be installed at different depths of the well, from surface to typically above the producing interval. These installations are sometimes part of Permanent Downhole Gauges (PDGs), and can provide valuable data especially after water breakthrough or gas production. Moreover, it can be used as targets in thermal PTA or full field simulations.

Temperature gauges are also run as part of PLT acquisitions. Whilst in the past these measurements were meant to provide zonal temperature for PVT calculations and qualitative indications of production/injection and integrity, this chapter will explain how the different thermal models can turn this data into profiles.

The most widely used temperature gauges for PLT applications are platinum resistance thermometers. The resistance of the metals increases pretty much linearly with temperature, and therefore by measuring the voltage of a circuit subject to a constant current, it is possible to obtain a temperature value from a calibrated device.

More recently Micro-Electro-Mechanical Systems (MEMS) started to be used in the industry, featuring monocrystalline sensing elements. These can be packed in small containers of different shapes. The image below shows one of these sensors, used for PLT applications.



Fig. 18.C.5 – MEMS Temperature gauge (Courtesy: OpenField)

18.D Theory review

The equations used to model the temperature in the wellbore and the reservoir are based on well-known heat transfer and thermodynamic principles. A revision of the physics involved is presented next.

18.D.1 Heat Conduction

Fourier's Law of heat conduction established that the heat flux (q) is proportional to the temperature gradient along certain material. The constant of proportionality λ is known as the thermal conductivity of the material or fluid. Fourier's law can be expressed as:

$$\vec{q} = -\lambda \nabla \mathrm{T}$$

Where the heat flux is a vector quantity and is of opposite sign to the temperature gradient, meaning that heat flows from warmer to cooler areas. This mechanism of heat conduction occurs as a concequence of the energy transfer caused by the molecules movement. In general terms, the thermal conductivity is an anisotropic scalar magnitude and temperature dependent $\lambda = \lambda(\mathrm{x}, \mathrm{y}, \mathrm{z}, \mathrm{T})$. However for the applications we will be dealing with, we will consider that λ is constant for the range of temperatures and isotropic. For the different materials and fluids found in an oil well, the magnitude of the heat conductivity can vary up to 4 orders of magnitude.

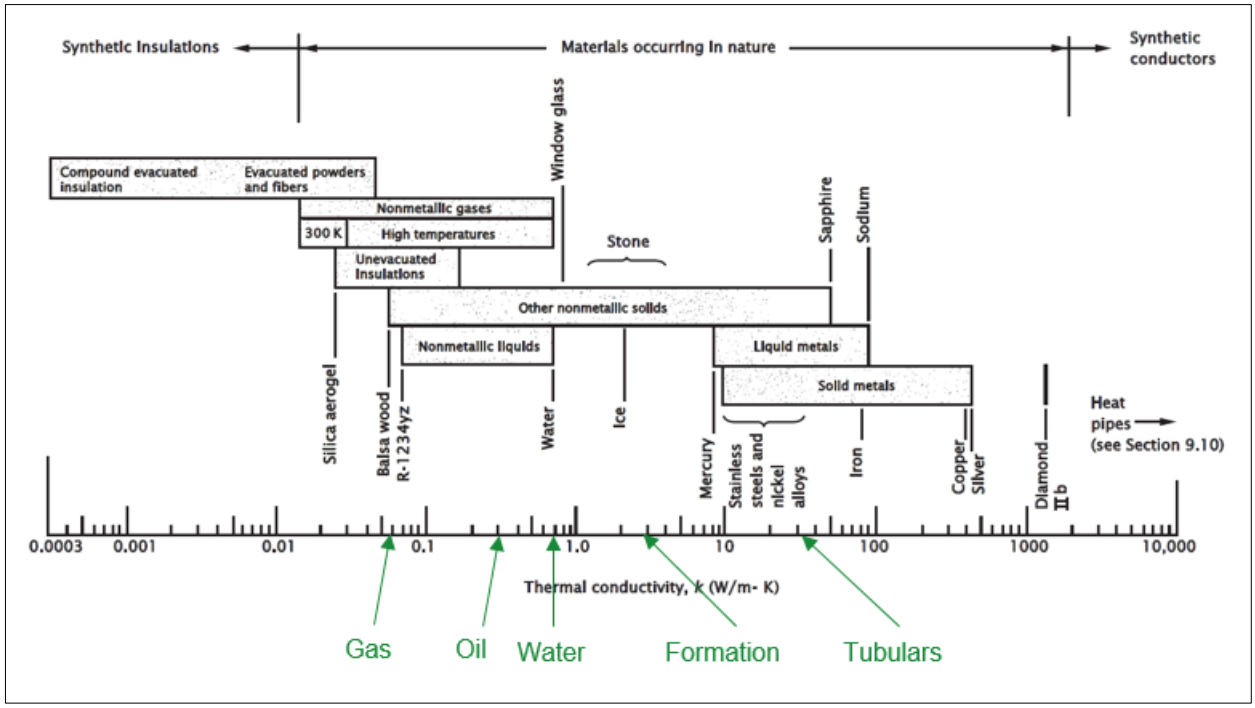


Fig. 18.D.1 – Thermal conductivity for different materials (from Lienhard, 2018)

In producing or injecting wells these different materials are connected in series as shown in the image below. A consequence of the large differences between the thermal conductivity of the materials involved is that the casing and tubing will be virtually isothermal and the largest temperature drops will occur in the fluids, since $\frac{dT}{dr} = \frac{q}{\lambda}$. A practical application of this is to fill

the casing-tubing annular with nitrogen to minimize the heat losses to avoid flow assurance issues, such as asphaltenes precipitation.

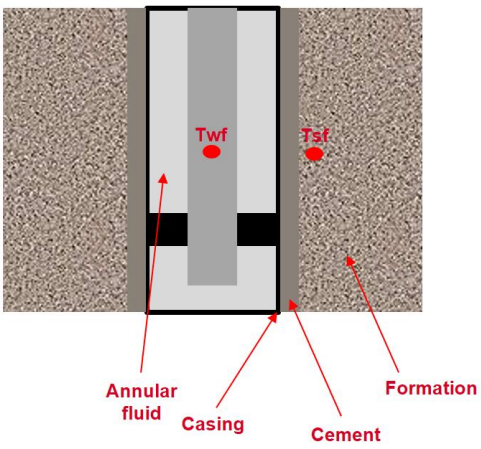


Fig. 18.D.2 – The thermal conductivity of the different components spans over 4 orders of magnitude.

18.D.2 Heat Convection

Convective heat transfer is described by the Newton's law of cooling. The equation indicates that, for a system composed of a body immersed in a fluid at a different temperature, the heat flux is proportional to the temperature difference between the body and the moving fluid. In this case the proportionality constant "h" is called Heat transfer coefficient or sometimes referred as "Film coefficient".

$$\vec{q} = \bar{h}\,(T_{body} - T_{\infty})$$

When the fluid is moving, for example due to a pressure difference or gravity, the heat transfer process is called "Forced convection". However, if the fluid is still, the molecules in contact with the hot body will increase their energy, will start to move faster and its density will decrease. This will create convective currents due to density differences in the fluid column. This is called "Free convection".

The Heat transfer coefficient depends on many factors, including the shape of the body, fluid velocity, temperature difference, thickness of boundary layer, etc.

18.D.3 Radiation

All the bodies emit energy through electromagnetic radiation. Bodies at high temperatures may emit energy in the visible spectrum (fire, the sun, etc.), but the radiation emitted by humans can only be seen with infrared cameras. Compared to conduction and convection, radiation does not require a medium.

Perfect radiators are called "Black Bodies" and they absorb all the energy and reflect none. The Stefan-Boltzmann law for a Black body states that the total energy emitted (integral for all wave lengths) is given by:

$$e(T) = \sigma\, T^4$$

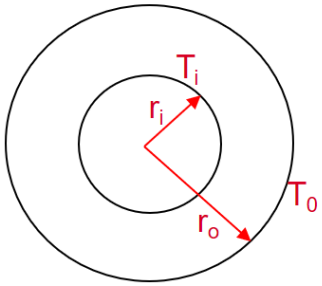
Were σ is the Stefan-Boltzmann constant. This expression implies that the energy emission is independent on the body characteristics and is a strong function of the temperature (fourth power). However, the materials that we consider in our heat transfer problems are not perfect black bodies. Therefore, an "emittance" coefficient is included in the Stefan-Boltzmann equation to account for real bodies.

In oilfield applications, radiation is the least important heat transfer mechanism for typical temperatures.

18.D.4 Heat Loss Coefficient

It is beyond the scope of this book to derive the thermal diffusivity equation. For cylindrical coordinates, the expression is:

$$\frac{1}{r}\frac{\partial}{\partial r}\left(r\frac{\partial T}{\partial r}\right)+\frac{1}{r^2}\frac{\partial^2 T}{\partial \theta^2}+\frac{\partial^2 T}{\partial z^2}$$



If we consider a hollow cylinder (i.e. a pipe) at steady state and where the axial (z) and azimuthal (θ) components are negligible, from the thermal diffusivity equation and the definition of conductive heat transfer (Fourier's law), it is possible to find that the heat decreases with the radius as:

$$q_{radial}=\frac{\lambda\,\Delta T}{ln\,(\frac{r_o}{r_i})}\,\frac{1}{r}$$

The total heat transfer in the cylinder of length *l* can then be calculated as:

$$Q(W)=\frac{2\pi\,\lambda\,l\,\Delta T}{ln\,(\frac{r_o}{r_i})}$$

This expression resembles other physical processes where a potential (pressure, voltage, concentration, etc.) leads to a flux. Equations of this type are Darcy, Ohm, Fick, etc. As an analogy with Ohm's law we can define the thermal resistance as:

$$R_{t_{cyl}}=\frac{ln\,(\frac{r_o}{r_i})}{2\pi\,\lambda\,l}$$

Starting again from the thermal diffusivity equation in radial coordinates, but replacing the external temperature (T_0) by a convective boundary condition, the total heat transfer can be calculated as follows:

$$Q=\frac{T_i-T_\infty}{\frac{1}{h\,2\,\pi\,r_o\,l}+\frac{ln\,(\frac{r_o}{r_i})}{2\,\pi\,\lambda\,l}}$$

The delta T is now divided by the sum of the convective and conductive thermal resistance. This concept becomes very useful when, apart from having a single cylinder, there are multiple concentric cylinders, like we find in wells with tubing, annulus, casing, cement, etc. The Heat transfer coefficient "U" is defined so:

$$Q=U\,A\,\Delta T$$

With the heat transfer coefficient U defined as the sum of all the different completion components, based on their geometry and thermal properties (*i*=inner, *o*=outer):

$$\frac{1}{U} = \frac{r_o \ln(r_o/r_i)}{\lambda_{tub}} + \frac{r_o \ln(r_{ci}/r_o)}{\lambda_{ann}} + \frac{r_o \ln(r_{co}/r_{ci})}{\lambda_{cas}} + \frac{r_o \ln(r_w/r_{co})}{\lambda_{cem}} + \frac{r_o}{r_{ci}\,(h_c + h_r)}$$

Where the first four terms are the conductive components of the tubing, annular, casing and cement. The terms h_c and h_r are corrective terms accounting for the annulus free convection and the annulus radiation respectively (Hassan and Kabir, 2002). Note that the presence of these corrective terms for the annulus introduces a dependence of *U* on the temperature, increasing the nonlinearity of the system.

For convenience, two other parameters are derived from the Heat transfer coefficient:

- Heat Loss Coefficient: $HLC = U\,2\pi\,r_w$
- Thermal Conductance: $D_{wb} = U\,2\pi\,dL\,r_w$

The required geometrical parameters and thermal properties for each completion element are entered either at the Well intake definition in Rubis or at the interpretation information in Emeraude. Tables with thermal properties for different materials are provided in the software for reference. However, it is important to understand the impact of the thermal and geometrical characteristics of the different components on the Heat transfer (or Heat loss) calculations.

Let's consider a completion composed by a 7'' casing (6.184'' ID) of thermal conductivity of 35 W/m °K, surrounded by cement OD=8.5'' of 1.3 W/m °K. This base case (BC) leads to a HLC= 41.4 W/m °K. The figure below on the left shows the variation of HLC for changes in either the cement or the casing thermal conductivity. Varying the casing conductivity from 5 to 100 W/m°K does not lead to a significant change in the HLC from the Base case. On the other hand, a change in cement conductivity of between 0.1 to 10 leads to a variation of 200 times of the HLC.

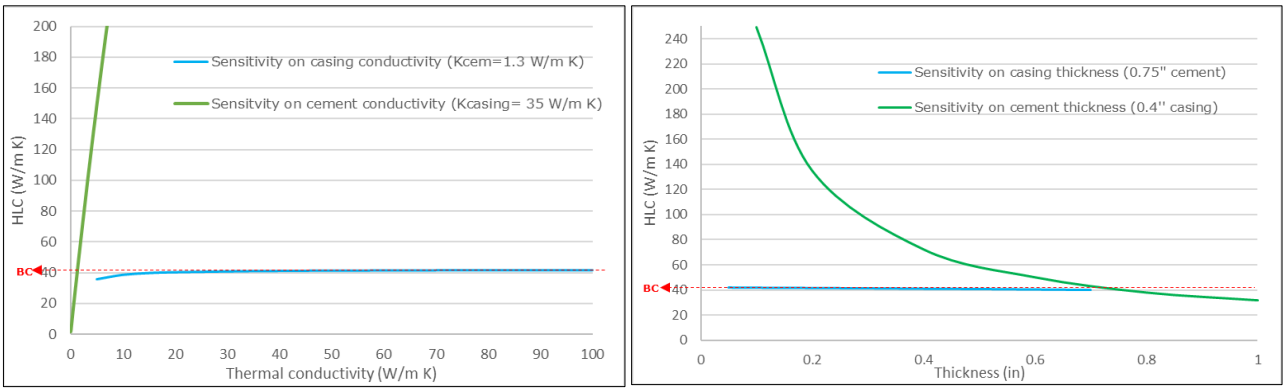


Fig. 18.D.3 – Sensitivities on the HLC estimations.

Similarly, the image on the right shows the variation on HLC for different casing and cement thickness. In this range of normal values, the casing thickness does not have a significant influence on the final HLC. However, an increase in the cement thickness leads to a rapid drop of the HLC.

These sensitivities show that, since the different completion components are connected in series, the influence of the material of lowest thermal conductivity will be preponderant. Errors in the thermal properties of the cement and annular fluids will have a large impact, while the casing and tubing won't have a large effect. A large HLC value favors the heat exchange with the formation, so the fluid between perforations will tend to come back quicker to the geothermal.

18.D.5 Geothermal Gradient

It is estimated that the earth's core temperature is between 5400 to 6000 °C. Clearly the surface of the earth is at a much lower temperature. As a consequence of this temperature gradient, and as shown by the Fourier's law, a net heat flux will exist. This heat flux is not isotropic, and in general is larger in areas where the tectonic plates are in contact, and where seismic or volcanic activity exists.

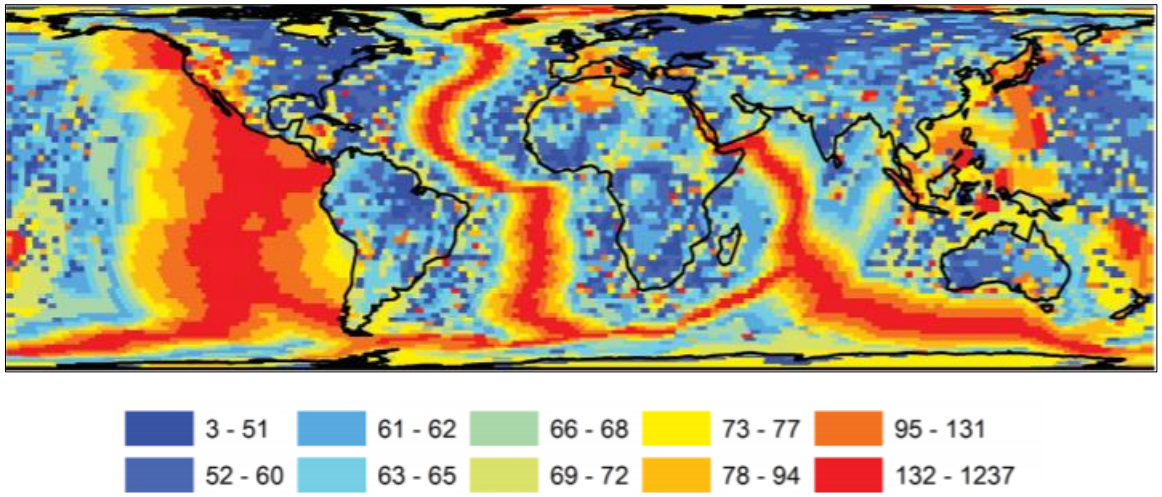


Fig. 18.D.4 – Heat flux map (mW/m2). From Davies (2003)

For a certain location in the earth the heat flux will be constant. When analysing the temperature variation vs. depth, the gradients will be given by $\frac{dT}{dz} = \frac{q}{\lambda}$. The thermal conductivity can be quite different depending on the mineralogy of the formation, with sandstones ~ 2.5 – 4.2 W/m K, shales ~ 1.05 – 1.45 W/m K and Claystone/siltstone ~ 0.8 – 1.25 W/m K. In general, away from the tectonic plates, the temperature increases 10-30 °C per km.

The determination of the geothermal gradient is very important, since the assumption will be that reservoir fluids far from the well are at thermal equilibrium with the formation, and thus at the geothermal temperature at that depth. Establishing the gradient would then consist in measuring an undisturbed formation temperature, during shut-in for example. While this is possible, due to the low thermal conductivity values of the formation, reaching the equilibrium would take a long time and wouldn't be operationally feasible in producing and injecting wells. Also geothermal gradients measured shortly after the well was drilled will be affected by the invasion and circulation of drilling and completion fluids.

The geothermal gradient can sometimes be measured in regions of the well with no fluid movement, like the sump below the bottom producing/injecting interval. Care must be exercised since the temperature in the sump might be affected by fluid movement behind casing or the vertical thermal conductivity due to the fluid production from the deepest perforation. This is shown in the image below, where the PL-derived flow profile shows the deepest perforation, however the temperature track shows temperature variations vs. depth, which could result in non-representative geothermal gradient estimations:

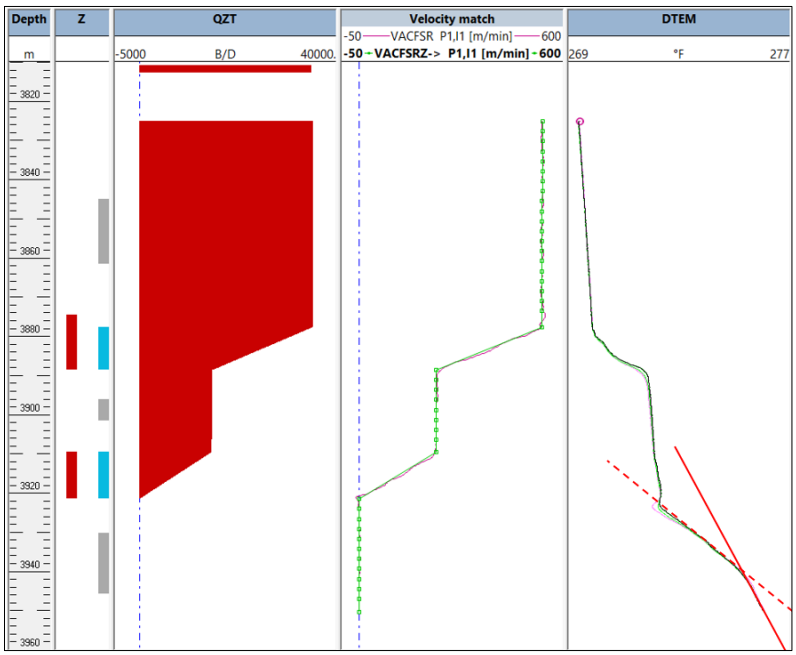


Fig. 18.D.5 – Temperature in the sump varying with depth

In high angle/horizontal wells it may not be possible to establish the geothermal temperature from measurements in the sump or during shut-in. Reference values for the area can be used as a first approach, even though the interpreter may need to treat these values more like a variable rather than a fixed parameter. In deviated wells it is necessary to enter the deviation survey for the gradient to be corrected vs. depth.

18.D.6 Joule-Thomson Effect

In the previous section it was mentioned that far field fluid temperature is equal to the geothermal temperature. However, as the fluid moves towards the well, it undergoes a pressure change (drop for producers) as given by the Darcy law in radial coordinates:

$$p(r) = p_{wf} + \frac{q\,\mu\,B}{k\,h}\ln\left(\frac{r}{r_w} + S\right)$$

The Joule-Thomson effect establishes that the temperature change is proportional to the pressure change, and the proportionality constant is given by the Joule-Thomson coefficient.

$$\Delta T = K_{JT}\,\Delta P$$

Strictly speaking the Joule-Thomson effect describes an isenthalpic process, which is achieved in steady state production conditions. The constant can be obtained from thermodynamic parameters as:

$$K_{JT} = (\frac{dT}{dP})_H = \frac{1}{C_P}(T\frac{dV}{dT} - V)$$

Where V is the specific volume (inverse density), $\frac{dV}{dT}$ is the thermal expansion and Cp is the specific heat.

Let's consider the production of single phase water. The change in volume for water is negligible in the temperature range that concerns us. Therefore, the expression of the Joule-Thomson coefficient can be reduced to $K_{JT} = \frac{-V}{C_P}$. From $\Delta T = K_{JT}\,\Delta P$ it is clear that as the water approaches the well it decompresses (negative ΔP) and since the K_{JT} is negative, the fluid will experience a warming. This is sometimes referred to as "Viscous heating".

The other extreme is to consider gas, which has a high compressibility and high thermal expansion. For typical downhole pressures the Joule-Thomson coefficient shows a positive sign. As a consequence, as the gas decompresses (negative ΔP), the temperature also drops. However, for high pressures (>7000 psia) there is an inversion point and K_{JT} will be negative, resulting in heating.

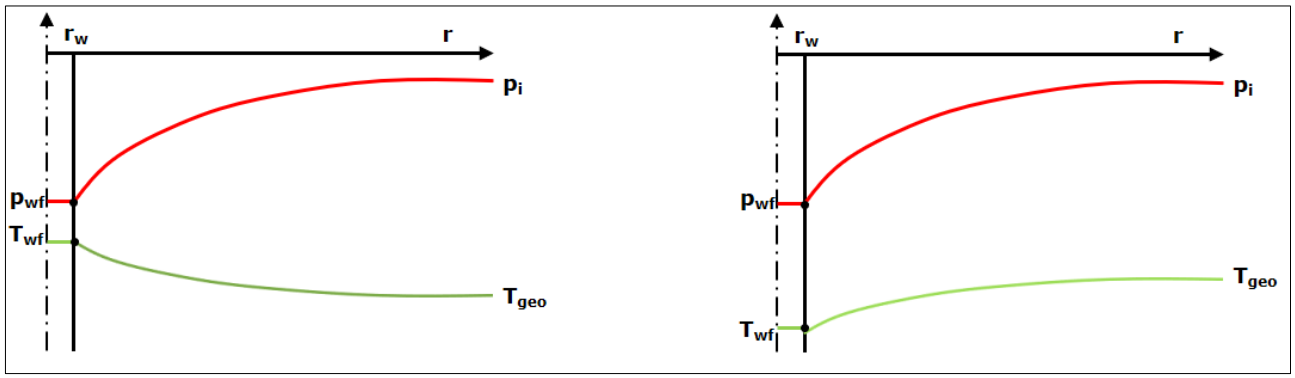


Fig. 18.D.6 – Reservoir Temperature profile predicted by Joule-Thomson for liquids or high pressure gas (left) and gas (right, pressure < 7000 psia)

Typical K_{JT} for water is around -0.0016 °C/psi, while for gas it can be around 0.016 to 0.032 °C/psi. This means that water requires a drawdown 10 times higher than gas to produce a similar ΔT. Oil would also have a negative K_{JT} (leading to heating). The temperature response of a layer producing gas and condensate would depend on the mass of both liquid and gas components, and might end up in cooling or warming.

The ΔP experienced by the fluid on its way to the well shows a sharp change around the wellbore, and it is influenced by the permeability of the formation and damage. From the thermal diffusivity equation, we can deduce that rapid changes in temperature when shutting-in the well can indicate skin. On the contrary, highly permeable formation or stimulated intervals would show very slow temperature changes.

In thermal interpretation, apart from dealing with the traditional PVT parameters used in PL or PTA interpretation, the definition of certain thermodynamic properties will have an impact on the simulations. The figure below shows the temperature profiles predicted in Emeraude when the produced fluid heat capacity (Cp_g) increases from 0.01 Btu/(lbm.°F) to 5 Btu/(lbm.°F), the zone contributions being unchanged and identical on each zone.

It can be seen that the higher the fluid heat capacity, the lower the cooling effect on the inflow zones as expected by the K_{JT} definition. But also, higher heat capacity means a more efficient convective heat transfer by the fluids coming from deeper depths, and this counterbalance the heat conduction between inflows.

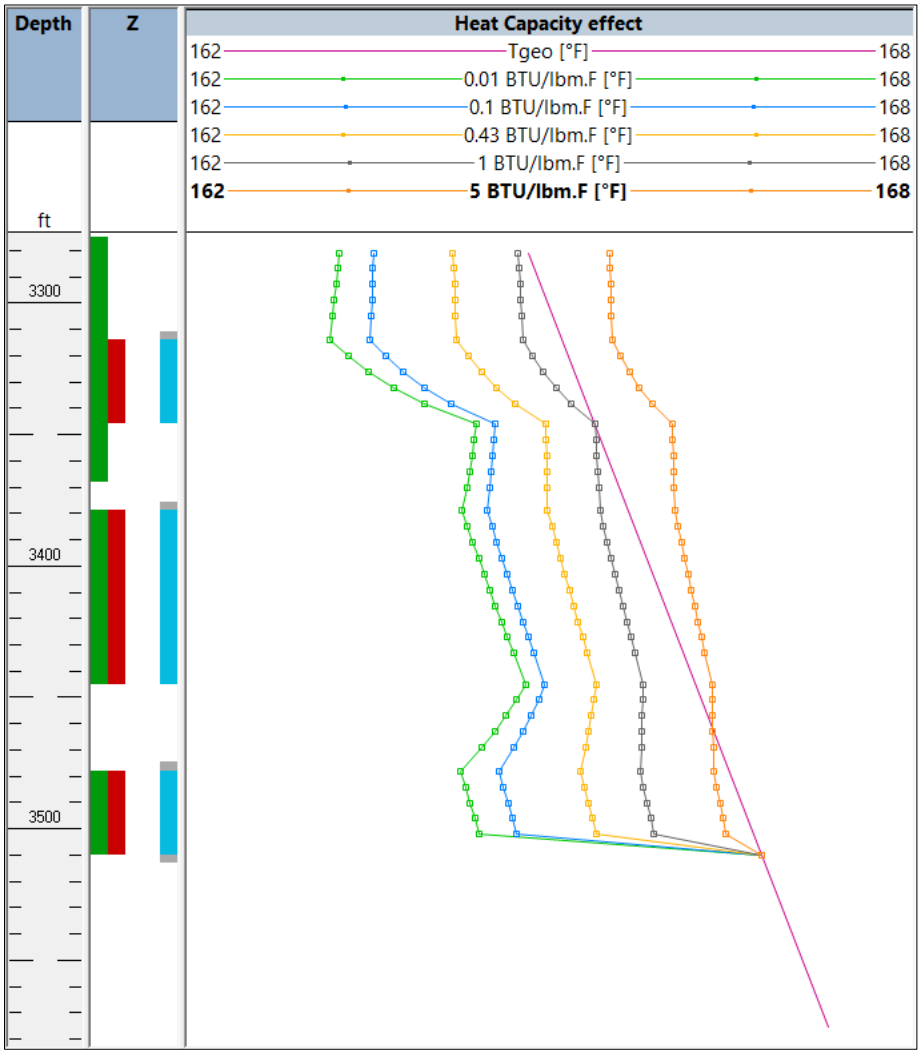


Fig. 18.D.7 – Effect of the fluid heat capacity on the simulated temperature (Gas producer)

18.D.7 Ramey Equation and qualitative analysis

Early models to predict the temperature profile in producing or injecting wells used the work of Ramey (1962) to model the temperature. Ramey's original work dealt mainly with water injectors, and therefore the assumptions are valid for single phase incompressible fluids. Moreover, the inflow/outflow itself is not modelled, and does not account for cooling or warming at the perforation interval.

The Ramey equation shows:

$$T(z,t) = T_{ge} - g_G z + g_G A$$

With the term A being a function of the rate (Q), density and heat capacity:

$$A = 1.66\, Q\, \rho_f C_f\, f(t)$$

and the time dependent term:

$$f(t) = -ln\left(\frac{r_{ce}}{2(\lambda t)^2}\right) - 0.29$$

For a producing well, considering no heating or cooling at the inflow point, the fluid will enter at the geothermal temperature. Above that depth the temperature will evolve as predicted by the Ramey equation. When the distance from the inflow "z" is much larger than A, the exponential in the last term of the equation tends to zero. Then the flowing temperature approaches an asymptote parallel to the geothermal, with the offset given by the rate and also time of production. This is shown in the figure below (I).

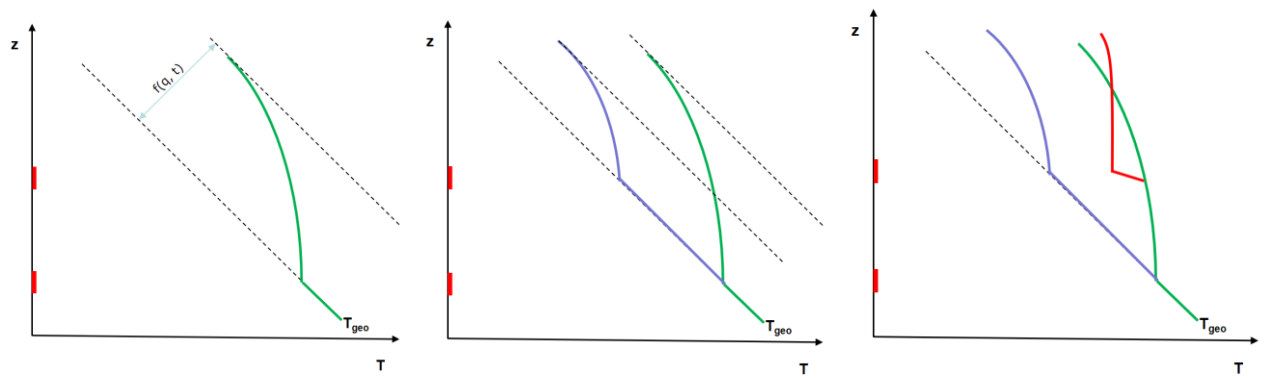


Fig. 18.D.8 – (I) Single inflow at the bottom perforation. (II) Two inflow zones producing independently. (III) Two inflow zones producing comingled.

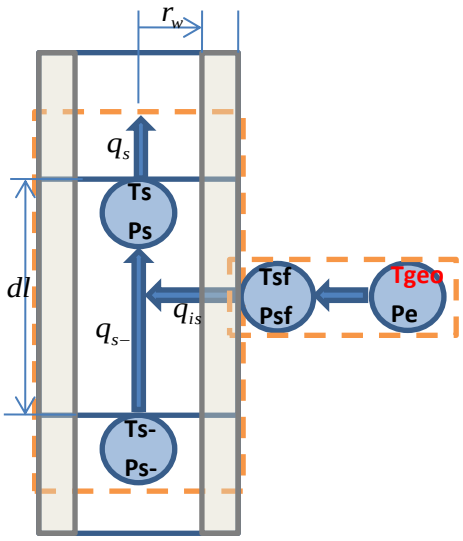
If now we consider the presence of two inflows producing independently of each other (II), from the offset of the temperature profile and the geothermal gradient it is clear that the bottom perforation produces a higher rate than the upper perforation (with all the rest of variables constant).

Finally, if we consider the commingled production of the two perforations (III), the final response is shown in red. The warmer fluid coming from the bottom perforation is mixed with cooler fluid coming from the upper perforation. This is seen as a temperature drop in the resulting red curve. The offset of the red curve from the geothermal will be given by the sum of the production from both perforations. In real cases, if the perforations are very close together or the rates are very large, it might be impossible to see the stabilization of the measured profile. This limits the applicability of this technique.

The first thermal model implemented in Emeraude was called "Segmented" model and used the Ramey equation plus an enthalpy balance with imposed pressure drops and the different inflows. This model is no longer available in Emeraude since it does not have any advantage compared to the method that will be described next.

18.D.8 Energy and mass balances

At the core of the Rubis thermal engine and Emeraude "Energy" model, equations of Energy and mass balance are solved in the reservoir and the wellbore. The implementation of these balances is different in both modules and will be explained in sections 18.E and 18.G.



Let's consider a small segment of the wellbore, of length dl, in front of a reservoir zone. The energy coming to the segment minus the energy leaving is equal to the energy accumulation:

$$\frac{dE}{dt} = E_{in} - E_{out}$$

The energy concentration "e" (energy divided by mass) of an infinitesimal volume of fluid is composed by internal energy "u" (thermal movements of molecules), kinetic and potential energy:

$$e = u + \frac{1}{2}v^2 + gdl$$

For a producing well, the energy coming into the segment (E_{in}) can be further expanded into the energy carried by the fluid coming from below in the pipe (q_{s-}), the energy transported by the fluid coming from the reservoir (q_{is}) and the energy transported as heat from the reservoir. Also, incorporating the concept of energy concentration and the expansion work, the energy balance can be expanded as:

$$\frac{dE}{dt} = q_{s-}\,\rho_{s-}\,e_{s-} + q_{is}\,\rho_{is}\,e_{is} - q_s\,\rho_s\,e_s + D\,\Delta T + q_{s-}\,\rho_{s-}\,(\frac{P_{s-}}{\rho_{s-}}) - q_s\,\rho_s\,(\frac{P_s}{\rho_s})$$

Grouping the terms of energy coming from below and going to the segment above, and the expansion work (last two terms), the concept of enthalpy is introduced as

$$h = u + \frac{P}{\rho}$$

Putting all together, the energy balance for a segment of the wellbore is defined by:

$$\frac{dE}{dt} = q_{s-}\,\rho_{s-}\,(h_{s-} + \frac{1}{2}(\frac{q_{s-}}{A\,\rho_{s-}})^2 + g\,dl) + q_{is}\,\rho_{is}\,(h_{sf} + \frac{1}{2}(\frac{q_{sf}}{A\,\rho_{sf}})^2 + g\,dl) - q_s\,\rho_s\,(h_s + \frac{1}{2}(\frac{q_s}{A\,\rho_s})^2) + D\,\Delta T$$

The same procedure is done for a small volume of the reservoir. This time it is necessary to consider that the energy accumulation (and thus the temperature change) occurs both in the fluid (contained in the porosity fraction, φ) and the rock fraction (1- φ). Using the concept of material derivative, the energy balance for a reservoir cell can be expressed as:

$$\varphi\rho\,\frac{\partial h}{\partial t} + (1-\varphi)\,\rho_r\,\frac{\partial h_r}{\partial t} + \rho\,v\,\nabla h - \frac{\partial P}{\partial t} = \rho g v + \nabla(\lambda\,\nabla T)$$

The terms on the left of the equality correspond to the accumulation and convection of enthalpy, while on the right is the energy transferred by the fluid and by heat conduction.

These balances were written for single phase but can be easily extended to multiphase by considering the holdup-weighted sum of the different phases.

For the mass balance, the conservation equation states:

$$\frac{dm}{dt} = m_{in} - m_{out}$$

This equation can be applied both to a small volume of reservoir and to a segment of the well. Clearly, the equations governing the fluid movement in the different media are well known.

18.E Emeraude "Energy" equation - Production and Injection profiling

The implementation of the thermal model in Emeraude is called "Energy" equation. This model consists on a direct simplification of the mass and energy balance equations presented in the previous section. The main assumption is that the flow is steady state, which allows setting the transient terms $\frac{\partial E}{\partial t}$ to zero. Also, in this formulation there is no vertical conduction within the reservoir.

Under steady state conditions, the reservoir is defined by two points:

- An outer point representing the undisturbed conditions at some distance r_e, where the temperature is given by the geothermal T_{geo} and the pressure is the external reservoir pressure P_e
- An inner point representing the sandface conditions at distance r_w, where the temperature is T_{sf} and the pressure is the external reservoir pressure P_{sf}

Having two nodes in the reservoir introduces the need of an extra equation to relate P_e and P_{sf}. This extra equation is Darcy under steady state conditions, that also allows accounting for the geometrical and mechanical skin terms.

$$\Delta P_{sf-e} = P_e - P_{sf} = \frac{(Q\ \mu)}{2\ \pi\ k_H\ h_T}\left[\frac{h_t}{L_w}\ S + \ln\left(\frac{r_e}{r_w}\right) +\ S_G\right]$$

The pressure drops are then computed iteratively at the average pressure point and at flowing wellbore temperature.

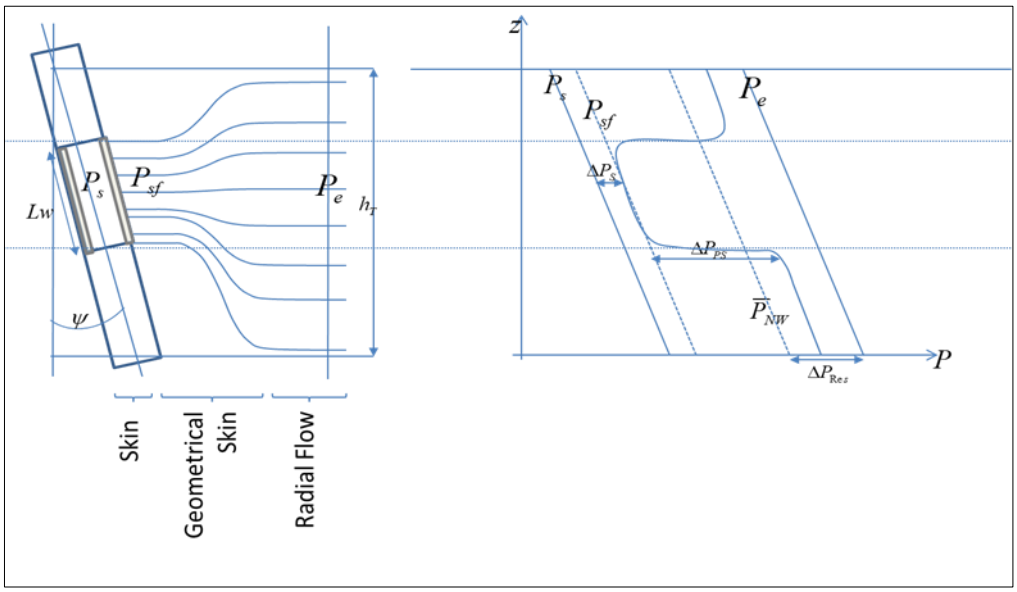


Fig. 18.E.1 – Pressure drop components

The Pseudo-skin, S_G, depends on the well deviation, the anisotropy, the geometry of the perforations and the formation. It is evaluated from Chen et al. (1995), with an anisotropic correction from Pucknell & Clifford (1991).

18.E.1 Resulting formulation of the Energy equation

The energy balances were obtained in the previous section for a generic case. Implementing the steady state assumption and removing the vertical thermal conductivity in the reservoir leads to the following expressions for the energy balance in the wellbore (E1) and reservoir (E2) for different wellbore conditions:

Energy equations for a **producer**

$$E1 = q_{s-}\,\rho_{s-}\,(h_{s-} + \frac{1}{2}(\frac{q_{s-}}{A\,\rho_{s-}})^2 + g\,dl) + q_{is}\,\rho_{is}\,(h_{sf} + \frac{1}{2}(\frac{q_{is}}{A\,\rho_{sf}})^2 + g\,\frac{dl}{2}) - q_s\,\rho_s\,(h_s + \frac{1}{2}\left(\frac{q_s}{A\,\rho_s}\right)^2) + D_{wb}\,(T_{sf} - \tilde{T}_s) = 0$$

$$E2 = q_{is}\,\rho_{is}\,(h_{sf} + \frac{1}{2}(\frac{q_{sf}}{A\,\rho_{sf}})^2 - h_{res}) + D_{wb}\,(T_{sf} - \tilde{T}_s) + D_{res}\,(T_{sf} - T_{geo}) = 0$$

Energy equations for a **producer with a thief zone**

$$E1 = q_{s-}\,\rho_{s-}\,(h_{s-} + \frac{1}{2}(\frac{q_{s-}}{A\,\rho_{s-}})^2 + g\,dl) - q_{is}\,\rho_{is}\,(\tilde{h} + \frac{1}{2}(\frac{q_{is}}{A\,\tilde{\rho}})^2 + g\,\frac{dl}{2}) - q_s\,\rho_s\,(h_s + \frac{1}{2}\left(\frac{q_s}{A\,\rho_s}\right)^2) + D_{wb}\,(T_{sf} - \tilde{T}_s) = 0$$

$$E2 = -\,q_{is}\,\rho_{is}\,(\tilde{h} + \frac{1}{2}(\frac{q_{sf}}{A\,\tilde{\rho}})^2 - h_{res}) + D_{wb}\,(T_{sf} - \tilde{T}_s) + D_{res}\,(T_{sf} - T_{geo}) = 0$$

Energy equations for an **injector**

$$E1 = -\,q_{s-}\,\rho_{s-}\,(h_{s-} + \frac{1}{2}(\frac{q_{s-}}{A\,\rho_{s-}})^2) + q_{is}\,\rho_{is}\left(\tilde{h} + \frac{1}{2}\left(\frac{q_{is}}{A\,\tilde{\rho}}\right)^2 - g\,\frac{dl}{2}\right) + q_s\,\rho_s\,(h_s + \frac{1}{2}\left(\frac{q_s}{A\,\rho_s}\right)^2 + g\,dl) + D_{wb}\,(T_{sf} - \tilde{T}_s) = 0$$

$$E2 = -\,q_{is}\,\rho_{is}\,(\tilde{h} + \frac{1}{2}(\frac{q_{sf}}{A\,\tilde{\rho}})^2 - h_{geo}) + D_{wb}\,(T_{sf} - \tilde{T}_s) + D_{res}\,(T_{sf} - T_{geo}) = 0$$

The resulting set of equations is solved simultaneously for the couple of unknown (T_s,T_{sf}), which is performed by an iterative method until convergence is achieved. For a producer, the temperature is updated starting from the lowest producing segment and going up the well to the top reservoir. For an injector, it is updated from the injection point going down the well.

These equations require the knowledge of the pressure and PVT properties. In Emeraude the pressure profile can be either an input (measured pressure) or simulated using a reference pressure (external reservoir, sandface, surface) and the corresponding equations to calculate the hydrostatic and frictional components in single or multiphase situations.

18.E.2 Summarized interpretation workflow

The temperature data to be used for qualitative purposes may come from different sources as explained in Section 18.C. If the interpretation is based on temperature only, the workflow will be almost identical, apart from the data loading and editing stages.

DTS data is loaded either in a single .las file containing multiple traces, or multiple .las files with a single trace per file, .csv files, etc. The traces may be time-referenced or not. The files may contain thousands of traces and not all of them might be of interest. Therefore, the data is "explored" to pick the traces at different times and these are used for the interpretation

purposes. The image below shows the "Explore" option of Emeraude, where it is possible to pick data at any time to display it vs. depth, and also at any depth to display it vs. time.

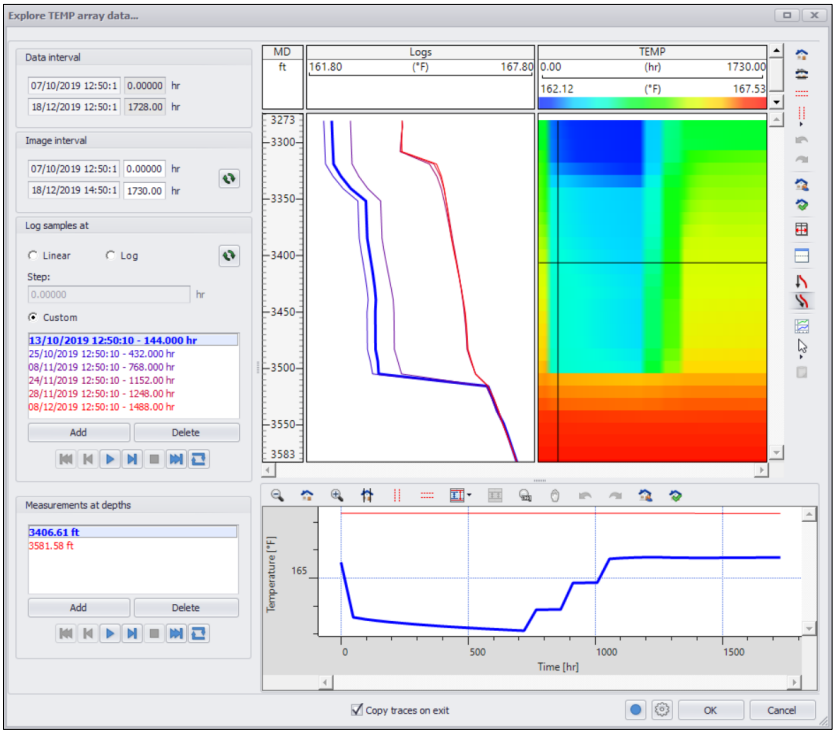


Fig. 18.E.2 – Emeraude "Explore" – Temperature traces of interest are selected for analysis

Once the traces of interest are exported, it is possible to save the rest of the DTS data as an image, which reduces considerably the size of the file and allows using the data for qualitative purposes.

The thermal interpretation is created. In Emeraude, the "Continuous" method (see PL chapter) is used, since the integral temperature response must be considered: the temperature at certain depth is a function of the temperature profile below (producer), or above (injector). From the traces extracted from the DTS array, it is necessary to define what trace is going to be analysed. This "reference channel" has to be selected bearing in mind the hypothesis of the Energy method, mainly the steady state assumption. Surface rates can be used as a reference of the trace condition.

The completion dimensions and thermal properties need to be entered for calculating the Heat loss coefficient. Emeraude includes a table with different materials and their thermal properties. It was mentioned in Section 18.D.4 that the material with smaller thermal conductivity dominates the magnitude of the HLC. Sensitivities will be presented in the next section. The image below shows a completion with a tubing down to 3200 ft. The completion dimensions and thermal properties can be defined in segments, to account for the different variations. However, if the temperature-derived flow profile is limited to the producing interval (bottom of the well) then it is not relevant to detail every single change in diameter occurring above this region. The image below also shows that the free annular convection option is checked. This induces a nonlinear calculation, since the heat transfer coefficient is a function of the temperature.

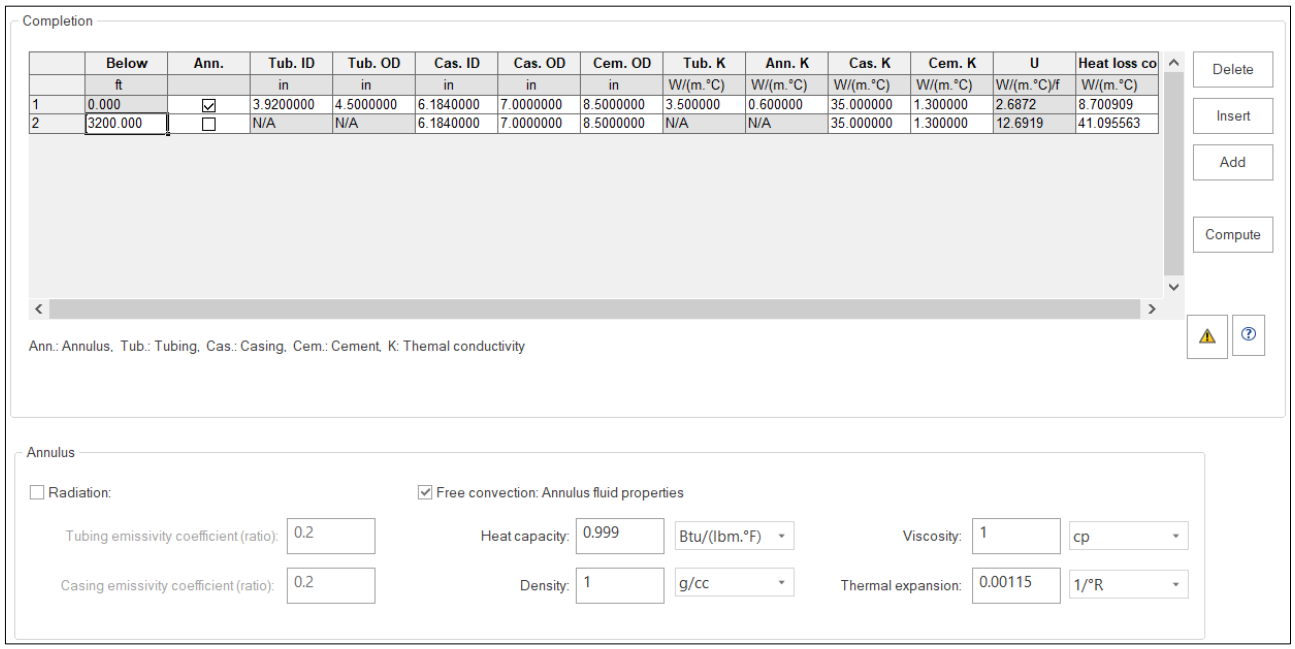


Fig. 18.E.3 – HLC calculation

The next step is to define the geothermal gradient. There are three options:

- Based on a reference depth and temperature, plus the gradient (slope)
- Based on an input curve: either a theoretical geothermal gradient or one of the traces (i.e. a stabilised temperature trace after a long shut-in)
- Based on a line fit in a region of thermal equilibrium. For example, in the image below we can assume that the sump represents the geothermal gradient and regress on the measure temperature (red curve, right track) to obtain the geothermal temperature (green curve, right track):

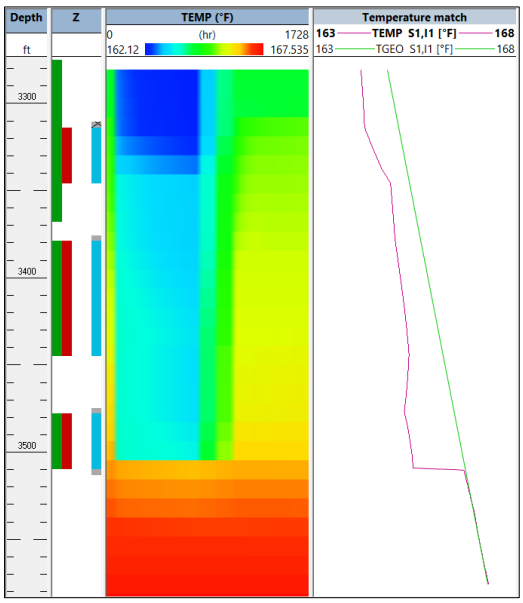
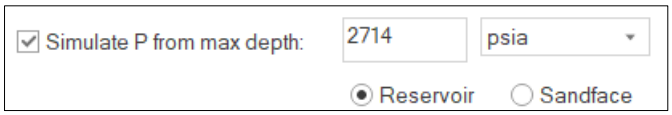


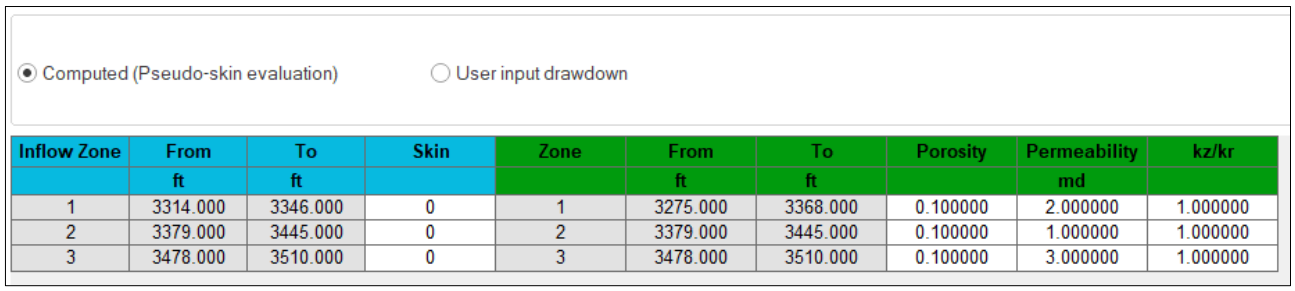
Fig. 18.E.4 – Geothermal gradient estimation from regression in the sump

As mentioned previously, the wellbore pressure is a necessary input. In case the user does not enter a pressure curve, then the pressure must be simulated. The image below indicates that reservoir pressure at maximum depth is equal to 2714 psia.



It is also necessary to enter the rock thermal conductivity, which in general will dominate the heat transfer to the formation since its thermal conductivity is very small. A transient correction is available (see Section 18.E.4).

Reservoir parameters, including external reservoir radius, permeability and skin are necessary since the pressure drop in the reservoir (from external pressure to sandface) is computed using the Darcy equation. The inflow length to reservoir length thickness will be used for the mechanical skin calculation.



Inflow Zone	From	To	Skin	Zone	From	To	Porosity	Permeability	kz/kr
	ft	ft			ft	ft		md	
1	3314.000	3346.000	0	1	3275.000	3368.000	0.100000	2.000000	1.000000
2	3379.000	3445.000	0	2	3379.000	3445.000	0.100000	1.000000	1.000000
3	3478.000	3510.000	0	3	3478.000	3510.000	0.100000	3.000000	1.000000

Fig. 18.E.5 – Petrophysical parameters

Having described the completion, reservoir and fluids properties, it is possible to run the regression on the temperature curve. When using temperature measurements only, the location of the rate calculation zones is irrelevant. From the Contributions tab, the contributions for the different zones are shown. The seeds value for the inflow rates of the different zones (1 to 3 in the image below) were all equal. When clicking on Global Improve the regression is launched, with the objective being to minimize the error between the measured and simulated temperature along the input temperature curve:

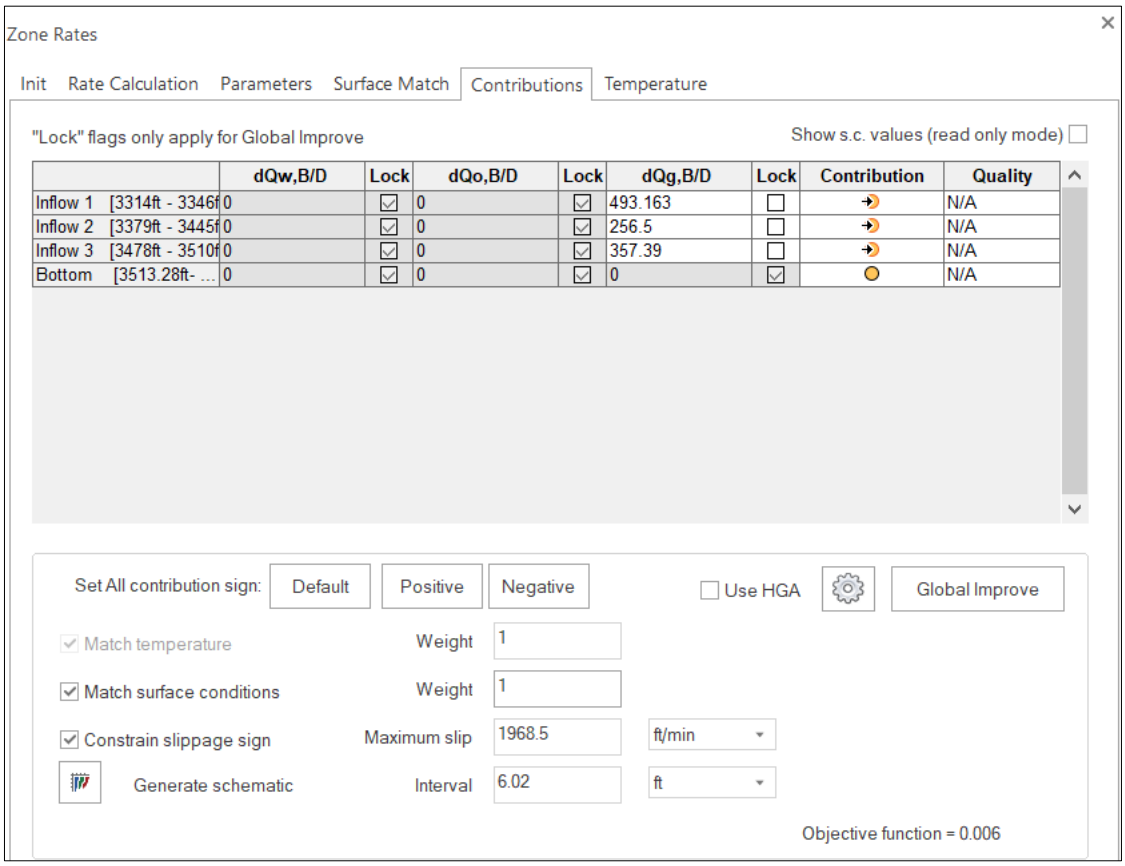


Fig. 18.E.6 – Inflow rates and Global regression

The regression also allows for extra constraints: in this case the "Match surface conditions" box is checked. However, there may be other curves or stations entered as part of the interpretation reference channels (passes or stations).

The image below shows the typical outputs of a temperature-based interpretation. The "Temperature match" track shows in red the input temperature curve, in green the geothermal gradient and in blue the simulated temperature. The QZT and QZI plots correspond to the cumulative flow profile and the contributions plot. Finally, the last track (Pres_KZ) shows the simulated pressure.

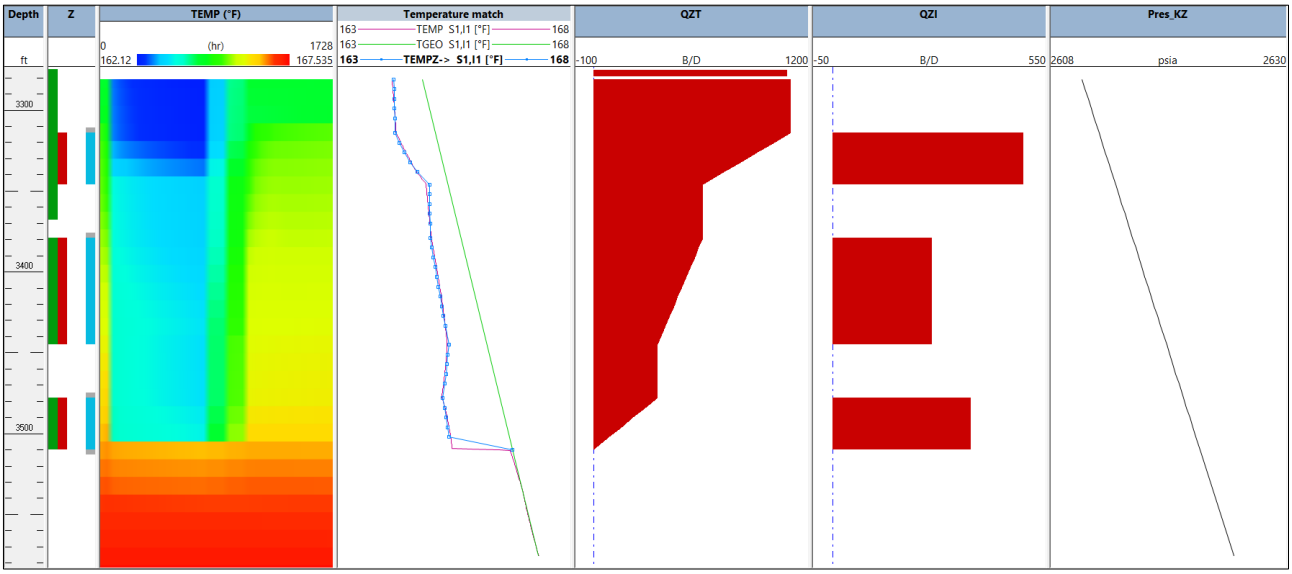


Fig. 18.E.7 – Resulting profile and simulated measurements

In a signals and systems theory context, this type of interpretation constitutes an inverse problem. The first iteration starts from a seed value of contribution per layer (assuming an even production). These layer rates are convolved with the system description, which includes all the thermal properties, completion details, user's decisions on the presence/absence of radiation and convection, the selection of the correlations, etc. The output of this operation is a temperature profile. In the first iteration the simulated temperature is likely to be off compared to the measured (reference) temperature. This difference constitutes the error, which can have weight if other constraints are used in the regression. The input is updated and a new iteration is run, until the convergence criteria is reached (i.e. the error E is minimized):

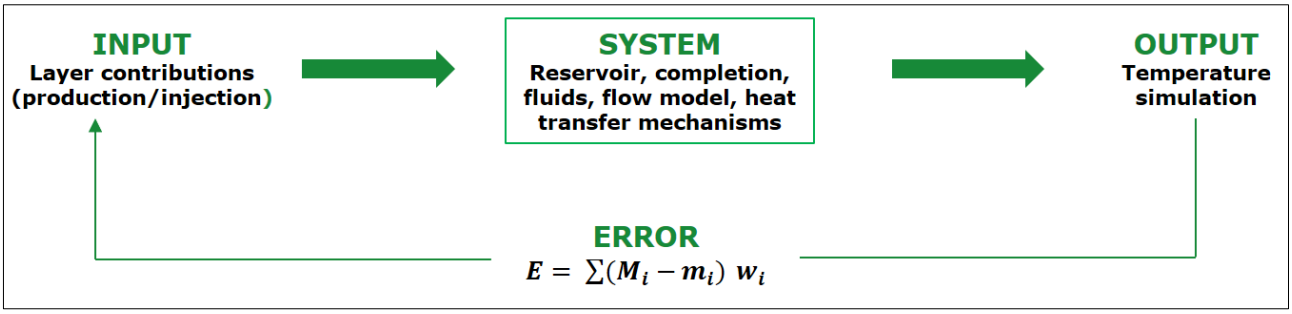


Fig. 18.E.8 – Diagram of the inverse problem for flow profiling

The profile obtained for a certain temperature is "a solution" of the error minimization process. The user must bear in mind the impact of the different inputs, and how these can affect the simulated profile. Compared to PL-based flow profiling, Temperature-based profiles require a larger number of numerical inputs, some of which can be constrained to small ranges, while others can be quite unknown. This is the subject of the next section.

18.E.3 Sensitivity to input parameters

Starting from the contributions obtained in the previous example, let's analyse how the simulated temperature would be affected by rock thermal conductivity (between 0.1 and 30 W/m K), Reservoir Radius (between 1 and 1E6 ft) and HLC (between 0.1 and 1000 W/m K). The image below shows the original temperature match in the first track and the sensitivity to the parameters in the other tracks:

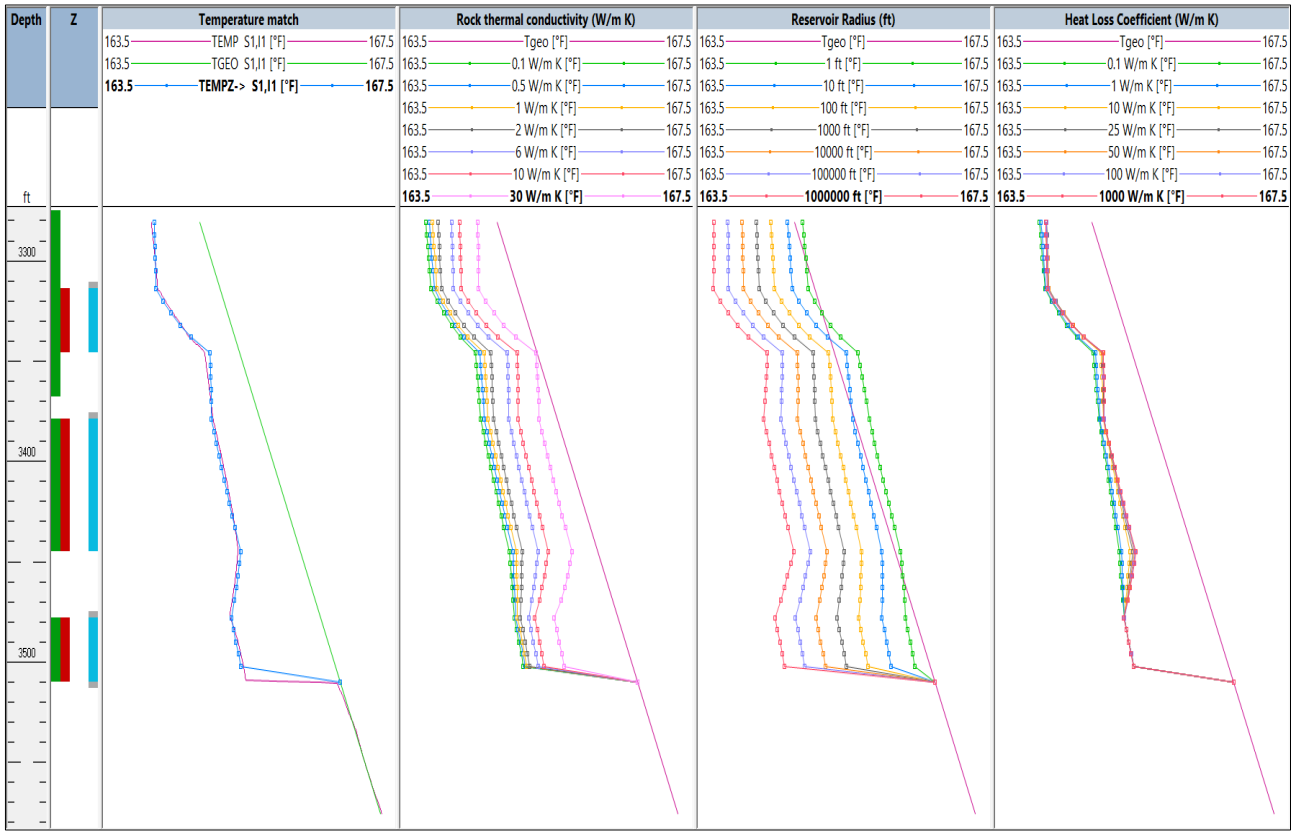


Fig. 18.E.9 – Sensitivities to reservoir thermal conductivity, external radius and HLC

- **Reservoir Thermal conductivity (λ_{res}):** Starting from the geothermal below the lowest inflow, a cooling can be seen over this inflow: it corresponds to an important pressure drop across the reservoir. One can notice that the higher the reservoir thermal conductivity, the smaller the cooling. Then, between the bottom inflow and the middle one, the temperature predicted by the Energy Model tends to the geothermal value, and this tendency increases with λ_{res}. As the reservoir thermal conductivity increases, the temperature in the well homogenizes faster and tends towards the geothermal value.

- **Reservoir Radius (r_e):** Increasing the reservoir radius means that the geothermal profile is reached further away from the wellbore: for a given set of parameters, the bigger the reservoir radius, the lower the temperature homogenization due to conduction.

- **Heat Loss Coefficient (HLC):** The factors affecting the HLC value were discussed previously. As the HLC increases, the temperature homogenizes slightly faster and tends towards the sandface temperature. However, this change is barely noticed for this range of HLC values, since this effect is strongly limited by the small reservoir thermal conductivity (λ_{res})**.** The HLC effect would be more pronounced for larger λ_{res} or smaller values of production time, for which the sandface temperature profile would be closer to the geothermal one.

The PVT properties of the fluid will also impact the final solution. Previously it was demonstrated that the gas heat capacity plays an important role in the Joule-Thomson coefficient, and also on the capacity of the fluid to transfer heat through convection. The Joule-Thomson coefficient is also a function of the thermal expansion, which is calculated through PVT correlations. The image below shows that the four different Z factor correlations available in Emeraude lead to none-unique results. The track on the right demonstrates that the effect of the thermal conductivity of the gas, in a range of logical values, has a smaller effect.

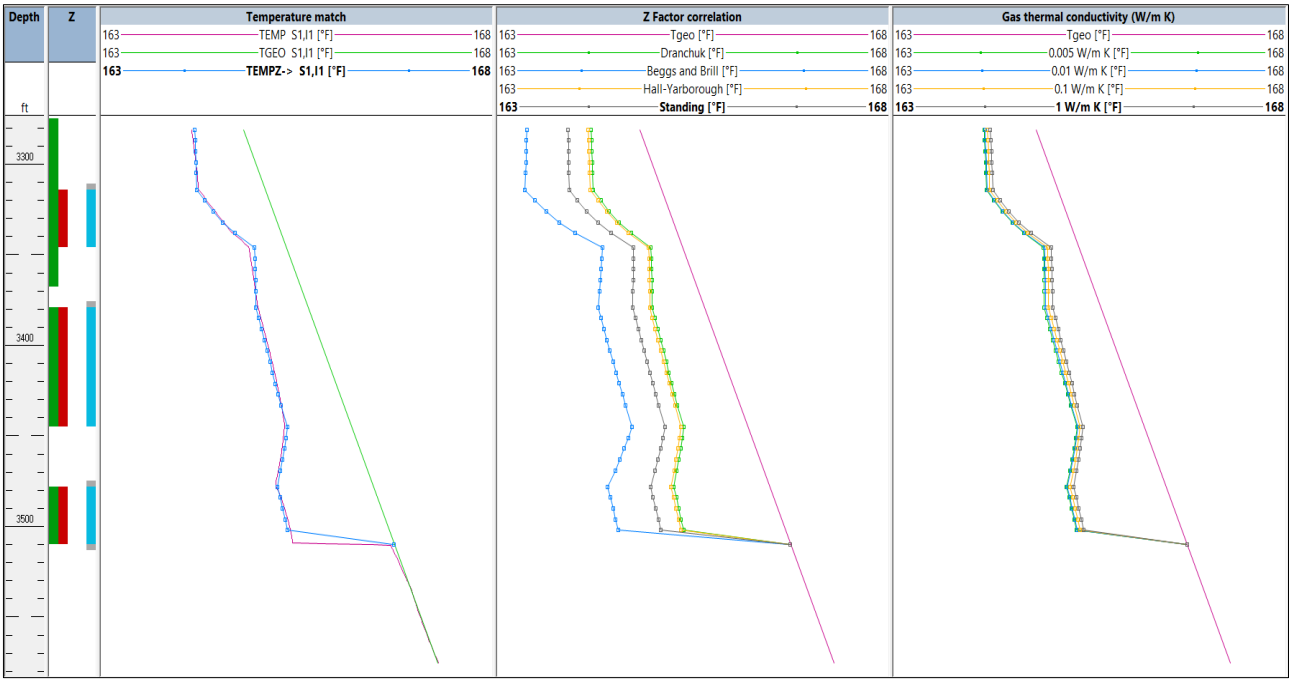


Fig. 18.E.10 – Sensitivities to the fluid properties

These sensitivities were meant to raise the awareness level on the impact of the different inputs, rather than discouraging the user on performing a temperature analysis. Since this type of analysis is an inverse problem solving, the validity of the resulting profile depends on the reliable characterization of all the parameters involved. Uncertainty in the input parameters will automatically translate into uncertainty in the answer. Given the large number of parameters, even single phase interpretation can turn out to be completely undefined and lead to random results. Clearly, hoping to solve in multiphase if only the temperature is supplied is totally unrealistic.

18.E.4 Time dependency

If the well has been shut-in for a long period, it would be fair to assume that the sandface temperature would be close to the geothermal temperature. Then, if we put the well in production, not only the temperature inside the wellbore will drop, but also the temperature in the reservoir, as explained in the Joule-Thomson section. Therefore, the magnitude of the heat flux due to conduction will also drop, because the sandface temperature will be closer to the wellbore temperature.

This phenomenon introduces a time dependency, which in principle is not compatible with the steady-state formulation of the Energy model in Emeraude. A transient correction on the conductive heat transfer was incorporated, which allows to account for the production time. The transient is modeled throughout a scaling of the reservoir thermal conductivity so that at early time the solution corresponds to the steady state solution obtained from a large reservoir thermal conductivity (sand face temperature close to the geothermal) and as time increases the solution tends toward the steady state solution obtained from the entered reservoir thermal conductivity:

$$\lambda^{*}_{res,trans} = \lambda_{res,0}\, max(1, \frac{ln\left(\frac{r_e}{r_w}\right)}{f(t)})$$

The figure below shows the temperature profile for different times of production, based on the layer rates obtained before. For short times, heat transfer is maximum and then the temperature tends to be closer to the geothermal gradient. This effect is reduced with the increase in production time:

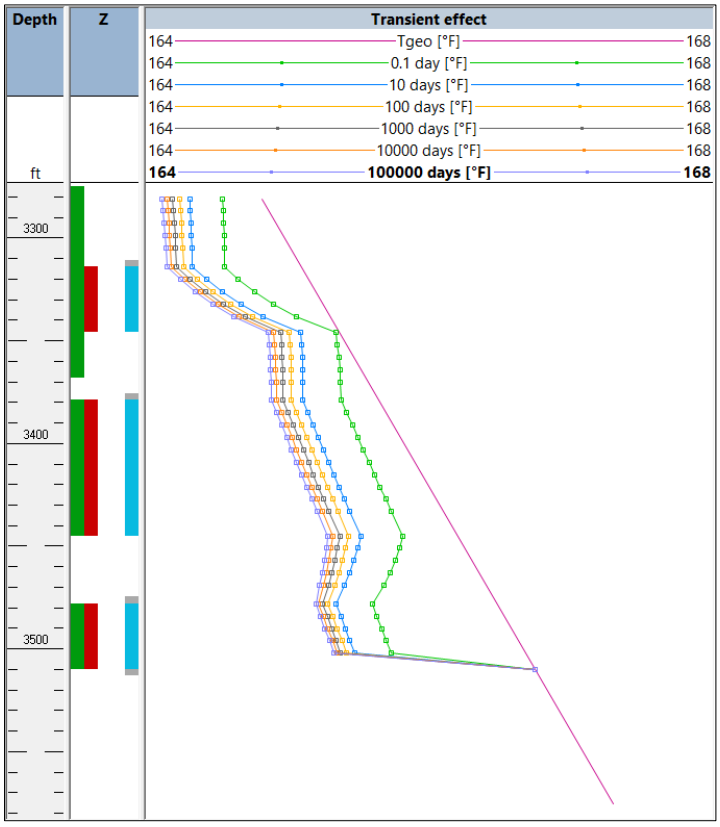


Fig. 18.E.11 – Sensitivity to the production time

18.E.5 Annular convection

The Energy Model allows considering annular free convection when evaluating heat transfer. This is often negligible, however it may have a significant impact on the solution when the annular fluid is particularly sensitive to the thermal gradient existing across and along the well (typically, when invaded with gas).

The following plot shows the multiphase field case described by Hassan & Kabir (SPE 22948). The red dots correspond to the measurements, the blue curve to the Energy Model without considering the annular free convection, and the green curve to the Energy Model while considering annular free convection.



Fig. 18.E.12 – Annular convection

This shows the importance of the annular free convection and it also provides a good assessment of the Energy Model in multiphase flow.

18.E.6 Multiphase profiling

Having analysed the sensitivities to the input parameters in single phase, it is easy to understand that the inverse problem in multiphase can only get worse. There is general agreement that the inverse problem is undefined in multiphase if the only available measurement is temperature.

The figure below provides an illustration where 2 completely different production profiles, one with 4% Water cut and the other with 55% Wcut, produce the same temperature profile:

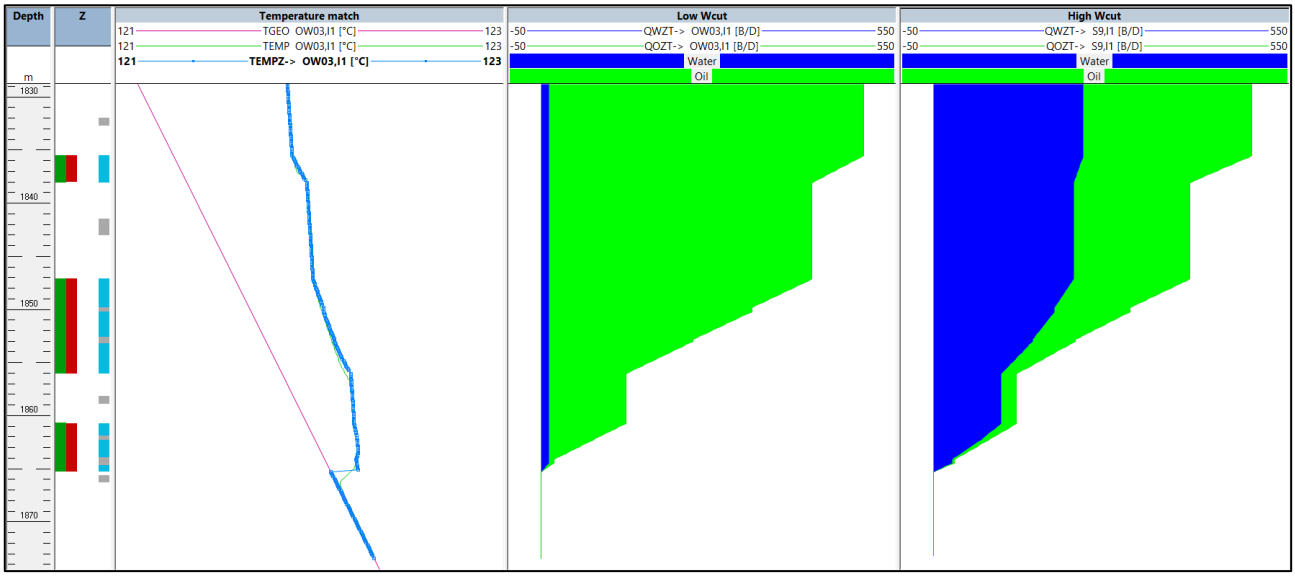


Fig. 18.E.13 – Completely different flow profiles lead to the same temperature response

Whilst in this case the interpreter can use the surface measurements to assess the validity of the different profiles, in other situations it might be impossible to choose one solution over another.

In multiphase situations it is necesseray to incorporate one or multiple holdup measurements (density, capacitance, holdup tools, DAS) or direct downhole rates. This way it will be possible to extend the balance equations to multiphase, using real measurement. The image below shows a multiphase flow profile obtained from the temperature measurement plus density and capacitance. The spinner was disregarded since it shows recirculation in the casing area and wouldn't reflect the production behind the tubing above the packer.

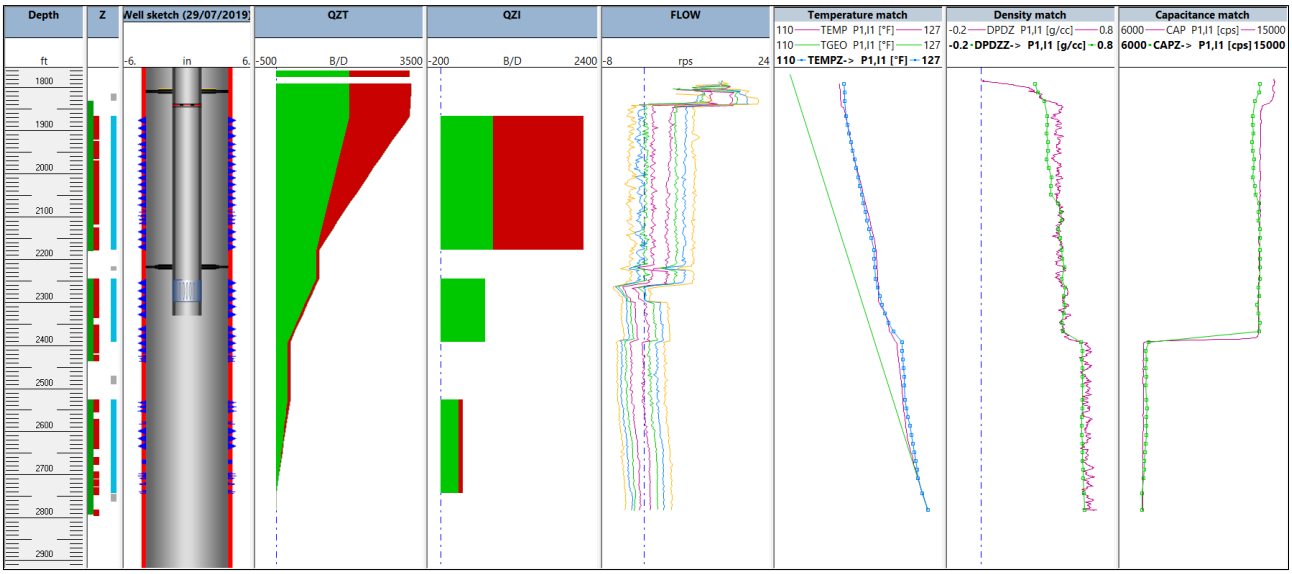


Fig. 18.E.14 – Multiphase profile from temperature, density and capacitance

The user can modify the weights given to the different measurements locally (in the rate calculation zones), since the representativeness of the holdup/velocity measurements will vary with the well deviation and flow conditions.

18.E.7 Horizontal wells

In liquid producers where the viscous heating is small, then the inflow fluid temperature will be equal to the geothermal temperature. In vertical wells, if the perforations are not too close together, then it should be possible to identify (and maybe quantify) the inflows from the different perforation, as seen in Section 18.D.7.

In horizontal wells with no TVD difference one should expect no geothermal temperature difference between the different inflow points. Therefore, unless there is considerable cooling or warming, the identification and quantification of the different inflows might be severely limited. Unfortunately, one of the characteristics of the horizontal wells is that the drawdown is smaller than vertical wells, which necessary leads to a smaller Joule-Thomson ΔT. The image below shows a PL-derived flow profile, with a total cumulative downhole rate of 9000 B/D (not small) and a TVD variation from heel to toe of 40 ft. Temperature variation in this range is 0.4 °F, which is slightly larger than the resolution of the temperature measurements.

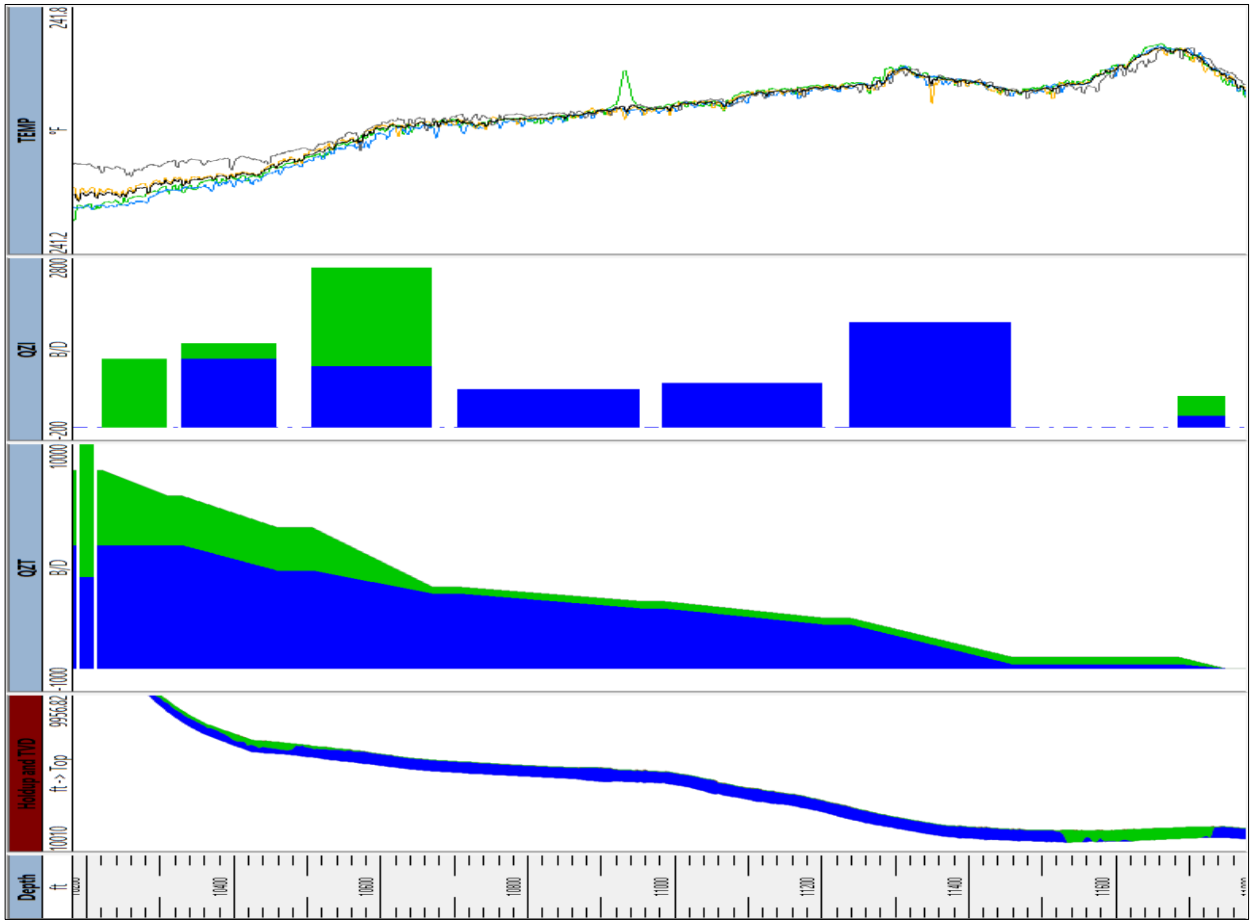


Fig. 18.E.15 – Temperature response of a horizontal Oil-water producer

When the temperature range is so small, the impact of the uncertainty of the inputs is even larger. Whilst the Energy model in Emeraude will still be available for any well deviation, it is up to the interpreter to understand the limitations of the measurements and the response to the different fluids.

In gas producers the Joule-Thomson constant will be 10 times larger than in liquids (and with positive sign), so for the same drawdown, gas producers will show a larger temperature response than in liquids. However, it should be remembered that the drawdown in long wells can be very small. Trying to quantify the production from every single perforation of a horizontal multifrac gas producer is in general completely unrealistic. In situations like this it is more convenient to lump the contributions of multiple perforations (or clusters) into a single zone.

18.E.8 Summary and limitations

As a conclusion, the Energy model allows going into great details in the definition of the fluid, completion and reservoir, for which it requires a number of input parameters, where the uncertainty on them is translated directly to the result. This thermal model allows accounting for the following energy transfer mechanisms:

- Enthalpy/convection
- Kinetic Energy
- Potential Energy
- Thermal Conduction (radial) in the well and reservoir

The required input parameters are:

- Geothermal temperature
- External reservoir pressure and radius
- Thermal conductivity of the completion and reservoir
- Permeability, skin, reservoir/perforation thickness

In terms of the limitations, analysing the hypothesis of the energy balance, it is clear that the far field temperature is the geothermal temperature. We can then say that the Energy works for geothermal fluid entries. However, if certain inflow produces fluid which external temperature is not the geothermal, the model has no means to know what temperature it is. The model does not work for **Non-geothermal fluid entries:**

- Injector – Producer connection
- Tgeo disturbed by drilling operations
- Exothermic reactions (acid jobs)
- Annular fluid movement (tubing leak)
- Cement channeling

Some other limitations that have been discussed in this section are:

- In the absence of an external holdup measurement input, the method remains single phase
- In Horizontal liquid producers with no Tgeo difference, it is normally not possible to quantify the inflow profile
- In injection conditions, there is normally very little heat exchange between the fluid and completion/formation. Normally not possible to quantify the injection profile.
- Vertical thermal conductivity is simulated

18.F Water Injection Fall-off – Emeraude

Recalling from the section on Joule-Thomson effect, the water has a negative coefficient, which in an injection case would lead to a small increase in temperature at the outflow depth. However, in most real life cases, the injection temperature is significantly lower than the formation temperature. Therefore, the temperature profile will be strongly influenced by the convective heat transfer of the colder water being injected to the reservoir. For example, the image below shows a PL-derived injection profile, with a total injection rate around 60000 BWPD. Even though some relatively small layers take up to 30000 B/D, the temperature measured by the 3 passes (track on the right) shows no response in front of the perforations. Only two things can be extracted from the temperature in this case: the surface injection temperature is changing (increasing) as the PL acquisition progresses (first pass in black, third pass in blue). The other thing is that below the bottom perforation there is no fluid movement, and the temperature will tend to be at equilibrium with the formation. Therefore, we can see the temperature going back to the geothermal.

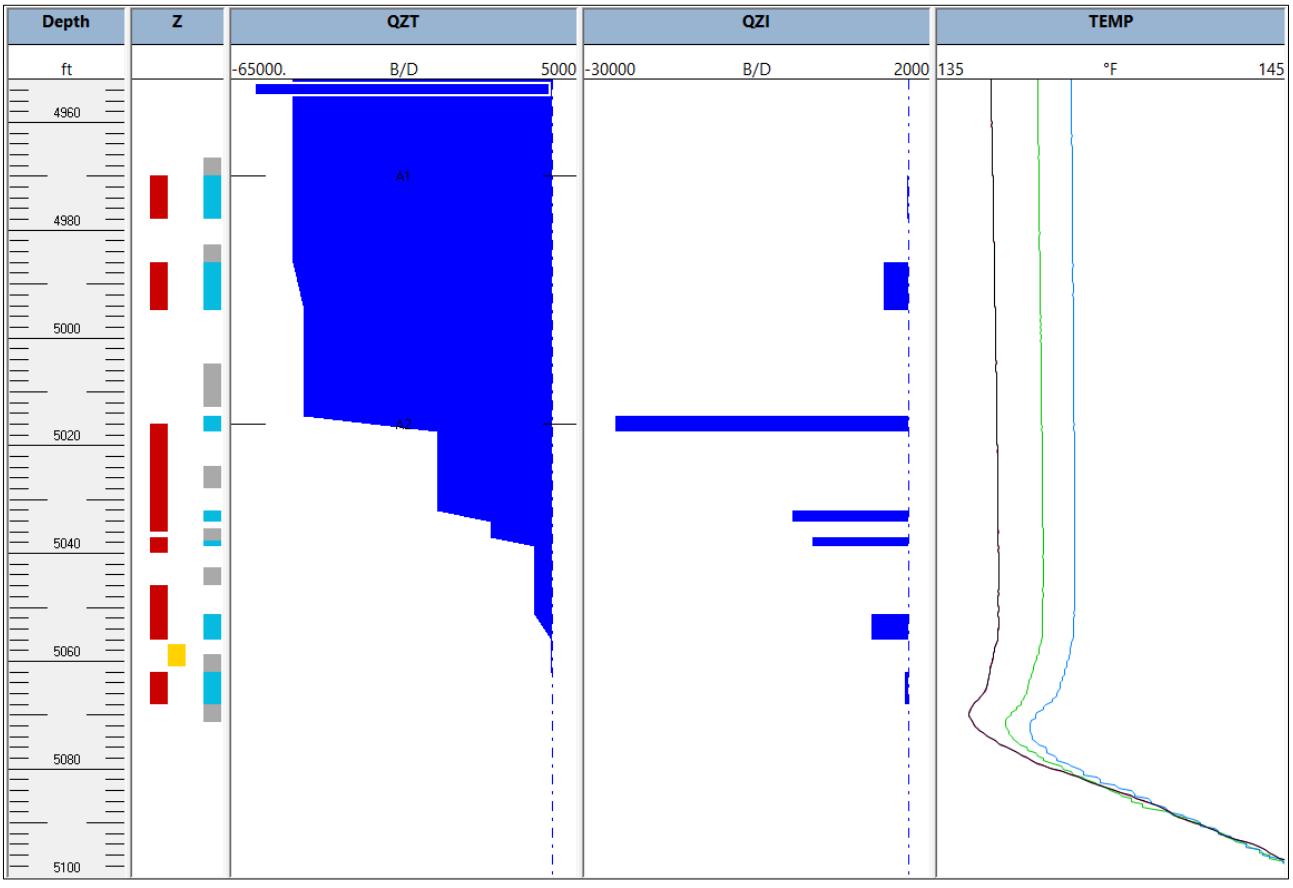


Fig. 18.F.1 – Temperature response while injecting

Temperature measurements while injecting can therefore provide very little information about the perforations injecting. It can only be used as a guide to understand what is the deepest outflow in the well, since below this depth the temperature will go back to the geothermal.

Fortunately, more information can be extracted from temperature with the injection well at shut-in conditions. As the water enters in the reservoir (while injecting) it will form a bank around the well, and heat will flow from the hotter reservoir to the cooler water. For layers that inject very little water, the reservoir will be very efficient at transferring heat since the gradients are very large. However, for layers that took large volumes of water, the cooler water bank will be larger and the heat transfer will be slower. When the well is finally closed, heat transfer will occur essentially by conduction (assuming no fluid movement). The temperature gradient between the reservoir and the wellbore will be larger in intervals that took zero (overburden) or little water. These zones will warm back quicker towards the geothermal temperature. This is the principle of the Warmback analysis.

This explanation referred to colder water and warmer reservoir. However, the model is not limited to that. If the injection water is warmer than the geothermal temperature (shallow injectors), then the model will predict the cool down of the fluid. That is why, the model is called "Water Injection Fall-off" and does not make reference to the evolution of the temperature during the test.

Thermal modelling of fall-off tests following water injection can be used for injectivity profiling in multilayered reservoirs, multiple perforation intervals or even a single long perforated interval or open-hole section. A semi-analytical model has been proposed in SPE 97023 (Pimenov et al., 2005) for horizontal wells using distributed temperature measurement along the wellbore. In Emeraude, this model has been modified and extended for other well configurations and also varying rock properties.

The basis of this model is a solution for the transient heat conduction problem in cylindrical coordinates as described by Carslaw and Jaeger (1959). Assuming conduction only in the radial direction, the temperature as a function of the elapsed time from the beginning of the shut-in can be calculated based on:

$$\frac{T_f - T(x,\tau_{sh})}{T_f - T(x,\tau_{in})} = \frac{1}{2\,\tau_{sh}} \int_0^\infty \exp\left(-\frac{\xi^2}{2\,\tau_{sh}}\right) \xi\, \psi(\xi, v, \tau_{in})\, d\xi$$

This equation contains a number of dimensional parameters which are detailed in the above-mentioned publication. However, as a summary it can be seen that the temperature at any depth, function of the elapsed shut-in time ($T(x,\tau_{sh})$), is calculated as a function of the mass rate injected to each perforation, which is actually what we are looking for, the injection profile. $\psi(\xi, v, \tau_{in})$ describes the radial temperature distribution at the end of the injection. Therefore, the injection time (τ_{in}) is also an input variable.

Compared to the Energy model, this is an approximation of a transient solution. If multiple temperature traces are recorded during the shut-in, then an injection profile can be established for each trace. Emeraude allows regressing on multiple traces at the same time, to reduce the uncertainty and account for possible quality issues of each individual trace. This method is also an inverse problem, where it is necessary to describe the system (reservoir properties) to obtain the Input (layered injection rates) based on the Output (Temperature profile).

The two main assumptions of the model were mentioned above: there is no vertical heat conduction, both across the formation and completion. In reality the temperature profile will be smoother than the one predicted by the model.

18.F.1 Summarized interpretation workflow

Temperature data can come from different sources, and the loading and quality check may vary as explained in the previous section. The image below shows the Explore option of Emeraude, where a DTS array image can be looked in detail, traces at different times can be extracted for analysis and profiles vs. time are displayed. In this case, the DTS acquisition encompasses the injection period (colder temperature trace) and nearly one month of shut-in. Temperature warms back and tends to be closer to the geothermal, but the warmback rate is not even for the different zones. This is clearly seen when displaying the data vs. time at different depths, shown at the bottom of the image.

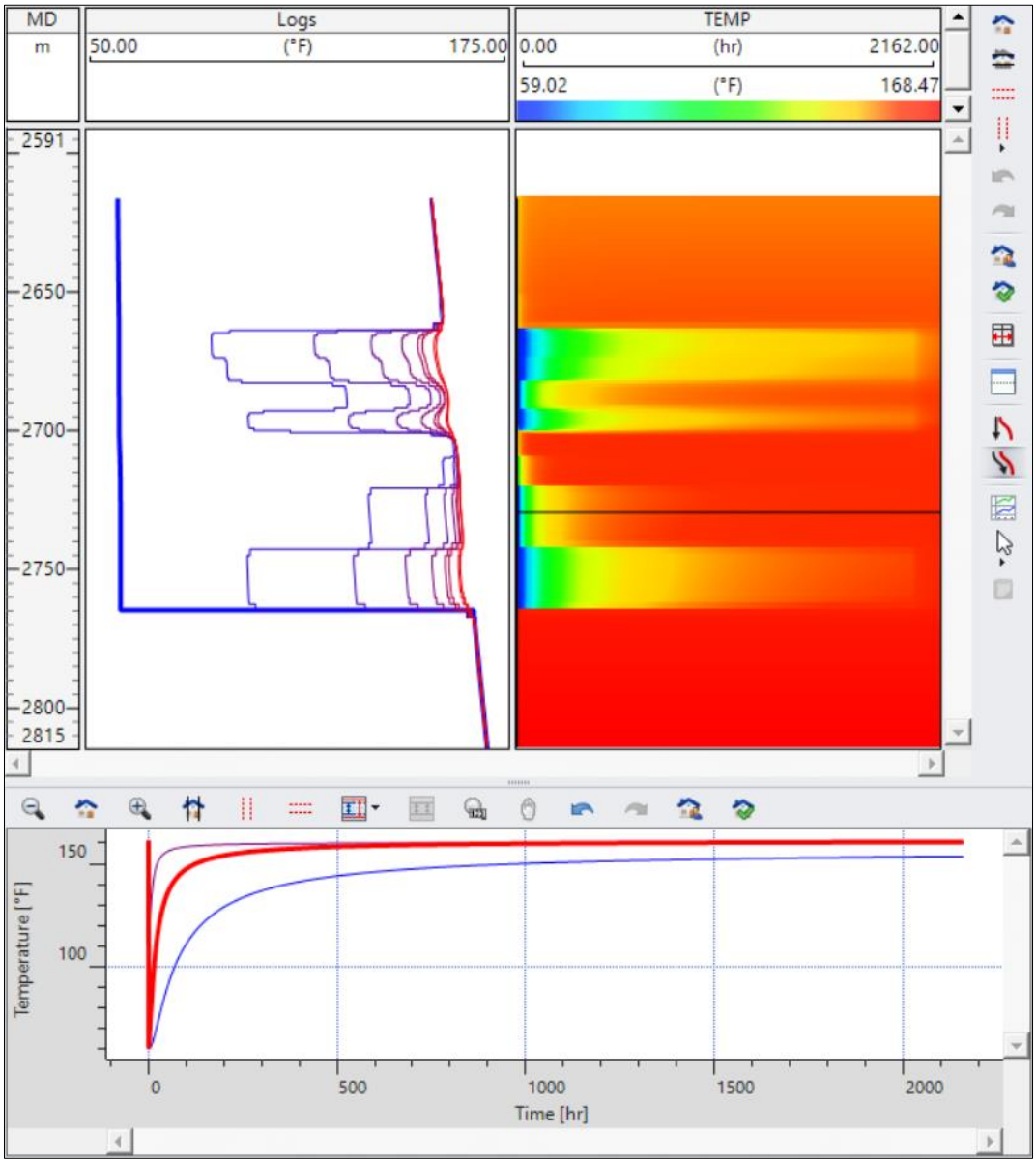
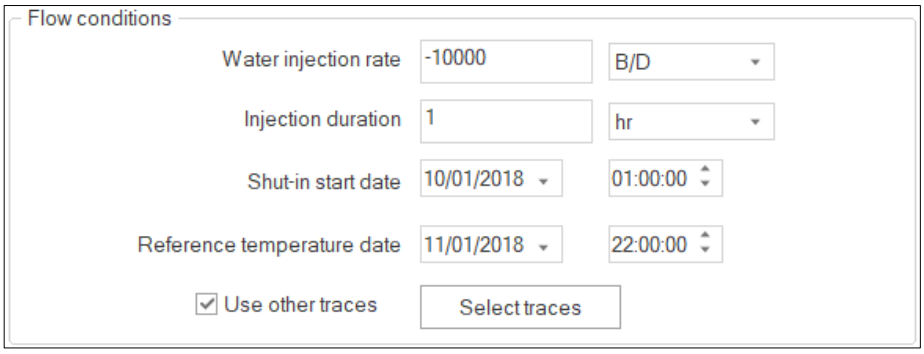


Fig. 18.F.2 – Temperature traces while injecting and warming back

Multiple traces are exported for analysis. Compared to the Energy model, all the traces can be used for a single analysis.

The traces are time referenced, which is needed for the model to calculate the elapsed time between the beginning of the shut-in and the measurement time. In case that the source of the temperature data is a pass recorded during an intervention (i.e. PLT, P&T survey), then the passes have to be referenced. It is also necessary to enter the duration of the injection period and the rate. For a long and more complex injection history these inputs are not so straightforward, and may require the use of an equivalent injection time/rate. This topic will be expanded in the following section.



In case of not having loaded a pressure measurement, this can be calculated based on surface or downhole (reservoir top) input parameters. Note that if surface conditions are entered, the Heat Loss coefficient needs to be defined from surface.

Finally, the number of thermal properties needed for this model is smaller than the Energy model. The wellbore is not accounted for by the use of the HLC (again, unless the pressure is calculated from wellhead). Reservoir heat conductivity and heat capacity are the two properties required.

The image below shows the resulting injection profile and simulated curves from the Water Injection Fall-off model. The Temperature match track shows one simulated curve per trace. The global error minimization uses all the traces at the same time. Also, this track shows the simulated water injection temperature, which can be compared to the measured temperature. Finally, the track on the right shows the simulated pressure. Similar to the Energy model, it is possible to add external constraints to the Global regression, such as downhole measurements or surface rates.

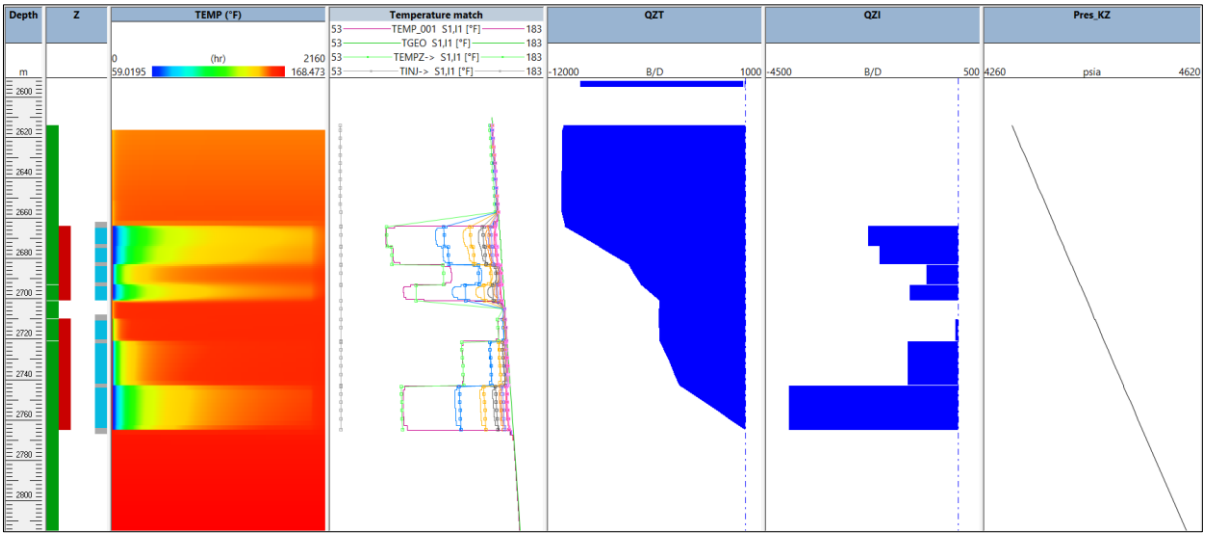


Fig. 18.F.3 – Resulting profile and simulated curves

18.F.2 Sensitivities to the input parameters

From an operational point of view, a key aspect is for how long the well should be closed for the temperature to show a significant and quantifiable response. We don't want the shut-in to be too short and the wellbore temperature to still be very close to the original injection profile. On the other hand, we don't want to stop the injection of the well for a period longer than needed. This is controlled by the rate of heat conduction, which as we have seen before is a function of the radial temperature gradient. The temperature gradient in the near wellbore region depends on the injection history (rates, duration, time) and thermal conductivity.

The sensitivities to the injection parameters are presented below. The second and third tracks show the wellbore temperature after 48 hs of shut-in as a function of the injection duration and water injection rate. These two parameters control the volume of water injected to the different layers, which in turn leads to a lower sandface temperature (in this case the water temperature is ~100 °F lower than the geothermal). In summary, the larger the injection times and/or rates, the smaller the difference between sandface and wellbore temperature, and thus the slower the warmback. If the warmback is too small, then the temperature measurement may not be used for quantitative purposes.

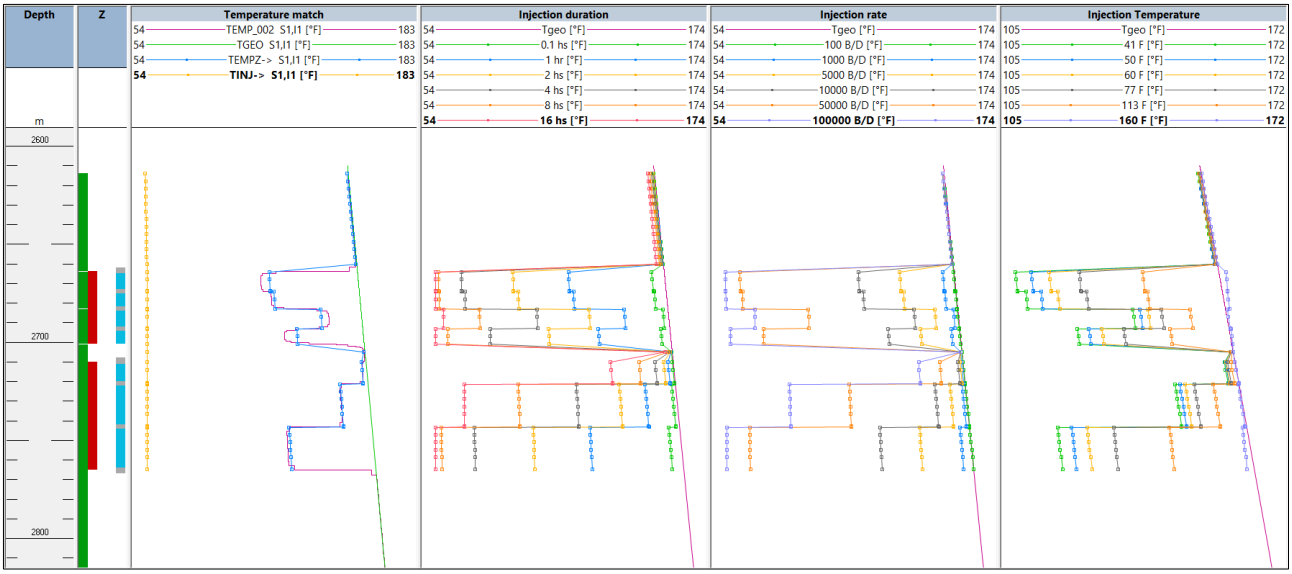


Fig. 18.F.4 – Sensitivities to injection parameters

The last track of Figure 18.F.4 shows the effect of changing the water injection temperature from 40 to 160 °F. The larger the difference between the injection and geothermal temperature, the larger will be the temperature disturbance in the wellbore. Note that as the injection temperature increase, the temperature variations between the injecting and non-injecting zones start to decrease. Eventually if the injection temperature becomes too close to the geothermal, the warmback would not be observed. This has implications in shallow water injectors, whose Tgeo can be around 25-30 °C, and the injection temperature coming from the water plant would be around the same temperature. In some cases, it has been decided to heat up the water and observe the cool down during the shut-in. Note that for the injection temperature at 160 °F, which is the same as the geothermal, there is an increase in

temperature at the top perforation. As explained in the section about Joule-Thomson, water temperature will increase as it decompresses (negative K_{JT}) on its way from the wellbore to the formation. Whilst at lower injection temperatures, convection dominates the heat exchange, at temperatures close to the geothermal, the model predicts the warming at the perforation level.

The tracks 2 and 3 of the image below show the sensitivity of the shut-in temperature (after 48 hrs of shut-in) and the injection temperature to a variation in reservoir thermal conductivity from 0.1 W/m K (a bit too low for reservoir rocks) to 8 W/m K (more than double the maximum theoretical values). The shut-in temperature after 48 hrs remains very close to the injection temperature when the thermal conductivity is small. The larger the thermal conductivity, the quicker will be the return of the wellbore temperature to the geothermal. For the injected water temperature, it can be seen that large thermal conductivities would lead to a quicker heat transfer and the water getting warmer due to the formation temperature. However, for normal reservoir rocks thermal conductivities (less than 3 W/m K) the effect is negligible (less than 0.5 °F in the simulation below). Finally, the heat capacity of the reservoir rock does not have a significant role on the shut-in temperature evolution.

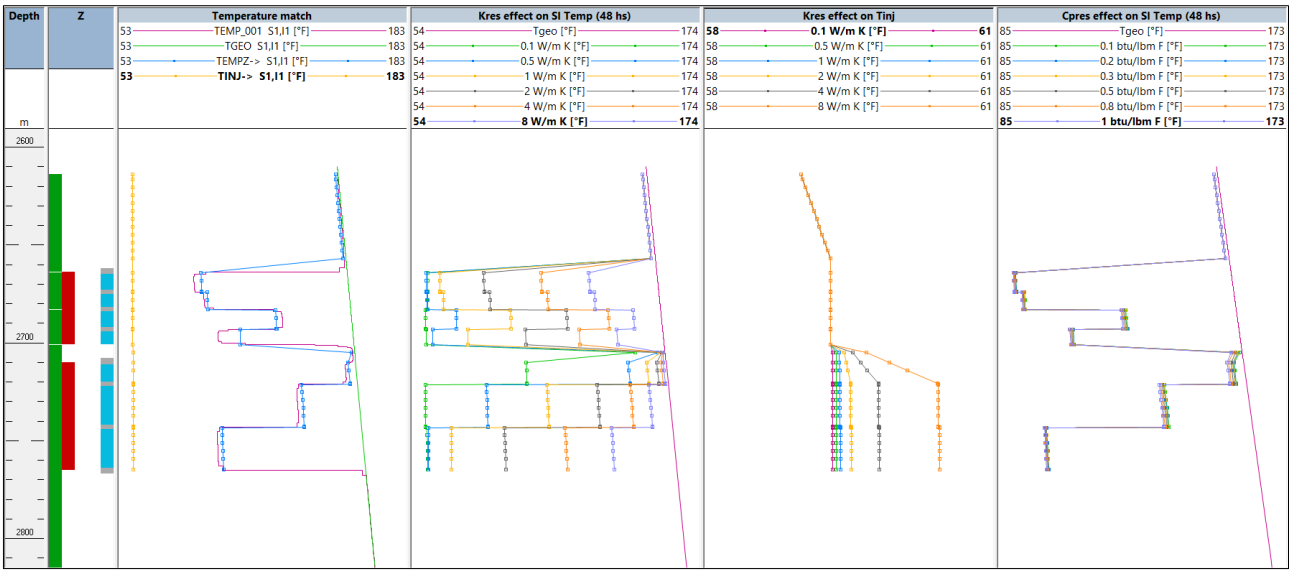


Fig. 18.F.5 – Sensitivities to thermal conductivity and heat capacity

18.G Numerical Simulation – Rubis

In Rubis thermal, the mass and energy balance equations are solved numerically for each reservoir cell and wellbore segment, which leads to a multiphase, transient, fully coupled wellbore-reservoir thermal simulator. Here are some characteristics:

- Single phase and multiphase compositional formulations
- Black Oil and compositional EOS PVT
- Full 3D resolution (no assumption of symmetry with respect to well axis)
- 3D Voronoi grid, with near-well refinement
- Finite volume formulation, fully implicit in pressure and temperature
- Heterogeneous media (permeability and thermal properties such as conductivity and specific heat capacity are not necessarily uniform).
- Multiwell
- Segmented well model(s) coupled to the reservoir, using a fully implicit formulation

Simulated temperatures and pressures can be output as a function of time at any input depth of the well (similar to a gauge), or as a function of depth along the well at specified times (similar to well logs). In the reservoir, pressure and temperature fields can also be output at user-specified time intervals.

18.G.1 Formulation

Notations

For a single phase case, the primary unknowns at any location of the reservoir are the pressure P and the temperature T. In a multiphase case, the additional unknowns of the problem are, for each phase p and each component k, the phase saturation S_p, and the phase composition C_p^k.

The main PVT coefficients are, for each phase p: the viscosity μ_p, the density ρ_p, the massic fluid enthalpy h_p, and the thermal conductivity λ_p. At any simulation time, and any location of the reservoir, these can be evaluated as functions of (P, T and C_p^k) the PVT module.

We also introduce the following rock properties: porosity φ, rock density ρ_r and rock thermal conductivity λ_r. The input distribution of these rock properties can be heterogeneous. The porosity depends on pressure, in order to account for the rock compressibility or unconsolidation, however its dependence on temperature is ignored.

Conservation equations and numerical discretization

In the reservoir, the kinetic energy of the fluid can be neglected, as well as the mechanical energy. Using these assumptions, a few derivations beyond the scope of this chapter lead from the first principle equation for the conservation of total energy to a simplified volumetric expression of the energy conservation. For a single phase, the following system of continuous conservation equations is obtained:

$$\frac{\partial}{\partial t}(\varphi\rho)+\nabla\cdot\left(\rho\cdot\vec{v}\right)=0 \qquad \text{(mass conservation)}$$

$$\varphi\rho\frac{\partial h}{\partial t}+(1-\Phi)\rho_r\frac{\partial h_r}{\partial t}+\rho\vec{v}\cdot\nabla h-\rho\vec{g}\vec{v}-\frac{\partial P}{\partial t}-\nabla\left(\lambda^*\nabla T\right)=0 \qquad \text{(energy conservation)}$$

Where $\vec{v}$ is the fluid velocity, h_r is the rock enthalpy and λ^* is the bulk thermal conductivity of the saturated medium, as detailed further below.

Rubis follows a finite-volume, fully implicit discretization approach. The mass conservation equation is integated over a cell *i* of volume V_i, as detailed in given in the chapter dedicated to numerical simulation [14]. If we note J_i, W_i and B_i the sets of reservoir cells, wells and reservoir bounds connected to the considered cell *i*, we obtain for each cell *i*, at the end of a time step *n+1*:

$$V_i\frac{\varphi_i^{n+1}\rho_i^{n+1}-\varphi_i^n\rho_i^n}{\Delta t}+\sum_{j\in J_i,W_i,B_i}q_{ij}^{n+1}=0$$

In the above equation, q_{ij} is the mass flux between the cell *i* and a neigbour cell, bound or well segment *j*. In the compositional context, this equation becomes:

$$\frac{V_i}{\Delta t}\cdot\sum_p\left[\left(\varphi_i^{n+1}S_{p,i}^{n+1}\rho_{p,i}^{n+1}C_{p,i}^{k,n+1}\right)-\left(\varphi_i^nS_{p,i}^n\rho_{p,i}^nC_{p,i}^{k,n}\right)\right]+\sum_{j\in J_i,W_i,B_i}\left(\sum_p q_{pij}^{k,n+1}\right)=0$$

Similarly, the equation for the conservation of energy is integrated over the cell volumes. We obtain for each cell *i*, at the end of a time step *n+1*:

$$\frac{V_i}{\Delta t}\left(\varphi_i^{n+1}\rho_i^{n+1}h_i^{n+1}-\varphi_i^n\rho_i^nh_i^n\right)+V_i(1-\varphi_i)\rho_{ri}\frac{h_{ri}^{n+1}-h_{ri}^n}{\Delta t}$$
$$-V_i\frac{P_i^{n+1}-P_i^n}{\Delta t}+\sum_{j\in J_i,W_i,B_i}\left(h_{ij}+g\Delta z_{ij}\right)q_{ij}+\sum_{j\in J_i,W_i,B_i}q_{ij}^T=0$$

In the above equation, Δz_{ij} is the difference of altitude between the upstream cell and the downstream cell - arising from the potential energy term.

In order to estimate the convective flux of energy between the cell *i* and one of its neighbors *j* (cell, well or boundary), the mixed enthalpy function h_{ij} is evaluated via the PVT module using the upstream values, i.e. $h_{ij} = h(P_i, T_i)$ if ^{i}is the upstream cell, otherwise $h_{ij} = h(P_j, T_j)$. We will see in paragraph 18.G.4 that this scheme can have some important consequences on the transient thermal simulation results and on the best choice for the simulation grid.

In the compositional context, this equation becomes:

$$\frac{V_i}{\Delta t}\cdot\sum_p\left(\varphi_i^{n+1}S_{p,i}^{n+1}\rho_{p,i}^{n+1}h_{p,i}^{n+1}-\varphi_i^nS_{p,i}^n\rho_{p,i}^nh_{p,i}^n\right)+V_i(1-\varphi_i)\rho_{ri}\frac{h_{r,i}^{n+1}-h_{r,i}^n}{\Delta t}-V_i\frac{P_i^{n+1}-P_i^n}{\Delta t}$$
$$+\sum_{j\in J_i,W_i,B_i}\sum_p\left(\left(h_{p,ij}+g\Delta z_{ij}\right)\cdot\sum_k q_{p,ij}^{k,n+1}\right)+\sum_{j\in J_i,W_i,B_i}D_{ij}\cdot\Delta T_{ij}=0$$

Where h_p is the mass enthalpy of phase *p*.

This discretization over all the cells leads to a (potentially large) single system of coupled equations (for each cell: one mass conservation equation per independent component + one

energy conservation), solved simultaneously by the non-linear solver (fully implicit coupling) at every simulation time step.

Enthalpy calculations

As previously mentioned, the massic fluid enthalpy h_p is obtained at any location via the PVT module, knowing the local values of (P, T and C_p^k)

In the EOS PVT context, for the hydrocarbon phases, the user inputs the heat capacity coefficients of single components, $Cp_{i,1}$, as well as the component's reference enthalpy H_{0i} at temperature T_{ref}. The single component molar enthalpy is then derived from:

$$H_i^* = H_{0i} + \sum_{l=1}^{hk} \frac{Cp_{i,l-1}}{l} \cdot (T - T_{ref})^l$$

,

from which we get the molar enthalpy of phase p:

$$H_p = \sum_{i=1}^{Nk} H_i^* \cdot x_i + H_p{}^{EOS} - P \cdot \sum_{i=1}^{Nk} x_i \cdot c_i$$

Where $x_i$are the molar compositions, the last right hand side term corresponds to the volume shift correction, and where:

$$H_p{}^{EOS} = R \cdot T \cdot (Z-1) + \frac{T \cdot \frac{\partial a}{\partial T} - a}{2\sqrt{2} \cdot b} \cdot \ln\left(\frac{Z + (1+\sqrt{2}) \cdot B}{Z + (1-\sqrt{2}) \cdot B}\right)$$

Finally, we get the massic enthalpy via:

$$h_p = \frac{1}{M_p} \cdot H_p$$

For all the other contexts (ex: black oil multiphase thermal, single phase thermal…), the enthalpy is simply derived from successive integrations, based on the input PVT correlations or tables for the density and compressibility, as explained below.

From the density function $\rho(P,T)$, accessible with the PVT module, the coefficient of thermal expansion of the fluid can be derived, for any values of P and T, with $\beta_T = -\frac{1}{\rho}\frac{\partial \rho}{\partial T}$. The massic specific heat capacity of the fluid (assumed constant at reference pressure $P0$) is a user input: c_f. In the Rubis interface, this reference pressure is assumed to be P0 = 1atm. These coefficients β_T and c_f are related to the enthalpy derivatives $\frac{\partial h}{\partial P} = \frac{1 - \beta_T T}{\rho}$ and $\left(\frac{\partial h}{\partial T}\right)_{P=P_0} = c_f$. The enthalpy $h(P,T)$ is then obtained using the following integration:

$$h(P,T) = h(P_0,T_0) + c_f (T - T_0) + \int_{P_0}^{P} \frac{1 + \frac{1}{\rho}\frac{\partial \rho}{\partial T}}{\rho} dP$$

This integration ensures the coherence of the PVT, i.e. $\frac{\partial h}{\partial P}$ is constrained by $\frac{\partial \rho}{\partial T}$. The Joule-Thomson coefficient, as well as the coefficient of isothermal compressibility $\chi = \frac{1}{\rho}\frac{\partial \rho}{\partial P}$, are not assumed to be constant during the simulation.

Rock Properties

The thermal conductivity, λ_r, the massic specific heat capacity, c_r, and the density of the rock are inputs from the user and are assumed to be constant and known. Since the rock density is constant, the coefficient of thermal expansion of the rock is equal to zero, so we have $\frac{\partial h_r}{\partial T} = c_r$ and $\frac{\partial h_r}{\partial P} = \frac{1}{\rho_r}$. The rock enthalpy is then obtained from:

$$h_r(P,T) = h_r(P_0,T_0) + \frac{(P-P_0)}{\rho_r} + \frac{(T-T_0)}{c_r}$$

NB - Arbitrary reference enthalpy values $h(P_0,T_0)$ and $h_r(P_0,T_0)$ appear in these integrations. These values have no consequence on the final result, since only enthalpy differences or derivatives will actually impact the global system.

Conduction

The conductive thermal flux of energy q_{ij}^T between cell *i* and a neighbour cell, well segment or bound *j* is given by: $q_{ij}^T = D_{ij}\,(T_i - T_j)$

Where D_{ij} is an analog for conduction to the "transmissibility" concept used to express the massic flux as a function of the pressure gradient (see numerical chapter [14]). D_{ij} depends only on the geometry of the cells (constant values) and on the bulk conductivity λ_i^* and λ_j^* of each connected cell. In the single-phase context, the following averaging model is chosen to express for the bulk thermal conductivity of the medium: $\lambda^* = \lambda_{fluid}^{\varphi} \cdot \lambda_r^{1-\varphi}$,

where the fluid thermal conductivity λ_{fluid}, input from the user, is assumed to be constant and known. Hence we see that D_{ij} is constant in the single-phase context. In the multiphase context, however, this assumption is no longer valid, and the model from Boris and Prat (1995) is followed:

$$\lambda^* = \lambda_{fluid}^{\varphi} \cdot \lambda_r^{1-\varphi} = \lambda_r^{1-\varphi} \prod_p \lambda_p^{(\varphi \cdot S_p)},$$

where phase thermal conductivities λ_f are user-inputs, assumed to be independent of *(P,T)*.

Reservoir boundary conditions

As described in the chapter on numerical simulation [14], three types of fluid flow conditions can be assigned to the reservoir lateral, bottom and top bounds for the mass equation: no flow, constant pressure or aquifer. Whatever boundary condition is chosen for the mass, Rubis assumes that the temperature of the boundary remains constant during the simulation – except for the specific case of the numerical aquifer, which is described further below.

The convection term between a cell *i* and a bound *b* is: $q_{ib}(h_{ib} + g\Delta z_{ib})$, where h_{ib} is evaluated upstream, i.e. the enthalpy of the fluid will be evaluated at the bound's values *(Tb, Pb)* when the flow comes from the boundary into the reservoir. When no-flow conditions prevail, this contribution by convection is of course equal to zero. In the potential energy term, $\Delta z_{ib}$is the relative altitude of the boundary with respect to the considered cell *i*.

When the reservoir boundary is no-flow, constant pressure or an analytical aquifer, the temperature is assumed to be constant inside the aquifer and along the aquifer/ reservoir limit. The conduction term from the boundary is then given by: $D_{ib}\,(T_i - T_b)$, where T_b is the constant bound temperature, T_i is the varying temperature of the connected reservoir cell, and the conductance D_{ib} is evaluated using the global conducvitiy λ_i^* of this cell (described above) - i.e. there is no need to input a conductivity for the aquifer.

When the reservoir boundary is a numerical aquifer, the constant temperature condition is not assigned to the aquifer/ reservoir limit, but to the outer boundaries of the aquifer itself. The conductivity and thermal capacity values inside the aquifer are assumed to be equal to those in the zone of the reservoir connected by the aquifer. As a consequence, the temperature is not necessarily constant inside the aquifer, nor at the boundary between the reservoir and the numerical aquifer.

Overburden, gaps and dead zones

In Rubis, it is possible to define "Dead" zones, where the 3D cells are simply deactivated and disappear from the system. These zones act both as perfect thermal isolant and absolute barrier to flow. At the boundary between a dead and an active zone, the flux of energy is hence null, and the temperature is not assumed to be constant.

It is also possible to define the geometry of any layer independently of its neighbors. In particular, it is possible to introduce a geometrical "gap" between two reservoir layers, as shown on Fig 18.G.1. Such gaps act as a pure thermal isolation.

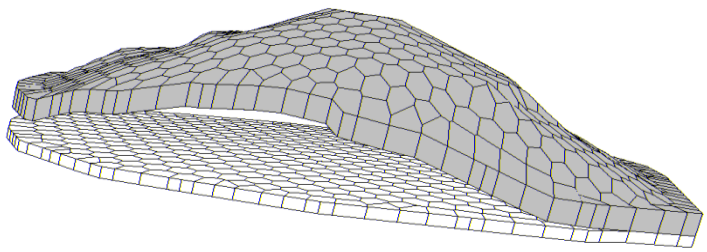


Fig. 18.G.1 – Two reservoir layers separated by a gap

In the example corresponding to the Fig 18.G.1, the bottom and the top sides of the reservoir will have constant temperature conditions, while the faces of cells pointing toward the gap will have "no thermal flux" conditions. As a consequence, these gaps are exactly equivalent to "dead" zones.

Because of these assumptions, it is recommended to avoid using dead zones or geometrical gaps in the thermal context. Instead, a standard property set can be used, with a net to gross value assigned to zero in this set. The corresponding zone will then act as an absolute barrier to flow with null porosity, but its thermal properties (rock conductivity and *Cp* values) will still be defined and accounted for. Hence, the temperature will not be uniform or constant in this zone. This is particularly useful in order to model the thermal effects of non-reservoir interlayers (Fig 18.G.2), or in order to include effect of the over/underburden in the simulation.

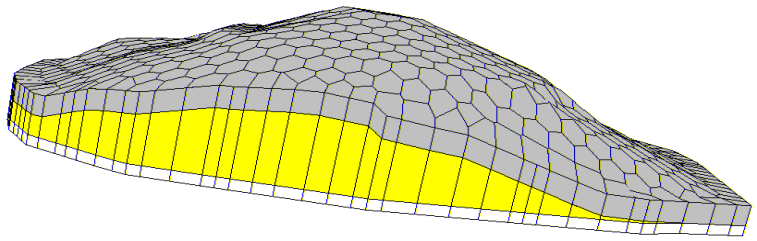


Fig. 18.G.2 – Non-reservoir interval layer explicity included in the model

Treatment of faults and fractures

Three kinds of faults can be defined in Rubis, which influence the flow along/across the fault: leaky, finite conductivity and infinite conductivity faults. Fractures (well hydraulic fractures or DFN) can be finite conductivity or infinite conductivity.

Leaky faults are simple transmissibility multipliers between all the reservoir cells separated by the fault. As a consequence, there is no flow occurring along these fault planes, and they only influence the convection fluxes, with no impact on thermal conduction.

On the contrary, flow occurs along the direction of finite or infinite conductivity and faults (or fractures), and thin 3D cells are associated to this type of faults (or fractures), with related pressure and temperature values. In Rubis, no thermal properties can be input for the faults and fractures, and several assumptions are made by the calcultor for the associated thermal conductivity connections:

For the connection between reservoir and fault (or fracture) cells, the thermal conduction across the fault is assumed to be infinite. In other words, the fault has no effect on the conductivity in this direction.

In the direction of a conductive fault (or fracture), the conduction effects are assumed to be small compared to convection effects. As a consequence, the thermal conductivity was neglected between two fault (or fracture) cells.

Dual porosity

No rigorous treatment of the double porosity has yet been implemented in Rubis for the thermal context. In particular, the matrix-fissure thermal connections are missing.

18.G.2 Wellbore coupling

Within the reservoir interval definition, the wellbore trajectory is divided into various segments *s*, honoring the perforated intervals and the intersections of the wellbore trajectory with the reservoir grid. The numerical well model implemented in Rubis assumes that all the phases travel at the same speed along the wellbore. As a consequence, global compositions instead of phase compositions are used, and the mass conservation equation for component *k* in a given segment *s* reduces to:

$$\frac{V_s}{\Delta t}\cdot\left[\left(\rho_s C_s^k\right)^n-\left(\rho_s C_s^k\right)^{n-1}\right]+q^k_{(s-1)s}\ -q^k_{s(s+1)}+\sum_i q^k_{is}=0\ ,$$

where C_s^k is the global composition and ρ_s is the global density in segment *s*.

Lets now consider the energy conservation equation into the wellbore. In order to simplify the model, the following assumptions will be made:

- The longitudinal conductivity exchange along the wellbore is negligible compared with other terms (especially longitudinal convection)
- The kinetic and potential energy change in the expansion term are negligible during a simulation time step
- The kinetic energy between cell *i* and segment s is negligible (kinetic energy is neglected in the reservoir part, as seen above.

The energy equation becomes:

$$\frac{V_s}{\Delta t}\cdot\left[\sum_p\left(\rho^{n-1}_{ps}h^{n-1}_{ps}-\rho^n_{ps}h^n_{ps}\right)-\left(P^{n-1}_s-P^n_s\right)\right]+\sum_p q_{p,(s-1)s}\cdot\left(h_{p(s-1)s}+ec_{p(s-1)s}+ep_{(s-1)s}\right)$$
$$-\sum_p q_{p,s(s+1)}\cdot\left(h_{ps(s+1)}+ec_{ps(s+1)}+ep_{s(s+1)}\right)+\sum_i\left[\sum_p q_{p,is}\cdot\left(h_{pis}+ep_{is}\right)+D_{is}\cdot\left(T_i\ -T_s\ \right)\right]=0$$

Compared to the Emeraude formulation, we see that the transient terms $\frac{\partial E}{\partial t}$ are kept (first left hand side block). We also see that the potential energy, kinetic energy and convective fluxes appear in the segment terms (no conduction between segments). The reservoir contribution involves convective fluxes, conduction and potential energy (kinetic energy neglected).

The conductive flux between the reservoir cell containing the well segment and the segment itself is obtained via a "composite" conductance D_{is} derived internally. This conductance, which depends on the geometry of the cell, combines the rock+fluid effective conductivity λ^* (previously defined) and the well Heat Transfer Coefficient defined earlier in this chapter.

As in the reservoir, the phase massic fluid enthalpy in any segment is evaluated via the PVT module, $h_{ps}(P_s,T_s,C_{ps}^k)$.

When using the thermal engine in Rubis, it is necessary to define the well intake. The pressure drops and rates between the segments are then related based on classical correlations accounting for slippage, frictions, etc. In the Rubis interface, the well intake definition also allows to define the completion geometry and the thermal parameters used to compute the Heat Loss Coefficient.

This discretization over all the segments leads to a system of coupled equations (for each segment: one mass conservation equation + one energy conservation, plus the constraint equations for each well). This system and the reservoir system described above are combined and solved simultaneously by the non-linear solver (fully implicit well-reservoir coupling) at every simulation time step.

18.G.3 Non-geothermal fluid entry

The Energy model in Emeraude is limited to single well simulations, and the assumption is that the far field temperature is equal to the geothermal temperature at that depth. For more complex situations, such as non-geothermal fluid entries or the influence of another well, then it is necessary to build and run a numerical model.

Let's consider the situation of a producing well, where shortly after water breakthrough from an injector well, a temperature drop is observed at the perforation level (through DTS, PLT or downhole gauge). Understanding the nature of the water breakthrough can be helpful to learn more about the flow pattern from the injector to the producer. Are they connected via a fault or fracture? Or is there a high permeability streak? This knowledge can have an impact on the production strategy and the way the waterflooding patterns are arranged.

The image below shows a cross section of the saturations (top) and temperature (bottom) maps, between the injector and producing wells. This simulation assumes that one of the layers (the one that shows the breakthrough) has a higher permeability than the other layers. From the saturations map is clear that that the water breakthrough has occurred, as the water saturation goes above the irreducible. The temperature map, on the other hand, shows that the "thermal front" is confined to the region close to the injector. The cold injection water exchanges heat with the formation as it moves away from the wellbore. When the permeability is large, the fluid diffusion will be much faster than the thermal diffusion. Eventually, the cold front may reach the producer but will definitely take more time and would not explain the temperature drop observed at the producer.

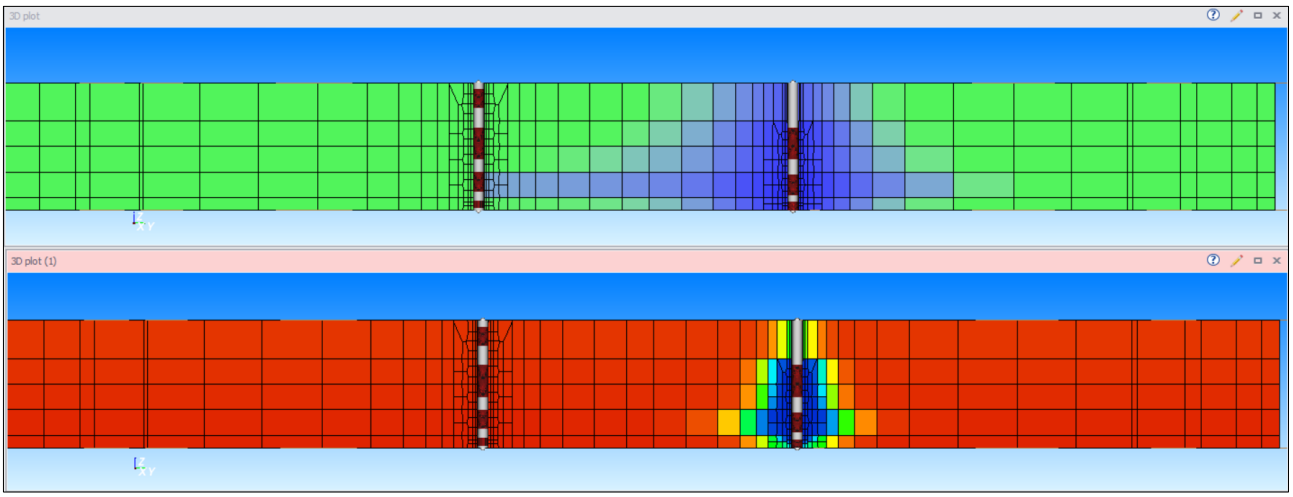


Fig. 18.G.3 – Saturation and temperature cross sections

If the high permeability streak is replaced by a fracture between the producer and injector, the water breakthrough would occur pretty much at the same time, so it would not be possible to note the difference if looking at the surface rates only. The image below shows the simulation results for this scenario. It is clear that when there is a fracture connection between wells, the cold temperature front propagation is much faster. The results can be displayed in the form of temperature gauges and production logs. This facilitates the comparison of the simulations with the different possible sources of temperature measurements.

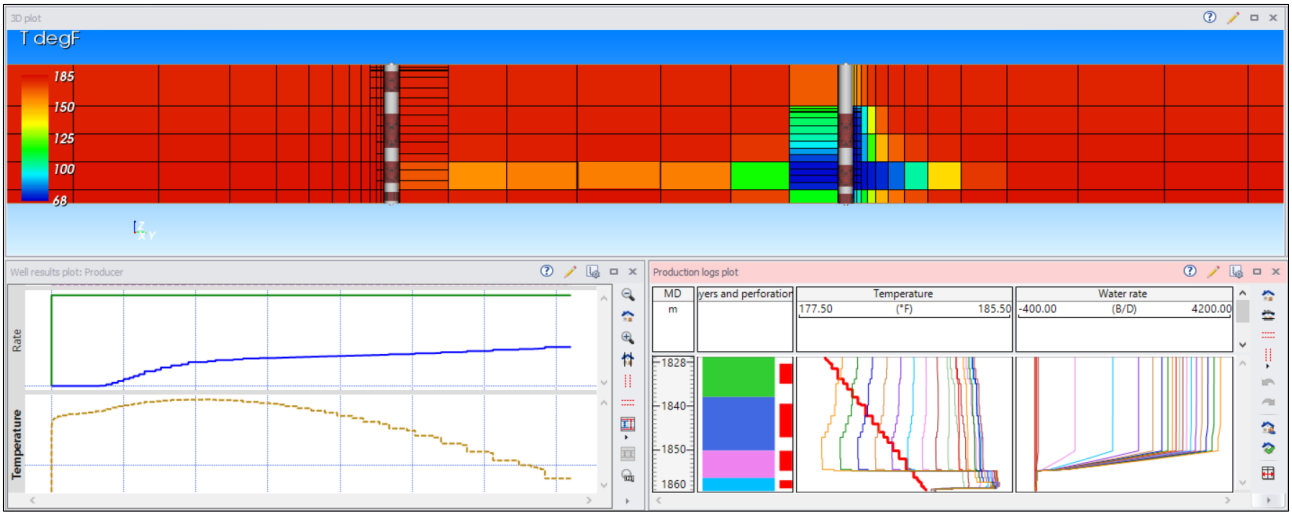


Fig. 18.G.4 – Simulation results – fracture connection

This type of what-if scenarios can be conducted relatively quickly in Rubis, keeping the complexity of the problem, including transient conditions, 3D, multiphase, etc.

18.G.4 Transient temperature logs

By fully coupling the segmented wellbore model to a complex reservoir system, the thermal numerical model is able to accurately capture the transient effects occurring in the vicinity of the wellbore.

Let us consider a vertical well perforated in two reservoir units, consisting of several layers with varying permeability and porosity (Fig 18.G.5). We simulate the injection of a cold fluid (15°C) at constant rate for one hour, followed by a long shut-in.

During the injection period, via convection, the cold temperature front associated to the injection fluid propagates further in the more permeabile layers, while in the layers of low permeability the temperature remains closer to the initial, geothermal value (Fig 18.G.6). Crossflow and thermal conduction across the communicating layers are rigorously captured.

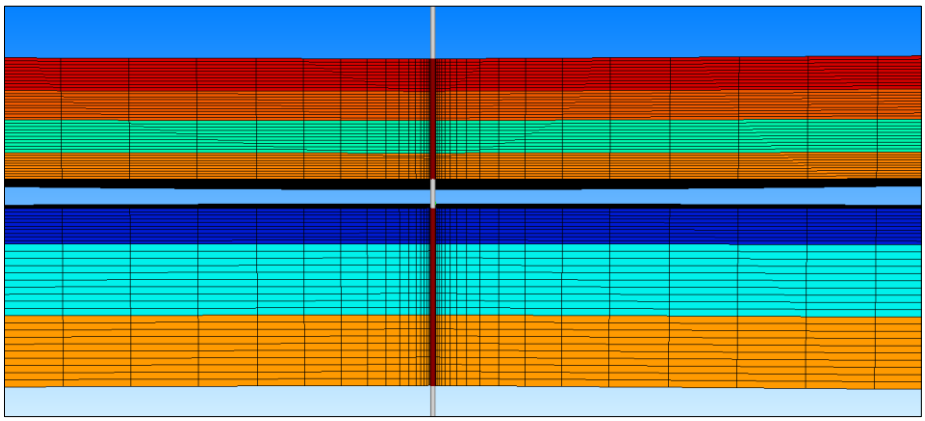


Fig. 18.G.5 – Vertical cross section and reservoir layers

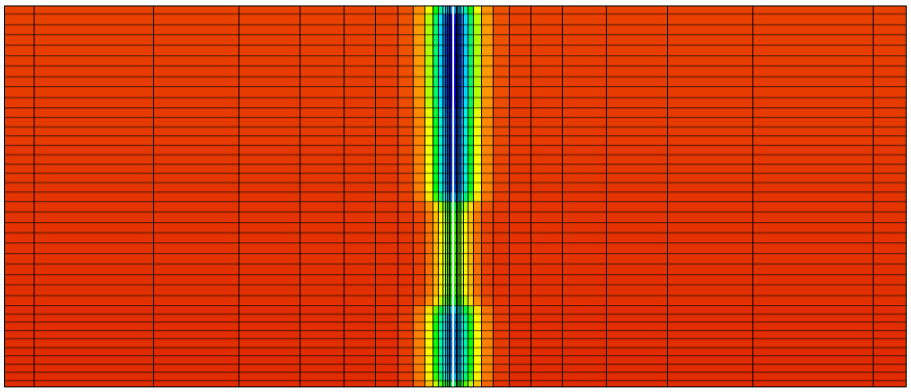


Fig. 18.G.6 – Temperature field after injection (1 hour) in the top unit

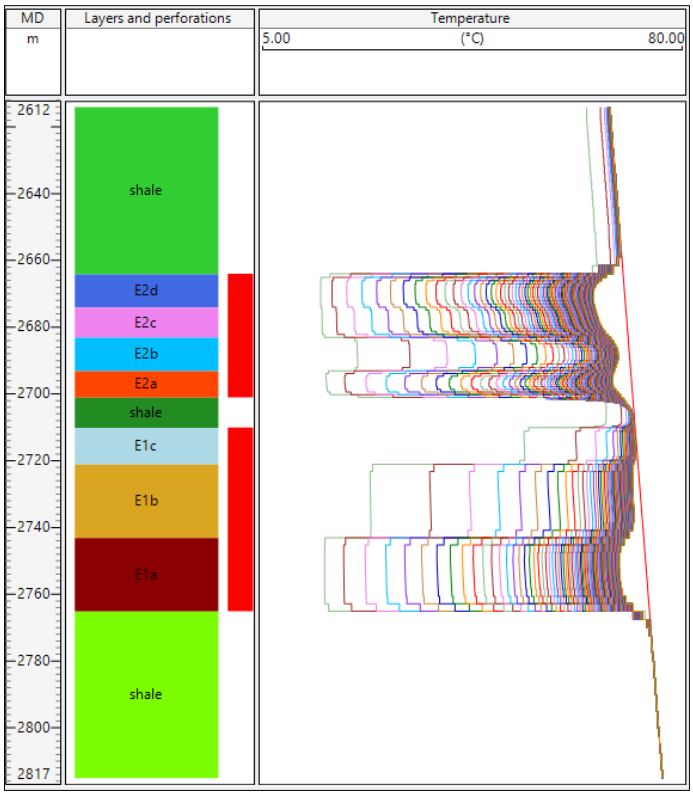


Fig. 18.G.7 – Temperature logs during shut-in

During the shutin period, thermal conduction becomes the principal mechanism, through which each layer will slowly warm back to the geothermal value. The warm back speed depends on the depth of penetration of the cold injection fluid in this layer – hence on its permeability. The corresponding evolution of the well temperature logs during warm back can be simulated, which gives acces to the permeability distribution of the intercepted layers (Fig 18.G.7). Here again, any crossflow and heat exchange occurring between the layers during the re-equilibrating process is captured by the simulator.

18.G.5 Gridding and transient thermal effects

As seen in the Numerical Simulation chapter [14], the grid resolution around wells can be easily modified in Rubis, with transmissibility and well index values being automatically adjusted via numerical near-well upscaling procedures. This approach is quite robust for non-thermal single-phase flow, even when very large coarsening factors and/or heterogeneity are considered. In the thermal context, however, the near-well temperature can remain transient for very long periods of time, and the simulation results become very sensitive to the near-well grid resolution. As a consequence, a significantly higher grid refinement is usually required in the thermal context.

This problem can be illustrated with a vertical producer located at the centre of a single layer, circular oil reservoir. This well is fully perforating the layer and produces at constant rate q_0. The lateral boundaries have constant pressure conditions, while no-flow conditions prevail at top and bottom boundaries. The model is simulated for various grid refinement levels. In the isothermal context, all the grid-dependent pressure transient effects are concentrated during the first hour of simulation, and the resulting well pressure history is shown to be fairly independent on the upscaling level. But when the same model is simulated in the thermal context, the transient temperature evolution at the well is shown to be very dependent to the grid size (see Fig 18.G.8). The time scale of the influence of near-well refinement, which was limited to about one hour in the isothermal case, becomes much larger. In this example, the simulated pressure remains insensitive to the grid refinement level. However, for some cases (ex: strong dependence of the viscosity to temperature), the error on temperature can also impacts the simulated pressure evolution.

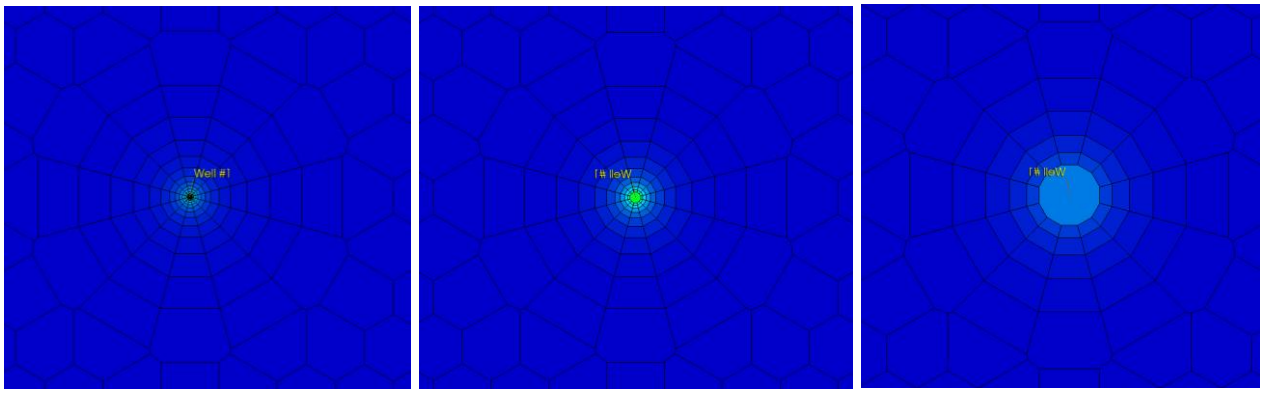


Fig. 18.G.8 – Temperature field around a producing vertical well for fine, intermediate and coarse simulation grids.

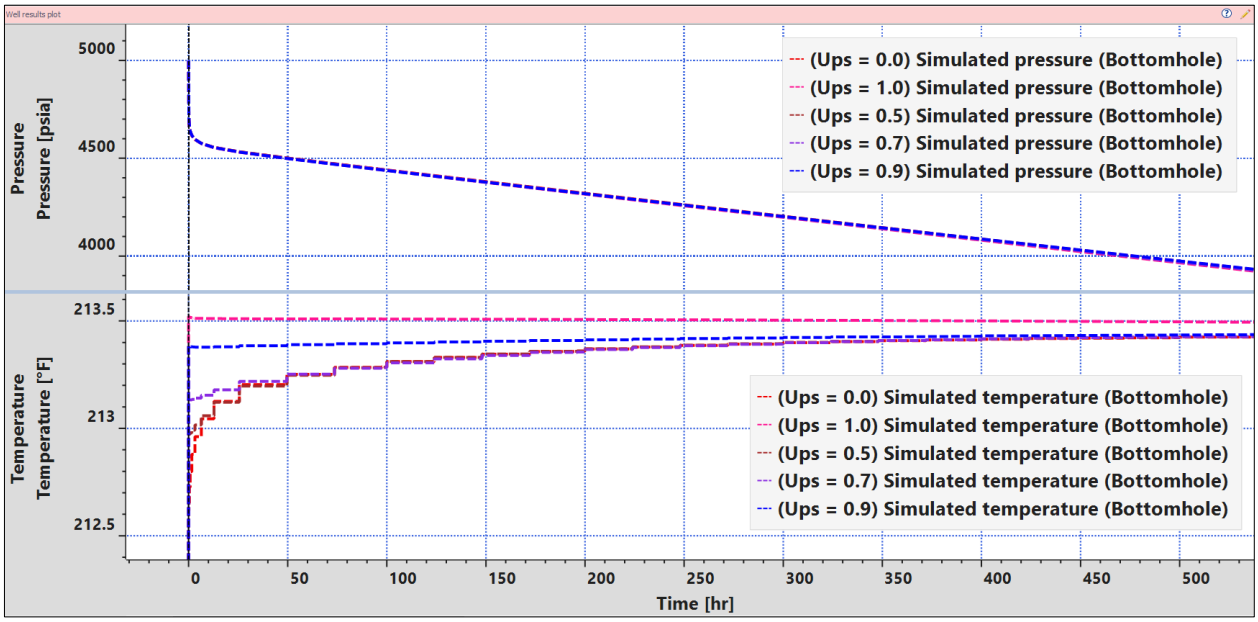


Fig. 18.G.9 – Simulated bottomhole pressure and temperature vs time for various upscaling levels in thermal case.

This dependence to the grid resolution is primarily influenced by the connections between well cells and reservoir cells. For these connections, as described previously, the convection term involves $q_{iw}\, h_{iw}$, where q_{iw} is the mass flux between the well cell and the wellbore, and h_{iw} is evaluated using the upstream value, which means for a producer: $h_{iw} = h_i$. When the enthalpy gradient is steep in the vicinity of the wellbore, we see (Fig 18.G.10) that a low resolution can lead to a discretization error on the value of the enthalpy flowing to the well - with the above described consequences on temperature estimations.

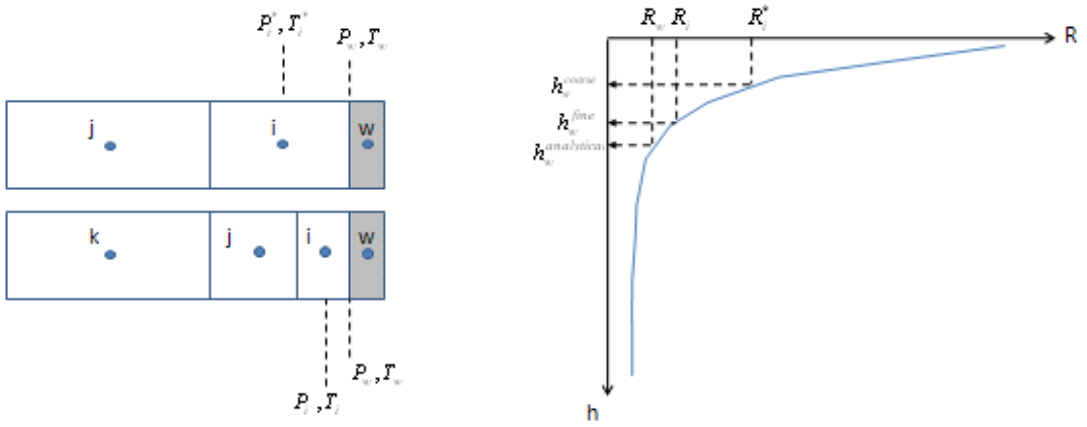


Fig. 18.G.10 – Enthalpy at well for two well cell radii, compared to the analytical value

18.H Forward Temperature simulation – Emeraude

In Forward simulation mode, the inputs are the layer rates (production or injection) plus the system description (Reservoir, wellbore, fluids, etc.). Using the Energy Equation and WIFO models, then it is possible to simulate the temperature response for any arbitrary production or injection profile.

Unless we have PL measurements, the layer rates are unknown. Therefore, this mode is useful for pre-job planning purposes, what-if scenarios or to understand what the impact of the uncertainty of different input parameters. All the sensitivities presented above for the Energy Equation and WIFO models can be obtained by conducting Forward simulations.

Emeraude presents two Forward simulation models which are based on the Energy equation, but the specific formulation is different to account for the particular wellbore flowing conditions. The Steam injection and Leak simulation methods are presented next.

18.H.1 Steam Injection

The main objective of steam injection is to maximise the amount of heat transfer between the steam and oil in the formation. The heat contained by the water is largely a function of its temperature. However, in this case since water exists in liquid and vapour form, the evaporation enthalpy or "latent heat" of the vapour will play a key role. Hot liquid water reaching the formation will transfer less energy than vapour at the same temperature.

As the hot vapour is injected from surface, heat exchange will occur, leading to a temperature drop and part of the vapour condensing to liquid water. At any depth of the well, the Steam quality is defined by the mass of steam divided by the total mass of injected water:

$$\chi = \frac{m_{vapour}}{m_{vapour} + m_{liquid}}$$

The objective of the steam injection design is then to maximise the steam quality reaching the perforations. This can be modelled in Emeraude, and sensitivities on the completion design and injection conditions can be carried out.

In this situation, liquid and vapour will coexist, and the system has only one degree of freedom, meaning that temperature and pressure are not independent. At equilibrium, in order to fully determine the state of the fluid it is necessary to know the pressure or temperature, plus the enthalpy (can be the entropy or specific volume too).

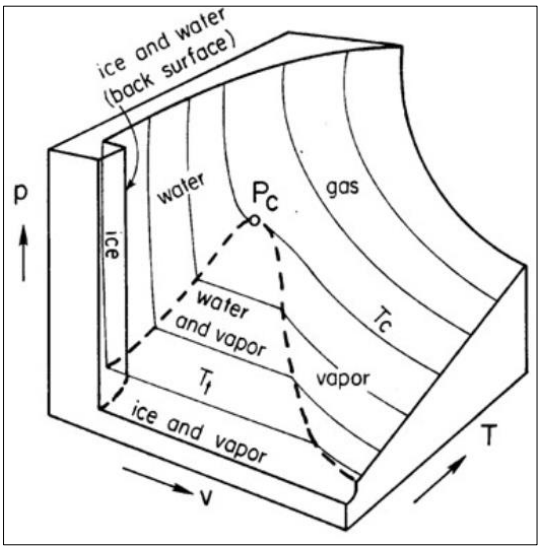


Fig. 18.H.1 – Water phase diagram – From Godson (1973)

In order to calculate the Enthalpy profile, it is necessary to define the surface injection conditions (rate, pressure and temperature) plus a tubing (or casing) pressure profile. Since liquid and vapour will travel at different velocities, multiphase flow correlations are used to compute the pressure profile.

Starting from the surface conditions, it is possible to apply the Energy equation to integrate downwards in order to obtain the temperature and the Steam quality profiles. The rate of injected water per layer is one of the inputs of the model, and this needs to be obtained by other means (i.e. reservoir simulation).

The results of a steam injection simulation are shown in the image below. The QZT and QZI tracks show the vapour fraction in red and liquid in blue. Steam quality drops from around 0.7 at surface to zero above the bottom perforation. This means that only hot water is injected at the bottom perforation.

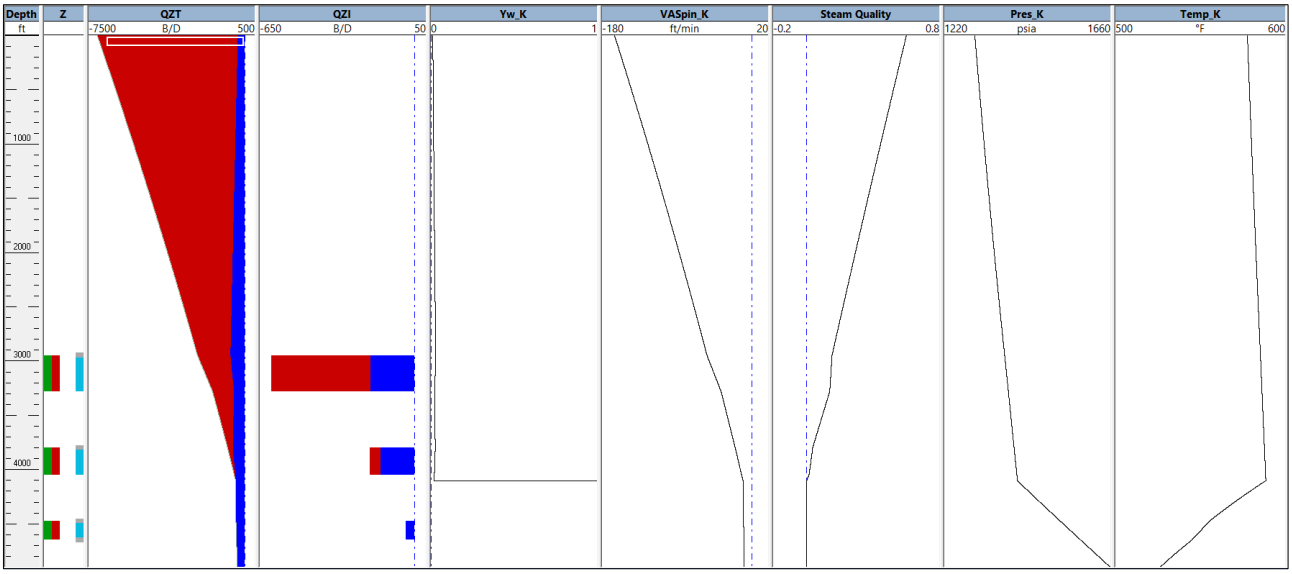


Fig. 18.H.2 – Steam injection simulation

From this base case it is possible to perform some sensitivities. When an annular is present, the fluid filling it will have a large impact. Liquid water has a large thermal conductivity compared to gases, which leads to a larger heat loss coefficient, facilitating the heat exchange. Also, based on the available surface injection facilities, the injection pressure and quality can be increased to maximise the steam quality at the perforation level.

18.H.2 Leak detection

Increased annular pressure detected at surface is likely to be an indication of tubing to casing leak. This may be a result of tubing corrosion, problem with valves, expansion joints, etc. Sustained annular pressure is an integrity concern, and the leak position has to be determined as soon as possible.

In general, leak rates are low and normally missed by conventional spinners. More specific cased hole logging tools can be run, such as Multifinger calipers, acoustic energy (noise) and temperature measurements. It is important to understand, before running the tools, what is the expected temperature response to different leak rates. This can be done in Emeraude. It has to be remembered that this simulation is exclusively for a tubing leak in a situation where water is injected through tubing and circulated back via annular.

The leak simulation is a specific formulation derived from the Energy Equation model. The temperature profile along the tubing and annulus are simulated. Also, as we are now interested in small localized features, the thermal conductivity in the axial condition is also accounted for. The diagram below shows the energy balance for a segment of the well. The arrows in red show conduction, both in the vertical (tubing, annular, casing) and in the horizontal direction. Forced convection in the tubing and annular are also taken into account (blue arrows):

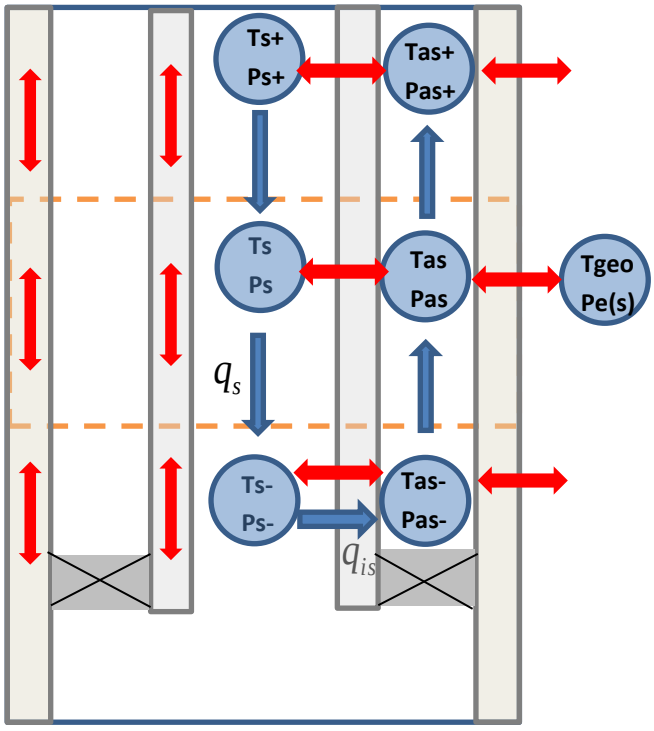


Fig. 18.H.3 – Energy balance for leak simulation

The image below shows a noise log indicating the possible depth of the tubing to annulus communication. The leak design option can be used, based on the injection conditions (rate, pressure, temperature) and the same heat transfer parameters used in the Energy model. The Temperature match track shows the simulation of the annular (blue) and tubing (green) temperature for a set of injection parameters. In this situation, both show an increase compared to the geothermal gradient.

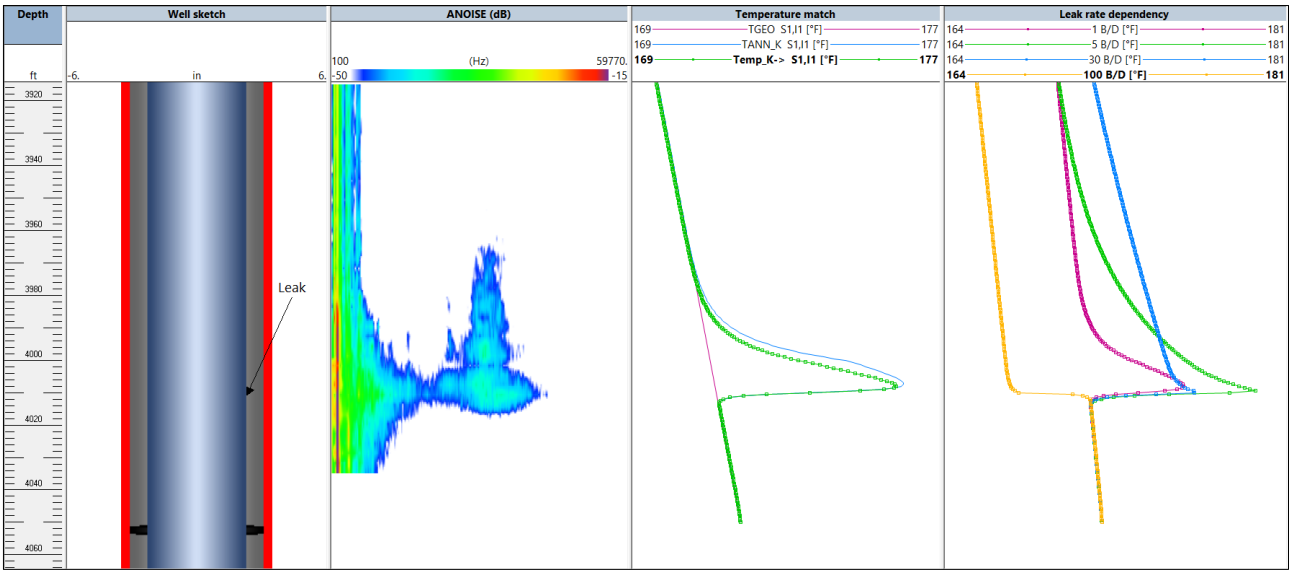


Fig. 18.H.4 – Leak simulation results and rate sensitivities

The last track shows a sensitivity of the temperature measured in the tubing for different leak rates. Similar to what is observed in traditional injection cases, when the injected water is colder than the downhole temperature, two mechanisms will be in play. The throttling effect through the leak (larger for increased delta P) leads to a localised increase in temperature. On the other hand, the convection of the colder water from surface leads to a decrease in temperature. Therefore, in the above picture, for rates of 1, 5 and 30 B/D, a temperature increase is observed. On the other hand, for 100 B/D the temperature decreases at the leak point. Clearly, the resulting temperature response is given by a balance of both mechanisms.

This type of simulation can help to set the expectations bar on the temperature response and optimise the surface injection conditions. Shallow leaks or warm injected water can lead to small delta T. In these cases, it will be possible to play with the Delta P at the leak, which in turn is given by the annular pressure (and therefore the bleeding rate).

TABLE OF CONTENTS

1 – INTRODUCTION 5

1.A WHAT IS THIS BOOK FOR? 5

1.B WHAT IS NEW IN THIS VERSION? 6

1.C WHAT IS DYNAMIC DATA ANALYSIS? 7

1.D BOOK CONTENT 11

1.E OTHER BOOKS FOR REFERENCE 12

1.F HOW MANY EQUATIONS DO YOU WANT? 13

2 – THEORY 15

2.A DIFFUSION EQUATION 15

2.A.1 Darcy's law 15

2.A.2 The diffusivity equation 16

2.A.3 Diffusion in a homogeneous isotropic reservoir 18

2.B INITIAL, WELL AND OUTER BOUNDARY CONDITIONS 20

2.B.1 Initial conditions 20

2.B.2 Well conditions 20

2.B.3 Outer boundary conditions 21

2.C LINE SOURCE SOLUTION IN A HOMOGENEOUS INFINITE RESERVOIR 22

2.C.1 The Line Source Solution 22

2.D WELLBORE STORAGE AND SKIN 24

2.D.1 Wellbore storage 24

2.D.2 Skin 25

2.D.3 Derivation 27

2.D.4 Behavior 29

2.E OUTER BOUNDARY CONDITIONS 30

2.E.1 Major types of boundaries 30

2.E.2 Derivation for a circular reservoir 31

2.E.3 Pseudo-Steady State flow 32

2.F COMPLEX PRODUCTION HISTORIES – SUPERPOSITION IN TIME 34

2.F.1 The principle of superposition 34

2.F.2 Build-up superposition *34*
2.F.3 Multirate superposition *35*
2.G OTHER MEANS TO SOLVE AND MODEL A DIFFUSION PROBLEM 36
2.G.1 Superposition in space of analytical models (image wells) *36*
2.G.2 Boundary elements *36*
2.G.3 Numerical models *37*
2.H PHYSICAL MEANING OF DIFFUSION 38
2.H.1 Reference case *38*
2.H.2 Effect of 'unknown' parameters *40*
2.H.2.a Wellbore storage 40
2.H.2.b Skin 41
2.H.2.c Permeability 42
2.H.2.d Reservoir size 43
2.H.3 Effect of 'known' parameters *44*
2.H.3.a Wellbore radius 44
2.H.3.b Porosity 45
2.H.3.c Total compressibility 46
2.H.3.d Viscosity 47
2.H.3.e Thickness 48
2.H.3.f How about rates? 49
2.H.4 Conclusions *50*
2.H.4.a on this series of designs 50
2.H.4.b on the equations 50
2.H.5 Effect of errors on the different input parameters *51*
2.I THE CASE OF DRY GAS 53
2.I.1 The PVT of real dry gas *53*
2.I.2 Derivation of the real dry gas diffusion *54*
2.I.3 Diffusion of real dry gas *55*
2.I.3.a Standard pseudopressures 55
2.I.3.b Normalized pseudopressures 56
2.I.4 Non-Darcy flow *56*
3 – PRESSURE TRANSIENT ANALYSIS (PTA) 59
3.A INTRODUCTION (WITH A SHORT HISTORY) 59
3.B THE OLD STUFF 63
3.B.1 IARF and Semilog plots *63*

3.B.2 Drawdown response and MDH plot 63
3.B.3 Build-up response and Horner plot 65
3.B.4 Shut-in after a complex production and superposition plot 67
3.B.5 Complex productions and rate normalized superposition plot 68
3.B.6 Using type-curves 68
3.B.7 Other specialized plots 70
3.B.8 IPR & AOF 71
3.C THE 'RIGHT' STUFF 72
3.C.1 Before the Bourdet Derivative 72
3.C.2 Definition of the Bourdet Derivative 73
3.C.3 Bourdet Derivative & Infinite Acting Radial Flow (IARF) 74
3.C.4 Bourdet Derivative & Wellbore Storage 75
3.C.5 The original idea behind the Bourdet Derivative 75
3.C.6 Bourdet Derivative & other flow regimes 76
3.C.7 Bourdet Derivative & Other models 77
3.C.8 Modeling 77
3.C.9 Other types of derivative 78
3.D THE USE OF MODERN DECONVOLUTION 79
3.D.1 What is deconvolution? Why do we need it? 79
3.D.1.a The need 79
3.D.1.b Mathematical formulation 80
3.D.2 Deconvolution Method 1 (von Schroeter et al., 2004) 81
3.D.2.a Problem unknowns 81
3.D.2.b Problem objective function 82
3.D.2.c Deconvolution in plain English 83
3.D.2.d Field data application 83
3.D.2.e Main limitation of von Schroeter et al. method 84
3.D.3 Deconvolution Method 2 (Levitan, 2005) 85
3.D.4 Deconvolution Method 3 (Houzé et al., 2006-2010) 87
3.D.4.a Variant 1: Using Levitan method after Method 3 88
3.D.4.b Variant 2: Using Method 3 on all build-ups 89
3.D.4.c Remaining limitations 89
3.D.5 Pi influence on the deconvolution 90
3.D.5.a Implementation in Saphir 5 91
3.D.6 Using sensitivity to assess the validity of a deconvolution 92
3.D.7 Conclusion 94

3.E MODERN PTA METHODOLOGY 95
3.E.1 Initialization 95
3.E.2 Loading Data 96
3.E.3 Quality Control 97
3.E.4 Editing data 98
3.E.5 Extraction and diagnostic 99
3.E.6 Deconvolution 100
3.E.7 Diagnostic 101
3.E.8 Model generation 101
3.E.9 Model refinement 103
3.E.10 Sensitivity study 103
3.E.11 Reporting Guidelines 104
3.F TEST DESIGN 105
3.F.1 Safety 105
3.F.2 Objectives 105
3.F.3 What data, what quality at what cost? 106
3.F.4 Type of test 108
3.F.5 Scenario 108
3.F.6 The final program 111
3.G OPERATIONAL CONSIDERATIONS: GATHERING DATA 112
3.H QUALITY ASSURANCE AND QUALITY CONTROL 113
3.H.1 Introduction 113
3.H.2 Background 113
3.H.3 The concept of Differential Pressure Analysis 114
3.H.4 Basics 115
3.H.5 Pressure correction 116
3.I MORE ON QA/QC 117
3.I.1 Diagnosing phase segregation from differential pressure 117
3.I.2 Impact on the diagnostic 119
3.I.3 Gauge drift 119
3.I.4 Phase redistribution 120
3.J THE CASE OF DRY GAS 122
3.J.1 Diffusion of real dry gas 122
3.J.2 Correcting the pressure to sandface 122

3.J.3 Gas material balance *123*
3.J.3.a Using pseudotime functions 124
3.J.3.b Integrating the material balance correction in the analytical model 124
3.J.3.c Using a numerical model 125
3.J.4 Non-Darcy flow *125*
3.J.4.a Simulating non-Darcy flow with a rate dependent skin model 125
3.J.4.b Simulating non-Darcy flow with a numerical model 127

4 – RATE TRANSIENT ANALYSIS (RTA) 129

4.A INTRODUCTION (WITH A SHORT HISTORY) 129
4.B THE OLD STUFF 131
4.B.1 Arps *131*
4.B.2 Fetkovich *134*
4.B.3 Gas material balance $\overline{P}/Z$ vs Q plot *136*
4.C THE RIGHT STUFF 137
4.C.1 Blasingame plot *137*
4.C.2 Loglog plot *140*
4.C.3 Material balance (Normalized rate-cumulative) plot *142*
4.C.4 Flowing gas material balance plot *143*
4.C.5 P-Q diagnostic plot *146*
4.C.6 History plot *147*
4.D THE CASE OF DRY GAS 148
4.D.1 Diffusion of real dry gas *148*
4.D.2 The old Stuff *148*
4.D.2.a Fetkovich 148
4.D.2.b Gas material balance $\overline{P}/Z$ vs Q plot 149
4.D.3 The right stuff *149*
4.D.3.a Blasingame plot 149
4.D.3.b Loglog plot 150
4.D.3.c Material balance (Normalized rate-cumulative) plot 151
4.D.3.d Flowing gas material balance plot and P-Q diagnostic plot 151
4.D.4 General major gas issues *152*
4.D.4.a Correcting the pressure to sandface 152
4.D.4.b Gas material balance correction 152
4.D.4.c Non-Darcy flow 154
4.E MODERN RTA METHODOLOGY 155

4.E.1 Preparing a project and loading data 156
4.E.2 Editing data 157
4.E.3 Extraction and diagnostics 157
4.E.4 Model generation 158
4.E.5 Model refinement 159
4.E.6 Deconvolution 159
4.E.6.a Principle 159
4.E.6.b Basic theory 159
4.E.6.c Model Regularization 160
4.E.6.d Implementation in Topaze 161
4.E.7 Forecast 162
4.E.8 Sensitivity study 162
4.E.9 Reporting Guidelines 163
4.F RTA VERSUS PTA 164
4.F.1 Introduction 164
4.F.2 Common tools 165
4.F.3 PSS vs. IARF 165
4.F.4 Diagnostic capabilities 165
4.F.5 Validity of the PTA hypothesis in Rate Transient Analysis 166

5 – WELLBORE MODELS 167

5.A INTRODUCTION 167
5.B CONSTANT WELLBORE STORAGE 168
5.B.1 Loglog analysis 168
5.B.2 Specialized analysis (Cartesian plot) 169
5.B.3 Sensitivity analysis on the wellbore storage coefficient 170
5.C CHANGING WELLBORE STORAGE 171
5.C.1 Analytical models 171
5.C.2 Combining pseudo-time and a constant storage model 172
5.C.3 Numerical pressure dependent wellbore storage 173

6 – WELL MODELS 175

6.A INTRODUCTION 175
6.B VERTICAL WELL WITH CONSTANT SKIN 176
6.C VERTICAL WELL WITH CHANGING SKIN 178
6.C.1 Rate dependent skin 178

6.C.2 Time dependent well model 179
6.C.3 Time dependent skin 180
6.D HIGH CONDUCTIVITY FRACTURE 181
6.D.1 Hypotheses 181
6.D.2 Behavior 182
6.D.3 Loglog Analysis 184
6.D.4 Sensitivity to different parameters 185
6.D.4.a Choice of fracture model 185
6.D.4.b Sensitivity to the half fracture length 185
6.D.4.c Sensitivity to the reservoir permeability 186
6.D.5 Specialized Analysis 187
6.D.6 Adding wellbore storage 188
6.D.7 Skin effect 188
6.D.7.a Fracture Geometrical Skin 188
6.D.7.b Model Skin and Total Equivalent Skin 189
6.D.7.c Influence of skin 190
6.E LOW CONDUCTIVITY FRACTURE 191
6.E.1 Hypothesis 191
6.E.2 Behavior 191
6.E.3 Loglog Analysis 192
6.E.4 Sensitivity to different parameters 193
6.E.4.a Sensitivity to $k_f w_f$ 193
6.E.4.b Sensitivity to the half fracture length 194
6.E.5 Specialized analysis 194
6.E.6 Adding wellbore storage 195
6.E.7 Skin effect 196
6.E.7.a Fracture Geometrical Skin 196
6.E.7.b Model Skin and Total Equivalent Skin 196
6.F LIMITED ENTRY WELL 198
6.F.1 Hypothesis 198
6.F.2 Behavior 198
6.F.3 Loglog Analysis 199
6.F.4 Sensitivity to different parameters 200
6.F.4.a Sensitivity to the anisotropy 200
6.F.4.b Sensitivity to the vertical distance to a constant pressure boundary 201
6.F.5 Specialized analysis 202

6.F.6 Adding wellbore storage 202
6.F.7 Skin effect 203
6.F.7.a Skin components 203
6.F.7.b Influence of skin 204
6.G HORIZONTAL WELLS 205
6.G.1 Hypothesis 205
6.G.2 Behavior 206
6.G.3 Loglog analysis 207
6.G.4 Sensitivity to different parameters 207
6.G.4.a Contributing horizontal section, h_w and position 207
6.G.4.b Sensitivity to the anisotropy 209
6.G.5 Adding wellbore storage 209
6.G.6 Skin effect 210
6.H MORE ON HORIZONTAL WELLS 211
6.H.1 The flow regimes and incomplete data 211
6.H.1.a Early time radial flow 211
6.H.1.b Linear flow 212
6.H.2 Horizontal anisotropy 214
6.H.3 Fractured horizontal well 215
6.H.3.a Sensitivity 215
6.H.3.b Adding wellbore storage 217
6.H.3.c Skin 218
6.H.4 Field examples 218
6.I SLANTED WELLS 219
6.I.1 Behavior 220
6.I.2 Sensitivity to different parameters 220
6.I.3 Adding wellbore storage 223
6.I.4 Skin 224
6.I.5 Slanted well multilayer 224
6.I.5.a Hypothesis 224
6.I.5.b Behavior 225
6.J MULTILATERAL WELLS 228
6.J.1 Hypothesis 228
6.J.2 The analytical multilateral well model 228
6.J.3 The numerical multilateral well model 229
6.J.4 Behavior 229

6.K INFLOW CONTROL DEVICE 230
6.K.1 Problems induced by a well completed in several formations 230
6.K.2 Solution proposed to optimize the drainage of the formation 230
6.K.3 ICD model principle 231
6.K.4 Behavior 233
6.K.5 Illustration 233

7 – RESERVOIR MODELS 235

7.A INTRODUCTION 235
7.B HOMOGENEOUS RESERVOIR 236
7.B.1 Homogeneous Sensitivity to parameters 238
7.B.1.a Skin 238
7.B.1.b Permeability 239
7.B.1.c Wellbore radius 240
7.B.1.d Porosity 241
7.B.1.e Total compressibility 242
7.B.1.f Viscosity 243
7.B.1.g Thickness 244
7.B.1.h … and how about rates? 245
7.C DOUBLE-POROSITY RESERVOIR 246
7.C.1 Hypothesis 246
7.C.2 Loglog behavior 247
7.C.3 Specialized analysis 251
7.C.4 Effect of wellbore storage 252
7.C.5 Skin 253
7.D EXTENSIONS OF THE DOUBLE-POROSITY RESERVOIR 254
7.D.1 Multiple porosities 254
7.D.2 Hypothesis 254
7.D.3 Loglog behavior 256
7.D.4 Effect of wellbore storage 257
7.D.5 Effect of skin 258
7.E DOUBLE-PERMEABILITY RESERVOIRS 259
7.E.1 Hypothesis 259
7.E.2 Loglog behavior 260
7.E.3 Effect of wellbore storage 262
7.E.4 Skin 262

7.E.5 Field examples 263
7.F EXTENSION OF DOUBLE-PERMEABILITY RESERVOIRS 264
7.F.1 Multiple layers 264
7.F.2 Numerical double permeability 265
7.G MULTILAYERED RESERVOIRS 267
7.G.1 Hypothesis 268
7.G.2 How to build a multilayer model 269
7.H COMPOSITE RESERVOIRS 272
7.H.1 Hypothesis 272
7.H.2 Loglog behavior 274
7.H.3 Specialized analysis 276
7.H.4 Effect of wellbore storage 277
7.H.5 Skin 278
7.H.6 Extensions of the composite reservoir 279
7.H.7 Polymer injection Fall Off model 281
7.H.7.a Objective of the model 281
7.H.7.b Description of the model and assumptions 281
7.H.7.c Method used in the solution 281
7.H.7.d Model input parameters 282
7.H.7.e Typical behavior 282
7.H.7.e.i Sensitivity to the input model parameters 283
7.H.7.e.i.1 Sensitivity to the polymer concentration Cp: 283
7.H.7.e.i.2 Sensitivity to the polymer viscosity coefficients a1, a2, a3 283
7.H.7.e.i.3 Sensitivity to the Shear rate coefficient gamma-c 284
7.H.8 Multiphase injection and fall off in a naturally fractured reservoir model 284
7.H.8.a Objectives of the model 284
7.H.8.b Definition and Assumptions 284
7.H.8.c Model Parameters 287
7.H.8.d Sensitivity to parameters and the injected volume 288
7.H.8.d.i Sensitivity to the mobility ratio 288
7.H.8.e Sensitivity to the fracture porosity 288
7.H.8.f Sensitivity to the matrix capillary pressure 289
7.H.8.g Sensitivity to the matrix permeability 289
7.H.9 Numerical models 290
7.H.10 When should we use a composite model? 290
7.H.10.a Changes of reservoir properties 290

7.H.10.b Fluid front 290
7.H.10.c Gravel packs and the invaded zone 290
7.H.10.d Match any old weird response 291
7.I RESERVOIR ANISOTROPIES 292
7.I.1 Vertical anisotropy 292
7.I.2 Horizontal anisotropy 293
7.J ANALYTICAL COMBINATIONS OF RESERVOIR MODELS 294
7.J.1 Double permeability radial composite 294
7.J.2 Double permeability double porosity layers 295
7.J.3 Double porosity radial composite 296
7.J.4 Just a comment on the above described models 296
8 – BOUNDARIES 297
8.A INTRODUCTION 297
8.B DIFFERENT TYPES OF BOUNDARIES 298
8.B.1 Description of a boundary behavior 298
8.B.2 No flow boundaries 299
8.B.3 Constant pressure boundaries 300
8.B.4 Aquifers 300
8.B.5 Leaky boundaries 301
8.B.6 Conductive boundaries 301
8.C SINGLE SEALING FAULT 302
8.C.1 Behavior 302
8.C.2 Semilog analysis 302
8.C.2.a Drawdown response 303
8.C.2.b Build-up response 303
8.C.3 Loglog analysis 304
8.C.4 Influence of the boundary distance 305
8.C.5 The case of shut-ins after a short production time 305
8.C.6 Remarks on the sealing fault model 306
8.D INTERSECTING FAULTS 307
8.D.1 Description 307
8.D.2 Behavior 307
8.D.3 Semilog analysis 308
8.D.3.a Drawdown response 308
8.D.3.b Build-up response 309

8.D.4 Loglog analysis 309
8.D.5 Remarks on the intersecting faults model 310
8.D.6 Example of intersecting faults match with field data 310
8.E TWO PARALLEL FAULTS 311
8.E.1 Description 311
8.E.2 Behavior 311
8.E.3 Semilog analysis 312
8.E.4 Loglog analysis 312
8.E.5 Specialized analysis 313
8.E.6 U-Shape reservoir 315
8.E.7 Remarks on the parallel faults model 316
8.E.8 Field example 316
8.F CLOSED SYSTEMS 317
8.F.1 Description 317
8.F.2 Behavior 318
8.F.3 Semilog analysis 319
8.F.4 Loglog analysis 319
8.F.5 Specialized analysis 320
8.F.6 Closed system versus drainage area 321
8.F.7 Other remarks on the closed systems 321
8.F.8 Example of matches with field data 322
8.G CONSTANT PRESSURE BOUNDARIES 323
8.G.1 Description 323
8.G.2 Behavior 323
8.G.3 Semilog analysis 324
8.G.4 Loglog analysis 324
8.G.4.a Drawdown response 324
8.G.4.b Build up response 325
8.G.5 Constant pressure vs. closed system 327
8.H LEAKY AND INCOMPLETE BOUNDARIES 329
8.H.1 Leaky fault 329
8.H.1.a Behavior 329
8.H.1.b Semilog analysis 330
8.H.1.c Loglog analysis 331
8.H.2 Incomplete boundary 332

8.H.2.a Behavior 332
8.H.2.b Semilog analysis 333
8.H.2.c Loglog analysis 334
8.I CONDUCTIVE FAULTS 335
8.I.1 Behavior 336
8.I.2 Semilog analysis 337
8.I.3 Loglog analysis 337
8.J COMBINATION WITH OTHER RESERVOIR AND WELL MODELS 340
8.K ASSESSING BOUNDARY EFFECTS 341
8.L RADIUS OF INVESTIGATION VS MINIMUM RESERVES 343
8.M SUPERPOSITION EFFECTS 344
8.M.1 Can we see a fault in a build-up and not in the drawdown? 344
8.M.2 Superposition effect consequence on the boundaries diagnosis 345
8.M.3 Conclusion 346
8.N TYPICAL ERRORS DIAGNOSING A BOUNDARY EFFECT 347
8.N.1 Incorrect production history 347
8.N.2 End effect in the derivative calculation 348
8.N.3 Gauge drift 349
8.N.4 Reservoir trends 349
8.N.5 Interference from other wells 349
8.O DECONVOLUTION 351
8.P CONCLUSION 353
9 – PVT 355
9.A INTRODUCTION 355
9.B PHASE EQUILIBRIUM 356
9.B.1 Single-component fluids 356
9.B.2 Multi-component fluids 357
9.C CLASSIFICATION OF RESERVOIR FLUIDS 359
9.D PHASE DESCRIPTION 361
9.D.1 Oil - Classical Black-Oil (BO) formulation 361
9.D.2 Wet gas 363
9.D.3 Modified Black Oil (MBO) PVT Formulation 363
9.D.4 Water production 365
9.E FLUID PROPERTIES 366

9.E.1 Gas properties 366
9.E.2 Oil properties 368
9.E.3 Water properties 369
9.F USE OF PVT DATA IN DDA (OIL) 371
9.F.1 Single-phase oil 371
9.F.2 Perrine 371
9.G USE OF PVT DATA IN DDA - CONTINUED (OIL) 373
9.G.1 Single phase oil pseudopressure 373
9.G.2 Multiphase pseudopressure 373
9.H USE OF PVT DATA IN DDA (GAS) 374
9.H.1 Dry gas 374
9.H.2 Wet gas and condensate single phase analog 374
9.I USE OF PVT DATA IN DDA - CONTINUED (GAS) 375
9.I.1 Multiphase pseudopressures for condensate 375
9.J GETTING PROPERTIES FROM PVT STUDIES 376
9.J.1 Constant Composition Expansion (CCE) 376
9.J.2 Differential Liberation Expansion (DLE) 377
9.J.3 Separator Tests 378
9.J.4 Converting Fluid Study Results 379
9.K OBTAINING PROPERTIES FROM PVT CORRELATIONS 380
9.K.1 Gas correlations 380
9.K.1.a Z factor 380
9.K.1.b Gas viscosity 381
9.K.2 Oil correlations 381
9.K.2.a Pb and Rs 381
9.K.2.b Oil FVF 382
9.K.2.c Oil viscosity 382
9.K.2.d Oil isothermal compressibility 383
9.K.3 Water correlations 383
9.K.3.a Water FVF 383
9.K.3.b Water Compressibility 383
9.K.3.c Gas solubility 383
9.K.3.d Water Viscosity 383
9.K.4 Correlation: feeding and matching 383
9.L 'COMPOSITIONAL' PVT FROM BO (AND MBO) MODEL 385

9.L.1 2-Phase envelope 385
9.M EQUATIONS OF STATE 388
9.N CONFINED PVT 389
9.N.1 Summary 389
9.N.2 Model description 389
9.N.2.a Capillary pressure 389
9.N.2.b Flash including capillary pressures 390
9.N.2.c Critical properties shift in nanopores 390
9.N.3 Results 391
9.N.3.a Influence on the phase envelope 391
9.N.3.b Influence on the PVT parameters; Density and Viscosity 393
9.N.3.c Influence on the production simulations 394
9.N.4 References 395
10 – UNCONVENTIONAL RESOURCES 397
10.A INTRODUCTION AND DEFINITIONS 397
10.A.1 Shale gas 398
10.A.2 Shale oil 399
10.A.3 Coal seam gas (not covered in this chapter) 401
10.A.4 Oil shale (not covered in this chapter) 401
10.A.5 Hydrates (not covered in this chapter) 402
10.B SPECIFICS OF SHALE PLAYS 403
10.B.1 Impact of the low permeability 405
10.B.2 Diffusion equations 406
10.B.2.a Desorption 407
10.B.2.b Molecular diffusion and diffusion between micropores 409
10.B.2.c Fracture diffusion 410
10.B.2.d Stress and pressure-dependent properties 412
10.B.2.e PVT issues 412
10.B.2.e.i Confined PVT solution 413
10.B.3 Fractured horizontal wells 415
10.B.4 Initial state of the system 416
10.B.5 Heterogeneities and DFN 417
10.B.6 Lack of quality data 418
10.C BASIC PRODUCTION BEHAVIOUR OF A SHALE WELL 419
10.C.1 'Early' linear flow 419

10.C.2 Transition from linear flow to SRV flow *420*
10.C.3 SRV flow *421*
10.C.4 Beyond SRV *422*
10.D Decline Curve Analysis (DCA) of unconventional plays 425
10.D.1 Main plots used in Decline Curve Analysis *425*
10.D.2 The Arps equations *428*
10.D.3 Power-law exponential *430*
10.D.4 Stretched exponential function *432*
10.D.5 The Duong model *434*
10.D.6 Logistic growth *436*
10.D.7 Stimulated Reservoir Volume Bounded decline curve *438*
10.D.8 Segmented DCA models *439*
10.D.8.a Segmented Power Law Model 439
10.D.8.b Segmented Hyperbolic DCA model 440
10.D.9 Conclusions *441*
10.E Rate Transient Analysis (RTA) for unconventional plays 442
10.E.1 Linear flow diagnostics *442*
10.E.2 Diagnostic of the SRV flow *444*
10.E.3 Simultaneous diagnostic of several flow regimes *445*
10.E.4 Matching data with a model *447*
10.E.5 History matching *449*
10.E.6 Production forecasting and EUR *451*
10.E.7 EUR statistics *451*
10.F Simple models 454
10.F.1 'Classic' Multi-Fractured Horizontal Well (MFHW) *454*
10.F.2 SRV bounded model *456*
10.F.3 Trilinear model *458*
10.G Field example – Demonstration of simple models 460
10.G.1 First eight months of production *460*
10.G.2 Linear flow model *461*
10.G.3 Analytical Multi Fractures Horizontal Well (MFHW) *462*
10.G.4 Numerical MFHW *462*
10.G.5 Comparing production forecasts *463*
10.G.6 Receiving ten more months of production data *465*
10.G.7 Discussion *467*

10.H ADVANCED MODELS 468
10.H.1 Complex geometries (analytical + numerical) 468
10.H.2 DFN models (numerical + analytical) 470
10.H.2.a Numerical DFN 470
10.H.2.b Stochastic DFN 472
10.H.2.c Analytical DFN 474
10.H.3 Modeling water flowback (numerical) 474
10.H.3.a Static initialization 474
10.H.3.b Dynamic initialization 476
10.H.4 Refrac jobs modeling 477
10.H.4.a Features for simple fracture system 478
10.H.4.b Features for complex fracture system 479
10.H.5 Multi-Zone Fractional Dimension 480
10.H.6 Anomalous Diffusion in a Tri-linear model 483
10.H.6.a Description and assumptions 483
10.H.6.b Model features and parameters 484
10.H.6.c General Anomalous Diffusion Behaviour 484
10.H.6.d The anomalous diffusion applied to a heterogeneous reservoir 487
10.I KAPPA RECOMMENDED WORKFLOW (2020) 492
10.I.1 Accessing data 492
10.I.2 Quality control (Citrine) 494
10.I.3 Diagnostic analysis, well grouping and selecting representative wells (Citrine) ... 494
10.I.4 Selection of representative wells (Citrine/Topaze) 498
10.I.5 Single well Rate Transient Analysis (Topaze) 498
10.I.6 Extension of the representative well model forecast to other wells 500

11 – FORMATION TESTS 503

11.A INTRODUCTION 503
11.B WHAT IS FORMATION TESTING (FT) USED FOR? 504
11.B.1 Pressure profiling 504
11.B.2 Sampling 512
11.B.3 Permeability determination 513
11.C TOOL DESCRIPTION 514
11.D TYPICAL FT JOB SEQUENCE 517
11.E DATA QUALITY CONTROL 518
11.F PRESSURE ANALYSIS 519

11.F.1 Data formats, data loading 519
11.F.2 Automatic determination of tests 520
11.F.3 Computation of rates from volumes 520
11.F.4 Pretest calculations (P_{dd}, P_{stop}, drawdown mobility) 522
11.F.5 Pretest quality assessment and rating 526
11.G STANDARD PRESSURE TRANSIENT ANALYSIS 527
11.G.1 Common features 527
11.G.2 Analytical model matching 528
11.G.3 Tool types, solutions and sensitivity 531
11.G.3.a Single circular active probe 531
11.G.3.b Single oval active probe 535
11.G.3.c Two sink probes (dual circular) 538
11.G.3.d Four oval probes – Schlumberger Saturn™ 541
11.G.4 Comparison of Behavior 544
11.H SPECIFIC FT ANALYSIS 545
11.H.1 Vertical Interference Tests 545
11.H.2 Formation Tester in Multilayers 548
11.H.2.a Model description 548
11.H.2.b Heterogeneous behavior 549
11.H.2.c Observation of the crossflow 550
11.H.2.d Effect of deviation 552

12 – PTA: SPECIAL TEST OPERATIONS 555

12.A INTRODUCTION 555
12.B SLUG TESTS 556
12.B.1 Test sequence in a DST 556
12.B.2 Build-up analysis using slug rates 557
12.B.3 Slug test analysis 558
12.C MULTILAYER TESTS 562
12.C.1 Introduction 562
12.C.2 Available models 562
12.C.3 Standard tests 564
12.C.4 Using Production Logs 565
12.C.4.a Stabilized rate acquisition 565
12.C.4.b Transient rate acquisition 565
12.C.5 Designing a multilayer test 566

12.C.6 Multilayer analysis workflow *567*
12.C.6.a Preparation of the data 567
12.C.6.b Getting the global results 568
12.C.6.c Multilayer model building and first run 569
12.C.6.d First improve of the model 570
12.C.6.e Final model adjustment 572
12.C.6.f The solution uniqueness 574
12.D INTERFERENCE TESTS 575
12.D.1 Homogeneous, sensitivity to parameters *577*
12.D.2 Influence of wellbore storage and skin *579*
12.D.3 Multilayer numerical: An overview *579*
12.D.4 Other application of the numerical model *581*
12.D.5 Interference testing and real life *583*
12.D.5.a The signal 583
12.D.5.b The tests 585
12.D.6 Pulse tests *587*
12.D.6.a The old stuff 588
12.D.6.b The right stuff 588
12.D.7 Vertical interference tests *589*
12.D.8 Permeability tensor determination from multiple interference *591*
12.E MINIFRAC TEST ANALYSIS INTRODUCTION 592
12.E.1 Minifrac analysis overview *592*
12.E.2 The G-Function analysis plot *593*
12.E.3 The square root of time analysis plot *594*
12.E.4 After Closure Analysis plot (A.C.A.) *594*
12.E.5 G-function Interpretation *594*
12.E.6 Additional analysis plot *596*
12.E.6.a Square root plot 596
12.E.6.b ACA analysis: Linear, Radial and Square linear plots 596
12.E.6.c LogLog Plot 599
12.E.6.d Loglog specialized lines 600
12.E.7 Parameters identification *601*
12.E.7.a G-Function and A.C.A. plot results 601
12.E.7.b Results equations 601
12.E.8 G-Function: Theoretical background *603*
12.E.8.a Fluid type assumption 605

12.E.8.b G-function simplification 605

13 – ANALYTICAL MODELS 609

13.A INTRODUCTION 609

13.B DIMENSIONLESS PROBLEMS 610

13.B.1 Derivation 610

13.C SUPERPOSITION IN TIME 612

13.C.1 The principle of superposition 612

13.C.2 Build-up superposition 613

13.C.3 Multirate superposition 614

13.D SUPERPOSITION IN SPACE 615

13.D.1 Superposition in space of analytical models (image wells) 615

13.D.2 Semi-analytical solutions 616

13.E THE USE OF PSEUDO FUNCTIONS 617

13.E.1 Definitions of the gas pseudo pressure and pseudo time 617

13.E.2 Behavior and usage of Pseudo pressures 620

13.E.3 Pseudo time for early time wellbore storage correction 622

13.E.4 Pseudo time for late time material balance correction 623

13.E.5 The case of unconventional formations 625

13.E.5.a Generalized Pseudo functions 625

13.E.5.b Taking into account the desorption effect 626

13.E.5.c Pseudo time calculation 627

13.E.5.d Dynamic Pseudo time 627

13.E.5.e Clarkson Dynamic drainage area Workflow 628

14 – NUMERICAL MODELS 631

14.A INTRODUCTION 631

14.B PRINCIPLES OF VORONOI, PEBI AND CPG GRIDS 632

14.B.1 Building complex geometries 632

14.B.2 What is a Voronoi grid 635

14.B.3 Building the Voronoi grid 636

14.B.4 Local 3D refinement for specific well geometries 640

14.B.4.a Vertical wells 640

14.B.4.b Fractured (fully penetrating) wells 641

14.B.4.c Limited entry wells 641

14.B.4.d Limited entry fractured wells 642

14.B.4.e Horizontal wells 643
14.B.4.f Complex well 644
14.B.5 Near-well upscaling 645
14.B.5.a Adjusting the grid resolution 645
14.B.5.b Numerical upscaling procedure 648
14.B.5.c Optimum upscaling factor 649
14.C FORMULATION 651
14.C.1 Formulation 651
14.C.2 Flux terms 652
14.C.3 Generalized transmissibility corrections (Saphir–Topaze–Rubis) 654
14.C.4 Solvers 655
14.D HANDLING LINEAR PROBLEMS 658
14.D.1 A 'super-analytical model' 658
14.D.2 Modeling composite zones 659
14.D.3 Using field data 660
14.D.4 Double-porosity reservoirs 663
14.D.5 Modeling permeability anisotropy 664
14.D.6 Modeling multi-layer reservoirs (with or without cross-flow) 666
14.E HANDLING NONLINEAR PROBLEMS 668
14.E.1 Non-Darcy flow 669
14.E.2 Flow with Water and Hydrocarbons (Oil OR Gas) 671
14.E.3 Unconsolidated formations 672
14.E.4 How about three-phase flow? 674
14.E.5 Thermal modelling 675
14.F NUMERICAL SETTINGS 676
14.F.1 Changing well controls 676
14.F.2 Change in time stepping for numerical models 677

15 – NODAL ANALYSIS 681

15.A INTRODUCTION 681
15.B INFLOW PERFORMANCE RELATIONSHIP AND A.O.F. 681
15.B.1 The IPR types 682
15.B.1.a Straight line Constant IPR: 682
15.B.1.b Darcy Equation 682
15.B.1.c C&n IPR 683
15.B.1.d Gas LIT IPR 684

15.B.1.e Vogel Oil IPR for Solution gas drive reservoir 684
15.B.2 Different types of multirate tests 685
15.B.3 Different IPR/AOF calculation methods 686
15.B.3.a The Rawlins and Shellhardt method (C&n) 686
15.B.3.b The LIT Method 687
15.B.3.c Jones method 688
15.C INTAKE MODELS IN PTA AND RTA 690
15.C.1 Classic pressure correction 690
15.C.2 Correction methods 690
15.C.3 Flow models and correlations 691
15.C.3.a Flow correlations for Liquid-Liquid 692
15.C.3.b Flow correlations for Liquid-Gas 692
15.C.3.c Flow correlations for dry gas 692
15.C.3.d Flow correlations for Three phase 692
15.C.3.e Lift curves 692
15.C.4 General calculation method 693
15.C.5 Correcting gauge data vs. correcting model 693
15.C.6 Well intake in multilateral wells 694

16 – PERMANENT GAUGES & INTELLIGENT FIELDS 695

16.A WHAT PDG DATA CAN BRING 695
16.B CHALLENGES OF PDG DATA 697
16.B.1 Storage and access 697
16.B.2 Smart reduction 697
16.C WAVELET FILTRATION – AN OVERVIEW 699
16.D WAVELET FILTRATION - THEORY 701
16.D.1 Wavelet and scaling functions 701
16.D.2 Wavelet filtration with a single frequency 702
16.D.3 Wavelet filtration with multiple frequencies 703
16.D.4 Parameters controlling wavelet processing 704
16.D.5 Selection of the initial time step / frequency 705
16.E WAVELET FILTRATION - PRACTICE 706
16.F PRESSURE TRANSIENT ANALYSIS OF PDG DATA 709
16.G RATE TRANSIENT ANALYSIS OF PDG DATA 712
16.H APPLICATIONS AND DATA FLOW 714
16.H.1 Accessing the historian, Client/Server solution 714

17 – PRODUCTION LOGGING 717

17.A INTRODUCTION 717

17.B WHAT PRODUCTION LOGGING IS USED FOR 718

17.C CLASSICAL PRODUCTION LOGGING TOOLS 720

17.C.1 Flowmeters (spinners) 721

17.C.2 Fluid identification tools 722

17.C.2.a Gradiomanometers 723

17.C.2.b Nuclear density tool 724

17.C.2.c Tuning Fork Density (TFD) 724

17.C.2.d Pseudo-density from pressure 725

17.C.2.e Capacitance tools for water holdup 725

17.C.2.f Gas holdup tools (GHT) 725

17.C.3 Pressure and Temperature sensors 726

17.C.4 Depth and ID devices 726

17.C.4.a Depth measurement 726

17.C.4.b Depth correction: Open Hole Gamma Ray 727

17.C.4.c Depth correction: Cased Hole CCL 727

17.C.4.d Depth correction: Cased Hole MML 727

17.C.4.e ID calculation: Calipers 727

17.D A TYPICAL PL JOB SEQUENCE 728

17.E TYPICAL JOB 729

17.F DATA LOADING, QA/QC, AND REFERENCE CHANNELS 730

17.G SPINNER CALIBRATION AND APPARENT VELOCITY CALCULATION 732

17.G.1 Spinner response 732

17.G.2 Spinner in-situ calibration 734

17.G.2.a Spinner Calibration application zones 735

17.G.3 Velocity from calibration: threshold handling and Vapparent 735

17.G.3.a Threshold options 735

17.G.3.b Apparent Velocity 736

17.G.4 Apparent velocity log 736

17.H SINGLE PHASE INTERPRETATION 737

17.H.1 Velocity profile correction factor 737

17.H.2 Single phase interpretation results 739

17.H.3 Matching surface conditions 740

17.I MULTIPHASE INTERPRETATION 741

17.I.1 Definitions 741

17.I.1.a Holdups 741
17.I.1.b Phase velocities 741
17.I.1.c Slippage velocity 741
17.I.2 Starting with 2-phase 742
17.I.3 General solution using non-linear regression 743
17.I.4 Flow models and correlations 744
17.I.5 Graphical presentation 745
17.I.6 Emeraude Zoned approach and the Zone Rates plot 746
17.I.7 Multiphase interpretation results 747
17.I.8 Zoned Approach and Global Regression 748
17.I.8.a Slippage compliance and Zoned method 749
17.I.9 The Continuous approach 750
17.I.9.a Illustration with a 3-Phase example 751
17.I.9.b So? 752
17.J SLANTED AND HORIZONTAL WELLS 753
17.J.1 Apparent down flow 753
17.J.2 Horizontal wells 753
17.K MULTIPLE PROBE TOOLS (MPT), OR ARRAY TOOLS 756
17.K.1 Schlumberger FloView – Courtesy Schlumberger 756
17.K.2 Schlumberger GHOST – Courtesy Schlumberger 757
17.K.3 Schlumberger FloScanner (FSI) – Courtesy Schlumberger 758
17.K.4 Baker Hughes-Sondex MAPS and PAI 759
17.K.4.a CAT: Capacitance Array Tool 759
17.K.4.b RAT: Resistance Array Tool 760
17.K.4.c SAT: Spinner Array Tool 761
17.K.4.d PAI 761
17.K.5 OpenField FAST 762
17.L MPT PROCESSING 764
17.L.1 Mapping models 764
17.L.1.a Linear model 764
17.L.1.b Polynomial model 765
17.L.1.c MapFlo holdup model 765
17.L.1.d Prandtl velocity model 766
17.L.1.e 2D interpolation model 767
17.L.2 Integration 767
17.L.3 Interpretation 768

17.M SIP 769
17.M.1 IPR Type 769

18 – THERMAL ANALYSIS AND SIMULATION 771

18.A Introduction 771
18.B What information can be extracted from Temperature data? 772
18.C Temperature Measurements 776
18.C.1 Distributed Temperature Sensing (DTS) 776
18.C.2 Discrete Temperature Sensors 778
18.C.3 Temperature gauges 779
18.D Theory review 780
18.D.1 Heat Conduction 780
18.D.2 Heat Convection 781
18.D.3 Radiation 781
18.D.4 Heat Loss Coefficient 782
18.D.5 Geothermal Gradient 784
18.D.6 Joule-Thomson Effect 785
18.D.7 Ramey Equation and qualitative analysis 787
18.D.8 Energy and mass balances 789
18.E Emeraude "Energy" equation - Production and Injection profiling 791
18.E.1 Resulting formulation of the Energy equation 792
18.E.2 Summarized interpretation workflow 792
18.E.3 Sensitivity to input parameters 798
18.E.4 Time dependency 800
18.E.5 Annular convection 801
18.E.6 Multiphase profiling 801
18.E.7 Horizontal wells 803
18.E.8 Summary and limitations 804
18.F Water Injection Fall-off – Emeraude 805
18.F.1 Summarized interpretation workflow 807
18.F.2 Sensitivities to the input parameters 809
18.G Numerical Simulation – Rubis 811
18.G.1 Formulation 811
18.G.2 Wellbore coupling 817
18.G.3 Non-geothermal fluid entry 818

18.G.4 Transient temperature logs 819
18.G.5 Gridding and transient thermal effects 821
18.H FORWARD TEMPERATURE SIMULATION – EMERAUDE 823
18.H.1 Steam Injection 823
18.H.2 Leak detection 825